MOLECULAR AND CELLULAR EFFECTORS IN THE RESOLUTION OF INFLAMMATION

EDITED BY: Amiram Ariel, Janos G. Filep, Sylvain Perruche and Sylvaine You
PUBLISHED IN: Frontiers in Immunology

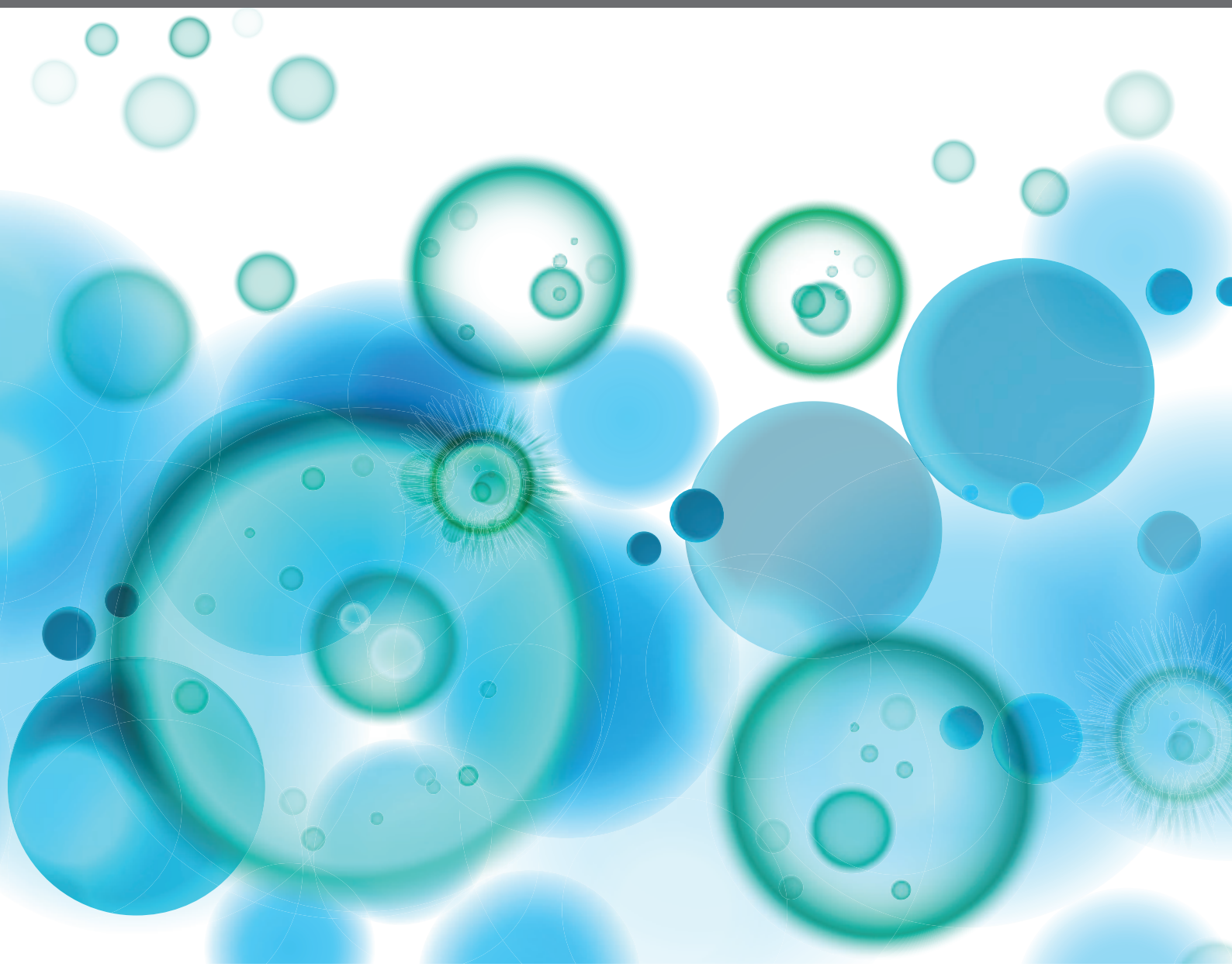

frontiers Research Topics

Frontiers eBook Copyright Statement

The copyright in the text of individual articles in this eBook is the property of their respective authors or their respective institutions or funders. The copyright in graphics and images within each article may be subject to copyright of other parties. In both cases this is subject to a license granted to Frontiers.

The compilation of articles constituting this eBook is the property of Frontiers.

Each article within this eBook, and the eBook itself, are published under the most recent version of the Creative Commons CC-BY licence. The version current at the date of publication of this eBook is CC-BY 4.0. If the CC-BY licence is updated, the licence granted by Frontiers is automatically updated to the new version.

When exercising any right under the CC-BY licence, Frontiers must be attributed as the original publisher of the article or eBook, as applicable.

Authors have the responsibility of ensuring that any graphics or other materials which are the property of others may be included in the CC-BY licence, but this should be checked before relying on the CC-BY licence to reproduce those materials. Any copyright notices relating to those materials must be complied with.

Copyright and source acknowledgement notices may not be removed and must be displayed in any copy, derivative work or partial copy which includes the elements in question.

All copyright, and all rights therein, are protected by national and international copyright laws. The above represents a summary only. For further information please read Frontiers' Conditions for Website Use and Copyright Statement, and the applicable CC-BY licence.

ISSN 1664-8714
ISBN 978-2-88976-387-0
DOI 10.3389/978-2-88976-387-0

About Frontiers

Frontiers is more than just an open-access publisher of scholarly articles: it is a pioneering approach to the world of academia, radically improving the way scholarly research is managed. The grand vision of Frontiers is a world where all people have an equal opportunity to seek, share and generate knowledge. Frontiers provides immediate and permanent online open access to all its publications, but this alone is not enough to realize our grand goals.

Frontiers Journal Series

The Frontiers Journal Series is a multi-tier and interdisciplinary set of open-access, online journals, promising a paradigm shift from the current review, selection and dissemination processes in academic publishing. All Frontiers journals are driven by researchers for researchers; therefore, they constitute a service to the scholarly community. At the same time, the Frontiers Journal Series operates on a revolutionary invention, the tiered publishing system, initially addressing specific communities of scholars, and gradually climbing up to broader public understanding, thus serving the interests of the lay society, too.

Dedication to Quality

Each Frontiers article is a landmark of the highest quality, thanks to genuinely collaborative interactions between authors and review editors, who include some of the world's best academicians. Research must be certified by peers before entering a stream of knowledge that may eventually reach the public - and shape society; therefore, Frontiers only applies the most rigorous and unbiased reviews.
Frontiers revolutionizes research publishing by freely delivering the most outstanding research, evaluated with no bias from both the academic and social point of view. By applying the most advanced information technologies, Frontiers is catapulting scholarly publishing into a new generation.

What are Frontiers Research Topics?

Frontiers Research Topics are very popular trademarks of the Frontiers Journals Series: they are collections of at least ten articles, all centered on a particular subject. With their unique mix of varied contributions from Original Research to Review Articles, Frontiers Research Topics unify the most influential researchers, the latest key findings and historical advances in a hot research area! Find out more on how to host your own Frontiers Research Topic or contribute to one as an author by contacting the Frontiers Editorial Office: frontiersin.org/about/contact

MOLECULAR AND CELLULAR EFFECTORS IN THE RESOLUTION OF INFLAMMATION

Topic Editors:
Amiram Ariel, University of Haifa, Israel
Janos G. Filep, Université de Montréal, Canada
Sylvain Perruche, Institut National de la Santé et de la Recherche Médicale (INSERM), France
Sylvaine You, Institut National de la Santé et de la Recherche Médicale (INSERM), France

Citation: Ariel, A., Filep, J. G., Perruche, S., You, S., eds. (2022). Molecular and Cellular Effectors in the Resolution of Inflammation. Lausanne: Frontiers Media SA. doi: 10.3389/978-2-88976-387-0

Table of Contents

06 ***Editorial: Molecular and Cellular Effectors in the Resolution of Inflammation***
Amiram Ariel, Sylvain Perruche, Sylvaine You and János G. Filep

10 ***A New E-Series Resolvin: RvE4 Stereochemistry and Function in Efferocytosis of Inflammation-Resolution***
Stephania Libreros, Ashley E. Shay, Robert Nshimiyimana, David Fichtner, Michael J. Martin, Nicholas Wourms and Charles N. Serhan

24 ***The Immunopathology of COVID-19 and the Cannabis Paradigm***
Nicole Paland, Antonina Pechkovsky, Miran Aswad, Haya Hamza, Tania Popov, Eduardo Shahar and Igal Louria-Hayon

37 ***CCR2 Is Dispensable for Disease Resolution but Required for the Restoration of Leukocyte Homeostasis Upon Experimental Malaria-Associated Acute Respiratory Distress Syndrome***
Emilie Pollenus, Thao-Thy Pham, Leen Vandermosten, Hendrik Possemiers, Sofie Knoops, Ghislain Opdenakker and Philippe E. Van den Steen

54 ***The Crucial Role of PPARγ-Egr-1-Pro-Inflammatory Mediators Axis in IgG Immune Complex-Induced Acute Lung Injury***
Chunguang Yan, Jing Chen, Yue Ding, Zetian Zhou, Bingyu Li, Chunmin Deng, Dong Yuan, Qi Zhang and Ximo Wang

66 ***GIPR Signaling in Immune Cells Maintains Metabolically Beneficial Type 2 Immune Responses in the White Fat From Obese Mice***
Irina Efimova, Inbar Steinberg, Isabel Zvibel, Anat Neumann, Dana Fernanda Mantelmacher, Daniel J. Drucker, Sigal Fishman and Chen Varol

79 ***αB-Crystallin Alleviates Endotoxin-Induced Retinal Inflammation and Inhibits Microglial Activation and Autophagy***
Fangyu Wang, Zhaoxin Jiang, Bingsheng Lou, Fang Duan, Suo Qiu, Zhixing Cheng, Xinqi Ma, Yao Yang and Xiaofeng Lin

93 ***Resolvin E1 Regulates Th17 Function and T Cell Activation***
Fatma Oner, Carla Alvarez, Wael Yaghmoor, Danielle Stephens, Hatice Hasturk, Erhan Firatli and Alpdogan Kantarci

108 ***Adenosine Diphosphate Improves Wound Healing in Diabetic Mice Through $P2Y_{12}$ Receptor Activation***
Paula Alvarenga Borges, Ingrid Waclawiak, Janaína Lima Georgii, Vanderlei da Silva Fraga-Junior, Janaína Figueiredo Barros, Felipe Simões Lemos, Thaís Russo-Abrahão, Elvira Maria Saraiva, Christina M. Takiya, Robson Coutinho-Silva, Carmen Penido, Claudia Mermelstein, José Roberto Meyer-Fernandes, Fábio B. Canto, Josiane Sabbadini Neves, Paulo A. Melo, Claudio Canetti and Claudia Farias Benjamim

126 ***Cells of the Immune System in Cardiac Remodeling: Main Players in Resolution of Inflammation and Repair After Myocardial Infarction***
Irina Kologrivova, Marina Shtatolkina, Tatiana Suslova and Vyacheslav Ryabov

145 ***Pro-Resolving Mediator Annexin A1 Regulates Intracellular Ca^{2+} and Mucin Secretion in Cultured Goblet Cells Suggesting a New Use in Inflammatory Conjunctival Diseases***
Anne V. Lyngstadaas, Markus V. Olsen, Jeffrey A. Bair, Robin R. Hodges, Tor P. Utheim, Charles N. Serhan and Darlene A. Dartt

159 ***12/15-Lipoxygenase Regulates IL-33-Induced Eosinophilic Airway Inflammation in Mice***
Jun Miyata, Yoshiyuki Yokokura, Kazuyo Moro, Hiroyuki Arai, Koichi Fukunaga and Makoto Arita

170 ***Specialized Pro-Resolving Mediators Mitigate Cancer-Related Inflammation: Role of Tumor-Associated Macrophages and Therapeutic Opportunities***
Margot Lavy, Vanessa Gauttier, Nicolas Poirier, Sophie Barillé-Nion and Christophe Blanquart

189 ***Butorphanol Promotes Macrophage Phenotypic Transition to Inhibit Inflammatory Lung Injury* via κ *Receptors***
Guangxin Luan, Fan Pan, Lina Bu, Kaixuan Wu, Aizhong Wang and Xiaotao Xu

206 ***Prostanoids and Resolution of Inflammation – Beyond the Lipid-Mediator Class Switch***
Tobias Schmid and Bernhard Brüne

215 ***Macrophage-Regulatory T Cell Interactions Promote Type 2 Immune Homeostasis Through Resistin-Like Molecule α***
Jiang Li, Sang Yong Kim, Nancy M. Lainez, Djurdjica Coss and Meera G. Nair

230 ***Protectins PCTR1 and PD1 Reduce Viral Load and Lung Inflammation During Respiratory Syncytial Virus Infection in Mice***
Katherine H. Walker, Nandini Krishnamoorthy, Thayse R. Brüggemann, Ashley E. Shay, Charles N. Serhan and Bruce D. Levy

245 ***Dysregulated Maresin Concentrations in Plasma and Nasal Secretions From Patients With Chronic Rhinosinusitis***
Issa Beegun, Duco S. Koenis, Ghassan Alusi and Jesmond Dalli

260 ***CNS-Spleen Axis – a Close Interplay in Mediating Inflammatory Responses in Burn Patients and a Key to Novel Burn Therapeutics***
Noorisah Khan, Supreet Kaur, Carly M. Knuth and Marc G. Jeschke

272 ***Critical Role of Synovial Tissue–Resident Macrophage and Fibroblast Subsets in the Persistence of Joint Inflammation***
Samuel Kemble and Adam P. Croft

289 ***High Na^+ Environments Impair Phagocyte Oxidase-Dependent Antibacterial Activity of Neutrophils***
Luka Krampert, Katharina Bauer, Stefan Ebner, Patrick Neubert, Thomas Ossner, Anna Weigert, Valentin Schatz, Martina Toelge, Agnes Schröder, Martin Herrmann, Markus Schnare, Anca Dorhoi and Jonathan Jantsch

301 ***The Antimicrobial Peptide Human β-Defensin-3 Accelerates Wound Healing by Promoting Angiogenesis, Cell Migration, and Proliferation Through the FGFR/JAK2/STAT3 Signaling Pathway***
Miho Takahashi, Yoshie Umehara, Hainan Yue, Juan Valentin Trujillo-Paez, Ge Peng, Hai Le Thanh Nguyen, Risa Ikutama, Ko Okumura, Hideoki Ogawa, Shigaku Ikeda and François Niyonsaba

318 ***Apoptotic Cells for Therapeutic Use in Cytokine Storm Associated With Sepsis– A Phase Ib Clinical Trial***
Peter Vernon van Heerden, Avraham Abutbul, Sigal Sviri, Eitan Zlotnick, Ahmad Nama, Sebastian Zimro, Raja el-Amore, Yehudit Shabat, Barak Reicher, Batla Falah and Dror Mevorach

335 ***Desmoglein2 Regulates Claudin2 Expression by Sequestering PI-3-Kinase in Intestinal Epithelial Cells***
Natalie Burkard, Michael Meir, Felix Kannapin, Christoph Otto, Maximilian Petzke, Christoph-Thomas Germer, Jens Waschke and Nicolas Schlegel

352 ***Monocyte Chemotactic Protein-Induced Protein 1 (MCPIP-1): A Key Player of Host Defense and Immune Regulation***
Zhuqing Jin, En Zheng, Candice Sareli, Pappachan E. Kolattukudy and Jianli Niu

363 ***Syndecan-1 Amplifies Ovalbumin-Induced Airway Remodeling by Strengthening TGFβ1/Smad3 Action***
Dong Zhang, Xin-rui Qiao, Wen-Jing Cui, Jin-tao Zhang, Yun Pan, Xiao-fei Liu and Liang Dong

380 ***LN Monocytes Limit DC-Poly I:C Induced Cytotoxic T Cell Response* via *IL-10 and Induction of Suppressor CD4 T Cells***
Anita Tewari, Miglena G. Prabagar, Sophie L. Gibbings, Kavita Rawat and Claudia V. Jakubzick

391 ***The Transcription Factor FRA-1/AP-1 Controls Lipocalin-2 Expression and Inflammation in Sepsis Model***
Shan Cao, Anne Schnelzer, Nicole Hannemann, Georg Schett, Didier Soulat and Aline Bozec

405 ***Pharmacological Activation Of Aldehyde Dehydrogenase 2 Protects Against Heatstroke-Induced Acute Lung Injury by Modulating Oxidative Stress and Endothelial Dysfunction***
Hsiao-Ya Tsai, Yu-Juei Hsu, Cheng-Yo Lu, Min-Chien Tsai, Wan-Chu Hung, Po-Chuan Chen, Jen-Chun Wang, Lung-An Hsu, Yung-Hsin Yeh, Pauling Chu and Shih-Hung Tsai

418 ***Regulation of T-Cell Immune Responses by Pro-Resolving Lipid Mediators***
Javier Perez-Hernandez, Valerio Chiurchiù, Sylvain Perruche and Sylvaine You

431 ***Transcriptional and Histochemical Signatures of Bone Marrow Mononuclear Cell-Mediated Resolution of Synovitis***
Bruno C. Menarim, Hossam El-Sheikh Ali, Shavahn C. Loux, Kirsten E. Scoggin, Theodore S. Kalbfleisch, James N. MacLeod and Linda A. Dahlgren

452 ***Pro-Resolving Factors Released by Macrophages After Efferocytosis Promote Mucosal Wound Healing in Inflammatory Bowel Disease***
Omayra Martin-Rodriguez, Thierry Gauthier, Francis Bonnefoy, Mélanie Couturier, Anna Daoui, Cécile Chagué, Séverine Valmary-Degano, Claire Gay, Philippe Saas and Sylvain Perruche

467 ***Hypoxia Promotes Neutrophil Survival After Acute Myocardial Infarction***
Maximilian Dölling, Markus Eckstein, Jeeshan Singh, Christine Schauer, Janina Schoen, Xiaomei Shan, Aline Bozec, Jasmin Knopf, Georg Schett, Luis E. Muñoz and Martin Herrmann

frontiers | Frontiers in Immunology

EDITORIAL
published: 26 May 2022
doi: 10.3389/fimmu.2022.938819

Editorial: Molecular and Cellular Effectors in the Resolution of Inflammation

Amiram Ariel[1,2*], *Sylvain Perruche*[3,4], *Sylvaine You*[5] *and János G. Filep*[6,7]

[1] The Department of Biology, The Faculty of Natural Sciences, University of Haifa, Haifa, Israel, [2] The Departments of Human Biology, The Faculty of Natural Sciences, University of Haifa, Haifa, Israel, [3] Univ. Bourgogne Franche-Comté, INSERM, EFS BFC, UMR1098 RIGHT, Interactions Hôte-Greffon-Tumeur/Ingénierie Cellulaire et Génique, Besançon, France, [4] MED'INN'Pharma, Besançon, France, [5] Université Paris Cité, CNRS, INSERM, Institut Cochin, Paris, France, [6] Department of Pathology and Cell Biology, University of Montreal, Montreal, QC, Canada, [7] Research Center, Maisonneuve-Rosemont Hospital, Montreal, QC, Canada

Keywords: resolution of inflammation, myeloid cells, lymphocytes, soluble mediators, intracellular signaling

Editorial on the Research Topic

Molecular and Cellular Effectors in the Resolution of Inflammation

OPEN ACCESS

Edited and reviewed by:
Pietro Ghezzi,
University of Urbino Carlo Bo, Italy

***Correspondence:**
Amiram Ariel
amiram@research.haifa.ac.il

Specialty section:
This article was submitted to Inflammation, a section of the journal Frontiers in Immunology

Received: *08 May 2022*
Accepted: *09 May 2022*
Published: *26 May 2022*

Citation:
Ariel A, Perruche S, You S and Filep JG (2022) Editorial: Molecular and Cellular Effectors in the Resolution of Inflammation. Front. Immunol. 13:938819. doi: 10.3389/fimmu.2022.938819

Acute inflammation is broadly defined as a protective response of the organism to invading pathogens and tissue injury. The reaction should ideally be localized and self-limited, enabling the elimination of pathogens and damaged cells, and resolve on its own, leading to tissue repair and restoration of normal tissue and organ function (1). Uncontrolled or excessive inflammation or failure of the initial response to resolve in a timely manner leads to nonresolving inflammation, which is often chronic, or transient and relapsing (2). This ongoing low-grade inflammation is thought to fail to activate the integrated process of resolution (3), which is increasingly being recognized as a critical component of numerous prevalent human diseases, including atherosclerosis, arthritis, pulmonary diseases, autoimmunity, diabetes and cancer (2, 4). The inflammatory response is a complex process, heterogeneous in nature and depends on the type of disease and organ in which it occurs. The sequence of events and signaling circuits activated during the initiation and resolution phase have received considerable attention, and are summarized in guiding maps for inflammation (5) and resolution pathways (6). Resolution is an active process governed by endogenous resolution programs driven by specialized pro-resolving mediators (SPMs) acting at pro-resolving receptors (7). As an example, lipoxins synthesized from arachidonic acid during the resolution of self-limited inflammation function as stop signals through the receptor ALX/FPR2 for neutrophil recruitment, facilitate neutrophil apoptosis and efferocytosis (4), pivotal events in efficient resolution. Given the dual nature of inflammation and the importance of the inflammatory response in survival, it is paramount to develop new treatments to overcome the limitations of currently available anti-inflammatory therapies, which are often accompanied with unwanted side effects and do not lead to repair of the affected tissues. Indeed, over the past few years a new branch of pharmacology termed "resolution pharmacology" (8, 9) has emerged, with the goal of developing strategies that promote resolution instead of blocking or inhibiting a mediator or pathway.

This Research Topic brings together thirty-two articles, both reviews and original research papers, which highlight recent advances in resolution biology, wound repair, metabolic disorders, and acquired immunity using a large variety of experimental models. Twenty-four articles report

original research on molecular mechanisms that underpin processes that limit inflammation and autoimmune disorders and/or promote tissue repair and return to homeostasis. These studies also provide profiles of the resolution process at the molecular and cellular levels, and discuss new avenues for potential therapeutic interventions based on enhancing pro-resolving mechanisms. Eight reviews summarize current knowledge on the complex molecular and cellular interactions between various immune cells, lipid and protein mediators, and intracellular signaling circuits, which may orchestrate the resolution of a broad spectrum of diseases, including COVID-19, inflammatory and autoimmune diseases, cardiac remodeling, burns, and cancer.

Pro-resolving lipid mediators, including lipoxins, resolvins, maresins and protectins, play central roles in orchestrating efficient resolution (7). Extending previous research, ten articles in this Research Topic discuss recent advances on lipid SPMs, their molecular characteristics, biosynthesis and functions in various pathologies. Libreros et al. describe the synthesis of a new member of the resolvin (Rv) E family, RvE4, its stereochemistry, and capacity to facilitate of the uptake of apoptotic cells (efferocytosis), an essential process to remove damaged cells and inflammatory cells from the inflamed site. Walker et al. report that Protectin Conjugates in Tissue Regeneration 1 (PCTR1) and protectin D1 (PD1) are produced during the resolution of RSV infection and, in turn, reduce viral load while limiting lung type 2 immunity in response to viral infection. Miyata et al. show that during type 2 immunity, activation of 12/15-lipoxygenase is essential for the production of SPMs during IL-33-induced lung inflammation. The SPM products 14(S)-HDoHE and 10(S), 17(S)-diHDoHE markedly reduced ILC2 proliferation and cytokine production to limit IL-33-driven eosinophilic inflammation. Oner et al. report that the SPM RvE1 is a potent inhibitor of Th17 cell differentiation, as well as IL-17 production by acting directly on naïve T cells or indirectly through dendritic cells. Beegun et al. identify dysregulated generation of another potent SPM, maresin 1 during chronic rhino-sinusitis. Maresin 1 reduces expression of adhesion molecules on phagocytes to promote inflammation resolution. Borges et al. demonstrate that adenosine diphosphate, a metabolic product released mainly by platelets at injury sites, plays a role in diabetic wound repair signaling through its receptor P2Y12 to limit inflammatory outcomes. Perez-Hernandez et al. present a critical review on the dual roles of SPM in tilting the effector to regulatory T cell pendulum towards beneficial outcomes and the diagnostic and prognostic value of these mediators in various experimental models and human diseases. Lavy et al. elaborate on this theme by providing an overview on the role of SPMs in the regulation of cancer immunity, with particular emphasis on the role of tumor-associated macrophages. They also discuss the ability of SPMs to re-educate macrophages for combating tumors. Schmid and Brune discuss prostanoids and their emerging functions in resolving inflammation and how they can be used for therapeutic purposes. Paland et al. summarize recent clinical advances in understanding the pathogenesis of COVID-19 and the development of potentially lethal cytokine storm and speculate how phytocannabinoids could be harnessed to treat severe cases and reduce mortality.

In addition to lipid SPMs, protein and peptide mediators have long been recognized as important regulators of resolution. Expanding our knowledge on these mediators, eight publications are dedicated to novel resolution-associated proteins or peptides and provide insight into their function. Martin-Rodriguez et al. describe novel potential therapeutic applications for mediators released by macrophages following efferocytosis in T cell-driven colitis. This secretome, named SuperMApo, notably contains TGF-β, IGF-I, and VEGF that act on intestinal epithelial cells to enhance wound repair and limit tissue damage. SuperMApo single treatment allows the resolution of ongoing experimental colitis. Takahashi et al. report that another wound healing effector, the anti-bacterial peptide beta-defensin 3, can promote angiogenesis, fibroblast migration, and proliferation through FGFR1. Lyngstadaas et al. identified novel functions for the well-known pro-resolving protein annexin A1 acting on conjunctival goblet cells. They report annexin A1 facilitation of calcium influx and mucin secretion from these cells *in vitro*, suggesting a protective role for this protein in inflammatory conjunctival diseases. Pollenus et al. unveil a dichotomic role for the chemokine receptor CCR2 critical for monocyte migration to inflamed and resolving sites in malaria-associated ARDS. They report that while CCR2 is essential for migration of inflammatory and non-classical monocytes during the onset and resolution of inflammation, respectively, CCR2-deficiency has no impact on ARDS development or resolution. Efimova et al. describe obesity as an inflammatory disorder regulated by myeloid cells. They argue for a previously unappreciated role for the glucagon-induced peptide receptor (GIPR) in myeloid cells to maintain a beneficial type II immune response in white adipose tissue. The ECM component syndecan-1, which was previously described as critical for the resolution of inflammation, exerts opposing actions in type II immunity-associated airway remodeling. Zhang et al. show that syndecan-1 enhances the TGF-β/SMAD3 pathway to promote ECM production and myofibroblast generation. Jin et al. review the complex role of chemokines, such as CCL2/MCP-1, and their products in the resolution of inflammation. While most inflammatory chemokines were previously solely considered to be potent pro-inflammatory and autoimmunity-driving effectors, recent data on the genes they induce requires revisiting this notion. For instance, MCP-1-induced peptide 1 (MCPIP1) is highlighted as a key pro-resolving agent that limits NF-kB activation and regulates the stability of specific mRNAs to promote resolution and the clearance of virus-infected apoptotic cells.

The phenotypic and functional heterogeneity of myeloid cells and macrophage subsets in particular, in resolving inflammation and wound repair have received considerable attention during the past years. Tewari et al. describe a novel role for lymph node monocytes in limiting poly I:C-induced, dendritic cell-mediated, T cell cytotoxicity through the induction of IL-10 production and the generation of $CD4^+$ suppressive T cells. Consistently,

blocking IL-10 in a melanoma-targeted immune response improved the therapeutic potential of poly I:C. Li et al. document another macrophage-regulatory T-cell circuit. This cell-cell interaction limited type 2 immunity by supporting the proliferation of Treg through myeloid production of resistin-like molecule α. Luan et al. show that the pain reliever butorphanol through the opioid κ receptor reduces LPS-induced acute lung injury by shifting the M1-like to M2-like macrophage balance and limiting the function of inflammatory effectors. Krampert et al. report that high sodium environments may hamper the anti-bacterial functions of neutrophils without affecting neutrophil viability. This response is likely mediated through NADPH oxidase-generated ROS and underscores the health hazard associated with high sodium intake. Kemble and Croft discuss the intricate local cell-cell interactions in the inflamed joints. Their overview focuses on synovial resident macrophages and fibroblasts, their mutual regulatory properties, and how their breakdown can lead to persisting pathology. They also discuss how these mechanisms can be harnessed to develop potential therapies. Khan et al. review another regulatory axis between the central nervous system and the spleen. They suggest that this axis is critical in regulating immune responses to thermal injury, and argue that a better understanding of its mechanistic aspects could provide opportunities for new therapies. Kologrivova et al. discuss the role of immune cells in tissue repair with a particular focus on cardiac remodeling and repair following myocardial infarction, with myeloid cells and lymphocytes considered for their dichotomic roles in injury generation and healing.

Six reports provide novel insights into intracellular mechanisms that control key events in inflammation and resolution. Burkard et al. show that desmoglein 2 (Dsg2) regulates the expression of the tight junction protein claudin 2 in intestinal inflammation, and thereby blocks changes in intestinal epithelial barrier induced by inflammatory conditions and PI3 kinase. Dolling et al. document that hypoxia promotes neutrophil survival and reduces NET formation potential following myocardial infarction in humans. The hypoxia-responsive transcription factor HIF-1α seems to be critical in mediating these responses. Cao et al. describe a new axis that governs the inflammatory response in endotoxemia. They identify a critical role for the transcription factor FRA-1 for optimal expression of the anti-inflammatory protein lipocalin 2 during LPS tolerance. Conversely, mice deficient in FRA-1 show deficiencies in resolution. Tsai et al. present evidence supporting a role for aldehyde dehydrogenase 2 (ALDH2) in limiting heat shock-induced endothelial damage and lung injury. The pharmacological stimulator of ALDH2, alda-1, increased enzymatic activity leading to a reduction of ROS production and alleviation of heat exposure-induced damage. Wang et al. reveal that another heat shock protein, αB-crystalline, alleviates LPS-induced uveitis by reducing production of inflammatory cytokines, activation of microglia, autophagy, inflammatory features, and loss of function in the retina. Yan et al. show that the anti-inflammatory transcription factor PPAR-γ limits damage in IgG-immune complex-induced lung inflammation, likely through the inhibition of EGR-1-induced cytokine production.

To illustrate the translational potential of resolution pharmacology, two articles present data from recent clinical studies. In a pilot study, van Heerden et al. report that treatment of patients with mild-to-moderate sepsis with preparations from early apoptotic cells (termed Allocetra™-OTS) led to early resolution of the cytokine storm, and survival of all subjects, as compared with a mortality rate of 27% of historically matched controls. No adverse effects have been observed. Menarim et al. provide detailed transcriptomic and histochemical analysis of bone marrow mononuclear cells recovered during the resolution of osteoarthritis. This report highlights PPAR-γ as a key effector, and hence a promising therapeutic target in resolving synovitis.

In conclusion, this Research Topic presents a selection of articles that underscore the resolution of inflammation as a tightly regulated process involving various lipid and protein effectors predominantly acting through specific surface receptors on responding cells. These effectors, in turn, activate transcriptional cascades that affect gene signatures leading to robust responses. Immune cells, particularly of the myeloid lineage, are key cellular contributors to the resolution of inflammation by regulating their local migration, cytokine production, debris clearance, NETosis, and cell death. Gaining a comprehensive understanding of these processes and identifying novel mediators and pathways that facilitate resolution will likely identify potential targets for development of novel therapeutic approaches for autoimmune, inflammatory, tissue repair, and fibrotic diseases.

AUTHOR CONTRIBUTIONS

This editorial was co-authored by all the indicated authors. All authors concur with its content and approve the submission.

REFERENCES

1. V Kumar, AK Abbas, JC Aster eds. *Robbins Basic Pathology*. Philadelphia, Pennsylvania, USA: Elsevier Saunders (2013). pp. 29–73.
2. Nathan C, Ding A. Nonresolving Inflammation. *Cell* (2010) 140:871–82. doi: 10.1016/j.cell.2010.02.029
3. Serhan CN, Savill J. Resolution of Inflammation: The Beginning Programs the End. *Nat Immunol* (2005) 6:1191–7. doi: 10.1038/ni1276
4. Serhan CN. Pro-Resolving Lipid Mediators Are Leads for Resolution Physiology. *Nature* (2014) 510:92–101. doi: 10.1038/nature13479
5. Netea MG, Balkwill B, Chonchol M, Cominelli F, Donath MY, Giamarellos-Bourboulis EJ, et al. A Guiding Map for Inflammation. *Nat Immunol* (2017) 18:826–31. doi: 10.1038/ni.3790
6. Serhan CN, Gupta SK, Perretti M, Godson C, Brennan E, Li Y, et al. The Atlas of Inflammation Resolution (AIR). *Mol Aspects Med* (2020) 74:894. doi: 10.1016/j.mam.2020.100894

7. Serhan CN, Levy BD. Resolvins in Inflammation: Emergence of the Pro-Resolving Superfamily of Mediators. *J Clin Invest* (2018) 128:2657–69. doi: 10.1172/JCI97943
8. Perretti M, Leroy X, Bland EJ, Montero-Melendez T. Resolution Pharmacology: Opportunities for Therapeutic Innovation in Inflammation. *Trends Pharmacol Sci* (2015) 36:737–55. doi: 10.1016/j.tips.2015.07.007
9. Perretti M, Godson C. Formyl Peptide Receptor Type 2 Agonists to Kick-Start Resolution Pharmacology. *Br J Pharmacol* (2020) 177:4595–600. doi: 10.1111/bph.15212

Conflict of Interest: SP is the CEO of MED'INN'Pharma.

The remaining authors declare that the research was conducted in the absence of any commercial or financial relationships that could be construed as a potential conflict of interest.

Publisher's Note: All claims expressed in this article are solely those of the authors and do not necessarily represent those of their affiliated organizations, or those of the publisher, the editors and the reviewers. Any product that may be evaluated in this article, or claim that may be made by its manufacturer, is not guaranteed or endorsed by the publisher.

Copyright © 2022 Ariel, Perruche, You and Filep. This is an open-access article distributed under the terms of the Creative Commons Attribution License (CC BY). The use, distribution or reproduction in other forums is permitted, provided the original author(s) and the copyright owner(s) are credited and that the original publication in this journal is cited, in accordance with accepted academic practice. No use, distribution or reproduction is permitted which does not comply with these terms.

frontiers in Immunology

ORIGINAL RESEARCH
published: 10 February 2021
doi: 10.3389/fimmu.2020.631319

A New E-Series Resolvin: RvE4 Stereochemistry and Function in Efferocytosis of Inflammation-Resolution

Stephania Libreros[1†], *Ashley E. Shay*[1†], *Robert Nshimiyimana*[1], *David Fichtner*[2], *Michael J. Martin*[2], *Nicholas Wourms*[2] *and Charles N. Serhan*[1*]

[1] Center for Experimental Therapeutics and Reperfusion Injury, Department of Anesthesiology, Perioperative and Pain Medicine, Brigham and Women's Hospital and Harvard Medical School, Boston, MA, United States, [2] Cayman Chemical, Research and Development Department, Ann Arbor, MI, United States

OPEN ACCESS

Edited by:
Janos G. Filep,
Université de Montréal, Canada

Reviewed by:
Gabrielle Fredman,
Albany Medical College, United States
Joan Clària,
Hospital, Clínic de Barcelona, Spain
Lucy V. Norling,
Queen Mary University of London, United Kingdom

***Correspondence:**
Charles N. Serhan
cserhan@bwh.harvard.edu

[†]These authors share first authorship

Specialty section:
This article was submitted to Inflammation, a section of the journal Frontiers in Immunology

Received: 19 November 2020
Accepted: 23 December 2020
Published: 10 February 2021

Citation:
Libreros S, Shay AE, Nshimiyimana R, Fichtner D, Martin MJ, Wourms N and Serhan CN (2021) A New E-Series Resolvin: RvE4 Stereochemistry and Function in Efferocytosis of Inflammation-Resolution. Front. Immunol. 11:631319. doi: 10.3389/fimmu.2020.631319

The resolution of the acute inflammatory response is governed by phagocytes actively clearing apoptotic cells and pathogens. Biosynthesis of the specialized pro-resolving mediators (SPMs) is pivotal in the resolution of inflammation *via* their roles in innate immune cells. Resolvin E4 (RvE4: 5S,15S-dihydroxy-eicosapentaenoic acid) is a newly uncovered member of the E-series resolvins biosynthesized from eicosapentaenoic acid (EPA) recently elucidated in physiologic hypoxia. This new resolvin was termed RvE4 given its ability to increase efferocytosis of apoptotic cells by macrophages. Herein, we report on the total organic synthesis of RvE4 confirming its unique structure, complete stereochemistry assignment and function. This synthetic RvE4 matched the physical properties of biogenic RvE4 material, i.e. ultra-violet (UV) absorbance, chromatographic behavior, and tandem mass spectrometry (MS^2) fragmentation, as well as bioactivity. We confirmed RvE4 potent responses with human M2 macrophage efferocytosis of human apoptotic neutrophils and senescent red blood cells. Together, these results provide direct evidence for the assignment of the complete stereochemistry of RvE4 as 5*S*,15*S*-dihydroxy-6*E*,8*Z*,11*Z*,13E,17*Z*-eicosapentaenoic acid and its bioactions in human phagocyte response.

Keywords: lipid mediator, phagocytes, M2 macrophages, pro-resolving mediator, omega-3 fatty acids, pro-resolving, eicosapentaenoic acid

INTRODUCTION

The acute inflammatory response is a critical and dynamic immunological process during infection and tissue injury (1). Human phagocytes play a pivotal role in host defense and acute inflammation *via* the production of endogenous lipid mediators (LMs), e.g. prostaglandins and leukotrienes, that are potent pro-inflammatory mediators (2). In recent years a novel superfamily of potent endogenous LMs has emerged, coined specialized pro-resolving mediators (SPMs: resolvins, maresins, protectins and lipoxins), which are derived from the essential omega(ω)-3 (docosahexaenoic acid; DHA and eicosapentaenoic acid; EPA) and omega(ω)-6 (arachidonic

acid; AA) polyunsaturated fatty acids (PUFAs) (3). SPMs play a fundamental role in the resolution of acute inflammation by governing the temporal and spatial regulation of leukocyte traffic and pro-inflammatory mediators, e.g. eicosanoids, cytokines, and chemokines (3). By definition, each SPM specifically limits neutrophil infiltration and increases the clearance of apoptotic cells by macrophages (3, 4). In this context, macrophages play a central function in the resolution phase of inflammation by actively clearing apoptotic cells (4) and biosynthesizing distinct families of LMs that can be either pro-inflammatory or anti-inflammatory and pro-resolving depending on the macrophage phenotypes and the specific agonists (5, 6). An example of this is with human macrophages: high-mobility group box 1 protein (HMGB1) stimulates the production of pro-inflammatory cytokines and leukotrienes, while high-mobility group box 1 protein together with complement component 1q (C1q) switches macrophages to produce SPMs (7).

EPA (8) is the precursor to the E-series resolvins. EPA's potential role and use in reducing cardiovascular disease (CVD) has been subject to much debate (9). Recently, using good manufacturing practice production of EPA as a U.S. Food and Drug Administration-approved Icosapent ethyl ester, a human clinical trial reported a substantial reduction in the risk of cardiovascular disease (CVD) (10). While this is a significant advancement for the field of ω-3 based therapeutics, the mechanism of EPA efficacy in reducing CVD remains to be established and its potential role in the resolution of human disease is currently not appreciated. Earlier, we found that hypoxic human vascular endothelial cells released and converted EPA to a novel 18-hydroxyeicosapentaenoic acid (18-HEPE) that is the precursor to resolvin E1 (RvE1) with the complete stereochemistry of 5*S*,12*R*,18*R*-trihydroxy-6*Z*,8*E*,10*E*,14*Z*,16*E*-eicosapentaenoic acid (11, 12). RvE1 is produced *via* transcellular biosynthesis with human neutrophils *via* acetylated cyclooxygenase-2 (COX-2) (12) or microbial cytochrome P450 (13). RvE1 (12) and resolvin E2 (RvE2: 5S,18R-dihydroxy-6*E*,8*Z*,11*Z*,14*Z*,16*E*-eicosapentaenoic acid) (14) both possess potent anti-inflammatory and pro-resolving actions. Resolvin E3 (RvE3: 17R,18R-dihydroxy-5*Z*,8*Z*,11*Z*,13*E*,15*E*-eicosapentaenoic acid) is a vicinal diol that also blocks neutrophil migration (15). The E-series resolvin precursor, 18-HEPE, is also a bioactive mediator with potent actions on cardiovascular tissues (16).

Recently, we encountered and elucidated a new member of the EPA–derived E-series resolvins that we termed Resolvin E4 (RvE4). The stereochemistry of RvE4 was deduced and the double-bond geometry proposed based on the activity of 15-lipoxygenase (15-LOX), namely: 5S,15S-dihydroxy-6*E*,8*Z*,11*Z*,13*E*,17*Z*-eicosapentaenoic acid (see **Illustration Scheme 1**). RvE4 is produced in physiologic hypoxia by human neutrophils and macrophages, and since it stimulates efferocytosis of both senescent erythrocytes (sRBCs) and apoptotic neutrophils, it classifies as a resolving function and with EPA as precursor belongs to the E-series resolvins. Hence, this novel bioactive structure was named RvE4. RvE4 also enhances the resolution of hemorrhagic exudate *in vivo* (17). Recently the biosynthesis of RvE4 was confirmed with purified recombinant human enzymes using 5-lipoxygenase (5-LOX) and 15-LOX with EPA substrate *in vitro* (18).

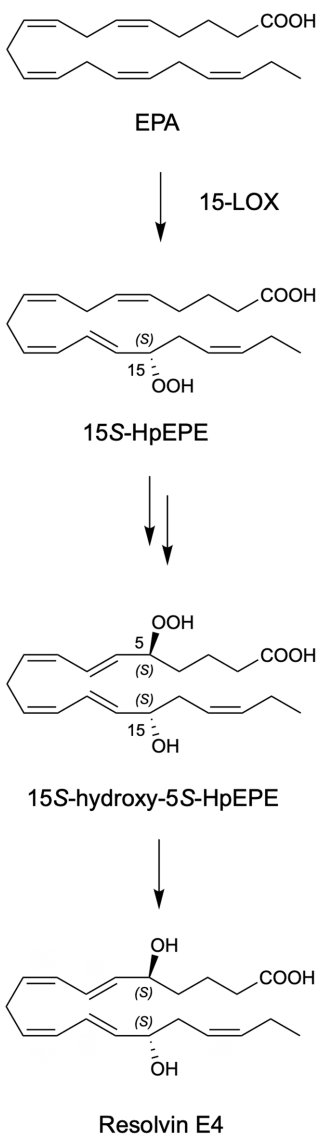

ILLUSTRATION SCHEME 1 | Proposed biosynthesis of Resolvin E4 (RvE4) by hypoxic human leukocytes. The proposed biosynthesis is initiated by lipoxygenation of EPA by 15-lipoxygenase (15-LOX) to 15*S*-hydroperoxy-EPE (15*S*-HpEPE); see (17). This intermediate can be further reduced to the corresponding hydroxyl intermediate 15*S*-HEPE. The resultant products are 15*S*-HpEPE or 15*S*-HEPE and can undergo a second enzymatic lipoxygenation to yield a hydroperoxyl group at the carbon C-5 position, which is reduced to form RvE4.

Herein, we establish and confirm the complete stereochemistry of RvE4 and its potent functions in human macrophage efferocytosis.

MATERIAL AND METHODS

Synthetic RvE4 Purification

The crude RvE4 was purified using an Agilent 1100 series Prep high-performance liquid chromatography (HPLC) system

equipped with a G1315B diode array detector using a Phenomenex Gemini C18 column with 250x21.2 mm dimension, a particle size of 5 micron, and a pore size of 110 angstroms. Resolvin E4 was further purified using methanol (Supelco/Sigma-Aldrich, St. Louis, MO, HPLC grade) and water with 0.1% acetic acid (JT Baker, glacial) mobile phase (68/32 MeOH/water w/0.1% AcOH) at a flow rate of 20 ml/min. The G1315B detector was monitoring 240 nm (bandwidth of 30 nm), 220nm (bandwidth of 30 nm), and 200 nm (bandwidth of 10 nm). The average retention time in these conditions was approximately 15 min.

Liquid Chromatography-Tandem Mass Spectrometry

The liquid chromatography-tandem mass spectrometry (LC-MS/MS) consists of a 5500 QTRAP mass spectrometer (Sciex, Framingham, MA) equipped with a LC-20AD ultra-fast liquid chromatography (UFLC) system (Shimadzu, Japan). A Poroshell 120 EC-C18 (4.6x100 mm, 2.7 micron, Agilent Technologies, Santa Clara, CA) was kept in a column oven maintained at 50˚C. Resolvin E4 was eluted from this column with a gradient of LC-MS grade methanol (Thermo Fisher, Waltham, MA)/water (Thermo Fisher, Waltham, MA)/acetic acid (Sigma-Aldrich, St. Louis, MO) from 50/50/0.01% *(vol/vol/vol)* to 98/2/0.01% *(vol/vol/vol)* at a flow rate of 0.5 ml/min (19). Targeted multiple reaction monitoring (MRM) for *m/z* 333>115 and enhanced product ion (EPI) mass spectra in negative polarity were used with the following parameters to identify resolvin E4: Collision Energy= −22, Collision Cell Exit Potential= −13, Entrance Potential= −10V, Declustering Potential= −80V, Curtain Gas= 25, Collision Gas= Medium, Ion Spray Voltage= −4,000 V, Temperature= 500°C, Ion Source Gas1 = 60 pounds per square inch (psi), and Ion Source Gas2 = 60 psi. Data were acquired and analyzed with Analyst software version 1.6.2 (Sciex, Framingham, MA) as in (17). Data represented as screen captures from Analyst software.

Human M2 Macrophages

Human peripheral blood mononuclear cells (PBMC) were obtained from de-identified healthy human volunteers from the Boston Children's Hospital Blood Bank under protocol # 1999-P-001297 approved by the Partners Human Research Committee. PBMCs were isolated by Ficoll-Histopaque-1077 density-gradient, followed by monocyte purification. Monocytes were then incubated for 7 days in RPMI-1640 medium (Lonza, NJ) containing 10% fetal calf serum, 2 mM L-glutamine, and 2 mM penicillin-streptomycin (Lonza, NJ) at 37°C and differentiated into macrophages through culturing with macrophage colony-stimulating factor (M-CSF) (20 ng/ml) (PeproTech, NJ), followed by polarization for 48 h with IL-4 (20 ng/ml) (PeproTech, NJ) (20, 21).

Human Neutrophil Purification

Human neutrophils were isolated by dextran sedimentation followed by Ficoll-Histopaque density centrifugation from human peripheral blood (22, 23). Whole blood was obtained from healthy human volunteers giving informed consent under protocol # 1999-P-001297 approved by the Partners Human Research Committee. Apoptotic neutrophils were prepared by plating 1 x 10^7 cells/ml in 5 ml DPBS (ThermoFisher Scientific, MA) for 24 h in a 100 mm X 20 mm petri dish (Corning, AZ). After 24 h, apoptotic neutrophils were removed from petri dishes with EDTA (5 mM) (Millipore Sigma, MO) and stained with Cell Trace™ Carboxyfluorescein succinimidyl ester (CFSE) at a concentration of 5μM for 30 min at 37°C (ThermoFisher Scientific, MA).

Human Erythrocyte Isolation

Human peripheral blood red blood cells (RBCs) from healthy human volunteers were isolated by centrifugation and aspiration of the platelet-rich plasma and buffy coat layer. Erythrocytes were purified by resuspension in RPMI-1640 (Lonza, NJ) [10% hematocrit] and centrifugation (500 X g) followed by aspiration of the top 10% of the erythrocyte layer (this purification procedure was carried out with six repetitions) (24). Purified erythrocytes were then resuspended (20% hematocrit) at 4°C for ~24–36 h to induce apoptosis. Erythrocytes were next washed twice with DPBS (ThermoFisher Scientific, MA) and then stained with Cell Trace™ Carboxyfluorescein succinimidyl ester (CFSE) at a concentration of 5mM for 30 min at 37°C (ThermoFisher Scientific, MA).

Human Efferocytosis of Apoptotic Neutrophils and Senescent Erythrocytes

Human M2 macrophages were seeded in a six-well Corning Costar Flat Bottom Cell culture plate (ThermoFisher Scientific, MA) at a cell density of 2 x 10^6 cells per well the night before the experiment. M2 macrophages were washed twice with DPBS (ThermoFisher Scientific, MA) to eliminate any cellular debris. Cells were treated with either synthetic RvE4 (10^{-11} M to 10^{-7}M), biogenic RvE4 (10^{-8} M) or vehicle control (0.01% ethanol vol/vol) 15 min before the addition of CFSE-labeled apoptotic neutrophils [1:3 (M2:apoptotic neutrophils) ratio] or CFSE-labeled senescent erythrocytes [1:50 (M2:sRBC) ratio]. After 60 min of co-incubation at 37°C, plates were washed thoroughly to remove non-ingested cells, and M2 macrophages were fixed with 4% paraformaldehyde for 15 min at 4°C. Cells were washed with DPBS and incubated with 5mM ethylenediaminetetraacetic acid (EDTA) for 15 min before cell scraping. These steps allowed for removal of undigested and membrane bound cells (25).

M2 macrophages were then permeabilized using the BD cytoperm™ permeabilization buffer (BD Biosciences, CA) for 45 min following the manufacturer's protocol. M2 macrophages were washed twice with BD Perm/Wash buffer (BD Biosciences, CA) and then resuspended in FACS buffer (DPBS, 5% FBS, 2mM EDTA, 2mM NaN_3). M2 macrophages were then taken to flow cytometry to assess efferocytosis (CFSE intensity). All flow cytometric samples were assessed using BD LSRFortessa (BD Biosciences, CA).

Software

Flow cytometric data was collected and then analyzed using FlowJo version X (BD Biosciences, CA) as in (17). The chemical structures of E-series resolvins and RvE4 were drawn using ChemDraw Level Professional (Version 16.0.1.4). RvE4 3D spatial filling was done using ChemBioDraw Level Ultra (Version 14.0.0.117) and ChemBio3D Level Ultra (Version 14.0.0.117) (PerkinElmer, Waltham, MA, USA). Graphs were prepared and non-linear regression carried out with Prism

software version 8 (GraphPad, CA). Graphic illustrations were created with BioRender software (https://biorender.com/).

Statistical Analysis

Individual sample incubations were compared by one-way ANOVA with Bonferroni multiple comparisons test or two-tailed student's t-test. The criterion for statistical significance was $p < 0.05$.

RESULTS

RvE4 Total Organic Synthesis and Stereochemistry

To assign the complete stereochemistry of RvE4 and determine whether synthetic RvE4 shares reported physical and biological functions (17), it was critical to establish the spectroscopic and physical properties of the new synthetic RvE4. The structure and stereochemistry of synthetic RvE4 were precise on the basis of its total organic synthesis from chiral starting materials of known stereochemistry as well as stereocontrolled chemical reactions as outlined in **Figure 1A**. Synthetic RvE4 was prepared to target RvE4 structure deduced earlier using the isolated well studied 15-lipoxygenase (LOX) enzyme that inserts molecular oxygen into 1,4-cis pentadiene predominantly in the *S* configuration (17). The total synthesis was accomplished in 21 steps to afford stereochemically pure 5*S*,15*S*-dihydroxy-6*E*,8*Z*,11*Z*,13*E*,17*Z*-eicosapentaenoic acid, RvE4. The synthesis began with defined building blocks of known stereochemistry to furnish the carbons C1-C7 fragment (**Figure 1A**, black). Next, the carbons C8-C20 fragment (**Figure 1A**, blue) was generated from chirally pure (*R*)-(+)-glycidol to unambiguously install the carbon C-15 position *S* alcohol chirality. With both the carbon C1–C7 and carbon C8–C20 key intermediates at hand, these fragments were joined together using a carbon-carbon cross-coupling reaction to form the eicosapentaenoate carbon backbone of RvE4 methyl ester.

The methyl ester was further hydrolyzed to afford crude RvE4 (**Figure 1A**). The product was isolated as in **Figure 1A** using HPLC [Gemini C18, 5 micron, 250 x 21.2 mm, 110Å, monitored at 240 nm (bandwidth of 30 nm), 220nm (bandwidth of 30 nm), and 200 nm (bandwidth of 10 nm), methanol/water/acetic acid (AcOH) 68/32/0.1%, 20 ml/min]. Further evidence for structural verification was obtained for this product from its full ^{1}H nuclear magnetic resonance (NMR) spectroscopy, and the *Z*/*E* configuration of the double bonds was determined and confirmed using 2D ^{1}H NMR (COSY) as shown in **Figure 1B** and **Supplementary Figure 1A**.

RvE4 Physical Properties: Matching of Organic Synthetic to Biogenic Material

To determine whether synthetic RvE4 shares the identical physical and biological properties of biogenic RvE4, it was essential to establish the chromatographic behavior, ultra-violet (UV) absorbance, and structural composition of both molecules. Biogenic RvE4 was prepared by incubating EPA with soybean 15-LOX and purified by high-performance liquid chromatography with a chiral column (HPLC) (17). This biogenic preparation of RvE4 matched endogenously biosynthesized RvE4 by human M2 macrophage-neutrophil co-incubations (17). The ultraviolet (UV)-chromophore of the biogenic RvE4 showed a single broad absorption band at $\lambda_{max}^{MeOH} = 244$ *nm* (solvent, methanol) (**Figure 2A**, inset), which is characteristic of two separate conjugated diene double bond systems in the RvE4 carbon backbone. This UV absorbance max in methanol was in accordance with our earlier published results obtained from M2 macrophage-neutrophil co-incubations, *i.e.* $\lambda_{max}^{MeOH} = 244$ *nm*, that produced RvE4 from endogenous stores of EPA (17). We next assessed the chromatographic behavior of biogenic RvE4 using reverse-phase ultra-fast liquid chromatography. Biogenic RvE4 eluted at 12.9 min as a single and major peak (**Figure 2A**). Tandem mass spectrometry analysis (MS/MS screen capture) of biogenic RvE4 revealed a fragmentation pattern with a parent ion of *m/z* 333=M-H and daughter ions of *m/z* 315=M-H-H_2O, *m/z* 271=M-H-H_2O-CO_2, *m/z* 253=M-H-2H_2O-CO_2, *m/z* 217 = 235-H_2O, *m/z* 199 = 217-H_2O, and *m/z* 173 = 235-H_2O-CO_2 as shown in **Figure 2B**.

Synthetic RvE4 demonstrated an essentially identical UV absorbance of $\lambda_{max}^{MeOH} = 244$ nm; see **Figure 2C**, inset, as well as the chromatographic behavior by obtaining an identical retention time of 12.9 min (**Figure 2C**) as biogenic RvE4. MS/MS direct screen capture analysis of synthetic RvE4 gave essentially the same fragmentation pattern as biogenic RvE4, i.e. with a parent ion of *m/z* 333=M-H and daughter ions of *m/z* 315=M-H-H_2O, *m/z* 271=M-H-H_2O-CO_2, *m/z* 253=M-H-2H_2O-CO_2, *m/z* 217 = 235-H_2O, *m/z* 199 = 217-H_2O, and *m/z* 173 = 235-H_2O-CO_2 (**Figure 2D**). This fragmentation pattern matches that of reported endogenous RvE4 isolated from human and murine leukocytes (17). Having matched these physical properties of biogenic RvE4 to those of the synthetic RvE4, we next sought evidence to determine if 50% co-injections of both compounds have identical physical properties in these same conditions. Co-injection of biogenic RvE4 with the synthetic RvE4 confirmed their identical chromatographic behavior, which co-eluted at 12.9 min beneath a single peak (**Figure 2E**). MS/MS direct screen capture analysis revealed that co-injection material has an identical fragmentation pattern (**Figures 2B, D**) as with parent ion of *m/z* 333=M-H and daughter ions of *m/z* 315=M-H-H_2O, *m/z* 271=M-H-H_2O-CO_2, *m/z* 253=M-H-2H_2O-CO_2, *m/z* 217 = 235-H_2O, *m/z* 199 = 217-H_2O, and *m/z* 173 = 235-H_2O-CO_2 (**Figure 2F**). RvE4 structure with major fragmentation points (*m/z* 115, *m/z* 217, and *m/z* 235) is shown in **Figure 2E**, inset. The present results with both biogenic and synthetic RvE4 confirmed the original reported physical properties of RvE4 and further verified its unique stereochemistry (see **Supplementary Figure 1**).

RvE4 Increases Efferocytosis in Human M2 Macrophages

Macrophage efferocytosis is one of the hallmarks of the resolution of inflammation, and pro-resolving mediators are key bioactive regulators of efferocytosis (3, 4). RvE4 is a potent stimulator of macrophage efferocytosis of senescent red blood cells (sRBCs) (17). Macrophage erythrophagocytosis is an essential mechanism for the removal of sRBCs in the spleen as this organ is the largest filter of RBCs in the human body (26). Therefore, we next determined whether the synthetic RvE4

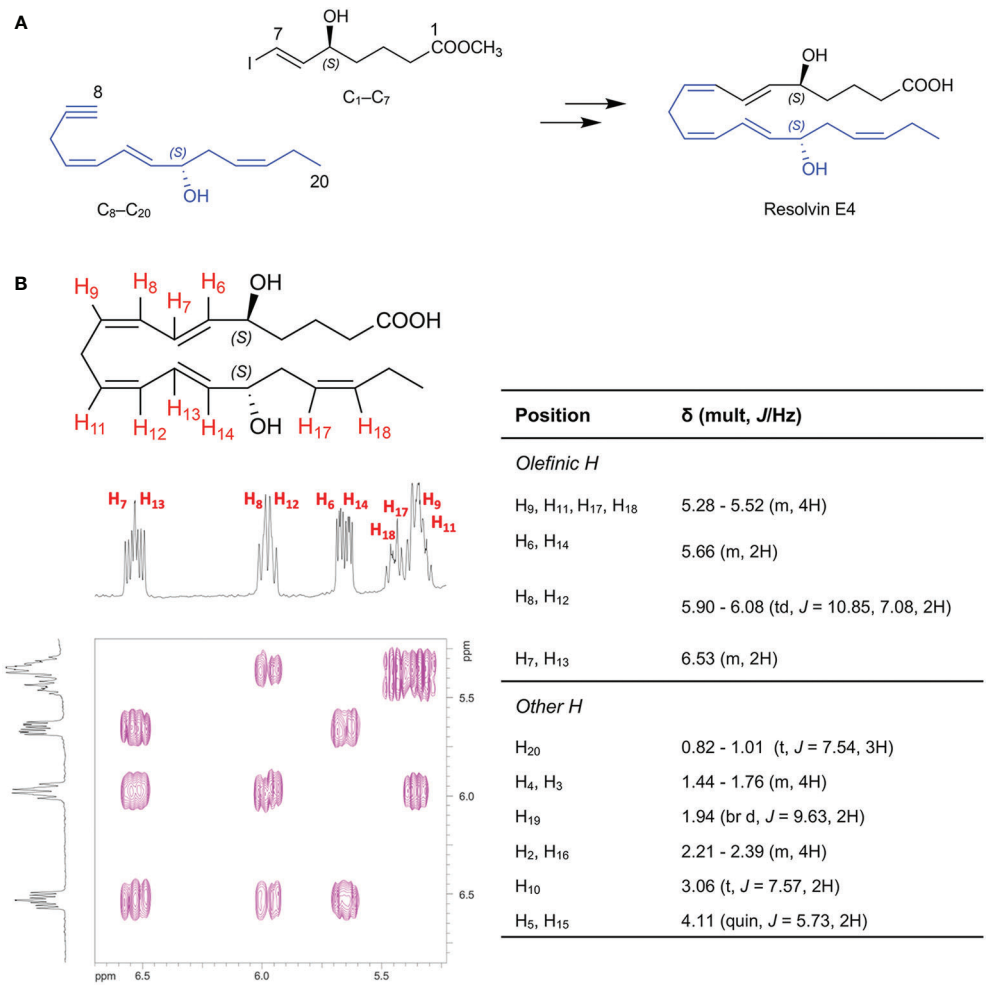

Position	δ (mult, *J*/Hz)
Olefinic H	
H_9, H_{11}, H_{17}, H_{18}	5.28 - 5.52 (m, 4H)
H_6, H_{14}	5.66 (m, 2H)
H_8, H_{12}	5.90 - 6.08 (td, *J* = 10.85, 7.08, 2H)
H_7, H_{13}	6.53 (m, 2H)
Other H	
H_{20}	0.82 - 1.01 (t, *J* = 7.54, 3H)
H_4, H_3	1.44 - 1.76 (m, 4H)
H_{19}	1.94 (br d, *J* = 9.63, 2H)
H_2, H_{16}	2.21 - 2.39 (m, 4H)
H_{10}	3.06 (t, *J* = 7.57, 2H)
H_5, H_{15}	4.11 (quin, *J* = 5.73, 2H)

FIGURE 1 | Retrosynthetic strategy for total organic synthesis and spectroscopic properties of Resolvin E4. The synthesis of RvE4 was accomplished by total organic synthesis from stereochemically pure starting building blocks and was characterized using NMR spectroscopy. **(A)** Synthetic precursors were prepared from enantiomerically pure commercially available starting materials and assembled using carbon-carbon bond coupling reactions between precursors C1–C7 (black), and C8–C20 (blue) to ensure absolute regio- and stereochemical control. **(B)** Double-bond geometry was assigned using two-dimensional ^{1}H-^{1}H NMR using a JNM ECZ-400S NMR spectrometer with a 400MHz magnet at 20.7°C on a JEOL ROYALPROBE^{TM} and referenced to the methanol-d_4 (CD_3OD) internal standard. The purple plot depicts positive contours of cross-peaks along the diagonal axis allowing for the full and detailed proton assignment. The enlarged region highlights the Z/E olefinic protons H_6-H_9, H_{11}-H_{14}, and H_{17}-H_{18}. This, in addition to the full ^{1}H-NMR spectrum of chemical shifts and coupling constants, confirmed the structure of Resolvin E4.

enhances macrophage efferocytosis of sRBCs. For this experiment, human M2 macrophages were incubated with synthetic RvE4 (0–100 nM) or vehicle control (0.01% ethanol *vol/vol)* prior to exposure with sRBCs to assess the direct actions on human M2 efferocytosis by flow cytometry. Representative flow cytometry gating strategy of M2 macrophages and histograms of intracellular CFSE-labeled sRBCs from vehicle control and synthetic RvE4 are reported in **Figures 3A, B**. Synthetic RvE4 increased macrophage efferocytosis of sRBCs in a concentration-dependent fashion with the highest statistically significant increase at 1nM and 10nM (**Figure 3C**) compared to vehicle, with an estimated EC_{50} of ~0.29 nM for synthetic RvE4. Since M2 macrophages treated with 10 nM of synthetic RvE4 had the highest increase in efferocytosis of sRBCs, we next examined if biogenic RvE4 at 10 nM had the same ability to stimulate efferocytosis in human M2 macrophages. Both synthetic RvE4 and biogenic RvE4 potently increased M2 efferocytosis of sRBCs by as much as ~40% at 10nM concentration (**Figure 3D**). There were no statistically significant differences noted between synthetic and biogenic RvE4 (p=0.73) by analysis of variance, indicating that both mediators gave an identical biological response. These results demonstrate that synthetic and biogenic RvE4 have essentially the same potencies in stimulating human macrophage efferocytosis of sRBCs.

Neutrophils are often the first leukocytes to infiltrate an inflammatory site in large numbers and therefore their effective

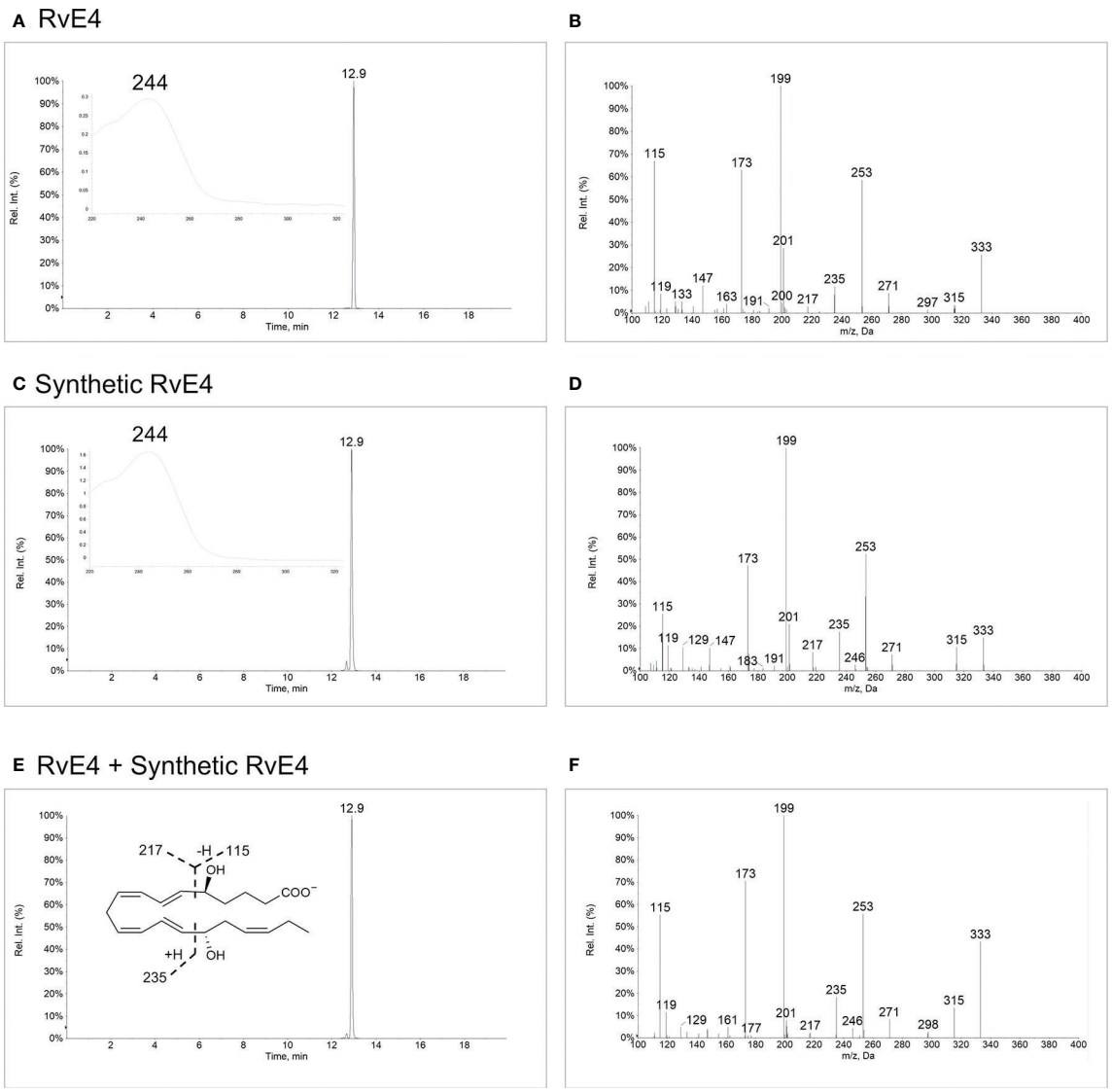

FIGURE 2 | Matching physical properties of biogenic and synthetic RvE4. Screen captures of **(A)** Biogenic RvE4 monitored by liquid chromatography-tandem mass spectrometry (LC-MS/MS) in negative ion MRM mode for *m/z* 333>115. *Inset:* UV spectrum with λ_{max}^{MeOH} = 244 *nm*. **(B)** MS/MS fragmentation spectrum with ions matching RvE4. **(C)** Synthetic RvE4 monitored by LC-MS/MS in negative ion MRM mode for *m/z* 333>115. *Inset:* UV spectrum with λ_{max}^{MeOH} = 244 *nm*. **(D)** MS/MS fragmentation spectrum with ions matching RvE4. **(E)** Biogenic and synthetic RvE4 were co-injected and monitored by LC-MS/MS in negative ion MRM mode for *m/z* 333>115. *Inset:* RvE4 structure with proposed fragmentations. **(F)** MS/MS fragmentation spectrum with ions matching RvE4. Arrows on y-axes indicate threshold; 5% for chromatograms **(A, C, E)**, 1% for spectrum **(B, D, F)**.

elimination is a prerequisite for the resolution of inflammation (3, 4, 27, 28). SPMs, including RvE4, enhance macrophage efferocytosis of apoptotic neutrophils *in vitro* and *in vivo* with both human cells and murine models of inflammation (3, 17). Given that RvE4 enhanced efferocytosis of sRBCs, we set out to determine if synthetic RvE4 enhances M2 macrophage efferocytosis of human apoptotic neutrophils. Human M2 macrophages were incubated with synthetic RvE4 (0–100 nM) or vehicle control (0.01% ethanol *vol/vol*) prior to exposure with CFSE-labeled apoptotic human neutrophils, and efferocytosis was assessed using flow cytometry. Representative flow cytometry gating strategy of M2 macrophages and histograms of intracellular CFSE-labeled apoptotic neutrophils from vehicle control and synthetic RvE4 are shown in **Figures 4A, B**. Synthetic RvE4 increased macrophage efferocytosis of apoptotic human neutrophils in a concentration-dependent fashion, with the highest statistically significant increase at 1nM and 10nM (**Figure 4C**) compared to vehicle control, with an estimated EC_{50} of ~0.23nM for synthetic RvE4. The increase of ~39% of M2 efferocytosis by the synthetic RvE4 at 10nM is in accordance with the published results of M2 macrophage efferocytosis of apoptotic neutrophils by the biogenic RvE4 (17). Taken together,

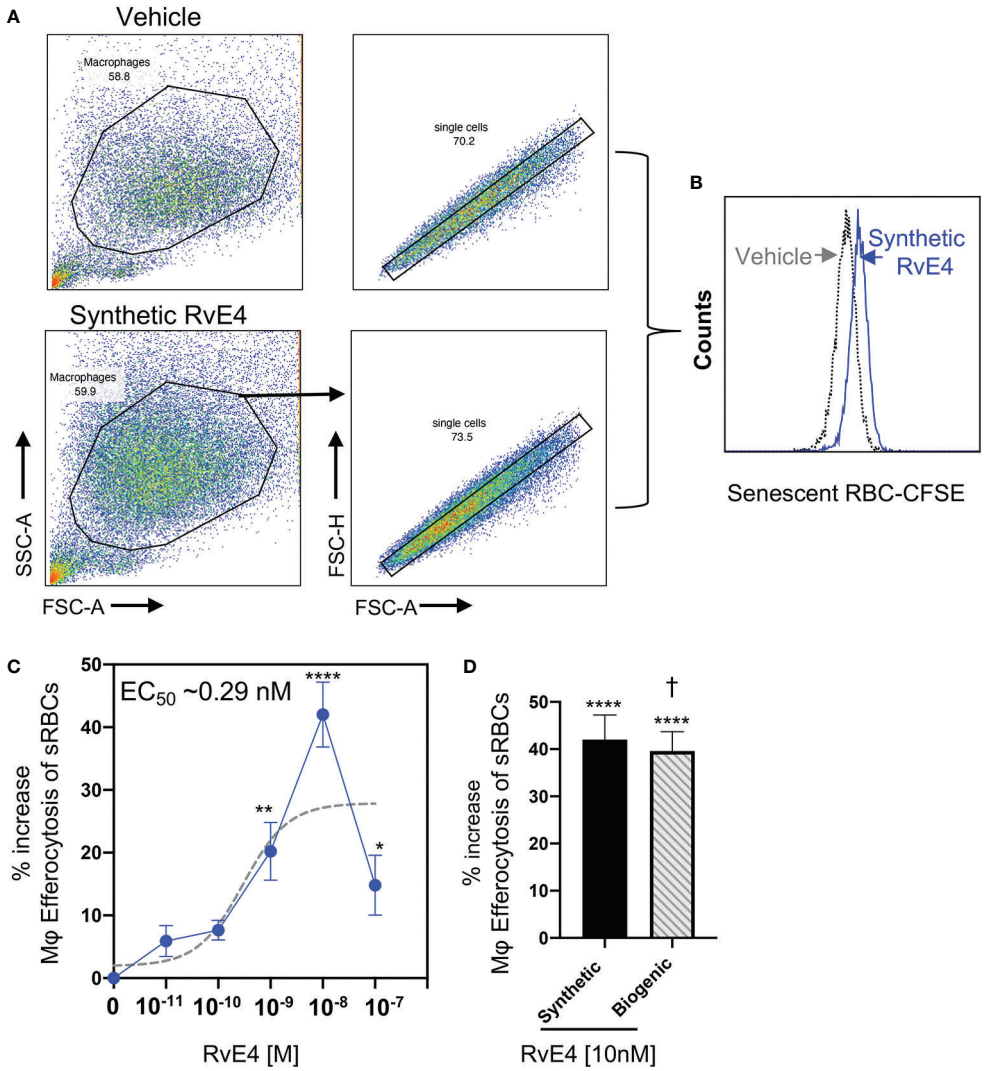

FIGURE 3 | RvE4 increases human M2 macrophage efferocytosis of senescent red blood cells. Human M2 macrophages were plated on a 6-well plate (2 x 10^6 cells/well), incubated with synthetic RvE4 (10^{-11}M to 10^{-7}M), biogenic RvE4 (10^{-7} M), or vehicle (0.01% ethanol *vol/vol*) for 15 min followed by CFSE-labeled senescent red blood cells (sRBCs) (1:50, M2:sRBCs). After 60 min of co-incubation at 37°C, plates were washed thoroughly to remove non-ingested sRBCs, and cells were fixed with DPBS containing 4% paraformaldehyde for 15 min on ice. Cells were washed with DPBS and removed from plates with a cell scraper in DPBS. M2 macrophages were then taken to flow cytometry to assess efferocytosis. **(A)** Flow cytometry gating strategy for M2 macrophages. **(B)** Representative histogram of intracellular CFSE-labeled sRBCs. **(C)** Dose-Response: percent increase in M2 efferocytosis of sRBCs above vehicle by synthetic RvE4 (solid blue line). EC_{50} was estimated using non-linear regression (dashed gray line) with log (agonist) vs. response (three parameters). **(D)** Comparison between synthetic RvE4 (10 nM) and biogenic RvE4 (10 nM): percent increase of M2 efferocytosis of sRBCs above the vehicle **(C, D)**. Results are the percent of efferocytosis above vehicle and expressed as mean ± SEM, n=5 (sRBCs). *p < 0.05, **p < 0.01, and ****p < 0.0001 when compared to vehicle (as control). † (p=0.73) no statistically significant differences when compared between synthetic and biogenic RvE4. Statistical analysis was carried out using one-way ANOVA with Bonferroni multiple comparisons test **(C)** or two-tailed Student's t-test **(D)**.

these results demonstrate the potent biological actions of synthetic RvE4 in enhancing efferocytosis with human M2 macrophages.

DISCUSSION

In the present report, we matched both the physical properties of RvE4 and its potent functions with human M2 macrophages to material produced *via* total organic synthesis permitting us to assign and confirm the proposed stereochemistry of RvE4 (17). Through matching studies using LC-MS/MS (co-elution and fragmentation), UV spectrum absorbance and biological actions, we have assigned the complete double-bond geometry of RvE4 as 5*S*,15*S*-dihydroxy-6*E*,8*Z*,11*Z*,13*E*,17*Z*-eicosapentaenoic acid (**Figures 1** and **2**). Therefore, synthetic RvE4 can be used as both a standard for LC-MS/MS-based mediator lipidomics as well

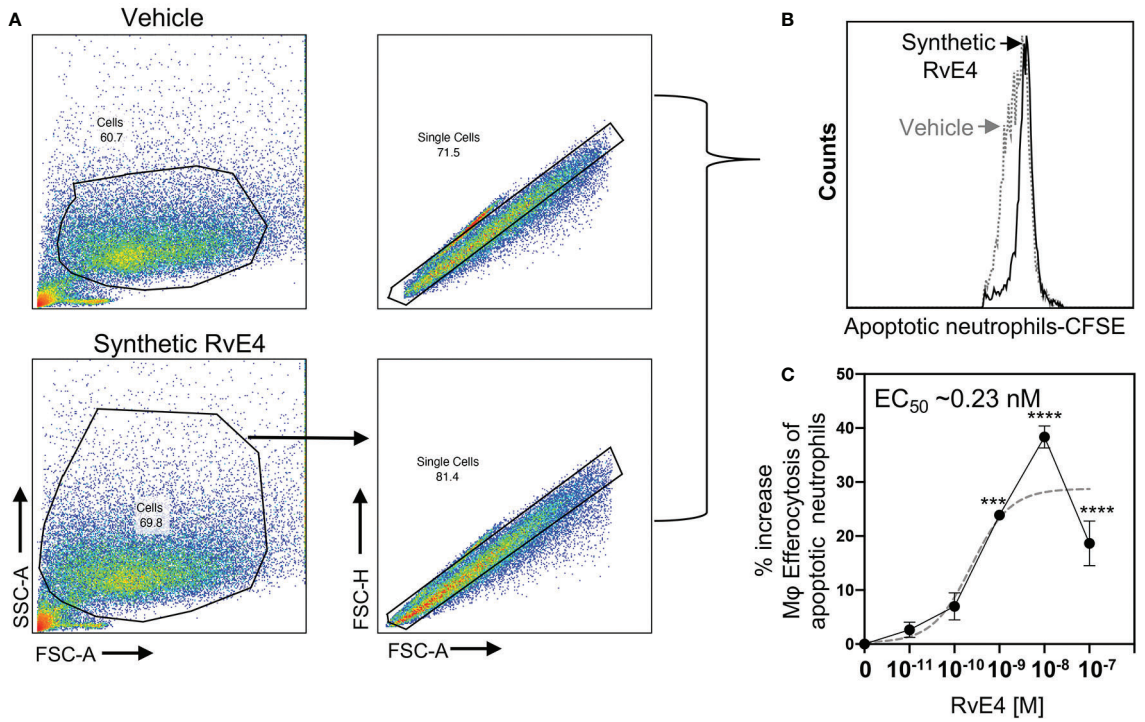

FIGURE 4 | Synthetic RvE4 increases human M2 macrophage efferocytosis of apoptotic human neutrophils. Human M2 macrophages were plated on a 6-well plate (2×10^6 cells/well), incubated with synthetic RvE4 (10^{-11} to 10^{-7}M) or vehicle (0.01% ethanol) for 15 min followed by CFSE-labeled apoptotic neutrophils (1:5 M2: apoptotic neutrophils). After 60 min of co-incubation at 37°C, plates were washed thoroughly to remove non-ingested neutrophils. M2 macrophages were fixed with DPBS containing 4% paraformaldehyde for 15 min on ice. Cells were washed with DPBS and removed from plates with a cell scraper in DPBS. Cells were then taken to flow cytometry to assess efferocytosis. **(A)** Flow cytometry gating strategy for M2 macrophages. **(B)** Representative histogram of intracellular CFSE-labeled apoptotic neutrophils. **(C)** Dose-Response: percent increases in M2 macrophage efferocytosis of apoptotic PMN above vehicle by synthetic RvE4 (solid black line). EC_{50} was estimated using non-linear regression (dashed gray line) with log (agonist) vs. response (three parameters). Results are represented as mean ± SEM. n=3 healthy human donors. ***p < 0.001 and ****p < 0.0001 compared to vehicle (as control). Statistical analysis was carried out using one-way ANOVA with Bonferroni multiple comparisons test.

as for further investigations to define potentially additional RvE4 functions in diverse biological systems.

RvE4 was uncovered from physiological hypoxic biosynthesis of EPA, *via* lipoxygenation, by human macrophages and neutrophils (17). M2 macrophages play critical roles in the resolution of inflammation by virtue of their capacity to carry out efferocytosis (3, 4), wound repair (3, 29), and production of SPMs (5). In the present experiments, RvE4 proved to be a potent agonist of M2 macrophage efferocytosis of neutrophils, giving an estimated EC_{50} ~0.23nM (**Figure 4**) and an EC_{50} ~0.29nM for the efferocytosis of sRBCs (**Figure 3**). In human macrophages and neutrophils, RvE4 biosynthesis is dependent on the substrate availability of EPA released from both phospholipases (PL) and triglycerides (17). EPA is converted by 15-LOX to 15S-HpEPE, which becomes a substrate for further lipoxygenation by either 5-LOX or a second enzymatic turn of 15-LOX to produce 15S-hydroxy-5S-HpETE; this is further reduced to RvE4 (**Figure 5**). This route of RvE4 biosynthesis by human phagocytes was recently confirmed by Kutzner et al. using recombinant human 5- and 15-LOX co-incubations *in vitro* (18). Recently, EPA was shown to be converted by wild type and recombinant engineered lipoxygenases to double dioxygenation products 5*S*,12*S*-diHEPE and RvE4 on large-scale studies (30). In addition, it is possible that the lipoxygenation of EPA is initiated *via* hydrogen abstraction at carbon position C7 by 5-LOX (**Figure 5**) to biosynthesize RvE4 in human neutrophils or by transcellular biosynthesis (31). Since earlier results demonstrate the conversion of EPA to 15*R*-HEPE *via* acetylated COX-2 (12, 13), it is plausible that lipoxygenation by 5-LOX and further conversion to the corresponding alcohol could give rise to 15*R*-RvE4. This 15*R*-RvE4 could be biosynthesized either from the acetylation of COX-2 by acetyl-CoA and sphingosine *via* sphingosine kinase 1 (SphK1) (32) or modified by S-nitrosylation by inducible nitric oxide synthase (33). Also, since 5-LOX can be phosphorylated to produce 15*R*-HETE and further converted to 15*R*-lipoxin A_4 (LXA_4) (34–36), it is likely that with EPA as a substitute phosphorylated 5-LOX can produce 15R-HEPE and subsequently be converted to 15*R*-RvE4.Therefore RvE4 can be biosynthesized from EPA potentially *via* multiple biosynthetic routes and now can be included in the E-series of pro-resolving mediators; see **Table 1**. The 15-LOX initiated route of RvE4 biosynthesis simplifies the production and biosynthesis of this mediator that can occur in the absence of enzyme

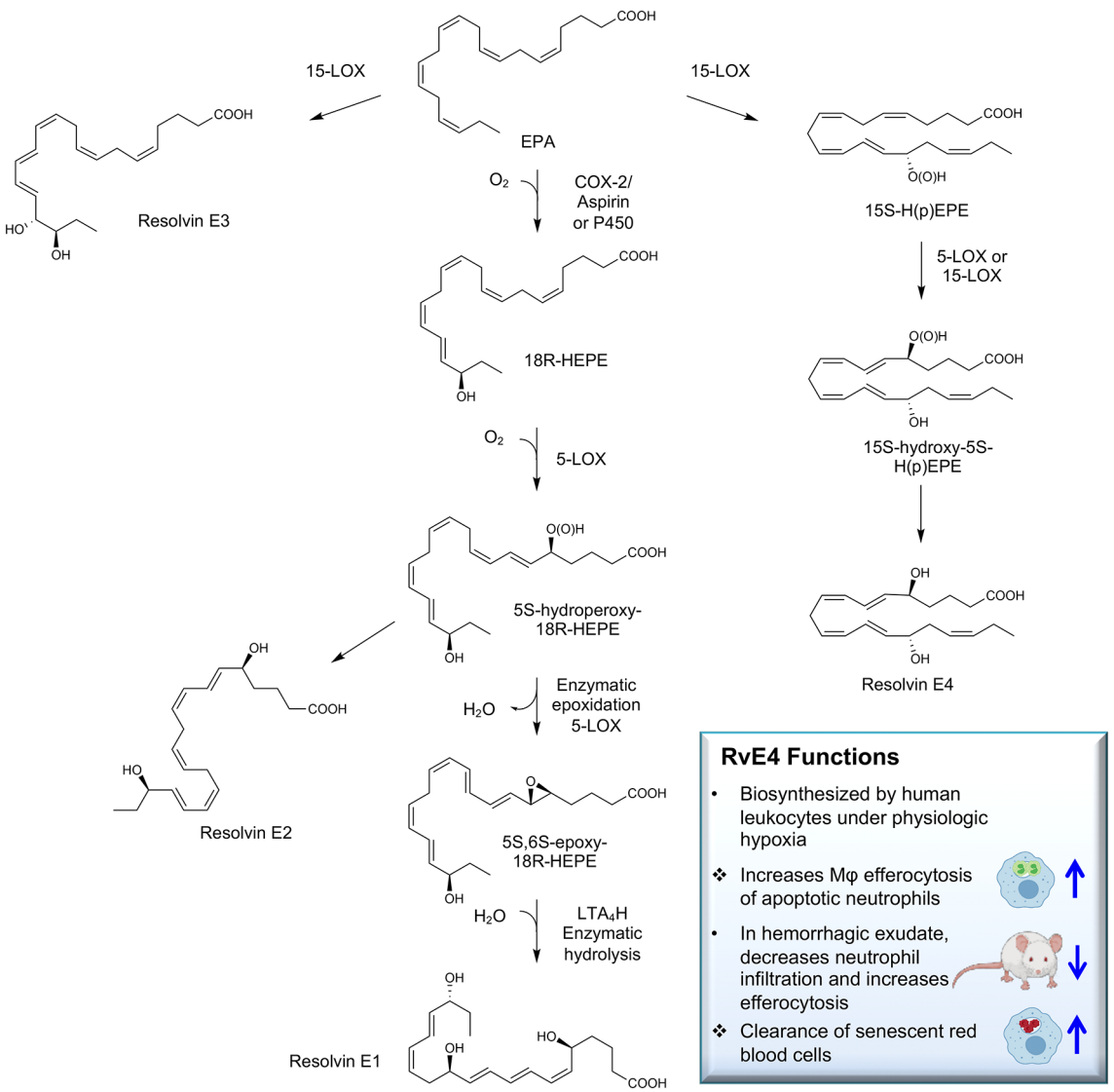

FIGURE 5 | Biosynthetic scheme for Resolvin E4 and E-series resolvins. Eicosapentaenoic acid (EPA) is converted to 18*R*-HEPE *via* acetylation of COX-2 by aspirin (12) or P450 (13), which is subsequently lipoxygenated by 5-LOX to produce the intermediate 5S-hydroperoxy-18*R*-HEPE. 5S-hydroperoxy-18*R*-HEPE can be either reduced to RvE2 (5*S*,18*R*-dihydroxy-6*E*,8*Z*,11*Z*,14*Z*,16*E*-eicosapentaenoic acid) (14) or to 5*S*,6*S*-epoxy-18*R*-HEPE by enzymatic epoxidation by 5-LOX confirmed by trapping experiments. 5S,6S-epoxy-18*R*-HEPE can be further hydrolyzed to produce RvE1 (5*S*,12*R*,18*R*-trihydroxy-6*Z*,8*E*,10*E*,14*Z*,16*E*-eicosapentaenoic acid) (11, 12). EPA can also be lipoxygenated by 15-LOX to produce RvE3 (17*R*,18*R*-dihydroxy-5*Z*,8*Z*,11*Z*,13*E*,15*E*-eicosapentaenoic acid) (15). Stereochemistry and proposed biosynthetic route of RvE4 and confirmed actions (❖ as demonstrated in the present paper) adding to the family of E-series resolvins derived from EPA.

modification (i.e. phosphorylation, acetylation, nitrosylation of COX-2) or aspirin therapy.

The main actions of RvE4 are to stimulate human macrophage efferocytosis of apoptotic neutrophils and senescent red blood cells, as well as reduce mouse hemorrhagic exudates by increasing efferocytosis and decreasing neutrophil infiltration *in vivo* (17). The ability of RvE4 to limit neutrophil tissue infiltration and to enhance efferocytosis are also functions shared by other members of the E-series resolvins (**Table 1**). For example, RvE1's pro-resolving actions include stopping neutrophil (12, 14, 37–39) and dendritic cell migration (11, 40), reducing pro-inflammatory cytokines (41), enhancing macrophage phagocytosis and efferocytosis (37, 38), enhancing bacterial clearance (41), modulating T cell responses (42) and regenerating periodontal ligament stem cells (43). RvE1 has unique actions on platelets by inhibiting adenosine diphosphate (ADP)-activated mobilization of P-selectin to minimize platelet aggregation. In addition, RvE1 has potent actions in the nanogram range *in vivo* including: organ protection, clearing infections, and stimulating resolution in, e.g., peritonitis (11, 12, 14, 37, 38), sepsis (45), ischemia-reperfusion

TABLE 1 | Eicosapentaenoic acid (EPA) derived specialized pro-resolving mediators (SPMs) and stable analogs: actions and human production.

Full name/ Abbreviation	Chemical name	Structure	Pro-resolving actions	Organ protection	Quantities in humans
Resolvin E1 (RvE1)	5*S*,12*R*,18*R*-trihydroxy-6*Z*,8*E*,10*E*,14*Z*,16*E*-eicosapentaenoic acid	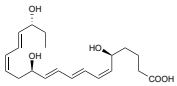	Stops PMN (12, 14, 37–39) and dendritic cell migration (11, 40). Reduces pro-inflammatory cytokines (41). Enhances macrophage phagocytosis & efferocytosis (37, 38). Enhances bacterial clearance (41). Inhibits TRP channels (42). Modulates T cell responses (42). Regeneration of periodontal ligament stem cells (43). Inhibits platelet aggregation (44).	Peritonitis (11, 12, 14, 37, 38), air pouch (12), CLP/sepsis (45), bacterial (41), I/R injury (46), diabetes (47), obesity (48), colitis (39, 49, 50), lung inflammation (51), kidney injury (52), depression (53, 54), atherosclerosis (55) (56), bone (57), reduces tumor growth (58), Dermatitis (59), *Candida albicans* (60), pain (61), and herpes (62).	Plasma 3.9–4.5 pg/ml (63) Plasma of Arthritis 96.1 pg/ml (64) Arthritis Synovial fluid 24.6 pg/ml (64) Plasma of Type 2 diabetes mellitus 45.9–50 pg/ml (65) Plasma of Peripheral artery disease (OMEGA-PAD II trial) 0.32–0.62 pg/ml (66) Cord Blood 34.1 pg/ml (67) Human Breast milk 8.8 pg/ml (68) Blister 0.1–0.3 pg/blister (69) Metabolic syndrome (weight loss program) 378-1339 pg/4.5 × 10^6 PMN (70)
18S-Resolvin E1 (18S-RvE1)	5*S*,12*R*,18*S*-trihydroxy-6*Z*,8*E*,10*E*,14*Z*,16*E*-eicosapentaenoic acid	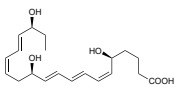	Stops PMN migration, reduces pro-inflammatory cytokines, and enhances macrophage phagocytosis & efferocytosis (38).	Peritonitis (38).	
18-oxo-Resolvin E1 (18-oxo-RvE1)	5*S*,12*R*-dihydroxy 6*Z*,8*E*,10*E*,14*Z*,16*E*-18-oxo-eicosapentaenoic acid	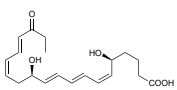	Stops PMN migration, reduces pro-inflammatory cytokines (71).	Peritonitis (71).	
Resolvin E2 (RvE2)	5*S*,18*R*-dihydroxy-6*E*,8*Z*,11*Z*,14*Z*,16*E*-eicosapentaenoic acid	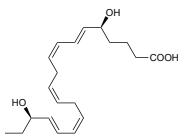	Stops PMN migration (14, 38). Down-regulates leukocyte integrins (72).	Peritonitis (14, 38), and depression (53).	Plasma 2.3–2.7 pg/ml (63) Plasma of Arthritis 68.8 pg/ml (64) Arthritis Synovial fluid 774.2 pg/ml (64) Plasma of Type 2 diabetes mellitus 59.7–82.3 pg/ml (65) Cord Blood 39.0 pg/ml (67) Plasma of Peripheral artery disease (OMEGA-PAD II trial) 9.7–13 pg/ml (66) Human Breast milk 321.2 pg/ml (68) Blister 1.8–2.1 pg/blister (69)
Ortho-Benzo-Resolvin E2 (*o*-BZ-RvE2)	(*S*,*E*)-5-hydroxy-8-(2-((*R*,*E*)-3-hydroxypent-1-en-1-yl)phenyl)oct-6-enoic acid	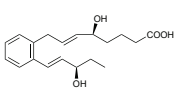	Stops PMN migration (73).	Peritonitis (73).	

(Continued)

TABLE 1 | Continued

Full name/ Abbreviation	Chemical name	Structure	Pro-resolving actions	Organ protection	Quantities in humans
18R-Resolvin E3 (18R-RvE3)	17*R*,18*R*-dihydroxy-5*Z*,8*Z*,11*Z*,13*E*,15*E*-eicosapentaenoic acid	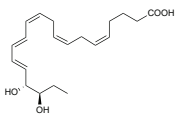	Stops PMN migration (15). Reduces IL-23 and IL-17 (74). BLT1R antagonist (74).	Peritonitis (15), lung inflammation (74), depression (75), and premature birth (76).	SARS-CoV-2 infection (77) Plasma 1.2–1.3 pg/ml (63) Plasma of Arthritis 13.9. pg/ml (64) Arthritis Synovial fluid 95.7 pg/ml (64) Plasma of Type 2 diabetes mellitus 36.9–50.6 pg/ml (65) Plasma of Peripheral artery disease (OMEGA-PAD II trial) 33-187 pg/ml (66) Cord Blood 106.8 pg/ml (67) Human Breast milk 444.9 pg/ml (68) Blister 5.8–11.7 pg/blister (69) Metabolic syndrome (weight loss program) 96–175 pg/4.5 × 10^6 PMN (70)
18S-Resolvin E3 (18S-RvE3)	17*R*,18*S*-dihydroxy-5*Z*,8*Z*,11*Z*,13*E*,15*E*-eicosapentaenoic acid	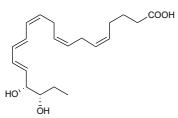	Stops PMN migration (15, 78).	Peritonitis (15, 78).	
18-deoxy-Resolvin E3 (18-deoxy-RvE3)	17*S*-hydroxy-5*Z*,8*Z*,11*Z*,13*E*,15*E*-eicosapentaenoic acid	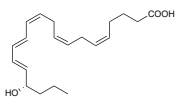	Stop PMN migration (79).	Peritonitis (79).	
18-hydroxy-eicosapenta-enoic acid (18-HEPE)	18*S*/*R*-hydroxy-5*Z*,8*Z*,11*Z*,14*Z*,16*E*-eicosapentaenoic acid	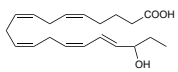	Reduces pro-inflammatory cytokines (16).	Prevents overload-induced maladaptive cardiac remodeling (16) and pulmonary metastasis (80).	

injury (46), diabetes (47), colitis (39, 49, 50), lung inflammation (51), obesity (48), atherosclerosis (55), tumor burden (58), dermatitis (59), *Candida albicans* (60), and herpes simplex virus infections (62) as well as in pain (61). In humans, RvE1 has been identified in the plasma of healthy individuals (63), plasma and synovial fluid from arthritic patients (64), plasma of type II diabetes mellitus patients (65), plasma of peripheral artery disease patients (66), cord blood (67), breast milk (68), and blisters induced by UV-killed *E. coli* (69). Recently, RvE1 was also found to be increased in human neutrophils from individuals with metabolic syndrome following weight loss upon stimulation (70). RvE1 analog 18-oxo-resolvin E1 was found to evoke anti-inflammatory actions by reducing neutrophil infiltration and pro-inflammatory cytokine/chemokine production *in vivo* (71). These results demonstrate tissue/organ- and cell type-specific actions of RvE1 in controlling a wide range of diseases where excessive or uncontrolled inflammation is an underlying pathobiology.

In the E-series cascade, RvE2 stops chemoattractant-induced PMN infiltration *in vivo* in murine peritonitis (14) and decreases depression-like behavior in mice (53). RvE2 has also been identified in the plasma of healthy individuals (63), plasma and synovial fluid of arthritis patients correlating with pain reduction in these patients (64), plasma of type II diabetes mellitus patients (65), plasma of peripheral artery disease patients, breast milk (68), and in human blisters induced by UV-killed *E. coli* (69). Of interest, RvE2 analog benzo-resolvin E2 was found to display exceptional potency in the femtomole range in reducing inflammation *in vivo* (73). RvE3 decreases allergic airway inflammation *via* the IL-23/IL-17A pathway (74), reduces depression-like behavior in mice (75), and lowers the incidence of preterm birth in lipopolysaccharide-exposed pregnant mice (76). RvE3 has been identified in the plasma and synovial fluid of arthritic patients (64), plasma of type II diabetes mellitus patients (65), cord blood (67), breast milk (68), and UV-killed *E. coli*-induced human blisters (69). Also, 18-HEPE, a precursor of the E-series resolvins, inhibits macrophage-mediated pro-inflammatory activation of cardiac fibroblasts and prevents overload-induced maladaptive cardiac remodeling *in vivo*, demonstrating its potent actions in cardiac tissue (16). This is further illustrated by the recent discovery of the potent bioactivity of 18-deoxy-resolvin E3 (18-deoxy-RvE3), which stops neutrophil infiltration and resolves peritonitis in mice

(79). Of interest, recent results demonstrated that RvE3 is reduced in severe compared to moderate COVID-19 patients (77), highlighting the significance of SPMs in human disease. It has been shown that E-series resolvins are also endogenous anti-depressants (81). These findings from many investigators emphasize the potent structure-based functions and actions of the E-series resolvin members listed in **Table 1**. Further investigations are needed to fully appreciate the structure-activity relationships of RvE4 produced *via* these different biosynthetic pathways discussed above in biological systems.

In summation, the EPA cascade to the E-series bioactive metabolome of resolvins produces several potent mediators within this biosynthesis pathway (**Table 1**) that target diverse cell types relevant to inflammation, resolution, and resolution of vascular inflammation. This EPA precursor cascade is likely to contribute to the clinical impact of omega(ω)-3 supplementation as in recent results from cardiovascular disease patients (82). In recent human randomized trials, omega(ω)-3 supplementation lowered systemic levels of key pro-inflammatory cytokines associated with inflammaging (83). Also, in humans omega(ω)-3 supplements increase RvE1 in serum and plasma of healthy individuals, RvE3 in plasma of patients with peripheral artery disease (66), and circulating RvE1, RvE2, and RvE3 (84). Taken together, our present results establish the complete stereochemistry of the newest member of the E-series resolvins, Resolvin E4 (RvE4: 5*S*,15*S*-dihydroxy-6*E*,8*Z*,11*Z*,13*E*,17*Z*-eicosapentaenoic acid), and confirm its potent bioactions stimulating human macrophage efferocytosis. Moreover, these results provide evidence that synthetic RvE4 can now be used as a standard for LC-MS/MS-based profiling, lipidomics/metabolomic studies as well as help to further define RvE4 specific functions in biological systems and cellular function *in vitro* and *in vivo*.

DATA AVAILABILITY STATEMENT

The original contributions presented in the study are included in the article/**Supplementary Material**. Further inquiries can be directed to the corresponding author.

ETHICS STATEMENT

Human peripheral blood mononuclear cells (PBMC) were obtained from de-identified healthy human volunteers from the Boston Children's Hospital Blood Bank under protocol # 1999-P001297 approved by the Partners Human Research Committee.

AUTHOR CONTRIBUTIONS

SL carried out the RvE4 bioactions, designed and performed experiments, analyzed the results, and contributed to manuscript and figure preparations. AS performed LC-MS/MS matching, analyzed results, and contributed to manuscript and figure preparations. RN analyzed NMR data and contributed to figure preparation. DF and NW carried out total organic synthesis. NW and MM acquired the NMR data. CS conceived and designed the experiments and contributed to manuscript and figure preparation. All authors contributed to the article and approved the submitted version.

FUNDING

This work was supported by the National Institutes of Health (grant nos. P01GM095467 to CS and F32HL142175 to SL).

ACKNOWLEDGMENTS

We thank M. H. Small for expert assistance in manuscript preparation.

SUPPLEMENTARY MATERIAL

The Supplementary Material for this article can be found online at: https://www.frontiersin.org/articles/10.3389/fimmu.2020.631319/full#supplementary-material

REFERENCES

1. Netea MG, Balkwill F, Chonchol M, Cominelli F, Donath MY, Giamarellos-Bourboulis EJ, et al. A guiding map forinflammation. *Nat Immunol* (2017) 18:826–31. doi: 10.1038/ni.3790
2. Haeggstrom JZ. Leukotriene biosynthetic enzymes as therapeutic targets. *J Clin Invest* (2018) 128:2680–90. doi: 10.1172/JCI97945
3. Serhan CN. Pro-resolving lipid mediators are leads for resolution physiology. *Nature* (2014) 510:92–101. doi: 10.1038/nature13479
4. Arienti S, Barth ND, Dorward DA, Rossi AG, Dransfield I. Regulation of Apoptotic Cell Clearance During Resolution of Inflammation. *Front Pharmacol* (2019) 10:891. doi: 10.3389/fphar.2019.00891
5. Werz O, Gerstmeier J, Libreros S, De la Rosa X, Werner M, Norris PC, et al. Human macrophages differentially produce specific resolvin or leukotriene signals that depend on bacterial pathogenicity. *Nat Commun* (2018) 9:59. doi: 10.1038/s41467-017-02538-5
6. Jordan PM, Gerstmeier J, Pace S, Bilancia R, Rao Z, Borner F, et al. Staphylococcus aureus-Derived alpha-Hemolysin Evokes Generation of Specialized Pro-resolving Mediators Promoting Inflammation Resolution. *Cell Rep* (2020) 33:108247. doi: 10.1016/j.celrep.2020.108247
7. Liu T, Xiang A, Peng T, Doran AC, Tracey KJ, Barnes BJ, et al. HMGB1-C1q complexes regulate macrophage function by switching between leukotriene and specialized proresolving mediator biosynthesis. *Proc Natl Acad Sci U.S.A.* (2019) 116:23254–63. doi: 10.1073/pnas.1907490116
8. Bracco U, Deckelbaum RJ Nestlé Nutrition Services. *Polyunsaturated fatty acids in human nutrition*. New York: Raven Press (1992).
9. De Caterina R. n-3 fatty acids in cardiovascular disease. *N Engl J Med* (2011) 364:2439–50. doi: 10.1056/NEJMra1008153
10. Bhatt DL, Steg PG, Miller M, Brinton EA, Jacobson TA, Ketchum SB, et al. Cardiovascular Risk Reduction with Icosapent Ethyl for Hypertriglyceridemia. *N Engl J Med* (2019) 380:11–22. doi: 10.1056/NEJMoa1812792
11. Arita M, Bianchini F, Aliberti J, Sher A, Chiang N, Hong S, et al. Stereochemical assignment, antiinflammatory properties, and receptor for the omega-3 lipid mediator resolvin E1. *J Exp Med* (2005) 201:713–22. doi: 10.1084/jem.20042031

12. Serhan CN, Clish CB, Brannon J, Colgan SP, Chiang N, Gronert K. Novel functional sets of lipid-derived mediators with antiinflammatory actions generated from omega-3 fatty acids via cyclooxygenase 2-nonsteroidal antiinflammatory drugs and transcellular processing. *J Exp Med* (2000) 192:1197–204. doi: 10.1084/jem.192.8.1197
13. Arita M, Clish CB, Serhan CN. The contributions of aspirin and microbial oxygenase to the biosynthesis of anti-inflammatory resolvins: novel oxygenase products from omega-3 polyunsaturated fatty acids. *Biochem Biophys Res Commun* (2005) 338:149–57. doi: 10.1016/j.bbrc.2005.07.181
14. Tjonahen E, Oh SF, Siegelman J, Elangovan S, Percarpio KB, Hong S, et al. Resolvin E2: identification and anti-inflammatory actions: pivotal role of human 5-lipoxygenase in resolvin E series biosynthesis. *Chem Biol* (2006) 13:1193–202. doi: 10.1016/j.chembiol.2006.09.011
15. Isobe Y, Arita M, Matsueda S, Iwamoto R, Fujihara T, Nakanishi H, et al. Identification and structure determination of novel anti-inflammatory mediator resolvin E3, 17,18-dihydroxyeicosapentaenoic acid. *J Biol Chem* (2012) 287:10525–34. doi: 10.1074/jbc.M112.340612
16. Endo J, Sano M, Isobe Y, Fukuda K, Kang JX, Arai H, et al. 18-HEPE, an n-3 fatty acid metabolite released by macrophages, prevents pressure overload-induced maladaptive cardiac remodeling. *J Exp Med* (2014) 211:1673–87. doi: 10.1084/jem.20132011
17. Norris PC, Libreros S, Serhan CN. Resolution metabolomes activated by hypoxic environment. *Sci Adv* (2019) 5:eaax4895. doi: 10.1126/sciadv.aax4895
18. Kutzner L, Goloshchapova K, Rund KM, Jubermann M, Blum M, Rothe M, et al. Human lipoxygenase isoforms form complex patterns of double and triple oxygenated compounds from eicosapentaenoic acid. *Biochim Biophys Acta Mol Cell Biol Lipids* (2020) 1865:158806. doi: 10.1016/j.bbalip.2020.158806
19. Jouvene CC, Shay AE, Soens MA, Norris PC, Haeggstrom JZ, Serhan CN. Biosynthetic metabolomes of cysteinyl-containing immunoresolvents. *FASEB J* (2019) 33:13794–807. doi10.1096/fj.201902003R
20. Martinez FO, Gordon S, Locati M, Mantovani A. Transcriptional profiling of the human monocyte-to-macrophage differentiation and polarization: new molecules and patterns of gene expression. *J Immunol* (2006) 177:7303–11. doi: 10.4049/jimmunol.177.10.7303
21. Murray PJ, Allen JE, Biswas SK, Fisher EA, Gilroy DW, Goerdt S, et al. Macrophage activation and polarization: nomenclature and experimental guidelines. *Immunity* (2014) 41:14–20. doi: 10.1016/j.immuni.2014.06.008
22. Calzetti F, Tamassia N, Arruda-Silva F, Gasperini S, Cassatella MA. The importance of being "pure" neutrophils. *J Allergy Clin Immunol* (2017) 139:352–5.e6. doi: 10.1016/j.jaci.2016.06.025
23. Nauseef WM. Isolation of human neutrophils from venous blood. *Methods Mol Biol* (2014) 1124:13–8. doi: 10.1007/978-1-62703-845-4_2
24. Dagur PK, McCoy JP Jr. Collection, Storage, and Preparation of Human Blood Cells. *Curr Protoc Cytom* (2015) 73:5.1.1–5.1.16. doi: 10.1002/0471142956.cy0501s73
25. Jersmann HP, Ross KA, Vivers S, Brown SB, Haslett C, Dransfield I. Phagocytosis of apoptotic cells by human macrophages: analysis by multiparameter flow cytometry. *Cytometry A* (2003) 51:7–15. doi: 10.1002/cyto.a.10005
26. Lewis SM, Williams A, Eisenbarth SC. Structure and function of the immune system in the spleen. *Sci Immunol* (2019) 4:eaau6085. doi: 10.1126/sciimmunol.aau6085
27. Cassatella MA, ed. The Neutrophil an Emerging Regulator of Inflammatory and Immune Response. Basel: Kargel (2003). doi: 10.1159/isbn.978-3-318-00952-1
28. Nauseef WM, Borregaard N. Neutrophils at work. *Nat Immunol* (2014) 15:602–11. doi: 10.1038/ni.2921
29. Okabe Y, Medzhitov R.Tissue biology perspective on macrophages. *Nat Immunol* (2016) 17:9–17. doi: 10.1038/ni.3320
30. Lee J, An J-U, Kim T-H, Ko Y-J, Park J-B, Oh D-K. Discovery and Engineering of a Microbial Double-Oxygenating Lipoxygenase for Synthesis of Dihydroxy Fatty Acids as Specialized Proresolving Mediators. *ACS Sustain Chem Eng* (2020) 8:16172–83. doi: 10.1021/acssuschemeng.0c04793
31. Claria J, Serhan CN. Aspirin triggers previously undescribed bioactive eicosanoids by human endothelialcell-leukocyte interactions. *Proc Natl Acad Sci USA* (1995) 92:9475–9. doi: 10.1073/pnas.92.21.9475
32. Lee JY, Han SH, Park MH, Song IS, Choi MK, Yu E, et al. N-AS-triggered SPMs are direct regulators of microglia in a model of Alzheimer's disease. *Nat Commun* (2020) 11:2358. doi: 10.1038/s41467-020-16080-4
33. Dalli J, Chiang N, Serhan CN. Elucidation of novel 13-series resolvins that increase with atorvastatin and clear infections. *Nat Med* (2015) 21:1071–5. doi: 10.1038/nm.3911
34. Radmark O, Werz O, Steinhilber D, Samuelsson B. 5-Lipoxygenase, a key enzyme for leukotriene biosynthesis in health and disease. *Biochim Biophys Acta* (2015) 1851:331–9. doi: 10.1016/j.bbalip.2014.08.012
35. He Z, Tao D, Xiong J, Lou F, Zhang J, Chen J, et al. Phosphorylation of 5-LOX: The Potential Set-point of Inflammation. *Neurochem Res* (2020) 45:2245–57. doi: 10.1007/s11064-020-03090-3
36. Ye Y, Lin Y, Perez-Polo JR, Uretsky BF, Ye Z, Tieu BC, et al. Phosphorylation of 5-lipoxygenase at ser523 by protein kinase A determines whether pioglitazone and atorvastatin induce proinflammatory leukotriene B4 or anti-inflammatory 15-epi-lipoxin a4 production. *J Immunol* (2008) 181:3515–23. doi: 10.4049/jimmunol.181.5.3515
37. Schwab JM, Chiang N, Arita M, Serhan CN. Resolvin E1 and protectin D1 activate inflammation-resolution programmes. *Nature* (2007) 447:869–74. doi: 10.1038/nature05877
38. Oh SF, Pillai PS, Recchiuti A, Yang R, Serhan CN. Pro-resolving actions and stereoselective biosynthesis of 18S E-series resolvins in human leukocytes and murine inflammation. *J Clin Invest* (2011) 121:569–81. doi: 10.1172/JCI42545
39. Arita M, Yoshida M, Hong S, Tjonahen E, Glickman JN, Petasis NA, et al. Resolvin E1, an endogenous lipid mediator derived from omega-3 eicosapentaenoic acid, protects against 2,4,6-trinitrobenzene sulfonic acid-induced colitis. *Proc Natl Acad Sci USA* (2005) 102:7671–6. doi: 10.1073/pnas.0409271102
40. Sawada Y, Honda T, Hanakawa S, Nakamizo S, Murata T, Ueharaguchi-Tanada Y, et al. Resolvin E1 inhibits dendritic cell migration in the skin and attenuates contact hypersensitivity responses. *J Exp Med* (2015) 212:1921–30. doi: 10.1084/jem.20150381
41. Lee CT, Teles R, Kantarci A, Chen T, McCafferty J, Starr JR, et al. Resolvin E1 Reverses Experimental Periodontitis and Dysbiosis. *J Immunol* (2016) 197:2796–806. doi: 10.4049/jimmunol.1600859
42. Park CK, Xu ZZ, Liu T, Lu N, Serhan CN, Ji RR. Resolvin D2 is a potent endogenous inhibitor for transient receptor potential subtype V1/A1, inflammatory pain, and spinal cord synaptic plasticity in mice: distinct roles of resolvin D1, D2, and E1. *J Neurosci* (2011) 31:18433–8. doi: 10.1523/JNEUROSCI.4192-11.2011
43. Albuquerque-Souza E, Schulte F, Chen T, Hasturk H, Van Dyke TE, et al. Maresin-1 and Resolvin E1 Promote Regenerative Properties of Periodontal Ligament Stem Cells Under Inflammatory Conditions. *Front Immunol* (2020) 11:585530. doi: 10.3389/fimmu.2020.585530
44. Fredman G, Van Dyke TE, Serhan CN. Resolvin E1 regulates adenosine diphosphate activation of human platelets. *Arterioscler Thromb Vasc Biol* (2010) 30:2005–13. doi: 10.1161/ATVBAHA.110.209908
45. Chen J, Purvis GSD, Collotta D, Al Zoubi S, Sugimoto MA, Cacace A, et al. RvE1 Attenuates Polymicrobial Sepsis-Induced Cardiac Dysfunction and Enhances Bacterial Clearance. *Front Immunol* (2020) 11:2080. doi: 10.3389/fimmu.2020.02080
46. Keyes KT, Ye Y, Lin Y, Zhang C, Perez-Polo JR, Gjorstrup P, et al. Resolvin E1 protects the rat heart against reperfusion injury. *Am J Physiol Heart Circ Physiol* (2010) 299:H153–64. doi: 10.1152/ajpheart.01057.2009
47. Freire MO, Dalli J, Serhan CN, Van Dyke TE. Neutrophil Resolvin E1 Receptor Expression and Function in Type 2 Diabetes. *J Immunol* (2017) 198:718–28. doi: 10.4049/jimmunol.1601543
48. Gonzalez-Periz A, Horrillo R, Ferre N, Gronert K, Dong B, Moran-Salvador E, et al. Obesity-induced insulin resistance and hepatic steatosis are alleviated by omega-3 fatty acids: a role for resolvins and protectins. *FASEB J* (2009) 23:1946–57. doi: 10.1096/fj.08-125674
49. Campbell EL, MacManus CF, Kominsky DJ, Keely S, Glover LE, Bowers BE, et al. Resolvin E1-induced intestinal alkaline phosphatase promotes resolution of inflammation through LPS detoxification. *Proc Natl Acad Sci USA* (2010) 107:14298–303. doi: 10.1073/pnas.0914730107
50. Quiros M, Feier D, Birkl D, Agarwal R, Zhou DW, Garcia AJ, et al. Resolvin E1 is a pro-repair molecule that promotes ntestinal epithelial wound healing. *Proc Natl Acad Sci USA* (2020) 117:9477–82. doi: 10.1073/pnas.1921335117
51. Haworth O, Cernadas M, Levy BD. NK cells are effectors for resolvin E1 in the timely resolution of allergic airway inflammation. *J Immunol* (2011) 186:6129–35. doi: 10.4049/jimmunol.1004007

52. Levy BD, Zhang QY, Bonnans C, Primo V, Reilly JJ, Perkins DL, et al. The endogenous pro-resolving mediators lipoxin A4 and resolvin E1 preserve organ function in allograft rejection. *Prostaglandins Leukot Essent Fatty Acids* (2011) 84:43–50. doi: 10.1016/j.plefa.2010.09.002
53. Deyama S, Shimoda K, Suzuki H, Ishikawa Y, Ishimura K, Fukuda H, et al. Resolvin E1/E2 ameliorate lipopolysaccharide-induced depression-like behaviors via ChemR23. *Psychopharmacol (Berl)* (2018) 235:329–36. doi: 10.1007/s00213-017-4774-7
54. Kantarci A, Aytan N, Palaska I, Stephens D, Crabtree L, Benincasa C, et al. Combined administration of resolvin E1 and lipoxin A4 resolves inflammation in a murine model of Alzheimer's disease. *Exp Neurol* (2018) 300:111–20. doi: 10.1016/j.expneurol.2017.11.005
55. Ho KJ, Spite M, Owens CD, Lancero H, Kroemer AH, Pande R, et al. Aspirin-triggered lipoxin and resolvin E1 modulate vascular smooth muscle phenotype and correlate with peripheral atherosclerosis. *Am J Pathol* (2010) 177:2116–23. doi: 10.2353/ajpath.2010.091082
56. Laguna-Fernandez A, Checa A, Carracedo M, Artiach G, Petri MH, Baumgartner R, et al. ERV1/ChemR23 Signaling Protects Against Atherosclerosis by Modifying Oxidized Low-Density Lipoprotein Uptake and Phagocytosis in Macrophages. *Circulation* (2018) 138:1693–705. oi: 10.1161/CIRCULATIONAHA.117.032801
57. Hasturk H, Kantarci A, Ohira T, Arita M, Ebrahimi N, Chiang N, et al. RvE1 protects from local inflammation and osteoclast- mediated bone destruction in periodontitis. *FASEB J* (2006) 20:401–3. doi: 10.1096/fj.05-4724fje
58. Sulciner ML, Serhan CN, Gilligan MM, Mudge DK, Chang J, Gartung A, et al. Resolvins suppress tumor growth and enhance cancer therapy. *J Exp Med* (2018) 215:115–40. doi: 10.1084/jem.20170681
59. Sawada Y, Honda T, Nakamizo S, Otsuka A, Ogawa N, Kobayashi Y, et al. Resolvin E1 attenuates murine psoriatic dermatitis. *Sci Rep* (2018) 8:11873. doi: 10.1038/s41598-018-30373-1
60. Haas-Stapleton EJ, Lu Y, Hong S, Arita M, Favoreto S, Nigam S, et al. Candida albicans modulates host defense by biosynthesizing the pro-resolving mediator resolvin E1. *PloS One* (2007) 2:e1316. doi: 10.1371/journal.pone.0001316
61. Xu ZZ, Zhang L, Liu T, Park JY, Berta T, Yang R, et al. Resolvins RvE1 and RvD1 attenuate inflammatory pain via central and peripheral actions. *Nat Med* (2010) 16:592–7, 1p following 597. doi: 10.1038/nm.2123
62. Rajasagi NK, Reddy PB, Suryawanshi A, Mulik S, Gjorstrup P, Rouse BT. Controlling herpes simplex virus-induced ocular inflammatory lesions with the lipid-derived mediator resolvin E1. *J Immunol* (2011) 186:1735–46. doi: 10.4049/jimmunol.1003456
63. Colas RA, Souza PR, Walker ME, Burton M, Zaslona Z, Curtis AM, et al. Impaired Production and Diurnal Regulation of Vascular RvDn-3 DPA Increase Systemic Inflammation and Cardiovascular Disease. *Circ Res* (2018) 122:855–63. doi: 10.1161/CIRCRESAHA.117.312472
64. Barden AE, Moghaddami M, Mas E, Phillips M, Cleland LG, Mori TA. Specialised pro-resolving mediators of inflammation in inflammatory arthritis. *Prostaglandins Leukot Essent Fatty Acids* (2016) 107:24–9. doi: 10.1016/j.plefa.2016.03.004
65. Barden A, Shinde S, Phillips M, Beilin L, Mas E, Hodgson JM, et al. The effects of alcohol on plasma lipid mediators of inflammation resolution in patients with Type 2 diabetes mellitus. *Prostaglandins Leukot Essent Fatty Acids* (2018) 133:29–34. doi: 10.1016/j.plefa.2018.04.004
66. Ramirez JL, Gasper WJ, Khetani SA, Zahner GJ, Hills NK, Mitchell PT, et al. Fish Oil Increases Specialized Pro-resolving Lipid Mediators in PAD (The OMEGA-PAD II Trial). *J Surg Res* (2019) 238:164–74. doi: 10.1016/j.jss.2019.01.038
67. See VHL, Mas E, Prescott SL, Beilin LJ, Burrows S, Barden AE, et al. Effects of prenatal n-3 fatty acid supplementation on offspring resolvins at birth and 12 years of age: a double-blind, randomised controlled clinical trial. *Br J Nutr* (2017) 118:971–80. doi: 10.1017/S0007114517002914
68. Arnardottir H, Orr SK, Dalli J, Serhan CN. Human milk proresolving mediators stimulate resolution of acute inflammation. *Mucosal Immunol* (2016) 9:757–66. doi: 10.1038/mi.2015.99
69. Motwani MP, Colas RA, George MJ, Flint JD, Dalli J, Richard-Loendt A, et al. Pro-resolving mediators promote resolution in a human skin model of UV-killed Escherichia coli-driven acute inflammation. *JCI Insight* (2018) 3:e94463. doi: 10.1172/jci.insight.94463
70. Barden A, Shinde S, Tsai IJ, Croft KD, Beilin LJ, Puddey IB, et al. Effect of weight loss on neutrophil resolvins in the metabolic syndrome. *Prostaglandins Leukot Essent Fatty Acids* (2019) 148:25–9. doi: 10.1016/j.plefa.2019.07.001
71. Arita M, Oh SF, Chonan T, Hong S, Elangovan S, Sun YP, et al. Metabolic inactivation of resolvin E1 and stabilization of its anti-inflammatory actions. *J Biol Chem* (2006) 281:22847–54. doi: 10.1074/jbc.M603766200
72. Oh SF, Dona M, Fredman G, Krishnamoorthy S, Irimia D, Serhan CN. Resolvin E2 formation and impact in inflammation resolution. *J Immunol* (2012) 188:4527–34. doi: 10.4049/jimmunol.1103652
73. Murakami Y, Fukuda H, Muromoto R, Hirashima K, Ishimura K, Fujiwara K, et al. Design and Synthesis of Benzene Congeners of Resolvin E2, a Proresolving Lipid Mediator, as Its Stable Equivalents. *ACS Med Chem Lett* (2020) 11:479–84. doi: 10.1021/acsmedchemlett.9b00596
74. Sato M, Aoki-Saito H, Fukuda H, Ikeda H, Koga Y, Yatomi M, et al. Resolvin E3 attenuates allergic airway inflammation via the interleukin-23-interleukin-17A pathway. *FASEB J* (2019) 33:12750–9. doi: 10.1096/fj.201900283R
75. Deyama S, Shimoda K, Ikeda H, Fukuda H, Shuto S, Minami M. Resolvin E3 attenuates lipopolysaccharide-induced depression-like behavior in mice. *J Pharmacol Sci* (2018) 138:86–8. doi: 10.1016/j.jphs.2018.09.006
76. Yamashita A, Kawana K, Tomio K, Taguchi A, Isobe Y, Iwamoto R, et al. Increased tissue levels of omega-3 polyunsaturated fatty acids prevents pathological preterm birth. *Sci Rep* (2013) 3:3113. doi: 10.1038/srep03113
77. Schwarz B, Sharma L, Roberts L, Peng X, Bermejo S, Leighton I, et al. Severe SARS-CoV-2 infection in humans is defined by a shift in the serum lipidome resulting in dysregulation of eicosanoid immune mediators. *Preprint medRxiv* (2020) 2020.07.09.20149849. doi: 10.1101/2020.07.09.20149849
78. Isobe Y, Arita M, Iwamoto R, Urabe D, Todoroki H, Masuda K, et al. Stereochemical assignment and anti-inflammatory properties of the omega-3 lipid mediator resolvin E3. *J Biochem* (2013) 153:355–60. doi: 10.1093/jb/mvs151
79. Fukuda H, Ikeda H, Muromoto R, Hirashima K, Ishimura K, Fujiwara K, et al. Synthesis of Resolvin E3, a Proresolving Lipid Mediator, and Its Deoxy Derivatives: Identification of 18-Deoxy-resolvin E3 as a Potent Anti-Inflammatory Agent. *J Org Chem* (2020) 85:14190–200. doi: 10.1021/acs.joc.0c01701
80. Li J, Chen CY, Arita M, Kim K, Li X, Zhang H, et al. An omega-3 polyunsaturated fatty acid derivative, 18-HEPE, protects against CXCR4-associated melanoma metastasis. *Carcinogenesis* (2018) 39:1380–8. doi: 10.1093/carcin/bgy117
81. Deyama S. Resolvins as novel targets for rapid-acting antidepressants. *Folia Pharmacologica Japonica* (2020) 155:381–5. doi: 10.1254/fpj.20044
82. Bhatt DL, Steg PG, Miller M. Cardiovascular Risk Reduction with Icosapent Ethyl. *Reply N Engl J Med* (2019) 380:1678. doi: 10.1056/NEJMc1902165
83. Tan A, Sullenbarger B, Prakash R, McDaniel JC. Supplementation with eicosapentaenoic acid and docosahexaenoic acid reduces high levels of circulating proinflammatory cytokines in aging adults: A randomized, controlled study. *Prostaglandins Leukot Essent Fatty Acids* (2018) 132:23–9. doi: 10.1016/j.plefa.2018.03.010
84. Souza PR, Marques RM, Gomez EA, Colas RA, De Matteis R, Zak A, et al. Enriched Marine Oil Supplements Increase Peripheral Blood Specialized Pro-Resolving Mediators Concentrations and Reprogram Host Immune Responses: A Randomized Double-Blind Placebo-Controlled Study. *Circ Res* (2020) 126:75–90. doi: 10.1161/CIRCRESAHA.119.315506

Conflict of Interest: The authors declare that the research was conducted in the absence of any commercial or financial relationships that could be construed as a potential conflict of interest.

Copyright © 2021 Libreros, Shay, Nshimiyimana, Fichtner, Martin, Wourms and Serhan. This is an open-access article distributed under the terms of the Creative Commons Attribution License (CC BY). The use, distribution or reproduction in other forums is permitted, provided the original author(s) and the copyright owner(s) are credited and that the original publication in this journal is cited, in accordance with accepted academic practice. No use, distribution or reproduction is permitted which does not comply with these terms.

frontiers in Immunology

REVIEW
published: 12 February 2021
doi: 10.3389/fimmu.2021.631233

The Immunopathology of COVID-19 and the Cannabis Paradigm

*Nicole Paland[1], Antonina Pechkovsky[1], Miran Aswad[1], Haya Hamza[1], Tania Popov[1], Eduardo Shahar[2] and Igal Louria-Hayon[1,3,4]**

[1] Medical Cannabis Research and Innovation Center, Rambam Health Care Campus, Haifa, Israel, [2] Clinical Immunology Unit, Rambam Health Care Campus, Haifa, Israel, [3] Clinical Research Institute at Rambam (CRIR), Rambam Health Care Campus, Haifa, Israel, [4] Department of Hematology, Rambam Health Care Campus, Haifa, Israel

Coronavirus disease-19 caused by the novel RNA betacoronavirus SARS-CoV2 has first emerged in Wuhan, China in December 2019, and since then developed into a worldwide pandemic with >99 million people afflicted and >2.1 million fatal outcomes as of 24th January 2021. SARS-CoV2 targets the lower respiratory tract system leading to pneumonia with fever, cough, and dyspnea. Most patients develop only mild symptoms. However, a certain percentage develop severe symptoms with dyspnea, hypoxia, and lung involvement which can further progress to a critical stage where respiratory support due to respiratory failure is required. Most of the COVID-19 symptoms are related to hyperinflammation as seen in cytokine release syndrome and it is believed that fatalities are due to a COVID-19 related cytokine storm. Treatments with anti-inflammatory or anti-viral drugs are still in clinical trials or could not reduce mortality. This makes it necessary to develop novel anti-inflammatory therapies. Recently, the therapeutic potential of phytocannabinoids, the unique active compounds of the cannabis plant, has been discovered in the area of immunology. Phytocannabinoids are a group of terpenophenolic compounds which biological functions are conveyed by their interactions with the endocannabinoid system in humans. Here, we explore the anti-inflammatory function of cannabinoids in relation to inflammatory events that happen during severe COVID-19 disease, and how cannabinoids might help to prevent the progression from mild to severe disease.

Keywords: SARS-CoV2, COVID-19, cytokine release syndrome, cytokine storm, inflammation, cannabis, cannabinoids, cannabinoid receptors

OPEN ACCESS

Edited by:
Amiram Ariel,
University of Haifa, Israel

Reviewed by:
Kuldeep Dhama,
Indian Veterinary Research Institute (IVRI), India
Abhilash Perisetti,
University of Arkansas for Medical Sciences, United States

***Correspondence:**
Igal Louria-Hayon
i_louriahayon@rambam.health.gov.il

Specialty section:
This article was submitted to Inflammation, a section of the journal Frontiers in Immunology

Received: *19 November 2020*
Accepted: *26 January 2021*
Published: *12 February 2021*

Citation:
Paland N, Pechkovsky A, Aswad M, Hamza H, Popov T, Shahar E and Louria-Hayon I (2021) The Immunopathology of COVID-19 and the Cannabis Paradigm. Front. Immunol. 12:631233. doi: 10.3389/fimmu.2021.631233

INTRODUCTION

Coronavirus disease 19 (COVID-19) caused by the novel severe acute respiratory syndrome-coronavirus 2 (SARS-CoV2) firstly emerged in December 2019 in Wuhan in China and has, since then, evolved into a global pandemic (1). It is a novel enveloped RNA betacoronavirus, which binds with its spike surface protein (S-protein) to angiotensin-converting enzyme 2 (ACE2) on the cellular host's surface. Entry of the virus to the host cell by endocytosis requires cleavage of the S-protein by the host cell transmembrane protease serine-2 (TMPRSS-2) (2). ACE2 is expressed in a diverse array of cells including cells of the upper respiratory, central nervous and vasculature system as well as of the eye, lung, liver, heart, kidney, and intestine contributing to the diverse clinical pulmonary and extra-pulmonary manifestations of COVID-19 including gastrointestinal involvement of COVID-19 [(3–5); **Figure 1**].

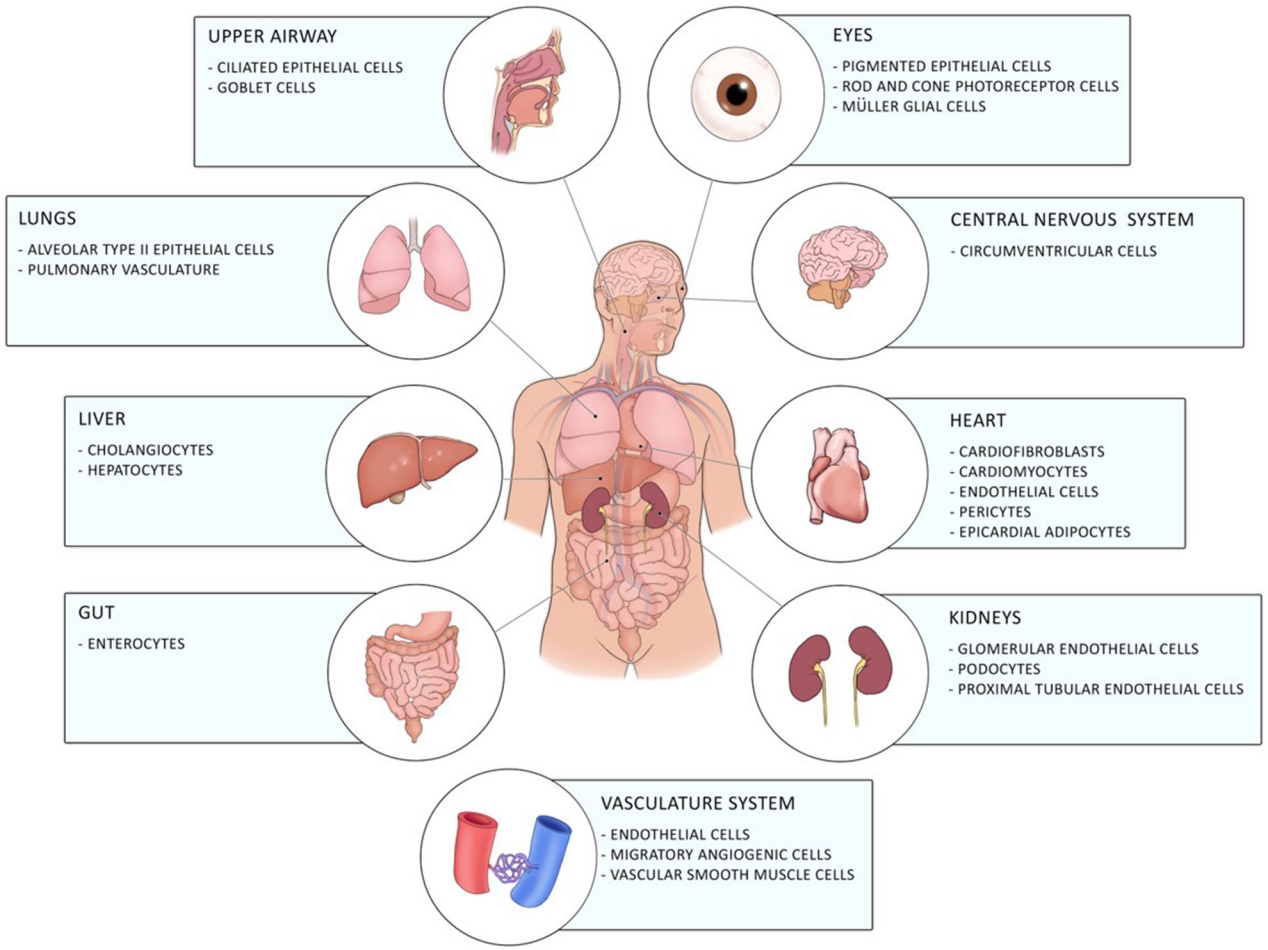

FIGURE 1 | Distribution of ACE2 in the human body. ACE2 is expressed in different cells of the eye, the upper airway, the lung, the liver, the gut, the central nervous system, the heart, the vasculature system, and of the kidneys.

SARS-CoV2 similarly to other coronavirus outbreaks SARS-CoV1 and Middle East Respiratory Syndrome (MERS) targets the lower respiratory tract system leading to pneumonia with fever, cough, and dyspnea (6). Most patients (80%) show only mild disease (either no or mild pneumonia), a smaller proportion (14%) develops severe symptoms with >50% pulmonary manifestations as observed on imaging tests including dyspnea and hypoxia. A small proportion (5%) develop a critical disease with respiratory failure, multi-organ failure or systemic shock. About 10–30% of hospitalized patients get into a critical stage where they require intensive care for respiratory support. Approximately 1% of all patients have a fatal outcome (7, 8). Patients who developed acute respiratory distress syndrome (ARDS) and required mechanical ventilation had a reported mortality rate of 88.1% in the New York City area in March 2020 (9). Interestingly, not only elderly, but also young patients with only mild comorbidities like hypertension, diabetes mellitus and obesity developed respiratory failure (10).

Epidemiological data show that differences in susceptibility and severity of COVID-19 widely depend on biological and socio-economic factors. A lower incidence of severe disease was observed in females with caucasian heritage (11, 12). This might be due to the fact that females are less susceptible to viral infections due to a higher macrophage and neutrophil activity and an increased antibody production and lower cytokine production (12). On the other hand seem ethnic minorities more susceptible to contract a SARS-CoV2 infection (11, 12). Ethnic minorities usually have less access to a functioning health care system, higher levels of medical comorbidities, and their lower socioeconomic status contributes to a weak cell-mediated immunity (11, 12).

Development of a severe disease progresses in two steps; mild symptoms at the start are followed by respiratory worsening after ∼10 days after onset of initial symptoms. This deterioration is accompanied with clinical presentations of ground-glass lung opacities on chest imaging, lymphocytopenia, high D-dimer, and high prothrombin (1). In patients with

moderate disease, a progressive reduction in inflammatory responses happens in convalescence while in patients with severe disease, these levels remain high and an additional cluster of inflammation appears (13) possibly due to a defective type I interferon response [(14); **Figure 2**]. Those systemic hyperinflammatory patterns in COVID-19 patients are similar to those in cytokine release syndrome (CRS) and the occurrence of CRS in severe disease was suggested (15).

Although certain patterns for the susceptibility to develop severe COVID-19 are recognizable (13, 16), the inflammatory response and the immune dynamics of the infected patient are still not fully understood. This makes the exact course of a SARS-CoV2 infection and the correlation to a certain clinical manifestation highly unpredictable. Effective and specific anti-viral drugs against SARS-CoV2 are not yet available. The usage of available repurposed anti-inflammatory medicines (17) and antibody-based immunotherapeutics targeting viral clearance (18, 19) is still experimental and applied only for the treatment of severely and critically ill patients (20–22). Safe and efficient treatment options that have the potential to halt disease progression at an early stage are needed. Cannabis and cannabinoids with their well-known anti-inflammatory properties may hold this potential.

Cannabis comprises various strains termed *Cannabis sativa*, *Cannabis ruderalis*, and *Cannabis indica*. It is not sure if they are three different species or whether ruderalis and indica are subspecies of *C. sativa*. During the history of the mankind, the cannabis plant was grown for varied uses as for production of fabric, for food, for recreational purposes and for medicinal use. Medically useful substances are produced in the trichomes that sit on the leaves and buds of the plant (23).

The cannabis plant contains more than 550 different components, of which are about 150 belongs to C21 or C22 terpenophenolic phitochemicals, which are predominantly expressed in the cannabis plant thus termed cannabinoids. The other 400 components are terpenes and phenolic compounds (24). The cannabinoids components contains both psychoactive [as 9-tetrahydrocannabinolic acid (THCA)] and non-psychoactive [as cannabidiolic acid (CBDA)] substances (24). The biological properties of the cannabinoids rely on their interaction with the endocannabinoid system includes G-proteins coupled receptors and Transient receptor potential chanels (TRP) (25).

Most interestingly, the anti-inflammatory properties especially of the non-psychoactive cannabidiol were recently explored as anti-viral agents. These effects were shown for the treatment of HIV (26), viral hepatitis (27), or influenza (28, 29) as well as orthopoxvirus, borna disease virus or vaccinia virus (30).

Here, we will explore the anti-inflammatory qualities of phytocannabinoids and discuss the possibility of applying cannabinoids as a treatment option for COVID-19 patients. We will explore the recent literature and emphasize the anti-inflammatory properties in relation to the events occurring during cytokine release syndrome (CRS) in mild or severe COVID-19 disease.

CYTOKINE RELEASE SYNDROME IN COVID-19 PATIENTS

Each infection with SARS-CoV2 is closely related to excessive inflammatory events with monocytes/macrophages and T cells playing a special role (31). Diffuse alveolar damage, pulmonary thrombi and vasculitis occurring predominantly in monocytes and myeloid tissue and an excess of plasma cells in lymph nodes, spleen, and lung was observed (15, 32). This leads to a severe increase in white blood cells with concomitant decrease in $CD4^+$ and $CD8^+$ lymphocytes resulting in an impaired neutrophil to lymphocyte ratio (33). Inflammatory cells infiltrate the sites of infection at an early stage of the infection with SARS-CoV2 and cause a stormy release of pro-inflammatory cytokines like IL-6, IL-17A, TNFα, IFNγ, IL-1α/β, and chemokines like CC-chemokine ligand 2 (CCL2) as well as CXC-chemokine ligand 10 (CXCL10) (13). The release of IL-6 by circulating monocytes into the bloodstream leads to an increased activation of T cells with a concomitant reduced total number of T cells. Monocyte-derived FNC1+ macrophages were found in bronchoalveolar lavage fluid (BALF) (13, 34) probably contribute to the hyperinflammation phenomenon (35). CRS can develop at every stage of infection beginning with the entry of the virus into the host causing innate and adaptive immune responses.

Induction of CRS During SARS-CoV2-ACE2 Interaction

Binding of the virus to ACE2 leads to the internalization of ACE2 and activation of angiotensin II resulting in the activation of nuclear factor kappa B (NF-κB). Subsequently, cytokines IL-6, TNFα, IL-1β, and IL-10 will be produced which might lead to local lung dysfunction including a rise in blood pressure, which contributes to lung injury and deterioration of pulmonary function as occurs in ARDS (36, 37).

Induction of CRS by Innate Immune Cells

ACE2 was found on $CD169^+$ macrophages in lymph nodes and spleen of COVID-19 patients and severe lymphocyte apoptosis was observed probably induced by viral antigens through Fas upregulation (38). $CD169^+$ cells control viral replication via type I interferon, and expose viral antigens to recognition by adaptive immune cells (39). Infection of $CD169^+$ macrophages enables the translocation of the virus to the spleen and lymph nodes, which contributes to the body-wide distribution of the virus resulting in accumulation of pro-inflammatory monocytes and macrophages at the sites of infection and at sites adjacent to the infection (40).

Monocyte derived *FCN1*+ macrophages that produce pro-inflammatory cytokines and chemokines were found in the BALF of patients with ARDS (34). This might contribute to the induction of T cell apoptosis, which might lead to pneumonia and disease progression to ARDS (41). Moreover, production of IL-6 in the spleen and lymph nodes, and of IL-6, TNFα, IL-10, and PD-1 by alveolar macrophages induces lymphocyte necrosis, further contributing to the development of lymphocytopenia and cytokine storm in the lung (38).

Monocytes and mononuclear cells in the peripheral blood and BALF are activated and secrete IL-6, IL-10, and TNFα,

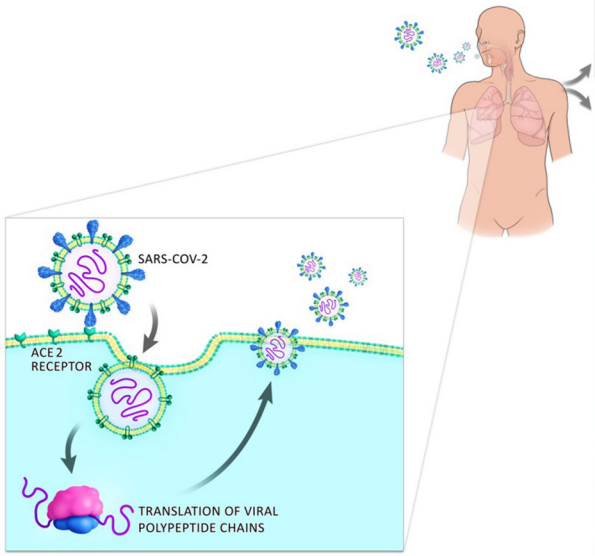

"Core" COVID-19 Inflammatory Response:

- Increase in inflammatory monocytes and neutrophils
- Decrease in lymphocytes
- Reduction of $CD4^+$ and $CD8^+$ T cell number and frequency due to apoptosis
- Increased activation of T cells due to the activity of circulating monocytes
- Increased IL-1α, IL-1β, IL-17A, IL-12p70 and IFNγ
- Monocyte derived FCN1+ macrophages in the bronchoalveolar lavage fluid

Severe Disease

- Additional inflammatory cluster: TPO, IL-5, IL-13, IL-33, IL-16, IL-21, IL-23, IFNγ, eotaxin-2
- Higher IL-1α, IL-1β, IL-6, IL-10, IL-18, TNFα, CC5/RANTES and IP-10 than in moderate disease
- Sustainment of high IFNγ and IL-12 levels
- Severe T cell depletion
- High levels of eosinophils and IgE
- Significant elevation of IL-6
- Increased plasma IL-17A and IL-22
- High viral load correlates with elevated levels of IFNα, IFNγ, TNFα and TRAIL
- Mortally ill patients exhibit elevated levels of cytokines IFNα, IFNλ and IL-Ra, and chemokines CCL1, CCL2, MCSF, IL-2, IL-16 and CCL21
- Aberrant levels of NETs
- Low numbers of T cells and T helper cells Th1, Th2 and Th17
- Infiltration of mononuclear cells to the interstitial area of the lung
- Low $CD4^+$ T cell levels and overactive $CD8^+$ cells
- Increased number of $CCR4^+$ and $CCR6^+$ Th17 cells

FIGURE 2 | Inflammatory responses in COVID-19 patients. Inflammatory responses to SARS-CoV2 comprise a "core" inflammatory response, which all COVID-19 patients experience. In patients with mild disease, the inflammatory response resolves on the way to convalescence. The appearance of additional inflammatory clusters is observed during progression to severe disease. This includes the release of a higher number of systemic pro-inflammatory cytokines, low numbers but over-reactive T cells, and infiltration of monocytes/macrophages to the sites of infection.

and chemoattractors of macrophages' IFN-induced protein 10 (IP-10), and MCP-1 (42). In peripheral blood mononuclear cells (PBMC) and BALF, high levels of neutrophil-attracting chemokines CXCL2 and CXCL8 attract neutrophils to the site of inflammation (43). Neutrophils secrete extracellular webs of DNA and histone to infectious particles, termed NETs, which are found aberrantly in patients with ARDS (44). They are believed to contribute to venous and arterial thrombosis in critical disease, multi-organ, and respiratory failure as well as coagulopathy due to their impact on the regulation of cytokine release (42).

Induction of CRS by Adaptive Immune Cells

Lymphocytopenia is a well-observed symptom in patients with severe COVID-19. It comprises a highly reduced number of circulating B and T cells combined with an increase in neutrophils and hyperactivation of monocytes and macrophages.

Patients with severe disease symptoms have low T cells and T helper cells, Th1, Th2, and Th17 numbers (45), either due to T cell apoptosis by high amounts of cytokines secreted by $CD4^+$ T cells (46, 47) or due to the redistribution to other tissues resulting in the infiltration of mononuclear cells into the interstitial area of the lung contributing to the development of interstitial pneumonitis (48).

In patients with ARDS, $CD4^+$, and $CD8^+$ T cells were found in the peripheral blood 14 days after disease onset. While $CD8^+$ T cells secrete primarily IFNγ, $CD4^+$ T cells secrete cytokines related to Th1 (IFNγ, TNFα, IL-2) and Th2 (IL-5, IL-9, IL-10) at normal levels (49) albeit at reduced levels in severe COVID-19 (50). Patients with ARDS had low but over-activated $CD8^+$ cells (51) leading to T cell exhaustion rendering the T cell response ineffective (50). In addition, activated T cells, including Th1 and Th17 helper cells, further stimulate the activation of monocytes enabling secretion of IL-1β, IL-6, and colony stimulating factor (CSF1 and CSF2) to contribute to the worsening of the cytokine storm resulting in organ failure (46).

Another important subset of T cells comprises regulatory T cells (Tregs). They are responsible for regulating the immune response to prevent hyperinflammation. To do so, they expand rapidly in antiviral immune responses (52). Inconsistent results have so far been obtained about the levels of Tregs in patients with severe COVID-19. Some observed higher levels of Tregs, while others reported reduced or unchanged levels (45).

As a result of the above, a significant elevation of a plethora of pro-inflammatory cytokine levels was reported. The most prominent elevated pro-inflammatory cytokine is IL-6 in patients with severe symptoms. This IL-6 production from $CD14^+$ and $CD16^+$ monocytes is driven by GM-CSF produced by Th1 cells (53) directly correlated with virus load (54). Moreover, IL-6 might influence lung-centric coagulopathy by inducing coagulation cascades (55).

Increased numbers of $CCR4^+$ and $CCR6^+$ Th17 cells were measured in COVID-19 patients with ARDS (56). Other

cytokines IL-1, IL-17, TNFα, and GM-CSF were associated with Th17 immune responses (57). These observations might explain the occurrence of a Th17-type cytokine storm, and the onset of multiple organ damage in patients with severe COVID-19 (56). Similarly, production of IP-10, CCL5/RANTES[41], CRP, and C-dimer were higher in patients with severe COVID-19 compared to mild COVID-19 (57). An increase of anti-inflammatory cytokines IL-10 and IL-4 hints to an elevated Th2 response, which might be involved in the development of pulmonary interstitial fibrosis (13, 58). Underlying bacterial infections might contribute to the development of CRS by exacerbating the inflammatory response (59).

TREATMENT OPTIONS FOR COVID-19 PATIENTS

No specific anti-viral drug for the successful treatment of COVID-19 is available. Several anti-inflammatory drugs are tested in pre-clinical and clinical trials as repurposed drugs for resolving CRS in patients with severe disease including steroids and corticosteroids like dexamethasone (60, 61), mono- and polyclonal antibodies normally used in rheumatology, i.e., the IL-6 inhibitor tocilizumab (62–65) including the "famous" monoclonal antibody cocktail REGN-COV2 (66), anti-viral drugs like remdesivir (67) or the HIV-drug combination lopinavir-ritonavir, the anti-parasitic drug hydroxychloroquine (68) as well as drugs against gastrointestinal diseases like famotidine (histamine-2 receptor antagonist), which showed antiviral properties for HIV or omeprazole (proton pump inhibitor) (69) in addition, the administration of convalescent plasma was tested (22).

Most of the drugs with the exception of remdesivir that was recently approved by the FDA, are still in clinical trials or could not reduce mortality (20–22). To prevent mortality, therapies halting disease progression at earlier stages are required. Cannabinoids with their anti-inflammatory function represent potential candidates to avoid CRS (70–72).

CANNABIS AND THE ENDOCANNABINOID SYSTEM

The cannabis plant comprises >550 different chemical constituents, ≈150 of these are cannabinoids and >400 non-cannabinoids. The main pharmacologically active compounds are the psychoactive tetrahydrocannabinols (THC), Δ^8-THC and Δ^9-THC, and other non-psychoactive cannabinoids like cannabinol (CBN), cannabidiol (CBD), or cannabigerol (CBG) to name only a few. CBN was the first cannabinoid that was isolated in 1899 (73). Non-cannabinoids are flavonoids, terpenes, and fatty acids [(23, 24); **Figure 3**].

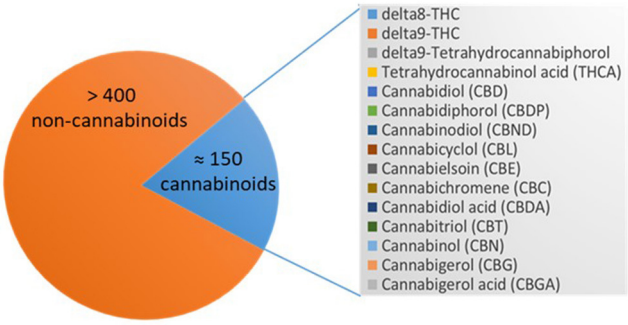

FIGURE 3 | Cannabinoids in *Cannabis sativa* spp. Depicted is the number of the compounds of the cannabis plant, which are >400 non-cannabinoids and ≈150 cannabinoids that are listed including their abbreviations.

Cannabinoid Receptors and Their Ligands

Cannabinoids convey their functions via cannabinoid receptors that are anchored in the cell membrane. Cannabinoid receptors bind to endo- (eCBs) and phytocannabinoids alike comprising the endocannabinoid system. The most studied endocannabinoids are 2-arachidonoylglycerol (2-AG) (74) and N-arachidonoylethanolamide (anandamide, AEA) (75). They belong to a group of lipid mediators that are either synthesized and released from membrane phospholipids "on demand" in response to physiological or pathological stimuli by many cell types in the brain or peripheral tissue or may be stored in organelles that might serve as potential platforms for trafficking and accumulation (76).

2-AG is a monoacylglycerol that serves as an intermediate in lipid metabolism (77). It is synthesized when needed by two major pathways, a signaling and a metabolic pathway. The signaling pathway starts from phosphatidylinositol-4,5-biphosphate (PIP_2) and the metabolic pathway starts from triglycerides that contain 2-arachidonate (78). Two second messengers are synthesized from PIP_2: diacylglycerol (DAG) and inositol-1,4,5-triphosphate (75). Triglycerides are hydrolyzed by hormone-sensitive lipase, other lipases, and carboxylesterase to diglycerides that contain 2-arachidonylglycerol (75). Diglycerides are then further processed by two isoforms of diacylglycerol lipase α and β (DAGL-α and -β) generating 2-AG and a fatty acid (79). Degradation of 2-AG is accomplished by the hydrolysis of the ester bond into arachidonic acid and glycerol by the enzyme monoacylglycerol lipase (MAGL) or α,β-hydrolase domain-containing proteins 12 and 6 (ABHD12 and ABHD6) (80).

The biosynthesis of AEA involves two steps: (i) the formation of N-arachidonoyl-phosphatidylethanolamine from phosphatidylethanolamine catalyzed by the calcium-dependent N-acyltransferase followed by (ii) the conversion of N-arachidonoylphosphatidylethanolamine to AEA or other N-acylethanolamines through five different metabolic pathways of which the most studied pathway involves N-acyl-phosphatidylethanolamine-hydrolyzing phospholipase D (76, 81). Degradation of AEA occurs through cleavage into arachidonic acid and ethanolamine by fatty acid amide hydrolase (FAAH) or N-acylethanolamine-hydrolyzing acid amidase (82).

Both, 2-AG and AEA, can be degraded by cyclooxygenase (COX), lipoxygenase (LOX), or cytochrome P450 resulting in the formation of oxidized compounds such as hydroxyl-anandamides and hydroxyeicosatetraenloyl-glycerol or

prostaglandin-ethanolamines and prostaglandin-glyceryl esters; all of them with different biological functions (76).

Two different classes of receptors are assigned as putative cannabinoid receptors, G-protein-coupled receptors (GPCRs) and transient receptor potential channels (TRP), which we present in further detail in the following two sections and in **Table 1**.

G Protein-Coupled Receptors

G protein-coupled receptors are a family of membrane proteins. They are characterized by seven membrane-spanning α-helical domains that are separated by alternating intra- and extracellular loops. GPCRs mediate the cellular response to neurotransmitters and hormones and are mostly responsible for taste, vision, and olfaction. The most prominent GPCRs that mediate endo- and phytocannabinoid signaling believed to be involved in signal transduction of the immune system are CB1R, CB2R, GPCR18, and GPCR55 (121).

Transient Receptor Potential Channels

Transient receptor potential (TRP) channels are a family of ion channels. They are membrane proteins which consist of channel subunits built of six putative transmembrane-spanning segments (S1-S6) with a pore-forming loop between S5 and S6 which assemble into tetramers to form functional channels (122). TRPs are involved in the signal transduction of numerous chemical and physical stimuli and regulate many neural signaling processes and other physiological functions such as temperature sensation, smell, taste, vision, pressure, or pain perception (123). Thus, they are potentially attractive targets for the therapeutic use of phytocannabinoids in the treatment of sensory, inflammatory or dermatological pathologies (124). Most TRPs can cause channelopathies which are risk factors for many disease states (125).

TRPs that are putative cannabinoid receptors are TRPV1-4, TRPA1, and TRPM8 (126).

Anti-inflammatory Properties of Cannabinoids and Their Potential to Downregulate COVID-19 Related CRS

First indications that cannabis has the potential to influence the disease course of COVID-19 were already published 3 years before the outbreak of the current pandemic. Researchers from Italy examined the potential of a hemp seed protein isolate that was prepared from defatted hemp seed by alkaline solubilization/acid precipitation as inhibitors for ACE-2. Four potentially bioactive peptides GVLY, IEE, LGV, and RVR were identified in the tested fraction by mono- and bidimensional NMR and LC-MS analyses. All four peptides had ACE-inhibitory activity rendering hemp seeds a potential agent to inhibit entry of SARS-CoV2 into the cells (127).

Recently, Canadian researchers have tested CBD extracts of 800 different *C. sativa* lines on 3D human models of oral, airways, and intestinal tissues and found 13 low THC/high CBD lines that modulated ACE2 and TMPRSS2 levels, which might lower the virus load (128). ACE2-reducing activity of cannabis-derived products were confirmed by a different group. They extracted a CBD, CBG, and THCV-containing fraction of a *C. sativa* strain and tested it *in vitro* in comparison to a standard phytocannabinoid agent. Both products reduced the secretion of pro-inflammatory cytokines IL-6, IL-8, CCL2, and CCL7 from the alveolar epithelial cell line A549, induced polarization of the macrophage cell line KG1 and increased the phagocytosis. CD36 and type II receptor for the Fc region of IgG (FcγRII) were upregulated. The researchers reported a certain superiority of the standard phytocannabinoids compared to the cannabis-derived fraction but cannot give recommendations for usage of cannabis in the treatment of COVID-19 (129). Another recent study simulated viral infections using the synthetic RNA Poly I:C and could show that Poly I:C-induced ARDS could be prevented by CBD (130) through the upregulation of apelin, a peptide regulating central and peripheral immunity that was severely downregulated in a murine model of ARDS (131). In the following two sections we will present the processes of regulation of the immune responses of endo- and phytocannabinoids.

Regulation of Immune Responses by Endocannabinoids via CB1 and CB2

The endocannabinoid system has anti-inflammatory activities in innate and adaptive immunity. It regulates migration and trafficking of different immune cells dependent on its receptors. Experiments with human bone marrow cells obtained by aspiration from healthy donors showed that the migration of human hematopoietic stem and progenitor cells was modulated by endocannabinoids. Endocannabinoids receptors CB1 and CB2 were expressed by bone marrow derived hematopoietic stem cells and $CD34^+$ cells. AEA and 2-AG were detected in the microenvironment of peripheral blood and bone marrow, which were secreted by bone marrow mesenchymal stem cells. Migration of hematopoietic stem cells was stimulated by AEA and 2-AG and blocked by CB receptor antagonists rendering endocannabinoids putative candidates for the enhancement of the migration of hematopoietic stem cells (132).

Cell trafficking of mature immune and effector cells, like lymphocytes, macrophages, neutrophils, and dendritic cells can be regulated by endocannabinoids [rev. in (133)]. It was reported that exogenously added 2-AG leads to the attenuation of lymphocyte proliferation through the decrease of Th1- and Th17-associated cytokines IL-6, IL-2, and TNFα. Moreover, activated B and T cells that produce high levels of 2-AG inhibit in a feedback loop T cell activation and proliferation, making exogenously applied 2-AG a putative candidate for therapeutic usage in Th1- or TH17-dependent diseases (134). Upon antigen activation by pathogens, macrophages, and dendritic cells produce and release 2-AG, which results in the upregulation of 2-AG levels in the serum and lymph nodes of mice during vaccination CB2 dependently. In a murine immunization model, transient administration of CB2 antagonist AM630 or inverse antagonist JTE907 increased the intensity of antigen-specific immune responses by upregulation of immunomodulatory genes in secondary lymphoid tissue (135). AEA inhibited macrophage-mediated killing of the TNFα-sensitive mouse alveolar macrophage cell line L929 (136). Correa

TABLE 1 | Cannabinoids receptors.

Receptor	Location in immune cells/tissue	Function in immunity	Ligands
CB1 and CB2	- Immune tissue (spleen and thymus) and leukocyte subpopulations like natural killer cells, B-cells, and peripheral blood mononuclear cells (83, 84)	- Reduces IL-2 synthesis (85) - Suppression of T cell activation (86–89) - Inhibition of lymphocyte proliferation and IL-17 secretion (86) - Regulation of function of intestinal neutrophils (90) - Regulation of acute trafficking of neutrophils to site of inflammation (91) - Retention of immature B cells in the bone marrow (92) - Immunosuppression in B cells after AEA or Δ^9-THC ligand binding (93)	*Endocannabinoids*: - 2-AG (94), AEA (95) *Phytocannabinoids*: - Δ^9-THC and Δ^8-THC as partial agonists regulating pain management (96, 97) - CBN as agonist (98) - CBD as a weak antagonist (99), as a negative allosteric modulator (100), and as an inhibitor of anandamide uptake (101) - CBG as a weak partial agonist (102, 103), and as an inhibitor of AEA uptake (101) - CBC as weak agonist (103), and as an inhibitor of AEA uptake (101) - Δ^9-THCV as an antagonist (104)
GPR18	- Spleen (105) - $CD4^+$- and $CD8^+$ T cells and $CD19^+$ B cells (106)	- Immune regulation in the small intestine for normal homeostasis of $CD8^+$ subsets of IELs ($CD8\alpha\alpha$ and $CD8\alpha\beta$ IELs) (107)	*Endocannabinoids*: - NAGly (105) *Phytocannabinoids*: - Δ^9-THC as an agonist (108) - CBD as antagonist (108)
GPR55	- Leukocytes	- T cell migration (109) - Hyperalgesia associated with inflammatory and neuropathic pain (110)	*Endocannabinoids*: - AEA, 2-AG, and virodhamine (111) *Phytocannabinoids*: - Δ^9-THC as an agonist (112) and LPI inhibitor (113) - CBD as antagonist (111) - CBG as weak LPI inhibitor (113) - Δ^9-THCV as a partial agonist and LPI inhibitor (113) - CBDV as a LPI inhibitor (113)
TRPV2	- Human and mouse B cells - Human dendritic cells and neutrophils - Mouse monocytes and macrophages	- Translocation of TRPV2 to the plasma membrane plays a role in the chemotaxis of macrophages and in phagocytosis (114) - Some analgesic and anti-proliferative properties of CBD may be mediated by TRPV2 activation (115)	*Phytocannabinoids*: - Δ^9-THC, CBD, CBG, Δ^9-THCV, and CBDV as agonists (101, 116)
TRPA1	- Expressed on human lung fibroblasts and epithelial cells (117)	- Agonist binding leads to release of IL-8 - Role in modulation of the release of chemokines in inflamed airways (117)	*Phytocannabinoids*: - Δ^9-THC, CBG (118) - CBN and CBC as antagonists (101)
TRPM8	- Co-expressed with several clusters of differentiation (CD) like CD38, CD79a, CD138, and in mature B-cell neoplasms (119)	- Role in cold hypersensitivity associated with inflammatory and neuropathic pain (120)	*Phytocannabinoids*: - Δ^9-THC, CBG (118) - CBN and CBC as antagonists (101)

CB, cannabinoid receptor; 2-AG, 2-arachidonoylglycerol; AEA, N-arachidonoylethanolamide; NADA, N-arachidonoyl dopamine; THC, tetrahydrocannabinols; CBN, cannabinol; CBD, cannabidiol; CBG, cannabigerol; CBC, cannabichromene; THCV, tetrahydrocannabinol; GPR, G protein-coupled receptor; LPI, lysophosphatidylinositol; CBDV, cannabidivarin; NAGly, N-arachidonyl glycine; TRPV2, transient receptor potential cation channel; subfamily V; member 2; IELs, intraepithelial lymphocytes; TRPA1, transient receptor potential cation channel; subfamily A; member 1; TRPM8, transient receptor potential cation channel; subfamily M, member 8.

et al. presented evidence that AEA inhibited expression of pro-inflammatory cytokines like IL-12 and IL-23 in *in vitro* models of immune disorders and increased the anti-inflammatory cytokine IL-10 in activated mouse microglia (137–139). In a model of acute intestinal inflammation it was shown that the transporter p-glycoprotein helped the influx of endocannabinoids into the intestinal lumen, which inhibited the migration of neutrophils by counteracting the pro-inflammatory neutrophil chemoattractant eicosanoid hepoxilin A3 (90). Similarly, the migration-related transcriptional profile of neutrophils was enhanced in $CB2^{-/-}$ mice. In response to Zymogen, the neutrophil, and lymphocyte antigen 6 complex was recruited to the dorsal air pouch and metalloproteinase 9 and CCL4 and CXCL10 increased (91).

Regulation of the Immune Response by Phytocannabinoids

Similarly, extracts of the phytocannabinoids CBD and THC could attenuate the proliferation of activated lymphocytes and the secretion of pro-inflammatory IL-17, thereby increasing secretion of the anti-inflammatory IL-10 (86). Additionally, the endocannabinoid AEA and the phytocannabinoid THC could also induce immunosuppression in B cells as was examined in both primary and secondary *in vitro* plaque-forming cell assays of antibody formation (93). Many reports have shown that exogenously applied CBD suppresses transcription factors involved in inflammation like NFAT, AP-1, and NF-κB, which results in a broad repression of cytokines

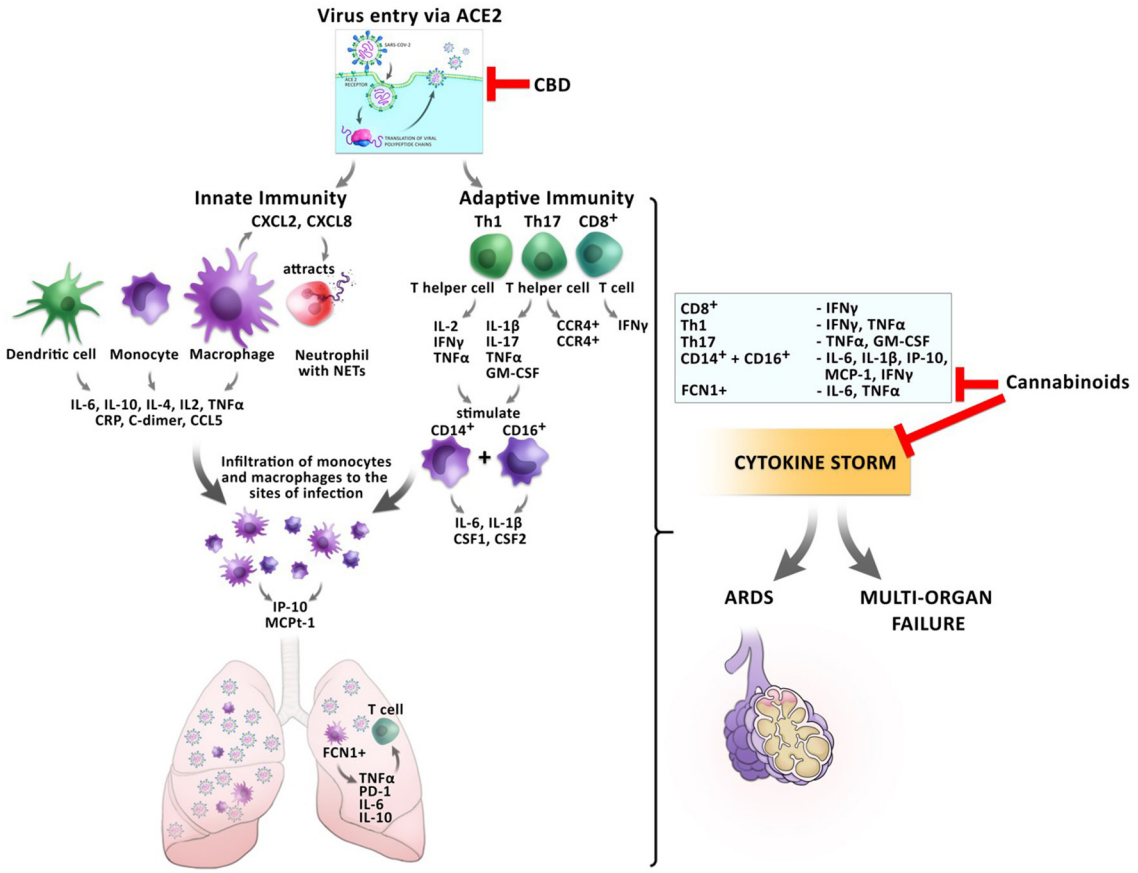

FIGURE 4 | Impact of cannabinoids on inflammatory responses during a SARS-CoV2 infection. The entry of the virus via ACE2 can be inhibited by CBD, reducing the virus load inside the cells. Infection with the virus triggers a cascade of inflammatory responses of the innate and adaptive immunity. Monocytes and macrophages secrete cytokines and chemokines. Activated macrophages secrete CXCL2 and CXCL8 which attract neutrophils, which release NETs to the site of infection. Infiltrating FCN1+ macrophages secrete IL-6, IL-10, and TNFα in the lung, which leads to T cell apoptosis. $CD8^+$ T cells secrete IFNγ and TNFα. T helper cells Th1 and Th17 stimulate CD14+ and CD16+ monocytes to secrete IL-6, IL-1β, and CSF1 and CSF2. This leads to the development of the cytokine storm, which might culminate in ARDS or multi-organ failure. Cannabinoids have the potential to inhibit the secretion of several pro-inflammatory cytokines resulting in prevention of CRS.

like IL-6, IL-1β, IL-1α, GM-CSF, and TNFα in diverse cells and tissues (140). These cytokines have a central role in the development of CRS in COVID-19. IL-6 promotes the differentiation of Th17 cells, which was shown to be suppressed by CBD (141). Moreover, CBD was shown to inhibit IFNγ (142).

A plethora of pre-clinical studies show that cannabinoids of certain cannabis strains can have an impact on the inflammatory response in mouse models of lung or inflammatory diseases, thus halting their progression. In a murine model of LPS-induced acute lung injury, CBD suppressed the vigorous immune response by three mechanisms: (i) inhibition of infiltration of leukocytes and neutrophils into lung tissue, (ii) inhibition of secretion of pro-inflammatory cytokines TNFα, IL-6, and the chemokines MCP-1 and MIP-2 into the BALF, (iii) inhibition of the activity of myeloperoxidase, an enzyme with antimicrobial activity abundantly expressed in neutrophils (143). In murine models of chronic asthma, cytokine levels of IL-4, IL-5, IL-6, IL-13, and TNFα were decreased by CBD, probably exerting its effect via the CB1 receptor. This led to the reduction of airway inflammation and fibrosis (144, 145). Moreover, the production of regulatory T cells were increased in murine models of inflammatory diseases (146).

These anti-inflammatory actions of cannabis might be beneficial for the prevention of CRS before the host inflammatory response turns pathological during the transition from mild to critical disease in COVID-19 patients (**Figure 4**).

CONCLUSION AND FUTURE PERSPECTIVES

According to the current state of available clinical data, most severe COVID-19 symptoms are related to CRS, which is also assumed to be responsible for the fatal outcome in COVID-19 patients. Here, we discuss the hypothesis that cannabinoids may have a great potential for the inhibition of hyperinflammation leading to CRS in COVID-19 patients. However, extensive

evidence from pre-clinical and clinical trials are still missing but urgently needed. This is because in spite of the medicinal potential of cannabis, it may be used in harmful or abusive manner. Cannabis is the most widely used illicit drug in the world. The United Nations Office On Drugs and Crime World Drug Report (UNODC) from 2020 measured around 192 million users in 2018 (147). An increased use among older adults was seen in the US between after legalization 2015 and 2018 (148) and known cannabis users increased their usage during first lockdown in the Netherlands (149) and in the US (150). The most common route of cannabis administration is smoking with or without tobacco. This raises concern in relation to the development of a severe/critical disease state in COVID-19 patients because smoking tobacco upregulates ACE-2 which increases the entry rate of the virus into the cells and leads to a worse outcome (151). While in Europe still 77.2–90.9% prefer tobacco-based smoking (152), the use of alternative routes of cannabis administration like vaporizing or edibles have increased in the US since legalization (153). However, whether vaping has an advantage over smoking for the likelihood of an infection with SARS-CoV2 and its outcome are still unknown (154).

Moreover, severe cardiovascular events were reported after acute usage of herbal cannabis (155) including an elevated risk of myocardial infarction in the presence of *Angina pectoris* (156) and reported cardiovascular deaths in 26% of users between 2006 and 2010 (157). In adolescent users, regular herbal cannabis use can lead to irreversible cognitive decline including loss of short-term memory, mood disorders, and schizophrenia (158).

However, increasing evidence shows a positive impact of cannabidiol on chronic pain in adult patients, as an antiemetic in chemotherapy-induced nausea and vomiting and in improving spasticity in multiple sclerosis based on patient's reports as well as in sleep improvement and fibromyalgia (159). However, many more precisely targeted clinical studies need to be performed in order to evaluate the benefit/risk ratio for cannabinoids. All together, these concerns emphasize the need of deeper science-based data that will allow the appropriate use of cannabis for medicinal purposes. Our studies at the Medical Cannabis Research and Innovation Center follow this route. We aim to become more knowledgeable about the exact anti-inflammatory capability of the cannabinoid's components of a chosen strain with the lowest potential to drug abuse and the least adverse effects so that we can administer cannabinoids more accurately targeted to the patients.

AUTHOR CONTRIBUTIONS

IL-H and NP conceptualized the manuscript and established the writing consortium. AP wrote the section about the cannabinoid receptors. MA wrote the section about the anti-inflammatory properties of cannabinoids. HH, TP, and ES contributed to the writing and reviewing process. All authors contributed to the article and approved the submitted version.

FUNDING

This work was supported by RAMBAM MED-TECH Milestone Grant Raphael Pharmaceutical Inc. Cannabinoids and Inflammation Research Grant.

ACKNOWLEDGMENTS

We want to thank Raphael Pharmaceutical Inc. for supporting this study. Acknowledgments go to Dr. Avraham Shtevi for editing the manuscript and to Yotam Giladi for creating the figures.

REFERENCES

1. Huang C, Wang Y, Li X, Ren L, Zhao J, Hu Y, et al. Clinical features of patients infected with 2019 novel coronavirus in Wuhan, China. *Lancet.* (2020) 395:497–506. doi: 10.1016/S0140-6736(20)30183-5
2. Hoffmann M, Kleine-Weber H, Schroeder S, Krüger N, Herrler T, Erichsen S, et al. SARS-CoV-2 cell entry depends on ACE2 and TMPRSS2 and is blocked by a clinically proven protease inhibitor. *Cell.* (2020) 181:271–80.e8. doi: 10.1016/j.cell.2020.02.052
3. Gheblawi M, Wang K, Viveiros A, Nguyen Q, Zhong J-C, Turner AJ, et al. Angiotensin-converting enzyme 2: SARS-CoV-2 receptor and regulator of the renin-angiotensin system: celebrating the 20th anniversary of the discovery of ACE2. *Circ Res.* (2020) 126:1456–74. doi: 10.1161/CIRCRESAHA.120.317015
4. Johnson KD, Harris C, Cain JK, Hummer C, Goyal H, Perisetti A. Pulmonary and extra-pulmonary clinical manifestations of COVID-19. *Front Med.* (2020) 7:526. doi: 10.3389/fmed.2020.00526
5. Perisetti A, Goyal H, Gajendran M, Boregowda U, Mann R, Sharma N. Prevalence, mechanisms, and implications of gastrointestinal symptoms in COVID-19. *Front Med.* (2020) 7:588711. doi: 10.3389/fmed.2020.588711
6. Mann R, Perisetti A, Gajendran M, Gandhi Z, Umapathy C, Goyal H. Clinical characteristics, diagnosis, and treatment of major coronavirus outbreaks. *Front Med.* (2020) 7:766. doi: 10.3389/fmed.2020.581521
7. Nanshan C, Zhou M, Dong X, Qu J, Gong F, Han Y, et al. Epidemiological and clinical characteristics of 99 cases of 2019 novel coronavirus pneumonia in Wuhan, China: a descriptive study. *Lancet.* (2020) 395:507–13. doi: 10.1016/S0140-6736(20)30211-7
8. Wu Z, McGoogan JM. Characteristics of and important lessons from the coronavirus disease 2019 (COVID-19) outbreak in China: summary of a report of 72 314 cases from the Chinese Center for Disease Control and Prevention. *JAMA.* (2020) 323:1239–42. doi: 10.1001/jama.2020.2648
9. Richardson S, Hirsch Richardson S, Hirsch JS, Narasimhan M, Crawford JM, McGinn T, et al. Consortium and the NC-19 R. presenting characteristics, comorbidities, and outcomes among 5700 patients hospitalized with COVID-19 in the New York city area. *JAMA.* (2020) 323:2052–59. doi: 10.1001/jama.2020.6775
10. Wu C, Chen X, Cai Y, Xia J, Zhou X, Xu S, et al. Risk factors associated with acute respiratory distress syndrome and death in patients with coronavirus disease 2019 pneumonia in Wuhan, China. *JAMA Intern Med.* (2020) 180:934–43. doi: 10.1001/jamainternmed.2020.0994
11. Garg S, Kim L, Whitaker M, O'Halloran A, Cummings C, Holstein R, et al. Hospitalization rates and characteristics of patients hospitalized with laboratory-confirmed coronavirus disease 2019—COVID-NET, 14 States, March 1–30, 2020. *MMWR Morb Mortal Wkly Rep.* (2020) 69:458–64. doi: 10.15585/mmwr.mm6915e3

12. Kopel J, Perisetti A, Roghani A, Aziz M, Gajendran M, Goyal H. Racial and gender-based differences in COVID-19. *Front Public Heal.* (2020) 8:418. doi: 10.3389/fpubh.2020.00418
13. Lucas C, Wong P, Klein J, Castro TBR, Silva J, Sundaram M, et al. Longitudinal analyses reveal immunological misfiring in severe COVID-19. *Nature.* (2020) 584:463–9. doi: 10.1038/s41586-020-2588-y
14. Hadjadj J, Yatim N, Barnabei L, Corneau A, Boussier J, Pere H, et al. Impaired type I interferon activity and exacerbated inflammatory responses in severe Covid-19 patients. *Science.* (2020) 369:718–24. doi: 10.1101/2020.04.19.20068015
15. Merad M, Martin JC. Pathological inflammation in patients with COVID-19: a key role for monocytes and macrophages. *Nat Rev Immunol.* (2020) 20:355–62. doi: 10.1038/s41577-020-0331-4
16. Franke L, (Severe C-19 GG). Genomewide association study of severe Covid-19 with respiratory failure. *N Engl J Med.* (2020) 383:1522–34. doi: 10.1056/NEJMoa2020283
17. Rabaan AA, Al-Ahmed SH, Sah R, Tiwari R, Yatoo MI, Patel SK, et al. SARS-CoV-2/COVID-19 and advances in developing potential therapeutics and vaccines to counter this emerging pandemic. *Ann Clin Microbiol Antimicrob.* (2020) 19:40. doi: 10.1186/s12941-020-00384-w
18. Sharun K, Tiwari R, Iqbal Yatoo M, Patel SK, Natesan S, Dhama J,. Antibody-based immunotherapeutics and use of convalescent plasma to counter COVID-19: advances and prospects. *Expert Opin Biol Ther.* (2020) 20:1033–46. doi: 10.1080/14712598.2020.1796963
19. Keam S, Megawati D, Patel SK, Tiwari R, Dhama K, Harapan H. Immunopathology and immunotherapeutic strategies in severe acute respiratory syndrome coronavirus 2 infection. *Rev Med Virol.* (2020) 30:e2123–3. doi: 10.1002/rmv.2123
20. RECOVERY. *No Clinical Benefit From Use of Lopinavir-Ritonavir in Hospitalised COVID-19 Patients Studied in RECOVERY*. (2020). Available online at: https://www.recoverytrial.net/news/no-clinical-benefit-from-use-of-lopinavir-ritonavir-in-hospitalised-covid-19-patients-studied-in-recovery (accessed September 14, 2020).
21. Group RC, Horby P, Mafham M, Linsell L, Bell JL, Staplin N, et al. Effect of hydroxychloroquine in hospitalized patients with Covid-19. *N Engl J Med.* (2020) 383:2030–40. doi: 10.1056/NEJMoa2022926
22. Agarwal A, Mukherjee A, Kumar G, Chatterjee P, Bhatnagar T, Malhotra P. Convalescent plasma in the management of moderate covid-19 in adults in India: open label phase II multicentre randomised controlled trial (PLACID Trial). *Br Med J.* (2020) 371:m3939. doi: 10.1136/bmj.m3939
23. Gould J. The Cannabis Crop. *Nature.* (2015) 525:S2–3. doi: 10.1038/525S2a
24. Andre CM, Hausman J-F, Guerriero G. *Cannabis sativa*: the plant of the thousand and one molecules. *Front Plant Sci.* (2016) 7:19. doi: 10.3389/fpls.2016.00019
25. Mechoulam R, Hanuš LO, Pertwee R, Howlett AC. Early phytocannabinoid chemistry to endocannabinoids and beyond. *Nat Rev Neurosci.* (2014) 15:757–64. doi: 10.1038/nrn3811
26. Costiniuk CT, Saneei Z, Routy J-P, Margolese S, Mandarino E, Singer J, et al. Oral cannabinoids in people living with HIV on effective antiretroviral therapy: CTN PT028-study protocol for a pilot randomised trial to assess safety, tolerability and effect on immune activation. *BMJ Open.* (2019) 9:e024793. doi: 10.1136/bmjopen-2018-024793
27. Lowe HIC, Toyang NJ, McLaughlin W. Potential of cannabidiol for the treatment of viral hepatitis. *Pharmacognosy Res.* (2017) 9:116–8. doi: 10.4103/0974-8490.199780
28. Karmaus PWF, Chen W, Crawford R, Kaplan BLF, Kaminski NE. Δ9-tetrahydrocannabinol impairs the inflammatory response to influenza infection: role of antigen-presenting cells and the cannabinoid receptors 1 and 2. *Toxicol Sci.* (2013) 131:419–33. doi: 10.1093/toxsci/kfs315
29. Buchweitz J, Karamaus P, Williams K, Harkema J, Kaminsky N. Targeted deletion of cannabinoid receptors CB1 and CB2 produced enhanced inflammatory responses to influenza A/PR/8/34 in the absence and presence of D9-tetrahydrocannabinol. *J Leukoc Biol.* (2008) 83:785–96. doi: 10.1189/jlb.0907618
30. Tahamtan A, Tavakoli-Yaraki M, Rygiel TP, Mokhtari-Azad T, Salimi V. Effects of cannabinoids and their receptors on viral infections. *J Med Virol.* (2016) 88:1–12. doi: 10.1002/jmv.24292
31. Grant RA, Morales-Nebreda L, Markov NS, Swaminathan S, Querrey M, Guzman ER, et al. Circuits between infected macrophages and T cells in SARS-CoV-2 pneumonia. *Nature.* (2021). doi: 10.1038/s41586-020-03148-w
32. Dorward DA, Russell CD, Um IH, Elshani M, Armstrong SD, Penrice-Randal R, et al. Tissue-specific tolerance in fatal Covid-19. *Am J Respir Crit Care Med.* (2020). 203:192–201. doi: 10.1101/2020.07.02.20145003
33. Liu J, Liu Y, Xiang P, Pu L, Xiong H, Li C, et al. Neutrophil-to-lymphocyte ratio predicts critical illness patients with 2019 coronavirus disease in the early stage. *J Transl Med.* (2020) 18:206. doi: 10.1186/s12967-020-02374-0
34. Liao M, Liu Y, Yuan J, Wen Y, Xu G, Zhao J, et al. Single-cell landscape of bronchoalveolar immune cells in patients with COVID-19. *Nat Med.* (2020) 26:842–4. doi: 10.1038/s41591-020-0901-9
35. Dhama K, Patel SK, Pathak M, Yatoo MI, Tiwari R, Malik YS, et al. An update on SARS-CoV-2/COVID-19 with particular reference to its clinical pathology, pathogenesis, immunopathology and mitigation strategies. *Travel Med Infect Dis.* (2020) 37:101755. doi: 10.1016/j.tmaid.2020.101755
36. Vaduganathan M, Vardeny O, Michel T, McMurray JJ V, Pfeffer MA, Solomon SD. Renin–angiotensin–aldosterone system inhibitors in patients with Covid-19. *N Engl J Med.* (2020) 382:1653–9. doi: 10.1056/NEJMsr2005760
37. Verdecchia P, Cavallini C, Spanevello A, Angeli F. The pivotal link between ACE2 deficiency and SARS-CoV-2 infection. *Eur J Intern Med.* (2020) 74:14–20. doi: 10.1016/j.ejim.2020.04.037
38. Chen Y, Feng Z, Diao B, Wang R, Wang G, Wang C, et al. The novel severe acute respiratory syndrome coronavirus 2 (SARS-CoV-2) directly decimates human spleens and lymph nodes. *medRxiv [Preprint].* (2020). doi: 10.1101/2020.03.27.20045427
39. Honke N, Shaabani N, Cadeddu G, Sorg UR, Zhang D-E, Trilling M, et al. Enforced viral replication activates adaptive immunity and is essential for the control of a cytopathic virus. *Nat Immunol.* (2012) 13:51–57. doi: 10.1038/ni.2169
40. Park MD. Macrophages: a Trojan horse in COVID-19? *Nat Rev Immunol.* (2020) 20:351. doi: 10.1038/s41577-020-0317-2
41. Channappanavar R, Fehr AR, Vijay R, Mack M, Zhao J, Meyerholz DK, et al. Dysregulated type I interferon and inflammatory monocyte-macrophage responses cause lethal pneumonia in SARS-CoV-infected mice. *Cell Host Microbe.* (2016) 19:181–93. doi: 10.1016/j.chom.2016.01.007
42. Xiong Y, Liu Y, Cao L, Wang D, Guo M, Jiang A, et al. Transcriptomic characteristics of bronchoalveolar lavage fluid and peripheral blood mononuclear cells in COVID-19 patients. *Emerg Microbes Infect.* (2020) 9:761–70. doi: 10.1080/22221751.2020.1747363
43. Koenig LM, Boehmer DFR, Metzger P, Schnurr M, Endres S, Rothenfusser S. Blocking inflammation on the way: rationale for CXCR2 antagonists for the treatment of COVID-19. *J Exp Med.* (2020) 217:e20201342. doi: 10.1084/jem.20201342
44. Zuo Y, Yalavarthi S, Shi H, Gockman K, Zuo M, Madison JA, et al. Neutrophil extracellular traps in COVID-19. *JCI Insight.* (2020) 5:e138999. doi: 10.1172/jci.insight.138999
45. Qin C, Zhou L, Hu Z, Zhang S, Yang S, Tao Y, et al. Dysregulation of immune response in patients with COVID-19 in Wuhan, China. *Clin Infect Dis.* (2020) 71:762–8. doi: 10.1093/cid/ciaa248
46. Wen W, Su W, Tang H, Le W, Zhang X, Zheng Y, et al. Immune cell profiling of COVID-19 patients in the recovery stage by single-cell sequencing. *Cell Discov.* (2020) 6:31. doi: 10.1038/s41421-020-0168-9
47. Gupta S, Bi R, Kim C, Chiplunkar S, Yel L, Gollapudi S. Role of NF-κB signaling pathway in increased tumor necrosis factor-α-induced apoptosis of lymphocytes in aged humans. *Cell Death Differ.* (2005) 12:177–183. doi: 10.1038/sj.cdd.4401557
48. Davis GS, Brody AR, Craighead JE. Analysis of airspace and interstitial mononuclear cell populations in human diffuse interstitial lung disease. *Am Rev Respir Dis.* (1978) 118:7–15. doi: 10.1164/arrd.1978.118.1.7
49. Weiskopf D, Schmitz KS, Raadsen MP, Grifoni A, Okba NMA, Endeman H, et al. Phenotype of SARS-CoV-2-specific T-cells in COVID-19 patients with acute respiratory distress syndrome. *Sci Immunol.* (2020) 5:eabd2071. doi: 10.1101/2020.04.11.20062349
50. Zheng H-Y, Zhang M, Yang C-X, Zhang N, Wang X-C, Yang X-P, et al. Elevated exhaustion levels and reduced functional diversity of T cells in

peripheral blood may predict severe progression in COVID-19 patients. *Cell Mol Immunol.* (2020) 17:541–3. doi: 10.1038/s41423-020-0401-3
51. Xu Z, Shi L, Wang Y, Zhang J, Huang L, Zhang C, et al. Pathological findings of COVID-19 associated with acute respiratory distress syndrome. *Lancet Respir Med.* (2020) 8:420–422. doi: 10.1016/S2213-2600(20)30076-X
52. Schorer M, Lambert K, Rakebrandt N, Rost F, Kao K-C, Yermanos A, et al. Rapid expansion of Treg cells protects from collateral colitis following a viral trigger. *Nat Commun.* (2020) 11:1522. doi: 10.1038/s41467-020-15309-6
53. Zhang D, Guo R, Lei L, Liu H, Wang Y, Wang Y, et al. COVID-19 infection induces readily detectable morphologic and inflammation-related phenotypic changes in peripheral blood monocytes. *J Leukoc Biol.* (2020) 109:13–22. doi: 10.1002/JLB.4HI0720-470R
54. Chen X, Zhao B, Qu Y, Chen Y, Xiong J, Feng Y, et al. Detectable serum severe acute respiratory syndrome coronavirus 2 viral load (RNAemia) is closely correlated with drastically elevated interleukin 6 level in critically ill patients with coronavirus disease 2019. *Clin Infect Dis.* (2020) 71:1937–42. doi: 10.1093/cid/ciaa449
55. Kerr R, Stirling D, Ludlam CA. Interleukin 6 and haemostasis. *Br J Haematol.* (2001) 115:3–12. doi: 10.1046/j.1365-2141.2001.03061.x
56. Wu D, Yang XO. TH17 responses in cytokine storm of COVID-19: an emerging target of JAK2 inhibitor Fedratinib. *J Microbiol Immunol Infect.* (2020) 53:368–70. doi: 10.1016/j.jmii.2020.03.005
57. Liu Y, Zhang C, Huang F, Yang Y, Wang F, Yuan J, et al. Elevated plasma levels of selective cytokines in COVID-19 patients reflect viral load and lung injury. *Natl Sci Rev.* (2020) 7:1003–11. doi: 10.1093/nsr/nwaa037
58. Chen G, Wu D, Guo W, Cao Y, Huang D, Wang H, et al. Clinical and immunological features of severe and moderate coronavirus disease 2019. *J Clin Invest.* (2020) 130:2620–9. doi: 10.1172/JCI137244
59. Wang J, Jiang M, Chen X, Montaner LJ. Cytokine storm and leukocyte changes in mild versus severe SARS-CoV-2 infection: review of 3939 COVID-19 patients in China and emerging pathogenesis and therapy concepts. *J Leukoc Biol.* (2020) 108:17–41. doi: 10.1002/JLB.3COVR0520-272R
60. Sterne, Jonathan AC, Murthy S, Diaz JV, Slutsky AS, Villar J, et al. Association between administration of systemic corticosteroids and mortality among critically ill patients with COVID-19: a meta-analysis. *JAMA.* (2020) 324:1–13. doi: 10.1001/jama.2020.17023
61. Sharun K, Tiwari R, Dhama J, Dhama K. Dexamethasone to combat cytokine storm in COVID-19: clinical trials and preliminary evidence. *Int J Surg.* (2020) 82:179–81. doi: 10.1016/j.ijsu.2020.08.038
62. Stebbing J, Phelan A, Griffin I, Tucker C, Oechsle O, Smith D, et al. COVID-19: combining antiviral and anti-inflammatory treatments. *Lancet Infect Dis.* (2020) 20:400–2. doi: 10.1016/S1473-3099(20)30132-8
63. Soy M, Keser G, Atagündüz P, Tabak F, Atagündüz I, Kayhan S. Cytokine storm in COVID-19: pathogenesis and overview of anti-inflammatory agents used in treatment. *Clin Rheumatol.* (2020) 39:2085–94. doi: 10.1007/s10067-020-05190-5
64. Boregowda U, Perisetti A, Nanjappa A, Gajendran M, Kutti Sridharan G, Goyal H. Addition of tocilizumab to the standard of care reduces mortality in severe COVID-19: a systematic review and meta-analysis. *Front Med.* (2020) 7:586221. doi: 10.3389/fmed.2020.586221
65. Liu B, Li M, Zhou Z, Guan X, Xiang Y. Can we use interleukin-6 (IL-6) blockade for coronavirus disease 2019 (COVID-19)-induced cytokine release syndrome (CRS)? *J Autoimmun.* (2020) 111:102452. doi: 10.1016/j.jaut.2020.102452
66. Baum A, Copin R, Ajithdoss D, Zhou A, Lanza K, Negron N, et al. REGN-COV2 antibody cocktail prevents and treats SARS-CoV-2 infection in rhesus macaques and hamsters. *Science.* (2020) 370:1110-5. doi: 10.1101/2020.08.02.233320
67. Beigel JH, Tomashek KM, Dodd LE, Mehta AK, Zingman BS, Kalil AC, et al. Remdesivir for the Treatment of Covid-19—preliminary report. *N Engl J Med.* (2020) 383:1813–26. doi: 10.1056/nejmoa2007764
68. White NJ, Watson JA, Hoglund RM, Chan XHS, Cheah PY, Tarning J. COVID-19 prevention and treatment: a critical analysis of chloroquine and hydroxychloroquine clinical pharmacology. *PLoS MED.* (2020) 17:e1003252. doi: 10.1371/journal.pmed.1003445
69. Aguila EJT, Cua IHY. Repurposed GI drugs in the treatment of COVID-19. *Dig Dis Sci.* (2020) 65:2452–3. doi: 10.1007/s10620-020-06430-z
70. Byrareddy SN, Mohan M. SARS-CoV2 induced respiratory distress: can cannabinoids be added to anti-viral therapies to reduce lung inflammation? *Brain Behav Immun.* (2020) 87:120–1. doi: 10.1016/j.bbi.2020.04.079
71. Esposito G, Pesce M, Seguella L, Sanseverino W, Lu J, Corpetti C, et al. The potential of cannabidiol in the COVID-19 pandemic. *Br J Pharmacol.* (2020) 177:4967–70. doi: 10.1111/bph.15157
72. Sexton M. Cannabis in the time of coronavirus disease 2019: the Yin and Yang of the endocannabinoid system in immunocompetence. *J Altern Complement Med.* (2020) 26:444–8. doi: 10.1089/acm.2020.0144
73. Pain S. A potted history. *Nature.* (2015) 525:S10–S11. doi: 10.1038/525S10a
74. Mechoulam R, Ben-Shabat S, Hanus L, Ligumsky M, Kaminski NE, Schatz AR, et al. Identification of an endogenous 2-monoglyceride, present in canine gut, that binds to cannabinoid receptors. *Biochem Pharmacol.* (1995) 50:83–90. doi: 10.1016/0006-2952(95)00109-D
75. Stella N, Schweitzer P, Piomelli D. A second endogenous cannabinoid that modulates long-term potentiation. *Nature.* (1997) 388:773–77.
76. Chiurchiù V, Battistini L, Maccarrone M. Endocannabinoid signalling in innate and adaptive immunity. *Immunology.* (2015) 144:352–64. doi: 10.1111/imm.12441
77. Murataeva N, Straiker A, Mackie K. Parsing the players: 2-arachidonoylglycerol synthesis and degradation in the CNS. *Br J Pharmacol.* (2014) 171:1379–91. doi: 10.1111/bph.12411
78. Farooqui AA, Rammohan KW, Horrocks LA. Isolation, characterization, and regulation of diacylglycerol lipases from the bovine brain. *Ann N Y Acad Sci.* (1989) 559:25–36. doi: 10.1111/j.1749-6632.1989.tb22596.x
79. Bisogno T, Howell F, Williams G, Minassi A, Cascio MG, Ligresti A, et al. Cloning of the first sn1-DAG lipases points to the spatial and temporal regulation of endocannabinoid signaling in the brain. *J Cell Biol.* (2003) 163:463–8. doi: 10.1083/jcb.200305129
80. Blankman JL, Simon GM, Cravatt BF. A comprehensive profile of brain enzymes that hydrolyze the endocannabinoid 2-arachidonoylglycerol. *Chem Biol.* (2007) 14:1347–56. doi: 10.1016/j.chembiol.2007.11.006
81. Okamoto Y, Morishita J, Tsuboi K, Tonai T, Ueda N. Molecular characterization of a phospholipase D generating anandamide and its congeners. *J Biol Chem.* (2004) 279:5298–305. doi: 10.1074/jbc.M306642200
82. McKinney MK, Cravatt BF. Structure and function of fatty acid amide hydrolase. *Annu Rev Biochem.* (2005) 74:411–32. doi: 10.1146/annurev.biochem.74.082803.133450
83. Zou S, Kumar U. Cannabinoid receptors and the endocannabinoid system: signaling and function in the central nervous system. *Int J Mol Sci.* (2018) 19:833. doi: 10.3390/ijms19030833
84. Benito C, Tolón RM, Pazos MR, Núñez E, Castillo AI, Romero J. Cannabinoid CB2 receptors in human brain inflammation. *Br J Pharmacol.* (2008) 153:277–85. doi: 10.1038/sj.bjp.0707505
85. Hoggatt J, Pelus LM. Eicosanoid regulation of hematopoiesis and hematopoietic stem and progenitor trafficking. *Leukemia.* (2010) 24:1993–2002. doi: 10.1038/leu.2010.216
86. Khuja I, Yekhtin Z, Or R, Almogi-Hazan O. Cannabinoids reduce inflammation but inhibit lymphocyte recovery in murine models of bone marrow transplantation. *Int J Mol Sci.* (2018) 20:668. doi: 10.3390/ijms20030668
87. Starnes T, Broxmeyer HE, Robertson MJ, Hromas R. Cutting Edge: IL-17D, a novel member of the IL-17 family, stimulates cytokine production and inhibits hemopoiesis. *J Immunol.* (2002) 169:642–6. doi: 10.4049/jimmunol.169.2.642
88. Chiricozzi A, Guttman-Yassky E, Suárez-Fariñas M, Nograles KE, Tian S, Cardinale I, et al. Integrative responses to IL-17 and TNF-α in human keratinocytes account for key inflammatory pathogenic circuits in psoriasis. *J Invest Dermatol.* (2011) 131:677–87. doi: 10.1038/jid.2010.340
89. Miossec P, Korn T, Kuchroo VK. Interleukin-17 and type 17 helper T cells. *N Engl J Med.* (2009) 361:888–98. doi: 10.1056/NEJMra0707449
90. Szabady RL, Louissaint C, Lubben A, Xie B, Reeksting S, Tuohy C, et al. Intestinal P-glycoprotein exports endocannabinoids to prevent inflammation and maintain homeostasis. *J Clin Invest.* (2018) 128:4044–56. doi: 10.1172/JCI96817
91. Kapellos TS, Taylor L, Feuerborn A, Valaris S, Hussain MT, Rainger GE, et al. Cannabinoid receptor 2 deficiency exacerbates inflammation and

neutrophil recruitment. *FASEB J.* (2019) 33:6154–67. doi: 10.1096/fj.201802524R
92. Pereira JP, An J, Xu Y, Huang Y, Cyster JG. Cannabinoid receptor 2 mediates the retention of immature B cells in bone marrow sinusoids. *Nat Immunol.* (2009) 10:403–11. doi: 10.1038/ni.1710
93. Eisenstein TK, Meissler JJ, Wilson Q, Gaughan JP, Adler MW. Anandamide and Delta9-tetrahydrocannabinol directly inhibit cells of the immune system via CB2 receptors. *J Neuroimmunol.* (2007) 189:17–22. doi: 10.1016/j.jneuroim.2007.06.001
94. Sugiura T, Kondo S, Sukagawa A, Nakane S, Shinoda A, Itoh K, et al. 2-arachidonoylgylcerol: a possible endogenous cannabinoid receptor ligand in brain. *Biochem Biophys Res Commun.* (1995) 215:89–97. doi: 10.1006/bbrc.1995.2437
95. Devane WA, Hanus L, Breuer A, Pertwee RG, Stevenson LA, Griffin G. Isolation and structure of a brain constituent that binds to the cannabinoid receptor. *Science.* (1992) 258:1946–9. doi: 10.1126/science.1470919
96. Boychuk DG, Goddard G, Mauro G, Orellana MF. The effectiveness of cannabinoids in the management of chronic nonmalignant neuropathic pain: a systematic review. *J Oral Facial Pain Headache.* (2015) 29:7–14. doi: 10.11607/ofph.1274
97. De Petrocellis L, Ligresti A, Moriello AS, Allarà M, Bisogno T, Petrosino S, et al. Effects of cannabinoids and cannabinoid-enriched Cannabis extracts on TRP channels and endocannabinoid metabolic enzymes. *Br J Pharmacol.* (2011) 163:1479–94. doi: 10.1111/j.1476-5381.2010.01166.x
98. Novack GD. Cannabinoids for treatment of glaucoma. *Curr Opin Ophthalmol.* (2016) 27**:**146–50. doi: 10.1097/ICU.0000000000000002:
99. JÄrbe TUC, Henriksson BG. Effects of Δ8-THC, and Δ9-THC on the acquisition of a discriminative positional habit in rats. *Psychopharmacologia.* (1973) 31:321–32. doi: 10.1007/BF00421276
100. Rhee M-H, Vogel Z, Barg J, Bayewitch M, Levy R, Hanuš L, et al. Cannabinol derivatives: binding to cannabinoid receptors and inhibition of adenylylcyclase. *J Med Chem.* (1997) 40:3228–33. doi: 10.1021/jm970126f
101. Kathmann M, Flau K, Redmer A, Tränkle C, Schlicker E. Cannabidiol is an allosteric modulator at mu- and delta-opioid receptors. *Naunyn Schmiedebergs Arch Pharmacol.* (2006) 372:354–61. doi: 10.1007/s00210-006-0033-x
102. Scuderi C, Steardo L, Esposito G. Cannabidiol promotes amyloid precursor protein ubiquitination and reduction of beta amyloid expression in SHSY5YAPP+ cells through PPARγ involvement. *Phyther Res.* (2014) 28:1007–13. doi: 10.1002/ptr.5095
103. Esposito G, Scuderi C, Valenza M, Togna GI, Latina V, De Filippis D, et al. Cannabidiol reduces Aβ-induced neuroinflammation and promotes hippocampal neurogenesis through PPARγ involvement. *PLoS ONE.* (2011) 6:e28668. doi: 10.1371/journal.pone.0028668
104. Rosenthaler S, Pöhn B, Kolmanz C, Huu CN, Krewenka C, Huber A, et al. Differences in receptor binding affinity of several phytocannabinoids do not explain their effects on neural cell cultures. *Neurotoxicol Teratol.* (2014) 46:49–56. doi: 10.1016/j.ntt.2014.09.003
105. Flegel C, Vogel F, Hofreuter A, Wojcik S, Schoeder C, Kieć-Kononowicz K, et al. Characterization of non-olfactory GPCRs in human sperm with a focus on GPR18. *Sci Rep.* (2016) 6:32255. doi: 10.1038/srep32255
106. Kohno M, Hasegawa H, Inoue A, Muraoka M, Miyazaki T, Oka K, et al. Identification of N-arachidonylglycine as the endogenous ligand for orphan G-protein-coupled receptor GPR18. *Biochem Biophys Res Commun.* (2006) 347:827–32. doi: 10.1016/j.bbrc.2006.06.175
107. Becker AM, Callahan DJ, Richner JM, Choi J, DiPersio JF, Diamond MS, et al. GPR18 controls reconstitution of mouse small intestine intraepithelial lymphocytes following bone marrow transplantation. *PLoS ONE.* (2015) 10:e0133854. doi: 10.1371/journal.pone.0133854
108. McHugh D, Page J, Dunn E, Bradshaw HB. Δ9-THC and N-arachidonyl glycine are full agonists at GPR18 and cause migration in the human endometrial cell line, HEC-1B. *Br J Pharmacol.* (2012) 165:2414–24. doi: 10.1111/j.1476-5381.2011.01497.x
109. Sumida H, Lu E, Chen H, Yang Q, Mackie K, Cyster JG. GPR55 regulates intraepithelial lymphocyte migration dynamics and susceptibility to intestinal damage. *Sci Immunol.* (2017) 2:eaao1135. doi: 10.1126/sciimmunol.aao1135
110. Whyte LS, Ryberg E, Sims NA, Ridge SA, Mackie K, Greasley PJ, et al. The putative cannabinoid receptor GPR55 affects osteoclast function *in vitro* and bone mass *in vivo*. *Proc Natl Acad Sci U S A.* (2009) 106:16511–6. doi: 10.1073/pnas.0902743106
111. Ryberg E, Larsson N, Sjögren S, Hjorth S, Hermansson N-O, Leonova J, et al. The orphan receptor GPR55 is a novel cannabinoid receptor. *Br J Pharmacol.* (2007) 152:1092–101. doi: 10.1038/sj.bjp.0707460
112. Howlett AC, Barth F, Bonner TI, Cabral G, Casellas P, Devane WA, et al. International union of pharmacology. XXVII. Classification of cannabinoid receptors. *Pharmacol Rev.* (2002) 54:161–202. doi: 10.1124/pr.54.2.161
113. Lauckner JE, Jensen JB, Chen H-Y, Lu H-C, Hille B, Mackie K. GPR55 is a cannabinoid receptor that increases intracellular calcium and inhibits M current. *Proc Natl Acad Sci U S A.* (2008) 105:2699–704. doi: 10.1073/pnas.0711278105
114. Blair NT, Carvacho I, Chaudhuri D, Clapham DE, DeCaen P, Delling M, et al. Transient receptor potential channels (version 2019.4) in the IUPHAR/BPS guide to pharmacology database. *IUPHAR/BPS Guid to Pharmacol CITE.* (2019) 1–59. doi: 10.2218/gtopdb/F78/2019.4
115. Nabissi M, Morelli MB, Santoni M, Santoni G. Triggering of the TRPV2 channel by cannabidiol sensitizes glioblastoma cells to cytotoxic chemotherapeutic agents. *Carcinogenesis.* (2012) 34:48–57. doi: 10.1093/carcin/bgs328
116. Sullivan SE, Kendall DA, Randall MD. Further characterization of the time-dependent vascular effects of Δ9-tetrahydrocannabinol. *J Pharmacol Exp Ther.* (2006) 317:428–438. doi: 10.1124/jpet.105.095828
117. Mukhopadhyay I, Gomes P, Aranake S, Shetty M, Karnik P, Damle M, et al. Expression of functional TRPA1 receptor on human lung fibroblast and epithelial cells. *J Recept Signal Transduct.* (2011) 31:350–358. doi: 10.3109/10799893.2011.602413
118. Vara D, Morell C, Rodríguez-Henche N, Diaz-Laviada I. Involvement of PPARγ in the antitumoral action of cannabinoids on hepatocellular carcinoma. *Cell Death Dis.* (2013) 4:e618. doi: 10.1038/cddis.2013.141
119. Hirai A, Aung NY, Ohe R, Nishida A, Kato T, Meng H, et al. Expression of TRPM8 in human reactive lymphoid tissues and mature B-cell neoplasms. *Oncol Lett.* (2018) 16:5930–8. doi: 10.3892/ol.2018.9386
120. McKemy DD. How cold is it? TRPM8 and TRPA1 in the molecular logic of cold sensation. *Mol Pain.* (2005) 1:16. doi: 10.1186/1744-8069-1-16
121. Rosenbaum DM, Rasmussen SGF, Kobilka BK. The structure and function of G-protein-coupled receptors. *Nature.* (2009) 459:356–63. doi: 10.1038/nature08144
122. Yu FH, Catterall WA. The VGL-chanome: a protein superfamily specialized for electrical signaling and ionic homeostasis. *Sci STKE.* (2004) 2004:re15. doi: 10.1126/stke.2532004re15
123. Moran MM, McAlexander MA, Bíró T, Szallasi A. Transient receptor potential channels as therapeutic targets. *Nat Rev Drug Discov.* (2011) 10:601–20. doi: 10.1038/nrd3456
124. Caterina MJ. TRP channel cannabinoid receptors in skin sensation, homeostasis, and inflammation. *ACS Chem Neurosci.* (2014) 5:1107–16. doi: 10.1021/cn5000919
125. Nilius B, Owsianik G. Transient receptor potential channelopathies. *Pflügers Arch Eur J Physiol.* (2010) 460:437–50. doi: 10.1007/s00424-010-0788-2
126. Storozhuk MV, Zholos AV TRP channels as novel targets for endogenous ligands: focus on endocannabinoids and nociceptive signalling. *Curr Neuropharmacol.* (2018) 16:137–50. doi: 10.2174/1570159X15666170424120802
127. Orio LP, Boschin G, Recca T, Morelli CF, Ragona L, Francescato P, et al. New ACE-inhibitory peptides from hemp seed (*Cannabis sativa* L.) proteins. *J Agric Food Chem.* (2017) 65:10482–8. doi: 10.1021/acs.jafc.7b04522
128. Wang B, Kovalchuk A, Li D, Ilnytskyy Y, Kovalchuk I, Kovalchuk O. In search of preventative strategies: novel anti-inflammatory high-CBD *Cannabis sativa* extracts modulate ACE2 expression in COVID-19 gateway tissues. *Preprints.* (2020). doi: 10.20944/preprints202004.0315.v1
129. Anil SM, Shalev N, Vinayaka AC, Nadarajan S, Namdar D, Belausov E, et al. Cannabis compounds exhibit anti-inflammatory activity *in vitro* in COVID-19-related inflammation in lung epithelial cells

and pro-inflammatory activity in macrophages. *Sci Rep.* (2021) 11:1462. doi: 10.1038/s41598-021-81049-2
130. Khodadadi H, Salles ÉL, Jarrahi A, Chibane F, Costigliola V, Yu JC, et al. Cannabidiol modulates cytokine storm in acute respiratory distress syndrome induced by simulated viral infection using synthetic RNA. *Cannabis Cannabinoid Res.* (2020) 5:197–201. doi: 10.1089/can.2020.0043
131. Salles ÉL, Khodadadi H, Jarrahi A, Ahluwalia M, Paffaro VA, Costigliola V, et al. Cannabidiol (CBD) modulation of apelin in acute respiratory distress syndrome. *J Cell Mol Med.* (2020) 24:12869–72. doi: 10.1111/jcmm.15883
132. Köse S, Aerts-Kaya F, Köprü ÇZ, Nemutlu E, Kuşkonmaz B, Karaosmanoglu B, et al. Human bone marrow mesenchymal stem cells secrete endocannabinoids that stimulate *in vitro* hematopoietic stem cell migration effectively comparable to beta-adrenergic stimulation. *Exp Hematol.* (2018) 57:30–41.e1. doi: 10.1016/j.exphem.2017.09.009
133. Almogi-Hazan O, Or R. Cannabis, the endocannabinoid system and immunity-the journey from the bedside to the bench and back. *Int J Mol Sci.* (2020) 21:4448. doi: 10.3390/ijms21124448
134. Sido JM, Nagarkatti PS, Nagarkatti M. Production of endocannabinoids by activated T cells and B cells modulates inflammation associated with delayed-type hypersensitivity. *Eur J Immunol.* (2016) 46:1472–9. doi: 10.1002/eji.201546181
135. Dotsey E, Ushach I, Pone E, Nakajima R, Jasinskas A, Argueta DA, et al. Transient cannabinoid receptor 2 blockade during immunization heightens intensity and breadth of antigen-specific antibody responses in young and aged mice. *Sci Rep.* (2017) 7:42584. doi: 10.1038/srep42584
136. Cabral GA, Toney DM, Fischer-Stenger K, Harrison MP, Marciano-Cabral F. Anandamide inhibits macrophage-mediated killing of tumor necrosis factor-sensitive cells. *Life Sci.* (1995) 56:2065–72. doi: 10.1016/0024-3205(95)00190-H
137. Correa F, Henangomez-Herrero M, Mestre L, Loria F, Docagne F, Guaza C. The endocannabinoid anandamide downregulates IL-23 and IL-12 subunits in a viral model of multiple sclerosis: evidence for a cross-talk between IL-12p70/IL-23 axis and IL-10 in microglial cells. *Brain, Behav Immun.* (2011) 25:736–49. doi: 10.1016/j.bbi.2011.01.020
138. Correa F, Docagne F, Clemente D, Mestre L, Becker C, Guaza C. Anandamide inhibits IL-12p40 production by acting on the promoter repressor element GA-12: possible involvement of the COX-2 metabolite prostamide E2. *Biochem J.* (2008) 409:761–70. doi: 10.1042/BJ20071329
139. Correa F, Hernangómez M, Mestre L, Loría F, Spagnolo A, Docagne F, et al. Anandamide enhances IL-10 production in activated microglia by targeting CB2 receptors: roles of ERK1/2, JNK, and NF-κB. *Glia.* (2010) 58:135–47. doi: 10.1002/glia.20907
140. Nichols JM, Kaplan BLF. Immune responses regulated by cannabidiol. *Cannabis Cannabinoid Res.* (2019) 5:12–31. doi: 10.1089/can.2018.0073
141. Zgair A, Lee JB, Wong JCM, Taha DA, Aram J, Di Virgilio D, et al. Oral administration of cannabis with lipids leads to high levels of cannabinoids in the intestinal lymphatic system and prominent immunomodulation. *Sci Rep.* (2017) 7:14542. doi: 10.1038/s41598-017-15026-z
142. Kaplan BLF, Springs AEB, Kaminski NE. The profile of immune modulation by cannabidiol (CBD) involves deregulation of nuclear factor of activated T cells (NFAT). *Biochem Pharmacol.* (2008) 76:726–37. doi: 10.1016/j.bcp.2008.06.022
143. Ribeiro A, Almeida VI, Costola-de-Souza C, Ferraz-de-Paula V, Pinheiro ML, Vitoretti LB, et al. Cannabidiol improves lung function and inflammation in mice submitted to LPS-induced acute lung injury. *Immunopharmacol Immunotoxicol.* (2015) 37:35–41. doi: 10.3109/08923973.2014.976794
144. Vuolo F, Petronilho F, Sonai B, Ritter C, Hallak JEC, Zuardi AW, et al. Evaluation of serum cytokines levels and the role of cannabidiol treatment in animal model of asthma. *Mediators Inflamm.* (2015) 2015:538670. doi: 10.1155/2015/538670
145. Vuolo F, Abreu SC, Michels M, Xisto DG, Blanco NG, Hallak JEC, et al. Cannabidiol reduces airway inflammation and fibrosis in experimental allergic asthma. *Eur J Pharmacol.* (2019) 843:251–9. doi: 10.1016/j.ejphar.2018.11.029
146. Hegde VL, Nagarkatti PS, Nagarkatti M. Role of myeloid-derived suppressor cells in amelioration of experimental autoimmune hepatitis following activation of TRPV1 receptors by cannabidiol. *PLoS ONE.* (2011) 6:e18281. doi: 10.1371/journal.pone.0018281
147. UNODC. *United Nations Office on Drugs and Crime World Drug Report 2020:2–Drug Use and Health Consequences*. (2020). Available online at: https://wdr.unodc.org/wdr2020/field/WDR20_Booklet_2.pdf (accessed January 20, 2021).
148. Han BH, Palamar JJ. Trends in cannabis use among older adults in the United States, 2015–2018. *JAMA Intern Med.* (2020) 180:609–11. doi: 10.1001/jamainternmed.2019.7517
149. van Laar MW, Oomen PE, van Miltenburg CJA, Vercoulen E, Freeman TP, Hall WD. Cannabis and COVID-19: reasons for concern. *Front Psychiatry.* (2020) 11:601653. doi: 10.3389/fpsyt.2020.601653
150. Cherkasova M. Addiction in the times of pandemic. *Can J Addict.* (2020) 11:9. doi: 10.1097/CXA.0000000000000082
151. Bourgonje AR, Abdulle AE, Timens W, Hillebrands J, Navis GJ, Gordijn SJ, et al. Angiotensin-converting enzyme-2 (ACE2), SARS-CoV-2 and pathophysiology of coronavirus disease 2019 (COVID-19). *J Pathol.* (2020) 251:228–48. doi: 10.1002/path.5471
152. Hindocha C, Freeman TP, Ferris JA, Lynskey MT, Winstock AR. No smoke without tobacco: a global overview of cannabis and tobacco routes of administration and their association with intention to quit. *Front Psychiatry.* (2016) 7:104. doi: 10.3389/fpsyt.2016.00104
153. Goodman S, Wadsworth E, Leos-Toro C, Hammond D, team ICPS. Prevalence and forms of cannabis use in legal vs. illegal recreational cannabis markets. *Int J Drug Policy.* (2020) 76:102658. doi: 10.1016/j.drugpo.2019.102658
154. Gaiha SM, Cheng J, Halpern-Felsher B. Association between youth smoking, electronic cigarette use, and COVID-19. *J Adolesc Heal.* (2020) 67:519–523. doi: 10.1016/j.jadohealth.2020.07.002
155. Aryana A, Williams MA. Marijuana as a trigger of cardiovascular events: speculation or scientific certainty? *Int J Cardiol.* (2007) 118:141–4. doi: 10.1016/j.ijcard.2006.08.001
156. Thomas G, Kloner RA, Rezkalla S. Adverse cardiovascular, cerebrovascular, and peripheral vascular effects of marijuana inhalation: what cardiologists need to know. *Am J Cardiol.* (2014) 113:187–90. doi: 10.1016/j.amjcard.2013.09.042
157. Jouanjus E, Lapeyre-Mestre M, Micallef J. Complications* FA of the RA and DMC (CEIP-AWG on C. Cannabis use: signal of increasing risk of serious cardiovascular disorders. *J Am Heart Assoc.* (2014) 3:e000638. doi: 10.1161/JAHA.113.000638
158. DeShazo RD, Parker SB, Williams D, Ingram JB, Elsohly M, Rodenmeyer K, et al. Marijuana's effects on brain structure and function: what do we know and what should we do? A brief review and commentary. *Am J Med.* (2019) 132:281–5. doi: 10.1016/j.amjmed.2018.09.006
159. National Academies of Sciences and Medicine E. *The Health Effects of Cannabis and Cannabinoids: The Current State of Evidence and Recommendations for Research*. Washington, DC: National Academies Press (2017).

Conflict of Interest: The authors declare that the research was conducted in the absence of any commercial or financial relationships that could be construed as a potential conflict of interest.

Copyright © 2021 Paland, Pechkovsky, Aswad, Hamza, Popov, Shahar and Louria-Hayon. This is an open-access article distributed under the terms of the Creative Commons Attribution License (CC BY). The use, distribution or reproduction in other forums is permitted, provided the original author(s) and the copyright owner(s) are credited and that the original publication in this journal is cited, in accordance with accepted academic practice. No use, distribution or reproduction is permitted which does not comply with these terms.

frontiers in Immunology

ORIGINAL RESEARCH
published: 16 February 2021
doi: 10.3389/fimmu.2020.628643

CCR2 Is Dispensable for Disease Resolution but Required for the Restoration of Leukocyte Homeostasis Upon Experimental Malaria-Associated Acute Respiratory Distress Syndrome

*Emilie Pollenus[1], Thao-Thy Pham[1], Leen Vandermosten[1], Hendrik Possemiers[1], Sofie Knoops[1], Ghislain Opdenakker[2] and Philippe E. Van den Steen[1]**

[1] Laboratory of Immunoparasitology, Department of Microbiology, Immunology and Transplantation, Rega Institute for Medical Research, KU Leuven, University of Leuven, Leuven, Belgium, [2] Laboratory of Immunobiology, Department of Microbiology, Immunology and Transplantation, Rega Institute for Medical Research, KU Leuven, University of Leuven, Leuven, Belgium

OPEN ACCESS

Edited by:
Janos G. Filep,
Université de Montréal, Canada

Reviewed by:
Rahul Vijay,
The University of Iowa, United States
Mathieu Paul Rodero,
UMR8601 Laboratoire de Chimie et Biochimie Pharmacologiques et Toxicologiques, France

***Correspondence:**
Philippe E. Van den Steen
Philippe.vandensteen@kuleuven.be

Specialty section:
This article was submitted to Inflammation, a section of the journal Frontiers in Immunology

Received: 12 November 2020
Accepted: 29 December 2020
Published: 16 February 2021

Citation:
Pollenus E, Pham T-T, Vandermosten L, Possemiers H, Knoops S, Opdenakker G and Van den Steen PE (2021) CCR2 Is Dispensable for Disease Resolution but Required for the Restoration of Leukocyte Homeostasis Upon Experimental Malaria-Associated Acute Respiratory Distress Syndrome. Front. Immunol. 11:628643. doi: 10.3389/fimmu.2020.628643

Malaria complications are often lethal, despite efficient killing of *Plasmodium* parasites with antimalarial drugs. This indicates the need to study the resolution and healing mechanisms involved in the recovery from these complications. *Plasmodium berghei* NK65-infected C57BL/6 mice develop malaria-associated acute respiratory distress syndrome (MA-ARDS) at 8 days post infection. Antimalarial treatment was started on this day and resulted in the recovery, as measured by the disappearance of the signs of pathology, in >80% of the mice. Therefore, this optimized model represents an asset in the study of mechanisms and leukocyte populations involved in the resolution of MA-ARDS. C-C chemokine receptor type 2 (CCR2) knock-out mice were used to investigate the role of monocytes and macrophages, since these cells are described to play an important role during the resolution of other inflammatory diseases. CCR2 deficiency was associated with significantly lower numbers of inflammatory monocytes in the lungs during infection and resolution and abolished the increase in non-classical monocytes during resolution. Surprisingly, CCR2 was dispensable for the development and the resolution of MA-ARDS, since no effect of the CCR2 knock-out was observed on any of the disease parameters. In contrast, the reappearance of eosinophils and interstitial macrophages during resolution was mitigated in the lungs of CCR2 knock-out mice. In conclusion, CCR2 is required for re-establishing the homeostasis of pulmonary leukocytes during recovery. Furthermore, the resolution of malaria-induced lung pathology is mediated by unknown CCR2-independent mechanisms.

Keywords: malaria, inflammation, resolution, monocytes, immunology, parasitology, eosinophils

INTRODUCTION

Malaria is a global health disease that caused 229 million clinical cases and 409,000 deaths in 2019 (1). Most of these deaths are caused by complications, such as cerebral malaria, severe malarial anemia, placental malaria, and malaria-associated acute respiratory distress syndrome (MA-ARDS) (2). Despite efficient and rapid parasite killing with artemisinin combination therapies, 15% of patients with severe malaria still dies. Some complications, such as MA-ARDS, may even develop during or after treatment (3, 4). Artemisinins have a short half-life and act rapidly by generating free radicals inside the parasite (5). Artesunate is a highly soluble artemisinin derivative with excellent bioavailability, and is the preferred first-line treatment for severe malaria. It is often combined with other longer-acting antimalarial drugs, including quinolones such as chloroquine, which inhibit the detoxification of heme to hemozoin.

MA-ARDS mainly occurs in adults in low-transmission areas or in non-immune travellers (4). It results in a poor prognosis with mortality rates up to 80%, and it affects 2–25% of adults with severe malaria. Currently, 40% of patients with MA-ARDS succumb despite treatment with a combination of antimalarial drugs and mechanical ventilation. MA-ARDS is characterized by excessive pulmonary inflammation, resulting in the disruption of the alveolar-capillary membrane integrity and subsequent alveolar edema, microhemorrhages, and hypoxemia (2). An exaggerated Th1 immune response is proposed to be the cause of this complication (6–8). In mouse models, a pathogenic role of $CD8^+$ T cells was identified, since depletion of $CD8^+$ T cells resulted in the prevention of MA-ARDS (7, 9). In patients with MA-ARDS, lung endothelial cells are activated, resulting in the secretion of cytokines and chemokines and subsequent leukocyte accumulation in the lungs (7). In addition, the endothelial cells cross-present parasite antigens in an MHC-I context. Upon antigen recognition, $CD8^+$ T cells produce interferon-γ (IFN-γ), granzyme B, and perforin, thereby causing apoptosis of endothelial cells and the breakdown of tight junctions of the alveolar-capillary membrane.

Resolution of inflammation is an active and coordinated process, which aims to restore normal functions of cells and tissues (10–12). During resolution, inflammatory cells such as neutrophils undergo apoptosis and are removed by phagocytosing macrophages, a process also known as efferocytosis (11). Wound healing mechanisms are crucial for the removal of debris and the restoration of tissue function. Monocytes and macrophages are thus suggested to play an important role during this resolution process (13). In the resolution process, monocytes may switch from an inflammatory phenotype (known as "M1" or $Ly6C^+$) to a more reparative phenotype (known as "M2-like" or $Ly6C^-$) or differentiate into macrophages or dendritic cells (DCs).

The study of resolution mechanisms is important, since new pro-resolving therapies might complement anti-inflammatory treatments (12, 14, 15). In fact, an adequate inflammatory response is often necessary for pathogen elimination and/or debris clearance. Pro-resolving approaches do not inhibit pathogen clearance in contrast to anti-inflammatory treatments. Pro-resolving agonists have a more broad mechanism of action involving modulation of the immune response and stimulation of repair, while anti-inflammatory molecules strongly inhibit the immune response (14, 15). Therefore, it is assumed that pro-resolving therapies are able to suppress inflammation with less unwanted side-effects, in comparison with anti-inflammatory treatments. At the same time, resolution processes promote the restoration of tissue function (14). Resolution of inflammation has been well-characterized in Th2-related diseases, such as helminth infections. Induction of the "M2-like" macrophage phenotype by interleukin-(IL-)4 and IL-13 does not only promote the control of helminth infection, but also the timely conversion of monocytes and macrophages from a pro-inflammatory "M1" to a reparative "M2-like" phenotype, which might be decisive in wound healing and tissue regeneration (16–19).

In contrast, much less is known about the resolution of Th1-related inflammation, in particular in malaria. The resolution mechanisms may be different in a Th1 *versus* a Th2-related disease. Only a few studies investigated the pro-resolving effects of exogenous molecules, such as lipoxin A4 and IL-33, in malaria (20–24). However, the complete resolution process and the endogenous players involved have not yet been studied in detail.

C-C chemokine receptor type 2 (CCR2) is crucial for the trafficking of monocytes in two ways (25). First, CCR2 is involved in the homeostatic release of monocytes from the bone marrow. Secondly, $CCR2^+$ $Ly6C^+$ inflammatory monocytes (iMOs) are recruited to the site of inflammation *via* the CCL2-CCR2 axis (25, 26). Therefore, CCR2 knock-out (KO) mice have lower numbers of circulating monocytes and are often used to study the roles of monocytes *in vivo*. In the development of MA-ARDS, the effect of CCR2 KO is limited (8, 27). In *Plasmodium berghei* ANKA-infected C57BL/6 mice, the wet:dry ratio of the lungs was slightly increased in CCR2 KO mice compared to wild-type (WT) mice, whereas no effect on alveolar edema was found (27). Also in *Plasmodium berghei* NK65 (*Pb*NK65)-infected C57BL/6 mice, no difference in survival between the CCR2 WT and KO mice was found (8). Despite the limited effect on the development of pathology, the effect of CCR2 on the resolution remains to be established. Interestingly, CCR2 was shown to be crucial for debris clearance and healing in a sterile thermal liver injury and a skin wound mouse model (28, 29).

Here, we adapted our mouse model to study the resolution of inflammation in the otherwise lethal MA-ARDS complication. Starting antimalarial treatment on the day that the first clinical disease symptoms appeared in *Pb*NK65-infected C57BL/6 mice, resulted in the efficient clearance of parasites followed by resolution of the inflammatory lung pathology. As 80% of the mice were rescued, this constitutes an excellent mouse model to study the mechanisms and leukocytes involved in the recovery from MA-ARDS. In addition, CCR2 KO mice were used to investigate the role of CCR2-dependent monocytes in the development and the resolution of malaria-induced lung pathology. Our data show that, although the CCR2 KO has no effect on the development nor the resolution of MA-ARDS,

CCR2 is crucial to re-establish the homeostasis of pulmonary leukocytes, since the reappearance of eosinophils and interstitial macrophages was mitigated in the lungs of *Pb*NK65-infected CCR2 KO mice.

MATERIALS AND METHODS

Mice and Dissections

Seven to eight weeks old C57BL/6 mice were purchased from Janvier Labs (Le Genest-Saint-Isle, France) and housed in a specific pathogen-free (SPF) facility. Seven to nine weeks old SPF CCR2 KO and CCR2 WT mice were bred in the animal house of the Rega Institute for Medical Research, KU Leuven. CCR2 KO mice were originally bought from The Jackson Laboratory (B6.129S4-Ccr2tm1Ifc/J; #004999; Bar Harbor, ME, USA) and C57BL/6J mice from Charles River (JAX™ C57BL/6J SOPF Mice; #680; Lyon, France). The CCR2 KO mice were mated with the C57BL/6J mice in order to generate F1 heterozygotes. These heterozygotes were inter-crossed to create CCR2 KO and matched CCR2 WT mice. All mice were housed in individually ventilated cages and received *ad libitum* high energy food (Ssniff Spezialdiäte GMBH, Soest, Germany) and water, which was supplemented with 0.422 mg/ml 4-amino-benzoic acid sodium (PABA; Sigma-Aldrich, Bornem, Belgium). All experiments were performed at the KU Leuven according to the regulations of the European Union (directive 2010/63/EU) and the Belgian Royal Decree of 29 May 2013, and were approved by the Animal Ethics Committee of the KU Leuven (License LA1210186, project P049/2018, Belgium). Mice were euthanized by intraperitoneal (i.p.) injection of 100 µl of dolethal (Vétoquinol, Aartselaar, Belgium; 200 mg/ml). Murine blood samples were obtained by cardiac puncture in heparinized (LEO, Pharma, Lier, Belgium) syringes. To obtain broncho-alveolar lavage fluid (BALF), 500 µl or 750 µl of Dulbecco's phosphate buffered saline was instilled through a catheter in the trachea in the right lungs after pinching off the left lung, or the complete lungs, respectively. After 30s the fluid was withdrawn. This was repeated and both lavages were pooled. The BALF was centrifuged (10 min, 314 g, 4°C) and the supernatant was collected for further analysis, whereas the cell pellet was combined with the cells isolated from the lungs for flow cytometry analysis. After transcardial perfusion, lungs and spleen were collected for analysis by flow cytometry or reverse transcriptase quantitative real time polymerase chain reaction (RT-qPCR).

Genotyping

DNA was isolated from the tails or ear snippets of CCR2 KO and CCR2 WT mice using the EZNA Tissue DNA Kit (Omega Bio-Tek, Norcross, GA, USA). PCR was performed followed by gel electrophoresis to confirm the CCR2 genotypes, according to the protocol of The Jackson Laboratory (WT primers: CCA CAG AAT CAA AGG AAA TGG and CAC AGC ATG AAC AAT AGC CAA G, KO primers: CCA CAG AAT CAA AGG AAA TGG and CCT TCT ATC GCC TTC TTG ACG). In order to confirm the effective C57BL/6J background in both the CCR2 KO and WT mice, background strain characterization through genome-wide SNP analysis was performed on tail or ear genomic DNA from two original CCR2 KO mice and two original C57BL/6J mice and from three CCR2 KO and 3 CCR2 WT mice after the backcross (Mouse Genome Scanning panel of 2050 SNPs, Taconic, Rensselaer, NY, USA).

Infection of Mice and Clinical Scoring

Mice were infected with *Pb*NK65 [Edinburgh strain (30, 31)] by i.p. injection of 10^4 infected red blood cells. Non-infected controls from the same sex and age were included in each experiment. The disease severity of the mice was evaluated based on body weight, parasitemia, and clinical score. The clinical score was calculated on the basis of different parameters: social activity (SA), limb grasping (LG), body tone (BT), trunk curl (TC), pilo-erection (PE), shivering (Sh), abnormal breathing (AB), dehydration (D), incontinence (I), and paralysis (P). In case of TC, PE, Sh and AB, a disease score of 0 (absent) or 1 (present) was given, while the other parameters received a score of 0 (normal), 1 (intermediate) or 2 (serious). The formula used to calculate the total clinical score was: SA + LG + BT + TC + PE + 3*(Sh + AB + D + I + P). Parasitemia was determined by staining blood smears with 10% Giemsa's Stain Improved R66 Solution (VWR, Heverlee, Belgium).

Antimalarial Treatment

Where indicated, mice were treated with antimalarial drugs. A combination of artesunate (ART, 10 mg/kg in 0.9% NaCl with 0.1% $NaHCO_3$; Sigma-Aldrich) and chloroquine diphosphate salt (CQ, 30 mg/kg in 0.9% NaCl; Sigma-Aldrich) was i.p. injected daily in a volume of 200 µl, starting at 8 days p.i. for a maximum of 5 days. In the experiments described in **Supplementary Figure 1**, a higher dose of 40 mg/kg of ART (without CQ) and a combination of 10 mg/kg of ART with 3 mg/kg of dexamethasone sodium phosphate (in 0.9% NaCl; Sigma-Aldrich) were also used.

Quantification of BALF protein concentration

Edema formation was assessed by determination of the protein concentration in the supernatant of the BALF samples using Bradford assay (Bio-Rad, Hercules, CA, USA).

Determination of mRNA Expression Levels

mRNA expression levels in left lungs were quantified with RT-qPCR. Therefore, RNA extraction was performed on the left lung using the QIAGEN's RNeasy Mini Kit (QIAGEN, Venlo, The Netherlands) according to the manufacturer's protocol. Next, cDNA was synthesized from the extracted RNA using the High Capacity cDNA Reverse Transcription Kit (Applied Biosystems, Life Technologies). The TaqMan® Fast Universal PCR master mix (Applied Biosystems) was used for the detection of the amplification of the targeted gene in combination with specific primers (**Supplementary Table 1**). The relative mRNA expression was determined using the $2^{-\Delta\Delta Ct}$ method (32), which reflected the fold change in gene expression compared

to the mean of the uninfected controls and was further normalized to the 18S housekeeping gene.

Isolation of Leukocytes From the Spleen

During dissection, spleens were removed and collected in phosphate buffered saline (PBS) + 2% fetal calf serum (FCS, Gibco) at 4°C. Single cells were obtained after mashing the spleen through a 70 µm nylon cell strainer (VWR) followed by treatment with a RBC lysis buffer (0.83% ammonium chloride (NH_4Cl; Acros Organics, Geel, Belgium)/10 mM Tris (Sigma) solution with pH 7.2) at 37°C. After washing with PBS + 2% FCS, cells were resuspended in PBS + 2% FCS and live leukocytes were counted in a Bürker chamber after 1/2 dilution in trypan blue (VWR).

Isolation of Leukocytes From the Lungs

Protocol 1

During dissection, lungs were removed and collected in HEPES buffer (10 mM HEPES-NaOH, 150 mM NaCl, 5 mM KCl, 1 mM $MgCl_2$, 1.8 mM $CaCl_2$, pH 7.4) at room temperature (RT) in gentle MACS C tubes (MACS Miltenyi Biotec, Leiden, The Netherlands). The lungs were homogenized in 5 ml of HEPES buffer with 2 mg/ml collagenase D (Sigma-Aldrich) and 0.04 mg/ml DNase I (Sigma-Aldrich) in the gentleMACS™ Dissociator (MACS Miltenyi Biotec) followed by incubation for 30 min at 37°C. After a second processing in the gentleMACS™ Dissociator, cells were passed through a 70 µm nylon cell strainer. After centrifugation (300 g, 7 min, RT), the non-leukocyte subsets were removed with a Percoll gradient [for 100% Percoll buffer: 90% Percoll (GE Healthcare, Upsala, Sweden)], 9 mM PBS, 0.01 M HEPES (Gibco, Thermo Fischer), and 0.005 N HCl). The cell pellet was resuspended in 40% Percoll buffer in PBS and dropwise added onto 72% Percoll buffer in PBS to get two distinct layers. After centrifugation (20 min, 491 g, RT, no break), leukocytes were collected from the interphase of the two Percoll layers. After washing with PBS + 2% FCS, cells were resuspended in PBS + 2% FCS and live leukocytes were counted in a Bürker chamber after 1/2 dilution in trypan blue.

Protocol 2

During dissection, lungs were removed and collected in RPMI buffer [RPMI GlutaMAX (Gibco) + 5% FCS + 1% penicillin/streptomycin (Gibco)] with 0.1% beta-mercaptoethanol at RT. Lungs were first minced with scissors and then incubated for 30 min at 37°C in digestion medium (2 mg/ml collagenase D and 0.1 mg/ml DNase I in RPMI buffer). Afterward, pieces of tissue were homogenized using a needle and syringe and fresh digestion medium was added for a second incubation at 37°C for 15 min. Lung tissue was homogenized again with the syringe and centrifuged (5 min, 708 g, RT). The cell pellet was resuspended using 10 mM EDTA and further diluted in PBS + 2% FCS. After a second centrifugation, cells were treated with 0.83% NH_4Cl/10 mM Tris to lyse RBCs at 37°C and passed through a 70 µm nylon cell strainer. Cells were washed and resuspended in PBS + 2% FCS and live leukocytes were counted in a Bürker chamber after 1/2 dilution in trypan blue.

Staining and Flow Cytometry of Leukocytes

1.5–3 million leukocytes per sample were transferred to 96 well plates and washed with PBS. Cells were incubated for 15 min at RT in the dark with a viability dye, Zombie Aqua (1/1,000; BioLegend, San Diego, CA, USA) or Zombie UV (1/1,000; BioLegend), together with Mouse Fc block (MACS Miltenyi Biotec). After washing twice with cold PBS + 2% FCS + 2 mM EDTA, the cells were stained with a panel of monoclonal antibodies (**Supplementary Table 2**) dissolved in Brilliant stain buffer (BD Biosciences; Erembodegem, Belgium) for 20 min at 4°C in the dark. Cells were transferred to FACS tubes, washed twice with PBS, and fixed in PBS + 0.4% formaldehyde.

100,000 or 200,000 live single cells were analyzed per sample with a BD LSR Fortessa Flow cytometer (BD Biosciences), depending on the panel (**Supplementary Table 2**). Data were analyzed with FlowJo v10 software (FlowJo LLC, Ashland, OR, USA) and cells were gated according to the gating strategies in supplementary methods. In the myeloid cell panel and the CCR2 panel, cells positive for lineage-specific markers were excluded using a dumpgate (with CD3, CD19, and NK1.1 as exclusion markers). In order to calculate the absolute numbers of each cell type, the frequency of this cell type among $CD45^+$ cells was multiplied by the total number of live leukocytes earlier counted using the Bürker chamber. In addition, uniform manifold approximation and projection (UMAP) plots were created of the flow cytometry data of the myeloid panel on the lungs. Here, cells of different samples were combined and unbiased clustering was performed using the FlowJo v10 software. Clusters were colored by cell class as defined in the figure legends.

Statistical Analysis

The data were analyzed using the GraphPad PRISM software (GraphPad, San Diego, California, USA, version 8.3.1). The non-parametric Mann-Whitney U test was performed followed by the Holm-Bonferroni correction. For the experiments in **Figures 1–5** and **Supplementary Figures 1-5**, significance was determined for the comparison of all groups compared to the uninfected controls at 0 days p.i. and of all infected groups from 9 days until 15 days p.i. compared to the untreated mice at 8 days. In the experiments with CCR2 KO and CCR2 WT mice (**Figures 6–9** and **Supplementary Figures 7-16**), significance was determined between each condition for the CCR2 WT and for the CCR2 KO mice and between the WT and KO mice within each condition. P-values were indicated as follows: *p<0.05, **p<0.01, ***p<0.001. The horizontal black line in each group indicates the median. Statistical differences compared to the corresponding uninfected control group are indicated with an asterisk above the individual data sets and horizontal lines with asterisk on top indicate significant differences between groups.

RESULTS

Antimalarial Treatment Induces Resolution of Experimental MA-ARDS

C57BL/6 mice were infected with *Pb*NK65, which resulted in the development of MA-ARDS (**Figure 1**). The first clinical disease

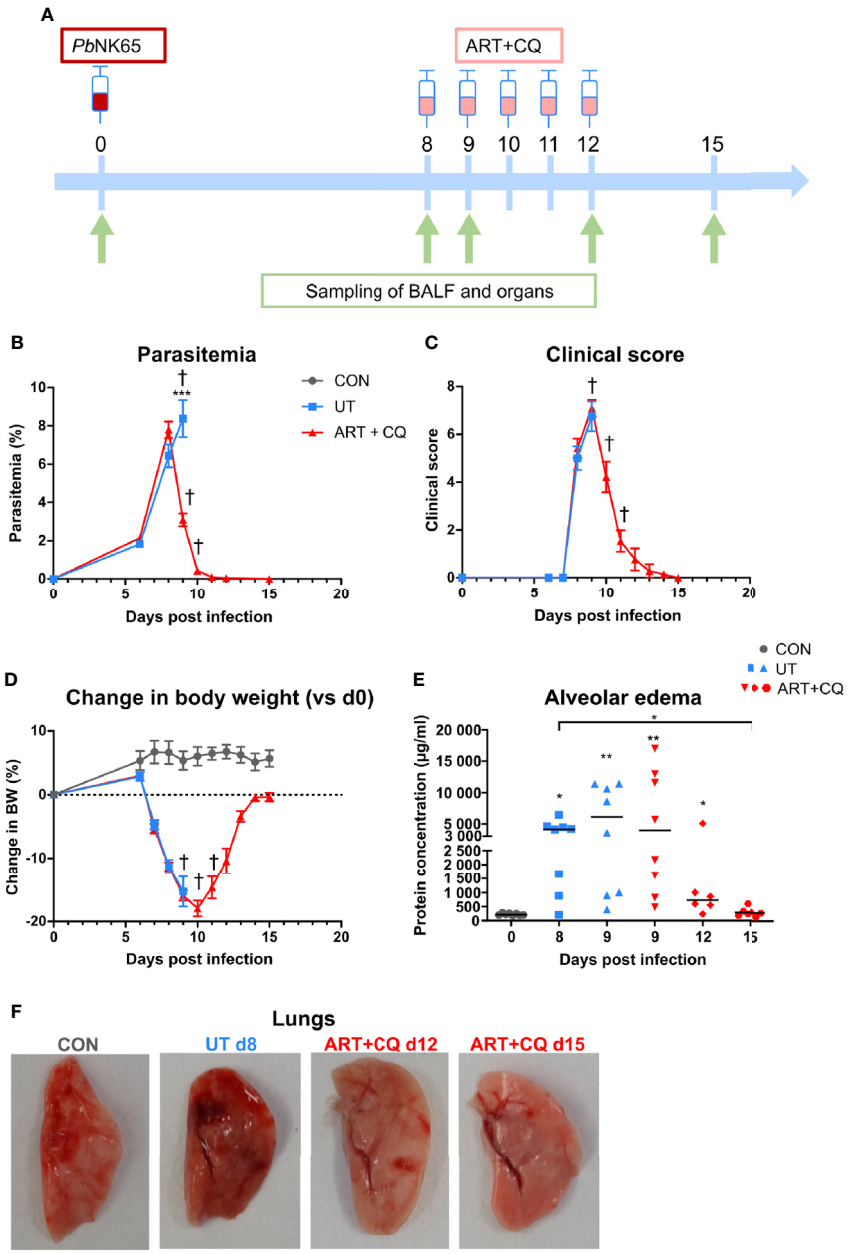

FIGURE 1 | A mouse model to study the resolution of malaria-associated acute respiratory distress syndrome (MA-ARDS) after antimalarial treatment. C57BL/6 mice were infected with *Pb*NK65. Mice were injected daily from 8 until 12 days p.i. with 10 mg/kg ART + 30 mg/kg CQ (ART+CQ). **(A)** Schematic representation of the timing of infection and antimalarial treatments in the mouse model. **(B)** Parasitemia was determined using Giemsa-stained blood smears. **(C)** The clinical score was monitored daily starting at 6 days p.i. **(D)** The change in body weight was calculated compared to day 0 p.i. starting at 6 days p.i. **(B, D)** Compilation of two experiments. Data are means ± SEM. n=8 for uninfected controls (CON), n=8–16 for the infected untreated group (UT), n=7–21 for the infected ART+CQ-treated group. **(E)** The protein concentration in the BALF was determined as a measure of alveolar edema. Compilation of two experiments. Each symbol represents data of an individual mouse. n=8 for CON on day 0, UT at 8 and 9 days p.i and ART+CQ at 9 days p.i., n=6 for ART+CQ at 12 days p.i., n=7 for ART+CQ at 15 days p.i. **(F)** Representative pictures of the left lung.

symptoms appeared 8 days p.i. (**Figure 1C**). MA-ARDS is characterized by the development of alveolar edema, which was measured by an increased protein concentration in the BALF in the untreated, *Pb*NK65-infected (UT) group compared to the uninfected controls (CON) on day 0 p.i. (**Figure 1E**) (31).

Artesunate (ART) is an antimalarial drug that efficiently and rapidly kills the parasites (5). To optimize the antimalarial

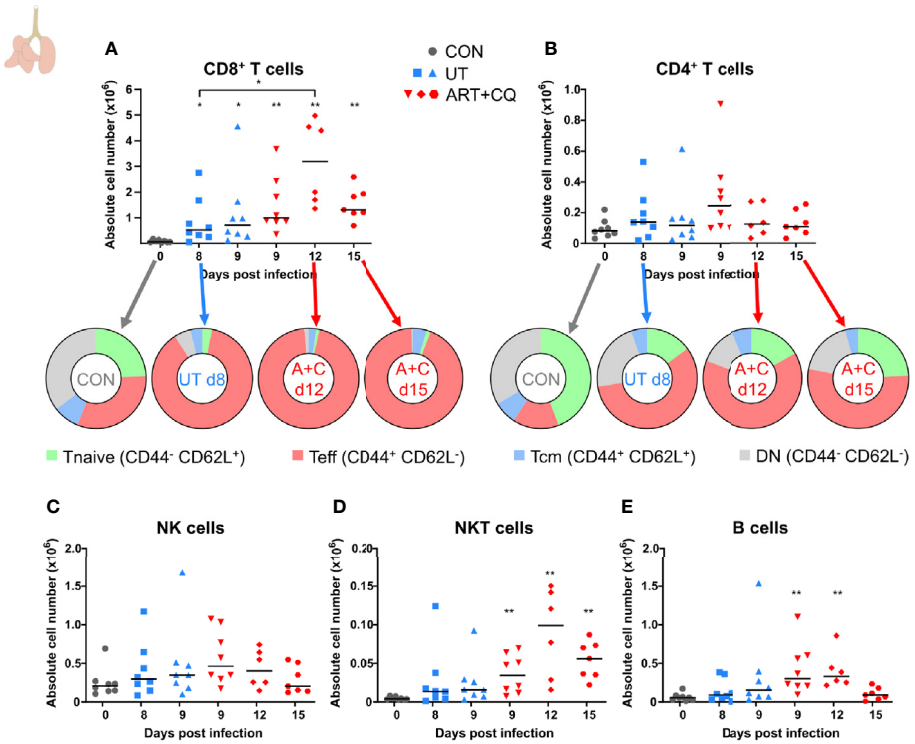

FIGURE 2 | Dynamics of the lymphocyte populations in the lungs during resolution of malaria-associated acute respiratory distress syndrome (MA-ARDS). C57BL/6 mice were infected with *Pb*NK65. Mice were injected daily from 8 until 12 days p.i. with 10 mg/kg ART + 30 mg/kg CQ. Mice were dissected at the indicated days p.i. Leukocytes were isolated from the lungs according to protocol 1 and flow cytometry was performed. **(A, B)** The absolute numbers of $CD8^+$ T cells ($CD45^+$ $CD3^+$ $NK1.1^-$ $CD8^+$) and $CD4^+$ T cells ($CD45^+$ $CD3^+$ $NK1.1^-$ $CD4^+$) and the proportions of Tnaive ($CD44^-$ $CD62L^+$), Teff ($CD44^+$ $CD62L^-$), and Tcm ($CD44^+$ $CD62L^+$) of the total cell population are shown. Percentages of these subsets are shown in **Supplementary Figure 3**. **(C–E)** The absolute numbers of NK cells ($CD45^+$ $CD3^-$ $NK1.1^+$), NKT cells ($CD45^+$ $CD3^+$ $NK1.1^+$), and B cells ($CD45^+$ $CD3^-$ $NK1.1^-$ $B220^+$) were calculated. Compilation of two experiments. Each symbol represents data of an individual mouse. n=8 for CON on day 0, UT at 8 and 9 days p.i and ART+CQ at 9 days p.i., n=6 for ART+CQ at 12 days p.i., n=7 for ART+CQ at 15 days p.i.

treatment in our mouse model, two dosages of 40 mg/kg and 10 mg/kg ART (ART 40 and ART 10) were tested. At 8 days p.i., when the first disease symptoms appeared in the *Pb*NK65-infected C57BL/6 mice, antimalarial treatment was started. Both dosages of ART significantly decreased parasitemias, clinical scores, and the levels of alveolar edema, resulting in survival rates of 80–100% from the otherwise lethal MA-ARDS complication (**Supplementary Figure 1**). A combination of 10 mg/kg of ART with 3 mg/kg of dexamethasone (DEX), a synthetic glucocorticoid, was also tested. This combination did not have a beneficial effect compared to ART alone, as parasites were cleared at a slower rate and the level of alveolar edema at 4 days post-treatment was not significantly decreased compared to the untreated group at 1 day post-treatment (**Supplementary Figure 1**). The efficiency of ART 10 was similar compared to ART 40. To limit the anti-inflammatory effects of ART, ART 10 was chosen as the preferred antimalarial treatment dosage. Besides clearing parasitemia, this treatment also resulted in a lower pulmonary mRNA expression of the inflammatory chemokines CCL2 and CXCL10, and of the cytokines tumor necrosis factor-α (TNF-α), IFN-γ, and IL-10 (**Supplementary Figure 2**).

Since recrudescences of parasitemia after the end of treatment with both ART dosages were often observed, for all subsequent experiments, treatment with ART 10 was combined with 30 mg/kg of chloroquine, a slower but longer-acting antimalarial drug (5). Starting this artesunate + chloroquine (ART+CQ) treatment for 5 days when the first disease symptoms appeared (8 days p.i.), resulted in a 60% decrease in parasitemia after one day of treatment (at day 9 p.i) and complete parasite clearance by the end of treatment (at day 12 p.i.) (**Figures 1A, B**). Upon antimalarial treatment, on average 80% of the mice were rescued from the otherwise lethal MA-ARDS complication (**Supplementary Figure 1B**). The clinical score still worsened from 8 to 9 days p.i., but started to decrease at 10 days p.i. until the mice appeared completely healthy again at 12 days p.i. (**Figure 1C**). The body weight recovered from 11 days p.i. onward (**Figure 1D**). An increase in the protein concentration in the BALF was observed at 8 and 9 days p.i. compared to the controls, showing that massive alveolar edema was present (**Figure 1E**). Thereafter, in the mice treated with ART+CQ, alveolar edema decreased and reached control levels at 15 days. Macroscopically, the development of the lung pathology and microhemorrhages were visible by the darkening of the lungs,

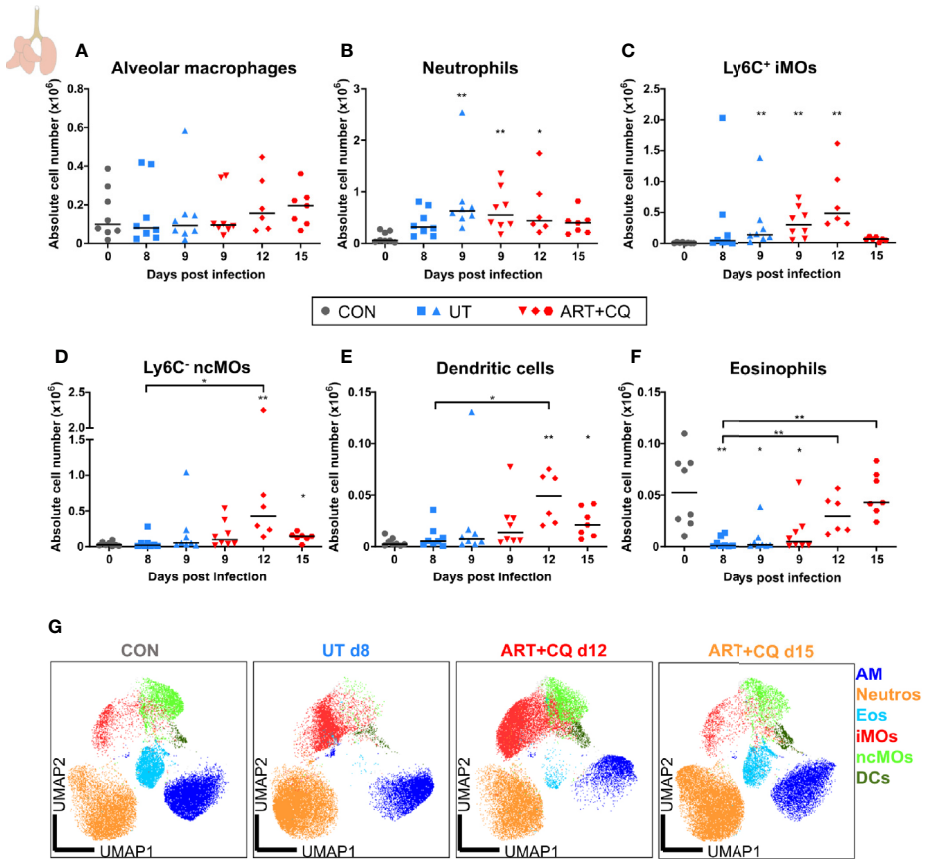

FIGURE 3 | Dynamics of the myeloid cell populations in the lungs during resolution of malaria-associated acute respiratory distress syndrome (MA-ARDS). C57BL/6 mice were infected with *Pb*NK65. Mice were injected daily from 8 until 12 days p.i. with 10 mg/kg ART + 30 mg/kg CQ. Mice were dissected at the indicated days p.i. Leukocytes were isolated from the lungs according to protocol 1 and flow cytometry was performed. **(A–F)** The absolute numbers of alveolar macrophages (AM; $CD45^+$ $SiglecF^+$ $CD11b^{int}$ $CD11c^+$), neutrophils (Neutros; $CD45^+$ Lin^- $CD11b^+$ $Ly6G^+$), $Ly6C^+$ inflammatory monocytes (iMOs; $CD45^+$ Lin^- $CD11b^{hi}$ MHC-II^- $Ly6C^+$), $Ly6C^-$ non-classical monocytes (ncMOs; $CD45^+$ Lin^- $CD11b^{hi}$ MHC-II^- $Ly6C^-$), dendritic cells (DCs; $CD45^+$ Lin^- $SiglecF^-$ MHC-II^+ $CD11c^+$), and eosinophils (Eos; $CD45^+$ $CD11b^+$ $SiglecF^+$ $CD11c^-$) in the lungs were calculated. Compilation of two experiments. Each symbol represents data of an individual mouse. n=8 for CON on day 0, UT at 8 and 9 days p.i and ART+CQ at 9 days p.i., n=6 for ART+CQ at 12 days p.i., n=7 for ART+CQ at 15 days p.i. **(G)** Clustering of 24,000 cells combined from four representative samples per condition, except ART+CQ d15 from two representative samples. The plots show a two-dimensional representation (UMAP) of the protein expression. Clusters are colored by cell class as defined in **(A–F)**.

which is due to microhemorrhages (31) (**Figure 1F**). These signs of pathology also resolved upon ART+CQ treatment.

Dynamics of Pulmonary Leukocyte Numbers and Activation During the Resolution of MA-ARDS

To determine the dynamics of leukocyte subpopulations in the lungs during the resolution of MA-ARDS, leukocytes were isolated from the lungs and analyzed by multicolor flow cytometry. $CD8^+$ T cells are known to be pathogenic in MA-ARDS (7, 9, 31) and their number was significantly increased in the lungs of *Pb*NK65-infected C57BL/6 mice at 8 and 9 days p.i. (**Figure 2A**). Interestingly, the absolute number of $CD8^+$ T cells further increased at 12 days p.i. compared to 8 days. At 15 days p.i., their numbers were still higher compared to controls. In contrast, no significant differences in the number of $CD4^+$ T cells were observed (**Figure 2B**). The activation phenotype of T cells in the lungs was investigated at 0, 8, 9, 12, and 15 days p.i. Both $CD8^+$ and $CD4^+$ T cells were activated during infection, resulting in an increased proportion of effector T (Teff) cells and a decreased proportion of naive T (Tnaive) cells (**Figures 2A, B**; **Supplementary Figure 3**). At 12 and 15 days p.i., the Teff cells remained the largest T cell subset in the lungs. No differences were found in the absolute number of NK cells (**Figure 2C**), whereas NKT cell counts were significantly increased after ART +CQ treatment (**Figure 2D**). Transient increases in B cell numbers were observed in ART+CQ-treated mice at 9 and 12 days p.i. compared to the uninfected controls (**Figure 2E**).

In these experiments, no differences in the number of alveolar macrophages (AM) were observed in the lungs (**Figure 3A**). The number of neutrophils increased in the lungs at 9 days p.i., irrespectively of the antimalarial treatment, and remained so at

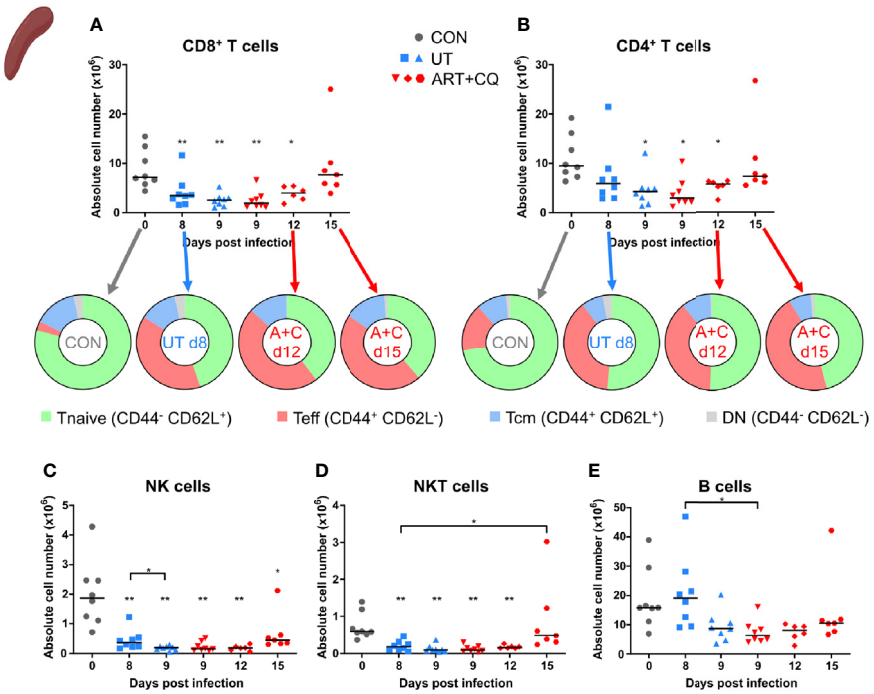

FIGURE 4 | Dynamics of the splenic lymphocyte populations during resolution of malaria-associated acute respiratory distress syndrome (MA-ARDS). C57BL/6 mice were infected with *Pb*NK65. Mice were injected daily from 8 until 12 days p.i. with 10 mg/kg ART + 30 mg/kg CQ. Mice were dissected at the indicated days p.i. Leukocytes were isolated from the spleen and flow cytometry was performed. **(A, B)** The absolute numbers of $CD8^+$ T cells ($CD45^+$ $CD3^+$ $NK1.1^-$ $CD8^+$) and $CD4^+$ T cells ($CD45^+$ $CD3^+$ $NK1.1^-$ $CD4^+$) and the proportions of Tnaive ($CD44^-$ $CD62L^+$), Teff ($CD44^+$ $CD62L^-$), and Tcm ($CD44^+$ $CD62L^+$) of the total cell population are shown. Percentages of these subsets are shown in **Supplementary Figure 5**. **(C–E)** The absolute numbers of NK cells ($CD45^+$ $CD3^-$ $NK1.1^+$), NKT cells ($CD45^+$ $CD3^+$ $NK1.1^+$), and B cells ($CD45^+$ $CD3^-$ $NK1.1^-$ $B220^+$) were calculated. Compilation of two experiments. Each symbol represents data of an individual mouse. n=8 for CON on day 0, UT at 8 and 9 days p.i and ART+CQ at 9 days p.i., n=6 for ART+CQ at 12 days p.i., n=7 for ART+CQ at 15 days p.i.

12 days p.i. (**Figure 3B**). The $Ly6C^+$ inflammatory monocytes (iMOs) were increased upon infection and remained increased until 12 days p.i. (**Figure 3C**). The numbers of $Ly6C^-$ non-classical monocytes (ncMOs) and dendritic cells (DCs) were increased during resolution (**Figures 3D–E**). Eosinophils largely disappeared from the lungs upon infection and gradually reappeared during resolution (**Figure 3F**). To analyze and depict the myeloid cell populations of the lungs in a more unbiased and gating-independent manner, UMAP plots were generated with the flow cytometry data (**Figure 3G**). The $Ly6C^+$ iMOs, $Ly6C^-$ ncMOs, and DCs clustered closely together, while the AM, neutrophil, and eosinophil clusters were more distinct. Moreover, clustering alterations were observed for the $Ly6C^+$ iMOs and AM upon infection and resolution. This was attributed to differences in the expression of specific markers, in particular CD64/FcγRI, which was increased at 8 days p.i. and decreased during resolution (**Supplementary Figure 4**). This reflects the activation of the monocytes during infection, which is also observed in humans (34, 35).

Overall, these data show that the first phase of resolution (at 12 days p.i.) was not characterized by a decrease of the infiltrating leukocytes. In fact, several leukocyte populations continued to increase during the first days of resolution, when both the alveolar edema and cytokines expression were already decreasing. At 15 days p.i., most leukocyte subpopulations were decreasing and approached control levels.

Dynamics of Splenic Leukocyte Numbers and Activation in the Resolution of MA-ARDS

The number of $CD8^+$ T cells, $CD4^+$ T cells, NK cells, and NKT cells were decreased in the spleens at 8 days p.i. compared to the uninfected controls (**Figures 4A–D**). During resolution, the absolute numbers of these cell types gradually increased. B cell numbers were slightly, but significantly downregulated after antimalarial treatment at 9 days p.i. compared to the untreated group at 8 days p.i. (**Figure 4E**). Similarly as in the lungs, the $CD8^+$ and $CD4^+$ T cells became activated in the spleen upon infection, as was shown by an increased proportion of Teff cells and a decreased proportion of Tnaive cells compared to the uninfected controls, without any change during resolution (**Figures 4A, B**; **Supplementary Figure 5**).

Most myeloid cell populations, such as DCs, eosinophils, iMOs, ncMOs, and red pulp macrophages, were also significantly depleted in the spleen upon infection and gradually increased again during resolution (**Figure 5**). The iMOs and ncMOs already reappeared at 12 days p.i., while it took until 15 days p.i. for the DCs, eosinophils, and red pulp

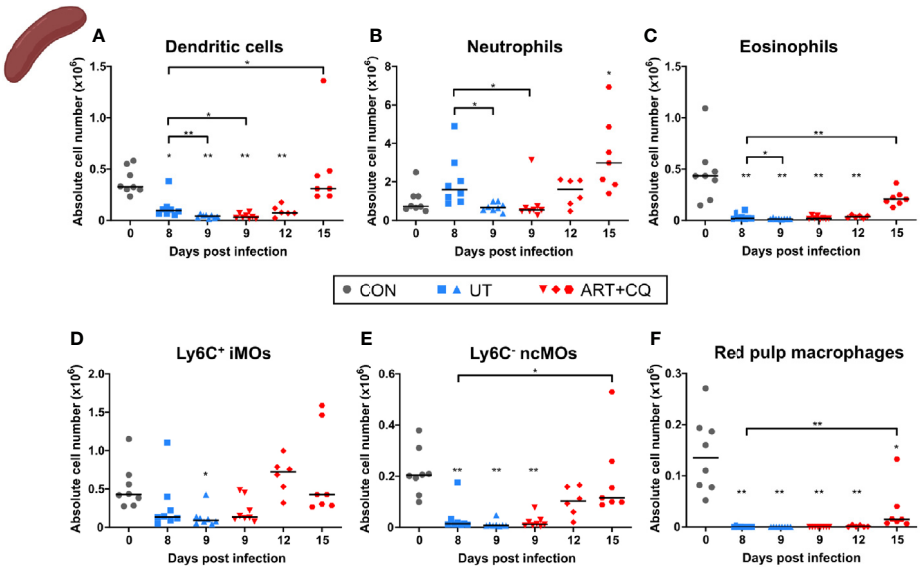

FIGURE 5 | Dynamics of the splenic myeloid cell populations during resolution of malaria-associated acute respiratory distress syndrome (MA-ARDS). C57BL/6 mice were infected with *Pb*NK65. Mice were injected daily from 8 until 12 days p.i. with 10 mg/kg ART + 30 mg/kg CQ. Mice were dissected at the indicated days p.i. Leukocytes were isolated from the spleen and flow cytometry was performed. **(A–F)** The absolute numbers of dendritic cells ($CD45^+$ Lin^- $MHC\text{-}II^+$ $CD11c^+$), neutrophils ($CD45^+$ Lin^- $CD11b^+$ $Ly6G^+$), eosinophils ($CD45^+$ $CD11b^+$ $MHC\text{-}II^-$ $CD11c^-$ $Ly6G^-$ $Ly6C^-$ $SSC\text{-}A^{hi}$), $Ly6C^+$ inflammatory monocytes (iMOs; $CD45^+$ Lin^- $CD11b^+$ $MHC\text{-}II^-$ $CD11c^-$ $SSC\text{-}A^{lo}$ $Ly6C^+$), $Ly6C^-$ non-classical monocytes (ncMOs; $CD45^+$ Lin^- $CD11b^+$ $MHC\text{-}II^-$ $CD11c^-$ $SSC\text{-}A^{lo}$ $Ly6C^-$), and red pulp macrophages [$CD45^+$ Lin^- $MHC\text{-}II^-$ $CD11c^-$ $CD11b^-$ $F4/80^+$ (33)] present in the spleen were calculated. Compilation of two experiments. Each symbol represents data of an individual mouse. n=8 for CON on day 0, UT at 8 and 9 days p.i and ART+CQ at 9 days p.i., n=6 for ART+CQ at 12 days p.i., n=7 for ART+CQ at 15 days p.i.

macrophages to return. Splenic neutrophils were not depleted by the infection and gradually increased during resolution (**Figure 5**).

Altogether, in this mouse model, we were able to rescue >80% of the mice from the otherwise lethal MA-ARDS complication, by starting antimalarial treatment (ART+CQ) on the day that the first clinical signs of disease appeared (at 8 days p.i.). The mice completely recovered and the lung inflammation fully resolved upon antimalarial treatment, as was shown by alveolar edema quantification, cytokine and chemokine expression and infiltrating cell determination. These results showed that this mouse model was useful to study the mechanisms and leukocyte involvement in the resolution of inflammation and pathology in MA-ARDS.

CCR2 Gene Knock-Out Has No Effect on the Development Nor the Resolution of MA-ARDS

Since monocytes and macrophages play important roles in the resolution of many inflammatory pathologies (12), their role was investigated with CCR2 KO mice. We carefully checked the CCR2 KO status at the protein and DNA levels (**Supplementary Figure 6**), and also confirmed that the genetic background of both CCR2 WT and KO mice was >99.95% C57BL/6 (**Supplementary Table 3**).

Parasitemia, clinical score, and loss of body weight were similar in CCR2 KO mice compared to CCR2 WT mice, both during infection and during/after antimalarial treatment (**Figures 6A–C**). Lung pathology, i.e., the amount of alveolar edema and the weight of the left lung, was similarly increased in both the WT and KO mice at 8 days p.i. (**Figures 6D–E**). Moreover, at 9 days p.i., both in the UT as in the ART+CQ group, no difference in lung pathology was observed between the CCR2 KO and CCR2 WT mice (**Supplementary Figure 7**). During resolution, alveolar edema was cleared from the lungs in both the CCR2 KO and CCR2 WT mice, while the weight of the left lung was still increased (**Figures 6D–E**). Also macroscopically, no differences in lung pathology were observed between CCR2 WT and KO mice (**Figure 6F**). In conclusion, CCR2 is neither required for the development of MA-ARDS, nor for the resolution of the pathology upon antimalarial treatment.

Effect of CCR2 Gene Knock-Out on the Dynamics of Pulmonary and Splenic Leukocyte Populations

Compared to the experiments above (protocol 1), a different isolation protocol (protocol 2) for the pulmonary leukocytes was further used. This adapted protocol allowed for the quantitative detection of DCs, IMs, and a more detailed appreciation of the dynamics of ncMOs, since it resulted in a higher number of total isolated leukocytes without affecting the overall dynamics of pulmonary leukocytes during MA-ARDS development and resolution.

The number of pulmonary iMOs was significantly lower at each time point in the CCR2 KO mice compared to the WT mice (**Figure 7A** and **Supplementary Figure 8**). Except for day 12 p.i.,

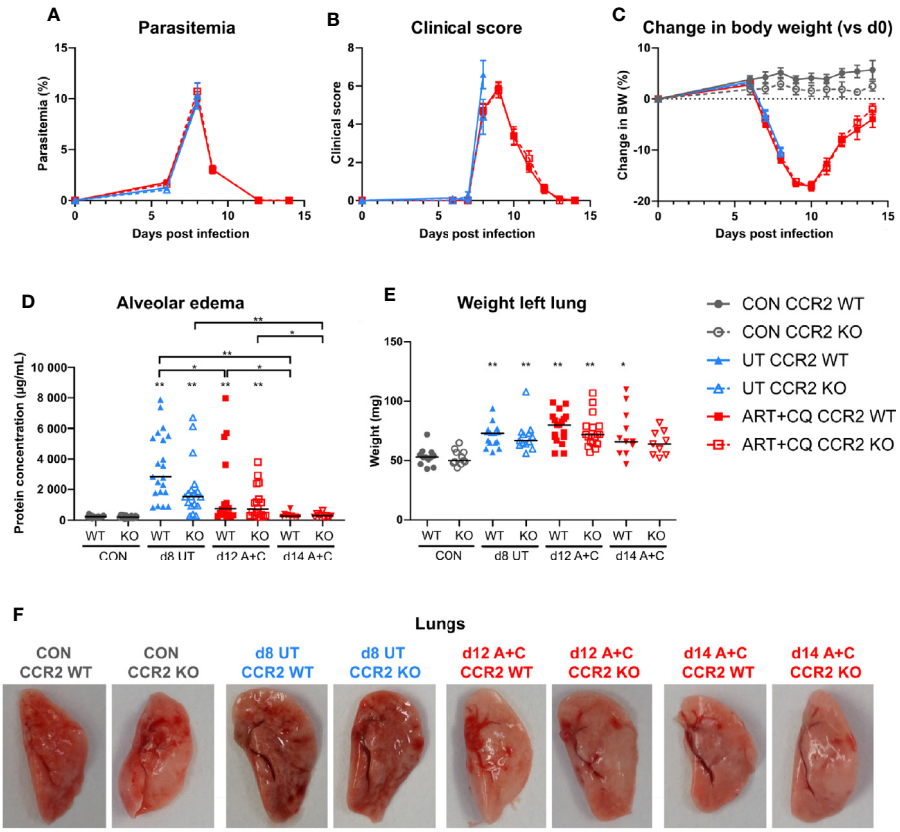

FIGURE 6 | The CCR2 knock-out had no effect on the development and the resolution of malaria-associated acute respiratory distress syndrome (MA-ARDS). CCR2 WT and CCR2 KO C57BL/6 mice were infected with *Pb*NK65. Mice were injected daily from 8 until 12 days p.i. with 10 mg/kg ART + 30 mg/kg CQ. **(A)** Parasitemia was determined daily using Giemsa-stained blood smears. **(B)** The clinical score was monitored daily starting at 6 days p.i. **(C)** The change in body weight was calculated compared to day 0 p.i. starting at 6 days p.i. **(A–C)** Compilation of five experiments. Data are shown as means ± SEM. n=6–12 for CON CCR2 WT, n=5–11 for CON CCR2 KO, n=15 for UT CCR2 WT, n=13 for UT CCR2 KO, n=10–32 for ART+CQ CCR2 WT, n=7–27 for ART+CQ CCR2 KO. **(D, E)** Lung pathology was quantified based on the protein concentration in the BALF **(D)** and the weight of the left lung **(E)** at 8 days p.i. for the UT group and at 12 and 14 days p.i. for the ART+CQ group. Compilation of five experiments. Each symbol represents data of an individual mouse. n=12–16 for CON CCR2 WT, n=11–15 for CON CCR2 KO, n=15–21 for UT CCR2 WT, n=13–18 for UT CCR2 KO, n=18 for ART+CQ CCR2 WT at 12 days p.i., n=17 for ART+CQ CCR2 KO at 12 days p.i., n=10–11 for ART+CQ CCR2 WT at 14 days p.i., n=9 for ART+CQ CCR2 KO at 14 days p.i. **(F)** Representative pictures of the left lung.

the numbers of ncMO were not affected by the CCR2 KO (**Figure 7B** and **Supplementary Figure 8**). At 12 days p.i., both iMOs and ncMOs were strikingly increased in the lungs of *Pb*NK65-infected WT mice, while this was largely abolished in the infected CCR2 KO group (**Figures 7A, B**). In the spleens of uninfected controls, a significant lower number of iMOs was found in the CCR2 KO compared to the WT mice, whereas no difference was observed for the ncMOs (**Figures 7C, D** and **Supplementary Figure 8**). The number of iMOs and ncMOs in the spleen similarly decreased in CCR2 KO and WT mice upon infection (8 and 9 days p.i.). The reappearance of both the iMOs and ncMOs in the spleen during resolution at 12 days p.i. was also similar in both the KO and WT mice, indicating that this is a CCR2-independent process.

In the spleens, except for the iMOs, none of the studied leukocyte populations showed significant differences between the CCR2 KO and WT mice at any time-point (**Supplementary Figures 9**-**12**).

In the lungs, no significant differences between the CCR2 KO and CCR2 WT mice were found, for any lymphocyte population at any of the analyzed time-points (**Figure 8**; **Supplementary Figures 13** and **14**). In addition, the CCR2 KO had no effect on the number of AM (**Figure 9A** and **Supplementary Figure 15A**). The $CD103^+$ and $CD11b^+$ DCs disappeared upon infection and reappeared during resolution, although it took until 9 days p.i. for the $CD103^+$ DCs to decrease, whereas the $CD11b^+$ DCs were already decreased at 8 days p.i. (**Figures 9B, C** and **Supplementary Figures 15B, C**). In CCR2 KO mice, a trend toward reduced numbers of $CD103^+$ and $CD11b^+$ DCs was observed compared to WT mice during resolution (at 12 days p.i.; **Figures 9B, C**; $p = 0.0684$ and $p = 0.0532$, respectively). Upon infection, the neutrophil numbers increased at 8 and 9 days p.i. in both the WT and KO group, whereas at 12 days p.i., less neutrophils were present in the lungs of the CCR2 KO mice compared to the WT mice (**Figure 9D** and **Supplementary Figure 15D**). The eosinophils disappeared from the lungs

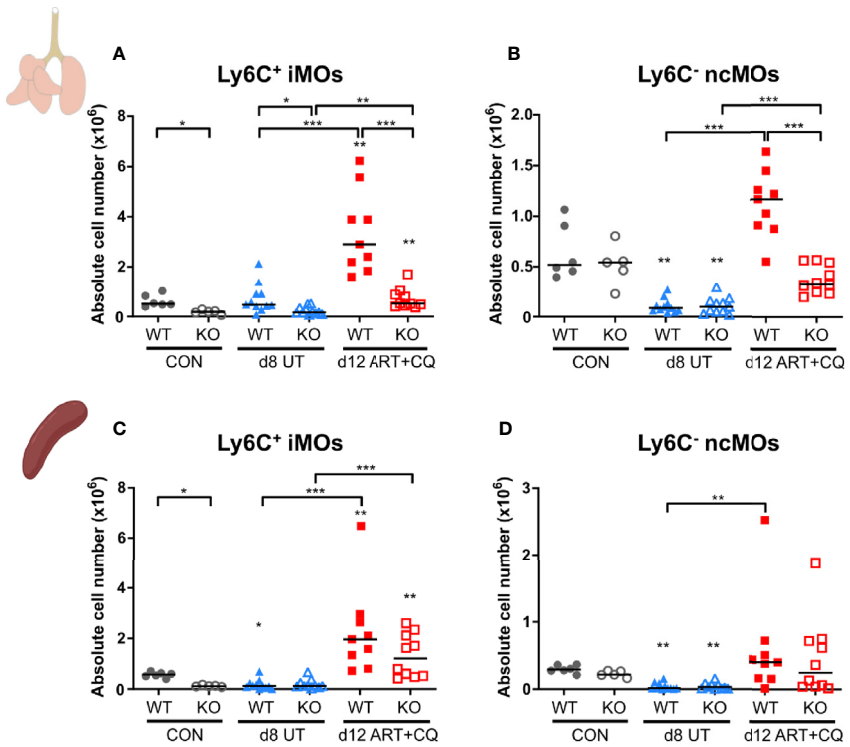

FIGURE 7 | The CCR2 knock-out resulted in less monocytes present in the lungs, but not in the spleen. CCR2 WT and CCR2 KO C57BL/6 mice were infected with *Pb*NK65. Mice were injected daily from 8 until 12 days p.i. with 10 mg/kg ART + 30 mg/kg CQ. Mice were dissected at the indicated days p.i. Leukocytes were isolated from the lungs according to protocol 2 and from the spleen and flow cytometry was performed. **(A–D)** The absolute numbers of Ly6C$^+$ iMOs **(A, C)** and Ly6C$^-$ ncMOs **(B, D)** present in the lungs **(A, B)** and spleen **(C, D)** were calculated. Compilation of two experiments. Each symbol represents data of an individual mouse. n=6 for CON CCR2 WT, n=5 for CON CCR2 KO, n=11 for UT CCR2 WT, n=11 for UT CCR2 KO, n=9 for ART+CQ CCR2 WT, n=10 for ART+CQ CCR2 KO.

upon infection and reappeared during resolution in the CCR2 WT mice (**Figure 9E** and **Supplementary Figure 15E**). Interestingly, their reappearance did not occur as efficiently in the CCR2 KO mice. The CCR2 KO thus had an effect on the presence of neutrophils and eosinophils in the lungs during resolution, despite the fact that the neutrophils and eosinophils do not express CCR2 in CCR2 WT mice (**Figures 9G, H**), in contrast to the Ly6C$^+$ iMOs (**Figure 9I**). This suggested that the mitigation of eosinophil reappearance during resolution was an indirect effect of the CCR2 KO, probably caused by the decreased numbers of monocytes present in the lungs. Interstitial macrophages decreased at 9 days p.i. and increased at 12 days p.i., but no increase occurred at 12 days p.i. in the CCR2 KO mice (**Figure 9F** and **Supplementary Figure 15F**). Also in the uninfected controls, reduced numbers of interstitial macrophages were observed in the lungs of CCR2 KO mice compared to WT mice. UMAP plots were generated to visualize these flow cytometry data (**Figure 9J**). Like before, the monocyte populations, the DC populations and the interstitial macrophages clustered closely, whereas the neutrophils, eosinophils, and AM clustered more separately. Also, shifts in the clusters between different time-points were observed for the AM and iMOs, and this was attributed to a change in expression of activation markers, in particular CD64. The expression of CD64 was increased on pulmonary iMOs and AM in both the WT and KO mice at 8 days p.i., and decreased again during resolution (**Supplementary Figure 16**).

In summary, the lower numbers of Ly6C$^+$ iMOs in the lungs in CCR2 KO mice did not affect the development and the resolution of the lung pathology of MA-ARDS. In contrast, the CCR2 gene deletion had an effect on the return to leukocyte homeostasis in the lungs, as was shown by the mitigation of the reappearance of eosinophils and the lack of increase in interstitial macrophages in the CCR2 KO mice compared to the WT mice. In addition, the decrease in neutrophil numbers was more pronounced in the lungs of CCR2 KO mice compared to the WT mice. The overall changes in the composition of pulmonary leukocytes during inflammation and resolution in our MA-ARDS model and the effects of the CCR2 KO on these dynamics are summarized in **Figure 10**.

DISCUSSION

Pro-resolving therapies have a broad mechanism of action involving modulation of the immune response and stimulation

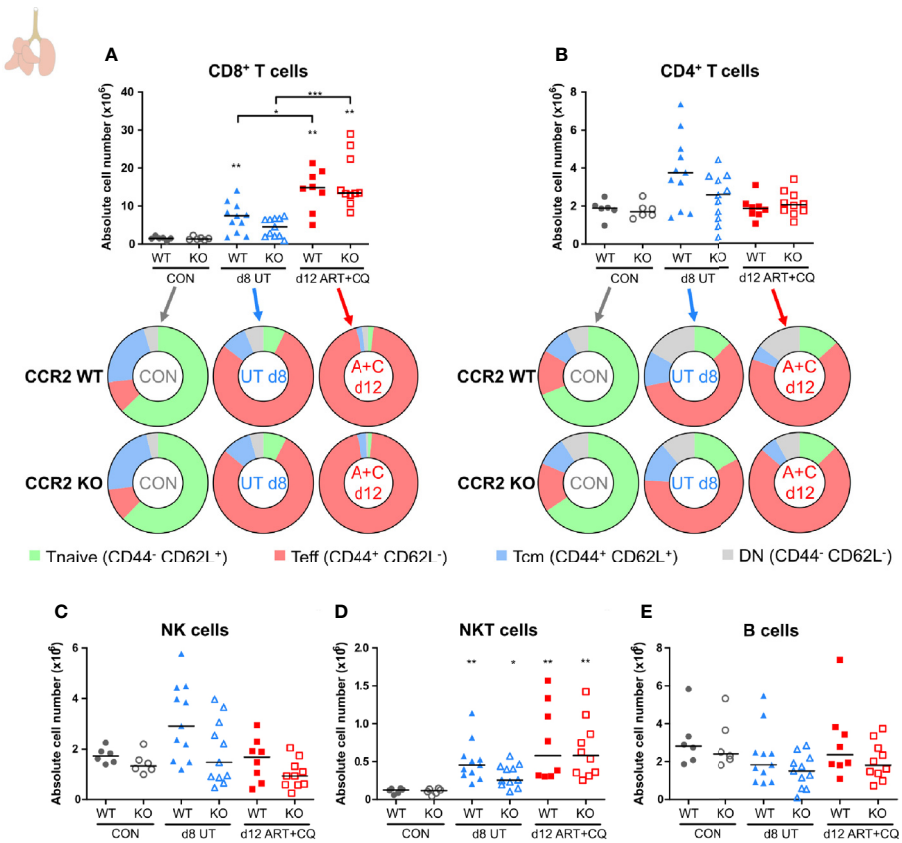

FIGURE 8 | CCR2 knock-out does not affect the number of pulmonary lymphocytes. CCR2 WT and CCR2 KO C57BL/6 mice were infected with *Pb*NK65. Mice were injected daily from 8 until 12 days p.i. with 10 mg/kg ART + 30 mg/kg CQ. Mice were dissected at the indicated days p.i. Leukocytes were isolated from the lungs according to protocol 2 and flow cytometry was performed. **(A, B)** The absolute numbers of $CD8^+$ T cells ($CD45^+$ $CD3^+$ $NK1.1^-$ $CD8^+$) and $CD4^+$ T cells ($CD45^+$ $CD3^+$ $NK1.1^-$ $CD4^+$) and the proportions of Tnaive ($CD44^-$ $CD62L^+$), Teff ($CD44^+$ $CD62L^-$), and Tcm ($CD44^+$ $CD62L^+$) of the total cell population are shown. Percentages of these subsets are shown in **Supplementary Figure 13**. **(C–E)** The absolute numbers of NK cells ($CD45^+$ $CD3^-$ $NK1.1^+$), NKT cells ($CD45^+$ $CD3^+$ $NK1.1^+$), and B cells ($CD45^+$ $CD3^-$ $NK1.1^-$ $B220^+$) were calculated. Compilation of two experiments. Each symbol represents data of an individual mouse. n=6 for CON CCR2 WT, n=6 for CON CCR2 KO, n=11 for UT CCR2 WT, n=11 for UT CCR2 KO, n=8 for ART+CQ CCR2 WT, n=10 for ART+CQ CCR2 KO.

of repair. This is in sharp contrast with anti-inflammatory treatments that merely induce a strong inhibition of the immune response (11, 12, 14). Therefore, pro-resolving therapies are considered to be more efficient than anti-inflammatory drugs to treat severe inflammatory pathologies. In this study, we developed a mouse model to study the resolution of MA-ARDS upon parasite killing. In this model, 80% of the *Pb*NK65-infected mice were rescued from the otherwise lethal MA-ARDS complication when ART+CQ was started on the day that the first disease symptoms appeared. In these mice, parasites were cleared and alveolar edema was resolved. This model allows us to study the molecular mechanisms and leukocyte populations involved in this recovery process, possibly offering a great asset for exploring novel therapies for malaria complications.

Previously, it was shown that 80 mg/kg of DEX, a potent glucocorticoid, resulted in increased survival and decreased lung pathology in *Pb*NK65-infected C57BL/6 (31). In the current study, we tested the effect of DEX on the resolution of MA-ARDS at a dosage of 3 mg/kg, in analogy with the maximum dosage for patients. The use of DEX in combination with ART was not beneficial in inducing resolution, as parasitemia and alveolar edema were cleared less efficiently. This is in line with the previous observation that DEX treatment increased parasitemia, which may explain the detrimental effect when combined with antimalarial treatment (31).

MA-ARDS is a Th1-mediated pathology in which $CD8^+$ T cells are pathogenic. Depletion of these cells resulted in the absence of pathology (7, 9, 31). In general, resolution mechanisms of such Th1-mediated pathologies remain poorly understood. Therefore, we performed detailed flow cytometry analyses to characterize the dynamics of leukocyte populations and their activation in lungs and spleen. During infection, both $CD4^+$ and $CD8^+$ T cells became activated, as was shown by a downregulation of CD62L expression and an upregulation of CD44 expression, which corresponded with a Teff phenotype. In fact, $CD8^+$ T cell numbers increased in the lungs during infection and further increased during resolution, while remaining

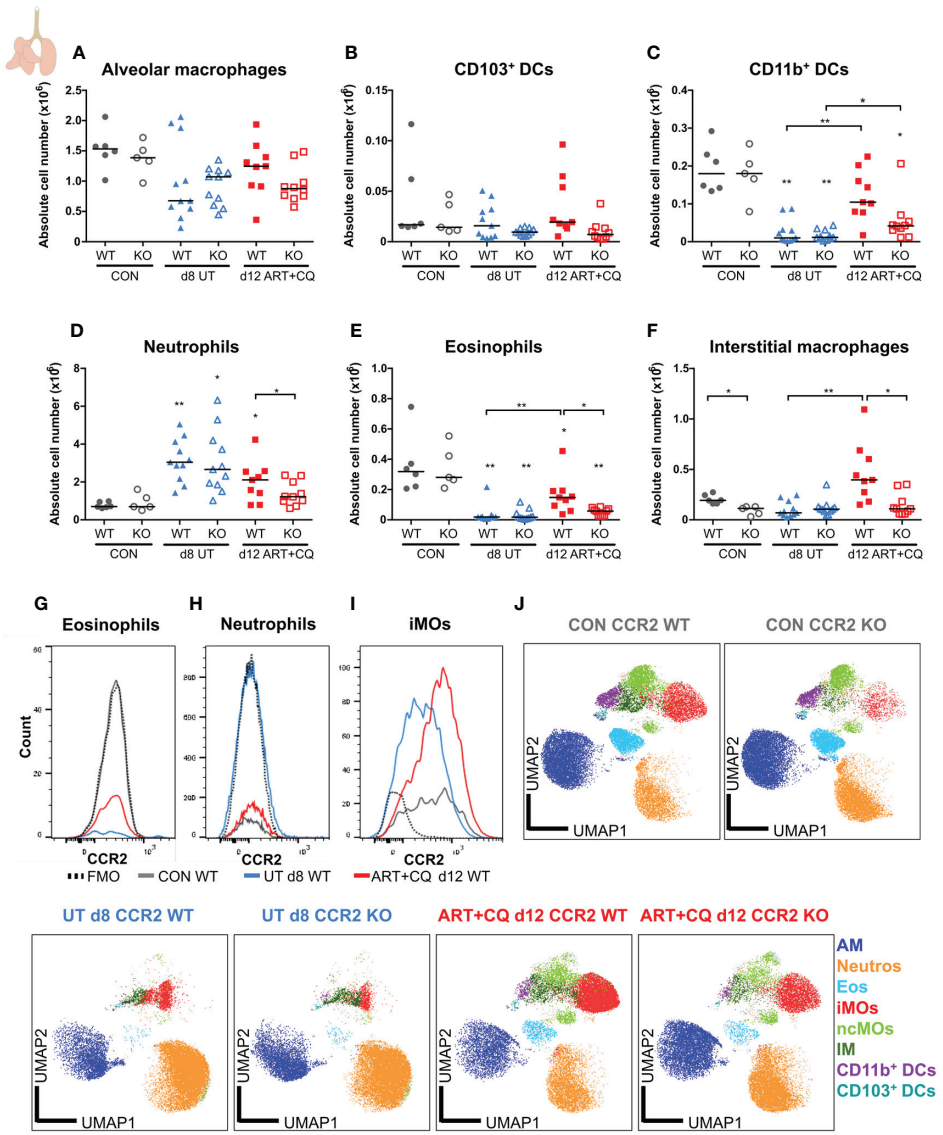

FIGURE 9 | CCR2 is crucial for the return to homeostasis for the myeloid cell populations in the lungs. CCR2 WT and CCR2 KO C57BL/6 mice were infected with *Pb*NK65. Mice were injected daily from 8 until 12 days p.i. with 10 mg/kg ART + 30 mg/kg CQ. Mice were dissected at the indicated days p.i. Leukocytes were isolated from the lungs according to protocol 2 and flow cytometry was performed. **(A–F)** The absolute numbers of alveolar macrophages (AM; CD45$^+$ SiglecF$^+$ CD11b^{int} CD11c$^+$), CD103$^+$ dendritic cells (CD103$^+$ DCs; CD45$^+$ Lin$^-$ SiglecF$^-$ MHC-II$^+$ CD11c$^+$ CD103$^+$ CD11b$^-$), CD11b$^+$ dendritic cells (CD11b$^+$ DCs; CD45$^+$ Lin$^-$ SiglecF$^-$ MHC-II$^+$ CD11c$^+$ CD103$^-$ CD11b$^+$ CD24$^+$ CD64$^-$), neutrophils (Neutros; CD45$^+$ Lin$^-$ CD11b$^+$ Ly6G$^+$), eosinophils (Eos; CD45$^+$ CD11b$^+$ SiglecF$^+$ CD11c$^-$), and interstitial macrophages (IM; CD45$^+$ Lin$^-$ CD11b^{hi} MHC-II$^+$ CD64$^+$ CD24$^-$) in the lungs were calculated. Compilation of two experiments. Each symbol represents data of an individual mouse. n=6 for CON CCR2 WT, n=5 for CON CCR2 KO, n=11 for UT CCR2 WT, n=11 for UT CCR2 KO, n=9 for ART+CQ CCR2 WT, n=10 for ART+CQ CCR2 KO. **(G, H)** Representative flow cytometry plots showing the CCR2 expression of eosinophils **(G)**, neutrophils **(H)**, and iMOs **(I)** in the lungs of CCR2 WT mice at the different time-points. **(J)** Clustering of 24,000 cells combined from two representative samples per condition for the CON CCR2 WT and CON CCR2 KO and from three representative samples per condition for the others. The plots show a two-dimensional representation (UMAP) of the protein expression. Clusters are colored by cell class as defined in panels **(A–F)** and **Figures 7A, B**.

activated. This was also observed by Claser et al. (7). They also demonstrated that IFN-γ is crucial to promote parasite antigen presentation in a MHC-I context by the endothelial cells. CD8$^+$ T cells are also a main source of IFN-γ in the lungs (8). Interestingly, we observed that although the number of CD8$^+$ T cells further increased during resolution, the expression of IFN-γ at 12 days p.i. was already decreased. Reduced parasite antigen presentation by the endothelial cells in the absence of IFN-γ may thus explain why lung pathology is already decreased at 12 days p.i.

In the lungs, Ly6C$^-$ ncMOs decreased during infection but increased during resolution, while Ly6C$^+$ iMOs were upregulated

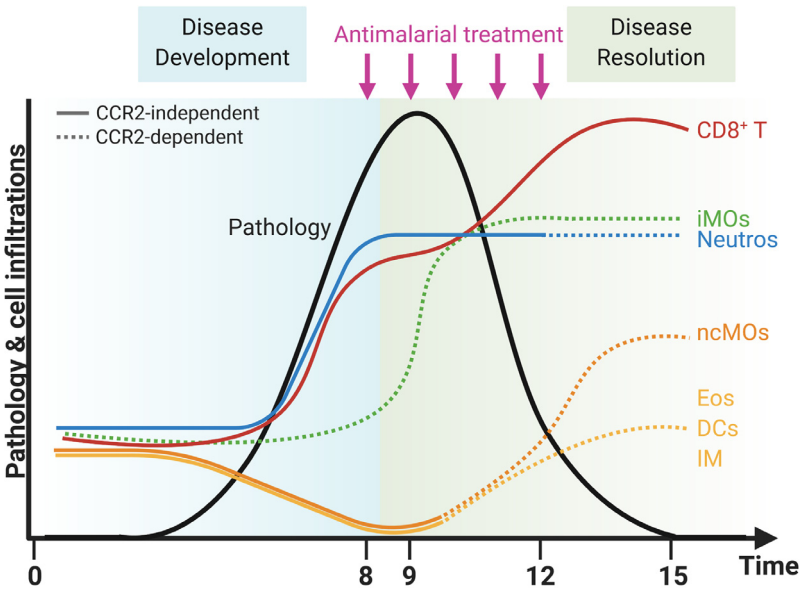

FIGURE 10 | CCR2-dependent dynamics of pulmonary leukocytes during inflammation and resolution. Upon infection with *Pb*NK65 parasites, C57BL/6 mice develop malaria-associated acute respiratory distress syndrome (MA-ARDS). This development of pathology is accompanied by an increase in the number of neutrophils (Neutros) and pathogenic $CD8^+$ T cells and a decrease in the number of eosinophils (Eos), dendritic cells (DCs), interstitial macrophages (IM), and non-classical $Ly6C^-$ monocytes (ncMOs) in the lungs. Late in the development of MA-ARDS, the number of pulmonary inflammatory $Ly6C^+$ monocytes (iMOs) increased as well. Upon antimalarial treatment, mice recover from MA-ARDS with a decrease in clinical symptoms and lung pathology. During resolution, the number of $CD8^+$ T cells further increased in the lungs, whereas the number of Neutros and iMOs remained high. In addition, the Eos, DCs, and IM reappeared in the lungs and the ncMOs increased even higher than in control mice during resolution. CCR2 gene KO inhibited several of these dynamic changes, and CCR2-dependent effects were indicated with dashed lines. The number of iMOs present in the lungs was decreased at each time-point in the CCR2 KO mice. In addition, the Neutros remained high during resolution in CCR2 WT mice, but decreased in the CCR2 KO mice. The Eos, DCs, IM, and ncMOs did not reappear or increase during resolution in the lungs of CCR2 KO mice. Created with BioRender.com.

both upon infection and during resolution. Moreover, CD64, an activation marker of monocytes, was increased on pulmonary $Ly6C^+$ iMOs and alveolar macrophages after infection. Increased CD64 expression on monocytes was also observed in patients with malaria, systemic lupus erythematosus (SLE) and sepsis (34–37). In malaria patients, CD64 upregulation was observed on circulating classical, intermediate and non-classical monocytes of malaria patients (34). CD64 expression correlated with a more severe pathology, such as decreased renal function and high CRP levels, in SLE patients (36). Interestingly, in severe septic patients, the expression on monocytes was higher in patients who survived, compared to patients who died (35, 37). During resolution of MA-ARDS in our model, CD64 expression started decreasing at 12 days p.i., and was fully downregulated to control levels at 15 days p.i. Therefore, similarly to lupus, CD64 expression also parallels the inflammation in MA-ARDS and its subsequent resolution (36).

Our data indicate that $CCR2^+$ $Ly6C^+$ iMOs are neither involved in the development nor the resolution of MA-ARDS. In the absence of CCR2, monocytes are retained in the bone marrow during homeostatic conditions and cannot migrate to the site of inflammation during infection or inflammation (25). In other studies on the effect of the CCR2 KO on the development of MA-ARDS or malaria-associated acute lung injury, similarly no or only modest differences between CCR2 WT and KO mice are detected (8, 27). Our data correspond largely to the data of Galvao-Filho et al., who also observed that the number of $Ly6C^+$ iMOs was lower in the lungs of *Pb*NK65-infected CCR2 KO mice compared to WT mice. Only at 9 days p.i., they observed a reappearance of $Ly6C^+$ iMOs in the CCR2 KO mice, which was not observed in our model (8). Our data indicate that during resolution (at 12 days p.i.), the number of $Ly6C^+$ iMOs increased in the lungs of both the CCR2 WT and KO mice, although to a much lower extent in the CCR2 KO mice. This may be explained by several processes, such as CCR2-independent egress from the bone marrow, local proliferation, or extramedullary hematopoiesis in the spleen.

Although monocytes and macrophages are important producers of cytokines, we confirm previous studies showing that CCR2 is not crucial in the development of MA-ARDS. Interestingly, Galvao-Filho et al. showed that the pathogenesis is mediated by CCR4-dependent tumor necrosis factor α- and inducible nitric oxide synthase-producing DCs (tip-DCs) (8). Importantly, the absence of a role for CCR2 in the recovery from MA-ARDS is surprising. Monocytes and macrophages are often described as essential players during resolution (13). In fact, several studies have shown that the CCL2/CCR2 axis is crucial for the resolution of various pathologies. In particular, in

atherosclerosis and myocardial infarction models, the use of siCCR2 and CCR2 KO mice resulted in a smaller necrotic area and delayed debris clearance with no occurrence of regression (28, 38, 39). The absence of CCR2 also prevented resolution in models of skin wounds, liver fibrosis, and post-operative ileus (29, 40, 41). CCL2 treatment, improved efferocytosis, and subsequent resolution in bacterial pneumonia and increased survival from bleomycin-induced lung injury (42, 43). This effect of CCL2 treatment was, at least in the bleomycin-induced lung injury model, mediated by CCR2, since CCR2 is the main receptor for CCL2 and CCL2 treatment was ineffective in CCR2 KO mice (43). Importantly, resolution of inflammation has been well-characterized in Th2-related diseases, such as helminth infections. In these studies, monocytes and macrophages are described to be crucial because of the switch in macrophage phenotype from the pro-inflammatory "M1" to the reparative "M2-like" phenotype. In contrast, much less is known about the resolution of Th1-related inflammation, in particular in malaria. Our results thus emphasize that different leukocyte populations and processes might be important for inducing resolution of Th1-related diseases, such as malaria, compared to Th2-related diseases. The CCR2 gene deletion resulted not only in reduced numbers of $Ly6C^+$ iMOs, but also of $Ly6C^-$ ncMOs and interstitial macrophages, and a trend for reduced $CD103^+$ and $CD11b^+$ DCs during resolution in the lungs. In CCR2 WT mice, a significant proportion of $Ly6C^-$ ncMOs, interstitial macrophages and DCs expresses CCR2. Therefore, CCR2 deficiency may have a direct effect on the absolute number of these populations. Alternatively, it may also be an indirect effect caused by the lower numbers of $Ly6C^+$ iMOs present in the lungs during resolution, since iMOs are considered precursors for DCs, ncMOs and monocyte-derived macrophages (44–46). Upregulation of $Ly6C^+$ iMOs in the circulation and monocyte-derived macrophages in the tissues is observed during inflammatory responses (44). During inflammation, the $Ly6C^+$ iMOs infiltrate the inflamed tissues to engulf dying cells and subsequently differentiate to $Ly6C^-$ ncMOs, which are involved in tissue repair mechanisms. $Ly6C^+$ iMOs are also thought to differentiate into cells resembling Tip-DCs or "M1" macrophages, whereas the $Ly6C^-$ ncMOs differentiate into "M2" macrophage-like cells (44–46). In contrast to the effect on interstitial macrophages, the deletion of CCR2 did not affect the number of AM. AM are under steady-state conditions derived from the yolk sac of the embryo or differentiated from fetal liver- or bone marrow-derived monocytes (44, 45). They also have a self-renewing capacity regulated by colony stimulating factor-1 (CSF-1) and granulocyte-macrophage colony stimulating factor (GM-CSF), so they do not necessarily rely on replenishment by iMOs during homeostasis and inflammation. The red pulp macrophages in the spleen also do not rely on CCR2, since they reappeared during resolution in both the CCR2 WT and KO mice.

Interestingly, the reappearance of pulmonary eosinophils, after their decrease during infection, was mitigated in CCR2 KO mice. Since eosinophils do not express CCR2, the indirect effect of the CCR2 KO is likely caused by the diminished number of $CCR2^+$ $Ly6C^+$ iMOs present in the lungs. Reparative "M2-like" macrophages may provide an ideal environment to attract eosinophils to the lungs, thus the lack of these cells in the CCR2 KO may explain the mitigated reappearance of eosinophils. Eosinophils are described to play a role during resolution by producing specialized pro-resolving lipid mediators, such as protectin D1, and cytokines, IL-4 and IL-13, resulting in the inhibition of neutrophil infiltration and the modulation of the macrophage phenotype (47–49). More specifically, IL-4 and IL-13 induce the "M1" to "M2-like" phenotype switch of macrophages, whereas protectin D1 stimulates macrophage activity to clear the apoptotic neutrophils (47, 50). However, our data suggest that eosinophils are not essential for resolution, since their delayed reappearance in the lungs does not affect the resolution of pathology. In contrast to pulmonary eosinophils, splenic eosinophils did reappear in the spleen during resolution, independently of CCR2. The pulmonary neutrophil numbers were decreased in CCR2 KO mice during resolution. Similarly to the eosinophils, neutrophils did not express CCR2 in CCR2 WT mice, suggesting that the effect observed in the CCR2 KO mice is an indirect consequence.

In conclusion, a new mouse model to study the mechanisms and the involvement of leukocyte populations in the resolution of MA-ARDS was established. This model offers a great asset to elucidate resolution mechanisms and to explore novel therapies for malaria complications, as pro-resolving therapies may be superior over anti-inflammatory therapies. Our data with the CCR2 KO mice indicated that $CCR2^+$ $Ly6C^+$ iMOs were neither involved in the development nor the resolution of MA-ARDS. In contrast, these cells were important for the leukocytes to return to homeostasis during resolution in CCR2 KO mice. This was indicated by a delayed replenishment of eosinophils and interstitial macrophages.

DATA AVAILABILITY STATEMENT

The original contributions presented in the study are included in the article/**Supplementary Material**. Further inquiries can be directed to the corresponding author.

ETHICS STATEMENT

The animal study was reviewed and approved by The Animal Ethics Committee of the KU Leuven (License LA1210186, project P049/2018, Belgium).

AUTHOR CONTRIBUTIONS

EP, T-TP, LV, HP, and SK performed the experiments. EP analyzed the data. PVdS, EP, and GO conceived the study. EP and PVdS wrote the first drafts of the manuscript. All authors

critically read and edited the manuscript. All authors contributed to the article and approved the submitted version.

FUNDING

This study was supported by Research Foundation-Flanders (F.W.O.-Vlaanderen, project G086215N and G097318N, G0C9720N) and the Research Fund of the KU Leuven (C1 project C16/17/010). EP is a recipient of the L'Oréal-Unesco Women for Sciences PhD fellowship, T-TP and HP are recipients of an aspirant PhD fellowship of the F.W.O.-Vlaanderen, LV holds a junior Postdoc fellowship of the F.W.O.-Vlaanderen and PVdS is a Research Professor at the KU Leuven.

ACKNOWLEDGMENTS

The authors thank Queeny Robalo for her excellent technical help, and Prof. G. Matteoli and Prof. P. Marques for interesting discussions.

SUPPLEMENTARY MATERIAL

The Supplementary Material for this article can be found online at: https://www.frontiersin.org/articles/10.3389/fimmu.2020.628643/full#supplementary-material

REFERENCES

1. World Health Organization. *WHO World Malaria Report 2020*. World Health Organization. (2020).
2. Van den Steen PE, Deroost K, Deckers J, Van Herck E, Struyf S, Opdenakker G. Pathogenesis of malaria-associated acute respiratory distress syndrome. *Trends Parasitol* (2013) 29(7):346–58. doi: 10.1016/j.pt.2013.04.006
3. White NJ. Qinghaosu (artemisinin): the price of success. *Science* (2008) 320 (5874):330–4. doi: 10.1126/science.1155165
4. Taylor WRJ, Hanson J, Turner GDH, White NJ, Dondorp AM. Respiratory manifestations of malaria. *Chest* (2012) 142(2):492–505. doi: 10.1378/chest.11-2655
5. Wiesner J, Ortmann R, Jomaa H, Schlitzer M. New Antimalarial Drugs. *Angew Chemie - Int Ed* (2003) 42(43):5274–93. doi: 10.1002/anie.200200569
6. Deroost K, Pham T-T, Opdenakker G, Van den Steen PE. The immunological balance between host and parasite in malaria. *FEMS Microbiol Rev* (2016) 40 (2):208–57. doi: 10.1093/femsre/fuv046
7. Claser C, Nguee SYT, Balachander A, Wu Howland S, Becht E, Gunasegaran B, et al. Lung endothelial cell antigen cross-presentation to CD8+T cells drives malaria-associated lung injury. *Nat Commun* (2019) 10(1):1–16. doi: 10.1038/s41467-019-12017-8
8. Galvão-Filho B, de Castro JT, Figueiredo MM, Rosmaninho CG, Antonelli LR do V, Gazzinelli RT. The emergence of pathogenic TNF/iNOS producing dendritic cells (Tip-DCs) in a malaria model of acute respiratory distress syndrome (ARDS) is dependent on CCR4. *Mucosal Immunol* (2019) 12 (2):312–22. doi: 10.1038/s41385-018-0093-5
9. Pham T-T, Verheijen M, Vandermosten L, Deroost K, Knoops S, Van den Eynde K, et al. Pathogenic CD8+ T Cells Cause Increased Levels of VEGF-A in Experimental Malaria-Associated Acute Respiratory Distress Syndrome, but Therapeutic VEGFR Inhibition Is Not Effective. *Front Cell Infect Microbiol* (2017) 7:416. doi: 10.3389/fcimb.2017.00416
10. Ortega-Gómez A, Perretti M, Soehnlein O. Resolution of inflammation: An integrated view. *EMBO Mol Med* (2013) 5(5):661–74. doi: 10.1002/emmm.201202382
11. Perretti M, Cooper D, Dalli J, Norling LV. Immune resolution mechanisms in inflammatory arthritis. *Nat Rev Rheumatol* (2017) 13(2):87–99. doi: 10.1038/nrrheum.2016.193
12. Fullerton JN, Gilroy DW. Resolution of inflammation: A new therapeutic frontier. *Nat Rev Drug Discov* (2016) 15(8):551–67. doi: 10.1038/nrd.2016.39
13. Hilgendorf I, Gerhardt LMS, Tan TC, Winter C, Holderried TAW, Chousterman BG, et al. Ly-6Chigh monocytes depend on Nr4a1 to balance both inflammatory and reparative phases in the infarcted myocardium. *Circ Res* (2014) 114(10):1611–22. doi: 10.1161/CIRCRESAHA.114.303204
14. Sugimoto MA, Vago JP, Perretti M, Teixeira MM. Mediators of the Resolution of the Inflammatory Response. *Trends Immunol* (2019) 40(3):212–27. doi: 10.1016/j.it.2019.01.007
15. Perretti M, Leroy X, Bland EJ, Montero-Melendez T. Resolution Pharmacology: Opportunities for Therapeutic Innovation in Inflammation. *Trends Pharmacol Sci* (2015) 36(11):737–55. doi: 10.1016/j.tips.2015.07.007
16. Chen F, Liu Z, Wu W, Rozo C, Bowdridge S, Van Rooijen N, et al. An essential role for the Th2-type response in limiting tissue damage during helminth infection. *Nat Med* (2012) 18(2):260–6. doi: 10.1038/nm.2628.An
17. Minutti CM, Jackson-Jones LH, García-Fojeda B, Knipper JA, Sutherland TE, Logan N, et al. Local amplifiers of IL-4Rα-mediated macrophage activation promote repair in lung and liver. *Science* (2017) 356(6342):1076–80. doi: 10.1126/science.aaj2067
18. Allen JE, Sutherland TE. Host protective roles of type 2 immunity: Parasite killing and tissue repair, flip sides of the same coin. *Semin Immunol* (2014) 26 (4):329–40. doi: 10.1016/j.smim.2014.06.003
19. Wynn TA, Vannella KM. Macrophages in Tissue Repair, Regeneration, and Fibrosis. *Immunity* (2016) 44(3):450–62. doi: 10.1016/j.immuni.2016.02.015
20. Pádua TA, Torres ND, Candéa ALP, Costa MFS, Silva JD, Silva-Filho JL, et al. Therapeutic effect of Lipoxin A $_4$ in malaria-induced acute lung injury. *J Leukoc Biol* (2018) 103(4):1–14. doi: 10.1002/JLB.3A1016-435RRR
21. Shryock N, McBerry C, Salazar Gonzalez RM, Janes S, Costa FTM, Aliberti J. Lipoxin A4 and 15-Epi-Lipoxin A4 Protect against Experimental Cerebral Malaria by Inhibiting IL-12/IFN-γ in the Brain. *PLoS One* (2013) 8(4):2–10. doi: 10.1371/journal.pone.0061882
22. Souza MC, Pádua TA, Torres ND, Souza Costa MF, Candéa AP, Maramaldo T, et al. Lipoxin A4attenuates endothelial dysfunction during experimental cerebral malaria. *Int Immunopharmacol* (2015) 24(2):400–7. doi: 10.1016/j.intimp.2014.12.033
23. Strangward P, Haley MJ, Albornoz MG, Barrington J, Shaw T, Dookie R, et al. Targeting the IL33–NLRP3 axis improves therapy for experimental cerebral malaria. *Proc Natl Acad Sci* (2018) 115(28):7404–9. doi: 10.1073/pnas.1801737115
24. Niewold P, Cohen A, van Vreden C, Getts DR, Grau GE, King NJC. Experimental severe malaria is resolved by targeting newly-identified monocyte subsets using immune-modifying particles combined with artesunate. *Commun Biol* (2018) 1(2018):227. doi: 10.1038/s42003-018-0216-2
25. Kratofil RM, Kubes P, Deniset JF. Monocyte conversion during inflammation and injury. *Arterioscler Thromb Vasc Biol* (2017) 37(1):35–42. doi: 10.1161/ATVBAHA.116.308198
26. Tacke F, Randolph GJ. Migratory fate and differentiation of blood monocyte subsets. *Immunobiology* (2006) 211(6–8):609–18. doi: 10.1016/j.imbio.2006.05.025
27. Lagassé HAD, Anidi IU, Craig JM, Limjunyawong N, Poupore AK, Mitzner W, et al. Recruited monocytes modulate malaria-induced lung injury through CD36-mediated clearance of sequestered infected erythrocytes. *J Leukoc Biol* (2016) 99(5):659–71. doi: 10.1189/jlb.4HI0315-130RRR
28. Dal-Secco D, Wang J, Zeng Z, Kolaczkowska E, Wong CHY, Petri B, et al. A dynamic spectrum of monocytes arising from the in situ reprogramming of CCR2 + monocytes at a site of sterile injury. *J Exp Med* (2015) 212(4):447–56. doi: 10.1084/jem.20141539
29. Boniakowski AE, Kimball AS, Joshi A, Schaller M, Davis FM, denDekker A, et al. Murine macrophage chemokine receptor CCR2 plays a crucial role in

macrophage recruitment and regulated inflammation in wound healing. *Eur J Immunol* (2018) 48(9):1445–55. doi: 10.1002/eji.201747400
30. Vandermosten L, Pham T-T, Possemiers H, Knoops S, Van Herck E, Deckers J, et al. Experimental malaria-associated acute respiratory distress syndrome is dependent on the parasite-host combination and coincides with normocyte invasion. *Malar J* (2018) 17(1):102. doi: 10.1186/s12936-018-2251-3
31. Van den Steen PE, Geurts N, Deroost K, Van Aelst I, Verhenne S, Heremans H, et al. Immunopathology and dexamethasone therapy in a new model for malaria-associated acute respiratory distress syndrome. *Am J Respir Crit Care Med* (2010) 181(9):957–68. doi: 10.1164/rccm.200905-0786OC
32. Livak KJ, Schmittgen TD. Analysis of relative gene expression data using real-time quantitative PCR and the 2-ΔΔCT method. *Methods* (2001) 25(4):402–8. doi: 10.1006/meth.2001.1262
33. Borges Da Silva H, Fonseca R, Pereira RM, Cassado AA, Álvarez JM, D'Império Lima MR. Splenic macrophage subsets and their function during blood-borne infections. *Front Immunol* (2015) 6:480. doi: 10.3389/fimmu.2015.00480
34. Loughland JR, Woodberry T, Field M, Andrew DW, SheelaNair A, Dooley NL, et al. Transcriptional profiling and immunophenotyping show sustained activation of blood monocytes in subpatent Plasmodium falciparum infection. *Clin Transl Immunol* (2020) 9(6):1–18. doi: 10.1002/cti2.1144
35. Ferreira da Mota NV, Colo Brunialti MK, Santos SS, Machado FR, Assuncao M, Pontes Azevedo LC, et al. Immunophenotyping of monocytes during human sepsis shows impairment in antigen presentation: A shift toward nonclassical differentiation and upregulation of FcGRI-receptor. *Shock* (2018) 50(3):293–300. doi: 10.1097/SHK.0000000000001078
36. Li Y, Lee PY, Sobel ES, Narain S, Satoh M, Segal MS, et al. Increased expression of FcγRI/CD64 on circulating monocytes parallels ongoing inflammation and nephritis in lupus. *Arthritis Res Ther* (2009) 11(1):1–13. doi: 10.1186/ar2590
37. Danikas DD, Karakantza M, Theodorou GL, Sakellaropoulos GC, Gogos CA. Prognostic value of phagocytic activity of neutrophils and monocytes in sepsis. Correlation to CD64 and CD14 antigen expression. *Clin Exp Immunol* (2008) 154(1):87–97. doi: 10.1111/j.1365-2249.2008.03737.x
38. Rahman K, Vengrenyuk Y, Ramsey SA, Vila NR, Girgis NM, Liu J, et al. Inflammatory Ly6Chi monocytes and their conversion to M2 macrophages drive atherosclerosis regression. *J Clin Invest* (2017) 127(8):2904–15. doi: 10.1172/JCI75005
39. Majmudar MD, Keliher EJ, Heidt T, Leuschner F, Truelove J, Sena BF, et al. Monocyte-directed RNAi targeting CCR2 improves infarct healing in atherosclerosis-prone mice. *Circulation* (2013) 127(20):2038–46. doi: 10.1161/CIRCULATIONAHA.112.000116
40. Farro G, Stakenborg M, Gomez-Pinilla PJ, Labeeuw E, Goverse G, Di Giovangiulio M, et al. CCR2-dependent monocyte-derived macrophages resolve inflammation and restore gut motility in postoperative ileus. *Gut* (2017) 66(12):2098–109. doi: 10.1136/gutjnl-2016-313144
41. Mitchell C, Couton D, Couty J, Anson M, Crain A, Bizet V, et al. Dual role of CCR2 in the constitution and the resolution of liver fibrosis in mice. *Am J Pathol* (2009) 174(5):1766–75. doi: 10.2353/ajpath.2009.080632
42. Amano H, Morimoto K, Senba M, Wang H, Ishida Y, Kumatori A, et al. Essential contribution of monocyte chemoattractant protein-1/C-C chemokine ligand-2 to resolution and repair processes in acute bacterial pneumonia. *J Immunol* (2004) 172(1):398–409. doi: 10.4049/jimmunol.172.1.398
43. Liang J, Jung Y, Tighe RM, Xie T, Liu N, Leonard M, et al. A macrophage subpopulation recruited by CC chemokine ligand-2 clears apoptotic cells in noninfectious lung injury. *Am J Physiol Cell Mol Physiol* (2012) 302(9):L933–40. doi: 10.1152/ajplung.00256.2011
44. Italiani P, Boraschi D. From monocytes to M1/M2 macrophages: Phenotypical vs. functional differentiation. *Front Immunol* (2014) 5:514 (OCT). doi: 10.3389/fimmu.2014.00514
45. Mitchell AJ, Roediger B, Weninger W. Monocyte homeostasis and the plasticity of inflammatory monocytes. *Cell Immunol* (2014) 291(1–2):22–31. doi: 10.1016/j.cellimm.2014.05.010
46. Murray PJ. Immune regulation by monocytes. *Semin Immunol* (2018) 35 (August 2017):12–8. doi: 10.1016/j.smim.2017.12.005
47. Yamada T, Tani Y, Nakanishi H, Taguchi R, Arita M, Arai H. Eosinophils promote resolution of acute peritonitis by producing proresolving mediators in mice. *FASEB J* (2011) 25(2):561–8. doi: 10.1096/fj.10-170027
48. Isobe Y, Kato T, Arita M. Emerging roles of eosinophils and eosinophil-derived lipid mediators in the resolution of inflammation. *Front Immunol* (2012) 3:270(AUG). doi: 10.3389/fimmu.2012.00270
49. Strandmark J, Rausch S, Hartmann S. Eosinophils in Homeostasis and Their Contrasting Roles during Inflammation and Helminth Infections. *Crit Rev Immunol* (2016) 36(3):193–238. doi: 10.1615/CritRevImmunol.2016018726
50. Jacobsen EA, Lee NA, Lee JJ. Re-defining the unique roles for eosinophils in allergic respiratory inflammation. *Clin Exp Allergy* (2014) 44(9):1119–36. doi: 10.1111/cea.12358

Conflict of Interest: The authors declare that the research was conducted in the absence of any commercial or financial relationships that could be construed as a potential conflict of interest.

Copyright © 2021 Pollenus, Pham, Vandermosten, Possemiers, Knoops, Opdenakker and Van den Steen. This is an open-access article distributed under the terms of the Creative Commons Attribution License (CC BY). The use, distribution or reproduction in other forums is permitted, provided the original author(s) and the copyright owner(s) are credited and that the original publication in this journal is cited, in accordance with accepted academic practice. No use, distribution or reproduction is permitted which does not comply with these terms.

frontiers in Immunology

ORIGINAL RESEARCH
published: 25 February 2021
doi: 10.3389/fimmu.2021.634889

The Crucial Role of PPARγ-Egr-1-Pro-Inflammatory Mediators Axis in IgG Immune Complex-Induced Acute Lung Injury

Chunguang Yan[1,2,3], Jing Chen[1], Yue Ding[1], Zetian Zhou[1], Bingyu Li[1], Chunmin Deng[1], Dong Yuan[4], Qi Zhang[3] and Ximo Wang[3]**

[1] Department of Pathogenic Biology and Immunology, Medical School of Southeast University, Nanjing, China, [2] Jiangsu Provincial Key Laboratory of Critical Care Medicine, Zhongda Hospital of Southeast University, Nanjing, China, [3] Tianjin Key Laboratory of Acute Abdomen Disease Associated Organ Injury and Integrated Chinese and Western Medicine (ITCWM) Repair, Institute of Integrative Medicine for Acute Abdominal Diseases, Integrated Chinese and Western Medicine Hospital, Tianjin University, Tianjin, China, [4] Emergency Department, Jintan Hospital, Jiangsu University, Changzhou, China

OPEN ACCESS

Edited by:
Amiram Ariel,
University of Haifa, Israel

Reviewed by:
Uzma Saqib,
Indian Institute of Technology Indore, India
Andreas Von Knethen,
Goethe University Frankfurt, Germany

***Correspondence:**
Chunguang Yan
ycgagcy@163.com
Ximo Wang
wangximo@126.com

Specialty section:
This article was submitted to Inflammation, a section of the journal Frontiers in Immunology

Received: 29 November 2020
Accepted: 20 January 2021
Published: 25 February 2021

Citation:
Yan C, Chen J, Ding Y, Zhou Z, Li B, Deng C, Yuan D, Zhang Q and Wang X (2021) The Crucial Role of PPARγ-Egr-1-Pro-Inflammatory Mediators Axis in IgG Immune Complex-Induced Acute Lung Injury. Front. Immunol. 12:634889. doi: 10.3389/fimmu.2021.634889

Background: The ligand-activated transcription factor peroxisome proliferator-activated receptor (PPAR) γ plays crucial roles in diverse biological processes including cellular metabolism, differentiation, development, and immune response. However, during IgG immune complex (IgG-IC)-induced acute lung inflammation, its expression and function in the pulmonary tissue remains unknown.

Objectives: The study is designed to determine the effect of PPARγ on IgG-IC-triggered acute lung inflammation, and the underlying mechanisms, which might provide theoretical basis for therapy of acute lung inflammation.

Setting: Department of Pathogenic Biology and Immunology, Medical School of Southeast University

Subjects: Mice with down-regulated/up-regulated PPARγ activity or down-regulation of Early growth response protein 1 (Egr-1) expression, and the corresponding controls.

Interventions: Acute lung inflammation is induced in the mice by airway deposition of IgG-IC. Activation of PPARγ is achieved by using its agonist Rosiglitazone or adenoviral vectors that could mediate overexpression of PPARγ. PPARγ activity is suppressed by application of its antagonist GW9662 or shRNA. Egr-1 expression is down-regulated by using the gene specific shRNA.

Measures and Main Results: We find that during IgG-IC-induced acute lung inflammation, PPARγ expression at both RNA and protein levels is repressed, which is consistent with the results obtained from macrophages treated with IgG-IC. Furthermore, both *in vivo* and *in vitro* data show that PPARγ activation reduces IgG-IC-mediated pro-inflammatory mediators' production, thereby alleviating lung injury. In terms of mechanism, we observe that the generation of Egr-1 elicited by IgG-IC is inhibited by PPARγ. As an important transcription factor, Egr-1 transcription is substantially increased by IgG-IC in both *in vivo* and *in vitro* studies, leading to augmented protein expression,

thus amplifying IgG-IC-triggered expressions of inflammatory factors *via* association with their promoters.

Conclusion: During IgG-IC-stimulated acute lung inflammation, PPARγ activation can relieve the inflammatory response by suppressing the expression of its downstream target Egr-1 that directly binds to the promoter regions of several inflammation-associated genes. Therefore, regulation of PPARγ-Egr-1-pro-inflammatory mediators axis by PPARγ agonist Rosiglitazone may represent a novel strategy for blockade of acute lung injury.

Keywords: acute lung injury, PPARγ, Egr-1, pro-inflammatory mediators, inflammation

BACKGROUND

Excessive formation of IgG immune complexes *in vivo* has been demonstrated to be associated with a variety of diseases, such as systemic lupus erythematosus, rheumatoid arthritis, acute glomerulonephritis, mixed cryoglobulinemia and vasculitis (1–7). Moreover, the pulmonary diseases, such as acute lung injury (ALI) and its more severe form—acute respiratory distress syndrome (ARDS), are also reported to be related with deposition of immune complexes in the tissue (8, 9). During IgG-IC induction of ALI/ARDS, the local macrophages are firstly activated through engagement of Fcγ receptors with the ligands, resulting in the release of numerous cytokines and chemokines. Then, under the action of the inflammatory factors, alveolar epithelial cells are activated and neutrophils are recruited into the pulmonary tissue. Finally, acute lung injury is triggered by the severe inflammatory response. However, the molecular events responsible for productions of inflammation-associated mediators are poorly understood.

PPARγ is a type II nuclear receptor, which is rich in adipose tissue. Actually, other types of cells and tissues also generate PPARγ (10–12). A large number of studies focus on its roles in regulation of gene expressions associated with lipid uptake and adipogenesis, and find that PPARγ is involved in a broad spectrum of lipid metabolism disorder-mediated diseases, such as obesity, diabetes and atherosclerosis (13–15). However, the importance of PPARγ in immune regulations has also been recognized. For example, PPARγ is required for IL-9 production in T_H2 cells, which might exert regulatory effects on acute allergic skin inflammatory response in human beings (16). Reddy et al. report that PPARγ activation has protective effects against cigarette smoke-stimulated inflammatory responses during chronic obstructive pulmonary disease (17). Except for its effect on chronic pulmonary disease, the role of PPARγ in acute lung injury has also been examined. There are data that ventilation- or LPS-induced acute lung injury is relieved by PPARγ, but the conclusions are obtained by using PPARγ antagonist or agonist (18–20). So, the nonspecific effects of the chemical reagents cannot be excluded. More importantly, the influence of PPARγ on IgG-IC-induced acute lung injury and the corresponding mechanism have not been elucidated.

Egr-1 also named as NGFI-A (nerve growth factor-induced protein A) is a nuclear protein acting as a transcription factor. Its expression can be induced by a variety of stimulus including cytokines, neurotransmitters and growth factors (21). However, the effect of IgG-IC treatment on its expression remains enigmatic. Aberrant Egr-1 expression or activity has been detected in various human diseases, such as atherosclerosis, cancer, ischemic injury and TGF-β-dependent pro-fibrotic responses (21). Notably, the role of Egr-1 in inflammatory responses has also been extensively investigated. For example, cigarette smoke-induced chemokine release from primary human lung fibroblasts is dependent on Egr-1 (22). In addition, the secretion of inflammatory cytokines induced by Mycoplasma pneumonia infection *in vitro* and *in vivo* is also positively regulated by Egr-1 (23). However, its influence on acute lung inflammation and the underlying mechanism after intrapulmonary deposition of IgG-IC remain mysterious.

Given the importance of PPARγ and Egr-1 in inflammatory responses, the present study intends to determine the roles of the two transcription factors in IgG-IC-induced acute lung injury, and the possible interaction between PPARγ and Egr-1. We find, for the first time, that PPARγ expression is downregulated, while Egr-1 expression is upregulated in IgG-IC-treated mouse lungs and macrophages. Furthermore, we prove that Egr-1 enhances IgG-IC-induced inflammatory response by directly binding to the promoter regions of the pro-inflammatory mediators, and PPARγ suppresses inflammation by inhibiting production of Egr-1. Taken together, the data show that during IgG-IC-induced acute lung injury, PPARγ may play an essential role in regulating inflammatory response by interfering with the expression of its downstream target Egr-1, and PPARγ agonist Rosiglitazone may be used clinically for blockade of acute lung injury in the future.

MATERIALS AND METHODS

Animals, Cell Culture, and Reagents

Pathogen-free male C57BL/6 mice that are 8–12 weeks old are obtained from Model Animal Research Center of Nanjing University (Nanjing, China), and all animal experiments are performed according to the protocol approved by Southeast University. RAW264.7 cells and HEK293 cells are purchased from American Type Culture Collection and cultured in DMEM supplemented with 10% fetal bovine serum (Gibico). Bovine serum albumin (BSA) and rabbit anti-BSA IgG (α-BSA) are purchased from Invitrogen and MP Biomedicals, respectively.

ELISA kit for mouse albumin is purchased from Bethyl Laboratories. ELISA kits for TNF-α, MCP-1, MIP-1α and MIP-2 are purchased from R&D Systems. PPARγ antagonist GW9662, PPARγ agonist Rosiglitazone (ROSI) and puromycin are purchased from Cayman Chemical.

IgG-IC-Induced Acute Lung Injury and Analysis of Bronchoalveolar Lavage Fluids (BALFs)

Mice are anesthetized by intraperitoneal injection of 1.5% sodium pentobarbital. Then rabbit anti-BSA antibodies are administrated into mouse lungs through the airways. Immediately after the operation, the mice are treated by intravenous injection of BSA dissolved in PBS. Four hours later, whole lungs or bronchoalveolar lavage fluids (BALFs) are collected.

BALFs are centrifuged at 3,000 rpm for 5 min at 4°C, and then cell-free supernatants are collected and subjected to analyze albumin, TNF-α, MCP-1, MIP-1α and MIP-2 levels by ELISA. Albumin contents derived from IgG-IC-treated mice are divided by those from the corresponding control mice to obtain values of lung permeability indexes. The remaining cell pellets are resuspended in HBSS containing 0.5% BSA. Total white blood cells are measured with hemocytometer. Cytospin centrifugation is used for preparation of samples for cell differentials. Samples are fixed and stained with Diff-Quik Stain (Solarbio® LIFE SCIENCES, China), which is followed by analysis of percentage of neutrophils.

Construction of Expression Vectors and Promoter-Driven Reporters

Adenoviral vectors promoting ectopic expression of PPARγ are constructed by following the instruction provided by BD Biosciences. Briefly, PPARγ-encoding sequences (Accession Number NM_001127330) are amplified from mouse lung cDNA library, and the DNA sequences are ligated with the shuttle vector—pShuttle2, to form the recombinational plasmids —pShuttle2-PPARγ. Enzyme-digested pShuttle2-PPARγ is extracted and linked with the adenoviral vector. Then the recombinational adenovirus vectors are linearized by the restriction enzyme PacI, which is followed by transfection of the linear DNA into HEK293 cells to make the infectious adenovirus (Ad-PPARγ). The obtained Ad-PPARγ is stored at −80°C, and tittered by utilizing the titer kit from BD Biosciences before use.

Control plasmid is constructed by ligating the amplified EGFP encoding fragment from pIRES-EGFP (Clontech) with pcDNA3.1-Myc-His (Invitrogen). Egr-1-encoding sequences (Accession Number NM_007913) are cloned from mouse lung cDNA library by PCR. The recombinational plasmids expressing Egr-1 are then formed by ligating the amplified DNA sequences with pcDNA3.1-Myc-His.

We firstly generate double-stranded oligos containing the PPARγ or Egr-1 interference sequence, and then link them to the vector—miRZip™ shRNA Expression Lentivector (System Biosciences). The transfer plasmids together with two other plasmids—pMD2.G and psPAX2 (Addgene plasmids 12259 and 12260) are co-transfected into HEK293 cells by using Lipofectamine 2000 (Invitrogen) to make mature viral particles that are titered by measuring GFP positivity after transduction.

The full length of TNF-α (Accession Number NC_000083)/ MCP-1 (Accession Number NC_000077)/MIP-1α (Accession Number) promoter region is amplified by using mouse genomic DNA as the template. Then TNF-α Luc, MCP-1 Luc and MIP-1α Luc are constructed by ligating their corresponding promoter fragments with pGL4-basic vector (Promega). Mutations are introduced to the Egr-1 binding sites in TNF-α, MCP-1 and MIP-1α promoter regions by using the Mut Express II Fast Mutagenesis Kit V2 (Vazyme, China). pRL-TK plasmids used as internal references are obtained from Promega.

Airway Injection of Recombinational Viral Vectors

Ad-GFP (BD Biosciences) or Ad-PPARγ is intratracheally administrated into mice. Three days later, the infected mice are used for the subsequent experiments. Mice receiving airway administration of shRNA NC or Egr-1 shRNA are used 5 days after infection.

Construction of Stable Cell Line

RAW264.7 cells are infected by control or PPARγ/Egr-1 shRNA lentiviral particles at a MOI of 30. Seventy-two hours later, the cells are treated with 3 μg/ml puromycin. The survival cells are selected, and the knockdown efficiency is confirmed by qPCR.

Western Blot Analysis

Total cellular or tissue proteins are extracted by using radioimmune precipitation assay buffer from Beyotime Biotechnology (China). Then 30 μg of proteins are run on a 12% SDS-polyacrylamide gel and examined by using the following antibodies: goat anti-PPARγ (Santa Cruz, catalog number sc-1984X), mouse anti-Egr-1 (Santa Cruz, catalog number sc-515830), and mouse anti-GAPDH (Proteintech, catalog number 60004-1-Ig).

Quantitative RT-PCR Assay

Total RNAs are extracted with Trizol (Invitrogen), and reverse transcribed into cDNAs using PrimeScript™ RT reagent Kit obtained from TaKaRa. qPCR assays are conducted with the following protocol: an initial step at 95°C for 3 min followed by 40 cycles of 95°C for 5 s and 60°C for 30 s. The primers used are as follows: PPARγ, 5′ primer, 5′-agg gcg atc ttg aca gga aa-3′, and 3′ primer, 5′-cga aac tgg cac cct tga aa-3′; Egr-1, 5′ primer, 5′-cga gtt atc cca gcc aaa cg-3′, and 3′ primer, 5′-gaa gac gat gaa gca gct gg-3′; TNF-α, 5′ primer, 5′-CGT CAG CCG ATT TGC TAT CT-3′, and 3′ primer, 5′-CGG ACT CCG CAA AGT CTA AG-3′; MCP-1, 5′ primer, 5′-AGG TCC CTG TCA TGC TTC TG-3′, and 3′ primer, 5′-TCT GGA CCC ATT CCT TCT TG-3′; MIP-1α, 5′ primer, 5′-ATG AAG GTC TCC ACC ACT GC-3′, and 3′ primer, 5′-CCC AGG TCT CTT TGG AGT CA-3′; GAPDH: 5′ primer, 5′-GCC TCG TCT CAT AGA CAA GAT G-3′, and 3′ primer, 5′-CAG TAG ACT CCA CGA CAT AC-3′.

Measurement of Pulmonary Myeloperoxidase (MPO) Activity

Four hours after airway deposition of IgG-IC, mouse lungs are harvested and homogenized in the buffer containing the following components: 0.5% hexadecyltrimethylammonium bromide, 50 mM potassium phosphate buffer and 5 mM EDTA. Then the homogenates are subjected to sonication. Cell-free supernatants are mixed with the MPO analysis buffer consisted of 5 μg/ml H_2O_2, 100 mM potassium, and 167 μg/ml *o*-dianisidine dihydrochloride. MPO contents are determined by measuring the change in optical density (at 450 nm) per min using the 96-well plate reader.

Luciferase Assays

Cells are cultured in 12-well plates. Twelve hours later, the cells are transfected with total of 0.5 μg plasmids using Fugene®6 Transfection Reagent (Promega) according to the manufacturer's guideline. Twenty-four hours after transfection, cells are lysed and the lysates are subjected to measurement of luciferase activities with the Dual-Luciferase Reporter Assay System purchased from Promega.

Statistical Assay

All data are represented as the mean ± S. E. M. Significance is indicated when p value is less than 0.05. Data sets are analyzed using Student's t test or one-way ANOVA, with individual group means being compared with the Student-Newman-Keuls multiple comparison test.

RESULTS

PPARγ Negatively Regulates IgG-IC-Induced Acute Lung Injury

The roles of PPARγ in pulmonary diseases have been extensively explored. However, during IgG-IC-stimulated acute lung injury, its expression and function have not been determined. So, we first examine if PPARγ production is changed in the mouse lung after intratracheal deposition of IgG-IC. As shown in **Figure S1A**, IgG-IC treatment leads to a 36% decrease in PPARγ production at mRNA level, which is consistent with the Western blot assay (**Figure S1B**).

We then investigate the role of PPARγ in IgG-IC-initiated acute lung injury which is reflected by lung permeability, and MPO activity—an indicator of neutrophil accumulation. Firstly, we overexpress PPARγ in the mouse pulmonary tissue by using adenovirus as the vector (24), and find that Ad-PPARγ greatly increases PPARγ expression even at a dose of 1×10^8 PFU (plaque forming unit) (**Figure 1A**). Importantly, mice receive intratracheal treatment of 1×10^8 PFU of adenoviral vectors do not show any signs of acute lung injury (**Figure S2**). Therefore, in the following studies, 1×10^8 PFU of Ad-PPARγ is applied to the animal experiments. As shown in **Figure 1B**, when compared with the control group, lung permeability index is increased by more than 2.5 folds after IgG-IC stimulation, which is almost reduced to basal level by ectopic expression of PPARγ. As expected, the increase in the pulmonary MPO activity caused by IgG-IC treatment is also significantly inhibited by PPARγ overexpression (**Figure 1C**).

Recruitment of white blood cells, especially neutrophils, into alveolar spaces plays a critical role in acute lung injury. We observe that influxes of total leukocytes and neutrophils into alveolar compartments are greatly induced by IgG-IC treatment (**Figures 1D, E**). However, 4 h after initiation of IgG-IC-induced acute lung injury, the numbers of total white blood cells and neutrophils recovered from BAL fluids of Ad-PPARγ mice are obviously reduced as compared with the control (**Figures 1D, E**).

We further elucidate the influence of PPARγ on expressions of pro-inflammatory mediators that are pivotal initiators of acute lung injury. We find that upon IgG-IC stimulation, expressions of TNF-α, MCP-1, MIP-1α and MIP-2 are dramatically induced in BAL fluids (**Figures 1F–I**). However, ectopic expression of PPARγ in the lung decreases IgG-IC-stimulated expressions of TNF-α, MCP-1, MIP-1α and MIP-2 by 43%, 67%, 36%, and 43%, respectively (**Figures 1F–I**).

To further elucidate the important role of PPARγ in IgG-IC-induced acute lung injury, chemical reagent GW9662—an antagonist of PPARγ, is used to block PPARγ activation. As shown in **Figure S3**, IgG-IC-induced elevation of acute lung injury-related indicators including lung permeability, MPO activity, alveolar recruitment of leukocytes, especially neutrophils, and expressions of pro-inflammatory mediators are further exacerbated in mice receiving GW9662 treatment. However, acute lung injury induced by IgG-IC is alleviated by PPARγ agonist—ROSI (**Figure S4**)

Inflammation Is Relieved by PPARγ in IgG-IC-Treated Macrophages

During IgG-IC-induced acute lung injury, macrophage is one of the most important positive regulators of the severity of tissue damage. Therefore, the role of PPARγ in IgG-IC-induced inflammatory response in macrophages is analyzed. Firstly, we investigate whether PPARγ expression in macrophages is affected by IgG-IC at mRNA level. As shown in **Figure 2A**, PPARγ expression in macrophages is decreased in a time-dependent manner within 6 h after onset of IgG-IC treatment. Even after 24 h of IgG-IC stimulation, PPARγ maintains at low level (**Figure 2A**). Furthermore, the above qPCR results are consistent with the data obtained from Western blot analysis (**Figure 2B**).

We then determine the effect of PPARγ on IgG-IC-stimulated pro-inflammatory mediators' generation by using PPARγ agonist Rosiglitasone (ROSI). We find that expressions of TNF-α, MCP-1 and MIP-1α at mRNA level are increased by 22-, 10-, and seven-folds, respectively in macrophages treated with IgG-IC (**Figures 2C–E**). ROSI treatment causes IgG-IC-mediated productions of TNF-α, MCP-1, and MIP-1α to decrease by 36%, 34%, and 32%, respectively (**Figures 2C–E**). We next verify the influence of ROSI on IgG-IC-initiated inflammatory reaction at protein level, and observe that the data obtained from ELISA are consistent with the qPCR results (**Figures 2F–H**).

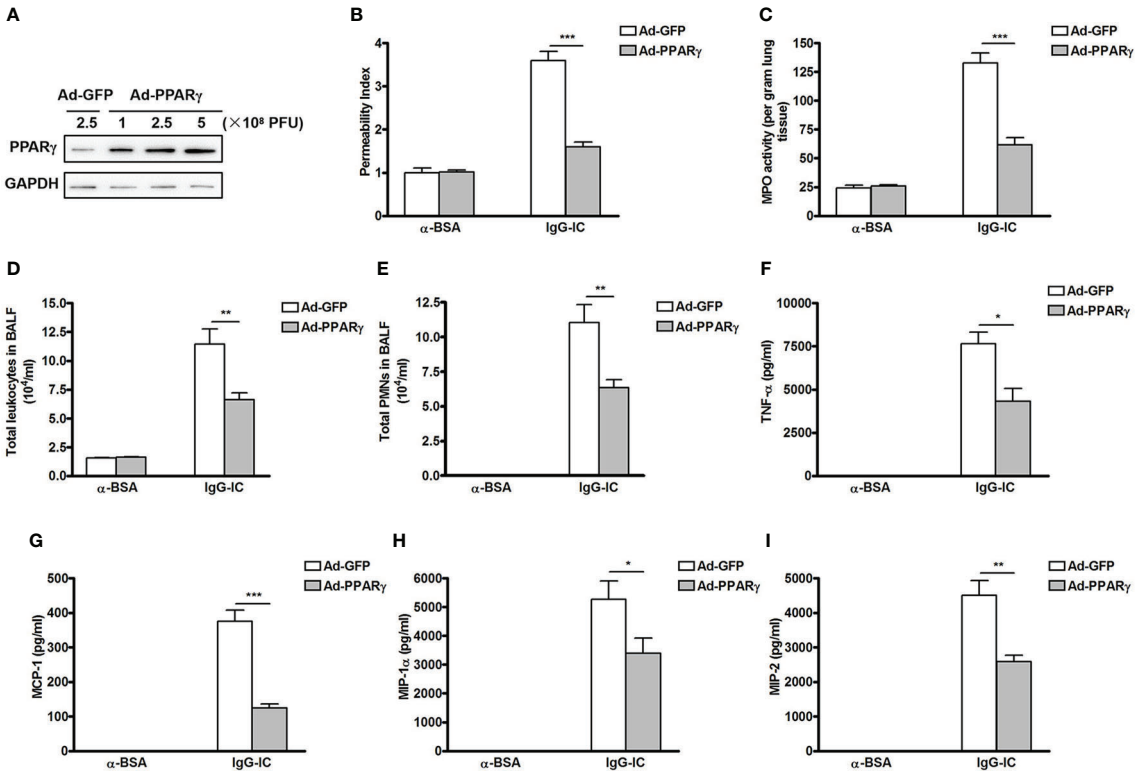

FIGURE 1 | Ectopic expression of peroxisome proliferator-activated receptor (PPAR)γ in the lung inhibits IgG immune complex (IgG-IC)-induced acute lung injury. **(A)** Different doses of adenovirus are injected into lungs *via* airways. Seventy-two hours later, lungs are harvested and total proteins are extracted. Then Western blot assays are conducted by using antibodies recognizing PPARγ and GAPDH, respectively. Mice are treated by airway administration of 1×10^8 PFU of Ad-GFP or Ad-PPARγ. Three days later, acute lung injury is induced by treating the mice with IgG-IC. Four hours later, bronchoalveolar lavage (BAL) fluids and whole lungs are collected to analyze lung permeability indexes **(B)**, measurement of pulmonary myeloperoxidase (MPO) contents **(C)**, total white blood cells **(D)**, and neutrophils counts **(E)** in BAL fluids, and levels of TNF-α **(F)**, MCP-1 **(G)**, MIP-1α **(H)**, and MIP-2 **(I)** in BAL fluids, respectively. Data are expressed as means ± S. E. M. N=3 for α-BSA-treated mice, N=5 for Ad-GFP+IgG-IC group, and N=6 for Ad-PPARγ+IgG-IC group. *, ** and *** indicate statistically significant difference—$p < 0.05$, $p < 0.01$, and $p < 0.001$, respectively.

To exclude the off-target effect of ROSI, we silence the expression of PPARγ in macrophages. As shown in **Figure 2I**, macrophages treated with PPARγ shRNA show a 73% decrease in PPARγ production when compared with the control cells. Of note, IgG-IC-mediated productions of TNF-α, MCP-1 and MIP-1α are no longer reduced by ROSI in macrophages expressing PPARγ specific shRNA (**Figures 2J–L**), indicating that ROSI negatively regulates IgG-IC-induced expressions of cytokine and chemokine *via* activating PPARγ.

Egr-1 Expression Is Reduced by PPARγ in Macrophages

To probe the mechanism by which PPARγ decreases IgG-IC-induced inflammatory response, we tend to find out a bridge molecule linking PPARγ with pro-inflammatory mediators. Time course experiment shows that Egr-1 mRNA level peaks after 6 h of IgG-IC stimulation, and then declines progressively (**Figure 3A**), which is consistent with Western blot results (**Figure 3B**). More importantly, we find that in the presence of IgG-IC, Egr-1 expression in ROSI-treated macrophages is only 37% of the control (**Figure 3C**). On the contrary, IgG-IC-stimulated Egr-1 expression is increased by approximately twofolds with downregulation of PPARγ production (**Figure 3D**), suggesting that Egr-1 might be the possible molecule connecting PPARγ with pro-inflammatory mediators.

Egr-1 Amplifies IgG-IC-Induced Expressions of Pro-Inflammatory Mediators in Macrophages by Binding to Their Promoter Regions

Egr-1 expression is controlled by PPARγ, but its effect on IgG-IC-triggered pro-inflammatory mediators' expressions remains elusive. Therefore, we first downregulate Egr-1 expression in macrophages by using lentivirus expressing Egr-1 specific shRNA (**Figure 4A**). In the presence of IgG-IC, TNF-α, MCP-1, and MIP-1α mRNA levels are increased by more than 20, 300, and 50 times, respectively (**Figures 4B–D**). Egr-1 shRNA treatment reduces the expressions of the above inflammatory mediators to 41%, 1%, and 74% of their respective controls (**Figures 4B–D**). Furthermore, the suppressive role of Egr-1 shRNA in inflammation is also confirmed at protein level in macrophages challenged by IgG-IC (**Figures 4E–G**).

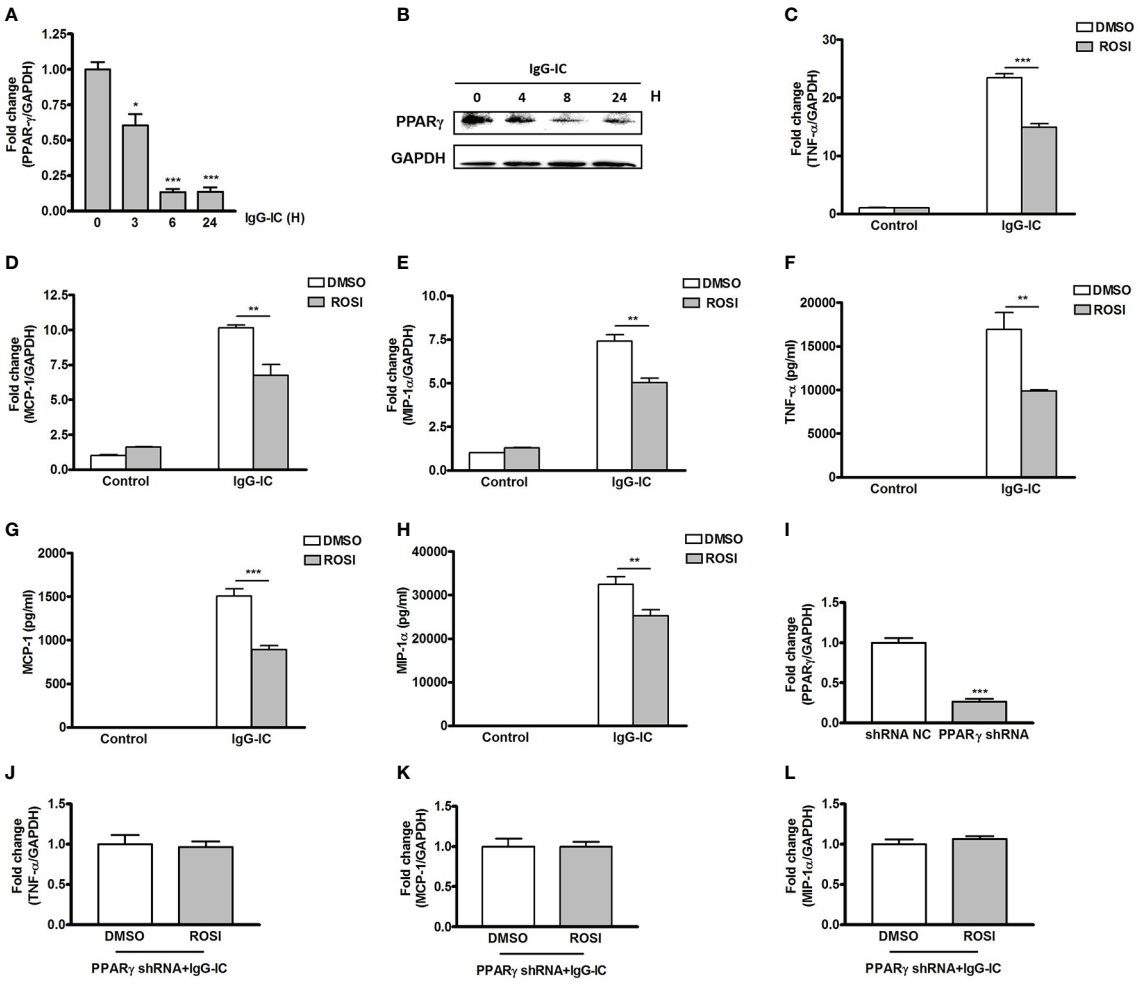

FIGURE 2 | Peroxisome proliferator-activated receptor (PPAR)γ decreases IgG immune complex (IgG-IC)-stimulated inflammatory response in macrophages. RAW264.7 cells are treated with 100 μg/ml of IgG-IC for different time points. Then RNAs and proteins are extracted, and qPCR **(A)** and Western blot **(B)** are performed to verify PPARγ generation at mRNA and protein levels, respectively. RAW264.7 cells are pre-treated with DMSO or 10 μM Rosiglitazon–ROSI. One hour later, the cells are further treated with IgG-IC. Then total cellular RNAs are isolated 4 h later, and cell-free supernatants are harvested 8 h later. TNF-α **(C, F)**, MCP-1 **(D, G),** and MIP-1α **(E, H)** expressions are examined at both RNA and protein levels. **(I)** RAW264.7 cells are infected by control or PPARγ shRNA lentiviral particles at a MOI of 30. Seventy-two hours later, the cells are treated with 3 μg/ml of puromycin. The survival cells are selected, and the knockdown efficiency is confirmed by qPCR. RAW264.7 cells expressing PPARγ shRNA are treated with DMSO or 10 μM ROSI for 1 h. Then the cells are treated with IgG-IC for 4 h, which is followed by measurement of TNF-α **(J)**, MCP-1 **(K)**, and MIP-1α **(L)** expressions. Data are expressed as means ± S. E. M. (N=3 for qPCR, and N=6 for ELISA). *, ** and *** indicate statistically significant difference—$p < 0.05$, $p < 0.01$, and $p < 0.001$, respectively.

To reveal the mechanism involved in Egr-1 regulation of pro-inflammatory mediators' generation, we firstly construct Egr-1 overexpression plasmid (**Figure 4H**). Then we investigate if productions of pro-inflammatory mediators are influenced by ectopic expression of Egr-1. As shown in **Figures 4I–K**, TNF-α, MCP-1, and MIP-1α promoter-driven luciferase activities are increased by Egr-1 to 242%, 277%, and 126% of their respective controls. According to software prediction (JASPAR), there are potential Egr-1 binding sites in the promoter regions of the above pro-inflammatory mediators. Thus, we further introduce mutations to the Egr-1 sites of the above inflammatory mediators' promoters, and find that Egr-1 site mutation causes TNF-α, MCP-1 and MIP-1α promoter-driven luciferase activities to decrease by 47%, 67%, and 47%, respectively (**Figures 4L–N**).

During IgG-IC-Induced Acute Lung Injury, Egr-1 Expression Is Reduced by PPARγ

To clarify the effect of PPARγ on Egr-1 expression *in vivo*, we first examine the production of Egr-1 during IgG-IC-induced acute lung injury. As shown in **Figure 5A**, Egr-1 mRNA level in the lung tissue is increased to 13.7-folds of the control group. Furthermore, IgG-IC also stimulates an obvious increase in Egr-1 protein expression when compared with the control treatment (**Figure 5B**). More importantly, during IgG-IC-induced acute lung injury, we find that mice receiving airway administration of

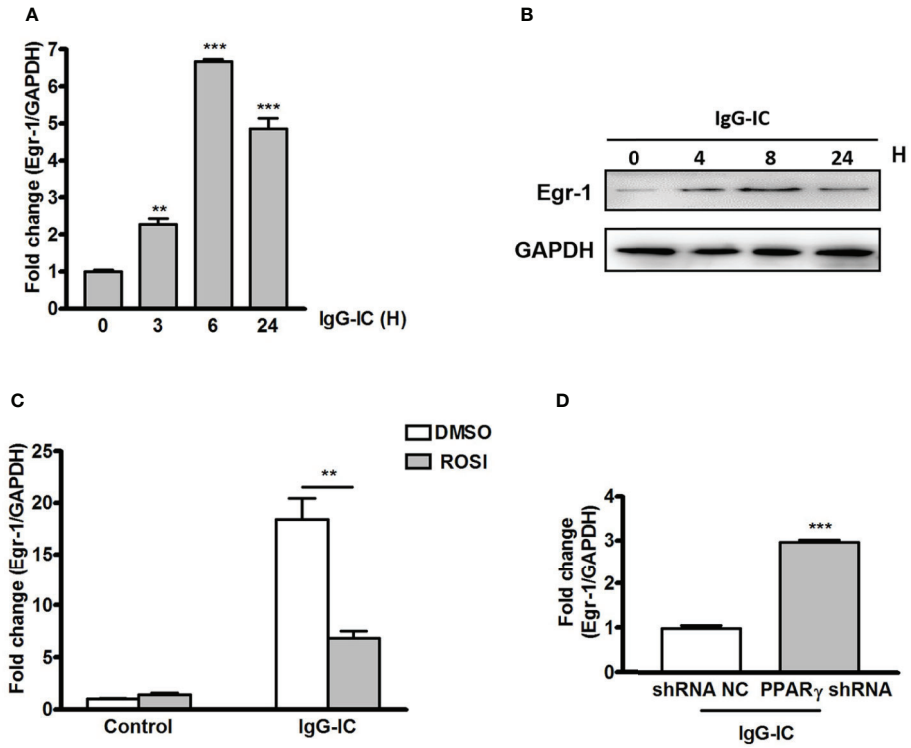

FIGURE 3 | Early growth response protein 1 (Egr-1) production is negatively regulated by peroxisome proliferator-activated receptor (PPAR)γ in macrophages. RAW264.7 cells are challenged by IgG immune complex (IgG-IC) for distinct time points. Then RNAs and proteins are extracted, and qPCR **(A)** and Western blot **(B)** are conducted to analyze Egr-1 expression. **(C)** RAW264.7 cells are pre-treated with DMSO or 10 μM Rosiglitazone (ROSI) for 1 h. Then the cells are incubated with IgG-IC for 3 h, and Egr-1 expression is examined. **(D)** RAW264.7 cells expressing control or PPARγ shRNA are treated with IgG-IC for 3 h, which is followed by measurement of Egr-1 generation. Data are expressed as means ± S. E. M. (N=3). ** and *** indicate statistically significant difference—$p < 0.01$, and $p < 0.001$, respectively.

Ad-PPARγ show a great reduction in Egr-1 generation when compared with their littermates treated by Ad-GFP (**Figure 5C**).

Egr-1 Aggravates IgG-IC-Induced Acute Lung Injury Through Amplifying Expressions of Pro-Inflammatory Mediators

Next, we analyze the role of Egr-1 in IgG-IC-induced acute lung injury by downregulating its expression with the lentiviral vector (25) (**Figure 6A**). Of note, lentiviral vector itself could not stimulate acute lung injury (**Figure S5**). We find that after airway deposition of IgG-IC, mice treated with Egr-1 shRNA display reduced tissue damage signs including lung permeability and MPO activity as compared with the control mice receiving shRNA NC treatment (**Figures 6B, C**). Additionally, IgG-IC-induced recruitment of white blood cells including neutrophils into the alveolar compartments is significantly relieved by downregulating Egr-1 expression in the lungs (**Figures 6D, E**).

Productions of pro-inflammatory mediators promote acute lung injury. So we examine the effect of Egr-1 on expressions of cytokine and chemokine. As shown in **Figures 6F–I**, IgG-IC stimulation dramatically elevates TNF-α, MCP-1, MIP-1α, and MIP-2 expressions in BAL fluids, which are significantly decreased with downregulation of Egr-1 generation in the lung tissue.

DISCUSSION

Due to lacking of specific therapy methods in clinic, the mortality rates of ALI/ARDS in the United States can be as high as 60%, despite the recent development of protective lung ventilation strategies (26, 27). Thus, we should further investigate the molecular mechanisms of ALI/ARDS to promote the development of specific therapies. In the present study, we utilize IgG-IC-induced acute lung injury model to reveal the underlying mechanism of acute lung injury. We have proved that IgG-IC treatment causes an obviously acute inflammatory response, characterized by the infiltration of neutrophils into the pulmonary tissue, and the elevated expressions of cytokine and chemokine, which are similar to clinical symptoms. Furthermore, we find that PPARγ-Egr-1-pro-inflammatory mediators axis is involved in IgG-IC-triggered pulmonary damage, and intervention of the axis might be a useful strategy for treatment of patients suffering from ALI/ARDS.

After intrapulmonary deposition of IgG-IC, local macrophages expressing high levels of Fcγ receptors, but not alveolar epithelial cells first perceive the stimulation. Then early response cytokines including TNF-α and IL-1β are released from the macrophages, which are crucial for stimulating lung endothelial cells to express adhesion molecules (28, 29). Moreover, the early response cytokines promote chemokine secretion in the lung tissue (30–32). Finally,

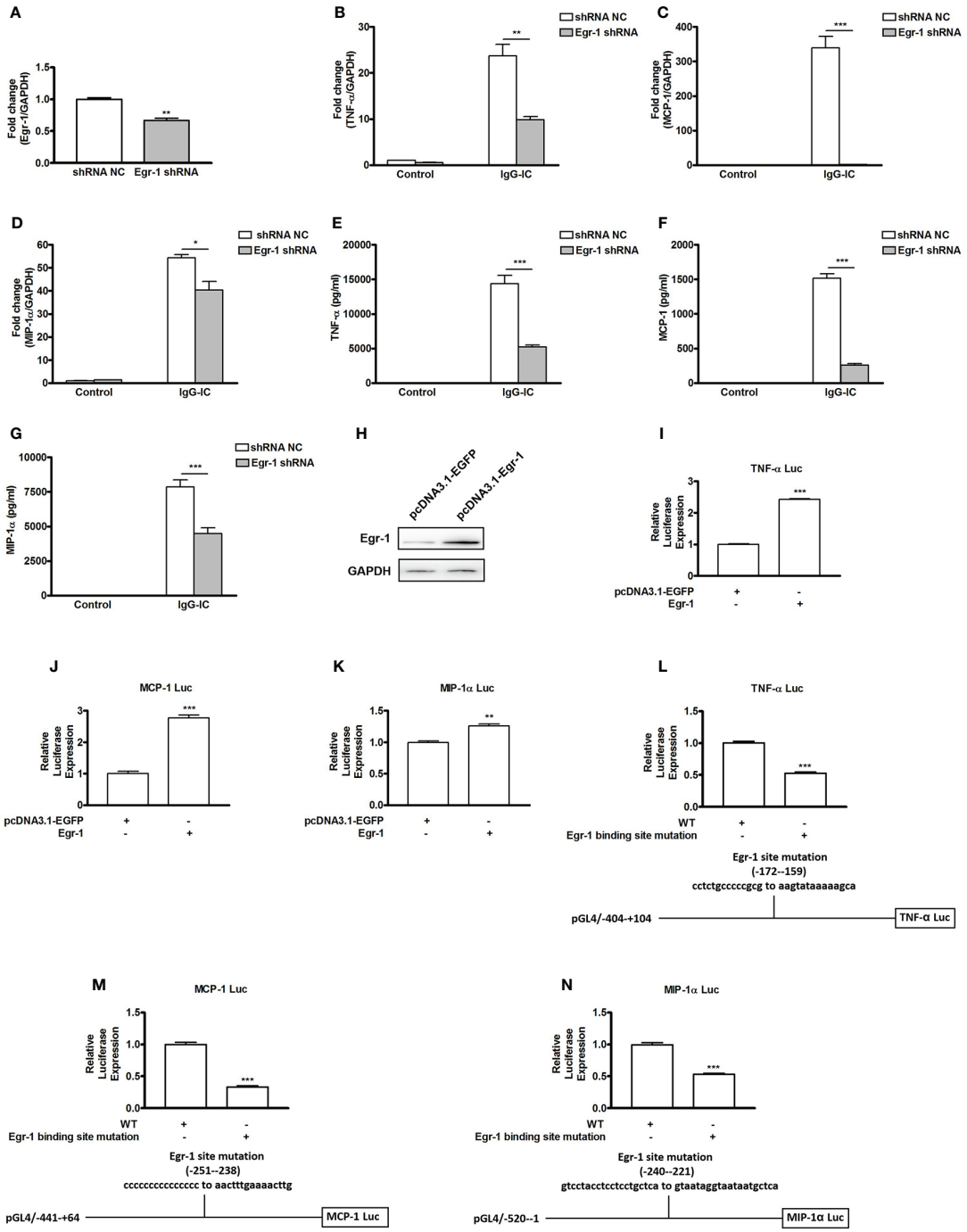

FIGURE 4 | Early growth response protein 1 (Egr-1) positively regulates IgG immune complex (IgG-IC)-triggered expressions of TNF-α, MCP-1, and MIP-1α in macrophages by binding to their promoter regions. **(A)** RAW264.7 cells are infected by control or Egr-1 shRNA lentiviral particles at a MOI of 30. Seventy-two hours later, the cells are treated with 3 μg/ml of puromycin. The survival cells are selected, and the knockdown efficiency is confirmed by qPCR. RAW264.7 cells expressing control or Egr-1 shRNA are treated with IgG-IC. Then RNAs and cell-free supernatants are harvested 4 and 8 h later, respectively. qPCR and ELISA are performed to analyze TNF-α **(B, E)**, MCP-1 **(C, F)**, and MIP-1α **(D, G)** expressions. **(H)** Egr-1-overexpressing plasmids are constructed, and confirmed in HEK293 cells by Western blot. **(I–N)** HEK293 cells are transfected with the indicated plasmids. Twenty-four hours later, the cells are lysed, and the lysates are subjected to luciferase assays. The detailed information about the luciferase-expressing constructs is indicated in the figures. The data are calculated by dividing the value of the indicated promoter-driven firefly luciferase by the corresponding value of thymidine kinase promoter-driven renilla luciferase, and then set to 1 in control cells. Data are expressed as means ± S. E. M. (N=3 for qPCR and luciferase assays, and N=6 for ELISA). *, ** and *** indicate statistically significant difference—$p < 0.05$, $p < 0.01$, and $p < 0.001$, respectively.

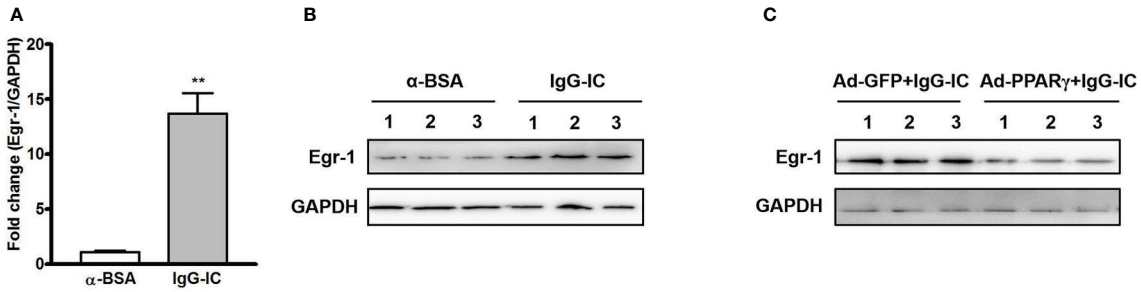

FIGURE 5 | IgG immune complex (IgG-IC)-mediated pulmonary early growth response protein 1 (Egr-1) expression is inhibited by ectopic production of peroxisome proliferator-activated receptor (PPAR)γ. Four hours after pulmonary deposition of IgG-IC, lungs are harvested. The tissue RNAs and proteins are isolated separately. Then the Egr-1 expression is examined by qPCR **(A)** and Western blot **(B)**, respectively. **(C)** Mice are treated with airway injection of Ad-GFP or Ad-PPARγ at a dose of 1×10^8 PFU. Seventy-two hours later, the mice are intratracheally challenged by IgG-IC for 4 h. Then the lungs are harvested, and proteins are extracted for Western blot analysis by using antibodies against Egr-1 and GAPDH, respectively. Data are expressed as means ± S. E. M. (For qPCR, N=3 for α-BSA treated mice, and N=5 for IgG-IC-treated mice; N=3 for Western blot). ** indicates statistically significant difference—$p < 0.01$.

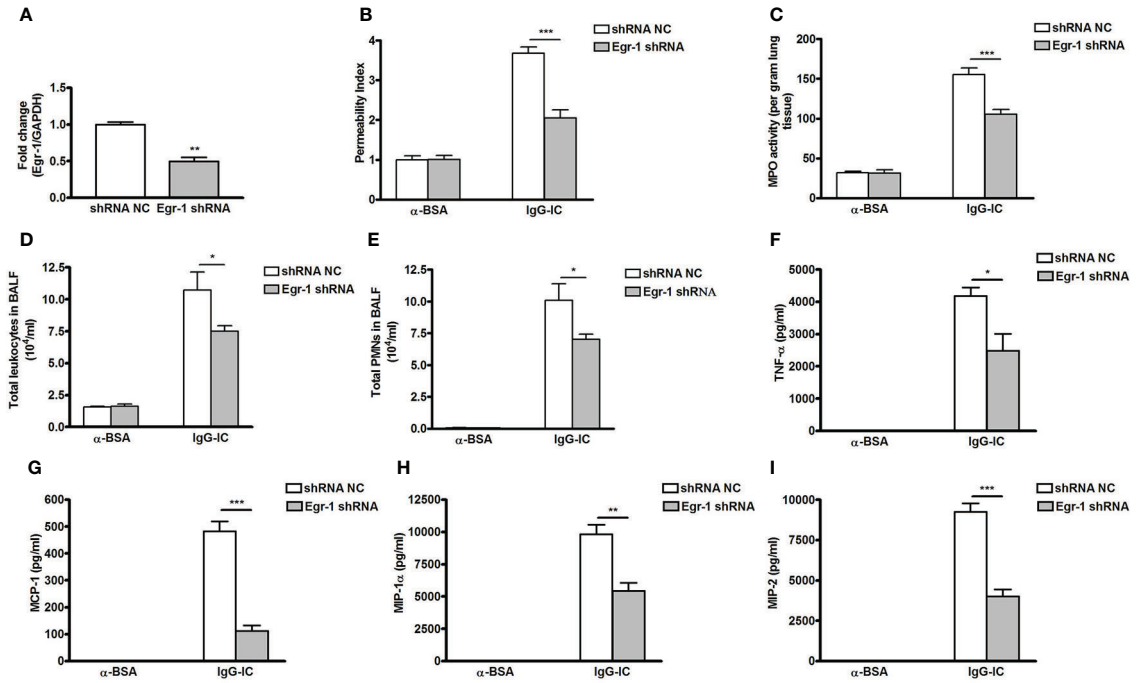

FIGURE 6 | Downregulating early growth response protein 1 (Egr-1) expression attenuates IgG immune complex (IgG-IC)-mediated acute lung injury. **(A)** Lentiviruses (3×10^7 TU—transduction unit) expressing control or Egr-1 shRNA are injected into mouse lungs through airways. Five days later, the lungs are harvested, and RNAs are extracted, which is followed by verification of Egr-1 expression by qPCR. Mice infected by control or Egr-1 shRNA lentiviral particles are intratracheally treated by IgG-IC for 4 h. Then bronchoalveolar lavage (BAL) fluids and whole lungs are harvested. Lung permeability index **(B)**, and measurement of pulmonary myeloperoxidase (MPO) activities **(C)** in whole lungs are measured. In addition, influxes of total leukocytes **(D)** and neutrophils **(E)** into alveolar spaces are counted. Also, productions of TNF-α **(F)**, MCP-1 **(G)**, MIP-1α **(H)**, and MIP-2 **(I)** in BAL fluids are assayed. Data are expressed as means ± S. E. M. (N=3 for qPCR; For ELISA, N=3 for α-BSA-treated mice, N=5 for shRNA NC+IgG-IC group, and N=6 for Egr-1 shRNA+IgG-IC group). *, ** and *** indicate statistically significant difference—$p < 0.05$, $p < 0.01$, and $p < 0.001$, respectively.

pulmonary injury and massive influx of neutrophils into the lung tissue are induced by the joint action of a variety of inflammation-related mediators including cytokines, chemokines and adhesion molecules. Actually, all the above processes are controlled by the network composed of various transcription factors. There are reports that the DNA binding activities of NF-κB and AP-1 are increased during IgG-IC-induced acute lung injury (31, 33). Both transcription factors can directly bind to a broad spectrum of pro-inflammatory mediators' promoter regions, and increase their productions. In addition, our findings demonstrate that both C/EBPβ and C/EBPδ, which belong to C/EBP family members, can increase IgG-IC-induced inflammation *via* association with the C/

EBP elements in the promoter regions of inflammatory genes (34, 35). In the present study, we find that PPARγ expression is significantly downregulated following IgG-IC treatment. However, as an important transcription factor, the role of PPARγ in IgG-IC-initiated inflammation has not been determined.

In the current paper, we find that PPARγ inhibits IgG-IC-induced TNF-α, MCP-1 and MIP-1α productions *in vitro* and *in vivo*. Previous studies have proved that PPARγ activation alleviates postoperative ileus-related gene expression through suppression of Egr-1 production (36). Also, Rosiglitazone-mediated PPARγ activation inhibits Egr-1 generation, leading to suppression of bleomycin-induced scleroderma and profibrotic responses (37). Thus, during IgG-IC-induced inflammatory responses, Egr-1 might be the potential bridge molecule linking PPARγ with pro-inflammatory mediators' productions. We find that Egr-1 expressions in macrophages and lungs are greatly upregulated by IgG-IC treatment. In addition, we observe that activation of PPARγ decreases Egr-1 expression, while lowing PPARγ level increases its generation, indicating that Egr-1 is negatively regulated by PPARγ. Furthermore, we demonstrate that during IgG-IC-induced acute inflammatory response, expressions of pro-inflammatory mediators are positively regulated by Egr-1. Thus, during IgG-IC-induced acute lung injury, PPARγ can negatively regulate IgG-IC-induced inflammation through an indirect way, which is similar to the method used by STAT3 (38). Of note, during IgG-IC-mediated acute lung injury, whether there are other PPARγ-regulated transcription factors that directly control inflammation responses remains an open question.

Egr-1, a critical transcription factor, belongs to the EGR family of Cys2His2-type zinc finger proteins. It is composed of transactivation and inhibitory domains, as well as three DNA-binding zinc finger domains which interact with GC-rich regions in the promoters of target genes (39). Its roles in lung diseases, especially in chronic lung diseases have been widely reported. Lee et al. find that Egr-1-mediated cell apoptosis is crucial for TGF-β-elicited lung fibrosis (40), indicating that Egr-1 plays a detrimental role in the disease. In contrast, Kramer et al. report that the deficiency of Egr-1 obviously exacerbates TGF-α-induced pulmonary fibrosis, which is independent of the tissue inflammatory response (41), which manifests the protective effect of Egr-1 in the disease. The above contradictory phenomena might be explained by the distinct stimulus used in the model. Therefore, the role of Egr-1 is complicated, and should be discussed in specific contexts. In the present paper, we observe that Egr-1 accelerates inflammation induced by IgG-IC through association with the promoter regions of pro-inflammatory mediators including TNF-α, MCP-1 and MIP-1α. Our previous data have demonstrated that the activities of both p38 MAPK and ERK1/2 are elicited, and are essential for cytokine/chemokine expressions during IgG-IC-induced inflammation (34). Others find that p38 MAPK activation is required for Egr-1-dependent expressions of pro-inflammatory mediators (42). Moreover, there are data that the IL-33-ERK/JNK/p38/Egr-1/TSLP (thymic stromal lymphopoietin) axis is involved in allergic skin Th2 inflammation (43). Thus, we speculate that there may be crosstalk between MAPK signaling pathway and PPARγ-Egr-1 axis during inflammatory reactions triggered by IgG-IC. However, this remains an open question, which should be supported by more studies. Additionally, the role of the inhibitory domain of Egr-1 in IgG-IC-induced inflammation should also be examined in the future.

On the basis of our present data, we conclude that PPARγ protects against the development of IgG-IC-induced acute lung injury through the reduction of inflammatory responses. This protection afforded by PPARγ features reduced cytokine/chemokine expressions and accumulation of neutrophils in the lung tissue. Furthermore, the anti-inflammatory effects of PPARγ after intrapulmonary deposition of IgG-IC are mediated by inhibiting generation of Egr-1, which can bind to the promoter regions of pro-inflammatory mediators including TNF-α, MCP-1, and MIP-1α. Therefore, PPARγ activation might represent a promising therapeutic option for IgG-IC-induced acute lung injury. Though PPARγ agonist Rosiglitazone has been used for treatment of type 2 diabetes in clinic, whether the protective effects of PPARγ detected in the animal model could be extrapolated to the clinical application is subject to the future clinical trials.

DATA AVAILABILITY STATEMENT

The raw data supporting the conclusions of this article will be made available by the authors, without undue reservation.

ETHICS STATEMENT

The animal study was reviewed and approved by Animal Experimental Ethical Committee of Southeast University.

AUTHOR CONTRIBUTIONS

CY, JC, YD, ZZ, BL, CD, and DY performed experiments. CY, QZ, and XW designed the experiments. CY and XW drafted the article. All authors contributed to the article and approved the submitted version.

FUNDING

This project is supported by the National Natural Science Foundation of China (grant numbers 81971858 and 31400751), Fundamental Research Funds for the Central Universities (grant number 3224002002C1), and the Scientific and Technological Project of Jintan District (grant number KJ201923).

SUPPLEMENTARY MATERIAL

The Supplementary Material for this article can be found online at: https://www.frontiersin.org/articles/10.3389/fimmu.2021.634889/full#supplementary-material

REFERENCES

1. Nydegger UE, Lambert PH, Gerber H, Miescher PA. Circulating Immune Complexes in the Serum in Systemic Lupus Erythematosus and in Carriers of Hepatitis B Antigen. Quantitation by binding to radiolabeled C1q. *J Clin Invest* (1974) 54:297–309. doi: 10.1172/JCI107765
2. Zubler RH, Nydegger U, Perrin LH, Fehr K, McCormick J, Lambert PH, et al. Circulating and intra-articular immune complexes in patients with rheumatoid arthritis. Correlation of 125I-Clq binding activity with clinical and biological features of the disease. *J Clin Invest* (1976) 57:1308–19. doi: 10.1172/JCI108399
3. Nangaku M, Couser WG. Mechanisms of immune-deposit formation and the mediation of immune renal injury. *Clin Exp Nephrol* (2005) 9:183–91. doi: 10.1007/s10157-005-0357-8
4. McInnes IB, Schett G. The Pathogenesis of Rheumatoid Arthritis. *N Engl J Med* (2011) 365:2205–19. doi: 10.1056/NEJMra1004965
5. Tsokos GC. Systemic Lupus Erythematosus. *N Engl J Med* (2011) 365:2110–21. doi: 10.1056/NEJMra1100359
6. Hijikata M, Shimizu YK, Kato H, Iwamoto A, Shih JW, Alter HJ, et al. Equilibrium centrifugation studies of hepatitis C virus: evidence for circulating immune complexes. *J Virol* (1993) 67:1953–8. doi: 10.1128/JVI.67.4.1953-1958.1993
7. Sansonno D, Dammacco F. Hepatitis C virus, cryoglobulinemia, and vasculitis: immune complex reactions. *Lancet Infect Dis* (2005) 5:227–36. doi: 10.1016/S1473-3099(05)70053-0
8. Bosmann M, Ward PA. Role of C3, C5 and anaphylatoxin receptors in acute lung injury and in sepsis. *Adv Exp Med Biol* (2012) 946:147–59. doi: 10.1007/978-1-4614-0106-3_9
9. Gao H, Neff T, Ward PA. Regulation of lung inflammation in the model of IgG immune-complex injury. *Annu Rev Pathol* (2006) 1:215–42. doi: 10.1146/annurev.pathol.1.110304.100155
10. Xie XM, Li SJ, Zhu YT, Liu L, Pan YL, Wang J, et al. MicroRNA-27a/b mediates endothelin-1-induced PPARγ reduction and proliferation of pulmonary artery smooth muscle cells. *Cell Tissue Res* (2017) 369:527–39. doi: 10.1007/s00441-017-2625-9
11. Xie XM, Li SJ, Zhu YT, Liu L, Ke R, Wang J, et al. Egr-1 mediates leptin-induced PPARγ reduction and proliferation of pulmonary artery smooth muscle cells. *Mol Biol Cell* (2018) 29:356–62. doi: 10.1091/mbc.E17-03-0141
12. Lu J, Liu L, Zhu YT, Zhang YH, Wu YY, Wang GZ, et al. PPAR-γ inhibits IL-13-induced collagen production in mouse airway fibroblasts. *Eur J Pharmacol* (2014) 737:133–9. doi: 10.1016/j.ejphar.2014.05.008
13. Yao Q, Liu J, Xiao L, Wang N. Peroxisome proliferator–activated receptor γ (PPARγ) induces the gene expression of integrin αVβ5 to promote macrophage M2 polarization. *J Biol Chem* 293(43):16572–82 (2018). doi: 10.1074/jbc.RA118.003161
14. Mukherjee R, Davies PJ, Crombie DL, Bischoff ED, Cesario RM, Jow L, et al. Sensitization of diabetic and obese mice to insulin by retinoid X receptor agonists. *Nature* (1997) 386:407–10. doi: 10.1038/386407a0
15. Gabunia K, Ellison S, Kelemen S, Kako F, Cornwell WD, Rogers TJ, et al. IL-19 halts progression of atherosclerotic plaque, polarizes, and increases cholesterol uptake and efflux in macrophages. *Am J Pathol* (2016) 186:1361–74. doi: 10.1016/j.ajpath.2015.12.023
16. Micosse C, von Meyenn L, Steck O, Kipfer E, Adam C, Simillion C, et al. Between Line 1176 and 1177: Human "TH9" cells are a subpopulation of PPAR-γ+ TH2 cells. *Sci Immunol* (2019) 4(31):1–13. doi: 10.1126/sciimmunol.aat5943
17. Reddy AT, Lakshmi SP, Banno A, Reddy RC. Role of GPx3 in PPARγ-induced protection against COPD-associated oxidative stress. *Free Radic Biol Med* (2018) 126:350–7. doi: 10.1016/j.freeradbiomed.2018.08.014
18. Hoetzel A, Dolinay T, Vallbracht S, Zhang YZ, Kim HP, Ifedigbo E, et al. Carbon monoxide protects against ventilator-induced lung injury via PPAR-γ and inhibition of Egr-1. *Am J Resp Crit Care* (2008) 177:1223–32. doi: 10.1164/rccm.200708-1265OC
19. He X, Hu JL, Li J, Zhao L, Zhang Y, Zeng YJ, et al. A feedback loop in PPARγ–adenosine A2A receptor signaling inhibits inflammation and attenuates lung damages in a mouse model of LPS-induced acute lung injury. *Cell Signal* (2013) 25:1913–23. doi: 10.1016/j.cellsig.2013.05.024
20. Wang GZ, Liu L, Zhang YH, Han D, Lu JM, Xu J, et al. Activation of PPARγ attenuates LPS-induced acute lung injury by inhibition of HMGB1-RAGE levels. *Eur J Pharmacol* (2014) 726:27–32. doi: 10.1016/j.ejphar.2014.01.030
21. Bhattacharyya S, Wu M, Fang F, Tourtellotte W, Feghali-Bostwick C, Varga J. Early growth response transcription factors: key mediators of fibrosis and novel targets for anti-fibrotic therapy. *Matrix Biol* (2011) 30:235–42. doi: 10.1016/j.matbio.2011.03.005
22. Li CJ, Ning W, Matthay MA, Feghali-Bostwick CA, Choi AM. MAPK pathway mediates EGR-1-HSP70-dependent cigarette smoke-induced chemokine production. *Am J Physiol Lung Cell Mol Physiol* (2007) 292:L1297–1303. doi: 10.1152/ajplung.00194.2006
23. Wang J, Cheng W, Wang Z, Xin L, Zhang W. ATF3 inhibits the inflammation induced by Mycoplasma pneumonia in vitro and in vivo. *Pediatr Pulmonol* (2017) 52:1163–70. doi: 10.1002/ppul.23705
24. Gao H, Hoesel LM, Guo RF, Rancilio NJ, Sarma JV, Ward PA. Adenoviral-mediated overexpression of SOCS3 enhances IgG immune complex-induced acute lung injury. *J Immunol* (2006) 177:612–20. doi: 10.4049/jimmunol.177.1.612
25. Wilson AA, Kwok LW, Porter EL, Payne JG, McElroy GS, Ohle SJ, et al. Lentiviral delivery of RNAi for in vivo lineage-specific modulation of gene expression in mouse lung macrophages. *Mol Ther* (2013) 21:825–33. doi: 10.1038/mt.2013.19
26. Goss CH, Brower RG, Hudson LD, Rubenfeld GD. Incidence of acute lung injury in the United States. *Crit Care Med* (2003) 31:1607–11. doi: 10.1097/01.CCM.0000063475.65751.1D
27. Angus DC, Linde-Zwirble WT, Lidicker J, Clermont G, Carcillo J, Pinsky MR. Epidemiology of severe sepsis in the United States: analysis of incidence, outcome, and associated costs of care. *Crit Care Med* (2001) 29:1303–10. doi: 10.1097/00003246-200107000-00002
28. Mulligan MS, Varani J, Dame MK, Lane CL, Smith CW, Anderson DC, et al. Role of endothelial-leukocyte adhesion molecule 1 (ELAM-1) in neutrophil-mediated lung injury in rats. *J Clin Invest* (1991) 88:1396–406. doi: 10.1172/JCI115446
29. Mulligan MS, Vaporciyan AA, Miyasaka M, Tamatani T, Ward PA. Tumor necrosis factor alpha regulates in vivo intrapulmonary expression of ICAM-1. *Am J Pathol* (1993) 142:1739–49. doi: 10.1097/00000433-199306000-00019
30. Guo RF, Ward PA. Mediators and regulation of neutrophil accumulation in inflammatory responses in lung: insights from the IgG immune complex model. *Free Radic Biol Med* (2002) 33:303–10. doi: 10.1016/S0891-5849(02)00823-7
31. Lentsch AB, Czermak BJ, Bless NM, Ward PA. NF-κB activation during IgG immune complex-induced lung injury: Requirements for TNF-α and IL-1β but not complement. *Am J Pathol* (1998) 152:1327–36. doi: 10.1016/S0098-1354(97)00258-5
32. Czermak BJ, Lentsch AB, Bless NM, Schmal H, Friedl HP, Ward PA. Synergistic enhancement of chemokine generation and lung injury by C5a or the membrane attack complex of complement. *Am J Pathol* (1999) 154:1513–24. doi: 10.1016/S0002-9440(10)65405-3
33. Guo RF, Lentsch AB, Sarma JV, Sun L, Riedemann NC, McClintock SD, et al. Activator Protein-1 Activation in Acute Lung Injury. *Am J Pathol* (2002) 161:275–82. doi: 10.1016/S0002-9440(10)64179-X
34. Yan C, Zhu M, Staiger J, Johnson PF, Gao H. C5a-regulated CCAAT/Enhancer-binding Proteins β and δ Are Essential in Fcγ Receptor-mediated Inflammatory Cytokine and Chemokine Production in Macrophages. *J Biol Chem* (2012) 287:3217–30. doi: 10.1074/jbc.M111.280834
35. Yan C, Wu M, Cao J, Tang H, Zhu M, Johnson PF, et al. Critical role for CCAAT/enhancer-binding protein β in immune complex-induced acute lung injury. *J Immunol* (2012) 189:1480–90. doi: 10.4049/jimmunol.1200877
36. De Backer O, Elinck E, Priem E, Leybaert L, Lefebvre RA. Peroxisome proliferator-activated receptor gamma activation alleviates postoperative ileus in mice by inhibition of Egr-1 expression and its downstream target genes. *J Pharmacol Exp Ther* (2009) 331:496–503. doi: 10.1124/jpet.109.155135
37. Wu M, Melichian DS, Chang E, Warner-Blankenship M, Ghosh AK, Varga J. Rosiglitazone Abrogates Bleomycin-Induced Scleroderma and Blocks Profibrotic Responses Through Peroxisome Proliferator-Activated Receptor-γ. *Am J Pathol* (2009) 174:519–33. doi: 10.2353/ajpath.2009.080574

38. Tang H, Yan C, Cao J, Sarma JV, Haura EB, Wu M, et al. An essential role for Stat3 in regulating IgG immune complex-induced pulmonary inflammation. *FASEB J* (2011) 25:4292–300. doi: 10.1096/fj.11-187955
39. Gashler A, Sukhatme VP. Early growth response protein 1 (Egr-1): prototype of a zinc-finger family of transcription factors. *Prog Nucleic Acid Res Mol Biol* (1995) 50:191–224. doi: 10.1016/S0079-6603(08)60815-6
40. Lee CG, Cho SJ, Kang MJ, Chapoval SP, Lee PJ, Noble PW, et al. Early Growth Response Gene 1-mediated Apoptosis Is Essential for Transforming Growth Factor 1-induced Pulmonary Fibrosis. *J Exp Med* (2004) 200:377–89. doi: 10.1084/jem.20040104
41. Kramer EL, Mushaben EM, Pastura PA, Acciani TH, Deutsch GH, Khurana Hershey GK, et al. Early growth response-1 suppresses epidermal growth factor receptor-Mediated Airway Hyperresponsiveness and Lung Remodeling in Mice. *Am J Respir Cell Mol Biol* (2009) 41:415–25. doi: 10.1165/rcmb.2008-0470OC
42. Braun L, Brenier-Pinchart MP, Yogavel M, Curt-Varesano A, Curt-Bertini RL, Hussain T, et al. AToxoplasmadense granule protein, GRA24, modulates the early immune response to infection by promoting a direct and sustained host p38 MAPK activation. *J Exp Med* (2013) 210:2071–86. doi: 10.1084/jem.20130103
43. Ryu WII, Lee H, Kim JH, Bae HC, Ryu HJ, Son SW. IL-33 induces Egr-1-dependent TSLP expression via the MAPK pathways in human keratinocytes. *Exp Dermatol* (2015) 24:857–63. doi: 10.1111/exd.12788

Conflict of Interest: The authors declare that the research was conducted in the absence of any commercial or financial relationships that could be construed as a potential conflict of interest.

Copyright © 2021 Yan, Chen, Ding, Zhou, Li, Deng, Yuan, Zhang and Wang. This is an open-access article distributed under the terms of the Creative Commons Attribution License (CC BY). The use, distribution or reproduction in other forums is permitted, provided the original author(s) and the copyright owner(s) are credited and that the original publication in this journal is cited, in accordance with accepted academic practice. No use, distribution or reproduction is permitted which does not comply with these terms.

frontiers in Immunology

ORIGINAL RESEARCH
published: 25 February 2021
doi: 10.3389/fimmu.2021.643144

GIPR Signaling in Immune Cells Maintains Metabolically Beneficial Type 2 Immune Responses in the White Fat From Obese Mice

Irina Efimova[1,2], Inbar Steinberg[1,2], Isabel Zvibel[1], Anat Neumann[1,2], Dana Fernanda Mantelmacher[1], Daniel J. Drucker[3], Sigal Fishman[1†] and Chen Varol[1,2*†]*

[1] The Research Center for Digestive Tract and Liver Diseases, Tel-Aviv Sourasky Medical Center Affiliated to Tel-Aviv University, Tel Aviv, Israel, [2] Department of Clinical Microbiology and Immunology, Sackler School of Medicine, Tel-Aviv University, Tel-Aviv, Israel, [3] The Lunenfeld-Tanenbaum Research Institute, Mount Sinai Hospital, University of Toronto, Toronto, ON, Canada

OPEN ACCESS

Edited by:
Amiram Ariel, University of Haifa, Israel

Reviewed by:
Makoto Fukuda, Baylor College of Medicine, United States
Dmitry Namgaladze, Goethe University Frankfurt, Germany

***Correspondence:**
Chen Varol
chenv@tlvmc.gov.il
Sigal Fishman
sigalf@tlvmc.gov.il

†These authors have contributed equally to this work and share last authorship

Specialty section:
This article was submitted to Inflammation, a section of the journal Frontiers in Immunology

Received: *17 December 2020*
Accepted: *14 January 2021*
Published: *25 February 2021*

Citation:
Efimova I, Steinberg I, Zvibel I, Neumann A, Mantelmacher DF, Drucker DJ, Fishman S and Varol C (2021) GIPR Signaling in Immune Cells Maintains Metabolically Beneficial Type 2 Immune Responses in the White Fat From Obese Mice. Front. Immunol. 12:643144. doi: 10.3389/fimmu.2021.643144

Glucose-dependent insulinotropic polypeptide (GIP) communicates information on energy availability from the gut to peripheral tissues. Disruption of its signaling in myeloid immune cells during high-fat diet (HFD)-induced obesity impairs energy homeostasis due to the unrestrained metabolically deleterious actions of S100A8/A9 alarmin. White adipose tissue (WAT) type 2 immune cell networks are important for maintaining metabolic and energy homeostasis and limiting obesity-induced inflammation. Nevertheless, the consequences of losing immune cell GIP receptor (GIPR) signaling on type 2 immunity in WAT remains unknown. Bone marrow (BM) chimerism was used to generate mice with GIPR ($Gipr^{-/-}$ BM) and GIPR/S100A8/A9 ($Gipr^{-/-}/S100a9^{-/-}$ BM) deletion in immune cells. These mice were subjected to short (5 weeks) and progressive (14 weeks) HFD regimens. GIPR-deficiency was also targeted to myeloid cells by crossing $Gipr^{fl/fl}$ mice and $Lyz2^{cre/+}$ mice ($LysM^{\Delta Gipr}$). Under both short and progressive HFD regimens, $Gipr^{-/-}$ BM mice exhibited altered expression of key type 2 immune cytokines in the epididymal visceral WAT (epiWAT), but not in subcutaneous inguinal WAT. This was further linked to declined representation of type 2 immune cells in epiWAT, such as group 2 innate lymphoid cells (ILC2), eosinophils, and $FOXP3^{+}$ regulatory T cells (Tregs). Co-deletion of S100A8/A9 in $Gipr^{-/-}$ immune cells reversed the impairment of type 2 cytokine expression in epiWAT, suggesting a mechanistic role for this alarmin in type 2 immune suppression. $LysM^{\Delta Gipr}$ mice on HFD also displayed altered expression of type 2 immune mediators, highlighting that GIPR-deficiency in myeloid immune cells is responsible for the impairment of type 2 immune networks. Finally, abrogated GIPR signaling in immune cells also affected adipocyte fraction cells, inducing their increased production of the beiging interfering cytokine IL-10 and stress- related type 2 cytokine IL-13. Collectively, these findings attribute an important role for GIPR in myeloid immune cells in supporting WAT type 2 immunity.

Keywords: glucose-dependent insulinotropic polypeptide receptor, obesity, type 2 immunity, white adipose tissue, S100A8/A9

INTRODUCTION

Integrated immunometabolic responses couple dietary intake, energy utilization, and storage to immune regulation of tissue function, and are therefore essential for the maintenance and restoration of homeostasis (1). Enteroendocrine cells (EECs) are strategically positioned along the entire gastrointestinal tract, where upon sensing ingested food, they produce hormonal messengers that transmit signals of nutrient availability to the brain and to metabolically important peripheral sites to allow the host to prioritize storage and/or utilize substrates for tissue growth, maintenance, and immune responses (2). Two gut hormones, Glucagon-like Peptide-1 (GLP-1) and Glucose-Dependent Insulinotropic Polypeptide (GIP), secreted by gut L and K cells, respectively, have attracted great interest in view of their metabolic roles and therapeutic potential (3, 4). Both hormones are known for their glucose-dependent insulinotropic actions on the pancreas *via* G-protein coupled receptors expressed on pancreatic islet cells (the incretin effect) (3). In addition, they both perform extra-pancreatic actions and differentially control metabolic homeostasis by modulation of satiety and food intake, potentially affecting energy expenditure (5).

Multiple immune cell subsets express receptors for both GLP-1 and GIP, pinpointing the immune system as another target for incretin action (6, 7). However, there is comparatively little comprehension of the precise roles of incretins in the control of immunometabolism. Specifically, the directional importance of GIP in obesity-associated inflammatory responses is surrounded by controversy, with studies reporting both pro- (8, 9) and anti-inflammatory (10, 11) effects in the white adipose tissue (WAT). These opposing results likely reflect the integrated pleiotropic functions of GIP in different tissues and cells, and the utilization in many studies of GIP analogues that can serve as both agonists and antagonists (12). Therefore, studying GIP biology in a cell-specific manner can benefit our comprehension of its immunometabolic pathways. In this respect, we have recently discovered a direct role for GIP in myeloid immune cells critical for controlling inflammation and body weight (11, 13). In contrast to the overall metabolic protection of mice with stimuli global germline inactivation of the GIPR (14), bone marrow (BM) chimeric mice with immune cell-targeted GIPR-deficiency (*Gipr*$^{-/-}$ BM) display greater weight gain during HFD feeding, despite similar food intake, concomitantly with increased insulin resistance and hepatic steatosis (13).

Thermogenesis is a process that dissipates energy as heat, and takes place in brown adipose tissue (BAT) and also in brown-like adipocytes (termed "beige" cells) in the inguinal WAT (ingWAT). Beige cells are generated from precursors or mature adipocytes in response to certain stimuli like chronic cold exposure, prolonged β-adrenergic stimulation or increased calorie intake (15, 16). Non-shivering thermogenesis generated by brown adipocytes and beiging is recognized as a relevant human physiological mechanism to offset obesity. The increased weight gain displayed by HFD-fed *Gipr*$^{-/-}$ BM is a result of impaired energy expenditure due to reduced ingWAT beiging (13). Targeting GIPR-deficiency to myeloid immune cells further pinpointed a mechanistic role for GIP in restraining the production of the alarmin S100A8/A9 (calprotectin), which hampers adaptive thermogenesis and ingWAT beiging. Nevertheless, the precise comprehension of how disruption of GIPR signaling in immune cell impairs energy balance remains elusive.

Type 2 immune cell networks are important for maintaining metabolic homeostasis and energy balance (17). Accordingly, eosinophil-derived IL-4 was suggested to maintain alternative M2 activation of adipose tissue macrophages (ATMs) to facilitate ingWAT beiging (18, 19), though other studies have challenged the contribution of ATMs to adaptive thermogenesis (20). Group 2 innate lymphoid cells (ILC2s) residing in the lean WAT activate eosinophils *via* IL-5 secretion and polarize ATMs towards M2 phenotype *via* IL-13 production (21, 22). ILC2s have also been shown to directly promote adipocyte beiging *via* production of Methionine-Enkephalin (MetEnk) peptides that upregulate UCP1 expression in adipocytes. The alarmin IL-33 is critical for priming the pro-beiging activity of ILC2s in WAT (21, 23). This type 2 cytokine also promotes proliferation of ST2 (IL-33 receptor)-expressing Tregs (24, 25), and acts directly on adipocytes to promote beiging and thermogenesis, thereby offsetting obesity (24, 26). IL-33 is locally produced within the epididymal visceral adipose tissue (epiWAT) mainly by mesenchymal stromal cell subtypes (27, 28). In light of this imperative crosstalk between metabolism and type 2 immune cells within fat depots, we examined here whether deletion of GIPR signaling in immune cells, and the resulted impairment in energy homeostasis during obesity, is due to the alteration of fat depot type 2 immunity. Indeed, we show here that targeted immune cell GIPR-deficiency results in a significant reduction of type 2 immune cells and pro-beiging mediators in the obese epiWAT, mediated in part through the unrestrained activity of the pro-inflammatory alarmin S100A8/A9. These results highlight a gut-immune axis governed by GIP, coupling nutrient availability to the control of metabolically beneficial type 2 immune responses in the obese epiWAT.

MATERIALS AND METHODS

Animals

C57BL/6J OlaHsd male mice (Envigo, Jerusalem, Israel), *Gipr*$^{-/-}$ mice (C57Bl/6 background, provided by Dr Y. Yamada, Akita University, Japan), *S100a9*$^{-/-}$ mice (C57Bl/6 background, provided by Prof. T. Vogl, Munster University, Germany), B6.129P2-*Lyz2*$^{tm1(cre)Ifo}$ (C57Bl/6 background, Jackson laboratory) and *Gipr*$^{fl/fl}$ mice (C57Bl/6 background, provided by Prof. D J Drucker, Mt. Sinai Hospital, University of Toronto, Canada) were maintained in specific pathogen-free animal facility and experiments were performed according to protocols approved by the Animal Care Use Committee of the Sourasky Medical Center. All mice were housed with 12 h light cycles and a constant temperature of 22°C, with free access to standard rodent chow (Ctrl, 5% kcal fat, 5010, Lab Diets) and

water. For the generation of BM chimeric mice, 6-week-old recipient C57BL/6J OlaHsd male mice were lethally irradiated with 950 rad using a TrueBeam linear accelerator (Varian Medical Systems). The next day, femurs were dissected from 6-weeks-old donor male mice (WT, *Gipr*$^{-/-}$ and *Gipr*$^{-/-}$*/S100a9*$^{-/-}$ mice), all born and raised in the same facility. About 5x10^6 of respective BM cells were injected into the tail vein of the recipients, and mice were allowed to reconstitute their BM-derived immune cells for 6 weeks. After reconstitution, weight-matched mice were fed with HFD (60% kcal from fat, Research Diets, D12492) for the indicated period. Male mice were used to exclude the effect of female hormones and hormonal cycling on insulin secretion and metabolism.

Cell Isolation of Stromal Vascular and Mature Adipocyte Fractions

Epididymal fat pads (epiWAT) and inguinal subcutaneous fat (ingWAT) were surgically removed from mice, weighted, cut into small pieces and subsequently incubated in a 50 ml conical vial with digestion buffer [DMEM, 12.5 mM HEPES pH 7.4, 2% BSA and 10 mg collagenase type II] for 40 min at 37^{0}C in a shaking bath at 150 rpm. The digested tissues were filtered through a 100 μM metal mesh and centrifuged at 1,400 g for 5 min: the lipid-containing mature adipocytes floated to the top, and the stromal vascular fraction (SVF) pelleted at the bottom. Mature adipocyte fraction was collected and stored at -80°C. The SVF pellet was resuspended in red blood cell lysis solution, and recovered cells were washed with cold 2% fetal bovine serum in phosphate-buffered saline (PBS). The SVF pellet was used for flow cytometry analysis and RNA extraction. For RNA isolation, cells were suspended in 1 ml of TRI Reagent (Sigma-Aldrich) and then stored at 80°C until further analysis.

Flow Cytometry Analysis and Sorting of Adipose Tissue Macrophages

Flow cytometry analysis was performed using BD FACSCanto™ II Cell Analyzer (BD Biosciences), and ATMs were sort-purified using BD FACSAria™ Fusion Cell Sorter (BD Biosciences). After blocking the Fc receptors with CD16/CD32 antibody (Bio-Legend), cell suspensions of WAT were incubated on ice with fluorochrome-conjugated antibodies in FACS buffer. The following antibodies were used to stain cells from mouse tissues: CD45 (30-F11), CD25 (PC61), CD90.2 (30-H12), IL-33Rα/ST2 (DIH9), CD5 (53-7.3), CD19 (1D3/CD19), CD11b (M1/70), CD11c (N418), FcεRI (MAR-1), NK1.1 (PK136), CD3ε (145-2C11), CD49b (DX5), SiglecF (E50-2440), CD31 (390), F4/80 (BM8), CD4 (RM4-5), CD8 (53-6.7), CD25 (PC61). Foxp3 (FJK-16S) was stained using the Foxp3 transcription factor staining buffer set (eBioscience). All antibodies used in flow cytometry were purchased from eBioscience, BioLegend, or BD Biosciences if not indicated otherwise above. Data were analyzed with FlowJo v10.4.1 software (TreeStar).

Intracellular Cytokine Analysis

To examine IL-10 production in immune cells, we cultured single-cell suspensions of SVF for 4 h ex vivo with phorbol 12-myristate 13-acetate (100 ng/ml; Sigma-Aldrich) and ionomycin (1 ug/ml; Sigma-Aldrich) in the presence of brefeldin A (10 μg/ml; Sigma-Aldrich) in a 37°C incubator (5% CO_2). Cells were washed with cold PBS and surface-stained before fixation and permeabilization using the Cytofix/Cytoperm Fixation/Permeabilization solution and Perm/Wash buffer according to the manufacturer's protocol (eBioscience). Intracellular staining was performed with IL-10 (JeS5-16E3) antibody (BioLegend).

Quantitative Real-Time Polymerase Chain Reaction

Frozen adipose tissue and mature adipocyte fraction were suspended in Qiazol (Qiagen) and homogenized using a Polytron (Kinematica). RNA was isolated using an RNeasy kit (Qiagen) following the manufacturer`s instructions. The SVF cells and sorted cells were homogenized in TRI Reagent (Sigma-Aldrich) and RNA-extracted according to the manufacturer`s protocol. Total RNA was reverse-transcribed using the High capacity cDNA RT kit (Applied Biosystems). Real time RT-PCR was performed with the Fast SYBR Green Master Mix (Applied Biosystems) using the Corbett rotor light cycler. Quantification of the PCR signals of each sample was performed by the ΔCt method and normalized to the housekeeping gene *Rplp0*. The following were the primer sets used: *Il33* F, 5'-ATTTCCCCGGCAAAGTTC-3'; *Il33* R, 5'- CTTATGG TGAGGCCAGAACG-3'; *Penk* F, 5'- GGAGGCTTCA TGAAACGGTA -3'; *Penk* R, 5'-TTCAGCAGAT CGGAGGAGTT-3'; *Il5* F, 5'- CACCAGCTATGCATTGGAG A-3'; *Il5* R, 5'- TAATCCAGGAACTGCCTCGT-3'; *Il13* F, 5'-TCCAATTGCAATGCCATCT A-3'; *Il13* R, 5'- TGGGCTAC TTCGATTTTGGT-3'; *Il10* F, 5'- TGCTATGCTGCCTGCTCT TA-3'; *Il10* R, 5'-ATGTTGTCCAGCTGGTCCTT-3'; *Atf4* F, 5'-CCTTCGACCAGTCGGGT TTG-3'; *Atf4* R, 5'- CTGTCCCG GAAAAGGCAT-3'; *Ddit3* F, 5'-CTGGAAGCCTGGTATG AGGAT-3'; *Ddit3* R, 5'- CAGGGTCAAGAGTAGTGAAGGT -3'; *Xbp1s* F, 5'- GAGTCCGC AGCAGGTG-3', *Xbp1s* R, 5'-GTGTCAGAGTCCATGGGA -3'; *Rplp0* F, 5'- CAACCCAGC TCTGGAGAAAC-3'; *Rplp0* R, 5'- GTTCTGAGCTG GCACAGTGA -3'.

Protein Immunoblots

Total protein from epiWAT tissue and epiWAT adipocyte fraction was extracted by homogenization in ice-cold RIPA buffer (PBS, 1% Igepal, 0.5% sodium deoxycholate, 0.1% sodium dodecyl sulfate, protease and phosphatase inhibitors cocktails 1:100). Homogenates were centrifuged for 20 min at 14,000 g, supernatants were collected and extracts were normalized to total protein content. Proteins were separated by sodium dodecyl sulfate polyacrylamide gel electrophoresis (SDS-PAGE), blotted onto nitrocellulose and blots were blocked for 1 h in 5% milk. Blots were incubated overnight at 4°C with antibodies to pEIF2α (Cell Signaling #119A11), XBP1s (BioLegend #647501), pIRE (Cell Signaling #3294) or P97 (BioLegend #636801), and then incubated with horseradish peroxidase-conjugated secondary antibodies and subjected to chemi-luminescent detection using the Micro Chemiluminescent imaging system (DNR Bio Imaging Systems). Densitometry was

performed using the Image J software and expression of the proteins normalized to the expression of housekeeping protein P97.

dAla2-GIP Administration

C57BL/6JOlaHsd 6 weeks old weight matched male mice were group-housed on 12:12 h light-dark cycle at 22°C, with free access to food and water. Mice were maintained on the HFD for 14 weeks and received a single daily i.p. injection of human dAla2-GIP analogue (60 nmol/kg body weight) (synthesized by Bio-Synthesis, Lewisville, Tx) or vehicle (saline) during the last 8 weeks of the obesogenic diet. Separate groups of mice were maintained on regular chow (RC) and received daily i.p. injections of human dAla2-GIP (60 nmol/kg body weight) or vehicle (saline) for 6 consecutive days. All injections were performed in the light cycle.

Cold Exposure

For cold-challenge experiments, individually housed mice with free access to chow were exposed to 4^0C in a temperature-controlled refrigerator (4–8°C) for 24 h. Rectal temperature was measured at indicated times (0 and 5 h) using a rectal thermometer (Vega Technologies, Taiwan). After completion of the challenge, mice were sacrificed, and their WAT samples were used for flow cytometry analysis or dissected and stored at -80°C.

Statistical Analysis

Statistical significance was determined between two groups using an unpaired two-tailed Student's t-test using GraphPad Prism 6.0 and differences between more than two groups were examined by one-way ANOVA with a Tukey post-hoc test. Significance was defined if p-value was less than 0.05 as following: * $p < 0.05$; ** $p < 0.01$; *** $p < 0.001$. Date are routinely represented as mean ± SEM, and the number of replicates per experiment can be found in the figure legends.

RESULTS

GIPR-Deficiency in Immune Cells Alters Expression of type 2 Immune Mediators in the Obese White Adipose Tissue

WAT is densely populated by various type 2 immune cells that maintain metabolic homeostasis and energy balance, but become dysregulated in obesity (17). Mice with targeted GIPR-deficiency to immune cells exhibit a deteriorated metabolic profile and significant myelopoiesis, concomitantly with impaired energy expenditure and ingWAT beiging under the setting of HFD-induced obesity (13). Hence, we hypothesized that their impaired beiging response may be due to the alteration in metabolically beneficial type 2 immune circuits. To explore this possibility, we implemented a BM chimerism approach to target GIPR-deficiency to immune cells. The BM of lethally irradiated wild type (WT) recipient mice was differentially reconstituted by transplantation of WT (WT BM) or *Gipr*$^{-/-}$ BM (*Gipr*$^{-/-}$ BM). Following immune cell reconstitution (6 weeks), weight-matched groups were subjected to 14 weeks of HFD (**Figure 1A**). In agreement with our previous findings (13), *Gipr*$^{-/-}$ BM mice displayed significantly increased weight gain starting already at the 3rd week of HFD feeding (**Figure 1B**), without a change in food consumption (**Figure 1C**). Further analysis revealed dysregulated gene expression of key type 2 immune mediators in the epiWAT of *Gipr*$^{-/-}$ BM mice. Notable was the impaired expression of IL-33 (*Il33*) and MetEnk (*Penk*) in epiWAT (**Figure 1D**), key pro-beiging mediators acting upstream on both adipocytes and local type 2 immune cells (21, 23–26). There was also a reduction of IL-5 mRNA (*Il5*) (**Figure 1D**), which was previously linked with the pro-beiging activity of ILC2 (23). In contrast, the expression of another type 2 immune mediator, IL-13, was upregulated in epiWAT (**Figure 1D**). These alterations were most prominent in epiWAT and were not observed in ingWAT (**Figure 1E**).

IL-10 is a type 2 cytokine classically known for its immunosuppressive role in immunity. In WAT, it was suggested as an essential promotor of M2-alternatively activated phenotype of ATMs (29–32). Yet, emerging evidence points to IL-10 as a pivotal suppressor of adipocyte thermogenesis capable of directly repressing the transcription of thermogenic genes in adipocytes (33). In this respect, IL-10 gene expression (*Il10*) was increased in the *Gipr*$^{-/-}$ BM epiWAT, and also in the ingWAT at 14 weeks of HFD (**Figure 1F**). Overall, these results suggest a role for GIPR signaling in immune cells as a promoter of type 2 immunity in the epiWAT.

GIPR-Deficiency in Immune Cells Reduces the Representation of Type 2 Immune Cells in the Obese White Adipose Tissue

Given the impairment in the production of type 2 immune mediators in the epiWAT during HFD induced by GIPR-deficiency in immune cells (**Figure 1**), we next examined the representation of key associated type 2 immune cells in the epiWAT stromal vascular fracture (SVF) of WT BM vs. *Gipr*$^{-/-}$ BM mice. Gating strategy for the various immune populations is shown in **Figure 2A**. In agreement with our earlier studies (13), the fraction (%) of ATMs (defined as $CD11b^+F4/80^+CD64^+$ cells) out of living $CD45^+$ was increased by about 2-fold in the *Gipr*$^{-/-}$ BM epiWAT (**Figure 2B**). In contrast, the fraction of eosinophils (defined as $CD11b^+SiglecF^+SSC^{hi}$) was reduced by two-fold (**Figure 2C**). Previous studies indicated an important role for IL-33 in maintaining WAT ILC2 and Tregs (21, 23–25). In alignment with the reduction in IL-33 in the epiWAT of *Gipr*$^{-/-}$ BM mice at 14 weeks of HFD (**Figure 1D**), the representation of ILC2 (defined as $Lin^-CD25^+CD90.2^+IL\text{-}33R^+$) trended lower (**Figure 2C**), and there was a five-fold decline in the levels of Tregs (defined as $CD4^+CD8^-CD25^+FOXP3^+$) (**Figure 2C**). IL-10 is produced by multiple immune cells in the WAT SVF, including ATMs (34), dendritic cells (35), Tregs (36), and regulatory B cells (37). Intracellular staining revealed increased expression of IL-10 in $F4/80^+$ ATMs in the epiWAT of *Gipr*$^{-/-}$ BM mice, while it was reduced among $F4/80^-$ immune cells (**Figure 2D**). Hence, the increased representation of ATMs in the *Gipr*$^{-/-}$ BM epiWAT (**Figure 2B**), and their expression of IL-10

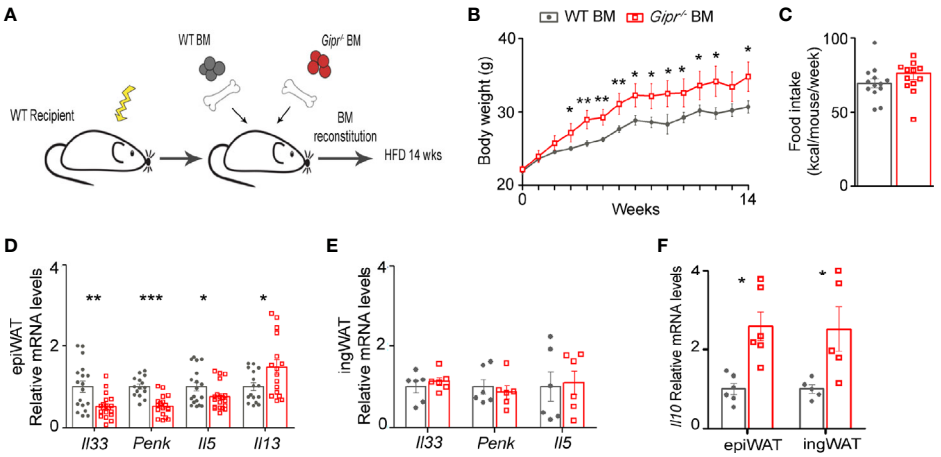

FIGURE 1 | Impaired production of type 2 immune mediators in the obese epiWAT of *Gipr*$^{-/-}$ BM mice. **(A)** Scheme illustrating experimental design. Lethally irradiated WT mice were reconstituted by transplantation of WT BM (gray circles) or *Gipr*$^{-/-}$ BM (red squares) for 6 weeks and then fed a HFD for 14 weeks. **(B)** Weekly measurements of body weight (g) (n≥6). **(C)** Average weekly food consumption (kcal) per mouse during a period of 14 weeks. **(D–E)** Expression of key type 2 immune mediators in **(D)** epiWAT (n ≥17) and **(E)** ingWAT (n=6) after 14 weeks of HFD, as analyzed by qRT-PCR and normalized to *Rplp0*. **(F)** Relative expression of *Il10* in epiWAT and ingWAT as determined by qRT-PCR. Data is compiled from three individual experiments **(D)** or from single individual experiment **(B, C, E, F),** and presented as mean ± SEM with significance: *p ≤ 0.05, **p ≤ 0.01, and ***p ≤ 0.001, unpaired two-tailed *t*-test, comparing between WT BM and *Gipr*$^{-/-}$ BM groups. WT, wild type mice; BM, bone marrow; HFD, high-fat diet; epiWAT, epididymal WAT; ingWAT, subcutaneous inguinal WAT.

(**Figure 2D**), can explain the upregulation of IL-10 in the *Gipr*$^{-/-}$ BM epiWAT SVF (**Figure 1F**).

Immune Cell-Derived S100A8/A9 Contributes to the Impairment of White Adipose Tissue Type 2 Immune Circuits in *Gipr*$^{-/-}$ Bone Marrow Mice

The pro-inflammatory dysregulated metabolic phenotype of *Gipr*$^{-/-}$ BM mice has been linked with the unrestrained activity of myeloid cell-derived S100A8/A9 (13). Hence, we next sought to investigate a possible mechanistic link between the alterations in type 2 immunity in the *Gipr*$^{-/-}$ BM epiWAT and the hyper-production of S100A8/A9 by GIPR-deficient BM-derived myeloid cells. To test this hypothesis, we studied a group of BM chimera mice reconstituted with BM from *Gipr*$^{-/-}$*S100a9*$^{-/-}$ double knockout mice (*Gipr*$^{-/-}$*S100a9*$^{-/-}$ BM) (**Figure 3A**). *S100a9*$^{-/-}$ mice were chosen given the lack of mature S100A8/A9 protein expression in these mice (38). Co-deletion of GIPR and S100A8/A9 reversed the decline in *Il33* and *Penk* expression detected in the epiWAT of *Gipr*$^{-/-}$ BM mice at 14 weeks of HFD feeding (**Figure 3B**). S100A8/A9 deletion also restored expression of *Il10* and *Il13* in the epiWAT of *Gipr*$^{-/-}$ BM mice to the levels observed in the control WT BM epiWAT (**Figure 3C**).

Time-resolved single cell characterization has recently discovered massive reorganization of the immune cell compartment in mouse epiWAT between 6 and 12 weeks of HFD feeding, with the most prominent changes including an expansion of ATMs and a reduction in type 2 immune cells, including Tregs and ILC2 (39). Hence, we next examined the effect of immune cell-GIPR-deficiency on type 2 immunity at an earlier time point, at 5 weeks of HFD feeding, followed by 5 h cold challenge at 4^{0}C to boost thermogenesis activity. Corroborating our earlier findings (**Figure 1A**), *Gipr*$^{-/-}$ BM mice exhibited increased body weight starting already at 4 weeks of HFD feeding (**Figure 3D**), despite similar food intake (**Figure 3E**). The co-deletion of S100A8/A9 (*Gipr-/-S100a9-/-* BM) normalized weight gain to that of the control group (**Figure 3D**). We have previously shown that S100A8/A9 directly impairs beiging (13). Indeed, *Gipr-/-* BM chimeric mice displayed reduced core temperature after 5 h of cold challenge, in comparison to the control group, and this defect was ameliorated by the co-deletion of S100A8/A9 (**Figure 3F**), indicating an etiologic role for S100A8/A9 in the failure of these mice to properly adapt thermogenesis. In support of this, the expression of S100A8 (*S100a8*) was profoundly elevated in the epiWAT, and also trended higher in the ingWAT of *Gipr-/-* BM mice, already at this early phase of HFD feeding (**Figure 3G**). Similar to the results obtained during the development of obesity (**Figure 3B**), the reduced expression of *Il33* and *Penk* in the epiWAT of *Gipr-/-* BM mice was restored to WT BM control levels in *Gipr-/-S100a9-/-BM* mice (**Figure 3H**). *Il10* was expressed at similar levels in the epiWAT of WT BM, *Gipr*$^{-/-}$ BM and *Gipr-/-S100a9-/-*BM mice after several weeks of HFD feeding. In contrast, *Il13* was profoundly upregulated in *Gipr*$^{-/-}$ BM group, and co-deletion of S100A8/A9 partially reverted *Il13* levels towards normal (**Figure 3I**). Flow cytometry analysis revealed a reduction in the fraction of ILC2 and eosinophils in the *Gipr-/-* BM epiWAT, while ATMs were similarly represented at this early phase (**Figure 3J**). We have previously shown that S100A8/A9 originates in the epiWAT SVF cells from ATMs and neutrophils. In line with the role of S100A8/A9 in driving impaired type 2 immunity in the *Gipr-/-* BM epiWAT, we next

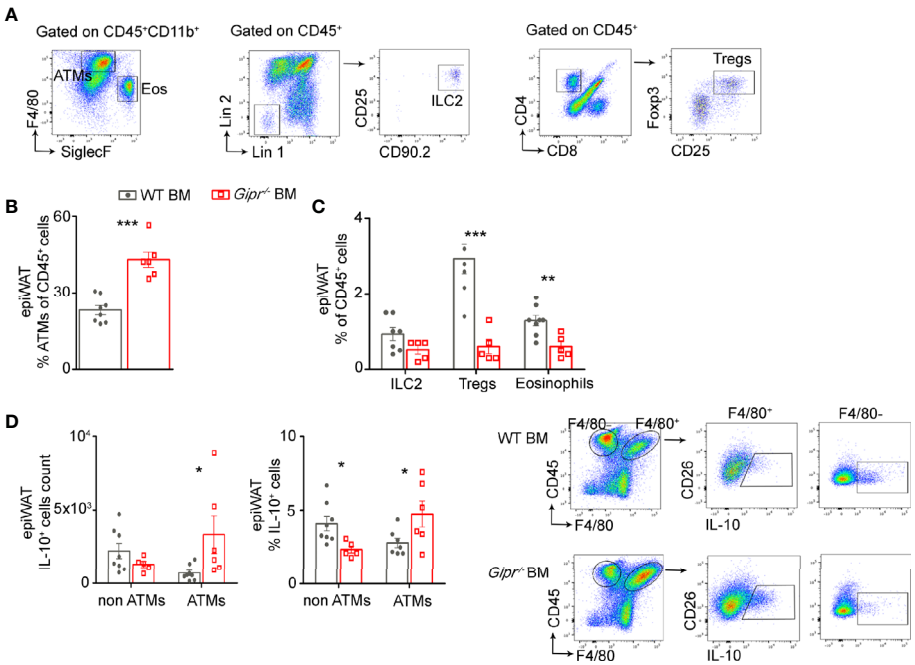

FIGURE 2 | Reduced frequency of type 2 immune cells in the obese epiWAT of *Gipr*$^{-/-}$ BM mice. Mice were reconstituted with WT BM (gray circles) or *Gipr*$^{-/-}$ BM (red squares) for 6 weeks and then fed a HFD for 14 weeks (n≥6). **(A)** Representative flow cytometry dot plots showing gating strategy for immune cell populations first gated on living CD45^{+} cells from epiWAT. ATMs were identified as CD11b^{+}F4/80^{+}CD64^{+}. Eosinophils were defined as CD11b^{+}SiglecF^{+}SSC^{hi}; ILC2 as Lin^{-} CD25^{+}CD90.2^{+}IL-33R^{+} and Tregs as CD4^{+}CD8^{-}CD25^{+}FOXP3^{+}. **(B)** Graph showing flow cytometry assessment of ATMs fraction out of total CD45^{+}. **(C)** Fraction of ILC2, Tregs and Eos out of total CD45^{+} cell population. **(D)** Proportion and numbers of IL-10^{+} cells among ATMs (F4/80^{+}) and non-ATMs (F4/80^{-}) cell populations, normalized to tissue mass in the epiWAT of HFD-fed chimeras. Right panel, representative flow cytometry images depicting the IL-10^{+}F4/80^{+} and IL-10^{+}F4/80^{-} immune cells. Data are analyzed by unpaired, two-tailed *t*-test, comparing between WT BM and *Gipr*$^{-/-}$ BM groups, and are presented as mean ± SEM. *p ≤ 0.05, **p ≤ 0.01 and ***p < 0.001 ATMs, adipose tissue macrophages; ILC2, innate lymphoid cells type 2; Eos, eosinophils; Tregs, T-regulatory cells.

examined whether treatment with the long-acting GIP analogue (dAla2-GIP) can reduce the S100A8/A9 production in the epiWAT ATMs following 14 weeks of HFD (**Figure 3K**). Indeed, dAla2-GIP administration reduced *S100a8* gene expression in the epiWAT ATMs (**Figure 3K**). Altogether, these results outline a pivotal role for GIP in balancing fat depot type 2 immune networks during the development of obesity, at least partially through its restraining of the immune cell-derived S100A8/A9.

GIPR-Deficiency in Myeloid Immune Cells Drives the Impairment of Type 2 Immune Networks in the Obese White Adipose Tissue

Myeloid immune cells are the main source of S100A8/A9 during inflammation (40). In the epiWAT from mice with obesity, GIP plays an important role in restraining the production of S100A8/A9 in ATMs (**Figure 3K**) (13), and the deficiency in GIPR in myeloid cells augments myelopoiesis and accumulation of S100A8/A9^{+} neutrophils and ATMs in the epiWAT (13). Therefore, we next examined whether deletion of GIPR specifically in the myeloid cells would be sufficient to induce alteration in type 2 immunity in the epiWAT. Accordingly, conditional *Gipr*$^{fl/fl}$ mice were crossed with *Lyz2*$^{cre/+}$ mice. The resulted *LysM*$^{\Delta Gipr}$ and their littermate *Gipr*$^{fl/fl}$ controls were subjected to eight and 14 weeks HFD regimens (**Figure 4A**). Similarly to *Gipr*-/- BM, *LysM*$^{\Delta Gipr}$ mice exhibit an aggravated metabolic phenotype in response to prolonged HFD, associated with increased weight gain, steatohepatitis, insulin resistance, myelopoiesis and S100A8/A9 production, as well as impaired ingWAT beiging (13). Compared to their *Gipr*$^{fl/fl}$ littermate controls, *LysM*$^{\Delta Gipr}$ mice displayed reduced levels of *Il33* in the epiWAT at 8 weeks and of *Penk* at 14 weeks of HFD feeding (**Figure 4B**). Similar to the results in *Gipr*-/- BM mice, increased expression of *Il10* was detected in the epiWAT of *LysM*$^{\Delta Gipr}$ mice compared to *Gipr*$^{fl/fl}$ littermate controls, but only after 14 weeks of HFD feeding (**Figure 4C**). Altogether, these results further consolidate an immunoregulatory role for GIP in myeloid cells.

GIPR-Deficiency in Immune Cells Alters the Expression of Type 2 Immune Mediators by Cells in the Adipocyte Fraction

In addition to WAT immune cells, adipocytes can also be a source for type 2 immune cytokines, such as IL-13 (41–43). Hence, we next examined the expression of *Il13* in the WAT of WT BM vs. *Gipr*$^{-/-}$ BM after 14 weeks of HFD feeding, while distinguishing between the adipocyte fraction and the SVF.

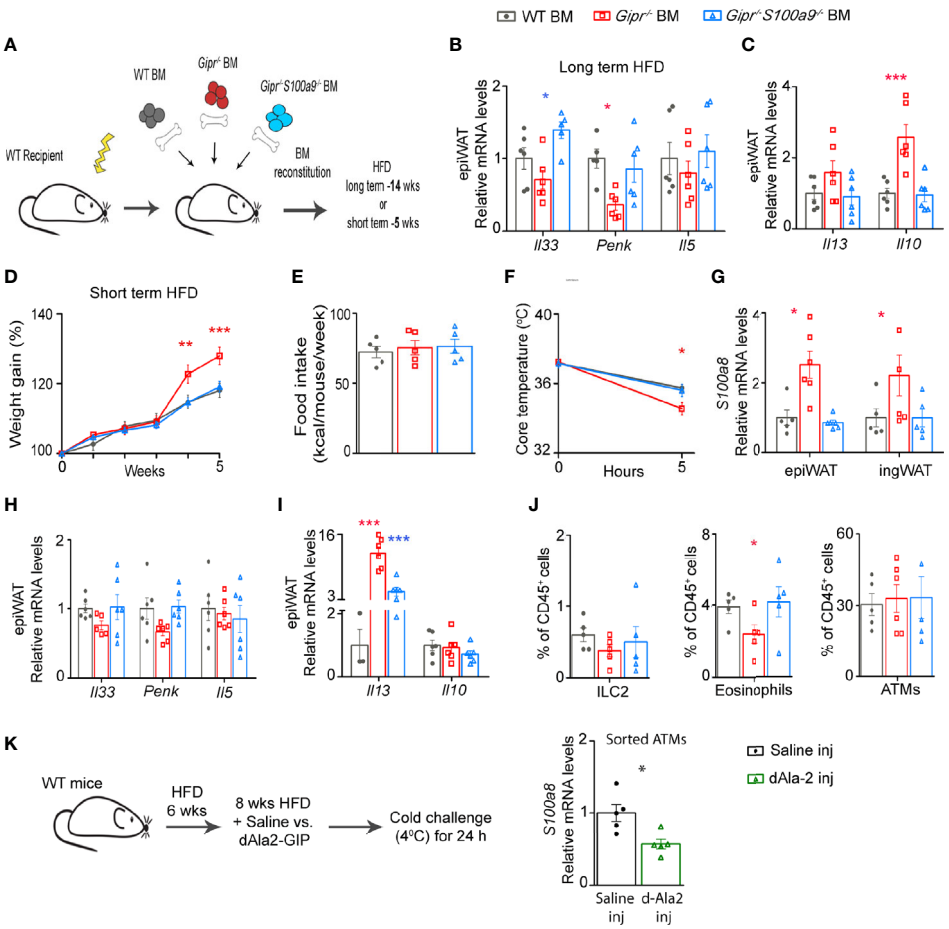

FIGURE 3 | Unrestrained production of S100A8/A9 by *Gipr*$^{-/-}$ immune cells impedes WAT type 2 immune circuits. **(A)** Scheme illustrating experimental design. Lethally irradiated WT mice were reconstituted with WT BM (gray circles), *Gipr*$^{-/-}$ BM (red squares) and *Gipr*$^{-/-}$/*S100a9*$^{-/-}$ BM (blue triangles) for 6 weeks and then fed with a HFD regime as indicated for **(B, C)** long-term (14 weeks) or **(D–J)** short-term (5 weeks). **(B, C)** qRT-PCR assessment of the expression of the indicated mediators normalized to *Rplp0* in epiWAT after 14 weeks of HFD (n=6). **(D, E)** Weekly measurements of body weight and food consumption (kcal/mouse/week) during 5 weeks HFD feeding (n≥6). **(F)** Body core temperature response (°C) to acute cold challenge after 5 h. **(G)** Expression of *S100a8* gene in epiWAT and ingWAT as determined by qRT-PCR. **(H, I)** Gene expression of indicated mediators in epiWAT after 5 weeks of a HFD as analyzed by qRT–PCR and normalized to *Rplp0*. **(J)** Graphs showing flow cytometry assessment of ILC2, eosinophils and ATMs fractions out of total CD45^{+} cell population (defined as shown in **Figure 2A**). **(K)** Scheme illustrating experimental design. WT mice were subjected to HFD feeding for 14 weeks and received daily i.p. injections of dAla2-GIP analogue (60 nmol/kg body weight) or vehicle (saline) during the last eight weeks (n= 8). Left panel, qRT-PCR analysis of *S100a8* expression in ATMs sorted from epiWAT of these mice. Data are from single experiment. Data are presented as mean ± SEM. Statistical analyses were conducted using one-way ANOVA followed by post-hoc Tukey test **(B, C)** or by unpaired two-tailed *t*-test **(K)** with significance: *p ≤ 0.05, **p ≤ 0.01 and ***p ≤ 0.001. Red or blue stars represent significance of *Gipr*$^{-/-}$ BM or *Gipr*$^{-/-}$/*S100a9*$^{-/-}$ BM groups vs. WT BM, respectively.

Levels of mRNA transcripts for the beiging-interfering cytokine *Il10* were profoundly elevated in both SVF and adipocyte fractions of the *Gipr*$^{-/-}$ BM WAT (**Figure 5A**). Notably, *Il13* expression was reduced in the SVF (p=0.06), but highly increased in the adipocyte fraction of the *Gipr*$^{-/-}$ BM WAT (**Figure 5B**), a phenomena associated with increased WAT inflammation during obesity (42). Moreover, we detected increased expression of *Il13* in the adipocyte fraction, but not the SVF, of the *LysM*$^{\Delta Gipr}$ epiWAT (**Figure 5C**).

Previous studies have shown that expression of IL-10 and IL-13 in WAT cells may be elevated by obesity-induced ER stress (43, 44). There are three major ER stress sensors, IRE1, PERK and ATF6, which transduce the mammalian unfolded protein response (UPR). Activated IRE1 splices the mRNA of XBP1 yielding the potent transcription factor spliced XBP1 (XBP1s). Activated PERK phosphorylates EIF2α (pEIF2α), which induces translation of ATF4 that further acts as a transcription factor for *Ddit3* (45). ER stress/UPR- related gene expression was assessed in the total epiWAT of WT BM and *Gipr*$^{-/-}$ BM mice after both short (5 weeks) and long-term (14 weeks) HFD regimens. Expression of ER stress/UPR markers was not altered after short-term HFD feeding in the epiWAT of *Gipr*$^{-/-}$ BM mice compared to expression in control WT BM mice (**Figure 5D**). In contrast, after 14 weeks of exposure to HFD, the expression of *Atf4*, *Ddit3*, and *Xbp1s*, were all enhanced in the epiWAT of *Gipr*$^{-/-}$ BM mice (**Figure 5E**). Fractionation of total epiWAT

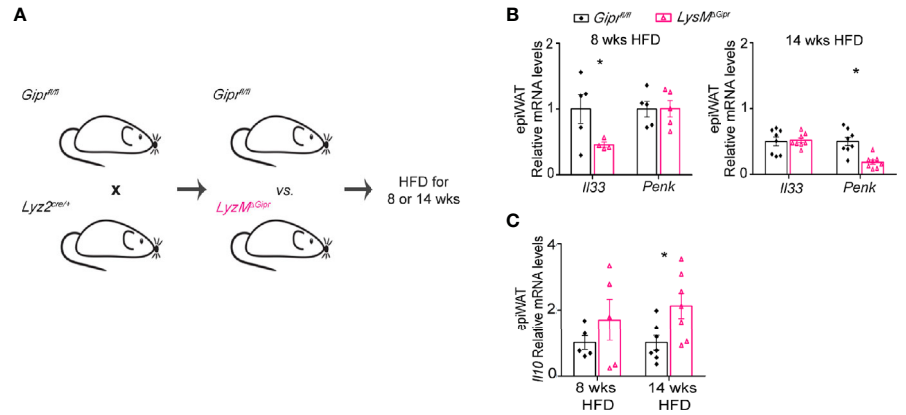

FIGURE 4 | Deficiency of GIP signaling in myeloid immune cells drives the impairment of type 2 immune networks in the obese epiWAT. **(A)** Scheme illustrating experimental design. Mice with targeted GIPR-deficiency to myeloid cells (*LysM*$^{\Delta Gipr}$, pink open triangles) and their littermate controls (*Gipr*$^{fl/fl}$, black rhombus) were fed a HFD for 8 and 14 weeks (n ≥6). **(B)** qRT-PCR assessment of the expression of *Il33* and *Penk* genes in epiWAT normalized to *Rplp0*. **(C)** qRT-PCR assessment of the expression of *Il10* in epiWAT of *LysM*$^{\Delta Gipr}$ and *Gipr*fl/fl mice after shorter (8 weeks) and longer (14 weeks) HFD-regimes. Data are analyzed by unpaired, two-tailed *t*-test and presented as mean ± SEM. *p ≤ 0.05.

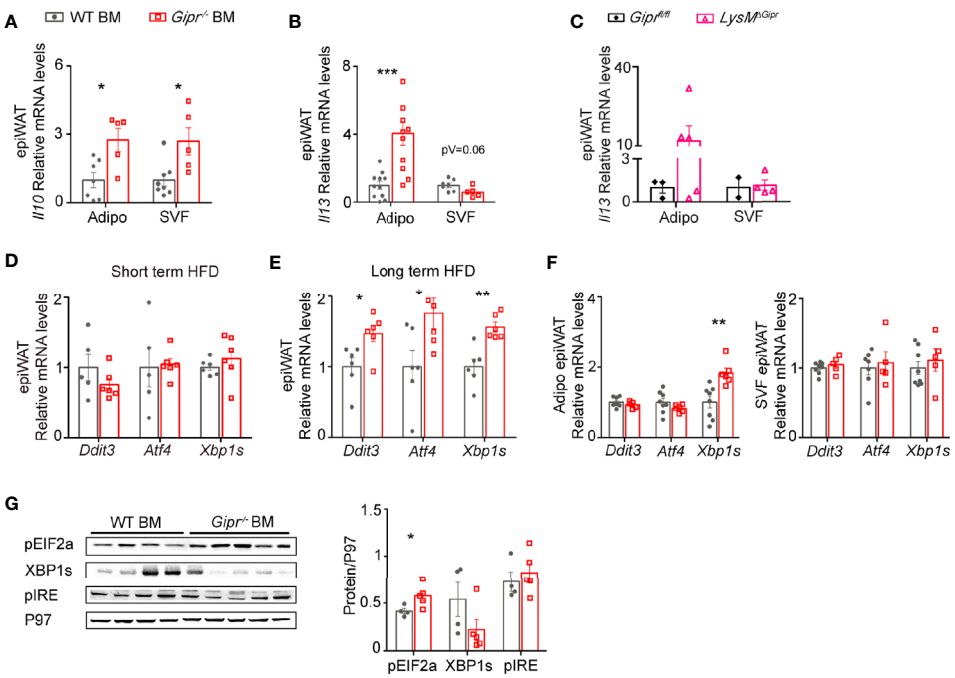

FIGURE 5 | Impairment of type 2 immune networks in *Gipr*$^{-/-}$ BM epiWAT involves adipocyte fraction cells. Expression of *Il10* **(A)** and *Il13* **(B)** in isolated adipocyte fraction and SVF in epiWAT of WT BM (gray circles) or *Gipr*$^{-/-}$ BM (red squares) mice after 14 weeks of HFD as determined by qRT-PCR analysis. **(C)** qRT-PCR assessment of the expression of *Il13* in isolated adipocyte fraction and SVF in epiWAT of *LysM*$^{\Delta Gipr}$ (pink open triangles) and *Gipr*$^{fl/fl}$ (black rhombus) obese mice after 14 weeks of HFD. **(D, E)** qRT-PCR assessment of the expression of indicated genes in epiWAT at shorter (5 weeks) and longer (14 weeks) HFD-regimes respectively, normalized to *Rplp0*. **(F)** qRT-PCR assessment of the expression of indicated genes in isolated adipocyte fraction and SVF in epiWAT of WT BM or *Gipr*$^{-/-}$ BM mice after 14 weeks of HFD. **(G)** Expression of phosphorylated EIF2 (pEIF2α), spliced form of XBP1 (XBP1s) and phosphorylated IRE (pIRE) in epiWAT from WT BM (n=4) and *Gipr*$^{-/-}$ BM (n=5) mice, as assessed by immunoblot analysis and was quantified using P97 as loading control (for pEIF2α, P=0.04, for XBP1s, p=0.15 and for pIRE, P=0.54), with densitometry presented below. Data are analyzed by unpaired, two-tailed *t*-test, and results are presented as mean ± SEM with significance: *p < 0.05, **p < 0.01, ***p < 0.001. Data in panel **(A)** are from two independent experiments, and in **(B–F)** are from one experiment. Adipo, adipocyte fraction; SVF, stromal vascular fraction.

revealed that mRNA expression of *Xbp1s* was elevated in the adipocyte fraction of *Gipr*$^{-/-}$ BM mice, but not in the SVF (**Figure 5F**). Western blot analysis revealed an increased phosphorylation of pEIF2α in the epiWAT of *Gipr*$^{-/-}$ BM mice (**Figure 5G**). In contrast, despite the increased gene expression of *Xbp1s*, the protein levels of XBP1s were reduced, and the expression level of its upstream activator pIRE did not vary (**Figure 5G**). pEIF2α is also required for expression of maximal stable spliced XBP1 protein *via* a mechanism that involves stabilization of *Xbp1s* mRNA (46). Hence, the increased expression of pEIF2α may explain the increase in *Xbp1s*. Altogether, these results reveal that absence of the GIPR signaling in immune cells alters the expression of type 2 immune mediators in adipocytes, associated with the induction of the PERK-EIF2a ER stress pathway during the development of obesity.

A Glucose-Dependent Insulinotropic Polypeptide Analogue Induces IL-33 and Penk in Epididymal Visceral White Adipose Tissue of Lean Mice During Cold-Induced Thermogenesis

To further substantiate the association between GIP and WAT type 2 immunity we next studied the impact of treatment with a GIP analogue on the production of type 2 immune mediators. IL-33 and Penk, both key stimulators of adaptive thermogenesis (23), were reduced in *Gipr*$^{-/-}$ BM epiWAT at both short (5 weeks) (**Figure 3H**) and long term (14 weeks) (**Figure 1D**) HFD. Hence, we next assessed the effect of GIP analogue treatment on IL-33 and Penk production in lean mice subjected to cold challenge (4°C). Accordingly, 7 weeks old C57BL/6J OlaHsd mice received daily i.p. injections of dAla2-GIP or vehicle (saline) for 6 days, and then were placed at 4°C for 24 h (**Figure 6A**). GIP treatment was sufficient to promote the expression of both *Il33* and *Penk* in the SVF, but not in the adipocyte fraction (**Figures 6B, C**). Given the increased expression of the beiging-interfering cytokine IL-10 in the epiWAT of *Gipr*$^{-/-}$ BM (**Figure 1F**) and *LysM*$^{\Delta Gipr}$ mice (**Figure 4C**) under prolonged HFD, we next examined the effect of the GIP analogue on cytokine expression in response to cold-challenge. Interestingly, dAla2-GIP treatment reduced IL-10 expression uniquely in the epiWAT adipocyte fraction, but not in the SVF fraction (**Figure 6C**). These results further substantiate a role for GIP in modulation of type 2 immune circuits in the epiWAT.

DISCUSSION

Here we uncover a new gut-immune axis showing that an absence of GIP signaling in immune cells during HFD hampers the production of key type 2 immune mediators and leads to the reduction of type 2 immune cells in the epiWAT, concomitantly with the augmented production of the beiging interfering cytokine IL-10 in both epiWAT adipocyte and SVF fractions. This impairment initiates already at the early stage of HFD feeding.

The WAT cellular ecosystem harbors, in addition to resident adipocytes and their mesenchymal progenitors, a unique blend of accessory immune cells, all intimately cooperating to regulate metabolic homeostasis (1, 17). During obesity, acute self-limiting inflammation allows healthy expansion of adipose tissue and adaptation to the altered metabolic demands derived from over-nutrition. However, in the course of a prolonged positive energy surplus, this physiological response becomes sustained and turns pathogenic, leading to pro-inflammatory transition of WAT resident and infiltrating immune cells (47). Type 2 immune cell networks are an essential factor directly affecting metabolic homeostasis and energy balance in WAT and limiting WAT inflammation during obesity. The numbers of WAT type 2 immune cells, such as ILC2, eosinophils, and Tregs, decline with progressing adiposity, thereby licensing obesity-induced inflammatory transition in the WAT (22, 39). We show here that the increased adiposity in *Gipr*$^{-/-}$ BM mice is associated with the impaired production of key type 2 immune mediators that are directly involved with both metabolic and immunoregulatory activities that balance nutrient overload. In this respect, *Gipr*$^{-/-}$ BM mice exhibit reduced expression of mediators that are indispensable for proper beiging response, such as IL-33 and Penk (24, 26). IL-33 is also crucial for the maintenance of WAT ILC2 and Tregs expressing its receptor (21, 23–25), and indeed there was a significant decline in the fraction of these cells as well as in eosinophils in the epiWAT of *Gipr*$^{-/-}$ BM mice. Importantly, we show that the alteration in type 2 immune networks in *Gipr*$^{-/-}$

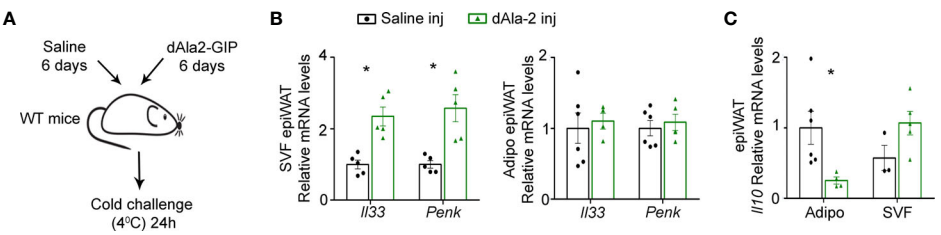

FIGURE 6 | GIP analogue enhances expression of type 2 mediators in epiWAT of lean mice during cold-induced thermogenesis. **(A)** Scheme illustrating experimental design. WT mice (n= 6) received daily i.p. injections of dAla2-GIP analogue (60 nmol/kg body weight) or vehicle (saline) for 6 days and after that were subjected to cold challenge (4°C) for 24 h. **(B)** qRT-PCR assessment of the expression of *Il33* and *Penk* genes in isolated adipocyte fraction and SVF of epiWAT normalized to *Rplp0*. **(C)** Expression of *Il10* in isolated adipocyte fraction and SVF of epiWAT of these mice was analyzed by qRT-PCR and normalized to *Rplp0*. Data are from a single experiment and analyzed by unpaired, 2-tailed *t*-test and presented as mean ± SEM. *p ≤ 0.05.

BM mice appears early during the development of obesity, subsequent to the acquisition of increased weight gain. Therefore, we believe that this impairment in type 2 immune pathways fuels the imbalanced energy expenditure and dysregulated beiging process previously linked to the GIP signaling loss in immune cells during DIO (13). Of note, we have not examined whether the alteration in type 2 immunity occurs prior to the increased weight gain, and therefore it remains unclear whether it is the initiating event disrupting energy expenditure. Moreover, the increased weight gain and associated inflammation may contribute to the impairment of type 2 immune networks in *Gipr*$^{-/-}$ BM mice. Importantly, we show here that alteration in type 2 immune networks in *Gipr*$^{-/-}$ BM mice appear mainly in the epiWAT, but not ingWAT. Hence, it remains mechanistically unclear whether and how these alterations in the epiWAT are associated with the impaired ingWAT beiging response previously reported in these mice (13).

Our previous studies have outlined an etiologic role for the inflammatory alarmin S100A8/A9 in the aggravated metabolic phenotype observed in *Gipr*$^{-/-}$ BM mice. Accordingly, the co-deletion of S100A8/A9 in *Gipr*$^{-/-}$ immune cells ameliorated the increased weight gain and impaired beiging displayed by *Gipr*$^{-/-}$ BM chimeric mice during HFD feeding (13). Moreover, a single S100A8/A9 injection was sufficient to impair the beiging response in cold-challenged lean WT mice (13). Here we provide an extended mechanistic insight into the importance of GIP-governed restraint of S100A8/A9 on the maintenance of energy balance, showing that S100A8/A9 drives some of the alterations in the production of type 2 immune mediators in the epiWAT of HFD-fed *Gipr*$^{-/-}$ BM mice. We show that *S100a8* gene expression is already increased in both epiWAT and ingWAT after 5 weeks in HFD-fed mice, and that co-deletion of S100A8/A9 restores the expression of type 2 mediators and the representation of type 2 immune cells to that of the control WT BM chimera mice. This coupling between S100A8/A9 overproduction by myeloid cells in the context of disrupted GIP signaling and the impairment of whole-body energy homeostasis and type 2 immunity has immediate translational relevance, as elevated S100A8/A9 expression in VAT and serum is also detected in people with type 2 diabetes mellitus (T2DM) and obesity (48, 49). Therefore, it will be necessary to determine further how S100A8/A9 affects type 2 immunity in the WAT. This may be challenging given that the S100A8 and S100A9 calgranulins can also appear as homodimers, which may differentially regulate adaptive thermogenesis either *via* effects on specific immune cells and/or *via* direct effects on beiging differentiation pathways in adipocytes. Moreover, S100A8, S100A9, and S100A8/A9 calgranulins can signal *via* multiple receptors, such as TLR4, RAGE, and Basigin (CD147) (50), which may be expressed by a broad spectrum of cells in the WAT.

Emerging studies outline direct immunoregulatory properties for GIP that are intertwined with its metabolic actions (6, 7). Therefore, there is a tremendous unmet need to dissect the exact repertoire of immune cells capable of sensing GIP, their location, and the resulting impact on central and peripheral metabolism. Mice with conditional targeting of GIPR-deficiency to myeloid immune cells exhibit abnormal metabolic phenotypes in response to sustained HFD feeding similar to that of *Gipr*$^{-/-}$ BM mice (13), suggesting that the GIP signaling is especially essential in myeloid cells for maintaining energy balance and tuning WAT inflammation. We have previously shown and corroborated here, that both *in vivo* and directly *ex vivo* treatments with a GIP analogue attenuate the expression of *S100a8* gene in ATMs from the obese epiWAT. In alignment with this, a direct anti-inflammatory role for GIP in macrophages has also been suggested in the context of atherosclerosis (51–53), as well as in microglia in neurodegenerative disorders of the central nervous system (54–58). It remains unclear however, whether WAT immune cells, specifically type 2 immune cells, directly respond to GIP. The lack of a reliable GIPR antibody has been a barrier in mapping cell-specific GIPR protein expression. Hence, GIPR expression is often determined at the transcript level combined with functional validation for GIP-induced Ca^{2+} influx and cAMP levels. Its expression in low copy number further excludes it from single cell Atlases of WAT immune and non-immune cells. Relative to the abundance of WAT adipocytes and ATMs, the scarcity of type 2 immune cells limits functional screenings of *Gipr* expression, therefore necessitating the generation of reporter mouse models and modified ligands that permit receptor labelling. Recently, transgenic mice allowing the conditional *Gipr* gene deletion in broad immune cell populations were used to map *Gipr* mRNA transcripts in various tissues. The immune expression of *Gipr* mRNA transcripts was most prominent in the BM, mainly among T cells, $Gr1^{+}CD11b^{+}$ myeloid cells and myeloid progenitor cells (7). Notably, the transgenic deletion of the *Gipr* gene in immune cells had no clear effect on the expression of *Gipr* mRNA transcripts in the lean epiWAT and mesenteric WAT, therefore challenging the idea that WAT type 2 immune cells are directly responding to GIP and suggesting the BM as the site for GIP immunoregulatory activity. Hence, the metabolic phenotypes observed within the WAT of HFD-fed *Gipr*$^{-/-}$ BM mice and *LysM*$^{\Delta Gipr}$ mice may be mediated by the lack of GIPR signaling in myeloid immune cells in the BM. In this respect, both Gipr$^{-/-}$ BM mice and *LysM*$^{\Delta Gipr}$ mice exhibit evidence for myelopoiesis and especially neutrophilia in peripheral blood and epiWAT during HFD, which may explain the increased expression of S100A8/A9 and its governed deleterious metabolic and inflammatory effects.

Utilizing a gain of function approach, we show here that treatment with the long-acting GIP analogue dAla2-GIP in weight-matched lean mice prior to their exposure to cold-induced thermogenesis resulted in increased expression of type 2 immune mediators IL-33 and Penk, both pivotal drivers of adaptive thermogenesis (23). These mediators are mainly produced by mesenchymal stromal cell subtypes (27, 28), suggesting non-immune pathway by which GIP can modulate type 2 immunity. Nevertheless, it remains elusive whether these cells can indeed directly recognize and respond to GIP. While loss-of-function studies indicate that GIP drives weight gain, when it comes to GIPR agonism and antagonism, compelling evidence paradoxically indicate that both approaches can reduce body weight, especially if combined with GLP-1 agonists (12, 59). This paradox may reflect the partial agonistic activity of certain antagonists (60), compensatory relationship and overlapping signaling axes

between GIPR and GLP-1R incretin receptors (59, 61), as well as desensitization of GIPR achieved by chronic agonism (62). With respect to the latter, in cultured mouse or human preadipocytes, exposure to 1 mM dAla2-GIP for 24 h decreased cAMP response to subsequent GIPR stimulation up to 48 h (62), indicating that chronic GIPR agonism functionally mimics GIPR antagonism. Therefore, it will be important to reconcile whether the GIP augmentation approach used here to achieve upregulation of IL-33 and Penk arises *via* GIPR agonism or antagonism. Noteworthy, despite the emerging concept that systemic GIP antagonism has a positive effect on body weight, similarly to the whole-body loss-of-function phenotypes of GIPR or GIP-deficiencies, targeting of GIPR-deficiency to myeloid immune cells produces the opposite effect with impaired energy expenditure and increased weight gain during nutrient overload. Hence, understanding the mechanisms behind the positive effects on body weight of therapies based on GIP analogues may benefit from incorporating knowledge of how GIPR signaling impacts different cell types within the immunological compartment, and specifically type 2 immunity.

In conclusion, we identified GIPR signaling as an important regulator of type 2 immunity networks in epiWAT and energy expenditure in ingWAT and a gatekeeper of the unrestrained activity of S100A8/A9 in myeloid cells during obesity. Our findings outline a pivotal gut-immune axis mediated by GIP in controlling immunometabolic crosstalk in response to energy intake.

DATA AVAILABILITY STATEMENT

The original contributions presented in the study are included in the article. Further inquiries can be directed to the corresponding authors.

ETHICS STATEMENT

The animal study was reviewed and approved by The Animal Care Use Committee of the Sourasky Medical Center.

AUTHOR CONTRIBUTIONS

The corresponding authors (CV and SF) confirm that all authors agreed to be accountable for the content of the work. IE, IZ, SF, and CV conceived the study, designed the experiments, and wrote the manuscript. IE, IS, IZ, and DM performed the experiments and analyzed the data. AN performed some of the RT–PCR and immunoblot analyses in the presented experiments. DD provided key scientific consultation, mouse tools, and carefully reviewed and edited the manuscript. CV and SF supervised the study. All authors contributed to the article and approved the submitted version.

FUNDING

CV and SF have received funding from the Israeli Science Foundation (grant nos. 1146/16 and 1114/20). CV is supported by the Joint Canada-Israel Health Research Program (grant no. 3416/19). DD is supported by a Banting and Best Diabetes Centre-Novo Nordisk Chair in Incretin Biology, the Novo Nordisk Foundation-Sinai Health Fund in Regulatory Peptides, CIHR grant 154321. These studies were directly supported by the Canada-Israel Health Research Initiative, jointly funded by the Canadian Institutes of Health Research, the Israel Science Foundation, International Development Research Centre, and the Azrieli Foundation, project 109150. Funding sources were not involved in the study design, collection, analysis, interpretation of data, preparation of the manuscript, and its submission.

ACKNOWLEDGMENTS

We would like to thank Ziv Itach Abramovich for his assistance with sorting experiments. We also thank Dr. Nathan Strauss for providing mouse irradiation services (Sourasky Medical Center) for radiation services. Finally, we would like to thank Prof. Thomas Vogl (University of Münster, Germany) for providing the *S100a9*$^{-/-}$ mice.

REFERENCES

1. Lee AH, Dixit VD. Dietary Regulation of Immunity. *Immunity* (2020) 53:510–23. doi: 10.1016/j.immuni.2020.08.013
2. Gribble FM, Reimann F. Enteroendocrine Cells: Chemosensors in the Intestinal Epithelium. *Annu Rev Physiol* (2016) 78:277–99. doi: 10.1146/annurev-physiol-021115-105439
3. Campbell JE, Drucker DJ. Pharmacology, physiology, and mechanisms of incretin hormone action. *Cell Metab* (2013) 17:819–37. doi: 10.1016/j.cmet.2013.04.008
4. Finan B, Ma T, Ottaway N, Muller TD, Habegger KM, Heppner KM, et al. Unimolecular dual incretins maximize metabolic benefits in rodents, monkeys, and humans. *Sci Transl Med* (2013) 5:209ra151. doi: 10.1126/scitranslmed.3007218
5. Nauck MA, Meier JJ. Incretin hormones: Their role in health and disease. *Diabetes Obes Metab* (2018) 20 Suppl 1:5–21. doi: 10.1111/dom.13129
6. Fishman S, Zvibel I, Varol C. Incretin Hormones in the Control of Immunometabolism. *Immunometabolism* (2019) 1:e190004. doi: 10.20900/immunometab20190004
7. Pujadas G, Varin EM, Baggio LL, Mulvihill EE, Bang KWA, Koehler JA, et al. The gut hormone receptor GIPR links energy availability to the control of hematopoiesis. *Mol Metab* (2020) 39:101008. doi: 10.1016/j.molmet.2020.101008
8. Chen S, Okahara F, Osaki N, Shimotoyodome A. Increased GIP signaling induces adipose inflammation via a HIF-1alpha-dependent pathway and impairs insulin sensitivity in mice. *Am J Physiol Endocrinol Metab* (2015) 308:E414–25. doi: 10.1152/ajpendo.00418.2014
9. Gogebakan O, Osterhoff MA, Schuler R, Pivovarova O, Kruse M, Seltmann AC, et al. GIP increases adipose tissue expression and blood levels of MCP-1 in humans and links high energy diets to inflammation: a randomised trial. *Diabetologia* (2015) 58:1759–68. doi: 10.1007/s00125-015-3618-4
10. Kim SJ, Nian C, Karunakaran S, Clee SM, Isales CM, McIntosh CH. GIP-overexpressing mice demonstrate reduced diet-induced obesity and steatosis,

and improved glucose homeostasis. *PloS One* (2012) 7:e40156. doi: 10.1371/journal.pone.0040156
11. Varol C, Zvibel I, Spektor L, Mantelmacher FD, Vugman M, Thurm T, et al. Long-acting glucose-dependent insulinotropic polypeptide ameliorates obesity-induced adipose tissue inflammation. *J Immunol* (2014) 193:4002–9. doi: 10.4049/jimmunol.1401149
12. Killion EA, Lu SC, Fort M, Yamada Y, Veniant MM, Lloyd DJ. Glucose-Dependent Insulinotropic Polypeptide Receptor Therapies for the Treatment of Obesity, Do Agonists = Antagonists? *Endocr Rev* (2020) 41(1):1–21. doi: 10.1210/endrevbnz002
13. Mantelmacher FD, Zvibel I, Cohen K, Epshtein A, Pasmanik-Chor M, Vogl T, et al. An enteroendocrine-myeloid cell S100A8/A9 axis controls inflammation and body weight. *Nat Metab* (2019) 1:58–69. doi: 10.1038/s42255-018-0001-z
14. Miyawaki K, Yamada Y, Ban N, Ihara Y, Tsukiyama K, Zhou H, et al. Inhibition of gastric inhibitory polypeptide signaling prevents obesity. *Nat Med* (2002) 8:738–42. doi: 10.1038/nm727
15. Rosen ED, Spiegelman BM. Adipocytes as regulators of energy balance and glucose homeostasis. *Nature* (2006) 444:847–53. doi: 10.1038/nature05483
16. Rosen ED, Spiegelman BM. What we talk about when we talk about fat. *Cell* (2014) 156:20–44. doi: 10.1016/j.cell.2013.12.012
17. Brestoff JR, Artis D. Immune regulation of metabolic homeostasis in health and disease. *Cell* (2015) 161:146–60. doi: 10.1016/j.cell.2015.02.022
18. Qiu Y, Nguyen KD, Odegaard JI, Cui X, Tian X, Locksley RM, et al. Eosinophils and type 2 cytokine signaling in macrophages orchestrate development of functional beige fat. *Cell* (2014) 157:1292–308. doi: 10.1016/j.cell.2014.03.066
19. Wu D, Molofsky AB, Liang HE, Ricardo-Gonzalez RR, Jouihan HA, Bando JK, et al. Eosinophils sustain adipose alternatively activated macrophages associated with glucose homeostasis. *Science* (2011) 332:243–7. doi: 10.1126/science.1201475
20. Fischer K, Ruiz HH, Jhun K, Finan B, Oberlin DJ, van der Heide V, et al. Alternatively activated macrophages do not synthesize catecholamines or contribute to adipose tissue adaptive thermogenesis. *Nat Med* (2017) 23:623–30. doi: 10.1038/nm.4316
21. Lee MW, Odegaard JI, Mukundan L, Qiu Y, Molofsky AB, Nussbaum JC, et al. Activated type 2 innate lymphoid cells regulate beige fat biogenesis. *Cell* (2015) 160:74–87. doi: 10.1016/j.cell.2014.12.011
22. Nussbaum JC, Van Dyken SJ, von Moltke J, Cheng LE, Mohapatra A, Molofsky AB, et al. Type 2 innate lymphoid cells control eosinophil homeostasis. *Nature* (2013) 502:245–8. doi: 10.1038/nature12526
23. Brestoff JR, Kim BS, Saenz SA, Stine RR, Monticelli LA, Sonnenberg GF, et al. Group 2 innate lymphoid cells promote beiging of white adipose tissue and limit obesity. *Nature* (2015) 519:242–6. doi: 10.1038/nature14115
24. Cipolletta D, Feuerer M, Li A, Kamei N, Lee J, Shoelson SE, et al. PPAR-gamma is a major driver of the accumulation and phenotype of adipose tissue Treg cells. *Nature* (2012) 486:549–53. doi: 10.1038/nature11132
25. Vasanthakumar A, Moro K, Xin A, Liao Y, Gloury R, Kawamoto S, et al. The transcriptional regulators IRF4, BATF and IL-33 orchestrate development and maintenance of adipose tissue-resident regulatory T cells. *Nat Immunol* (2015) 16:276–85. doi: 10.1038/ni.3085
26. Odegaard JI, Lee MW, Sogawa Y, Bertholet AM, Locksley RM, Weinberg DE, et al. Perinatal Licensing of Thermogenesis by IL-33 and ST2. *Cell* (2017) 171:1707. doi: 10.1016/j.cell.2017.12.003
27. Mahlakoiv T, Flamar AL, Johnston LK, Moriyama S, Putzel GG, Bryce PJ, et al. Stromal cells maintain immune cell homeostasis in adipose tissue via production of interleukin-33. *Sci Immunol* (2019) 4(35):eaax0416. doi: 10.1126/sciimmunol.aax0416
28. Spallanzani RG, Zemmour D, Xiao T, Jayewickreme T, Li C, Bryce PJ, et al. Distinct immunocyte-promoting and adipocyte-generating stromal components coordinate adipose tissue immune and metabolic tenors. *Sci Immunol* (2019) 4(35):eaaw3658. doi: 10.1126/sciimmunol.aaw3658
29. Gao M, Zhang C, Ma Y, Bu L, Yan L, Liu D. Hydrodynamic delivery of mIL10 gene protects mice from high-fat diet-induced obesity and glucose intolerance. *Mol Ther* (2013) 21:1852–61. doi: 10.1038/mt.2013.125
30. Lumeng CN, Bodzin JL, Saltiel AR. Obesity induces a phenotypic switch in adipose tissue macrophage polarization. *J Clin Invest* (2007) 117:175–84. doi: 10.1172/JCI29881
31. Xie L, Fu Q, Ortega TM, Zhou L, Rasmussen D, O'Keefe J, et al. Overexpression of IL-10 in C2D macrophages promotes a *macrophage phenotypic switch in adipose tissue environments*. *PloS One* (2014) 9:e86541. doi: 10.1371/journal.pone.0086541
32. Hong EG, Ko HJ, Cho YR, Kim HJ, Ma Z, Yu TY, et al. Interleukin-10 prevents diet-induced insulin resistance by attenuating macrophage and cytokine response in skeletal muscle. *Diabetes* (2009) 58:2525–35. doi: 10.2337/db08-1261
33. Rajbhandari P, Thomas BJ, Feng AC, Hong C, Wang J, Vergnes L, et al. IL-10 Signaling Remodels Adipose Chromatin Architecture to Limit Thermogenesis and Energy Expenditure. *Cell* (2018) 172:218–233 e17. doi: 10.1016/j.cell.2017.11.019
34. Acosta JR, Tavira B, Douagi I, Kulyte A, Arner P, Ryden M, et al. Human-Specific Function of IL-10 in Adipose Tissue Linked to Insulin Resistance. *J Clin Endocrinol Metab* (2019) 104:4552–62. doi: 10.1210/jc.2019-00341
35. Macdougall CE, Wood EG, Loschko J, Scagliotti V, Cassidy FC, Robinson ME, et al. Visceral Adipose Tissue Immune Homeostasis Is Regulated by the Crosstalk between Adipocytes and Dendritic Cell Subsets. *Cell Metab* (2018) 27:588–601 e4. doi: 10.1016/j.cmet.2018.02.007
36. Feuerer M, Herrero L, Cipolletta D, Naaz A, Wong J, Nayer A, et al. Lean, but not obese, fat is enriched for a unique population of regulatory T cells that affect metabolic parameters. *Nat Med* (2009) 15:930–9. doi: 10.1038/nm.2002
37. Nishimura S, Manabe I, Takaki S, Nagasaki M, Otsu M, Yamashita H, et al. Adipose Natural Regulatory B Cells Negatively Control Adipose Tissue Inflammation. *Cell Metab* (2013) 18:759–66. doi: 10.1016/j.cmet.2013.09.017
38. Ehrchen JM, Sunderkotter C, Foell D, Vogl T, Roth J. The endogenous Toll-like receptor 4 agonist S100A8/S100A9 (calprotectin) as innate amplifier of infection, autoimmunity, and cancer. *J Leukoc Biol* (2009) 86:557–66. doi: 10.1189/jlb.1008647
39. Jaitin DA, Adlung L, Thaiss CA, Weiner A, Li B, Descamps H, et al. Lipid-Associated Macrophages Control Metabolic Homeostasis in a Trem2-Dependent Manner. *Cell* (2019) 178:686–698 e14. doi: 10.1016/j.cell.2019.05.054
40. Wang S, Song R, Wang Z, Jing Z, Wang S, Ma J. S100A8/A9 in Inflammation. *Front Immunol* (2018) 9:1298. doi: 10.3389/fimmu.2018.01298
41. Kang K, Reilly SM, Karabacak V, Gangl MR, Fitzgerald K, Hatano B, et al. Adipocyte-derived Th2 cytokines and myeloid PPARdelta regulate macrophage polarization and insulin sensitivity. *Cell Metab* (2008) 7:485–95. doi: 10.1016/j.cmet.2008.04.002
42. Kwon H, Laurent S, Tang Y, Zong H, Vemulapalli P, Pessin JE. Adipocyte-specific IKKbeta signaling suppresses adipose tissue inflammation through an IL-13-dependent paracrine feedback pathway. *Cell Rep* (2014) 9:1574–83. doi: 10.1016/j.celrep.2014.10.068
43. Suzuki T, Gao J, Ishigaki Y, Kondo K, Sawada S, Izumi T, et al. ER Stress Protein CHOP Mediates Insulin Resistance by Modulating Adipose Tissue Macrophage Polarity. *Cell Rep* (2017) 18:2045–57. doi: 10.1016/j.celrep.2017.01.076
44. LaMarche NM, Kane H, Kohlgruber AC, Dong H, Lynch L, Brenner MB. Distinct iNKT Cell Populations Use IFNgamma or ER Stress-Induced IL-10 to Control Adipose Tissue Homeostasis. *Cell Metab* (2020) 32:243–258 e6. doi: 10.1016/j.cmet.2020.05.017
45. Ron D, Walter P. Signal integration in the endoplasmic reticulum unfolded protein response. *Nat Rev Mol Cell Biol* (2007) 8:519–29. doi: 10.1038/nrm2199
46. Majumder M, Huang C, Snider MD, Komar AA, Tanaka J, Kaufman RJ, et al. A novel feedback loop regulates the response to endoplasmic reticulum stress via the cooperation of cytoplasmic splicing and mRNA translation. *Mol Cell Biol* (2012) 32:992–1003. doi: 10.1128/MCB.06665-11
47. Lee YS, Wollam J, Olefsky JM. An Integrated View of Immunometabolism. *Cell* (2018) 172:22–40. doi: 10.1016/j.cell.2017.12.025
48. Kim SJ, Chae S, Kim H, Mun DG, Back S, Choi HY, et al. A protein profile of visceral adipose tissues linked to early pathogenesis of type 2 diabetes mellitus. *Mol Cell Proteomics* (2014) 13:811–22. doi: 10.1074/mcp.M113.035501
49. Mortensen OH, Nielsen AR, Erikstrup C, Plomgaard P, Fischer CP, Krogh-Madsen R, et al. Calprotectin–a novel marker of obesity. *PloS One* (2009) 4:e7419. doi: 10.1371/journal.pone.0007419
50. Tomonobu N, Kinoshita R, Sakaguchi M. S100 Soil Sensor Receptors and Molecular Targeting Therapy Against Them in Cancer Metastasis. *Transl Oncol* (2020) 13:100753. doi: 10.1016/j.tranon.2020.100753
51. Nagashima M, Watanabe T, Terasaki M, Tomoyasu M, Nohtomi K, Kim-Kaneyama J, et al. Native incretins prevent the development of atherosclerotic

lesions in apolipoprotein E knockout mice. *Diabetologia* (2011) 54:2649–59. doi: 10.1007/s00125-011-2241-2
52. Nogi Y, Nagashima M, Terasaki M, Nohtomi K, Watanabe T, Hirano T. Glucose-dependent insulinotropic polypeptide prevents the progression of macrophage-driven atherosclerosis in diabetic apolipoprotein E-null mice. *PloS One* (2012) 7:e35683. doi: 10.1371/journal.pone.0035683
53. Kahles F, Liberman A, Halim C, Rau M, Mollmann J, Mertens RW, et al. The incretin hormone GIP is upregulated in patients with atherosclerosis and stabilizes plaques in ApoE(-/-) mice by blocking monocyte/macrophage activation. *Mol Metab* (2018) 14:150–7. doi: 10.1016/j.molmet.2018.05.014
54. Spielman LJ, Gibson DL, Klegeris A. Incretin hormones regulate microglia oxidative stress, survival and expression of trophic factors. *Eur J Cell Biol* (2017) 96:240–53. doi: 10.1016/j.ejcb.2017.03.004
55. Duffy AM, Holscher C. The incretin analogue D-Ala2GIP reduces plaque load, astrogliosis and oxidative stress in an APP/PS1 mouse model of Alzheimer's disease. *Neuroscience* (2013) 228:294–300. doi: 10.1016/j.neuroscience.2012.10.045
56. Faivre E, Holscher C. Neuroprotective effects of D-Ala(2)GIP on Alzheimer's disease biomarkers in an APP/PS1 mouse model. *Alzheimers Res Ther* (2013) 5:20. doi: 10.1186/alzrt174
57. Li Y, Liu W, Li L, Holscher C. Neuroprotective effects of a GIP analogue in the MPTP Parkinson's disease mouse model. *Neuropharmacology* (2016) 101:255–63. doi: 10.1016/j.neuropharm.2015.10.002
58. Yuan Z, Li D, Feng P, Xue G, Ji C, Li G, et al. A novel GLP-1/GIP dual agonist is more effective than liraglutide in reducing inflammation and enhancing GDNF release in the MPTP mouse model of Parkinson's disease. *Eur J Pharmacol* (2017) 812:82–90. doi: 10.1016/j.ejphar.2017.06.029
59. Campbell JE. Targeting the GIPR for obesity: To agonize or antagonize? Potential mechanisms. *Mol Metab* (2020), 101139. doi: 10.1016/j.molmet.2020.101139
60. Sparre-Ulrich AH, Hansen LS, Svendsen B, Christensen M, Knop FK, Hartmann B, et al. Species-specific action of (Pro3)GIP - a full agonist at human GIP receptors, but a partial agonist and competitive antagonist at rat and mouse GIP receptors. *Br J Pharmacol* (2016) 173:27–38. doi: 10.1111/bph.13323
61. Svendsen B, Capozzi ME, Nui J, Hannou SA, Finan B, Naylor J, et al. Pharmacological antagonism of the incretin system protects against diet-induced obesity. *Mol Metab* (2020) 32:44–55. doi: 10.1016/j.molmet.2019.11.018
62. Killion EA, Chen M, Falsey JR, Sivits G, Hager T, Atangan L, et al. Chronic glucose-dependent insulinotropic polypeptide receptor (GIPR) agonism desensitizes adipocyte GIPR activity mimicking functional GIPR antagonism. *Nat Commun* (2020) 11:4981. doi: 10.1038/s41467-020-18751-8

Conflict of Interest: DD has served as an advisor or consultant or speaker within the past 12 months to Boehringer Ingelheim Inc., Forkhead Biotherapeutics, Intarcia Therapeutics, Kallyope, Merck Research Laboratories, Eli Lilly Inc., Novo Nordisk Inc. Neither DD nor his family members hold stock directly or indirectly in any of these companies. GLP-2 is the subject of a patent license agreement between Shire Inc and the University of Toronto, Toronto General Hospital (UHN), and Daniel Drucker.

The remaining authors declare that the research was conducted in the absence of any commercial or financial relationships that could be construed as a potential conflict of interest.

Copyright © 2021 Efimova, Steinberg, Zvibel, Neumann, Mantelmacher, Drucker, Fishman and Varol. This is an open-access article distributed under the terms of the Creative Commons Attribution License (CC BY). The use, distribution or reproduction in other forums is permitted, provided the original author(s) and the copyright owner(s) are credited and that the original publication in this journal is cited, in accordance with accepted academic practice. No use, distribution or reproduction is permitted which does not comply with these terms.

frontiers in Immunology

ORIGINAL RESEARCH
published: 11 March 2021
doi: 10.3389/fimmu.2021.641999

αB-Crystallin Alleviates Endotoxin-Induced Retinal Inflammation and Inhibits Microglial Activation and Autophagy

Fangyu Wang[1†], Zhaoxin Jiang[1†], Bingsheng Lou[1], Fang Duan[1], Suo Qiu[1], Zhixing Cheng[2], Xinqi Ma[1], Yao Yang[1] and Xiaofeng Lin[1*]*

[1] State Key Laboratory of Ophthalmology, Zhongshan Ophthalmic Center, Sun Yat-sen University, Guangzhou, China,
[2] Guangdong Provincial People's Hospital, Guangdong Academy of Medical Sciences, Guangzhou, China

αB-Crystallin, a member of the small heat shock protein (sHSP) family, plays an immunomodulatory and neuroprotective role by inhibiting microglial activation in several diseases. However, its effect on endotoxin-induced uveitis (EIU) is unclear. Autophagy may be associated with microglial activation, and αB-crystallin is involved in the regulation of autophagy in some cells. The role of αB-crystallin in microglial autophagy is unknown. This study aimed to explore the role of αB-crystallin on retinal microglial autophagy, microglial activation, and neuroinflammation in both cultured BV2 cells and the EIU mouse model. Our results show that αB-crystallin reduced the release of typical proinflammatory cytokines at both the mRNA and protein level, inhibited microglial activation in morphology, and suppressed the expression of autophagy-related molecules and the number of autophagolysosomes *in vitro*. In the EIU mouse model, αB-crystallin treatment alleviated the release of ocular inflammatory cytokines and the representative signs of inflammation, reduced the apoptosis of ganglion cells, and rescued retinal inflammatory structural and functional damage, as evaluated by optical coherence tomographic and electroretinography. Taken together, these results indicate that αB-crystallin inhibits the activation of microglia and supresses microglial autophagy, ultimately reducing endotoxin-induced neuroinflammation. In conclusion, αB-crystallin provides a novel and promising option for affecting microglial autophagy and alleviating symptoms of ocular inflammatory diseases.

Keywords: αB-crystallin, microglial activation, autophagy, endotoxin-induced uveitis, ocular inflammatory diseases

OPEN ACCESS

Edited by:
Sylvaine You,
Institut National de la Santé et de la Recherche Médicale (INSERM), France

Reviewed by:
Ravikanth Velagapudi,
Duke University, United States
Sanja Arandjelovic,
University of Virginia, United States

***Correspondence:**
Yao Yang
yangyao22@163.com
Xiaofeng Lin
linxiaof@mail.sysu.edu.cn

[†]These authors have contributed equally to this work

Specialty section:
This article was submitted to Inflammation, a section of the journal Frontiers in Immunology

Received: *15 December 2020*
Accepted: *09 February 2021*
Published: *11 March 2021*

Citation:
Wang F, Jiang Z, Lou B, Duan F, Qiu S, Cheng Z, Ma X, Yang Y and Lin X (2021) αB-Crystallin Alleviates Endotoxin-Induced Retinal Inflammation and Inhibits Microglial Activation and Autophagy. Front. Immunol. 12:641999. doi: 10.3389/fimmu.2021.641999

INTRODUCTION

Uveitis, a common ocular inflammatory disease, is a leading cause of blindness worldwide affecting individuals regardless of age, sex, or race (1, 2). Corticosteroids are the main treatment option for noninfectious uveitis (3, 4). In addition to poor response by 30% of patients (5), corticosteroid treatment is also accompanied by inevitable systemic as well as ocular side effects (6, 7). Therefore, there is a need for an efficient and safe intervention for uveitis. Microglia, the primary resident population of innate immune cells in the brain and retina, activates under stress and produces proinflammatory neurotoxic cytokines such as the tumor necrosis factor (TNF) and nitric oxide (NO), leading to a cascade of inflammation, which results in irreversible neurodegeneration in

various diseases (8, 9), including uveitis (10), glaucoma (11), age-related macular degeneration (AMD) (12), and retinitis pigmentosa (RP) (13). Thus, microglial activation plays an important role in a large number of inflammatory diseases.

Recently, interventions aimed at inhibiting the activation of microglia in neuroinflammatory disease have gained considerable interest. αB-Crystallin (CRYAB/HSPB5), a member of the small heat shock protein (sHSP) family, has been a recent target of interest for therapy. sHSP family members, induced by numerous stressors, are observed throughout the species (14). Recent studies have shown that αB-crystallin is not only an intracellular chaperone (stabilizing the correct protein conformation, folding, and translocation from multiple stresses) (15), but also acts as a signaling molecule in the extracellular space, communicating with other cells such as microglia, to regulate immune response and inflammation (16, 17). As an immunomodulatory neuroprotectant, αB-crystallin is involved in several stress-related statuses such as stroke (18), spinal cord contusion (19), and autoimmune demyelination (20). Furthermore, studies report that αB-crystallin alleviates neuroinflammation through inhibition of microglial activation in the anterior ischemic optic neuropathy (AION) (21) and experimental autoimmune encephalomyelitis (EAE) (17). Interestingly, retinal αB-crystallin is upregulated in *Staphylococcus aureus*-induced endophthalmitis and protects the retina from damage. Thus, modulation of the microglial activation by αB-crystallin in ocular inflammatory disease requires further investigation, which may lead to promising new therapy for uveitis.

Autophagy is a cellular process that eliminates aggregated or unfolded proteins to maintain protein homeostasis. It also removes excess or damaged organelles in the cells through several processes, including macroautophagy, microautophagy, and chaperone-mediated autophagy (CMA) (22, 23). In addition to maintaining natural innate proteostasis, molecular chaperones also participate in autophagy. As a form of molecular chaperone, αB-crystallin is closely linked with autophagy. Studies suggest that αB-crystallin not only modulates the autophagy of retinal pigment epithelium (RPE) in AMD (16) and the astrocyte in Parkinson's disease (24), but also the autophagy of cardiomyocytes in cardiomyopathy (25). Moreover, an increasing number of studies have shown that the upregulated levels of autophagy could promote microglial activation, leading to neuroinflammation, for example, in HIV associated encephalitis (26), intracerebral hemorrhage (ICH) (27), and cocaine exposure (23). In addition, one investigator reported that suppressing autophagy could inhibit microglial classical activation (28). Therefore, the role that αB-crystallin plays in microglial autophagy requires additional investigation; particularly, as microglial autophagy may provide a potential method of influencing microglial activation and ultimately ocular neuroinflammation.

Whether exogenous αB-crystallin can play a role in microglial autophagy and inhibit microglial activation in acute ocular inflammation remains unclear. Based on existing studies, we hypothesized that αB-crystallin may suppress microglial activation and influence autophagy to alleviate neuroinflammation. We aimed to explore the potential of αB-crystallin in the alleviation of ocular inflammatory diseases such as uveitis. For this purpose, the endotoxin-induced uveitis (EIU) mouse model, a mature model developed for acute ocular inflammation, was chosen. We divided our study into two parts, *in vitro* and *in vivo*. This study aimed to investigate the role of exogenous αB-crystallin in regulating microglial autophagy and activation in the BV2 microglia cells and the EIU mouse model.

MATERIALS AND METHODS

Cell Culture and Treatment

BV2 cell lines (mouse microglial cell lines) were purchased from a commercial cell bank (DMSZ, Germany). The cells were cultured in Dulbecco's Modified Eagle Medium (DMEM) (C11330500BT, Gibco), containing 10% fetal bovine serum (FBS) (LB-10270, Roby), at 37°C in a humidified incubator with 5% CO_2. BV2 microglial cells were randomly divided into three groups: (1) a control group, (2) a group treated with phosphate buffered saline (PBS)+ lipopolysaccharides (LPS), and (3) a group treated with αB-crystallin + LPS. The BV2 cells were seeded in six-well plates, followed by the addition of recombined human αB-crystallin (C7944-53, Us Biologycal) (1 μg/ml) or sterile PBS (C10010500BT, Gibco) 12 h before treatment with LPS. The selection for appropriate concentration of αB-crystallin was shown in the **Supplementary Figure 1A**. For LPS stimulation, LPS (L6529, Sigma) (100 ng/ml) was added into the six-well plates for the PBS+LPS or αB+LPS groups. The cells from one well were harvested at 6 h or 12 h after LPS stimulation for further analysis.

EIU Mouse Model and Treatment

All animal studies were conducted in accordance with the Association for Research in Vision and Ophthalmology resolution and approved by the Zhongshan Ophthalmic Center Animal Care and Use Committee, Sun Yat-sen University, Guangzhou, China (authorization number 2019164). The C57BL/6J mice (6–8 weeks old) were maintained in a 12 h light/dark cycle at 23°C with *ad libitum* access to food and water. They were randomly divided into three groups: (1) a control group, (2) a PBS+LPS group, and (3) an αB+LPS group. The right eyes of mice in the PBS+LPS and αB+LPS groups were intravitreally injected with PBS and LPS (PBS+LPS group) or αB-crystallin and LPS (αB+LPS group). The EIU mouse model was induced by a single intravitreal injection of 1 μl LPS (200 μg/ ml). Twenty four hour before the LPS injection, mice in the PBS+LPS group received one intravitreal injection of 1 μl PBS. Mice in the αB+LPS group received one intravitreal injection of 1 μl αB-crystallin (500 μg/ml). For further analysis, mice in each group were sacrificed and the right eyeballs were enucleated at 6, 12, and 24 h after the LPS stimulation. The results for single intravitreous injection of αB-crystallin were shown in the **Supplementary Figures 1B–D**.

Quantitative Real-Time Polymerase Chain Reaction (qRT-PCR)

Total RNA was isolated from the BV2 microglia of one well of six-well plates ($n = 3$) or the mouse retinas ($n = 3$) using RNAiso Plus (9108, Takara). RNA was subject to reverse

TABLE 1 | Primer sequences for qRT-PCR.

Gene		Primer sequence (3′∼ 5′)
IL6	Forward	TAGTCCTTCCTACCCCAATTTCC
	Reverse	TTGGTCCTTAGCCACTCCTTC
TNFα	Forward	TGCCTATGTCTCAGCCTCTT
	Reverse	GAGGCCATTTGGGAACTTCT
COX2	Forward	TCA TTC ACC AGA CAG ATT GCT
	Reverse	AAG CGT TTG CGG TAC TCA TT
iNOS	Forward	CCC TTC AAT GGT TGG TAC ATG G
	Reverse	ACA TTG ATC TCC GTG ACA GCC
Beclin1	Forward	GCACCATGCAGGTGAGCTTC
	Reverse	TTTCGCCTGGGCTGTGGTAA
GAPDH	Forward	GGTTGTCTCCTGCGACTTCA
	Reverse	TGGTCCAGGGTTTCTTACTCC

transcription to cDNA using the PrimeScriptTMRT reagent kit (RR036B, Takara). The nucleic acid purity was quantified and analyzed using spectrophotometry (NanoDrop Technologies, Wilmington, DE). Primer sequences are presented in **Table 1**. Gene expression levels were measured using the LightCycler 480 system (Roche, Switzerland). The PCR procedure was as follows: pre-incubation for 5 min at 95°C, followed by 40 cycle amplification of denaturation for 10 s at 95°C, and annealing for 15 s at 60°C. The expression level of each gene was expressed as the fold expression after normalization to the internal control glyceraldehyde 3-phosphate dehydrogenase (GAPDH).

Western Blotting

The total protein was extracted from the BV2 cells of one well of six-well plates ($n = 3$) or the mouse retinas ($n = 3$) using lysis buffer (KGP250, KeyGen) containing protease and phosphatase inhibitors. The protein concentration was measured using the PierceTM BCA Protein Assay Kit (23227, Thermo Scientific). An equal amount of protein from each sample was mixed with 5X SDS loading buffer (KGP101, KeyGen), subjected to 12% SDS gel, and then transferred to PVDF membranes (ISEQ00010, Merck Millipore). The membranes were blocked with 5% non-fat milk (MB3217, Meilunbio) in PBS for 1.5 h at room temperature and then incubated with primary antibodies against a nitric oxide synthase (iNOS) (ab15323, Abcam), cyclooxygenase 2 (COX2) (12282S, CST), Beclin1 (3738S, CST), Light Chain 3 (LC3) (3868S, CST), and GAPDH (ab8245, Abcam) overnight at 4°C. The membranes were then incubated with secondary antibodies (ab6802, Abcam; ab6789, Abcam) for 1 h. Protein bands were visualized using the ChemiDoc Touch Imaging System (Bio-Rad, USA). The band intensity was quantified using Image J software (NIH, USA).

Enzyme-Linked Immunosorbent Assay (ELISA)

The cellular supernatant and intraocular liquid from mice were collected. Cardiac perfusion was performed with PBS on the anesthetized mice before they were sacrificed, followed by removal of the right eyes. The extraocular muscle and fascia were cleared. The eyeball was washed with PBS and dried with gauze. The eyeball was carefully dissected to remove the cornea, iris, lens, retina, and choroid; the intraocular liquid was then collected with tips. The cellular supernatant or intraocular fluid was collected and centrifuged at 16,000 *g* for 30 min at 4°C. The supernatant was removed and stored at −80°C until further analysis. The cell supernatant ($n = 3$) and intraocular fluid ($n = 9$) were collected 12 h after LPS stimulation. The cellular supernatant (1:50 diluted by PBS) and intraocular fluid (1:20 diluted by PBS) of each group were measured using ELISA kits for tumor necrosis factor alpha (TNF-α) (MTA00B, R&D) and interleukin-6 (IL-6) (M6000B, R&D), following the manufacturer's instructions.

Immunofluorescent Staining

Cells were seeded onto 8-well glass chamber slides (PEZGS0816, Merck Millipore) for fixation and further staining. Cells were fixed with 4% paraformaldehyde (PFA) (DF0133-4, Leagene) for 15 min and washed by PBS three times. For cryosections, eyeballs were carefully removed, fixed in 4% PFA at 4°C overnight, subjected to gradient dehydration with sucrose solution (10, 20, and 30%), and embedded in an OCT compound (4583, Sakura) at −80°C. The frozen samples were sliced transversely (12 μm) with a cryostat (CM1950, Leica) at −20°C and then washed by PBS three times. For retinal flat mounts, the eyeballs were fixed in 4% PFA for 1 h at room temperature, and the retina was dissected out as a cup. The cells, cryosections, and retinal cups were blocked with PBS containing 0.1% Triton-X100 (1139ML100, Biosharp) and 5% bovine serum albumin (BSA) (4240GR100, Biofoxx) at room temperature for 1 h. The cells and cryosections were incubated with primary antibodies at 4°C overnight, and the retinal cups, for 24 h. The primary antibodies were diluted in blocking buffer. The primary antibody included anti-Iba1 (011-27991, Woka), anti-Beclin1 (ab207612, Abcam), and anti-LC3 (3868, CST). The reason we excluded P62 antibody was shown in the **Supplementary Figure 1E**. After washing with PBS three times, the cells, cryosections, and retinal cups were incubated with secondary antibodies for 2 h at room temperature. The secondary antibodies were conjugated with Alexa Fluor 488 (ab150129, Abcam) and Alexa Fluor 555 (A32794, Invitrogen). The cells and cryosections were counterstained with 4′,6-diamidino-2-phenylindole (DAPI) (C0065-50, Solarbio) for 5 min and washed by PBS three times. The retinal cups were cut into four pieces and flat-mounted with an anti-fade mounting medium (S2100, Solarbio). Images were captured using a confocal microscope (LSM880, Carl Zeiss). The immunofluorescent intensity was quantified using Image J software.

Clinical Evaluation of Ocular Inflammation

After LPS injection for 24 h, the mice were anesthetized with an appropriate dose of phenobarbitone (50 mg/kg, intraperitoneal injection). The mice were administered tetracaine and tropicamide before the examination. The severity of the anterior and posterior segmental inflammation of the right eye was evaluated with slit lamp biomicroscopy (SL-D7/DC-3/IMAGEnet, Topcon) and the fundus imaging system

(MicronIV, Phoenix). For the anterior segmental images, the eyeball was adjusted to a suitable position to observe and photograph the inflammation in the anterior segment. For the posterior segmental images, methylcellulose was applied to the ocular surface to maintain contact with the lens, and to acquire the fundus image. Tobramycin ointment was then applied to protect the cornea until palinesthesia. Images were captured for further analysis. The data were shown in the **Supplementary Materials**.

Optical Coherence Tomographic (OCT) Imaging

Mice ($n = 6$) were anesthetized with pentobarbital (50 mg/kg, intraperitoneal injection), and their pupils were dilated with tropicamide. Retinal structure was assessed using an OCT imaging system (SpectralisOCT, Germany). The scan area centered on the optic nerve was 9 x 9 mm (496 data points/A scan, 1536 A-scans/horizontal B-scan, 85000 A scan/s, $30^\circ \times 30^\circ$, an average of three frames per B-scan). Saline was used to keep the cornea moist for the transparence of optical media to guarantee the image acquisition quality to be above 15. Retinal thicknesses (range of one diameter of optic disc distant from the margin of optic nerve head) were measured using the "measure" tool in the software. Total retinal thickness was measured from the nerve fiber layer to the RPE layer.

Histopathological Analysis

The enucleated eyes ($n = 6$) were fixed in FAS solution (G1109, Guge) for 24 h, washed with PBS, dehydrated using gradient reagent alcohol (65, 75, 85, 95, and 100%), and then embedded in paraffin. Mice eye sections throughout the optic disc were cut at 5 μm thickness, deparaffinized, and stained with hematoxylin and eosin (H&E) (DH0006-2, Leagene) for histopathologic analysis. The number of intraocular inflammatory cells was calculated to assess the severity of uveitis symptoms. The sections throughout the optic disc were photographed using a microscope (Leica DM4000, Germany). Each image was captured with the optic disc as the center for counting inflammatory cells. A marquee of the same size (length: 6.5 times the scale, width: 5.5 times the scale) was applied across the optic disc and the number of inflammatory cells in it was counted. The counting was performed separately by two experienced researchers and the average of the numbers from each researcher were documented.

Apoptosis by Terminal Deoxynucleotidyl Transferase dUTP Nick End Labeling (TUNEL) Assay

Cryosections were obtained using the before mentioned method. A TUNEL kit (12156792910, Roche) was used. The cryosections ($n = 6$) were washed by PBS three times and incubated the cryosections with 0.1% Triton-100 at 4°C for 5 min. The sections were incubated with the TUNEL reaction mixture at room temperature for 1 h, and then washed with PBS three times. The sections were then stained with DAPI for 5 min and washed three times. Finally, the sections were mounted with an anti-fade mounting medium and photographed using a confocal microscope (LSM880, Carl Zeiss). Images of the mid-peripheral retina were taken to count TUNEL positive cells in the visual field. The counting was performed by two researchers and the average numbers were documented.

Visual Evoked Potential (VEP)

VEP recordings of mice ($n = 6$) were performed using an electrophysiological system (Diagnosys Celeris, USA). All experimental mice underwent a dark adaptation for 12 h prior to the daytime tests. Mice were anesthetized with pentobarbital (50 mg/kg, intraperitoneal injection). Pupils were dilated with tropicamide, and the cornea was anesthetized with tetracaine. VEP was recorded using a gold-plated wire loop electrode contacting the cornea as an active electrode. Stainless steel needles inserted under the skin at the middle part of the skull and the tail were the reference and ground electrodes, respectively. The amplitudes of the VEP wave were recorded as the average of three responses under 0.05 cd·s/m^2 flash stimuli intensity. Examination parameters were as follows: LED intensity, 100%; frame rate, 6 ms; waveform contrast, 100%; and waveform frequency, 0.5 Hz.

Transmission Electron Microscopy (TEM)

BV2 cells ($n = 3$) were collected from the six-well plates, pelleted by centrifugation and fixed with TEM fixative (G1102, Servicebio) at 4°C. Pellets were then washed with 0.1 M phosphate buffer (PB) (pH 7.4) three times before being pre-embedded in 1% agarose and fixed with 1% osmium tetroxide (OsO_4) (Ted Pella Inc., USA) for 2 h at room temperature. Following fixation, samples were washed 3 times with PB and then dehydrated using an alcohol gradient (30, 70, 80, 95, and 100%) and two washes with 100% acetone (Sinopharm Chemical Reagent Co., China). To embed samples in resin, two different ratios of acetone to EMBed 812 (Structure Probe Inc., USA) were used; either 1:1 for 2 h or 1:2 overnight. Resin blocks were placed at 65°C for 48 h to polymerize. Blocks were sectioned into 60–80 nm slices using the EM UC7 ultramicrotome (Leica, Wetzlar, Germany). Slices were fixed onto cuprum grids (150 mesh) with formvar film and then stained with 2% uranium acetate and 2.6% lead citrate to avoid CO_2 exposure. Grids were left to dry overnight at room temperature before being imaged using the HT7700 TEM system (Hitachi, Japan). Five fields were randomly selected for each sample and photographed. The number of autophagolysosomes in the field was recorded. Finally, the average number of the five fields was recorded as the result for the sample. Autophagolysosome is a single membrane hybrid structure generated by the fusion of autophagosome and lysosome, containing partially or fully degraded organelles as well as cytoplasmic material, and containing electron-dense regions representing undegraded residuals (29–33).

Statistical Analyses

Statistical analyses were performed using SPSS 22.0 (IBM, USA). The mean ± SEM value comparisons of multiple groups were analyzed using one-way analysis of variance (ANOVA) followed by Tukey's *post hoc* test. A value of $p < 0.05$ was considered statistically significant.

RESULTS

αB-Crystallin Inhibited the Release of Inflammatory Cytokines and the Activation of BV2 Cells

After the cultured BV2 microglia cell lines were stimulated by LPS for 6 and 12 h, the mRNA and the protein levels of inflammatory cytokines (including COX2, iNOS, TNFα, and IL6) were significantly upregulated when compared with those in the control group. Pre-treatment of cells with αB-crystallin reduced the expression of inflammatory cytokines at the mRNA and protein levels (**Figures 1A–D**). In terms of cell morphology, the control BV2 cells were flat with filopodia. When challenged with LPS, BV2 cells were activated, as represented by a round shape with retracted filopodia. Pre-treatment with αB-crystallin sustained the ramified microglial morphology (**Figure 1E**). In conclusion, αB-crystallin efficiently suppressed the activation of microglia and blocked the inflammation *in vitro*.

αB-Crystallin Suppressed Autophagy of BV2 Cells

Beclin1 and LC3II play an important role in the autophagy process. Beclin1 contributes to the maturation of the autophagosome, whereas LC3II is an indispensable molecule for the formation of the autophagosome membrane. After the LPS stimulation, the Beclin1 mRNA in BV2 increased at 6 h (**Figure 2A**); furthermore, a Beclin1 protein increase was observed at 12 h (**Figures 2B,C**). The transformation of LC3I to LC3II increased at 12 h at the protein level (**Figures 2B,D**). Autophagolysosomes (the end product of autophagy) were also observed, and LPS increased the number of autophagolysosomes in the cells (**Figures 2E,F**). Therefore, LPS led to an increase in autophagy. Nevertheless, pre-treating cells with αB-crystallin significantly inhibited the autophagy level in cells, as confirmed by the mRNA and protein levels and the intracellular ultrastructure (**Figures 2A–F**).

αB-Crystallin Alleviated Inflammation of C57BL/6J Mice

After the 24 h intraocular injection of LPS, we observed anterior and posterior segmental ocular inflammation. Anterior segmental images showed that LPS induced inflammatory reactions such as congestion, hypopyon, hyphema, and pupil synechia. Treatment with αB-crystallin suppressed the anterior ocular inflammation (**Supplementary Figure 2A**). Regarding the posterior inflammation, the image showed that LPS led to significant inflammation, including vitreous opacity, vascular white scabbard, optic disc edema, and inflammatory cell infiltration, whereas αB-crystallin inhibited these reactions (**Supplementary Figure 2B**). H&E pictures and the scatter diagram showed that αB-crystallin decreased the number of inflammatory cells infiltrating into the vitreous body caused by LPS (**Figures 3A,B**).

αB-Crystallin Inhibited the Release of Inflammatory Cytokines and the Activation of Microglia in C57BL/6J Mice

The C57BL/6J mice were sacrificed, and the retina and vitreous fluid were tested for inflammatory cytokines (including COX2, iNOS, TNFα, and IL6). After LPS injection at 6 h and 12 h, the mRNA and protein levels of these inflammatory factors were significantly upregulated compared with those in the control group. Pre-treatment with αB-crystallin reduced the expression of inflammatory cytokines at both the mRNA and protein levels (**Figures 4A–D**). In terms of cellular morphology, retinal flat mounts showed that naive microglia presented a ramified shape with a large covering area and several branches. The activated microglia caused by LPS had an amoeboid shape with a small covering area and little branches. The ramified microglial morphology was sustained by αB-crystallin (**Figure 4E**). In addition to the direct morphologic changes, the statistical results of the subtended area and branches of each cell further confirmed the αB-crystallin suppression of microglial activation (**Figures 4F,G**).

αB-Crystallin Suppressed Autophagy of Retinal Microglia in C57BL/6J Mice

After the C57BL/6J mice were sacrificed, their eyeballs were collected for immunofluorescence assessment. The eyeball sections were double-stained for Iba1/Beclin1 or Iba1/LC3. The immunofluorescent images showed that Beclin1 and LC3 were mainly expressed in microglia, rather than other retinal cells, indicating that autophagy was an active biological process in the microglia cells. The results showed that LPS increased Beclin1 and LC3 expression compared with that in the control group, whereas αB-crystallin inhibited the expression of these autophagy-related proteins (**Figures 5A–D**).

αB-Crystallin Contributed to Protecting the Structure of the Retina and Visual Function of C57BL/6J Mice

Finally, we evaluated the protective effect of αB-crystallin on the mice retina. Intravitreal injection of LPS was performed 24 h later, and OCT was performed to detect the retinal thickness. LPS caused marked retinal thickening as well as increased retinal internal reflection indicating a severe retinal inflammatory reaction. Nevertheless, αB-crystallin decreased retinal thickness and retinal internal reflection. After 7 days, the thickness of the retina for the PBS+LPS group was reduced compared with that in the control group; thus, the inflammation might have caused further damage to the retinal structure. Regarding the LPS+αB-crystallin group, the retina was thicker than in the PBS+LPS group (**Figures 6A,B**). The TUNEL experiments showed that LPS induced retinal ganglion cell (RGC) death, whereas αB-crystallin reduced the TUNEL-positive cells (**Figures 6C,D**). In order to evaluate the function of the retina, we tested the VEP for mice at 7 d. Lower VEP amplitude showed that LPS induced functional impairment. This impairment was reduced by αB-crystallin, and the VEP amplitude for the αB+LPS group was higher than that for the PBS+LPS group (**Figures 6E,F**).

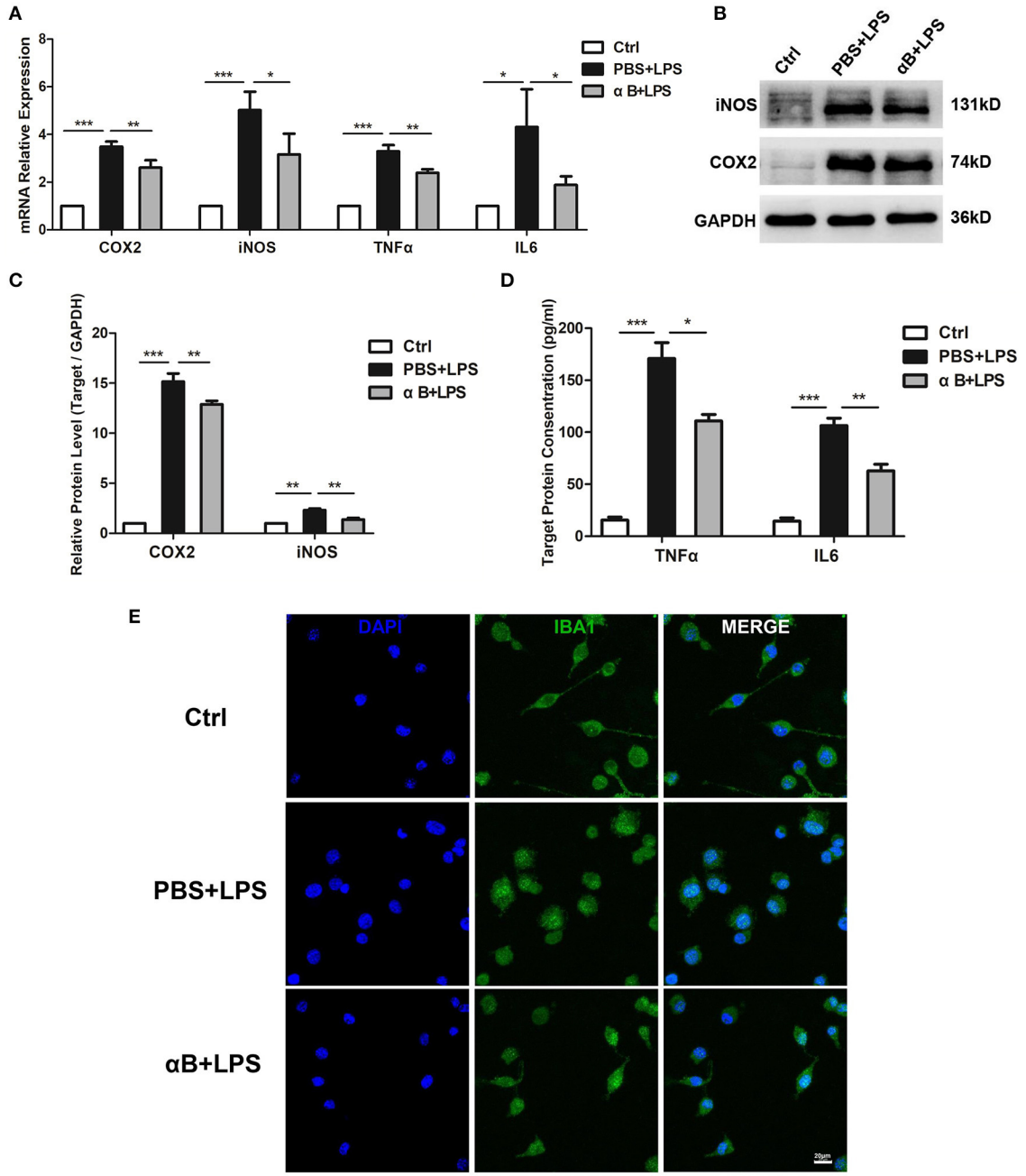

FIGURE 1 | αB-Crystallin inhibits the release of inflammatory cytokine and the activation of microglia *in vitro*. **(A)** αB-Crystallin decreased the expression of COX2, iNOS, TNFα, and IL6, at the mRNA level, in BV2 cells exposed to LPS. **(B–D)** αB-Crystallin reduced the expression of inflammatory cytokines at the protein level caused by LPS. **(B,C)** Western bolt results for COX2 and iNOS. **(D)** ELISA results for TNFα and IL6. **(E)** αB-Crystallin inhibited the activation of BV2 cells by morphology. LPS induced BV2 cells to show an amoeboid appearance, while αB-crystallin suppressed this transformation. Scale bar 20 μm. $^{*}p < 0.05$, $^{**}p < 0.01$, and $^{***}p < 0.001$ (one-way ANOVA).

DISCUSSION

To determine the effect of αB-crystallin exposure on LPS-induced inflammation, microglial activation, and microglial autophagy, we utilized indicators representing inflammatory reaction, microglial activation, microglial autophagy, and retinal structure and function. We first examined whether αB-crystallin influences microglial activation and autophagy, and then investigated whether αB-crystallin can be used as an effective *in vivo* intervention for ocular inflammatory disease. We hypothesized that modulating microglial autophagy may provide a potential target for suppressing LPS-induced neuroinflammation.

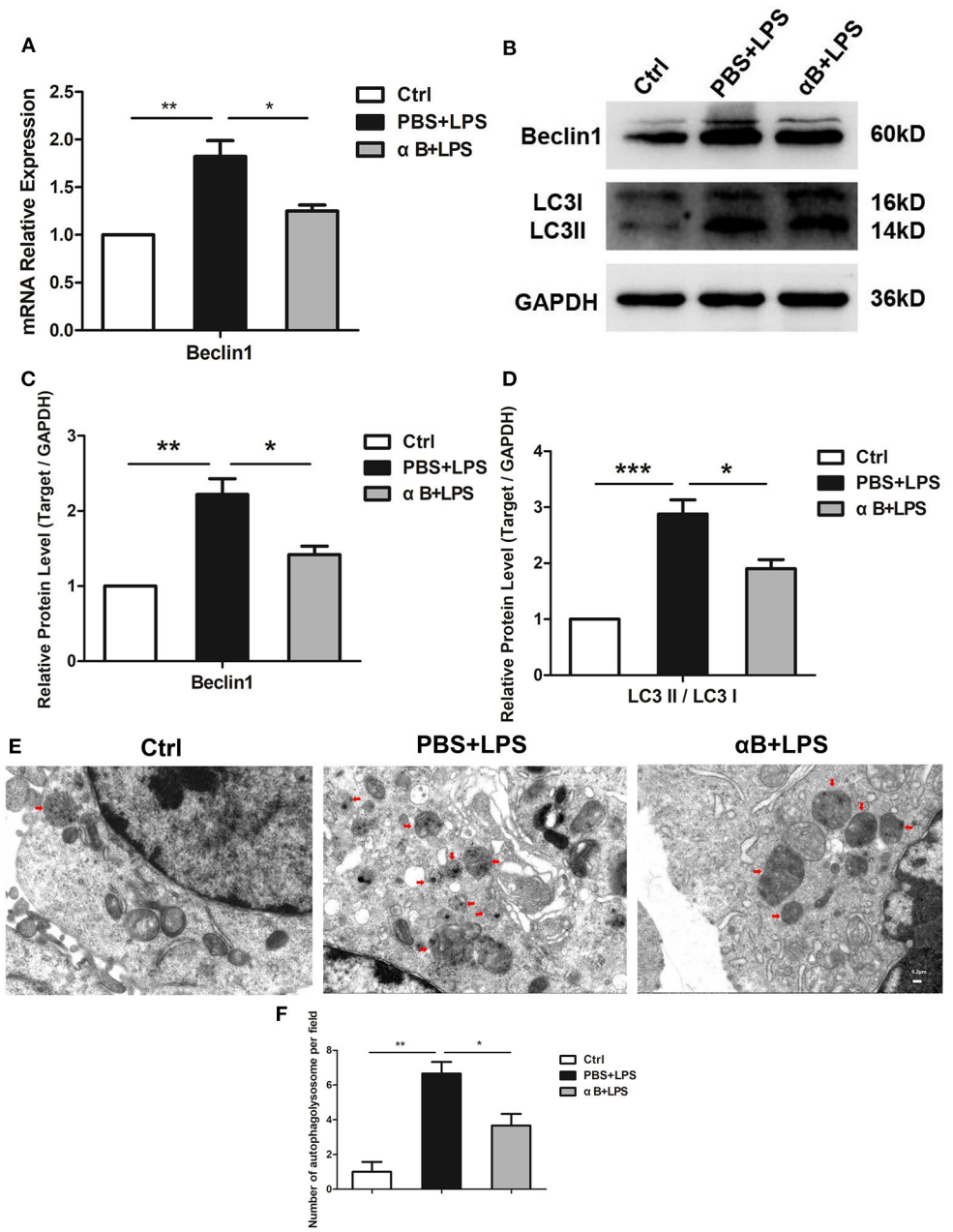

FIGURE 2 | αB-Crystallin suppresses the autophagy of microglia *in vitro*. **(A)** LPS increased the mRNA expression of Beclin1(autophagy-related gene) in BV2 cells; αB-crystallin decreased its expression caused by LPS. **(B–D)** LPS increased the Beclin1 expression and the conversion of LC3I to LC3II at the protein level in BV2 cells. **(E)** The electron micrograph images and **(F)** the statistical results for the number of autophagolysosome showed that the rest of the BV2 microglia maintained low levels of autophagy. LPS induced obvious autophagy in BV2 cells. αB-Crystallin inhibited the autophagic level caused by LPS. Red arrows indicate autophagolysosomes in cells. Scale bar 0.2 μm. $^{*}p < 0.05$, $^{**}p < 0.01$, and $^{***}p < 0.001$ (one-way ANOVA).

Our results showed that prophylactic αB-crystallin treatment effectively reduced the inflammation and the activation of microglia *in vitro*. Similarly, Guo et al. (17) reported that αB-crystallin inhibited the expression of IL1β, IL6, and TNFα in microglia under stress conditions. Pangratz-Fuehrer et al. (21) concluded that αB-crystallin could dampen microglial activation. Holtman et al. (34) found that human microglia exposed to αB-crystallin induced a series of anti-inflammatory signals based on hub gene research. These results are consistent with the anti-inflammatory effects of αB-crystallin for sustaining cellular internal environment homeostasis. Differently, Bsibsi et al. (35) showed that microglia exposed to αB-crystallin (50 μg/ml) could induce IL6, TNF, and COX2 expression. Additionally, Bhat and Sharma (36) showed that α-crystallin could induce microglial

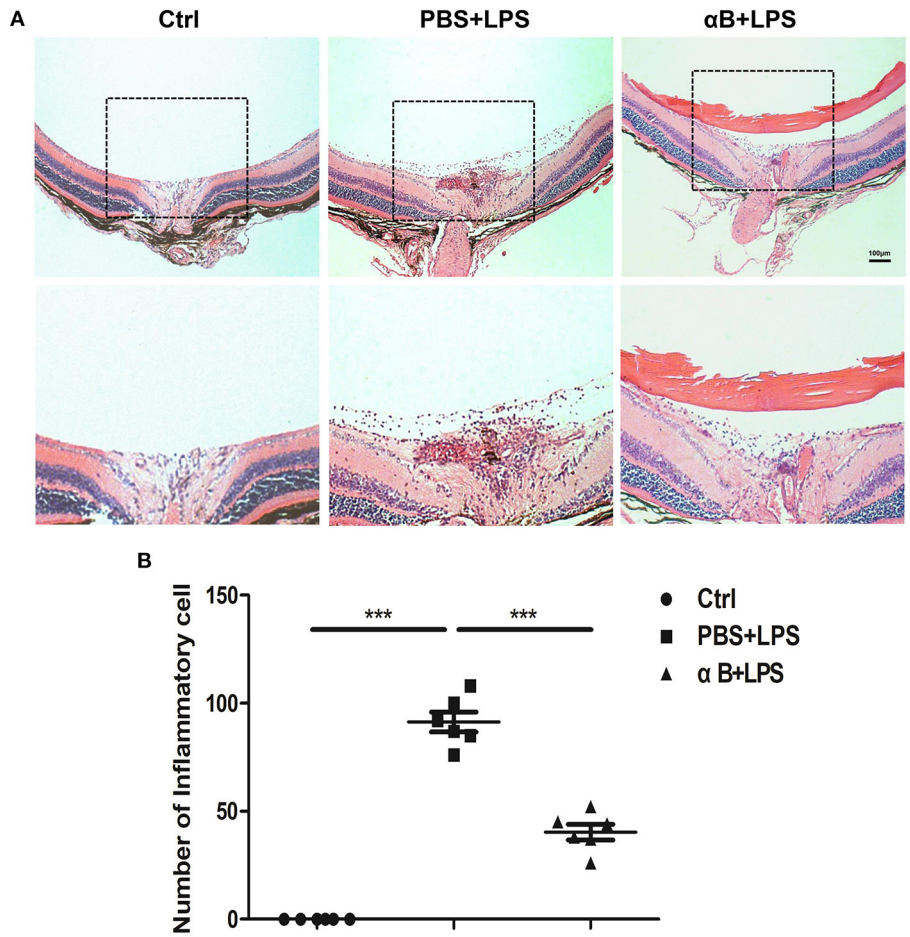

FIGURE 3 | αB-Crystallin alleviates inflammation *in vivo*. **(A,B)** αB-Crystallin relieved inflammatory infiltration in C57BL/6J mice. **(A)** H&E staining images showed that αB-crystallin decreased the number of inflammatory infiltrating cells in the vitreous cavity of C57BL/6J mice caused by LPS. Scale bar 100 μm. **(B)** The scatter diagram of infiltrating cells. ***$p < 0.001$ (one-way ANOVA).

activation. The likely reasons for this are as follows: the α-crystallin used was extracted from the bovine lens, whereas we used pure recombinant αB-crystallin. In their study (35, 36), they exposed microglia to α-crystallin (0–50 μg/ml) and found that a high concentration (50 μg/ml) of α-crystallin induced inflammation in microglia, whereas a low concentration of the protein did not. Thus, purity and protein concentration may influence the role of αB-crystallin in inflammation. In order to exert its protective effect, investigators need to ensure its purity and the appropriate concentration.

To the best of our knowledge, no reports currently exist for αB-crystallin in an EIU mouse model. In our study, we found that αB-crystallin reduced intraocular inflammation and inhibited the activation of microglia *in vivo*. Similarly, Holtman et al. (34) showed that systemic administration of αB-crystallin inhibited neuroinflammation. Arac et al. (18) demonstrated that αB-crystallin reduced both the stroke volume and the inflammatory cytokines. Wu et al. (37) reported that α-Crystallin inhibited microglial activation after the optic nerve crush. Despite the administration route (intravenous, intravitreal, or intraperitoneal) of exogenous αB-crystallin, the results show that αB-crystallin has a strong anti-inflammatory effect in various diseases, providing promising evidence for its use in alleviating ocular inflammatory diseases. This differs from the findings of Arac et al. (18) who showed that after stroke, the number of microglia cells was similar to the wild type. They only described the total number of microglia between the different groups and did not highlight the activated microglia of the CRYAB $^{-/-}$mice. Furthermore, Rao et al. (38) reported that αB-crystallin did not show a protective effect in experimental autoimmune uveitis (EAU). Their EAU mouse model was induced by subcutaneous injection of interphotoreceptor retinoid binding protein in B10.RIII mice, and the protective effect of crystallin was only evaluated on day 21 (EAU is a chronic process); this approach differed from ours. Studies suggest that the effect of α-crystallin might depend on the severity of oxidative stress and the duration of the stimulus (18). Moreover, results might differ between acute and chronic oxidative stress (39, 40). Therefore, the

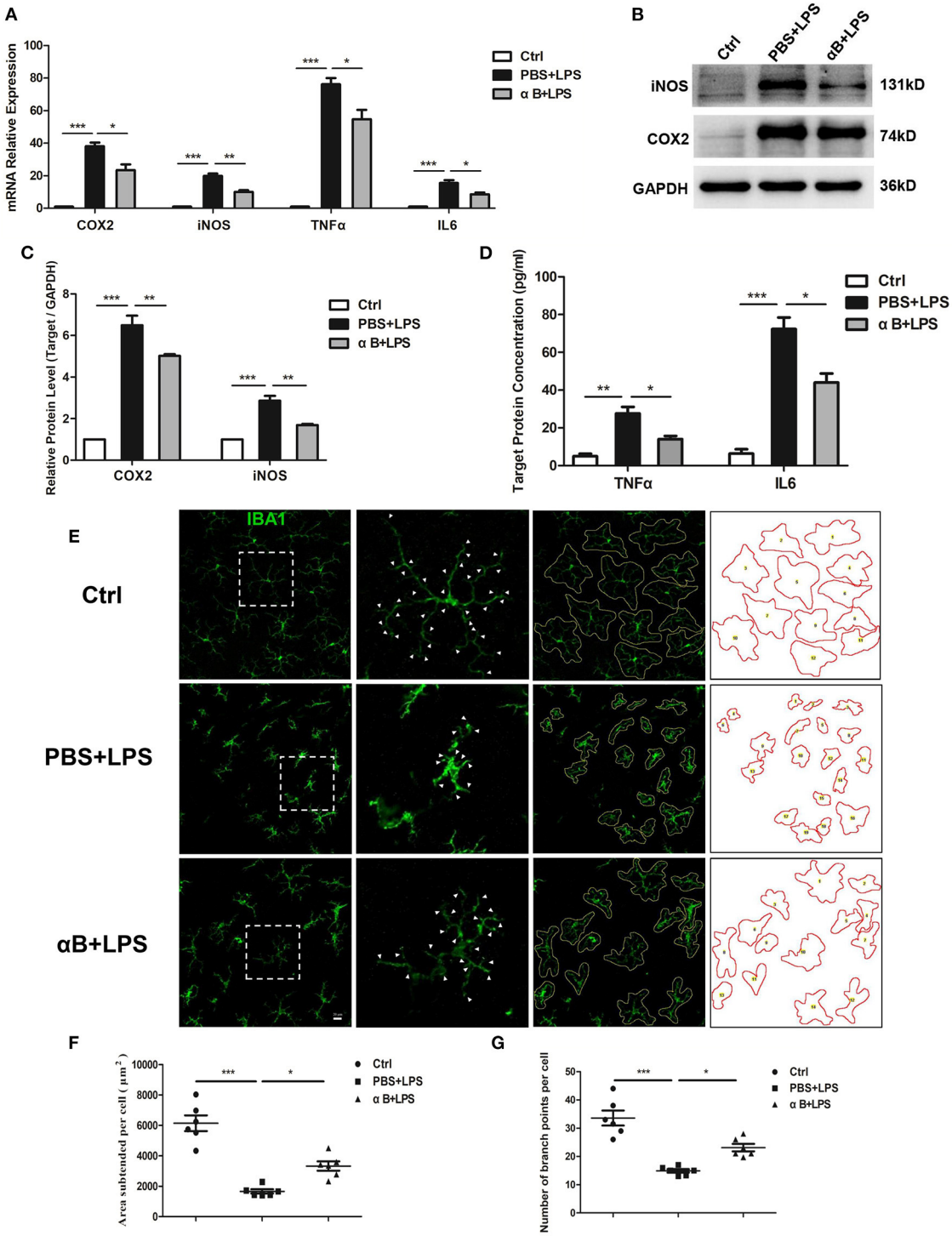

FIGURE 4 | αB-Crystallin inhibits the release of inflammatory cytokine and the activation of microglia *in vivo*. **(A–D)** αB-Crystallin decreased the expression of COX2, iNOS, TNFα, and IL6, at mRNA level, in the retina exposed to LPS. **(B–D)** αB-Crystallin reduced the expression of these inflammatory cytokines at the protein level caused by LPS. **(B,C)** Western bolt results for COX2 and iNOS in the retina. **(D)** ELISA results for TNFα and IL6 in the intraocular fluid. **(E)** αB-Crystallin inhibited the activation of microglia in C57BL/6J mice caused by LPS. LPS changed the microglial morphology (less covering area and branches), whereas αB-crystallin suppressed this morphological transformation. Scale bar 20 μm. **(F)** The scatter diagram of area subtended per cell and **(G)** the number of branch points per cell. $^{*}p < 0.05$, $^{**}p < 0.01$, and $^{***}p < 0.001$ (one-way ANOVA).

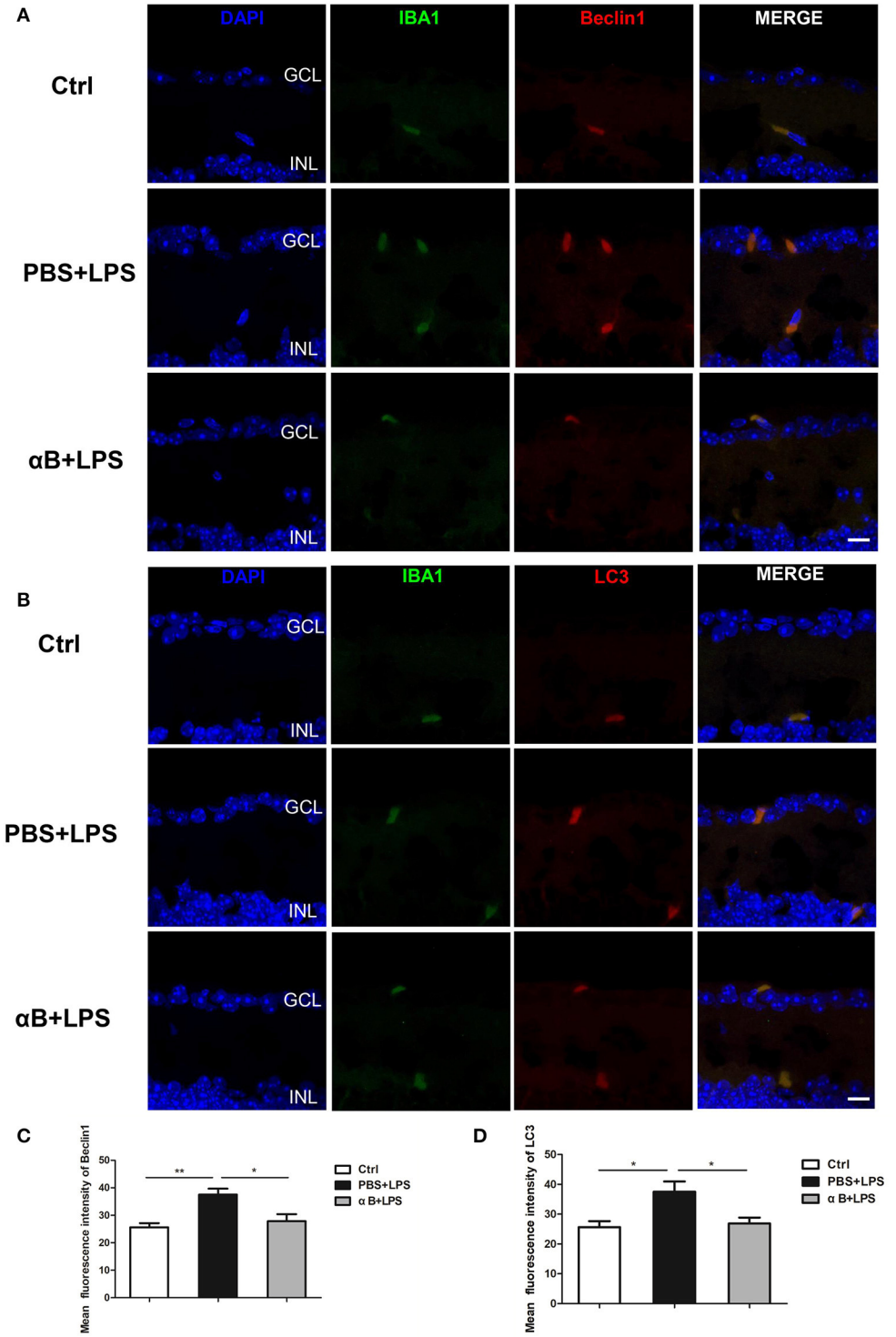

FIGURE 5 | αB-Crystallin inhibits the autophagy of microglia *in vivo*. **(A)** Representative immunofluorescence images and **(C)** the histogram for mean fluorescence intensity of Beclin 1 showed that LPS increased the Beclin1 expression in microglia compared with that in the control group, and αB-crystallin inhibited the expression of Beclin1. **(B)** Representative immunofluorescence images and **(D)** the histogram for the mean fluorescence intensity of LC3 showed that LPS increased the LC3 expression in microglia, and αB-crystallin suppressed its expression. Scale bar 10 μm. GCL, ganglion cell layer. INL, inner nuclear layer. $^{*}p < 0.05$ and $^{**}p < 0.01$ (one-way ANOVA).

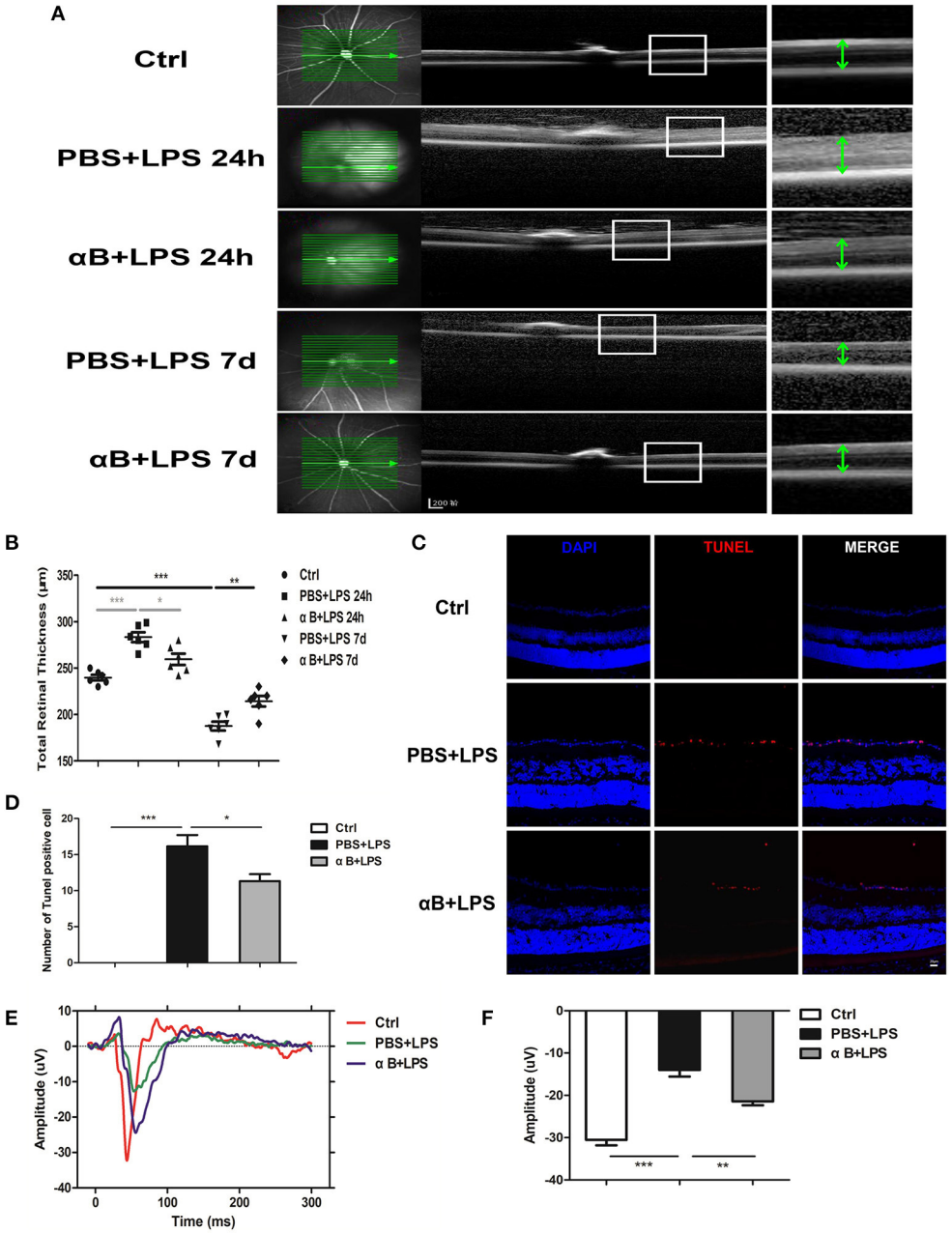

FIGURE 6 | αB-Crystallin protects the structure of the retina and visual function of C57BL/6J mice. **(A,B)** Images of OCT **(A)** and scatter diagram **(B)** showed that retinal thickness increased at 24 h but decreased at 7 d in the PBS+LPS group, whereas αB-crystallin suppressed these changes. Scale bar 200 μm. **(C)** Representative immunofluorescence images and **(D)** the statistical results showed that LPS increased the TUNEL-positive cells in the retinal ganglion cell layer, whereas αB-crystallin decreased these cells. Scale bar 20 μm. **(E)** The waveform of VEP and **(F)** the statistical results showed that LPS decreased the amplitude of VEP, whereas αB-crystallin inhibited this decrease. OCT, optical coherence tomography. VEP, visual evoked potential. $^{*}p < 0.05$, $^{**}p < 0.01$, and $^{***}p < 0.001$ (one-way ANOVA). GCL, ganglion cell layer. INL, inner nuclear layer. ONL, outer nuclear layer.

immunoregulatory role of αB-crystallin in different types of disease deserves further investigation.

The mechanism underlying αB-crystallin-mediated inhibition of microglial activation is still unclear (17). Studies show that increased autophagy might promote the activation of microglia and increase neuroinflammation in several instances, such as acute infection (41), acute electric stimulation (42), hypoxia (43), and traumatic brain injury (44). Yang et al. (45) found that suppressing autophagy decreased the microglial activation and inflammatory injury in ICH. Besides, François, et al. (46) found that through tri-culturing microglia, astrocytes, and neurons with LPS, only microglia exhibited an increased level

of autophagy combined with upregulation of an inflammatory reaction. Therefore, autophagy might play an important role in the regulation of microglial activation and neuroinflammation (46). For this reason, we observed microglial autophagy in our study. Our results showed that αB-crystallin suppressed the microglial autophagy *in vitro* and *in vivo*. Similarly, Lu et al. (24) reported that CRYAB knockdown in astrocytes resulted in a marked augmentation of autophagy activity. In contrast, Kannan (16) concluded that extracellular αB-crystallin present in drusen increased the autophagy-mediated clearance. Pattison et al. (25) found that the mutation of αB-crystallin decreased the expression of Atg7 and reduced the autophagic function of rat cardiomyocytes. Therefore, αB-crystallin may either promote or inhibit cellular autophagy in different cells. To date, there have been several studies on autophagy, but no unanimous conclusion has been reached regarding its mechanism. Mizushima et al. (22) reported the apparent conundrum that autophagy had dual effects on cells, which might be either beneficial or detrimental. Numerous studies have shown that persistent, inefficient, or excessive induction of autophagy is detrimental and promotes cellular injury (47). Based on our results, αB-crystallin may prevent microglial immoderate autophagy, which may influence microglial activation (23). However, the specific relationship between microglial autophagy and microglial activation requires further investigation.

To our surprise, our results showed that autophagic markers were detected almost exclusively in microglia (in the retina) (**Figures 5A,B**). Therefore, autophagy played an active and vital role in the microglial biological process. Further studies are required to understand the effect of αB-crystallin on microglial autophagy, such as the possible pathway. It has been reported in the literature that αB-crystallin is the ligand for TLR2 (35, 48), and based on our results it can inhibit microglial autophagy induced by LPS (ligand for TLR4). Furthermore, both TLR2 and TLR4 participate in microglial autophagy (41, 45). Whether there is a connection between the two receptors during autophagy is unclear. A deeper understanding of αB-crystallin combined with preliminary clinical application provides a potential therapy not only for uveitis but also for other inflammatory diseases.

In summary, the present study showed that prophylactic αB-crystallin treatment can suppress the LPS-induced inflammation. It reduced the release of proinflammatory cytokines as well as the activation of microglia, both *in vitro* and *in vivo*. Simultaneously, we found that αB-crystallin inhibits microglial autophagy. Microglial autophagy may therefore play a role in microglial activation. Finally, we demonstrate its beneficial effects for protecting the structure and function of the retina in the EIU model. Taken together, the use of αB-crystallin could be considered a novel potential interventional strategy for acute ocular inflammatory diseases induced by microglial activation. Additionally, the regulation of microglial autophagy may be a new effective target for the alleviation of inflammatory diseases.

DATA AVAILABILITY STATEMENT

The original contributions presented in the study are included in the article/**Supplementary Material**, further inquiries can be directed to the corresponding author/s.

ETHICS STATEMENT

The animal study was reviewed and approved by Zhongshan Ophthalmic Center Animal Care and Use Committee, Sun Yat-sen University, Guangzhou, China.

AUTHOR CONTRIBUTIONS

FW and ZJ performed experiments, analyzed data, and wrote the manuscript. XL designed and supervised the experiments. YY supervised the experiments and revised the manuscript. BL, FD, SQ, ZC, and XM performed part of the experiments. All authors contributed to the article and approved the submitted version.

FUNDING

This project was supported by the National Natural Science Foundation of China (Nos. 81900851 and 82000910) and the Fundamental Research Funds of the State Key Laboratory of Ophthalmology (Nos. 30306020240020130 and 3030902113030).

ACKNOWLEDGMENTS

The authors would like to thank Editage (www.editage.com) for English language editing.

SUPPLEMENTARY MATERIAL

The Supplementary Material for this article can be found online at: https://www.frontiersin.org/articles/10.3389/fimmu.2021.641999/full#supplementary-material

REFERENCES

1. Read RW. Uveitis: advances in understanding of pathogenesis and treatment. *Curr Rheum Rep*. (2006) 8:260–6. doi: 10.1007/s11926-006-0006-6
2. Jabs DA, Nussenblatt RB, Rosenbaum JT. Standardization of uveitis nomenclature for reporting clinical data. Results of the First International Workshop. *Am J Ophthalmol.* (2005) 140:509–16. doi: 10.1016/j.ajo.2005.03.057
3. Foster CS, Kothari S, Anesi SD, Vitale AT, Chu D, Metzinger JL, et al. The Ocular Immunology and Uveitis Foundation preferred practice patterns of uveitis management. *Surv Ophthalmol.* (2016) 61:1–17. doi: 10.1016/j.survophthal.2015.07.001
4. Engelhard SB, Patel V, Reddy AK. Intermediate uveitis, posterior uveitis, and panuveitis in the Mid-Atlantic USA. *Clin Ophthalmol.*. (2015) 9:1549–55. doi: 10.2147/opth.s89428
5. Kovaleva M, Johnson K, Steven J, Barelle CJ, Porter A. Therapeutic potential of shark anti-ICOSL VNAR domains is exemplified in a murine model of autoimmune non-infectious uveitis. *Front Immunol.* (2017) 8:1121. doi: 10.3389/fimmu.2017.01121

6. Knickelbein JE, Armbrust KR, Kim M, Sen HN, Nussenblatt RB. Pharmacologic treatment of noninfectious uveitis. *Handb Exp Pharm.* (2017) 242:231–68. doi: 10.1007/164_2016_21
7. Barnes PJ. Glucocorticosteroids: current and future directions. *Br J Pharm.* (2011) 163:29–43. doi: 10.1111/j.1476-5381.2010.01199.x
8. Silverman SM, Wong WT. Microglia in the retina: roles in development, maturity, and disease. *Ann Rev Vis Sci.* (2018) 4:45–77. doi: 10.1146/annurev-vision-091517-034425
9. Cheng Z, Yang Y, Duan F, Lou B, Zeng J, Huang Y, et al. Inhibition of notch1 signaling alleviates endotoxin-induced inflammation through modulating retinal microglia polarization. *Front Immunol.* (2019) 10:389. doi: 10.3389/fimmu.2019.00389
10. Rao NA, Kimoto T, Zamir E, Giri R, Wang R, Ito S, et al. Pathogenic role of retinal microglia in experimental uveoretinitis. *Invest Ophthalmol Vis Sci.* (2003) 44:22–31. doi: 10.1167/iovs.02-0199
11. Agarwal R, Agarwal P. Rodent models of glaucoma and their applicability for drug discovery. *Exp Opin Drug Dis.* (2017) 12:261–70. doi: 10.1080/17460441.2017.1281244
12. Ma W, Zhang Y, Gao C, Fariss RN, Tam J, Wong WT. Monocyte infiltration and proliferation reestablish myeloid cell homeostasis in the mouse retina following retinal pigment epithelial cell injury. *Sci Rep.* (2017) 7:8433. doi: 10.1038/s41598-017-08702-7
13. Roque RS, Imperial CJ, Caldwell RB. Microglial cells invade the outer retina as photoreceptors degenerate in Royal College of Surgeons rats. *Invest Ophthalmol Vis Sci.* (1996) 37:196–203.
14. Kappé G, Leunissen J, de Jong W. Evolution and diversity of prokaryotic small heat shock proteins. *Prog Mol Subcell Biol.* (2002) 28:1–17. doi: 10.1007/978-3-642-56348-5_1
15. Derham B, Harding J. Alpha-crystallin as a molecular chaperone. *Prog Retinal Eye Res.* (1999) 18:463–509. doi: 10.1016/s1350-9462(98)00030-5
16. Kannan R, Sreekumar PG, Hinton DR. Novel roles for α-crystallins in retinal function and disease. *Prog Retinal Eye Res.* (2012) 31:576–604. doi: 10.1016/j.preteyeres.2012.06.001
17. Guo YS, Liang PZ, Lu SZ, Chen R, Yin YQ, Zhou JW. Extracellular αB-crystallin modulates the inflammatory responses. *Biochem Biophys Res Commun.* (2019) 508:282–8. doi: 10.1016/j.bbrc.2018.11.024
18. Arac A, Brownell SE, Rothbard JB, Chen C, Ko RM, Pereira MP, et al. Systemic augmentation of alphaB-crystallin provides therapeutic benefit twelve hours post-stroke onset via immune modulation. *Proc Natl Acad Sci USA.* (2011) 108:13287–92. doi: 10.1073/pnas.1107368108
19. Klopstein A, Santos-Nogueira E, Francos-Quijorna I, Redensek A, David S, Navarro X, et al. Beneficial effects of αB-crystallin in spinal cord contusion injury. *J Neurosci.* (2012) 32:14478–88. doi: 10.1523/jneurosci.0923-12.2012
20. Ousman SS, Tomooka BH, van Noort JM, Wawrousek EF, O'Connor KC, Hafler DA, et al. Protective and therapeutic role for alphaB-crystallin in autoimmune demyelination. *Nature.* (2007) 448:474–9. doi: 10.1038/nature05935
21. Pangratz-Fuehrer S, Kaur K, Ousman SS, Steinman L, Liao YJ. Functional rescue of experimental ischemic optic neuropathy with alphaB-crystallin. *Eye.* (2011) 25:809–17. doi: 10.1038/eye.2011.42
22. Mizushima NL, evine B, Cuervo AM, Klionsky DJ. Autophagy fights disease through cellular self-digestion. *Nature.* (2008) 451:1069–75. doi: 10.1038/nature06639
23. Guo ML, Liao K, Periyasamy P, Yang L, Cai Y, Callen SE, et al. Cocaine-mediated microglial activation involves the ER stress-autophagy axis. *Autophagy.* (2015) 11:995–1009. doi: 10.1080/15548627.2015.1052205
24. Lu SZ, Guo YS, Liang PZ, Zhang SZ, Yin S, Yin YQ, et al. Suppression of astrocytic autophagy by alphaB-crystallin contributes to alpha-synuclein inclusion formation. *Transl Neurodegen.* (2019) 8:3. doi: 10.1186/s40035-018-0143-7
25. Pattison JS, Osinska H, Robbins J. Atg7 induces basal autophagy and rescues autophagic deficiency in CryABR120G cardiomyocytes. *Circ Res.* (2011) 109:151–60. doi: 10.1161/circresaha.110.237339
26. Zhou D, Masliah E, Spector SA. Autophagy is increased in postmortem brains of persons with HIV-1-associated encephalitis. *J Infect Dis.* (2011) 203:1647–57. doi: 10.1093/infdis/jir163
27. Yuan B, Shen H, Lin L, Su T, Zhong L, Yang Z. Autophagy promotes microglia activation through Beclin-1-Atg5 pathway in intracerebral hemorrhage. *Mol Neurobiol.* (2017) 54:115–24. doi: 10.1007/s12035-015-9642-z
28. Hu Z, Zhou L, Yang S, Chen M, Yu H, Tao R, et al. FTY720 modulates microglia toward anti-inflammatory phenotype by suppressing autophagy via STAT1 pathway. *Cell Mol Neurobiol.* (2021) 41:353–64. doi: 10.1007/s10571-020-00856-9
29. Chauhan S, Goodwin JG, Chauhan S, Manyam G, Wang J, Kamat AM, et al. ZKSCAN3 is a master transcriptional repressor of autophagy. *Mol cell.* (2013) 50:16–28. doi: 10.1016/j.molcel.2013.01.024
30. Gulbins A, Schumacher F, Becker K, Wilker B, Soddemann M, Boldrin F, et al. Antidepressants act by inducing autophagy controlled by sphingomyelin-ceramide. *Mol Psychiatry.* (2018) 23:2324–46. doi: 10.1038/s41380-018-0090-9
31. Teves JMY, Bhargava V, Kirwan KR, Corenblum MJ, Justiniano R, Wondrak GT, et al. Parkinson's disease skin fibroblasts display signature alterations in growth, redox homeostasis, mitochondrial function, and autophagy. *Front Neurosci.* (2018) 11:737. doi: 10.3389/fnins.2017.00737
32. Aivazidis S, Jain A, Rauniyar AK, Anderson CC, Marentette JO, Orlicky DJ, et al. SNARE proteins rescue impaired autophagic flux in Down syndrome. *PLoS ONE.* (2019) 14:e0223254. doi: 10.1371/journal.pone.0223254
33. Mineharu Y, King GD, Muhammad AKMG, Bannykh S, Kroeger KM, Liu C, et al. Engineering the brain tumor microenvironment enhances the efficacy of dendritic cell vaccination: implications for clinical trial design. *Clin Cancer Res.* (2011) 17:4705–18. doi: 10.1158/1078-0432.CCR-11-0915
34. Holtman I, Bsibsi M, Gerritsen W, Boddeke H, Eggen B, van der Valk P, et al. Identification of highly connected hub genes in the protective response program of human macrophages and microglia activated by alpha B-crystallin. *Glia.* (2017) 65:460–73. doi: 10.1002/glia.23104
35. Bsibsi M, Holtman IR, Gerritsen WH, Eggen BJ, Boddeke E, van der Valk P, et al. Alpha-B-crystallin induces an immune-regulatory and antiviral microglial response in preactive multiple sclerosis lesions. *J Neuropathol Exp Neurol.* (2013) 72:970–9. doi: 10.1097/NEN.0b013e3182a776bf
36. Bhat NR, Sharma KK. Microglial activation by the small heat shock protein, alpha-crystallin. *Neuroreport.* (1999) 10:2869–73. doi: 10.1097/00001756-199909090-00031
37. Wu N, Yu J, Chen S, Xu J, Ying X, Ye M, et al. α-Crystallin protects RGC survival and inhibits microglial activation after optic nerve crush. *Life Sci.* (2014) 94:17–23. doi: 10.1016/j.lfs.2013.10.034
38. Rao NA, Saraswathy S, Pararajasegaram G, Bhat SP. Small heat shock protein αA-crystallin prevents photoreceptor degeneration in experimental autoimmune uveitis. *PLoS ONE.* (2012) 7:e33582. doi: 10.1371/journal.pone.0033582
39. Shin J, Kim S, Lim C, Jeong J, Piao C, Lee J. alphaB-crystallin suppresses oxidative stress-induced astrocyte apoptosis by inhibiting caspase-3 activation. *Neurosci Res.* (2009) 64:355–61. doi: 10.1016/j.neures.2009.04.006
40. Yaung J, Jin M, Barron E, Spee C, Wawrousek E, Kannan R, et al. alpha-Crystallin distribution in retinal pigment epithelium and effect of gene knockouts on sensitivity to oxidative stress. *Mol Vis.* (2007) 13:566–77.
41. Arroyo DS, Soria JA, Gaviglio EA, Garcia-Keller C, Cancela LM, Rodriguez-Galan MC, et al. Toll-like receptor 2 ligands promote microglial cell death by inducing autophagy. *FASEB J.* (2013) 27:299–312. doi: 10.1096/fj.12-214312
42. Bie M, Lv Y, Ren C, Xing F, Cui Q, Xiao J, et al. Lycium barbarum polysaccharide improves bipolar pulse current-induced microglia cell injury through modulating autophagy. *Cell Trans.* (2015) 24:419–28. doi: 10.3727/096368915x687453
43. Yang Z, Zhao TZ, Zou YJ, Zhang JH, Feng H. Hypoxia Induces autophagic cell death through hypoxia-inducible factor 1α in microglia. *PLoS ONE.* (2014) 9:e96509. doi: 10.1371/journal.pone.0096509
44. Park Y, Liu C, Luo T, Dietrich WD, Bramlett H, Hu B. Chaperone-mediated autophagy after traumatic brain injury. *J Neurotr.* (2015) 32:1449–57. doi: 10.1089/neu.2014.3694
45. Yang Z, Liu B, Zhong L, Shen H, Lin C, Lin L, et al. Toll-like receptor-4-mediated autophagy contributes to microglial activation and inflammatory injury in mouse models of intracerebral haemorrhage. *Neuropathol Appl Neurobiol.* (2015) 41:e95–106. doi: 10.1111/nan.12177
46. François A, Terro F, Janet T, Rioux Bilan A, Paccalin M, Page G. Involvement of interleukin-1β in the autophagic process of microglia:

relevance to Alzheimer's disease. *J Neuroinflammation.* (2013) 10:151. doi: 10.1186/1742-2094-10-151

47. Chen Z, Wu Y, Wang P, Wu Y, Li Z, Zhao Y, et al. Autophagy is essential for ultrafine particle-induced inflammation and mucus hyperproduction in airway epithelium. *Autophagy.* (2016) 12:297–311. doi: 10.1080/15548627.2015.1124224
48. van Noort J, Bsibsi M, Nacken P, Verbeek R, Venneker E. Therapeutic intervention in multiple sclerosis with alpha B-crystallin: a randomized controlled phase IIa trial. *PLoS ONE.* (2015) 10:e0143366. doi: 10.1371/journal.pone.0143366

Conflict of Interest: The authors declare that the research was conducted in the absence of any commercial or financial relationships that could be construed as a potential conflict of interest.

Copyright © 2021 Wang, Jiang, Lou, Duan, Qiu, Cheng, Ma, Yang and Lin. This is an open-access article distributed under the terms of the Creative Commons Attribution License (CC BY). The use, distribution or reproduction in other forums is permitted, provided the original author(s) and the copyright owner(s) are credited and that the original publication in this journal is cited, in accordance with accepted academic practice. No use, distribution or reproduction is permitted which does not comply with these terms.

frontiers in Immunology

ORIGINAL RESEARCH
published: 17 March 2021
doi: 10.3389/fimmu.2021.637983

Resolvin E1 Regulates Th17 Function and T Cell Activation

*Fatma Oner[1,2], Carla Alvarez[1,3], Wael Yaghmoor[1,4], Danielle Stephens[1], Hatice Hasturk[1], Erhan Firatli[2] and Alpdogan Kantarci[1,5]**

[1] The Forsyth Institute, Cambridge, MA, United States, [2] Department of Periodontology, School of Dentistry, Istanbul University, Istanbul, Turkey, [3] Faculty of Dentistry, Universidad de Chile, Santiago, Chile, [4] Faculty of Dentistry, Umm Al-Qura University, Makkah, Saudi Arabia, [5] School of Dental Medicine, Harvard University, Boston, MA, United States

Resolvin E1 (RvE1) is a specialized pro-resolving lipid mediator derived from eicosapentaenoic acid and plays a critical role in resolving inflammation and tissue homeostasis. T_h17 cells are a distinct group of T helper (T_h) cells with tissue-destructive functions in autoimmune and chronic inflammatory diseases *via* the secretion of IL-17. Dendritic cell (DC)-mediated antigen presentation regulates the T_h17-induced progression of inflammation and tissue destruction. In this study, we hypothesized that the RvE1 would restore homeostatic balance and inflammation by targeting the T_h17 function. We designed three experiments to investigate the impact of RvE1 on different phases of T_h17 response and the potential role of DCs: First $CD4^+$ T cells were induced by IL-6/TGF_β to measure the effect of RvE1 on T_h17 differentiation in an inflammatory milieu. Second, we measured the impact of RvE1 on DC-stimulated T_h17 differentiation in a co-culture model. Third, we measured the effect of RvE1 on DC maturation. RvE1 blocked the CD25, CCR6 and IL-17 expression; IL-17, IL-21, IL-10, and IL-2 production, suggesting inhibition of T cell activation, T_h17 stimulation and chemoattraction. RvE1 also suppressed the activation of DCs by limiting their pro-inflammatory cytokine production. Our findings collectively demonstrated that the RvE1 targeted the T_h17 activation and the DC function as a potential mechanism for inflammatory resolution and acquired immune response.

Keywords: RvE1, T helper (T) 17 cells H, resolution of inflammation, resolvin, T cell - DC interactions

OPEN ACCESS

Edited by:
Sylvaine You,
Institut National de la Santé et de la Recherche Médicale (INSERM), France

Reviewed by:
Valerio Chiurchiù,
Italian National Research Council, Italy
Akio Morinobu,
Kyoto University, Japan

****Correspondence:***
Alpdogan Kantarci,
akantarci@forsyth.org

Specialty section:
This article was submitted to Inflammation, a section of the journal Frontiers in Immunology

Received: *04 December 2020*
Accepted: *01 March 2021*
Published: *17 March 2021*

Citation:
Oner F, Alvarez C, Yaghmoor W, Stephens D, Hasturk H, Firatli E and Kantarci A (2021) Resolvin E1 Regulates Th17 Function and T Cell Activation. Front. Immunol. 12:637983. doi: 10.3389/fimmu.2021.637983

INTRODUCTION

The resolution is critical for homeostatic balance to counteract the chronicity of inflammation (1, 2). Specialized pro-resolving lipid mediators (SPMs) regulate the cellular and molecular mechanisms to terminate the inflammatory process and restore pre-inflammatory conditions of health. This process, known as the resolution of inflammation, is a highly programmed and active stage mediated by lipoxins, maresins, protectins, and resolvins (3, 4). Resolvins are biosynthesized from omega-3 polyunsaturated fatty acids where E-series are derived from eicosapentaenoic acid, and D-series are derived from docosahexaenoic acid (5, 6). Studies in humans have demonstrated an association between defective levels of resolvins and inflammatory diseases (7, 8) and therapeutic effects of omega-3 polyunsaturated fatty acids in chronic inflammatory diseases (9). In preclinical studies, RvE1 prevented bone loss and regenerated tissue architecture (10, 11) by blocking osteoclast differentiation (12) through the RANKL/OPG pathway (13). The impact of RvE1 and other

resolvins on neutrophils and macrophages suggests a de-regulatory function on the acute inflammation and innate immunity (14). The therapeutic and regenerative effects of RvE1 in animal models also imply that the impact of the SPMs is not limited to the prevention of acute inflammation from becoming chronic. The chronicity of the inflammatory response is highly regulated by the antigen-presenting cells such as dendritic cells (DCs) and subsequent activation of the T helper lymphocytes (T_h) (15). In line with this approach, promoting effects of Lipoxin A4 (LXA4) and leukotriene B4 (LTB4) on T follicular helper cells show the role of SPMs on antigen-specific immune response (16) and functionally active receptor expression of LTB4 (BLT1) on effector T cells may link early immune activation and acquired immune response (17). Thus, it is plausible that the therapeutic effects of the SPMs would involve a direct impact on the DC-T_h axis.

In chronic inflammatory diseases, T lymphocytes control and regulate the host response by taking advantage of their memory properties and high cytokine-producing capacities (18). T lymphocytes are categorized into a variety of T helper (Th) subgroups, including T_h1, T_h2, T_h17, and regulatory T cells (Treg), showing anti-inflammatory or pro-inflammatory properties (19) among these subgroups. T_h17 cells have protective roles in controlling mucosal infections while presenting destructive functions in autoimmune and chronic inflammatory diseases (20, 21). T_h17 cells further acquire phenotypic instability and transforming capacity from one cell to another, explaining their dual roles in inflammatory processes (22). T_h17 cells produce a wide range of cytokine profiles, including IL-17, IL-21, IL-23, IL-22, IL-26, IL-6, IL-1βTGF$_\beta$, TNF$_\alpha$ and GM-CSF of which IL-17 is pivotal for their pro-inflammatory activation (23–25). As in the case of the other T cells, T_h17 cells require antigen presentation for activation. Dendritic cells (DC) located at mucosal surfaces or in circulation are critical for T_h17 cell function (26, 27). It is unknown how DC-induced T_h17 cell activity is impacted during the resolution of the inflammatory process, which is an essential step for the homeostatic restoration.

In this study, we hypothesized that as a pro-resolution mediator, RvE1 will suppress T_h17 differentiation, and this will be mediated through the DC-activity. To test this hypothesis, we analyzed the impact of RvE1 on several stages of T_h17 activation, including T_h17 polarization and DC-induced naïve T cell activation.

MATERIALS AND METHODS

Reagents

CD11c Microbeads UltraPure kit, CD4+ T cell isolation kit, T cell medium (TexMACs), TGF$_\beta$ recombinant protein and anti-chemR23 (APC) were purchased from MACS Miltenyi Biotec. Purified anti-mouse CD3 and CD28, recombinant mouse IL-6 (carrier-free), monoclonal anti-mouse antibodies; CD4 (APC), CD25 (FITC), *CCR6 (PE-Cy7)*, FoxP3 (Pacific Blue), IL-17 (R-PE), I-A^k MHC class II (PE), CD40 (PE/Cy5), CD86 (FITC) and CD80 (APC) were purchased from Biolegend. RORγt antibody (PerCP-Cy5.5) was purchased from R&D system, ionomycin and PMA were purchased from Sigma Aldrich. Dilutions of antibodies were as follows: RORγt was at 1/100; CD4, IL-17, CD40, and MHC II were at 1.25/100; CD25, CD86, and FoXP3 were at 2/100; CCR6 was at 5/100, and chemR23 was at 10/100. Monensin (1×) was purchased from Thermofisher Scientific. Pam_3CSK_4 was purchased from InvivoGen. RvE1 was purchased from Cayman Chemicals; RvE1 was stored in -80°C and immediately before use diluted in ethanol for the final concentration. IL-2 LUMINEX kit was purchased from Millipore Sigma. AYOXXA multiplex analysis kit was purchased from AYOXXA (Cologne, Germany).

Animals

Male and female FVB, BALB/CBYJ type mice, were purchased from Jackson Laboratories and Charles River Laboratories. All animals were housed under standard pathogen-free conditions and kept feeding at the Forsyth Institute Animal Facility, Cambridge, MA. Six to ten-week-old mice were used in the experiments. The protocols were approved by the Forsyth Institute's Institutional Animal Care and Use Committee (IACUC).

Cell Purification and Sorting

Wild type mice without any genetic differences were sacrificed, and their spleen was excised. Spleen specimens were ground in sterile PBS with ACK lysis buffer (NH_4Cl, Na_2EDTA, $KHCO_3$, ph 7.4) to eliminate red blood cells and filtered using 70 μm and 40 μm nylon mesh filters to achieve purity of splenocytes. Splenocytes were then passed through immune-magnetic depletion for specific cell type isolation. CD11c+ dendritic cells were isolated by CD11c MicroBeads UltraPure kit by positive selection through a midiMACS separator. CD4+ T cells were isolated by CD4+ T cell isolation kit (including monoclonal antibodies against CD8a, CD11b, CD11c, CD19, CD45R (B220), CD49b (DX5), CD105, Anti-MHC Class II, Ter-119, and TCRγ/δ) by negative selection through midiMACS separator. $CD4^+$ T cells and $CD11c^+$ dendritic cells had purity over 95%, confirmed by flow cytometry.

T_h17 Polarization

To identify the impact of RvE1 on T cell activation, we generated three different groups; 1) Unstimulated T cells, 2) T cell activation group, 3) RvE1 treatment group. 10^5 CD4+ T cells were incubated in 200 μl final T cell medium (TeXMACS) with 10% FBS and 1% Penicillin-Streptomycin in triplicate for 5 days. For T cell activation, U-bottom 96-well plates were covered with 30 μl of anti-CD3(10 μg/ml) in 200 μl total volume with sterile PBS. After 4 hours incubation period at 37°C, plates were washed with 200 μl sterile PBS twice, and 1.5 μg/ml anti-CD28-alone was added to the medium for the next days. For RvE1 treatment; additionally, 10 nM RvE1 was added to the assigned groups on day 0 and 3. To evaluate the effect of RvE1 on T_h17 polarization, we tested the following experimental groups: 1) Unstimulated T cells, 2) T_h17 cell polarization group, 3) 10 nM RvE1 treatment group. Highly purified naïve CD4+ T cells were polarized into

T_h17 cells as described (28). Briefly, 10^5 CD4+ T cells were incubated in 200 µl final T cell medium (TeXMACS) with 10% FBS and 1% Penicillin-Streptomycin in triplicate for each condition. TeXMACS is a serum-free cell culture medium without animal-derived components and contains pre-selected human serum albumin, stable glutamine, and phenol red. It provides enhanced T cell viability, consistency, and growth (29). In polarization and RvE1 treatment groups, U-bottom 96-well plates were covered with 30 µl of anti-CD3(10 µg/ml) in 200 µl total volume with sterile PBS. After 4 hours incubation period at 37°C, plates were washed with 200 µl sterile PBS twice. For the T_h17 polarization group, a mixture of 20 ng/ml IL-6, 5 ng/ml TGFβ and 1.5 µg/ml anti-CD28 were prepared, and 100 µl of this mix were added to each well. For the RvE1 treatment group, in addition to the T_h17 polarization mix, 10 nM RvE1 was added on day 0 and 3. All cells were incubated at 37°C for five days. Cells for FACS analysis and supernatants for Multiplex analysis were collected on day 5.

T_h17 Stimulation by DC

To determine the ability of DCs to stimulate naïve CD4+ T cells into T_h17 cells and evaluate the impact of RvE1, we co-cultured naive CD4+ T cells (50,000/200 µl) with CD11c+ DC (1000/200 µl) in U-bottom 96-well plates in 200 µl RPMI containing 10% FBS and 1% Penicillin-Streptomycin. Recent publications show that toll-like receptor (TLR) signaling regulated by DCs was sufficient for T helper cell stimulation and Th17 differentiation (30, 31); Pam_3CSK_4 is a TLR activator necessary for Th17 polarization (32, 33). Thus, Pam_3CSK_4 (100 ng) was used to stimulate cells. Six experimental groups were tested: 1) Unstimulated CD4+ T cells 2) CD4+ T cells+ Pam_3CSK_4 3) DCs+CD4+ T cells 4) DCs+CD4+ T cells+ RvE1 5) DCs+CD4+ T cells+ Pam_3CSK_4 6) DCs+ CD4+ T cells+ Pam_3CSK_4+ RvE1. All cells were incubated at 37°C for 5 days. First, cells were treated with 10 nM RvE1 for 24 hours and then stimulated with 100 ng Pam_3CSK_4. Another dose of RvE1 was applied to the cells on day 3. Cells and supernatants were collected for FACS analysis and Multiplex analysis on day 5.

DC Maturation

CD11c+ DCs were stimulated with Pam_3CSK_4 in the presence or absence of RvE1 to evaluate its impact on the activation of DC. $2x10^5$ cells were incubated in 48-well plates in 500 µl RPMI containing 10% FBS and 1% Penicillin-Streptomycin at 37°C for three days. First cells were treated with 10 nM RvE1 for 24 hours, and then 100 ng Pam_3CSK_4 was added. An additional dose of RvE1 was applied on day 2. Cells-alone or treated only with RvE1 were used as control. All cells were collected for FACS analysis on day 3.

Expression of Surface Receptors and Antigens on Th Cells and DCs

Cell viabilities were checked by trypan blue before analyzing surface receptor expressions at the end of the experiments. CD4, CD25, CCR6, chemR23, FoxP3, RORγt and IL-17 expressions on T cells were measured on day 5. T cells in triplicate were pooled in 24-well culture plates in 1 ml final volume for each condition. PMA (phorbol myristate acetate) (50 ng/ml), ionomycin (1µM) and monensin (1×) were added to each well for 6 hours at 37°C. CD4, CD25, and CCR6 antibodies were added to the cells for 30 minutes on ice. After washing, cells were fixed with 4% paraformaldehyde for 10 minutes at room temperature. Then, 0.1% Triton for permeabilization and 0.5% BSA for blocking was applied for 10 minutes at room temperature and on ice, respectively. Antibody cocktail containing FoxP3, RORγt, and IL-17 were added for intracellular staining, and FACS analysis was performed. CD80, CD86, CD40, MHC II expressions on DC were measured on day 3; antibody cocktail was added to cells for 30 minutes on ice. Then, 4% paraformaldehyde, 0.5% BSA, and 0.1% Triton was applied as described above before performing FACS analysis. For all the experiments, the cell population was selected in the FSC/SSC plot according to their expected cell size and granularity. Singlets were gated to eliminate doublets and then proceeded to the individual analysis of the markers. All analyses were made by Attune NXT Flow Cytometer Software.

Multiplex Analysis

To determine the cytokine release, IL-2, IL-17A, IL-17F, IL-21, CCL20, IL-6, and $TGF_β$ were measured. IL-2 assay was performed according to the manufacturer's instructions (Millipore) and assayed on Luminex (BioRad). The other cytokines were measured by AYOXXA multiplexing, as described by the manufacturer.

Statistical Analyses

ANOVA was used for statistical analyses. Tukey's posthoc analysis was used for multiple comparisons. Differences were considered statistically significant when p was less than 0.05.

RESULTS

To test the impact of RvE1 on T cell activation, naive CD4+ T cells obtained from the spleen were activated with anti-CD3 and soluble anti-CD28 in the presence or absence of RvE1. PMA and ionomycin were added for 6 hours on day five, and FACS analysis was performed. RvE1 did not change CD4+ T cell expressions; the frequency of CD4+ T cells was high without any noticeable difference between groups. Meanwhile, CD25+ T cells in response to RvE1 were decreased significantly (**Figure 1**). There was no statistical change in the viability of cells due to stimulation or RvE1 treatment.

RvE1 Suppresses T_h17 Proliferation Under Polarizing Conditions

Splenic $CD4^+$ T cells were polarized into T_h17 cells under specific polarizing conditions (CD3/CD28 activation and IL6/TGFβ stimulation). RvE1 was applied baseline and on day 3. Cells were cultured for five days, and data was analyzed (**Figure 2A**). $CD4^+$ T cell percentage was similar in all experimental groups (**Figure 2B**). To determine the impact of RvE1 on T_h17 stimulation from naive CD4+ T cells, we analyzed RORγt and IL-17 expressions. Th17 polarizing increased the expression of RORγt and IL-17; RvE1 prevented the impact of polarization and

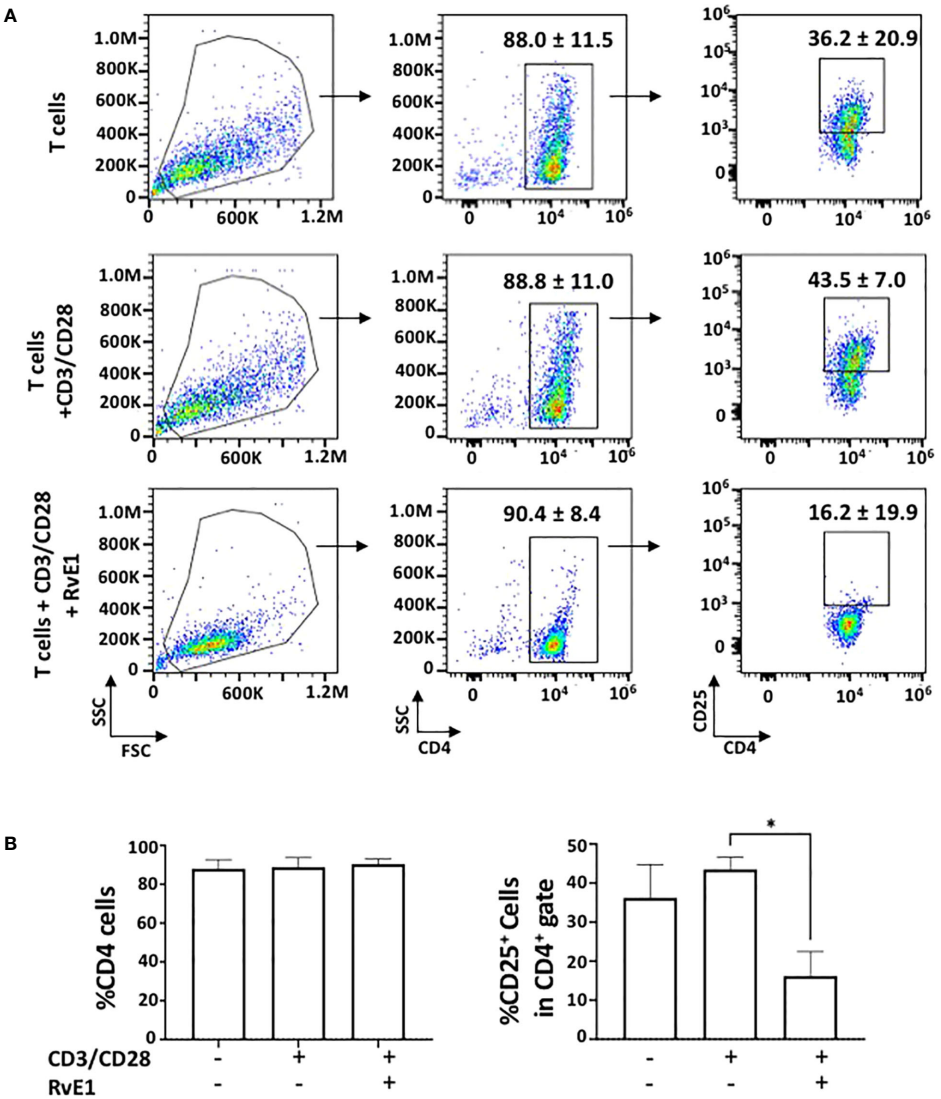

FIGURE 1 | RvE1 suppresses T cell activation by decreasing $CD25^+$ cells. **(A)** There is an example of gating strategies **(A)** shows representative flow cytometric data and **(B)** shows proportion of $CD4^+$ cells and $CD25^+$ cells in $CD4^+$ gate in unstimulated T cells, activated T cells and RvE1 treatment groups Data showed are ± sem for six independent experiments. *$p < 0.05$.

significantly decreased IL-17^+ cells. Simultaneously, there was a decrease in RORγt^+ cells in response to RvE1, the difference was not statistically significant. We also analyzed the cc chemokine receptor 6 (CCR6) and its ligand CCL20 to measure the chemotactic migration of T_h17 cells. The highest CCR6 expression was observed in unstimulated cells, and RvE1 decreased these levels significantly. RvE1 resulted in a significant decrease in CD25 expression by the T_h cells. CD25 expression was observed in unstimulated groups and reached a peak level after the polarization. RvE1 prevented the expression of these receptors. To analyze the impact of RvE1, we then gated $CD4^+CD25^+$ cells and analyzed IL-17 and RORγt expressions. RvE1 decreased the frequency of $CD4^+CD25^+$ cells, but in contrast with its effect gated on only $CD4^+$ cells, there was an increasing trend on IL-17^+ and RORγt^+ cells in response to RvE1 with no statistical significance (**Figure 2C**).

We then measured IL-17A, IL-17F, IL-21, and IL-10 content in supernatants (**Figure 3**). The highest cytokine secretion was observed by CD4 polarized T_h17 cells; levels of IL-17A, IL-17F, IL-21, and IL-10 were limited in unstimulated groups. There was a substantial increase in their secretion levels after polarization. RvE1 led to a significant decrease in IL-17A. IL-17F decline was also noteworthy, while the change was not statistically significant. IL-10 and IL-21 generation by the T_h17 cells significantly decreased in response to RvE1. Consistent with the CCR6 expression, RvE1 reduced the CCL20 secretion to

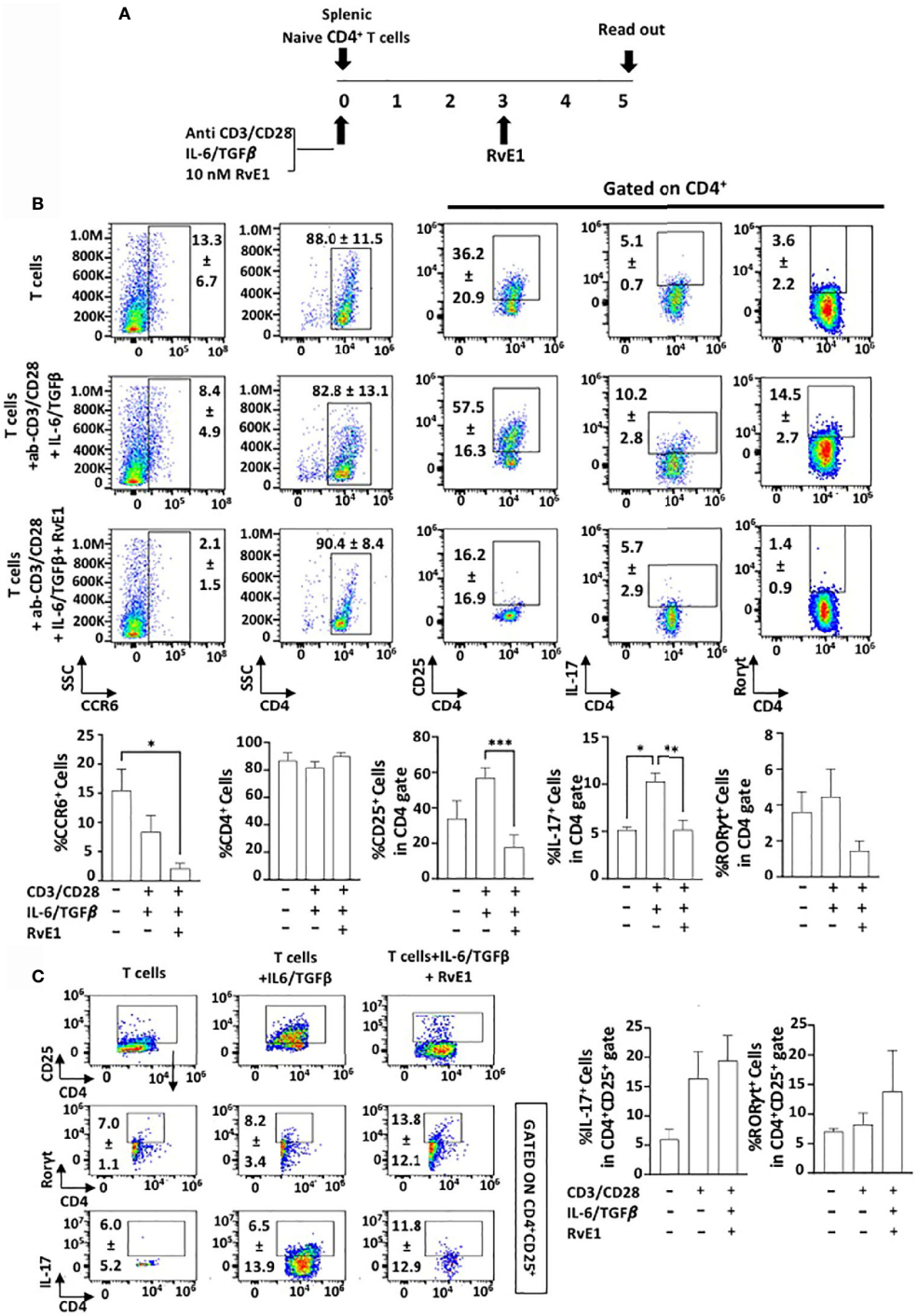

FIGURE 2 | RvE1 prevents Th17 differentiation by inhibiting IL-17 expression and T cell activation by decreasing CD25 expression. RvE1 regulates the migration of Th17 cells by decreasing CCR6 expression. **(A)** Experimental design protocol. Naïve $CD4^+$ T cells were stimulated to Th17 cells under Th17 polarizing conditions. T cells were cultured alone for control groups. For the Th17 stimulation group, ab-CD3/CD28 and IL-6/TGFβ was applied, and for the RvE1 treatment group, besides these polarizing conditions 10 nM RvE1 was used baseline and on day 3. All cells were incubated for five days at 37°C. Cells were induced with PMA/ionomycin and monensin for 6 hours on day five and analyzed by flow cytometry. **(B)** Representative flow cytometric data (above) and proportion (below) of $CCR6^+$ cells, $CD4^+$ cells and $CD25^+$, $IL\text{-}17^+$ and $ROR\gamma t^+$ cells in $CD4^+$ gate in unstimulated T cells, Th17-polarized cells and RvE1 treatment groups. **(C)** shows flow cytometric data (left) of $CD4^+CD25^+$ cells, $IL\text{-}17^+$ and $ROR\gamma t^+$ cells gated in $CD4^+CD25^+$ cells and proportion (right) of $IL\text{-}17^+$ and $ROR\gamma t^+$ cells gated in $CD4^+CD25^+$ in unstimulated T cells, Th17-polarized cells and RvE1 treatment groups. Results are ± sem for six independent experiments *$p < 0.05$, **$p < 0.01$, ***$p < 0.001$.

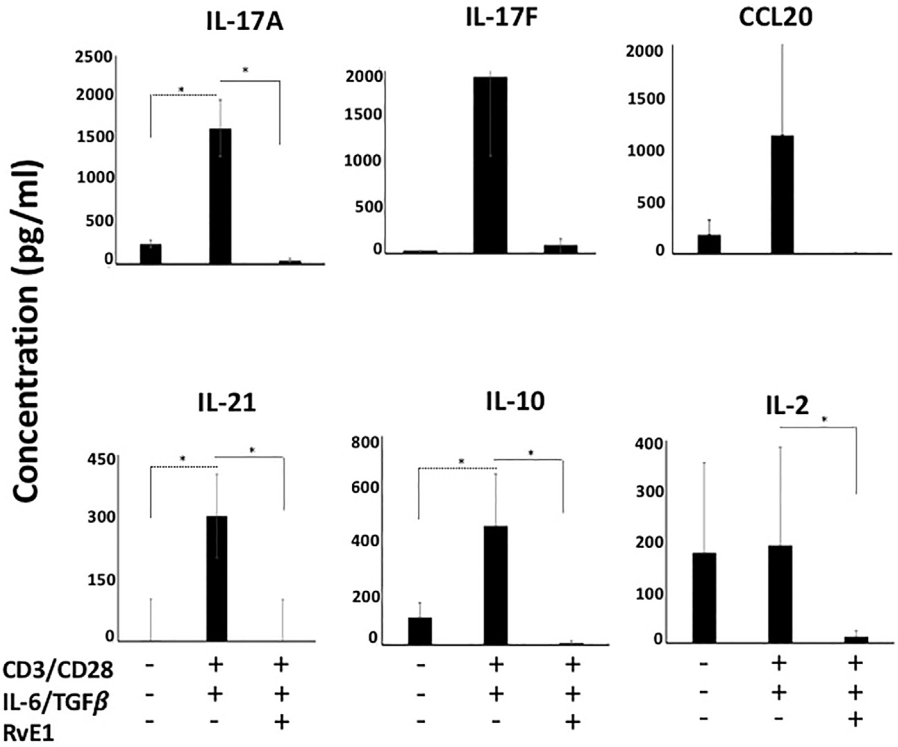

FIGURE 3 | RvE1 suppresses cytokine secretion from Th17 cells. IL-17A, IL-17F, CCL20, IL-21, IL-10 and IL-2 secretions from unstimulated T cells, Th17-polarized cells and RvE1 treatment groups were analyzed. IL-17A, IL-17F, CCL20, IL-21 and IL-10 were analyzed by AYOXXA and IL-2 was analyzed by Luminex. Results are ± sem for six independent experiments, *$p < 0.05$.

the levels of the unstimulated group. We also analyzed the levels of secreted IL-2, which, in line with its receptor (CD25) activation, showed a significant decrease after RvE1 treatment.

Effect of RvE1 on DC-Stimulated T_h17 Proliferation

We analyzed the impact of RvE1 when naive $CD4^+$ T cells were stimulated by DCs (**Figures 4** and **5**). As the optimal IL-17 production by the T_h17 cells was reported in the presence of Pam_3CSK_4 in co-culture experiments (34), we incubated $CD11c^+$ DCs with naïve $CD4^+$ T cells (1000 DC/50000 T cells in 200 µl total medium) in the presence of Pam_3CSK_4 (100 ng) with or without RvE1 (10 nM) for five days. RvE1 was applied to the cells for 24 hours, and then Pam_3CSK_4 was added (**Figure 4A**). Before performing the FACS analysis, PMA, ionomycin, and monensin were added for 6 hours. The percentage of $CD4^+$ T cells was similar in each group (**Figure 4B**). To evaluate the impact of RvE1 on T_h17 stimulation, we analyzed RORγt and IL-17 expressions. Pam_3CSK_4 stimulation significantly increased $ROR\gamma t^+$ cells; RvE1 application did not cause any further change in these levels, same as its effect on $IL\text{-}17^+$ cells. We then analyzed IL-17A secretion from Th17 cells. Pam_3CSK_4 stimulation increased IL-17A levels, which were decreased in response to RvE1, while the changes were not statistically significant (**Figure 5B**). Pam_3CSK_4 stimulation and RvE1 treatment increased the CCR6 expression (**Figure 4B**) in contrast with its ligand-CCL20 that decreased after RvE1 treatment (**Figure 5B**); the changes due to RvE1 was not statistically significant (**Figures 4B** and **5C**). We also stimulated T cells alone with Pam_3CSK_4 and measured $ROR\gamma t^+$ and $IL\text{-}17^+$ cells. Pam_3CSK_4 stimulated $ROR\gamma t^+$, $IL\text{-}17^+$ cells expressed by T cells independently from DCs (data not shown) similarly suggesting a toll-like receptor signaling on T cells that may promote T helper cell differentiation independent from antigen-presenting cells (33, 34). In a similar pattern, Pam_3CSK_4 stimulation significantly increased CD25 expression but differing from CD4-polarized Th17 cells applying RvE1 did not affect these levels (**Figure 4B**). same as its effects on IL-2 secretion. IL-2 secretions by T cells co-cultured with DCs were at similar levels independent from Pam_3CSK_4 stimulation or RvE1 treatment (**Figure 4C**). We then gated $CD4^+CD25^+$ T cells; similar to CD25 expressions, CD4+CD25+ cells slightly increased in response to RvE1. A decreasing trend was observed on IL-17 and RORγt expressions by $CD4^+CD25^+$ T cells (**Figure 5A**).

ChemR23/ERV1 Receptor Is Expressed on DCs and T_h17 Cells

Figure 6 shows the expression of ChemR23/ERV1 (receptor for the RvE1) on DCs and T cells. ChemR23 expression was previously reported on DCs and lymphocytes (35). In line with

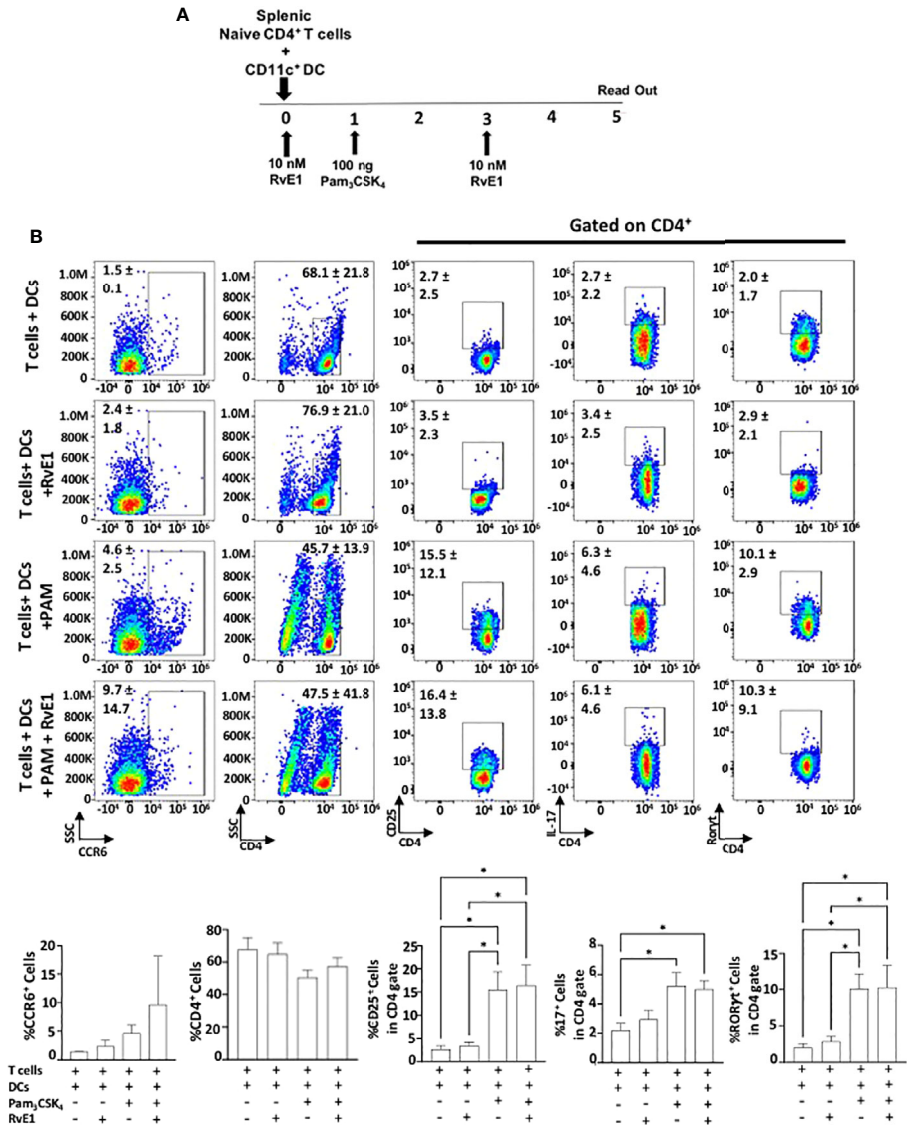

FIGURE 4 | **(A)** Experimental design protocol. $CD4^+$ T cells were co-cultured with dendritic cells (1000 DC/50000 T cell) in the presence or absence of PAM_3CSK_4 (100 ng) and RvE1 (10 nM). RvE1 was applied baseline and on day 3; PAM_3CSK_4 was applied on day 1. All cells were incubated at 37°C for 5 days **(B)** Representative flow cytometric data (above) and proportion (below) of $CCR6^+$ cells, $CD4^+$ cells and $CD25^+$, IL-17^+, RORγt^+ cells in $CD4^+$ gate in T cells+ DCs, T cells+DCs+RvE1, T cells+ DCs+ PAM_3CSK_4 and T cells+ DCs+ PAM_3CSK_4+ RvE1. Results are ± sem for four independent experiments, *$p < 0.05$.

previous studies, both T cells and DCs expressed substantial levels of receptors for SPMs in unstimulated/stimulated conditions (36, 37). Th17-polarized cells expressed more receptors compared with Th0 (CD3/CD28 activated T cells). In a similar pattern, Pam_3CSK_4 stimulated the expression of chemR23 on both T cells and DCs. (**Figure 6**). The overall changes, however, were not statistically significant among groups.

Effect of RvE1 on FoXP3 Levels

FoXP3 is the transcription factor necessary for differentiation of regulatory T cells (Treg), which are crucial to prevent autoimmune disorders and the extent of inflammation (38) with suppressive functions on Th17 cells (39). **Figure 7** demonstrates FoXP3 expression on DC-stimulated T helper cells. There was a limited FoXP3 expression on T cells co-cultured with DCs; this was significantly increased with Pam_3CSK_4 stimulation where RvE1 did not further change the percentage of $FoXP3^+$ cells (**Figure 7A**). We also measured FoXP3 expression in CD4-polarized Th17 cells; however, very low expressions were detected as expected (data not shown).

RvE1 Suppresses the Activation of DCs

Our results showed the effect of RvE1 on T_h17 polarization either directly by specific T_h17 proliferative reagents or by DC

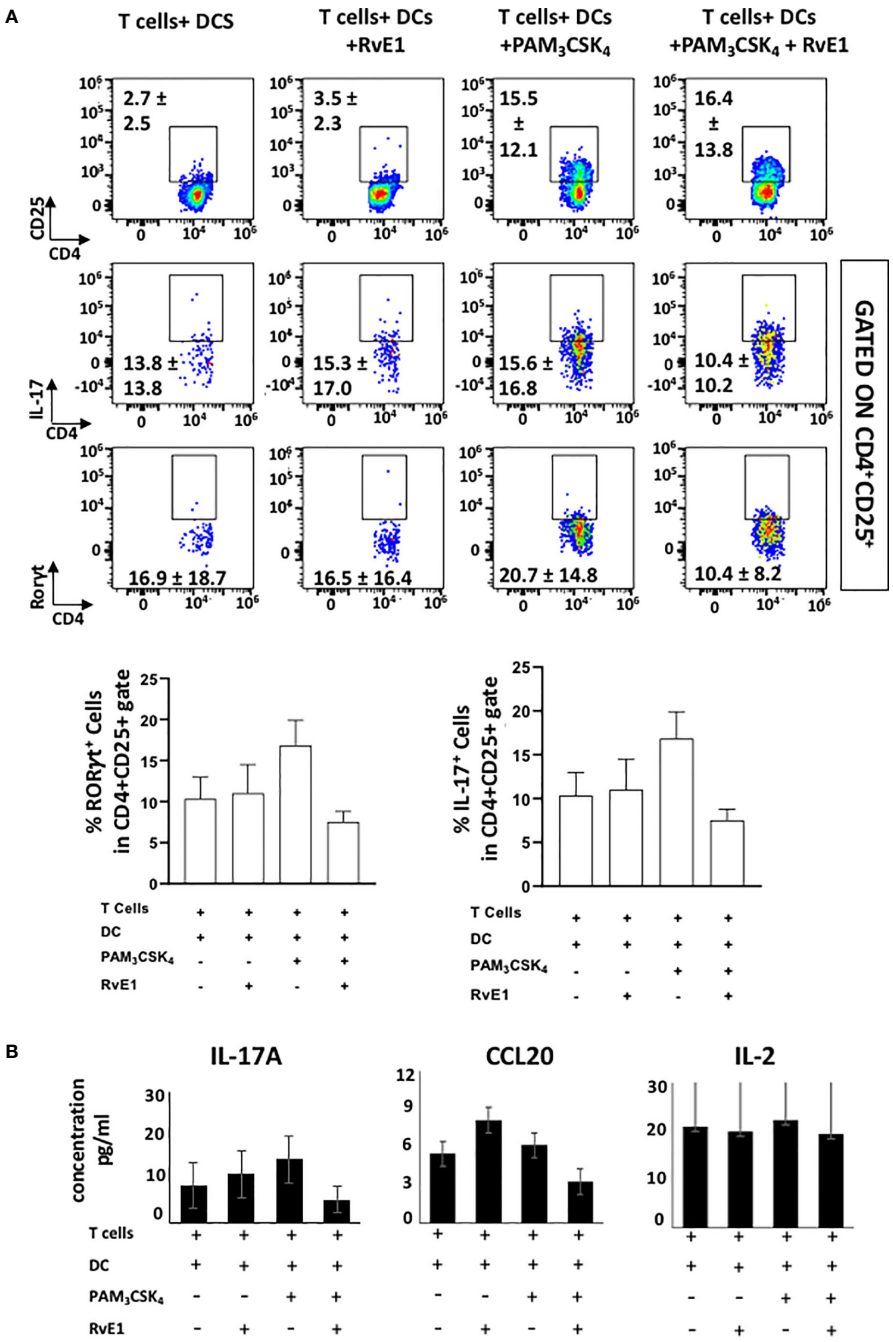

FIGURE 5 | **(A)** shows flow cytometric data (above) of $CD4^+CD25^+$ cells, IL-17^+ and $ROR\gamma t^+$ cells gated in $CD4^+CD25^+$ cells and proportion (below) of IL-17^+ and $ROR\gamma t^+$ cells gated in $CD4^+CD25^+$ cells T cells+ DCs, T cells+DCs+RvE1, T cells+ DCs+ PAM_3CSK_4 and T cells+ DCs+ PAM_3CSK_4+ RvE1. **(B)** shows IL-17A, CCL20 and IL-2 secretions by Th17 cells. CCL20 and IL-17A were analyzed by AYOXXA and IL-2 was analyzed by LUMINEX. Results are ± sem for four independent experiments.

stimulation. Thus, we measured the effect of RvE1 on the maturation and activation of DCs. DCs were stimulated with Pam_3CSK_4 (100 ng) with or without RvE1 (10 nM) for three days and analyzed (**Figure 7B**). CD80/86, CD40, and MHC II expressions were analyzed by flow cytometry to measure the DC maturation and the effect of RvE1. Although expression of CD40, CD80, and MHC II increased after PAM_3CSK_4 stimulation, reduction by the RvE1 was not significant (**Supplementary Figure 1**). We then examined IL-6, IL-2, and TGFβ content secreted by DCs; secretion of these cytokines was

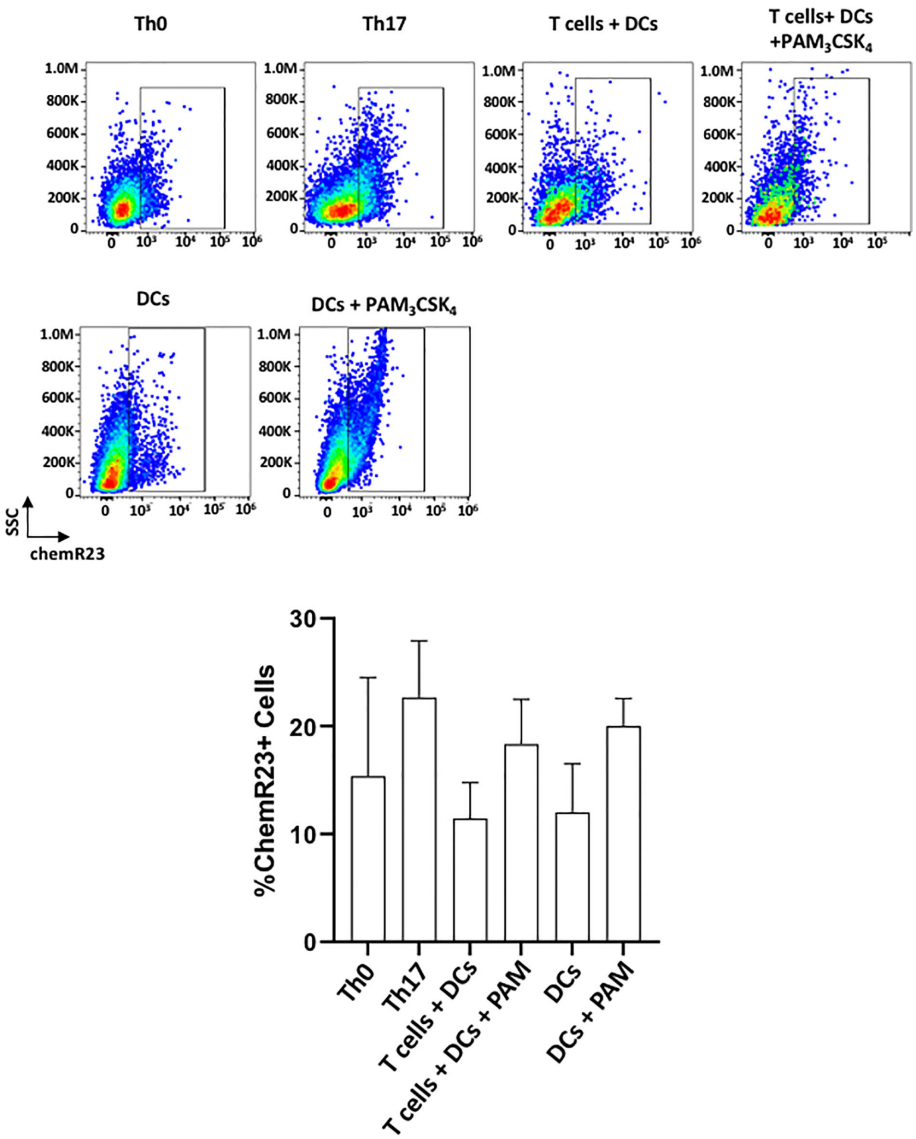

FIGURE 6 | chemR23/ERV1 is expressed on T cells$^+$ and DCs. Representative flow cytometric data (above) and proportion (below) of cells showing chemR23 expression on Th0 cells (CD4$^+$ T cells + ab-CD3/CD28), Th17 cells (CD4$^+$ T cells+ ab-CD3/CD28+ TGFβ/IL-6), T cells-DCs coculture, T cells-DCs co-culture with PAM_3CSK_4 stimulation, DCs and DCs with PAM_3CSK_4 stimulation. Results shown are ± sem for three independent experiments.

limited in DCs; after stimulation with Pam_3CSK_4, there was a substantial and significant increase in IL-6 and IL-2 levels, which RvE1 significantly reduced. TGFβ levels reached peak levels after RvE1 treatment in T cell-DCs groups stimulated with Pam_3CSK_4 (**Figure 7B**).

DISCUSSION

Since the discovery of RvE1 in exudates from murine dorsal pouches treated with aspirin and EPA (40), resolvins and other SPMs have been extensively used as mediators of resolution in chronic inflammatory diseases. Many of these studies focused on the cellular and molecular mechanisms of innate immunity. We tested the hypothesis that the RvE1 will restore homeostatic balance and inflammation by targeting the T_h17 activation, a critical step in the chronicity of inflammation. We used the splenocyte-derived CD4$^+$ T cells and CD11c$^+$ DCs (41–45) and minimized inter-individual variations. We applied the RvE1 at baseline and day 3 since supplementary doses were necessary to show its impact. Administering the other day would be another way to test the effect (37), but as Th17 polarization is achieved either on day 3 or 5 (28); we decided to repeat the application on day 3 when we added a fresh medium to the cell culture and possibly providing a new model for future research. We used three different doses of RvE1 (1 nM, 10 nM, and 100 nM) and

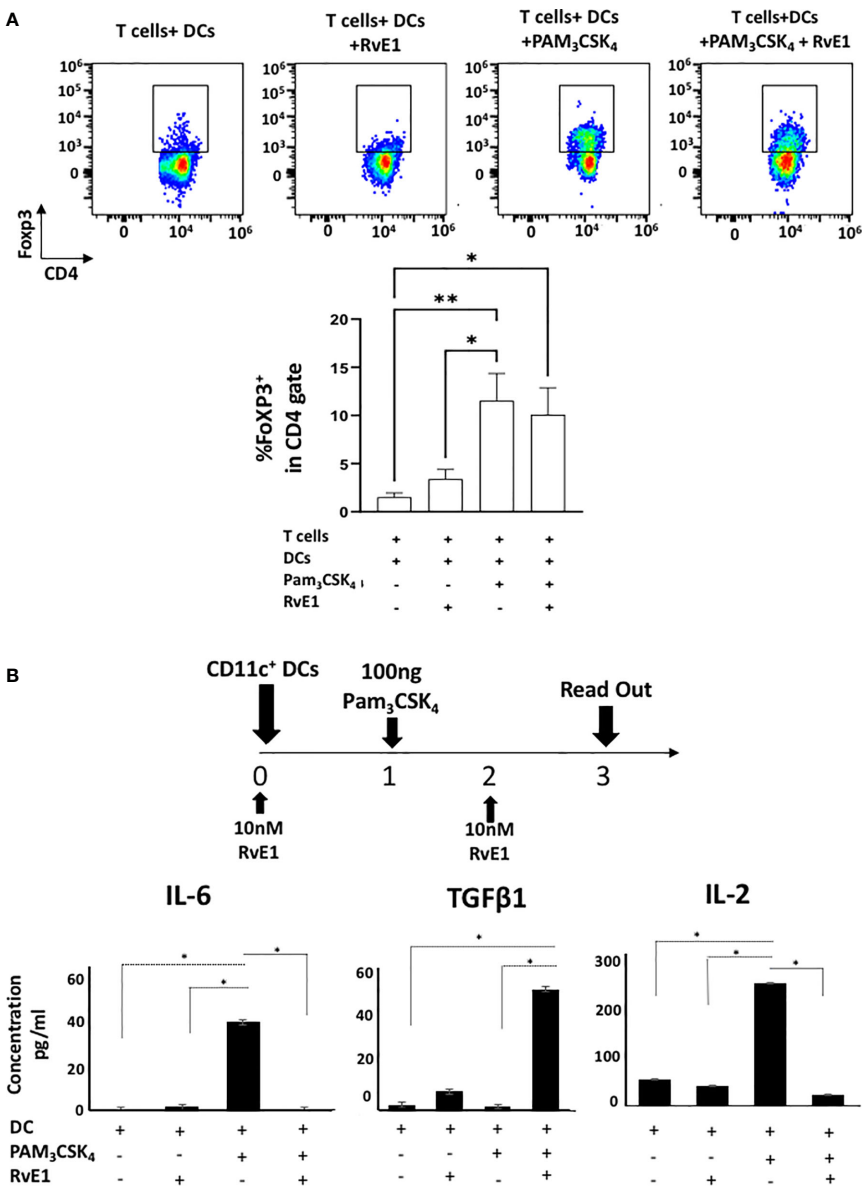

FIGURE 7 | **(A)** shows representative flow cytometric data (above) and proportion (below) of FoXP3$^+$ cells in CD4$^+$ gate in T cells+ DCs, T cells+DCs+RvE1, T cells+ DCs+ PAM_3CSK_4 and T cells+ DCs+ PAM_3CSK_4+ RvE1. Naive CD4$^+$ T cells were cocultured with dendritic cells and stimulated by PAM_3CSK_4, RvE1 treatment was applied baseline and on day 3 to the assigned groups. Cells were incubated at 37°C for five days, and on day 5. PMA/ionomycin and monensin were applied to the cells for 6 hours before performing FACS analysis. **(B)** CD11c+ dendritic cells (2x10^5 cells/500 ?l) were treated with 10 nM RvE1 for 24 hours and then induced with 100 ng PAM_3CSK_4 for 48 hours. One more dose of RvE1 was applied on day 2. **(B)** shows secreted cytokine levels by dendritic cells; Supernatants were collected on day 3; IL-6 and TGF_β were analyzed by AYOXXA and IL-2 by LUMINEX. Results shown are means ± sem for at least four independent experiments *$p < 0.05$, **$p < 0.01$.

analyzed Th17 polarization from naive CD4$^+$ T cells. These experiments were used to optimize the RvE1 dose in this study. The most efficient results were achieved by 10 nM RvE1; the effects of 1 and 100 nM doses were similar to 10 nM. None of the doses had any significant impact on the viability of cells. Therefore, we chose to use the 10 nM RvE1 treatment for the rest of the assays, including the DC-mediated Th17 proliferation and DC maturation. We only checked the viability of cells under the microscope and during FACS analysis. This is a limitation of our study; however, based on the flow dot plots in the figures, we can interpret that the viability of our cells was high.

Receptor-mediated production of cytokines is critical for T_h17 function. RORγt receptor expression is necessary for effector T_h17 cells and an efficient cytokine production such as IL-17 (23–25, 44–48). In addition to the IL-17, IL-21 is generated by T cells in the

inflammatory milieu and provides an alternative pathway for pathogenic T_h17 differentiation (49). In our study, RvE1 prevented IL-17 expression and IL-17A secretion by T_h17 cells, consistent with the findings of RvD1, RvD2 and maresin (37), suggesting that the SPMs may use common intracellular and post-receptor signaling pathways regulating the T_h17 function. However, these data contrasted with the findings that another SPM, LTB4, increases IL-17 secretion and RORγt expression suggesting a promoter effect on Th17 cells (50). Our data also showed a substantial increase in IL-21 levels when T_h17 cells were polarized, where RvE1 completely prevented this increase and restored the IL-21 secretion. Meanwhile, IL-10, another critical anti-inflammatory cytokine (51), was decreased in response to RvE1. Currently, there is no consensus on the impact of resolvins on IL-10 secretion. While some studies suggested that resolvins increased IL-10 secretion (13, 37, 52), others reported an opposite effect (53). This could be due to a complex interplay between the pro-inflammatory and anti-inflammatory cytokine production by the T_h17 cells; It is known that IL-1β increases IL-17 production while inhibiting IL-10 secretion (54). In the absence of an inflammatory milieu, however, the resolution phase-associated cytokines of the inflammation may be similarly reduced as the pro-inflammatory cytokines as a function of the non-pathogenic T_h17 cell population, which secrete IL-10 cytokines (55, 56).

The effect of RvE1 on T_h17 cells is not only limited to their proliferation capacity but also inhibition of their attractivity with decreased CCR6 receptor expression and CCL20 cytokine secretion. $CCR6^+$ cell populations together with $CXCR3^+$ cells produce both IL-17 and IFN-γ. Therefore, $CCR6^+$ cells are also T_h17/T_h1 cells (57). Meanwhile Treg cells express CCR6 receptor but not CCL20 (58, 59). The highest CCR6 expression with almost no CCL20 secretion observed in unstimulated T cells may suggest that different T cell groups can express CCR6 but not CCL20. Our data suggested that RvE1 restore the chemoattraction of T_h17 cells by targeting both CCR6 and CCL20 levels under T_h17 polarizing conditions. In a recent *in vivo* study, RvE1 was shown to decrease the number of DCs and T_h17 cells in the inflamed area without impacting the CCL20 levels (60), suggesting additional compensatory mechanisms regulating the CCR6 activation in tissues.

DC-T cell interaction is a highly organized process starting with the engagement of Toll-like receptor (TLR) and peptide-loaded major histocompatibility complex (MHC), following with the activation of co-stimulatory molecules CD40, CD80/CD86, and ending up with cytokine secretion (61). In DC-mediated T_h17

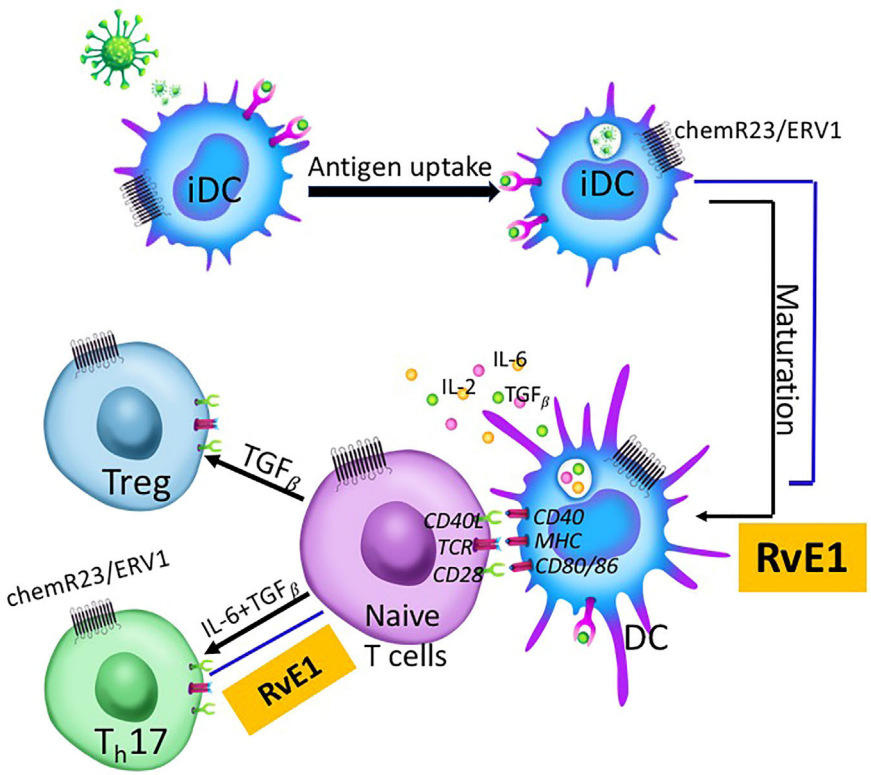

FIGURE 8 | Immature dendritic cells (iDC) located at mucosal surfaces or in circulation are the antigen-presenting cells coming across with the antigen initially. After taking up the antigen, they undergo maturation and migrate to lymphoid tissues where naive T cells are present. DC-T cell cross-talk is a three-step process involving TCR-MHC binding and resulting in cytokine production. T cells differentiate into T helper subgroups for effector functions depending on the cytokines produced by DCs and T cells. IL-6 and TGFβ induce T_h17 proliferation while TGFβ-alone induces Treg proliferation. RvE1 impacts this process at two different levels; 1) DC maturation, and 2) T_h17 proliferation from naive T cells. RvE1 receptor chemR23/ERV1 is expressed both on DCs and T cells. RvE1 prevents DC maturation by regulating cytokine production from DCs, and T_h17 differentiation from naive T cells, Th17 chemoattractiom and T cell activation.

polarization, the inhibitory impact of the RvE1 on RORγt, IL-17, and CD25 expression and cytokine secretion were not as effective as it was under T_h17-polarizing conditions suggesting that DCs decrease the responsiveness of T cells against RvE1. The role of DCs in this system is not clear; our data revealed that Pam_3CSK_4 stimulation increased the IL-6 and IL-2 secretion by the DC, and RvE1 reversed this effect while increasing the TGF_β levels. A similar mechanism for the inhibition of T cell activation through blocking monocyte activation in health but not in chronic inflammatory conditions has been linked to Annexin A1, which acts as endogenous anti-inflammatory mediator (62). In parallel with our findings, other researchers have demonstrated that in response to RvE1, DC maturation was suppressed, IL-12 and TNFα generation was decreased and DCs generated from precursor molecules in the presence of RvE1 secreted less IL-17 from pre-activated T cells (52). In an *in vivo* sepsis study, RvD1 decreased IL-6, TNF_α, $IL\text{-}1_\beta$ and IFN_γ levels significantly (53). Overall, the DC-mediated T cell response to the SPMs seems to be pathology-specific and may differentially involve the activity of other cell types including the DCs in health and disease.

IL-2 production by $CD4^+$ T helper cells is increased following antigen activation; CD25 expression increased during T cell activation increases the IL-2 receptor's affinity for its ligands (63–65). Our work demonstrated that the stimulation of naïve $CD4^+$ T cells with either Pam_3CSK_4 in co-cultures or Th17 polarizing reagents resulted in the most profound increase in CD25 expression; RvE1 significantly decreased this under T_h17 polarizing conditions. This finding was in parallel with a significantly reduced IL-2 cytokine secretion by T cells under the same conditions by the RvE1, which may suggest that RvE1 suppressed IL-2 secretion leading to a decrease of CD25 expression (66). $CD4^+CD25^+$ T cells are known as "natural suppressor cells," showing anergic, suppressing functions by inhibiting transcription of IL-2 *via* TCR, Exposing to antigen stimulation or polyclonal T cell receptor stimulation activates these cells ($CD4^+CD25^+$) to mediate their suppressive functions (67, 68), which may be the reason for increased $CD4^+CD25^+$ T cell populations under Th17 polarizing conditions and DC-mediated Th17 polarization. Our data showed that RvE1 does not have effect on $CD4^+CD25^+$ cells or on $CD4^+CD25^+IL\text{-}17^+$ and $CD4^+CD25^+ROR\gamma t^+$ cells. While further studies are required to elucidate the effector functions of these cells during the resolution phase of the inflammation, previous reports on CD25 expression by Th17 cells ($CD25^+CCR6^+$) showed anti-inflammatory properties *via* high CTLA1 expression and suppress the activity of $CD8^+$ T cells and IFNγ production (69).

$CD4^+CD25^+$ T cells express FoxP3 to become regulatory T (Treg) cells and reach higher phenotypic stability; FoxP3 is a necessary transcription factor for Treg ($CD4^+CD25^+FOXP3^+$) cells to maintain immunosuppressive and anti-inflammatory functions (70). Low levels of FoXP3 expression were detected under Th17 polarizing conditions as expected; however, FoXP3 was significantly increased in DC-mediated Th17 polarization showing that Treg cell populations also increased following Pam_3CSK_4 stimulation. Although it was not significant, there was a tendency towards decreasing the FoXP3 expression due to RvE1. It was previously reported that in the resolution of inflammation mediated by a non-SPM agonist-Annexin, there was no effect on Treg cell populations ($CD4^+FoXP3^+$) (62). While our data is not sufficient to conclusively predict the effect of RvE1 on Treg cells, as the IL-2 is critical for the generation, survival, and function of Treg cells (71), decreased CD25 and IL-2 levels by RvE1 may lead to lower FoXP3 expression. Collectively, these data suggested that RvE1 may inhibit Treg differentiation in addition to T_h17 differentiation. SPMs may be expected to increase FoxP3 and Treg populations in a targeted polarization (37). Recently animal models demonstrated the regulatory function of Maresin 1 on Treg/Th17 balance through transcription factors (72, 73) suggesting a role for the inflammatory milieu in which T_h17 and Treg cells work counterregulatory of each other's function. Our data are in line with findings suggesting that IL-2-mediated mechanism by Treg cells may lead to an increase of both T_h17 and Treg cells at the same time by preventing inhibition capacity of IL-2 over T_h17 cells (74). In this scenario, a reduced IL-2 level may be preventing the IL-2-mediated suppression of RORγt expression and T_h17 differentiation (75), suggesting that the IL-2 is an essential cytokine in RvE1-dependent regulation of T cell class switch.

Our data demonstrated that the RvE1 blocked the CD25, IL-17, and CCR6 expression; IL-17, IL-21, IL-10, and IL-2 production by T_h17 cells. RvE1 prevented IL-6 and IL-2 production and stimulated TGF_β production by DC. The data present two critical outcomes: 1) SPMs regulate the chronicity of inflammation by reversing T_h17 activation, and 2) Antigen-presenting DCs that are involved in T_h17 activation could not be a therapeutic target in preventing the lymphocytic involvement of acquired immune responses during inflammation as they decrease the responsiveness of T cells (**Figure 8**).

CONCLUSION

Immune response orchestrated by T cells is a highly complex process due to the engagement of different molecules. Our results showed that RvE1 inhibited T helper cell activation by decreasing CD25 expression while suppressing the T_h17 proliferation. A parallel decrease in IL-6 and an increase in TGFβ secreted by DCs with a critical role of IL-2 suggested that the RvE1-mediated resolution of T_h17 cell activity.

DATA AVAILABILITY STATEMENT

The original contributions presented in the study are included in the article/**Supplementary Material**. Further inquiries can be directed to the corresponding author.

ETHICS STATEMENT

The animal study was reviewed and approved by Forsyth Institute`s Animal Care and Use Committee in accordance with Institutional Animal Care and Use Committee with Animal Assurance Number; A3051-01/D16-00029.

AUTHOR CONTRIBUTIONS

FO and AK conceptualized the study and wrote the original draft. FO performed the experiments. WY collected the animal samples. FO, CA and AK contributed to assembly data, FO, CA and DS performed data analysis. EF and HH provided administrative support. All authors contributed to the article and approved submitted version.

FUNDING

This project was supported by the NIH R01AG062496 grant and doctoral award by the Scientific and Technological Research Council of Turkey (BIDEB 2214-105B141600394).

SUPPLEMENTARY MATERIAL

The Supplementary Material for this article can be found online at: https://www.frontiersin.org/articles/10.3389/fimmu.2021.637983/full#supplementary-material

Supplementary Figure 1 | CD11c+ dendritic cells (2x10^5 cells/500 ?l) were treated with 10 nM RvE1 for 24 hours and then induced with 100 ng PAM_3CSK_4 for 48 hours. One more dose of RvE1 was applied on day 2. Cells were collected for analysis on day 3; antibody cocktail was added to cells for 30 minutes on ice. Then, 4% paraformaldehyde, 0.5% BSA, and 0.1% Triton was applied as described before performing FACS analysis. Graphs above show the percentage of CD86/80, CD40 and MHC II expression on DCs. results shown are means ± sem for three independent experiments *p < 0.05.

REFERENCES

1. Serhan CN, Brain SD, Buckley CD, Gilroy DW, Haslett C, O'Neill LAJ, et al. Resolution of inflammation: state of the art, definitions and terms. *FASEB J* (2007) 21(2):325–32. doi: 10.1096/fj.06-7227rev
2. Serhan CN. Novel pro-resolving lipid mediator in inflammation are leads for Resolution Physiology. *Nature* (2014) 510(7503):92–101. doi: 10.1038/nature13479
3. Oh SF, Pillai PS, Recchiuti A, Yang R, Serhan CN. Pro-resolving actions and stereoselective biosynthesis of 18 E-series resolvins in human leukocytes and murine inflammation. *J Clin Invest* (2011) 121:569–81. doi: 10.1172/JCI42545
4. Serhan CN, Savill J. Resolution of inflammation: The beginning programs the end. *Nat Immunol* (2005) 6(12):1191–7. doi: 10.1038/ni1276
5. Yang R, Chiang N, Oh SF, Serhan CN. Metabolomics-lipidomics of eicosanoids and docosanoids generated by phagocytosis. *Curr Protoc Immunol* (2011) 95:1–26. doi: 10.1002/0471142735.im1426s95
6. Bannenberg G, Serhan CN. Specialized pro-resolving lipid mediators in the inflammatory response: An update. *Biochim Biophys Acta - Mol Cell Biol Lipids* (2010) 1801(12):1260–73. doi: 10.1016/j.bbalip.2010.08.002
7. Hsiao HM, Thatcher TH, Colas RA, Serhan CN, Phipps RP, Sime PJ. Resolvin D1 reduces emphysema and chronic inflammation. *Am J Pathol* (2015) 185(12):3189–201. doi: 10.1016/j.ajpath.2015.08.008
8. Chiurchiù V, Leuti A, Saracini S, Fontana D, Finamore P, Giua R, et al. Resolution of inflammation is altered in chronic heart failure and entails a dysfunctional responsiveness of T lymphocytes. *FASEB J* (2018) 33(1):909–16. doi: 10.1096/fj.201801017R
9. Yates CM, Calder PC, Ed Rainger G. Pharmacology and therapeutics of omega-3 polyunsaturated fatty acids in chronic inflammatory disease. *Pharmacol Ther* (2014) 141(3):272–82. doi: 10.1016/j.pharmthera.2013.10.010
10. Hasturk H, Kantarci A, Ohira T, Arita M, Ebrahimi N, Chiang N, et al. RvE1 protects from local inflammation and osteoclast- mediated bone destruction in periodontitis. *FASEB J* (2006) 20(2):401–3. doi: 10.1096/fj.05-4724fje
11. Hasturk H, Kantarci A, Goguet-Surmenian E, Blackwood A, Andry C, Serhan CN, et al. Resolvin E1 Regulates Inflammation at the Cellular and Tissue Level and Restores Tissue Homeostasis In Vivo. *J Immunol* (2007) 179(10):7021–9. doi: 10.4049/jimmunol.179.10.7021
12. Herrera BS, Ohira T, Gao L, Omori K, Yang R, Zhu M, et al. An endogenous regulator of inflammation, resolvin E1, modulates osteoclast differentiation and bone resorption. *Br J Pharmacol* (2008) 155(8):1214–23. doi: 10.1038/bjp.2008.367
13. Mizraji G, Heyman O, Van Dyke TE, Wilensky A. Resolvin D2 restrains Th1 immunity and prevents alveolar bone loss in murine periodontitis. *Front Immunol* (2018) 9(APR):1–10. doi: 10.3389/fimmu.2018.00785
14. Herrera BS, Hasturk H, Kantarci A, Freire MO, Nguyen O, Kansal S, et al. Impact of resolvin E1 on murine neutrophil phagocytosis in type 2 diabetes. *Infect Immun* (2015) 83(2):792–801. doi: 10.1128/IAI.02444-14
15. Bourque J, Hawiger D. Immunomodulatory bonds of the partnership between dendritic cells and T cells. *Crit Rev Immunol* (2018) 38:379–401. doi: 10.1615/CritRevImmunol.2018026790
16. Nagaya T, Kawata K, Kamekura R, Jitsukawa S, Kubo T, Kamei M, et al. Lipid mediators foster the differentiation of T follicular helper cells. *Immunol Lett* (2017) 181:51–7. doi: 10.1016/j.imlet.2016.11.006
17. Tager AM, Bromley SK, Medoff BD, Islam SA, Bercury SD, Friedrich EB, et al. Leukotriene B4 receptor BLT1 mediates early effector T cell recruitment. *Nat Immunol* (2003) 4(10):982–90. doi: 10.1038/ni970
18. Schorer M, Kuchroo VK, Joller N. Role of co-stimulatory molecules in T helper cell differentiation. *Adv Exp Med Biol* (1189) 2019):153–77. doi: 10.1007/978-981-32-9717-3_6
19. Annunziato F, Cosmi L, Santarlasci V, Maggi L, Liotta F, Mazzinghi B, et al. Phenotypic and functional features of human Th17 cells. *J Exp Med* (2007) 204(8):1849–61. doi: 10.1084/jem.20070663
20. Veldhoen M. Interleukin 17 is a chief orchestrator of immunity. *Nat Immunol* (2017) 18(6):612–21. doi: 10.1038/ni.3742
21. Khader SA, Gaffen SL, Kolls JK. Th17 cells at the crossroads of innate and adaptive immunity against infectious diseases at the mucosa. *Mucosal Immunol* (2009) 2(5):403–11. doi: 10.1038/mi.2009.100
22. Zenobia C, Hajishengallis G. Basic biology and role of interleukin-17 in immunity and inflammation. *Periodontol 2000* (2016) 69(1):142–59. doi: 10.1111/prd.12083
23. Miossec P, Kolls JK. Targeting IL-17 and T H 17 cells in chronic inflammation. *Nat Rev Drug Discov* (2012) 11(10):763–76. doi: 10.1038/nrd3794
24. Korn T, Bettelli E, Oukka M, Kuchroo VK. IL-17 and Th17 Cells. *Annu Rev Immunol* (2009) 27(1):485–517. doi: 10.1146/annurev.immunol.021908.132710
25. Bettelli E, Korn T, Oukka M, Kuchroo VK. Induction and effector functions of TH17 cells. *Nature* (2008) 453(7198):1051–7. doi: 10.1038/nature07036
26. Mellman I, Steinman RM, Haven N. Dendritic cells; specialized and regulated antigen processing machines. *Cell* (2001) 106:255–8. doi: 10.1016/S0092-8674(01)00449-4
27. Leal Rojas IM, Mok WH, Pearson FE, Minoda Y, Kenna TJ, Barnard RT, et al. Human blood cD1c+dendritic cells promote Th1 and Th17 effector function in memory cD4+T cells. *Front Immunol* (2017) 8(AUG):1–11. doi: 10.3389/fimmu.2017.00971
28. Bedoya SK, Wilson TD, Collins EL, Lau K, Larkin J. Isolation and th17 differentiation of naïve CD4 T lymphocytes. *J Vis Exp* (2013) 79:e50765. doi: 10.3791/50765
29. Bacher P, Schink C, Teutschbein J, Kniemeyer O, Assenmacher M, Brakhage AA, et al. Antigen-Reactive T Cell Enrichment for Direct, High-Resolution Analysis of the Human Naive and Memory Th Cell Repertoire. *J Immunol* (2013) 190(8):3967–76. doi: 10.4049/jimmunol.1202221
30. Napolitani G, Rinaldi A, Bertoni F, Sallusto F, Antonio L. Selected TLR agonist combinations synergistically trigger a TH1 polarizing program in dendritic cells. *Nat Immunol* (2005) 6(8):769–76. doi: 10.1038/ni1223
31. Yu C-F, Peng W-M, Oldenburg J, Hoch J, Bieber T, Limmer A, et al. Human Plasmacytoid Dendritic Cells Support Th17 Cell Effector Function in Response to TLR7 Ligation. *J Immunol* (2010) 184(3):1159–67. doi: 10.4049/jimmunol.0901706
32. Ferreira TB, Hygino J, Wing AC, Kasahara TM, Sacramento PM, Camargo S, et al. Different interleukin-17-secreting Toll-like receptor + T-cell subsets are

associated with disease activity in multiple sclerosis. *Immunology* (2018) 154 (2):239–52. doi: 10.1111/imm.12872
33. Reynolds JM, Pappu BP, Peng J, Martinez GJ, Chung Y, Ma L, et al. Toll-like receptor 2 signaling in CD4+ T lymphocytes promotes T helper 17 responses and regulates the pathogenesis of autoimmune disease. *Immunity* (2011) 32 (5):692–702. doi: 10.1016/j.immuni.2010.04.010
34. Ye J, Wang Y, Liu X, Li L, Opejin A, Hsueh EC, et al. TLR7 Signaling Regulates Th17 Cells and Autoimmunity: Novel Potential for Autoimmune Therapy. *J Immunol* (2017) 199(3):941–54. doi: 10.4049/jimmunol.1601890
35. Serhan C, Chiang N, Van Dyke T. Resolving inflammation: dual anti-inflammatory and pro-resolution lipid mediators. *Nat Rev Immuno* (2008) 8(5):349–61. doi: 10.1038/nri2294
36. Hua J, Jin Y, Chen Y, Inomata T, Lee HS, Chauhan SK, et al. The resolvin D1 analogue controls maturation of dendritic cells and suppresses alloimmunity in corneal transplantation. *Investig Ophthalmol Vis Sci* (2014) 55(9):5944–51. doi: 10.1167/iovs.14-14356
37. Chiurchiu VA, Leuti S, Dalli J, Jacobson A, Battistini L, Maccarone M, et al. Pro-resolving lipid mediators Resolvin D1, Reesolvin D2 and Maresin 1 are critical in modulating T cell responses. *Sci Transl Med* (2016) 8:353ra111. doi: 10.1126/scitranslmed.aaf7483
38. Josefowicz SZ, Lu LF, Rudensky AY. Regulatory T cells; mechanisms of differentiation and function. *Annu Rev Immunol* (2012) 30:531–64. doi: 10.1146/annurev.immunol.25.022106.141623
39. Chaudhry A, Rudra D, Treuting P, Samstein RM, Kas A, Rudensky AY. CD4+ regulatory T cells control Th17 response in a STAT3-dependent manner. *Science* (2009) 326(5955):986–91. doi: 10.1126/science.1172702
40. Serhan CN, Hong S, Gronert K, Colgan SP, Devchand PR, Mirick G, et al. Resolvins. *J Exp Med* (2002) 196(8):1025–37. doi: 10.1084/jem.20020760
41. Lim TS, Goh JKH, Mortellaro A, Lim CT, Hämmerling GJ, Ricciardi-Castagnoli P. CD80 and CD86 Differentially Regulate Mechanical Interactions of T-Cells with Antigen-Presenting Dendritic Cells and B-Cells. *PLoS One* (2012) 7(9):1–8. doi: 10.1371/journal.pone.0045185
42. Fujii S, Liu K, Smith C, Bonito AJ, Steinman RM. The Linkage of Innate to Adaptive Immunity via Maturing Dendritic Cells In Vivo Requires CD40 Ligation in Addition to Antigen Presentation and CD80/86 Costimulation. *J Exp Med* (2004) 199(12):1607–18. doi: 10.1084/jem.20040317
43. Aggarwal S, Ghilardi N, Xie MH, De Sauvage FJ, Gurney AL. Interleukin-23 promotes a distinct CD4 T cell activation state characterized by the production of interleukin-17. *J Biol Chem* (2003) 278(3):1910–4. doi: 10.1074/jbc.M207577200
44. Ivanov II, McKenzie BS, Zhou L, Tadokoro CE, Lepelley A, Lafaille JJ, et al. The Orphan Nuclear Receptor RORγt Directs the Differentiation Program of Proinflammatory IL-17+T Helper Cells. *Cell* (2006) 126(6):1121–33. doi: 10.1016/j.cell.2006.07.035
45. He Z, Wang F, Zhang J, Sen S, Pang Q, Luo S, et al. Regulation of Th17 Differentiation by IKKα-Dependent and -Independent Phosphorylation of RORγt. *J Immunol* (2017) 199(3):955–64. doi: 10.4049/jimmunol.1700457
46. Lubberts E. IL-17/Th17 targeting: On the road to prevent chronic destructive arthritis? *Cytokine* (2008) 41(2):84–91. doi: 10.1016/j.cyto.2007.09.014
47. Chung Y, Chang SH, Martinez GJ, Yang XO, Nurieva R, Kang HS, et al. Critical Regulation of Early Th17 Cell Differentiation by Interleukin-1 Signaling. *Immunity* (2009) 30(4):576–87. doi: 10.1016/j.immuni.2009.02.007
48. Yang XO, Panopoulos AD, Nurieva R, Seon HC, Wang D, Watowich SS, et al. STAT3 regulates cytokine-mediated generation of inflammatory helper T cells. *J Biol Chem* (2007) 282(13):9358–63. doi: 10.1074/jbc.C600321200
49. Zhou L, Ivanov II, Spolski R, Min R, Shenderov K, Egawa T, et al. IL-6 programs TH-17 cell differentiation by promoting sequential engagement of the IL-21 and IL-23 pathways. *Nat Immunol* (2007) 8(9):967–74. doi: 10.1038/ni1488
50. Chen H, Qin J, Wei P, Zhang J, Li Q, Fu L, et al. Effects of leukotriene B4 and prostaglandin E2 on the differentiation of murine Foxp3+ T regulatory cells and Th17 cells. *Prostaglandins Leukot Essent Fat Acids* (2009) 80(4):195–200. doi: 10.1016/j.plefa.2009.01.006
51. Maynard CL, Harrington LE, Janowski KM, Oliver JR, Zindl CL, Rudensky AY, et al. Regulatory T cells expressing interleukin 10 develop from Foxp3+ and Foxp3- precursor cells in the absence of interleukin 10. *Nat Immunol* (2007) 8(9):931–41. doi: 10.1038/ni1504
52. Vassiliou EK, Kesler OM, Tadros JH, Ganea D. Bone Marrow-Derived Dendritic Cells Generated in the Presence of Resolvin E1 Induce Apoptosis of Activated CD4+ T Cells. *J Immunol* (2008) 181(7):4534–44. doi: 10.4049/jimmunol.181.7.4534
53. Chen F, Fan XH, Wu YP, Zhu JL, Wang F, Bo LL, et al. Resolvin D1 improves survival in experimental sepsis through reducing bacterial load and preventing excessive activation of inflammatory response. *Eur J Clin Microbiol Infect Dis* (2014) 33(3):457–64. doi: 10.1007/s10096-013-1978-6
54. Zielinski CE, Mele F, Aschenbrenner D, Jarrossay D, Ronchi F, Gattorno M, et al. Pathogen-induced human TH17 cells produce IFN-γ or IL-10 and are regulated by IL-1β. *Nature* (2012) 484(7395):514–8. doi: 10.1038/nature10957
55. Tang L, Yang X, Liang Y, Xie H, Dai Z, Zheng G. Transcription factor retinoid-related orphan receptor γt: A promising target for the treatment of psoriasis. *Front Immunol* (2018) 9:1210. doi: 10.3389/fimmu.2018.01210
56. McGeachy MJ, Bak-Jensen KS, Chen Y, Tato CM, Blumenschein W, McClanahan T, et al. TGF-β and IL-6 drive the production of IL-17 and IL-10 by T cells and restrain TH-17 cell-mediated pathology. *Nat Immunol* (2007) 8(12):1390–7. doi: 10.1038/ni1539
57. Acosta-Rodriguez EV, Rivino L, Geginat J, Jarrossay D, Gattorno M, Lanzavecchia A, et al. Surface phenotype and antigenic specificity of human interleukin 17-producing T helper memory cells. *Nat Immunol* (2007) 8 (6):639–46. doi: 10.1038/ni1467
58. Yamazaki T, Yang XO, Chung Y, Fukunaga A, Nurieva R, Pappu B, et al. CCR6 regulates the migration of inflammatory and regulatory T cells. *J Immunol* (2008) 181(12):8391–401. doi: 10.4049/jimmunol.181.12.8391
59. Afzali B, Mitchell P, Lechler RI, John S, Lombardi G. Translational mini-review series on Th17 cells: Induction of interleukin-17 production by regulatory T cells. *Clin Exp Immunol* (2010) 159(2):120–30. doi: 10.1111/j.1365-2249.2009.04038.x
60. Sawada Y, Honda T, Nakamizo S, Otsuka A, Ogawa N, Kobayashi Y, et al. Resolvin E1 attenuates murine psoriatic dermatitis. *Sci Rep* (2018) 8(1):1–9. doi: 10.1038/s41598-018-30373-1
61. Hubo M, Trinschek B, Kryczanowsky F, Tuettenberg A, Steinbrink K, Jonuleit H. Costimulatory molecules on immunogenic versus tolerogenic human dendritic cells. *Front Immunol* (2013) 4(APR):1–14. doi: 10.3389/fimmu.2013.00082
62. Colamatteo A, Maggioli E, Azevedo Loiola R, Hamid Sheikh M, Calì G, Bruzzese D, et al. Reduced Annexin A1 Expression Associates with Disease Severity and Inflammation in Multiple Sclerosis Patients. *J Immunol* (2019) 203(7):1753–65. doi: 10.4049/jimmunol.1801683
63. Malek TR. The Biology of Interleukin-2. *Annu Rev Immunol* (2008) 26 (1):453–79. doi: 10.1146/annurev.immunol.26.021607.090357
64. Boyman O, Sprent J. The role of interleukin-2 during homeostasis and activation of the immune system. *Nat Rev Immunol* (2012) 12(3):180–90. doi: 10.1038/nri3156
65. Létourneau S, Krieg C, Pantaleo G, Boyman O. IL-2- and CD25-dependent immunoregulatory mechanisms in the homeostasis of T-cell subsets. *J Allergy Clin Immunol* (2009) 123(4):758–62. doi: 10.1016/j.jaci.2009.02.011
66. Ono Y, Tsuboi H, Moriyama M, Asashima H, Kudo H, Takahashi H, et al. RORγt antagonist improves Sjögren's syndrome-like sialadenitis through downregulation of CD25. *Oral Dis* (2020) 26(4):766–77. doi: 10.1111/odi.13255
67. Sakaguchi S, Sakaguchi N, Shimizu J, Yamazaki S, Sakihama T, Itoh M, et al. Immunologic tolerance maintained by CD25+ CD4+ regulatory T cells: Their common role in controlling autoimmunity, tumor immunity, and transplantation tolerance. *Immunol Rev* (2001) 182(7):18–32. doi: 10.1034/j.1600-065X.2001.1820102.x
68. Shevach EM. CD4+CD25+ suppressor T cells: more questions than answers. *Nat Rev Immunol* (2002) 2(6):389–400. doi: 10.1038/nri821
69. Lang C, Wang J, Chen L. CD25-expressing Th17 cells mediate CD8+ T cell suppression in CTLA-4 dependent mechanisms in pancreatic ductal adenocarcinoma. *Exp Cell Res* (2017) 360(2):384–9. doi: 10.1016/j.yexcr.2017.09.030
70. Kitagawa Y, Sakaguchi S. Molecular control of regulatory T cell development and function. *Curr Opin Immunol* (2017) 49:64–70. doi: 10.1016/j.coi.2017.10.002
71. Abbas AK, Trotta E R, Simeonov D, Marson A, Bluestone JA. Revisiting IL-2: Biology and therapeutic prospects. *Sci Immunol* (2018) 3(25):eaat1482. doi: 10.1126/sciimmunol.aat1482
72. Xia H, Wang F, Wang M, Wang J, Sun S, Chen M, et al. Maresin1 ameliorates acute lung injury induced by sepsis through regulating Th17/Treg balance. *Life Sci* (2020) 254(February):117773. doi: 10.1016/j.lfs.2020.117773

73. Kim JY, Lim K, Kim KH, Kim JH, Choi JS, Shim SC. N-3 polyunsaturated fatty acids restore Th17 and Treg balance in collagen antibody-induced arthritis. *PLoS One* (2018) 13(3):1–14. doi: 10.1371/journal.pone.0194331
74. Chen Y, Haines CJ, Gutcher I, Hochweller K, Blumenschein WM, McClanahan T, et al. Foxp3+ regulatory T cells promote T helper 17 cell development in vivo through regulation of interleukin-2. *Immunity* (2011) 34 (3):409–21. doi: 10.1016/j.immuni.2011.02.011
75. Kryczek I, Wei S, Vatan L, Escara-Wilke J, Szeliga W, Keller ET, et al. Cutting Edge: Opposite Effects of IL-1 and IL-2 on the Regulation of IL-17 + T Cell Pool IL-1 Subverts IL-2-Mediated Suppression. *J Immunol* (2007) 179 (3):1423–6. doi: 10.4049/jimmunol.179.3.1423

Conflict of Interest: The authors declare that the research was conducted in the absence of any commercial or financial relationships that could be construed as a potential conflict of interest.

Copyright © 2021 Oner, Alvarez, Yaghmoor, Stephens, Hasturk, Firatli and Kantarci. This is an open-access article distributed under the terms of the Creative Commons Attribution License (CC BY). The use, distribution or reproduction in other forums is permitted, provided the original author(s) and the copyright owner(s) are credited and that the original publication in this journal is cited, in accordance with accepted academic practice. No use, distribution or reproduction is permitted which does not comply with these terms.

frontiers in Immunology

ORIGINAL RESEARCH
published: 22 March 2021
doi: 10.3389/fimmu.2021.651740

Adenosine Diphosphate Improves Wound Healing in Diabetic Mice Through $P2Y_{12}$ Receptor Activation

Paula Alvarenga Borges[1,2†], Ingrid Waclawiak[1†], Janaína Lima Georgii[1†], Vanderlei da Silva Fraga-Junior[3], Janaína Figueiredo Barros[1], Felipe Simões Lemos[1], Thaís Russo-Abrahão[4], Elvira Maria Saraiva[5], Christina M. Takiya[3], Robson Coutinho-Silva[3], Carmen Penido[6,7], Claudia Mermelstein[1], José Roberto Meyer-Fernandes[4], Fábio B. Canto[8], Josiane Sabbadini Neves[1], Paulo A. Melo[1], Claudio Canetti[3‡] and Claudia Farias Benjamim[1,3‡]*

[1] Institute of Biomedical Sciences, Center of Health Sciences, Federal University of Rio de Janeiro (UFRJ), Rio de Janeiro, Brazil, [2] Fluminense Federal Institute (IFF), Rio de Janeiro, Brazil, [3] Institute of Biophysics Carlos Chagas Filho (IBCCF), Center of Health Sciences, UFRJ, Rio de Janeiro, Brazil, [4] Institute of Medical Biochemistry Leopoldo de Meis, Center of Health Sciences, UFRJ, Rio de Janeiro, Brazil, [5] Institute of Microbiology Paulo de Góes, Center of Health Sciences, UFRJ, Rio de Janeiro, Brazil, [6] Center for Technological Development in Health, Oswaldo Cruz Foundation, Rio de Janeiro, Brazil, [7] Laboratory of Applied Pharmacology, Institute of Drug Technology, Farmanguinhos, Oswaldo Cruz Foundation, Rio de Janeiro, Brazil, [8] Department of Immunobiology, Institute of Biology, Fluminense Federal University (UFF), Niterói, Brazil

Chronic wounds are a public health problem worldwide, especially those related to diabetes. Besides being an enormous burden to patients, it challenges wound care professionals and causes a great financial cost to health system. Considering the absence of effective treatments for chronic wounds, our aim was to better understand the pathophysiology of tissue repair in diabetes in order to find alternative strategies to accelerate wound healing. Nucleotides have been described as extracellular signaling molecules in different inflammatory processes, including tissue repair. Adenosine-5'-diphosphate (ADP) plays important roles in vascular and cellular response and is immediately released after tissue injury, mainly from platelets. However, despite the well described effect on platelet aggregation during inflammation and injury, little is known about the role of ADP on the multiple steps of tissue repair, particularly in skin wounds. Therefore, we used the full-thickness excisional wound model to evaluate the effect of local ADP application in wounds of diabetic mice. ADP accelerated cutaneous wound healing, improved new tissue formation, and increased both collagen deposition and transforming growth factor-β (TGF-β) production in the wound. These effects were mediated by $P2Y_{12}$ receptor activation since they were inhibited by Clopidogrel (Clop) treatment, a $P2Y_{12}$ receptor antagonist. Furthermore, $P2Y_1$ receptor antagonist also blocked ADP-induced wound closure until day 7, suggesting its involvement early in repair process. Interestingly, ADP treatment increased the expression of $P2Y_{12}$ and $P2Y_1$

OPEN ACCESS

Edited by:
Amiram Ariel, University of Haifa, Israel

Reviewed by:
Ronald Sluyter, University of Wollongong, Australia
Edyta Gendaszewska-Darmach, Lodz University of Technology, Poland

***Correspondence:**
Claudia Farias Benjamim
cfbenjamim@biof.ufrj.br; cfbenjamim@gmail.com

†These authors have contributed equally to this work and share first authorship

‡These authors have contributed equally to this work and share last authorship

Specialty section:
This article was submitted to Inflammation, a section of the journal Frontiers in Immunology

Received: *10 January 2021*
Accepted: *01 March 2021*
Published: *22 March 2021*

Citation:
Borges PA, Waclawiak I, Georgii JL, Fraga-Junior VdS, Barros JF, Lemos FS, Russo-Abrahão T, Saraiva EM, Takiya CM, Coutinho-Silva R, Penido C, Mermelstein C, Meyer-Fernandes JR, Canto FB, Neves JS, Melo PA, Canetti C and Benjamim CF (2021) Adenosine Diphosphate Improves Wound Healing in Diabetic Mice Through $P2Y_{12}$ Receptor Activation. Front. Immunol. 12:651740. doi: 10.3389/fimmu.2021.651740

receptors in the wound. In parallel, ADP reduced reactive oxygen species (ROS) formation and tumor necrosis factor-α (TNF-α) levels, while increased IL-13 levels in the skin. Also, ADP increased the counts of neutrophils, eosinophils, mast cells, and gamma delta (γδ) T cells ($V\gamma4^+$ and $V\gamma5^+$ cells subtypes of $\gamma\delta^+$ T cells), although reduced regulatory T (Tregs) cells in the lesion. In accordance, ADP increased fibroblast proliferation and migration, myofibroblast differentiation, and keratinocyte proliferation. In conclusion, we provide strong evidence that ADP acts as a pro-resolution mediator in diabetes-associated skin wounds and is a promising intervention target for this worldwide problem.

Keywords: adenosine diphosphate (ADP), wound healing, mice, skin, diabetes, inflammation, purinergic signaling, $P2Y_{12}$ recepor

INTRODUCTION

Wound healing is a complex, dynamic and multi-mediated process characterized by a highly regulated cascade of events requiring the interaction of many cell types, including inflammatory and immune cells. Normal healing process occurs over a range of overlapping events: inflammation, granulation tissue formation, and remodeling. Impaired wounds are often associated with pathologic inflammation due to a persistent, incomplete, or uncoordinated healing process (1, 2).

Patients suffer from abnormalities of wound healing worldwide; in particular, under conditions such as senescence, diabetes, ischemia, peripheral vascular disease, and cancer (3, 4). Chronic wounds are reported to affect around 8.2 million patients just in the USA, based on a 2018 retrospective analysis of Medicare beneficiaries; the estimated annual cost for healthcare system to treat wound-related complications is more than US$ 28 billion (5, 6). In Brazil, the most populous country in Latin America, about 40 to 60% of non-traumatic lower limb amputations occur in diabetic patients, whereas, about 85% are related to foot ulcers (7–9).

Among inflammatory mediators, nucleotides play important roles in host defense and tissue repair; however, little is known about their role in wounds (10). The nucleotide adenosine-5'-diphosphate (ADP) plays a pivotal role in the physiologic process of hemostasis and platelet aggregation. ADP activates $P2Y_1$, $P2Y_{12}$, and $P2Y_{13}$ receptors, which are expressed by monocytes, macrophages, lymphocytes, mast cells, fibroblasts, keratinocytes, endothelial cells, eosinophils, platelets, neutrophils, and dendritic cells (11–13). Neuroprotective function for ADP was demonstrated in zebrafish retina since it mitigates the excessive cell death and tissue damage; additionally, it stimulated cellular proliferation after injury (14). In addition, ADP induced the proliferation of mouse fibroblasts (3T3 and 3T6), suggesting a positive effect on wound healing (15). Since purinergic system has been involved in pro-inflammatory, cell proliferative and pro-resolution effects, we aim to explore the role of ADP in accelerating wound healing in diabetic mice, considering that chronic wounds are a relevant health problem evidenced by the lack of an effective treatment, especially in diabetic patients.

Abbreviations: ADO, adenosine; ADP, adenosine diphosphate; ATP, adenosine triphosphate; AMP, adenosine monophosphate; BrdU, 5-bromo-2'-deoxyuridine; CBA, cytometric bead array; CCL2, C-C motif chemokine ligand 2; Clop, clopidogrel; DAPI, 4',6-diamidino-2-phenylindole; FACS – Foxp3- forkhead box protein p3; gamma delta T cells, γδ T cells; IFN, interferon; IHC, immunohistochemistry; IL, interleukin; PBS, phosphate buffer saline; ROS, reactive oxygen species; α-SMA, α-smooth muscle actin; TGF-β, transforming growth factor-β; TNF-α, tumor necrosis factor-α; Tregs, regulatory T cells; WB, western blotting.

MATERIALS AND METHODS

Mice

Male Swiss (8-10 weeks) and C57BL/6 mice (10-14 weeks) weighing 25-30 g obtained from the Institute of Science and Technology in Bio Models at Oswaldo Cruz Foundation, were used for full-thickness excisional wound models. For the cutaneous leishmaniasis lesion model, we used male BALB/c mice (10-14 weeks), obtained from the Microbiology and Parasitology Department animal facility at Biomedical Institute in Fluminense Federal University. All procedures described were approved by the Ethics Committee for the Use of Animals of the Federal University of Rio de Janeiro (CEUA/UFRJ: 093/15 and IMPPG 128/15).

Induction of Diabetes Mellitus

Diabetes was induced by alloxan (65 mg/kg, i.v. in 100 μL of saline) in mice fasted for 12 h (16, 17). Non-diabetic mice were injected with saline (100 μL). Diabetes was confirmed 7 days later when blood glucose concentration was at least 350 mg/dl. The glucose levels were still elevated (over 350 mg/dl) at day 30 after alloxan injection.

Full-Thickness Excisional Wound Model

At day 7 after alloxan or saline administration, mice were intraperitoneally (i.p. - 10 μL/10 g) anesthetized (ketamine 112 mg/kg and xylazine 7.5 mg/kg) and a full-thickness excisional wound (10 mm in diameter) was executed on the dorsum using biopsy punch. Wounds were treated once a day for 14 days (or until sample collection) with topical application by a micropipette of adenosine-5'-monophosphate (AMP), ADP, adenosine-5'-triphosphate (ATP), adenosine, or pyrophosphate (Sigma-Aldrich, St Louis, MO) at 30 μM (30 μL/mouse - 15.2 μg/kg), or vehicle (30 μL of saline/mouse). In another set

of experiments, a dose-response curve of ADP at 30 μM (15.2 μg/kg), 100 μM (51.2 μg/kg) or 300 μM (153.6 μg/kg), administrated topically in 30 μL, was performed. After the application on the wound, mice were placed alone under a glass funnel for 5 min until the solution was absorbed.

Wound Area Quantification

To determine the wound closure rate, the wound area was evaluated at days 0, 3, 7, 10, and 14 after wounding. Photographs were taken at a standard distance using a tripod and were analyzed using ImageJ software (National Institutes of Health – NIH). Data were expressed as a percentage of the initial wound area.

Treatments

The administration of Clopidogrel® (Clop - 5 mg/kg) was performed daily by oral gavage, 1 h before ADP administration for 14 days. Antagonists of $P2Y_1$ (MRS 2179 - 30 μM/30 μL/mouse - Tocris, Bioscience, UK) and $P2Y_{12}$ (MRS 2395 - 30 μM/30 μL/mouse - Sigma-Aldrich) receptors, and ATP diphosphohydrolase (apyrase - 6 U/mL, 30 μL/mouse - Sigma-Aldrich – A6535-100UN) were topically applied for 14 days, 30 min before ADP administration. The apyrase used in our work was purified from potato and has predominantly the low ATPase/ADPase ratio of ~1:1 (Sigma-Aldrich).

Hematoxylin & Eosin Staining and Total Collagen Quantification

Wound tissues were paraffin-embedded and cut in 5-μm thick sections. Hematoxylin and eosin staining was performed as described elsewhere. Skin sample sections (7-μm) were stained with Picro Sirius Red for total amount of collagen, as previously reported (18). The quantification was determined by morphometric analysis using a quantitative imaging software (ImagePro Plus, version 4.5.1). The percentage of collagen per field was obtained by dividing the total area by the fibrosis area.

Ecto-Nucleotidase Activity

Ecto-nucleotidase activity was determined in wound homogenates by the rate of inorganic phosphate (Pi) released using the malachite green reactions, as previously described (19). The concentration of Pi released in the reaction was determined by a Pi standard curve and expressed as nucleotidase activity (nmol Pi x h^{-1} x mg ptn^{-1}).

Immunohistochemistry (IHC)

Wound samples collected at day 7 were paraffin-embedded, cut in sections (7-μm) and immunostained for several markers, as described previously (20). The specific markers are detailed in the **Supplementary Material**. Data were expressed as number of positive cells per field. For collagen type markers, we employed a score method described by Calvi et al. (21), for the semi-quantification of collagen deposits performed by two different observers, as reported in the **Supplementary Material**.

Immunofluorescence

Wound sections (5-μm) were immunostained against α-smooth muscle actin (α-SMA; A-2547, 1:200, Sigma-Aldrich) as previously reported (22). Control experiments with no primary antibodies showed only faint background staining (data not shown).

Fibroblast Purification and Proliferation Assay

Primary neonate dermal fibroblasts were purified from the abdomen and dorsal skin of C57BL/6 male mice as previously described, with few modifications (23). Briefly, the skin was cut into small pieces and digested with 0.1% dispase (Roche, Mannheim, Germany) at 4°C for 24 h. After removal of the epidermal layers, the remaining dermal parts were incubated with 0.1% collagenase D (Sigma-Aldrich) at 37°C for 1 h. Next, the digested cells were passed through a 40-μm cell strainer. Fibroblasts (2 x 10^4 cells) were cultured for 5-bromo-2'-deoxyuridine (BrdU) staining proliferation assay, as previously described (24). The images were captured using a fluorescence microscope and analyzed using ImageJ software. Results were expressed as the percentage of $BrdU^+$ cells by total number of cells labeled with 4',6-diamidino-2-phenylindole (DAPI).

Wound Scratch Assay

Primary dermal fibroblasts were seeded and grown until 90% confluence to evaluate migration-induced effect of ADP (10, 30, or 100 μM), as previously reported (25). Pictures of the scratched areas were taken at 0, 6, 12, 18, and 24 h using an inverted microscope equipped with a digital camera (BEL Engineering - Monza, Italy). The areas were measured using the ImageJ software and the fibroblast migration was expressed as % of open area compared to the initial area (0 h – 100%).

Flow Cytometry

Flow cytometry of the wound tissues was performed as previously described (26). Briefly, wound tissues were digested by an enzyme cocktail (reported in **Supplementary Material**) and the cells (10^6 cells/mL) were subjected to flow cytometry procedure, stained, and analyzed. Lymphocyte populations recovered from skin and draining inguinal, axillary, and brachial lymph nodes were also analyzed. For skin regulatory T (Tregs) cells analysis, samples were enriched by Percoll gradient for mononuclear cells. Samples were acquired with BD FACS Canto II (BD Biosciences, San Jose, CA) and then analyzed with FlowJo software. Gating strategy and the list of antibodies are described in the **Supplementary Material**.

Eosinophil and mast cell infiltrates

Skin sections (5-μm) were stained with modified Sirius Red or Alcian Blue for eosinophils and mast cells, respectively, as described elsewhere (27, 28). Images were taken using a digital camera coupled to the microscope (Olympus BX53) at 40x magnification. Twenty fields were analyzed per wound/animal (n=3) and the data were expressed as number of eosinophils or mast cells/mm^2.

Myeloperoxidase Activity

The number of neutrophils was indirectly determined by myeloperoxidase enzyme activity in the wounds removed 7 days after wounding, as previously described (29). The number of neutrophil was estimated by a standard curve, using neutrophils obtained 6 h after i.p. administration of 3% thioglycolate (>90% of

neutrophils). Total protein extract was quantified by the Bradford method. Results were expressed as number of neutrophils/mg of protein.

ELISA

Cytokine quantification was performed in protein extracts from wounds obtained at day 3 and 7 after wounding using PeproTech kits following manufacturer's instructions. The results were expressed as pg or ng of cytokine/mg of protein.

Superoxide Assay

The superoxide production assay was performed by the nitroblue tetrazolium (NBT) reaction with reactive oxygen species resulting in formazan as final product (30). Briefly, the wounds were removed at day 7 and homogenized in phosphate buffer saline (PBS) containing protease inhibitors. The formazan formed was measured by ELISA plate reader (620 nm, Spectra Max-250, Molecular Devices). Results were expressed as μg of formazan/mg of protein.

Cytometric Bead Array (CBA)

Cytokine concentration in the wounds was determined by flow cytometry using the kit CBA Mouse Inflammation (BD Biosciences, San Diego, CA), following manufacturer's instructions. This CBA kit allows measurements of interleukin-6 (IL-6), IL-10, C-C motif chemokine ligand 2 (CCL2), interferon-γ (IFN-γ), TNF-α, and IL-12p70. Sample processing and data analysis were acquired by FACS Calibur flow cytometer (BD Bioscences) and FCAP Array software, respectively. Results were expressed as pg or ng of cytokine/mg of protein.

Western Blotting (WB)

Wound homogenates (30 mg of skin tissue – 20 μg of protein loaded per gel lane) collected at day 7 were prepared as previously described (31). Immunoreactive bands for α-SMA (1:1000 - Sigma-Aldrich) and β-actin (1:1000 - Cell Signaling, Danvers, MA) were visualized using an enhanced chemiluminescence reagent (Amersham ECL, Biosciences) and pictures were recorded using Healthcare ImageQuant LAS 4000 (GE Healthcare Life Sciences). Densitometry analysis was performed using ImageJ software and the results were expressed as the ratio of α-SMA/β-actin (housekeeping).

Statistical Analysis

Statistical differences in the wound closure experiments were determined using two-way ANOVA followed by Bonferroni post-test. The significance of other experiments was determined by one-way ANOVA followed by Tukey post-test or unpaired Student's t test, as stated in the legends. The statistical tests were performed by GraphPad Prism software.

A more detailed description can be found in **Supplementary Material**.

RESULTS

ADP Improves Wound Healing in Diabetic Mice

Diabetic and non-diabetic male Swiss mice were topically treated with saline or ADP 30 μM (30 μL - 15.4 μg/kg), every day for 14 days after wounding. ADP was effective in accelerating the wound closure in diabetic mice compared to the respective saline-treated mice (**Figure 1A**), but did not change the wound healing in non-diabetic mice (**Figure 1B**). ADP-treated diabetic mice presented 60% wound closure versus 2% in saline-treated mice at day 7 (**Figure 1A** - graph). More importantly, the wound closure profile of the diabetic animals treated with ADP was similar to that of saline-treated non-diabetic mice (**Figure 1B** – first row of photographs). Moreover, the only effective dose able to accelerate wound closure was 30 μM (**Figure 1C**-table). Indeed, higher ADP doses tested delayed wound healing when observed at day 14, compared to the saline-treated wound.

Clop Impairs ADP-Induced Wound Closure

To assess the role of $P2Y_{12}$ and ADP in our model, the $P2Y_{12}$ irreversible antagonist Clop was administrated (5 mg/kg) daily by gavage. This treatment impaired the ADP-mediated wound closure in diabetic mice (**Figure 1A**). It was characterized by an increase of the lesion size and a worsening of the wound general aspects, at all the time-points evaluated. Furthermore, Clop administration also worsened the saline-treated wound of diabetic mice (**Supplementary Figure 1**). Still, an endogenous and physiological critical role in tissue repair of ADP/$P2Y_{12}$ axis was suggested, since Clop treatment also impaired healing of both saline- (**Supplementary Figure 1**) and ADP-treated wounds (**Figure 1B**) of non-diabetic mice. Taking into consideration that ADP is the major agonist of $P2Y_{12}$ receptor (32, 33) and Clop treatment prevented ADP-induced wound closure, these observations provide an unequivocal proof of ADP's role in accelerating wound closure of diabetic mice.

$P2Y_1$ Also Seems to Mediate ADP Effects

The involvement of ADP receptors in wound healing was verified by the use of another $P2Y_{12}$ antagonist (MRS2395) and by a $P2Y_1$ antagonist (MRS2179). Both antagonists, used at 30 μM (30 μL/wound), impaired the wound closure induced by ADP until day 7. However, at day 10 and 14 the wound healing profile was identical to that observed in ADP-treated group without antagonists administration (**Figures 2A, B**). $P2Y_1$ and $P2Y_{12}$ receptor antagonists alone did not accelerate or worsen the wound closure in diabetic mice (**Figures 2A, B**). Since Clop treatment impaired the wound healing in the presence (**Figure 1A**) and absence (**Supplementary Figure 1**) of ADP in diabetic mice, we expected to observe the same response with MSR2395 treatment. Indeed, such divergence could be partially explained by different administration routes (systemic *versus* local) between these drugs; in addition, while Clop is an irreversible antagonist, MRS2395 is a competitive antagonist.

Apyrase Worsens Wound Healing

Apyrase removes the γ-phosphate from ATP and the β-phosphate from ADP, yielding AMP (34). Apyrase treatment worsened wound healing in diabetic mice, when compared to either saline- or ADP-treated diabetic wounds (**Figure 2C**), confirming the crucial role of this nucleotide in tissue repair.

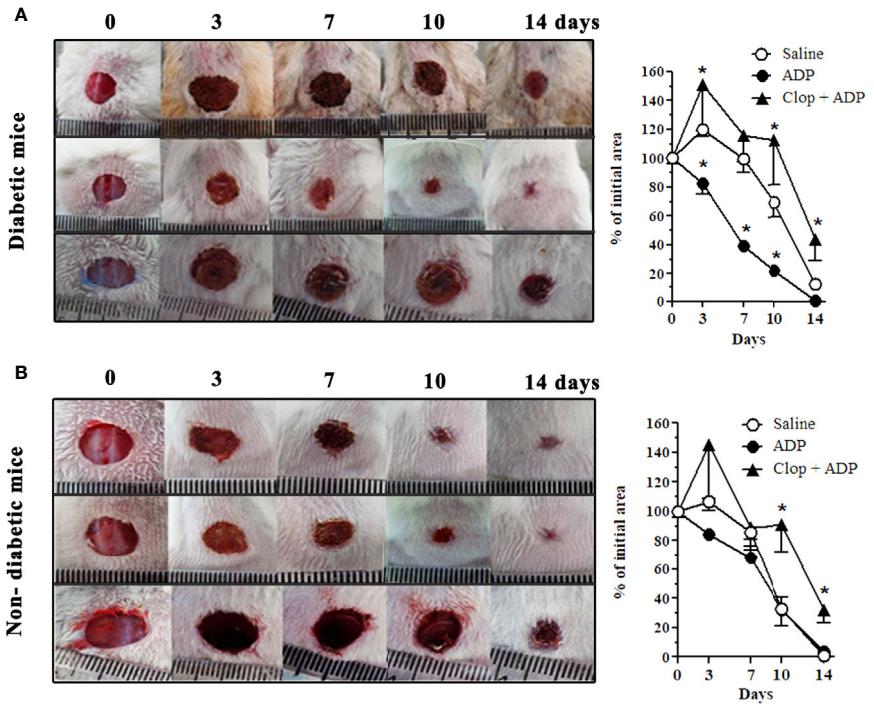

C

Treatments	% of initial area			
	3rd	7th	10th	14th days
Saline	107.7 ± 13.8	62.1 ± 14.9	52.3 ± 27.2	15.2 ± 17.9
ADP 15.2 µg/kg 30 µM	76.8 ±10.6*	35.7 ± 7.2*	18.5 ± 3.4*	0.1± 0.3*
ADP 51.2 µg/kg 100 µM	75.3 ± 2.3	86.3 ± 18.9	53.7±16.7	45.6 ± 9.6*
ADP 153.6 µg/kg 300 µM	102.2 ± 11.7	76.6 ± 3.2	51 ± 4.3	39.8 ± 0.5*

FIGURE 1 | ADP accelerates wound healing in diabetic mice *via* $P2Y_{12}$. Representative images and graphs of diabetic **(A)** and non-diabetic **(B)** mice that were subjected to excisional full-thickness wounding, and then, topically treated with ADP 30 µM (30 µL - 15.4 µg/kg) or saline every day for 14 days. One group of mice was treated by gavage with Clop (5 mg/kg) 1 h before ADP and saline, both once a day for 14 days. Open wound area was measured at days 0, 3, 7, 10 and 14. The areas at day 0 were considered 100%, and the subsequent areas measured at different time-points were calculated as percentages (%) of the initial value. **(C)** Dose-effect data of ADP treatment followed at days 3, 7, 10, and 14 after wounding. Data are expressed as mean ± standard error of the mean. *P < 0.05 by two-way ANOVA followed by Bonferroni post-test, compared to saline-treated mice; n=7-10 per group. Panels A and B are representative of three or more experiments; panel **(C)** represents one experiment.

Different Nucleotides Do Not Accelerate the Wound Healing

In order to test the effect of other nucleotides in our model, adenosine, AMP, pyrophosphate or ATP were topically applied on the wounds of diabetic mice at 30 µM/mouse, the same optimal concentration previously used for ADP. None of the nucleotides tested improved the wound healing (**Figures 2D–F**), except for ATP treatment, which showed a slight improvement of wound closure at day 7 (**Figure 2G**).

ADP Reduces Ecto-Nucleotidase Activity in the Wounds of Diabetic Mice

To assess a possible enzyme deregulation related to the metabolism of extracellular ADP during diabetes, the ecto-nucleotidase activity was evaluated in wounds at day 7 after wounding. The enzyme activity detected in the ADP-treated wounds obtained from diabetic mice was reduced compared to saline-treated wounds from diabetic mice, and when compared to wounds from non-diabetic mice (**Figure 2H**). The same

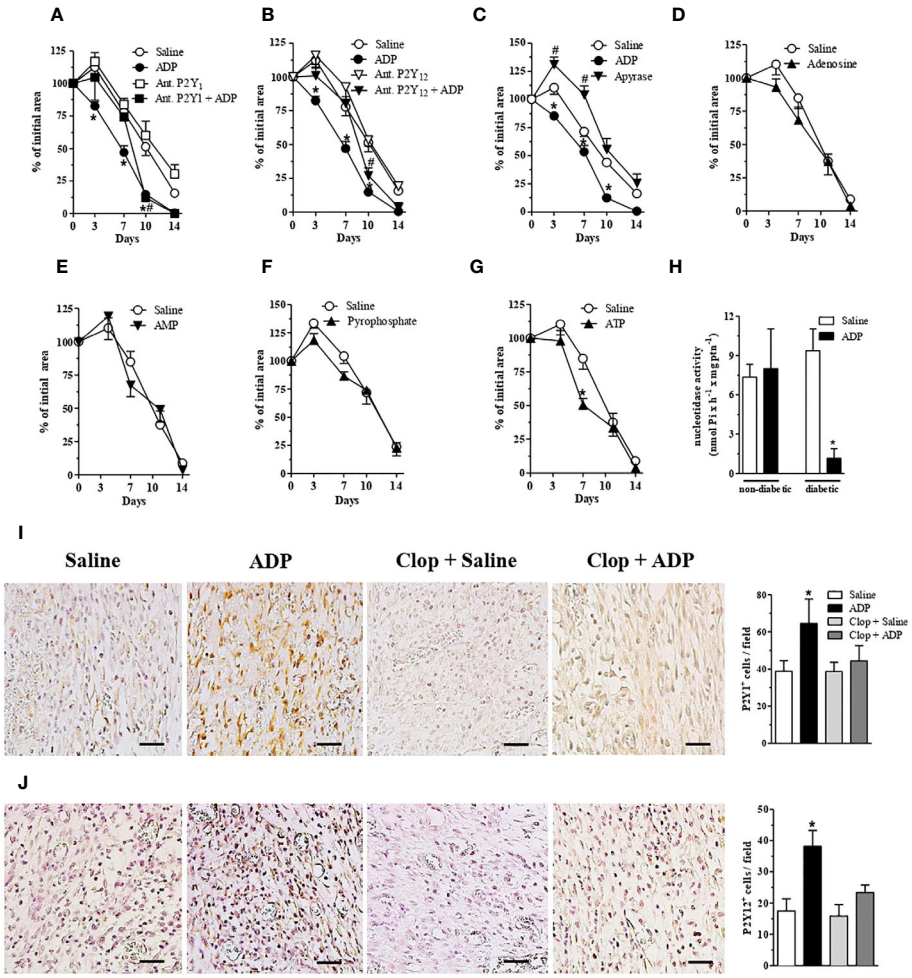

FIGURE 2 | Central role of ADP, $P2Y_1$ and $P2Y_{12}$ during wound healing of diabetic mice. **(A, B)** Diabetic mice were subjected to excisional full-thickness wounding and then, topically treated with $P2Y_1$ or $P2Y_{12}$ antagonists (30 μM/mouse - 30 μL) 30 min before ADP (30 μM/mouse) or saline administration. Both antagonists were applied every day for 14 days. Open wound area was followed over time as described in **Figure 1**. *P < 0.05 by two-way ANOVA followed by Bonferroni post-test, compared to saline-treated mice; #P < 0.05 by two-way ANOVA followed by Bonferroni post-test compared between $P2Y_1$ or $P2Y_{12}$ antagonists + ADP and saline-treated mice, n=7-10 per group. **(C–G)** Diabetic mice were subjected to excisional full-thickness wounding and then topically treated with apyrase (6 U/mL), ATP, ADP, AMP, adenosine, pyrophosphate (30 μM/mouse - 30 μL) or saline every day for 14 days. Open wound areas were followed over time as described in **Figure 1**. Data are expressed as mean ± standard error of the mean. *P < 0.05 by two-way ANOVA followed by Bonferroni post-test, compared to saline-treated mice; #P < 0.05 by two-way ANOVA followed by Bonferroni post-test compared between apyrase- and saline-treated mice, n=8-10 per group. **(H)** Non-diabetic and diabetic mice were subjected to excisional full-thickness wounding and then topically treated with ADP (30 μM/mouse) or saline every day for 7 days. The nucleotidase activity was evaluated in the wound tissue harvested at day 7. *P < 0.05 by Student's t test, compared to saline-treated diabetic mice, n=6 per group. **(I, J)** Photomicrographs and bar graphs of $P2Y_1^+$ and $P2Y_{12}^+$ cell numbers per field, respectively. Diabetic mice subjected to excisional full-thickness wounding were topically treated with ADP (30 μM/mouse) or saline every day for 7 days. Both groups were treated by gavage with Clop (5 mg/kg) 1 h before saline or ADP treatment of the wounds. The wound tissues were harvested at day 7 and stained by IHC for $P2Y_1$ and $P2Y_{12}$ receptors. Scale bars: 50μm. Data are expressed as mean ± standard error of the mean. *P < 0.05 by one-way ANOVA followed by Tukey post-test, compared to saline-treated mice, n=6 per group.

profile was observed in blood samples obtained from ADP-treated diabetic mice (data not shown). It seems that ADP treatment downregulates ecto-nucleotidase activity only in diabetic mice, which seems to favor wound healing. Indeed, we did not investigate if the ecto-nucleotidase activity reduction by ADP is due to a decrease in enzyme expression or a direct effect on enzyme activity. Further experiments are necessary to elucidate the mechanism involved.

ADP Increases $P2Y_1^+$ and $P2Y_{12}^+$ Cells in the Wounds of Diabetic Mice

ADP-treated diabetic wounds presented higher expression of $P2Y_1$ and $P2Y_{12}$ at day 7, when compared to saline-treated wounds (**Figures 2I, J**). Moreover, Clop treatment impaired ADP-induced $P2Y_1$ and $P2Y_{12}$ expression, whereas it did not change the expression of such receptors in saline-treated diabetic mice (**Figures 2I, J**). These data suggest that exogenous ADP

positively modulates its own response in the wounded skin of diabetic mice.

ADP Improves Tissue Formation in the Wounds of Diabetic Mice

Saline-treated wounds of diabetic mice presented edematous dermis, leukocyte infiltration (predominantly by mononuclear cells), and null (or partial) formation of epidermis at day 7. In the reticular dermis, exuberant formation of granulation tissue and congested neovessels were observed (**Figure 3A**). Interestingly, ADP-treated wounds presented the epidermis regenerated and integrated to the underlying dermis, with hyperplasic suprabasal layers, and hyperkeratosis. In the dermis, there was a dense granulation tissue with inflammatory cell infiltrate comprising eosinophils, mast cells, myeloid progenitors, neutrophils, and mononuclear cells. Clop administration impaired tissue regeneration in saline-treated wounds, where denuded epidermis areas, necrotic dermis with an inflammatory infiltrate composed predominantly of polymorphonuclear cells, striking bleeding, and the absence of granulation tissue were

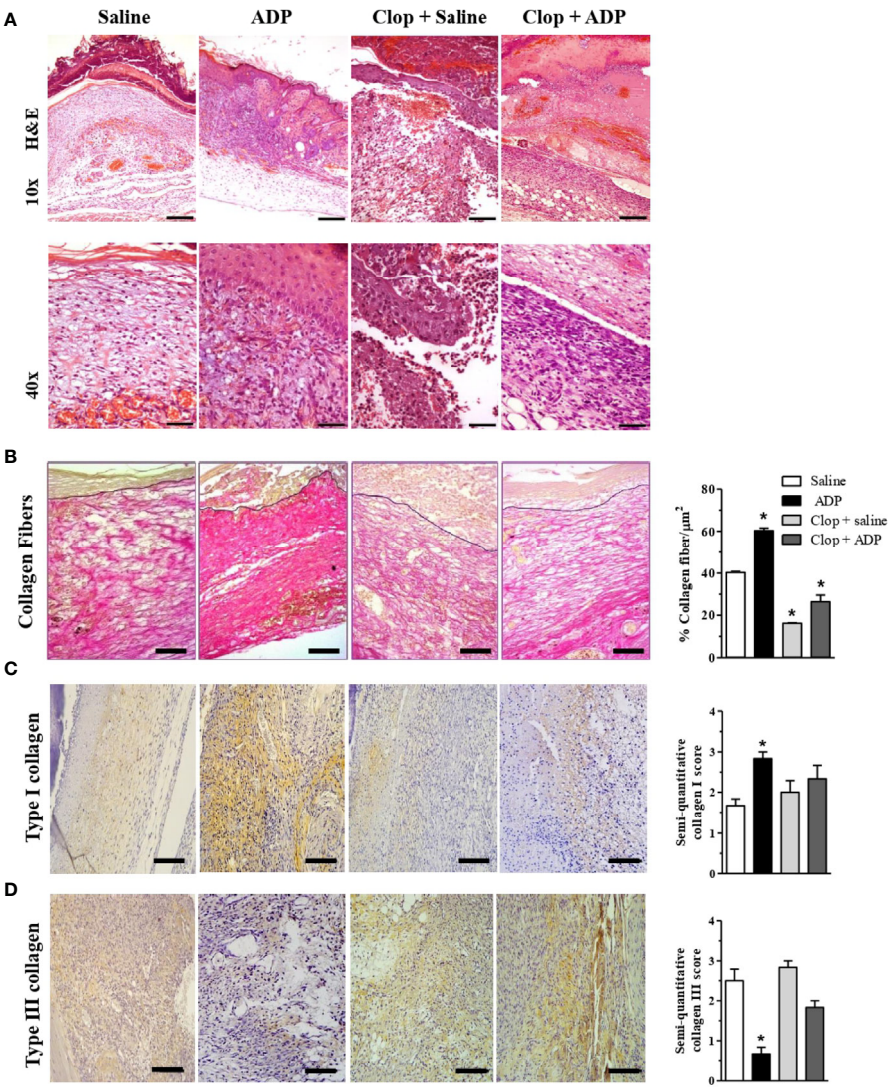

FIGURE 3 | ADP-treated wounds present an improved tissue repair and an increased collagen depo9sition. **(A)** Diabetic mice subjected to excisional full-thickness wounding were treated by gavage with Clop (5 mg/kg) 1 h before ADP (30 µM/mouse - 30 µL) or saline administration, once a day for 7 days. Wounds were harvested at day 7 and stained with hematoxylin and eosin. Representative images of 4-5 mice per group. Scale bars: 10x=200 µm; 20x=100 µm; 40x=50 µm. **(B)** Collagen deposit (red staining) in wounds at day 7 stained with Picro Sirius Red and the representative images are shown; bar graph summarizes data from 5-6 mice per group, representative of three independent experiments. Scale bars: 50 µm. *P < 0.05 by one-way ANOVA followed by Tukey post-test, compared to saline-treated mice. **(C, D)** Type I and type III collagen staining by IHC. Scale bar 50 µm. Graphs with semi-quantification score for type I and type III collagen deposit. Data from one experiment with 3-4 mice per group.

observed. Clop administration also impaired the tissue formation in ADP-treated mice, however, performing milder effects. In this case, wounds displayed a more organized reticular dermis, with collagen bundles parallel to the skin surface and interspersed with fibroblasts; a few vessels and inflammatory infiltrate were also noticed (**Figure 3A**).

Picro Sirius Red stained tissue photomicrographs (red staining) showed higher deposition of collagen fibers in ADP-treated wounds of diabetic animals compared to the saline-treated wounds (**Figure 3B**). Clop administration impaired collagen deposit in both ADP and saline-treated wounds. Collagen fibers quantification confirmed that ADP treatment enhanced collagen deposition while Clop administration impaired its accumulation (**Figure 3B**-graph). ADP seemed to accelerate the switch of type III to type I collagen, a more mature fiber (**Figures 3C, D**). Nevertheless, Clop administration reduced type I collagen deposit, without changing type III collagen deposit in both saline- and ADP-treated wounds. The results depicted in the bar graphs represent the photomicrographs (**Figures 3C, D**-graphs).

ADP Induces Keratinocyte Proliferation in Diabetic Wounds

We next evaluated if ADP enhances re-epithelization. At day 7 after wounding, ADP-treated wounds presented a higher number of cells expressing Ki67, a cell proliferation marker, in the layer adjacent to the basal membrane when compared to saline-treated wounds in diabetic mice. At day 14, the frequency of $Ki67^+$ cells was still higher than that of saline-treated wounds, but to a lesser extent (**Figure 4A**). The percentage of proliferating cells, observed at days 7 and 14 post wounding, is shown as bar charts (**Figure 4A**-graphs). Corroborating this result, epidermis area was also larger in ADP-treated wounds at day 7 compared to saline-treated wounds, while at day 14 it returned to normal (**Figure 4B**).

ADP Modulates the Inflammatory Response

We observed a reduction in the production of reactive oxygen species at day 7 post-wounding after in ADP-treated mice, while Clop administration restored reactive oxygen species production (**Figure 4C**), suggesting again the participation of $P2Y_{12}$. At day 3 after wounding, ADP treatment promoted an increase of IFN-γ and a reduction of TNF-α levels without affecting IL-10 levels, while increased IL-10 and IL-13 levels were observed at day 7 (**Figure 4D**). No differences were detected in IL-6, IL-12p70 and CCL2 levels between the groups (data not shown). These results suggest that ADP treatment controls inflammatory response associated with pro-resolution effects.

ADP Increases Myofibroblasts Population and Transforming Growth Factor- β (TGF-β) Production

Myofibroblasts present high ability of extracellular matrix protein production and wound contraction (1). We observed that ADP treatment increased α-SMA expression in the dermis, which was reduced by Clop; in the Clop + ADP group a less dramatic reduction of myofibroblasts was observed by immunofluorescence (**Figure 5A**). The ADP-induced α-SMA expression in diabetic wound was confirmed by WB analysis (**Figure 5B**). In accordance, ADP at 30 μM (but not at other concentrations tested) also induced proliferation of murine fibroblasts *in vitro* (**Figure 5C**). In addition, fibroblasts treated with ADP at 30 μM presented a better migration capacity when compared to saline-treated cells or with cells treated with ADP at 10 and 100 μM, suggesting a dose-dependent effect of ADP on wound healing, in accordance with earlier data (**Figures 5D, E**).

TGF-β is a pivotal cytokine that regulates myofibroblast differentiation and activation, re-epithelization, and activation of alternative macrophages, which are essential steps for wound healing (1, 2). ADP treatment seemed to increase TGF-β production by keratinocytes in the epidermis (**Figure 5F**) and the number of $TGF\text{-}\beta^+$ cells in the dermis (**Figure 5G**). These results reinforce the pro-resolution role of ADP in wound healing.

ADP-Treated Wounds Present a Different Leukocyte Profile

The presence and involvement of inflammatory and immune cells in wound healing are well described (35). Unbalanced numbers and/or activation of local leukocytes are common in diabetes, which compromises tissue repair (36). Interestingly, we observed an increase of neutrophil ($CD11b^+CD11c^-Ly6G^+F4/80^-CD68^-$ cell population, indicated in pink) recruitment in ADP-treated wounds by flow cytometry (**Figure 6A** - upper graph). Consistent with that, the enhancement of myeloperoxidase (MPO) activity seen in ADP-treated wounds, relative to saline-treated wounds, was significantly reduced by Clop administration (**Figure 6B**). In parallel, a decrease in the inducible nitric oxide $synthase^+$ cells and an increase in the $arginase^+$ cells were detected in the ADP-treated wounds (**Figures 6C, D**). This result suggests that monocyte/macrophage population ($CD11b^+CD11c^-Ly6G^-F4/80^+CD68^+$, indicated in blue) may have switched towards an alternatively-activated phenotype, since its frequency was similar between groups (**Figure 6A** - bottom graph). Clop treatment prevented the ADP-induced change of macrophage phenotype in the wound (**Figures 6C, D**). Therefore, our data suggest an ADP-mediated skewed response towards pro-resolution scenario in the context of tissue injury.

Moreover, histological examination of the skin sections from ADP-treated wounds showed increased number of eosinophils (**Figure 6E**) and mast cells (**Figure 6F**) compared to saline-treated wounds. Clop administration did not modify eosinophil and mast cell populations in the saline-treated wounds, although impairs ADP-induced accumulation of both cell types, indicating $P2Y_{12}$ involvement in their recruitment and/or survival.

T cells are resident in normal human and mouse skin and participate in cutaneous immunosurveillance, contributing to skin homeostasis (36, 37). Thus, we evaluated T cell profile in the skin and wound-draining lymph nodes of diabetic mice after ADP treatment. Interestingly, the percentage of Tregs (forkhead

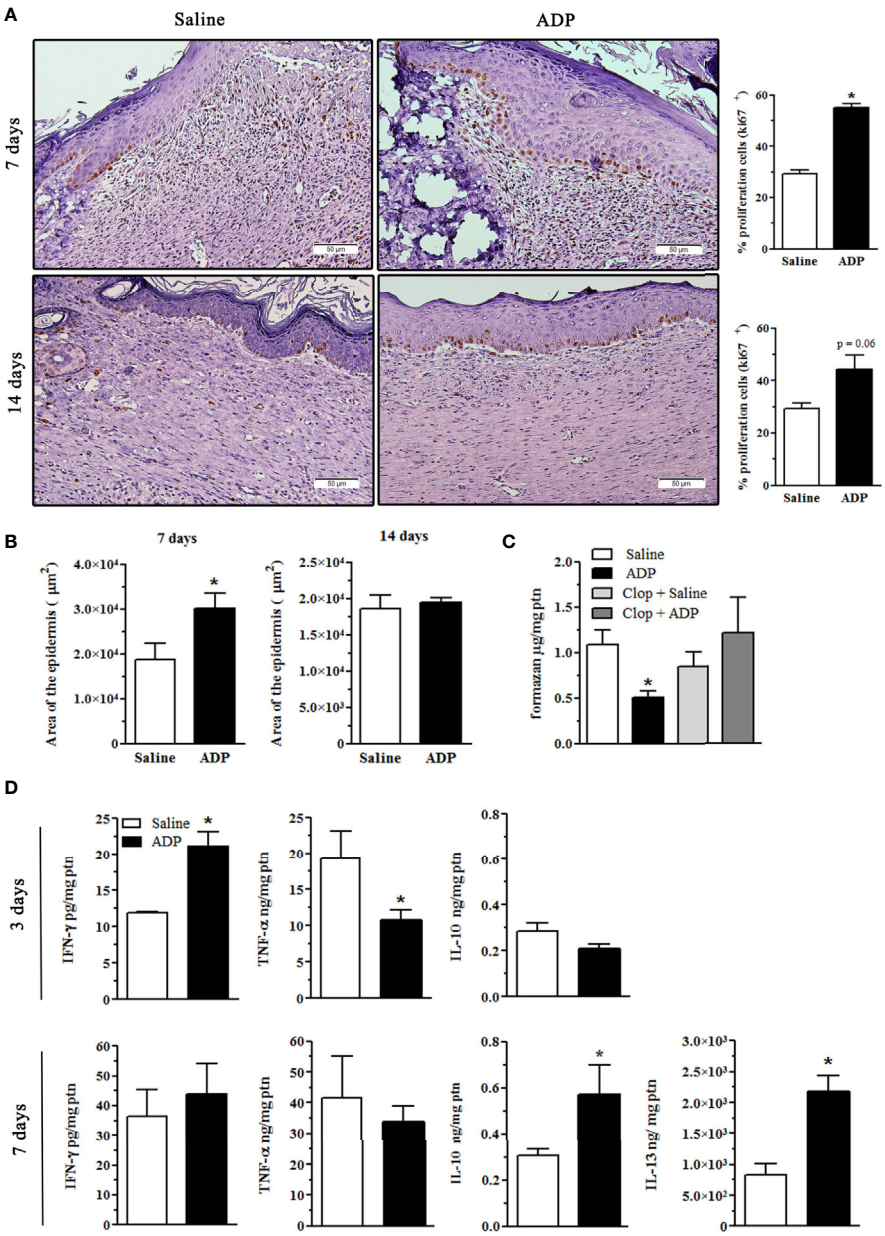

FIGURE 4 | ADP induces keratinocyte proliferation and modulates cytokine and free-radical production. Diabetic mice were subjected to excisional full-thickness wounding, and then, topically treated with ADP (30 µM/mouse - 30 µL) or saline every day for up to 14 days. **(A, B)** Wound tissues were harvested from diabetic mice at days 7 and 14 after wounding, and stained for Ki67 by IHC and with hematoxylin and eosin. Scale bar: 50 µm. The percentage of proliferating keratinocytes ($Ki67^+$) and the area of epidermis were represented in bar graphs. Data are expressed as mean ± standard error of the mean. *$P < 0.001$ by Student's t test, compared to saline-treated mice; n= 6 per group. **(C)** Superoxide radical production was indirectly evaluated in the wounds obtained at day 7 after wounding by f9ormazan generation as final product. Some animals were treated by gavage with Clop (5 mg/kg) 1 h before ADP or saline wound topic treatment. *$P < 0.05$ by one-way ANOVA followed by Tukey post-test, compared to saline-treated mice, n=4-5 per group. **(D)** Wound tissues were harvested from diabetic mice at days 3 and 7 after wounding and cytokine levels were evaluated by ELISA. *$P < 0.05$ by Student's t test, compared to saline-treated mice, n=4-6 per group.

box protein P3 [$FoxP3^+$]/$CD4^+CD3^+$) was selectively reduced in the ADP-treated wounds relative to saline-treated wounds, but not in the draining lymph nodes (**Figure 7A**).

In parallel, ADP did not alter $CD4^+$ and $CD8^+$ T cells frequencies in the skin and lymph nodes; however, ADP-treated wounds showed increased proportions of skin-associated gamma delta (γδ) T cells subtypes as $V\gamma4^+$ and $V\gamma5^+$ (**Figure 7B**). Again, no changes in overall T cell populations were seen in the draining lymph nodes after wounding.

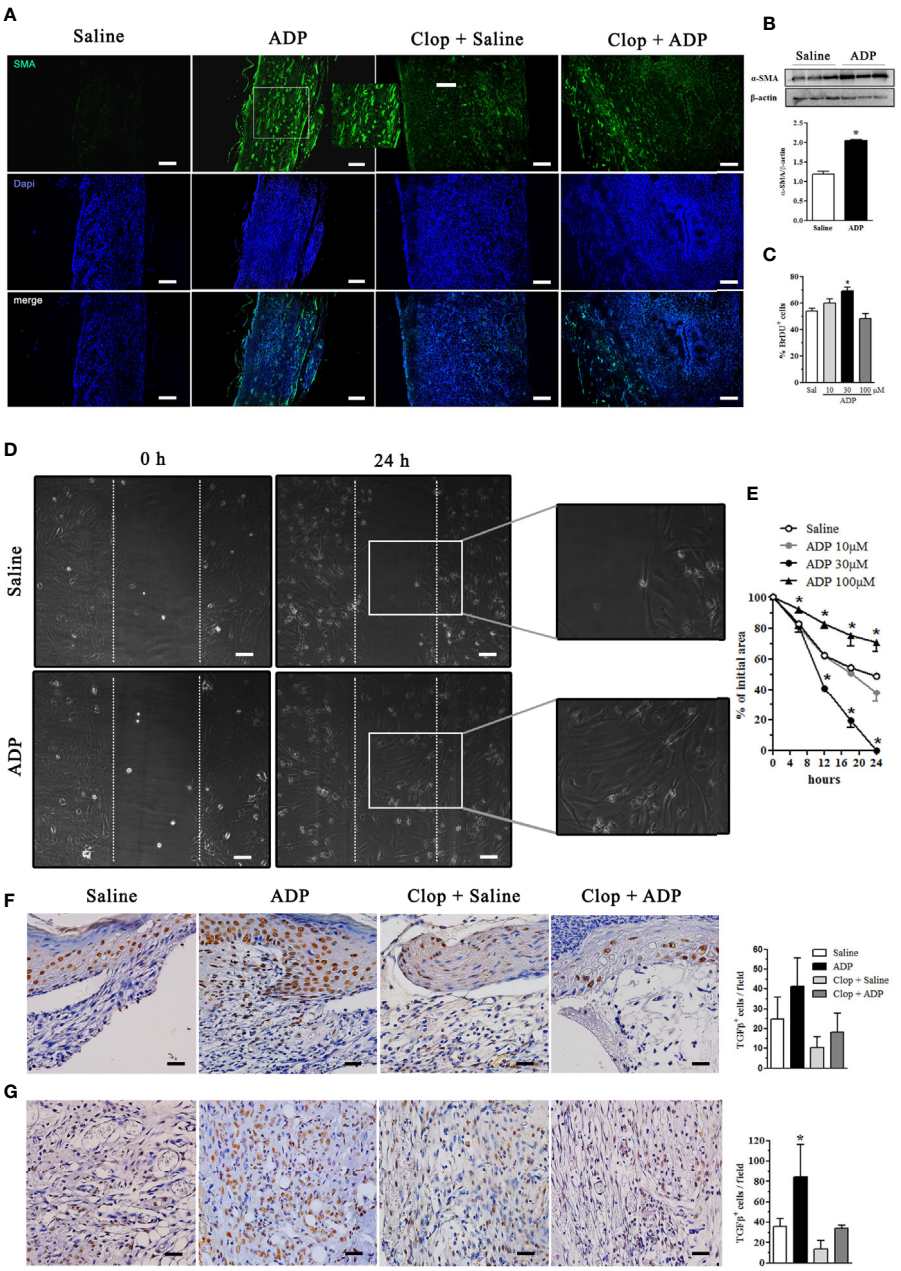

FIGURE 5 | ADP activates myofibroblasts/fibroblasts and increases the amount of TGF-β$^+$cells in the wounds of diabetic mice. Diabetic mice were subjected to excisional full-thickness wounding and then, topically treated with ADP (30 μM/mouse - 30 μL) or saline every day for 7 days. Some mice were treated by gavage with Clop (5 mg/kg) 1 h before ADP or saline administration, once a day for 7 days. **(A)** Wound tissues harvested at day 7 were stained for α-SMA (green) and DAPI (blue) and analyzed by immunofluorescence. **(B)** Gel bands and graphs depicting the semi-quantification of α-SMA by WB. Each bar represents a pool of skin-derived protein extracts obtained from at least 5 mice. *P<0.05 by Student's t test compared to saline-treated mice; data are representative of two independent experiments. **(C)** Primary culture of neonate murine dermal fibroblasts was plated for 24 h, incubated with BrdU for more 24 h and the cell proliferation was evaluated by immunofluorescence. *P<0.05 by one-way ANOVA followed by Tukey post-test, compared to saline-treated mice; data are representative of three independent experiments. **(D, E)** Primary dermal murine fibroblasts were plated for 24 h, pre-incubated with mitomycin-C 5 μg/mL for 2 h and then incubated with different concentrations of ADP. The open ar9ea between the front edges of the scratch were evaluated at 0, 6, 12, 18 and 24 h after scratch and expressed as % of initial area. Fibroblast culture images represent only the first and last time points evaluated for cell migration. *P < 0.05 by two-way ANOVA followed by Bonferroni post-test, compared to saline-treated mice, the data are representative of three independent experiments. Photomicrographs and bar graphs of TGF-β$^+$ cells determined by IHC in the **(F)** epidermis and **(G)** dermis obtained at day 7 after wounding. *P < 0.05 by one-way ANOVA followed by Tukey post-test, compared to saline-treated mice, n=8 per group.

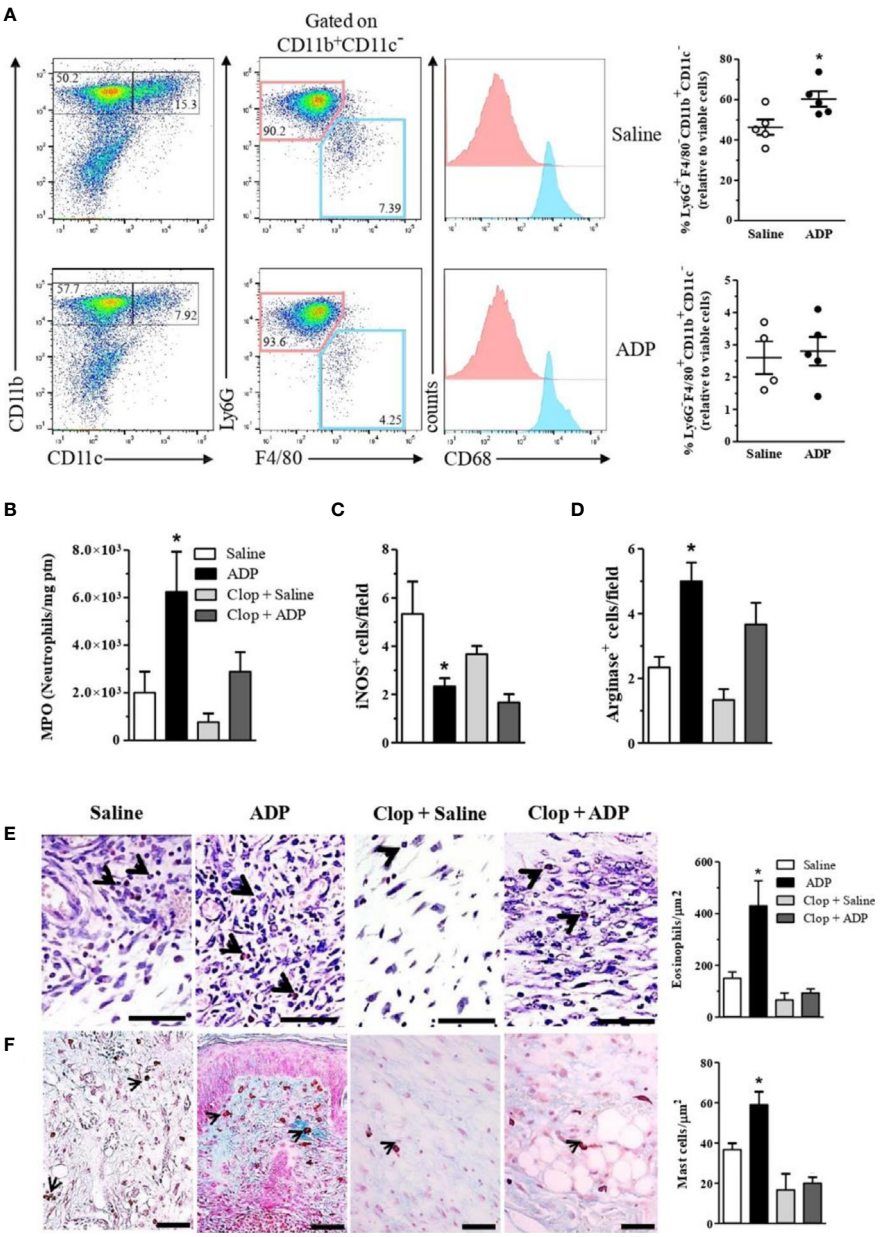

FIGURE 6 | ADP-treated wounds present an increase of neutrophils, arginine$^+$ cells, eosinophils and mast cells. Diabetic mice were subjected to excisional full-thickness wounding and then, topically treated with ADP (30 µM/mouse - 30 µL) or saline every day for 7 days. Some mice were treated by gavage with Clop (5 mg/kg) 1 h before ADP or saline administration, once a day for 7 days. Wound tissues were harvested at day 7 after wounding and cell suspensions were analyzed by flow cytometry. **(A)** Dot-plots (left) and graphs (right) show Ly6G$^+$F4/80$^-$ and Ly6G$^-$F4/80$^+$ populations (gated on live CD11b$^+$CD11c$^-$ cells) in the wounded skin. Graphs show the frequency of each cell population relative to gated live cells; for that, percentages of Ly6G$^+$F4/80$^-$ [neutrophils – depicted in pink] or Ly6G$^-$F4/80$^+$ [macrophages – depicted in blue] cells were multiplied by the percentage of live CD11b$^+$CD11c$^-$ cells; intracellular CD68 staining confirms macrophage identity; data representative of one experiment with n=4-5 mice per group; *P < 0.05 by Studen9t's t test compared to saline-treated mice **(B)** Wound tissues were harvested at day 7 and prepared for myeloperoxidase quantification; and bar graphs are representative of three independent experiments with n=6 per group; **(C)** Wound tissues were evaluated by IHC for inducible nitric oxide synthase$^+$ or **(D)** arginase$^+$ cells at day 7 after wounding. *P < 0.05 by one-way ANOVA followed by Tukey post-test, data are representative of two independent experiments with n=6 per group. Skin histological sections of wound tissues harvested at day 7 and stained with **(E)** modified Sirius Red stain for eosinophil or with **(F)** Alcian Blue stain for mast cells. Bar graphs represent the number of eosinophils or mast cells per µm^2. Scale bars=50µm. *P < 0.05 by one-way ANOVA followed by Tukey post-test, compared to saline-treated mice. Data are representative of one experiment with 5-6 mice per group.

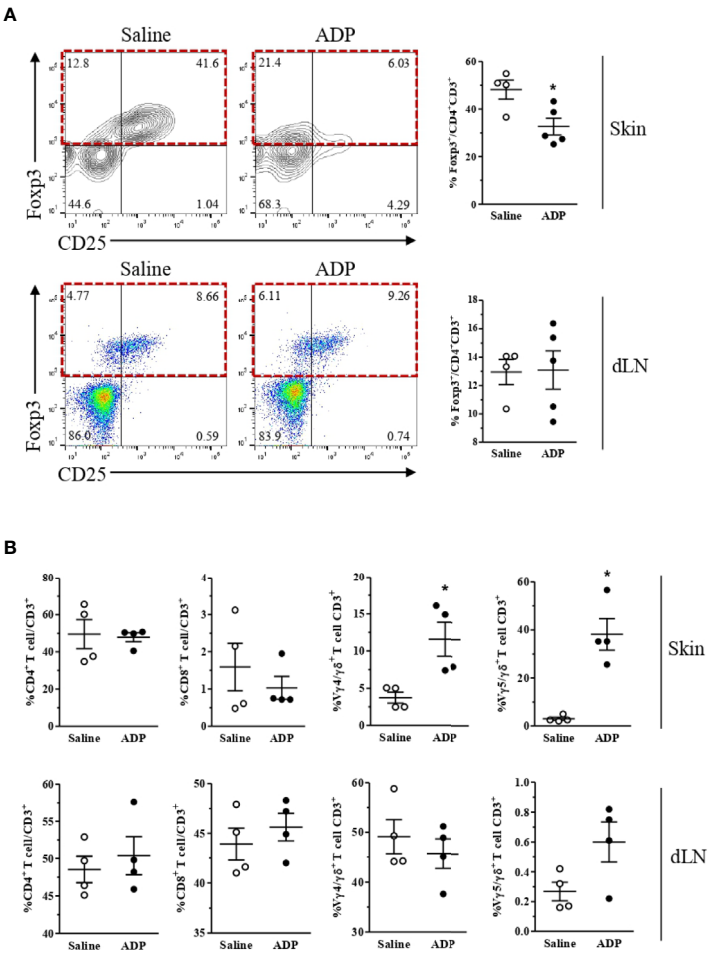

FIGURE 7 | ADP-treated wounds present a reduced population of Tregs and an increase of Vγ4 and Vγ5 T cells. Diabetic mice were subjected to excisional full-thickness wounding and then topically treated with ADP (30 μM/mouse – 30 μL) or saline every day for 7 days. Wound tissues and the skin-draining lymph nodes were harvested at day 7 after wounding and cell suspensions were analyzed by flow cytometry. **(A)** Contour-plots (top left), dot-plots (bottom left), and respective graphs (right) show the frequencies of Foxp3$^+$Tregs (relative to CD4$^+$CD3$^+$population) in the skin and draining lymph nodes (dLN); **(B)** CD4$^+$ 9and CD8$^+$ T cells (relative to total CD3$^+$ lymphocytes), Vγ4$^+$, and Vγ5$^+$ cells (relative to total γδ$^+$T lymphocytes) in the skin and dLN. Data were expressed as mean ± standard error of the mean. *P < 0.05 by Student's t test compared to saline-treated mice; n=4-5 per group, data are representative of two independent experiments, except for the γδ$^+$ T lymphocyte data, which represent one experiment.

ADP Does Not Improve Wound Healing of Cutaneous Ulcer Induced by *Leishmania amazonensis*

We also evaluated the effect of ADP on cutaneous ulcer induced by experimental *Leishmania amazonensis* infection and no improvement was observed (**Figure 8**). These results indicate that ADP may be context-dependent and possibly effective just in wounds of individuals with metabolic diseases such as diabetes.

DISCUSSION

In this paper, we provide the first evidence that ADP plays a pivotal role as a potent agent that accelerates cutaneous wound healing in diabetic mice. Due to the large number of patients suffering from diabetes worldwide that present a poor quality of life and high risk of complications as chronic wounds, we emphasize the importance of a better comprehension of the pathophysiology and the mediators involved in wound healing.

ADP is an endogenous nucleotide which acts as a potent mediator in platelet aggregation and inflammation, being quickly metabolized. The role of ADP in tissue repair has was always been related to platelet aggregation, since ADP is rapidly released from activated platelets, acting in an autocrine way together with histamine, serotonin, calcium and several other mediators for platelet aggregation, driving the return to homeostasis (38). Besides, other authors have previously described an effect of ADP on cell proliferation, such as on cell culture of murine fibroblasts (3T3 and 3T6), isolated rat chondrocytes and

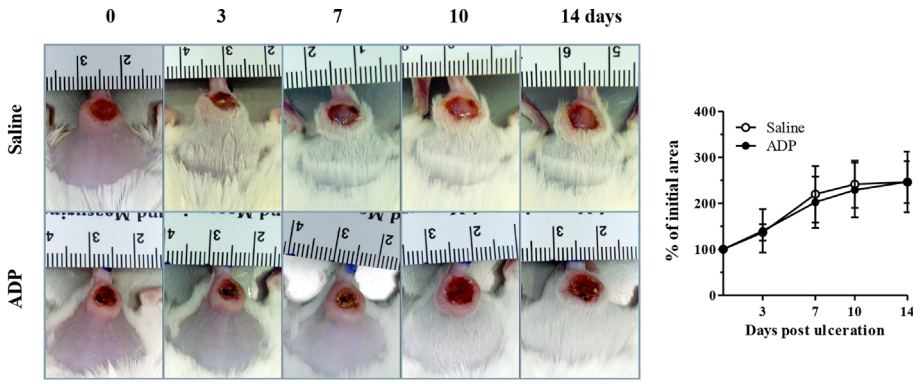

FIGURE 8 | ADP did not accelerate wound healing of cutaneous leishmaniasis. BALB/c mice were intradermally inoculated with 10^6 promastigote/mouse/50 µL (2×10^8/mL). After wound ulceration, animals were topically treated every day with saline or ADP (30 µM/mouse – 30 µL) per 10 days. Open wound area was measured at days 0, 3, 7, 10, and 14. Representative images and graph of cutaneous leishmaniasis-associated wound treated with saline or ADP. The areas at day 0 were considered 100%, and the subsequent areas were proportional (%) to the initial wound area; n=7 per group.

zebrafish retinal cells (14, 15, 39, 40), suggesting that ADP may improve healing and regeneration due to these properties. Corroborating with literature data, nucleotides, including ADP, induce epithelial cell migration in an *in vitro* model of wound healing using a quiescent monkey kidney epithelial culture (41). Similar data was observed in a study with non-transformed small intestine epithelial cell line IEC-6 using the same *in vitro* wound model, where ADP and ATP stimulate epithelial migration (42).

Given the above findings, we hypothesized that ADP modulates many other molecular and cellular aspects of inflammation during tissue repair, promoting an efficient wound healing. Therefore, our study reports an important role of exogenous ADP in stimulating immune cells activation, resolution of inflammation, and restoration of tissue integrity in non-healing wounds of diabetic mice.

Controlled inflammation is one of the major steps for wound healing. The absence of inflammatory response or its exaggerated activation impair the natural progression of wound healing towards the proliferative and remodeling/healing phases. An unbalanced ADP production/action, which is observed in diabetes, could impact on inflammation process. Thus, exogenous ADP seems to adequately modulate this process in our model, recovering the normal evolution of healing. Therefore, it is reasonable to observe that, when topically applied during the initial healing phase, ADP just improved the wound healing of diabetic mice but not of healthy non-diabetic animals, which are already extremely competent in tissue repair. Of note, ADP-treated wounds in diabetic mice heal at the same rate seen in wounds of non-diabetic mice. Interestingly, we found that a 5-day treatment protocol with ADP was also effective in accelerating wound healing (data not shown) as observed to the 14-days treatment. This result support the role of ADP in the initial healing steps.

Taking these data into account, we suggested a possible failure in the nucleotide pathway during diabetes. Thus, in an attempt to explain this phenomenon, we raised some possibilities such as: (i) deficient ADP production; (ii) upregulation of ADP degradation by ecto-nucleotidases; (iii) inefficient expression/activation of purinergic receptors in the skin of diabetic mice. First, we addressed ADP production in the skin by HPLC, however we found low levels of ADP in the wounds since it is a liable molecule that is metabolized in less than 5 minutes, which makes its quantification unfeasible (data not shown). Second, regarding the enzymes that degrade extracellular nucleotides, the ecto-nucleoside triphosphate diphosphohydrolase-1 (CD39) hydrolyses extracellular ATP and ADP into AMP, which is subsequently converted to adenosine (ADO) by the action of ecto-5'-nucleotidase (CD73) (43, 44). Previous studies have demonstrated that the nucleotidase activity is increased in diabetic patients and associated pathologies. Moreover, hydrolysis of adenine nucleotides is increased in platelets from diabetic patients (45), which can partly explain beneficial effect exogenous ADP. In our data, exogenous ADP treatment inhibited overall nucleotidase activity in the wound of diabetic animals, favoring the ADP effect in wound healing. Lastly, the increased expression of $P2Y_1$ and $P2Y_{12}$ receptors in the diabetic wound observed after ADP treatment suggests a possible deficiency in the expression of nucleotide receptors during diabetes. Altogether, part of the beneficial effects of ADP on diabetic wounds appear to be by up regulating its own receptors in the skin and by reducing the nucleotidase activity.

We explored several strategies in order to demonstrate the major role of ADP on wound healing in diabetic mice. Initially, we demonstrated that ATP, AMP, ADO, and pyrophosphate were not as effective as ADP at the low concentration of 30 µM. Furthermore, the role of ADP in our system was also confirmed using apyrase, enzyme responsible for degrading ATP and ADP into AMP. In fact, apyrase administration worsened wound healing of diabetic mice, excluding at the same time the role of

AMP accumulation derived from ADP degradation as a possible mechanism for ADP-induced tissue repair.

ADP poses several advantages among other nucleotides. Studies already demonstrated the role of ADO and its receptors in wound healing. For instance, daily treatment of healthy and diabetic rats with A2A receptor agonist accelerated wound healing by stimulating fibroblast and endothelial cell migration to the injured area and by reducing inflammation (46, 47). Surprisingly, Montesinos et al. (47), using A2A receptor knockout mice, also demonstrated the importance of A2A receptor to the formation of uniform granulation tissue and angiogenesis (47). ATP was also described to accelerate wound healing. ATP-containing vesicles promote a massive influx and *in situ* proliferation of macrophages, the release of pro-inflammatory cytokines and vascular endothelial growth factor, neovascularization and collagen production (48). Meanwhile, it is important to stress that ATP directly excites primary sensory neurons, triggering pain signaling, a fact that undermines its therapeutically use for wound healing (49). Also, it was already described that *Staphylococcus aureus* USA300, one of the most prevalent bacterial species identified in chronic wounds, exploits the immunomodulatory characteristics of ADO to subvert host immune response (50), retarding the healing of infected wounds. Lastly, ADO and ATP also promote fibrosis when released in high concentrations or chronically (51–53), which denotes a negative aspect in the case of topically application.

To confirm our findings, we used an ADP receptor antagonist. Clop is a prodrug used widely as a platelet aggregation inhibitor and exerts its action by irreversibly antagonizing the $P2Y_{12}$ receptor (54). It is worthy to state that ADP is the major ligand of $P2Y_{12}$ receptor (31, 32). Our study showed that Clop impaired the effect of exogenous ADP in diabetic wounds, and more strikingly, also in non-diabetic mice, which revealed the role of endogenous ADP and $P2Y_{12}$ receptor in tissue repair. Similarly, the same profile was observed with a $P2Y_1$R antagonist (MRS2179) and a different $P2Y_{12}$R antagonist (MRS2395), confirming the role of both receptors in wound healing. Remarkably, the effect of those ADP receptor antagonists was lost after day 7. One explanation for that could be an increase in tissue sensitivity due to topic ADP application, since we already demonstrated an ADP-driven up regulation of $P2Y_1$ and $P2Y_{12}$ receptors, which may be due to a recruitment of purinergic receptor-expressing cells to the tissue or by an up regulation of those receptors by resident cells. We could also not discard a possible involvement of $P2Y_{13}$ receptor in the final stage of wound healing, although unfortunately the $P2Y_{13}$ antagonist was not available.

The role of ADP in wound healing is expected since $P2Y_1$, $P2Y_{12}$, and $P2Y_{13}$ receptors are expressed in all kinds of cell types important for tissue repair (leukocytes, endothelial cells, keratinocytes, fibroblasts, and platelets). They are involved in cell activation, migration, and proliferation (12, 31, 35). However, the exact effects of these receptors and ADP in wound healing are not well determined. A successful healing results in the reconstitution of skin tension, resistance, and function to a similar degree as those of the original tissue, relying on (i) deposition of extracellular matrix proteins, such as collagen; (ii) formation of basal membrane, epidermis and new vessels, and (iii) repopulation of resident cells (1). Here, we showed that ADP improved the tissue formation by promoting less edema, accelerated re-epithelization, increased cell infiltration, and collagen deposit. ADP-treated wounds were characterized by a significant cell migration, such as leukocytes and fibroblasts, from the edge towards the center of the lesion. Note that the arrival of these cells marks the formation of granulation tissue, which is crucial for the healing process. These results suggest that ADP acts as a pro-inflammatory and pro-resolution molecule, providing a tissue formation of superior quality and organization compared to that observed in untreated wounds of diabetic mice. In rats, $P2Y_1$ receptor is expressed by cells of the basal layer, which is the site of keratinocyte proliferation (55). Yoshida et al. (56), demonstrated mRNA expression for $P2Y_1$ e $P2Y_{12}$ receptors in a culture of keratinocytes, whereas others reported that fibroblasts express $P2Y_1$, $P2Y_{12}$, and $P2Y_{13}$ receptors (49, 56, 57). Thus, ADP receptors are widely expressed in the skin corroborating the pleiotropic effect of ADP in wound healing during diabetes.

Fibroblasts/myofibroblasts are cells that approach the edges of the wounds and produce extracellular matrix, primarily collagen, which is the major component of the mature scar (58). An increase in the number of myofibroblasts induced by ADP treatment helps to explain the accelerated tissue repair, the increase in the collagen deposit, and its correlation with the increase of TGF-β^+ cells in the dermis and epidermis. Again, by inhibiting $P2Y_{12}$ receptor several parameters were reduced in the injured skin of diabetic mice, including myofibroblast differentiation/activation, TGF-β production and collagen deposit, which in turn diminished granulation tissue formation, resulting in impairment of wound healing. Moreover, the shift from type III to type I collagen, triggered by ADP treatment, provided a more mature connective tissue and scar. Type I collagen is the most abundant collagen type in health skin and is associated with scar maturation (59, 60). The positive effect of ADP on fibroblast was also confirmed by *in vitro* experiments, since this nucleotide induced fibroblast proliferation and migration.

The balance of pro- and anti-inflammatory cytokines is essential for successful healing, while an overwhelming cytokine production as well as no production impair wound healing (61). Of note, Lin et al. (62), demonstrated that IL-6 knockout mice present a delay in the wound closure, a reduction in leukocyte infiltration, re-epithelialization, angiogenesis, and collagen deposition, compared to wild type mice (62). Others demonstrated that $TNF^{-/-}$ mice have a better granulation tissue formation but a compromised re-epithelialization (63). Also, CCL2 knockout mice exhibit a delay in re-epithelialization, angiogenesis, and collagen synthesis (64). In our analyzes, the increased levels of IFN-γ at day 3 and an increase of IL-10 and IL-13 at day 7 after wounding suggest an anticipation in the shift of inflammatory to resolution phase induced by ADP treatment. The increased amount of TGF-β in the skin after ADP treatment supports the idea of transition to an earlier resolution phase (65).

An intense inflammatory infiltrate in the wound tissues was observed after ADP application. It is noteworthy that the inflammatory process during normal wound healing is characterized by spatial and temporal changes in leukocytes' patterns. The well-defined chronology of these events is essential for ideal repair (66). Tissue macrophages are activated by IL-4 and IL-13 cytokines and converted in a cell-type programmed to promote wound healing (67). The high concentration of IL-13 at day 7 together with a shift of macrophage phenotype from M1 to M2 after ADP treatment corroborates with our hypothesis that ADP is a pro-resolution molecule. Similarly, mast cells are skin-resident cells that accumulate and are necessary for wound healing (68). However, according to the literature mast cells can favor or impair wound healing, depending on the stimulus intensity (69). In our diabetes model, the increased mast cell population after ADP treatment suggests a positive role in wound healing, but other experiments must be done to confirm this correlation.

Studies demonstrated that neutrophils, isolated from wound sites, can also regulate the innate immune response during healing (66). Zhang et al. (70), showed that neutrophils have a regulatory role in the inflammatory response by secreting IL-10 (70). The neutrophil accumulation in the wound after ADP treatment at day 7, together with increased IL-10 levels at the same time-point supports our hypothesis that ADP drives the neutrophil activation to a tissue-repair profile. Another polymorphonuclear cell type, the eosinophil, also infiltrates into wounds (often in close proximity with fibroblasts), stores TGF-β and seems to release it, as demonstrated in a rabbit cutaneous open wound model (71, 72). Therefore, the eosinophils recruited by ADP at day 7 may contribute to accelerate the wound healing *via* TGF-β production and collagen deposition. Here we demonstrated that ADP promoted an exuberant accumulation of eosinophils within wounds of diabetic mice, which correlated with improved tissue recovery.

Skin also hosts αβ and γδ T lymphocytes, which maintain tissue homeostasis by modulating keratinocyte differentiation (re-epithelization), responding to infection, and regulating wound repair. A balance between Tregs, Th17 cells, and γδ T cells plays an important role in skin homeostasis (35). The reduction of Tregs and increase of $V\gamma4^+$ and $V\gamma5^+$ cells (two γδ T cells subtypes) in the skin after ADP treatment provide evidence for recovery of epidermal barrier function, as well as of the innate immune response. Strikingly, mice deficient for γδ T cells, including dendritic epidermal T cells (which express the $V\gamma5^+$ TCR), present a delay in wound healing and a defect in their ability to clear intradermal *S. aureus* infection (73). This type of cell produces insulin growth factor-1 and keratinocyte growth factor-2, molecules related to re-epithelization and skin wound repair (74). $V\gamma4^+$ cells migrate to murine dermis and epidermis after wounding and are the major source of IL-17A, which in turn enhances neutrophil migration and induces IL-1 and IL-23 production from epidermal cells to initiate local inflammation, necessary for wound healing (75).

Finally, our findings suggest that ADP has beneficial effects mainly in diabetic wounds, since ADP did not accelerate wound healing neither in naive mice nor in *Leishmania amazonensis*-induced skin lesion.

In conclusion, we provide novel insights into the pathophysiology of wounds that are difficult to heal, as well as the crucial role of endogenous and exogenous ADP on tissue repair. The real mechanism underlying the effect of ADP on wound repair in diabetes is not completely understood, but we provide the evidence that ADP promotes skin homeostasis by inducing a brief and balanced inflammatory process and by recruiting and/or activating immune cells, followed by a switch to adequate proliferation and remodeling phases (**Figure 9**). Still, another point to be raised and that deserves caution is related to Clop, since our data also brings out a potential harmful effect for thrombosis patients who have wounds.

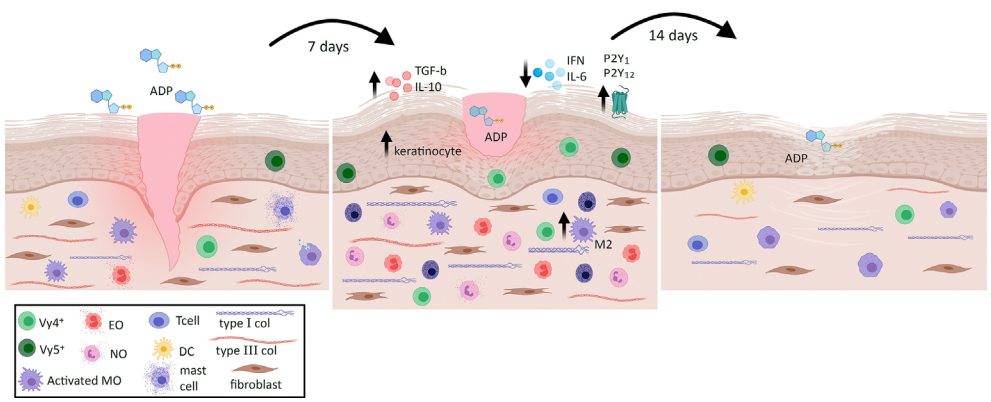

FIGURE 9 | Summary of the pleiotropic effects of ADP on skin wound in diabetic mice. ADP topical instillation accelerates wound closure and improves tissue repair represented by type I collagen deposit and adequate reepithelization. The mechanisms seem to involve the increase of neutrophils, eosinophils, mast cells, M2 macrophages, myofibroblasts and $V\gamma4^+$ and $V\gamma5^+$ cells in the wound, besides its ability in modulating cytokine release. ADP plays pivotal role within inflammation, proliferation and remodeling phases during skin tissue repair in diabetes wounds.

DATA AVAILABILITY STATEMENT

The raw data supporting the conclusions of this article will be made available by the authors, without undue reservation.

ETHICS STATEMENT

The animal study was reviewed and approved by Ethics Committee for the Use of Animals of the Federal University of Rio de Janeiro, protocol number 093/15.

AUTHOR CONTRIBUTIONS

PB, JG and IW: conceptualization, formal analysis, investigation, methodology, writing–original draft, and editing. JB, VF-J, FL, and TR-A: collected and analyzed the data for this work. ES: designed and performed the Leishmania experiment. CT: performed and analyzed the histology data. RC-S and JM-F: formal analysis and investigation of purinergic biology. CP: conceptualization formal analysis of γδ T cells assay. JN and PM: conceived the project. FC: performed and analyzed all FACs data. CM: performed and analyzed IF data. CC: investigation, writing–review and editing. CB: conceived the project, formal analysis, investigation, project administration, resources, supervision, writing–original draft, writing–review and editing. All authors contributed to the article and approved the submitted version.

FUNDING

This work was supported by grants from National Council for Scientific and Technological Development (Conselho Nacional de Desenvolvimento Científico e Tecnológico - CNPq), Research Support Foundation of the State of Rio de Janeiro (Fundação de Amparo à Pesquisa do Estado do Rio de Janeiro – FAPERJ), Coordination of the Improvement of Higher Education Personnel – (Coordenação de Aperfeiçoamento de Pessoal de Nível Superior CAPES) and Health Ministry.

ACKNOWLEDGMENTS

We greatly acknowledge Ariane Rennó Brogliato for her contribution to the conception, design, analysis, and interpretation of the manuscript, and as a mentor to Paula Borges and Ingrid Waclawiak, it was of great significance. We thank Dr Isabela Ramos to kindly provide the pyrophosphate used in the *in vivo* wound healing experiment. This manuscript has been released as a preprint at BioRxiv (76).

SUPPLEMENTARY MATERIAL

The Supplementary Material for this article can be found online at: https://www.frontiersin.org/articles/10.3389/fimmu.2021.651740/full#supplementary-material

REFERENCES

1. Gurtner GC, Werner S, Barrandon Y, Longaker MT. Wound repair and regeneration. *Nature* (2008) 453:314–21. doi: 10.1038/nature07039
2. Järbrink K, Ni G, Sönnergren H, Schmidtchen A, Pang C, Bajpai R, et al. Prevalence and incidence of chronic wounds and related complications: a protocol for a systematic review. *Syst Rev* (2016) 5:152. doi: 10.118/s13643-016-0329-y
3. Singer AJ, Clark RAF. Cutaneous wound healing. *N Engl J Med* (1999) 341:738–46. doi: 10.1056/nejm199909023411006
4. Stadelmann WK, Digenis AG, Tobin GR. Physiology and healing dynamics of chronic cutaneous wounds. *Am J Surg* (1998) 176(2A Suppl):26S–38S. doi: 10.1016/s0002-9610(98)00183-4
5. Sen CK. Human Wounds and its burden an updated compendium of estimates. *Adv Wound Care* (2019) 8:39–48. doi: 10.1089/wound.2019.0946
6. Nussbaum SR, Carter MJ, Fife CE, DaVanzo J, Haught R, Nusgart M, et al. Na economic evaluation of the impact, cost, and medicare policy implication of chronic nonhealing wounds. *Value Health* (2018) 21:27–32. doi: 10.1016/j.jval.2017.07.007
7. Tavares DMS, Dias FA, Araújo LR, Pereira GA. Perfil de clientes submetidos a amputações relacionadas ao diabetes mellitus. *Rev Bras Enferm* (2009) 62:825–30. doi: 10.1590/S0034-71672009000600004
8. Toscano MC, Sugita HT, Rosa MQM, Pedrosa HC, Rosa RS, Bahia LR. Annual direct medical costs of diabetic foot disease in Brazil: A cost of illness study. *Int J Environ Res Public Health* (2018) 15:89. doi: 10.3390/ijerph15010089
9. van Battum P, Schaper N, Prompers L, Apelqvist J, Jude E, Piaggesi A, et al. Differences in minor amputation rate in diabetic foot disease throughout Europe are in part explained by differences in disease severity at presentation. *Diabetes Med* (2011) 28:199–205. doi: 10.1111/j.1464-5491.2010.03192.x
10. Giuliani AL, Sarti AC, Virgilio FD. Extracellular nucleotides and nucleosides as signalling molecules. *Immunol Lett* (2019) 205:16–24. doi: 10.1016/j.imlet.2018.11.006
11. Gachet C. P2 receptors, platelet function and pharmacological implications. *J Thromb Haemost* (2008) 99(3):466–72. doi: 10.1160/th07-11-0673
12. Gendaszewska-Darmach E, Kucharska M. Nucleotide receptors as targets in the pharmacological enhancement of dermal wound healing. *Purinergic Signal* (2011) 7:193–206. doi: 10.1007/s11302-011-9233-z
13. Shen J, DiCorleto PE. ADP stimulates human endothelial cell migration via P2Y1 nucleotide receptor-mediated mitogen-activated protein kinase pathways. *Circ Res* (2008) 102:448–56. doi: 10.1161/circresaha.107.165795
14. Battista AG, Ricatti MJ, Pafundo DE, Gautier MA, Faillace MP. Extracellular ADP regulates lesion-induced in vivo cell proliferation and death in the zebrafish retina. *J Neurochem* (2009) 111:600–13. doi: 10.1111/j.1471-4159.2009.06352.x
15. Huang N, Wang D, Heppel LA. Extracellular ATP is a mitogen for 3T3, 3T6 and A431 cells and acts synergistically with other growth factors. *Proc Natl Acad Sci* (1989) 86:7904–8. doi: 10.1073/pnas.86.20.7904
16. Vadlamudi RVSV, Rodgers RL, McNeill JH. The effect of chronic alloxana and streptozotocin-induced diabetes on isolated rat heart performance. *Can J Physiol Pharmacol* (1982) 60:902–11. doi: 10.1139/y82-127
17. imWalde SS, Dohle C, Schott-Ohly P, Gleichmann H. Molecular target structures in alloxan-induced diabetes in mice. *Life Sci* (2002) 71:1681–94. doi: 10.1016/s0024-3205(02)01918-5
18. Barros JF, Waclawiak I, Pecli C, Borges P, Georgii JL, Ramos-Junior ES, et al. Role of chemokine receptor CCR4 and regulatory T cells in wound healing of diabetic mice. *J Invest Dermatol* (2019) 139:1161–70. doi: 10.1016/j.jid.2018.10.039
19. Lanzetta PA, Alvarez LJ, Reinach OS, Candia OA. An improved assay for nanomole amounts of inorganic phosphate. *Anal Biochem* (1979) 100:95–7. doi: 10.1016/0003-2697(79)90115-5
20. Lemos FS, Pereira JX, Carvalho VF, Bernardes ES, Chammas R, Pereira TM, et al. Galectin-3 orchestrates the histology of mesentery and protects liver

during lupus like syndrome induced by pristane. *Sci Rep* (2019) 9(1):14620. doi: 10.1038/s41598-019-50564-8
21. Calvi ENC, Nahas FX, Barbosa MVJ, Ihara SSM, Calil JÁ, Ferreira LM. Immunohistochemical analysis of collagen content and types in the rectus abdominis muscle of cadavers of different ages. *Acta Cir Bras* (2011) 26:3–7. doi: 10.1590/S0102-86502011000800002
22. Kapoor M, Liu S, Huh K, Parapuram S, Kennedy L, Leask A. Connective tissue growth factor promoter activity in normal and wounded skin. *Fibrogenesis Tissue Repair* (2008) 1:3. doi: 10.1186/1755-1536-1-3
23. Chen FG, Zhang WJ, Bi D, Liu W, Wei X, Chen FF, et al. Clonal analysis of nestin$^-$vimentin$^+$ multipotent fibroblasts isolated from human dermis. *J Cell Sci* (2007) 120:2875–83. doi: 10.1242/jcs.03478
24. Pavel M, Renna M, Park SJ, Menzies FM, Ricketts T, Füllgrabe J, et al. Contact inhibition controls cell survival and proliferation via YAP/TAZ-autophagy axis. *Nat Commun* (2018) 9:2961. doi: 10.1038/s41467-018-05388-x
25. Beyeler J, Schnyder I, Katsaros C, Chiquet M. Accelerated wound closure in vitro by fibroblasts from a subgroup of cleft lip/palate patients: role of transforming growth factor-a. *PloS One* (2014) 9:e111752. doi: 10.1371/journal.pone.0111752
26. Brubaker AL, Schneider DF, Palmer JL, Faunce DE, Kovacs EJ. An improved cell isolation method for flow cytometric and functional analyses of cutaneous wound leukocytes. *J Immunol Methods* (2011) 373:161–66. doi: 10.1016/j.jim.2011.08.013
27. Meyerholz DK, Griffin MA, Castilow EM, Vargas SM. Comparison of histochemical methods for murine eosinophil detection in an RSV vaccine-enhanced inflammation model. *Toxicol Pathol* (2009) 37:249–55. doi: 10.1177/0192623308329342
28. Carson LF, Hladik C. *Histotechnology: A self-instructional text*. Am Soc Clin Pathol (2009) Chicago, IL, USA p. 188.
29. Devalaraja RM, Nanney LB, Du J, Qian Q, Yu Y, Devalaraja MN, et al. Delayed wound healing in CXCR2 knockout mice. *J Invest Dermatol* (2000) 115:234–44. doi: 10.1046/j.1523-1747.2000.00034.x
30. Choi HS, Kim JW, Cha YN, Kim C. A quantitative nitroblue tetrazolium assay for determining intracellular superoxide anion production in phagocytic cells. *J Immunoassay Immunochem* (2006) 27:31–44. doi: 10.1080/15321810500403722
31. Yeh CJ, Chen CC, Leu YL, Lin MW, Chiu MM, Wang SH. The effects of artocarpin on wound healing: in vitro and in vivo studies. *Sci Rep* (2017) 7:15599. doi: 10.1038/s41598-017-15876-7
32. Burnstock G, Knight GE, Greig AVH. Purinergic signaling in healthy and diseased skin. *J Invest Dermatol* (2012) 132:526–46. doi: 10.1038/jid.2011.344
33. Le Duc D, Schulz A, Lede V, Schulze A, Thor D, Brüser A, et al. P2Y receptors in Immune response and inflammation. *Adv Immunol* (2017) 136:85–121. doi: 10.1016/bs.ai.2017.05.006
34. Smith TM, Kirley TL. The calcium activated nucleotidases: A diverse family of soluble and membrane associated nucleotide hydrolyzing enzymes. *Purinergic Signal* (2006) 2:327–33. doi: 10.1007/s11302-005-5300-7
35. Xu F, Zhang C, Graves DT. Abnormal cell responses and role of TNF-α in impaired diabetic wound healing. *BioMed Res Int* (2013) 2013:754802. doi: 10.1155/2013/754802
36. Nestle FO, Di Meglio P, Qin J-Z, Nickoloff BJ. Skin immune sentinels in health and disease. *Nat Rev Immunol* (2009) 9:679–91. doi: 10.1038/nri2622
37. Cañedo-Dorantes L, Cañedo-Ayala M. Skin acute wound healing: a comprehensive review. *Int J Inflamm* (2019) 2019:3706315. doi: 10.1155/2019/3706315
38. Rodrigues M, Kosaric N, Bonham CA, Gurtner GC. Wound Healing: a cellular perspective. *Physiol Rev* (2019) 99:665–706. doi: 10.1152/physrev.00067.2017
39. Wang D, Huang N, Heppel LA. Extracellular ATP shows synergistic enhancement of DNA synthesis when combined with agents that are active in wound healing or as neurotransmitters. *Biochem Biophys Res Commun* (1990) 166(1):251–8. doi: 10.1016/0006-291X(90)91938-O
40. Zhou Q, Xu C, Cheng X, Liu Y, Yue M, Hu M, et al. Platelets promote cartilage repair and chondrocyte proliferation via ADP in a rodent model of osteoarthritis. *Platelets* (2015) 27:212–22. doi: 10.3109/09537104.2015.1075493
41. Kartha S, Toback G. Adenine nucleotides stimulate migration in wounded cultures of kidney epithelial cells. *J Clin Invest* (1992) 90:288–92. doi: 10.1172/JCI115851
42. Dignass AU, Becker A, Spiegler S, Goebell H. Adenine nucleotides modulate epithelial wound healing in vitro. *Eur J Clin Invest* (1998) 28:554–61. doi: 10.1046/j.1365-2362.1998.00330.x
43. Vuerich M, Robson SC, Longhi MS. Ectonucleotidases in intestinal and hepatic inflammation. *Front Immunol* (2019) 10:507:507. doi: 10.3389/fimmu.2019.00507
44. Chia JSJ, McRae JL, Cowan PJ, Dwyer KM. The CD39-adenosinergic axis in the pathogenesis of immune and nonimmune diabetes. *J BioMed Biotechnol* (2012) 2012:320495. doi: 10.1155/2012/320495
45. Lunkes GI, Lunkes DS, Leal D, Araújo MC, Corrêa M, Becker L, et al. Effect of high glucose levels in human platelet NTPDase and 5'-nucleotidase activities. *Diabetes Res Clin Pract* (2008) 81(3):351–57. doi: 10.1016/j.diabres.2008.06.001
46. Montesinos MC, Gadangi P, Longaker M, Sung J, Levine J, Nilsen D, et al. Wound healing is accelerated by agonists of adenosine A2 (G alpha s-linked) receptors. *J Exp Med* (1997) 186:1615–20. doi: 10.1084/jem.186.9.1615
47. Montesinos MC, Desai A, Chen J-F, Yee H, Schwarzschild MA, Fink JS, et al. Adenosine promotes wound healing and mediates angiogenesis in response to tissue injury via occupancy of A(2A) receptors. *Am J Pathol* (2002) 160:2009–18. doi: 10.1016/S0002-9440(10)61151-0
48. Kotwal GJ, Sarojini H, Chien S. Pivotal role of ATP in macrophages fast tracking wound repair and regeneration. *Wound Repair Regen* (2015) 23:724–7. doi: 10.1111/wrr.12323
49. Inoue K, Tsuda M, Koizumi S. ATP receptors in pain sensation: Involvement of spinal microglia and $P2X_4$ receptors. *Purinergic Signal* (2005) 1:95–100. doi: 10.1007/s11302-005-6210-4
50. Thammavongsa V, Kern JW, Missiakas DM, Schneewind O. Staphylococcus aureus synthesizes adenosine to escape host immune responses. *J Exp Med* (2009) 206:2417–27. doi: 10.1084/jem.20090097
51. Shaikh G, Cronstein B. Signaling pathways involving adenosine A2A and A2B receptors in wound healing and fibrosis. *Purinergic Signal* (2016) 12:191–7. doi: 10.1007/s11302-016-9498-3
52. Perera LMB, Sekiguchi A, Uchiyama A, Uehara A, Fujiwara C, Yamazaki S, et al. The regulation of skin fibrosis in systemic sclerosis by extracellular ATP via $P2Y_2$. *J Invest Dermatol* (2019) 139:890–9. doi: 10.1016/j.jid.2018.10.027
53. Ferrari D, Gambari R, Idzko M, Müller T, Albanesi C, Pastore S, et al. Purinergic signaling in scarring. *FASEB J* (2016) 30:3–12. doi: 10.1096/fj.15-274563
54. Cattaneo M. P2Y12 receptor antagonists: a rapidly expanding group of antiplatelet agents. *Eur Heart J* (2006) 27:1010–2. doi: 10.1093/eurheartj/ehi851
55. Greig AV, Linge C, Cambrey A, Burnstock G. Purinergic receptors are part of a signaling system for keratinocyte proliferation, differentiation, and apoptosis in human fetal epidermis. *J Invest Dermatol* (2003) 121:1145–9. doi: 10.1046/j.1523-1747.2003.12567.x
56. Yoshida H, Kobayashi D, Ohkubo S, Nakahata N. ATP stimulates interleukin-6 production via P2Y receptors in human HaCaT keratinocytes. *Eur J Pharmacol* (2006) 540:1–9. doi: 10.1016/j.ejphar.2006.04.008
57. Solini A, Chiozzi P, Morelli A, Passaro A, Felin R, Di Virgilio F. Defective. P2Y purinergic receptor function: a possible novel mechanism for impaired glucose transport. *J Cell Physiol* (2003) 197:435–44. doi: 10.1002/jcp.10379
58. Werner S, Krieg T, Smola H. Keratinocyte–fibroblast interactions in wound healing. *J Invest Dermatol* (2007) 127:998–1008. doi: 10.1038/sj.jid.5700786
59. Sorushanova A, Delgado LM, Wu Z, Shologu N, Kshirsagar A, Raghunath R, et al. The collagen suprafamily: from biosynthesis to advanced biomaterial development. *Adv Mater* (2018) 31:1801651. doi: 10.1002/adma.201801651
60. Cheng W, Yan-hua R, Fang-gang N, Guo-an Z. The content and ratio of type I and III collagen in skin differ with age and injury. *Afr J Biotechnol* (2011) 10:2524–9. doi: 10.5897/AJB10.1999
61. Kondo T, Ohshima T. The dynamics of inflammatory cytokines in healing process of mouse skin wound: a preliminary study for possible wound age determination. *Intern J Leg Med* (1996) 108:231–6. doi: 10.1007/bf01369816
62. Lin ZQ, Kondo T, Ishida Y, Takayasu T, Mukaida N. Essential involvement of IL-6 in the skin wound-healing process as evidenced by delayed wound healing in IL-6-deficient mice. *J Leukoc Biol* (2003) 73:713–21. doi: 10.1189/jlb.0802397
63. Shinozaki M, Okada Y, Kitano A, Ikeda K, Saika S, Shinozaki M. Impaired cutaneous wound healing with excess granulation tissue formation in TNF alpha-null mice. *Arch Dermatol Res* (2009) 301:531–7. doi: 10.1007/s00403-009-0969-z
64. Dipietro LA, Reintjes MG, Low QE, Levi B, Gamelli RL. Modulation of macrophage recruitment into wounds by monocyte chemoattractant

protein-1. *Wound Repair Regen* (2001) 9:28–33. doi: 10.1046/j.1524-475x.2001.00028.x
65. Ishida Y, Kondo T, Takayasu T, Iwakura Y, Mukaida N. The essential involvement of crosstalk between IFN-gamma and TGF-beta in the skin wound-healing process. *J Immunol* (2004) 172:1848–55. doi: 10.4049/jimmunol.172.3.1848
66. Eming SA, Krieg T, Davidson JM. Inflammation in wound repair: molecular and cellular mechanisms. *J Invest Dermatol* (2007) 127:514–25. doi: 10.1038/sj.jid.5700701
67. Mosser DM, Edwards JP. Exploring the full spectrum of macrophage activation. *Nat Rev Immunol* (2008) 8:958–69. doi: 10.1038/nri2448
68. Weller K, Foitzik K, Paus R, Syska W, Maurer M. Mast cells are required for normal healing of skin wounds in mice. *FASEB J* (2006) 20:2366–8. doi: 10.1096/fj.06-5837fje
69. Tellechea A, Leal EC, Kafanas A, Auster ME, Kuchibhotla S, Ostrovsky Y, et al. Mast cells regulate wound healing in diabetes. *Diabetes* (2016) 65:2006–19. doi: 10.2337/db15-0340
70. Zhang X, Majlessi L, Deriaud E, Leclerc C, Lo-man R. Coactivation of Syk kinase and MyD88 adaptor protein pathways by bacteria promotes regulatory properties of neutrophils. *Immunity* (2009) 31:761–71. doi: 10.1016/j.immuni.2009.09.016
71. Todd R, Donoff BR, Chiang T, Chou MY, Elovic A, Gallagher GT, et al. The eosinophil as a cellular source of transforming growth factor alpha in healing cutaneous wounds. *Am J Pathol* (1991) 138:1307–13.
72. Basset EG, Baker JR, De Souza P. A light microscopical study of healing incised dermal wounds in rats, with special reference to eosinophil leucocytes and to the collagenous fibers of the periwound areas. *Br J Exp Pathol* (1977) 58:581–605.
73. Cho JS, Pietras EM, Garcia NC, Ramos RI, Farzam DM, Monroe HR, et al. IL-17 is essential for host defense against cutaneous Staphylococcus aureus infection in mice. *J Clin Invest* (2010) 120(1 Supplement):1762–73. doi: 10.1172/JCI40891
74. Girardi M, Lewis JM, Filler RB, Hayday AC, Tigelaar RE. Environmentally responsive and reversible regulation of epidermal barrier function by gammadelta T cells. *J Invest Dermatol* (2006) 126:808–14. doi: 10.1038/sj.jid.5700120
75. Li Y, Wu J, Luo G, He W. Functions of Vγ4 T cells and dendritic epidermal T cells on skin wound healing. *Front Immunol* (2018) 9:1099:1099. doi: 10.3389/fimmu.2018.01099
76. Borges PA, Waclawiak I, Georgii JL, Barros JF, Fraga-Junior V, Lemos FS, et al. Adenosine diphosphate contributes to wound healing in diabetic mice through $P2Y_1$ and $P2Y_{12}$ receptors activation. *BioRxiv* (2020). doi: 10.1101/2020.10.22.350785

Conflict of Interest: The authors declare that the research was conducted in the absence of any commercial or financial relationships that could be construed as a potential conflict of interest.

Copyright © 2021 Borges, Waclawiak, Georgii, Fraga-Junior, Barros, Lemos, Russo-Abrahão, Saraiva, Takiya, Coutinho-Silva, Penido, Mermelstein, Meyer-Fernandes, Canto, Neves, Melo, Canetti and Benjamim. This is an open-access article distributed under the terms of the Creative Commons Attribution License (CC BY). The use, distribution or reproduction in other forums is permitted, provided the original author(s) and the copyright owner(s) are credited and that the original publication in this journal is cited, in accordance with accepted academic practice. No use, distribution or reproduction is permitted which does not comply with these terms.

frontiers in Immunology

REVIEW
published: 02 April 2021
doi: 10.3389/fimmu.2021.664457

Cells of the Immune System in Cardiac Remodeling: Main Players in Resolution of Inflammation and Repair After Myocardial Infarction

Irina Kologrivova[1], Marina Shtatolkina[2], Tatiana Suslova[1] and Vyacheslav Ryabov[2,3]*

[1] Department of Clinical Laboratory Diagnostics, Cardiology Research Institute, Tomsk National Research Medical Centre, Russian Academy of Sciences, Tomsk, Russia, [2] Department of Emergency Cardiology, Cardiology Research Institute, Tomsk National Research Medical Centre, Russian Academy of Sciences, Tomsk, Russia, [3] Division of Cardiology, Department of Professional Development and Retraining, Siberian State Medical University, Tomsk, Russia

OPEN ACCESS

Edited by:
Sylvaine You, Institut National de la Santé et de la Recherche Médicale (INSERM), France

Reviewed by:
Dominik Rückerl, The University of Manchester, United Kingdom
Juliana Priscila Vago, Radboud University Nijmegen, Netherlands

***Correspondence:**
Irina Kologrivova
ikologrivova@gmail.com

Specialty section:
This article was submitted to Inflammation, a section of the journal Frontiers in Immunology

Received: *05 February 2021*
Accepted: *16 March 2021*
Published: *02 April 2021*

Citation:
Kologrivova I, Shtatolkina M, Suslova T and Ryabov V (2021) Cells of the Immune System in Cardiac Remodeling: Main Players in Resolution of Inflammation and Repair After Myocardial Infarction. Front. Immunol. 12:664457. doi: 10.3389/fimmu.2021.664457

The burden of heart failure (HF), developing after myocardial infarction MI, still represents a major issue in clinical practice. Failure of appropriate resolution of inflammation during post-myocardial injury is associated with unsuccessful left ventricular remodeling and underlies HF pathogenesis. Cells of the immune system have been shown to mediate both protective and damaging effects in heart remodeling. This ambiguity of the role of the immune system and inconsistent results of the recent clinical trials question the benefits of anti-inflammatory therapies during acute MI. The present review will summarize knowledge of the roles that different cells of the immune system play in the process of post-infarct cardiac healing. Data on the phenotype, active molecules and functions of the immune cells, based on the results of both experimental and clinical studies, will be provided. For some cellular subsets, such as macrophages, neutrophils, dendritic cells and lymphocytes, an anti-inflammatory activity has been attributed to the specific subpopulations. Activity of other cells, such as eosinophils, mast cells, natural killer (NK) cells and NKT cells has been shown to be highly dependent of the signals created by micro-environment. Also, new approaches for classification of cellular phenotypes based on the single-cell RNA sequencing allow better understanding of the phenotype of the cells involved in resolution of inflammation. Possible perspectives of immune-mediated therapy for AMI patients are discussed in the conclusion. We also outline unresolved questions that need to be solved in order to implement the current knowledge on the role of the immune cells in post-MI tissue repair into practice.

Keywords: myocardial infarction, myocardial remodeling, inflammation, resolution, immune cells, cellular heterogeneity, immune metabolism

INTRODUCTION

Study of treatment and prevention of atherosclerosis complications represents one of the most cutting-edge problems in the modern world. Despite the fact that modern interventional and pharmacological approaches allowed to greatly reduce mortality and morbidity after myocardial infarction (MI), patients remain at the high risk for the recurrent events in both short- and long-term (1). Even more so, the burden of heart failure (HF), developing after MI, still represents a major issue in clinical practice, especially HF with preserved ejection fraction (HFpEF) holding a high frequency in the population with no trends to decline (2, 3).

Left ventricular remodeling is the underlying basis of HF pathogenesis in patients after acute MI (AMI). The term "remodeling" was coined by N. Sharp in the end of 70s of the 20th century to describe structural and geometrical changes after AMI. Later on, it became more general term. Nowadays, heart remodeling means the complex process of disturbances in myocardial structure and function in response to the damaging myocardial overload and loss of the functioning myocardium (4).

Restoration of the myocardial blood flow with thrombolytic therapy and primary percutaneous coronary intervention, being an obligatory step in myocardial treatment, increases tissue deterioration even further and leads to ischemia/reperfusion myocardial injury (5). Deeper understanding of tissue remodeling post-MI may be the basis of the successful management of cardiac reparative processes.

Nowadays approaches to influence cardiac healing in the clinical practice are absent. Meanwhile state-of-the-art data emphasize an important role of immune system in orchestration of reparation and post-infarction tissue remodeling after AMI (6, 7). It determines both the degree of myocardial injury and the subsequent course of the disease. On the one hand inflammatory changes may favor death of cardiomyocytes and infarction expansion. But on the other hand, angiogenic and regenerative immune reactions may benefit resolution of inflammation and regeneration of injured myocardium. Immune cells remove necrotic cell debris and create milieu necessary for migration, proliferation, differentiation of fibroblasts and endothelial cells, which is required for reconstruction of extracellular matrix, neo-vascularization, scar formation and, hence, heart recovery (8).

Understanding of the key processes in the immune system during AMI may allow to create new diagnostic and therapeutic approaches to predict and prevent further HF development. Unfortunately, knowledge of the immune mechanisms during heart remodeling is incomplete and even clinical trials sometimes show contradictory results. Partially this may be explained by the fact, that many cells, which originally were considered to be proinflammatory and harmful by default, also may display powerful healing properties. The current therapeutic approaches are missing techniques which would have not only suppressed inflammation, but rather targeted its resolution. In the present review we will summarize knowledge of the roles that different cells of the immune system play in the process of post-MI inflammation development and resolution and the subsequent cardiac remodeling. In the end we will outline possible perspectives of immune-mediated therapy for AMI patients and outline pending questions concerning implementation of the current knowledge into practice.

PATHOPHYSIOLOGY OF POST-INFARCTION HEART HEALING

Cardiac repair after AMI consists of several phases: early inflammatory phase (first 72 hours after AMI), late reparative and proliferative phase (days 7-10), which are followed by maturation phase (9, 10).

The initial processes activated in the early phase are related to the maintenance of the cardiac output and normalization of the left ventricular wall strain. Left ventricular radius of curvature changes, which determinates different wall stiffness and distribution of the intraventricular volume. "Stretching" and thinning of the myocardium in the injured zone takes place, followed by inflammation and resorption of necrotic tissue. This ultimately leads to the so-called "myocardial infarct expansion". Release of the intracellular content and destruction of extracellular matrix during inflammatory phase are associated with generation of danger-associated molecular patterns (DAMPs), non-specific stereotypic signals, which when recognized by pattern-recognition receptors (PRRs), lead to activation of the immune cells (10). The ultimate result of the inflammatory phase is degradation of extracellular matrix and phagocytosis of dead cells, also known as efferocytosis if it is associated with sensing of the 'eat-me' signals on apoptotic cells, such as phosphatidylserine (11).

Inflammatory phase should be followed by the reparative and proliferative phases to provide a wound healing and a proper scar formation. Intact myocardium is actively involved in the processes of the late remodeling. The aim of scar is prevention of myocardial rupture and partial limitation of the functional deterioration. Anti-inflammatory signaling, depletion of inflammatory neutrophils, fibroblasts proliferation and deposition of granulation tissue should be switched on to achieve this (12).

The final phase is maturation, associated with remodeling of extracellular matrix and lasting several months. This phase depends on the events that had occurred in the previous phases and is critical for the restoration of the heart function. Unsuccessful maturation may lead to the increase of myocardial stiffness, diastolic dysfunction and development of HF (10).

Cells of the immune system are present in myocardium at all the stages of heart repair. But the original dogma of their exclusively deteriorating role has been significantly shattered in the last decades. Many cellular populations have been shown to encompass both inflammatory and anti-inflammatory subsets, while properties of others have been shown to depend on the signals received from microenvironment. Timely switching from inflammatory to anti-inflammatory activity of the immune systems is crucial during post-myocardial healing. Meer inhibition of inflammation appeared to be harmful to the

myocardial function and may even lead to the rupture of myocardium. On the contrary, adequate resolution of inflammation, defined as degradation of the inflammatory products, leading to cessation of inflammation and restoration of homeostasis (13), is essential to prevent the chronization of the inflammatory process. Key targets of inflammation resolution in AMI are limitation of infiltration of myocardial tissue with polymorphonuclear cells, decrease of the vascular permeability and proper clearance of the destroyed cells and components of extracellular matrix. Understanding the role which immune cells play in inflammation resolution will allow to elaborate appropriate diagnostic and therapeutic approaches to improve AMI outcomes.

SPECIALIZED PRO-RESOLVING LIPID MEDIATORS AS GUIDES FOR RESOLUTION OF INFLAMMATION IN INJURED MYOCARDIUM

Cellular traffic in the development of any inflammation is governed by the chemical mediators. Sterile inflammation developing in the course of acute MI is not an exception. The most potent mediators of inflammation are produced from the essential polyunsaturated fatty acids (PUFAs). Splenic leukocytes recruited to the myocardium represent an important source of these mediators, with macrophages being the major cellular subtype being involved (14). While acute phase of inflammation is primarily governed by prostaglandins and leukotrienes, recently identified specialized pro-resolving lipid mediators (SPM) participate in the resolution of inflammation (15). The timely switching of lipid metabolism from leukotriene B4 (LTB4) production to the synthesis of SPM limits attraction of pro-inflammatory leukocytes to the myocardium and provides efficient resolution of inflammation. SPM are classified into several subsets: lipoxins, resolvins, protectins and maresins. This classification is based on the nature of the precursor polyunsaturated fatty acid (16). SPM production becomes possible only in the course of intercellular interactions: formation of interactome between neutrophils and macrophages, neutrophils and platelets, neutrophils and eosinophils or endothelial cells provides the required sequence in the biosynthesis of lipid metabolites (17, 18). Synthesis of SPM leads to the termination of polymorphonuclear neutrophil (PMN) transmigration, alternative polarization of the macrophage phenotype and enhancement of efferocytosis of the apoptotic neutrophils (19). Even more so, these SPM have the capacity to modulate the functioning of the adaptive immune system, skewing activation towards regulatory T-cells' subsets (20).

Myocardial infarction was associated with redistribution of leukocytes from the spleen to the heart tissue at day 1 together with the increased SPM generation in myocardium (21). STEMI patients presented with increase of SPM plasma levels already in the first hours after infarction, even before reaching the peak of high-sensitive troponin T (hsTnT), highlighting that processes of inflammation resolution are initiated in unison with its development (16). Production of pro-resolving mediators during MI possessed race- and sex-dependent signature patterns: black patients were characterized by the lowest level of resolving E1, while white males had the lowest production of protectin D1 (22). Administration of resolvin E1 (RvE1) to rats after ischemia/reperfusion limited the infarct size in a dose-dependent manner, while RvE1 treatment of cardiomyocytes *in vitro* significantly increased their viability and limited the rate of apoptosis (23). Injection of resolving D1 (RvD1) also improved heart function after the coronary artery ligation in mice and prompted synthesis of the internal RvD1, RvD2, maresin 1 (MaR1) and lipoxin A4 (LXA4) in the murine spleens (24). Of note, RvE1 administration during days 7-14 post-MI, on the contrary, adversely affected the myocardial function, due to the impaired recruitment of the monocytes/macrophages and reduced neovascularization (25). Lipoxins produced from arachidonic acid have been shown to upregulate the production of inflammatory cytokines IL-1β and IL-6 at day 1 post-MI (14).

Artificially induced impairment of the SPM signaling was associated with failure of inflammation resolution and dysfunction of leukocytes in the model of post-myocardial decompensated heart failure (26).

Besides lipid mediators the traffic of immune cells post-MI is also guided by other bioactive substances including annexin A1 (27), antimicrobial peptides (28), acute-phase proteins (29), and, obviously, various cytokines and chemokines (30). This creates a complex cross-talk between cells of the immune system, which, when unperturbed by aggravating factors, leads to the successful resolution of inflammation and restoration of myocardial function. Each cellular subset makes its unique input in the scenario of the development/resolution of inflammation following myocardial infarction.

NEUTROPHILS

Neutrophils (or polymorphonuclear neutrophils) represent the most abundant subpopulation of polymorphonuclear cells in the blood and are the first cells of the immune system arriving to the site of infraction (31). In humans their phenotype is described as CD11b+CD16+CD62L+ (CD11b+ Ly6G+F4/80 in mice) (32). They contain granules with proteases and biologically active substances. Granules are classified into azurophilic primary (contain cathepsin G, myeloperoxidase (MPO), defensins, neutrophilic elastase), specific secondary (contain NADPH oxidase, lysozyme, lactoferrin) and tertiary (contain metalloproteinases (MMP)).

Neutrophils are recruited to the infarcted myocardium during the first few hours, initiating local inflammation and tissue destruction (31). Of interest is that rather a large pool of the resident cardiac neutrophils has also been described, which primarily perform the surveillance role in the myocardium (33). The main function of the recruited neutrophils is to clear the site of myocardial injury from the necrotic tissue. Unfortunately this process is also associated with further tissue

destruction. Neutrophilic activity is majorly mediated by phagocytosis, degranulation, production of reactive oxygen species and NETosis, recently described process, characterized by the release of chromatin fibers into extracellular space and formation of neutrophilic extracellular traps (NETs) (34). The neutrophilic role in post-infarct inflammatory response is so important that clearance of neutrophils from the myocardial tissue is considered to be one of the major signs of resolution of inflammation (35).

Elevated neutrophils are associated with bad prognosis in MI patients. The major detrimental effects are dependent upon the function of myeloperoxidase (MPO) secreted by neutrophils into the extracellular space (36). NETs released by neutrophils consist of chromatin, histones and granules with proteolytic enzymes. The intensity of NETs formation in the culprit lesion has been shown to directly correlate with the infarction size. Besides, NETs induced differentiation of monocytes into intermediate subset, associated with poorer prognosis (the role of monocytes will be discussed in the further chapter) (37). Crosslinking of NETs with plasma fibrinogen leads to thrombosis and "no-reflow" phenomenon (38).

However, neutrophils' recruitment has been shown to be an obligatory requirement for the successful switching from inflammatory response to its resolution. This dual function of neutrophils may explain unsuccessful attempts of translation of anti-neutrophilic therapies into clinics (39). Apoptosis of neutrophils after degranulation represents a powerful stimulus to polarization of macrophages into anti-inflammatory phenotype, through the secretion of annexin A1, lipocalin, lactoferrin, cathelicidin and formation of apoptotic bodies (29). Release of these pro-resolving substances also suppresses further recruitment of polymorphonuclear cells in the infarct zone (32). Neutrophils may secrete annexin A1, lactoferrin and participate in chemokine scavenging, thus terminating transmigration of granulocytes to the infarcted myocardium (40). IFN-γ produced by natural killer (NK) cells and T-lymphocytes has been shown to be tightly involved in this process, stimulating resident macrophages to attract neutrophils to myocardial tissue (41). Prolonged lifespan of neutrophils under the influence of tumor necrosis factor (TNF) and IL-1β was associated with increased endothelial damage and adverse myocardial healing (42), while matrix metalloproteinase (MMP)-12 seems to favor neutrophilic apoptosis (17). Overall, MMP-12 has been shown to possess potent pro-resolving properties, influencing inflammatory signaling and controlling cellular clearance, and neutrophils appeared to be the source of MMP-12 themselves (43).

Switching between the production of inflammatory and pro-resolving lipid mediators also explains the dual role of neutrophils in the MI. Neutrophils are the main cells, expressing 5-lipoxigenase (LOX), which is responsible both for the synthesis of leukotriens and production of the various SPM initiated in the course of intercellular interactions in tissues (17, 18). As a result, neutrophils enhance the recruitment of other PMNs at the beginning of the development of inflammation, while suppress further PMN migration and facilitate efferocytosis in the resolution phase. We have encountered no studies describing the role of neutrophilic SPM in resolution of post-MI inflammation. However, lack or deficiency of 5-LOX was associated with the increased mortality of mice after chronic coronary ligation (44).

It has been shown that neutrophils undergo the continual change of the proteome in the first week after AMI, with Day 1 cells predominantly producing metalloproteinases, switching to upregulation of apoptosis and ECM reorganization phenotype at Day 3 and predominant expression of the reparative substances, including fibronectin, galectin-3, and fibrinogen at Day 7 (45).

Even more so, according to the recent data neutrophils may be subcategorized into N1- and N2-subpopulations, with CD206-N1-neutrophils being inflammatory and CD206+ N2-neutrophils – ant-inflammatory cells (31). In mice N1-neutrophils prevailed during the initial phase of infarction and N2-neutrophils peaked at days 5-7 after MI (31). In the model of chronic MI total depletion of neutrophils was associated with increased fibrosis and worsening of the heart function (29).

Current studies provided information that neutrophils are characterized by the even more significant heterogeneity than it was originally thought. In humans there were recognized CD177+, olfactomedin 4 (OLFM4)+, T cell receptor αβ+, CD49d+CXCR4 +vascular endothelial growth factor (VEGFR)+ neutrophilic subsets. Neutrophils expressing programmed death-ligand (PD-L)1, arginase 1(ARG1), CD10 are reported to have potent immunosuppressive activity (46). However, it is still unclear, either newly identified neutrophilic phenotypes represent the true subsets, or rather refer to the definite functional state of neutrophils. Data concerning the functions of the recently identified subpopulations of neutrophils in myocardial infarction are presently absent.

EOSINOPHILS

Another subpopulation of granulocytes which role in myocardial infarction is usually overlooked is represented by eosinophils. In steady state they constitute 1-3% of leukocytes in peripheral blood and contain primary and secondary granules, as well as lipid bodies (47). Main active substances produced by eosinophils are galectin-10, major basic protein (MBP), eosinophil-derived neurotoxin (EDN), eosinophil cationic protein (ECP), eosinophil peroxidase (EPO) and derivatives of arachidonic acid. These substances are released in the course of degranulation, phagocytosis and formation of extracellular DNA traps (the process named EETosis), enabling eosinophils to kill extracellular parasites and participate in allergic reactions (47). Even more so, eosinophils are capable of presentation of antigens to Th2-lymphocytes and may even activate dendritic cells through the production of eosinophil peroxidase (EPO) (48). Eosinophils were also shown to be involved in the pathogenesis of myocardial infarction, reaching the peak in plasma by days 2-3 post-AMI (49). They may increase damage of myocardial tissue through the production of ROS by eosinophil peroxidase or induction of cellular cytotoxicity by granules' contents or antibody-mediated cellular cytotoxicity (47).

Meanwhile, patients with low eosinophilic cell count were characterized by the bigger infarct size and higher rate of cardiac events during long-term follow-up (50). Thus, eosinophils have also been shown to mediate anti-inflammatory effects and input

resolution of inflammation. Even though until recently they were regarded as a simple short-lived post-mitotic cellular subpopulation, nowadays a potent regulatory potential of eosinophils has been widely appreciated. Eosinophils possess a potential to produce variable growth factors, including TGF-α and -β, fibroblast growth factor (FGF), epidermal growth factor (EGF), platelet-derived growth factor (PDGF) and vascular-endothelial growth factor (VEGF), participating in angiogenesis and myocardial repair (51). However, balance between production of eosinophilic IL-5 and growth factors is pertinent, as mice overexpressing IL-5 were characterized by the insufficient production of ECM components and impaired wound healing (52). Eosinophils have also been confirmed to be the main source of protectin D1 and a range of resolvins, including novel resolvin RvE3, limiting infiltration of tissue with neutrophils (13).

Eosinophils also secrete IL-4, cytokine playing an essential role in differentiation of macrophages towards M2 phenotype, and regulating myocardial tissue regeneration (53, 54). Eosinophilic cationic protein mEar1 together with IL-4 was able to inhibit apoptosis is cardiomyocytes and prevent adhesion of neutrophils to endothelial wall, improving cardiac dysfunction (49). Most likely production of IL-4 is a key feature providing beneficial effects of eosinophils during AMI, as injection of the recombinant IL-4 to eosinophil-deficient mice rescued adverse remodeling of the left ventricle after the permanent ligation of the left coronary artery (54). However, the potency of treatment with IL-4 appeared to be time-dependent: administration of IL-4 lost its efficiency when injected at the advanced stages of the post-MI remodeling (55). Thus, time frame of the intercellular interactions has been shown to be critical for the successful myocardial healing following infarction. These findings highlight the importance of the proper "treatment window" choice when elaborating therapeutic approaches to manipulate inflammation and immune cells' kinetics in AMI.

Distinct regulatory subpopulation of murine Siglec-F^{int}CD62L+$CD101^{lo}$ eosinophils (rEos, corresponding to human Siglec-8+CD62L+$IL\text{-}3R^{lo}$ cells) with homeostatic functions has recently been described in lungs (48). They were also detected in gastro-intestinal tract, Peyer's patches, adipose tissue, thymus and uterus, but there are currently no data on whether these cells exist in humans' heart. Aforementioned rEos produce IL-4 in high quantities (48) and represent the cellular subset that potentially may be involved in resolution of post-infarct inflammation.

There still remains many unresolved questions in the role of eosinophils in post-infarct inflammation, such as gender bias, as many aspects of homeostatic and anti-inflammatory activity of eosinophils have only been confirmed in males, and were not established in females yet (49).

MONOCYTES/MACROPHAGES

The role of monocytes and macrophages in post-infarct inflammation has been described the most explicitly. Myocardium contains resident macrophages (about 7-8% of all non-cardiomyocytes), arising either from the yolk sac or fetal liver, and providing immune surveillance and regulation of cardiac functions (12, 56). Even though in steady state resident macrophages may proliferate to maintain their pool, they are rapidly depleted after myocardial injury (57). It is circulating monocytes that are going to be recruited and subsequently differentiate into macrophages to mediate development and resolution of inflammation. Myocardial infarction already in the first 30 minutes is characterized by the significant mobilization and influx of monocytes to the myocardial tissue, first from the patrolling pool in the peripheral blood and then from the splenic reservoir through the signaling *via* angiotensin II Type 1a receptor (58). These initially recruited monocytes may even be regarded as one of the stimuli that further attract neutrophils to the infarcted myocardium, as depletion of CCR2+ monocytes and macrophages was associated with impaired neutrophils extravasation during ischemia reperfusion injury in mice (59).

Several subsets of monocytes have been described based on their phenotype, however there is no consistency in the understanding of the further fate of these monocytic subpopulations. In men classification is based on the expression of molecules CD14 (lipopolysaccharide-receptor) and CD16 (low-affinity Fcγ-receptor). Classical monocytes in humans are described as $CD14{+}{+}CD16^{neg}$; in mice – $Ly\text{-}6C^{hi}$. They constitute about 90% of all circulating monocytes and are characterized by high expression of CD62 and CCR2, which enables their recruitment to the site of injury towards the gradient of MCP-1 and chemokines CCL2 and CCL7. Classical monocytes produce inflammatory cytokines and nitric oxide and are able to differentiate into macrophages and dendritic cells. They peak at Day 3 after MI, and are involved in breakdown of necrotic myocardium (12). Even though there is no direct evidence that classical monocytes are precursors to macrophages with a certain phenotype, they are often called "inflammatory monocytes" (35). Blockage of CCR2 in mice was associated with increase of left ventricular ejection fraction (LVEF) and decrease of left ventricular end-diastolic volume (LVEDV) (60). Increased levels of classical monocytes were associated with impaired left ventricular functions six months after AMI (61). Meanwhile, the total depletion of monocytes and infiltrating macrophages during the 1^{st} week following myocardial injury in mice was associated with enhanced heart rupture and increased mortality (62).

Human non-classical monocytes are $CD14{+}CD16^{hi}$ and murine non-classical monocytes are $Ly\text{-}6C^{lo}$. High expression of chemokine receptor CX3CR1 is typical for non-classical monocytes, allowing their homing to the infarction site by gradient of chemokine fractalkine. Their function and origin are less clear than classical monocytes. Mainly they represent a patrolling monocyte population, being found close to the vessel wall in the circulation and scavenging oxidized lipids, cellular debris and pathogens (58). According to our data the frequency of non-classical monocytes inversely correlates with the severity of atherosclerosis in patients with stable coronary artery disease (63). One may speculate that it is non-classical monocytes that are essential for the resolution of inflammation in AMI, as late recruitment of monocytes in the models of acute inflammation

did not depend on the CCR2 expression (64). Even though there is no direct evidence of the subsequent differentiation of non-classical monocytes into M2-macrophages, loss of fractalkine receptors was associated with skewing of macrophage balance to inflammatory subset in epididymal white adipose tissue (65). It has been shown that transcription factor NR4A1 (also known as Nur77) plays role in re-differentiation of classical monocytes into non-classical subpopulation. Absence of Nr4a1 in mice was associated with impaired LV function after AMI (66). Non-classical monocytes reach the peak at Day 5 after MI, but classical monocytes still predominate in numbers through all the course of infarction progression (12). Non-classical monocytes may regulate scar formation, angiogenesis and myocardial healing, through the secretion of VEGF and TGF-β (67). Absence of increase of non-classical monocytes is an unfavorable sign which was associated with reduction of LVEF (68).

There may be also identified so called intermediate monocytes (CD14++CD16^{hi}), absent in mice. Most likely these cells represent a transition step between classical and non-classical monocytes. Their function is described primarily as inflammatory (12, 58). Intermediate monocytes also express CCR2 and angiopoietin-2 receptor (TIE-2), and thus are involved in regulation of angiogenesis (56). Levels of intermediate monocytes in AMI patients correlated with troponin concentration (69).

Differentiation of monocytes to macrophages is accompanied by increase of CD68 and MHC II expression in humans and F4/80 in mice, and reduction of CD14 expression (12). Macrophages play dual role in resolution of inflammation: clearing the tissue from necrotic remnants on one hand, and secreting pro-resolving mediators on the other hand (35). Similarly to monocytes, macrophages are characterized by heterogeneity, with different subsets involved in resolution of inflammation unequally. The common and most widely used approach to classify macrophages depends on the stimuli used to polarize macrophages *in vitro*. Monocytes will differentiate towards M1 macrophages under the influence of granulocyte-macrophage colony-stimulating factor GM-CSF and towards M2 macrophages under the influence of macrophage colony-stimulating factor (M-CSF) also known as colony stimulating factor 1 (CSF-1). The following post-differentiation stimulation with either LPS/IFN-gamma/TNF-alpha or IL-4/IL-13 will respectively initiate transition of M1/M2 macrophages into the activated state (70, 71). In vivo it is cytokines, DAMPs and growth factors that play the role of the polarizing agents (35).

M1 macrophages are characterized by the inflammatory phenotype and produce cytokines such as IL-1β, IL-6 and TNF-α, while alternatively activated M2 macrophages are anti-inflammatory and may activate fibroblasts, induce cell proliferation, collagen deposition and angiogenesis (12, 70). M2 macrophages may be further subcategorized into M2a, M2b and M2c cells, where M2a and M2c macrophages primarily cooperate with cells of the adaptive immunity and M2b cells play the role in regulation of inflammation (72).

Various types of cell death have been identified in the infarcted myocardium, including necrosis, apoptosis, necroptosis, autophagy-related cell death, pyroptosis and ferroptosis (11). M2 macrophages have been shown to be tightly involved in efferocytosis – a process of engulfment of the apoptic bodies, essential in the resolution of inflammation after AMI (73). The main feature of efferocytosis is clearance of the dead cells in the "immunologically silent" manner, as production of inflammatory cytokines is suppressed by efferocytic mechanisms (74, 75). Instead, macrophages switch to the production of TGF-β, IL-10, lipoxins, resolvins and other SPM (75). The growth-arrest specific gene 6 (Gas6)/myeloid-epithelial-reproductive tyrosine kinase (MerTK) pathway is employed by macrophages to recognize phosphatidylserine (PtdSer) on the surface of the dead cells and proceed to efferocytosis (11). Deficiency of MerTK was associated with impairment of efferocytosis and increase of the infarct size after the coronary occlusion in mice (76). Expression of MerTK appeared to be tightly associated with the monocytic scavenger receptor CD36: mice lacking CD36 were characterized by the reduced expression of MerTK on macrophages. The double knock out of CD36 and MerTK led to the increased post-infarct myocardial rupture (77).

In our previous collaborative works it has been shown that stabilin-1+ M2 macrophages peaked in patients' heart tissue in the regenerative phase of MI (days 4-10) and did not decrease further on, predominating in the infarct area (78). Specific targeting of genes responsible for M2 polarization was followed by the impairment of left ventricular function after coronary artery ligation in mice (79). Meanwhile, blocking of M1 polarization pathways led to the reduced LV dilation at 3 weeks post-coronary artery ligation (80).

However, M1-M2 paradigm still carries some inconsistency. Unexpected results were obtained by Yang M. et al. (81), who knocked out GATA3, a transcription factor that appeared to be involved in the development of M2-phenotype (81). This was associated with the prolonged persistence of CCR2+/Ly-6C^{hi} inflammatory macrophages in the post-infarct myocardial tissue. Yet, animals performed improved LV function in 2 months of observation compared to intact animals, thus, questioning the detrimental role of Ly-6C^{hi} macrophages in cardiac remodeling. It is worth noting that the decreased accumulation of neutrophils was also observed in animals after GATA3-knock out, thus representing the confounding issue of the study (81).

One of the alternatives is to avoid classification of macrophages into M1 and M2, but rather indicate the stimulus used to activate macrophages: M_LPS, M_IFN-γ, M_IL-4, M_IL-10, M_IL-6, etc. RNA expression profile and CD markers vary greatly between M_LPS and M_IFN-γ (previously reported together as M1 subpopulation) and between M_IL-4 and M_IL-10 (previously reported together as M2 macrophages) (82). The use of single-cell RNA sequencing (scRNA-seq) allowed to identify as many as 11 clusters of mononuclear phagocytes with distinct gene expression profiles in the heart of naïve mice (57). There was observed predominantly inflammatory gene expression at day 3 post-coronary artery ligation, and reparative genes expression at day 7, accompanied by mixed expression of M1 and M2 marker-genes, further

emphasizing over-simplification of macrophages categorization into M1 and M2 cells (83).

MAST CELLS

Mast cells represent cells of immune system of myeloid origin, residing in mucosa and connective tissue and mainly being involved in development of allergic conditions. They are abundant in human heart and coronary lesions and were shown to participate both in plaque rupture and processes of myocardial remodeling after infarction (84–87). Mast cells are able to produce various inflammatory cytokines including TNF-α, IFN-γ, IL-6, amines (mainly histamine) and proteases, regulating activity of matrix metalloproteases, collagen degradation and thus playing role in organization and resolution of inflammation and fibrosis in myocardium (87).

Phenotype of mast cells is characterized by expression of c-Kit, Fc-εRI and various mast-cell-specific proteases (84). Depending on the proteases contained in granules mast cells have been classified into two subsets: MC_T (with granules containing only tryptase) and MC_{CT} (with granules containing tryptase, chymase, cathepsin G, and carboxypeptidase). Heart mast cells have been described to have MCct phenotype (87). Biological activity of mast cells may be realized through degranulation and secretion of the granules' content, secretion of cytokines or production of lipid mediators, depending on the nature of the stimuli received during activation (84). Main route of mast cells activation is represented by the cross-linking of FcεRI with IgE (85). Secretagogues of mast cells, mediating unspecific degranulation, include complement components, stem cell factor (SCF), defensins produced by neutrophils, substance P, neurotensin, endothelin-1, reactive oxygen species, IL-33 (ligand of ST2 receptor) (85, 87). Estrogen has been shown to down-regulate mast cell activity (87).

Mast cells have been found in media of infarct-related and infarct-unrelated arteries at different stages of infarction, and in myocardial tissue itself, implying that they may participate both in initiation and termination of the post-infarct inflammation (86). Treatment of isolated rat heart with ketotifen (mast cell membrane stabilizer) reduced ischemia/reperfusion injury (88). Retrospective and prospective studies investigating effects of histamine type 2 receptors (H2) antagonists showed reduction of brain-natriuretic peptide (BNP) production and decrease of the left ventricular dilation together with improvement of the heart failure in patients (89).

Despite evident inflammatory properties of mast cells, their main function during cardiac tissue remodeling remains to be associated with regulation of fibrous tissue metabolism (84). Mast cells may be both enhancers and inhibitors of post-myocardial fibrosis, reaching their pick at day 7 after MI. Pro-fibrotic properties are mediated primarily by chymase and tryptase, which are known to be activators of TGF-β and angiotensin II, the well-known promoters of fibroblasts activity. In addition, MC store basic fibroblast growth factor (bFGF) in their granules. MC also produce and secrete anti-fibrotic mediators such as IL-10, IL-13, CXCL-10 and VEGF-A (84).

Another input of MC in resolution of inflammation is mediated by activation of protease activated receptor (PAR)-2 on cardiomyocytes by tryptase. As a result of this activation anti-inflammatory 15-deoxy 12,14 prostaglandin J2 (15-d-PGJ2) is produced from Cyclooxygenase-2 (COX-2) (90). 15-d-PGJ2 regulates timely resolution of inflammation at the level of transcription, inhibiting proinflammatory factors NF-κB, STAT3, and activator protein 1 (AP1) and stimulating pro-resolving E2-related factor 2 (Nrf2). Besides, it inhibits protein translation, thus limiting the development of inflammation (91).

DENDRITIC CELLS

Dendritic cells (DCs) represent an extremely heterogeneous population of immune cells, both of myeloid and lymphoid origin. Their main function is presentation of antigens to T-lymphocytes. DCs express MHC II, similarly to monocytes and macrophages, but belong to a distinct cellular population (92). They also secrete various cytokines and growth factors, regulating immune response and inflammatory processes (92).

Two major DC subpopulations were identified in men and mice, such as plasmacytoid DCs (pDCs) and conventional DCs (cDCs), further classified into CD141+/CD103+ cDCs1 and CD1c/CD11b+ cDCs2 lineages (93). Both pDC and cDC subsets may be found in myocardium in steady state, as well as double-negative CD103-CD11b- pre-cDCs and poorly characterized population of monocyte-derived CD64+CD11c +MHCII+ DCs (moDCs) (94). Myocardial infarction was associated with the increase of cDCs and moDCs in the heart (95). But only cDCs2 increased expression of co-stimulatory molecule CD86 and migrated into the draining lymph nodes initiating activation of autoreactive IL-17+/IFN-γ+ T-lymphocytes (95).

DCs may modify the process of post-MI healing through activation of T-lymphocytes in draining lymph nodes, production of inflammatory cytokines and direct activation of fibroblasts (94). Besides antigen presentation to T-lymphocytes DCs may also influence the development of inflammation through the production of exosomes enriched in micro (mi)-RNA (96, 97). Infiltration of myocardium with DCs after left anterior descending coronary artery ligation in mice was characterized by spatial-temporal dynamics: DCs could be found in ventricle and septum at day 3, and appeared in the left atrium at day 7 (94).

Experimental works using depletion of DCs to study their function show inconsistent results. Depletion of conventional DCs in chimeric mice was associated with decrease of macrophages at day 7 post-MI, followed by reduction of infarct size, prevention of ventricular remodeling and improvement of cardiac function (94). However, in the series of other works DCs depletion was also associated with decrease of anti-inflammatory T-regulatory lymphocytes and impairment of the myocardial healing. Mixtures of cytokines

IL-37 and troponin I led to the creation of tolerogenic DCs, which beneficially influenced the process of post-MI remodeling (98). Local injection of tolerogenic DCs induced activation of M2 macrophages through T-regulatory lymphocytes and favored resolution of inflammation, wound healing and ventricular systolic function (99). Biologically active molecules mediating pro-resolving functions of tolerogenic DCs include galectin-1 and pentraxin 3 (100, 101).

Thus, the ultimate result of the DCs activity in the course of AMI depends on the dendritic cells' subpopulation being involved and subsequent type of the recruited effector cells. Ideally, activation of the conventional DCs should be followed by the increase of the tolerogenic DCs' activity to provide timely resolution of inflammation.

T-LYMPHOCYTES

T-lymphocytes are the cells of the adaptive immunity. Presentation of the specific antigen by antigen-presenting cells in secondary lymphoid organs is an obligatory stage in their activation and clonal expansion (102). Population of T-lymphocytes may further be subdivided into helper CD4+T-lymphocytes, secreting cytokines, and cytotoxic CD8+ T-lymphocytes, able to lyse pathologically changed cells directly (103). Each population may play either inflammatory or regulatory role (102).

Cells of the adaptive immunity attracted attention of the researchers not so long ago, and their function during MI remains elusive and stem from experimental works. It has been shown that RAG1 knock-out (KO) mice, which lacked T-lymphocytes, developed infarction of smaller sizes, compared to the wild-type animals. The primary role for modulation of the injury size has been ascribed to CD4+ T-lymphocytes, with interferon-γ (IFN-γ) and IL-17 being tightly involved in the process (104, 105). These cytokines amplify death of cardiac cells and stimulate proliferation of fibroblasts. Deficiency of IL-17A or γδ-T cells (main producers of IL-17 in the heart) alleviated left ventricular dysfunction after myocardial infarction (105). Meanwhile, decrease of Th2 lymphocytes was associated with increased severity of STEMI and high risk of adverse cardiovascular events (106), while administration of IL-4, the Th2 key-stone cytokine, had pro-resolving effects (55).

There is an opinion that activation of CD4+ T-lymphocytes during AMI is antigen-independent, associated with the recruitment and activation of effector memory T-cells through recognition of alarmins by TLR (107). Another pathway of T-lymphocytes' activation is mediated by MMP-9 *via* cleavage of CD31, which normally inhibits signaling through T-cell receptor (TCR) (108).

At the same time, pro-inflammatory milieu, formed during MI, creates conditions favorable for activation of autoreactive clones of T-lymphocytes, which may trigger autoimmune destruction of the myocardial tissue (109). Heart-specific T-lymphocytes receive positive signal for differentiation while polyclonal inhibition of other T-lymphocytes' clones is observed (110). Priming of T-cells takes place in mediastinal (heart-draining) lymph nodes, which enlarge after MI. Myosin heavy chain α (MYHCA), missing in thymus and not participating in negative selection of T clones, was shown to be the dominant epitope associated with activation of T-lymphocytes during MI (110).

T-lymphocytes are attracted to injured myocardium and are detained there. One of the possible chemokines, involved in this process, is fractalkine, recognized by T-lymphocytes' receptor CX3CR1 (111). T-cells may also participate in microvascular-obstruction during ischemia-reperfusion injury, release inflammatory cytokines and increase cellular infiltration of the myocardial tissue even further ultimately leading to the aggravation of myocardial injury (111). This activation of CD4+ T-lymphocytes is a prerequisite process after MI, as absence of CD4+ cells in animals was associated with poorer outcome (102).

Cytotoxic CD8+ T-lymphocytes were also shown to be involved in post-infarction inflammation (112). CD8+ T-cells as well may have both beneficial and detrimental effects in myocardial infarction. Deficiency of cytotoxic T-cells was associated with better restoration of heart physiology, but scar formation was impaired. Mice deficient for CD8+ T-lymphocytes died post-MI due to the myocardial rupture caused by dysregulated fibrosis and increased inflammation (113).

Protective effects mediated by T-lymphocytes may be mediated by the distinct CD4+ and CD8+ subsets positive for expression of angiotensin receptor AT2 (114, 115). But primary protective function during MI is, of course, mediated by subpopulation of T-regulatory lymphocytes.

Tregs represent a distinct subpopulation of CD4+ T-lymphocytes, characterized by anti-inflammatory activity. Their major role in infarction is repair of myocardial tissue through suppression of inflammatory processes and activation of fibrosis (102). Natural Tregs appear in the infarction zone already in the first hours after MI and persist for at least 7 days (116). Treg recruitment most likely involves chemokine receptor CCR5 (117). Myosin-specific T-helper lymphocytes are attracted to the site of myocardial infarction and undergo *in situ* conversion to Tregs, which were characterized by enhanced expression of inhibitory check-point molecules, such as CTLA-4, TIGIT (T cell immunoreceptor with Ig and ITIM domains), PD-1, BTLA (B- and T-lymphocyte attenuator) (110).

Ectoenzymes CD39 and CD73 are expressed on the membrane of Tregs. Ectonucleoidase activity of these molecules input to the increase of the local adenosine concentration, which has been shown to suppress inflammatory activity of conventional CD4+ T-lymphocytes in myocardial injury (104, 118). Tregs can influence the differentiation of macrophages in the site of myocardial infarction, and direct it towards M2 phenotype, inducing expression of arginase-1, interleukin-13, osteopontin, and TGF-β (119). Disruption of this interaction was associated with failures in the formation of extracellular matrix in scar region and myocardial rupture (120). Crosstalk between Tregs and macrophages promoted efferocytosis in the models of acute inflammation (121). However no data is available on this effect of T-regulatory lymphocytes in AMI. Tregs may also improve cardiac

tissue remodeling in a paracrine manner directly stimulating proliferation of cardiomyocytes through the secretion of six main factors (Cst7, Tnfsf11, Il33, Fgl2, Matn2, and Igf2) (116).

Statin intake before percutaneous interventions after MI was associated with the increase of Tregs among PBMC (122). Expansion of Tregs *via* agonistic antibodies led to the reduction of the recruitment of neutrophils, monocytes and lymphocytes to the site of myocardial injury and suppressed activation of CD8+ lymphocytes (123). Artificial depletion of Tregs was associated with unfavorable remodeling of the left ventricle, development of apical aneurisms and even cardiac ruptures (116, 120). This underscores an important role of Tregs in reparation of the injured myocardium.

MYELOID-DERIVED SUPPRESSOR CELLS

Myeloid-derived suppressor cells (MDSC) represent a recently described subpopulation of cells that originate from myeloid precursors in bone marrow, blocked at different steps of their development. This subpopulation is highly heterogeneous and at present includes polymorphonuclear MDSC (PMN-MDSC), monocytic (M-MDSC) and early-derived MDSC (eMDSC) (124). In steady state they may be found in bone marrow, but do not possess any suppressive activity. In the course of inflammatory disorders and tumorigenesis they appear in the secondary lymphoid organs and peripheral tissues (125). Role of these cells in the course of development of MI is not yet studied, but most likely they exhibit pro-resolving functions, suppressing T cell mediated immune responses (126).

Administration of rapamycin suppressed activation of the mammalian target of rapamycin (mTOR) and activated MDSC during acute kidney injury (127). This activation was accompanied by the decrease of CD4+ and CD8+ T-lymphocytes infiltration and decrease of inflammatory cytokines production (IL-1β, IL-6 and IFN-γ). Production of anti-inflammatory TGF-β increased on the contrary (127). Expression of indoleamine 2,3-dioxygenase (IDO) by MDSCs was associated with metabolic starvation of T cells and directed development of DCs towards tolerogenic subset (128). MDSC also exhibited anti-hypertrophic and anti-inflammatory effects when co-cultured with cardiomyocytes, through the secretion of IL-10 and nitric oxide (129).

MDSCs were elevated in patients with HF, and their depletion aggravated heart function (129). The kinetics of MDSCs' recruitment to myocardial tissue and potential factors being involved in regulation still need to be elucidated.

B-LYMPHOCYTES

B-lymphocytes represent cells of the adaptive immunity, characterized by the production of antibodies and mediating humoral immune response. Two major types of B-lymphocytes have been described: B1-lymphocytes (functioning in T-independent manner; also called "innate-like" B-lymphocytes) and B2-lymphocytes (interaction with T-lymphocytes is required for proper function; also called conventional B lymphocytes) (130). B2 lymphocytes predominate in circulation. Surprisingly, B-lymphocytes are the most abundant lymphoid cells in myocardium, both in mice, and in men (131, 132). After myocardial infarction their numbers gradually increase nearly 5-fold. The time of reaching the peak values will depend on the presence of ischemia-reperfusion (day 7 – in non-reperfused myocardium; day 3 – after ischemia-reperfusion injury of the myocardium) (133).

The main effector molecules produced by B-lymphocytes are antibodies. Antibody production in performed by plasma cells – the terminal stage of B-lymphocyte differentiation. Antibodies increased destruction of myocardial tissue, as blocking of IgM led to the significant reduction in ischemia-reperfusion injury (134). At the same time, specialized pro-resolving mediators 17-hydroxydocosahexaenoic acid (17-HDHA) and resolvin D1 increased production of IgM and IgG from B-cells, suppressing secretion of B-derived IL-6 and IL-10 (135). Potentially, balanced antibody production may benefit resolution of inflammation through clearance of cellular debris.

Besides antibodies, B cells are also capable to secrete cytokines and chemokines. The production of CCL7, attracting Ly-6C^{high} monocytes to myocardium, has been shown to be dependent upon B-lymphocytes. Depletion of B2-lymphocytes from circulation by anti-BAFF of anti-CD20 antibodies disrupted monocytes recruitment and was associated with the reduction of infarct size and favorable heart remodeling (136).

Meanwhile, injection of B-lymphocytes into early post-infarcted myocardium reduced apoptosis in cardiomyocytes and preserved left ventricular function, while other cells of myeloid and lymphoid lineage as well as combinations of bone marrow cell subsets had no effect (137). Recently described population of IL-10 producing CD5+ "regulatory B-lymphocytes" may be the one to play anti-inflammatory function (138). However, an exact mechanism mediating this protecting effect of B-lymphocytes has not yet been described.

NK CELLS

Natural killer (NK) cells constitute 2-5% of all peripheral blood leukocytes and belong to the heterogeneous group of innate lymphoid cells (ILC), type I ILC in particular. They exhibit lymphoid cellular morphology, but do not have antigen specificity. Instead, they express a great variability of invariant receptors, recognizing both self and non-self antigens. NK activation depends on the balance between activation and inhibitory signals they receive during interaction with their target cells. NK cells express transcriptional factor T-bet and produce IFN-γ, perforin and granzyme B (139).

NKs' role during MI still remains poorly characterized. NK cells appeared to be the major source of IFN-γ during angiotensin (AT) II induced vascular dysfunction (140). NK cells may interact with inflammatory macrophages through the

cytokine axis IFN-γ/TNF-α/IL-12 whereby potentiating activity of one another and increasing inflammation in infarction zone (141).

At the same time there are data pointing to the possibility of insufficient NK function during MI. Patients with acute coronary syndrome were characterized by the lower numbers of NK cells in the peripheral blood compared to patients with stable angina (142). One of the possible explanations of the decreased NK numbers in CAD patients is high susceptibility of these cells to apoptosis induced by various stimuli (143). Observed NK deficiency during MI was associated with the reduced capacity to limit cardiac cell apoptosis and modulate development of fibrosis in post-infarcted myocardium (144). Thus, NK cells may also fulfil protective function in CAD patients. Most likely the balance between various stimuli will determine the ultimate role of the NK cells in infarct and peri-infarct zones.

iNKT CELLS

A distinct minor subpopulation of invariant natural killer T (iNKT) cells (0.01 – 0.5% of all peripheral blood leukocytes) simultaneously expresses NK activating and inhibitory receptors and an invariant αβ TCR which can recognize lipid and glycolipid antigens (mainly DAMPs) (145). Infiltration of activated iNKT into post-infarcted myocardium ameliorated left ventricular (LV) remodeling and development of heart failure after MI (145). Absolute numbers of circulating iNKT in AMI patients were decreased and could have been used to predict restenosis in long-term follow-up (146).

Mechanisms of iNKT protective effects during MI were not identified yet, but in the case of sterile inflammation in the liver iNKT have been shown to infiltrate the injured site and orchestrated healing *via* production of IL-4 and switching of macrophages to patrolling phenotype (147). Similar pattern of iNKT activity may exist in post-MI injury, but further research to prove this concept is required.

Glycosphingolipid α-galactosylceramide (αGC) is one of the most potent stimulators of both NK and iNKT activity. Administration of αGC to mice with ischemia/reperfusion reduced the infarction size, but whether this effect was mediated by iNKT cells or represents epiphenomenon remains disputable (148).

FUTURE DIRECTIONS

Thus, cells of the immune system are unequivocally involved in development and resolution inflammation during myocardial infarction. The main features of the phenotypes, active molecules and effector activity of the immune cells during AMI are summarized in **Table 1**. The same cellular population may exhibit both inflammatory and pro-resolving properties (**Figure 1**), which, being combined with the excessive complexity of intercellular interactions, creates a well-tuned, but highly susceptible to perturbations, system of immune regulation in myocardial remodeling. This may explain unsuccessful attempts of remodeling modulation *via* targeting of the single signaling pathways or definite cellular populations (39). Besides, the majority of data concerning the role of immune cells in myocardial infarction have been obtained in experiment. Clinical context complicates existing regularities of immune cell functioning during AMI with such confounding variables as aging, comorbid conditions, variable genetic background, etc. (40).

However, results obtained in COLCOT and CANTOS clinical trials show the potential of anti-inflammatory therapy in AMI patients (150, 151), even though the benefits of approaches used up to date may seem not so large-scale and limited to the narrow group of patients. In our opinion relatively modest success of these trials is associated with a fact that inflammatory phase is obligatory at the early stage of MI to clear the necrotic cellular debris and create favorable circumstances for the development of reparative phase. Thereby, complete suppression of inflammation which may be beneficial during autoimmune conditions, may be inappropriate in patients after cardiovascular events at the early stages of treatment. New approaches for patient's follow-up and treatment targeting resolution of inflammation should be elaborated.

One of the modern concepts of immune modulation represents metabolic reprogramming of immune cells (152). All the inflammatory cells' subpopulations have been shown to be dependent upon aerobic glycolysis, while anti-inflammatory subpopulations normally produce energy through oxidative phosphorylation (152). Rewiring of the cellular metabolism determines direction of cellular differentiation and may be used to selectively and specifically regulate the power of immune responses. Activation of AMP-activated protein kinase (AMPK) is known to increase fatty acid oxidation and promote differentiation of cells with pro-resolving activity (M2 macrophages, Tregs, N2 neutrophils), while stimulation of mammalian target of rapamycin (mTOR) and hypoxia induced factor (HIF) 1-α is associated with an increase of inflammatory profile of the immune cells (M1 macrophages, mature DCs, activated B cells, Th1, Th17) (**Figure 2**) (152–154).

Cellular metabolism is tightly linked to epigenetic reprogramming of the immune cells, which, in turn, represents another powerful tool of the cell fate control. Chromatin-modifying enzymes include multiple types of histone acetyltransferases and deacetylases. Moreover, some of these enzymes display non-catalytic activity, governing the direction of inflammatory responses. Recent work by Nguyen H.C.B. et al. demonstrated that histone deacetylase 3 (HDAC3) may activate either inflammatory or anti-inflammatory genes depending on the nature of the transcription factor being recruited (155).

The issue of targeted delivery of immune-modulating medications during MI also needs to be elaborated to avoid undesirable systemic effects. Current approaches propose to use hydrogels, patches, inhaled nano-particles, extracellular vesicles including exosomes and are reviewed in detail elsewhere (156).

TABLE 1 | Summary characteristics of immune cells involved in development and resolution of inflammation in acute myocardial infarction.

Cell types	Development of inflammation				References	Resolution of inflammation				References
	Subpopulations	Surface Markers	Active molecules	Effector activity		Subpopulations	Surface Markers	Active molecules	Effector activity	
Neutrophils	N1-neutrophils	CD11b CD16 CD15 CD87	MPO ROS leukotrines	NETosis Degranulation Phagocytosis	(31, 34, 36, 37)	N2-neutrophils	CD11b CD206+ ?	VEGF MMP-9 MMP-12	Macrophages polarization Angiogenesis	(31, 43, 45, 149)
						N1-neutrophils	CD11b CD16 CD15 CD87	resolvins annexin A1 lipocalin lactoferrin cathelicidin	SPM synthesis Formation of apoptotic bodies	(17, 18, 29, 31, 32, 40)
Eosinophils	Inflammatory eosinophils?	Siglec-F^{hi} (mice)	ROS	EETosis	(47, 52)	Regulatory eosinophils?	Siglec-F^{int} (mice)	IL-4	Macrophages polarization	(13, 49, 51, 53, 54)
		CD62L–	major basic protein	Degranulation			Siglec-8+ (humans)	TGF-β	Angiogenesis	
		CD49d	eosinophil cationic protein	Oxidative burst			CD62L+	VEGF		
		CD101^{hi}	eosinophil peroxidase				CD101^{lo}	FGF		
			arachidonic acid derivatives				?	resolvin RvE3 protectin D1		
			IL-5							
Monocytes	Classical monocytes	CD14++CD16^{neg}/ Ly-6C^{hi} (mice)	TNF-α	Secretion of inflammatory cytokines	(12, 67)	Non-classical monocytes	CD14+CD16^{hi}/Ly-6C^{lo}	VEGF	Secretion of anti-inflammatory and angiogeneic cytokines	(12, 67)
	Intermediate monocytes	CD14++CD16^{hi}	IL-1β				CXC3R1	TGF-β		
		CCR2	IL-6							
		TIE-2	NO							
Macrophages	M1-macrophages?	CD68	IL-12	Phagocytosis	(12, 70)	M2- macrophages (M2a, M2b, M2c)?	CD206	IL-10	Secretion of anti-inflammatory and angiogeneic cytokines	(72, 73, 75, 78)
		MHC II	IL-23	Secretion of inflammatory cytokines		CD163	IL-1Ra			
		CD86	ROS			Stabilin-1	TGF-β			
			NO				VEGF			
			leukotriens				Arginase			
							SPM (resolvins, maresins, lipoxins, protectins)	SPM synthesis Efferocytosis		
Mast cells	MC$_{CT}$	CD64	cathepsin G	Secretion of inflammatory cytokines	(84, 87)	?	?	chymase	Regulation of fibrosis	(84, 90, 91)
		CD117	carboxypeptidase histamine TNF-α IL-6 IFN-γ	Degranulation Collagen degradation				tryptase bFGF IL-10 IL-13 VEGF-A		
Dendritic cells	pDC	MHC II	IL-23	Antigen presentation to Th1/Th2/TH17	(92, 93, 95)	Tolerogenic DC	MHC IIlow	IDO	Antigen presentation to Treg	(98–101)
	cDC	CD80/CD86		Secretion of inflammatory cytokines			CD80/CD86low	IL-10	Inhibition of TCR signaling	
	moDC	CD1c/CD11b (mice) CD141/CD103 (mice)					PDL-1,-2	TGF-β		
							CTLA-4	galectin-1		
								pentraxin 3		

(Continued)

TABLE 1 | Continued

Cell types	Development of inflammation				References	Resolution of inflammation				References
	Subpopulations	Surface Markers	Active molecules	Effector activity		Subpopulations	Surface Markers	Active molecules	Effector activity	
T-lymphocytes	CD4+ T-helper	CD3	IFN-γ (in CD4+ Th)	Autoreactivity	(104, 105, 109, 111, 112)	Tregs	CTLA-4	TGF-β	Secretion of anti-inflammatory cytokines	(102, 104, 110, 114, 115, 118)
	CD8+ T-cytotoxic	CD4	IL-17 (in CD4+ Th and γδ T cells)	Secretion of inflammatory cytokines		AT2R+ T cells	PD-1	IL-10	Apoptosis of inflammatory cells	
	γδ T cells	CD8	perforins (in CD8+ Tc)	Cytotoxicity in cardiomyocytes?			BTLA	IL-35	Increase of extracellular adenosine	
		γδ TCR	granzymes (in CD8+ Tc)				CD39			
							CD73			
Myeloid-derived suppressor cells	?	?	?	?	?	PMN-MDSC	HLADR-CD14-CD15 +CD11b+	IL-10	Immune suppression?	(124, 126–128)
						M-MDSC	CD33+CD14+CD11b+	NO		
						eMDSC	Lin-CD33+CD11b+	TGF-β		
								IDO		
								arginase 1		
B-lymphocytes	B1-lymphocytes	CD19	IgM	Antibody production	(134, 136)	regulatory B-lymphocytes	Tim-1	IL-10	Secretion of anti-inflammatory cytokines?	(138)
	B2-lymphocytes		IgG	Chemokines production				TGF-β?		
			CCL7					IL-35?		
NK-cells	?	CD69	IFN-γ	Secretion of inflammatory cytokines	(139–141)	?	Inhibitory receptors:	IL-13	Secretion of anti-inflammatory cytokines	(139, 143, 144)
		Activating receptors:	TNF-α	Recognition of DAMPs			KIR	IL-10	Recognition of "self"-molecules	
		NKp44	perforin	Cytolysis			NKG-2A		Prevention of cytolysis	
		NKG2D	granzyme							
		CD226								
iNKT	?	Activating receptors	IL-17	Secretion of inflammatory cytokines	(145)	?	Inhibitory receptors	IL-4	Secretion of anti-inflammatory cytokines	(147)
		Invariant αβ-TCR	IFN-γ	Recognition of DAMPs				IL-10	Recognition of "self"-molecules	
				Cytolysis					Prevention of cytolysis	

BTLA, B- and T-lymphocyte attenuator; CCL, CC chemokine ligand; CCR, C-C chemokine receptor; CD, cluster of differentiation; CTLA, cytotoxic T-lymphocyte-associated protein; DAMP, damage associated molecular pattern; DC, dendritic cells; IDO, indoleamine 2,3-dioxygenase; IFN, interferon; Ig, immunoglobulin; IL, interleukin; KIR, killer cell immunoglobulin-like receptor; Lin, lineage; MC, mast cell; MHC, major histocompatibility complex; MMP, matrix metalloproteinase; MPO, myeloperoxidase; NKG2D, natural killer group 2 member D; NO, nitric oxide; PDL, programmed death ligand; ROS, reactive oxygen species; SPM, specialized pro-resolving mediators; TCR, T-cell receptor; TGF, transforming growth factor; TNF, tumor necrosis factor; VEGF, vascular endothelial growth factor. Question marks indicate absent or incomplete data and facts that have not been sufficiently studied for myocardial infarction.

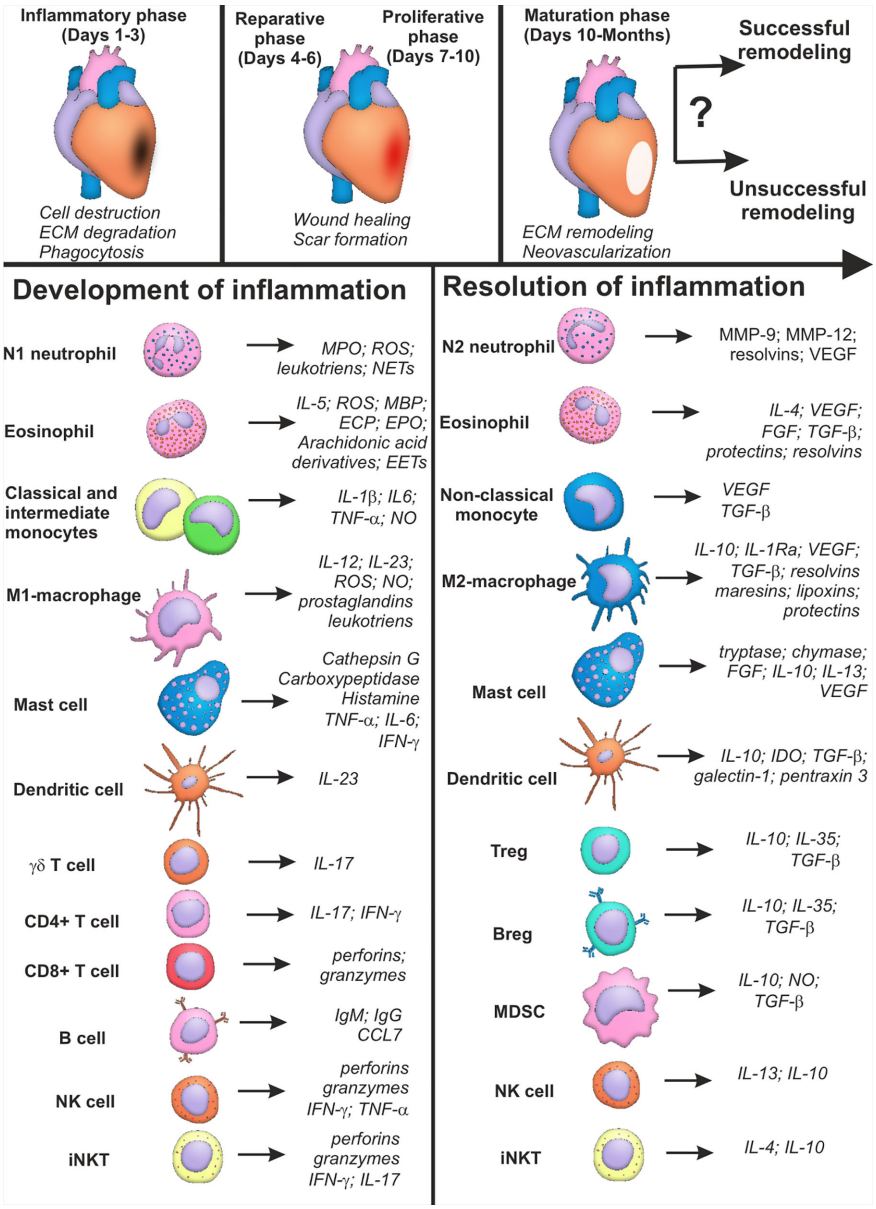

FIGURE 1 | Summary characteristics of immune cells involved in development and resolution of inflammation post-myocardial infarction. Cells of the immune system may input either successful or unsuccessful myocardial remodeling after myocardial infarction, being involved in all the three phases of cardiac repair: inflammatory phase; reparative and proliferative phase; maturation phase. Some cellular populations (monocytes, macrophages, lymphocytes) are represented by two or more subsets with opposite or complementary effects. At the same time, some immune cells may exhibit either inflammatory or reparative properties, depending on the nature of the signal and cellular milieu (eosinophils, dendritic cells, mast cells, NK cells, iNKT cells). Possibility exists that new distinct subpopulations of immune cells are yet to be described, and inflammatory and reparative functions will further be ascribed to different cellular subsets. CCL CC, Chemokine ligand; CD, Cluster of differentiation; ECP, Eosinophil cationic protein; FGF, Fibroblast growth factor; IFN, Interferon; Ig, Immunoglobulin; IL, Interleukin; IL-1Ra, Interleukin-1 receptor antagonist; MBP, Major basic protein; MMP, Matrix metalloproteinase; MPO, Myeloperoxidase; NO, Nitric oxide; ROS, Reactive oxygen species; TGF, Transforming growth factor; TNF, Tumor necrosis factor; VEGF, Vascular endothelial growth factor; Question marks indicate absent or incomplete data and facts that have not been sufficiently studied for myocardial infarction.

All the above mentioned techniques have certain dangers and drawbacks and require further studies of the bioavailability and safety in clinics.

New diagnostic approaches, such as fluorescence-based techniques, single-cell RNA sequencing and mass spectrometry imaging and profiling, which become more and more widespread and affordable, allow to evaluate single cell metabolomics and transcriptomics and propose personalized targeted ways of metabolic and epigenetic reprogramming depending on the initial state of immunometabolism (157, 158).

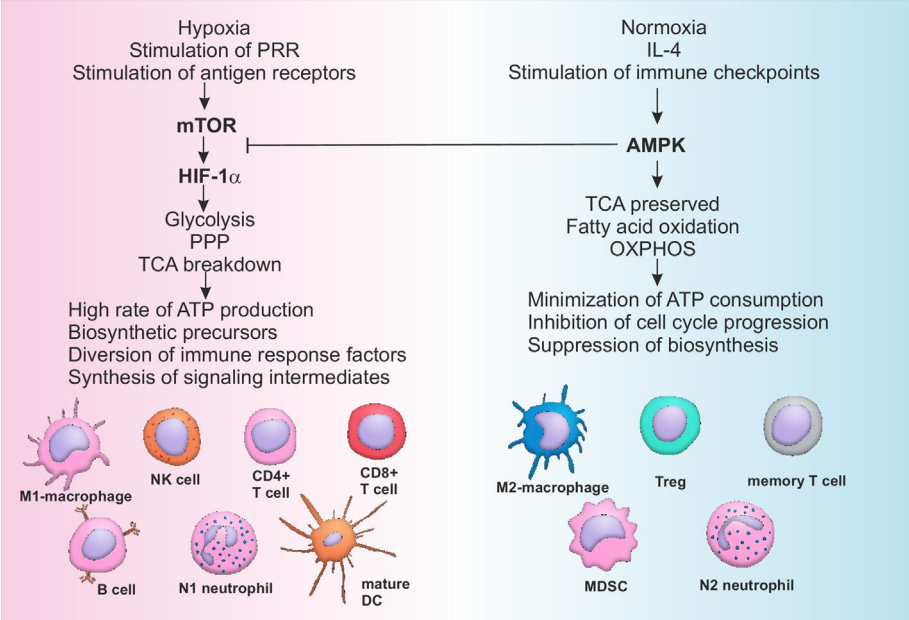

FIGURE 2 | Pathways of metabolic reprogramming in immune cells. Activation of mTOR during hypoxia and stimulation of PRR by DAMPs or antigen receptors on T- and B-lymphocytes by antigens leads to the sustained stimulation of HIF-1α, which in turn activates glycolysis and pentose-phosphate pathway, breaking down tricarboxylic acid (TCA) cycle. All of the above mentioned metabolic pathways are associated with high rate of ATP production, generation of biosynthetic precursors (nucleotides, fatty acids, ribose, amino acids), diversion of immune suppressive factors such as phosphoenolpyruvate into glycolytic pathway and production of cofactors (such as NADH). As a consequence cells of the immune system are activated and acquire inflammatory phenotype. Restoration of the normal oxygen supply or anti-inflammatory signaling, sometimes combined with checkpoint (PD-1) activation, stimulates AMPK, characterized by the suppressive activity towards mTOR. AMPK supports integrity of TCA, stimulates OXPHOS and fatty acid oxidation, minimizing ATP consumption and inhibiting cell cycle and biosynthesis. Switching from catabolism to anabolism represents a stimulus for the development of anti-inflammatory and memory cells. AMPK, AMP activated protein kinase; ATP, Adenosine triphosphate; CD, Cluster of differentiation; DC, Dendritic cell; HIF, Hypoxia induced factor; IL, Interleukin; MDSC, Myeloid derived suppressor cell; mTOR, Mammalian target of rapamycin; OXPHOS, Oxidative phosphorylation; PPP, Pentose phosphate pathway; PRR, Pattern recognition receptors; TCA, Tricarboxylic acid cycle; Treg, T regulatory lymphocytes.

In the perspective it might be possible to find a powerful signaling mechanism to manipulate cellular heterogeneity in the course of the immune response during AMI and influence not only a single subpopulation, but redirect functional activity of the whole cellular diversity in a desired way. Identification of molecules that may be used during AMI to obtain time-dependent equilibrium in immune regulation through metabolic and epigenetic rearrangement represents a promising area of future research.

CONCLUDING REMARKS

Increase of patients' survival after AMI is associated with spread of HF frequency in population. Hence study of consequences of cellular response to myocardial injury will remain an important research area withholding both fundamental and practical significance. Summarizing our review, we can state that there are no "good" or "bad" players in the realm of the immune cells involved in myocardial remodeling after infarction. Each subset of immune cells present in the heart may either increase injury and inflammation or initiate healing of the cardiac tissue. Suppression of inflammation *via* total depletion of a definite cellular subset has not been associated with a more favorable outcome, or has led to inconsistent results. Rather, keeping a time-dependent balance in the work of immune cells, when inflammatory activity is followed by timely switching on of the resolution and reparative mechanisms, is what matters in the successful heart healing and remodeling following infarction.

The substantial question remains, which is the nature of the factors that orchestrate the preservation of the balanced immune response during myocardial infarction, and which are the factors that lead to the impairments in this process? We need to keep in mind, that patients face myocardial infarction already having a dramatic background of various health problems, including but not limited to atherosclerosis, other chronic inflammatory disorders, metabolic disturbances, increased blood pressure, aging, history of smoking and chronic stress, etc., all of which being associated with immune dysregulation of various kind and different scale. The amount of fundamental and clinical data obtained in the field up to date is enormous, but does not lead to the significant improvements. We need to admit that further breakthrough in management of post-infarction remodeling

requires a novel instrument to systematize an exciting data. Possible solution may be the use of high-throughput methods and artificial intelligence to develop "digital counterparts" of inflammation which will allow creation of "inflammatory portrait" for each patient and identification of an existing gap in the work of immune cells in each single case. As a matter of fact, this foreshadows the end of the population-based medicine and beginning of the personalized medicine era.

AUTHOR CONTRIBUTIONS

VR and TS conceived the concept and designed the manuscript outline. IV and MS wrote the manuscript. IV prepared figures. TS and VR performed critical evaluation of the manuscript. IV prepared manuscript for publication. All authors contributed to the article and approved the submitted version.

FUNDING

This work was supported by the Ministry of Science and Higher Education of the Russian Federation [theme of fundamental research AAAA-A15-115123110026-3].

ACKNOWLEDGMENTS

The authors thank Anna Anikina for technical assistance in the production of figures in the manuscript.

REFERENCES

1. Johansson S, Rosengren A, Young K, Jennings E. Mortality and morbidity trends after the first year in survivors of acute myocardial infarction: a systematic review. *BMC Cardiovasc Disord* (2017) 17:53. doi: 10.1186/s12872-017-0482-9
2. Bahit MC, Kochar A, Granger CB. Post-Myocardial Infarction Heart Failure. *J Am Coll Cardiol HF* (2018) 6:179–86. doi: 10.1016/j.jchf.2017.09.015
3. Gerber Y, Weston SA, Berardi C, McNallan SM, Jiang R, Redfield MM, et al. Contemporary trends in heart failure with reduced and preserved ejection fraction after myocardial infarction: a community study. *Am J Epidemiol* (2013) 178:1272–80. doi: 10.1093/aje/kwt109
4. van der Bijl P, Abou R, Goedemans L, Gersh BJ, Holmes DR, Marsan NA, et al. Left ventricular post-infarct remodeling. *J Am Coll Cardiol HF* (2020) 8:131–40. doi: 10.1016/j.jchf.2019.08.014
5. Neri M, Riezzo I, Pascale N, Pomara C, Turillazzi E. Ischemia/reperfusion injury following acute myocardial infarction: a critical issue for clinicians and forensic pathologists. *Mediators Inflamm* (2017) 2017:7018393. doi: 10.1155/2017/7018393
6. Karpov RS, Popov SV, Markov VA, Suslova TE, Ryabov VV, Poponina YS, et al. Autologous mononuclear cells in restorative regeneration during acute myocardial infarction. *Bull Exp Biol Med* (2005) 4:239–43. doi: 10.1007/s10517-006-0043-1
7. Gori AM, Cesari F, Marcucci R, Giusti B, Paniccia R, Antonucci E, et al. The balance between pro- and anti-inflammatory cytokines is associated with platelet aggregability in acute coronary syndrome patients. *Atherosclerosis* (2009) 202:255–62. doi: 10.1016/j.atherosclerosis.2008.04.001
8. Frangogiannis NG. The inflammatory response in myocardial injury, repair, and remodeling. *Nat Rev Cardiol* (2014) 11:255–65. doi: 10.1038/nrcardio.2014.28
9. Sutton MG, Sharpe N. Left ventricular remodeling after myocardial infarction: pathophysiology and therapy. *Circulation* (2000) 101:2981–8. doi: 10.1161/01.cir.101.25.2981
10. Prabhu SD, Frangogiannis NG. The biological basis for cardiac repair after myocardial infarction. *Circ Res* (2016) 119:91–112. doi: 10.1161/CIRCRESAHA.116.303577
11. Yoshimura C, Nagasaka A, Kurose H, Nakaya M. Efferocytosis during myocardial infarction. *J Biochem* (2020) 168(1):1–6. doi: 10.1093/jb/mvaa051
12. Peet C, Ivetic A, Bromage DI, Shah AM. Cardiac monocytes and macrophages after myocardial infarction. *Cardiovasc Res* (2020) 116:1101–12. doi: 10.1093/cvr/cvz336
13. Isobe Y, Kato T, Arita M. Emerging roles of eosinophils and eosinophil-derived lipid mediators in the resolution of inflammation. *Front Immunol* (2012) 3:270. doi: 10.3389/fimmu.2012.00270
14. Halade GV, Tourki B. Specialized pro-resolving mediators directs cardiac healing and repair with activation of inflammation and resolution program in heart failure. *Adv Exp Med Biol* (2019) 1161:45–64. doi: 10.1007/978-3-030-21735-8_6
15. Serhan CN, Levy BD. Resolvins in inflammation: emergence of the pro-resolving superfamily of mediators. *J Clin Invest* (2018) 128(7):2657–69. doi: 10.1172/JCI97943
16. Fosshaug LE, Colas RA, Anstensrud AK, Gregersen I, Nymo S, Sagen EL, et al. Early increase of specialized pro-resolving lipid mediators in patients with ST-elevation myocardial infarction. *EBioMedicine* (2019) 46:264–73. doi: 10.1016/j.ebiom.2019.07.024
17. Jadapalli JK, Halade GV. Unified nexus of macrophages and maresins in cardiac reparative mechanisms. *FASEB J* (2018) 32:5227–37. doi: 10.1096/fj.201800254R
18. Markworth JF, Maddipati KR, Cameron-Smith D. Emerging roles of pro-resolving lipid mediators in immunological and adaptive responses to exercise-induced muscle injury. *Exerc Immunol Rev* (2016) 22:110–34. Available at: https://pubmed.ncbi.nlm.nih.gov/26856678.
19. Buckley CD, Gilroy DW, Serhan CN. Proresolving lipid mediators and mechanisms in the resolution of acute inflammation. *Immunity* (2014) 40(3):315–27. doi: 10.1016/j.immuni.2014.02.009
20. Chiurchiù V, Leuti A, Dalli J, Jacobsson A, Battistini L, Maccarrone M, et al. Proresolving lipid mediators resolvin D1, resolvin D2, and maresin 1 are critical in modulating T cell responses. *Sci Transl Med* (2016) 8(353):353ra111. doi: 10.1126/scitranslmed.aaf7483
21. Halade GV, Norris PC, Kain V, Serhan CN, Ingle KA. Splenic leukocytes define the resolution of inflammation in heart failure. *Sci Signal* (2018) 11(520):eaao1818. doi: 10.1126/scisignal.aao1818
22. Halade GV, Kain V, Dillion C, Beasley M, Dudenbostel T, Oparil S, et al. Race-based and sex-based differences in bioactive lipid mediators after myocardial infarction. *ESC Heart Fail* (2020) 7(4):1700–10. doi: 10.1002/ehf2.12730
23. Keyes KT, Ye Y, Lin Y, Zhang C, Perez-Polo JR, Gjorstrup P, et al. Resolvin E1 protects the rat heart against reperfusion injury. *Am J Physiol Heart Circ Physiol* (2010) 299(1):H153–64. doi: 10.1152/ajpheart.01057.2009
24. Kain V, Ingle KA, Colas RA, Dalli J, Prabhu SD, Serhan CN, et al. Resolvin D1 activates the inflammation resolving response at splenic and ventricular site following myocardial infarction leading to improved ventricular function. *J Mol Cell Cardiol* (2015) 84:24–35. doi: 10.1016/j.yjmcc.2015.04.003
25. Liu G, Liu Q, Shen Y, Kong D, Gong Y, Tao B, et al. Early treatment with Resolvin E1 facilitates myocardial recovery from ischaemia in mice. *Br J Pharmacol* (2018) 175(8):1205–16. doi: 10.1111/bph.14041
26. Tourki B, Kain V, Pullen AB, Norris PC, Patel N, Arora P, et al. Lack of resolution sensor drives age-related cardiometabolic and cardiorenal defects and impedes inflammation-resolution in heart failure. *Mol Metab* (2020) 31:138–49. doi: 10.1016/j.molmet.2019.10.008
27. de Jong RCM, Pluijmert NJ, de Vries MR, Pettersson K, Atsma DE, Jukema JW, et al. Annexin A5 reduces infarct size and improves cardiac function

after myocardial ischemia-reperfusion injury by suppression of the cardiac inflammatory response. *Sci Rep* (2018) 8(1):6753. doi: 10.1038/s41598-018-25143-y
28. Wu Y, Zhang Y, Zhang J, Zhai T, Hu J, Luo H, et al. Cathelicidin aggravates myocardial ischemia/reperfusion injury via activating TLR4 signaling and P2X7R/NLRP3 inflammasome. *J Mol Cell Cardiol* (2020) 139:75–86. doi: 10.1016/j.yjmcc.2019.12.011
29. Horckmans M, Ring L, Duchene J, Santovito D, Schloss MJ, Drechsler M, et al. Neutrophils orchestrate post-myocardial infarction healing by polarizing macrophages towards a reparative phenotype. *Eur Heart J* (2017) 38:187–97. doi: 10.1093/eurheartj/ehw002
30. Chen B, Frangogiannis NG. Chemokines in myocardial infarction. *J Cardiovasc Transl Res* (2021) 14(1):35–52. doi: 10.1007/s12265-020-10006-7
31. Ma Y, Yabluchanskiy A, Lindsey ML. Neutrophil roles in left ventricular remodeling following myocardial infarction. *Fibrogen Tissue Repair* (2013) 6:11. doi: 10.1093/cvr/cvw024
32. Jung M, Dodsworth M, Thum T. Inflammatory cells and their non-coding RNAs as targets for treating myocardial infarction. *Basic Res Cardiol* (2019) 114:4. doi: 10.1007/s00395-018-0712-z
33. Daseke MJ, Valerio FM, Kalusche WJ, Ma Y, DeLeon-Pennell KY, Lindsey ML. Neutrophil proteome shifts over the myocardial infarction time continuum. *Basic Res Cardiol* (2019) 114:37. doi: 10.1007/s00395-019-0746-x
34. Hoyer FF, Nahrendorf M. Neutrophil contributions to ischaemic heart disease. *Eur Heart J* (2017) 38:465–72. doi: 10.1093/eurheartj/ehx017
35. Tourki B, Halade G. Leukocyte diversity in resolving and nonresolving mechanisms of cardiac remodeling. *FASEB J* (2017) 31:4226–39. doi: 10.1096/fj.201700109R
36. Koeth RA, Haselden V, Tang WH. Myeloperoxidase in cardiovascular disease. *Adv Clin Chem* (2013) 62:1–32. doi: 10.1016/b978-0-12-800096-0.00001-9
37. Mangold A, Hofbauer TM, Ondracek AS, Artner T, Scherz T, Speidl WS, et al. Neutrophil extracellular traps and monocyte subsets at the culprit lesion site of myocardial infarction patients. *Sci Rep* (2019) 9:16304. doi: 10.1038/s41598-019-52671-y
38. Ge L, Zhou X, Ji WJ, Lu RY, Zhang Y, Zhang YD, et al. Neutrophil extracellular traps in ischemia-reperfusion injury-induced myocardial no-reflow: therapeutic potential of DNase-based reperfusion strategy. *Am J Physiol Heart Circ Physiol* (2015) 308:H500–9. doi: 10.1152/ajpheart.00381.2014
39. Faxon DP, Gibbons RJ, Chronos NA, Gurbel PA, Sheehan F. The effect of blockade of the CD11/CD18 integrin receptor on infarct size in patients with acute myocardial infarction treated with direct angioplasty: the results of the HALT-MI study. *J Am Coll Cardiol* (2002) 40:1199–204. doi: 10.1016/s0735-1097(02)02136-8
40. Frangogiannis NG. Regulation of the inflammatory response in cardiac repair. *Circ Res* (2012) 110:159–73. doi: 10.1161/CIRCRESAHA.111.243162
41. Hoyer FF, Nahrendorf M. Interferon-c regulates cardiacmyeloid cells in myocardial infarction. *Cardiovasc Res* (2019) 115:1815–16. doi: 10.1093/cvr/cvz143
42. Cross A, Moots RJ, Edwards SW. The dual effects of TNFalpha on neutrophil apoptosis are mediated via differential effects on expression of Mcl-1 and Bfl-1. *Blood* (2018) 111:878–84. doi: 10.1182/blood-2007-05-087833
43. Mouton AJ, Rivera Gonzalez OJ, Kaminski AR, Moore ET, Lindsey ML. Matrix metalloproteinase-12 as an endogenous resolution promoting factor following myocardial infarction. *Pharmacol Res* (2018) 137:252–8. doi: 10.1016/j.phrs.2018.10.026
44. Blömer N, Pachel C, Hofmann U, Nordbeck P, Bauer W, Mathes D, et al. 5-Lipoxygenase facilitates healing after myocardial infarction. *Basic Res Cardiol* (2013) 108(4):367. doi: 10.1007/s00395-013-0367-8
45. Daseke MJ, Valerio FM, Kalusche WJ, Ma Y, DeLeon-Pennell KY, Lindsey ML. Neutrophil proteome shifts over the myocardial infarction time continuum. *Basic Res Cardiol* (2019) 114:37. doi: 10.1007/s00395-019-0746-x
46. Silvestre-Roig C, Fridlender ZG, Glogauer M, Scapini P. Neutrophil diversity in health and disease. *Trends Immunol* (2019) 40:565–83. doi: 10.1016/j.it.2019.04.012
47. Ramirez GA, Yacoub MR, Ripa M, Mannina D, Cariddi A, Saporiti N, et al. Eosinophils from physiology to disease: a comprehensive review. *BioMed Res Int* (2018) 2018:9095275. doi: 10.1155/2018/9095275
48. Mesnil C, Raulier S, Paulissen G, Xiao X, Birrell MA, Pirottin D, et al. Lung-resident eosinophils represent a distinct regulatory eosinophil subset. *J Clin Invest* (2016) 126:3279–95. doi: 10.1172/JCI85664
49. Liu J, Yang C, Liu T, Deng A, Fang W, Zheng X, et al. Eosinophils improve cardiac function after myocardial infarction. *Nat Commun* (2020) 11:6396. doi: 10.1038/s41467-020-19297-5
50. Rios-Navarro C, Gavara J, Vidal V, Bonanad C, Racugno P, Bayes-Genis A, et al. Characterization and implications of the dynamics of eosinophils in blood and in the infarcted myocardium after coronary reperfusion. *PLoS One* (2018) 13:e0206344. doi: 10.1371/journal.pone.0206344
51. Wen T, Rothenberg ME. The regulatory function of eosinophils. *Microbiol Spectr* (2016) 4:1. doi: 10.1128/microbiolspec.MCHD-0020-2015
52. Leitch VD, Strudwick XL, Matthaei KI, Dent LA, Cowin AJ. IL-5-overexpressing mice exhibit eosinophilia and altered wound healing through mechanisms involving prolonged inflammation. *Immunol Cell Biol* (2009) 87:131–40. doi: 10.1038/icb.2008.72
53. Xu JY, Xiong YY, Lu XT, Yang YJ. Regulation of Type 2 Immunity in Myocardial Infarction. *Front Immunol* (2019) 10:62. doi: 10.3389/fimmu.2019.00062
54. Toor IS, Rückerl D, Mair I, Ainsworth R, Meloni M, Spiroski AM, et al. Eosinophil deficiency promotes aberrant repair and adverse remodeling following acute myocardial infarction. *JACC Basic Transl Sci* (2020) 5(7):665–81. doi: 10.1016/j.jacbts.2020.05.005
55. Shintani Y, Ito T, Fields L, Shiraishi M, Ichihara Y, Sato N, et al. IL-4 as a Repurposed Biological Drug for Myocardial Infarction through Augmentation of Reparative Cardiac Macrophages: Proof-of-Concept Data in Mice. *Sci Rep* (2017) 7:6877. doi: 10.1038/s41598-017-07328-z
56. Arfvidsson J, Ahlin F, Vargas KG, Thaler B, Woijta J, Huber K. Monocyte subsets in myocardial infarction: A review. *Int J Cardiol* (2017) 231:47–53. doi: 10.1016/j.ijcard.2016.12.182
57. Dick SA, Macklin JA, Nejat S, Momen A, Clemente-Casares X, Althagafi MG, et al. Self-renewing resident cardiac macrophages limit adverse remodeling following myocardial infarction. *Nat Immunol* (2019) 20:29–39. doi: 10.1038/s41590-018-0272-2
58. Dutta P, Nahrendorf M. Monocytes in myocardial infarction. *Arterioscler Thromb Vasc Biol* (2015) 35:1066–70. doi: 10.1161/ATVBAHA.114.304652
59. Li W, Hsiao H-M, Higashikubo R, Saunders BT, Bharat A, Goldstein SR, et al. Heart-resident CCR2+ macrophages promote neutrophil extravasation through TLR9/MyD88/CXCL5 signaling. *JCI Insight* (2016) 1(12):e87315. doi: 10.1172/jci.insight.87315
60. Majmudar MD, Keliher EJ, Heidt T, Leuschner F, Truelove J, Sena BF, et al. Monocyte-directed RNAi targeting CCR2 improves infarct healing in atherosclerosis-prone mice. *Circulation* (2013) 127:2038–46. doi: 10.1161/CIRCULATIONAHA.112.000116
61. Tsujioka H, Imanishi T, Ikejima H, Kupri A, Takarada S, Tanimoto T, et al. Impact of heterogeneity of human peripheral blood monocyte subsets on myocardial salvage in patients with primary acute myocardial infarction. *J Am Coll Cardiol* (2009) 54:130–8. doi: 10.1016/j.jacc.2009.04.021
62. van Amerongen MJ, Harmsen MC, van Rooijen N, Petersen AH, van Luyn MJ. Macrophage depletion impairs wound healing and increases left ventricular remodeling after myocardial injury in mice. *Am J Pathol* (2007) 170(3):818–29. doi: 10.2353/ajpath.2007.060547
63. Kologrivova I, Suslova T, Koshelskaya O, Trubacheva O, Haritonova O, Vinnitskaya I. Frequency of monocyte subsets is linked to the severity of atherosclerosis in patients with ischemic heart disease: A case-control study. *BioMedicine* (2020) 10:36–47. doi: 10.37796/2211-8039.1015
64. Serbina NV, Pamer EG. Monocyte emigration from bone marrow during bacterial infection requires signals mediated by chemokine receptor CCR2. *Nat Immunol* (2006) 7:311–7. doi: 10.1038/ni1309
65. Nagashimada M, Ni Y, Ota T. Loss of Fractalkine-CX3CR1 Signaling Exacerbates Obesity-Induced Adipose Tissue Inflammation and Insulin Resistance through M1 Dominant Shift in Macrophages. *Diabetes* (2018) 67(1):1989. doi: 10.2337/db18-1989-P
66. Hilgendorf I, Gerhardt LMS, Tan TC, Winter C, Holderried TAW, Chousterman BG, et al. Ly-6C high monocytes depend on Nr4a1 to balance

both inflammatory and reparative phases in the infarcted myocardium. *Circ Res* (2014) 114:1611–22. doi: 10.1161/CIRCRESAHA.114.303204
67. Weinberger T, Schulz C. Myocardial infarction: a critical role of macrophages in cardiac remodeling. *Front Physiol* (2015) 16:107. doi: 10.3389/fphys.2015.00107
68. Panizzi P, Swirski FK, Figueiredo JL, Waterman P, Sosnovik DE, Aikawa E, et al. Impaired infarct healing in atherosclerotic mice with Ly-6C(hi) monocytosis. *J Am Coll Cardiol* (2010) 55:1629–38. doi: 10.1016/j.jacc.2009.08.089
69. Tapp LD, Shantsila E, Wrigley BJ, Pamukcu B, Lip GY. The CD14++CD16+ monocytes subset and monocyte-platelet interactions in patients with ST-elevation myocardial infarction. *J Thromb Haemost* (2012) 10:1231–41. doi: 10.1111/j.1538-7836.2011.04603.x
70. Beyer M, Mallmann MR, Xue J, Staratschek-Jox A, Vorholt D, Krebs W, et al. High-Resolution Transcriptome of Human Macrophages. *PLoS One* (2012) 7(9):e45466. doi: 10.1371/journal.pone.0045466
71. Murray PJ, Allen JE, Biswas SK, Fisher EA, Gilroy DW, Goerdt S, et al. Macrophage activation and polarization: nomenclature and experimental guidelines. *Immunity* (2014) 41(1):14–20. doi: 10.1016/j.immuni.2014.06.008
72. Gombozhapova A, Rogovskaya Y, Shurupov V, Rebenkova M, Kzhyshkowska J, Popov SV, et al. Macrophage activation and polarization in post-infarction cardiac remodeling. *J BioMed Sci* (2017) 24:13. doi: 10.1186/s12929-017-0322-3
73. Korns D, Frasch SC, Fernandez-Boyanapalli R, Henson PM, Bratton DL. Modulation of macrophage efferocytosis in inflammation. *Front Immunol* (2011) 2:57. doi: 10.3389/fimmu.2011.00057
74. Green D, Oguin T, Martinez J. The clearance of dying cells: table for two. *Cell Death Differ* (2016) 23:915–26. doi: 10.1038/cdd.2015.172
75. DeBerge M, Zhang S, Glinton K, Grigoryeva L, Hussein I, Vorovich E, et al. Efferocytosis and outside-in signaling by cardiac phagocytes. Links to repair, cellular programming, and intercellular crosstalk in heart. *Front Immunol* (2017) 8:1428. doi: 10.3389/fimmu.2017.01428
76. Wan E, Yeap XY, Dehn S, Terry R, Novak M, Zhang S, et al. Enhanced efferocytosis of apoptotic cardiomyocytes through myeloid-epithelial-reproductive tyrosine kinase links acute inflammation resolution to cardiac repair after infarction. *Circ Res* (2013) 113(8):1004–12. doi: 10.1161/CIRCRESAHA.113.301198
77. Dehn S. Thorp EB Myeloid receptor CD36 is required for early phagocytosis of myocardial infarcts and induction of Nr4a1-dependent mechanisms of cardiac repair. *FASEB J* (2018) 32:254–64. doi: 10.1096/fj.201700450R
78. Ryabov V, Gombozhapova A, Rogovskaya Y, Kzhyshkowska J, Rebenkova M, Karpov R. Cardiac CD68+ and stabilin-1+ macrophages in wound healing following myocardial infarction: From experiment to clinic. *Immunobiology* (2018) 223:413–21. doi: 10.1016/j.imbio.2017.11.006
79. Shiraishi M, Shintani Y, Shintani Y, Ishida H, Saba R, Yamaguchi A, et al. Alternatively activated macrophages determine repair of the infarcted adult murine heart. *J Clin Invest* (2016) 126:2151–66. doi: 10.1172/JCI85782
80. Courties G, Heidt T, Sebas M, Iwamoto Y, Jeon D, Truelove J, et al. In vivo silencing of the transcription factor IRF5 reprograms the macrophage phenotype and improves infarct healing. *J Am Cardiol* (2014) 40:274–88. doi: 10.1016/j.jacc.2013.11.023
81. Yang M, Song L, Wang L, Yukht A, Ruther H, Li F, et al. Deficiency of GATA3-positive macrophages improves cardiac function following myocardial infarction or pressure overload hypertrophy. *J Am Coll Cardiol* (2018) 72:885–904. doi: 10.1016/j.jacc.2018.05.061
82. Roussel M, Ferrell PBJr, Greenplate AR, Lhomme F, Le Gallou S, Diggins KE, et al. Mass cytometry deep phenotyping of human mononuclear phagocytes and myeloid-derived suppressor cells from human blood and bone marrow. *J Leukoc Biol* (2017) 102:437–47. doi: 10.1189/jlb.5MA1116-457R
83. Walter W, Alonso-Herranz L, Trappetti V, Crespo I, Ibberson M, Cedenilla M, et al. Deciphering the dynamic transcriptional and post-transcriptional networks of macrophages in the healthy heart and after myocardial injury. *Cell Rep* (2018) 23:622–36. doi: 10.1016/j.celrep.2018.03.029
84. Legere SA, Haidl ID, Légaré JF, Marshall JS. Mast cells in cardiac fibrosis: new insights suggest opportunities for intervention. *Front Immunol* (2019) 10:580. doi: 10.3389/fimmu.2019.00580
85. Hermans MAW, Roeters van Lennep JE, van Daele PLA, Bot I. Mast cells in cardiovascular disease: from bench to bedside. *Int J Mol Sci* (2019) 20:3395. doi: 10.3390/ijms20143395
86. Kupreishvili K, Fuijkschot WW, Vonk AB, Smulders YM, Stooker W, Van Hinsbergh VW, et al. Mast cells are increased in the media of coronary lesions in patients with myocardial infarction and may favor atherosclerotic plaque instability. *J Cardiol* (2017) 69:548–54. doi: 10.1016/j.jjcc.2016.04.018
87. Janicki JS, Brower GL, Levick SP. The emerging prominence of the cardiac mast cell as a potent mediator of adverse myocardial remodeling. *Methods Mol Biol* (2015) 1220:121–39. doi: 10.1007/978-1-4939-1568-2_8
88. Jaggi AS, Singh M, Sharma A, Singh D, Singh N. Cardioprotective effects of mast cell modulators in ischemia-reperfusion- induced injury in rats. *Methods Find Exp Clin Pharmacol* (2007) 29:593–600. doi: 10.1358/mf.2007.29.9.1161005
89. Kim J, Ogai A, Nakatani S, Hashimura K, Kanzaki H, Komamura K, et al. Impact of blockade of histamine H2 receptors on chronic heart failure revealed by retrospective and prospective randomized studies. *J Am Coll Cardiol* (2006) 48:1378–84. doi: 10.1016/j.jacc.2006.05.069
90. Murray DB, McLarty-Williams J, Nagalla KT, Janicki JS. Tryptase activates isolated adult cardiac fibroblasts via protease activated receptor-2 (PAR-2). *J Cell Commun Signal* (2012) 6(1):45–51. doi: 10.1007/s12079-011-0146-y
91. Sugimoto MA, Sousa LP, Pinho V, Perretti M, Teixeira MM. Resolution of Inflammation: What Controls Its Onset? *Front Immunol* (2016) 7:160. doi: 10.3389/fimmu.2016.00160
92. Patente TA, Pinho MP, Oliveira AA, Evangelista GCM, Bergami-Santos PC, Barbuto JAM. Human dendritic cells: their heterogeneity and clinical application potential in cancer immunotherapy. *Front Immunol* (2019) 9:3176. doi: 10.3389/fimmu.2018.03176
93. Musumeci A, Lutz K, Winheim E, Krug AB. What makes a pDC: recent advances in understanding plasmacytoid DC development and heterogeneity. *Front Immunol* (2019) 10:1222. doi: 10.3389/fimmu.2019.01222
94. Lee JS, Jeong SJ, Kim S, Chalifour L, Yun TJ, Miah MA, et al. Conventional dendritic cells impair recovery after myocardial infarction. *J Immunol* (2018) 201:1784–98. doi: 10.4049/jimmunol.1800322
95. Van der Borght K, Scott CL, Nindl V, Bouché A, Martens L, Sichien D, et al. Myocardial infarction primes autoreactive T cells through activation of dendritic cells. *Cell Rep* (2017) 18:3005–17. doi: 10.1016/j.celrep.2017.02.079
96. Liu H, Gao W, Yuan J, Wu C, Yao K, Zhang L, et al. Exosomes derived from dendritic cells improve cardiac function via activation of CD4(+) T lymphocytes after myocardial infarction. *J Mol Cell Cardiol* (2016) 91:123–33. doi: 10.1016/j.yjmcc.2015.12.028
97. Wei G, Jie Y, Haibo L, Chaoneng W, Dong H, Jianbing Z, et al. Dendritic cells derived exosomes migration to spleen and induction of inflammation are regulated by CCR7. *Sci Rep* (2017) 7:42996. doi: 10.1038/srep42996
98. Zhu R, Sun H, Yu K, Zhong Y, Shi H, Wei Y, et al. Interleukin-37 and dendritic cells treated with interleukin-37 plus troponin I ameliorate cardiac remodeling after myocardial infarction. *J Am Heart Assoc* (2016) 5:e004406. doi: 10.1161/JAHA.116.004406
99. Choo EH, Lee JH, Park EH, Park HE, Jung NC, Kim TH, et al. Infarcted myocardium-primed dendritic cells improve remodeling and cardiac function after myocardial infarction by modulating the regulatory T cell and macrophage polarization. *Circulation* (2017) 135:1444–57. doi: 10.1161/CIRCULATIONAHA.116.023106
100. Barbati E, Specchia C, Villella M, Rossi ML, Barlera S, Bottazzi B, et al. Influence of pentraxin 3 (PTX3) genetic variants on myocardial infarction risk and PTX3 plasma levels. *PLoS One* (2012) 7(12):e53030. doi: 10.1371/journal.pone.0053030
101. Sundblad V, Morosi LG, Geffner JR, Rabinovich GA. Galectin-1: A Jack-of-All-Trades in the Resolution of Acute and Chronic Inflammation. *J Immunol* (2017) 199(11):3721–30. doi: 10.4049/jimmunol.1701172
102. Hofmann U, Frantz S. Role of T-cells in myocardial infarction. *Eur Heart J* (2016) 37:873–9. doi: 10.1093/eurheartj/ehv639
103. Lai S, Marín-Juez R, Stainier DYR. Immune responses in cardiac repair and regeneration: a comparative point of view. *Cell Mol Life Sci* (2019) 76:1365–80. doi: 10.1007/s00018-018-2995-5

104. Yang Z, Day YJ, Toufektsian MC, Xu Y, Ramos SI, Marshall MA, et al. Myocardial infarct-sparing effect of adenosine A2A receptor activation is due to its action on CD4+ T lymphocytes. *Circulation* (2006) 114:2056–64. doi: 10.1161/CIRCULATIONAHA.106.649244
105. Yan X, Shichita T, Katsumata Y, Matsuhashi T, Ito H, Ito K, et al. Deleterious effect of the IL-23/IL-17A axis and γδT cells on left ventricular remodeling after myocardial infarction. *J Am Heart Assoc* (2012) 1:e004408. doi: 10.1161/JAHA.112.004408
106. Li C, Zong W, Zhang M, Tu Y, Zhou Q, Ni M, et al. Increased Ratio of Circulating T-Helper 1 to T-Helper 2 Cells and Severity of Coronary Artery Disease in Patients with Acute Myocardial Infarction: A Prospective Observational Study. *Med Sci Monit* (2019) 25:6034–42. doi: 10.12659/MSM.913891
107. Reynolds JM, Dong C. Toll-like receptor regulation of effector T lymphocyte function. *Trends Immunol* (2013) 34:511–9. doi: 10.1016/j.it.2013.06.003
108. Angelini G, Flego D, Vinci R, Pedicino D, Trotta F, Ruggio A, et al. Matrix metalloproteinase-9 might affect adaptive immunity in non-ST segment elevation acute coronary syndromes by increasing CD31 cleavage on CD4 + T-cells. *Eur Heart J* (2018) 39:1089–97. doi: 10.1093/eurheartj/ehx684
109. Liao YH, Cheng X. Autoimmunity in myocardial infarction. *Int J Cardiol* (2006) 112:21–6. doi: 10.1016/j.ijcard.2006.05.009
110. Rieckmann M, Delgobo M, Gaal C, Büchner L, Steinau P, Reshef D, et al. Myocardial infarction triggers cardioprotective antigen-specific T helper cell responses. *J Clin Invest* (2019) 129:4922–36. doi: 10.1172/JCI123859
111. Boag SE, Das R, Shmeleva EV, Bagnall A, Egred M, Howard N, et al. T lymphocytes and fractalkine contribute to myocardial ischemia/reperfusion injury in patients. *J Clin Invest* (2015) 125:3063–76. doi: 10.1172/JCI80055
112. Savva GM, Pachnio A, Kaul B, Morgan K, Huppert FA, Brayne C, et al. Cytomegalovirus infection is associated with increased mortality in the older population. *Aging Cell* (2013) 12:381–7. doi: 10.1111/acel.12059
113. Ilatovskaya DV, Pitts C, Clayton J, Domondon M, Troncoso M, Pippin S, et al. CD8+ T-cells negatively regulate inflammation post-myocardial infarction. *Am J Physiol Heart Circ Physiol* (2019) 317:H581–96. doi: 10.1152/ajpheart.00112.2019
114. Curato C, Slavic S, Dong J, Skorska A, Altarche-Xifró W, Miteva K, et al. Identification of noncytotoxic and IL-10-producing CD8+AT2R+ T cell population in response to ischemic heart injury. *J Immunol* (2010) 185:6286–93. doi: 10.4049/jimmunol.0903681
115. Skorska A, von Haehling S, Ludwig M, Lux CA, Gaebel R, Kleiner G, et al. The CD4(+) AT2R(+) T cell subpopulation improves post-infarction remodelling and restores cardiac function. *J Cell Mol Med* (2015) 19:1975–85. doi: 10.1111/jcmm.12574
116. Zacchigna S, Martinelli V, Moimas S, Colliva A, Anzini M, Nordio A, et al. Paracrine effect of regulatory T cells promotes cardiomyocyte proliferation during pregnancy and after myocardial infarction. *Nat Commun* (2018) 9:2432. doi: 10.1038/s41467-018-04908-z
117. Dobaczewski M, Xia Y, Bujak M, Gonzalez-Quesada C, Frangogiannis NG. CCR5 signaling suppresses inflammation and reduces adverse remodeling of the infarcted heart, mediating recruitment of regulatory T cells. *Am J Pathol* (2010) 176:2177–87. doi: 10.2353/ajpath.2010.090759
118. Xia N, Jiao J, Tang TT, Lv BJ, Lu YZ, Wang KJ, et al. Activated regulatory T-cells attenuate myocardial ischaemia/reperfusion injury through a CD39-dependent mechanism. *Clin Sci (Lond)* (2015) 128:679–93. doi: 10.1042/CS20140672
119. Weirather J, Hofmann UD, Beyersdorf N, Ramos GC, Vogel B, Frey A, et al. Foxp3+ CD4+ T cells improve healing after myocardial infarction by modulating monocyte/macrophage differentiation. *Circ Res* (2014) 115:55–67. doi: 10.1161/CIRCRESAHA.115.303895
120. Saxena A, Dobaczewski M, Rai V, Haque Z, Chen W, Li N, et al. Regulatory T cells are recruited in the infarcted mouse myocardium and may modulate fibroblast phenotype and function. *Am J Physiol Heart Circ Physiol* (2014) 307:H1233–42. doi: 10.1152/ajpheart.00328.2014
121. Doran AC, Yurdagul A, Tabas I. Efferocytosis in health and disease. *Nat Rev Immunol* (2020) 20:254–67. doi: 10.1038/s41577-019-0240-6
122. Forero-Peña DA, Gutierrez FR. Statins as modulators of regulatory T-cell biology. *Mediators Inflammation* (2013) 2013:167086. doi: 10.1155/2013/167086
123. Tang TT, Yuan J, Zhu ZF, Zhang WC, Xiao H, Xia N, et al. Regulatory T cells ameliorate cardiac remodeling after myocardial infarction. *Basic Res Cardiol* (2012) 107:232. doi: 10.1007/s00395-011-0232-6
124. Bronte V, Brandau S, Chen SH, Colombo MP, Frey AB, Greten TF, et al. Recommendations for myeloid-derived suppressor cell nomenclature and characterization standards. *Nat Commun* (2016) 7:12150. doi: 10.1038/ncomms12150
125. Gabrilovich DI, Nagaraj S. Myeloid-derived suppressor cells as regulators of the immune system. *Nat Rev Immunol* (2009) 9(3):162–74. doi: 10.1038/nri2506
126. Kim T-H, Kang K, Kim EM, Park HE, Park EH, Kim I, et al. Mesenchymal stem cells promote the infiltration of myeloid derived suppressor cells in a mouse myocardial infarction model. *Atherosclerosis* (2017) 263:e60. doi: 10.1016/j.atherosclerosis.2017.06.201
127. Zhang C, Wang S, Li J, Zhang W, Zheng L, Yang C, et al. The mTOR signal regulates myeloid-derived suppressor cells differentiation and immunosuppressive function in acute kidney injury. *Cell Death Dis* (2017) 8:e2695. doi: 10.1038/cddis.2017.86
128. Li F, Zhao Y, Wei L, Li S, Liu J. Tumor-infiltrating Treg, MDSC, and IDO expression associated with outcomes of neoadjuvant chemotherapy of breast cancer. *Cancer Biol Ther* (2018) 19(8):695–705. doi: 10.1080/15384047.2018.1450116
129. Zhou L, Miao K, Yin B, Li H, Fan J, Zhu Y, et al. Cardioprotective role of myeloid-derived suppressor cells in heart failure. *Circulation* (2018) 138:181–97. doi: 10.1161/CIRCULATIONAHA.117.030811
130. Cano RLE, Lopera HDE. "Introduction to T and B lymphocytes". In: JM Anaya, Y Shoenfeld, A Rojas-Villarraga, RA Levy and R Cervera, editors. *Autoimmunity: From Bench to Bedside*. Colombia: El Rosario University Press (2013). p. 77–95.
131. Yu YR, O'Koren EG, Hotten DF, Kan MJ, Kopin D, Nelson ER, et al. A protocol for the comprehensive flow cytometric analysis of immune cells in normal and inflamed murine non-lymphoid tissues. *PloS One* (2016) 11:e0150606. doi: 10.1371/journal.pone.0150606
132. Hofmann U, Frantz S. Role of lymphocytes in myocardial injury, healing, and remodeling after myocardial infarction. *Circ Res* (2015) 116:354–67. doi: 10.1161/CIRCRESAHA.116.304072
133. Yan X, Anzai A, Katsumata Y, Matsuhashi T, Ito K, Endo J, et al. Temporal dynamics of cardiac immune cell accumulation following acute myocardial infarction. *J Mol Cell Cardiol* (2013) 62:24–35. doi: 10.1016/j.yjmcc.2013.04.023
134. Haas MS, Alicot EM, Schuerpf F, Chiu I, Li J, Moore FD, et al. Blockade of self-reactive IgM significantly reduces injury in a murine model of acute myocardial infarction. *Cardiovasc Res* (2010) 87:618–27. doi: 10.1093/cvr/cvq141
135. Ramon S, Gao F, Serhan CN, Phipps RP. Specialized proresolving mediators enhance human B cell differentiation to antibody-secreting cells. *J Immunol* (2012) 189(2):1036–42. doi: 10.4049/jimmunol.1103483
136. Zouggari Y, Ait-Oufella H, Bonnin P, Simon T, Sage AP, Guérin C, et al. B lymphocytes trigger monocyte mobilization and impair heart function after acute myocardial infarction. *Nat Med* (2013) 19:1273–80. doi: 10.1038/nm.3284
137. Goodchild TT, Robinson KA, Pang W, Tondato F, Cui J, Arrington J, et al. Bone marrow-derived B cells preserve ventricular function after acute myocardial infarction. *JACC Cardiovasc Interv* (2009) 2:1005–16. doi: 10.1016/j.jcin.2009.08.010
138. Wu L, Dalal R, Cao CD, Postoak JL, Yang G, Zhang Q, et al. IL-10–producing B cells are enriched in murine pericardial adipose tissues and ameliorate the outcome of acute myocardial infarction. *Proc Natl Acad Sci U S A* (2019) 116:21673–84. doi: 10.1073/pnas.1911464116
139. Ong S, Rose NR, Čihák ová D. Natural killer cells in inflammatory heart disease. *Clin Immunol* (2017) 175:26–33. doi: 10.1016/j.clim.2016.11.010
140. Kossmann S, Schwenk M, Hausding M, Karbach SH, Schmidgen MI, Brandt M, et al. Angiotensin II-induced vascular dysfunction depends on interferon-gamma-driven immune cell recruitment and mutual activation of monocytes and NK-cells. *Arterioscler Thromb Vasc Biol* (2013) 33:1313–9. doi: 10.1161/ATVBAHA.113.301437
141. Knorr M, Munzel T, Wenzel P. Interplay of NK cells and monocytes in vascular inflammation and myocardial infarction. *Front Physiol* (2014) 5:295. doi: 10.3389/fphys.2014.00295

142. Backteman K, Andersson C, Dahlin LG, Ernerudh J, Jonasson L. Lymphocyte subpopulations in lymph nodes and peripheral blood: a comparison between patients with stable angina and acute coronary syndrome. *PLoS One* (2012) 7:e32691. doi: 10.1371/journal.pone.0032691
143. Li W, Lidebjer C, Yuan XM, Szymanowski A, Backteman K, Ernerudh J, et al. NK cell apoptosis in coronary artery disease: relation to oxidative stress. *Atherosclerosis* (2008) 19:65–72. doi: 10.1016/j.atherosclerosis.2007.10.031
144. Boukouaci W, Lauden L, Siewiera J, Dam N, Hocine HR, Khaznadar Z, et al. Natural killer cell crosstalk with allogeneic human cardiac-derived stem/progenitor cells controls persistence. *Cardiovasc Res* (2014) 104:290–302. doi: 10.1093/cvr/cvu208
145. Sobirin MA, Kinugawa S, Takahashi M, Fukushima A, Homma T, Ono T, et al. Activation of natural killer T cells ameliorates postinfarct cardiac remodeling and failure in mice. *Circ Res* (2012) 111:1037–47. doi: 10.1161/CIRCRESAHA.112.270132
146. Liu LL, Lu JL, Chao PL, Lin LR, Zhang ZY, Yang TC. Lower prevalence of circulating invariant natural killer T (iNKT) cells in patients with acute myocardial infarction undergoing primary coronary stenting. *Int Immunopharmacol* (2011) 11:480–4. doi: 10.1016/j.intimp.2010.12.019
147. Liew PX, Lee W-Y, Kubes P. iNKT Cells Orchestrate a Switch from Inflammation to Resolution of Sterile Liver Injury. *Immunity* (2017) 47:752–65. doi: 10.1016/j.immuni.2017.09.016
148. Homma T, Kinugawa S, Takahashi M, Sobirin MA, Saito A, Fukushima A, et al. Activation of invariant natural killer T cells by alpha-galactosylceramide ameliorates myocardial ischemia/reperfusion injury in mice. *J Mol Cell Cardiol* (2013) 62C:179–88. doi: 10.1016/j.yjmcc.2013.06.004
149. Sánchez-Alonso S, Alcaraz-Serna A, Sánchez-Madrid F, Alfranca A. Extracellular vesicle-mediated immune regulation of tissue remodeling and angiogenesis after myocardial infarction. *Front Immunol* (2018) 9:2799. doi: 10.3389/fimmu.2018.02799
150. Tardif JC, Kouz S, Waters DD, Bertrand OF, Diaz R, Maggioni AP, et al. Efficacy and Safety of Low-Dose Colchicine after Myocardial Infarction. *N Engl J Med* (2019) 381:2497–505. doi: 10.1056/NEJMoa1912388
151. Ridker PM, Everett BM, Thuren T, MacFadyen JG, Chang WH, Ballantyne C, et al. CANTOS Trial Group. Antiinflammatory therapy with canakinumab for atherosclerotic disease. *N Engl J Med* (2017) 377:1119–31. doi: 10.1056/NEJMoa1707914
152. Palsson-McDermott EV, O'Neill LAJ. Targeting immunometabolism as an anti-inflammatory strategy. *Cell Res* (2020) 30:300–14. doi: 10.1038/s41422-020-0291-z
153. Zhang S, Bories G, Lantz C, Emmons R, Becker A, Liu E, et al. Immunometabolism of phagocytes and relationships to cardiac repair. *Front Cardiovasc Med* (2019) 6:42. doi: 10.3389/fcvm.2019.00042
154. O'Neill LA, Kishton RJ, Rathmell J. A guide to immunometabolism for immunologists. *Nat Rev Immunol* (2016) 16:553–65. doi: 10.1038/nri.2016.70
155. Nguyen HCB, Adlanmerini M, Hauck AK, Lazar MA. Dichotomous engagement of HDAC3 activity governs inflammatory responses. *Nature* (2020) 584:286–90. doi: 10.1038/s41586-020-2576-2
156. Leoni G, Soehnlein O. (Re) Solving Repair After Myocardial Infarction. *Front Pharmacol* (2018) 9:1342. doi: 10.3389/fphar.2018.01342
157. Yang Y, Huang Y, Wu J, Liu N, Deng J, Luan T. Single-cell analysis by ambient mass spectrometry. *TrAC Trends Anal Chem* (2017) 90:14–26. doi: 10.1016/j.trac.2017.02.009
158. Chaudhry F, Isherwood J, Bawa T, Patel D, Gurdziel K, Lanfear DE, et al. Single-cell RNA sequencing of the cardiovascular system: new looks for old diseases. *Front Cardiovasc Med* (2019) 6:173. doi: 10.3389/fcvm.2019.00173

Conflict of Interest: The authors declare that the research was conducted in the absence of any commercial or financial relationships that could be construed as a potential conflict of interest.

Copyright © 2021 Kologrivova, Shtatolkina, Suslova and Ryabov. This is an open-access article distributed under the terms of the Creative Commons Attribution License (CC BY). The use, distribution or reproduction in other forums is permitted, provided the original author(s) and the copyright owner(s) are credited and that the original publication in this journal is cited, in accordance with accepted academic practice. No use, distribution or reproduction is permitted which does not comply with these terms.

frontiers in Immunology

ORIGINAL RESEARCH
published: 22 April 2021
doi: 10.3389/fimmu.2021.618653

Pro-Resolving Mediator Annexin A1 Regulates Intracellular Ca^{2+} and Mucin Secretion in Cultured Goblet Cells Suggesting a New Use in Inflammatory Conjunctival Diseases

Anne V. Lyngstadaas[1,2,3], Markus V. Olsen[1,2,3], Jeffrey A. Bair[1], Robin R. Hodges[1†], Tor P. Utheim[1,3,4], Charles N. Serhan[5] and Darlene A. Dartt[1]*

[1] Schepens Eye Research institute/Massachusetts Eye and Ear, Department of Ophthalmology, Harvard Medical School, Boston, MA, United States, [2] Institute of Clinical Medicine, Faculty of Medicine, University of Oslo, Oslo, Norway, [3] Department of Medical Biochemistry, Oslo University Hospital, Oslo, Norway, [4] Department of Plastic and Reconstructive Surgery, University of Oslo, Oslo, Norway, [5] Center for Experimental Therapeutics and Reperfusion Injury, Department of Anesthesia, Brigham and Women's Hospital and Harvard Medical School, Boston, MA, United States

OPEN ACCESS

Edited by:
Mats Bemark,
University of Gothenburg, Sweden

Reviewed by:
Harry D. Dawson,
Agricultural Research Service (USDA), United States
Kathryn A. Knoop,
Mayo Clinic, United States

***Correspondence:**
Darlene A. Dartt
Darlene_dartt@meei.harvard.edu

[†]Deceased

Specialty section:
This article was submitted to Mucosal Immunity, a section of the journal Frontiers in Immunology

Received: 17 October 2020
Accepted: 11 March 2021
Published: 22 April 2021

Citation:
Lyngstadaas AV, Olsen MV, Bair JA, Hodges RR, Utheim TP, Serhan CN and Dartt DA (2021) Pro-Resolving Mediator Annexin A1 Regulates Intracellular Ca^{2+} and Mucin Secretion in Cultured Goblet Cells Suggesting a New Use in Inflammatory Conjunctival Diseases. Front. Immunol. 12:618653. doi: 10.3389/fimmu.2021.618653

The amount of mucin secreted by conjunctival goblet cells is regulated to ensure the optimal level for protection of the ocular surface. Under physiological conditions lipid specialized pro-resolving mediators (SPM) are essential for maintaining tissue homeostasis including the conjunctiva. The protein Annexin A1 (AnxA1) can act as an SPM. We used cultured rat conjunctival goblet cells to determine if AnxA1 stimulates an increase in intracellular $[Ca^{2+}]$ ($[Ca^{2+}]_i$) and mucin secretion and to identify the signaling pathways. The increase in $[Ca^{2+}]_i$ was determined using fura2/AM and mucin secretion was measured using an enzyme-linked lectin assay. AnxA1 stimulated an increase in $[Ca^{2+}]_i$ and mucin secretion that was blocked by the cell-permeant Ca^{2+} chelator BAPTA/AM and the ALX/FPR2 receptor inhibitor BOC2. AnxA1 increased $[Ca^{2+}]_i$ to a similar extent as the SPMs lipoxin A_4 and Resolvin (Rv) D1 and histamine. The AnxA1 increase in $[Ca^{2+}]_i$ and mucin secretion were inhibited by blocking the phospholipase C (PLC) pathway including PLC, the IP_3 receptor, the Ca^{2+}/ATPase that causes the intracellular Ca^{2+} stores to empty, and blockade of Ca^{2+} influx. Inhibition of protein kinase C (PKC) and Ca^{2+}/calmodulin-dependent protein kinase also decreased the AnxA1-stimulated increase in $[Ca^{2+}]_i$ and mucin secretion. In contrast inhibitors of ERK 1/2, phospholipase A_2 (PLA_2), and phospholipase D (PLD) did not alter AnxA1-stimulated increase in $[Ca^{2+}]_i$, but did inhibit mucin secretion. Activation of protein kinase A did not decrease either the AnxA1-stimulated rise in $[Ca^{2+}]_i$ or secretion. We conclude that in health, AnxA1 contributes to the mucin layer of the tear film and ocular surface homeostasis by activating the PLC signaling pathway to increase $[Ca^{2+}]_i$ and stimulate mucin secretion and ERK1/2, PLA_2, and PLD to stimulate mucin secretion from conjunctival goblet cells.

Keywords: ocular surface, annexin A1, secretion, specialized pro resolving mediators, mucin

INTRODUCTION

Inflammation is a component in common to both allergic conjunctivitis and dry eye disease – two frequently occurring diseases of the ocular surface (cornea and conjunctiva) (1). In allergic conjunctivitis allergens penetrate the conjunctival epithelium and initiate the production of pro-inflammatory mediators including histamine, leukotrienes, and prostaglandins. These compounds cause vasodilation, pain, edema and recruitment of neutrophils, macrophages, and mast cells into the conjunctiva (2). In acute inflammation, the infiltrating leukocytes switch from producing pro-inflammatory mediators to generate the specialized pro-resolving lipid mediators (SPMs) lipoxins, resolvins, protectins, and maresins (2–6). These SPMs actively terminate inflammation by blocking the effects of the pro-inflammatory mediators on their target tissues, including the conjunctival goblet cells. The protein annexin A1 (AnxA1) is also pro-resolving (6, 7). In general, failed endogenous resolution mechanisms lead to uncontrolled and chronic inflammation (1). In addition to resolving inflammation, the SPMs also maintain homeostasis of the conjunctival epithelium to keep the ocular surface healthy.

Conjunctival goblet cells synthesize and secrete large, high molecular weight, gel forming mucins (8). These mucins make up the innermost layer of the tear film (9). MUC5AC, the major mucin secreted by conjunctival goblet cells, can trap and remove ocular allergens and airborne pathogens (8). An optimum amount of MUC5AC secreted into the tear film is critical for ocular surface health, as a depleted number of goblet cells and mucin secretion lead to corneal and conjunctival damage (8). Conversely, MUC5AC overproduction is a symptom of allergic conjunctivitis and unhealthy for the ocular surface (8). Lipid SPMs including D-series and E-series resolvins, lipoxins, and maresins act by blocking excess mucin secretion from conjunctival goblet cells during inflammation, as well as stimulating mucin secretion under physiological conditions, thus maintaining ocular surface homeostasis (10–12).

AnxA1 is an anti-inflammatory, pro-resolving protein originally described as a mediator of glucocorticoid action (13). The synthesis of AnxA1 is a primary anti-inflammatory mechanism of glucocorticoids. AnxA1 works at least partly by suppressing phospholipase A_2 activity, thus blocking the production of pro-inflammatory eicosanoids (14). During inflammation, endogenous glucocorticoids are secreted from the adrenal gland to avoid an excessively vigorous inflammatory response that could potentially damage the host (15). Glucocorticoids can stimulate both the synthesis and secretion of AnxA1 (16). After being synthesized AnxA1 is mobilized to the plasma membrane and secreted by three different mechanisms: 1) the ATP-binding (ABC) transporter, 2) direct phosphorylation of serine-27 that localizes it to the plasma membrane, and 3) exocytosis by granule fusion with the cell membrane (17). The secreted AnxA1 can then interact with the ALX/FPR2 receptor in a paracrine, autocrine, or juxtacrine fashion.

As an effector molecule of glucocorticoids, AnxA1 has potential as an endogenous anti-inflammatory drug, and the use of AnxA1 therapeutically likely has fewer side effects than the use of glucocorticoids. AnxA1 contributes to the regulation of a wide variety of cellular events, including both acute and chronic inflammation, ischemic injury, fever, pain, and the release of arachidonic acid (14). AnxA1, as well as its N-terminal peptides, have also been found to potently inhibit neutrophil trafficking in mice (7). AnxA1 could prevent development of pro-inflammatory disease in the conjunctiva.

To determine if AnxA1 plays a role in maintaining the mucous layer in ocular surface health we investigated if exogenous addition of AnxA1 can increase intracellular [Ca^{2+}] and stimulate MUC5AC secretion in cultured primary conjunctival goblet cells from rats and determined which signaling pathways AnxA1 activates in these cells.

MATERIALS AND METHODS

Materials

AnxA1 was obtained from MyBiosource (San Diego, CA). The compound was stored at -20°C. Prior to use, AnxA1 was immediately diluted in Krebs-Ringer bicarbonate buffer with HEPES (KRB-HEPES, 119 mM NaCl, 4.8 mM KCl, 1.0 mM $CaCl_2$, 1.2 mM $MgSO_4$, 1.2 mM KH_2PO_4, 25 mM $NaHCO_3$, 10 mM HEPES, and 5.5 mM glucose [pH 7.45]) to the required concentration and added to the conjunctival goblet cells. RPMI-1640 cell culture medium, penicillin/streptomycin, trypsin, and L-glutamine were purchased from Lonza (Walkerville, IL). Fetal bovine serum (FBS) was from Atlanta Biologicals (Norcross, GA). Fura-2 was from Life Technologies (Grand Island, NY). U73122 and U73343, KN92 and KN93 were purchased from Tocris Bioscience (Ellisville, MO). The lectin Ulex Europaeus Agglutinin (UEA-1), histamine, BAPTA/AM, 2-aminoethyl diphenylborinate (2-APB), 1-butanol (1-but), *t*-butanol (*t*-but), carbachol, aristolochic acid (AA), thapsigargin and RO317549 were all purchased from Sigma-Aldrich (St Louis, MO). UO126 was obtained from R&D Systems (Minneapolis, MN). H89 and synthetic lipoxin A_4 (LXA_4, 5(S),6(R),15(S)-TriHETE) were from EMD Millipore (Billerica, MA). Resolvin (Rv) D1 (7S, 8R, 17S-trihydroxy-4Z, 9E 11E, 13Z, 19Z-docosahexaenoic acid) was purchased from Cayman Chemical, Ann Arbor, MI). N-Boc-Phe-Leu-Phe-Leu-Phe (BOC2) was obtained from Genscript Corp in Piscataway, NJ.

Animals

Four- to eight-week-old male Sprague-Dawley rats (Taconic Farms, Germantown, NY, USA) were anesthetized with CO_2 and decapitated. The bulbar and forniceal conjunctival epithelium was surgically removed from both eyes. All experiments were in accordance with the US National Research Council's Guide for the Care and Use of Laboratory Animals, the US Public Health Service's Policy on Humane Care and Use of Laboratory Animals, and Guide for the Care and Use

of Laboratory Animals and were approved by the Schepens Eye Research Institute Animal Care and Use of Committee.

Culture of Conjunctival Goblet Cells

Goblet cells from rat conjunctiva were grown in organ culture as described previously (3). The conjunctiva was dissected free of underlying connective tissue. The conjunctival explants were grown on six-well plates in RPMI 1640 medium supplemented with 10% fetal bovine serum (FBS), 2 mM glutamine, and 100 μg/mL penicillin-streptomycin for approximately one week. The goblet cells were then trypsinized and plated onto glass bottom petri dishes or 24 well plates, for $[Ca^{2+}]_i$ measurements or mucin secretion measurements, respectively. First passage goblet cells were used in all experiments. The identity of the cultured cells was checked by evaluating staining with antibody to cytokeratin 7 (detects goblet cell bodies) and the lectin UEA-1 (detects goblet cell secretory products) to ensure that goblet cells predominated in the cultures.

Measurement of cDNA Expression by Semi-Quantitative PCR

Cultured goblet cells were homogenized in TRIzol and total RNA isolated according to manufacturer's instructions. One microgram of total RNA was used for complementary DNA (cDNA) synthesis using the Superscript First-Strand Synthesis system for RT-PCR (Invitrogen, Carlsbad, CA). The cDNA was amplified by the polymerase chain reaction (PCR) using primers specific to AnxA1 using the Jumpstart REDTaq Readymix Reaction Mix (Sigma-Aldrich, St. Louis, MO) in a thermal cycler (Master Cycler, Eppendorf, Hauppauge, NY). The forward primer was GTG ATC GCT GTG AGG ATA TGA G, and the reverse primer was TAC AGA GCA GTT GGG ATG TTT AG. These primers generated 504 bp fragments. β-Actin primers, the positive control, were forward CGT CAT ACT CCT GCT TGC TGA TCC A and the reverse primer was ATC TGG CAC CAC ACC TTC TAC AAT GG CT and generated a 790 bp fragment. The conditions were as follows: 5 min at 95°C followed by 35 cycles of 1 min at 94°C, 30 seconds at annealing temperature for 1 min at 72°C with a final hold at 72°C for 10 min. Samples with no cDNA served as the negative control. Amplification products were separated by electrophoresis on a 1.5% agarose gel and visualized by ethidium bromide staining.

Measurement of Mucin Secretion

Cultured rat goblet cells were plated in 24-well plates and grown to confluence (1, 10–12, 18, 19). After serum starving cultured goblet cells for 2 h, the goblet cells were stimulated with AnxA1 in increasing concentrations in serum-free RPMI 1640 supplemented with 0.5% BSA for 2 h. The inhibitors were added 30 minutes prior to stimulation with AnxA1. An enzyme-linked lectin assay (ELLA) with the lectin UEA-1 was used to measure high molecular weight glycoprotein secretion that included MUC5AC produced by goblet cells. The supernatants were collected and analyzed for the total amount of lectin-detectable glycoconjugates, which quantifies the amount of goblet cell secretion as described previously (1, 3, 10–12, 20–22). The cells were scraped, and the cell homogenate was analyzed for the total amount of protein by using the Bradford protein assay. High molecular weight glycoconjugate secretion was normalized to total protein in the homogenate. Secretion was expressed as fold increase above basal that was set to 1.

Measurement of Intracellular $[Ca^{2+}]$

Cultured rat conjunctival goblet cells were transferred to 35-mm glass bottom culture dishes and incubated overnight. The goblet cells were then incubated for 1 h at 37°C with Krebs-Ringer bicarbonate buffer with HEPES (KRB-HEPES) (119 mM NaCl, 4.8 mM KCl, 1.0 mM $CaCl_2$, 1.2 mM $MgSO_4$, 1.2 mM KH_2PO_4, 25 MM $NaHCO_3$, 10 mM HEPES, and 5.5 mM glucose) (pH 7.45) plus 0.5% BSA containing 0.5 fura-2/AM (Invitrogen, Grand Island, NY), 8 μM pluronic acid F127 (Sigma-Aldrich, St. Louis, MO, USA) and 250 μM sulfinpyrazone (Sigma-Aldrich), followed by washing in KRB-HEPES containing sulfinpyrazone. Ca^{2+} measurements were made with a ratio imaging system (InCyt Im2; Intracellular Imaging, Cincinnati, OH) using excitation wavelengths of 340 and 380 nm and an emission wavelength of 505 nm. A minimum of 10 cells were selected in each experimental condition. AnxA1 was added either alone or after incubation with inhibitors for 15 or 30 min and intracellular $[Ca^{2+}]$ ($[Ca^{2+}]_i$) measured. After addition of agonist, data were collected in real time. The data are presented as $[Ca^{2+}]_i$ over time and peak $[Ca^{2+}]_i$, calculated by subtracting the average value before the agonist AnxA1 was added (basal) from the peak $[Ca^{2+}]_i$.

Statistical Analysis

Results were expressed as the fold-increase above basal. Data are expressed as mean ± SEM. Data were analyzed by Student's t-test. $p < 0.05$ was considered statistically significant.

RESULTS

AnxA1 Is Expressed in Rat Conjunctival Goblet Cells

The protein AnxA1 was detected in a wide range of tissues, including the lung, intestine and bone marrow (14). We used PCR to investigate the expression of AnxA1 in cultured rat conjunctival goblet cells (**Figure 1**). A single band at the correct size of 504 bp was found in cDNA isolated from the conjunctivas of three individual animals. Expression of β-actin was used as a control. As AnxA1 is a protein, this is the first pro-resolving mediator whose presence in rat conjunctival goblet cells was verified by PCR.

AnxA1 Stimulates Mucin Secretion in Rat Conjunctival Goblet Cells

Lipid specialized pro-resolving mediators (SPM) such as LXA_4, RvD1, and RvE1 stimulate mucin secretion from cultured rat conjunctival goblet cells (10–12). To explore if the protein AnxA1 stimulates secretion, goblet cells were stimulated for two h with AnxA1 (10^{-11}-10^{-8} M) or a positive control

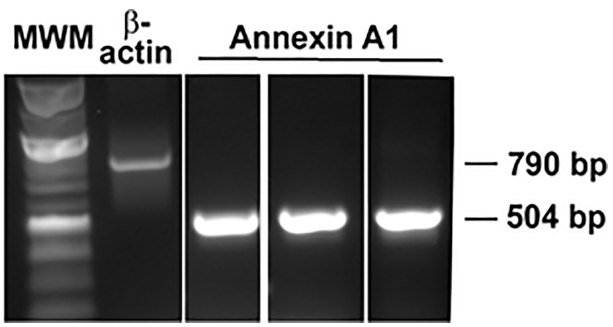

FIGURE 1 | AnxA1 expression is detected in cultured rat conjunctival goblet cells by RT-PCR. Each lane represents cDNA from a different animal. β-Actin was used as a control.

histamine (10^{-5} M) (18, 23) and the amount of secretion was then measured (**Figure 2**). Histamine is known to stimulate glycoconjugate secretion from conjunctival goblet cells (22, 24). AnxA1 increased mucin secretion in a concentration-dependent manner with a maximum increase at 10^{-10} M. Significant increases occurred from 10^{-11} M to 10^{-9} M AnxA1 and were 1.7 ± 0.2, 3.2 ± 0.3 and 2.0 ± 0 fold above basal, respectively from three independent experiments. In comparison histamine significantly increased mucin secretion from basal by 2.2 ± 0.4 fold.

AnxA1 Increases $[Ca^{2+}]i$ in Rat Conjunctival Goblet Cells

As AnxA1 stimulates conjunctival goblet cells to secrete mucins, we determined if AnxA1 alters the $[Ca^{2+}]_i$. Cultured goblet cells were incubated with fura-2/AM before stimulation with AnxA1 (10^{-11} -10^{-8} M). AnxA1 increased $[Ca^{2+}]_i$ in a time and concentration-dependent manner (**Figures 3A–C**). All

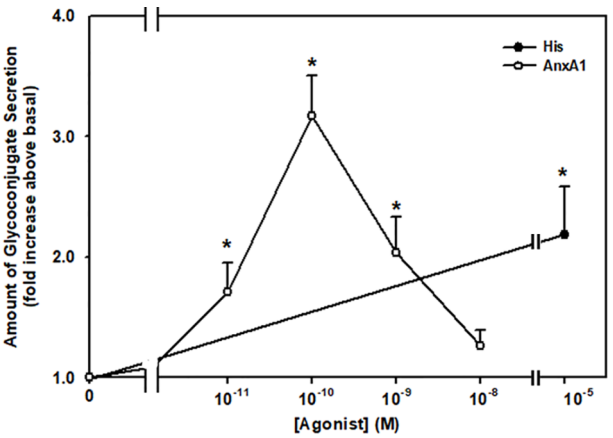

FIGURE 2 | AnxA1 increases glycoconjugate secretion from cultured rat conjunctival goblet cells. Goblet cells were incubated with increasing concentrations of annexin A1 (AnxA1, 10^{-11} - 10^{-8} M) or histamine (His, 10^{-5} M). Data are presented as mean ± SEM from three independent experiments. * Indicates significant difference from basal.

concentrations of AnxA1 significantly increased $[Ca^{2+}]_i$ with the highest increase of 467.3 ± 95.1 nM occurring at 10^{-9} M (**Figure 3C**). These data are from five independent experiments. Therefore, AnxA1 increased $[Ca^{2+}]_i$ in conjunctival goblet cells.

To compare the $[Ca^{2+}]_i$ responses induced by other known mediators with that of AnxA1, goblet cells were stimulated with AnxA1, the lipid SPMs LXA_4 and RvD1, and the allergic mediator histamine. All compounds were used at the concentrations previously found to result in the highest increase in $[Ca^{2+}]_i$ (10, 12). Each mediator significantly increased $[Ca^{2+}]_i$ over basal and to the same extent, as there was no significant difference between them (n=4, **Figures 3D, E**).

AnxA1 Uses Intracellular Ca^{2+} to Stimulate Secretion in Rat Conjunctival Goblet Cells

To determine if the AnxA1-stimulated increase in $[Ca^{2+}]_i$ leads to mucin secretion, rat goblet cells were incubated with the intracellular calcium chelator BAPTA/AM (10^{-4} M) for 30 minutes prior to AnxA1 (10^{-9} M) stimulation. The cholinergic agonist carbachol (Cch) at 10^{-4} M was used as a control. To ensure that BAPTA chelated $[Ca^{2+}]_i$ and prevented the increase in $[Ca^{2+}]_i$ induced by AnxA1 and Cch, $[Ca^{2+}]_i$ was measured (**Supplemental Figure 1**). AnxA1 significantly increased $[Ca^{2+}]_i$ to a peak of 128.8 ± 11.5 nM.When goblet cells were preincubated with BAPTA/AM, the AnxA1-stimulated increase in $[Ca^{2+}]_i$ was significantly inhibited to 30.1 ± 7.5 nM. The Ca^{2+} response to Cch, a positive control, was also significantly inhibited from 227.0 ± 54.8 nM to 29.3 ± 50.2 nM in the presence of BAPTA. These results were from 4 independent experiments.

We then investigated if AnxA1 uses Ca_i^{2+} to increase mucin secretion. Rat cultured goblet cells were treated with BAPTA/AM (10^{-4} M), stimulated by AnxA1 (10^{-10} M) and secretion measured. In three independent experiments, AnxA1 alone significantly increased glycoconjugate secretion by 1.5 ± 0.05 fold above basal (**Figure 3F**). BAPTA/AM significantly inhibited AnxA1-stimulated mucin secretion to 0.9 ± 0.06 fold above basal. Cch (10^{-4} M)-stimulated glycoconjugate secretion was also significantly inhibited from 1.7 ± 0.2 fold to 1.1 ± 0.1 fold above basal. These findings demonstrate that AnxA1 increases $[Ca^{2+}]_i$ to stimulate mucin secretion in conjunctival goblet cells.

AnxA1 Uses Both Intracellular Ca^{2+} Stores and Extracellular Ca^{2+} to Increase $[Ca^{2+}]_i$ in Rat Conjunctival Goblet Cells

To examine the role that intracellular Ca^{2+} stores play in AnxA1 stimulation, goblet cells were incubated with the Ca^{2+} reuptake inhibitor thapsigargin. Thapsigargin depletes the ER of Ca^{2+} by blocking the Ca^{2+}/ATPase in the endoplasmic reticulum (ER) that inhibits Ca^{2+} from being taken up by the ER (25). The ER store of Ca^{2+} is depleted as Ca^{2+} passively leaks out of the ER and is not replaced as shown by the increase in $[Ca^{2+}]_i$ over time (**Figure 4A**). AnxA1 added alone induced a peak increase in $[Ca^{2+}]_i$ of 166.8 ± 26.7 nM (**Figures 4A, B**, n=6). The AnxA1-induced Ca^{2+} response was significantly blocked by thapsigargin pre-treatment and was 24.6 ± 9.7 nM. In the same cells, Cch was

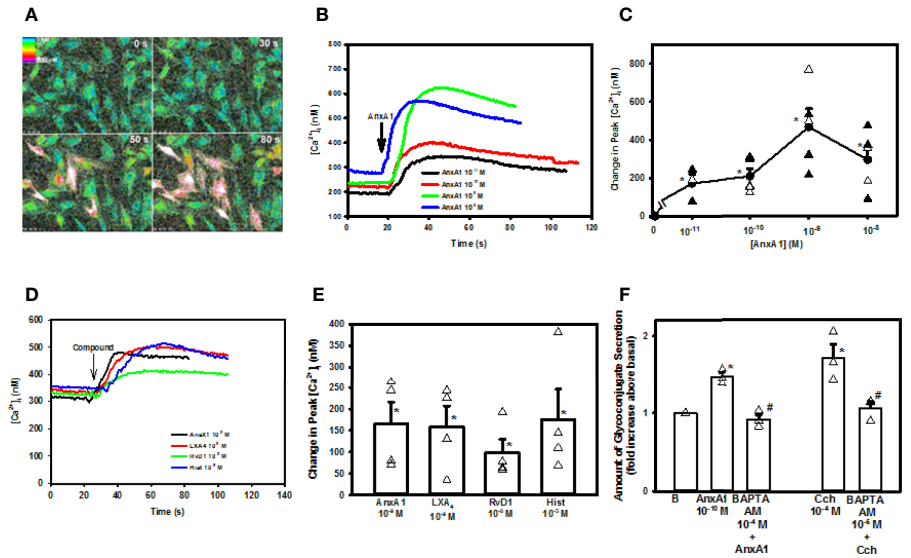

FIGURE 3 | AnxA1 elevates $[Ca^{2+}]_i$ to stimulate glycoconjugate secretion in cultured rat conjunctival goblet cells. Cultured goblet cells were incubated with fura-2/AM and stimulated with increasing concentrations of Annexin A1 (AnxA1, 10^{-11} M to 10^{-8} M). Pseudo color images of $[Ca^{2+}]_i$ of goblet cells stimulated by AnxA1 10^{-9} M at four times are shown in **(A)** The increase in $[Ca^{2+}]_i$ over time with AnxA1 (10^{-11} M to 10^{-8} M) is shown in **(B)** The change in peak $[Ca^{2+}]_i$ after stimulation with AnxA1 (10^{-11} M to 10^{-8} M) is shown in **(C)** Increase in $[Ca^{2+}]_i$ over time in response to AnxA1 (10^{-9} M), LXA_4 (10^{-9} M), RvD1 (10^{-9} M) and histamine (hist, 10^{-5} M) is shown in **(D)** The change in peak $[Ca^{2+}]_i$ with AnxA1, LXA_4, RvD1, and histamine is shown in **(E)** Glycoconjugate secretion from goblet cells treated vehicle, AnxA1 (10^{-10} M), with the Ca^{2+} chelator BAPTA-AM (10^{-4} M) followed by stimulation with AnxA1, carbachol (Cch, 10^{-4} M) or BAPTA-AM (10^{-4} M) followed by carbachol is shown in **(F)** Data are mean ± SEM from 4 independent experiments **(A–E)** or 3 **(F)** independent experiments. *indicates significant difference from basal; #indicates significant difference from AnxA1 or Cch alone.

used as a control and increased $[Ca^{2+}]_i$ to 243.4 ± 24.0 nM. Cch-stimulated increase in $[Ca^{2+}]_i$ was also blocked by pre-treatment with thapsigargin and was 44.4 ± 21.2 nM. These experiments indicate that AnxA1 works by mobilizing Ca^{2+} from the ER to increase cytoplasmic $[Ca^{2+}]_i$.

After an agonist depletes intracellular Ca^{2+} stores, this depletion activates STIM1 and Orai to induce Ca^{2+} influx to replace those stores. Since AnxA1 used intracellular Ca^{2+} stores, we investigated if AnxA1 used extracellular Ca^{2+}. Cells were incubated in KRB with and without extracellular $CaCl_2$. AnxA1 (10^{-9} M) added to the KRB containing $CaCl_2$ significantly increased $[Ca^{2+}]_i$ by 124.1 ± 23.0 nM (**Figures 4C, D**, n=4). This increase in $[Ca^{2+}]_i$ was significantly reduced to 44.0 ± 23.7 nM when AnxA1 was added to KRB without $CaCl_2$, indicating that AnxA1 stimulates influx of extracellular Ca^{2+} to increase $[Ca^{2+}]_i$. Cch (10^{-4} M), a control, elevated $[Ca^{2+}]_i$ to 160.4 ± 40.9 nM. Cch-stimulated increase in $[Ca^{2+}]_i$ was significantly blocked by the $CaCl_2$-free solution and was 11.8 ± 2.1 nM. Based on these results, AnxA1 releases Ca^{2+} from intracellular Ca^{2+} stores and stimulates extracellular Ca^{2+} influx to increase the $[Ca^{2+}]_i$ in conjunctival goblet cells.

AnxA1 Uses the ALX/FPR2 Receptor to Increase $[Ca^{2+}]_i$ and Stimulate Secretion in Rat Conjunctival Goblet Cells

In tissues and cells examined, AnxA1 works through the G-protein coupled formyl peptide receptor 2 (ALX/FPR2) (14, 26). To confirm that AnxA1 uses this receptor in goblet cells, cultured rat conjunctival goblet cells were incubated with the ALX/FPR2 antagonist BOC-2 (10^{-4} M) for 30 minutes before stimulating the goblet cells with AnxA1 (10^{-9} M) or LXA_4 (10^{-9} M), which is known to bind to ALX/FPR2 and is a positive control (12). AnxA1 added alone significantly increased $[Ca^{2+}]_i$ with a peak of 265.4 ± 61.0 nM (**Figures 5A, C**, n=5). BOC-2 significantly blocked AnxA1's increase in $[Ca^{2+}]_i$ to 54.1 ± 23.9 nM. The LXA_4 response was 180.8 ± 52.4 nM (**Figures 5B, C**). In the presence of BOC-2, the LXA_4 response was significantly reduced to 47.7 ± 20.0 nM.

To determine if AnxA1 uses the ALX/FPR2 receptor to stimulate high molecular weight glycoprotein secretion, cells were preincubated with BOC-2 (10^{-4} M) followed by AnxA1 (10^{-10} M) (**Figure 5D**, n=3). LXA_4 (10^{-9} M) was again used as a positive control. Secretion was significantly increased by 1.5 ± 0.05 fold above basal when AnxA1 (10^{-10} M) was added by itself. AnxA1 stimulated secretion was significantly inhibited by BOC-2 to 0.74 ± 0.16 fold above basal. LXA_4 stimulated secretion was also inhibited by BOC-2. These data indicate that AnxA1 uses the ALX/FPR2 receptor to stimulate an increase in $[Ca^{2+}]_i$ and secretion in conjunctival goblet cells.

AnxA1 Activates the PLC Pathway and Its Downstream Effectors IP_3 and PKC to Increase $[Ca^{2+}]_i$ and Stimulate Secretion in Rat Conjunctival Goblet Cells

The phospholipase C (PLC) pathway is critical for cellular Ca^{2+} signaling as activation of PLC generates both inositol 1,4,5-

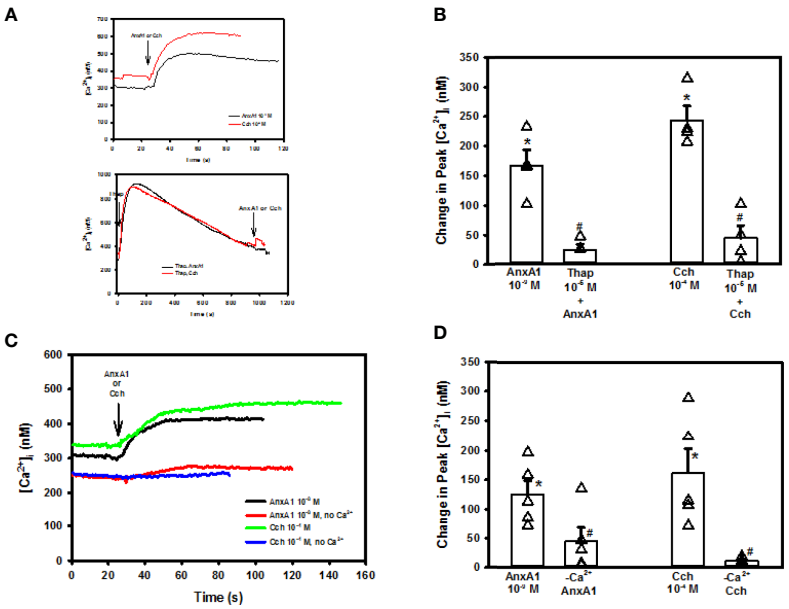

FIGURE 4 | Annexin A1 (Anx1, 10-9 M) or carbachol (Cch, 10-4 M) (A top panel) or AnxA1 uses intracellular and extracellular Ca^{2+} to increase $[Ca^{2+}]_i$ in cultured rat conjunctival goblet cells. Cultured rat goblet cells were treated with thapsigargin (10^{-5} M) (first arrow) for 15 minutes before stimulation indicated by second arrow with annexin A1 (AnxA1, 10^{-9} M) or Cch (10^{-4} M). (A bottom panel), $[Ca^{2+}]_i$ over time is shown in **(A)** Change in peak $[Ca^{2+}]_i$ is shown in **(B)** Goblet cells were incubated in KRB solution with and without $CaCl_2$ and stimulated with AnxA1 (10^{-9} M) or Carbachol (Cch, 10^{-4} M). $[Ca^{2+}]_i$ over time is shown in **(C)** Change in peak $[Ca^{2+}]_i$ is shown in **(D)** Data are mean ± SEM from 4 **(A, B)** or 6 **(C, D)** independent experiments. *indicates significant difference from basal; #indicates significance from AnxA1 or Cch alone.

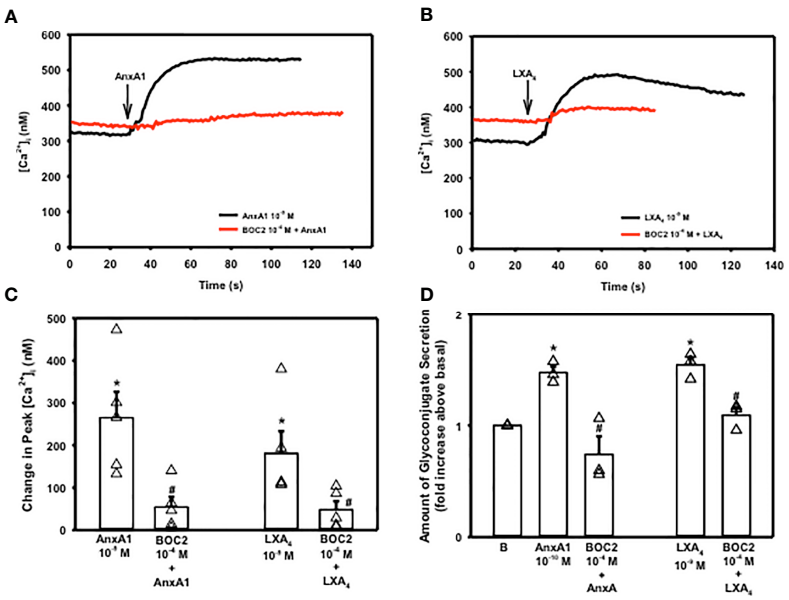

FIGURE 5 | AnxA1 uses the ALX/FPR2 receptor to increase $[Ca^{2+}]_i$ and stimulate secretion in cultured rat conjunctival goblet cells. Goblet cells were preincubated with BOC2 (10^{-4} M) for 30 minutes and stimulated with vehicle or annexin A1 (AnxA1, 10^{-9} M) shown in **(A, C)** and vehicle or the control LXA_4 (10^{-9} M) shown in **(B, C)** $[Ca^{2+}]_i$ over time is shown in **(A, B)** Change in peak $[Ca^{2+}]_i$ is shown in **(C)** Amount of glycoconjugate secretion is shown in **(D)** with AnxA1 at 10^{-10} M. B indicates basal (vehicle) in **(D)** Data in are mean ± SEM from 4 **(A–C)** or 3 **(D)** independent experiments. *indicates significant difference from basal; #indicates significance from AnxA1 or LXA_4 alone.

trisphosphate (IP_3) and diacylglycerol (DAG) (27). IP_3 interacts with its receptors on the ER to release Ca^{2+} from intracellular stores, while DAG activates protein kinase C (PKC). To explore if AnxA1 activates the PLC pathway in rat conjunctival goblet cells, these cells were preincubated with either the PLC inhibitor U73122 or its negative control U73343 at 10^{-7} M, before addition of AnxA1 (10^{-9} M) or a positive control Cch [10^{-4} M) (28)]. AnxA1 added alone significantly increased $[Ca^{2+}]_i$ with a peak of 217.1 ± 34.6 nM (**Figure 6A**, n=3) The active inhibitor U73122 significantly decreased the AnxA1 stimulated increase in $[Ca^{2+}]_i$ to 63 ± 10.0 nM, while the inactive inhibitor U73343 did not significantly block AnxA1. The Cch response was also inhibited by U73122, but not U73343 (28).

The effects of U73122 and U73143 on secretion were then determined. AnxA1 (10^{-10} M) increased secretion 2.0 ± 0.3 fold above basal (**Figure 6B**, n=3). AnxA1-stimulated response was completely inhibited by preincubation with U73122 (10^{-7} M), but not U73143 (10^{-7} M). U73122, but not U73143, also significantly inhibited secretion stimulated by Cch (10^{-4} M), which was a positive control. These data show that AnxA1 stimulates PLC to increase $[Ca^{2+}]_i$ and stimulate secretion.

To further explore the PLC pathway, goblet cells were incubated for 30 min with 2APB (10^{-5} M), an inhibitor of IP_3 receptors on the ER (29). AnxA1 (10^{-9} M) added alone significantly increased $[Ca^{2+}]_i$ by 160.6 ± 43.4 nM (**Figure 6C**, n=4). AnxA1-induced $[Ca^{2+}]_i$ increase was significantly

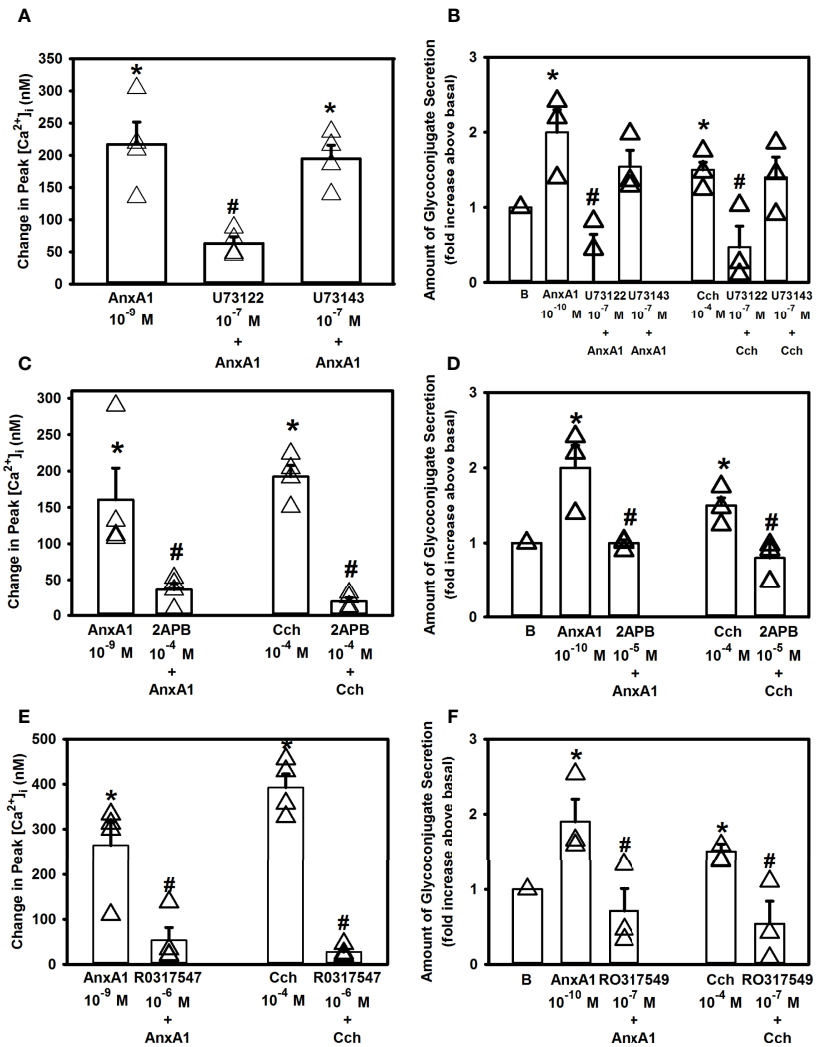

FIGURE 6 | AnxA1 activates the Phospholipase C (PLC) pathway and its downstream effectors to increase $[Ca^{2+}]_i$ in cultured rat conjunctival goblet cells. Cultured goblet cells were treated with vehicle, the PLC inhibitor U73122, its inactive analog U73343 (both at 10^{-7} M, **A**, **B**), 2APB (10^{-5} M, **C**, **D**), or the PKC inhibitor RO317549 (10^{-7} M, **E**, **F**) for 30 minutes before stimulation with annexin A1 (AnxA1, 10^{-9} M) in **(A, C, E)** or with AnxA1 at 10^{-10} M in **(B, D, F)** or the positive control carbachol (Cch, 10^{-4}). Change in peak $[Ca^{2+}]_i$ are shown in **(A, C, E)** while glycoconjugate secretion is shown in **(B, D, F)**. B (vehicle) indicates basal in **(B, D, F)**. Data are mean ± SEM from three **(A, B, D, F)**, four **(C, E)** independent experiments. *indicates significant difference from basal; #indicates significance from AnxA1 or carbachol alone.

decreased to 35.7 ± 9.6 nM after 30 minutes of incubation with 2APB. Cch (10^{-4} M) was used as a positive control and its stimulation of $[Ca^{2+}]_i$ was significantly blocked by 2APB as well.

A similar effect of 2APB was found when secretion was examined. AnxA1 (10^{-10} M) increased secretion 2.0 ± 0.3 fold above basal (**Figure 6D**, n=3). AnxA1-stimulated response was significantly inhibited by incubation with 2APB, which also significantly inhibited secretion stimulated by Cch (10^{-4} M), the positive control.

Next, we investigated the effect of the PKC inhibitor RO317549. Goblet cells were incubated for 30 minutes with RO317549 (10^{-7} M) before stimulation with AnxA1 (10^{-9} M) or a positive control Cch (10^{-4} M). $[Ca^{2+}]_i$ was significantly increased when AnxA1 was added alone (263.7 ± 51.8 nM, **Figure 6E**, n=4). RO317549 significantly blocked the effect of AnxA1 on $[Ca^{2+}]_i$ and was 27.0 ± 6.3 nM)). Cch-stimulated increase in $[Ca^{2+}]_i$ was also significantly inhibited.

Inhibition of PKC with RO317549 also blocked AnxA1-stimulated secretion. AnxA1 increased secretion by 1.9 ± 0.3 fold above basal (**Figure 6F**, n=3). RO317549 significantly reduced AnxA1-induced secretion to 0.7 ± 0.3 fold above basal. As a positive control, Cch stimulated secretion was also significantly inhibited

In conjunctival goblet cells inhibitors of PLC activity, IP_3 interaction with its receptors, and PKC each blocked the AnxA1-stimulated function measured. Based on these findings, AnxA1 activates the PLC pathway both to increase intracellular Ca^{2+} and stimulate secretion through the production of IP_3 and activation of PKC.

AnxA1 Increases $[Ca^{2+}]_i$ and Secretion Through Activation of Ca^{2+}/CaMK II in Conjunctival Goblet Cells

Free intracellular Ca^{2+} can bind to calmodulin, to create a calmodulin/calcium complex. This complex can bind to different proteins such as Ca^{2+}/calmodulin dependent protein kinase II (Ca^{2+}/CaMK) (30). We have previously shown that LXA_4, through the ALX/FPR2 receptor, increases $[Ca^{2+}]_i$ through Ca^{2+}/CaMK (12). To investigate if AnxA1 also activates Ca^{2+}/CaMK, goblet cells were preincubated with the Ca^{2+}/CaMK inhibitor KN93 or the inactive analog KN92 at 10^{-7} M for 30 minutes. AnxA1 (10^{-9} M) significantly increased $[Ca^{2+}]_i$ to a peak of 235.6 ± 50.0 nM (**Figure 7A**). KN93 but not KN92 significantly blocked AnxA1-stimulated increase in $[Ca^{2+}]_i$ and was 97.6 ± 19.6 (**Figure 7A**, n=4). A positive control Cch (10^{-4} M) significantly increased $[Ca^{2+}]_i$ by 203.5 ± 40.2 nM. KN 93, but not KN92, significantly decreased Cch-stimulated increase in $[Ca^{2+}]_i$.

KN93 also significantly decreased 10^{-10} M AnxA1-stimulated secretion from 1.6 ± 0.1 to 0.9 ± 0.1 fold above basal (**Figure 7B**, n=3). KN92 had no effect on AnxA1-stimulated secretion. KN93, but not KN92, also significantly inhibited 10^{-4} M Cch-stimulated secretion. These data indicate that AnaX1 uses Ca^{2+}/CaMK to increase $[Ca^{2+}]_i$ and stimulate glycoconjugate secretion.

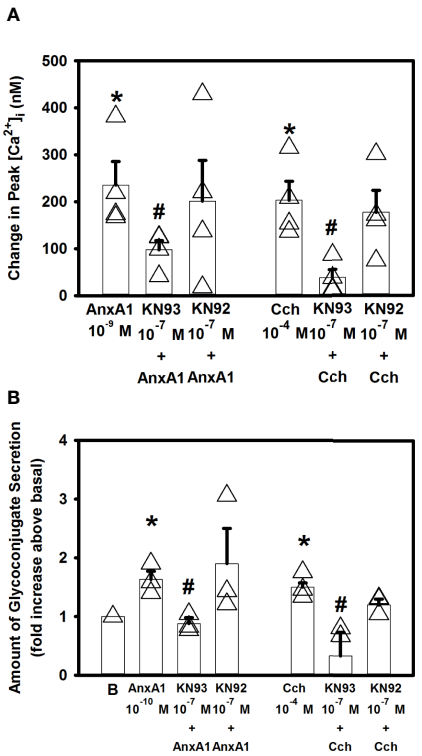

FIGURE 7 | AnxA1 activates the calcium/calmodulin-dependent protein kinase (Ca^{2+}/CaMK) to increase $[Ca^{2+}]_i$ and stimulate glycoconjugate secretion in cultured rat conjunctival goblet cells. Goblet cells were treated with the Ca^{2+}/CaMK inhibitor KN93, its inactive analog KN92,or vehicle for 30 minutes prior to stimulation with annexin A1 (AnxA1, 10^{-9} M) or carbachol (Cch, 10^{-4} M). Change in peak $[Ca^{2+}]_i$ is shown in **(A)** AnxA1 (10^{-10} M)-stimulated glycoconjugate secretion is shown in **(B)** indicates basal (vehicle) in **(B)** Data are mean ± SEM from 4 **(A)** or 3 **(B)** independent experiments. *indicates significant difference from basal. #indicates significance from Cch alone.

AnxA1 Does Not Increase $[Ca^{2+}]_i$ But Does Increase Secretion Through Activation of ERK 1/2 in Rat Conjunctival Goblet Cells

The ERK 1/2 pathway is a component of a signaling cascade that is activated in cells by a variety of stimuli (18, 31, 32). To determine if the ERK 1/2 pathway plays a role in AnxA1-stimualted increase in $[Ca^{2+}]_i$ the ERK 1/2 inhibitor UO126 was used. Rat conjunctival goblet cells were incubated with UO126 (10^{-8}–10^{-6} M) for 30 minutes (**Figure 8A**, n=3). AnxA1 (10^{-9} M) added alone significantly increased $[Ca^{2+}]_i$ by 152.5 ± 37.2 nM. AnxA1-induced $[Ca^{2+}]_i$ increase was not significantly blocked by UO126 at any concentration. Histamine (10^{-5} M), which is known to activate ERK 1/2 was used as a control (22) and was significantly blocked by all three concentrations of UO126.

To examine the effects of UO126 on glycoconjugate secretion, goblet cells were incubated with AnxA1 with and without UO126 (10^{-7} M). AnxA1(10^{-10} M) alone increased secretion by 2.0 ± 0.3

fold above basal (**Figure 8B**, n=3). UO126 significantly decreased AnxA1-stimulated response and was 0.6 ± 0.3 fold above basal. In contrast to previous studies (31) U0126 did not inhibit the carbachol-induced secretory response. These data indicate that AnxA1 does not activate ERK1/2 to increase $[Ca^{2+}]_i$ but does activate it to stimulate glycoconjugate secretion.

AnxA1 Does Not Use PKA to Increase $[Ca^{2+}]_i$ in Rat Conjunctival Goblet Cells

To determine if AnxA1 increases cAMP levels to activate protein kinase A (PKA) to increase $[Ca^{2+}]_i$ and stimulate secretion, goblet cells were preincubated with the PKA inhibitor H89 (10^{-5} M) for 30 minutes before stimulating the cells with AnxA1 (10^{-9} M) (**Supplemental Figure 2A**, n=9). AnxA1 added alone significantly increased $[Ca^{2+}]_i$ by 420 ± 111.9 nM. H89 did not significantly inhibit AnxA1 stimulated increase in $[Ca^{2+}]_i$. Vasoactive intestinal peptide (VIP, 10^{-8} M), which is known to increase cAMP (19), was used as a control. VIP-stimulated increase in $[Ca^{2+}]_i$ was 548.1 ± 110.6 nM. H89 significantly blocked VIP-stimulated increase in $[Ca^{2+}]_i$ and was 252.5 ± 39.6 nM.

Similar to the effects on $[Ca^{2+}]_i$ H89 did not significantly inhibit AnxA1-stimulated glycoconjugate secretion (**Supplemental Figure 2B**, n=3). However, the positive control, VIP-stimulated secretion was inhibited by H89. These data indicate that activation of PKA does not play a role in AnxA1-stimulated increase in $[Ca^{2+}]_i$ or secretion.

AnxA1 Does Not Increase $[Ca^{2+}]_i$ But Does Stimulate Secretion Through the PLD Pathway in Rat Conjunctival Goblet Cells

Phospholipase D (PLD) is an important regulator of several critical aspects of cell physiology, and is involved in cell functions like endocytosis, exocytosis, cell migration and mitosis (33). We previously showed that the other SPMs such as RvD1, RvE1 and LXA_4 work through PLD (10–12). To explore if AnxA1 uses PLD, cultured rat conjunctival goblet cells were incubated for 15 minutes with either the PLD inhibitor 1-but or the inactive inhibitor *t*-but, both at 0.3% (**Figure 9A**). AnxA1 (10^{-9} M) alone significantly increased $[Ca^{2+}]_i$ to a peak of 141.2 ± 50.0 nM (n=4). Neither preincubation with 1-but or *t*-but altered the effect of AnxA1 on the Ca^{2+} response. The increase in $[Ca^{2+}]_i$ stimulated by the positive control carbachol (10^{-4} M) was significantly blocked by the active inhibitor 1-but, but not the inactive inhibitor *t*-but.

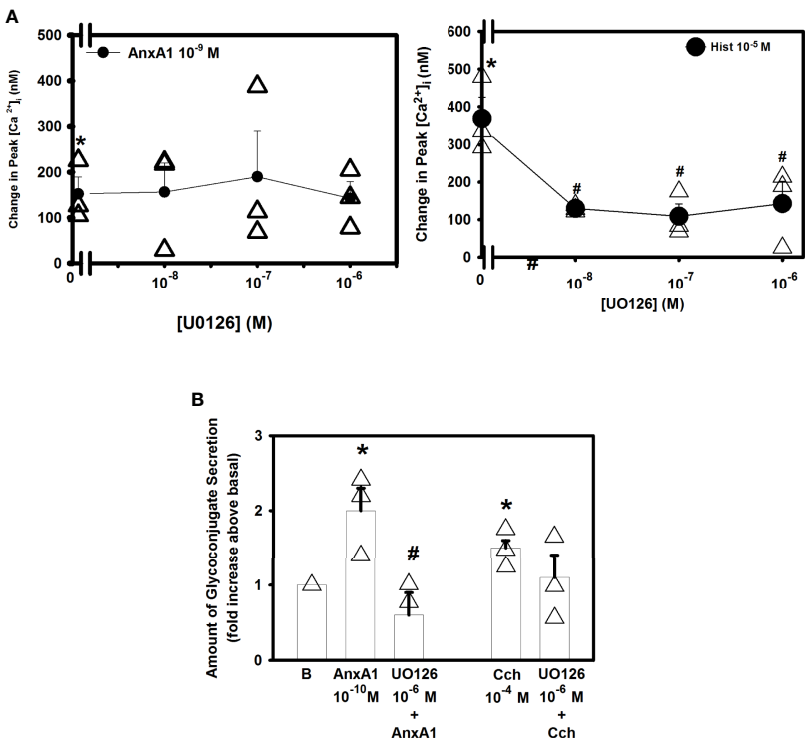

FIGURE 8 | AnxA1 does not activate extracellular regulated protein kinase (ERK) 1/2 to increase $[Ca^{2+}]_i$ but does activate it to stimulate glycoconjugate secretion in cultured rat conjunctival goblet cells. Rat conjunctival goblet cells were treated with vehicle or the ERK 1/2 inhibitor UO126 (10^{-8} - 10^{-6} M) for 30 minutes prior to stimulation with either annexin A1 (AnxA1, 10^{-9} M) in **(A)** or with AnxA1 at 10^{-10} M in **(B)**, or the control histamine (Hist, 10^{-5} M) or carbachol (Cch, 10^{-4} M). Change in peak $[Ca^{2+}]_i$ is shown in **(A)** Glycoconjugate secretion is shown in **(B)** B indicates basal (vehicle) in **(B)** Data are mean ± SEM from 4 **(A)** or 3 **(B)** independent experiments. *indicates significant difference from basal. #indicates significance from either AnxA1 or histamine alone.

When secretion was measured, AnxA1 (10^{-10} M) alone increased secretion 1.9 ± 0.3 fold above basal (**Figure 9B**, n=3)). Incubation with 1-but, but not t-but, significantly decreased this response that was 0.9 ± 0.1 fold above basal. Similarly to AnxA1, stimulation of secretion by Cch (10^{-4} M) was significantly decreased by 1-but, but not t-but. Based on these findings we conclude that AnxA1 does not active the PLD pathway to stimulate an increase in $[Ca^{2+}]_i$ but does activate PLD to stimulate secretion in cultured rat conjunctival goblet cells.

AnxA1 Does Not Increase $[Ca^{2+}]_i$ But Does Stimulate Secretion Through PLA2 Pathway in Cultured Rat Goblet Cells

Another phospholipase that is present and can be activated in goblet cells is the PLA2 pathway (10–12). To determine if AnxA1 utilizes PLA2 to increase $[Ca^{2+}]_i$ and secretion, goblet cells were incubated with the PLA2 inhibitor aristolochic acid (AA) for 30 min prior to stimulation with AnxA1 (**Figure 10A**). AnxA1 (10^{-9} M) significantly increased peak $[Ca^{2+}]_i$ by 530.0 ± 109.2 nM (n=4). Preincubation with AA at 10^{-6} M significantly altered the AnxA1-stimulated response that was 228.1 ± 60.7 nM. AA at 10^{-5} M did not significantly alter the AnxA1 response. The positive control Cch (10^{-4} M)-stimulated response was significantly decreased with AA 10^{-6} and 10^{-5} M from 542.6 ± 78.6 nM to 217.7 ± 65.4 nM and 257.1 ± 52.6 nM, respectively.

AnxA1 (10^{-10} M) increased glycoconjugate secretion by 1.9 ± 0.3 fold above basal (**Figure 10B**, n=3). This response was significantly inhibited by AA (10^{-5} M) to 0.5 ± 0.4. Thus AnxA1 does not active the PLA2 pathway to stimulate an increase in $[Ca^{2+}]_i$ but does activate PLA2 to stimulate secretion in cultured rat conjunctival goblet cells.

DISCUSSION

In the present study, we showed that AnxA1 contributes to tear film and ocular surface homeostasis by activating the PLC pathway, including its downstream effectors IP_3 and PKC, through interaction with the ALX/FPR2 receptor (**Figure 11**). This results agrees with findings in Hodges et al. (12) using a desensitization protocol that indicates that AnxA1 interacts with the same receptor as LXA4 and RvD1, the ALX/FPR2 receptor. This interaction increases $[Ca^{2+}]_i$ and stimulates glycoconjugate

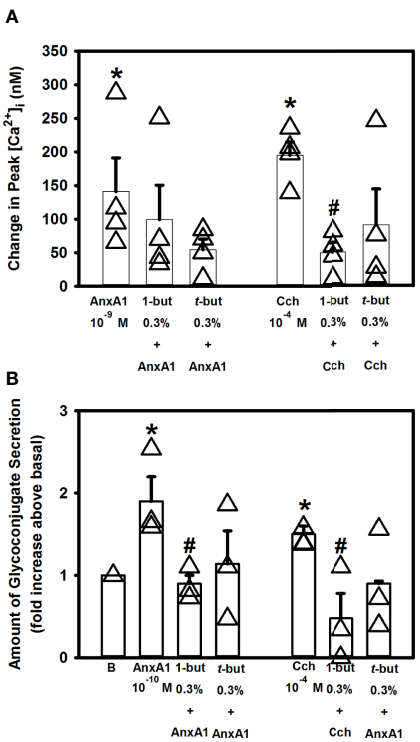

FIGURE 9 | AnxA1 does not active the phospholipase D (PLD) pathway to increase $[Ca^{2+}]_i$ but activates it to stimulate secretion in cultured rat conjunctival goblet cells. Rat conjunctival goblet cells were treated with vehicle, the PLD inhibitor 1-butanol (1-but) or the inactive inhibitor *t*-butanol (*t*-but) for 15 minutes prior to stimulation with annexin A1 (AnxA1, 10^{-9} M) in **(A)** or with AnxA1 at 10^{-10} M in **(B)**, or carbachol (Cch, 10^{-4} M). Change in peak $[Ca^{2+}]_i$ is shown in **(A)** Glycoconjugate secretion is shown in **(B)** Data are mean ± SEM from 4 **(A)** or 3 **(B)** independent experiments. *indicates significant difference from basal. #indicates significant difference from either AnxA1 or Cch alone.

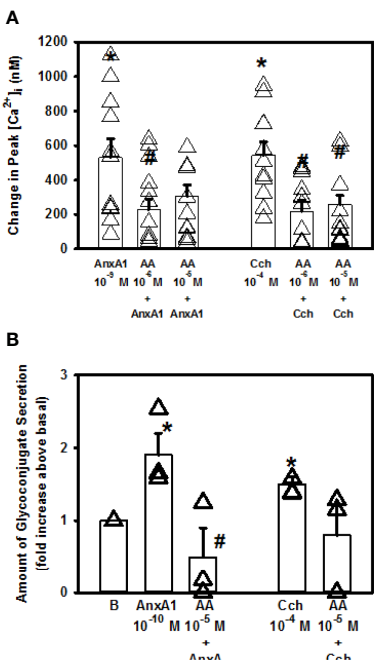

FIGURE 10 | AnxA1 does not active the phospholipase A_2 (PLA_2) pathway to increase $[Ca^{2+}]_i$ but activates it to stimulate secretion in cultured rat conjunctival goblet cells. Rat conjunctival goblet cells were preincubated with either vehicle or the PLA_2 inhibitor aristolochic acid (AA, 10^{-5} M) for 30 minutes prior to stimulation with annexin A1 (AnxA1, 10^{-9} M) in **(A)** or with AnxA1 at 10^{-10} M in **(B)**, or carbachol (Cch, 10^{-4} M). Change in peak $[Ca^{2+}]_i$ is shown in **(A)** Glycoconjugate secretion is shown in **(B)** Data are mean ± SEM from 4 **(A)** or 3 **(B)** independent experiments. *indicates significant difference from basal. #indicates significant difference from AnxA1 alone.

secretion including the protective mucin MUC5AC from conjunctival goblet cells. AnxA1-stimulated increase in $[Ca^{2+}]_i$ is dependent on both intracellular Ca^{2+} stores and influx of extracellular Ca^{2+} consistent with an interaction with Orai and STIM-1 known to regulate these processes in most tissues in which stimulation of G-protein-coupled receptors activates PLC (34).

AnxA1 is present in a variety of other tissues like bone marrow, the intestine and lungs (14, 35). In this study, we showed by RT-PCR that AnxA1 is expressed in conjunctival goblet cells and thus is available to activate these cells. This indicates that AnxA1 not only works during ocular inflammation, but also under physiological conditions, by secreting a basal level of mucins to the tear film and thus maintaining ocular homeostasis. We have demonstrated this for other SPMs including LXA_4, RvD1, RvD2, maresin 1, and RvE1 (10–12). Unlike the lipid SPMs AnxA1 is a protein, thus we were able to verify its expression by RT-PCR. In contrast, complex lipidomic measurements are needed to detect the presence of the lipid SPMs. As the lipid LXA_4 is produced by the cornea, it is possible that LXA_4 could diffuse *via* tears to goblet cells in order to stimulate glycoconjugate secretion. In contrast, AnxA1 is found in conjunctival goblet cells and could be secreted to act upon goblet cells or stratified squamous cells. As AnxA1 is both present and has a role in goblet cell function, AnxA1 likely plays a role in ocular health under physiological conditions as well as preventing or treating the multitude of ocular surface inflammatory diseases. Future study of the regulation of AnxA1 synthesis and secretion in conjunctival goblet cells is warranted.

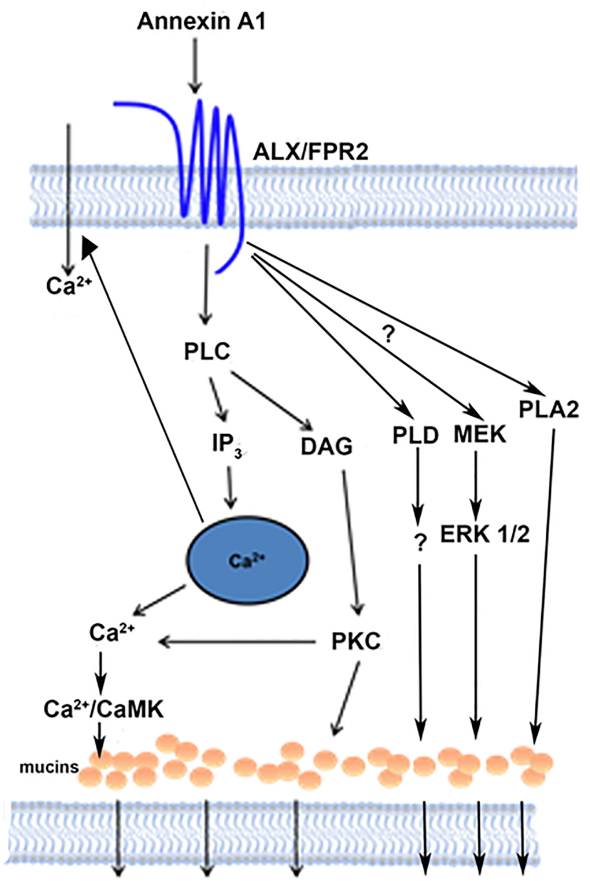

FIGURE 11 | Schematic diagram of signaling pathways activated by AnxA1. AnxA1 binds to the ALX/FPR2 receptor to active the PLC, PLD, and PLA2 pathways, and consequently the secretion of mucins from conjunctival goblet cells. AnxA1 also stimulates influx of Ca^{2+}. PLC, phospholipase C; DAG, diacylglycerol; IP_3, inositol triphosphate; PKC, protein kinase C; Ca^{2+}/CamK, calcium/calmodulin-dependent kinase; PLD, phospholipase D; MEK, mitogen-activated protein kinase kinase; ERK 1/2, extracellular regulated kinase; PLA2, phospholipase A2.

The ALX/FPR2 receptor is a G-protein-coupled receptor and is the receptor to which AnxA1 binds (36). In addition to its presence on goblet cells (12) the ALX/FPR2 receptor has been identified in human neutrophils, epithelial cells, endothelial cells and monocytes (37, 38). Using ALX/FPR2, AnxA1 functions to resolve diverse inflammatory events, including reduction of joint injury in experimental arthritis (39), lessening of salivary gland inflammation (40), and contributes to corneal wound healing (41). AnxA1 in uterine epithelial cells also activates the ALX/FPR2 receptor to upregulate the membrane-spanning mucin MUC1, tight junction molecules claudin-1 and occludens 1 to increase adherence of trophoblast steroids, a model for embryo implantation (42). Herein we showed that AnxA1 activates the ALX/FPR2 receptor in rat conjunctival goblet cells and that this activation leads to the increase in $[Ca^{2+}]_i$ and secretion of mucins into the tear film. We previously studied the SPMs LXA_4 and RvD1, which also activate the ALX/FPR2 receptor in rats. Cooray et al. have shown that the ALX/FPR2 receptors can homodimerize or heterodimerize with FPR1 or FPR3 depending on which agonist is bound (43). In addition, ALX/FPR2 has multiple binding sites notably different lipid and protein sites and binds to multiple compounds (44). AnxA1, a protein, and RvD1 and LXA_4, which are lipids, bind to different receptor regions in addition to inducing dissimilar receptor conformations (45). This differential binding and a potential difference in FPR receptor family dimerization could explain the complex desensitization we obtained with addition of AnxA1, LXA_4, and RvD1 (46). These dissimilarities could make the three compounds differ in their effectiveness to treat ocular allergy and other forms of ocular inflammation.

This differential binding of AnxA1, LXA_4, and RvD1 to bind to the same receptor in conjunctival goblet cells could also lead to ligand-specific activation of signaling pathways. In fact, the AnxA1, LXA_4, and RvD1 activation of downstream signaling cascades are not fully similar. While AnxA1, LXA_4, and RvD1 each activate the PLC pathway, only LXA_4 and RvD1 activate PLD, PLA_2 and ERK 1/2 (10, 12) to stimulate an increase both in $[Ca^{2+}]_i$ and mucin secretion. This pattern of pathway activation is consistent with AnxA1 activating the peptide site on ALX/FPR2, whereas LXA_4 and RvD1 activate the lipid site or overlapping sites.

In the present study, we found AnxA1 to have a peak increase in $[Ca^{2+}]_i$ at a 10^{-9} M concentration, while the maximum

response for secretion was at 10^{-10} M. Furthermore, AnxA1 at 10^{-8} M did not even increase secretion. These findings could be due to several factors. The increase in $[Ca^{2+}]_i$ occurs very rapidly, within seconds, and is measured in the time frame of seconds. In contrast, secretion, although it can occur rapidly, is measured after 2 hours. The rapid increase in $[Ca^{2+}]_i$ may not directly link to secretion. The peak $[Ca^{2+}]_i$ measured is primarily a function of Ca^{2+} release from intracellular stores whereas stimulation of secretion also is regulated by the subsequent influx of Ca^{2+} as well as the size of the intracellular Ca^{2+} stores. The maximum concentration of AnxA1 used to increase the $[Ca^{2+}]_i$ compared to that used for secretion may result from the differential dependence on the use of distinct mechanisms of Ca^{2+} handling in the goblet cells.

In further support of the independence of AnxA1 concentration on peak $[Ca^{2+}]$ and secretion is that secretion, but not peak $[Ca^{2+}]$ is stimulated by AnxA1 activation of PLA_2, PLD, and ERK1/2. Thus the increase in peak $[Ca^{2+}]$ and secretion are differentially regulated by AnxA1. This is in contrast to the increase in peak $[Ca^{2+}]$ and secretion that when stimulated by LXA_4 or RvD1 are both dependent on activation of the PLC, PLD, and PLA_2 pathways. This finding is also consistent with binding of the protein and the lipids to different sites on ALX/FPR2.

In the present study we found that AnxA1 was able to significantly increase $[Ca^{2+}]_i$ at a notably low concentration (10^{-12} M) in conjunctival goblet cells. In contrast, LXA_4 increased $[Ca^{2+}]_i$ at 10^{-8} M (10). Unfortunately the effect of RvD1 concentration on $[Ca^{2+}]_i$ was not performed at concentrations below 10^{-10} M (unpublished data, DA Dartt 2020). The differential effect of AnxA1 and LXA_4 concentration on $[Ca^{2+}]_i$ is consistent with their binding to different areas on the ALX/FPR2 receptor.

Furthermore, we found that AnxA1 was not dependent on either the ERK 1/2, PLA2, or the PLD pathway to increase $[Ca^{2+}]_i$ although AnxA1 does utilize these pathways to stimulate secretion. In conjunctival goblet cells AnxA1 did not activate ERK 1/2 pathway to increase $[Ca^{2+}]_i$, but rather more likely AnxA1 increased $[Ca^{2+}]_i$ to activate ERK1/2. ERK1/2 activity can be Ca^{2+}-dependent *via* activation of PLC by a G-protein-coupled receptor or can be independent of Ca^{2+} when activated by β-arrestin-dependent down regulation of G-protein-coupled receptors (47). Published literature showed that in multiple tissues the binding of AnxA1 to the ALX/FPR2 receptor leads to the transient phosphorylation of ERK 1/2 (7, 13, 48, 49), which is associated with a prompt increase in $[Ca^{2+}]_i$ (7, 38, 50). This suggests that in goblet cells, the activation of ERK 1/2 occurs downstream of the rise of $[Ca^{2+}]_i$ after activation of PLC. Similarly for AnxA1 activation of PLD, the rise in Ca^{2+} occurs before activation of PLD. An increase in Ca^{2+} and activation of PKC as could occur by PLC stimulation could activate PLD in the goblet cells as documented in a mast cell line (51). The signaling pathways activated by AnxA1 are complex, cell specific, and species dependent.

The function of AnxA1 has been studied in a variety of disease models in order to explore this agonist's potential as a novel anti-inflammatory therapeutic agent, including models of inflammatory bowel disease (52), rheumatoid arthritis (53), chronic atherogenesis (54), myocardial reperfusion injury (55), myocardial infarction (56), and now ocular inflammation. AnxA1 is thought to have potential as a new treatment option for inflammation by being an effector molecule of glucocorticoids (57). Synthetic glucocorticoids play an extensive and crucial role in the treatment of unwanted and uncontrolled inflammation but come with potentially harmful metabolic side effects with long-term use (57). It is believed that therapeutic application of endogenous anti-inflammatory mediators like AnxA1 will be effective and cause fewer side effects by inducing natural pathways of resolution of inflammation (58–60). AnxA1 could be used therapeutically to treat the multiple inflammatory diseases of the ocular surface especially dry eye and ocular allergy as well as to prevent these diseases or to maintain ocular surface homeostasis in health.

In conclusion, our findings demonstrate that the glucocorticoid effector protein AnxA1 has potential in prevention or as a new treatment for dry eye, allergic conjunctivitis and other forms of ocular surface inflammation through its effect on conjunctival goblet cells. AnxA1 works through activation of the ALX/FPR2 receptor to stimulate multiple signaling pathways, ultimately leading to the secretion of high molecular weight glycoconjugates including mucins into the ocular tear film. These mucins are a crucial component of a healthy tear film, and thus the regulation of mucin secretion from conjunctival goblet cells by AnxA1 is an important contributor to ocular surface health, and prevention of ocular surface disease and treatment of these diseases.

AUTHOR'S NOTE

This manuscript is dedicated to Robin R. Hodges who passed away on March 13, 2021. For over 30 years she managed the Dartt laboratory ensuring its excellence. She was respected and beloved by all.

DATA AVAILABILITY STATEMENT

The raw data supporting the conclusions of this article will be made available by the authors, without undue reservation.

ETHICS STATEMENT

The animal study was reviewed and approved by Schepens Eye Research Institute Animal Care and Use of Committee.

AUTHOR CONTRIBUTIONS

AL, MO, JB, and RH performed experiments. AL, RH, TU, CS, and DD wrote the manuscript. All authors contributed to the article and approved the submitted version.

FUNDING

This work was supported by Norwegian Research Council to AL and by NIH R01 EY019470 to DD and RO1GM038765 to CS.

SUPPLEMENTARY MATERIAL

The Supplementary Material for this article can be found online at: https://www.frontiersin.org/articles/10.3389/fimmu.2021.618653/full#supplementary-material

Supplementary Figure 1 | Chelation of Ca_i^{2+} blocks AnxA1-stimulated increase in $[Ca^{2+}]_i$ in cultured rat conjunctival goblet cells. Cultured rat goblet cells were preincubated with the Ca^{2+} chelator BAPTA/AM (10^{-4} M) prior to stimulation with either AnxA1 (10^{-9} M) or carbachol (Cch, 10^{-4} M) and change in peak $[Ca^{2+}]_i$ shown. Data are mean ± SEM from 4 independent experiments. * indicates significant difference from basal; # indicates significant difference from either AnxA1 or Cch alone.

Supplementary Figure 2 | AnxA1 is not dependent on protein kinase A (PKA) to increase $[Ca^{2+}]_i$ in cultured rat conjunctival goblet cells. Goblet cells were preincubated with the PKA inhibitor H89 for 30 minutes before stimulation with vehicle, annexin A1 (AnxA1, 10^{-9} M) in **(A)** or with AnxA1 (10^{-10} M) in **(B)**, or vasoactive intestinal peptide (VIP, 10^{-8} M). Change in peak $[Ca^{2+}]_i$ is shown in **(A)**. Glycoconjugate secretion is shown in **(B)**. B indicates basal (vehicle) in **(B)**. Data are mean ± SEM from 9 (A) or 3 **(B)** independent experiments. * indicates significant difference from zero; # indicates significance from AnxA1 or VIP alone.

REFERENCES

1. Li D, Hodges RR, Jiao J, Carozza RB, Shatos MA, Chiang N, et al. Resolvin D1 and aspirin-triggered resolvin D1 regulate histamine-stimulated conjunctival goblet cell secretion. *Mucosal Immunol* (2013) 6(6):1119–30. doi: 10.1038/mi.2013.7
2. Fredman G, Serhan CN. Specialized proresolving mediator targets for RvE1 and RvD1 in peripheral blood and mechanisms of resolution. *Biochem J* (2011) 437(2):185–97. doi: 10.1042/BJ20110327
3. Dartt DA, Hodges RR, Li D, Shatos MA, Lashkari K, Serhan CN. Conjunctival goblet cell secretion stimulated by leukotrienes is reduced by resolvins D1 and E1 to promote resolution of inflammation. *J Immunol* (2011) 186(7):4455–66. doi: 10.4049/jimmunol.1000833
4. Serhan CN, Chiang N, Van Dyke TE. Resolving inflammation: dual anti-inflammatory and pro-resolution lipid mediators. *Nat Rev Immunol* (2008) 8 (5):349–61. doi: 10.1038/nri2294
5. Serhan CN, Arita M, Hong S, Gotlinger K. Resolvins, docosatrienes, and neuroprotectins, novel omega-3-derived mediators, and their endogenous aspirin-triggered epimers. *Lipids* (2004) 39(11):1125–32. doi: 10.1007/s11745-004-1339-7
6. Serhan CN, Savill J. Resolution of inflammation: the beginning programs the end. *Nat Immunol* (2005) 6(12):1191–7. doi: 10.1038/ni1276
7. Perretti M, D'Acquisto F. Annexin A1 and glucocorticoids as effectors of the resolution of inflammation. *Nat Rev Immunol* (2009) 9(1):62–70. doi: 10.1038/nri2470
8. Dartt DA, Masli S. Conjunctival epithelial and goblet cell function in chronic inflammation and ocular allergic inflammation. *Curr Opin Allergy Clin Immunol* (2014) 14(5):464–70. doi: 10.1097/ACI.0000000000000098
9. Dartt DA. Control of mucin production by ocular surface epithelial cells. *Exp eye Res* (2004) 78(2):173–85. doi: 10.1016/j.exer.2003.10.005
10. Lippestad M, Hodges RR, Utheim TP, Serhan CN, Dartt DA. Resolvin D1 Increases Mucin Secretion in Cultured Rat Conjunctival Goblet Cells *via* Multiple Signaling Pathways. *Investigative Ophthalmol Vis Sci* (2017) 58: (11):4530–44. doi: 10.1167/iovs.17-21914
11. Lippestad M, Hodges RR, Utheim TP, Serhan CN, Dartt DA. Signaling pathways activated by resolvin E1 to stimulate mucin secretion and increase intracellular Ca(2+) in cultured rat conjunctival goblet cells. *Exp Eye Res* (2018) 173:64–72. doi: 10.1016/j.exer.2018.04.015
12. Hodges RR, Li D, Shatos MA, Bair JA, Lippestad M, Serhan CN, et al. Lipoxin A4 activates ALX/FPR2 receptor to regulate conjunctival goblet cell secretion. *Mucosal Immunol* (2017) 10(1):46–57. doi: 10.1038/mi.2016.33
13. Hayhoe RP, Kamal AM, Solito E, Flower RJ, Cooper D, Perretti M. Annexin 1 and its bioactive peptide inhibit neutrophil-endothelium interactions under flow: indication of distinct receptor involvement. *Blood* (2006) 107(5):2123–30. doi: 10.1182/blood-2005-08-3099
14. Gavins FNE, Hickey MJ. Annexin A1 and the regulation of innate and adaptive immunity. *Front Immunol* (2012) 3:1–11. doi: 10.3389/fimmu.2012.00354
15. Sapolsky RM, Romero LM, Munck AU. How do glucocorticoids influence stress responses? Integrating permissive, suppressive, stimulatory, and preparative actions. *Endocrine Rev* (2000) 21(1):55–89. doi: 10.1210/er.21.1.55
16. Yazid S, Norling LV, Flower RJ. Anti-inflammatory drugs, eicosanoids and the annexin A1/FPR2 anti-inflammatory system. *Prostaglandins Other Lipid Mediat* (2012) 98(3-4):94–100. doi: 10.1016/j.prostaglandins.2011.11.005
17. Purvis GSD, Solito E, Thiemermann C. Annexin-A1: Therapeutic Potential in Microvascular Disease. *Front Immunol* (2019) 10:938. doi: 10.3389/fimmu.2019.00938
18. He M, Lippestad M, Li D, Hodges RR, Utheim TP, Dartt DA. Activation of the EGF Receptor by Histamine Receptor Subtypes Stimulates Mucin Secretion in Conjunctival Goblet Cells. *Invest Ophthalmol Visual Sci* (2018) 59(8):3543–53. doi: 10.1167/iovs.18-2476
19. Li D, Jiao J, Shatos MA, Hodges RR, Dartt DA. Effect of VIP on intracellular [Ca2+], extracellular regulated kinase 1/2, and secretion in cultured rat conjunctival goblet cells. *Invest Ophthalmol Vis Sci* (2013) 54(4):2872–84. doi: 10.1167/iovs.12-11264
20. Dartt DA, Rios JD, Kanno H, Rawe IM, Zieske JD, Ralda N, et al. Regulation of conjunctival goblet cell secretion by Ca(2+)and protein kinase C. *Exp Eye Res* (2000) 71(6):619–28. doi: 10.1006/exer.2000.0915
21. Hodges RR, Dartt DA. Tear Film Mucins: Front Line Defenders of the Ocular Surface; Comparison with Airway and Gastrointestinal Tract Mucins. *Exp eye Res* (2013) 117:62–78. doi: 10.1016/j.exer.2013.07.027
22. Li D, Carozza RB, Shatos MA, Hodges RR, Dartt DA. Effect of histamine on Ca(2+)-dependent signaling pathways in rat conjunctival goblet cells. *Invest Ophthalmol Visual Sci* (2012) 53(11):6928–38. doi: 10.1167/iovs.12-10163
23. Contreras-Ruiz L, Ghosh-Mitra A, Shatos MA, Dartt DA, Masli S. Modulation of Conjunctival Goblet Cell Function by Inflammatory Cytokines. *Mediators Inflamm* (2013) 2013:1–11. doi: 10.1155/2013/636812
24. Hayashi D, Li D, Hayashi C, Shatos M, Hodges RR, Dartt DA. Role of histamine and its receptor subtypes in stimulation of conjunctival goblet cell secretion. *Invest Ophthalmol Visual Sci* (2012) 53(6):2993–3003. doi: 10.1167/iovs.11-8748
25. Luo D, Broad LM, Bird GS, Putney JW Jr. Signaling pathways underlying muscarinic receptor-induced [Ca2+]i oscillations in HEK293 cells. *J Biol Chem* (2001) 276(8):5613–21. doi: 10.1074/jbc.M007524200
26. Walther A, Riehemann K, Gerke V. A novel ligand of the formyl peptide receptor: annexin I regulates neutrophil extravasation by interacting with the FPR. *Mol Cell* (2000) 5(5):831–40. doi: 10.1016/S1097-2765(00)80323-8
27. Putney JW, Tomita T. Phospholipase C Signaling and Calcium Influx. *Adv Biol Regul* (2012) 52(1):152–64. doi: 10.1016/j.advenzreg.2011.09.005
28. Olsen MV, Lyngstadaas AV, Bair JA, Hodges RR, Utheim TP, Serhan CN, et al. Maresin 1, a specialized proresolving mediator, stimulates intracellular [Ca(2+)] and secretion in conjunctival goblet cells. *J Cell Physiol* (2021) 236 (1):340–53. doi: 10.1002/jcp.29846
29. Mikoshiba K. Role of IP3 receptor signaling in cell functions and diseases. *Adv Biol Regul* (2015) 57:217–27. doi: 10.1016/j.jbior.2014.10.001
30. Marcelo KL, Means AR, York B. The Ca(2+)/Calmodulin/CaMKK2 Axis: Nature's Metabolic CaMshaft. *Trends Endocrinol metabol: TEM* (2016) 27 (10):706–18. doi: 10.1016/j.tem.2016.06.001
31. Kanno H, Horikawa Y, Hodges RR, Zoukhri D, Shatos MA, Rios JD, et al. Cholinergic agonists transactivate EGFR and stimulate MAPK to induce goblet cell secretion. *Am J Physiol Cell Physiol* (2003) 284(4):C988–98. doi: 10.1152/ajpcell.00582.2001

32. Dartt DA, Kanno H, Rios J, Zoukhri D. Role of mitogen-activated protein kinase in cholinergic stimulation of conjunctival goblet cell secretion. *Adv Exp Med Biol* (2002) 506(Pt A):297–300. doi: 10.1007/978-1-4615-0717-8_41
33. Foster DA, Xu L. Phospholipase D in cell proliferation and cancer. *Mol Cancer Research: MCR* (2003) 1(11):789–800.
34. Bird GS, Putney JW. "Pharmacology of Store-Operated Calcium Entry Channels". In: JA Kozak, JW Putney, editors. *Calcium Entry Channels in Non-Excitable Cells*. Boca Raton: CRC Press (2018). p. 311–24.
35. Trentin PG, Ferreira TPT, Arantes ACS, Ciambarella BT, Cordeiro RSB, Flower RJ, et al. Annexin A1 mimetic peptide controls the inflammatory and fibrotic effects of silica particles in mice. *Br J Pharmacol* (2015) 172(12):3058–71. doi: 10.1111/bph.13109
36. Spurr L, Nadkarni S, Pederzoli-Ribeil M, Goulding NJ, Perretti M, D'Acquisto F. Comparative analysis of Annexin A1-formyl peptide receptor 2/ALX expression in human leukocyte subsets. *Int Immunopharmacol* (2011) 11 (1):55–66. doi: 10.1016/j.intimp.2010.10.006
37. Chiang N, Serhan CN, Dahlen SE, Drazen JM, Hay DW, Rovati GE, et al. The lipoxin receptor ALX: potent ligand-specific and stereoselective actions *in vivo*. *Pharmacol Rev* (2006) 58(3):463–87. doi: 10.1124/pr.58.3.4
38. Babbin BA, Lee WY, Parkos CA, Winfree LM, Akyildiz A, Perretti M, et al. Annexin I regulates SKCO-15 cell invasion by signaling through formyl peptide receptors. *J Biol Chem* (2006) 281(28):19588–99. doi: 10.1074/jbc.M513025200
39. Odobasic D, Jia Y, Kao W, Fan H, Wei X, Gu R, et al. Formyl peptide receptor activation inhibits the expansion of effector T cells and synovial fibroblasts and attenuates joint injury in models of rheumatoid arthritis. *Int Immunopharmacol* (2018) 61:140–9. doi: 10.1016/j.intimp.2018.05.028
40. Wang CS, Baker OJ. The G-Protein-Coupled Receptor ALX/Fpr2 Regulates Adaptive Immune Responses in Mouse Submandibular Glands. *Am J Pathol* (2018) 188(7):1555–62. doi: 10.1016/j.ajpath.2018.04.003
41. Leedom AJ, Sullivan AB, Dong B, Lau D, Gronert K. Endogenous LXA4 circuits are determinants of pathological angiogenesis in response to chronic injury. *Am J Pathol* (2010) 176(1):74–84. doi: 10.2353/ajpath.2010.090678
42. Hebeda CB, Sandri S, Benis CM, Md P-S, RA L, Reutelingsperger C, et al. Annexin A1/Formyl Peptide Receptor Pathway Controls Uterine Receptivity to the Blastocyst. *Cells* (2020) 9(5):1188. doi: 10.3390/cells9051188
43. Cooray SN, Gobbetti T, Montero-Melendez T, McArthur S, Thompson D, Clark AJ, et al. Ligand-specific conformational change of the G-protein-coupled receptor ALX/FPR2 determines proresolving functional responses. *Proc Natl Acad Sci U S A* (2013) 110(45):18232–7. doi: 10.1073/pnas.1308253110
44. Back M, Powell WS, Dahlen SE, Drazen JM, Evans JF, Serhan CN, et al. Update on leukotriene, lipoxin and oxoeicosanoid receptors: IUPHAR Review 7. *Br J Pharmacol* (2014) 171(15):3551–74. doi: 10.1111/bph.12665
45. Le Y, Ye RD, Gong W, Li J, Iribarren P, Wang JM. Identification of functional domains in the formyl peptide receptor-like 1 for agonist-induced cell chemotaxis. *FEBS J* (2005) 272(3):769–78. doi: 10.1111/j.1742-4658.2004.04514.x
46. Maderna P, Cottell DC, Toivonen T, Dufton N, Dalli J, Perretti M, et al. FPR2/ALX receptor expression and internalization are critical for lipoxin A4 and annexin-derived peptide-stimulated phagocytosis. *FASEB J* (2010) 24 (11):4240–9. doi: 10.1096/fj.10-159913
47. Lin A, DeFea KA. beta-Arrestin-kinase scaffolds: turn them on or turn them off? *Wiley Interdiscip Rev Syst Biol Med* (2013) 5(2):231–41. doi: 10.1002/wsbm.1203
48. He R, Sang H, Ye RD. Serum amyloid A induces IL-8 secretion through a G protein-coupled receptor, FPRL1/LXA4R. *Blood* (2003) 101(4):1572–81. doi: 10.1182/blood-2002-05-1431
49. Cattaneo F, Parisi M, Ammendola R. Distinct Signaling Cascades Elicited by Different Formyl Peptide Receptor 2 (FPR2) Agonists. *Int J Mol Sci* (2013) 14 (4):7193–230. doi: 10.3390/ijms14047193
50. Solito E, Kamal A, Russo-Marie F, Buckingham JC, Marullo S, Perretti M. A novel calcium-dependent proapoptotic effect of annexin 1 on human neutrophils. *FASEB J* (2003) 17(11):1544–6. doi: 10.1096/fj.02-0941fje
51. Chahdi A, Choi WS, Kim YM, Fraundorfer PF, Beaven MA. Serine/threonine protein kinases synergistically regulate phospholipase D1 and 2 and secretion in RBL-2H3 mast cells. *Mol Immunol* (2002) 38(16-18):1269–76. doi: 10.1016/S0161-5890(02)00074-3
52. Leoni G, Neumann PA, Kamaly N, Quiros M, Nishio H, Jones HR, et al. Annexin A1-containing extracellular vesicles and polymeric nanoparticles promote epithelial wound repair. *J Clin Invest* (2015) 125(3):1215–27. doi: 10.1172/JCI76693
53. Yang YH, Morand E, Leech M. Annexin A1: potential for glucocorticoid sparing in RA. *Nat Rev Rheumatol* (2013) 9(10):595–603. doi: 10.1038/nrrheum.2013.126
54. Kusters DH, Chatrou ML, Willems BA, De Saint-Hubert M, Bauwens M, van der Vorst E, et al. Pharmacological Treatment with Annexin A1 Reduces Atherosclerotic Plaque Burden in LDLR-/- Mice on Western Type Diet. *PLoS One* (2015) 10(6):e0130484. doi: 10.1371/journal.pone.0130484
55. Qin C, Buxton KD, Pepe S, Cao AH, Venardos K, Love JE, et al. Reperfusion-induced myocardial dysfunction is prevented by endogenous annexin-A1 and its N-terminal-derived peptide Ac-ANX-A1(2-26). *Br J Pharmacol* (2013) 168 (1):238–52. doi: 10.1111/j.1476-5381.2012.02176.x
56. Qin C, Yang YH, May L, Gao X, Stewart AG, Tu Y, et al. Cardioprotective potential of annexin-A1 mimetics in myocardial infarction. *Pharmacol Ther* (2015) 148:47–65. doi: 10.1016/j.pharmthera.2014.11.012
57. Perretti M, Gavins FN. Annexin 1: an endogenous anti-inflammatory protein. *News Physiol Sci: an Int J Physiol Produced Jointly by Int Union Physiol Sci Am Physiol Soc* (2003) 18:60–4. doi: 10.1152/nips.01424.2002
58. Perretti M, Dalli J. Exploiting the Annexin A1 pathway for the development of novel anti-inflammatory therapeutics. *Br J Pharmacol* (2009) 158(4):936–46. doi: 10.1111/j.1476-5381.2009.00483.x
59. Sugimoto MA, Vago JP, Teixeira MM, Sousa LP. Annexin A1 and the Resolution of Inflammation: Modulation of Neutrophil Recruitment, Apoptosis, and Clearance. *J Immunol Res* (2016) 2016:1–13. doi: 10.1155/2016/8239258
60. Perretti M. Endogenous interaction. *Trends Pharmacol Sci* (1997) 18(11):418–25. mediators that inhibit the leukocyte-endothelium. doi: 10.1016/S0165-6147(97)01116-4

Conflict of Interest: The authors declare that the research was conducted in the absence of any commercial or financial relationships that could be construed as a potential conflict of interest.

Copyright © 2021 Lyngstadaas, Olsen, Bair, Hodges, Utheim, Serhan and Dartt. This is an open-access article distributed under the terms of the Creative Commons Attribution License (CC BY). The use, distribution or reproduction in other forums is permitted, provided the original author(s) and the copyright owner(s) are credited and that the original publication in this journal is cited, in accordance with accepted academic practice. No use, distribution or reproduction is permitted which does not comply with these terms.

frontiers in Immunology

ORIGINAL RESEARCH
published: 19 May 2021
doi: 10.3389/fimmu.2021.687192

12/15-Lipoxygenase Regulates IL-33-Induced Eosinophilic Airway Inflammation in Mice

Jun Miyata[1,2,3], *Yoshiyuki Yokokura*[4], *Kazuyo Moro*[5,6,7], *Hiroyuki Arai*[4], *Koichi Fukunaga*[2] *and Makoto Arita*[1,8,9*]

[1] Laboratory of Metabolomics, RIKEN Center for Integrative Medical Sciences, Yokohama, Japan, [2] Division of Pulmonary Medicine, Department of Medicine, Keio University School of Medicine, Tokyo, Japan, [3] Division of Infectious Diseases and Respiratory Medicine, Department of Internal Medicine, National Defense Medical College, Tokorozawa, Japan, [4] Graduate School of Pharmaceutical Sciences, The University of Tokyo, Tokyo, Japan, [5] Laboratory for Innate Immune Systems, RIKEN Center for Integrative Medical Sciences (IMS), Yokohama, Japan, [6] Laboratory for Innate Immune Systems, Department of Microbiology and Immunology, Graduate School of Medicine, Osaka University, Osaka, Japan, [7] Laboratory for Innate Immune Systems, Immunology Frontier Research Center, Osaka University, Osaka, Japan, [8] Division of Physiological Chemistry and Metabolism, Keio University Faculty of Pharmacy, Tokyo, Japan, [9] Cellular and Molecular Epigenetics Laboratory, Graduate School of Medical Life Science, Yokohama City University, Yokohama, Japan

OPEN ACCESS

Edited by:
Amiram Ariel,
University of Haifa, Israel

Reviewed by:
Nan Chiang,
Brigham and Women's Hospital and Harvard Medical School, United States
Michelle Amantea Sugimoto,
University College London, United Kingdom

***Correspondence:**
Makoto Arita
makoto.arita@riken.jp

Specialty section:
This article was submitted to Inflammation, a section of the journal Frontiers in Immunology

Received: *29 March 2021*
Accepted: *04 May 2021*
Published: *19 May 2021*

Citation:
Miyata J, Yokokura Y, Moro K, Arai H, Fukunaga K and Arita M (2021) 12/15-Lipoxygenase Regulates IL-33-Induced Eosinophilic Airway Inflammation in Mice. Front. Immunol. 12:687192. doi: 10.3389/fimmu.2021.687192

Dysregulated fatty acid metabolism is clinically associated with eosinophilic allergic diseases, including severe asthma and chronic rhinosinusitis. This study aimed to demonstrate the role of 12/15-lipoxygenase (12/15-LOX) in interleukin (IL)-33-induced eosinophilic airway inflammation; to this end, we used 12/15-LOX-deficient mice, which displayed augmented IL-33-induced lung inflammation, characterized by an increased number of infiltrated eosinophils and group 2 innate lymphoid cells (ILC2s) in the airway. Liquid chromatography-tandem mass spectrometry (LC-MS/MS)-based lipidomics revealed that the levels of a series of 12/15-LOX-derived metabolites were significantly decreased, and application of 14(S)-hydroxy docosahexaenoic acid (HDoHE), a major 12/15-LOX-derived product, suppressed IL-33-mediated eosinophilic inflammation in 12/15-LOX-deficient mice. Using bioactive lipid screening, we found that 14(S)-HDoHE and 10(S),17(S)-diHDoHE markedly attenuated ILC2 proliferation and cytokine production at micromolar concentration *in vitro*. In addition, maresin 1 (MaR1) and resolvin D1 (RvD1), 12/15-LOX-derived specialized proresolving mediators (SPMs), inhibited cytokine production of ILC2s at nanomolar concentration. These findings demonstrate the protective role of endogenous 12/15-LOX-derived lipid mediators in controlling ILC2-mediated eosinophilic airway inflammation and related diseases. Thus, 12/15-LOX-derived lipid mediators may represent a potential therapeutic strategy for ameliorating airway inflammation-associated conditions.

Keywords: 12/15-lipoxygenase, IL-33, docosahexaenoic acid, 14(S)-HDoHE, group 2 innate lymphoid cell, lipidomics, maresin, specialized proresolving mediator

INTRODUCTION

Asthma is a common disease affecting more than 300 million people worldwide, and the number of patients with asthma is rapidly increasing (1, 2). Genetic and environmental factors induce diverse immune responses that are classified into atopic and non-atopic phenotypes, mainly characterized by eosinophilic airway inflammation. Severe asthma is characterized by resistance to standardized treatments, including corticosteroids, and frequent exacerbation, which could worsen the quality of life in these patients. However, the exact mechanism underlying severe asthma has not been fully elucidated. Thus, it is necessary to elucidate its pathophysiological process.

Dysregulated metabolism of polyunsaturated fatty acids [arachidonic acid (AA), eicosapentaenoic acid (EPA), and docosahexaenoic acid (DHA)] is observed in allergic diseases, including severe asthma and its related diseases, such as aspirin-exacerbated respiratory disease and eosinophilic chronic rhinosinusitis (3, 4). This abnormality is partly characterized by impaired synthesis of specialized proresolving mediators (SPMs; lipoxins (LXs; LXA_4 and LXB_4), protectins (PD1 and PDX), resolvin D series (RvDs; RvD1-6), and maresins (MaRs; MaR1-2), which promote the resolution of inflammation. SPMs inhibit the migration of polymorphonuclear cells to inflammatory sites and enhance the phagocytic activity of apoptotic cells *via* macrophages (5, 6). These mediators are mainly biosynthesized *via* 15-lipoxygenase (LOX) in humans and 12/15-LOX, an ortholog of 15-LOX in mice, that are highly expressed in eosinophils and specific types of macrophages (7–10). Previously, we observed downregulated biosynthesis of 15-LOX-derived SPMs in eosinophils isolated from patients with severe asthma and eosinophilic chronic rhinosinusitis (7, 11–13). Systemic administration of SPMs suppressed pulmonary eosinophilic inflammation in murine models of asthma (14–18). These findings suggest the regulatory roles of 15-LOX and 12/15-LOX in eosinophilic inflammation in the lungs, although the causal relationships between these enzymes and severe allergic diseases remain unclear.

Interleukin (IL)-33 is an IL-1 family cytokine with potent inflammatory properties (19). The gene encoding ST2, an IL-33 receptor, is closely related to asthma susceptibility (20, 21). Group 2 innate lymphoid cells (ILC2s) are potent producers of type 2 cytokines, including IL-5 and IL-13, in response to IL-33 (22–24). Other cell types, including eosinophils, basophils, mast cells, and dendritic cells also respond to IL-33, showing proinflammatory reactions (25–35). IL-33 is highly expressed in airway mucosa or nasal polyps isolated from patients with asthma, and its expression level is well correlated with disease severity (36–39). Therefore, IL-33 is considered a pivotal regulator and potential therapeutic target in respiratory diseases with type-2 airway inflammation, including severe asthma.

In the present study, we investigated the regulatory roles of 12/15-LOX-derived lipid mediators in IL-33-induced eosinophilic airway inflammation in mice. Lipidomic analysis of inflamed lung tissue and *in vitro* lipid screening analysis using ILC2s were performed to demonstrate the roles of 12/15-LOX.

Abbreviations: Alox15, 12/15-lipoxygenase; AA, arachidonic acid; BALF, bronchial alveolar lavage fluid; DHA, docosahexaenoic acid; EPA, eicosapentaenoic acid; HDoHE, hydroxy docosahexaenoic acid; HE, hematoxylin eosin; HETE, hydroxyeicosatetraenoic acid; IL, interleukin; LC, liquid chromatography; LOX, lipoxygenase; LT, leukotriene; MaRs, maresins; MS/MS, tandem mass spectrometry; PAS, periodic acid Schiff; PD1, protectin D1; PDX, protectin DX; PG, prostaglandin; RT-PCR, reverse transcription-PCR; Rv, resolvin; SPM, specialized proresolving mediator.

MATERIALS AND METHODS

Mouse Experiments

Specific pathogen- and virus-antibody-free, 6-8-week-old, male C57BL/6J (C57BL/6) mice, weighing 25-30 g, were purchased from Charles River Laboratories, Japan. 12/15-LOX-deficient mice were obtained from the Jackson Laboratory (002778, Bar Harbor, ME, USA). All animals were housed at the facility in bubble barrier units (bioBubble, Fort Collins, Colo., USA) under positive pressure. The experimental protocol was reviewed and approved by the Laboratory Animal Care and Use Committee of Keio University of Medicine, the Animal Committee of the University of Tokyo, and the Animal Care and Use Committee of the RIKEN.

Administration of Reagents *In Vivo*

We administered 40 μL of PBS or IL-33 (R&D, 500 ng per mouse) *via* intranasal administration under anesthesia with intraperitoneal administration of ketamine (100 mg/kg) and xylazine (10 mg/kg). In some experiments, we simultaneously administered 5 μg/day of 14(S)-HDoHE (Cayman Chemical, Ann Arbor, MI, USA) *via* intraperitoneal injection.

Establishment of IL-33-Induced Airway Inflammation

We administered IL-33 (R&D Systems, Minneapolis, MN, 500 ng per mouse) for 3 consecutive days and analyzed them 1 or 4 days after the last challenge as previously described (40) with technical modification. Bronchoalveolar lavage fluid (BALF) was collected for cell counts and flow cytometric analysis, and lung tissue for the measurement of mRNA expression and histopathologic analysis. Formalin-fixed paraffin-embedded lung slides were stained with hematoxylin and eosin (HE) or periodic acid Schiff (PAS).

Collection of BALF

The mice were sacrificed by an overdose of intravenous pentobarbital at the indicated times after the last challenge. The trachea was cannulated, and the lungs were lavaged by washing twice with 0.7 mL of ice-cold PBS with EDTA (0.6 mM). The total number of cells in BALF was counted using a hemocytometer, and a differential cell count of 200 cells was determined on Diff-Quik-stained cytospin slides (Baxter Scientific Products, McGraw Park, Ill., USA) prepared with Auto Smear CF12D (Sakura Finetek, Tokyo, Japan). Flow cytometric analysis was performed for cell counts of specific types of lymphocytes (ILC2s and Th2 cells).

Targeted Liquid Chromatography Tandem Mass Spectrometry (LC-MS/MS)-Based Lipidomics

LC-MS/MS-based mediator lipidomics was performed as previously described (41). Lung tissues were homogenized in ice-cold methanol and kept in -20°C overnight. The methanolic extract was then diluted with water, acidified with HCl to a pH of 3.5, and applied to Sep-Pak C18 cartridges (Waters) for solid phase extraction. Deuterated internal standards (1 ng of leukotriene (LT) B_4-d4, LTD_4-d5, prostaglandin (PG) E_2-d4, and 15-HETE-d8 (Cayman Chemical, Ann Arbor, MI, USA) were added to the supernatants prior to extraction. For LC-MS/MS analysis, a triple quadrupole linear ion trap mass spectrometer (QTRAP 5500; AB Sciex, Foster City, CA) equipped with a 1.7-μm, 1.0 × 150 mm Acquity UPLC™ BEH C18 column (Waters Corp., Milford, MA) was used. MS/MS analyses were conducted in negative ion mode, and the eicosanoids and docosanoids were identified and quantified by multiple reaction monitoring. Calibration curves were obtained over a range of 1–1,000 pg. The LC retention times for each compound were determined using the corresponding synthetic standards. PD1 and PDX, stereoisomers, were not separable under this LC-MS/MS setting.

Functional Assays of ILC2s *In Vitro*

Mouse ILC2s were isolated from mesentery using a previously reported method (42). Purified ILC2s were cultured in 96-well round-bottom plates in 200 μL RPMI-1640 media containing 10% FCS, HEPES buffer, non-essential amino acids, penicillin, streptomycin, and 2-mercaptoethanol in the presence of IL-2 (10 ng/mL) at 37°C. To comprehensively evaluate the effect of lipid metabolites, cultured ILC2s were seeded at a density of 10,000 cells per well into 96-well round-bottom plates in the absence of IL-2, and IL-33 was added to the culture medium at a final concentration of 10 ng/mL after pretreatment for 30 min with lipid metabolites (10^{-11} M – 10^{-5} M). One hundred microliters of supernatant were collected for the cytokine assay, and ILC2s were counted by flow cytometry on day 4. For apoptosis analysis, ILC2s were stained with Annexin V and propidium iodide (PI) according to the manufacturer's protocols (Apoptosis Detection Kit, BD Pharmingen), and then analyzed by flow cytometry on day 1 and day 4. All data were analyzed using FlowJo software (TreeStar, Ashland, OR, USA).

Statistical Analysis

Data are presented as the mean ± SEM. Dose-response relationships of lipid metabolites on ILC2 activities were analyzed with repeated measures of analysis of variance, followed by the Bonferroni/Dunn procedure as a *post hoc* test. Data were analyzed using GraphPad Prism version 4.0c (GraphPad Software, San Diego, CA). Statistical significance was set at $P < 0.05$.

RESULTS

12/15-LOX Deficiency Augmented IL-33-Induced Airway Eosinophilic Inflammation

To determine whether 12/15-LOX affects the disease onset and/or progression of airway eosinophilic inflammation, we used mice deficient in the gene encoding 12/15-LOX (*alox15*) in a murine model of IL-33-induced innate airway eosinophilic inflammation. 12/15-LOX-deficient (12/15-$LOX^{-/-}$) mice developed more severe airway inflammation associated with an increased number of eosinophils and lymphocytes in BALF compared to controls (**Figure 1A**). Lymphocyte subset analysis revealed a significant increase in the number of ILC2s and Th2 cells ($CD4^+ST2^+$ cells) in BALF from IL-33-challenged 12/15-$LOX^{-/-}$ mice compared to wild-type mice (**Figure 1B**). Importantly, the number of ILC2s was greater than that of Th2 cells (**Figure 1B**). Expression of mRNA levels of type 2 cytokines (*il5*, *il13*) and chemokines for eosinophils (*ccl11*, *ccl24*, *and ccl26*), which are critical inducers of eosinophilic inflammation, in the lungs was significantly higher in IL-33-treated 12/15-$LOX^{-/-}$ mice than in wild-type mice (**Figure 1C**). Histological analysis demonstrated prominent accumulation of inflammatory cells around the bronchus and increased mucus production in the lung tissue stained with HE and PAS, respectively (**Figures 1D, E**). In addition, the absence of 12/15-LOX had no impact on the number of cells and lymphocyte subset including Th2 cells and ILC2s in BALF at the steady state (Supplementary **Figures 1A, B**).

Lipidomic Profile of Lung Tissue During IL-33-Induced Airway Eosinophilic Inflammation

To investigate the lipid mediator profiles in the lungs during IL-33-induced eosinophilic pulmonary inflammation, LC-MS/MS-based mediator lipidomics was performed. The amounts of lipid mediators on days 1 and 4 following the last challenge are summarized in **Supplementary Table 1**. COX-derived products such as PGE_2, PGD_2, and $PGF_{2\alpha}$, thromboxane B_2, and 12-HHT were abundantly produced in the inflamed lung tissue on day 1, and these amounts were almost the same between wild-type and 12/15-$LOX^{-/-}$ mice (**Figure 2A**). Among the LOX-derived products, 14-HDoHE, 17-HDoHE, and 12-hydroxyeicosatetraenoic acid (HETE) were generated at substantial levels on day 1. Additionally, their biosynthesis was dependent on 12/15-LOX (**Figure 2A**). Among the monohydroxylated forms of DHA (4-, 7-, 10-, 13-, 14-, 17-, 20-, and 21-HDoHE), the amount of 14-HDoHE was the highest on day 1 (**Figure 2B**). The amounts of fatty acids, precursors of lipid mediators (AA, EPA, and DHA), in the lungs did not differ between wild-type and 12/15-$LOX^{-/-}$ mice on day 1 (**Figure 2C**). Among the downstream lipid mediators (AA-, EPA-, and DHA-derived dihydroxy- or trihydroxy-fatty acids), PD1/PDX, RvD2, RvD5, and RvE3 were also present in a 12/15-LOX-dependent manner on day 1 (**Figure 2D**). PD1/PDX was relatively abundant compared to other mediators.

14(S)-HDoHE and 10(S),17(S)-diHDoHE Suppress ILC2 Cell Activation *In Vitro*

To further understand the molecular mechanism of 12/15-LOX in the regulation of innate eosinophilic pulmonary inflammation, we performed lipid screening using AA-, EPA-, and DHA-derived metabolites. Their suppressive effects on the

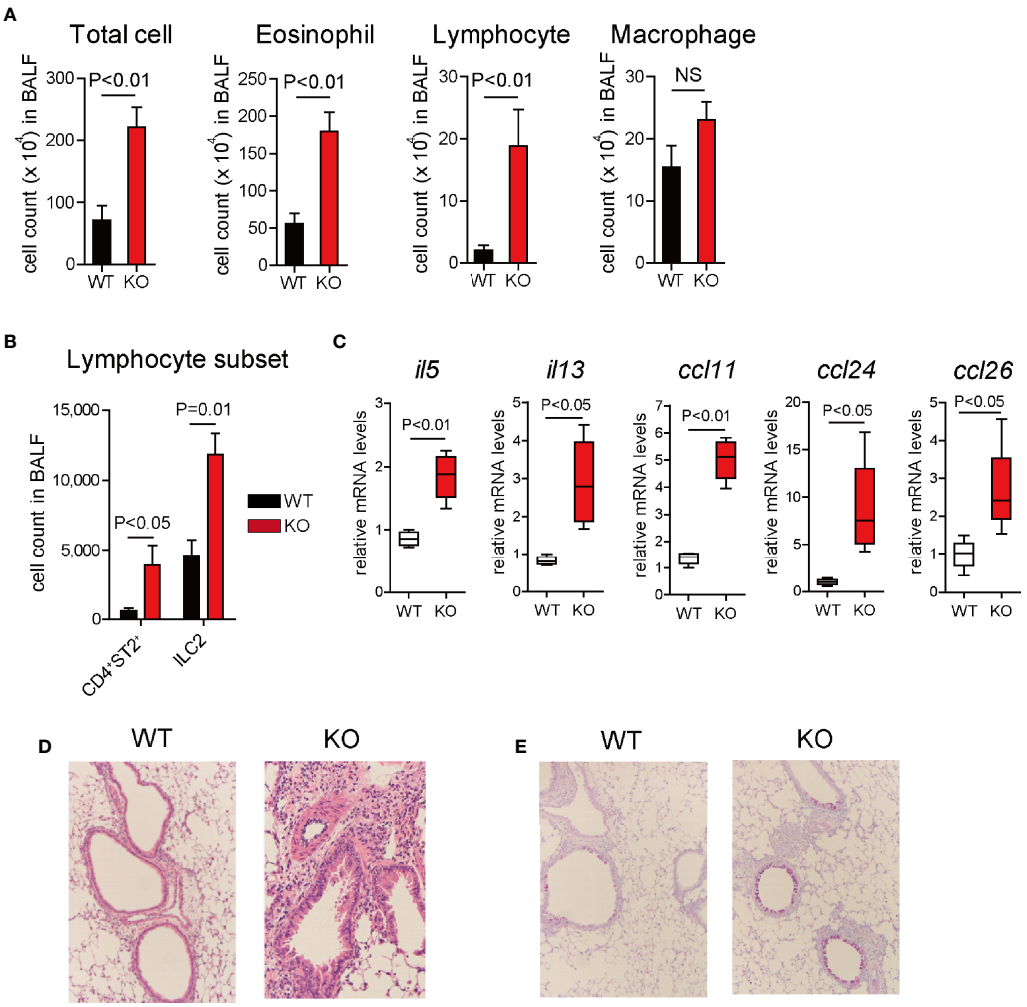

FIGURE 1 | 12/15-lipoxygenase deficiency augments IL-33-induced airway eosinophilic inflammation. Airway inflammation was induced by administration of IL-33 (500 ng per mouse, intranasal), for 3 consecutive days, in C57BL/6 and 12/15-lipoxygenase deficient mice. Analysis was performed 4 days after the final administration of IL-33. **(A)** Number of total cells, eosinophils, lymphocytes, and macrophages in BALF. **(B)** Number of ILC2 and Th2 cells in BALF by flow cytometric analysis. **(C)** Relative mRNA expression of cytokines (*il5*, *il13*, *ccl11*, *ccl24*, and *ccl26*) was determined by RT-PCR and quantitative real-time PCR analysis. Airway histology was assessed by **(D)** hematoxylin and eosin and **(E)** periodic acid–Schiff (PAS)-Alcan blue staining. The data are representative of three independent experiments. Mean ± SEM, n=4 for each group.

proliferation of ILC2 cells *in vitro* in response to IL-33 were investigated by flow cytometry. The lipid screening assay demonstrated that 14(S)-HDoHE was a potent suppressor of cellular proliferation of ILC2s among DHA-derived monohydroxy metabolites (4-, 7-, 10-, 13-, 14-, 17-, 20-, and 21-HDoHE) (**Figure 3A**). In addition, among DHA-derived SPMs, including RvDs, PDs, MaRs, and other AA- or EPA-derived dihydroxy or trihydroxy metabolites, 10(S),17(S)-diHDoHE (PDX) most potently suppressed the proliferation of ILC2 cells (**Figure 4A**).

14(S)-HDoHE suppressed ILC2 cell proliferation in a concentration-dependent manner (**Figure 3B**). In addition, cytokine release (IL-5) from ILC2 cells was suppressed by 14(S)-HDoHE in a concentration-dependent manner (**Figure 3C**). The inhibitory effect of 14(S)-HDoHE on IL-5 production was more potent than other related structural isomers such as 12(S)-HETE, 12(R)-HETE, 12(S)-HEPE, and 12(R)-HEPE (**Figure 3D**). Flow cytometric analysis of Annexin V- and PI-stained ILC2 cells upon stimulation with IL-33 revealed the pro-apoptotic effects of 14(S)-HDoHE on ILC2s after stimulation with IL-33 for 1 or 4 days (**Figures 3E–G**). PDX similarly inhibited ILC2 proliferation and IL-5 production in a concentration-dependent manner. PDX displayed more potent suppressive effect than its related metabolites including 17(S)-HDoHE and 10(S/R)-HDoHE (**Figures 4B, C**). The suppressive effects of PD1, RvD1, and RvD2, were also evaluated at nanomolar concentrations. Unlike the others, RvD1 slightly inhibited the proliferation and IL-5 production of ILC2s (**Figures 4D–G**). In addition, the suppressive effects of MaR1 were evaluated at nanomolar to micromolar concentrations. MaR1 inhibited IL-5 production, not

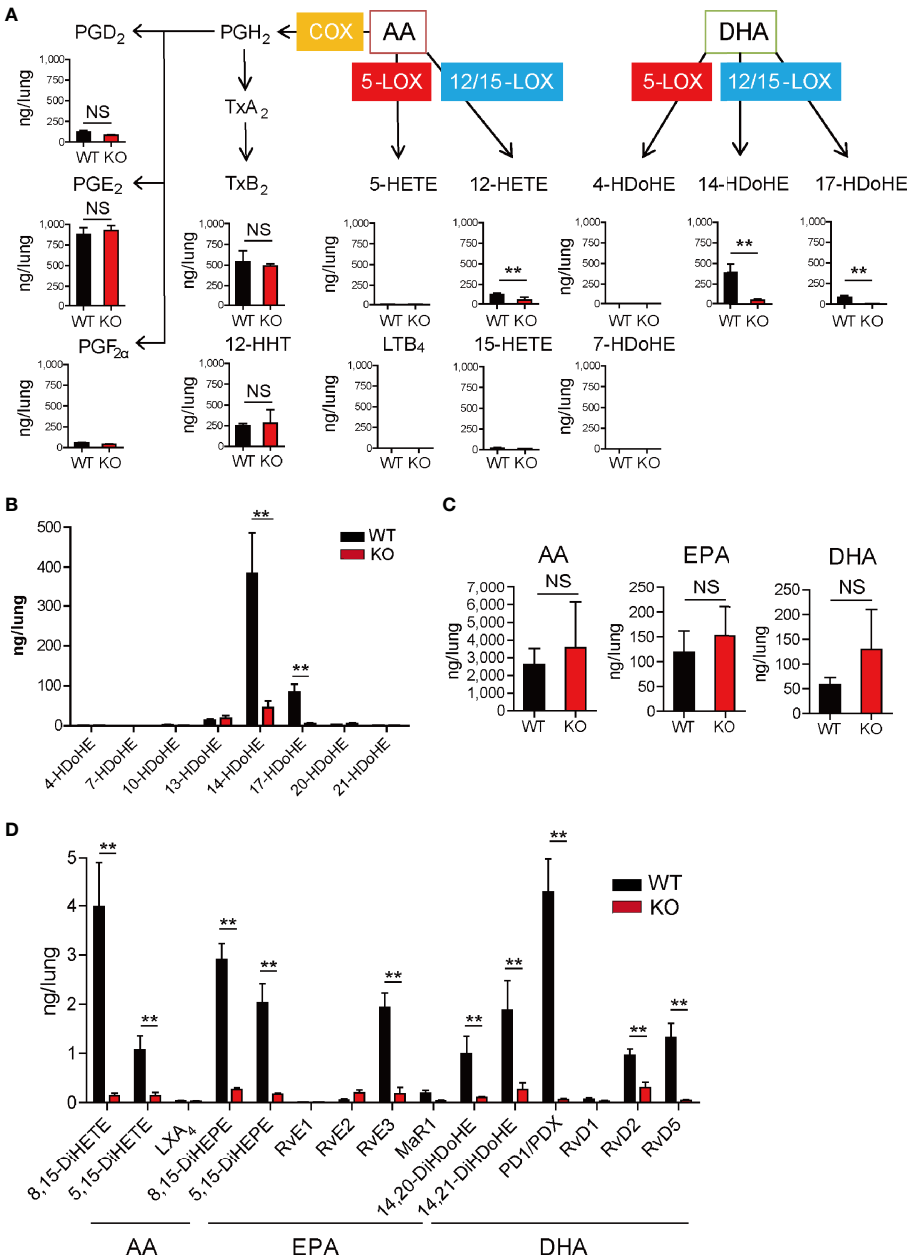

FIGURE 2 | Lipidomic profiles of lungs during IL-33-induced airway eosinophilic inflammation. Airway inflammation was induced by administration of IL-33 (500 ng per mouse, intranasal), for 3 consecutive days, in C57BL/6 and 12/15-lipoxygenase (LOX)-deficient mice. Analysis was performed 1 day after the final administration of IL-33. **(A)** Lipidomic analysis showed quantitative alterations of arachidonic acid (AA) and docosahexaenoic acid (DHA)-derived metabolites *via* cyclooxygenase (COX), 5-LOX, and 12/15-LOX, including prostaglandins (PG), thromboxanes (Tx), 12- hydroxyheptadecatrienoic acid (HHT), hydroxyeicosatetraenoic acid (HETE), leukotriene B_4 (LTB_4), and hydroxy docosahexaenoic acid (HDoHE). **(B)** Comparative analysis of DHA-derived monohydroxy metabolites in wild-type or 12/15-LOX deficient mice. **(C)** Comparative analysis of the amounts of polyunsaturated fatty acids [AA, DHA, and eicosapentaenoic acid (EPA)] in wild-type or 12/15-LOX deficient mice. **(D)** Comparative analysis of 12/15-LOX-derived dihydroxy- or trihydroxy-lipid metabolites, including lipoxin (LX), Rv, MR, and protectin (PD). Mean ± SEM, n=3 for each group. **P < 0.01 (Student's t-test). NS, not significant.

cell proliferation, of ILC2s at nanomolar concentrations (**Figures 4H, I**). These results suggest that the DHA-derived 12/15-LOX metabolites collectively regulates ILC2 functions to control innate type-2 airway inflammation.

14(S)-HDoHE Suppressed IL-33-Induced Airway Eosinophilic Inflammation *In Vivo*

Next, we determined the potential preventive effect of 14(S)-HDoHE, a major product of 12/15-LOX in the lung during

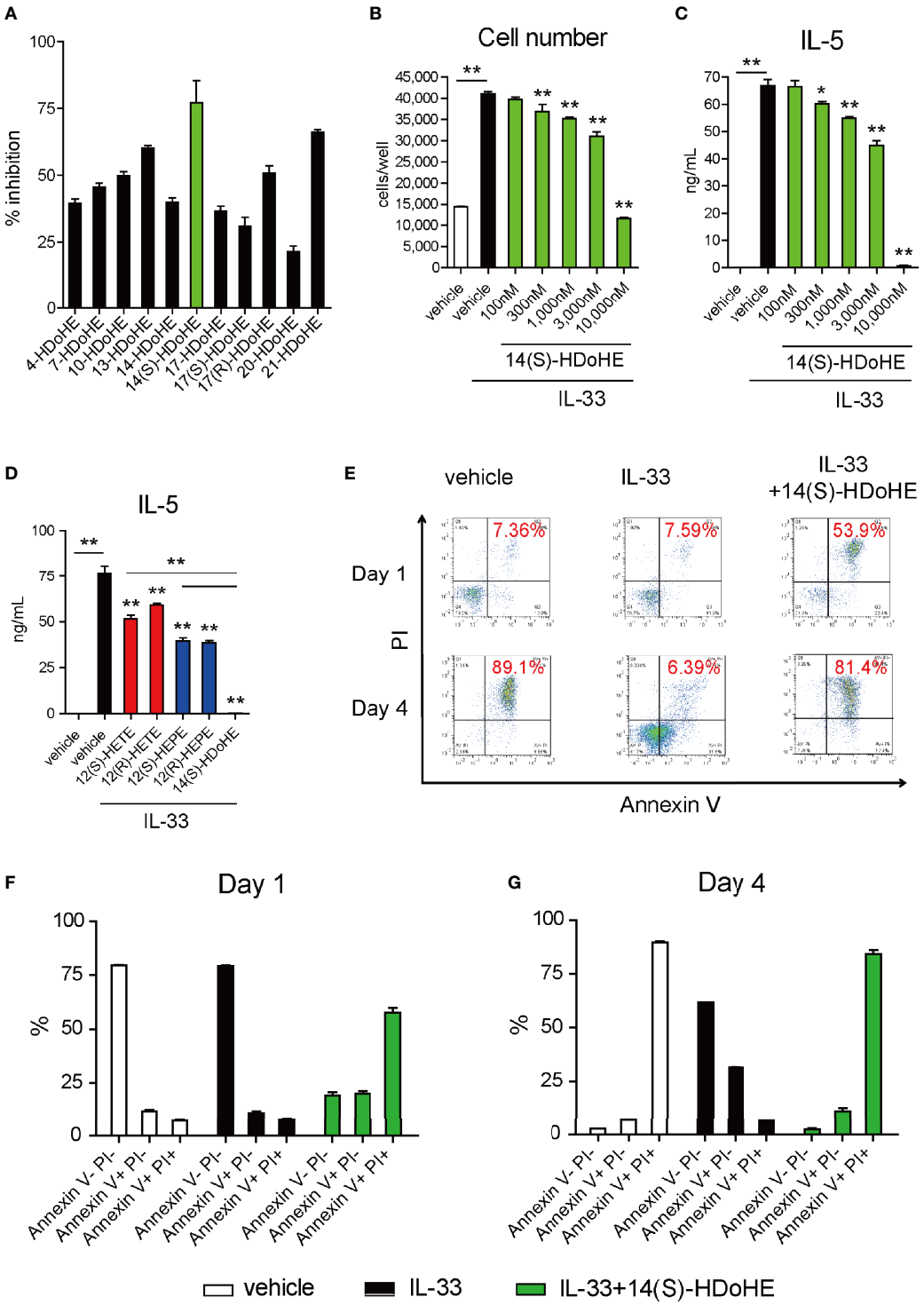

FIGURE 3 | 14(S)-HDoHE inhibit proliferation and cytokine production of ILC2s, with pro-apoptotic effects. ILC2 cells (10,000 cells per well) were cultured with IL-33 (10 ng/mL) for 1 or 4 days in the presence or absence of **(A)** DHA-derived monohydroxy-lipid metabolites (HDoHE, hydroxy docosahexaenoic acid: 10^{-5} M) or **(B–G)** in the presence or absence of 14(S)-HDoHE (3×10^{-7} – 10^{-5} M: **(B, C)**; or 10^{-5} M: **(D–G)**, **(D)** 12-hydroxyeicosatetraenoic acid (HETE) and 12-hydroxyeicosapentaenoic acid (HEPE). The total cell count **(A, B)** and concentrations of IL-5 **(C, D)** in the culture supernatant were measured. **(E–G)** Flow cytometric analysis of Annexin V- and PI-stained ILC2 cells cultured with or without IL-33 (10 ng/mL) in the presence or absence of 14(S)-HDoHE (10^{-5} M) for 1 or 4 days. The data are representative of three independent experiments. Mean ± SEM, n=3-8 for each group. *P < 0.05, **P < 0.01 (Student's t-test).

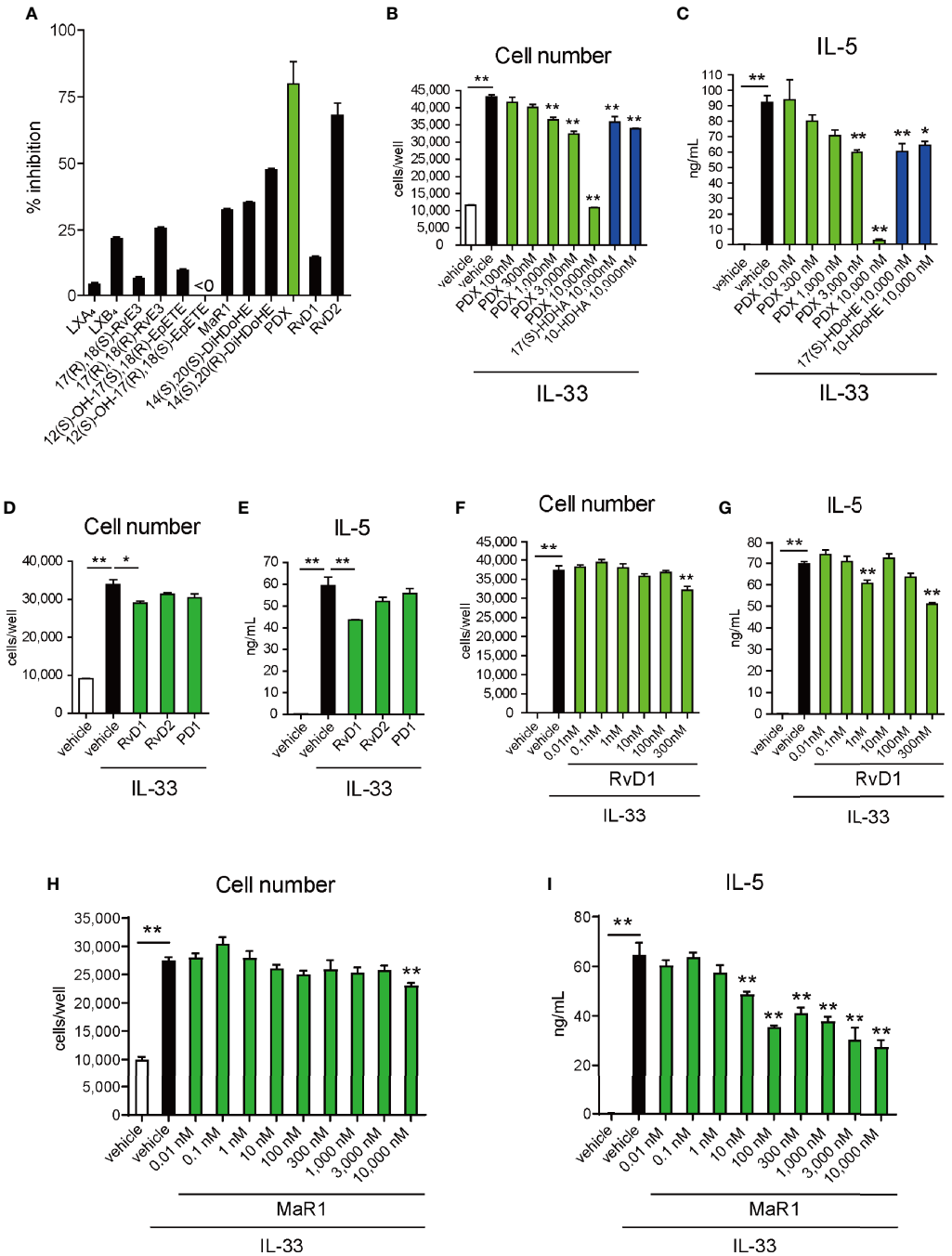

FIGURE 4 | Effects of SPMs on proliferation and cytokine production of ILC2s. **(A)** ILC2 cells (10,000 cells per well) were cultured with IL-33 (10 ng/mL) for 4 days in the presence or absence of **(A)** dihydroxy- or trihydroxy-lipid metabolites (LX, lipoxin; Rv, resolvin; MR, maresin; PD, protectin D: 10^{-5} M) or in the presence or absence of **(B, C)** 10(S),17(S)-diHDoHE (PDX, $3 \times 10^{-7} - 10^{-5}$ M), **(D, E)** 17(S)-HDoHE-derived SPMs (RvD1, resolvin D1; RvD2, resolvin D2; PD1, protectin D1: 3 x 10^{-7} nM), **(F, G)** RvD1 ($1 \times 10^{-11} - 3 \times 10^{-7}$ M: **(D, E)**, or **(H, I)** MaR1 (MaR1; maresin 1: $10^{-11} - 10^{-5}$ M). The total cell count **(A, B, D, F, H)** and concentrations of IL-5 **(C, E, G, I)** in the culture supernatant were measured. Data are shown as Mean ± SEM, n = 3 for each group. *P < 0.05, **P < 0.01 (Student's *t*-test).

inflammation, *in vivo* on IL-33-induced airway eosinophilic inflammation. Intraperitoneal administration of 14(S)-HDoHE reduced the number of eosinophils and macrophages in BALF compared with that in vehicle-treated mice in 12/15-LOX$^{-/-}$ mice (**Figure 5A**). 14(S)-HDoHE administration also decreased the number of ILC2 and CD4^{+}ST2^{+} Th2 cells present in BALF in 12/15-LOX$^{-/-}$ mice (**Figure 5B**). Also, 14(S)-HDoHE reduced the number of ILC2 and Th2 cells in BALF of WT mice (**Figure 5B**).

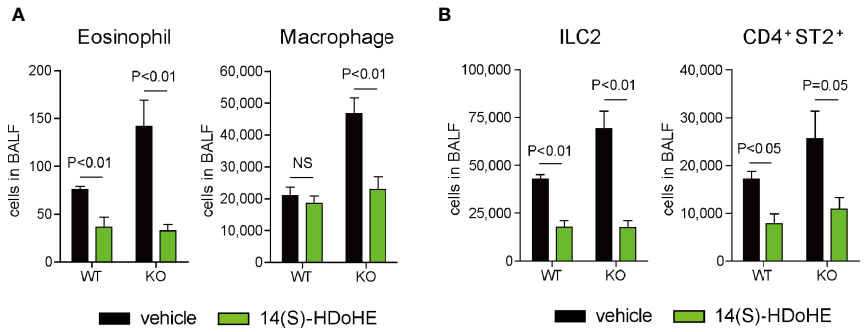

FIGURE 5 | 14(S)-HDoHE suppresses IL-33-induced airway eosinophilic inflammation. Airway inflammation was induced by administration of IL-33 (500 ng per mouse, intranasal), for 3 consecutive days, in C57BL/6 and 12/15-lipoxygenase deficient mice. 14(S)-hydroxy docosahexaenoic acid (HDoHE) was administered *via* intraperitoneal injection prior to IL-33 administration. Flow cytometric analysis was performed 4 days after the final administration of IL-33. **(A)** Number of eosinophils and macrophages in the BALF. **(B)** Number of lymphocyte subsets, including ILC2 and Th2 cells, in the BALF. Mean ± SEM, n=4 for each group. NS, not significant.

DISCUSSION

In the present study, we demonstrated that 12/15-LOX, a key enzyme for the biosynthesis of specialized pro-resolving lipid mediators (SPMs), conferred a protective effect on innate pulmonary eosinophilic inflammation *in vivo*. Lipidomic analysis revealed a series of 12/15-LOX-derived mediators present at substantial levels in the inflamed lung. Using bioactive lipid screening, the potent effect of 14(S)-HDoHE and 10(S),17(S)-diHDoHE in suppressing ILC2 function was observed *in vitro*. These findings demonstrate the direct effect of DHA-derived pro-resolving mediators in suppressing ILC2 activation. 14(S)-HDoHE also displayed potent anti-inflammatory effects on IL-33-induced eosinophilic airway inflammation when administered *in vivo*. These results provide a new therapeutic option for 12/15-LOX-derived pro-resolving mediators in ILC2-mediated allergic diseases.

Previous studies have shown the regulatory effects of 14(S)-HDoHE on murine platelets and human alveolar macrophages *in vitro* (43, 44). PD1/PDX also possesses potent anti-inflammatory functions in regulating neutrophil activation *in vitro* (45, 46) and ameliorates pulmonary inflammation and fibrosis *in vivo* (47, 48). Interestingly, we previously reported that peripheral blood eosinophils isolated from patients with severe asthma had a defective biosynthetic capacity of 14(S)-HDoHE, 17(S)-HDoHE, and PD1/PDX (7). Similarly, their biosynthetic capacities have been reported to be impaired in obese mice, and systemic administration of these metabolites ameliorated obesity-induced inflammatory states (49). These findings highlight the therapeutic potential of 14(S)-HDoHE and related SPMs in the regulation of chronic inflammation through DHA metabolism. However, the precise mechanism underlying the 14(S)-HDoHE-mediated effects thorough specific receptors and/or downstream metabolites remains undetermined.

IL-33 induces ILC2 proliferation and activation, which orchestrate innate type-2 inflammation as the dominant IL-5-producing cell *in vitro* and *in vivo* (22, 23, 50–55). IL-5 plays a central role in prolonging eosinophils survival and activating eosinophils to elicit degranulation, superoxide generation, cytokine release, and cysteinyl leukotriene synthesis (12, 56). In this study, 14(S)-HDoHE, 17(S)-HDoHE, and other DHA-derived SPMs, such as RvDs, PDs, and MaRs, differentially exerted regulatory effects on cellular functions of ILC2 cells at micromolar or nanomolar concentrations. In humans, LXA_4, an AA-derived SPM, decreased IL-13 release from ILC2s stimulated with IL2/IL25/IL-33/PGD_2 at nanomolar concentrations (57). In addition, MaR1, a DHA-derived SPM, regulated IL-13 release from ILC2 *in vitro* at nanomolar concentration and *in vivo* at ng/mouse administration in a murine model of asthma (58). Also, regulatory T cells synergistically exerted inhibitory effects on ILC2 in the presence of MaR1 (58). Other cell types, including regulatory T cells, may enhance the suppressive effects of SPMs on ILC2s. Additionally, our study suggests that RvD1 and MaR1 can inhibit ILC2 function at nanomolar concentration. Thus, we speculate that these bioactive SPMs collectively, not individually, orchestrate the regulatory circuit for ILC2-mediated eosinophilic inflammation.

The cellular sources of 12/15-LOX-derived mediators during allergic inflammation are of particular interest. 12/15-LOX-expressing eosinophils play pro-resolving functions by enhancing the resolution of neutrophilic inflammation in acute peritonitis (8, 9) and by promoting corneal wound healing in the eye (59). In addition, 12/15-LOX-expressing resident macrophages play an important role in the efferocytosis of apoptotic neutrophils in acute peritonitis (10). Further studies are required to identify the cell types that locally produce 12/15-LOX-derived SPMs to suppress ILC-2-mediated eosinophilic inflammation.

In conclusion, our results demonstrate that 12/15-LOX-derived mediators regulate IL-33-induced eosinophilic airway inflammation. Bioactive lipid screening identified 14(S)-HDoHE and 10(S),17(S)-diHDoHE as potent endogenous suppressors of ILC2 activation. These findings contribute to a better understanding of the cellular and molecular mechanisms underlying the resolution of eosinophilic airway inflammation. Thus, 12/15-LOX-derived lipid mediators and/or 12/15-LOX-mediated lipid metabolism may represent a potential therapeutic strategy for ameliorating airway inflammation-associated conditions.

DATA AVAILABILITY STATEMENT

The raw data supporting the conclusions of this article will be made available by the authors, without undue reservation.

ETHICS STATEMENT

The animal study was reviewed and approved by the Animal Care and Use Committee of the RIKEN, the Animal Committee of the University of Tokyo, the Laboratory Animal Care and Use Committee of Keio University of Medicine.

AUTHOR CONTRIBUTIONS

JM and MA designed the experiments. JM and YY performed most of the experiments and compiled the data. KM provided murine group 2 innate lymphoid cells. MA, KF, and HA supervised the project. JM and MA wrote the manuscript, and all authors provided feedback on the manuscript. All authors contributed to the article and approved the submitted version.

FUNDING

This work was supported by the JSPS Grant-in-Aid for Scientific Research on Innovative Areas (15H05897, 15H05898 to MA), the RIKEN Special Postdoctoral Researchers Program (to JM), and the Grant-in-Aid for research of ONO Medical Research Foundation (to JM).

ACKNOWLEDGMENTS

We thank Yosuke Isobe (RIKEN-IMS) for advice and critical input regarding this study; Mie Honda, Kanako Igarashi, and Kazutaka Ikeda (RIKEN-IMS) for technical assistance with LC-MS-based lipidomics.

SUPPLEMENTARY MATERIAL

The Supplementary Material for this article can be found online at: https://www.frontiersin.org/articles/10.3389/fimmu.2021.687192/full#supplementary-material

REFERENCES

1. Bousquet J, Clark TJ, Hurd S, Khaltaev N, Lenfant C, O'Byrne P, et al. GINA Guidelines on Asthma and Beyond. *Allergy* (2007) 62(2):102–12. doi: 10.1111/j.1398-9995.2006.01305.x
2. Masoli M, Fabian D, Holt S, Beasley R. The Global Burden of Asthma: Executive Summary of the GINA Dissemination Committee Report. *Allergy* (2004) 59(5):469–78. doi: 10.1111/j.1398-9995.2004.00526.x
3. Yamamoto T, Miyata J, Arita M, Fukunaga K, Kawana A. Current State and Future Prospect of the Therapeutic Strategy Targeting Cysteinyl Leukotriene Metabolism in Asthma. *Respir Invest* (2019) 57(6):534–43. doi: 10.1016/j.resinv.2019.08.003
4. Miyata J, Fukunaga K, Kawashima Y, Ohara O, Kawana A, Asano K, et al. Dysregulated Metabolism of Polyunsaturated Fatty Acids in Eosinophilic Allergic Diseases. *Prostaglandins Other Lipid Mediat* (2020) 150:106477. doi: 10.1016/j.prostaglandins.2020.106477
5. Serhan CN. Pro-Resolving Lipid Mediators are Leads for Resolution Physiology. *Nature* (2014) 510(7503):92–101. doi: 10.1038/nature13479
6. Serhan CN, Levy BD. Resolvins in Inflammation: Emergence of the Pro-Resolving Superfamily of Mediators. *J Clin Invest* (2018) 128(7):2657–69. doi: 10.1172/jci97943
7. Miyata J, Fukunaga K, Iwamoto R, Isobe Y, Niimi K, Takamiya R, et al. Dysregulated Synthesis of Protectin D1 in Eosinophils From Patients With Severe Asthma. *J Allergy Clin Immunol* (2013) 131(2):353–60 e1-2. doi: 10.1016/j.jaci.2012.07.048
8. Tani Y, Isobe Y, Imoto Y, Segi-Nishida E, Sugimoto Y, Arai H, et al. Eosinophils Control the Resolution of Inflammation and Draining Lymph Node Hypertrophy Through the Proresolving Mediators and CXCL13 Pathway in Mice. *FASEB J* (2014) 28(9):4036–43. doi: 10.1096/fj.14-251132
9. Yamada T, Tani Y, Nakanishi H, Taguchi R, Arita M, Arai H. Eosinophils Promote Resolution of Acute Peritonitis by Producing Proresolving Mediators in Mice. *FASEB J* (2011) 25(2):561–8. doi: 10.1096/fj.10-170027
10. Lim CS, Porter DW, Orandle MS, Green BJ, Barnes MA, Croston TL, et al. Resolution of Pulmonary Inflammation Induced by Carbon Nanotubes and Fullerenes in Mice: Role of Macrophage Polarization. *Front Immunol* (2020) 11:1186. doi: 10.3389/fimmu.2020.01186
11. Miyata J, Fukunaga K, Kawashima Y, Watanabe T, Saitoh A, Hirosaki T, et al. Dysregulated Fatty Acid Metabolism in Nasal Polyp-Derived Eosinophils From Patients With Chronic Rhinosinusitis. *Allergy* (2019) 74(6):1113–24. doi: 10.1111/all.13726
12. Miyata J, Fukunaga K, Kawashima Y, Ohara O, Arita M. Cysteinyl Leukotriene Metabolism of Human Eosinophils in Allergic Disease. *Allergol Int Off J Japanese Soc Allergol* (2020) 69(1):28–34. doi: 10.1016/j.alit.2019.06.002
13. Miyata J, Arita M. Role of Omega-3 Fatty Acids and Their Metabolites in Asthma and Allergic Diseases. *Allergol Int Off J Japanese Soc Allergol* (2015) 64(1):27–34. doi: 10.1016/j.alit.2014.08.003
14. Levy BD, Lukacs NW, Berlin AA, Schmidt B, Guilford WJ, Serhan CN, et al. Lipoxin A4 Stable Analogs Reduce Allergic Airway Responses Via Mechanisms Distinct From CysLT1 Receptor Antagonism. *FASEB J* (2007) 21(14):3877–84. doi: 10.1096/fj.07-8653com
15. Levy BD, Kohli P, Gotlinger K, Haworth O, Hong S, Kazani S, et al. Protectin D1 Is Generated in Asthma and Dampens Airway Inflammation and Hyperresponsiveness. *J Immunol* (2007) 178(1):496–502. doi: 10.4049/jimmunol.178.1.496
16. Rogerio AP, Haworth O, Croze R, Oh SF, Uddin M, Carlo T, et al. Resolvin D1 and Aspirin-Triggered Resolvin D1 Promote Resolution of Allergic Airways Responses. *J Immunol* (2012) 189(4):1983–91. doi: 10.4049/jimmunol.1101665
17. Levy BD, De Sanctis GT, Devchand PR, Kim E, Ackerman K, Schmidt BA, et al. Multi-Pronged Inhibition of Airway Hyper-Responsiveness and Inflammation by Lipoxin a(4). *Nat Med* (2002) 8(9):1018–23. doi: 10.1038/nm748
18. Mochimaru T, Fukunaga K, Miyata J, Matsusaka M, Masaki K, Kabata H, et al. 12-OH-17,18-Epoxyeicosatetraenoic Acid Alleviates Eosinophilic Airway Inflammation in Murine Lungs. *Allergy* (2018) 73(2):369–78. doi: 10.1111/all.13297
19. Schmitz J, Owyang A, Oldham E, Song Y, Murphy E, McClanahan TK, et al. Il-33, an Interleukin-1-Like Cytokine That Signals Via the IL-1 Receptor-Related Protein ST2 and Induces T Helper Type 2-Associated Cytokines. *Immunity* (2005) 23(5):479–90. doi: 10.1016/j.immuni.2005.09.015
20. Moffatt MF, Gut IG, Demenais F, Strachan DP, Bouzigon E, Heath S, et al. A Large-Scale, Consortium-Based Genomewide Association Study of Asthma. *N Engl J Med* (2010) 363(13):1211–21. doi: 10.1056/NEJMoa0906312
21. Gudbjartsson DF, Bjornsdottir US, Halapi E, Helgadottir A, Sulem P, Jonsdottir GM, et al. Sequence Variants Affecting Eosinophil Numbers

Associate With Asthma and Myocardial Infarction. *Nat Genet* (2009) 41 (3):342–7. doi: 10.1038/ng.323
22. Bartemes KR, Iijima K, Kobayashi T, Kephart GM, McKenzie AN, Kita H. Il-33-responsive Lineage- CD25+ CD44(Hi) Lymphoid Cells Mediate Innate Type 2 Immunity and Allergic Inflammation in the Lungs. *J Immunol* (2012) 188(3):1503–13. doi: 10.4049/jimmunol.1102832
23. Moro K, Yamada T, Tanabe M, Takeuchi T, Ikawa T, Kawamoto H, et al. Innate Production of T(H)2 Cytokines by Adipose Tissue-Associated c-Kit(+) Sca-1(+) Lymphoid Cells. *Nature* (2010) 463(7280):540–4. doi: 10.1038/nature08636
24. Neill DR, Wong SH, Bellosi A, Flynn RJ, Daly M, Langford TK, et al. Nuocytes Represent a New Innate Effector Leukocyte That Mediates Type-2 Immunity. *Nature* (2010) 464(7293):1367–70. doi: 10.1038/nature08900
25. Besnard AG, Togbe D, Guillou N, Erard F, Quesniaux V, Ryffel B. IL-33-Activated Dendritic Cells Are Critical for Allergic Airway Inflammation. *Eur J Immunol* (2011) 41(6):1675–86. doi: 10.1002/eji.201041033
26. Eiwegger T, Akdis CA. Il-33 Links Tissue Cells, Dendritic Cells and Th2 Cell Development in a Mouse Model of Asthma. *Eur J Immunol* (2011) 41 (6):1535–8. doi: 10.1002/eji.201141668
27. Kurokawa M, Matsukura S, Kawaguchi M, Ieki K, Suzuki S, Odaka M, et al. Expression and Effects of IL-33 and ST2 in Allergic Bronchial Asthma: IL-33 Induces Eotaxin Production in Lung Fibroblasts. *Int Arch Allergy Immunol* (2011) 155 Suppl 1:12–20. doi: 10.1159/000327259
28. Cherry WB, Yoon J, Bartemes KR, Iijima K, Kita H. A Novel IL-1 Family Cytokine, IL-33, Potently Activates Human Eosinophils. *J Allergy Clin Immunol* (2008) 121(6):1484–90. doi: 10.1016/j.jaci.2008.04.005
29. Rank MA, Kobayashi T, Kozaki H, Bartemes KR, Squillace DL, Kita H. Il-33-activated Dendritic Cells Induce an Atypical TH2-type Response. *J Allergy Clin Immunol* (2009) 123(5):1047–54. doi: 10.1016/j.jaci.2009.02.026
30. Saglani S, Lui S, Ullmann N, Campbell GA, Sherburn RT, Mathie SA, et al. Il-33 Promotes Airway Remodeling in Pediatric Patients With Severe Steroid-Resistant Asthma. *J Allergy Clin Immunol* (2013) 132(3):676–85 e13. doi: 10.1016/j.jaci.2013.04.012
31. Bouffi C, Rochman M, Zust CB, Stucke EM, Kartashov A, Fulkerson PC, et al. IL-33 Markedly Activates Murine Eosinophils by an NF-kappaB-Dependent Mechanism Differentially Dependent Upon an IL-4-driven Autoinflammatory Loop. *J Immunol* (2013) 191(8):4317–25. doi: 10.4049/jimmunol.1301465
32. Komai-Koma M, Gilchrist DS, McKenzie AN, Goodyear CS, Xu D, Liew FY. Il-33 Activates B1 Cells and Exacerbates Contact Sensitivity. *J Immunol* (2011) 186(4):2584–91. doi: 10.4049/jimmunol.1002103
33. Kurowska-Stolarska M, Kewin P, Murphy G, Russo RC, Stolarski B, Garcia CC, et al. Il-33 Induces Antigen-Specific IL-5+ T Cells and Promotes Allergic-Induced Airway Inflammation Independent of IL-4. *J Immunol* (2008) 181 (7):4780–90. doi: 10.4049/jimmunol.181.7.4780
34. Yagami A, Orihara K, Morita H, Futamura K, Hashimoto N, Matsumoto K, et al. Il-33 Mediates Inflammatory Responses in Human Lung Tissue Cells. *J Immunol* (2010) 185(10):5743–50. doi: 10.4049/jimmunol.0903818
35. Suzukawa M, Koketsu R, Iikura M, Nakae S, Matsumoto K, Nagase H, et al. Interleukin-33 Enhances Adhesion, CD11b Expression and Survival in Human Eosinophils. *Lab Invest* (2008) 88(11):1245–53. doi: 10.1038/labinvest.2008.82
36. Fux M, Pecaric-Petkovic T, Odermatt A, Hausmann OV, Lorentz A, Bischoff SC, et al. Il-33 is a Mediator Rather Than a Trigger of the Acute Allergic Response in Humans. *Allergy* (2014) 69(2):216–22. doi: 10.1111/all.12309
37. Hardman CS, Panova V, McKenzie AN. Il-33 Citrine Reporter Mice Reveal the Temporal and Spatial Expression of IL-33 During Allergic Lung Inflammation. *Eur J Immunol* (2013) 43(2):488–98. doi: 10.1002/eji.201242863
38. Prefontaine D, Nadigel J, Chouiali F, Audusseau S, Semlali A, Chakir J, et al. Increased IL-33 Expression by Epithelial Cells in Bronchial Asthma. *J Allergy Clin Immunol* (2010) 125(3):752–4. doi: 10.1016/j.jaci.2009.12.935
39. Prefontaine D, Lajoie-Kadoch S, Foley S, Audusseau S, Olivenstein R, Halayko AJ, et al. Increased Expression of IL-33 in Severe Asthma: Evidence of Expression by Airway Smooth Muscle Cells. *J Immunol* (2009) 183 (8):5094–103. doi: 10.4049/jimmunol.0802387
40. Kabata H, Moro K, Fukunaga K, Suzuki Y, Miyata J, Masaki K, et al. Thymic Stromal Lymphopoietin Induces Corticosteroid Resistance in Natural Helper Cells During Airway Inflammation. *Nat Commun* (2013) 4:2675. doi: 10.1038/ncomms3675
41. Arita M. Mediator Lipidomics in Acute Inflammation and Resolution. *J Biochem* (2012) 152(4):313–9. doi: 10.1093/jb/mvs092
42. Moro K, Ealey KN, Kabata H, Koyasu S. Isolation and Analysis of Group 2 Innate Lymphoid Cells in Mice. *Nat Protoc* (2015) 10(5):792–806. doi: 10.1038/nprot.2015.047
43. Yamaguchi A, Stanger L, Freedman CJ, Standley M, Hoang T, Adili R, et al. Dha 12-LOX-derived Oxylipins Regulate Platelet Activation and Thrombus Formation Through a PKA-dependent Signaling Pathway. *J Thromb Haemost* (2021) 19(3):839–51. doi: 10.1111/jth.15184
44. Wendell SG, Golin-Bisello F, Wenzel S, Sobol RW, Holguin F, Freeman BA. 15-Hydroxyprostaglandin Dehydrogenase Generation of Electrophilic Lipid Signaling Mediators From Hydroxy ω-3 Fatty Acids. *J Biol Chem* (2015) 290 (9):5868–80. doi: 10.1074/jbc.M114.635151
45. Serhan CN, Gotlinger K, Hong S, Lu Y, Siegelman J, Baer T, et al. Anti-Inflammatory Actions of Neuroprotectin D1/protectin D1 and Its Natural Stereoisomers: Assignments of Dihydroxy-Containing Docosatrienes. *J Immunol* (2006) 176(3):1848–59. doi: 10.4049/jimmunol.176.3.1848
46. Stein K, Stoffels M, Lysson M, Schneiker B, Dewald O, Krönke G, et al. A Role for 12/15-Lipoxygenase-Derived Proresolving Mediators in Postoperative Ileus: Protectin DX-Regulated Neutrophil Extravasation. *J leukocyte Biol* (2016) 99(2):231–9. doi: 10.1189/jlb.3HI0515-189R
47. Li H, Hao Y, Zhang H, Ying W, Li D, Ge Y, et al. Posttreatment With Protectin DX Ameliorates Bleomycin-Induced Pulmonary Fibrosis and Lung Dysfunction in Mice. *Sci Rep* (2017) 7:46754. doi: 10.1038/srep46754
48. Xia H, Ge Y, Wang F, Ming Y, Wu Z, Wang J, et al. Protectin DX Ameliorates Inflammation in Sepsis-Induced Acute Lung Injury Through Mediating Pparγ/Nf-κb Pathway. *Immunologic Res* (2020) 68(5):280–8. doi: 10.1007/s12026-020-09151-7
49. Crouch MJ, Kosaraju R, Guesdon W, Armstrong M, Reisdorph N, Jain R, et al. Frontline Science: A Reduction in DHA-Derived Mediators in Male Obesity Contributes Toward Defects in Select B Cell Subsets and Circulating Antibody. *J leukocyte Biol* (2019) 106(2):241–57. doi: 10.1002/jlb.3hi1017-405rr
50. Kondo Y, Yoshimoto T, Yasuda K, Futatsugi-Yumikura S, Morimoto M, Hayashi N, et al. Administration of IL-33 Induces Airway Hyperresponsiveness and Goblet Cell Hyperplasia in the Lungs in the Absence of Adaptive Immune System. *Int Immunol* (2008) 20(6):791–800. doi: 10.1093/intimm/dxn037
51. Snelgrove RJ, Gregory LG, Peiro T, Akthar S, Campbell GA, Walker SA, et al. Alternaria-Derived Serine Protease Activity Drives IL-33 Mediated Asthma Exacerbations. *J Allergy Clin Immunol* (2014) 134(3):583–92.e6. doi: 10.1016/j.jaci.2014.02.002
52. Ikutani M, Yanagibashi T, Ogasawara M, Tsuneyama K, Yamamoto S, Hattori Y, et al. Identification of Innate IL-5-producing Cells and Their Role in Lung Eosinophil Regulation and Antitumor Immunity. *J Immunol* (2012) 188 (2):703–13. doi: 10.4049/jimmunol.1101270
53. Salmond RJ, Mirchandani AS, Besnard AG, Bain CC, Thomson NC, Liew FY. Il-33 Induces Innate Lymphoid Cell-Mediated Airway Inflammation by Activating Mammalian Target of Rapamycin. *J Allergy Clin Immunol* (2012) 130(5):1159–66.e6. doi: 10.1016/j.jaci.2012.05.018
54. Barlow JL, Peel S, Fox J, Panova V, Hardman CS, Camelo A, et al. IL-33 Is More Potent Than IL-25 in Provoking IL-13-producing Nuocytes (Type 2 Innate Lymphoid Cells) and Airway Contraction. *J Allergy Clin Immunol* (2013) 132(4):933–41. doi: 10.1016/j.jaci.2013.05.012
55. Kim HY, Chang YJ, Subramanian S, Lee HH, Albacker LA, Matangkasombut P, et al. Innate Lymphoid Cells Responding to IL-33 Mediate Airway Hyperreactivity Independently of Adaptive Immunity. *J Allergy Clin Immunol* (2012) 129(1):216–27.e1-6. doi: 10.1016/j.jaci.2011.10.036
56. Pelaia C, Paoletti G, Puggioni F, Racca F, Pelaia G, Canonica GW, et al. Interleukin-5 in the Pathophysiology of Severe Asthma. *Front Physiol* (2019) 10:1514. doi: 10.3389/fphys.2019.01514
57. Barnig C, Cernadas M, Dutile S, Liu X, Perrella MA, Kazani S, et al. Lipoxin A4 Regulates Natural Killer Cell and Type 2 Innate Lymphoid Cell Activation in Asthma. *Sci Transl Med* (2013) 5(174):174ra26. doi: 10.1126/scitranslmed.3004812
58. Krishnamoorthy N, Burkett PR, Dalli J, Abdulnour RE, Colas R, Ramon S, et al. Cutting Edge: Maresin-1 Engages Regulatory T Cells to Limit Type 2 Innate Lymphoid Cell Activation and Promote Resolution of Lung Inflammation. *J Immunol* (2015) 194(3):863–7. doi: 10.4049/jimmunol.1402534

59. Ogawa M, Ishihara T, Isobe Y, Kato T, Kuba K, Imai Y, et al. Eosinophils Promote Corneal Wound Healing Via the 12/15-Lipoxygenase Pathway. *FASEB J* (2020) 34(9):12492–501. doi: 10.1096/fj.202000483R

Conflict of Interest: The authors declare that the research was conducted in the absence of any commercial or financial relationships that could be construed as a potential conflict of interest.

Copyright © 2021 Miyata, Yokokura, Moro, Arai, Fukunaga and Arita. This is an open-access article distributed under the terms of the Creative Commons Attribution License (CC BY). The use, distribution or reproduction in other forums is permitted, provided the original author(s) and the copyright owner(s) are credited and that the original publication in this journal is cited, in accordance with accepted academic practice. No use, distribution or reproduction is permitted which does not comply with these terms.

frontiers in Immunology

REVIEW
published: 30 June 2021
doi: 10.3389/fimmu.2021.702785

Specialized Pro-Resolving Mediators Mitigate Cancer-Related Inflammation: Role of Tumor-Associated Macrophages and Therapeutic Opportunities

Margot Lavy[1], *Vanessa Gauttier*[1], *Nicolas Poirier*[1], *Sophie Barillé-Nion*[2*†] *and Christophe Blanquart*[2*†]

[1] OSE Immunotherapeutics, Nantes, France, [2] Université de Nantes, Inserm UMR 1232, CRCINA, Nantes, France

OPEN ACCESS

Edited by:
Sylvain Perruche,
Institut National de la Santé et de la Recherche Médicale (INSERM), France

Reviewed by:
Dipak Panigrahy,
Harvard Medical School, United States
Paola Allavena,
University of Milan, Italy

***Correspondence:**
Sophie Barillé-Nion
sophie.barille@univ-nantes.fr
Christophe Blanquart
christophe.blanquart@univ-nantes.fr

[†]These authors have contributed equally to this work

Specialty section:
This article was submitted to Inflammation, a section of the journal Frontiers in Immunology

Received: 29 April 2021
Accepted: 15 June 2021
Published: 30 June 2021

Citation:
Lavy M, Gauttier V, Poirier N, Barillé-Nion S and Blanquart C (2021) Specialized Pro-Resolving Mediators Mitigate Cancer-Related Inflammation: Role of Tumor-Associated Macrophages and Therapeutic Opportunities. Front. Immunol. 12:702785. doi: 10.3389/fimmu.2021.702785

Inflammation is a fundamental physiological response orchestrated by innate immune cells to restore tissue homeostasis. Specialized pro-resolving mediators (SPMs) are involved in active resolution of inflammation but when inflammation is incomplete, chronic inflammation creates a favorable environment that fuels carcinogenesis and cancer progression. Conventional cancer therapy also strengthens cancer-related inflammation by inducing massive tumor cell death that activate surrounding immune-infiltrating cells such as tumor-associated macrophages (TAMs). Macrophages are key actors of both inflammation and its active resolution due to their plastic phenotype. In line with this high plasticity, macrophages can be hijacked by cancer cells to support tumor progression and immune escape, or therapy resistance. Impaired resolution of cancer-associated inflammation supported by TAMs may thus reinforces tumor progression. From this perspective, recent evidence suggests that stimulating macrophage's pro-resolving functions using SPMs can promote inflammation resolution in cancer and improve anticancer treatments. Thus, TAMs' re-education toward an antitumor phenotype by using SPMs opens a new line of attack in cancer treatment. Here, we review SPMs' anticancer capacities with special attention regarding their effects on TAMs. We further discuss how this new therapeutic approach could be envisioned in cancer therapy.

Keywords: inflammation, cancer, specialized pro-resolving mediators, macrophages, phagocytosis, tumor microenvironment

Abbreviations: AA, Arachidonic acid; APCs, Antigen-presenting cells; AT-SPM, Aspirin-triggered SPM; cAMP, Cyclic adenosine monophosphate; CAFs, Cancer-associated fibroblasts; CAR, Chimeric antigen receptor; COXs, Cyclooxygenases; CSF-1, Colony-stimulating factor 1; DHA, Docosahexaenoic acid; EGF, Epidermal growth factor; EPA, Eicosapentaenoic acid; GM-CSF, Granulocyte-macrophage colony-stimulating factor; GPCRs, G protein-coupled receptors; IFN, Interferon; IL, Interleukin; iNOS, Inducible nitric oxide synthase; LOXs, Lipoxygenases; LPS, Lipopolysaccharides; LTs, Leukotrienes; LTB4, Leukotriene B4; LXs, Lipoxins; MaR, Maresin; MDSC, Myeloid-derived suppressor cells; MHC, Major histocompatibility complex; NF-kB, nuclear factor-kappa B; NK, Natural Killer; NO, Nitric oxide; NSAID, Nonsteroidal anti-inflammatory drugs; PGs, Prostaglandins; PGE2, Prostaglandin E2; PMNs, Polymorphonuclear neutrophils; PUFA, Polyunsaturated fatty acids; ROS, Reactive oxygen species; Rv, Resolvins; SPMs, Specialized pro-resolving mediators; TAMs, Tumor-associated macrophages; TANs, Tumor-associated neutrophils; TGF-β, Transforming growth factor beta; TLR, Toll-like receptor; TME, Tumor microenvironment; TNF-α, Tumor Necrosis Factor; VEGF, Vascular Endothelial Growth Factor.

INTRODUCTION

Inflammation is now recognized as a hallmark of cancer (1) and several lines of evidence have highlighted the significance of chronic inflammation in fueling tumor progression and influencing tumor response to treatment in many cancers. Rudolf Virchow was the first to describe leukocytes within tumor in the 19th century (2). A century later, Dvorak evidenced common features shared by inflammation and carcinogenesis proposing tumors as "wounds that do not heal" (3). This new inflammatory vision of tumor biology is now well supported by numerous studies that have highlighted the main contribution of chronic inflammation in cancer progression (4, 5). Inflammation is a defensive and protective reaction that aims to heal and repair damaged tissues. This physiological response is self-limited to prevent further detrimental over-reactions for tissue homeostasis. When inflammation is improperly regulated, deleterious signals may appear in inflamed tissues, supporting chronic inflammation setting up and fostering the development of many diseases, including autoimmune disorders, cardiovascular diseases or cancers. Resolution of inflammation is therefore a fundamental mechanism which allows damaged tissues to return to homeostasis in a process termed catabasis (6, 7). This active process mainly relies on a recently discovered array of molecules named specialized pro-resolving mediators (SPMs), including lipoxins, resolvins, protectins and maresins, which production is temporally and spatially regulated during acute inflammation (8, 9). SPMs mediate an effective inflammation resolution by transducing anti-inflammatory and pro-resolving signals that stop leukocytes recruitment in inflamed tissues and increase removal of apoptotic polymorphonuclear neutrophils (PMNs) (10). These events are crucial to break down further inflammatory signals and ensure restoration of tissue integrity. Among their target cells, SPMs have shown the ability to modulate macrophages' biology by notably increasing their nonphlogistic (*i.e.* noninflammatory) phagocytosis of apoptotic PMNs. This phenomenon is named efferocytosis, from the Latin word '*effere*' that translates to 'to take to the grave' (9, 11). Macrophages display tumor supporting roles and immunosuppressive functions that are exacerbated during carcinogenesis and tumor response to conventional anticancer treatments. SPMs may thus offer the opportunity to re-educate tumor-associated macrophages (TAMs) by promoting their pro-resolving activities and turning them toward an antitumoral phenotype.

Here, we summarize the recent findings on SPMs and cancer-focused macrophage biology as well as their connections. We further discuss the therapeutic opportunities to manipulate tumor and inflammation dialogue during cancer progression or therapeutic pressure especially through TAMs re-education using SPM-based therapies to improve anticancer treatments.

SPMs MEDIATE RESOLUTION OF INFLAMMATION

SPMs' Roles in Inflammation Resolution

Acute inflammation is a finely regulated physiological process initiated within minutes to hours in response to tissue injury or infection, where cellular and chemical mediators are operating. Pro-inflammatory lipid mediators including prostaglandins (PGs) and leukotrienes (LTs) are first secreted during the initiation step. Prostaglandin E2 (PGE2) contributes to the dilatation and increase in permeability of vascular vessels, and leukotriene B4 (LTB4) to leukocyte chemotaxis, both mechanisms are necessary for inflammation amplification (7, 12, 13). Increased blood flow and vessels permeability induce fluid, proteins and leukocytes to migrate to the inflammatory site, resulting in swelling (edema) (**Figure 1**). The first cellular effector recruited in damaged site are neutrophils (9) that kill pathogens due to their microbicidal activities and ensure debris removal by phagocytosis. Monocytes are subsequently recruited by chemotactic factors and differentiate locally into macrophages that clear cellular debris and apoptotic PMNs. Importantly, during inflammation progression, a switch in lipid mediator synthesis from pro-inflammatory (PGs and LTs) to pro-resolving mediators (SPMs) occurs in order to trigger inflammation resolution. Lipoxins' (LXs) production first occurs both locally and systemically to stop leukocyte recruitment and is then completed by a production of other SPMs to exert their pro-resolving effects. These effects include the cessation of neutrophils' recruitment and the increase of apoptotic PMNs removal by macrophages (7, 18–20). Efferocytosis is an important physiological process where phagocytes engulf apoptotic cells before they become necrotic and release danger molecules, thus preventing further exacerbated inflammatory signals (21). In addition, apoptotic PMNs' efferocytosis by macrophages induces a reparative phenotype by triggering intracellular signaling that further contribute to inflammation resolution through production of TGF-β and VEGF, that are necessary for tissue repair (7). Therefore, the switch in bioactive lipid production from PGs and LTs to SPMs is fundamental to prevent inflammation exacerbation. This mechanism is required for complete resolution and return to tissue homeostasis (9).

SPMs' Biosynthesis and Interactive Network

SPMs are a set of recently identified lipid mediators that act locally as endogenous agonists to stimulate the resolution of inflammation. Four subclasses of SPMs have been identified so far: lipoxins, resolvins (Rv), protectins and maresins (MaR) (10, 22). The discovery of these new bioactive lipids changed the comprehensive view of inflammation resolution as it was initially considered a passive process where inflammatory cells and chemical mediators were locally diluted (23). The emergence of the SPM family as omega-3 polyunsaturated fatty-acid (PUFA) derived bioactive lipids revealed their crucial role in actively "turning off" the inflammatory response by stopping neutrophils infiltration and enhancing their efferocytosis by macrophages (9). This active catabatic process is temporally and spatially regulated to sustain tissue homeostasis (8). However, evidence of chronic inflammation in different clinical contexts that initiates or fuels pathogenesis, reflects a defect in the temporal regulation of inflammation resolution. Under these conditions, SPMs may represent actionable targets to "switch on" resolving mechanisms and improve treatment outcome. Recent studies have highlighted the potential antitumor roles of SPMs in carcinogenesis and cancer

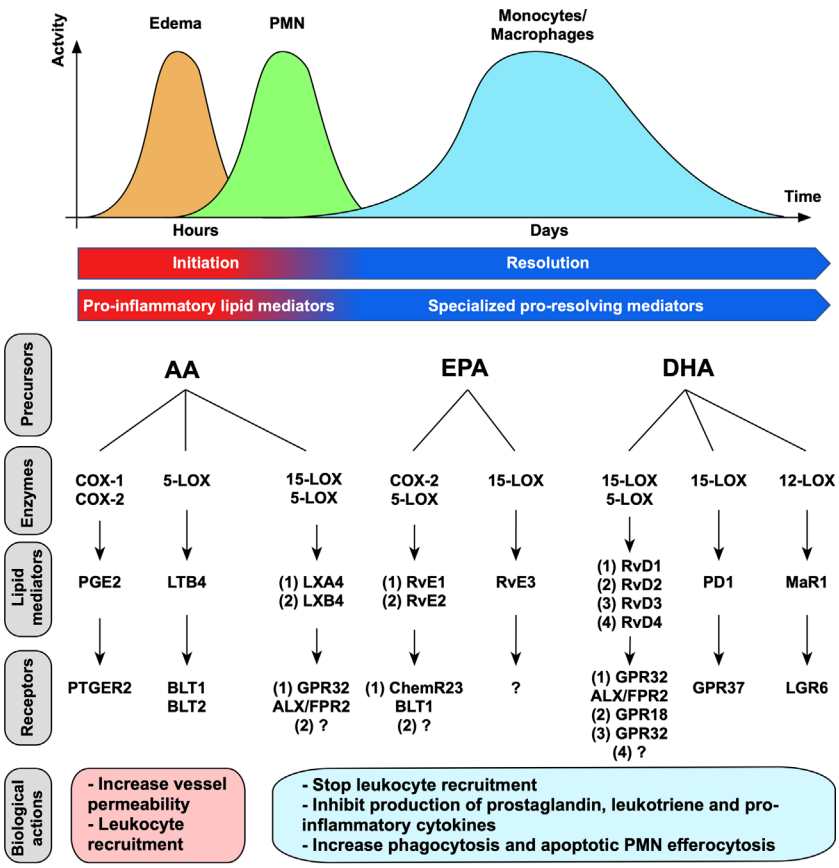

FIGURE 1 | Lipid mediators' time-course, synthesis and biological actions. Lipid mediators are produced sequentially through action of specific enzymes. Pro-inflammatory lipid mediators (prostaglandins and leukotrienes) are first produced during inflammation initiation. During inflammation resolution, a switch in lipid mediator synthesis occurred and promote SPMs' synthesis. Each SPM execute its functions by binding to a specific receptor. The receptors for LXB4, RvE2, RvE3, RvD4 have not been characterized yet (14–17).

progression including tumor response to treatment. Therefore, a comprehensive understanding of their biology is required to manipulate them for therapeutic purposes.

Lipid mediators include both pro-inflammatory (PGs and LTs) as well as anti-inflammatory and pro-resolving mediators (SPMs). They are generated through the action of the specific enzymes cyclooxygenases (COXs) and lipoxygenases (LOXs) from PUFA, including arachidonic acid (AA), eicosapentaenoic acid (EPA) and decosahexaenoic acid (DHA) (6) (**Figure 1**). Among COXs, COX-1 is constitutively expressed in several tissues and is responsible for basal level of PGs that are necessary for the maintenance of homeostasis, whereas COX-2 expression is triggered under inflammatory or tumorigenic signals (24). LOX enzymes present cell-specificity as 5-LOX is expressed in both myeloid (DC, monocytes and macrophages) and lymphoid (T- and B-cells) cells, 12-LOX in platelets and macrophages, and 15-LOX in vascular cells (12). Importantly, SPMs' production involves sequential enzymatic reactions that occur during cell-cell interactions. Arachidonic acid is metabolized to lipoxins through action of 15-LOX and 5-LOX during interactions between inflammatory (neutrophils or macrophages) and vascular cells (endothelial cells or platelets) (8). Resolvins are either named E-series or D-series resolvins that are respectively derived from EPA or DHA (14). Among E-series resolvins, RvE1 and RvE2 are produced by sequential actions of cytochrome P450 or COX-2 acetylated by aspirin in endothelial cells, and 5-LOX in human PMNs (25). D-series resolvins are produced through successive actions of 15-LOX and 5-LOX. Importantly, systemic administration of aspirin promotes acetylation of COX-2 which changes its enzymatic activity (*i.e.* stopping prostaglandins' production) to generate epimeric forms of SPMs termed aspirin-triggered SPM (AT-SPM) (25). Of note, AT-LXA4 and AT-RvD1-2-3-4 have been described to date (14). Protectins are derived from DHA and produced through action of 15-LOX in leukocytes (14). Maresin is the latest SPM family discovered and is derived from DHA, and MaR1 is synthesized *via* 12-LOX by macrophages (26). SPMs' synthesis is finely orchestrated to guarantee their right sequence of actions locally to resolve acute protective inflammation.

Of importance, SPMs are short-lived molecules that are further metabolized and inactivated by various enzymatic pathways involving β-oxidation, ω-oxidation, dehydrogenation and reduction (27). They act through specific G-protein-coupled receptors (GPCRs) (23) in a picogram to nanogram dose range (**Figure 1**). GPCRs represent the largest family of cell surface receptors, counting around 800 members (28), and a complex network of interactions has been already described between SPMs and GPCRs. In fact, two SPMs can bind to the same GPCR. For example, LXA4 and RvD1 both bind GPR32 and ALX/FPR2 expressed on PMNs and monocytes (6, 29–32). In addition, one SPM can bind to two GPCRs with different affinity. For instance, RvE1 binds to ChemR23 on myeloid cells, including macrophages and dendritic cells, and acts as a partial agonist for BLT1 expressed on PMNs to counteract LTB4's pro-inflammatory actions (8, 33). GPCRs can also interact with ligands of different nature, as evidenced for ChemR23, that binds both RvE1 and the chemoattractant protein chemerin, consequently strengthening the complexity of this network. The deep understanding of the interconnected systems linking SPMs to their specific GPCRs still offers many approaches for targeting these inflammation controlling networks.

SPMs and Tumor: Clinical Correlations

Importantly, unresolved inflammatory process leads to chronic inflammation with significant pathogenic consequences such as organ damages, auto-immune diseases or cancer initiation and progression (6, 32). Deficiency in SPMs' synthesis or biological activities participates to chronic inflammation establishment that sets the stage for tissue damage. For example, LXA4 deficiency is associated with cystic fibrosis and severe asthma (34, 35). Regarding cancers, overexpression of COX-2, 5-LOX and high levels of PG- and LT-derived metabolites that have important roles in tumor progression have been reported in many tumors (36, 37). Contrarily, to date, few studies have investigated the potential relationship between SPM levels and cancer. Decreased levels of LXA4 induced by 15-LOX down-regulation in serum and tumor from patients with colorectal cancer (38, 39) have been reported, suggesting the anti-tumorigenic potential of 15-LOX-derived metabolites in colon carcinogenesis (38). In another study, lower serum levels of RvD1 were found in patients with colon cancer compared to healthy volunteers and were reversely correlated with advanced cancer stage (40). These serum levels were further correlated with better survival in patients with endometrial cancer, suggesting that RvD1 could be a predictive biomarker of high tumor blood flow (41). Altogether, these clinical data demonstrated that impaired SPM activity coincides with promotion of carcinogenesis. Of note, the non-steroidal anti-inflammatory drug (NSAID) aspirin has shown protective effects in colorectal cancer and reduced the risk of developing other cancers such as lung and breast cancers (42, 43). Importantly, anticancer effects of aspirin were in part mediated through irreversible COX-2 acetylation and the generation of AT-SPM (44). These data emphasize the therapeutic potential of preventing inflammation in cancer, especially by using SPMs or their mimetics, as developed in the fourth part of this review.

MACROPHAGES ARE GUARDIANS OF TISSUE HOMEOSTASIS AND KEY REGULATORS OF PRO-TUMOR INFLAMMATION

Diversity of Macrophages Phenotypes and Functions

Macrophages are part of innate immune cells that possess important functions in organ development and tissue homeostasis. Macrophages can refer to either tissue-resident or monocytes-derived macrophages, that have different functions in tissues. Tissue-resident macrophages mainly originate from the embryonic yolk sac and fetal liver progenitors (45). These macrophages activate a unique transcriptional program dependent on their tissue of residence, as illustrated by specialized liver Kuppfer cells, brain microglia, lung alveolar macrophages or bone osteoclasts (46, 47). They maintain their pool by local homeostatic proliferation (48) and can be enriched locally from peripheral monocytes recruitment upon inflammatory signals. In contrast, monocyte-derived macrophages are continuously produced in bone marrow during hematopoiesis, and are recruited from blood circulation during inflammatory process. Both types of macrophages differentially exert their functions in damaged tissues. In sterile microlesions, tissue-resident macrophages prevented initiation of inflammation by sequestrating cell debris. When tissue-resident macrophages could not control the surging inflammatory signals (macrolesions or successive microlesions), PMNs' swarming triggered monocytes recruitment that in turn, engaged resolving and reparative programs (49). Distinctively from tissue-resident macrophages that have a major first-line homeostatic function, monocytes-derived macrophages are involved in pro-resolving mechanisms.

To ensure tissue homeostasis, macrophages have a myriad of functions, including host defense against pathogens or damage and regulation of immune responses to ensure tissue repair in these contexts. Macrophages are part of classical antigen-presenting cells (APCs) and mediate cellular immune responses through the processing and presentation of antigens to lymphocytes (50). In addition, macrophages are professional phagocytes that engulf either foreign particles (microbes) or altered self-particles or cells (dying or dead cells) (51, 52). They can quickly produce a large array of cytokines and chemokines that orchestrate local acute inflammatory process (52, 53).

Both diversity and plasticity define macrophages since they can acquire different phenotypes and functions depending on the stimuli present in the surrounding environment. Such properties are supported by plasticity of the epigenetic modifications that can rapidly modify macrophages' identity and destiny depending on external stimuli (54, 55). Those modifications includes DNA methylation, histone modifications and non-coding RNA (56). Of note, microRNA generated in response to various environmental stimuli have been reported to modulate macrophages' final differentiation (54).

Macrophages are generally classified as pro-inflammatory M1-like or anti-inflammatory M2-like macrophages (47) (**Figure 2A**). M1-like macrophages exert pro-inflammatory properties and are involved in microbicidal and tumoricidal activities. They can be

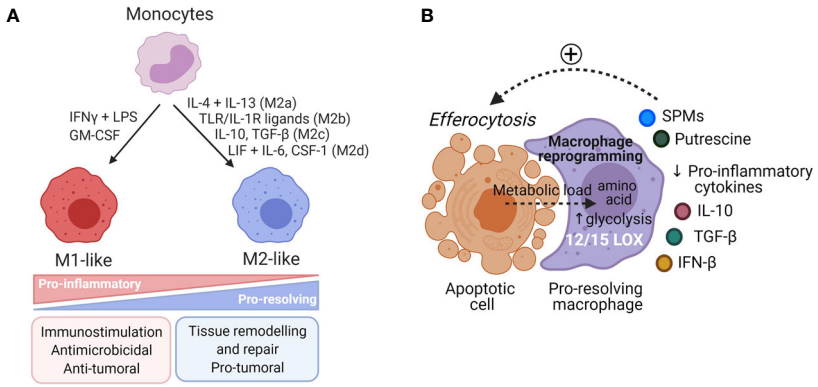

FIGURE 2 | Diversity of macrophages' phenotypes. **(A)** Monocytes can be differentiated *in vitro* either in pro-inflammatory M1-like macrophages or in anti-inflammatory M2-like macrophages upon various external stimuli. M1-like macrophages are involved in microbicidal and tumoricidal activities. M2-like macrophages have pro-resolving functions and are involved in tissue repair. In cancer settings, TAM, associated to a M2-like phenotype, support tumor progression and mitigate tumor response to anticancer treatments through production of proteases, angiogenic and growth factors. **(B)** During efferocytosis of apoptotic cells, macrophages undergo a reprogramming toward a pro-resolving phenotype. Macrophages receive an important metabolic load from these engulfed cells that induce metabolic modifications such as activation of the putrescine pathway or increased glycolysis that supports actin polymerization and cell clearance. Pro-resolving macrophages express 12/15-LOX and turn off production of pro-inflammatory cytokines for production of IL-10, TGF-β and IFN-β that participate in inflammation resolution.

generated *in vitro* in response to IFN-γ, GM-CSF or Toll-like receptors (TLR) agonists. They are characterized by secretion of high level of IL-12 and low levels of IL-10, production of nitric oxide (NO) and reactive oxygen species (ROS), secretion of pro-inflammatory cytokines including TNF-α and IL-1β (57, 58). In contrast to M1-like macrophages, in physiological contexts, M2-like macrophages are involved in inflammation resolution and wound healing. Mantovani et al. proposed a classification for M2-like phenotypes depending on stimuli used for monocyte-derived macrophages differentiation. Monocytes stimulation by: (1) IL-4 and IL-13 leads to M2a phenotype involved in tissue repair and killing of extracellular pathogens (59, 60); (2) Immune complexes or TLR or IL-1R ligands to M2b phenotype involved in immune regulation (61); (3) Glucocorticoids or IL-10 to M2c phenotype involved in efferocytosis of apoptotic PMNs and resolution of inflammation (62); and (4) CSF-1 or adenosine or IL-6 plus LIF to M2d phenotype involved in angiogenesis and immunosuppression. M2d macrophages reflect *in vivo* TAM phenotype with pro-tumorigenic properties (63).

Regarding phagocytic properties, M2-like macrophages can phagocyte more microbial particles and cancer cells than M1-like macrophages. Of interest, macrophage expression of specific surface markers can reflect their phagocytic capability (CD14, CD206 and CD163) or even their phagocytic capacity (i.e. amount of particles; CD209) as evidenced by a mass cytometry-based phagocytosis assay (64).

Importantly, M1-like and M2-like monocyte-derived macrophages produce distinct lipid mediator profiles. For example, upon bacterial stimulation, human M1-like macrophages display increased production of 5-LOX-derived LT including LTB4 and COX-2-derived PGs including PGE2, which production was 20 times higher in M1-like compared to M2-like macrophages. In contrast, M2-like macrophages exhibit increased 15-LOX expression resulting in SPM production that represent 50% of their total lipid mediators synthesis (65–67).

Generally, M1-like macrophages are associated with pro-inflammatory, antiviral, antibacterial, antitumor phenotypes and with production of pro-inflammatory lipid mediators (PGs and LTs). For their part, M2-like macrophages are defined by anti-inflammatory and reparative phenotypes related to their production of pro-resolving SPMs, but are also associated to a protumoral phenotype in cancers. However, this M1/M2 *in vitro* polarization model has shown its limitation as it does not authentically reflect macrophages' polarization occurring in tissues. It rather is a continuum between M1-like and M2-like phenotypes depending on cytokines present in the surrounding environment (68) and the origin of macrophages (69). This classification is still useful to study macrophages' biology *in vitro* but for greater clarity, Murray et al. suggested to adopt a specific nomenclature that specifies the stimuli used for monocyte activation [i.e. M(IL-4) for macrophages activated *in vitro* by IL-4] (70).

Pro-Resolving Functions of Macrophages

Removal of apoptotic cells by macrophage-dependent efferocytosis is a key step to achieve complete local inflammation resolution and return to tissue homeostasis. Efferocytosis of apoptotic PMN increased macrophages' SPMs biosynthesis (RvE1, PD1, LXA4, MaR1) (71) that in turn acts as a positive feedback loop, as evidenced by LXA4, that enhanced nonphlogistic PMN engulfment by macrophages (65, 72). Moreover, SPMs production by macrophages is enhanced through the release of microparticles that contain metabolic precursors, derived from dying neutrophils at the inflammatory site (65). Both efferocytosis and microparticles derived from apoptotic cells trigger macrophages' reprogramming from a pro-inflammatory to a pro-resolving hybrid phenotype between M1-like and M2-like macrophages (**Figure 2B**) (65, 73). Pro-resolving macrophages undergo continuous efferocytosis of apoptotic cells to prevent

their evolution toward necrosis until complete inflammation resolution. This process is upregulated by metabolites loaded from apoptotic cells during the first round of efferocytosis and the putrescine pathway (74). Apoptotic cells ingestion induces a deep metabolic reprogramming in efferocytic macrophages (75) that blocks the production of pro-inflammatory cytokines. Moreover, this process triggers the secretion of factors including IL-10, TGF-β, CCL-5 and protein S that promotes the clearance of apoptotic cells, prevents autoimmunity, and further supports macrophages' reprogramming (76–79).

So far, pro-resolving macrophages' phenotypes and functions have been mainly described in murine models of acute inflammatory diseases. Macrophages isolated from resolving acute peritonitis produced high levels of anti-inflammatory IL-10 and expressed M1-like markers such as iNOS and COX-2. They also expressed high level of cAMP that triggers COX-2 dependent lymphocyte repopulation necessary to restore homeostasis post inflammation, and prevent further reinfection (80). Importantly, transcriptomic analyses revealed that murine resolution-phase macrophages possess a unique phenotype that cannot fit the conventional M1/M2 classification, conferring them a hybrid phenotype with shared characteristics of M1-like and M2-like macrophages (81). Resolution-phase macrophages are enriched with molecules involved in antigen presentation and T-/B-cell chemotaxis, they produce SPMs, and they are involved in phagocytosis of apoptotic cells (82). Of particular interest, a specific population of "satiated" macrophages have been described among resolution-phase macrophages in zymosan-A induced peritonitis. This population is characterized by downregulation of CD11b expression induced by efferocytosis, production of high levels of anti-inflammatory and pro-resolving cytokines, including TGF-β, and high expression of 12/15-LOX. $CD11b^{low}$ macrophages were termed "satiated" as they have ingested many apoptotic PMNs but are no longer capable of phagocytosis, contrarily to $CD11b^{hi}$ macrophages from which they derive. $CD11b^{low}$ macrophages then migrate out of the inflammatory site (83). These data were reinforced by transcriptomic analyses that demonstrated a down regulation of gene clusters involved in phagocytosis and cytoskeleton configuration, and increased expression of gene clusters involved in myeloid cell migration (84). Moreover, non-phagocytic macrophages produce IFN-β that actively increases PMNs' apoptosis and removal by efferocytosis and participates in phagocytotic macrophage reprogramming (85). These results obtained in inflammatory murine models have clarified the vision of pro-resolving macrophages and the importance of their phenotypic and functional switch that finely regulates inflammation resolution. Of major interest, restoring pro-resolving functions of macrophages using SPMs in murine models of cancer deeply impaired tumor progression (86, 87). However, since mouse and human macrophages exhibit different gene signatures and metabolisms, efforts must now be concentrated on unraveling the profile of human pro-resolving macrophages (88). It would also demonstrate that promoting resolution of inflammation represent a promising strategy for the treatment of inflammatory diseases including cancers.

Macrophages Have Pro- But Also Anti-Tumor Activities in Cancer

Many observations have revealed tight links between cancers and inflammation (4). Inflammation may initially arise from cancer-associated exogenous pathogens (5) or from tumor cells secreting various pro-inflammatory factors (2, 89). When persisting, inflammation feeds carcinogenesis and cancer progression. Importantly, anticancer treatments including chemotherapies and radiotherapies can also trigger an inflammatory response at the tumor site resulting in a protumoral environment that supplies tumor progression and immunosuppression (86, 90).

Macrophages infiltrated in tumors are defined as tumor-associated macrophages (TAMs). TAMs first arise from tissue-resident macrophages (91) but various tumor-produced chemokines (CCL-2, CCL-5) and cytokines (CSF-1) also recruit circulating monocytes and further promote their differentiation into TAMs (92–94).

Importantly, macrophages are the major immune infiltrating component of tumor microenvironment (TME) in many solid tumors, representing up to 36% of total immune cells in breast tumors (95–97). TAMs high density coincides with a poor prognosis in many cancers (bladder, prostrate, ovarian and breast cancer) excepted for colorectal cancer (98). Recently, new technologies based on deconvolution of gene expression profiles or single cell analysis by RNA or mass-cytometry have gained great interest in studying TAMs (99, 100). Using these approaches, TAMs have been classified in clusters, characterized by differential expression levels of M2 markers such as CD163, MARCO and CCL-18 (101–103). Infiltration of M2-like TAMs has been associated with lower overall survival in non-small cell lung cancer (NSCLC) (104), lung adenocarcinoma (105) and gastric cancer (106). Importantly, these recent data demonstrated that TAMs expressed both M1 and M2 gene signatures (101, 102, 107, 108) and that presence of M1-like TAM was associated with increased survival in NSCLC (109) and in advanced ovarian cancers (110). Interestingly, upregulation of genomic signatures associated with immune cell activation and antigen presentation or phagocytosis, immune responses and blood vessels formation has been revealed in TAMs, respectively isolated from breast and endometrial cancer patients, compared with tissues-resident macrophages (111). Of note, a specific TAM subset associated with a phagocytic pattern has been reported in lung, colorectal, ovarian and breast cancer (108).

Those data have weakened our vision of the binary macrophage polarization model since TAMs may represent a specific "cancer-associated" spectrum of alternative polarization states between M1-like and M2-like macrophages. These data have also provided a new perception of TAMs' complexity as they demonstrated that TAMs both express pro- and anti-tumor markers (112).

Many studies have reported that TAMs display strong tumor supportive activities during both primary tumor development and its metastatic progression (**Figure 3**). TAMs produce prosurvival factors that protect tumor cells from apoptosis (PGE2, IL-10, TGF-β and IL-6) (119–121), including from chemotherapies-induced cell death (122). TAMs accumulate

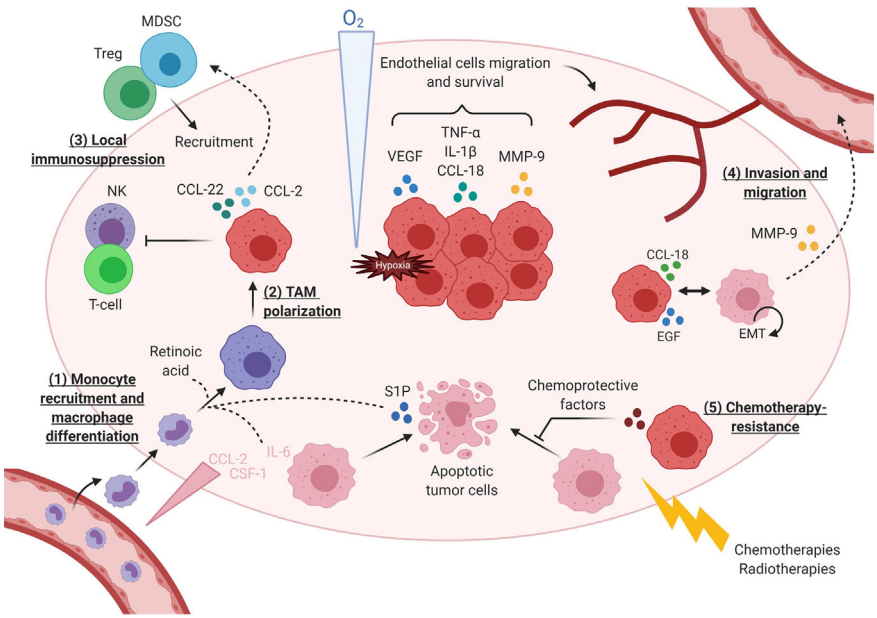

FIGURE 3 | TAMs execute diverse activities during tumor initiation and its immune escape. (1) Macrophages are first recruited in tumor under the action of chemokines secreted by tumor cells. Some factors such as retinoic acid (113) and IL-6 (114) favor monocytes differentiation toward macrophages instead of dendritic cells. (2) Macrophages become TAMs with immunosuppressive activity, in particular due to sphingosine 1 phosphatase (S1P) released by dying tumor cells. (3) TAMs support local immunosuppression by: secreting immunosuppressive cytokines, inhibiting effector T-cells (115) and NK cells (116), recruiting Tregs though CCL22-CCR4 axis or MDSC through CCL2-CCR2. (4) Under hypoxia, macrophages produce various cytokines, including CCL-18 (117) triggered by tumor cells at the tumor invasive front, and proteases that induce EMT in tumor cells and favor their invasion and migration. Additional paracrine loops between tumor cells and TAMs, as described for EGF and CSF-1, amplify TAM-dependent cancer cell motility (94, 118). (5) Finally, TAMs contribute to anticancer treatment resistance by secreting factors protecting tumor cells from death.

particularly in hypoxic areas (123, 124) where they secrete proangiogenic factors and proteases (VEGF, β-FGF, TP, TNFα, CXCL18, uPA, CCL18) that support endothelial cells' survival and migration for the development of a high-density vascular network (95, 124). Among proteases, TAMs produce MMP-9 that induce extracellular matrix remodeling further supporting tumor cell invasion (125, 126). TAMs also operate at distant sites during metastatic processes as observed in murine breast tumor cells that, when reaching lung capillaries, secrete CSF-1 to recruit new macrophages that in turn, help them to invade the lung parenchyma (127). In addition, TAMs actively participate in promoting an immunosuppressive TME through expression of immune checkpoints (PD-1 and B7-H4), production of immunosuppressive cytokines (IL-10 and TGF- β) (128), recruitment of immunosuppressive cells (Tregs and MDSC) (116, 126), and inhibition of effector immune cells (NK and T-cell) (115, 116). Importantly, chemotherapies often induce macrophages' recruitment in tumors, as seen by increased CD68+ macrophages infiltration in matched breast tumor samples before and after neoadjuvant chemotherapy (90, 122). Recruited macrophages presented a reinforced M2-like phenotype (90, 129, 130). Moreover, macrophage abundance in treated tumors was correlated with a low cytotoxic T cell infiltrate, suggesting that chemo-recruited TAMs increase immunosuppression by limiting T-cell responses to anticancer treatment (90).

Despite their tumor-supporting roles, macrophages constitute a high proportion of immune effectors in the majority of liquid and solid tumors, particularly in the so called "cold" tumors, and can be manipulated to eradicate tumors. Macrophages can exert direct (cell-contact, independent of phagocytosis) or indirect (soluble effectors) cytotoxicity toward tumor cells, at least *in vitro* (94, 131). They can recognize tumor cell through expression of various receptors (lectins, phosphatidylserine, integrins) (132) and produce when activated, various cytotoxic molecules [NO (94)] and cytokines [TNF-α (133)] that trigger tumor cells apoptosis and phagocytosis. Macrophages within tumors can be activated by tumor-associated antigens that they can further process and present *via* their MHC-II to CD4+ helper T cells and CD8+ cytotoxic T cells (132), to promote effective antitumor adaptive immune responses. Loss of efficient antitumor functions of macrophages due to their hijacking by cancer cells is critical for the development of antitumor immune responses. For example, increased expression of CD47 by tumor cells triggers an inhibitory signaling in macrophages through the immune checkpoint SIRPα, that limits macrophage-dependent phagocytosis (134) and lymphocyte chemotaxis (135). Restoring and/or stimulating antitumor functions of macrophages within tumors may counterbalance their tumor-supporting roles and help to promote an efficient immune antitumor response.

TAMs Are Preferentially Associated With a Pro-Inflammatory Lipid Mediator Profile in Cancer Context

Because of highly specialized approaches to detect and quantify lipidic mediators in biological specimens, TAM-related lipid mediators' profile has not been extensively studied. However, metabolic enzymes and receptors involved in activities of these mediators can be appraised using transcriptomic analyses. As such, TAMs isolated from ascites of patients with ovarian cancer revealed that TAMs expressed *PTGS2* (coding for COX-2), PGE2 and LTB4 receptors, contrarily to tumor cells (136). These results suggest that TAMs could be associated with a pro-inflammatory lipid mediator profile based on PGs and LTs, that supports their pro-tumorigenic functions.

Of importance, cancer cells indirect interactions with TAM-like *in vitro* alter the lipid mediator profile produced by cancer cells toward the synthesis of pro-inflammatory PGs and LTs, with pro-tumorigenic properties (36, 137). Among PGs, PGE2 largely contributes to tumor progression and promotes an immunosuppressive TME, particularly in macrophages (37, 138). Reversely, cancer cells also affect macrophages' lipid mediator profile through induction of COX-2 expression and release of sphingosine 1-phosphate (S1P) when dying. COX-2-derived PGE2 from both TAMs and cancer cells reinforce macrophages' immunosuppressive phenotype and inhibit their phagocytic capability (139). Moreover, TAM-like recognition of apoptotic cancer cells induced reduction of 5-LOX expression in TAMs in breast tumor spheroid models. This result is in line with lower 5-LOX expression in macrophages from human breast invasive tumors compared with macrophages from normal breast tissues (137). TAMs with reduced 5-LOX expression have reduced capacity to recruit effector T cells, suggesting an antitumor role for 5-LOX (137). These data demonstrated that cancer cells set up an inflammatory environment supported by the generation of pro-inflammatory and tumor-supporting bioactive lipids. Importantly, it has been reported that TAM indirect interactions with lung cancer cells induced SPM production (RvE3, RvD2, RvD5) (66), but to a lower extent than PGs and LTs. To strengthen the switch of bioactive lipid mediators occurring during inflammation resolution, the promotion of SPMs synthesis within tumors would reduce inflammation and restore antitumor functions of macrophages in the TME. Indeed, as developed below, SPMs demonstrated the capacity to induce anti-inflammatory and antitumor responses in cancer context. Further studies are needed to fully characterize the expression of SPMs and their specific receptors in TAMs to better understand the implications of these pro-resolving molecules in cancers.

TARGETING TAMs USING SPMs AS AN ANTICANCER STRATEGY

Since inflammation fuels cancer progression, use of anti-inflammatory drugs such as NSAID was first envisioned to interfere with this deleterious process (140). However, new insights in inflammation biology suggest that promoting its active resolution rather than achieving its complete inhibition may help to foster an effective antitumoral immune response, in particular during anticancer treatments (89). In this regard, recent studies demonstrated that SPMs exerted intrinsic antitumor activities mainly through macrophages and greatly improve tumor response to chemotherapies in various murine cancer models (86). This innovative concept strengthened by the fundamental role of macrophages in both inflammation resolution and cancer progression, has gained great interest in cancer treatment (141). Macrophages depletion and/or recruitment inhibition using specific monoclonal antibodies, such as anti-CSF1R, were first investigated to breakdown their growth-supportive roles. However, important toxicity have been reported and linked to a depletion of all macrophages in the body (142). Instead of their therapeutic eradication, repolarization of TAMs toward an antitumoral phenotype based on high phenotypic plasticity opens new possibilities in cancer treatment (143). From this perspective, recent approaches are being evaluated: epigenetic reprogramming of M2-like TAMs into M1-like TAMs (144); increasing phagocytic activity by CD47/SIRPα blockade (145, 146); engineering Chimeric Antigen Receptors for Phagocytosis (CAR-P) to increase tumor cell killing (147, 148). Recent reports also illustrate that macrophages can be involved in immunotherapy resistance mechanisms such as T-cell exclusion by impeding CD8 T-cells from reaching tumor cells (149). Moreover, relieving the SIRPα break on macrophages promotes intra-tumoral chemokine secretion, T-cell migration in tumor bed and improves T-cell immunotherapy responses (135).

SPMs Shape Macrophages Functions

In view of their crucial role in inflammation resolution, early studies using SPMs were first conducted in inflammatory contexts and aimed to understand SPMs' pro-resolving effects on macrophages. Of note, some effects were mediated by SPM mimetics including SPM analogs and receptor agonists (named in bold in **Table 1**) that will be further developed in part 4. Even though experimental conditions vary between studies (*i.e.* type of macrophages, SPM concentration and time of incubation) they all demonstrated that SPMs increased macrophages' phagocytosis of microbicidal particles and efferocytosis of apoptotic PMNs (**Table 1**). Those effects were accompanied by decreased macrophages' secretion of pro-inflammatory cytokines (153, 156, 159) mediated in part by reducing the nuclear factor-κB (NF-κB) activation (33, 156, 159, 163), a transcription factor involved in the development and maintenance of chronic inflammation (164). SPMs such as RvD1 and RvD2 can also induce macrophages' secretion of anti-inflammatory cytokines including IL-10 and TGF-β (156, 160), two cytokines involved in resolving and reparative mechanisms. In addition, LXA4 exerted death protective effects on macrophages (150), allowing them to ensure complete functions during inflammation resolution. These results underline a SPM-based phenotypic switch in macrophages toward an intermediate phenotype between M1-like and M2-like (155, 157, 159) with pro-resolving functions.

TABLE 1 | SPMs' *in vitro* effects on human macrophages in inflammatory contexts.

Macrophages	SPMs	Effects	References
Human monocyte-derived macrophages (M1-like, M2-like)	LXA4 (250nM)	Protect macrophages from apoptosis	(150)
	LXA4 (0.1-10nM)	Increase phagocytosis of zymosan particles	(151)
Human monocytes	LXA4 **(ATL-1)** (1-100μM)	Inhibit monocytes' apoptosis	(152)
Primary human macrophages	LXA4 **(ATL-1)** (100μM)	Increase phagocytosis Decrease secretion of pro-inflammatory cytokines	(153)
Human monocyte-derived macrophages (M1-like)	RvD1 (0.1-1nM)	Increase phagocytosis of microbial particles and apoptotic PMN	(154)
	RvD1 (0.1-10nM)	Increase phagocytosis of zymosan particles	(151)
	RvD1 (10nM)	Switch M1-like to M2-like macrophages	(155)
Human alveolar macrophages	RvD1 and RvD2 (100 nM)	Increase phagocytosis of microbial particles (E. coli) Decrease secretion of pro-inflammatory cytokines	(156)
Primary human macrophages	RvD1 (10nM)	Polarize resting primary macrophages and repolarize M1-like macrophages to a pro-resolving phenotype	(157)
M1-like macrophages	RvD5 (10nM)	Increase phagocytosis of microbial particles	(67)
Human monocyte-derived macrophages (M1-like)	RvE1 (10nM)	Increase phagocytosis of microbial particles	(158)
Primary human macrophages	RvE1 (10nM)	Induce a pro-resolving phenotype	(159)
Human monocyte derived macrophages (GM-CSF)	RvE2 (1-10nM)	Increase phagocytosis of zymosan particles	(160)
Human macrophages (M2-like)	MaR1 (1 nM)	Increase efferocytosis of apoptotic PMN	(161)
Human monocyte-derived macrophages (M1-like, M2-like)	MaR1 (10pM-10nM)	Increase phagocytosis (E. coli, zymosan) and efferocytosis of apoptotic PMN	(19)
Human monocyte-derived macrophages (M1-like)	MaR1 (10 nM)	Switch M1-like to M2-like macrophages	(155)
Human macrophages	PD-1 **(22-F-PD1)** (0.001-10nM)	Increase macrophages' efferocytosis of apoptotic PMN	(162)

Bold, SPM analogs or receptor agonists.

Importantly, as inflammation is an integrated part of cancer biology, SPMs' effects on human macrophages have started to be evaluated in cancer contexts (**Table 2**). To better mimic macrophages' polarization within tumors, biological fluids from cancer patients or conditioned media from tumor cells, are now used for *in vitro* monocytes differentiation into TAM-like macrophages (63, 165, 168). In such settings, SPMs including LXA4, RvD1 and RvD2 suppressed TAM-like phenotype, suggesting that SPMs can modulate macrophages' polarization in cancer context (165, 167). Interestingly, SPMs' functions have been tested in *in vitro* models of chemotherapy-mimicking inflammation (86). Incubation of monocyte-derived macrophages with chemotherapies-induced tumor cell debris in presence of RvD1, RvD2, or RvE1 increased their efferocytotic activity and reduced their secretion of pro-inflammatory cytokines (86). Moreover, LXA4's analog decreased TAM-like's production of IL-10, a cytokine associated with immunosuppressive properties in TME (165). This result seems to contradict the observed effects of SPMs on the increased production of such cytokines (IL-10, TGF-b) by macrophages, in a pro-resolving context, thus questioning about a potential immunosuppressive role of SPMs when modulating immune related activities in TAMs. However, these diverging effects were not observed in the same context, *i.e.* non-tumor versus tumor environment. Such results should consider the global environment, as other cytokines may also operate in regulating those mechanisms. Further studies are needed to establish a broader secretion profile of cytokines produced by macrophages upon SPM treatment in tumor context. In addition, no immunosuppressive effects have been reported in experimental models using SPMs so far, contrarily to their anti-inflammatory and pro-resolving functions. Dedicated experiments should be conducted to confirm the absence of immunosuppressive events associated with the use of SPMs in cancer context.

Overall, SPMs turn out to be potent modulators of TAMs' phenotype toward a more phagocytic and less inflammatory

TABLE 2 | SPMs' effects on human macrophages in a cancer context.

Macrophages	SPMs	Effects	References
Human monocyte-derived macrophages	RvD1 – RvD2 – RvE1 (1pM – 100nM)	Increase phagocytosis of tumor cell debris and reduce pro-inflammatory cytokine secretion	(86)
Human monocyte-derived TAM	LX4 **(ATL-1)** (10nM)	Suppress TAM phenotype Decrease IL-10 secretion	(165)
Human monocyte-derived macrophages	LXA4 - RvD1 – RvD3 (AT-SPM) (100pM-100nM)	Increase phagocytosis of tumor cell debris and reduce pro-inflammatory cytokines secretion	(166)
THP-1 monocytes	RvD1-RvD2 (1-100nM)	Suppress TAM phenotype	(167)

Bold, SPM analogs or receptor agonists.

phenotype that may boost their intrinsic antitumor activities. Altogether, these data evidenced that SPMs can directly act on macrophages and modulate their phenotype and biological activities. However, it still remains difficult to reach a consensus on a well-defined macrophage phenotype induced by SPM due to the complexity of macrophages' polarization in *in vitro* experiments, in direct relation with their high intrinsic plasticity. Indeed, several parameters such as inter-donor variability, variety in protocols to perform *in vitro* macrophage differentiation, diversity in M1/M2 markers used for phenotype analyses by flow cytometry and/or cytokine secretion in response to LPS stimulation, all together, these discrepancies feed inter-laboratory results diversity that complicates a synthetic view of macrophage biology (70, 169). As discussed earlier in this review, there is a need for the deep characterization of pro-resolving macrophages in human context. More data about SPMs' production by macrophages or TAMs and their effects on these cells would allow a better understanding of how SPMs modulate regulatory functions of macrophages, particularly in the context of immune networks.

SPMs Restrict Carcinogenesis and Cancer Progression

SPMs' anticancer effects have been evaluated in different *in vitro* and *in vivo* cancer models during either carcinogenesis or tumor progression, and are listed and referenced by SPMs and type of cancer in **Table 3**. First, SPMs can prevent inflammation-induced carcinogenesis due to their pro-resolving properties. For instance, LXA4 suppressed early development of colorectal cancer and cancer transformation in skin papillomas (38, 174) and MaR1 prevented cancer transformation after UVB-long exposure (181). Secondly, all SPM subfamilies were shown to reduce tumor growth in different murine tumor models as exposed in **Table 3**. As such, LXA4 was efficient in reducing colorectal, hepatocellular, melanoma, lung and breast carcinoma tumor growth *in vivo* (38, 165, 166, 170, 171, 180). Resolvins of series D and E also exhibited antitumor activities on primary tumor growth in lung, lymphoma, melanoma, pancreatic and prostate cancer (86, 180). In oral squamous cell carcinoma, RvD2 showed *in vitro* and *in vivo* dose-dependent antitumor effects but RvD1 appeared less efficient to induce tumor reduction, possibly underlining cancer or specific SPMs effects (179). LXA4 and D-series resolvins also exhibited anti-metastatic effects in various murine tumor models including lung, liver and pancreatic cancers (86, 172, 176, 180).

Importantly, these studies showed that SPMs mediate their antitumor actions in part by counteracting pro-tumorigenic properties of TAMs, including stimulation of tumor cell proliferation and migration, epithelial-mesenchymal transition (EMT), angiogenesis and production of tumor growth-supportive cytokines and chemokines (38, 165, 167, 172, 173). As mentioned above, SPMs altered TAMs' phenotype both *in vitro* and *in vivo* (165, 175) and stimulated apoptotic tumor cell clearance (179).

In addition, SPMs can directly modulate various cancer cell autonomous mechanisms, including proliferation, cell death decision or invasive phenotype, as previously reported (176–178, 182). Some effects were mediated by down-regulation of the NF-κB pathway (178), also involved in cancer progression (183) and transcription of tumor-promoting genes in TAMs (164). However, no direct evidence of SPMs' effects on NF-κB were reported on TAMs so far. Of note, beyond acting on

TABLE 3 | List of publications reporting SPMs' antitumor activity in murine cancer models.

SPMs	Cancer Models	Molecules	Effects	References
LXA4	Colorectal cancer	Native	Suppress early development of colorectal cancer (Mϕ)	(38)
		BML-111 or AT-LXA4	Inhibit tumor growth	(166, 170)
	Hepatocellular carcinoma	**BML-111**	Inhibit tumor growth	(170, 171)
		BML-111	Inhibit EMT and metastasis (Mϕ)	(172)
		BML-111	Inhibit proliferation, invasion and angiogenesis of cancer cells (Mϕ)	(173)
	Papillomas	Native	Inflammation resolution Reduce the risk of cancer transformation	(174)
	Melanoma	**ATL-1, BML-111**	Inhibit tumor growth Alter TAM phenotype *in vivo* (Mϕ)	(165, 170)
		ATL-1	Decrease monocyte infiltration in tumor (Mϕ) Alters TAM phenotype *in vivo* (Mϕ)	(175)
	Pancreatic	**BML-111**	Reduce liver metastases	(176)
RvD1	Hepatocellular carcinoma	Native	Block CAF pro-tumor effects on tumor growth and metastases	(177)
		Native	Prevent liver injury and cancer transformation	(178)
	Melanoma	Native	Reduce pulmonary metastasis	(86)
RvD2	OSCC	Native	Tumor growth reduction (Mϕ)	(179)
	Lung, Melanoma	Native	Reduce pulmonary metastasis	(86)
RvE1	Hepatocellular carcinoma	Native	Prevent liver injury and cancer transformation	(178)
RvD2, RvD3, RvD4	Lung, Lymphoma, Melanoma	Native	Reduce metastases and improve survival (preoperative context)	(180)
RvD1, RvD2, RvE1	Lung, Pancreatic cancer, Prostate	Native	Inhibit tumor growth	(86)
RvD1, RvD3	Lung	**AT-RvD1, AT-RvD3**	Inhibit tumor growth	(176)
MaR1	Skin inflammation	Native	Prevent cancer risk following UVB irradiation	(181)

Bold, SPM analogs or receptor agonists.

Please refer to Prevete et al. (182) for previous studies reported SPMs' anticancer effects (182). Mϕ indicated studies where SPM anticancer effects were mediated through counter regulation of TAM protumor functions or TAM repolarization.

macrophages, SPMs can also modulate other immune cells present in TME such as T- or B-lymphocytes (170), cancer-associated fibroblasts (CAFs) (177) or tumor-associated neutrophils (TANs) (184) to unlock their antitumoral activities.

Altogether, these data suggest that SPMs exhibit potent anticancer activities through both direct effects on tumor cells and/or through the modulation of TAMs toward a less immunosuppressive and antitumoral phenotype (**Figure 4**). Since macrophages represent the major component of immune cells in many tumors and are key actors in SPMs' biology, developing new therapeutic strategies based on SPM-induced stimulation of TAMs pro-resolving functions could be envisioned as a new perspective in cancer treatment.

HOW TO USE SPMs IN CANCER TREATMENT?

SPMs as Anticancer Molecules

As mentioned above, counteracting inflammation has been viewed as a therapeutic opportunity in cancer treatment for many years. NSAID and among them aspirin have already achieved encouraging results in clinical trials, showing protective effects in many cancers (42, 43). Nevertheless, the lack of specificity of NSAID gave rise to significant side effects (bleedings, cardiovascular and kidney toxicity) and infectious complications, therefore compromising their use in cancer patients (86, 89, 140). In contrast, SPMs have not shown immunosuppressive effects in experimental models of pain and inflammation (185) or cancer (86) so far. Thus, SPMs would reduce intrinsic cancer-associated inflammation and reinforce antitumor immune responses while avoiding NSAID deleterious side effects.

Surgery is often the first approach for therapeutic care practiced in several cancers such as breast and colorectal cancer (186, 187). However, several studies highlighted the risk of early metastatic occurrence after surgery by outgrowth stimulation of dormant metastasis. The surgical procedure is not immune silent as it triggered local and systemic inflammatory reactions as evidenced by increased inflammatory circulating monocytes and pro-inflammatory cytokines (188). Preventing inflammatory events and stimulating inflammation resolution by preoperative administration of RvD2, RvD3 and RvD4 inhibited the development of micro-metastases in several murine resection tumor models (180). More generally, resolvins have been shown to inhibit metastasis in cancer murine models with higher efficacy when combined to chemotherapy (**Table 3**) (86). Thus, SPMs could be used in oncology as a preoperative strategy to resolve surgery related-inflammation and to prevent metastases relapse.

Importantly, anticancer treatments (chemo- and radio-therapies or immunotherapies) induce direct or indirect tumor cell death resulting in the generation of apoptotic tumor cell debris (86). Those debris largely contribute to fuel local inflammation by activating macrophages that further support cancer progression. Breaking down this vicious circle by resolving tumor-associated inflammation would stop further inflammatory and pro-tumorigenic signals. From this perspective, Sulciner and colleagues have studied the anticancer effects of resolvins in murine models of tumor cell debris-stimulated tumor growth (86). RvD1, RvD2 and RvE1 inhibited tumor growth at a higher extent than conventional

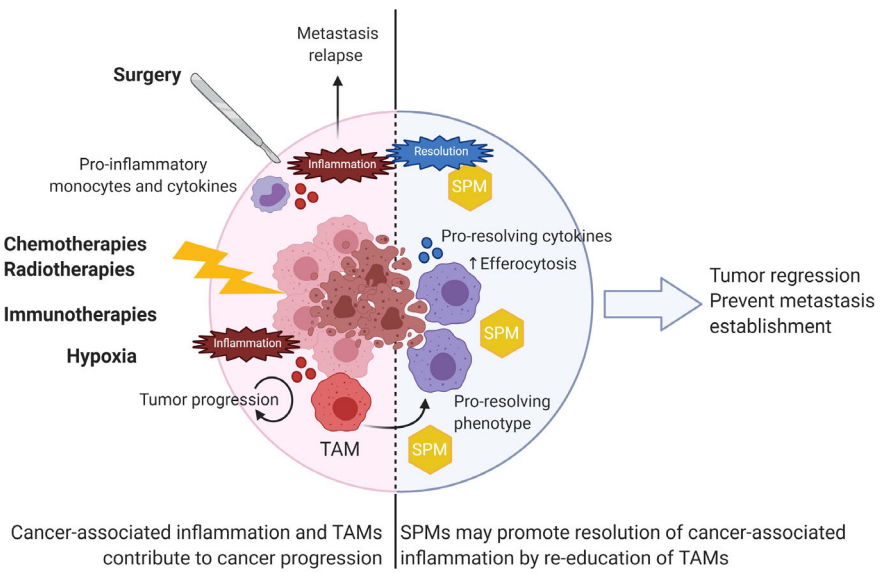

FIGURE 4 | SPMs as anticancer agents to resolve cancer-associated inflammation. Various extrinsic factors such as surgery and anticancer treatments as well as intrinsic hypoxia contribute to local inflammation within tumors. TAMs largely contribute to fuel tumor progression by various functions described in **Figure 3**. Use of SPM would resolve cancer-associated inflammation by repolarizing TAMs toward a pro-resolving phenotype with increased efferocytosis capabilities. As a result, SPMs could induce tumor regression and prevent further metastasis establishment.

chemotherapies or anti-inflammatory drugs. Moreover, synergistic antitumoral effects were observed when mice were treated with chemotherapies (gemcitabine or cisplatin) or relevant targeted anticancer therapies (cetuximab or erlotinib) in combination with resolvins, in both debris-stimulated tumor models, or spontaneous cancer models (86). Therefore, resolvins could be added as a complement to anticancer treatments to enhance therapeutic efficacy. Interestingly, compared to inflammatory drugs, resolvins have not shown immunosuppressive effects yet and were able to stimulate macrophages' efferocytosis. Thus, resolvins represent a great alternative to the use of anti-inflammatory drugs to stimulate TAM dependent pro-resolving mechanisms during anticancer treatments without apparent immunosuppressive side effects.

Hence, several possible approaches could be envisioned to include SPM in cancer care: (1) SPM could replace anti-inflammatory drugs in perioperative surgery to prevent further inflammatory events; (2) SPM could be administered combined with chemo- and radio-therapy or immunotherapies to resolve resulting inflammation and dampen anticancer treatment side effects; (3) SPM could be envisioned in metastatic cancer treatment to prevent further metastatic relapse. Further studies are needed to evaluate the feasibility and efficacy of such approaches in human clinical studies.

Engineering SPM Mimetics

One drawback of SPM is their short lifespan due to their lipidic nature and rapid metabolic inactivation, which can make them difficult to use. For instance, LXA4 added to macrophages results in LXA4 loss within minutes of its exposure (189). There has been an impetus for the development of small molecules or analogs capable of mimicking their biological activities but with a greater stability (**Tables 4**, **5**).

SPM Analogs: Chemical Modifications of Native SPMs

In the late 1990's, Serhan and colleagues designed the first LXA4 analogs with chemical modifications of native LXA4, resulting in increased stability due to enzyme conversion resistance (189). AT-SPM generated by low-dose aspirin also present increased stability compared to native SPM (44). Since several SPM analogs characterized by a higher stability both *in vitro* and *in vivo* have been developed (27, 189). Importantly, these analogs demonstrated similar biological activities than native SPMs *in vitro* and *in vivo*. They were able to stimulate macrophages pro-resolving functions and induce inflammation resolution in a GPCR-dependent manner in *in vitro* and *in vivo* inflammatory models (19, 162, 191). These analogs also exerted antitumor effects, including inhibition of primary tumor growth and metastasis as previously detailed in **Tables 2** and **3** (165, 170, 175, 193). Of note, analogs displayed biological activities at doses lower than native SPMs (189). Specifically, AT-RvD1, AT-RvD3 and AT-LXA4 have been shown to inhibit tumor growth in colorectal, lung, and breast murine models at doses 1,000-fold lower than aspirin (166).

SPM Receptor Agonists: Targeting SPM Specific Receptors

Among identified SPM receptors to date, ChemR23 (RvE1), ALX/FPR2 (LXA4, RvD1), GPR32 (LXA4, RvD1, RvD3), GPR18 (RvD2) and LGR6 (MaR1) are GPCRs that are often

TABLE 4 | SPMs or AT-SPM analogs and receptor agonists.

Nature	SPMs	Name	Reference
Analogs	LXA4	15(R/S)-methyl-LXA4, 16-phenoxy-LXA4	(190)
	PD-1	22-F-PD1	(162)
	MaR1	7S-MaR1	(191)
	RvE1	19-(*p*-fluorophenoxy)-RvE1 methyl ester	(27)
AT-SPM analogs	LXA4	ATL-1 (15-epi-16-(para-fluoro)phenoxy-LXA4)	(152, 153, 165, 175)
Receptor agonists	FPR2/LXA4	BML-111 (5(S),6®,7- trihydroxyheptanoic acid methyl ester)	(170–173)
	GPR32	NCGC00120943 (C1A), NCGC00135472 (C2A) pMPPF, and pMPPI	(19)
	ChemR23	Monoclonal antibody	(192)

Here are listed SPM mimetics, including analogs, AT-SPM analogs and receptor agonists that show increased stability and biological activities in inflammation resolution settings.

TABLE 5 | Therapeutic approaches for the development and use of SPM mimetics in cancer treatments.

			Disadvantages	Advantages
SPMs	Native		Short half-life	Biological activities
	Analogs		Short half-life	Increased Stability Biological activities
	Receptor agonists	Small molecules	Short half-life	Increased Stability Easy to develop Biological activities
		Monoclonal antibodies	Manufacturing costs	Long exposure for chronic disease Easy to develop Specificity and selectivity

TABLE 6 | SPMs and SPM mimetics tested in human.

SPMs	Analog/Receptor agonist	Clinical trials	Effects	References
RvE1	RX-10045 **(analog)**	Combined Phase I and II in patients with dry eye symptoms	Safe and well tolerated	NCT00799552
LXA4	15(R/S)-methyl-lipoxin A_4 **(analog)**	Study in Infantine eczema	Well tolerated Reduction of eczema severity	(198)
LXA4	BLXA4-ME **(analog)**	Phase I/II in patients with gingivitis (on going)	Assess safety and preliminary efficacy	NCT02342691
LXA4	LXA4 **(native)**	Study in patients with asthma	LXA_4 attenuated leukotriene C4-induced bronchoconstriction	(199)
LXA4	5(S),6(R)-LXA_4 methyl ester **(analog)**, BML-111 **(agonist)**	Pilot study in asthmatic children	Safe and well tolerated Improvement of pulmonary functions	(200)

expressed on macrophages' surface (19, 194). Development of specific agonists for SPM receptors would mimic SPMs' activities on macrophages and could be used to modulate their biological activities. Of note, GPCRs are currently the most important group of targets for approved drugs (195).

As SPM and their corresponding binding pockets in GPCRs are small, it is thus quite easy to develop specific receptor agonists (28) (**Tables 4** and **5**). This process requires a high understanding of the targeted receptors' pharmacology as underlined by functional selectivity for one ligand to certain downstream signaling pathways (referred as ligand bias theory) (28). Drug discovery and challenges regarding GPCRs in relation to inflammation resolution have been extensively reviewed here (15).

Among receptor agonists, BML-111 is a commercially available synthetic molecule that targets the LXA4 and RvD1 receptor ALX/FPR2 (196). BML-111 has shown antitumor activities in murine colorectal, hepatocellular and melanoma tumor models (170) (**Table 3**).

Therapeutic antibodies can also be used as agonists to activate GPCRs (192). They offer several advantages: longer life span than small molecules, specificity and selectivity (197). In a recent report, Trilleaud et al. illustrated that a selected and optimized agonist monoclonal antibody can exercise pro-resolving RvE1 actions on pro-resolving macrophages' polarization, neutrophils migration inhibition and acceleration of neutrophils' apoptosis. While this pro-resolving agonist antibody accelerates inflammation resolution *in vivo* in various models, and was also able to trigger efficient resolution in non-resolving chronic inflammatory models, Trilleaud et al. also reported that such pro-resolving agonist antibody can significantly limits colon carcinogenesis induced by inflammation and eradicate established colorectal tumors in some mice in monotherapy or combination with chemotherapy (192). Developing specific and lasting agonists may be a promising approach for the modulation of both inflammation resolution and antitumor responses in chronic diseases such as cancers.

SPM Mimetics in Clinic

As SPM and their mimetics have shown encouraging results in preclinical models, these molecules have been further tested in human and shown both safety and efficacy (**Table 6**). SPMs are immunoresolvent rather than immunosuppressive molecules that exert their pro-resolving and anti-inflammatory actions at low doses without deleterious side effects, which makes them very interesting molecules on the clinical level (201). Those results in human are encouraging to pursue the development of small molecules capable of mimicking SPM to stimulate pro-resolving functions of macrophages/TAM.

CONCLUSION

Cancer and inflammation are closely related not only during initial steps of carcinogenesis but also during cancer progression as well as tumor response to anticancer treatment including modern immunotherapies. Hijacked macrophages within tumor microenvironment largely support tumor growth in part by sustaining local immunosuppression. Due to the emerging central role of SPMs in inflammation resolution, SPM biology is now a trending field of study in human diseases that emerge as potent therapeutic targets not only in chronic inflammatory diseases but also in cancers. Due to macrophages' high plasticity, SPMs may indeed represent a new approach for cancer treatment by repolarizing TAMs toward antitumor macrophages with the advantage of using bioactive molecules, supposedly without immunosuppressive properties and deleterious side-effects. Developing stable and lasting SPM, these data confirm the value of targeting SPMs by promoting pro-resolving responses in a context of cancer treatment.

AUTHOR CONTRIBUTIONS

ML performed the scientific literature search, design the figures and wrote the review. VG and NP completed the review. SB-N and CB completed and finalized the review. All authors contributed to the article and approved the submitted version.

ACKNOWLEDGMENTS

This work was supported by INSERM and CNRS. The authors thank Association Nationale Recherche et Technology (ANRT) for Lavy M grant. Many thanks to Raphaël Rispal for proofreading the manuscript. **Figures 2–4** were created with Biorender.com.

REFERENCES

1. Hanahan D, Weinberg RA. The Hallmarks of Cancer. *Cell* (2000) 100:57–70. doi: 10.1016/S0092-8674(00)81683-9
2. Balkwill F, Mantovani A. Inflammation and Cancer: Back to Virchow? *Lancet* (2001) 357:539–45. doi: 10.1016/S0140-6736(00)04046-0
3. Flier JS, Underhill LH, Dvorak HF. Tumors: Wounds That Do Not Heal. *N Engl J Med* (1986) 315:1650–9. doi: 10.1056/NEJM198612253152606
4. Korniluk A, Koper O, Kemona H, Dymicka-Piekarska V. From Inflammation to Cancer. *Ir J Med Sci* (2017) 186:57–62. doi: 10.1007/s11845-016-1464-0
5. Parkin DM. The Global Health Burden of Infection-Associated Cancers in the Year 2002. *Int J Cancer* (2006) 118:3030–44. doi: 10.1002/ijc.21731
6. Basil MC, Levy BD. Specialized Pro-Resolving Mediators: Endogenous Regulators of Infection and Inflammation. *Nat Rev Immunol* (2016) 16:51–67. doi: 10.1038/nri.2015.4
7. Serhan CN, Savill J. Resolution of Inflammation: The Beginning Programs the End. *Nat Immunol* (2005) 6:1191–7. doi: 10.1038/ni1276
8. Bannenberg G, Serhan CN. Specialized Pro-Resolving Lipid Mediators in the Inflammatory Response: An Update. *Biochim Biophys Acta* (2010) 1801:1260–73. doi: 10.1016/j.bbalip.2010.08.002
9. Serhan CN. Pro-Resolving Lipid Mediators Are Leads for Resolution Physiology. *Nature* (2014) 510:92–101. doi: 10.1038/nature13479
10. Serhan CN, Chiang N, Van Dyke TE. Resolving Inflammation: Dual Anti-Inflammatory and Pro-Resolution Lipid Mediators. *Nat Rev Immunol* (2008) 8:349–61. doi: 10.1038/nri2294
11. Doran AC, Yurdagul A, Tabas I. Efferocytosis in Health and Disease. *Nat Rev Immunol* (2020) 20:254–67. doi: 10.1038/s41577-019-0240-6
12. Freire MO, Van Dyke TE. Natural Resolution of Inflammation. *Periodontol 2000* (2013) 63:149–64. doi: 10.1016/S0140-6736(00)04046-0
13. Ricciotti E, FitzGerald GA. Prostaglandins and Inflammation. *Arterioscler Thromb Vasc Biol* (2011) 31:986–1000. doi: 10.1161/ATVBAHA.110.207449
14. Kohli P, Levy BD. Resolvins and Protectins: Mediating Solutions to Inflammation. *Br J Pharmacol* (2009) 158:960–71. doi: 10.1111/j.1476-5381.2009.00290.x
15. Park J, Langmead CJ, Riddy DM. New Advances in Targeting the Resolution of Inflammation: Implications for Specialized Pro-Resolving Mediator Gpcr Drug Discovery. *ACS Pharmacol Transl Sci* (2020) 3:88–106. doi: 10.1021/acsptsci.9b00075
16. Kim N, Lannan KL, Thatcher TH, Pollock SJ, Woeller CF, Phipps RP, et al. Lipoxin B_4 Enhances Human Memory B Cell Antibody Production Via Upregulating Cyclooxygenase-2 Expression. *J Immunol* (2018) 201:3343–51. doi: 10.4049/jimmunol.1700503
17. Edin ML, Zeldin DC. Commercial Scale Production of RvD4 Opens the Resolving Door to New Research. *J Leukoc Biol* (2018) 103:991–3. doi: 10.1002/JLB.3CE0118-032R
18. Bannenberg G, Moussignac R-L, Gronert K, Devchand PR, Schmidt BA, Guilford WJ, et al. Lipoxins and Novel 15-Epi-Lipoxin Analogs Display Potent Anti-Inflammatory Actions After Oral Administration. *Br J Pharmacol* (2004) 143:43–52. doi: 10.1038/sj.bjp.0705912
19. Chiang N, Libreros S, Norris PC, de la Rosa X, Serhan CN. Maresin 1 Activates LGR6 Receptor Promoting Phagocyte Immunoresolvent Functions. *J Clin Invest* (2019) 129:5294–311. doi: 10.1172/JCI129448
20. Schwab JM, Chiang N, Arita M, Serhan CN. Resolvin E1 and Protectin D1 Activate Inflammation-Resolution Programmes. *Nature* (2007) 447:869–74. doi: 10.1038/nature05877
21. Werfel TA, Cook RS. Efferocytosis in the Tumor Microenvironment. *Semin Immunopathol* (2018) 40:545–54. doi: 10.1007/s00281-018-0698-5
22. Serhan CN, Levy BD. Resolvins in Inflammation: Emergence of the Pro-Resolving Superfamily of Mediators. *J Clin Invest* (2018) 128:2657–69. doi: 10.1172/JCI97943
23. Dalli J, Serhan C. Macrophage Proresolving Mediators—The When and Where. *Microbiol Spectr* (2016) 4(3). doi: 10.1128/microbiolspec.MCHD-0001-2014
24. Greenhough A, Smartt HJM, Moore AE, Roberts HR, Williams AC, Paraskeva C, et al. The COX-2/PGE2 Pathway: Key Roles in the Hallmarks of Cancer and Adaptation to the Tumour Microenvironment. *Carcinogenesis* (2009) 30:377–86. doi: 10.1093/carcin/bgp014
25. Serhan CN, Chiang N. Endogenous Pro-Resolving and Anti-Inflammatory Lipid Mediators: A New Pharmacologic Genus. *Br J Pharmacol* (2008) 153 (Suppl 1):S200–15. doi: 10.1038/sj.bjp.0707489
26. Hwang S-M, Chung G, Kim YH, Park C-K. The Role of Maresins in Inflammatory Pain: Function of Macrophages in Wound Regeneration. *IJMS* (2019) 20:5849. doi: 10.3390/ijms20235849
27. Arita M, Oh SF, Chonan T, Hong S, Elangovan S, Sun Y-P, et al. Metabolic Inactivation of Resolvin E1 and Stabilization of Its Anti-Inflammatory Actions. *J Biol Chem* (2006) 281:22847–54. doi: 10.1074/jbc.M603766200
28. van der Vorst EPC, Peters LJF, Müller M, Gencer S, Yan Y, Weber C, et al. G-Protein Coupled Receptor Targeting on Myeloid Cells in Atherosclerosis. *Front Pharmacol* (2019) 10:531. doi: 10.3389/fphar.2019.00531
29. Buckley CD, Gilroy DW, Serhan CN. Pro-Resolving Lipid Mediators and Mechanisms in the Resolution of Acute Inflammation. *Immunity* (2014) 40:315–27. doi: 10.1016/j.immuni.2014.02.009
30. Cash JL, Norling LV, Perretti M. Resolution of Inflammation: Targeting GPCRs That Interact With Lipids and Peptides. *Drug Discov Today* (2014) 19:1186–92. doi: 10.1016/j.drudis.2014.06.023
31. Chiang N, Serhan CN, Dahlén S-E, Drazen JM, Hay DWP, Rovati GE, et al. The Lipoxin Receptor ALX: Potent Ligand-Specific and Stereoselective Actions In Vivo. *Pharmacol Rev* (2006) 58:463–87. doi: 10.1124/pr.58.3.4
32. Fukunaga K, Kohli P, Bonnans C, Fredenburgh LE, Levy BD. Cyclooxygenase 2 Plays a Pivotal Role in the Resolution of Acute Lung Injury. *J Immunol* (2005) 174:5033–9. doi: 10.4049/jimmunol.174.8.5033
33. Ishida T, Yoshida M, Arita M, Nishitani Y, Nishiumi S, Masuda A, et al. Resolvin E1, an Endogenous Lipid Mediator Derived From Eicosapentaenoic Acid, Prevents Dextran Sulfate Sodium–Induced Colitis. *Inflammatory Bowel Dis* (2010) 16(1):87–95. doi: 10.1002/ibd.21029
34. Karp CL, Flick LM, Park KW, Softic S, Greer TM, Keledjian R, et al. Defective Lipoxin-Mediated Anti-Inflammatory Activity in the Cystic Fibrosis Airway. *Nat Immunol* (2004) 5:388–92. doi: 10.1038/ni1056
35. Levy BD, Levy C, Levy ES, Palmer LJ, Marigowda G, Israel E, et al. Diminished Lipoxin Biosynthesis in Severe Asthma. *Am J Respir Crit Care Med* (2005) 172:824–30. doi: 10.1164/rccm.200410-1413OC
36. Werner M, Pace S, Czapka A, Jordan PM, Gerstmeier J, Koeberle A, et al. Communication Between Human Macrophages and Epithelial Cancer Cell Lines Dictates Lipid Mediator Biosynthesis. *Cell Mol Life Sci* (2020) 77 (21):4365–78. doi: 10.1007/s00018-019-03413-w
37. Hashemi Goradel N, Najafi M, Salehi E, Farhood B, Mortezaee K. Cyclooxygenase-2 in Cancer: A Review. *J Cell Physiol* (2019) 234:5683–99. doi: 10.1002/jcp.27411
38. Liu H, Zeng J, Huang W, Xu Q, Ye D, Sun R, et al. Colorectal Cancer Is Associated With a Deficiency of Lipoxin A_4, an Endogenous Anti-Inflammatory Mediator. *J Cancer* (2019) 10(19):4719–30. doi: 10.7150/jca.32456
39. Tian R, Zuo X, Jaoude J, Mao F, Colby J, Shureiqi I, et al. ALOX15 as a Suppressor of Inflammation and Cancer: Lost in the Link. *Prostaglandins Other Lipid Mediat* (2017) 132:77–83. doi: 10.1016/j.prostaglandins.2017.01.002
40. Zhuang Q, Meng Q, Xi Q, Wu G. [Association of Serum Inflammatory Cytokines and Resolvin D1 Concentration With Pathological Stage of Colon Cancer]. *Zhonghua Wei Chang Wai Ke Za Zhi* (2018) 21:1285–90. doi: 10.1038/nrclinonc.2011.199
41. Eritja N, Jové M, Fasmer KE, Gatius S, Portero–Otin M, Trovik J, et al. Tumour-Microenvironmental Blood Flow Determines a Metabolomic Signature Identifying Lysophospholipids and Resolvin D as Biomarkers in Endometrial Cancer Patients. *Oncotarget* (2017) 8:109018–26. doi: 10.18632/oncotarget.22558
42. Cuzick J, Otto F, Baron JA, Brown PH, Burn J, Greenwald P, et al. Aspirin and Non-Steroidal Anti-Inflammatory Drugs for Cancer Prevention: An International Consensus Statement. *Lancet Oncol* (2009) 10(5):501–7. doi: 10.1016/S1470-2045(09)70035-X
43. Thun MJ, Jacobs EJ, Patrono C. The Role of Aspirin in Cancer Prevention. *Nat Rev Clin Oncol* (2012) 9:259–67. doi: 10.1038/nrclinonc.2011.199
44. Serhan CN, Fredman G, Yang R, Karamnov S, Belayev LS, Bazan NG, et al. Novel Proresolving Aspirin-Triggered DHA Pathway. *Chem Biol* (2011) 18 (8):976–87. doi: 10.1016/j.chembiol.2011.06.008
45. Gordon S, Martinez-Pomares L. Physiological Roles of Macrophages. *Pflugers Arch* (2017) 469:365–74. doi: 10.1007/s00424-017-1945-7

46. Kierdorf K, Prinz M, Geissmann F, Gomez Perdiguero E. Development and Function of Tissue Resident Macrophages in Mice. *Semin Immunol* (2015) 27:369–78. doi: 10.1016/j.smim.2016.03.017
47. Mills CD, Kincaid K, Alt JM, Heilman MJ, Hill AM. M-1/M-2 Macrophages and the Th1/Th2 Paradigm. *J Immunol* (2000) 164:6166–73. doi: 10.4049/jimmunol.164.12.6166
48. Hashimoto D, Chow A, Noizat C, Teo P, Beasley MB, Leboeuf M, et al. Tissue-Resident Macrophages Self-Maintain Locally Throughout Adult Life With Minimal Contribution From Circulating Monocytes. *Immunity* (2013) 38:792–804. doi: 10.1016/j.immuni.2013.04.004
49. Uderhardt S, Martins AJ, Tsang JS, Lämmermann T, Germain RN. Resident Macrophages Cloak Tissue Microlesions to Prevent Neutrophil-Driven Inflammatory Damage. *Cell* (2019) 177:541–55.e17. doi: 10.1016/j.immuni.2016.02.026
50. Kumar V. Macrophages: The Potent Immunoregulatory Innate Immune Cells. In: K Hussain Bhat, editor. *Macrophage Activation - Biology and Disease*. London, United Kingdom: IntechOpen (2020).
51. Hirayama D, Iida T, Nakase H. The Phagocytic Function of Macrophage-Enforcing Innate Immunity and Tissue Homeostasis. *IJMS* (2017) 19:92. doi: 10.3390/ijms19010092
52. Gordon S. Phagocytosis: An Immunobiologic Process. *Immunity* (2016) 44:463–75. doi: 10.1016/j.immuni.2016.02.026
53. Jeannin P, Paolini L, Adam C, Delneste Y. The Roles of CSFs on the Functional Polarization of Tumor-Associated Macrophages. *FEBS J* (2018) 285:680–99. doi: 10.1111/febs.14343
54. Locati M, Curtale G, Mantovani A. Diversity, Mechanisms, and Significance of Macrophage Plasticity. *Annu Rev Pathol Mech Dis* (2020) 15:123–47. doi: 10.1146/annurev-pathmechdis-012418-012718
55. Van den Bossche J, Saraber DL. Metabolic Regulation of Macrophages in Tissues. *Cell Immunol* (2018) 330:54–9. doi: 10.1016/j.cellimm.2018.01.009
56. Davis FM, Gallagher KA. Epigenetic Mechanisms in Monocytes/Macrophages Regulate Inflammation in Cardiometabolic and Vascular Disease. *Arterioscler Thromb Vasc Biol* (2019) 39:623–34. doi: 10.1161/ATVBAHA.118.312135
57. Mantovani A, Sica A, Sozzani S, Allavena P, Vecchi A, Locati M, et al. The Chemokine System in Diverse Forms of Macrophage Activation and Polarization. *Trends Immunol* (2004) 25:677–86. doi: 10.1016/j.it.2004.09.015
58. Viola A, Munari F, Sánchez-Rodríguez R, Scolaro T, Castegna A. The Metabolic Signature of Macrophage Responses. *Front Immunol* (2019) 10:1462. doi: 10.3389/fimmu.2019.01462
59. Italiani P, Boraschi D. From Monocytes to M1/M2 Macrophages: Phenotypical vs. Functional Differentiation. *Front Immunol* (2014) 5. doi: 10.3389/fimmu.2014.00514
60. Na YR, Stakenborg M, Seok SH, Matteoli G. Macrophages in Intestinal Inflammation and Resolution: A Potential Therapeutic Target in IBD. *Nat Rev Gastroenterol Hepatol* (2019) 16:531–43. doi: 10.1038/s41575-019-0172-4
61. Edholm E-S, Rhoo KH, Robert J. Evolutionary Aspects of Macrophages Polarization. *Results Probl Cell Differ* (2017) 62:3–22. doi: 10.1007/978-3-319-54090-0_1
62. Zizzo G, Hilliard BA, Monestier M, Cohen PL. Efficient Clearance of Early Apoptotic Cells by Human Macrophages Requires M2c Polarization and MerTK Induction. *J Immunol* (2012) 189:3508–20. doi: 10.4049/jimmunol.1200662
63. Duluc D, Delneste Y, Tan F, Moles M-P, Grimaud L, Lenoir J, et al. Tumor-Associated Leukemia Inhibitory Factor and IL-6 Skew Monocyte Differentiation Into Tumor-Associated Macrophage-Like Cells. *Blood* (2007) 110:4319–30. doi: 10.1182/blood-2007-02-072587
64. Schulz D, Severin Y, Zanotelli VRT, Bodenmiller B. In-Depth Characterization of Monocyte-Derived Macrophages Using a Mass Cytometry-Based Phagocytosis Assay. *Sci Rep* (2019) 9:1925. doi: 10.1038/s41598-018-38127-9
65. Dalli J, Serhan CN. Specific Lipid Mediator Signatures of Human Phagocytes: Microparticles Stimulate Macrophage Efferocytosis and Pro-Resolving Mediators. *Blood* (2012) 120:e60–72. doi: 10.1182/blood-2012-04-423525
66. Werner M, Jordan PM, Romp E, Czapka A, Rao Z, Kretzer C, et al. Targeting Biosynthetic Networks of the Proinflammatory and Proresolving Lipid Metabolome. *FASEB J* (2019) 33(5):6140–53. doi: 10.1096/fj.201802509R
67. Werz O, Gerstmeier J, Libreros S, De la Rosa X, Werner M, Norris PC, et al. Human Macrophages Differentially Produce Specific Resolvin or Leukotriene Signals That Depend on Bacterial Pathogenicity. *Nat Commun* (2018) 9:59. doi: 10.1038/s41467-017-02538-5
68. Sica A, Mantovani A. Macrophage Plasticity and Polarization: In Vivo Veritas. *J Clin Invest.* (2012) 122:787–95. doi: 10.1172/JCI59643
69. Bowman RL, Klemm F, Akkari L, Pyonteck SM, Sevenich L, Quail DF, et al. Macrophage Ontogeny Underlies Differences in Tumor-Specific Education in Brain Malignancies. *Cell Rep* (2016) 17(9):2445–59. doi: 10.1016/j.celrep.2016.10.052
70. Murray PJ, Allen JE, Biswas SK, Fisher EA, Gilroy DW, Goerdt S, et al. Macrophage Activation and Polarization: Nomenclature and Experimental Guidelines. *Immunity* (2014) 41(1):14–20. doi: 10.1016/j.immuni.2014.06.008
71. Norling LV, Serhan CN. Profiling in Resolving Inflammatory Exudates Identifies Novel Anti-Inflammatory and Pro-Resolving Mediators and Signals for Termination. *J Internal Med* (2010) 268:15–24. doi: 10.1111/j.1365-2796.2010.02235.x
72. Godson C, Mitchell S, Harvey K, Petasis NA, Hogg N, Brady HR, et al. Cutting Edge: Lipoxins Rapidly Stimulate Nonphlogistic Phagocytosis of Apoptotic Neutrophils by Monocyte-Derived Macrophages. *J Immunol* (2000) 164:1663–7. doi: 10.4049/jimmunol.164.4.1663
73. Ariel A, Serhan CN. New Lives Given by Cell Death: Macrophage Differentiation Following Their Encounter With Apoptotic Leukocytes During the Resolution of Inflammation. *Front Immunol* (2012) 3:4. doi: 10.3389/fimmu.2012.00004
74. Yurdagul A, Subramanian M, Wang X, Crown SB, Ilkayeva OR, Darville L, et al. Macrophage Metabolism of Apoptotic Cell-Derived Arginine Promotes Continual Efferocytosis and Resolution of Injury. *Cell Metab* (2020) 31:518–533.e10. doi: 10.4049/jimmunol.1502542
75. Kourtzelis I, Hajishengallis G, Chavakis T. Phagocytosis of Apoptotic Cells in Resolution of Inflammation. *Front Immunol* (2020) 11:553. doi: 10.3389/fimmu.2020.00553
76. Bonnefoy F, Gauthier T, Vallion R, Martin–Rodriguez O, Missey A, Daoui A, et al. Factors Produced by Macrophages Eliminating Apoptotic Cells Demonstrate Pro-Resolutive Properties and Terminate Ongoing Inflammation. *Front Immunol* (2018) 9:2586. doi: 10.3389/fimmu.2018.02586
77. Aswad M, Assi S, Schif-Zuck S, Ariel A. Ccl5 Promotes Resolution-Phase Macrophage Reprogramming in Concert With the Atypical Chemokine Receptor D6 and Apoptotic Polymorphonuclear Cells. *J Immunol* (2017) 199:1393–404. doi: 10.4049/jimmunol.1502542
78. Lumbroso D, Soboh S, Maimon A, Schif–Zuck S, Ariel A, Burstyn–Cohen T, et al. Macrophage-Derived Protein S Facilitates Apoptotic Polymorphonuclear Cell Clearance by Resolution Phase Macrophages and Supports Their Reprogramming. *Front Immunol* (2018) 9:358. doi: 10.3389/fimmu.2018.00358
79. Zhang Y, Kim H-J, Yamamoto S, Kang X, Ma X. Regulation of Interleukin-10 Gene Expression in Macrophages Engulfing Apoptotic Cells. *J Interferon Cytokine Res* (2010) 30:113–22. doi: 10.1089/jir.2010.0004
80. Bystrom J, Evans I, Newson J, Stables M, Toor I, van Rooijen N, et al. Resolution-Phase Macrophages Possess a Unique Inflammatory Phenotype That Is Controlled by Camp. *Blood* (2008) 112:4117–27. doi: 10.1182/blood-2007-12-129767
81. Stables MJ, Shah S, Camon EB, Lovering RC, Newson J, Bystrom J, et al. Transcriptomic Analyses of Murine Resolution-Phase Macrophages. *Blood* (2011) 118:e192–208. doi: 10.1182/blood-2011-04-345330
82. Ortega-Gómez A, Perretti M, Soehnlein O. Resolution of Inflammation: An Integrated View. *EMBO Mol Med* (2013) 5:661–74. doi: 10.1002/emmm.201202382
83. Schif-Zuck S, Gross N, Assi S, Rostoker R, Serhan CN, Ariel A, et al. Satiated-Efferocytosis Generates Pro-Resolving CD11blow Macrophages: Modulation by Resolvins and Glucocorticoids. *Eur J Immunol* (2011) 41(2):366–79. doi: 10.1002/eji.201040801
84. Butenko S, Satyanarayanan SK, Assi S, Schif–Zuck S, Barkan D, Sher N, et al. Transcriptomic Analysis of Monocyte-Derived Non-Phagocytic Macrophages Favors a Role in Limiting Tissue Repair and Fibrosis. *Front Immunol* (2020) 11:405. doi: 10.3389/fimmu.2020.01003
85. Kumaran Satyanarayanan S, El Kebir D, Soboh S, Butenko S, Sekheri M, Saadi J, et al. Ifn-β Is a Macrophage-Derived Effector Cytokine Facilitating

the Resolution of Bacterial Inflammation. *Nat Commun* (2019) 10:3471. doi: 10.1038/s41467-019-10903-9
86. Sulciner ML, Serhan CN, Gilligan MM, Mudge DK, Chang J, Gartung A, et al. Resolvins Suppress Tumor Growth and Enhance Cancer Therapy. *J Exp Med* (2018) 215:115–40. doi: 10.1084/jem.20170681
87. Fishbein A, Wang W, Yang H, Yang J, Hallisey VM, Deng J, et al. Resolution of Eicosanoid/Cytokine Storm Prevents Carcinogen and Inflammation-Initiated Hepatocellular Cancer Progression. *Proc Natl Acad Sci USA* (2020) 117:21576–87. doi: 10.1073/pnas.2007412117
88. Saas P, Chagué C, Maraux M, Cherrier T. Toward the Characterization of Human Pro-Resolving Macrophages? *Front Immunol* (2020) 11:593300. doi: 10.3389/fimmu.2020.593300
89. Zhang Q, Zhu B, Li Y. Resolution of Cancer-Promoting Inflammation: A New Approach for Anticancer Therapy. *Front Immunol* (2017) 8:71. doi: 10.3389/fimmu.2017.00071
90. DeNardo DG, Brennan DJ, Rexhepaj E, Ruffell B, Shiao SL, Madden SF, et al. Leukocyte Complexity Predicts Breast Cancer Survival and Functionally Regulates Response to Chemotherapy. *Cancer Discov* (2011) 1:54–67. doi: 10.1158/2159-8274.CD-10-0028
91. Zhou K, Cheng T, Zhan J, Peng X, Zhang Y, Wen J, et al. Targeting Tumor −Associated Macrophages in the Tumor Microenvironment (Review). *Oncol Lett* (2020) 20:1–1. doi: 10.3892/ol.2020.12097
92. Murdoch C, Muthana M, Coffelt SB, Lewis CE. The Role of Myeloid Cells in the Promotion of Tumour Angiogenesis. *Nat Rev Cancer* (2008) 8:618–31. doi: 10.1038/nrc2444
93. Sica A, Schioppa T, Mantovani A, Allavena P. Tumour-Associated Macrophages Are a Distinct M2 Polarised Population Promoting Tumour Progression: Potential Targets of Anti-Cancer Therapy. *Eur J Cancer* (2006) 42:717–27. doi: 10.1016/j.ejca.2006.01.003
94. Goswami KK. Tumor Promoting Role of Anti-Tumor Macrophages in Tumor Microenvironment. *Cell Immunol* (2017) 316:1–10. doi: 10.1016/j.cellimm.2017.04.005
95. Panni RZ, Linehan DC, DeNardo DG. Targeting Tumor-Infiltrating Macrophages to Combat Cancer. *Immunotherapy* (2013) 5:1075–87. doi: 10.2217/imt.13.102
96. Koelzer VH, Canonica K, Dawson H, Sokol L, Karamitopoulou–Diamantis E, Lugli A, et al. Phenotyping of Tumor-Associated Macrophages in Colorectal Cancer: Impact on Single Cell Invasion (Tumor Budding) and Clinicopathological Outcome. *OncoImmunology* (2016) 5:e1106677. doi: 10.1080/2162402X.2015.1106677
97. Zhang S-C, Hu Z-Q, Long J-H, Zhu G-M, Wang Y, Jia Y, et al. Clinical Implications of Tumor-Infiltrating Immune Cells in Breast Cancer. *J Cancer* (2019) 10:6175–84. doi: 10.7150/jca.35901
98. Zhang Q, Liu L, Gong C, Shi H, Zeng Y, Wang X, et al. Prognostic Significance of Tumor-Associated Macrophages in Solid Tumor: A Meta-Analysis of the Literature. *PloS One* (2012) 7:e50946. doi: 10.1371/journal.pone.0050946
99. Wu K, Lin K, Li X, Yuan X, Xu P, Ni P, et al. Redefining Tumor-Associated Macrophage Subpopulations and Functions in the Tumor Microenvironment. *Front Immunol* (2020) 11:1731. doi: 10.3389/fimmu.2020.01731
100. Saadatpour A, Lai S, Guo G, Yuan G-C. Single-Cell Analysis in Cancer Genomics. *Trends Genet* (2015) 31:576–86. doi: 10.1016/j.tig.2015.07.003
101. Azizi E, Carr AJ, Plitas G, Cornish AE, Konopacki C, Prabhakaran S, et al. Single-Cell Map of Diverse Immune Phenotypes in the Breast Tumor Microenvironment. *Cell* (2018) 174:1293–308.e36. doi: 10.3892/etm.2019.8068
102. Qiu S-Q, Waaijer SJH, Zwager MC, de Vries EGE, van der Vegt B, Schröder CP, et al. Tumor-Associated Macrophages in Breast Cancer: Innocent Bystander or Important Player? *Cancer Treat Rev* (2018) 70:178–89. doi: 10.1016/j.ctrv.2018.08.010
103. Chung W, Eum HH, Lee H-O, Lee K-M, Lee H-B, Kim K-T, et al. Single-Cell RNA-Seq Enables Comprehensive Tumour and Immune Cell Profiling in Primary Breast Cancer. *Nat Commun* (2017) 8:15081. doi: 10.1038/ncomms15081
104. Sumitomo R, Hirai T, Fujita M, Murakami H, Otake Y, Huang C-L, et al. M2 Tumor-Associated Macrophages Promote Tumor Progression in Non-Small-Cell Lung Cancer. *Exp Ther Med* (2019) 18:4490–8. doi: 10.3892/etm.2019.8068
105. Zhang B, Yao G, Zhang Y, Gao J, Yang B, Rao Z, et al. M2-Polarized Tumor-Associated Macrophages Are Associated With Poor Prognoses Resulting From Accelerated Lymphangiogenesis in Lung Adenocarcinoma. *Clinics* (2011) 66:1879–86. doi: 10.1590/S1807-59322011001100006
106. Wang J, Zhang J, Li J-H, Liu X, Wang J-Z, Qu H-Y, et al. High Tumor-Associated Macrophages Infiltration Is Associated With Poor Prognosis and may Contribute to the Phenomenon of Epithelial–Mesenchymal Transition in Gastric Cancer. *OTT Volume* (2016) 9:3975–83. doi: 10.2147/OTT.S103112
107. Wagner J, Rapsomaniki MA, Chevrier S, Anzeneder T, Langwieder C, Dykgers A, et al. A Single-Cell Atlas of the Tumor and Immune Ecosystem of Human Breast Cancer. *Cell* (2019) 177(5):1330–1345.e18. doi: 10.1038/s41598-020-63276-1
108. Qian J, Olbrecht S, Boeckx B, Vos H, Laoui D, Etlioglu E, et al. A Pan-Cancer Blueprint of the Heterogeneous Tumor Microenvironment Revealed by Single-Cell Profiling. *Cell Res* (2020) 30(9):745–62. doi: 10.1038/s41422-020-0355-0
109. Ohri CM, Shikotra A, Green RH, Waller DA, Bradding P. Macrophages Within NSCLC Tumour Islets Are Predominantly of a Cytotoxic M1 Phenotype Associated With Extended Survival. *Eur Respir J* (2009) 33:118–26. doi: 10.1183/09031936.00065708
110. Macciò A, Gramignano G, Cherchi MC, Tanca L, Melis L, Madeddu C, et al. Role of M1-Polarized Tumor-Associated Macrophages in the Prognosis of Advanced Ovarian Cancer Patients. *Sci Rep* (2020) 10:6096. doi: 10.1038/s41598-020-63276-1
111. Cassetta L, Fragkogianni S, Sims AH, Swierczak A, Forrester LM, Zhang H, et al. Human Tumor-Associated Macrophage and Monocyte Transcriptional Landscapes Reveal Cancer-Specific Reprogramming, Biomarkers, and Therapeutic Targets. *Cancer Cell* (2019) 35(4):588–602.e10. doi: 10.1016/j.ccr.2009.01.001
112. Chevrier S, Levine JH, Zanotelli VRT, Silina K, Schulz D, Bacac M, et al. An Immune Atlas of Clear Cell Renal Cell Carcinoma. *Cell* (2017) 169(4):736–749.e18. doi: 10.1016/j.imbio.2015.11.010
113. Devalaraja S, To TKJ, Folkert IW, Natesan R, Alam MZ, Li M, et al. Tumor-Derived Retinoic Acid Regulates Intratumoral Monocyte Differentiation to Promote Immune Suppression. *Cell* (2020) 180:1098–114.e16. doi: 10.1101/gad.180331.111
114. Chomarat P, Banchereau J, Davoust J, Karolina Palucka A. IL-6 Switches the Differentiation of Monocytes From Dendritic Cells to Macrophages. *Nat Immunol* (2000) 1:510–4. doi: 10.1038/82763
115. Rodriguez PC, Zea AH, DeSalvo J, Culotta KS, Zabaleta J, Quiceno DG, et al. L-Arginine Consumption by Macrophages Modulates the Expression of CD3ζ Chain in T Lymphocytes. *J Immunol* (2003) 171:1232–9. doi: 10.4049/jimmunol.171.3.1232
116. Petty AJ, Yang Y. Tumor-Associated Macrophages: Implications in Cancer Immunotherapy. *Immunotherapy* (2017) 9:289–302. doi: 10.2217/imt-2016-0135
117. Su S, Liu Q, Chen J, Chen J, Chen F, He C, et al. A Positive Feedback Loop Between Mesenchymal-Like Cancer Cells and Macrophages Is Essential to Breast Cancer Metastasis. *Cancer Cell* (2014) 25:605–20. doi: 10.1016/j.ccr.2014.03.021
118. Wyckoff JB, Wang Y, Lin EY, Li J-F, Goswami S, Stanley ER, et al. Direct Visualization of Macrophage-Assisted Tumor Cell Intravasation in Mammary Tumors. *Cancer Res* (2007) 67:2649–56. doi: 10.1158/0008-5472.CAN-06-1823
119. Li H, Yang B, Huang J, Lin Y, Xiang T, Wan J, et al. Cyclooxygenase-2 in Tumor-Associated Macrophages Promotes Breast Cancer Cell Survival by Triggering a Positive-Feedback Loop Between Macrophages and Cancer Cells. *Oncotarget* (2015) 6(30):29637–50. doi: 10.18632/oncotarget.4936
120. Grivennikov S, Karin E, Terzic J, Mucida D, Yu G-Y, Vallabhapurapu S, et al. IL-6 and Stat3 Are Required for Survival of Intestinal Epithelial Cells and Development of Colitis-Associated Cancer. *Cancer Cell* (2009) 15:103–13. doi: 10.1016/j.ccr.2009.01.001
121. Jeong SK, Kim JS, Lee CG, Park Y-S, Kim SD, Yoon SO, et al. Tumor Associated Macrophages Provide the Survival Resistance of Tumor Cells to Hypoxic Microenvironmental Condition Through IL-6 Receptor-Mediated Signals. *Immunobiology* (2017) 222:55–65. doi: 10.1016/j.imbio.2015.11.010

122. Shree T, Olson OC, Elie BT, Kester JC, Garfall AL, Simpson K, et al. Macrophages and Cathepsin Proteases Blunt Chemotherapeutic Response in Breast Cancer. *Genes Dev* (2011) 25:2465–79. doi: 10.1101/gad.180331.111
123. Leek RD, Lewis CE, Whitehouse R, Greenall M, Clarke J, Harris AL, et al. Association of Macrophage Infiltration With Angiogenesis and Prognosis in Invasive Breast Carcinoma. *Cancer Res* (1996) 56:4625–9. doi: 10.1016/j.ccr.2012.02.017
124. Mantovani A, Schioppa T, Porta C, Allavena P, Sica A. Role of Tumor-Associated Macrophages in Tumor Progression and Invasion. *Cancer Metastasis Rev* (2006) 25:315–22. doi: 10.1007/s10555-006-9001-7
125. Biswas SK, Allavena P, Mantovani A. Tumor-Associated Macrophages: Functional Diversity, Clinical Significance, and Open Questions. *Semin Immunopathol* (2013) 35:585–600. doi: 10.1007/s00281-013-0367-7
126. Chanmee T, Ontong P, Konno K, Itano N. Tumor-Associated Macrophages as Major Players in the Tumor Microenvironment. *Cancers* (2014) 6:1670–90. doi: 10.3390/cancers6031670
127. Qian B, Deng Y, Im JH, Muschel RJ, Zou Y, Li J, et al. A Distinct Macrophage Population Mediates Metastatic Breast Cancer Cell Extravasation, Establishment and Growth. *PloS One* (2009) 4. doi: 10.1371/journal.pone.0006562
128. DeNardo DG, Ruffell B. Macrophages as Regulators of Tumour Immunity and Immunotherapy. *Nat Rev Immunol* (2019) 19:369–82. doi: 10.1038/s41577-019-0127-6
129. Dijkgraaf EM, Heusinkveld M, Tummers B, Vogelpoel LTC, Goedemans R, Jha V, et al. Chemotherapy Alters Monocyte Differentiation to Favor Generation of Cancer-Supporting M2 Macrophages in the Tumor Microenvironment. *Cancer Res* (2013) 73:2480–92. doi: 10.1158/0008-5472.CAN-12-3542
130. Nakasone ES, Askautrud HA, Kees T, Park J-H, Plaks V, Ewald AJ, et al. Imaging Tumor-Stroma Interactions During Chemotherapy Reveals Contributions of the Microenvironment to Resistance. *Cancer Cell* (2012) 21(4):488–503. doi: 10.1016/j.ccr.2012.02.017
131. Hamaidia M, Gazon H, Hoyos C, Hoffmann GB, Louis R, Duysinx B, et al. Inhibition of EZH2 Methyltransferase Decreases a PD-1–Dependent Mechanism. *JCI Insight* (2019) 4(18):e128474. doi: 10.1007/s10555-018-9731-3
132. Gautam PK, Deepak P, Kumar S, Acharya A. Role of Macrophage in Tumor Microenvironment: Prospect in Cancer Immunotherapy. *Eur J Inflamm* (2013), 1–14. doi: 10.1177/1721727X1301100101
133. Keller R, Keist R, Wechsler A, Leist TP, van der Meide PH. Mechanisms of Macrophage-Mediated Tumor Cell Killing: A Comparative Analysis of the Roles of Reactive Nitrogen Intermediates and Tumor Necrosis Factor. *Int J Cancer* (1990) 46:682–6. doi: 10.1002/ijc.2910460422
134. Feng M, Jiang W, Kim BYS, Zhang CC, Fu Y-X, Weissman IL, et al. Phagocytosis Checkpoints as New Targets for Cancer Immunotherapy. *Nat Rev Cancer* (2019) 19:568–86. doi: 10.1038/s41568-019-0183-z
135. Gauttier V, Pengam S, Durand J, Biteau K, Mary C, Morello A, et al. Selective Sirpα Blockade Reverses Tumor T Cell Exclusion and Overcomes Cancer Immunotherapy Resistance. *J Clin Invest* (2020) 130:6109–23. doi: 10.1038/nrd.2018.169
136. Reinartz S, Finkernagel F, Adhikary T, Rohnalter V, Schumann T, Schober Y, et al. A Transcriptome-Based Global Map of Signaling Pathways in the Ovarian Cancer Microenvironment Associated With Clinical Outcome. *Genome Biol* (2016) 17(1):108. doi: 10.1186/s13059-016-0956-6
137. Ringleb J, Strack E, Angioni C, Geisslinger G, Steinhilber D, Weigert A, et al. Apoptotic Cancer Cells Suppress 5-Lipoxygenase in Tumor-Associated Macrophages. *J Immunol* (2018) 200:857–68. doi: 10.4049/jimmunol.1700609
138. Weigert A, Strack E, Snodgrass RG, Brüne B. mPGES-1 and ALOX5/-15 in Tumor-Associated Macrophages. *Cancer Metastasis Rev* (2018) 37:317–34. doi: 10.1007/s10555-018-9731-3
139. Lee SP, Serezani CH, Medeiros AI, Ballinger MN, Peters-Golden M. Crosstalk Between Prostaglandin E2 and Leukotriene B4 Regulates Phagocytosis in Alveolar Macrophages Via Combinatorial Effects on Cyclic Amp. *J Immunol* (2009) 182:530–7. doi: 10.4049/jimmunol.182.1.530
140. Bacchi S, Palumbo P, Sponta A, Coppolino MF. Clinical Pharmacology of Non-Steroidal Anti-Inflammatory Drugs: A Review. *Antiinflamm Antiallergy Agents Med Chem* (2012) 11(1):52–64. doi: 10.2174/187152312803476255
141. Serhan CN, Brain SD, Buckley CD, Gilroy DW, Haslett C, O'Neill LAJ, et al. Resolution of Inflammation: State of the Art, Definitions and Terms. *FASEB J* (2007) 21:325–32. doi: 10.1096/fj.06-7227rev
142. Cassetta L, Pollard JW. Targeting Macrophages: Therapeutic Approaches in Cancer. *Nat Rev Drug Discov* (2018) 17:887–904. doi: 10.1038/nrd.2018.169
143. Lopez-Yrigoyen M, Cassetta L, Pollard JW. Macrophage Targeting in Cancer. *Ann NY Acad Sci* (2020) 14377. doi: 10.1111/nyas.14377
144. Guerriero JL, Sotayo A, Ponichtera HE, Castrillon JA, Pourzia AL, Schad S, et al. Class IIa HDAC Inhibition Reduces Breast Tumours and Metastases Through Anti-Tumour Macrophages. *Nature* (2017) 543:428–32. doi: 10.1038/nature21409
145. Yang H, Shao R, Yang H, Huang X, Wang Z, Rong Y, et al. Engineering Macrophages to Phagocytose Cancer Cells by Blocking the CD47/SIRPα Axis. *Cancer Med* (2019) 8:4245–53. doi: 10.1002/cam4.2332
146. Jalil AR, Andrechak JC, Discher DE. Macrophage Checkpoint Blockade: Results From Initial Clinical Trials, Binding Analyses, and CD47-Sirpα Structure–Function. *Antibody Ther* (2020) 3:80–94. doi: 10.1093/abt/tbaa006
147. Morrissey MA, Williamson AP, Steinbach AM, Roberts EW, Kern N, Headley MB, et al. Chimeric Antigen Receptors That Trigger Phagocytosis. *eLife* (2018) 7:e36688. doi: 10.7554/eLife.36688
148. Klichinsky M, Ruella M, Shestova O, Lu XM, Best A, Zeeman M, et al. Human Chimeric Antigen Receptor Macrophages for Cancer Immunotherapy. *Nat Biotechnol* (2020) 38(8):947–53. doi: 10.4049/jimmunol.1103652
149. Peranzoni E, Lemoine J, Vimeux L, Feuillet V, Barrin S, Kantari–Mimoun C, et al. Macrophages Impede CD8 T Cells From Reaching Tumor Cells and Limit the Efficacy of Anti-PD-1 Treatment. *Proc Natl Acad Sci USA* (2018) 115(17):E4041–50. doi: 10.1073/pnas.1720948115
150. Prieto P, Cuenca J, Través PG, Fernández–Velasco M, Martín–Sanz P, Boscá L, et al. Lipoxin A4 Impairment of Apoptotic Signaling in Macrophages: Implication of the PI3K/Akt and the ERK/Nrf-2 Defense Pathways. *Cell Death Differ* (2010) 17:1179–88. doi: 10.1038/cdd.2009.220
151. Pierdomenico AM, Recchiuti A, Simiele F, Codagnone M, Mari VC, Davì G, et al. MicroRNA-181b Regulates Alx/Fpr2 Receptor Expression and Proresolution Signaling in Human Macrophages. *J Biol Chem* (2015) 290(6):3592–600. doi: 10.1074/jbc.M114.592352
152. Simões RL, Niconi-de-Almeida Y, da-Fé AR, Barja-Fidalgo C, Fierro IM. A Synthetic Analog of 15-Epi-Lipoxin A4 Inhibits Human Monocyte Apoptosis: Involvement of ERK-2 and PI3-Kinase. *Prostaglandins Other Lipid Mediators* (2010) 91:10–7. doi: 10.1016/j.prostaglandins.2009.12.001
153. Prescott D, McKay DM. Aspirin-Triggered Lipoxin Enhances Macrophage Phagocytosis of Bacteria While Inhibiting Inflammatory Cytokine Production. *Am J Physiol Gastrointest Liver Physiol* (2011) 301:11. doi: 10.1152/ajpgi.00042.2011
154. Krishnamoorthy S, Recchiuti A, Chiang N, Yacoubian S, Lee C-H, Yang R, et al. Resolvin D1 Binds Human Phagocytes With Evidence for Proresolving Receptors. *PNAS* (2010) 107:1660–5. doi: 10.1073/pnas.0907342107
155. Dalli J, Zhu M, Vlasenko NA, Deng B, Haeggström JZ, Petasis NA, et al. The Novel 13S,14S-Epoxy-Maresin Is Converted by Human Macrophages to Maresin 1 (MaR1), Inhibits Leukotriene A4 Hydrolase (LTA4H), and Shifts Macrophage Phenotype. *FASEB J* (2013) 27:2573–83. doi: 10.1096/fj.13-227728
156. Croasdell A, Thatcher TH, Kottmann RM, Colas RA, Dalli J, Serhan CN, et al. Resolvins Attenuate Inflammation and Promote Resolution in Cigarette Smoke-Exposed Human Macrophages. *Am J Physiol Lung Cell Mol Physiol* (2015) 309(8):L888–901. doi: 10.1152/ajplung.00125.2015
157. Schmid M, Gemperle C, Rimann N, Hersberger M. Resolvin D1 Polarizes Primary Human Macrophages Toward a Proresolution Phenotype Through GPR32. *J Immunol* (2016) 196:3429–37. doi: 10.4049/jimmunol.1501701
158. Ohira T, Arita M, Omori K, Recchiuti A, Van Dyke TE, Serhan CN, et al. Resolvin E1 Receptor Activation Signals Phosphorylation and Phagocytosis. *J Biol Chem* (2010) 285:3451–61. doi: 10.1074/jbc.M109.044131
159. Herová M, Schmid M, Gemperle C, Hersberger M. ChemR23, the Receptor for Chemerin and Resolvin E1, Is Expressed and Functional on M1 But Not on M2 Macrophages. *J Immunol* (2015) 194:2330–7. doi: 10.4049/jimmunol.1402166
160. Oh SF, Dona M, Fredman G, Krishnamoorthy S, Irimia D, Serhan CN, et al. Resolvin E2 Formation and Impact in Inflammation Resolution. *J Immunol* (2012) 188:4527–34. doi: 10.4049/jimmunol.1103652

161. Serhan CN, Dalli J, Karamnov S, Choi A, Park C-K, Xu Z-Z, et al. Macrophage Proresolving Mediator Maresin 1 Stimulates Tissue Regeneration and Controls Pain. *FASEB J* (2012) 26(4):1755–65. doi: 10.1096/fj.11-201442
162. Tungen JE, Aursnes M, Ramon S, Colas RA, Serhan CN, Olberg DE, et al. Synthesis of Protectin D1 Analogs: Novel Pro-Resolution and Radiotracer Agents. *Org Biomol Chem* (2018) 16(36):6818–23. doi: 10.1039/C8OB01232F
163. Walker J, Dichter E, Lacorte G, Kerner D, Spur B, Rodriguez A, et al. Lipoxin A4 Increases Survival by Decreasing Systemic Inflammation and Bacterial Load in Sepsis. *Shock* (2011) 36:410–6. doi: 10.1097/SHK.0b013e31822798c1
164. Biswas SK, Lewis CE. Nf-κb as a Central Regulator of Macrophage Function in Tumors. *J Leukocyte Biol* (2010) 88:877–84. doi: 10.1189/jlb.0310153
165. Simões RL, De–Brito NM, Cunha–Costa H, Morandi V, Fierro IM, Roitt IM, et al. Lipoxin A_4 Selectively Programs the Profile of M2 Tumor-Associated Macrophages Which Favour Control of Tumor Progression: Lipoxin Analog Modulates Tumor-Associated Macrophages. *Int J Cancer* (2017) 140:346–57. doi: 10.1002/ijc.30424
166. Gilligan MM, Gartung A, Sulciner ML, Norris PC, Sukhatme VP, Bielenberg DR, et al. Aspirin-Triggered Proresolving Mediators Stimulate Resolution in Cancer. *Proc Natl Acad Sci USA* (2019) 116:6292–7. doi: 10.1073/pnas.1804000116
167. Shan K, Feng N, Cui J, Wang S, Qu H, Fu G, et al. Resolvin D1 and D2 Inhibit Tumour Growth and Inflammation Via Modulating Macrophage Polarization. *J Cell Mol Med* (2020) 24:8045–56. doi: 10.1111/jcmm.15436
168. Chéné A-L, d'Almeida S, Blondy T, Tabiasco J, Deshayes S, Fonteneau J-F, et al. Pleural Effusions From Patients With Mesothelioma Induce Recruitment of Monocytes and Their Differentiation Into M2 Macrophages. *J Thoracic Oncol* (2016) 11:1765–73. doi: 10.1016/j.jtho.2016.06.022
169. Murray PJ. Macrophage Polarization. *Annu Rev Physiol* (2017) 79:541–66. doi: 10.1146/annurev-physiol-022516-034339
170. Wang Z, Cheng Q, Tang K, Sun Y, Zhang K, Zhang Y, et al. Lipid Mediator Lipoxin A4 Inhibits Tumor Growth by Targeting IL-10-producing Regulatory B (Breg) Cells. *Cancer Lett* (2015) 364(2):118–24. doi: 10.1016/j.canlet.2015.04.030
171. Chen Y, Hao H, He S, Cai L, Li Y, Hu S, et al. Lipoxin A_4 and Its Analogue Suppress the Tumor Growth of Transplanted H22 in Mice: The Role of Antiangiogenesis. *Mol Cancer Ther* (2010) 9:2164–74. doi: 10.1158/1535-7163.MCT-10-0173
172. Xu F, Zhou X, Hao J, Dai H, Zhang J, He Y, et al. Lipoxin A4 and its Analog Suppress Hepatocarcinoma Cell Epithelial-Mesenchymal Transition, Migration and Metastasis Via Regulating Integrin-Linked Kinase Axis. *Prostaglandins Other Lipid Mediators* (2018) 137:9–19. doi: 10.1016/j.prostaglandins.2018.05.007
173. Hao H, Liu M, Wu P, Cai L, Tang K, Yi P, et al. Lipoxin A4 and its Analog Suppress Hepatocellular Carcinoma Via Remodeling Tumor Microenvironment. *Cancer Lett* (2011) 309:85–94. doi: 10.1016/j.canlet.2011.05.020
174. Wang C, Xiao M, Liu X, Ni C, Liu J, Erben U, et al. Ifn- -Mediated Downregulation of LXA4 Is Necessary for the Maintenance of Nonresolving Inflammation and Papilloma Persistence. *Cancer Res* (2013) 73:1742–51. doi: 10.1158/0008-5472.CAN-12-2801
175. de-Brito NM, da-Costa HC, Simões RL, Barja-Fidalgo C. Lipoxin-Induced Phenotypic Changes in CD115+LY6Chi Monocytes TAM Precursors Inhibits Tumor Development. *Front Oncol* (2019) 9:540. doi: 10.3389/fonc.2019.00540
176. Zong L, Chen K, Jiang Z, Chen X, Sun L, Ma J, et al. Lipoxin A4 Attenuates Cell Invasion by Inhibiting Ros/Erk/Mmp Pathway in Pancreatic Cancer. *Oxid Med Cell Longevity* (2016) 2016:e6815727. doi: 10.1155/2016/6815727
177. Sun L, Wang Y, Wang L, Yao B, Chen T, Li Q, et al. Resolvin D1 Prevents Epithelial-Mesenchymal Transition and Reduces the Stemness Features of Hepatocellular Carcinoma by Inhibiting Paracrine of Cancer-Associated Fibroblast-Derived COMP. *J Exp Clin Cancer Res* (2019) 38:170. doi: 10.1186/s13046-019-1163-6
178. Kuang H, Hua X, Zhou J, Yang R. Resolvin D1 and E1 Alleviate the Progress of Hepatitis Toward Liver Cancer in Long-Term Concanavalin A-Induced Mice Through Inhibition of NF-κb Activity. *Oncol Rep* (2016) 35:307–17. doi: 10.3892/or.2015.4389
179. Ye Y, Scheff NN, Bernabé D, Salvo E, Ono K, Liu C, et al. Anti-Cancer and Analgesic Effects of Resolvin D2 in Oral Squamous Cell Carcinoma. *Neuropharmacology* (2018) 139:182–93. doi: 10.1016/j.neuropharm.2018.07.016
180. Panigrahy D, Gartung A, Yang J, Yang H, Gilligan MM, Sulciner ML, et al. Preoperative Stimulation of Resolution and Inflammation Blockade Eradicates Micrometastases. *J Clin Invest* (2019) 129(7):2964–79. doi: 10.1172/JCI127282
181. Cezar TLC, Martinez RM, Rocha C, Melo CPB, Vale DL, Borghi SM, et al. Treatment With Maresin 1, a Docosahexaenoic Acid-Derived Pro-Resolution Lipid, Protects Skin From Inflammation and Oxidative Stress Caused by UVB Irradiation. *Sci Rep* (2019) 9:3062. doi: 10.1038/s41598-019-39584-6
182. Prevete N, Liotti F, Amoresano A, Pucci P, de Paulis A, Melillo RM, et al. New Perspectives in Cancer: Modulation of Lipid Metabolism and Inflammation Resolution. *Pharmacol Res* (2018) 128:80–7. doi: 10.1016/j.phrs.2017.09.024
183. Xia Y, Shen S, Verma IM. Nf-κb, an Active Player in Human Cancers. *Cancer Immunol Res* (2014) 2:823–30. doi: 10.1158/2326-6066.CIR-14-0112
184. Mattoscio D, Isopi E, Lamolinara A, Patruno S, Medda A, De Cecco F, et al. Resolvin D1 Reduces Cancer Growth Stimulating a Protective Neutrophil-Dependent Recruitment of Anti-Tumor Monocytes. *J Exp Clin Cancer Res* (2021) 40(1):129. doi: 10.1186/s13046-021-01937-3
185. Chiang N, Serhan CN. Structural Elucidation and Physiologic Functions of Specialized Pro-Resolving Mediators and Their Receptors. *Mol Aspects Med* (2017) 58:114–29. doi: 10.1016/j.mam.2017.03.005
186. Maughan KL, Lutterbie MA, Ham PS. Treatment of Breast Cancer. *Breast Cancer* (2010) 81:8. doi: 10.4161/mabs.2.6.13420
187. Brenner H, Kloor M, Pox CP. Colorectal Cancer. *Lancet* (2014) 383:1490–502. doi: 10.1016/S0140-6736(13)61649-9
188. Krall JA, Reinhardt F, Mercury OA, Pattabiraman DR, Brooks MW, Dougan M, et al. The Systemic Response to Surgery Triggers the Outgrowth of Distant Immune-Controlled Tumors in Mouse Models of Dormancy. *Sci Transl Med* (2018) 10(436):eaan3464. doi: 10.1126/scitranslmed.aan3464
189. Serhan CN, Maddox JF, Petasis NA, Akritopoulou–Zanze I, Papayianni A, Brady HR, et al. Design of Lipoxin A4 Stable Analogs That Block Transmigration and Adhesion of Human Neutrophils. *Biochemistry* (1995) 34:14609–15. doi: 10.1021/bi00044a041
190. Maddox JF, Hachicha M, Takano T, Petasis NA, Fokin VV, Serhan CN, et al. Lipoxin A4 Stable Analogs Are Potent Mimetics That Stimulate Human Monocytes and THP-1 Cells Via a G-Protein-Linked Lipoxin A4 Receptor. *J Biol Chem* (1997) 272(11):6972–8. doi: 10.1074/jbc.272.11.6972
191. Francos–Quijorna I, Santos–Nogueira E, Gronert K, Sullivan AB, Kopp MA, Brommer B, et al. Maresin 1 Promotes Inflammatory Resolution, Neuroprotection, and Functional Neurological Recovery After Spinal Cord Injury. *J Neurosci* (2017) 37:11731–43. doi: 10.1523/JNEUROSCI.1395-17.2017
192. Trilleaud C, Gauttier V, Biteau K, Girault I, Belarif L, Mary C, et al. Agonist Anti-ChemR23 mAb Reduces Tissue Neutrophil Accumulation and Triggers Chronic Inflammation Resolution. *Sci Adv* (2021) 7(14):eabd1453. doi: 10.1126/sciadv.abd1453
193. Zong L, Chen K, Jiang Z, Chen X, Sun L, Ma J, et al. Lipoxin A4 Reverses Mesenchymal Phenotypes to Attenuate Invasion and Metastasis Via the Inhibition of Autocrine TGF-β1 Signaling in Pancreatic Cancer. *J Exp Clin Cancer Res* (2017) 36(1):181. doi: 10.1186/s13046-017-0655-5
194. Dalli J, Serhan CN. Identification and Structure Elucidation of the Pro-Resolving Mediators Provides Novel Leads for Resolution Pharmacology. *Br J Pharmacol* (2019) 176:1024–37. doi: 10.1111/bph.14336
195. Sriram K, Insel PA. G Protein-Coupled Receptors as Targets for Approved Drugs: How Many Targets and How Many Drugs? *Mol Pharmacol* (2018) 93:251–8. doi: 10.1124/mol.117.111062
196. Zhang L, Wan J, Li H, Wu P, Jin S, Zhou X, et al. Protective Effects of BML-111, a Lipoxin A_4 Receptor Agonist, on Carbon Tetrachloride-Induced Liver Injury in Mice. *Hepatol Res* (2007) 37(11):948–56. doi: 10.1111/j.1872-034X.2007.00154.x
197. Hutchings CJ, Koglin M, Marshall FH. Therapeutic Antibodies Directed at G Protein-Coupled Receptors. *mAbs* (2010) 2:594–606. doi: 10.4161/mabs.2.6.13420
198. Wu S-H, Chen X-Q, Liu B, Wu H-J, Dong L. Efficacy and Safety of 15(R/s)-Methyl-Lipoxin A4 in Topical Treatment of Infantile Eczema. *Br J Dermatol* (2013) 168:172–8. doi: 10.1111/j.1365-2133.2012.11177.x

199. Christie PE, Spur BW, Lee TH. The Effects of Lipoxin A_4 on Airway Responses in Asthmatic Subjects. *Am Rev Respir Dis* (1992) 145:1281–4. doi: 10.1164/ajrccm/145.6.1281
200. Kong X, Wu S-H, Zhang L, Chen X-Q. Pilot Application of Lipoxin A4 Analog and Lipoxin A4 Receptor Agonist in Asthmatic Children With Acute Episodes. *Exp Ther Med* (2017) 14:2284–90. doi: 10.3892/etm.2017.4787
201. Fattori V, Zaninelli TH, Rasquel-Oliveira FS, Casagrande R, Verri WA. Specialized Pro-Resolving Lipid Mediators: A New Class of non-Immunosuppressive and Non-Opioid Analgesic Drugs. *Pharmacol Res* (2020) 151:104549. doi: 10.1016/j.phrs.2019.104549

Conflict of Interest: ML, VG, and NP are employees and/or shareholders of OSE Immunotherapeutics, a company developing pro-resolutive agonist monoclonal antibodies. VG and NP are patent owners on ChemR23 agonist monoclonal antibodies.

The remaining authors declare that the research was conducted in the absence of any commercial or financial relationships that could be construed as a potential conflict of interest.

Copyright © 2021 Lavy, Gauttier, Poirier, Barillé-Nion and Blanquart. This is an open-access article distributed under the terms of the Creative Commons Attribution License (CC BY). The use, distribution or reproduction in other forums is permitted, provided the original author(s) and the copyright owner(s) are credited and that the original publication in this journal is cited, in accordance with accepted academic practice. No use, distribution or reproduction is permitted which does not comply with these terms.

frontiers in Immunology

ORIGINAL RESEARCH
published: 07 July 2021
doi: 10.3389/fimmu.2021.692286

Butorphanol Promotes Macrophage Phenotypic Transition to Inhibit Inflammatory Lung Injury *via* κ Receptors

Guangxin Luan[†], *Fan Pan*[†], *Lina Bu*[†], *Kaixuan Wu*, *Aizhong Wang*[*] *and Xiaotao Xu*[*]

Department of Anesthesiology, Affiliated Shanghai Sixth People's Hospital, Shanghai Jiao Tong University, Shanghai, China

OPEN ACCESS

Edited by:
Sylvaine You,
Institut National de la Santé et de la Recherche Médicale (INSERM), France

Reviewed by:
Murugesan Rajaram,
The Ohio State University, United States
Bing Du,
East China Normal University, China

***Correspondence:**
Aizhong Wang
wangaz@sjtu.edu.cn
Xiaotao Xu
xuxiaotao08@163.com

[†]*These authors have contributed equally to this work*

Specialty section:
This article was submitted to Inflammation, a section of the journal Frontiers in Immunology

Received: *08 April 2021*
Accepted: *21 June 2021*
Published: *07 July 2021*

Citation:
Luan G, Pan F, Bu L, Wu K, Wang A and Xu X (2021) Butorphanol Promotes Macrophage Phenotypic Transition to Inhibit Inflammatory Lung Injury via κ Receptors. Front. Immunol. 12:692286. doi: 10.3389/fimmu.2021.692286

Acute lung injury (ALI)/acute respiratory distress syndrome (ARDS) is characterized by diffuse inflammation of the lung parenchyma and refractory hypoxemia. Butorphanol is commonly used clinically for perioperative pain relief, but whether butorphanol can regulate LPS-induced alveolar macrophage polarization is unclear. In this study, we observed that butorphanol markedly attenuated sepsis-induced lung tissue injury and mortality in mice. Moreover, butorphanol also decreased the expression of M1 phenotype markers (TNF-α, IL-6, IL-1β and iNOS) and enhanced the expression of M2 marker (CD206) in alveolar macrophages in the bronchoalveolar lavage fluid (BALF) of LPS-stimulated mice. Butorphanol administration reduced LPS-induced numbers of proinflammatory (M1) macrophages and increased numbers of anti-inflammatory (M2) macrophages in the lungs of mice. Furthermore, we found that butorphanol-mediated suppression of the LPS-induced increases in M1 phenotype marker expression (TNF-α, IL-6, IL-1β and iNOS) in bone marrow-derived macrophages (BMDMs), and this effect was reversed by κ-opioid receptor (KOR) antagonists. Moreover, butorphanol inhibited the interaction of TLR4 with MyD88 and further suppressed NF-κB and MAPKs activation. In addition, butorphanol prevented the Toll/IL-1 receptor domain-containing adaptor inducing IFN-β (TRIF)-mediated IFN signaling pathway. These effects were ameliorated by KOR antagonists. Thus, butorphanol may promote macrophage polarization from a proinflammatory to an anti-inflammatory phenotype secondary to the inhibition of NF-κB, MAPKs, and the TRIF-mediated IFN signaling pathway through κ receptors.

Keywords: butorphanol, acute lung injury, inflammation, macrophage, κ receptor

Abbreviations: ALI, Acute lung injury; ARDS, Acute respiratory distress syndrome; VALI, Ventilator-associated lung injury; TLR4, Toll-like receptor 4; TRIF, Toll/IL-1 receptor domain-containing adaptor inducing IFN-β; PAMPs, Pathogen-associated molecular patterns; DAMPs, Damage-associated molecular patterns; LPS, Lipopolysaccharide; MPO, Myeloperoxidase; BALF, Bronchoalveolar lavage fluid; KOR, κ-opioid receptor; MOR, μ-opioid receptor; CNS, Central nervous system.

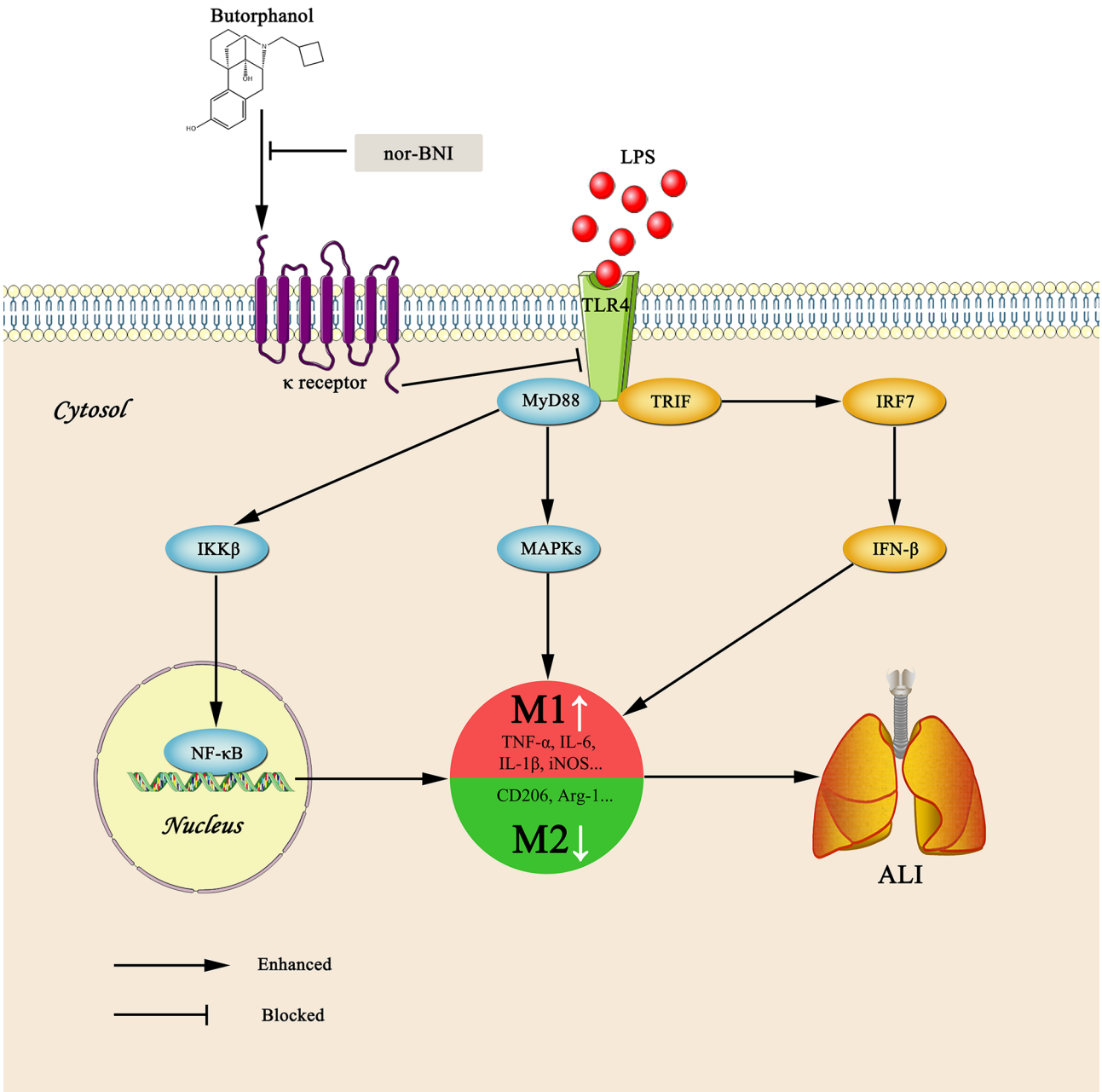

GRAPHICAL ABSTRACT | Graphical summary of the effects and mechanisms of butorphanol on sepsis-induced ALI. Upon binding of LPS to TLR4, macrophages are activated and accumulated at the site of infection where they are polarized into the M1 (a pro-inflammatory) and M2 (an anti-inflammatory) phenotypes. However, butorphanol may mitigate sepsis-induced ALI by promoting macrophage transition from M1 to M2 phenotype secondary to the inhibition of NF-κB and MAPKs, and the TRIF-mediated IFN signaling pathway through κ receptors.

INTRODUCTION

Inflammatory responses are initiated by tissue injury or infection (1). Despite their role in clearing pathogens, uncontrolled inflammatory responses can lead to tissue structure damage (2). Sepsis is induced by potentially fatal systemic inflammatory responses secondary to infections and is the primary cause of death in intensive care units (ICUs) (3). Studies have illustrated that coagulation dysfunction, immune dysregulation and inflammatory reactions contribute to sepsis pathogenesis (4). In addition, ALI or ARDS may occur during severe sepsis (5, 6). Excessive macrophage activation has been

viewed as one of the most important factors that exacerbate sepsis-induced ALI (7).

Macrophages in ALI are activated *via* Toll-like receptors (TLRs) through the recognition of damage-associated molecular patterns (DAMPs) and pathogen-associated molecular patterns (PAMPs). LPS-induced TLR4 activation in macrophages triggers the production of proinflammatory cytokines, including TNF-α, IL-6 and IL-1β, which leads to the recruitment of neutrophils and lymphocytes to the site of infection and contributes to pathogen clearance (8, 9). However, as an essential part of the innate immune system, macrophages exhibit marked plasticity and functional heterogeneity based on the cytokines to which they are exposed (10, 11). Macrophages are divided into alternatively activated (M2) macrophages and classically activated (M1) macrophages. In the early stage of inflammation, LPS can convert macrophages to an M1 phenotype, and M1 macrophages produce proinflammatory factors such as reactive oxygen intermediates and reactive nitrogen intermediates and the cytokines TNF-α, IL-6 and IL-1β (12, 13). Therefore, M1 macrophages are involved in inhibiting cellular proliferation and causing tissue injury. M2 macrophages are polarized in response to IL-10, glucocorticoids, and IL-4 (9, 11, 14) and produce anti-inflammatory cytokines and other effectors, such as IL-10, Mrc 1 (CD206), and arginase-1 (Arg-1), which take part in wound healing and tissue repair (13, 15). Although the mechanism of macrophage polarization *in vivo* is poorly understood, TLR4 induces the activation of NF-κB and further increases the induction of specific cytokines and transcription factors, which may play vital roles in controlling macrophage plasticity (9, 16–19).

Butorphanol is a lipid-soluble anesthetic drug that is a strong κ-opioid receptor (KOR) agonist and a weak μ-opioid receptor (MOR) agonist-antagonist (20). As a partial MOR and complete KOR agonist, butorphanol is widely used in the clinic as an analgesic, while the incidence of vomiting, gastrointestinal nausea and respiratory depression is less than that of pure MOR agonists (remifentanil, fentanyl, and sufentanil). In recent years, a large number of studies have confirmed the protective effect of KOR on the heart, brain, lung, and other important organs (21–24). The mechanisms may include inhibiting inflammation and oxidative stress (24). Moreover, TLR4 and opioid receptor interactions occur in the central nervous system (CNS), and effects on peripheral immune cells have also been demonstrated (25). However, whether butorphanol can regulate macrophage polarization in sepsis-induced ALI is not clear.

We examined the role of butorphanol in macrophage polarization and neutralizing sepsis-induced ALI in mice. We found that butorphanol was vital in promoting macrophage conversion and reducing the LPS-induced inflammatory response. We also demonstrated that butorphanol-induced macrophage reprogramming was crucial in the resolution of ALI. Butorphanol increased the expression of M2 markers (CD206 and Arg-1) but decreased the expression of M1 markers (TNF-α, IL-6, IL-1β and iNOS) in LPS-stimulated bone marrow-derived macrophages (BMDMs). This finding shows that butorphanol plays an important role in the alleviation of inflammatory lung injury *in vivo* and *in vitro* by promoting macrophage phenotypic transition.

METHODS AND MATERIALS

Reagents and Antibodies

Butorphanol was obtained from Hengrui (Jiangsu, China). SB203580, PD98059, SP600125, Naloxegol, and Norbinaltorphimine dihydrochloride (nor-BNI) were obtained from MedChemExpress (Monmouth Junction, NJ, USA). LPS (Escherichia coli 055:B5) and DAPI were obtained from Sigma-Aldrich (St. Louis, MO, USA). CCK-8 kit was obtained from Dojindo (Kumamoto, Japan). TNF-α, IL-6 and IL-1β Elisa Kits were obtained from Novus (USA). TRIzol reagent, random hexamers and MultiScribe reverse transcriptase and SYBR Green PCR Master Mix were obtained from Thermo Fisher (USA). The primary antibodies include: phospho-JNK (1:1000; Cell Signaling Technology, Danvers, MA, USA), JNK (1:1000; Cell Signaling Technology, Danvers, MA, USA), phospho-ERK (1:1000; Cell Signaling Technology, Danvers, MA, USA), ERK (1:1000; Cell Signaling Technology, Danvers, MA, USA), phospho-p38 (1:1000; Cell Signaling Technology, Danvers, MA, USA), p38 (1:1000; Cell Signaling Technology, Danvers, MA, USA), phospho-STAT6 (1:1000; Cell Signaling Technology, Danvers, MA, USA), STAT6 (1:1000; Cell Signaling Technology, Danvers, MA, USA), Arg-1 (1:1000; Cell Signaling Technology, Danvers, MA, USA), F4/80 (1:1000; Cell Signaling Technology, Danvers, MA, USA), iNOS (1:1000; HUABIO, China), CD206 (1:1000; Abcam, Cambridge, UK), TLR4 (1:200; Novus, USA), MyD88 (1:200, Santa Cruz Biotechnology, CA), NF-κB (1:200; Cell Signaling Technology, Danvers, MA, USA) and β-Tubulin (1:1000; Cell Signaling Technology, Danvers, MA, USA). The secondary antibodies include: Alexa Fluor 488-conjugated anti-mouse (1:400; Abcam, Cambridge, UK), Alexa Fluor 594-conjugated anti-rabbit (1:400; Abcam, Cambridge, UK), and horseradish peroxidase (HRP)-conjugated anti-rabbit (1:10000; Cell Signaling Technology, Danvers, MA, USA).

Animals

All studies involving animals were performed in compliance with the ARRIVE guidelines. C57BL/6J mice (males, 6-8 weeks old, 20-25 g body weight; Fudan University Medical Animal Center, Shanghai, China) were used. All mice were housed at a constant room temperature of 22-23°C with an alternating 12 h light/dark cycle and free access to water and standard food.

Endotoxin-Induced ALI

Age- and weight-matched mice received a single intraperitoneal (i.p.) dose of LPS (10 $mg{\cdot}kg^{-1}$ body weight) (26). Butorphanol (4 $mg{\cdot}kg^{-1}$ or 8 $mg{\cdot}kg^{-1}$ body weight) was administered 30 min after LPS injection. Saline alone was similarly administered to control

mice. For survival studies, mice were injected i.p. with 20 mg·kg^{-1} LPS and monitored four times daily for up to 3 d (26).

Bone Marrow-Derived Macrophage Cultures

Bone marrow cells were collected by flushing the femur and tibia cavities of mice, plated at approximately 2×10^6 cells/mL and incubated in Dulbecco's modified Eagle's medium supplemented with 10% (vol/vol) FBS, 1% (vol/vol) streptomycin/penicillin, and 10% (vol/vol) L929-conditioned media as previously described (27). Cells were used for experiments on day 7 of culture.

Isolation of CD11b+ Alveolar Macrophages

CD11b+ alveolar macrophages were isolated according to the manufacturer's instructions (28). Briefly, the cells were collected from total bronchoalveolar lavage fluid (BALF) and incubated with CD11b+ magnetic beads (Miltenyi Biotec). Then, the cells were applied to an MS column (Miltenyi) to select CD11b+ cells.

CCK-8 Cell Viability Assay

A CCK-8 cell viability assay was used to measure cell viability as previously described (29). Briefly, BMDMs were treated with butorphanol (0, 1, 2, 4, and 8 μM) for 24 h. Next, 10 μl of CCK-8 solution was added to each well and incubated for 2 h. The absorbance of each well was measured at 450 nm using an automatic porous spectrophotometer (Molecular Devices, USA).

Histological Examination

The lungs were isolated from mice in all groups, perfused and fixed with 4% paraformaldehyde, embedded, and cut into 5-μm sections. The sections were stained with hematoxylin and eosin (HE), and ten microscopic fields were used to assess the lung injury score based on a previous study (30). A semiquantitative scoring system was used to analyze lung injury, and the scoring criteria were as follows: 0: normal appearance; 1: mild interstitial hyperemia and polymorphonuclear leukocyte infiltration; 2: paravascular edema and moderate pulmonary structural damage; 3: massive cell infiltration and moderate alveolar structure destruction; and 4: massive cell infiltration and severe lung structural damage.

Immunofluorescence Analysis

The sections were blocked with 3% goat serum (Millipore, S26-LITER) in Tris-buffered saline (TBS) containing 0.1% Triton X-100 for 1 h at room temperature. The slides were incubated with anti-F4/80, anti-iNOS or anti-CD206 overnight and then with secondary antibodies for 1 h at room temperature. The nuclei were stained with DAPI for 3 min at room temperature. BMDMs were cultured and seeded on 24-well glass coverslips. The cells were incubated with LPS with or without butorphanol for 24 h, washed three times with ice-cold phosphate-buffered saline (PBS), fixed with paraformaldehyde for 10 min, and then blocked with 3% bovine serum albumin in PBS for 1 h at room temperature. The cells were incubated with anti-TLR4, anti-MyD88 or anti-NF-κB antibodies at 4°C overnight, washed with 1% PBST three times and incubated with secondary antibodies for 1 h at room temperature. The nuclei were stained with DAPI for 3 min at room temperature. Then, images were obtained by a Zeiss LSM 710 confocal microscope (Athens, GA, USA).

MPO Assay

Myeloperoxidase (MPO) activity in lung tissue was measured as described previously (31). Briefly, lungs were perfused with PBS to remove all blood, weighed and homogenized in 1 mL of PBS with 0.5% hexadecyltrimethylammonium bromide. The supernatant was then collected and mixed 1/30 (vol/vol) with assay buffer (0.2 mg·mL^{-1} o-dianisidine hydrochloride and 0.0005% H_2O_2) after the homogenates were sonicated and centrifuged at 40,000 × g for 20 min. The change in absorbance was measured at 460 nm for 3 min, and MPO activity was calculated as the change in absorbance over time.

Western Blotting

Protein lysates (30 μg) were resolved by 8-15% SDS-polyacrylamide gels and transferred to polyvinylidene fluoride (PVDF) membranes. The membrane was blocked with 5% dry milk in TBS containing 0.1% Tween-20 for 1 h at room temperature. The membranes were then probed with the indicated primary antibodies overnight at 4°C. Next, the membranes were washed three times and then incubated with an HRP-conjugated secondary antibody for 1 h and developed using an enhanced chemiluminescence (ECL) detection kit (Millipore, USA). Images were acquired using ImageQuant LAS 4000 mini (GE Healthcare Life Sciences, USA). Band intensity was determined by densitometric analysis with ImageJ software.

Cytokine ELISA

Cytokines (TNF-α, IL-6 and IL-1β) in BALF were measured with a commercially available ELISA kit according to the manufacturer's instructions.

RNA Extraction and qRT-PCR

Total RNA was isolated from cells and reverse-transcribed with random hexamers and MultiScribe reverse transcriptase. The obtained cDNA was mixed with SYBR Green PCR Master Mix, and GAPDH served as an internal control. Relative gene expression was calculated and normalized using the 2-ΔΔCt method. The following mouse primers were used:

iNOS (forward, 5'-AGTCTCAGACATGGCTTGCCCCT-3'; reverse, 5'-GCTGCGGGGAGCCATTTTGGT-3'), IL-6 (forward, 5'-TCCAGTTGCCTTCTTGGGACTG-3'; reverse, 5'-AGCC TCCGACTTGTGAAGTGGT-3'), TNF-α (forward, 5'-GACCC TCACACTCAGATCATCT-3'; reverse, 5'-CCTCCACTTG GTGGTTTGCT-3'), IL-1β (forward, 5'-GAATCTATACCTGT CCTGTG-3'; reverse, 5'-TTATGTCCTGACCACTGTTG-3'), CD206 (forward, 5'-CCACGGATGACCTGTGCTCGAG-3'; reverse, 5'- ACACCAGAGCCATCCGTCCGA-3'), and Arg-1 (forward, 5'-GAATGGAAGAGTCAGTGTGG-3'; reverse, 5'-AATGACACATAGGTCAGGGT-3'), IRF7 (forward, 5'-GCTC

CAAACCCCAAGCCCTCTG-3'; reverse, 5'-GACAGCTT CCACCTGCCATGCT-3'), IRF3 (forward, 5'-ACGGCAGGACG CACAGATGG-3'; reverse, 5'- TCCAGGTTGACACGTCCGGC-3'), IFN-β (forward, 5'-GGATCCTCCACGCTGCGTTCC-3'; reverse, 5'-CCGCCCTGTAGGTGAGGTTGA-3').

Lung Wet/Dry Weight Ratio

The wet/dry weight (W/D) ratios were calculated as an indicator of pulmonary edema (32). Briefly, the right upper lung of each mouse was removed, rinsed in saline and then weighed to determine the wet weight. The lung was then dried at 80°C in an oven for 48 h and reweighed to obtain the dry weight. The W/D ratios were then calculated by dividing the wet weight by the dry weight.

Collection of BALF and Cells

BALF was collected at 24 h by cannulating a catheter into the trachea, which was then lavaged three times with 0.8 mL of cold PBS. Samples were centrifuged at 700 ×g for 5 min at 4°C. The collected supernatant was further analyzed for inflammatory cytokine levels.

Statistical Analysis

All data are expressed as the means ± SEM. Statistical significance was determined using GraphPad Prism 8 software (GraphPad Software Inc., San Diego, CA, USA). Statistical comparisons among multiple groups were carried out using one-way ANOVA followed by Tukey's *post hoc* test and the log-rank test. A value of $P < 0.05$ was considered to be statistically significant.

RESULTS

Butorphanol Alleviates LPS-Induced ALI/ARDS by Regulating Macrophage Polarization *In Vivo*

To explore the role of butorphanol in macrophage polarization and the inflammatory response *in vivo*, we established a mouse ALI/ARDS model induced by LPS (33). Histopathological analysis showed that butorphanol (4 mg·kg^{-1} or 8 mg·kg^{-1}) attenuated LPS-induced lung tissue damage (**Figures 1A, B**). LPS increased the W/D ratio of lung tissues at 24 h, and this effect was reversed by butorphanol (**Figure 1C**). In addition, neutrophil sequestration in lung tissue was measured by determining MPO levels. We found that MPO activity was significantly increased in lung tissue in mice stimulated with LPS, and this effect was also neutralized by butorphanol (**Figure 1D**). In addition, butorphanol (4 mg·kg^{-1} or 8 mg·kg^{-1}) significantly reversed the decrease in total protein in BALF in LPS-injected mice (**Figure 1E**). The ELISA results showed that LPS increased proinflammatory cytokine expression levels (TNF-α, IL-6, and IL-1β) in BALF. Conversely, butorphanol (4 mg·kg^{-1} or 8 mg·kg^{-1}) injection decreased the LPS-induced increases in proinflammatory cytokine expression levels (TNF-α, IL-6, and IL-1β) in BALF (**Figures 1F–H**). qRT-PCR analysis showed that LPS increased the induction of proinflammatory gene (TNF-α, IL-6, IL-1β and iNOS) and reduced anti-inflammatory markers (CD206) in CD11b+ alveolar macrophages isolated from the BALF of mice. Conversely, butorphanol decreased the LPS-induced induction of proinflammatory gene (TNF-α, IL-6, IL-1β and iNOS) and enhanced anti-inflammatory markers (CD206) in cells (**Figures 1I–M**). Moreover, all mice subjected to LPS died within 48 h. The administration of butorphanol (4 mg·kg-1 or 8 mg·kg-1) resulted in 50% and 80% survival in LPS-induced mice, respectively (**Figure 1N**). We further examined the numbers of M1 and M2 macrophages in the lung by immunofluorescence. LPS increased the number of F4/80^{+}iNOS^{+} M1 alveolar macrophages and decreased the number of F4/80^{+}CD206^{+} M2 alveolar macrophages in lung tissues, and this effect was counteracted by butorphanol (**Figures 2A, B**; **3A, B**). These data showed that butorphanol could relieve septic ALI/ARDS by modulating macrophage polarization and inhibiting the inflammatory response *in vivo*.

Butorphanol Inhibits M1 Macrophage Polarization

To further investigate the role of butorphanol in the balance of M1/M2 macrophage polarization in LPS-induced ALI, BMDMs were stimulated with LPS. The results showed that butorphanol (8 mu;Mu;) did not cause cytotoxicity in BMDMs (**Figure 4A**). We found that LPS obviously increased the expression levels of iNOS, IL-6, TNF-α and IL-1β in M1-polarized BMDMs. In contrast, 8 mu;Mu; butorphanol significantly reduced the expression levels of iNOS, IL-6, TNF-α and IL-1β in M1-polarized BMDMs stimulated with LPS (**Figures 4B–H**). The western blot results demonstrated that LPS significantly increased the level of iNOS in M1-polarized BMDMs. However, butorphanol significantly decreased the expression of iNOS in M1-polarized BMDMs stimulated with LPS (**Figures 4I, J**). This result suggests that the effect of butorphanol is TLR4-dependent. Furthermore, whether butorphanol reduced interferon (IFN)-γ-induced M1 polarization was also examined. IFN-γ significantly increased the expression levels of TNF-α, IL-6, IL-1β and iNOS in M1-polarized BMDMs. However, 8 mu;Mu; butorphanol significantly reduced the expression levels of TNF-α, IL-6, IL-1β and iNOS in M1-polarized BMDMs subjected to IFN-γ (**Figures 4K–N**). Collectively, these results showed that butorphanol alleviated the inflammatory response by inhibiting LPS- or IFN-γ-induced M1 activation of BMDMs.

Butorphanol Promotes M2 Macrophage Polarization

To explore the role of butorphanol in LPS-induced M2 macrophage polarization, BMDMs were treated with LPS. The results showed that LPS obviously decreased the expression of Arg-1 and CD206 in BMDMs. In contrast, butorphanol significantly reversed the LPS-induced decrease in the expression of CD206 and Arg-1 in BMDMs (**Figures 5A, B**). Furthermore, we used IL-4 to stimulate BMDMs toward the M2 phenotype. The results showed that butorphanol increased the expression of CD206 and Arg-1 (**Figures 5C, D**). The western blot results showed that LPS significantly decreased the

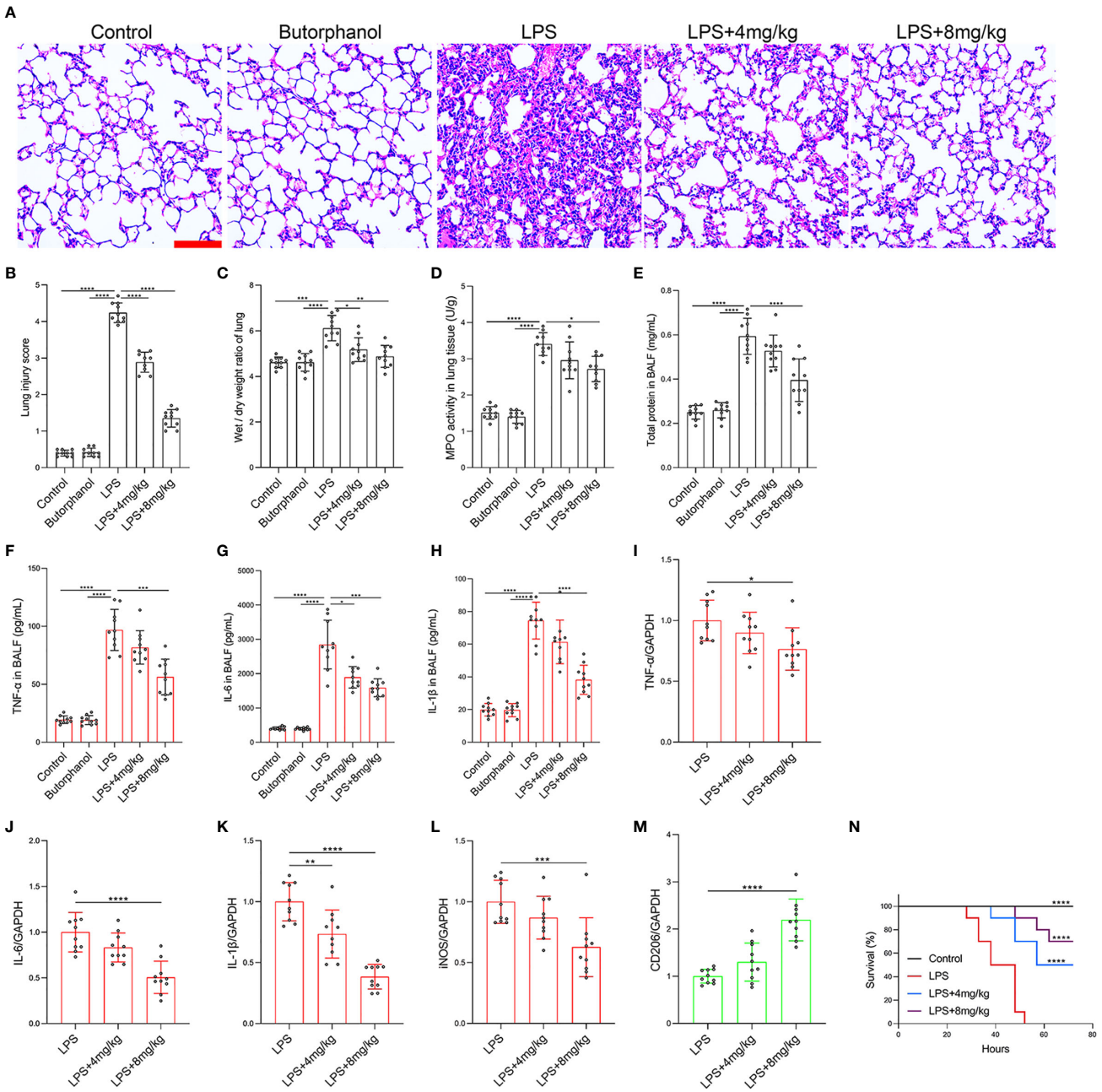

FIGURE 1 | Butorphanol ameliorated LPS-induced inflammatory lung injury. Mice were injected with LPS (10 mg·kg^{-1} i.p.) or butorphanol (8 mg·kg^{-1} i.p.) or butorphanol (4 mg·kg^{-1} i.p. or 8 mg·kg^{-1} i.p.) plus LPS (10 mg·kg^{-1} i.p.) and analyzed after 24 h. **(A)** Hematoxylin and eosin staining of lung sections. Scale bar: 50 μm. **(B)** Lung injury score. **(C, D)** Lungs obtained at 24 h after LPS challenge were used to determine the wet/dry weight ratio and MPO activity. **(E)** The total protein level in BALF was measured with a BCA assay. **(F–H)** The BALF expression levels of TNF-α, IL-6, and IL-1β were determined by ELISA. **(I–M)** The mRNA levels of TNF-α, IL-6, IL-1β, iNOS, and CD206 in CD11b+ alveolar macrophages in the BALF of mice were measured with qRT-PCR. **(N)** Mouse survival was monitored for 72 h after a lethal dose of LPS (20 mg·kg^{-1} i.p.) alone or in combination with butorphanol (4 mg·kg^{-1} i.p. or 8 mg·kg^{-1} i.p.) 30 min after LPS challenge. n = 10 per group. The results are the means ± SEM of ten independent experiments. Statistical analysis was performed by one-way ANOVA followed by Tukey's *post hoc* test when comparing multiple independent groups and the log-rank test. *P < 0.05, **P < 0.01, ***P < 0.001, ****P < 0.0001.

expression of CD206 in M1-polarized BMDMs. However, butorphanol significantly increased the expression of CD206 in M1-polarized BMDMs stimulated with LPS (**Figures 5E, F**). The western blot results also demonstrated that IL-4 significantly enhanced the expression of CD206 and Arg-1 in M2-polarized BMDMs. Moreover, butorphanol enhanced the expression of

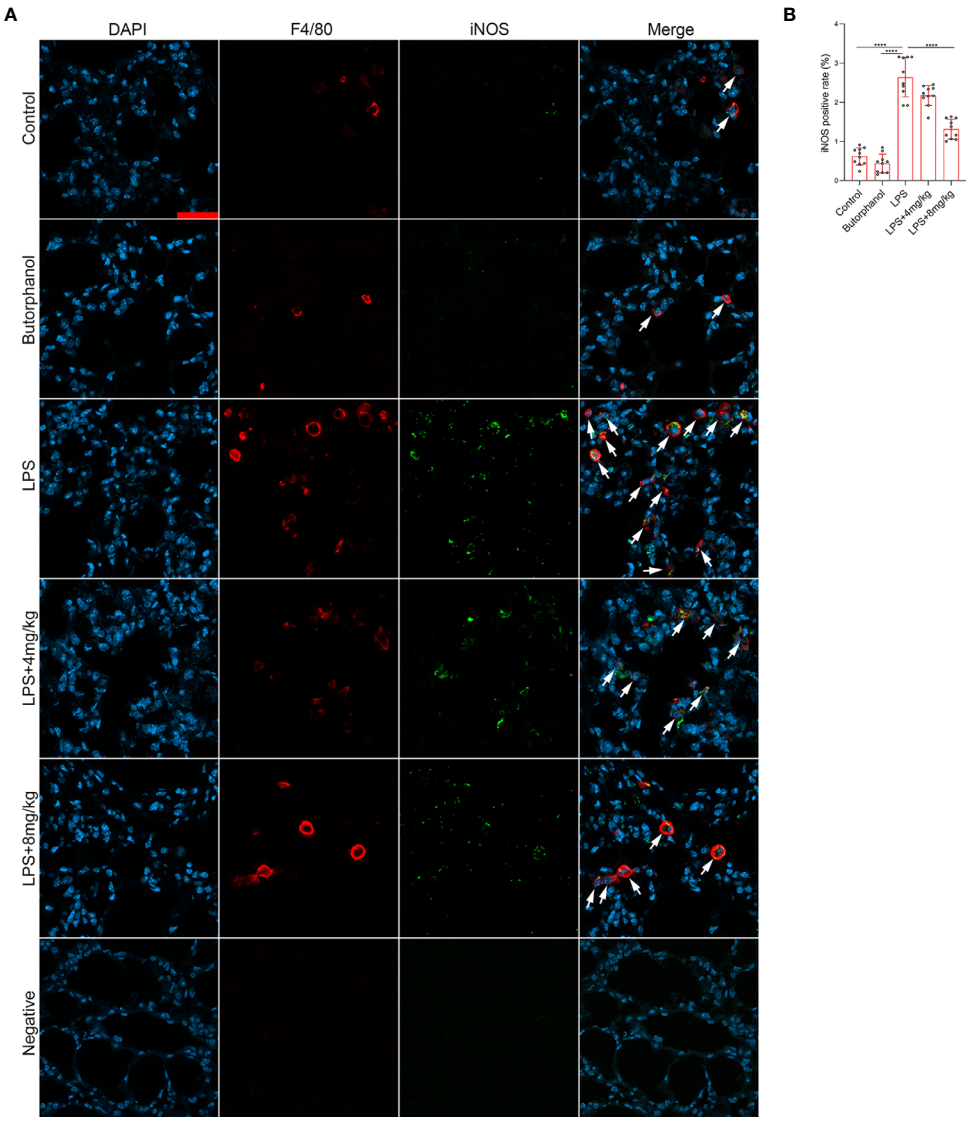

FIGURE 2 | Butorphanol administration inhibited M1 macrophage polarization in LPS-induced lung injury. Mice were injected with LPS (10 mg·kg^{-1} i.p.) or butorphanol (8 mg·kg^{-1} i.p.) or butorphanol (4 mg·kg^{-1} i.p. or 8 mg·kg^{-1} i.p.) plus LPS (10 mg·kg^{-1} i.p.) and analyzed after 24 h. **(A)** Sections were stained with antibodies against F4/80 (red) and iNOS (green). Scale bar: 25 μm. **(B)** The image analysis results are presented as the percentage of iNOS-positive F4/80 cells. The results are the means ± SEM of ten independent experiments. Statistical analysis was performed by one-way ANOVA followed by Tukey's *post hoc* test when comparing multiple independent groups. ****P < 0.0001.

CD206 and Arg-1 (**Figures 5G–I**). It is well known that the activation of signal transducer and activator of transcription 6 (STAT6) is associated with M2 macrophage polarization (34). Therefore, the phosphorylation level of STAT6 was analyzed by western blotting. The results showed that IL-4 significantly increased the phosphorylation level of STAT6 in M2-polarized BMDMs. However, butorphanol further increased the phosphorylation level of STAT6 in M2-polarized BMDMs in the presence of IL-4 (**Figures 5J, K**). These results suggested that butorphanol was crucial in contributing to the M2 polarization of BMDMs.

Butorphanol Modulates Macrophage Polarization Through KOR in LPS-Induced BMDMs

It has been demonstrated that the activation of MOR can alleviate LPS-induced ALI through the PI3K/Akt pathway (35). To further explore which opioid receptors are involved in butorphanol-mediated macrophage polarization in LPS-induced ALI, we used MOR and KOR antagonists to block the effect of butorphanol. Compared with that in control macrophages, LPS markedly increased the expression of IL-6,

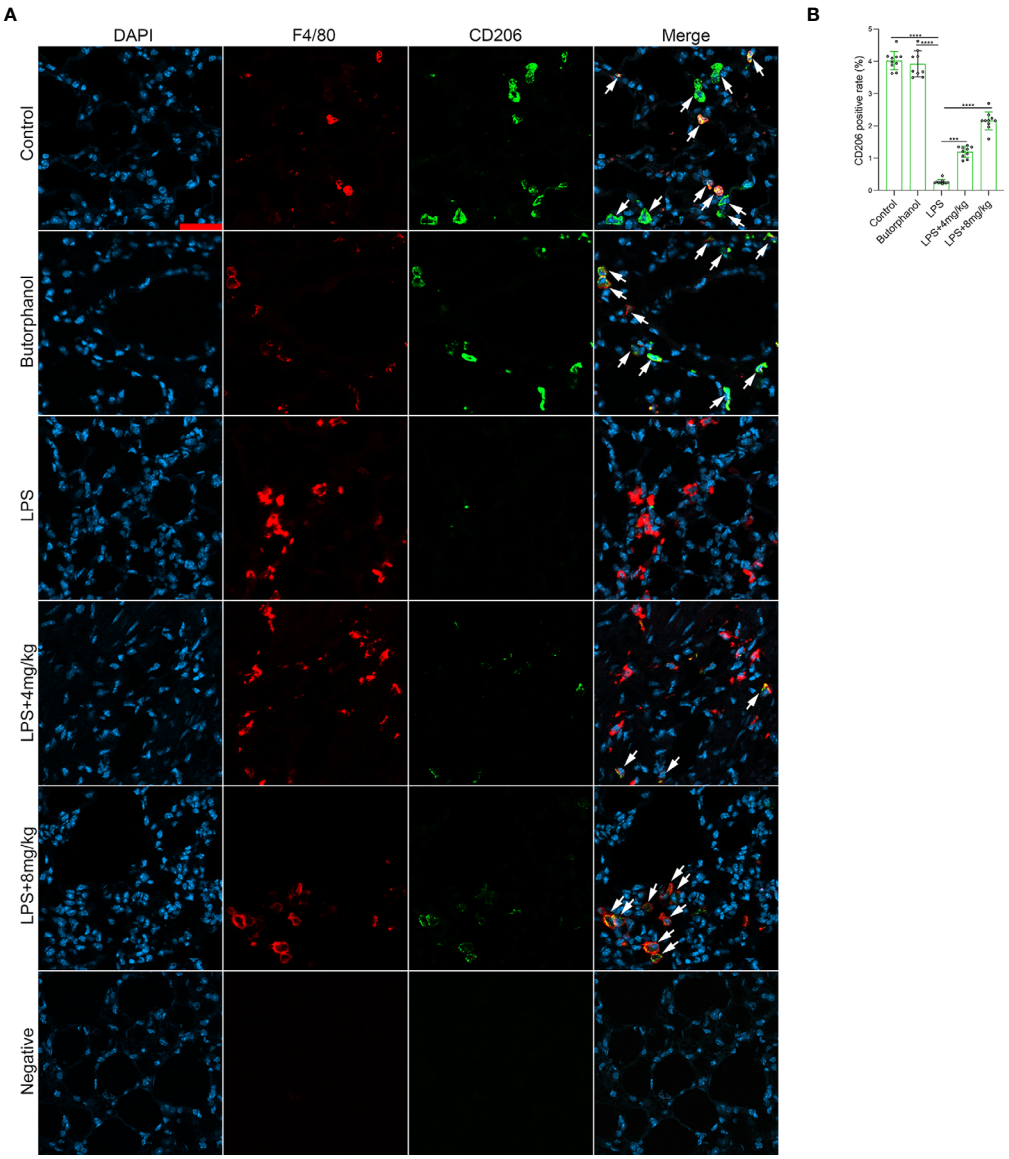

FIGURE 3 | Butorphanol administration promoted M2 macrophage polarization in LPS-induced lung injury. Mice were injected with LPS (10 mg·kg^{-1} i.p.) or butorphanol (8 mg·kg^{-1} i.p.) or butorphanol (4 mg·kg^{-1} i.p. or 8 mg·kg^{-1} i.p.) plus LPS (10 mg·kg^{-1} i.p.) and analyzed after 24 h. **(A)** Sections were stained with antibodies against F4/80 (red) and CD206 (green). Scale bar: 25 μm. **(B)** The image analysis results are presented as the percentage of CD206-positive F4/80 cells. The results are the means ± SEM of ten independent experiments. Statistical analysis was performed by one-way ANOVA followed by Tukey's *post hoc* test when comparing multiple independent groups. ***P < 0.001, ****P < 0.0001.

TNF-α, and iNOS in BMDMs; however, butorphanol treatment notably decreased the expression of IL-6, TNF-α, and iNOS in LPS-induced BMDMs. Moreover, the inhibitory effect of butorphanol on the levels of IL-6, TNF-α, and iNOS was reversed by the KOR antagonist but not the MOR antagonist (**Figures 6A–E**). Compared with that in control macrophages, LPS markedly reduced the expression of anti-inflammatory markers (CD206) in BMDMs; however, butorphanol treatment significantly increased the expression of anti-inflammatory markers (CD206) in LPS-induced BMDMs. Moreover, the effect of butorphanol on the level of anti-inflammatory markers (CD206) was reversed by the KOR antagonist but not the MOR antagonist (**Figure 6F**).

Butorphanol Inhibits MyD88-Dependent Signaling Pathways Through KOR in M1-Polarized BMDMs

We explored whether butorphanol prevented TLR4 signaling, which induces the nuclear translocation of NF-κB *via* MyD88-independent and MyD88-dependent pathways

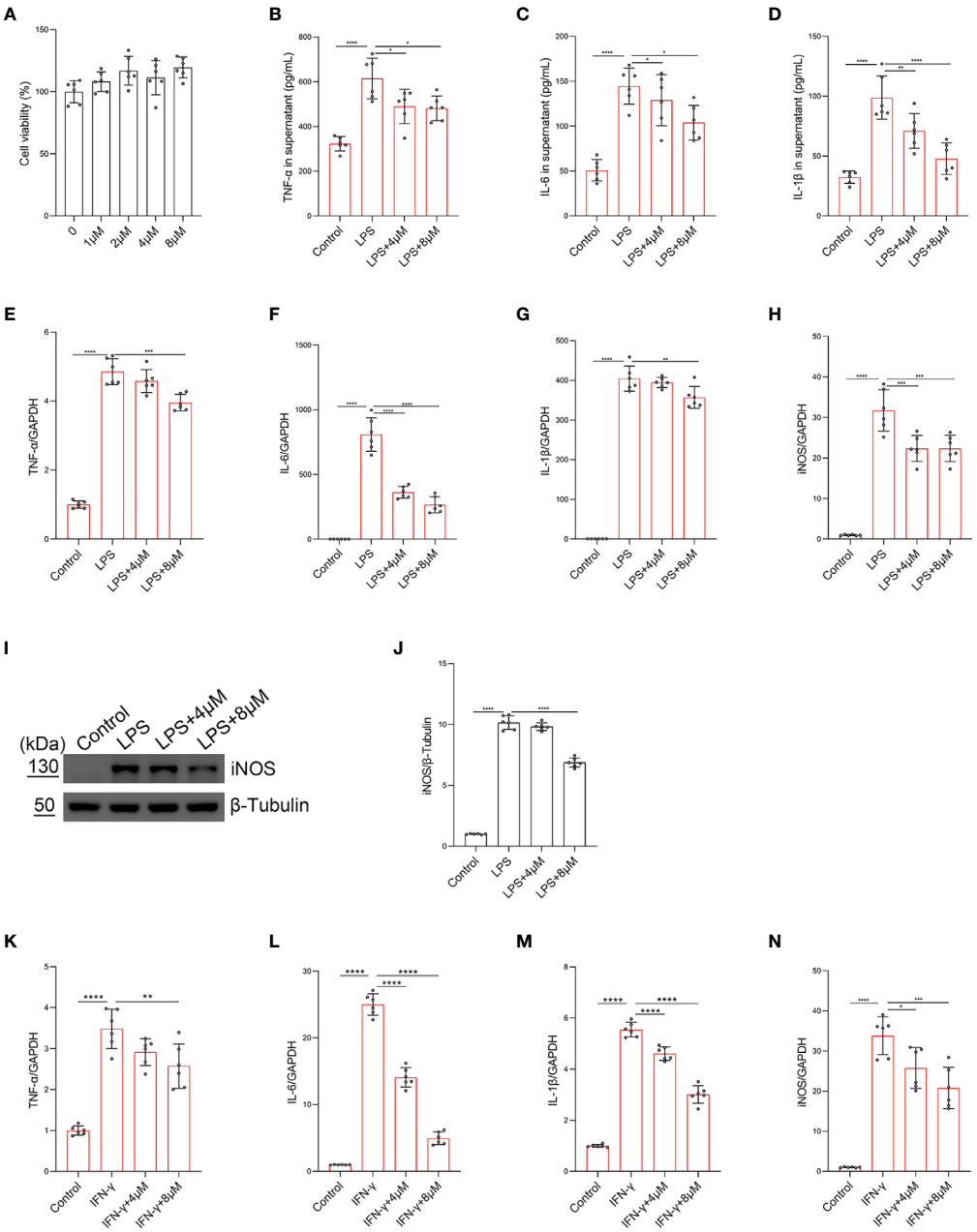

FIGURE 4 | Butorphanol inhibited M1 macrophage activation. Macrophages were collected and cultured from the bone marrow of mice and treated with different concentrations of butorphanol (0-8 μM) for 24 h. **(A)** CCK-8 analysis of cell viability. Cells were incubated with LPS (1 μg·mL^{-1}) alone or butorphanol (4 μM or 8 μM) plus LPS (1 μg·mL^{-1}) for 24 h. **(B–D)** TNF-α, IL-6, and IL-1β protein levels in the supernatant of macrophage cultures were determined by ELISA. **(E–H)** The mRNA expression of proinflammatory cytokines (TNF-α, IL-6, IL-1β, and iNOS) in cells was measured by qRT-PCR. **(I)** The levels of iNOS were measured by western blot analysis. **(J)** Densitometric analysis of iNOS levels in **(I)** was performed with normalization to β-tubulin. Cells were incubated with IFN-γ (100 ng·mL^{-1}) alone or butorphanol (4 μM or 8 μM) plus IFN-γ (100 ng·mL^{-1}) for 24 h. **(K–N)** The mRNA expression of proinflammatory cytokines (TNF-α, IL-6, IL-1β, and iNOS) in cells was measured by qRT-PCR. The results are the means ± SEM of six independent experiments. Statistical analysis was performed by one-way ANOVA followed by Tukey's *post hoc* test when comparing multiple independent groups. *P < 0.05, **P < 0.01, ***P < 0.001, ****P < 0.0001.

(36). In our study, LPS induced a strong TLR4-MyD88 association within 15 min and IκB kinase β (IKKβ) phosphorylation and NF-κB translocation within 30 min. However, butorphanol inhibited the association of MyD88 with TLR4, IKKβ phosphorylation and NF-κB translocation (**Figures 7A–D**); thus, butorphanol prevents MyD88-dependent NF-κB activation. The role of butorphanol in preventing the association of TLR4 with MyD88, IKKβ

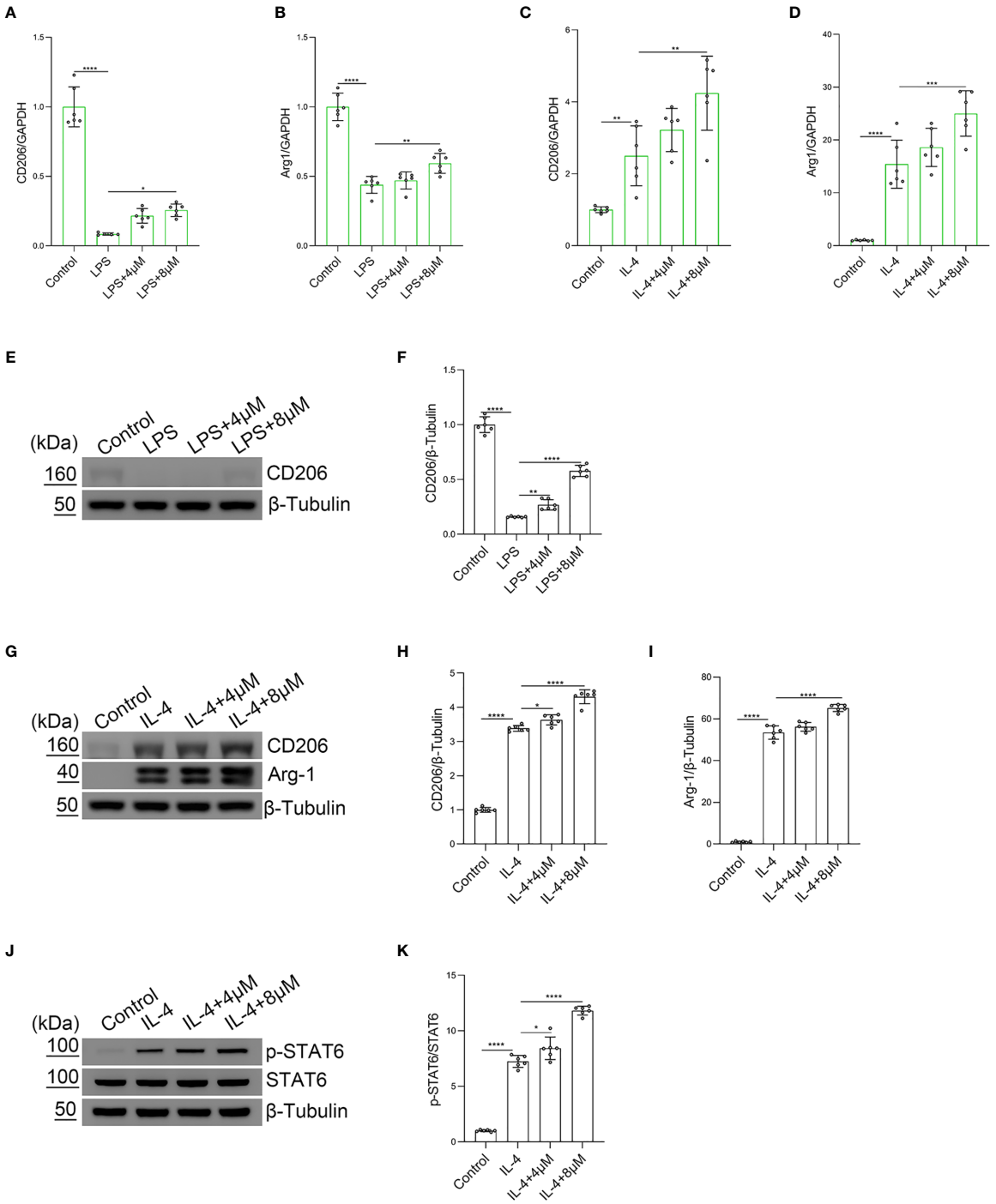

FIGURE 5 | Butorphanol promoted M2 macrophage polarization. Macrophages were collected and cultured from the bone marrow of mice and incubated with LPS (1 μg·mL^{-1}) alone or butorphanol (4 μM or 8 μM) plus LPS (1 μg·mL^{-1}) for 24 h. **(A, B)** The mRNA expression of M2 markers (CD206 and Arg-1) in cells was measured by qRT-PCR. **(E)** The protein levels of CD206 were measured by western blot analysis. **(F)** Densitometric analysis of CD206 expression in **(E)** was performed with normalization to β-tubulin. Macrophages were incubated with IL-4 (20 ng·mL^{-1}) alone or butorphanol (4 μM or 8 μM) plus IL-4 (20 ng·mL^{-1}) for 24 h. **(C, D)** The mRNA expression of M2 markers (CD206 and Arg-1) in cells was measured by qRT-PCR. **(G)** The protein levels of CD206 and Arg-1 were measured by western blot analysis. **(H, I)** Densitometric analysis of CD206 and Arg-1 levels in **(G)** was performed with normalization to β-tubulin. Macrophages were incubated with IL-4 (20 ng·mL^{-1}) alone or butorphanol (4 μM or 8 μM) plus IL-4 (20 ng·mL^{-1}) for 30 min. **(J)** The protein levels of phosphorylated STAT6 and total STAT6 were measured by western blot analysis. **(K)** Densitometric analysis of the phosphorylated STAT6 levels in **(J)** was performed with normalization to the respective total protein. The results are the means ± SEM of six independent experiments. Statistical analysis was performed by one-way ANOVA followed by Tukey's *post hoc* test when comparing multiple independent groups. *P < 0.05, **P < 0.01, ***P < 0.001, ****P < 0.0001.

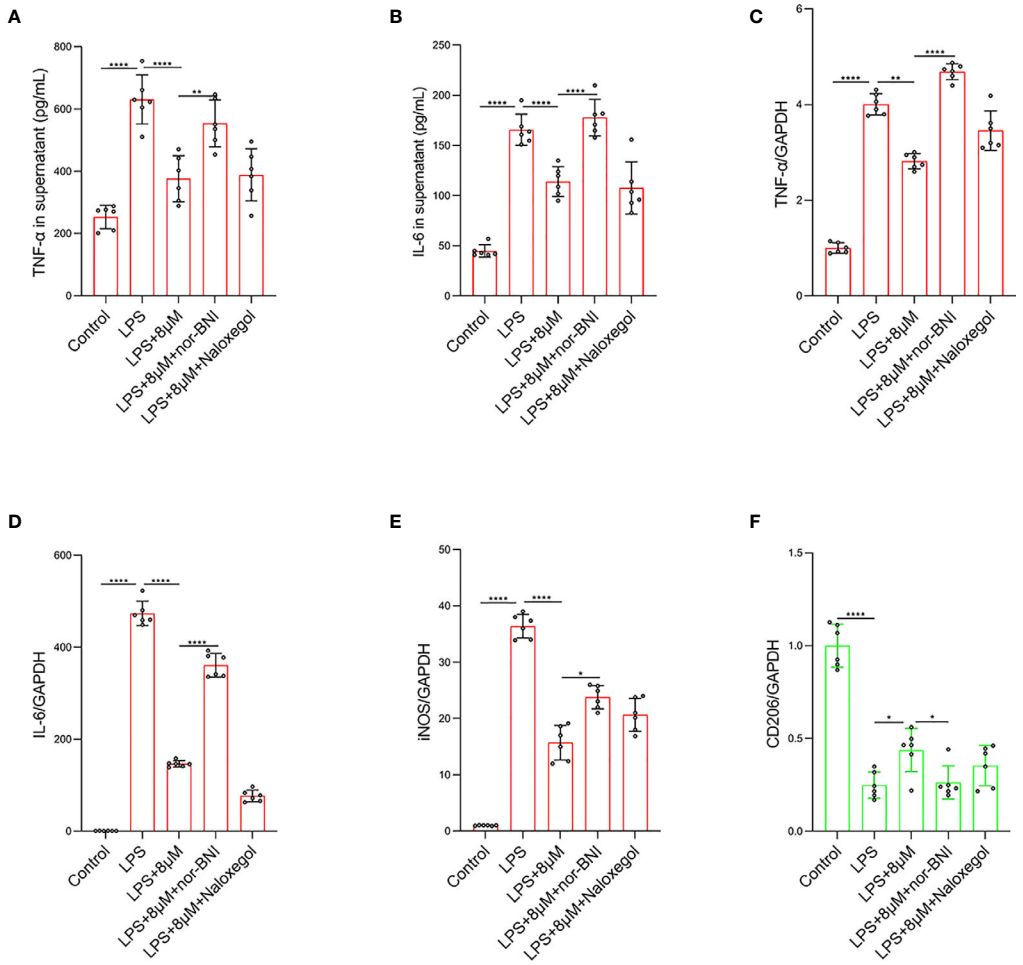

FIGURE 6 | Butorphanol regulated macrophage polarization through the KOR in LPS-induced BMDMs. Macrophages were collected and cultured from the bone marrow of mice and incubated with LPS (1 μg·mL^{-1}) alone or butorphanol (8 μM) plus LPS (1 μg·mL^{-1}), nor-BNI (KOR antagonist, 5 μM) plus butorphanol (8 μM) plus LPS (1 μg·mL^{-1}), or naloxegol (MOR antagonist, 5 μM) plus butorphanol (8 μM) plus LPS (1 μg·mL^{-1}) for 24 h. Cells were pretreated with nor-BNI or naloxegol for 30 min. **(A, B)** TNF-α and IL-6 protein levels in the supernatant of macrophage cultures were determined by ELISA. **(C–F)** The mRNA levels of TNF-α, IL-6, iNOS and CD206 in cells were measured by qRT-PCR. The results are the means ± SEM of six independent experiments. Statistical analysis was performed by one-way ANOVA followed by Tukey's *post hoc* test when comparing multiple independent groups. *P < 0.05, **P < 0.01, ****P < 0.0001.

phosphorylation and NF-κB activation was alleviated by a KOR antagonist (**Figures 7A–D**).

Butorphanol Inhibits M1 Macrophage Polarization Through the MAPK Signaling Pathway in M1-Polarized BMDMs

To confirm that the JNK/ERK/P38 pathway was involved in the effect of butorphanol on M1 macrophage polarization, we examined the effect of butorphanol on LPS-induced JNK, ERK and P38 phosphorylation in BMDMs. Compared with those of control macrophages, LPS increased the phosphorylation levels of JNK, P38 and ERK within 30 min. However, LPS-induced JNK, P38 and ERK phosphorylation was decreased by butorphanol treatment (**Figures 8A–D**). Furthermore, we used the JNK inhibitor SP600125 (10 μM), the ERK inhibitor PD98059 (10 μM) and the P38 inhibitor SB203580 (10 μM) to block the phosphorylation of JNK, ERK and P38, respectively (37). As shown in **Figures 8E–I**, the JNK, ERK and P38 inhibitors significantly inhibited the expression of IL-1β, IL-6, and iNOS in LPS-treated BMDMs. Moreover, the levels of inflammatory cytokines (IL-1β, IL-6, and iNOS) in the JNK, ERK and P38 inhibitor groups were similar to those in the butorphanol treatment group. Taken together, our results demonstrated that butorphanol inhibited M1 macrophage polarization through the JNK/ERK/P38 signaling pathway in M1-polarized BMDMs.

Butorphanol Prevents the Phosphorylation of MAPKs in M1-Polarized BMDMs Through KOR

Moreover, we found that butorphanol (8 mu;Mu;) administration significantly inhibited the phosphorylation of MAPKs in LPS-

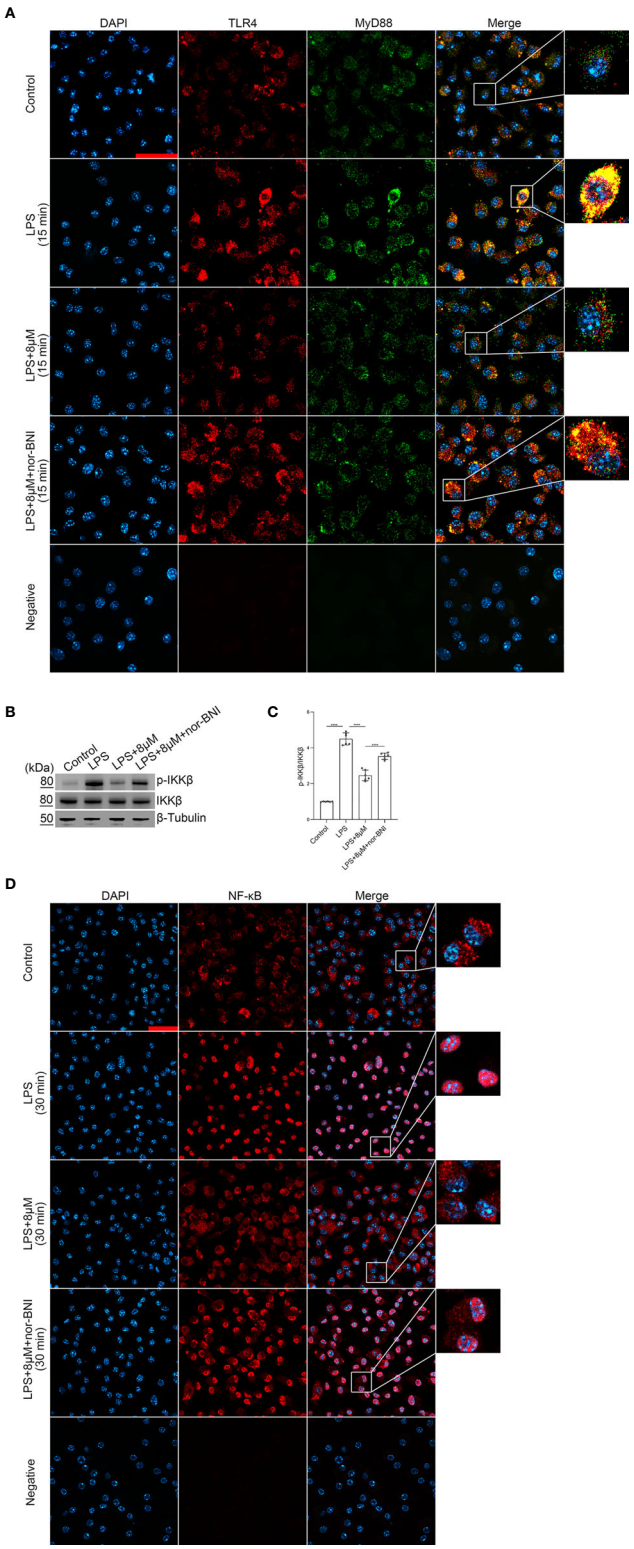

FIGURE 7 | Continued

FIGURE 7 | Butorphanol prevented the interaction of MyD88 with TLR4 and inhibited NF-κB activation through KOR in M1-polarized BMDMs. Macrophages were collected and cultured from the bone marrow of mice and incubated with LPS (1 μg·mL^{-1}) alone, butorphanol (8 μM) plus LPS (1 μg·mL^{-1}), or nor-BNI (KOR antagonist, 5 μM) plus butorphanol (8 μM) and LPS (1 μg·mL^{-1}) for 15 min or 30 min. Cells were pretreated with nor-BNI for 30 min. **(A)** To observe the interaction of MyD88 with TLR4, cells were fixed, permeabilized, and stained, and images were obtained by confocal microscopy. Scale bar: 25 μm. **(B)** The levels of phosphorylated IKKβ and total IKKβ were measured by western blot analysis. **(C)** Densitometric analysis of the phosphorylated IKKβ levels in **(B)** was performed with normalization to the respective total protein. **(D)** The translocation of NF-κB in cells was examined by confocal microscopy. Scale bar: 25 μm. The results are the means ± SEM of six independent experiments. Statistical analysis was performed by one-way ANOVA followed by Tukey's *post hoc* test when comparing multiple independent groups. ****P < 0.0001.

induced BMDMs. The effect of butorphanol on inhibiting the phosphorylation of MAPKs in LPS-induced BMDMs was counteracted by pretreatment with a KOR antagonist (**Figures 9A–D**). Taken together, our results demonstrated that butorphanol inhibited the phosphorylation of MAPKs through KOR in M1-polarized BMDMs.

Butorphanol Inhibits TRIF-Dependent Signaling Pathways Through KOR in M1-Polarized BMDMs

In addition, TLR4 mediates the expression of inflammatory genes through TRIF-dependent signaling pathways in LPS-treated macrophages (38). In our study, the mRNA level of IFN-regulated factor-3 (IRF3) was not significantly increased at 6 h, whereas LPS significantly increased the elevation of IRF7 at 6 h, which are involved in the TLR4-mediated TRIF-dependent IFN signaling pathway in LPS-induced macrophages (38). Butorphanol decreased the LPS-induced elevation of IRF7 in BMDMs. The effect of butorphanol on inhibiting elevation of IRF7 was alleviated by a KOR antagonist (**Figures 10A, B**). Moreover, LPS significantly increased the mRNA level of IFN-β in BMDMs. Butorphanol significantly reduced the mRNA level of IFN-β in LPS-induced BMDMs, the effect of which was attenuated by the KOR antagonist (**Figure 10C**). Thus, butorphanol functions by inhibiting TRIF-dependent IFN signaling pathways through KOR in M1-polarized BMDMs.

DISCUSSION

The present study was performed to verify the hypothesis that butorphanol contributes to M2 macrophage polarization to alleviate sepsis-induced ALI and explore the potential mechanisms. Our results demonstrated that butorphanol ameliorated pathological lung damage, decreased the inflammatory response, and promoted M2 macrophage polarization in LPS-induced ALI.

Furthermore, we showed that butorphanol suppressed M1 polarization in LPS-induced BMDMs and reduced the

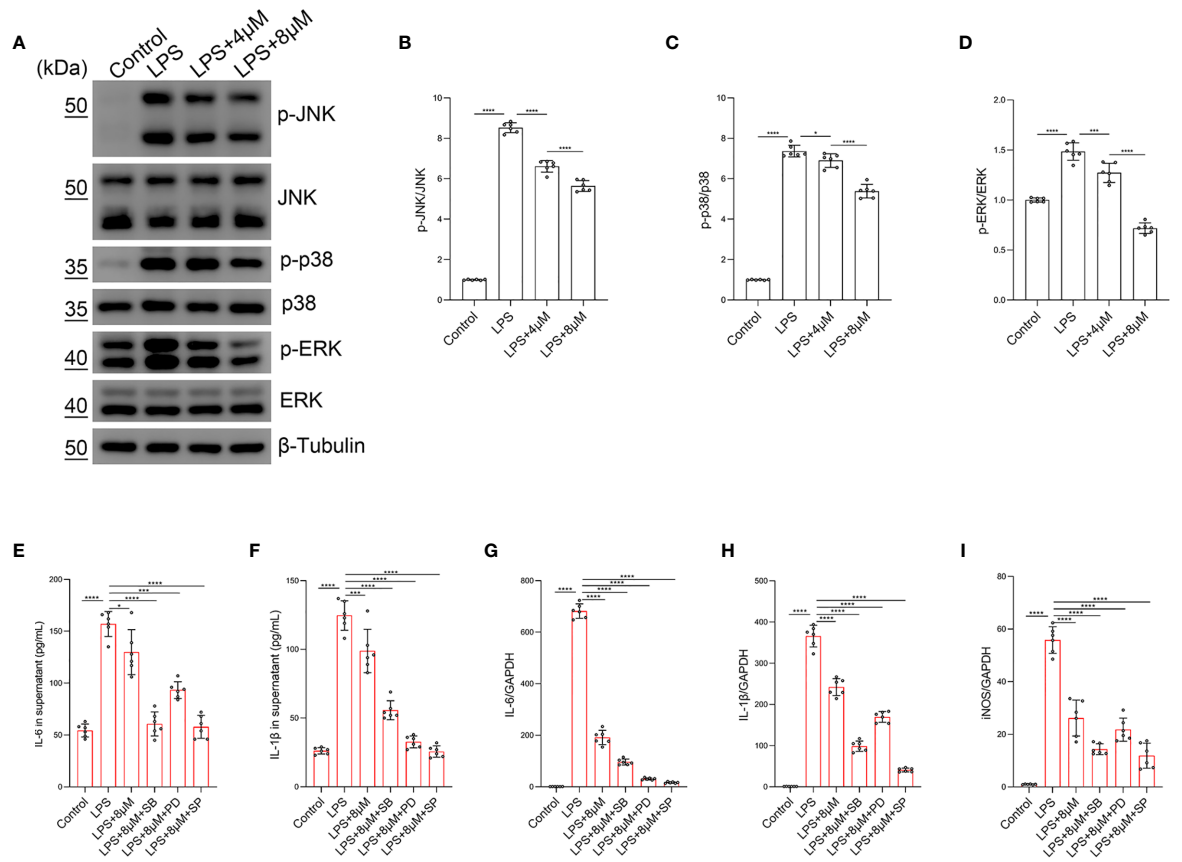

FIGURE 8 | Butorphanol inhibited M1 phenotype macrophage polarization through the MAPK signaling pathway. Macrophages were collected and cultured from the bone marrow of mice and treated with LPS (1 μg·mL^{-1}) alone or butorphanol (4 μM or 8 μM) plus LPS (1 μg·mL^{-1}) for 30 min. **(A)** The levels of phosphorylated MAPKs and their respective total proteins were measured by western blot analysis. **(B–D)** Densitometric analysis of the phosphorylated MAPKs levels in **(A)** was performed with normalization to the respective total proteins. Macrophages were incubated with LPS (1 μg·mL^{-1}) alone, butorphanol (8 μM) plus LPS (1 μg·mL^{-1}), the p38 inhibitor SB203580 (10 μM) plus LPS (1 μg·mL^{-1}), the ERK inhibitor PD98059 (10 μM) plus LPS (1 μg·mL^{-1}), or the JNK inhibitor SP600125 (10 μM) plus LPS (1 μg·mL^{-1}) for 24 h. **(E, F)** IL-6 and IL-1β protein levels in the supernatant of macrophage cultures were determined by ELISA. **(G–I)** The mRNA levels of IL-6, IL-1β, and iNOS in cells were measured by qRT-PCR. The results are the means ± SEM of six independent experiments. Statistical analysis was performed by one-way ANOVA followed by Tukey's *post hoc* test when comparing multiple independent groups. *P < 0.05, ***P < 0.001, ****P < 0.0001.

expression of proinflammatory cytokines (IL-1β, IL-6, and TNF-α). Moreover, butorphanol increased M2 macrophage polarization by upregulating the expression of CD206 and Arg-1 in BMDMs induced by LPS or IL-4. Furthermore, butorphanol inhibited NF-κB and MAPK activation and the TRIF-mediated IFN signaling pathway through KOR in LPS-induced M1-polarized BMDMs.

Accumulating evidence has suggested that macrophage polarization plays an important role in the progression of inflammatory diseases, such as sepsis and ALI (39, 40). M1 macrophages are characterized as toxic, while M2 macrophages are considered to be protective (18). It has been demonstrated that butorphanol also has therapeutic effects on ventilator-associated lung injury (VALI) (24). The main pathological change in VALI is the destruction of pulmonary vascular endothelial cells and the increase in pulmonary vascular permeability, which is particularly significant in obese patients (41). It was suggested that butorphanol could reduce lung injury and improve intraoperative oxygenation in obese patients by inhibiting inflammation and reducing vascular injury (24). Moreover, it has been shown that butorphanol can relieve sepsis-induced brain injury by inhibiting the NF-κB signaling pathway (42). However, we further demonstrated that butorphanol promoted macrophage phenotypic transition to alleviate sepsis-induced lung injury secondary to the inhibition of NF-κB and MAPK signaling, as well as the TRIF-mediated IFN signaling pathway through KOR.

To estimate the bioactivity of butorphanol *in vivo*, we established a mouse model of LPS-induced ALI (43). The results showed that butorphanol notably increased the survival rates of mice subjected to LPS and decreased the levels of lung inflammatory cytokines. It has been noted that the lungs are susceptible to infection during sepsis (44). Therefore, preventing lung infection may be an effective therapeutic approach in sepsis.

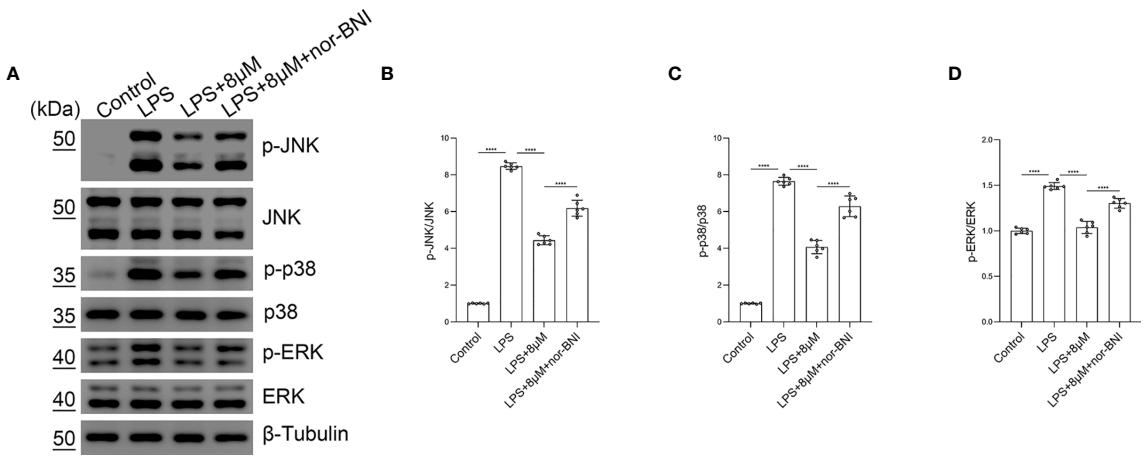

FIGURE 9 | Butorphanol prevented the phosphorylation of MAPKs through KOR in M1-polarized BMDMs. Macrophages were collected and cultured from the bone marrow of mice and incubated with LPS (1 μg·mL^{-1}) alone, butorphanol (8 μM) plus LPS (1 μg·mL^{-1}) or nor-BNI (KOR antagonist, 5 μM) plus butorphanol (8 μM) plus LPS (1 μg·mL^{-1}) for 30 min. Cells were pretreated with nor-BNI for 30 min. **(A)** The levels of phosphorylated MAPKs and their respective total proteins were measured by western blot analysis. **(B–D)** Densitometric analysis of the phosphorylated MAPKs levels in **(A)** was performed with normalization to the respective total proteins. The results are the means ± SEM of six independent experiments. Statistical analysis was performed by one-way ANOVA followed by Tukey's *post hoc* test when comparing multiple independent groups. ****P < 0.0001.

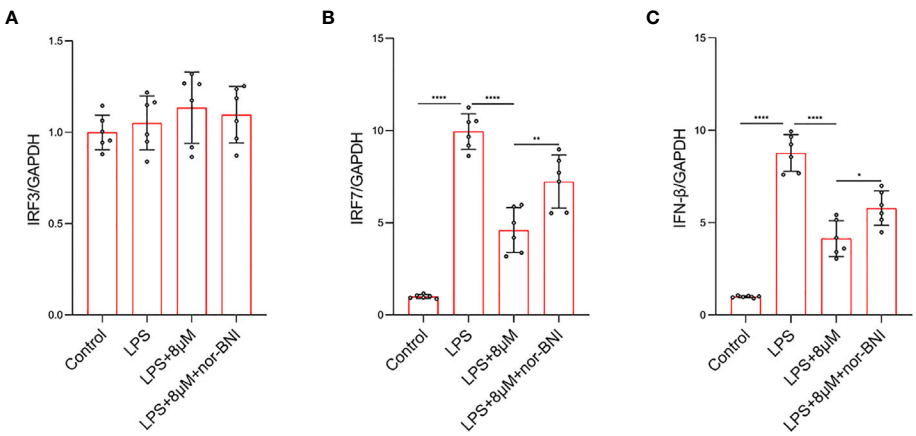

FIGURE 10 | Butorphanol decreased LPS-induced the elevation of IRF7 and IFN-β through KOR in M1-polarized BMDMs. Macrophages were collected and cultured from the bone marrow of mice and incubated with LPS (1 μg·mL^{-1}) alone, butorphanol (8 μM) plus LPS (1 μg·mL^{-1}) or nor-BNI (KOR antagonist, 5 μM) plus butorphanol (8 μM) plus LPS (1 μg·mL^{-1}) for 6 h. Cells were pretreated with nor-BNI for 30 min. **(A–C)** The mRNA levels of IRF3, IRF7, and IFN-β in cells were measured by qRT-PCR. The results are the means ± SEM of six independent experiments. Statistical analysis was performed by one-way ANOVA followed by Tukey's *post hoc* test when comparing multiple independent groups. *P < 0.05, **P < 0.01, ****P < 0.0001.

Our results demonstrated that butorphanol modified lung tissue injury, inhibited M1 macrophage polarization, and enhanced M2 macrophage polarization in the lungs of LPS-injected mice. In addition, butorphanol administration significantly enhanced the number of M2 macrophages and decreased the number of M1 macrophages in the lungs of LPS-injected mice.

The present study also verified that butorphanol significantly converted macrophages to the M2 phenotype. The features of M1 or M2 macrophage polarization include the expression of M1- or M2-associated molecular markers, respectively. For instance, M1 macrophage markers are iNOS, pSTAT1, pSTAT3, TNF-α, IL-6, IFNγ, IL-12p70, and IL-1β, whereas M2 macrophage markers are Arg-1, Chi3l3, pSTAT6, IL-4, and IL-10 (45). Butorphanol inhibited LPS-induced M1-associated molecular markers and enhanced M2-associated molecular markers in BMDMs. These results showed that butorphanol could promote M2 macrophage polarization both *in vivo* and *in vitro*. Furthermore, butorphanol treatment markedly reduced the expression of IL-6, TNF-α, and iNOS in LPS-induced BMDMs. Moreover, the inhibitory effect of butorphanol on the levels of IL-

6, TNF-α, and iNOS was reversed by a KOR antagonist but not an MOR antagonist.

Potential interactions can occur between TLR4 and opioid receptors (μ, δ and κ). These interactions are involved in immune function, opioid analgesia, and intestinal motility (25). The TLR4 signaling pathway was directly activated by opioid receptor agonists in the CNS in the absence of LPS, indicating interactions within the cell membrane. Opioids bind to and activate TLR4, which in turn increases the production of proinflammatory cytokines in the CNS (46). However, opioid receptor agonists inhibit LPS-induced TLR4 signaling and decrease the inflammatory response in peripheral immune cells, indicating that the TLR4 and opioid receptor interaction is dependent on the cell type and activator (47, 48). In addition, NF-κB activation plays a central role in driving inflammatory signaling (49). Under normal conditions, NF-κB is inhibited by IκB and maintained in an inactive state in the cytoplasm (49). IKK-β induces IκBα phosphorylation (at Ser32), which causes its dissociation and degradation, promoting NF-κB release and subsequent reactive oxygen species (ROS) and cytokine production (50, 51). The formation of inactive dimers of the p50 subunit of NF-κB is essential for promoting macrophage polarization to the anti-inflammatory phenotype, resulting in the suppression of NF-κB-induced macrophage polarization (17). We demonstrated that butorphanol prevented the association of TLR4 with MyD88 and inhibited the phosphorylation of IKK-β, which restrained NF-κB signaling activation (49) and further promoted macrophages to shift to the anti-inflammatory M2 phenotype. These results demonstrated that the inhibitory effect of butorphanol on the interaction between TLR4 and MyD88, the phosphorylation of IKK-β and the activation of NF-κB were reversed by the KOR antagonist.

In addition, the MAPK pathway is downstream of the opioid receptor and TLR4 signaling pathways, and opioid receptors can also induce neuroinflammation in the CNS through the activation of MAPK signals (25). Different opioid receptors have distinct roles in different cell types and diseases. MAPK phosphorylation in murine macrophages promoted M1 macrophage polarization, resulting in cytotoxic and inflammatory effects such as NO production. MAPKs have been viewed as potential targets of sepsis. Briefly, LPS binds to TLR4 and induces the activation of MAPK-dependent intracellular signaling (41, 43, 44). In our study, the phosphorylation of JNK, ERK, and p38 was significantly increased after LPS stimulation, but butorphanol decreased the phosphorylation levels of JNK, ERK, and p38. In our study, inhibition of the phosphorylation levels of MAPKs completely blocked LPS-induced M1 macrophage polarization, demonstrating that the suppression of M1 polarization by butorphanol to exert anti-inflammatory effects may inhibit the JNK, ERK, and p38 pathways. In addition, we found that butorphanol-mediated inhibition of MAPK phosphorylation in LPS-induced BMDMs was counteracted by pretreatment with a KOR antagonist. Moreover, we demonstrated that butorphanol inhibited LPS-induced the elevation of IRF7 and IFN-β, which was attenuated by a KOR antagonist.

In summary, our study demonstrates that butorphanol alleviates LPS-induced ALI by contributing to M2 macrophage polarization and inhibiting M1 macrophage polarization. Moreover, butorphanol significantly decreases M1 polarization and increases M2 polarization in macrophages secondary to inhibition of the NF-κB and MAPKs and the TRIF-mediated IFN signaling pathway through KOR. Our results demonstrate that butorphanol may be an anti-inflammatory agent for the treatment of sepsis and ALI.

DATA AVAILABILITY STATEMENT

The original contributions presented in the study are included in the article/supplementary material. Further inquiries can be directed to the corresponding authors.

ETHICS STATEMENT

All the procedures and all animal experiments carried out in this study were performed in accordance with the Guide for the Care and Use of Laboratory Animals (eighth edition) published by the National Research Council (United States) and were approved by the Institutional Animal Care and Use Committee of Sixth People's Hospital affiliated with Shanghai Jiao Tong University.

AUTHOR CONTRIBUTIONS

GL and XX designed and performed most of the experiments, analyzed and interpreted the data, and wrote the manuscript. FP, LB and KW assisted during the acquisition, analysis, and interpretation of data and revised the manuscript. XX and AW assisted with data acquisition and manuscript revision. XX is responsible for the integrity of the work as a whole. All authors contributed to the article and approved the submitted version.

FUNDING

This work was supported by the National Natural Science Foundation of China (81772062).

REFERENCES

1. Takeuchi O, Akira S. Pattern Recognition Receptors and Inflammation. *Cell* (2010) 140(6):805–20. doi: 10.1016/j.cell.2010.01.022
2. Medzhitov R. Origin and Physiological Roles of Inflammation. *Nature* (2008) 454(7203):428–35. doi: 10.1038/nature07201
3. Dellinger RP, Levy MM, Rhodes A, Annane D, Gerlach H, Opal SM, et al. Surviving Sepsis Campaign Guidelines Committee Including the Pediatric, Surviving Sepsis Campaign: International Guidelines for Management of Severe Sepsis and Septic Shock: 2012. *Crit Care Med* (2013) 41(2):580–637. doi: 10.1007/s00134-012-2769-8
4. Huang M, Cai S, Su J. The Pathogenesis of Sepsis and Potential Therapeutic Targets. *Int J Mol Sci* (2019) 20(21):5376. doi: 10.3390/ijms20215376

5. Rubenfeld GD, Caldwell E, Peabody E, Weaver J, Martin DP, Neff M, et al. Incidence and Outcomes of Acute Lung Injury. *N Engl J Med* (2006) 354 (4):416–7. doi: 10.1056/NEJMoa050333
6. Zhao H, Chen H, Xiaoyin M, Yang G, Hu Y, Xie K, et al. Autophagy Activation Improves Lung Injury and Inflammation in Sepsis. *Inflammation* (2019) 42(2):426–39. doi: 10.1007/s10753-018-00952-5
7. Fan EKY, Fan J. Regulation of Alveolar Macrophage Death in Acute Lung Inflammation. *Respir Res* (2018) 19(1):50. doi: 10.1186/s12931-018-0756-5
8. Kawai T, Akira S. Toll-Like Receptors and Their Crosstalk With Other Innate Receptors in Infection and Immunity. *Immunity* (2011) 34(5):637–50. doi: 10.1016/j.immuni.2011.05.006
9. Murray PJ, Allen JE, Biswas SK, Fisher EA, Gilroy DW, Goerdt S, et al. Macrophage Activation and Polarization: Nomenclature and Experimental Guidelines. *Immunity* (2014) 41(1):14–20. doi: 10.1016/j.immuni.2014.06.008
10. Hussell T, Bell TJ. Alveolar Macrophages: Plasticity in a Tissue-Specific Context. *Nat Rev Immunol* (2014) 14(2):81–93. doi: 10.1038/nri3600
11. Kopf M, Schneider C, Nobs SP. The Development and Function of Lung-Resident Macrophages and Dendritic Cells. *Nat Immunol* (2015) 16(1):36–44. doi: 10.1038/ni.3052
12. Bouhlel MA, Derudas B, Rigamonti E, Dievart R, Brozek J, Haulon S, et al. Ppargamma Activation Primes Human Monocytes Into Alternative M2 Macrophages With Anti-Inflammatory Properties. *Cell Metab* (2007) 6 (2):137–43. doi: 10.1016/j.cmet.2007.06.010
13. Arora S, Dev K, Agarwal B, Das P, Syed MA. Macrophages: Their Role, Activation and Polarization in Pulmonary Diseases. *Immunobiology* (2018) 223(4–5):383–96. doi: 10.1016/j.imbio.2017.11.001
14. Mosser DM, Edwards JP. Exploring the Full Spectrum of Macrophage Activation. *Nat Rev Immunol* (2008) 8(12):958–69. doi: 10.1038/nri2448
15. Wang N, Liang H, Zen K. Molecular Mechanisms That Influence the Macrophage M1-M2 Polarization Balance. *Front Immunol* (2014) 5:614. doi: 10.3389/fimmu.2014.00614
16. Lawrence T, Natoli G. Transcriptional Regulation of Macrophage Polarization: Enabling Diversity With Identity. *Nat Rev Immunol* (2011) 11 (11):750–61. doi: 10.1038/nri3088
17. Porta C, Rimoldi M, Raes G, Brys L, Ghezzi P, Di Liberto D, et al. Tolerance and M2 (Alternative) Macrophage Polarization Are Related Processes Orchestrated by P50 Nuclear Factor KappaB. *Proc Natl Acad Sci USA* (2009) 106(35):14978–83. doi: 10.1073/pnas.0809784106
18. Sica A, Mantovani A. Macrophage Plasticity and Polarization: *In Vivo* Veritas. *J Clin Invest* (2012) 122(3):787–95. doi: 10.1172/JCI59643
19. Mantovani A, Biswas SK, Galdiero MR, Sica A, Locati M. Macrophage Plasticity and Polarization in Tissue Repair and Remodelling. *J Pathol* (2013) 229(2):176–85. doi: 10.1002/path.4133
20. Jose DE, Ganapathi P, Anish Sharma NG, Shankaranarayana P, Aiyappa DS, Nazim M. Postoperative Pain Relief With Epidural Buprenorphine Versus Epidural Butorphanol in Laparoscopic Hysterectomies: A Comparative Study. *Anesth Essays Res* (2016) 10(1):82–7. doi: 10.4103/0259-1162.173612
21. Wu Y, Wan J, Zhen WZ, Chen LF, Zhan J, Ke JJ, et al. The Effect of Butorphanol Postconditioning on Myocardial Ischaemia Reperfusion Injury in Rats. *Interact Cardiovasc Thorac Surg* (2014) 18(3):308–12. doi: 10.1093/icvts/ivt516
22. Huang LH, Li J, Gu JP, Qu MX, Yu J, Wang ZY. Butorphanol Attenuates Myocardial Ischemia Reperfusion Injury Through Inhibiting Mitochondria-Mediated Apoptosis in Mice. *Eur Rev Med Pharmacol Sci* (2018) 22(6):1819–24. doi: 10.26355/eurrev_201803_14601
23. Yang L, Sun DF, Wu Y, Han J, Liu RC, Wang LJ. Intranasal Administration of Butorphanol Benefits Old Patients Undergoing H-Uvulopalatopharyngoplasty: A Randomized Trial. *BMC Anesthesiol* (2015) 15:20. doi: 10.1186/1471-2253-15-20
24. Wang XL, Zeng S, Li XX, Zhao Y, Wang XH, Li T, et al. The Protective Effects of Butorphanol on Pulmonary Function of Patients With Obesity Undergoing Laparoscopic Bariatric Surgery: A Double-Blind Randomized Controlled Trial. *Obes Surg* (2020) 30(10):3919–29. doi: 10.1007/s11695-020-04755-2
25. Zhang P, Yang M, Chen C, Liu L, Wei X, Zeng S. Toll-Like Receptor 4 (TLR4)/Opioid Receptor Pathway Crosstalk and Impact on Opioid Analgesia, Immune Function, and Gastrointestinal Motility. *Front Immunol* (2020) 11:1455. doi: 10.3389/fimmu.2020.01455
26. Mittal M, Tiruppathi C, Nepal S, Zhao YY, Grzych D, Soni D, et al. Tnfalpha-Stimulated Gene-6 (TSG6) Activates Macrophage Phenotype Transition to Prevent Inflammatory Lung Injury. *Proc Natl Acad Sci USA* (2016) 113(50): E8151–8. doi: 10.1073/pnas.1614935113
27. Carow B, Gao Y, Teran G, Yang XO, Dong C, Yoshimura A, et al. CISH Controls Bacterial Burden Early After Infection With Mycobacterium Tuberculosis in Mice. *Tuberculosis (Edinb)* (2017) 107:175–80. doi: 10.1016/j.tube.2017.09.007
28. Nemeth K, Leelahavanichkul A, Yuen PS, Mayer B, Parmelee A, Doi K, et al. Bone Marrow Stromal Cells Attenuate Sepsis *via* Prostaglandin E(2)-Dependent Reprogramming of Host Macrophages to Increase Their Interleukin-10 Production. *Nat Med* (2009) 15(1):42–9. doi: 10.1038/nm.1905
29. Zhao J, Xie F, Chen R, Zhang Z, Dai R, Zhao N, et al. Transcription Factor NF-KappaB Promotes Acute Lung Injury *via* MicroRNA-99b-Mediated PRDM1 Down-Regulation. *J Biol Chem* (2020) 295(52):18638–48. doi: 10.1074/jbc.RA120.014861
30. Vettorazzi S, Bode C, Dejager L, Frappart L, Shelest E, Klassen C, et al. Glucocorticoids Limit Acute Lung Inflammation in Concert With Inflammatory Stimuli by Induction of Sphk1. *Nat Commun* (2015) 6:7796. doi: 10.1038/ncomms8796
31. Gong H, Rehman J, Tang H, Wary K, Mittal M, Chaturvedi P, et al. HIF2alpha Signaling Inhibits Adherens Junctional Disruption in Acute Lung Injury. *J Clin Invest* (2015) 125(2):652–64. doi: 10.1172/JCI77701
32. Eckle T, Fullbier L, Wehrmann M, Khoury J, Mittelbronn M, Ibla J, et al. Identification of Ectonucleotidases CD39 and CD73 in Innate Protection During Acute Lung Injury. *J Immunol* (2007) 178(12):8127–37. doi: 10.4049/jimmunol.178.12.8127
33. Cheng KT, Xiong S, Ye Z, Hong Z, Di A, Tsang KM, et al. Caspase-11-Mediated Endothelial Pyroptosis Underlies Endotoxemia-Induced Lung Injury. *J Clin Invest* (2017) 127(11):4124–35. doi: 10.1172/JCI94495
34. Goenka S, Kaplan MH. Transcriptional Regulation by STAT6. *Immunol Res* (2011) 50(1):87–96. doi: 10.1007/s12026-011-8205-2
35. Ji S, Wang L. Mu-Opioid Receptor Signalling *via* PI3K/Akt Pathway Ameliorates Lipopolysaccharide-Induced Acute Respiratory Distress Syndrome. *Exp Physiol* (2019) 104(10):1555–61. doi: 10.1113/EP087783
36. Andreakos E, Sacre SM, Smith C, Lundberg A, Kiriakidis S, Stonehouse T, et al. Distinct Pathways of LPS-Induced NF-Kappa B Activation and Cytokine Production in Human Myeloid and Nonmyeloid Cells Defined by Selective Utilization of Myd88 and Mal/TIRAP. *Blood* (2004) 103(6):2229–37. doi: 10.1182/blood-2003-04-1356
37. Hammaker D, Boyle DL, Topolewski K, Firestein GS. Differential Regulation of Anti-Inflammatory Genes by P38 MAP Kinase and MAP Kinase Kinase 6. *J Inflamm (Lond)* (2014) 11:14. doi: 10.1186/1476-9255-11-14
38. Xia MZ, Liang YL, Wang H, Chen X, Huang YY, Zhang ZH, et al. Melatonin Modulates TLR4-Mediated Inflammatory Genes Through Myd88- and TRIF-Dependent Signaling Pathways in Lipopolysaccharide-Stimulated RAW264.7 Cells. *J Pineal Res* (2012) 53(4):325–34. doi: 10.1111/j.1600-079X.2012.01002.x
39. Stearns-Kurosawa DJ, Osuchowski MF, Valentine C, Kurosawa S, Remick DG. The Pathogenesis of Sepsis. *Annu Rev Pathol* (2011) 6:19–48. doi: 10.1146/annurev-pathol-011110-130327
40. Guo W, Liu W, Chen Z, Gu Y, Peng S, Shen L, et al. Tyrosine Phosphatase SHP2 Negatively Regulates NLRP3 Inflammasome Activation *via* ANT1-Dependent Mitochondrial Homeostasis. *Nat Commun* (2017) 8(1):2168. doi: 10.1038/s41467-017-02351-0
41. Shah RJ, Wickersham N, Lederer DJ, Palmer SM, Cantu E, Diamond JM, et al. Preoperative Plasma Club (Clara) Cell Secretory Protein Levels Are Associated With Primary Graft Dysfunction After Lung Transplantation. *Am J Transplant* (2014) 14(2):446–52. doi: 10.1111/ajt.12541
42. Meng J, Jiang SJ, Jiang D, Zhao Y. Butorphanol Attenuates Inflammation *via* Targeting NF-KappaB in Septic Rats With Brain Injury. *Eur Rev Med Pharmacol Sci* (2019) 23(3 Suppl):161–70. doi: 10.26355/eurrev_201908_18643
43. Feng L, Song P, Zhou H, Li A, Ma Y, Zhang X, et al. Pentamethoxyflavanone Regulates Macrophage Polarization and Ameliorates Sepsis in Mice. *Biochem Pharmacol* (2014) 89(1):109–18. doi: 10.1016/j.bcp.2014.02.016
44. Day J, Friedman A, Schlesinger LS. Modeling the Immune Rheostat of Macrophages in the Lung in Response to Infection. *Proc Natl Acad Sci USA* (2009) 106(27):11246–51. doi: 10.1073/pnas.0904846106
45. Martinez FO, Helming L, Gordon S. Alternative Activation of Macrophages: An Immunologic Functional Perspective. *Annu Rev Immunol* (2009) 27:451–83. doi: 10.1146/annurev.immunol.021908.132532

46. Grace PM, Ramos KM, Rodgers KM, Wang X, Hutchinson MR, Lewis MT, et al. Activation of Adult Rat CNS Endothelial Cells by Opioid-Induced Toll-Like Receptor 4 (TLR4) Signaling Induces Proinflammatory, Biochemical, Morphological, and Behavioral Sequelae. *Neuroscience* (2014) 280:299–317. doi: 10.1016/j.neuroscience.2014.09.020
47. Roy S, Cain KJ, Chapin RB, Charboneau RG, Barke RA. Morphine Modulates NF Kappa B Activation in Macrophages. *Biochem Biophys Res Commun* (1998) 245(2):392–6. doi: 10.1006/bbrc.1998.8415
48. Welters ID, Menzebach A, Goumon Y, Cadet P, Menges T, Hughes TK, et al. Morphine Inhibits NF-KappaB Nuclear Binding in Human Neutrophils and Monocytes by a Nitric Oxide-Dependent Mechanism. *Anesthesiology* (2000) 92(6):1677–84. doi: 10.1097/00000542-200006000-00027
49. Taniguchi K, Karin M. NF-KappaB, Inflammation, Immunity and Cancer: Coming of Age. *Nat Rev Immunol* (2018) 18(5):309–24. doi: 10.1038/nri.2017.142
50. Christian F, Smith EL, Carmody RJ. The Regulation of NF-Kappab Subunits by Phosphorylation. *Cells* (2016) 5(1):12. doi: 10.3390/cells5010012
51. Li D, Wang X, Huang Q, Li S, Zhou Y, Li Z. Cardioprotection of CAPE-Ono2 Against Myocardial Ischemia/Reperfusion Induced ROS Generation *via* Regulating the SIRT1/eNOS/NF-KappaB Pathway *In Vivo* and *In Vitro*. *Redox Biol* (2018) 15:62–73. doi: 10.1016/j.redox.2017.11.023

Conflict of Interest: The authors declare that the research was conducted in the absence of any commercial or financial relationships that could be construed as a potential conflict of interest.

Copyright © 2021 Luan, Pan, Bu, Wu, Wang and Xu. This is an open-access article distributed under the terms of the Creative Commons Attribution License (CC BY). The use, distribution or reproduction in other forums is permitted, provided the original author(s) and the copyright owner(s) are credited and that the original publication in this journal is cited, in accordance with accepted academic practice. No use, distribution or reproduction is permitted which does not comply with these terms.

frontiers in Immunology

MINI REVIEW
published: 12 July 2021
doi: 10.3389/fimmu.2021.714042

Prostanoids and Resolution of Inflammation – Beyond the Lipid-Mediator Class Switch

Tobias Schmid[1*] *and Bernhard Brüne*[1,2,3,4]

[1] *Institute of Biochemistry I, Faculty of Medicine, Goethe-University Frankfurt, Frankfurt, Germany,* [2] *German Cancer Consortium (DKTK) Partner Site Frankfurt, Frankfurt, Germany,* [3] *Frankfurt Cancer Institute, Goethe-University Frankfurt, Frankfurt, Germany,* [4] *Fraunhofer Institute for Translational Medicine and Pharmacology ITMP, Frankfurt, Germany*

Bioactive lipid mediators play a major role in regulating inflammatory processes. Herein, early pro-inflammatory phases are characterized and regulated by prostanoids and leukotrienes, whereas specialized pro-resolving mediators (SPM), including lipoxins, resolvins, protectins, and maresins, dominate during the resolution phase. While pro-inflammatory properties of prostanoids have been studied extensively, their impact on later phases of the inflammatory process has been attributed mainly to their ability to initiate the lipid-mediator class switch towards SPM. Yet, there is accumulating evidence that prostanoids directly contribute to the resolution of inflammation and return to homeostasis. In this mini review, we summarize the current knowledge of the resolution-regulatory properties of prostanoids and discuss potential implications for anti-inflammatory, prostanoid-targeted therapeutic interventions.

Keywords: prostaglandin, prostacyclin, thromboxane, specialized pro-resolving mediator, inflammation, resolution, macrophage

OPEN ACCESS

Edited by:
Amiram Ariel,
University of Haifa, Israel

Reviewed by:
Eoin Brennan,
University College Dublin, Ireland
Valerio Chiurchiù,
Italian National Research Council, Italy

***Correspondence:**
Tobias Schmid
t.schmid@biochem.uni-frankfurt.de

Specialty section:
This article was submitted to Inflammation, a section of the journal Frontiers in Immunology

Received: *24 May 2021*
Accepted: *30 June 2021*
Published: *12 July 2021*

Citation:
Schmid T and Brüne B (2021) Prostanoids and Resolution of Inflammation – Beyond the Lipid-Mediator Class Switch. Front. Immunol. 12:714042. doi: 10.3389/fimmu.2021.714042

INTRODUCTION

Inflammation is an integral part of protective host responses against pathogens or injury (1). Herein, inflammatory processes usually follow a defined sequence of reactions characterized by the rapid induction of a pro-inflammatory response, which is closely followed by an anti-inflammatory response. To regain homeostasis resolution of inflammation represents an integral and crucial part of acute inflammation. In fact, failure to completely resolve inflammatory processes is associated with the emergence of chronic inflammatory conditions. While resolution was considered to merely represent the downregulation or inactivation of inflammatory mediators for a long time, it is now appreciated to be active and complex, involving the formation of pro-resolving mediators (2). Moreover, it is widely accepted that resolution processes are initiated early during inflammation, and classical pro-inflammatory mediators have been shown to directly impact on resolution as well (3). Therefore, pro-resolving therapeutic approaches are increasingly being considered rather than anti-inflammatory ones as the latter might diminish the host response against pathogenic challenges (4, 5). Since lipid mediators play a crucial, yet often ambivalent role during the inflammatory process, and prostanoid synthesis represents a major target for anti-inflammatory therapies, the present mini review aims to recapitulate the current understanding of the role of prostanoids in the context of resolution of inflammation.

THE COURSE OF INFLAMMATION

Cellular Mediators

Upon an insult (e.g., pathogen contact, injury) local resident immune cells are the first responders. Among these, tissue resident macrophages (MΦ) represent not only an important first line of defense but even more importantly they establish an environment prone to recruit neutrophils and monocytes from the circulation. Neutrophils are main executers in the acute inflammatory environment, i.e. they produce high amounts of reactive oxygen and nitrogen species to eliminate pathogens, and secrete a plethora of inflammatory mediators (6). Within the inflammatory environment neutrophils rapidly die by apoptotic processes and are phagocytosed by MΦ in a process termed efferocytosis (7, 8). Importantly, uptake of apoptotic cells (AC) induces a shift in MΦ polarization from a pro-inflammatory to an anti-inflammatory and immunomodulatory phenotype (9–14). MΦ and other antigen-presenting cells such as dendritic cells (DC) eventually activate adaptive immune responses, which ensures complete removal of the invading pathogens and enables accelerated responses upon anew contact to the triggering stimulus (15). The return to cellular homeostasis further requires successful emigration of infiltrated immune cells from the cleared site of inflammation (16). In contrast to the concept of a rapid return to homeostasis, recent reports provided evidence that resolution is followed by a longer lasting, immune-suppressive post-resolution phase characterized by infiltrating regulatory T cells (Treg) and myeloid-derived suppressor cells (MDSC), but also MΦ, which might be decisive for a successful adaptation vs. chronic inflammation and/or autoimmunity (17–19).

Lipid Mediators

Regulation and execution of inflammatory reactions is mediated by soluble mediators, such as cytokines and chemokines. In addition, bioactive lipids emerged as crucial factors during all phases of the inflammatory process (20, 21). Specifically, while leukotrienes and prostaglandins appear early during the onset of inflammation, specialized pro-resolving mediators (SPM), such as lipoxins, resolvins, and maresins, are produced later on, facilitating the resolution of inflammation (22). Prostanoids, like leukotrienes, belong to the eicosanoid family of lipid mediators (23). Both classes are synthesized from arachidonic acid (AA) after the latter is released from membrane phospholipids by phospholipase A_2 (24). While leukotrienes are synthesized by the lipoxygenases, prostanoid formation initially requires conversion of AA to the unstable prostaglandin H_2 (PGH_2) *via* the bifunctional cyclooxygenases 1 (Cox-1) and 2 (25, 26). In line with the established pro-inflammatory function of the prostanoids, the cyclooxgenases became an important target in the therapy of inflammatory diseases, and as of today, non-steroidal anti-inflammatory drugs (NSAIDs) rank amongst the most important anti-inflammatory drugs (27, 28). Of note, while Cox-1 is constitutively expressed in most cells, Cox-2 often is inducible and emerged as the more important cyclooxygenase in the context of inflammation. Consequently Cox inhibitors (Coxibs) selectively targeting Cox-2 emerged as promising novel anti-inflammatory therapeutics (29, 30). The short-lived Cox product PGH_2 is then substrate to specific synthases, which produce potent prostanoids including PGD_2, PGE_2, $PGF_{2\alpha}$, and PGI_2, as well as thromboxane A_2 (TXA_2) (**Figure 1**).

Interestingly, the production of the different lipid mediators appears to be tightly connected across the course of inflammation. For example, the presumably pro-inflammatory PGE_2 was shown to attenuate the synthesis of leukotrienes and to induce the production of SPM, thus initiating the so-called lipid-mediator class switch (31). While the SPM-regulatory impact of prostanoids on the resolution of inflammation is rather well characterized, there is accumulating evidence that prostanoids also directly impinge on other aspects of the resolution process. In the following sections, we will therefore summarize the current understanding of the role of the most prominent prostanoids in resolution of inflammation, aside from the aforementioned lipid-mediator class switch, with a special focus on PGE_2.

PROSTANOIDS IN THE RESOLUTION OF INFLAMMATION

Thromboxane A_2

TXA_2 is predominantly produced by platelets, but also at appreciable amounts by MΦ (32). Interestingly, while thromboxane A synthase (TXAS) appears to be coupled to the activity of Cox-1 and Cox-2 constitutes the dominant Cox in inflammatory conditions, the activity of TXA_2 is largely pro-inflammatory (33, 34). In fact, there is little evidence that TXA_2 might contribute to the resolution of inflammation. In line, Kupffer cell-derived TXA_2 was shown to contribute to liver fibrosis, a common outcome of ineffective resolution (35). The observation that TXA_2 synthesis is induced by pro-inflammatory stimuli, while it is suppressed upon inflammatory restimulation (36), further suggest that the prevention of TXA_2, e.g. *via* redirection of Cox-1-provided PGH_2 towards PGE_2 synthesis, might be part of the immune-suppressive environment typical for the post-resolution phase (18).

Prostaglandin I_2 (Prostacyclin)

PGI_2 (prostacyclin) has been characterized as the counterpart of TXA_2 as it inhibits platelet aggregation and acts as a potent vaso- and bronchodilator (37). It is produced primarily by vascular endothelial and smooth muscle cells, yet other cells such as fibroblasts and dendritic cells also synthesize PGI_2 (38). In the context of inflammation, PGI_2 was shown to inhibit LPS-induced expression of pro-inflammatory cytokines in MΦ, DC, $CD4^+$ T cells, and endothelial cells (39–42). PGI_2 further synergizes with anti-inflammatory cytokines interleukin-4 (IL-4) and IL-13 to suppress pro-inflammatory cytokines (43). Along the same lines, PGI_2 receptor (IP) deficient mice displayed stronger allergic inflammation, which was attributable to enhanced Th2 cell function (44). Thus, PGI_2 emerges as a predominant anti-inflammatory mediator, positioning it also as a counterpart of TXA_2 in the context of inflammation.

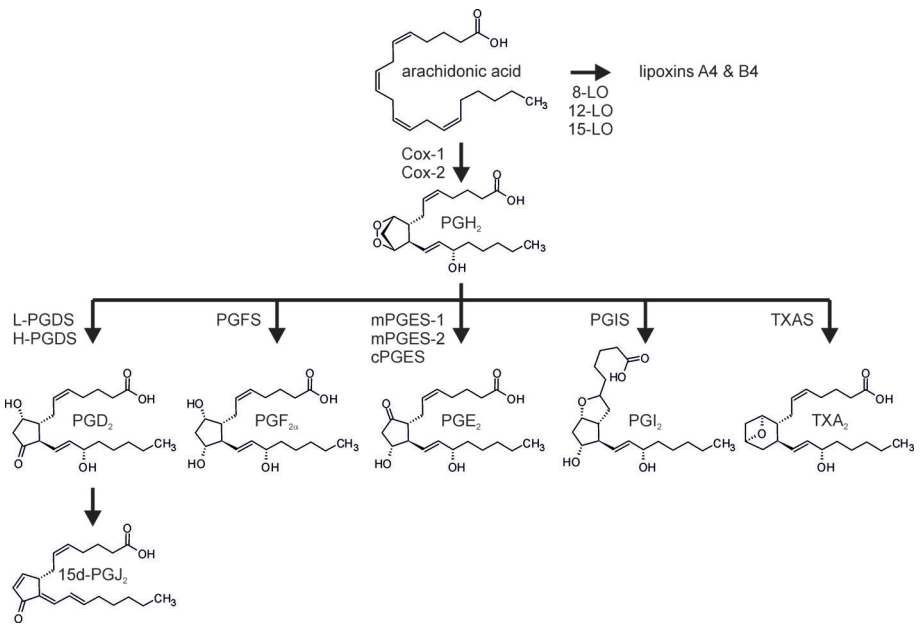

FIGURE 1 | Prostanoid synthesis. Arachidonic acid, liberated from membrane phospholipids by phospholipase A_2, is converted to prostaglandin H_2 (PGH_2) by the dual peroxidase/cyclooxygenase activity of the cyclooxygenases (Cox-1, Cox-2). PGH_2 serves as the substrate for the terminal synthases to produce PGD_2, PGE_2, $PGF_{2\alpha}$, PGI_2, and thromboxane A_2 (TXA_2). PGD_2 is further dehydrated and isomerized spontaneously to 15-deoxy–$\Delta^{12,14}$-PGJ_2 (15d-PGJ_2). Alternatively, arachidonic acid can be converted to lipoxins, i.e. SPM, *via the* activity of the lipoxygenases (LO). L-PGDS, lipocalin-type PGD synthase; H-PGDS, hematopoietic-type PGDS; mPGES, microsomal PGES; cPGES, cytosolic PGES; TXAS, TXA synthase.

Prostaglandin D_2

PGD_2 is produced by numerous immune cells including activated MΦ, DC, Th2 cells, eosinophils, platelets, but also endothelial cells (45). However, since its main source are mast cells (46, 47), PGD_2 has been characterized extensively in the context of allergic reactions (48). PGD_2 can further be metabolized to the cyclopentenone, PGJ_2-type prostanoids, including PGJ_2 and 15d-PGJ_2, which also display biological activity in the context of resolution of inflammation (49). PGD_2 binds to the PGD_2 receptors 1 (DP1) and DP2 [also known as chemoattractant receptor-homologous molecule expressed on Th2 cells (CRTH2)] (50). Activation of DP2 is of specific importance in allergic inflammation, where mast cell-derived PGD_2 stimulates the recruitment of innate lymphoid type 2 cells (51) and Th2 cells (52), and causes activation of these as well as of basophils and eosinophils (53). While PGD_2 was shown to contribute to allergic inflammation, PGD_2 synthase (PGDS) decreases during the acute inflammatory phase, while it rises again at later stages corresponding to the resolution phase in animal models (54). PGD_2 and 15d-PGJ_2 both exert pro-inflammatory functions *via* CRTH2 (55). In contrast, PGD_2-dependent activation of DP1 as well as 15d-PGJ_2-mediated activation of peroxisome proliferator-activated receptor γ (PPARγ) inhibit the production of inflammatory cytokines and chemokines by antigen-presenting cells including DC or MΦ by interfering with inflammatory transcription factors nuclear factor kappa B (NFκB), activator protein 1 (AP1), and signal transducer and activator of transcription 3 (STAT3) (56–58) and additionally by enhancing the activity of anti-inflammatory nuclear factor erythroid 2-like 2 (Nrf2) (59, 60). Consequently, PGD_2 and 15d-PGJ_2 support emigration of MΦ to the draining lymph nodes and attenuate the recruitment of leukocytes (54). They further inhibit effector functions of and induce apoptosis in T lymphocytes (57). Thus, PGD_2 contributes to normalize the local environment, an important aspect of the resolution of inflammation (61).

Prostaglandin $F_{2\alpha}$

$PGF_{2\alpha}$ is produced by the aldo-keto reductase (AKR) 1C3, also known as $PGF_{2\alpha}$ synthase (PGFS) using PGH_2 or PGD_2 (62). Alternatively, PGE_2 can be converted to $PGF_{2\alpha}$ by AKR1C1 or AKR1C2 (63). While $PGF_{2\alpha}$ is synthesized in most tissues (64), its prime site of production is the female reproductive system (65), where $PGF_{2\alpha}$ has been shown to be of functional importance (66, 67). Nevertheless, $PGF_{2\alpha}$ also appears to be involved in inflammatory processes (64, 68). $PGF_{2\alpha}$ is elevated in rheumatoid arthritis (69) and was shown to contribute to and correlate with fibrosis (70, 71), which is characteristic for insufficient resolution. Interestingly though, PGFS expression and concomitantly $PGF_{2\alpha}$ levels decrease similar to PGD_2 during acute inflammation, only to increase again in the resolution phase (72), which might be indicative for an active role of $PGF_{2\alpha}$ in the resolution of inflammation. Yet, the exact role of $PGF_{2\alpha}$ in inflammation-resolving processes remains to be determined.

Prostaglandin E_2

The best characterized and presumably most important prostanoid in the context of inflammation is PGE_2. It can be

synthesized by all cell types. In the context of inflammation the prime producers are fibroblasts, epithelial cells, and immune cells (73). PGE_2 exerts its functions *via* four G-protein-coupled PGE_2 receptors (EP1-4) (74). While EP2 and 4 represent $G\alpha_s$-coupled receptors increasing cAMP levels upon activation (75), the $G\alpha_i$-coupled EP3 variants inhibit adenylate cyclase, thus reducing cAMP (76), and $G\alpha_q$ EP1 enhances intracellular Ca^{2+} levels (74). The distinct downstream signals as well as the cell type-specific distribution of the receptors, and their differential sensitivity for PGE_2 account for the diverse functions of PGE_2 also in inflammation (77).

Upon inflammatory stimulation, both the expression of Cox-2 and microsomal PGE_2 synthase 1 (mPGES-1) are induced in MΦ (78), skewing the prostanoid spectrum towards PGE_2 production in the acute inflammatory phase (73). PGE_2 signals towards enhanced recruitment of neutrophils, MΦ, and mast cells (79–81) and enhances the expression and secretion of pro-inflammatory cytokines in DC, MΦ, and T cells (82–84). Its NFκB-activating properties further support neutrophil survival, thereby extending the pro-inflammatory impact of neutrophils in the inflammatory niche (85, 86). Yet, this initial increase in PGE_2 is only moderate and transient in character, and PGE_2 levels rise again during the resolution phase, eventually increasing to much higher levels in the post-resolution phase (18, 87, 88). This seemingly biphasic regulation of PGE_2 might at least in part be due to a shift from transcriptional to post-transcriptional programs governing not only PGE_2 production, but more generally the course of inflammation (89). With respect to the regulation of PGE_2 synthesis, Cox-2 rapidly accumulates during early inflammation. In a negative feedback loop, elevated PGE_2 induces the expression of dual specificity phosphatase 1 (DUSP1), thereby enhancing the activity of the RNA-binding protein tristetraprolin (TTP), which destabilizes the mRNA of Cox-2, but also of pro-inflammatory tumor necrosis factor (TNF) (90). The second wave of PGE_2 production by MΦ appears to be facilitated by another increase of Cox-2 expression induced by sphingosine-1-phosphate released from apoptotic cells, which activates the RNA-stabilizing protein human antigen R (HuR) in MΦ to increase Cox-2 expression (91). As a side note, while PGE_2 is predominantly produced in a Cox-2/mPGES-1 dependent manner during the inflammatory and early resolution phase, PGE_2 levels during the post-resolution phase are approx. 3-fold higher, which is due to enhanced Cox-1/mPGES-1 expression in MΦ (18). While these findings might explain the kinetics of PGE_2 production and even some of the inhibitory effects of PGE_2 on pro-inflammatory mediators, further evidence for an immunosuppressive function of MΦ-derived PGE_2 emerged in the tumor context, where PGE_2 inhibits CD80 expression *via* EP2, thereby attenuating activation of cytotoxic T cells (92, 93). Similarly, PGE_2 suppresses cytolytic functions of NK cells (94, 95) and inhibits phagocytic and bacteria killing activities of MΦ, thus preventing the establishment of appropriate inflammatory, anti-microbial responses largely *via* EP2-dependent cAMP induction (96–98). In line, EP2- and EP4-signaling limits secretion of TNF and IL-1β, and enhances expression of anti-inflammatory IL-10 in response to LPS by microglia (99), i.e. resident MΦ of the central nervous system (100). In general, EP2- and EP4-activation by PGE_2 appears to be crucial to establish an anti-inflammatory and resolving MΦ phenotype (101, 102), which is characterized by further immune-modulatory factors such as transforming growth factor β (TGFβ) (103). Nevertheless, there are contradictory reports regarding the exact impact of PGE_2 on T cell functions. On the one hand, PGE_2 appears to inhibit IL-2 production by T cells, thereby attenuating both T cell activation and activation-dependent apoptosis (104–106). On the other hand, while PGE_2 appears to contribute to sustained inflammation by differentiation and activation of Th1 and γδ T cells, considered to support inflammation (107–109), other findings indicate that PGE_2 selectively inhibits Th1 cytokine production leaving Th2 cytokines, such as IL-4 and IL-5, unaffected (110, 111), thus provoking a PGE_2-dependent shift towards Th2 responses, which are associated with repair mechanisms instead (112–114). This notion is substantiated by the high levels of PGE_2 observed in Th2-driven diseases such as atopic allergy (115). Indeed, the intricate impact of PGE_2 on the balance between different T cell subtypes might be one of the key mechanisms how PGE_2 affects a self-limiting inflammation throughout resolution and post-resolution phases. Elevated PGE_2 impairs interferon γ (IFN γ) synthesis, thereby directly attenuating Th1 responses, while leaving Th2 responses unaltered (110, 111). PGE_2 further favors Th17 responses *via* EP2 and EP4 by shifting the IL-12/IL-23 balance towards Th17-supportive IL-23 (116–118). While Th17 cells are largely inflammatory in nature contributing to severe inflammatory diseases (107, 119), they have been shown to be highly plastic, being able to trans-differentiate into Treg thereby contributing to resolution of inflammation (120). Yet, PGE_2 not only promotes differentiation of naïve T cells or Th17 cells towards Tregs (121, 122), it also supports further expansion of differentiated Tregs (123). Conclusively, the concentration, source, and timing of PGE_2 appear critical to determine the exact T cell response in the context of inflammatory responses. Moreover, while the pro-resolving activity of cyclooxygenase metabolites has long been attributed predominantly to PGD_2 and 15d-PGJ_2 (124), PGE_2 emerged as an important facilitator of the lipid-mediator class switch inducing not only the production of PGD_2 and its derivatives, but also of the so-called specialized pro-resolving mediators (SPM) (20). SPM, synthesized by 15-lipoxygenase (ALOX15) (31, 125–127), are key players in the resolution of inflammation (114, 128). PGE_2 induces the expression of the relevant lipoxygenases, thereby skewing the balance towards a pro-resolving lipid mediator profile (129, 130). While SPM levels are mostly considered to reciprocally reflect PGE_2 levels during the course of inflammation, they in fact coexist (131). The exact temporal and spatial distribution of both PGE_2 and SPM might eventually determine the course of the resolution of inflammation. Of note, SPM also have been shown to affect the T cell balance (132–134). Yet, there is mounting evidence that PGE_2 also directly supports further resolution-associated functions. Along these lines, PGE_2 has been shown to inhibit pro-inflammatory cytokine production (99, 135) and to stimulate the expression of anti-inflammatory cytokines (136, 137), thereby

contributing to the early steps of the resolution process (138). Furthermore, blocking PGE_2 synthesis attenuated efficient resolution in a peritonitis model by preventing the emigration of MΦ from the site of inflammation in a CX3CL1-dependent manner (87). Extending beyond its impact on the resolution phase, PGE_2 contributes to the immune suppressive post-resolution phase, where PGE_2 suppresses innate immune responses, inhibits lymphocyte functions, and contributes to the generation and activity of Treg (121, 139) and MDSC (140). While these immune suppressive effects appear negative in the context of novel infections, they lower the risk of autoimmune responses (18, 19) (**Figure 2**). The complexity of the resolution of inflammation both at cellular as well as (lipid) mediator level, highlights the need for further studies unraveling details of the resolution phase to allow for the development of refined therapeutic intervention strategies, especially for chronic inflammatory diseases lacking proper resolution mechanisms.

THERAPEUTIC CONSIDERATIONS

Cox inhibitors are amongst the most widely used over the counter anti-inflammatory drugs worldwide (141). Despite the undisputed beneficial effects of the broad spectrum Cox inhibitors, specific Cox-2 inhibitors (Coxibs) were developed to more selectively interfere with the production of inflammation-associated prostanoids (142). Due to the prominent role of PGE_2 in the establishment of inflammatory processes, recent therapeutic approaches aimed at inhibiting the inflammation-associated terminal PGE_2 synthase mPGES-1 to selectively block the production of PGE_2 only (73, 143, 144). Yet, considering the major impact of PGE_2 on successful resolution of inflammation, therapeutic approaches targeting PGE_2 synthesis should be critically revisited as continued PGE_2 inhibition in inflammatory diseases might be expected to lead to chronic diseases due to insufficient resolution. In fact, even attenuating inflammation itself might interfere with successful resolution, since the process of resolution is initiated already very early during the inflammatory process (3). Thus, it might be warranted to focus on therapeutic approaches promoting resolution rather than on anti-inflammatory ones in the future (4, 145). Indeed, there are numerous efforts to target SPM production or receptors (146). Considering promising effects of PGE_2 receptor antagonists (e.g. EP4) in the context of chronic inflammatory diseases (147), it will be interesting to see combinatorial approaches in the future.

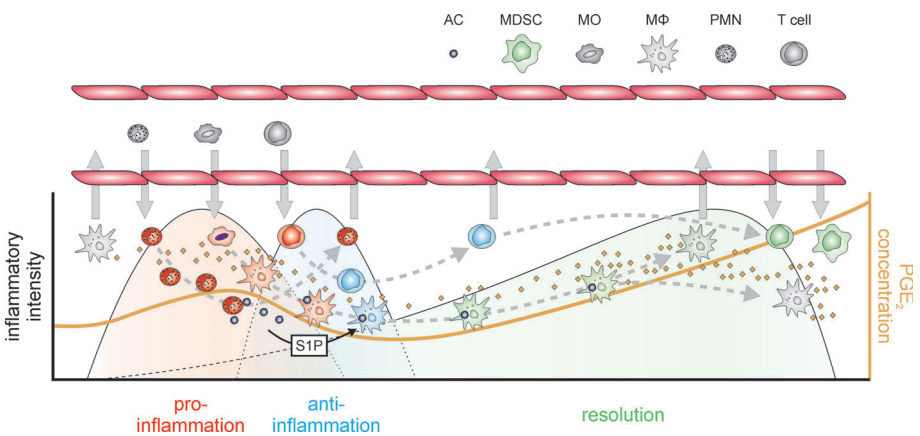

FIGURE 2 | PGE_2 in the context of inflammation. An inflammatory insult is recognized by resident immune cells such as resident MΦ. Upon inflammatory stimulation Cox-2 and mPGES-1 are induced in MΦ resulting in increased PGE_2 synthesis. PGE_2 then contributes to the MΦ-mediated recruitment of neutrophils, which act as a first line of defense to eliminate the pathogenic stimulus and incite further inflammatory responses. Already at this early stage of the inflammatory process PGE_2 initiates the lipid mediator class switch towards the production of specialized pro-resolving mediators (SPM) including lipoxins, resolvins, maresins, and protectins e.g. in neutrophils. Neutrophils are rapidly followed by monocytes again facilitated by PGE_2, which upon infiltration into the affected tissue differentiate into pro-inflammatorily activated MΦ and release soluble mediators including cytokines and chemokines, as well as further PGE_2. PGE_2-triggered transcriptional programs eventually induce post-transcriptional feedback circuits, which reduce Cox-2 mRNA stability and thus protein expression to eventually inhibit PGE_2 production, and also attenuate the expression of pro-inflammatory cytokines such as TNF. In addition, anti-inflammatory mediators (including IL-10) are induced restricting the intensity of the inflammatory reactions. Within the inflammatory niche, activated neutrophils rapidly undergo apoptotic cell death and are phagocytosed by MΦ, which causes a shift in MΦ polarization towards an alternatively activated, immune-modulatory, resolution phenotype characterized by the secretion of e.g. TGFβ. Apoptotic cells further release sphingosine-1-phosphate (S1P), which enhances the mRNA stability of Cox-2 again, resulting in increasing PGE_2 production. Within the resolving environment PGE_2 supports a shift from Th1 T cells to the repair-associated Th2-type further supporting tissue normalization. In addition, PGE_2 attenuates expression of CX3CL1 in MΦ, thereby eventually allowing their emigration from the resolving tissue. PGE_2 further supports the recruitment of T cells and myeloid cells, which differentiate into regulatory T cells and myeloid-derived suppressor cells, respectively, thereby establishing an immune-suppressive post-resolution environment. *Lower part*: During inflammation, PGE_2 levels transiently increase in the acute inflammatory phase. After a decrease during the anti-inflammatory and the early resolution phase, PGE_2 tends to increase again during the progress of resolution, reaching highest levels in the post-resolution phase. AC, apoptotic cells; MΦ, macrophages (gray – naïve, resident; red – pro-inflammatory; blue – anti-inflammatory; green – resolution phase); MDSC, myeloid-derived suppressor cells; MO, monocytes; PMN, neutrophils (gray – naïve, red – inflammatory); T cells (red – Th1; blue – Th2; green – Treg); ⇨, infiltration/emigration; →, development within the inflammatory niche.

AUTHOR CONTRIBUTIONS

TS and BB wrote and edited the manuscript. All authors contributed to the article and approved the submitted version.

FUNDING

This work was supported by grants of the DFG (GRK 2336 TP6, SCHM2663/7, SFB1039 B04).

REFERENCES

1. Medzhitov R. Origin and Physiological Roles of Inflammation. *Nature* (2008) 454(7203):428–35. doi: 10.1038/nature07201
2. Buckley CD, Gilroy DW, Serhan CN, Stockinger B, Tak PP. The Resolution of Inflammation. *Nat Rev Immunol* (2013) 13(1):59–66. doi: 10.1038/nri3362
3. Serhan CN, Savill J. Resolution of Inflammation: The Beginning Programs the End. *Nat Immunol* (2005) 6(12):1191–7. doi: 10.1038/ni1276
4. Fullerton JN, Gilroy DW. Resolution of Inflammation: A New Therapeutic Frontier. *Nat Rev Drug Discov* (2016) 15(8):551–67. doi: 10.1038/nrd.2016.39
5. Dalli J. Does Promoting Resolution Instead of Inhibiting Inflammation Represent the New Paradigm in Treating Infections? *Mol Aspects Med* (2017) 58:12–20. doi: 10.1016/j.mam.2017.03.007
6. Smith JA. Neutrophils, Host Defense, and Inflammation: A Double-Edged Sword. *J Leukoc Biol* (1994) 56(6):672–86. doi: 10.1002/jlb.56.6.672
7. Savill JS, Wyllie AH, Henson JE, Walport MJ, Henson PM, Haslett C. Macrophage Phagocytosis of Aging Neutrophils in Inflammation. Programmed Cell Death in the Neutrophil Leads to its Recognition by Macrophages. *J Clin Invest* (1989) 83(3):865–75. doi: 10.1172/JCI113970
8. Fadok VA, Voelker DR, Campbell PA, Cohen JJ, Bratton DL, Henson PM. Exposure of Phosphatidylserine on the Surface of Apoptotic Lymphocytes Triggers Specific Recognition and Removal by Macrophages. *J Immunol (Baltimore Md: 1950)* (1992) 148(7):2207–16.
9. Fadok VA, Bratton DL, Konowal A, Freed PW, Westcott JY, Henson PM. Macrophages That Have Ingested Apoptotic Cells *In Vitro* Inhibit Proinflammatory Cytokine Production Through Autocrine/Paracrine Mechanisms Involving TGF-Beta, PGE2, and PAF. *J Clin Invest* (1998) 101(4):890–8. doi: 10.1172/JCI1112
10. Johann AM, Knethen Av, Lindemann D, Brüne B. Recognition of Apoptotic Cells by Macrophages Activates the Peroxisome Proliferator-Activated Receptor-Gamma and Attenuates the Oxidative Burst. *Cell Death Differ* (2006) 13(9):1533–40. doi: 10.1038/sj.cdd.4401832
11. Weigert A, Johann AM, Knethen Av, Schmidt H, Geisslinger G, Brüne B. Apoptotic Cells Promote Macrophage Survival by Releasing the Antiapoptotic Mediator Sphingosine-1-Phosphate. *Blood* (2006) 108 (5):1635–42. doi: 10.1182/blood-2006-04-014852
12. Mora J, Schlemmer A, Wittig I, Richter F, Putyrski M, Frank A-C. Et alInterleukin-38 Is Released From Apoptotic Cells to Limit Inflammatory Macrophage Responses. *J Mol Cell Biol* (2016) 8(5):426–38. doi: 10.1093/jmcb/mjw006
13. Kourtzelis I, Li X, Mitroulis I, Grosser D, Kajikawa T, Wang B, et al. DEL-1 Promotes Macrophage Efferocytosis and Clearance of Inflammation. *Nat Immunol* (2019) 20(1):40–9. doi: 10.1038/s41590-018-0249-1
14. Watanabe S, Alexander M, Misharin AV, Budinger GRS. The Role of Macrophages in the Resolution of Inflammation. *J Clin Invest* (2019) 129 (7):2619–28. doi: 10.1172/JCI124615
15. Newson J, Stables M, Karra E, Arce-Vargas F, Quezada S, Motwani M, et al. Resolution of Acute Inflammation Bridges the Gap Between Innate and Adaptive Immunity. *Blood* (2014) 124(11):1748–64. doi: 10.1182/blood-2014-03-562710
16. Sugimoto MA, Sousa LP, Pinho V, Perretti M, Teixeira MM. Resolution of Inflammation: What Controls Its Onset? *Front Immunol* (2016) 7:160. doi: 10.3389/fimmu.2016.00160
17. Rajakariar R, Lawrence T, Bystrom J, Hilliard M, Colville-Nash P, Bellingan G, et al. Novel Biphasic Role for Lymphocytes Revealed During Resolving Inflammation. *Blood* (2008) 111(8):4184–92. doi: 10.1182/blood-2007-08-108936
18. Newson J, Motwani MP, Kendall AC, Nicolaou A, Muccioli GG, Alhouayek M, et al. Inflammatory Resolution Triggers a Prolonged Phase of Immune Suppression Through COX-1/mPGES-1-Derived Prostaglandin E2. *Cell Rep* (2017) 20(13):3162–75. doi: 10.1016/j.celrep.2017.08.098
19. Motwani MP, Newson J, Kwong S, Richard-Loendt A, Colas R, Dalli J, et al. Prolonged Immune Alteration Following Resolution of Acute Inflammation in Humans. *PLoS One* (2017) 12(10):e0186964. doi: 10.1371/journal.pone.0186964
20. Buckley CD, Gilroy DW, Serhan CN. Proresolving Lipid Mediators and Mechanisms in the Resolution of Acute Inflammation. *Immunity* (2014) 40 (3):315–27. doi: 10.1016/j.immuni.2014.02.009
21. Serhan CN, Haeggström JZ, Leslie CC. Lipid Mediator Networks in Cell Signaling: Update and Impact of Cytokines. *FASEB J* (1996) 10(10):1147–58. doi: 10.1096/fasebj.10.10.8751717
22. Serhan CN, Chiang N, Dalli J, Levy BD. Lipid Mediators in the Resolution of Inflammation. *Cold Spring Harb Perspect Biol* (2015) 7(2):a016311. doi: 10.1101/cshperspect.a016311
23. Korotkova M, Jakobsson P-J. Persisting Eicosanoid Pathways in Rheumatic Diseases. *Nat Rev Rheumatol* (2014) 10(4):229–41. doi: 10.1038/nrrheum.2014.1
24. Dennis EA. Phospholipase A2 in Eicosanoid Generation. *Am J Respir Crit Care Med* (2000) 161(2 Pt 2):S32–5. doi: 10.1164/ajrccm.161.supplement_1.ltta-7
25. Samuelsson B, Granström E, Green K, Hamberg M, Hammarström S. Prostaglandins. *Annu Rev Biochem* (1975) 44:669–95. doi: 10.1146/annurev.bi.44.070175.003321
26. Dubois RN, Abramson SB, Crofford L, Gupta RA, Simon LS, van de Putte LB, et al. Cyclooxygenase in Biology and Disease. *FASEB J* (1998) 12 (12):1063–73. doi: 10.1096/fasebj.12.12.1063
27. Rainsford KD. Anti-Inflammatory Drugs in the 21st Century. *Subcell Biochem* (2007) 42:3–27. doi: 10.1007/1-4020-5688-5_1
28. Bacchi S, Palumbo P, Sponta A, Coppolino MF. Clinical Pharmacology of non-Steroidal Anti-Inflammatory Drugs: A Review. *Antiinflamm Antiallergy Agents Med Chem* (2012) 11(1):52–64. doi: 10.2174/187152312803476255
29. Mazaleuskaya LL, Ricciotti E. Druggable Prostanoid Pathway. *Adv Exp Med Biol* (2020) 1274:29–54. doi: 10.1007/978-3-030-50621-6_3
30. Ferrer MD, Busquets-Cortés C, Capó X, Tejada S, Tur JA, Pons A, et al. Cyclooxygenase-2 Inhibitors as a Therapeutic Target in Inflammatory Diseases. *Curr Med Chem* (2019) 26(18):3225–41. doi: 10.2174/0929867325666180514112124
31. Levy BD, Clish CB, Schmidt B, Gronert K, Serhan CN. Lipid Mediator Class Switching During Acute Inflammation: Signals in Resolution. *Nat Immunol* (2001) 2(7):612–9. doi: 10.1038/89759
32. Ricciotti E, FitzGerald GA. Prostaglandins and Inflammation. *Arterioscler Thromb Vasc Biol* (2011) 31(5):986–1000. doi: 10.1161/ATVBAHA.110.207449
33. Kobayashi T, Tahara Y, Matsumoto M, Iguchi M, Sano H, Murayama T, et al. Roles of Thromboxane A2 and Prostacyclin in the Development of Atherosclerosis in apoE-Deficient Mice. *J Clin Invest* (2004) 114(6):784–94. doi: 10.1172/JCI200421446
34. Nakahata N. Thromboxane A2: Physiology/Pathophysiology, Cellular Signal Transduction and Pharmacology. *Pharmacol Ther* (2008) 118(1):18–35. doi: 10.1016/j.pharmthera.2008.01.001
35. Miller AM, Masrorpour M, Klaus C, Zhang JX. LPS Exacerbates Endothelin-1 Induced Activation of Cytosolic Phospholipase A2 and Thromboxane A2 Production From Kupffer Cells of the Prefibrotic Rat Liver. *J Hepatol* (2007) 46(2):276–85. doi: 10.1016/j.jhep.2006.08.026
36. Naraba H, Murakami M, Matsumoto H, Shimbara S, Ueno A, Kudo I, et al. Segregated Coupling of Phospholipases A2, Cyclooxygenases, and Terminal Prostanoid Synthases in Different Phases of Prostanoid Biosynthesis in Rat Peritoneal Macrophages. *J Immunol (Baltimore Md: 1950)* (1998) 160(6):2974–82.
37. Camacho M, Rodríguez C, Guadall A, Alcolea S, Orriols M, Escudero J-R, et al. Hypoxia Upregulates PGI-Synthase and Increases PGI_2 Release in Human Vascular Cells Exposed to Inflammatory Stimuli. *J Lipid Res* (2011) 52(4):720–31. doi: 10.1194/jlr.M011007
38. Dorris SL, Peebles RS. PGI2 as a Regulator of Inflammatory Diseases. *Mediators Inflamm* (2012) 2012:926968. doi: 10.1155/2012/926968
39. Luttmann W, Herzog V, Virchow JC, Matthys H, Thierauch KH, Kroegel C. Prostacyclin Modulates Granulocyte/Macrophage Colony-Stimulating Factor Release by Human Blood Mononuclear Cells. *Pulm Pharmacol* (1996) 9(1):43–8. doi: 10.1006/pulp.1996.0005

40. Zhou W, Blackwell TS, Goleniewska K, O'Neal JF, FitzGerald GA, Lucitt M, et al. Prostaglandin I2 Analogs Inhibit Th1 and Th2 Effector Cytokine Production by CD4 T Cells. *J Leukoc Biol* (2007) 81(3):809–17. doi: 10.1189/jlb.0606375
41. Zhou W, Hashimoto K, Goleniewska K, O'Neal JF, Ji S, Blackwell TS, et al. Prostaglandin I2 Analogs Inhibit Proinflammatory Cytokine Production and T Cell Stimulatory Function of Dendritic Cells. *J Immunol (Baltimore Md: 1950)* (2007) 178(2):702–10. doi: 10.4049/jimmunol.178.2.702
42. Di Francesco L, Totani L, Dovizio M, Piccoli A, Di Francesco A, Salvatore T, et al. Induction of Prostacyclin by Steady Laminar Shear Stress Suppresses Tumor Necrosis Factor-Alpha Biosynthesis via Heme Oxygenase-1 in Human Endothelial Cells. *Circ Res* (2009) 104(4):506–13. doi: 10.1161/CIRCRESAHA.108.191114
43. Luttmann W, Herzog V, Matthys H, Thierauch KH, Virchow JC, Kroegel C. Modulation of Cytokine Release From Mononuclear Cells by Prostacyclin, IL-4 and IL-13. *Cytokine* (1999) 11(2):127–33. doi: 10.1006/cyto.1998.0410
44. Takahashi Y, Tokuoka S, Masuda T, Hirano Y, Nagao M, Tanaka H, et al. Augmentation of Allergic Inflammation in Prostanoid IP Receptor Deficient Mice. *Br J Pharmacol* (2002) 137(3):315–22. doi: 10.1038/sj.bjp.0704872
45. Marone G, Galdiero MR, Pecoraro A, Pucino V, Criscuolo G, Triassi M, et al. Prostaglandin D2 Receptor Antagonists in Allergic Disorders: Safety, Efficacy, and Future Perspectives. *Expert Opin Investig Drugs* (2019) 28 (1):73–84. doi: 10.1080/13543784.2019.1555237
46. Lewis RA, Soter NA, Diamond PT, Austen KF, Oates JA, Roberts LJ. Prostaglandin D2 Generation After Activation of Rat and Human Mast Cells With Anti-IgE. *J Immunol (Baltimore Md: 1950)* (1982) 129(4):1627–31.
47. Urade Y, Ujihara M, Horiguchi Y, Igarashi M, Nagata A, Ikai K, et al. Mast Cells Contain Spleen-Type Prostaglandin D Synthetase. *J Biol Chem* (1990) 265(1):371–5. doi: 10.1016/S0021-9258(19)40239-1
48. Kupczyk M, Kuna P. Targeting the PGD2/CRTH2/DP1 Signaling Pathway in Asthma and Allergic Disease: Current Status and Future Perspectives. *Drugs* (2017) 77(12):1281–94. doi: 10.1007/s40265-017-0777-2
49. Surh Y-J, Na H-K, Park J-M, Lee H-N, Kim W, Yoon I-S, et al. 15-Deoxy-Δ^{1214};-Prostaglandin J^2, an Electrophilic Lipid Mediator of Anti-Inflammatory and Pro-Resolving Signaling. *Biochem Pharmacol* (2011) 82 (10):1335–51. doi: 10.1016/j.bcp.2011.07.100
50. Pettipher R, Hansel TT, Armer R. Antagonism of the Prostaglandin D2 Receptors DP1 and CRTH2 as an Approach to Treat Allergic Diseases. *Nat Rev Drug Discov* (2007) 6(4):313–25. doi: 10.1038/nrd2266
51. Wojno EDT, Monticelli LA, Tran SV, Alenghat T, Osborne LC, Thome JJ, et al. The Prostaglandin D_2 Receptor CRTH2 Regulates Accumulation of Group 2 Innate Lymphoid Cells in the Inflamed Lung. *Mucosal Immunol* (2015) 8(6):1313–23. doi: 10.1038/mi.2015.21
52. Hirai H, Tanaka K, Yoshie O, Ogawa K, Kenmotsu K, Takamori Y, et al. Prostaglandin D2 Selectively Induces Chemotaxis in T Helper Type 2 Cells, Eosinophils, and Basophils *via* Seven-Transmembrane Receptor CRTH2. *J Exp Med* (2001) 193(2):255–61. doi: 10.1084/jem.193.2.255
53. Nagata K, Hirai H, Tanaka K, Ogawa K, Aso T, Sugamura K, et al. CRTH2, an Orphan Receptor of T-Helper-2-Cells, is Expressed on Basophils and Eosinophils and Responds to Mast Cell-Derived Factor(s). *FEBS Lett* (1999) 459(2):195–9. doi: 10.1016/S0014-5793(99)01251-X
54. Rajakariar R, Hilliard M, Lawrence T, Trivedi S, Colville-Nash P, Bellingan G, et al. Hematopoietic Prostaglandin D2 Synthase Controls the Onset and Resolution of Acute Inflammation Through PGD2 and 15-Deoxydelta12 14 PGJ2. *Proc Natl Acad Sci U S A* (2007) 104(52):20979–84. doi: 10.1073/pnas.0707394104
55. Xue L, Gyles SL, Wettey FR, Gazi L, Townsend E, Hunter MG, et al. Prostaglandin D2 Causes Preferential Induction of Proinflammatory Th2 Cytokine Production Through an Action on Chemoattractant Receptor-Like Molecule Expressed on Th2 Cells. *J Immunol (Baltimore Md: 1950)* (2005) 175(10):6531–6. doi: 10.4049/jimmunol.175.10.6531
56. Herlong JL, Scott TR. Positioning Prostanoids of the D and J Series in the Immunopathogenic Scheme. *Immunol Lett* (2006) 102(2):121–31. doi: 10.1016/j.imlet.2005.10.004
57. Appel S, Mirakaj V, Bringmann A, Weck MM, Grünebach F, Brossart P. PPAR-Gamma Agonists Inhibit Toll-Like Receptor-Mediated Activation of Dendritic Cells *via* the MAP Kinase and NF-kappaB Pathways. *Blood* (2005) 106(12):3888–94. doi: 10.1182/blood-2004-12-4709
58. Jennewein C, Kuhn A-M, Schmidt MV, Meilladec-Jullig V, Knethen Av, Gonzalez FJ, et al. Sumoylation of Peroxisome Proliferator-Activated Receptor Gamma by Apoptotic Cells Prevents Lipopolysaccharide-Induced NCoR Removal From kappaB Binding Sites Mediating Transrepression of Proinflammatory Cytokines. *J Immunol (Baltimore Md: 1950)* (2008) 181 (8):5646–52. doi: 10.4049/jimmunol.181.8.5646
59. Itoh K, Mochizuki M, Ishii Y, Ishii T, Shibata T, Kawamoto Y, et al. Transcription Factor Nrf2 Regulates Inflammation by Mediating the Effect of 15-Deoxy-Delta(12,14)-Prostaglandin J(2). *Mol Cell Biol* (2004) 24(1):36–45. doi: 10.1128/MCB.24.1.36-45.2004
60. Kuhn A-M, Tzieply N, Schmidt MV, Knethen Av, Namgaladze D, Yamamoto M, et al. Antioxidant Signaling *via* Nrf2 Counteracts Lipopolysaccharide-Mediated Inflammatory Responses in Foam Cell Macrophages. *Free Radic Biol Med* (2011) 50(10):1382–91. doi: 10.1016/j.freeradbiomed.2011.02.036
61. Burstein SH. The Chemistry, Biology and Pharmacology of the Cyclopentenone Prostaglandins. *Prostaglandins other Lipid Mediators* (2020) 148:106408. doi: 10.1016/j.prostaglandins.2020.106408
62. Suzuki-Yamamoto T, Nishizawa M, Fukui M, Okuda-Ashitaka E, Nakajima T, Ito S, et al. cDNA Cloning, Expression and Characterization of Human Prostaglandin F Synthase. *FEBS Lett* (1999) 462(3):335–40. doi: 10.1016/S0014-5793(99)01551-3
63. Nishizawa M, Nakajima T, Yasuda K, Kanzaki H, Sasaguri Y, Watanabe K, et al. Close Kinship of Human 20alpha-Hydroxysteroid Dehydrogenase Gene With Three Aldo-Keto Reductase Genes. *Genes Cells* (2000) 5(2):111–25. doi: 10.1046/j.1365-2443.2000.00310.x
64. Basu S. Novel Cyclooxygenase-Catalyzed Bioactive Prostaglandin F2alpha From Physiology to New Principles in Inflammation. *Med Res Rev* (2007) 27 (4):435–68. doi: 10.1002/med.20098
65. Hao C-M, Breyer MD. Physiological Regulation of Prostaglandins in the Kidney. *Annu Rev Physiol* (2008) 70:357–77. doi: 10.1146/annurev.physiol.70.113006.100614
66. Poyser NL. The Control of Prostaglandin Production by the Endometrium in Relation to Luteolysis and Menstruation. *Prostaglandins Leukot Essential Fatty Acids* (1995) 53(3):147–95. doi: 10.1016/0952-3278(95)90115-9
67. Sugimoto Y, Yamasaki A, Segi E, Tsuboi K, Aze Y, Nishimura T, et al. Failure of Parturition in Mice Lacking the Prostaglandin F Receptor. *Science (New York N Y)* (1997) 277(5326):681–3. doi: 10.1126/science.277.5326.681
68. Basu S. Bioactive Eicosanoids: Role of Prostaglandin F(2α) and F_2-Isoprostanes in Inflammation and Oxidative Stress Related Pathology. *Mol Cells* (2010) 30(5):383–91. doi: 10.1007/s10059-010-0157-1
69. Basu S, Whiteman M, Mattey DL, Halliwell B. Raised Levels of F(2)-Isoprostanes and Prostaglandin F(2alpha) in Different Rheumatic Diseases. *Ann Rheum Dis* (2001) 60(6):627–31. doi: 10.1136/ard.60.6.627
70. Oga T, Matsuoka T, Yao C, Nonomura K, Kitaoka S, Sakata D, et al. Prostaglandin F(2alpha) Receptor Signaling Facilitates Bleomycin-Induced Pulmonary Fibrosis Independently of Transforming Growth Factor-Beta. *Nat Med* (2009) 15(12):1426–30. doi: 10.1038/nm.2066
71. Aihara K, Handa T, Oga T, Watanabe K, Tanizawa K, Ikezoe K, et al. Clinical Relevance of Plasma Prostaglandin F2α Metabolite Concentrations in Patients With Idiopathic Pulmonary Fibrosis. *PLoS One* (2013) 8(6): e66017. doi: 10.1371/journal.pone.0066017
72. Colville-Nash PR, Gilroy DW, Willis D, Paul-Clark MJ, Moore AR, Willoughby DA. Prostaglandin F2alpha Produced by Inducible Cyclooxygenase may Contribute to the Resolution of Inflammation. *Inflammopharmacology* (2005) 12(5-6):473–6; discussion 477-80. doi: 10.1163/156856005774382616
73. Park JY, Pillinger MH, Abramson SB. Prostaglandin E2 Synthesis and Secretion: The Role of PGE2 Synthases. *Clin Immunol (Orlando Fla)* (2006) 119(3):229–40. doi: 10.1016/j.clim.2006.01.016
74. Hata AN, Breyer RM. Pharmacology and Signaling of Prostaglandin Receptors: Multiple Roles in Inflammation and Immune Modulation. *Pharmacol Ther* (2004) 103(2):147–66. doi: 10.1016/j.pharmthera.2004.06.003
75. Fujino H, Salvi S, Regan JW. Differential Regulation of Phosphorylation of the cAMP Response Element-Binding Protein After Activation of EP2 and EP4 Prostanoid Receptors by Prostaglandin E2. *Mol Pharmacol* (2005) 68 (1):251–9. doi: 10.1124/mol.105.011833
76. Yang J, Xia M, Goetzl EJ, An S. Cloning and Expression of the EP3-Subtype of Human Receptors for Prostaglandin E2. *Biochem Biophys Res Commun* (1994) 198(3):999–1006. doi: 10.1006/bbrc.1994.1142

77. Tsuge K, Inazumi T, Shimamoto A, Sugimoto Y. Molecular Mechanisms Underlying Prostaglandin E2-Exacerbated Inflammation and Immune Diseases. *Int Immunol* (2019) 31(9):597–606. doi: 10.1093/intimm/dxz021
78. Claveau D, Sirinyan M, Guay J, Gordon R, Chan C-C, Bureau Y, et al. Microsomal Prostaglandin E Synthase-1 is a Major Terminal Synthase That is Selectively Up-Regulated During Cyclooxygenase-2-Dependent Prostaglandin E2 Production in the Rat Adjuvant-Induced Arthritis Model. *J Immunol (Baltimore Md: 1950)* (2003) 170(9):4738–44. doi: 10.4049/jimmunol.170.9.4738
79. Yu Y, Chadee K. Prostaglandin E2 Stimulates IL-8 Gene Expression in Human Colonic Epithelial Cells by a Posttranscriptional Mechanism. *J Immunol (Baltimore Md: 1950)* (1998) 161(7):3746–52.
80. Weller CL, Collington SJ, Hartnell A, Conroy DM, Kaise T, Barker JE, et al. Chemotactic Action of Prostaglandin E2 on Mouse Mast Cells Acting via the PGE2 Receptor 3. *Proc Natl Acad Sci U S A* (2007) 104(28):11712–7. doi: 10.1073/pnas.0701700104
81. Treutlein E-M, Kern K, Weigert A, Tarighi N, Schuh C-D, Nüsing RM, et al. The Prostaglandin E2 Receptor EP3 Controls CC-Chemokine Ligand 2-Mediated Neuropathic Pain Induced by Mechanical Nerve Damage. *J Biol Chem* (2018) 293(25):9685–95. doi: 10.1074/jbc.RA118.002492
82. Sheibanie AF, Yen J-H, Khayrullina T, Emig F, Zhang M, Tuma R, et al. The Proinflammatory Effect of Prostaglandin E2 in Experimental Inflammatory Bowel Disease is Mediated Through the IL-23–IL-17 Axis. *J Immunol (Baltimore Md: 1950)* (2007) 178(12):8138–47. doi: 10.4049/jimmunol.178.12.8138
83. Raucci F, Saviano A, Casillo GM, Guerra-Rodriguez M, Mansour AA, Piccolo M, et al. IL-17-Induced Inflammation Modulates the mPGES-1/PPAR-γ Pathway in Monocytes/Macrophages. *Br J Pharmacol* (2021). doi: 10.1111/bph.15413
84. Schiffmann S, Weigert A, Männich J, Eberle M, Birod K, Häussler A, et al. PGE2/EP4 Signaling in Peripheral Immune Cells Promotes Development of Experimental Autoimmune Encephalomyelitis. *Biochem Pharmacol* (2014) 87(4):625–35. doi: 10.1016/j.bcp.2013.12.006
85. Poligone B, Baldwin AS. Positive and Negative Regulation of NF-kappaB by COX-2: Roles of Different Prostaglandins. *J Biol Chem* (2001) 276 (42):38658–64. doi: 10.1074/jbc.M106599200
86. Ward C, Walker A, Dransfield I, Haslett C, Rossi AG. Regulation of Granulocyte Apoptosis by NF-Kappab. *Biochem Soc Trans* (2004) 32 (Pt3):465–7. doi: 10.1042/bst0320465
87. Rappl P, Rösser S, Maul P, Bauer R, Huard A, Schreiber Y, et al. Inhibition of mPGES-1 Attenuates Efficient Resolution of Acute Inflammation by Enhancing CX3CL1 Expression. *Cell Death Dis* (2021) 12(2):135. doi: 10.1038/s41419-021-03423-2
88. Gilroy DW, Colville-Nash PR, Willis D, Chivers J, Paul-Clark MJ, Willoughby DA. Inducible Cyclooxygenase may Have Anti-Inflammatory Properties. *Nat Med* (1999) 5(6):698–701. doi: 10.1038/9550
89. Rappl P, Brüne B, Schmid T. Role of Tristetraprolin in the Resolution of Inflammation. *Biology (Basel)* (2021) 10(1):66. doi: 10.3390/biology10010066
90. Tang T, Scambler TE, Smallie T, Cunliffe HE, Ross EA, Rosner DR, et al. Macrophage Responses to Lipopolysaccharide are Modulated by a Feedback Loop Involving Prostaglandin E2, Dual Specificity Phosphatase 1 and Tristetraprolin. *Sci Rep* (2017) 7(1):4350. doi: 10.1038/s41598-017-04100-1
91. Johann AM, Weigert A, Eberhardt W, Kuhn A-M, Barra V, Knethen Av, et al. Apoptotic Cell-Derived Sphingosine-1-Phosphate Promotes HuR-Dependent Cyclooxygenase-2 mRNA Stabilization and Protein Expression. *J Immunol (Baltimore Md: 1950)* (2008) 180(2):1239–48. doi: 10.4049/jimmunol.180.2.1239
92. Sha W, Olesch C, Hanaka H, Rådmark O, Weigert A, Brüne B. Necrosis in DU145 Prostate Cancer Spheroids Induces COX-2/mPGES-1-Derived PGE2 to Promote Tumor Growth and to Inhibit T Cell Activation. *Int J Cancer* (2013) 133(7):1578–88. doi: 10.1002/ijc.28181
93. Olesch C, Sha W, Angioni C, Sha LK, Açaf E, Patrignani P, et al. MPGES-1-Derived PGE2 Suppresses CD80 Expression on Tumor-Associated Phagocytes to Inhibit Anti-Tumor Immune Responses in Breast Cancer. *Oncotarget* (2015) 6(12):10284–96. doi: 10.18632/oncotarget.3581
94. Walker W, Rotondo D. Prostaglandin E2 Is a Potent Regulator of Interleukin-12- and Interleukin-18-Induced Natural Killer Cell Interferon-Gamma Synthesis. *Immunology* (2004) 111(3):298–305. doi: 10.1111/j.1365-2567.2004.01810.x
95. Joshi PC, Zhou X, Cuchens M, Jones Q. Prostaglandin E2 Suppressed IL-15-Mediated Human NK Cell Function Through Down-Regulation of Common Gamma-Chain. *J Immunol (Baltimore Md: 1950)* (2001) 166 (2):885–91. doi: 10.4049/jimmunol.166.2.885
96. Serezani CH, Chung J, Ballinger MN, Moore BB, Aronoff DM, Peters-Golden M. Prostaglandin E2 Suppresses Bacterial Killing in Alveolar Macrophages by Inhibiting NADPH Oxidase. *Am J Respir Cell Mol Biol* (2007) 37(5):562–70. doi: 10.1165/rcmb.2007-0153OC
97. Aronoff DM, Canetti C, Peters-Golden M. Prostaglandin E2 Inhibits Alveolar Macrophage Phagocytosis Through an E-Prostanoid 2 Receptor-Mediated Increase in Intracellular Cyclic AMP. *J Immunol (Baltimore Md: 1950)* (2004) 173(1):559–65. doi: 10.4049/jimmunol.173.1.559
98. O'Brien AJ, Fullerton JN, Massey KA, Auld G, Sewell G, James S, et al. Immunosuppression in Acutely Decompensated Cirrhosis is Mediated by Prostaglandin E2. *Nat Med* (2014) 20(5):518–23. doi: 10.1038/nm.3516
99. Brenneis C, Coste O, Altenrath K, Angioni C, Schmidt H, Schuh C-D, et al. Anti-Inflammatory Role of Microsomal Prostaglandin E Synthase-1 in a Model of Neuroinflammation. *J Biol Chem* (2011) 286(3):2331–42. doi: 10.1074/jbc.M110.157362
100. Ginhoux F, Prinz M. Origin of Microglia: Current Concepts and Past Controversies. *Cold Spring Harb Perspect Biol* (2015) 7(8):a020537. doi: 10.1101/cshperspect.a020537
101. Takayama K, García-Cardena G, Sukhova GK, Comander J, Gimbrone MA, Libby P. Prostaglandin E2 Suppresses Chemokine Production in Human Macrophages Through the EP4 Receptor. *J Biol Chem* (2002) 277(46):44147–54. doi: 10.1074/jbc.M204810200
102. Bystrom J, Evans I, Newson J, Stables M, Toor I, van Rooijen N, et al. Resolution-Phase Macrophages Possess a Unique Inflammatory Phenotype That is Controlled by cAMP. *Blood* (2008) 112(10):4117–27. doi: 10.1182/blood-2007-12-129767
103. Korns D, Frasch SC, Fernandez-Boyanapalli R, Henson PM, Bratton DL. Modulation of Macrophage Efferocytosis in Inflammation. *Front Immunol* (2011) 2:57. doi: 10.3389/fimmu.2011.00057
104. Walker C, Kristensen F, Bettens F, deWeck AL. Lymphokine Regulation of Activated (G1) Lymphocytes. I. Prostaglandin E2-Induced Inhibition of Interleukin 2 Production. *J Immunol (Baltimore Md: 1950)* (1983) 130(4):1770–3.
105. Kolenko V, Rayman P, Roy B, Cathcart MK, O'Shea J, Tubbs R, et al. Downregulation of JAK3 Protein Levels in T Lymphocytes by Prostaglandin E2 and Other Cyclic Adenosine Monophosphate-Elevating Agents: Impact on Interleukin-2 Receptor Signaling Pathway. *Blood* (1999) 93(7):2308–18. doi: 10.1182/blood.V93.7.2308.407k16_2308_2318
106. Porter BO, Malek TR. Prostaglandin E2 Inhibits T Cell Activation-Induced Apoptosis and Fas-Mediated Cellular Cytotoxicity by Blockade of Fas-Ligand Induction. *Eur J Immunol* (1999) 29(7):2360–5. doi: 10.1002/(SICI)1521-4141(199907)29:07<2360::AID-IMMU2360>3.0.CO;2-A
107. Yao C, Sakata D, Esaki Y, Li Y, Matsuoka T, Kuroiwa K, et al. Prostaglandin E2-EP4 Signaling Promotes Immune Inflammation Through Th1 Cell Differentiation and Th17 Cell Expansion. *Nat Med* (2009) 15(6):633–40. doi: 10.1038/nm.1968
108. Yao C, Hirata T, Soontrapa K, Ma X, Takemori H, Narumiya S. Prostaglandin E_2 Promotes Th1 Differentiation *via* Synergistic Amplification of IL-12 Signalling by cAMP and PI3-Kinase. *Nat Commun* (2013) 4:1685. doi: 10.1038/ncomms3315
109. Du B, Zhu M, Li Y, Li G, Xi X. The Prostaglandin E2 Increases the Production of IL-17 and the Expression of Costimulatory Molecules on γδ T Cells in Rheumatoid Arthritis. *Scand J Immunol* (2020) 91(5):e12872. doi: 10.1111/sji.12872
110. Betz M, Fox BS. Prostaglandin E2 Inhibits Production of Th1 Lymphokines But Not of Th2 Lymphokines. *J Immunol (Baltimore Md: 1950)* (1991) 146 (1):108–13.
111. Snijdewint FG, Kaliński P, Wierenga EA, Bos JD, Kapsenberg ML. Prostaglandin E2 Differentially Modulates Cytokine Secretion Profiles of Human T Helper Lymphocytes. *J Immunol (Baltimore Md: 1950)* (1993) 150(12):5321–9.
112. Kalinski P. Regulation of Immune Responses by Prostaglandin E2. *J Immunol (Baltimore Md: 1950)* (2012) 188(1):21–8. doi: 10.4049/jimmunol.1101029
113. Placek K, Schultze JL, Aschenbrenner AC. Epigenetic Reprogramming of Immune Cells in Injury, Repair, and Resolution. *J Clin Invest* (2019) 129 (8):2994–3005. doi: 10.1172/JCI124619

114. Snodgrass RG, Benatzy Y, Schmid T, Namgaladze D, Mainka M, Schebb NH, et al. Efferocytosis Potentiates the Expression of Arachidonate 15-Lipoxygenase (ALOX15) in Alternatively Activated Human Macrophages Through LXR Activation. *Cell Death Differ* (2021) 28(4):1301–16. doi: 10.1038/s41418-020-00652-4
115. Kapsenberg ML, Hilkens CM, Wierenga EA, Kalinski P. The Paradigm of Type 1 and Type 2 Antigen-Presenting Cells. Implications for Atopic Allergy. *Clin Exp Allergy* (1999) 29(Suppl 2):33–6. doi: 10.1046/j.1365-2222.1999.00006.x-i2
116. Khayrullina T, Yen J-H, Jing H, Ganea D. *In Vitro* Differentiation of Dendritic Cells in the Presence of Prostaglandin E2 Alters the IL-12/IL-23 Balance and Promotes Differentiation of Th17 Cells. *J Immunol (Baltimore Md: 1950)* (2008) 181(1):721–35. doi: 10.4049/jimmunol.181.1.721
117. Boniface K, Bak-Jensen KS, Li Y, Blumenschein WM, McGeachy MJ, McClanahan TK, et al. Prostaglandin E2 Regulates Th17 Cell Differentiation and Function Through Cyclic AMP and EP2/EP4 Receptor Signaling. *J Exp Med* (2009) 206(3):535–48. doi: 10.1084/jem.20082293
118. Maseda D, Banerjee A, Johnson EM, Washington MK, Kim H, Lau KS, et al. mPGES-1-Mediated Production of PGE2 and EP4 Receptor Sensing Regulate T Cell Colonic Inflammation. *Front Immunol* (2018) 9:2954. doi: 10.3389/fimmu.2018.02954
119. Maseda D, Johnson EM, Nyhoff LE, Baron B, Kojima F, Wilhelm AJ, et al. Mpges1-Dependent Prostaglandin E2 (PGE2) Controls Antigen-Specific Th17 and Th1 Responses by Regulating T Autocrine and Paracrine PGE2 Production. *J Immunol (Baltimore Md: 1950)* (2018) 200(2):725–36. doi: 10.4049/jimmunol.1601808
120. Gagliani N, Amezcua Vesely MC, Iseppon A, Brockmann L, Xu H, Palm NW, et al. Th17 Cells Transdifferentiate Into Regulatory T Cells During Resolution of Inflammation. *Nature* (2015) 523(7559):221–5. doi: 10.1038/nature14452
121. Baratelli F, Lin Y, Zhu L, Yang S-C, Heuzé-Vourc'h N, Zeng G, et al. Prostaglandin E2 Induces FOXP3 Gene Expression and T Regulatory Cell Function in Human CD4+ T Cells. *J Immunol (Baltimore Md: 1950)* (2005) 175(3):1483–90. doi: 10.4049/jimmunol.175.3.1483
122. Soontrapa K, Honda T, Sakata D, Yao C, Hirata T, Hori S, et al. Prostaglandin E2-Prostaglandin E Receptor Subtype 4 (EP4) Signaling Mediates UV Irradiation-Induced Systemic Immunosuppression. *Proc Natl Acad Sci U S A* (2011) 108(16):6668–73. doi: 10.1073/pnas.1018625108
123. Banerjee DK, Dhodapkar MV, Matayeva E, Steinman RM, Dhodapkar KM. Expansion of FOXP3high Regulatory T Cells by Human Dendritic Cells (DCs) *In Vitro* and After Injection of Cytokine-Matured DCs in Myeloma Patients. *Blood* (2006) 108(8):2655–61. doi: 10.1182/blood-2006-03-011353
124. Willoughby DA, Moore AR, Colville-Nash PR, Gilroy D. Resolution of Inflammation. *Int J Immunopharmacol* (2000) 22(12):1131–5. doi: 10.1016/S0192-0561(00)00064-3
125. Serhan CN, Chiang N, van Dyke TE. Resolving Inflammation: Dual Anti-Inflammatory and Pro-Resolution Lipid Mediators. *Nat Rev Immunol* (2008) 8(5):349–61. doi: 10.1038/nri2294
126. Bannenberg G, Serhan CN. Specialized Pro-Resolving Lipid Mediators in the Inflammatory Response: An Update. *Biochim Biophys Acta* (2010) 1801 (12):1260–73. doi: 10.1016/j.bbalip.2010.08.002
127. Snodgrass RG, Brüne B. Regulation and Functions of 15-Lipoxygenases in Human Macrophages. *Front Pharmacol* (2019) 10:719. doi: 10.3389/fphar.2019.00719
128. Serhan CN, Gupta SK, Perretti M, Godson C, Brennan E, Li Y, et al. The Atlas of Inflammation Resolution (AIR). *Mol Aspects Med* (2020) 74:100894. doi: 10.1101/2020.01.27.921882
129. Mancini AD, Di Battista JA. The Cardinal Role of the Phospholipase A(2)/cyclooxygenase-2/Prostaglandin E Synthase/Prostaglandin E(2) (PCPP) Axis in Inflammostasis. *Inflammation Res* (2011) 60(12):1083–92. doi: 10.1007/s00011-011-0385-7
130. Loynes CA, Lee JA, Robertson AL, Steel MJ, Ellett F, Feng Y, et al. PGE2 Production at Sites of Tissue Injury Promotes an Anti-Inflammatory Neutrophil Phenotype and Determines the Outcome of Inflammation Resolution *In Vivo*. *Sci Adv* (2018) 4(9):eaar8320. doi: 10.1126/sciadv.aar8320
131. Chiurchiù V, Leuti A, Maccarrone M. Bioactive Lipids and Chronic Inflammation: Managing the Fire Within. *Front Immunol* (2018) 9:38. doi: 10.3389/fimmu.2018.00038
132. Chiurchiù V, Leuti A, Dalli J, Jacobsson A, Battistini L, Maccarrone M, et al. Proresolving Lipid Mediators Resolvin D1, Resolvin D2, and Maresin 1 are Critical in Modulating T Cell Responses. *Sci Transl Med* (2016) 8 (353):353ra111. doi: 10.1126/scitranslmed.aaf7483
133. Jin S, Chen H, Li Y, Zhong H, Sun W, Wang J, et al. Maresin 1 Improves the Treg/Th17 Imbalance in Rheumatoid Arthritis Through miR-21. *Ann Rheum Dis* (2018) 77(11):1644–52. doi: 10.1136/annrheumdis-2018-213511
134. Cheng T, Ding S, Liu S, Li X, Tang X, Sun L. Resolvin D1 Improves the Treg/Th17 Imbalance in Systemic Lupus Erythematosus Through miR-30e-5p. *Front Immunol* (2021) 12:668760. doi: 10.3389/fimmu.2021.668760
135. Ratcliffe MJ, Walding A, Shelton PA, Flaherty A, Dougall IG. Activation of E-Prostanoid4 and E-Prostanoid2 Receptors Inhibits TNF-Alpha Release From Human Alveolar Macrophages. *Eur Respir J* (2007) 29(5):986–94. doi: 10.1183/09031936.00131606
136. Strassmann G, Patil-Koota V, Finkelman F, Fong M, Kambayashi T. Evidence for the Involvement of Interleukin 10 in the Differential Deactivation of Murine Peritoneal Macrophages by Prostaglandin E2. *J Exp Med* (1994) 180(6):2365–70. doi: 10.1084/jem.180.6.2365
137. Takayama K, Sukhova GK, Chin MT, Libby P. A Novel Prostaglandin E Receptor 4-Associated Protein Participates in Antiinflammatory Signaling. *Circ Res* (2006) 98(4):499–504. doi: 10.1161/01.RES.0000204451.88147.96
138. Serhan CN, Brain SD, Buckley CD, Gilroy DW, Haslett C, O'Neill LAJ, et al. Resolution of Inflammation: State of the Art, Definitions and Terms. *FASEB J* (2007) 21(2):325–32. doi: 10.1096/fj.06-7227rev
139. Mahic M, Yaqub S, Johansson CC, Taskén K, Aandahl EM. FOXP3+CD4+CD25+ Adaptive Regulatory T Cells Express Cyclooxygenase-2 and Suppress Effector T Cells by a Prostaglandin E2-Dependent Mechanism. *J Immunol (Baltimore Md: 1950)* (2006) 177(1):246–54. doi: 10.4049/jimmunol.177.1.246
140. Obermajer N, Muthuswamy R, Lesnock J, Edwards RP, Kalinski P. Positive Feedback Between PGE2 and COX2 Redirects the Differentiation of Human Dendritic Cells Toward Stable Myeloid-Derived Suppressor Cells. *Blood* (2011) 118(20):5498–505. doi: 10.1182/blood-2011-07-365825
141. Fuentes AV, Pineda MD, Venkata KCN. Nagulapalli. Comprehension of Top 200 Prescribed Drugs in the US as a Resource for Pharmacy Teaching, Training and Practice. *Pharm (Basel Switzerland)* (2018) 6(2):43. doi: 10.3390/pharmacy6020043
142. Hinz B, Brune K. Cyclooxygenase-2–10 Years Later. *J Pharmacol Exp Ther* (2002) 300(2):367–75. doi: 10.1124/jpet.300.2.367
143. Hara S. Prostaglandin Terminal Synthases as Novel Therapeutic Targets. *Proc Japan Academy Ser B Phys Biol Sci* (2017) 93(9):703–23. doi: 10.2183/pjab.93.044
144. Bergqvist F, Morgenstern R, Jakobsson P-J. A Review on mPGES-1 Inhibitors: From Preclinical Studies to Clinical Applications. *Prostaglandins other Lipid Mediators* (2020) 147:106383. doi: 10.1016/j.prostaglandins.2019.106383
145. Werner M, Jordan PM, Romp E, Czapka A, Rao Z, Kretzer C, et al. Targeting Biosynthetic Networks of the Proinflammatory and Proresolving Lipid Metabolome. *FASEB J* (2019) 33(5):6140–53. doi: 10.1096/fj.201802509R
146. Park J, Langmead CJ, Riddy DM. New Advances in Targeting the Resolution of Inflammation: Implications for Specialized Pro-Resolving Mediator GPCR Drug Discovery. *ACS Pharmacol Transl Sci* (2020) 3(1):88–106. doi: 10.1021/acsptsci.9b00075
147. Chen Q, Muramoto K, Masaaki N, Ding Y, Yang H, Mackey M, et al. A Novel Antagonist of the Prostaglandin E(2) EP(4) Receptor Inhibits Th1 Differentiation and Th17 Expansion and Is Orally Active in Arthritis Models. *Br J Pharmacol* (2010) 160(2):292–310. doi: 10.1111/j.1476-5381.2010.00647.x

Conflict of Interest: The authors declare that the research was conducted in the absence of any commercial or financial relationships that could be construed as a potential conflict of interest.

Copyright © 2021 Schmid and Brüne. This is an open-access article distributed under the terms of the Creative Commons Attribution License (CC BY). The use, distribution or reproduction in other forums is permitted, provided the original author(s) and the copyright owner(s) are credited and that the original publication in this journal is cited, in accordance with accepted academic practice. No use, distribution or reproduction is permitted which does not comply with these terms.

frontiers in Immunology

ORIGINAL RESEARCH
published: 19 July 2021
doi: 10.3389/fimmu.2021.710406

Macrophage-Regulatory T Cell Interactions Promote Type 2 Immune Homeostasis Through Resistin-Like Molecule α

*Jiang Li, Sang Yong Kim, Nancy M. Lainez, Djurdjica Coss and Meera G. Nair**

Division of Biomedical Sciences, School of Medicine, University of California Riverside, Riverside, CA, United States

RELMα is a small, secreted protein expressed by type 2 cytokine-activated "M2" macrophages in helminth infection and allergy. At steady state and in response to type 2 cytokines, RELMα is highly expressed by peritoneal macrophages, however, its function in the serosal cavity is unclear. In this study, we generated RELMα TdTomato (Td) reporter/knockout ($R\alpha^{Td}$) mice and investigated RELMα function in IL-4 complex (IL-4c)-induced peritoneal inflammation. We first validated the $RELM\alpha^{Td/Td}$ transgenic mice and showed that IL-4c injection led to the significant expansion of large peritoneal macrophages that expressed Td but not RELMα protein, while $RELM\alpha^{+/+}$ mice expressed RELMα and not Td. Functionally, $RELM\alpha^{Td/Td}$ mice had increased IL-4 induced peritoneal macrophage responses and splenomegaly compared to $RELM\alpha^{+/+}$ mice. Gene expression analysis indicated that $RELM\alpha^{Td/Td}$ peritoneal macrophages were more proliferative and activated than $RELM\alpha^{+/+}$ macrophages, with increased genes associated with T cell responses, growth factor and cytokine signaling, but decreased genes associated with differentiation and maintenance of myeloid cells. We tested the hypothesis that $R\alpha^{Td/Td}$ macrophages drive aberrant T cell activation using peritoneal macrophage and T cell co-culture. There were no differences in $CD4^+$ T cell effector responses when co-cultured with $RELM\alpha^{+/+}$ or $RELM\alpha^{Td/Td}$ macrophages, however, $RELM\alpha^{Td/Td}$ macrophages were impaired in their ability to sustain proliferation of $FoxP3^+$ regulatory T cells (Treg). Supportive of the *in vitro* results, immunofluorescent staining of the spleens revealed significantly decreased $FoxP3^+$ cells in the $RELM\alpha^{Td/Td}$ spleens compared to $RELM\alpha^{+/+}$ spleens. Taken together, these studies identify a new RELMα regulatory pathway whereby RELMα-expressing macrophages directly sustain Treg proliferation to limit type 2 inflammatory responses.

Keywords: splenomegaly, peritonitis, Treg, Th2 cytokine, M2 macrophage

OPEN ACCESS

Edited by:
Amiram Ariel,
University of Haifa, Israel

Reviewed by:
Benjamin G. Dewals,
University of Liège, Belgium
David Voehringer,
University of Erlangen Nuremberg, Germany

***Correspondence:**
Meera G. Nair
meera.nair@medsch.ucr.edu

Specialty section:
This article was submitted to Inflammation, a section of the journal Frontiers in Immunology

Received: *16 May 2021*
Accepted: *29 June 2021*
Published: *19 July 2021*

Citation:
Li J, Kim SY, Lainez NM, Coss D and Nair MG (2021) Macrophage-Regulatory T Cell Interactions Promote Type 2 Immune Homeostasis Through Resistin-Like Molecule α. Front. Immunol. 12:710406. doi: 10.3389/fimmu.2021.710406

INTRODUCTION

Macrophages are a dominant resident population within the peritoneal cavity with critical immune surveillance and homeostatic functions (1). As sentinels, they are rapid responders to microbial invasion resulting from injury of the serous organs, such as the spleen, liver and intestinal tract, and can be mobilized to traffic to the injured organ and mediate tissue repair (2). Peritoneal

macrophages also perform homeostatic functions to support innate B1 cells (3), clear debris and apoptotic cells (4, 5), and dampen inflammation (6–8). On the other hand, dysregulated peritoneal macrophage responses are associated with diseases including peritonitis, bacterial dissemination, and cancer metastases (9–12). Identification of peritoneal macrophage-derived factors and activation markers that cause beneficial or pathologic outcomes would provide insight into their biology and identify targets for treatment of serous cavity-associated disease.

Peritoneal macrophages, especially the monocyte-derived small peritoneal macrophages, express Resistin-like molecule α (RELMα) under homeostatic conditions (13). In type 2 cytokine-polarized environments such as helminth infection or *in vivo* IL-4 complex injection, RELMα expression is dramatically elevated reaching 100% expression by small and large peritoneal macrophages (14). RELMα, also known as FIZZ1 and HIMF, was originally identified as a highly secreted protein in the lung during allergic airway inflammation (15), however, it is now well-recognized that RELMα is pleiotropically expressed throughout the body, and a signature gene expressed by M2-polarized macrophages in response to multiple helminth infections (16, 17). RELMα expression is also triggered by other signals in addition to type 2 cytokines, for example by phagocytosis of apoptotic cells through scavenger receptors (18), or in response to hypoxia (19). Studies in pulmonary inflammation, hypertension and fibrosis, point to an inflammatory function for RELMα by promoting immune cell recruitment, fibroblast activation and proliferation associated with pathogenic fibrosis (20, 21). On the other hand, in response to tissue migratory helminth parasites, RELMα critically prevents fatal lung tissue damage, granulomatous inflammation, and promotes tissue repair (22–28). Downstream regulatory mechanisms for RELMα include limiting $CD4^+$ T cell polarization, promoting anti-inflammatory responses, and mediating collagen cross-linking associated with tissue healing (26, 29, 30). RELMα also exhibits antibacterial properties by disrupting bacterial membranes for certain bacterial species (31).

Despite high expression levels of RELMα by peritoneal macrophages, whether RELMα affects the role of these cells in immune surveillance or homeostasis is unknown. In this study, we generated transgenic mice where RELMα is deleted and replaced with the TdTomato reporter protein ($R\alpha^{Td}$) and investigated the consequence of RELMα deletion in a polarized type 2 cytokine environment caused by injection of IL-4 complexes. We first validated the Rα transgenic mice and demonstrated successful deletion of RELMα and expression of TdTomato protein, which had an equivalent expression pattern to RELMα. Next, we compared PBS and IL-4c injected $R\alpha^{+/+}$ and $R\alpha^{Td/Td}$ mice, where we identify a critical role for RELMα in limiting IL-4-induced peritoneal macrophage expansion, M1 macrophage activation, and splenomegaly. Gene expression analysis of sorted macrophages from $R\alpha^{+/+}$ and $R\alpha^{Td/Td}$ mice revealed that RELMα deficiency leads the induction of genes promoting T cell response, growth factor and cytokine signaling, but decreased genes associated with differentiation and maintenance of myeloid cells. Combining macrophage-T cell co-cultures, and investigation of *ex vivo* T cell responses, we further identify a role for macrophage-derived RELMα in promoting regulatory T cell proliferation and the production of IL-10 and GM-CSF. Together, results from these studies validate the utility of $R\alpha^{Td/Td}$ mice to track RELMα expression and identify a dual role for RELMα in limiting type 2 cytokine immunopathology by cell-intrinsic effects on macrophages and regulatory T cells.

MATERIALS AND METHODS

Mice

Retnla^{Td} transgenic mice were generated by genOway (Lyon, France) by homologous recombination in C57BL/6 embryonic stem cells. *Retnla* Exon 2-4 was targeted using cre recombinase and Flp-mediated excision and replacement with the Td reporter gene, with a WPRE site (32) to enhance reporter expression and stability. The mice were crossed with the genOway proprietary cre-deleter mouse (pCMV driven cre) to generate constitutive $Retnla^{Td}$ mice. $Retnla^{Td/+}$ heterozygote mice were crossed with C57BL/6 mice to generate littermate homozygote (Td/Td) and WT (+/+) mice after three generations, then bred in-house. $Arginase^{YFP}$ (Yarg) mice were available from Jackson labs. Mice were age matched (6 to 14 weeks old), sex-matched for experiments, and housed under an ambient temperature with a 12 hours light/12 hours dark cycle.

IL-4 Complex (IL-4c) Injection

Mice were injected intraperitoneally (i.p.) with 2.5μg of recombinant mouse IL-4 (Peprotech, Rock Hill, NJ) complexed to 12μg 11B11 (Bio X Cell) in 100μl PBS or 100μl PBS (vehicle control) on days 0 and 2 and peritoneal cells and spleen were recovered at day 4, according to published studies (17).

RNA Isolation and qPCR

Cells were washed twice with ice-cold PBS and lysed with RLT buffer. RNA was extracted by using the Aurum total RNA mini kit (Bio-Rad, San Diego, CA). cDNA was generated by iScript reverse transcriptase (Bio-Rad, San Diego, CA). RT-qPCR was performed with the Bio-Rad CFX Connect system using Bio-Rad CFX Manager 3.1 software. RELMα primers were purchased from Qiagen, Td Tomato primer sequence were (F: 5'-CCA CCT GTT CCT GGG GCA-3', R: 5'-ACT CTT TGA TGA CGG CCA TGT-3'), and 18s primer sequences were (F: 5'-ACG GAA GGG CAC CAC CAG GA-3', R: 5'-CAC CAC CAC CCA CGG AAT CG-3')

Immunofluorescence

Spleens were recovered and immediately immersed in 4% PFA. After 24 hours, tissue was removed from 4% PFA and incubated for 24 hours in 30% sucrose. For immunofluorescent staining, sections were incubated with rabbit anti-RELMα [2.5ug/ml; (Peprotech, Rock Hill, NJ)] or rabbit anti-TdTomato (Rockland Immunochemicals, Limerick, PA, USA), PE-anti CD3 (BioLegend, San Diego, CA) and FITC Rat anti-Foxp3 (eBioscience, Santa Clara, CA) overnight at 4°C. Sections were incubated with Cy5 anti-Rabbit fluorochrome-

conjugated antibodies for 2 hours at room temperature (Abcam, Cambridge, Ma), then counterstained with DAPI (BioLegend, San Diego, CA). FoxP3$^+$ cells were quantified by the ImageJ software.

Flow Cytometry and t-SNE Analysis

Peritoneal cavity cells (PECs) were recovered in a total of 5 mL of ice-cold PBS. Splenic macrophage isolation were performed according to previous studies (33).Visceral fat was dissected and single cell dissociation and staining performed as previously described (34). For flow cytometry, cells were blocked with 0.6 μg Rat IgG and 0.6 μg α-CD16/32 (2.4G2) 5 min, stained for 25 min with antibodies to CD11b (M1/70), MHCII (M5/114.15.2), CD11c (N418), CD4(RM4-5), Ly6C(HK 1.4), Ly6G(1A8), CD19(1D3) and CD8(53-6.7) (all from BioLegend, San Diego, CA); SiglecF (E50-2440) (BD Bioscience, San Jose, CA); F4/80 (BM8) (eBioscience, Santa Clara, CA). Cells were analyzed on a Novocyte (ACEA Biosciences, San Diego, CA) or LSRII instrument (BD Bioscience, San Jose, CA) followed by data analysis using FlowJo v10 (Tree Star Inc.; Ashland, OR). t-SNE analyses were performed with FlowJo v10, involving concatenation of samples (5000 cells per biological replicate) from all groups before running the t-SNE analyses to generate plots consistent between groups. This was followed by analysis of separated groups for expression of the desired markers. The parameters used to run the t-SNE analyses are in **Supplementary Table 1**. Arg, Rα or TdTomato were excluded as parameters given that their expression was being analyzed, and they were negative in the some of the transgenic mouse groups.

Cytokine Quantification

For sandwich ELISA, capture and biotinylated detection antibodies were used according to previously described protocols (25). IL-23, IL-1α, IFN-γ, TNF-α, MCP-1, IL-12p70, IL-1β, IL-10, IL-6, IL-27, IL-17A, IFN-β and GM-CSF were detected by the Mouse Inflammation Panel (13-plex) (BioLegend, San Diego, CA) and analyzed on the LSRII instrument (BD Bioscience) and LEGENDplex™ software.

Splenocyte Stimulation

Spleens were harvested from PBS or IL4c treated mice at day 4. Single cell suspensions were generated from whole spleen, and red blood cells lysed with ACK lysis buffer. Cells were stimulated in 48 well plates at 5x10^6 cells/well with 1μg/ml of α-CD3 and α-CD28 (eBioscience) as described previously (29). Supernatants were recovered at day 3 for cytokine measurement.

Macrophage and Splenocyte Co-Cultures

Peritoneal cells from naïve Rα$^{+/+}$ or Rα$^{Td/Td}$ mice were recovered and treated *in vitro* with IL-4 (20ng/ml) or equivalent control PBS in complete DMEM media (Invitrogen, Gaithersburg, MD). After 24hrs, supernatants were recovered for RELMα ELISA, cells were washed with PBS to remove non-adherent cells, followed by recovery of adherent macrophages with TrypLE™ Express (Invitrogen, Gaithersburg, MD) and plated in a 96-well flat bottom plate at 2x10^4 cells/well. In vivo-derived M2 macrophages were generated by one i.p. injection of IL-4c, recovery of the peritoneal cells, and F4/80 bead purification using MS columns with >90% purity (Miltenyi Biotec, Inc). Splenocytes were recovered from naïve Rα$^{+/+}$ mice, and single cell suspensions prepared as above. Splenocytes were CFSE-labelled (5μM, 15 minutes) as previously described (29) (Invitrogen, Gaithersburg, MD), then added to the macrophages (Mac : Splenocyte 1:10) with 0.5μg/ml α-CD3 (5 replicate wells per condition). After 3 and 6 days, non-adherent splenocytes were recovered for flow cytometry analysis on the LSRII (BD Bioscience), and supernatants were recovered for cytokine measurement.

Nanostring Gene Expression Analysis

Peritoneal macrophages (CD11b$^+$F4/80$^+$) were sorted with the MoFlo Astrios cell sorter (Beckman Coulter). 5000 macrophages from PBS mice or IL-4c-injected mice were lysed with 1/3 RLT buffer diluted with ddH_20 (Qiagen). Lysed cells were processed and quantified by the Myeloid Innate Immunity v2 panel according to manufacturer's instructions (Nanostring). Gene expression analysis was conducted using the Advanced Analysis Nanostring software. Raw counts were normalized to internal controls (4 housekeeping genes, *Eef1g, Gusb, Oaz1* and *Rpl19*), then normalized transcripts with n>30 counts were included for analysis (a total of 309 out of 734 genes). The Nanostring Advanced Analysis algorithm generated biological pathway scores by extracting pathway-level information from a group of genes using the first principal component (PC) of their expression data (35). Pathway scores of Rα$^{+/+}$ or Rα$^{Td/Td}$ naive and IL-4c-injected mice were analyzed by an unpaired t-test and chosen pathways (p value ≤ 0.05) are represented as the difference in pathway score between the Rα$^{+/+}$ or Rα$^{Td/Td}$ groups (n=4/group). Differentially expressed (DE) genes (p ≤ 0.05) in each pathway were graphed as heatmaps (36).

Statistical Analysis

Data are presented as mean ± SEM and statistical analysis was performed by Graphpad Prism 9 software. Data was assessed by one-way ANOVA followed by post-hoc Tukey's test for multiple comparison, or by unpaired t-test for 2-group comparisons. For data collected over several time points, two-way ANOVA with post-Sidak multiple test was performed. *, p ≤ 0.05; **, p ≤ 0.01; ***, p ≤ 0.001. Experiments were repeated 2-4 times with n=2-8 per group for *in vivo* experiments, or 3-5 replicate wells for *in vitro* studies, apart from Nanostring gene expression analysis, which was performed once (n=2 for naïve and n=4 for IL-4c injected per group).

Mouse and Data Availability

RELMα transgenic mice are available at MMRC repository (067014-UCD, https://mmrrc.ucdavis.edu).

RESULTS

Generation and Validation of RELMα Transgenic Mice

RELMα is a pleiotropic protein expressed by both immune and non-immune cells, and is detectable in the serum of naïve mice (16). In the serosal cavities, resident macrophages express

RELMα in homeostatic conditions, however, RELMα expression is dramatically elevated in a type 2 cytokine environment such as helminth infection or IL-4c injection (17). We sought to address RELMα function in the peritoneal cavity by generating transgenic mice in which cre and flp recombinase mediates RELMα (exons 2-4) deletion and replacement with the TdTomato reporter protein (**Figure 1A**). To validate the targeting strategy and enable tracking of RELMα-expressing cells, these founder mice were crossed to a universal cre deleter mouse line so that RELMα expression can be tracked by Td reporter protein in heterozygote mice ($R\alpha^{Td/+}$), while homozygote mice ($R\alpha^{Td/Td}$) are used to investigate RELMα function. Quantification of RELMα protein in the serum and peritoneal cavity fluid indicated high levels of circulating RELMα under homeostatic conditions in $R\alpha^{+/+}$ mice, detectable but significantly reduced RELMα in heterozygote ($R\alpha^{Td/+}$) mice, and no RELMα in homozygote mice ($R\alpha^{Td/Td}$) (**Figure 1B**). RELMα and Td mRNA levels were also quantified in adherent peritoneal cells from naïve mice treated *in vitro* with IL-4 (**Figure 1C**). Both $R\alpha^{+/+}$ and $R\alpha^{Td/+}$ macrophages had equivalent IL-4 induced RELMα expression. In IL-4 treated $R\alpha^{Td/Td}$ and $R\alpha^{Td/+}$ macrophages, Td expression was increased. Although the Td expression pattern was similar to RELMα in the heterozygote mice, the fold induction of Td was much lower than that of RELMα. This suggests differences in PCR efficiency, mRNA stability, or that deletion of RELMα has feedback consequences on the RELMα promoter and gene expression. We investigated if these potential differences in RNA levels were also observed at the protein level by flow cytometry. Intracellular RELMα and Td protein was evaluated by flow cytometry of peritoneal cells recovered from PBS or IL-4 complex (IL4c) injected mice (**Figure 1D** and **Figure S1A**). As expected, the main cellular sources of RELMα protein following IL4c injection were the small and large peritoneal macrophages (SPM and LPM) with >95% expression of RELMα in $R\alpha^{+/+}$ and $R\alpha^{Td/+}$. In the $R\alpha^{Td/+}$ heterozygote mice, Td protein was induced by IL-4 with 50% expression in LPM and 85% expression in SPM. We also observed IL-4c induced expression of RELMα and Td by eosinophils and $CD5^+$ B1 cells (**Figure 1D** and **Figure S1B**). Finally, we examined RELMα and Td expression in other organs such as the visceral fat and the spleen (**Figure S2A**), where we observed some IL-4 induced RELMα or Td expression by macrophages, but this was much lower in magnitude compared to the peritoneal cells.

To evaluate heterogeneity in serosal macrophage populations, we generated t-SNE plots on flow cytometry data from IL-4c-treated Arginase-YFP/Rα dual reporter mice (**Figure 1E**). The main subsets observed were LPM (red), SPM (blue) and B1 cells (cyan). When comparing heterozygote $R\alpha^{Td/+}Yarg^{+/+}$ and $R\alpha^{Td/Td}Yarg^{+/+}$, RELMα was expressed in SPM and LPM of heterozygote $R\alpha^{Td/+}$ but not in homozygote $R\alpha^{Td/Td}$ mice. $R\alpha^{Td/Td}$ mice showed instead Td protein expression with similar expression pattern to RELMα. While SPM were a homogenous population with high level RELMα (or Td) expression, LPM exhibited more heterogeneity with mid and high level RELMα-expressing subsets (green vs yellow/red) (**Figure 1F**). In contrast, Arginase was more homogeneously expressed in both SPM and LPM (yellow/red). Together, these data validate effective RELMα deletion and replacement with TdTomato and indicate potential heterogeneity of RELMα compared to Arginase expression in the LPM. We also demonstrate that $R\alpha^{Td/+}$ heterozygote mice have robust Td and RELMα protein expression, supporting the utility of this transgenic mouse model to track RELMα expression.

$RELM\alpha^{Td/Td}$ Mice Suffer From Increased IL-4c Induced Pathology

Serosal macrophages that reside in the peritoneal cavity have important surveillance roles as sentinels for pathogen infections, but also regulate inflammation and can migrate to visceral organs to mediate repair (37). Peritoneal macrophages are main cellular sources with up to 100% RELMα expression following IL-4c injection, however, the function of RELMα in the peritoneal cavity has not been investigated. Wild-type ($R\alpha^{+/+}$) or RELMα-deficient ($R\alpha^{Td/Td}$) mice were injected with PBS or IL-4c. IL-4c injection led to significantly increased RELMα protein in the serum and RELMα mRNA in the peritoneal cells of $R\alpha^{+/+}$ mice, while Td mRNA was significantly elevated in peritoneal cells of $R\alpha^{Td/Td}$ mice (**Figure 2A**). As previously reported (14), IL-4c caused increased peritoneal cell numbers in $R\alpha^{+/+}$ mice, but peritoneal inflammation was exacerbated in $R\alpha^{Td/Td}$ mice (**Figure 2B**). Flow cytometric analysis revealed that LPM were the main cell-type affected by RELMα deficiency (**Figure 2C**). In the $R\alpha^{+/+}$ mice, peritoneal B cell numbers were significantly decreased by IL4c treatment (**Figure 2C**), and further subsetting into $CD5^+$ B1 cells and $CD23^+$ B2 cells revealed that the decrease was significant in B2 cells (**Figure S2B**). In contrast, neither B1 nor B2 cells were reduced by IL-4c in $R\alpha^{Td/Td}$ mice, and B1 cells were significantly higher in IL-4c treated $R\alpha^{Td/Td}$ mice compared to IL-4c treated $R\alpha^{+/+}$ mice (**Figure S2B**), suggesting that RELMα is downstream of IL-4c mediated reduction in B cells. Other peritoneal cell subsets were not affected by IL-4c treatment nor RELMα deficiency. IL-4c induces significant LPM proliferation, therefore we evaluated Ki67 expression as a marker for proliferation. There was a significant increase in Ki67 positive LPM and SPM in IL-4c injected $R\alpha^{Td/Td}$ mice but no changes in B cells (**Figure 2D**). RELMα-deficient mice also exhibited IL-4 induced splenomegaly, which was more severe than observed in wild-type mice (**Figures 2E, F**). This suggested an exacerbated response in RELMα deficiency, similar to the macrophage activation syndrome caused by sustained IL-4 exposure (38). Proinflammatory cytokine measurement in the serum revealed that $R\alpha^{Td/Td}$ mice had increased circulating cytokines compared to $R\alpha^{+/+}$ mice, with significant increases in IL1α under homeostatic conditions, and increased TNFα, IFNγ and IL-6 following IL-4 treatment, but no changes in circulating type 2 cytokine IL-5 (**Figure 2G**). We also performed the same cytokine bead array analysis on peritoneal lavage fluid but did not observe detectable cytokine levels. Together, these data reveal that RELMα critically mitigates IL-4-induced inflammatory effects including LPM and SPM proliferation, splenomegaly and systemic proinflammatory cytokine expression.

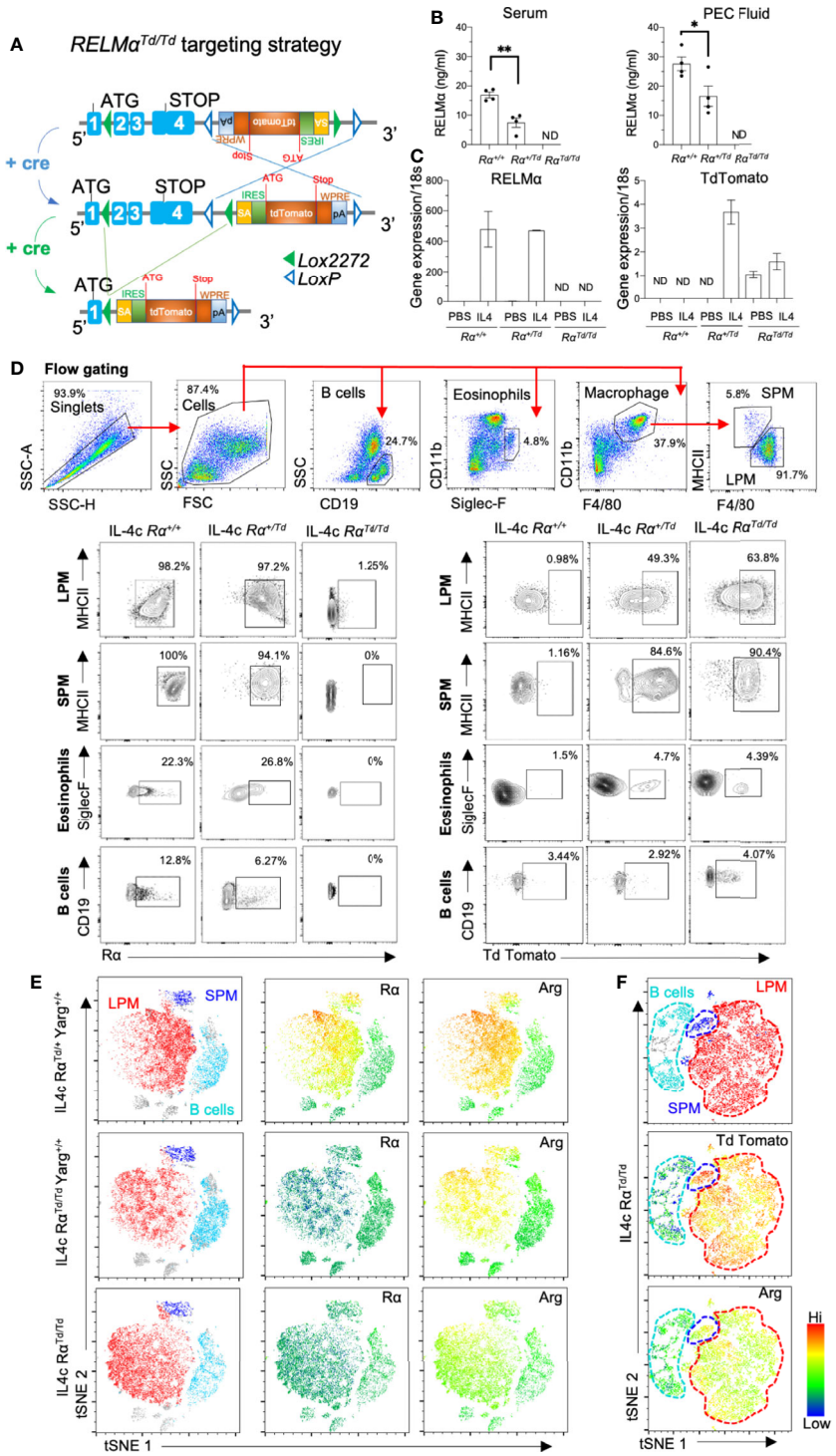

FIGURE 1 | Validation of RELMα reporter transgenic mice. RELMα (Rα) or TdTomato (Td) reporter homozygote and heterozygote mice were intraperitoneally injected with PBS or IL-4c (2.5μg IL4/mouse) at day 0 and 2, then sacrificed at day 4. **(A)** Targeting strategy for RELMα deletion and replacement with Td reporter gene. **(B)** RELMα ELISA of serum and peritoneal fluid of 6–8 weeks mice. **(C)** RELMα and Td qRT-PCR of peritoneal cells treated *in vitro* for 24h with IL-4 (20ng/ml), presented as relative expression to PBS and normalized to 18s transcript. Rα expression was normalized to the PBS $Rα^{+/+}$group (set at "1") **(D)** Flow cytometry gating and analysis of large and small peritoneal cells (LPM and SPM), eosinophils and B cells from IL4c-injected mice for Td and RELMα protein. **(E, F)** t-SNE -guided analysis of peritoneal cavity cells subsets gated according to 1D (LPM, red; SPM, blue; B1 cell, cyan) for expression of Rα, Arg^{YFP} and Td employing $Rα^{Td}$ and Yarg reporter mice. Results shown are combined from 2-3 independent experiments (n=4-12), apart from **(C, E)** which is one experiment, n=3 replicates. ND, not detected. *, $p \leq 0.05$; **, $p \leq 0.01$.

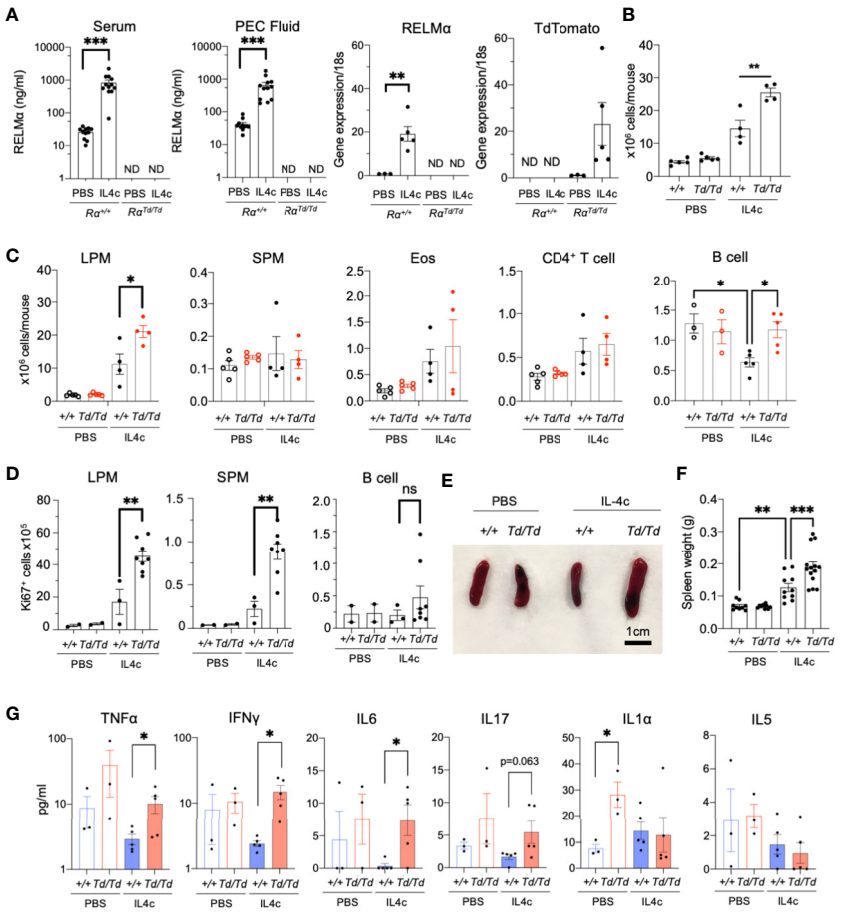

FIGURE 2 | Increased IL-4-induced pathology in RELMα$^{Td/Td}$ mice. PBS or IL4c-injected Rα$^{+/+}$ or Rα$^{Td/Td}$ mice were sacrificed at day 4 followed by evaluation of spleen and peritoneal cavity responses. **(A)** Peritoneal fluid and serum RELMα levels measured by ELISA, and RELMα and Td RNA was measured by peritoneal cell qRT-PCR as relative expression to PBS and normalized to 18s transcript. Rα expression was normalized to the PBS Rα$^{+/+}$group (set at "1") **(B, C)** Peritoneal inflammation and subset frequency evaluated by cell counts and flow cytometry analysis for small and large peritoneal macrophages (SPM and LPM), eosinophils, CD4^{+} T cells and B cells. **(D)** Peritoneal cell proliferation assessed by Ki67 staining. **(E, F)** Spleen size and weight were measured. **(G)** Serum cytokines were quantified. Results shown are representative of 3 independent experiments (n=4-8 per group). ND, not detected. *, p ≤ 0.05; **, p ≤ 0.01; ***, p ≤ 0.001.

RELMα Deficiency Leads to Dysregulated IL-4 Induced Myeloid Gene Expression Associated With T Cell Response, Growth Factor and Cytokine Signaling, and Myeloid Differentiation

To identify mechanisms underlying RELMα regulation of peritoneal macrophage responses, gene expression analysis was performed in F4/80^{+}CD11b^{+} peritoneal macrophages sorted from PBS or IL-4c treated Rα$^{+/+}$ or Rα$^{Td/Td}$ mice, using the Nanostring myeloid immunity panel (734 genes) (**Figure 3A**). Principal component analysis (PCA) demonstrated clustering according to genotype and treatment, with IL-4 treatment driving the greatest transcriptional differences regardless of genotype (**Figure 3B**). Out of four mice, macrophages from one IL-4c-treated Rα$^{+/+}$ mice appeared as an outlier and clustered with the PBS-treated group (**Figure 3B**, red circle). Retrospective analysis revealed that this mouse had less RELMα in the PEC fluid, and lower peritoneal cell numbers likely because of ineffective IL-4c delivery (**Figure S3A**), therefore this sample was removed from gene expression analyses.

Investigation of the most differentially expressed genes indicated that Chil3/4 (Ym1/Ym2) and Rnase2a (Ear11) were highly upregulated by IL-4 for both mouse genotypes (**Figures 3C, D**). As signature M2 macrophage genes, RELMα and Ym1/2 are reported to have equivalent expression patterns, but Ym1 can also promote RELMα expression (24). Ear11 is an eosinophil-associated ribonuclease that is secreted by M2 macrophages and promotes neutrophil chemotaxis (39). Consistent with IL-4 induced resident macrophage proliferation, genes associated with the cell cycle (Top2a, Cdc20, Kif20a, Ccnb2) were upregulated. Consistent with an anti-inflammatory function for M2 macrophages, both Rα$^{+/+}$ and Rα$^{Td/Td}$ macrophages from IL-4c treated mice had reduced expression of genes associated with chemotaxis (Cxcl13, Cxcl14,

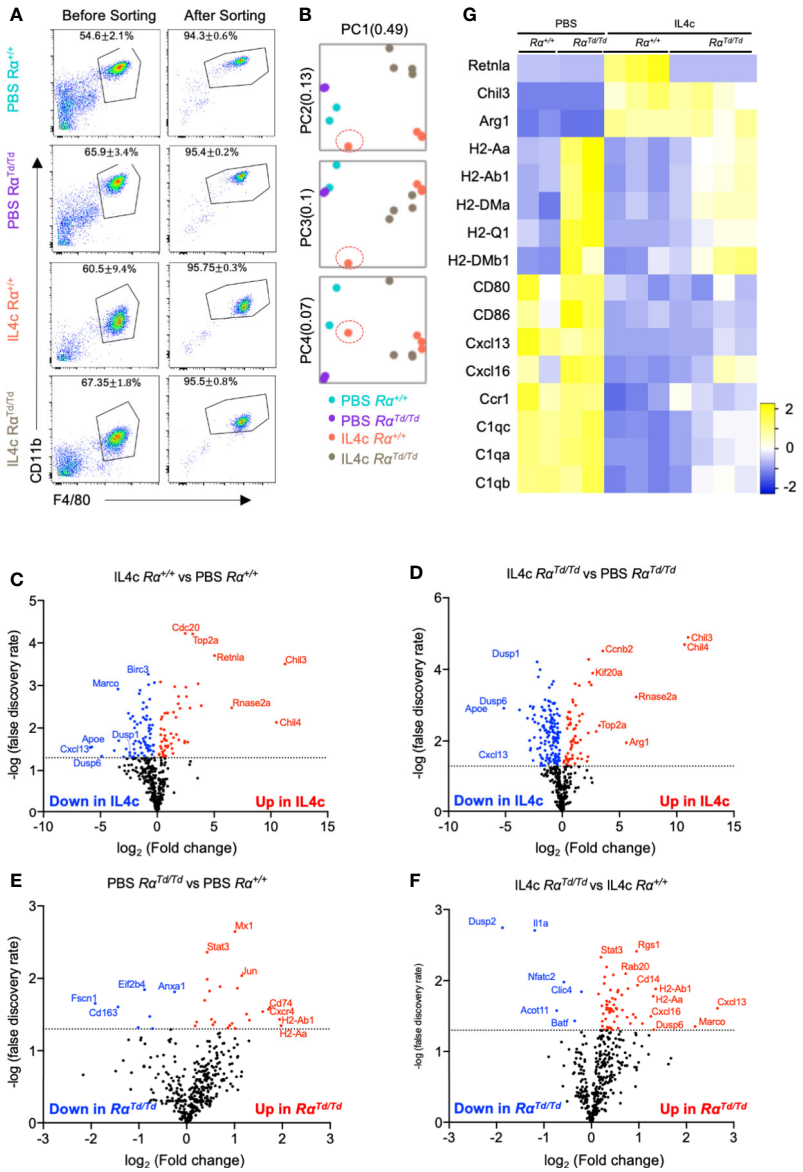

FIGURE 3 | Gene expression analysis of peritoneal macrophages identify IL-4-induced and suppressed genes that are regulated by RELMα. Peritoneal macrophages were sorted from PBS or IL4c-injected Rα$^{+/+}$ or Rα$^{Td/Td}$ mice and analyzed by using the Nanostring myeloid gene expression panel. **(A)** Flow cytometry gating strategy and purity. **(B)** Principal component analysis demonstrates sample clustering. **(C–F)** Volcano plot of genes that are most changed in response based on IL-4c treatment **(C, D)** or genotype **(E, F)**. **(G)** Heatmap of canonical macrophage activation genes in different groups. Nanostring gene expression data are from a single experiment (n=2 for PBS and n=4 for IL-4c injected).

Cxcl2), complement responses (C1qa, C1qb, C1qc) and innate immune activation (Birc3, CD80, CD86) (**Figures 3C, D, G**). Unexpectedly, the dual-specificity protein phosphatases (Dusp1, Dusp6), and Apoe were also suppressed by IL-4, although these have proposed anti-inflammatory and repair functions (40). These expression patterns likely reflect *in vivo* macrophage plasticity and the unique response of resident peritoneal macrophages to repeated treatment with IL-4, which may lead to negative feedback pathways for type 2 cytokine signaling. Overall, these genes were similarly induced or suppressed by IL-4 in both Rα$^{+/+}$ and Rα$^{Td/Td}$ mice, suggesting that these resident M2 macrophage activation programs occur even in the absence of RELMα.

We next evaluated RELMα-regulated genes (**Figures 3E–G**). The most consistently upregulated genes in PBS or IL-4-induced Rα$^{Td/Td}$ macrophages were MHC class II genes associated with antigen presentation (H2 genes, CD74), suggesting enhanced antigen presentation function by macrophages in RELMα-deficient mice even in homeostatic conditions. RELMα-deficient macrophages also had increased expression of

chemokine/chemokine receptors (Ccl6, Cxcl13, Cxcl16) (**Figure 4A**). Cxcl13, involved in B1 cell maintenance (41), was the most upregulated gene in IL-4c induced Rα$^{Td/Td}$ macrophages compared to Rα$^{+/+}$ macrophages, consistent with the increased B1 cell numbers in RELMα-deficient mice. Conversely Dusp2, which negatively regulates cell proliferation (42, 43), was the most downregulated in the Rα$^{Td/Td}$ macrophages (**Figure 4A**), consistent with their enhanced proliferation. Advanced pathway analysis (35) was performed to determine functional pathways that were significantly altered by RELMα following IL-4 treatment (**Figure 4B**). Consistent with upregulation of genes associated with macrophage hyperactivation, functional pathways that were significantly induced in RELMα-deficient macrophages involved enhanced T cell responses (Th1 activation, T-cell activation, antigen presentation). RELMα-deficient macrophages also induced genes associated with cytokine and growth factor signaling (Pdgfb, Jak3, Syk), which may have contributed to their increased expansion in response to IL-4 (**Figure 4C**). This increased macrophage proliferation and frequency in Rα$^{Td/Td}$ mice may therefore result from dual effects of increased growth factor expression and responsiveness, and decreased expression of downregulatory checkpoints, such as Dusp2 and Batf (**Figure 4C**). Rα$^{Td/Td}$ macrophages showed a reduction in genes associated with differentiation of myeloid cells (Mafb, Cebpa, Laptm5), which may reflect the enhanced proliferation rather than differentiation or maturation of these macrophages in the absence of RELMα.

Genes associated with angiogenesis (Fn1, Pdgfb) (44), phagocytosis (MerTK, Timd4, MHCII, C1q, CD16/32, Rab20 and Anxa1) (45–47), and the scavenger receptors (Marco, CD163) were increased in Rα$^{Td/Td}$ macrophages (**Figure 4C**).

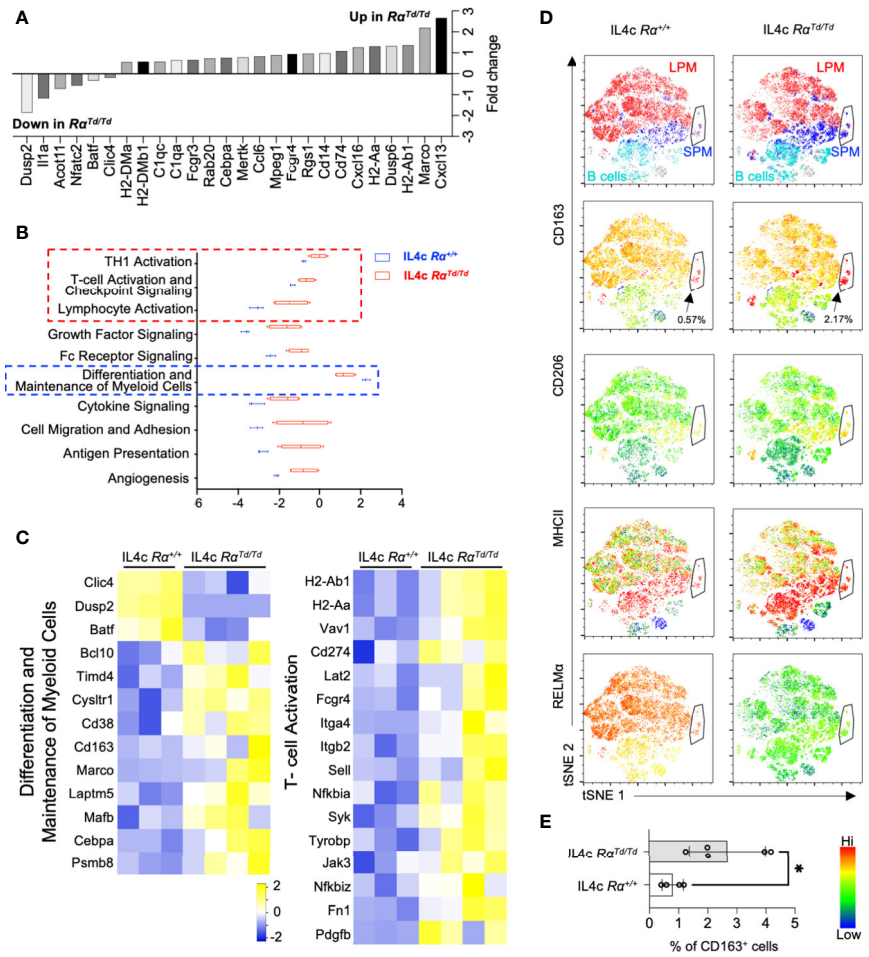

FIGURE 4 | RELMα-deficient M2 macrophages exhibit a hyperactivated macrophage phenotype. Differential expression of genes associated with functional pathways was evaluated in macrophages sorted from IL-4c injected Rα$^{+/+}$ or Rα$^{Td/Td}$ mice. **(A)** Genes with highest Log2 fold change differences between IL4c injected Rα$^{+/+}$ and IL4c Rα$^{Td/Td}$ identified by Nanostring advanced analysis ($p < 0.05$). **(B)** Advanced pathway analysis performed on IL4c Rα$^{+/+}$ and IL4c Rα$^{Td/Td}$ macrophage RNA reveals significantly increased or decreased pathway scores ($p<0.05$). **(C)** Heatmap of differentially expressed genes within the functional pathways. **(D)** t-SNE-guided flow cytometry analysis of peritoneal cell subsets (LPM, red; SPM, blue; B1 cell, cyan). Black arrow and outline indicate a separate subset with SPM and LPM characteristics. Subsets were evaluated for expression of CD163, CD206, MHCII and RELMα. **(E)** Frequency of CD163^{+} macrophages in IL4c-treated Rα$^{+/+}$ and Rα$^{Td/Td}$ mice. *, $p \leq 0.05$.

This was consistent with the IL-4 treated Rα$^{Td/Td}$ mice exhibiting characteristics of macrophage activation syndrome, associated with splenomegaly and erythrophagocytosis (38). To further analyze and validate some of these genes and their association with RELMα at the single cell and protein level, we use t-SNE mapping of flow cytometry data of peritoneal cells (**Figure 4D**). The t-SNE plots indicated the presence of a small subset that shared SPM and LPM characteristics (black arrow). This subset had the highest expression of CD163 and MHC class II, and co-expressed RELMα in the Rα$^{+/+}$ mice. Further, it was increased by four-fold in the Rα$^{Td/Td}$ mice, suggesting that RELMα expression by this subset may provide an autocrine negative feedback to limit its own expansion. Consistent with the Nanostring data, the MHCII^{hi} expressing subsets (**Figure 4D**, red) were expanded in the Rα$^{Td/Td}$ macrophages, especially in the SPM and SPM->LPM subsets, consistent with the significantly increased MHCII MFI in SPM but not LPM in Rα$^{Td/Td}$ mice (**Figure S2C**). however, there was heterogeneous distribution in LPM reflecting two functionally distinct LPM subsets in response to IL-4. Anti-CD163 surface staining confirmed the Nanostring data that Rα$^{Td/Td}$ macrophages had significantly elevated CD163 expression in the SPM, LPM and the SPM to LPM cell subset, and was co-expressed with the M2 macrophage marker CD206 (**Figure 4D**). CD163 is a scavenger receptor for hemoglobin and is increased in M2 macrophages associated with hemophagocytic syndromes (48). Combined with the increased expression of genes associated with phagocytosis and scavenger functions, our observations that CD163^{+} M2 macrophages are significantly expanded in Rα$^{Td/Td}$ mice (**Figure 4E**) point to a causal link between enhanced macrophage scavenging and the exacerbated IL-4 induced inflammation and splenomegaly in Rα$^{Td/Td}$ mice (38, 49–51).

RELMα-Expressing M2 Macrophages Support Regulatory T Cell Responses

Our *in vivo* data suggests that RELMα mice suffer from increased proinflammatory cytokine expression that is associated with enhanced macrophage activation, including increased expression of genes involved in T cell activation. We therefore investigated if macrophage-intrinsic RELMα dampens pro-inflammatory T cell responses using *in vitro* co-culture of peritoneal macrophages with splenocytes. Resident peritoneal macrophages from naive Rα$^{+/+}$ or Rα$^{Td/Td}$ mice were recovered and activated *in vitro* with IL-4, leading to significant RELMα secretion by Rα$^{+/+}$ macrophages (**Figure 5A**). The macrophages were then recovered and co-cultured with CFSE-labeled splenocytes activated with anti-CD3. After 3 days of co-culture, only modest proliferation of effector CD4 T cells (CD4^{+}CD25^{-}) was observed (~15%) (**Figures 5B, C**), although robust proliferation was observed by day 6 (~70%) (**Figure S3C**). Although there were no differences in effector T cell proliferation, CD4^{+}CD25^{+}Foxp3^{+} regulatory T cells (Treg) exhibited robust proliferation (60-80%), which was significantly higher when co-cultured with IL-4 treated Rα$^{+/+}$ macrophages compared to PBS treated Rα$^{+/+}$ macrophages (**Figure 5D**). PBS-treated Rα$^{Td/Td}$ macrophages supported equivalent Treg proliferation compared to PBS Rα$^{+/+}$ macrophages, however IL-4 treated Rα$^{Td/Td}$ macrophages were unable to enhance Treg proliferation (**Figure 5D**).

We evaluated the downstream effects of macrophage-Treg interaction by quantifying cytokine secretion. Macrophages or splenocytes cultured alone did not produce cytokines (**Figure 5E** and data not shown). Both PBS or IL-4 treated Rα$^{+/+}$ macrophages-splenocyte co-cultures resulted in robust and equivalent secretion of IL-10, GM-CSF, and IFNγ, while IL-4-treated macrophages promoted enhanced secretion of IL-1α, MCP-1, IL-6. Co-cultures with PBS-treated Rα$^{Td/Td}$ macrophages induced equivalent cytokine secretion to PBS-treated Rα$^{+/+}$ macrophages, however, IL-4-treated Rα$^{Td/Td}$ macrophages were unable to promote cytokines associated with Treg differentiation and function (IL-10 and GM-CSF). Instead, IL-4-treated Rα$^{Td/Td}$ macrophages promoted secretion of MCP-1, IL-6. We also observed a reduction in IFNγ and IL-1α secretion in co-cultures with IL-4 treated Rα$^{Td/Td}$ macrophages. Given that the co-cultures consisted of macrophages and splenocytes, the cellular source of the cytokines is unclear. Since the splenocytes are treated with anti-CD3, we conclude that most of the cytokines detected are directly from T cells, or indirectly from T cells activating other splenocytes or the peritoneal macrophages to produce cytokines.

We also investigated *in vivo*-derived M2 macrophages by IL-4c intraperitoneal injection, followed by recovery and purification of F4/80^{+} macrophages at day 1, and co-culture with anti-CD3 stimulated splenocytes (**Figure 5F**). Similar to the *in vitro*-derived M2 macrophages, co-culture with Rα$^{Td/Td}$ macrophages led to significantly reduced Treg proliferation compared to Rα$^{+/+}$ macrophages, with no significant effect on effector T cells. The Rα$^{Td/Td}$ co-cultures also had significantly reduced IL-2 levels compared with the Rα$^{+/+}$ macrophage co-cultures (**Figure 5G**), which may explain the reduced Treg proliferation. Together, this data suggests that macrophage-derived RELMα promotes Treg responses and suppresses myeloid expression of chemokines and proinflammatory cytokines, but has a mixed effect on T cell polarization and inflammasome activation.

Dysregulated Splenic T Cell Responses and Reduced Regulatory T Cells in RELMα-Deficient Mice

Based on the co-culture results that demonstrated a direct effect of macrophage-derived RELMα in supporting Treg responses, we sought to determine the *in vivo* relevance of this novel regulatory function for RELMα. We therefore evaluated peritoneal macrophage and splenic T cell responses in PBS or IL-4c-treated Rα$^{+/+}$ or Rα$^{Td/Td}$ mice. We observed significantly increased CD25 expression in the Rα$^{Td/Td}$ LPM and SPM (**Figure 6A**), which may provide one mechanism for limiting IL-2 availability to Tregs (52). t-SNE mapping showed that most IL-4c induced Rα$^{Td/Td}$ SPM and a small subset of Rα$^{Td/Td}$ LPM expressed CD25, compared to low expression in IL-4c induced Rα$^{+/+}$ macrophages (**Figure 6B**). To validate the *in vitro* finding of impaired Treg responses in the absence of RELMα, we quantified Treg frequencies in the spleens of PBS or IL-4c-treated Rα$^{+/+}$ and Rα$^{Td/Td}$ mice. Immunofluorescent analysis of the periarteriolar lymphoid sheath of the spleen confirmed that IL4c-treated Rα$^{Td/Td}$ mice had significantly reduced Foxp3^{+} cells (**Figures 6C, D**). Additionally, IL-4c

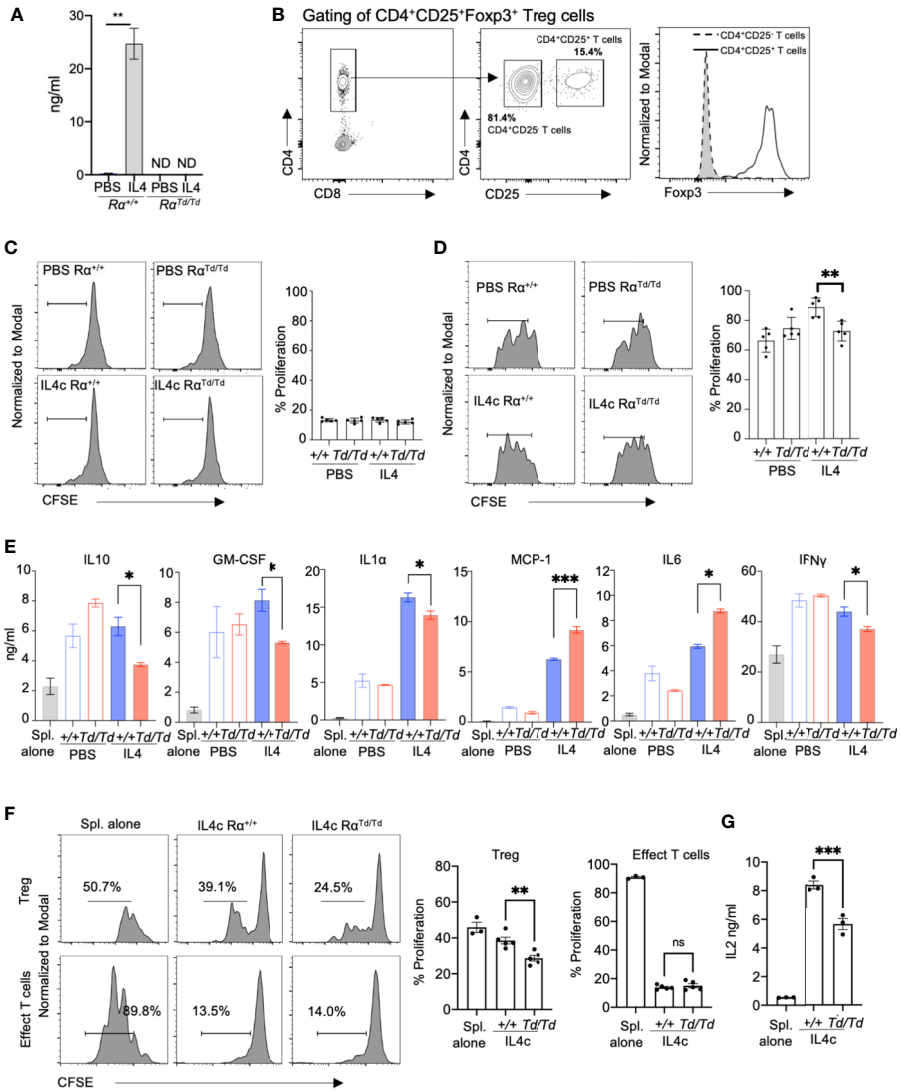

FIGURE 5 | Macrophage-derived RELMα promotes regulatory T cell responses. Peritoneal macrophages from $R\alpha^{+/+}$ or $R\alpha^{Td/Td}$ mice were treated with PBS or IL-4 (20ng/mL) for 24h, washed then adherent macrophages were co-cultured for three days with CFSE-labeled splenocytes with anti-CD3 at a 1:10 (Mac : Splen ratio). **(A)** RELMα secretion by peritoneal macrophages treated *in vitro* with PBS or activated with IL-4. **(B)** T cell gating strategy. **(C, D)** Proliferation of $CD4^+CD25^-$ T cells **(C)** and $CD4^+CD25^+FoxP3^+$ Tregs **(D)** when splenocytes are co-cultured with peritoneal macrophages treated *in vitro* with PBS or IL4 **(E)** Cytokine secretion measured at day 3 post-culture. **(F)** Proliferation of $CD4^+CD25^-$ T cells and $CD4^+CD25^+FoxP3^+$ Tregs when splenocytes are co-cultured with F4/80+ peritoneal macrophages purified from *in vivo* IL-4c-treated mice. **(G)** IL-2 secretion measured at day 3 post-culture. ND, not detected; NS, not significant. *, $p \leq 0.05$; **, $p \leq 0.01$; ***, $p \leq 0.001$.

treatment led to detectable RELMα protein expression in $R\alpha^{+/+}$ mice and Td protein in $R\alpha^{Td/Td}$ mice (**Figure 6C**), suggesting local effects of RELMα on the spleen. Flow cytometry analysis of the spleen also revealed significant reductions in $CD4^+CD25^+$ Tregs in IL4c-treated $R\alpha^{Td/Td}$ mice compared to $R\alpha^{+/+}$ mice (**Figures 6E, F**).

We next evaluated if the Treg deficiency in $R\alpha^{Td/Td}$ mice was associated with dysregulated T cell polarization in the spleen. Anti-CD3 stimulation of splenocytes from IL-4c-treated $R\alpha^{Td/Td}$ mice led to significantly increased secretion of IL-17A, TNFα and IL-1α compared to splenocytes from the counterpart $R\alpha^{+/+}$ mice (**Figure 6G**). Combined, these *in vitro* and *in vivo* data reveal a previously unappreciated role for peritoneal macrophage-derived RELMα in mitigating IL-4 induced inflammation and immunopathology through promoting Treg responses and limiting proinflammatory macrophage and T cell responses.

DISCUSSION

As critical sentinels of the peritoneal cavity and visceral organs, the biology of peritoneal macrophages is increasingly being investigated (2, 53–56). These studies highlight the complexity and importance

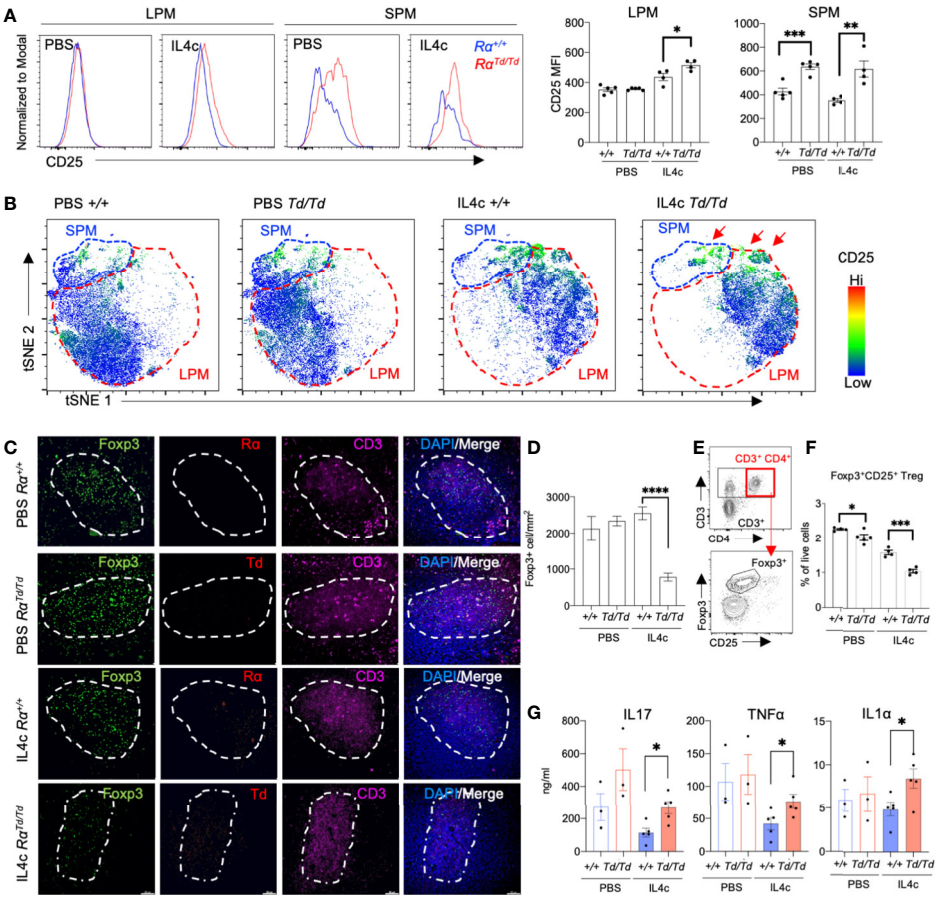

FIGURE 6 | Impaired splenic regulatory T cell responses in RELMα-deficient mice are associated with increased inflammatory cytokines. Peritoneal cells and spleens from $R\alpha^{+/+}$ or $R\alpha^{Td/Td}$ mice treated with PBS or IL-4c were recovered for evaluation of macrophage and T cell responses. **(A)** CD25 expression in SPM and LPM. **(B)** t-SNE -guided gating of peritoneal cavity LPM and SPM and analysis of CD25. **(C, D)** Immunofluorescent staining for CD3, Foxp3, RELMα and Td was performed on spleen sections and Foxp3+ cells were quantified. Bar: 50μm. **(E)** Gating strategy for effector and regulatory splenic T cells. **(F)** Frequency of Tregs in spleen evaluated *ex vivo* by intracellular staining for Foxp3. **(G)** Cytokine secretion was quantified from splenocytes stimulated with αCD3/αCD28 for 72 hours. *, $p \leq 0.05$; **, $p \leq 0.01$; ***, $p \leq 0.001$; ****, $p < 0.0001$.

of these cells in response to infection and inflammation (55, 57), but also reveal their role in immune homeostasis (1, 2, 58, 59). Peritoneal macrophages follow similar activation pathways to other macrophage lineages, where M1 macrophages activated by IFNγ and TNFα have enhanced microbicidal or tumoricidal capacity and secrete high levels of pro-inflammatory cytokines and mediators (60), while IL-4 activated M2 macrophages reduce inflammation and contribute to tissue repair through secretion of IL-10 and TGF-β (61, 62). Although M2 macrophages have anti-inflammatory roles, dysregulation of these signaling pathways also induce inflammation and immunopathology (38), which we investigated using the *in vivo* model of IL-4c induced peritonitis. RELMα is a signature marker of small peritoneal macrophages under homeostatic conditions and is highly expressed by small and large peritoneal macrophages in a type 2 cytokine environment. However, the potential contribution of RELMα to peritoneal macrophage activation, function, or effects on other immune or resident cells are unknown. We addressed this question by generating RELMα transgenic mice and found that RELMα expressed by peritoneal macrophages acts back to limit macrophage proliferation and activation. Macrophage-derived RELMα was also critical to support regulatory T cell proliferation and function.

Genetically deficient RELMα mice have been previously investigated (28, 29, 31), and one study generated a RELMα-cre recombinase mouse line that enabled fate mapping of RELMα-expressing cells and diphtheria toxin-induced deletion of these cells (23). In the fate mapping RELMα-cre mice, any cell in which the *Retnla* promoter has been active at any time, will have constitutive reporter protein expression throughout its lifespan, therefore potentially overrepresenting RELMα expression. In contrast, the reporter mouse model described here can reflect temporal changes in *Retnla* promoter activity. Here, we validate its utility as a faithful reporter by side-by-side analysis of TdTomato reporter and RELMα mRNA and protein expression. Compared to the RELMα-cre mice, or other studies

in helminth infection, we found that peritoneal macrophages were the dominant source of RELMα, while eosinophils and B1 cells only expressed modest levels of RELMα in response to IL-4. Our data is consistent with RNA-seq and Immgen datasets that evaluate naïve immune cell subsets (13), where small peritoneal macrophages are the highest RELMα expressors. Compared to other mouse models, these mice offer the potential to specifically delete RELMα within individual cells. Furthermore, this alleviates the need for diphtheria toxin, that causes apoptosis and can have pathologic consequences independent of RELMα function. In this study, we validated our transgenic mice by crossing them to a universal cre-deleter mouse line, however, this transgenic mouse model provides the valuable opportunity in future studies to delete RELMα in specific cell-types.

Consistent with other studies demonstrating a protective and anti-inflammatory role for RELMα, we show that RELMα is only expressed in naïve small peritoneal macrophage but is expressed by small and large peritoneal macrophages in IL-4-induced peritonitis. Within the peritoneal cavity, the main cell target of RELMα was the large peritoneal macrophage (LPM), where RELMα limited LPM proliferation and activation. This suggests that the same cell-type that produces RELMα is also its target, suggesting a macrophage-intrinsic negative feedback loop. Since IL-4 drives significant expansion of peritoneal resident macrophages, it may be important for immune homeostasis and energy conservation to have internal feedback mechanisms, such as RELMα, to keep this process in-check. For instance, sustained IL-4 exposure leads to immunopathology such as the macrophage activation syndrome, where splenomegaly is observed (38). The treatment regime in our studies involved only two IL-4c injections, however, $R\alpha^{Td/Td}$ mice had already begun to exhibit immunopathologic features such as splenomegaly.

Gene expression analysis of the peritoneal macrophages from wild-type or RELMα-deficient mice indicated dual effects for RELMα in limiting proliferation and promoting survival, while also regulating macrophage polarization. RELMα-deficient macrophages had reduced expression of checkpoint inhibitors Dusp2, Batf (43, 63), but increased expression of anti-apoptotic signals such as Bcl2, Ctss and Pim2 (**Figure S3B**) (64, 65). RELMα-deficient macrophages exhibited increased genes associated with functional myeloid pathways compared to wild-type macrophages, suggesting overall enhanced myeloid activation. These included increased expression of Cd74, Cd14, Mpeg1, Ccl6 and MHCII, increased complement factors associated with the coagulation cascade (C1qa, C1qb, C1qc), and higher expression of phagocytic and scavenger receptors (Mertk, Cd32, Cd16, Marco). Most of RELMα-deficient macrophages upregulated genes associated M1 macrophage activation and antimicrobial function, including Cybb (66), Ifnar2 (67), Birc3 (68), Ccr5 (69) and Cd84 (70) (**Figure S3B**). In contrast, RELMα deficiency did not affect expression of other M2 macrophage signature genes such as Ym1 or Arginase, suggesting a regulatory effect of RELMα through inhibiting M1 activation, rather than promoting M2 activation.

Although gene expression analysis was performed on bulk-sorted peritoneal macrophages and did not distinguish monocyte-derived SPM from resident LPM, RELMα deficiency resulted in a heterogeneous macrophage phenotype with SPM and LPM markers. These included increased expression in RELMα-deficient macrophages of LPM-specific genes such as Timd4 and Cxcl13, but also SPM-associated genes MHCII, CD62L (Sell), CD38 and CD74 (71, 72). IL-4c-induced peritonitis has been previously shown to be caused by resident LPM proliferation rather than the recruitment of blood monocytes (17, 73). In our studies both $R\alpha^{Td/Td}$ SPM and LPM showed evidence of increased proliferative capacity with elevated Ki67 expression compared to $R\alpha^{+/+}$ macrophages, yet we did not observe significantly increased SPM numbers. It is possible that in the $RELM\alpha^{-/-}$ environment, SPM were transitioning to LPM, as has been reported in inflammatory environments (71–73). Indeed, the absence of RELMα led to increased circulating inflammatory cytokines including TNFα, IFNγ, IL-6 and IL-1α, and exacerbated splenomegaly. Gene expression analysis revealed increased genes associated with growth factor signaling and angiogenesis (e.g. Pdgfb, Ncf2 and Fn1) in the RELMα-deficient macrophages, which could have contributed to the splenomegaly.

The main regulatory effects of RELMα in limiting inflammation and immunopathology were observed following IL-4 treatment, however, MHCII genes (H2-Aa, H2-Ab1 and H2-DMa) were consistently elevated in the RELMα-deficient macrophages in both PBS and IL-4c treatment, suggesting a potential effect of RELMα on antigen presentation in a homeostatic or type 2 cytokine environment. To investigate the role of macrophage-intrinsic RELMα in T cell responses, we performed splenocyte co-cultures with peritoneal macrophages from wild-type or RELMα-deficient mice. RELMα deficiency had no significant effect on effector T cell responses, however, was unable to support optimal regulatory T cell proliferation. The direct mechanism underlying this defect is unclear, however, cytokine quantification revealed decreased Treg-associated cytokines GM-CSF (74) and IL-10, and conversely increased IL-6 in RELMα-deficient macrophage co-cultures. These co-culture findings were supported by the *in vivo* studies, where there was reduced Treg frequency in the spleen, but enhanced Th17 cell responses. RELMα-deficient macrophages had increased expression of the IL-2R (CD25), suggesting that they may limit IL-2 availability to the Tregs (75, 76), which was supported by our finding that IL-2 levels were significantly reduced in RELMα-deficient macrophage co-cultures. However, further experiments are needed to functionally link CD25 expression with IL-2 consumption by RELMα-deficient macrophages. Also, future investigation of the Tregs is warranted, such as their ability to suppress naïve T cells, and how their function is altered by RELMα. Immunofluorescent staining validated Treg reduction in the spleen, which may have contributed to the splenomegaly by removal of this regulatory brake. Macrophages in the spleen express RELMα, therefore splenic macrophage function may be similar to what was observed for the peritoneal cavity macrophages. An alternative possibility is that peritoneal macrophages migrate to the spleen, as prior studies observed peritoneal macrophage migration to other organs such as the liver in response to injury (2). Previous studies used bone marrow-derived macrophages or dendritic cells and *in vivo* helminth infection to address RELMα function in T cell

polarization (28–30). Findings from these studies revealed many effects of RELMα on T cells, such as limiting Th2 cell polarization and promoting T cell-derived IL-10. Our studies support an immune regulatory role for RELMα on Tregs. However, we did not observe any differences in Th2 cell polarization, potentially because we interrogated the effect of RELMα on IL-4-induced responses, compared to the more complex outcomes and regulatory networks in helminth infection. Here, we further demonstrate the *in vivo* significance of resident peritoneal macrophages, which express significantly higher levels of RELMα than *in vitro* bone marrow-derived cells. We also identify a targeted effect of RELMα on promoting Treg proliferation with functional consequences to limit spleen immunopathology. Overall, these studies identify dual effects of macrophage-intrinsic RELMα in limiting macrophage activation while supporting Treg responses with the overall effect of limiting type 2 cytokine-mediated immunopathology. Investigation of this macrophage-Treg axis, and how it is influenced by RELMα, will be an important future direction to assess the biological significance of this interaction beyond IL-4c injection. Specifically, this immune regulatory role for RELMα in the peritoneal cavity may critically influence the outcome of type 2 cytokine-biased diseases such as helminth infection, injury and repair to visceral organs (77–80), but conversely may have impact in other settings where peritoneal macrophages and Tregs are detrimental such as in cancer metastases (81, 82).

DATA AVAILABILITY STATEMENT

The data has been uploaded to NCBI - accession number is GSE174606.

ETHICS STATEMENT

The animal study was reviewed and approved by University of California Riverside Institutional Animal Care and Use Committee.

AUTHOR CONTRIBUTIONS

MN and JL conceptualized the study. JL and NL developed the methodology. JL, SK, and NL performed the investigation. MN and JL performed the formal analysis. MN and JL wrote the article. SK and DC edited the manuscript. MN and DC supervised the study. All authors contributed to the article and approved the submitted version.

FUNDING

This research was supported by the UCR School of Medicine (to MN), and the National Institutes of Health (NIAID, R01AI153195 to MN). DC was supported in part by the National Institutes of Health (NICHD, R01HD091167).

SUPPLEMENTARY MATERIAL

The Supplementary Material for this article can be found online at: https://www.frontiersin.org/articles/10.3389/fimmu.2021.710406/full#supplementary-material

REFERENCES

1. Bain CC, Jenkins SJ. The Biology of Serous Cavity Macrophages. *Cell Immunol* (2018) 330:126–35. doi: 10.1016/j.cellimm.2018.01.003
2. Wang J, Kubes P. A Reservoir of Mature Cavity Macrophages That Can Rapidly Invade Visceral Organs to Affect Tissue Repair. *Cell* (2016) 165 (3):668–78. doi: 10.1016/j.cell.2016.03.009
3. Jackson-Jones LH, Bénézech C. Control of Innate-Like B Cell Location for Compartmentalised IgM Production. *Curr Opin Immunol* (2018) 50:9–13. doi: 10.1016/j.coi.2017.10.006
4. Wong K, Valdez PA, Tan C, Yeh S, Hongo JA, Ouyang W. Phosphatidylserine Receptor Tim-4 Is Essential for the Maintenance of the Homeostatic State of Resident Peritoneal Macrophages. *Proc Natl Acad Sci USA* (2010) 107 (19):8712–7. doi: 10.1073/pnas.0910929107
5. Rodriguez-Manzanet R, Sanjuan MA, Wu HY, Quintana FJ, Xiao S, Anderson AC, et al. T and B Cell Hyperactivity and Autoimmunity Associated With Niche-Specific Defects in Apoptotic Body Clearance in TIM-4-Deficient Mice. *Proc Natl Acad Sci USA* (2010) 107(19):8706–11. doi: 10.1073/pnas.0910359107
6. Newson J, Stables M, Karra E, Arce-Vargas F, Quezada S, Motwani M, et al. Resolution of Acute Inflammation Bridges the Gap Between Innate and Adaptive Immunity. *Blood* (2014) 124(11):1748–64. doi: 10.1182/blood-2014-03-562710
7. Huynh ML, Fadok VA, Henson PM. Phosphatidylserine-Dependent Ingestion of Apoptotic Cells Promotes TGF-Beta1 Secretion and the Resolution of Inflammation. *J Clin Invest* (2002) 109(1):41–50. doi: 10.1172/JCI11638
8. Butenko S, Satyanarayanan SK, Assi S, Schif-Zuck S, Sher N, Ariel A. Transcriptomic Analysis of Monocyte-Derived Non-Phagocytic Macrophages Favors a Role in Limiting Tissue Repair and Fibrosis. *Front Immunol* (2020) 11:405. doi: 10.3389/fimmu.2020.00405
9. Jorch SK, Surewaard BG, Hossain M, Peiseler M, Deppermann C, Deng J, et al. Peritoneal GATA6+ Macrophages Function as a Portal for Staphylococcus Aureus Dissemination. *J Clin Invest* (2019) 129(11):4643–56. doi: 10.1172/JCI127286
10. Cailhier JF, Partolina M, Vuthoori S, Wu S, Ko K, Watson S, et al. Conditional Macrophage Ablation Demonstrates That Resident Macrophages Initiate Acute Peritoneal Inflammation. *J Immunol* (2005) 174(4):2336–42. doi: 10.4049/jimmunol.174.4.2336
11. Noy R, Pollard JW. Tumor-Associated Macrophages: From Mechanisms to Therapy. *Immunity* (2014) 41(1):49–61. doi: 10.1016/j.immuni.2014.06.010
12. Jin Z, Zhu Z, Liu S, Hou Y, Tang M, Zhu P, et al. TRIM59 Protects Mice From Sepsis by Regulating Inflammation and Phagocytosis in Macrophages. *Front Immunol* (2020) 11:263. doi: 10.3389/fimmu.2020.00263
13. Kim KW, Williams JW, Wang YT, Ivanov S, Gilfillan S, Colonna M, et al. MHC II+ Resident Peritoneal and Pleural Macrophages Rely on IRF4 for Development From Circulating Monocytes. *J Exp Med* (2016) 213(10):1951–9. doi: 10.1084/jem.20160486
14. Jenkins SJ, Ruckerl D, Thomas GD, Hewitson JP, Duncan S, Brombacher F, et al. IL-4 Directly Signals Tissue-Resident Macrophages to Proliferate Beyond Homeostatic Levels Controlled by CSF-1. *J Exp Med* (2013) 210(11):2477–91. doi: 10.1084/jem.20121999
15. Holcomb IN, Kabakoff RC, Chan B, Baker TW, Gurney A, Henzel W, et al. FIZZ1, a Novel Cysteine-Rich Secreted Protein Associated With Pulmonary Inflammation, Defines a New Gene Family. *EMBO J* (2000) 19(15):4046–55. doi: 10.1093/emboj/19.15.4046
16. Pine GM, Batugedara HM, Nair MG. Here, There and Everywhere: Resistin-Like Molecules in Infection, Inflammation, and Metabolic Disorders. *Cytokine* (2018) 110:442–51. doi: 10.1016/j.cyto.2018.05.014

17. Jenkins SJ, Ruckerl D, Cook PC, Jones LH, Finkelman FD, van Rooijen N, et al. Local Macrophage Proliferation, Rather Than Recruitment From the Blood, is a Signature of TH2 Inflammation. *Science* (2011) 332(6035):1284–8. doi: 10.1126/science.1204351
18. Bosurgi L, Cao YG, Cabeza-Cabrerizo M, Tucci A, Hughes LD, Kong Y, et al. Macrophage Function in Tissue Repair and Remodeling Requires IL-4 or IL-13 With Apoptotic Cells. *Science* (2017) 356(6342):1072–6. doi: 10.1126/science.aai8132
19. Torres-Capelli M, Marsboom G, Li QO, Tello D, Rodriguez FM, Alonso T, et al. Role of Hif2α Oxygen Sensing Pathway in Bronchial Epithelial Club Cell Proliferation. *Sci Rep* (2016) 6. doi: 10.1038/srep25357
20. Liu T, Yu H, Ullenbruch M, Jin H, Ito T, Wu Z, et al. The *In Vivo* Fibrotic Role of FIZZ1 in Pulmonary Fibrosis. *PloS One* (2014) 9(2):e88362. doi: 10.1371/journal.pone.0088362
21. Lin Q, Fan C, Skinner JT, Hunter EN, Macdonald AA, Illei PB, et al. Relmα Licenses Macrophages for Damage-Associated Molecular Pattern Activation to Instigate Pulmonary Vascular Remodeling. *J Immunol* (2019) 203 (11):2862–71. doi: 10.4049/jimmunol.1900535
22. Batugedara HM, Li J, Chen G, Lu D, Patel JJ, Jang JC, et al. Hematopoietic Cell-Derived Relmα Regulates Hookworm Immunity Through Effects on Macrophages. *J Leukoc Biol* (2018) 104(4):855–69. doi: 10.1002/JLB.4A0917-369RR
23. Krljanac B, Schubart C, Naumann R, Wirtz S, Culemann S, Krönke G, et al. Relmα-Expressing Macrophages Protect Against Fatal Lung Damage and Reduce Parasite Burden During Helminth Infection. *Sci Immunol* (2019) 4 (35). doi: 10.1126/sciimmunol.aau3814
24. Sutherland TE, Rückerl D, Logan N, Duncan S, Wynn TA, Allen JE. Ym1 Induces Relmα and Rescues IL-4rα Deficiency in Lung Repair During Nematode Infection. *PloS Pathog* (2018) 14(11):e1007423. doi: 10.1371/journal.ppat.1007423
25. Chen G, Wang SH, Jang JC, Odegaard JI, Nair MG. Comparison of Relmα and Relmβ Single- and Double-Gene-Deficient Mice Reveals That Relmα Expression Dictates Inflammation and Worm Expulsion in Hookworm Infection. *Infect Immun* (2016) 84(4):1100–11. doi: 10.1128/IAI.01479-15
26. Knipper JA, Willenborg S, Brinckmann J, Bloch W, Maaß T, Wagener R, et al. Interleukin-4 Receptor α Signaling in Myeloid Cells Controls Collagen Fibril Assembly in Skin Repair. *Immunity* (2015) 43(4):803–16. doi: 10.1016/j.immuni.2015.09.005
27. Kim SY, Nair MG. Macrophages in Wound Healing: Activation and Plasticity. *Immunol Cell Biol* (2019) 97(3):258–67. doi: 10.1111/imcb.12236
28. Pesce JT, Ramalingam TR, Wilson MS, Mentink-Kane MM, Thompson RW, Cheever AW, et al. Retnla (Relmalpha/Fizz1) Suppresses Helminth-Induced Th2-Type Immunity. *PloS Pathog* (2009) 5(4):e1000393. doi: 10.1371/journal.ppat.1000393
29. Nair MG, Du Y, Perrigoue JG, Zaph C, Taylor JJ, Goldschmidt M, et al. Alternatively Activated Macrophage-Derived RELM-{Alpha} Is a Negative Regulator of Type 2 Inflammation in the Lung. *J Exp Med* (2009) 206(4):937–52. doi: 10.1084/jem.20082048
30. Cook PC, Jones LH, Jenkins SJ, Wynn TA, Allen JE, MacDonald AS. Alternatively Activated Dendritic Cells Regulate CD4+ T-Cell Polarization *In Vitro* and In Vivo. *Proc Natl Acad Sci USA* (2012) 109(25):9977–82. doi: 10.1073/pnas.1121231109
31. Harris TA, Gattu S, Propheter DC, Kuang Z, Bel S, Ruhn KA, et al. Resistin-Like Molecule α Provides Vitamin-A-Dependent Antimicrobial Protection in the Skin. *Cell Host Microbe* (2019) 25(6):777–88.e8. doi: 10.1016/j.chom.2019.04.004
32. Xu ZL, Mizuguchi H, Mayumi T, Hayakawa T. Woodchuck Hepatitis Virus Post-Transcriptional Regulation Element Enhances Transgene Expression From Adenovirus Vectors. *Biochim Biophys Acta* (2003) 1621(3):266–71. doi: 10.1016/s0304-4165(03)00078-3
33. Fujiyama S, Nakahashi-Oda C, Abe F, Wang Y, Sato K, Shibuya A. Identification and Isolation of Splenic Tissue-Resident Macrophage Sub-Populations by Flow Cytometry. *Int Immunol* (2019) 31(1):51–6. doi: 10.1093/intimm/dxy064
34. Chen KE, Lainez NM, Nair MG, Coss D. Visceral Adipose Tissue Imparts Peripheral Macrophage Influx Into the Hypothalamus. *J Neuroinflamm* (2021) 18(1):140. doi: 10.1186/s12974-021-02183-2
35. Tomfohr J, Lu J, Kepler TB. Pathway Level Analysis of Gene Expression Using Singular Value Decomposition. *BMC Bioinf* (2005) 6:225. doi: 10.1186/1471-2105-6-225
36. Babicki S, Arndt D, Marcu A, Liang Y, Grant JR, Maciejewski A, et al. Heatmapper: Web-Enabled Heat Mapping for All. *Nucleic Acids Res* (2016) 44 (W1):W147–53. doi: 10.1093/nar/gkw419
37. Liu M, Silva-Sanchez A, Randall TD, Meza-Perez S. Specialized Immune Responses in the Peritoneal Cavity and Omentum. *J Leukoc Biol* (2021) 109 (4):717–29. doi: 10.1002/JLB.5MIR0720-271RR
38. Milner JD, Orekov T, Ward JM, Cheng L, Torres-Velez F, Junttila I, et al. Sustained IL-4 Exposure Leads to a Novel Pathway for Hemophagocytosis, Inflammation, and Tissue Macrophage Accumulation. *Blood* (2010) 116 (14):2476–83. doi: 10.1182/blood-2009-11-255174
39. Panova V, Gogoi M, Rodriguez-Rodriguez N, Sivasubramaniam M, Jolin HE, Heycock MWD, et al. Group-2 Innate Lymphoid Cell-Dependent Regulation of Tissue Neutrophil Migration by Alternatively Activated Macrophage-Secreted Ear11. *Mucosal Immunol* (2021) 14(1):26–37. doi: 10.1038/s41385-020-0298-2
40. Dickinson RJ, Keyse SM. Diverse Physiological Functions for Dual-Specificity MAP Kinase Phosphatases. *J Cell Sci* (2006) 119(22):4607–15. doi: 10.1242/jcs.03266
41. Ansel KM, Harris RB, Cyster JG. CXCL13 is Required for B1 Cell Homing, Natural Antibody Production, and Body Cavity Immunity. *Immunity* (2002) 16(1):67–76. doi: 10.1016/s1074-7613(01)00257-6
42. Wei W, Jiao Y, Postlethwaite A, Stuart JM, Wang Y, Sun D, et al. Dual-Specificity Phosphatases 2: Surprising Positive Effect at the Molecular Level and a Potential Biomarker of Diseases. *Genes Immun* (2013) 14(1):1–6. doi: 10.1038/gene.2012.54
43. Lin SC, Chien CW, Lee JC, Yeh YC, Hsu KF, Lai YY, et al. Suppression of Dual-Specificity Phosphatase-2 by Hypoxia Increases Chemoresistance and Malignancy in Human Cancer Cells. *J Clin Invest* (2011) 121(5):1905–16. doi: 10.1172/JCI44362
44. Zhang J, Lo C. Regulation of Fibronectin Expression by PDGF-BB and IGF-I in Cultured Rat Thoracic Aortic Adventitial Fibroblasts. *Cell Biol Int* (1995) 19 (6):517–25. doi: 10.1006/cbir.1995.1096
45. A-Gonzalez N, Quintana JA, García-Silva S, Mazariegos M, González de la Aleja A, Nicolás-Ávila JA, et al. Phagocytosis Imprints Heterogeneity in Tissue-Resident Macrophages. *J Exp Med* (2017) 214(5):1281–96. doi: 10.1084/jem.20161375
46. Egami Y. Molecular Imaging Analysis of Rab GTPases in the Regulation of Phagocytosis and Macropinocytosis. *Anat Sci Int* (2016) 91(1):35–42. doi: 10.1007/s12565-015-0313-y
47. Mantegazza AR, Magalhaes JG, Amigorena S, Marks MS. Presentation of Phagocytosed Antigens by MHC Class I and II. *Traffic* (2013) 14(2):135–52. doi: 10.1111/tra.12026
48. Schaer DJ, Schleiffenbaum B, Kurrer M, Imhof A, Bächli E, Fehr J, et al. Soluble Hemoglobin-Haptoglobin Scavenger Receptor CD163 as a Lineage-Specific Marker in the Reactive Hemophagocytic Syndrome. *Eur J Haematol* (2005) 74(1):6–10. doi: 10.1111/j.1600-0609.2004.00318.x
49. Fuentes-Duculan J, Suárez-Fariñas M, Zaba LC, Nograles KE, Pierson KC, Mitsui H, et al. A Subpopulation of CD163-Positive Macrophages is Classically Activated in Psoriasis. *J Invest Dermatol* (2010) 130(10):2412–22. doi: 10.1038/jid.2010.165
50. Culemann S, Grüneboom A, Nicolás-Ávila J, Weidner D, Lämmle KF, Rothe T, et al. Locally Renewing Resident Synovial Macrophages Provide a Protective Barrier for the Joint. *Nature* (2019) 572(7771):670–5. doi: 10.1038/s41586-019-1471-1
51. Skytthe MK, Graversen JH, Moestrup SK. Targeting of CD163. *Int J Mol Sci* (2020) 21(15):1–32. doi: 10.3390/ijms21155497
52. Li J, Lu E, Yi T, Cyster JG. EBI2 Augments Tfh Cell Fate by Promoting Interaction With IL-2-Quenching Dendritic Cells. *Nature* (2016) 533 (7601):110–4. doi: 10.1038/nature17947
53. Ghosn EE, Cassado AA, Govoni GR, Fukuhara T, Yang Y, Monack DM, et al. Two Physically, Functionally, and Developmentally Distinct Peritoneal Macrophage Subsets. *Proc Natl Acad Sci USA* (2010) 107(6):2568–73. doi: 10.1073/pnas.0915000107
54. Cassado A, D'Império Lima MR, Bortoluci KR. Revisiting Mouse Peritoneal Macrophages: Heterogeneity, Development, and Function. *Front Immunol* (2015) 6:225. doi: 10.3389/fimmu.2015.00225
55. Zhang N, Czepielewski RS, Jarjour NN, Erlich EC, Esaulova E, Saunders BT, et al. Expression of Factor V by Resident Macrophages Boosts Host Defense in the Peritoneal Cavity. *J Exp Med* (2019) 216(6):1291–300. doi: 10.1084/jem.20182024

56. Zindel J, Peiseler M, Hossain M, Deppermann C, Lee WY, Haenni B, et al. Primordial GATA6 Macrophages Function as Extravascular Platelets in Sterile Injury. *Science* (2021) 371(6533):1–12. doi: 10.1126/science.abe0595
57. Dahdah A, Gautier G, Attout T, Fiore F, Lebourdais E, Msallam R, et al. Mast Cells Aggravate Sepsis by Inhibiting Peritoneal Macrophage Phagocytosis. *J Clin Invest* (2014) 124(10):4577–89. doi: 10.1172/JCI75212
58. Roberts AW, Lee BL, Deguine J, John S, Shlomchik MJ, Barton GM. Tissue-Resident Macrophages Are Locally Programmed for Silent Clearance of Apoptotic Cells. *Immunity* (2017) 47(5):913–27.e6. doi: 10.1016/j.immuni.2017.10.006
59. Okabe Y, Medzhitov R. Tissue-Specific Signals Control Reversible Program of Localization and Functional Polarization of Macrophages. *Cell* (2014) 157 (4):832–44. doi: 10.1016/j.cell.2014.04.016
60. Mosser DM, Edwards JP. Exploring the Full Spectrum of Macrophage Activation. *Nat Rev Immunol* (2008) 8(12):958–69. doi: 10.1038/nri2448
61. Liu Q, Tian Y, Zhao X, Jing H, Xie Q, Li P, et al. NMAAP1 Expressed in BCG-Activated Macrophage Promotes M1 Macrophage Polarization. *Mol Cells* (2015) 38(10):886–94. doi: 10.14348/molcells.2015.0125
62. Mao R, Wang C, Zhang F, Zhao M, Liu S, Liao G, et al. Peritoneal M2 Macrophage Transplantation as a Potential Cell Therapy for Enhancing Renal Repair in Acute Kidney Injury. *J Cell Mol Med* (2020) 24(6):3314–27. doi: 10.1111/jcmm.15005
63. Quigley M, Pereyra F, Nilsson B, Porichis F, Fonseca C, Eichbaum Q, et al. Transcriptional Analysis of HIV-Specific CD8+ T Cells Shows That PD-1 Inhibits T Cell Function by Upregulating BATF. *Nat Med* (2010) 16 (10):1147–51. doi: 10.1038/nm.2232
64. Salpeter SJ, Pozniak Y, Merquiol E, Ben-Nun Y, Geiger T, Blum G. A Novel Cysteine Cathepsin Inhibitor Yields Macrophage Cell Death and Mammary Tumor Regression. *Oncogene* (2015) 34(50):6066–78. doi: 10.1038/onc.2015.51
65. Asano J, Nakano A, Oda A, Amou H, Hiasa M, Takeuchi K, et al. The Serine/Threonine Kinase Pim-2 Is a Novel Anti-Apoptotic Mediator in Myeloma Cells. *Leukemia* (2011) 25(7):1182–8. doi: 10.1038/leu.2011.60
66. Gerrick KY, Gerrick ER, Gupta A, Wheelan SJ, Yegnasubramanian S, Jaffee EM. Transcriptional Profiling Identifies Novel Regulators of Macrophage Polarization. *PloS One* (2018) 13(12):e0208602. doi: 10.1371/journal.pone.0208602
67. Orecchioni M, Ghosheh Y, Pramod AB, Ley K. Macrophage Polarization: Different Gene Signatures in M1(LPS+) vs. *Classically M2(LPS-) Vs Alternatively Activated Macrophages Front Immunol* (2019) 10:1084. doi: 10.3389/fimmu.2019.01084
68. Conte D, Holcik M, Lefebvre CA, Lacasse E, Picketts DJ, Wright KE, et al. Inhibitor of Apoptosis Protein Ciap2 is Essential for Lipopolysaccharide-Induced Macrophage Survival. *Mol Cell Biol* (2006) 26(2):699–708. doi: 10.1128/MCB.26.2.699-708.2006
69. Shaheen ZR, Christmann BS, Stafford JD, Moran JM, Buller RML, Corbett JA. CCR5 is a Required Signaling Receptor for Macrophage Expression of Inflammatory Genes in Response to Viral Double-Stranded RNA. *Am J Physiol Regul Integr Comp Physiol* (2019) 316(5):R525–34. doi: 10.1152/ajpregu.00019.2019
70. Sintes J, Romero X, de Salort J, Terhorst C, Engel P. Mouse CD84 is a Pan-Leukocyte Cell-Surface Molecule That Modulates LPS-Induced Cytokine Secretion by Macrophages. *J Leukoc Biol* (2010) 88(4):687–97. doi: 10.1189/jlb.1109756
71. Louwe PA, Badiola Gomez L, Webster H, Perona-Wright G, Bain CC, Forbes SJ, et al. Recruited Macrophages That Colonize the Post-Inflammatory Peritoneal Niche Convert Into Functionally Divergent Resident Cells. *Nat Commun* (2021) 12(1):1770. doi: 10.1038/s41467-021-21778-0
72. Bain CC, Gibson DA, Steers NJ, Boufea K, Louwe PA, Doherty C, et al. Rate of Replenishment and Microenvironment Contribute to the Sexually Dimorphic Phenotype and Function of Peritoneal Macrophages. *Sci Immunol* (2020) 5 (48). doi: 10.1126/sciimmunol.abc4466
73. Liu Z, Gu Y, Chakarov S, Bleriot C, Kwok I, Chen X, et al. Fate Mapping *via* Ms4a3-Expression History Traces Monocyte-Derived Cells. *Cell* (2019) 178 (6):1509–1525.e19. doi: 10.1016/j.cell.2019.08.009
74. Kared H, Leforban B, Montandon R, Renand A, Layseca Espinosa E, Chatenoud L, et al. Role of GM-CSF in Tolerance Induction by Mobilized Hematopoietic Progenitors. *Blood* (2008) 112(6):2575–8. doi: 10.1182/blood-2008-02-140681
75. Kryczek I, Wei S, Zou L, Altuwaijri S, Szeliga W, Kolls J, et al. Cutting Edge: Th17 and Regulatory T Cell Dynamics and the Regulation by IL-2 in the Tumor Microenvironment. *J Immunol* (2007) 178(11):6730–3. doi: 10.4049/jimmunol.178.11.6730
76. Driesen J, Popov A, Schultze JL. CD25 as an Immune Regulatory Molecule Expressed on Myeloid Dendritic Cells. *Immunobiology* (2008) 213(9-10). doi: 10.1016/j.imbio.2008.07.026
77. Spellberg B, Edwards JE. Type 1/Type 2 Immunity in Infectious Diseases. *Clin Infect Dis* (2001) 32(1):76–102. doi: 10.1086/317537
78. Boothby IC, Cohen JN, Rosenblum MD. Regulatory T Cells in Skin Injury: At the Crossroads of Tolerance and Tissue Repair. *Sci Immunol* (2020) 5(47). doi: 10.1126/sciimmunol.aaz9631
79. Xiao F, Liu X, Guo SW. Platelets and Regulatory T Cells May Induce a Type 2 Immunity That Is Conducive to the Progression and Fibrogenesis of Endometriosis. *Front Immunol* (2020) 11:610963. doi: 10.3389/fimmu.2020.610963
80. Wang Z, Hao C, Zhuang Q, Zhan B, Sun X, Huang J, et al. Excretory/Secretory Products From *Trichinella Spiralis* Adult Worms Attenuated DSS-Induced Colitis in Mice by Driving PD-1-Mediated M2 Macrophage. *Front Immunol* (2020) 11:563784. doi: 10.3389/fimmu.2020.563784
81. Mikuła-Pietrasik J, Uruski P, Tykarski A, Książek K. The Peritoneal "Soil" for a Cancerous "Seed": A Comprehensive Review of the Pathogenesis of Intraperitoneal Cancer Metastases. *Cell Mol Life Sci* (2018) 75(3):509–25. doi: 10.1007/s00018-017-2663-1
82. Movahedi K, Laoui D, Gysemans C, Baeten M, Stangé G, Van den Bossche J, et al. Different Tumor Microenvironments Contain Functionally Distinct Subsets of Macrophages Derived From Ly6C(high) Monocytes. *Cancer Res* (2010) 70(14):5728–39. doi: 10.1158/0008-5472.CAN-09-4672

Conflict of Interest: The authors declare that the research was conducted in the absence of any commercial or financial relationships that could be construed as a potential conflict of interest.

Copyright © 2021 Li, Kim, Lainez, Coss and Nair. This is an open-access article distributed under the terms of the Creative Commons Attribution License (CC BY). The use, distribution or reproduction in other forums is permitted, provided the original author(s) and the copyright owner(s) are credited and that the original publication in this journal is cited, in accordance with accepted academic practice. No use, distribution or reproduction is permitted which does not comply with these terms.

frontiers in Immunology

ORIGINAL RESEARCH
published: 19 August 2021
doi: 10.3389/fimmu.2021.704427

Protectins PCTR1 and PD1 Reduce Viral Load and Lung Inflammation During Respiratory Syncytial Virus Infection in Mice

Katherine H. Walker[1], Nandini Krishnamoorthy[1], Thayse R. Brüggemann[1], Ashley E. Shay[2], Charles N. Serhan[2] and Bruce D. Levy[1]**

[1] Pulmonary and Critical Care Medicine, Department of Medicine, Brigham and Women's Hospital and Harvard Medical School, Boston, MA, United States, [2] Center for Experimental Therapeutics and Reperfusion Injury, Department of Anesthesiology, Perioperative and Pain Medicine, Brigham and Women's Hospital and Harvard Medical School, Boston, MA, United States

Viral pneumonias are a major cause of morbidity and mortality, owing in part to dysregulated excessive lung inflammation, and therapies to modulate host responses to viral lung injury are urgently needed. Protectin conjugates in tissue regeneration 1 (PCTR1) and protectin D1 (PD1) are specialized pro-resolving mediators (SPMs) whose roles in viral pneumonia are of interest. In a mouse model of Respiratory Syncytial Virus (RSV) pneumonia, intranasal PCTR1 and PD1 each decreased RSV genomic viral load in lung tissue when given after RSV infection. Concurrent with enhanced viral clearance, PCTR1 administration post-infection, decreased eosinophils, neutrophils, and NK cells, including NKG2D$^+$ activated NK cells, in the lung. Intranasal PD1 administration post-infection decreased lung eosinophils and *Il-13* expression. PCTR1 increased lung expression of cathelicidin anti-microbial peptide and decreased interferon-gamma production by lung CD4$^+$ T cells. PCTR1 and PD1 each increased interferon-lambda expression in human bronchial epithelial cells *in vitro* and attenuated RSV-induced suppression of interferon-lambda in mouse lung *in vivo*. Liquid chromatography coupled with tandem mass spectrometry of RSV-infected and untreated mouse lungs demonstrated endogenous PCTR1 and PD1 that decreased early in the time course while cysteinyl-leukotrienes (cys-LTs) increased during early infection. As RSV infection resolved, PCTR1 and PD1 increased and cys-LTs decreased to pre-infection levels. Together, these results indicate that PCTR1 and PD1 are each regulated during RSV pneumonia, with overlapping and distinct mechanisms for PCTR1 and PD1 during the resolution of viral infection and its associated inflammation.

Keywords: resolution, interferon, pro-resolving, docosahexaenoic acid, viral

OPEN ACCESS

Edited by:
Amiram Ariel,
University of Haifa, Israel

Reviewed by:
Christianne Bandeira-Melo,
Federal University of Rio de Janeiro, Brazil
Jun Miyata,
National Defense Medical College, Japan

***Correspondence:**
Nandini Krishnamoorthy
nkrishnamoorthy@bwh.harvard.edu
Bruce D. Levy
blevy@bwh.harvard.edu

Specialty section:
This article was submitted to Inflammation, a section of the journal Frontiers in Immunology

Received: *02 May 2021*
Accepted: *06 July 2021*
Published: *19 August 2021*

Citation:
Walker KH, Krishnamoorthy N, Brüggemann TR, Shay AE, Serhan CN and Levy BD (2021) Protectins PCTR1 and PD1 Reduce Viral Load and Lung Inflammation During Respiratory Syncytial Virus Infection in Mice. Front. Immunol. 12:704427. doi: 10.3389/fimmu.2021.704427

Abbreviations: 17-HDHA, 17-hydroxydocosahexaenoic acid; ANOVA, Analysis of Variance; BAL, Bronchoalveolar Lavage; CAMP, Cathelicidin Anti-Microbial Peptide (previously LL-37 in humans); cys-, cysteinyl; DHA, Docosahexaenoic Acid; EPI, Enhanced product ion; GSTM4, Glutathione S-transferase Mu 4; IFN, Interferon; IL, Interleukin; i.n., intranasal; LC-MS/MS, Liquid Chromatography coupled with tandem Mass Spectrometry; LOX, Lipoxygenase; LT, Leukotriene; LTC_4S, Leukotriene C_4 synthase; Ly6G, Lymphocyte antigen 6 complex locus G6D; mGST, microsomal glutathione S-transferase; NKG2D, Natural Killer Group 2D; NK1.1, Natural Killer cell marker, also known as Killer Cell Lectin-like Receptor subfamily B member (KLRB1C) or CD161; ns, not significant; PBS, Phosphate Buffered Saline; PCTR1, Protectin conjugates in tissue regeneration 1: 16*R*-glutathionyl, 17*S*-hydroxy-4*Z*,7*Z*,10*Z*,12*E*,14*E*,19*Z*-docosahexaenoic acid; PD1, protectin D1: 10*R*,17*S*-dihydroxy-4*Z*,7*Z*,11*E*,13*E*,15*Z*,19*Z*-docosahexaenoic acid; PDx, protectin Dx: 10*S*,17*S*-dihydroxy-4*Z*,7*Z*,11*E*,13*Z*,15*E*,19*Z*-docosahexaenoic acid; p.i., post infection; RSV, Respiratory Syncytial Virus; SiglecF, Sialic acid-binding immunoglobulin-like lectin F; SPM, Specialized pro-resolving mediator; Veh, Vehicle.

INTRODUCTION

The resolution of inflammation is an actively regulated process in which specialized pro-resolving mediators (SPMs) play a prominent role. SPMs are endogenous lipid mediators that include lipoxins, resolvins, maresins, and protectins, which are enzymatically produced from essential polyunsaturated fatty acids (1). SPMs can drive the resolution of acute inflammatory processes to restore tissue homeostasis after sterile or infectious injury and can enhance pathogen clearance in animal infection models (2, 3). Of particular interest is the docosahexaenoic acid (DHA)-derived protectin family of SPMs, including protectin conjugates in tissue regeneration 1 (PCTR1: 16*R*-glutathionyl, 17*S*-hydroxy-4*Z*,7*Z*,10*Z*,12*E*,14*E*,19*Z*-docosahexaenoic acid) (4) and protectin D1 (PD1: 10*R*,17*S*-dihydroxy-4*Z*,7*Z*,11*E*,13*E*, 15*Z*,19*Z*-docosahexaenoic acid) (5) (see **Figure 1**).

DHA is converted to 17*S*-hydro(peroxy)-docosahexaenoic acid (17*S*-H(p)DHA) *via* 15-lipoxygenase (LOX) in human cells and 12/15-LOX in mice (5, 6). Enzymatic epoxidation of 17*S*-H(p)DHA produces the 16*S*,17*S*-epoxy-protectin intermediate (5, 6). Enzymatic hydrolysis of the 16*S*,17*S*-epoxy-protectin intermediate generates protectin D1 (PD1) (5, 6) and glutathione S-transferase-mediated (LTC_4S, leukotriene C_4 synthase; GSTM4, glutathione S-transferase Mu 4; mGST3, microsomal glutathione S-transferase 3) S_N2 reaction with glutathione produces protectin conjugates in tissue regeneration 1 (PCTR1) (4, 7, 8). Because of structural similarities between PCTRs and other cysteinyl-SPMs (cys-SPMs) such as maresin conjugates in tissue regeneration, PCTR1 is proposed to be subsequently converted to PCTR2 by γ-glutamyl transferase, followed by conversion to PCTR3 by dipeptidases (9). Of note, this biosynthetic pathway can be influenced by neuronal stimuli such as acetylcholine (10). Protectins act through G-coupled receptors (11) and intracellular mediators such as TNF receptor associated factor 3 (12).

Importantly, PCTR1 is present in human lung tissue (13) and decreases neutrophil migration while increasing macrophage recruitment and efferocytosis (4). PD1 is present in human exhaled breath condensates and decreases during acute airway inflammation such as asthma exacerbation (14); PD1 decreases T cell migration, promotes T cell apoptosis, and reduces inflammatory cytokine production (15).

Respiratory Syncytial Virus (RSV) is a leading cause of viral lower respiratory tract infection in children and elderly patients, causing over 34 million estimated infections and 3.5 million estimated hospitalizations annually across the globe (16, 17). The most severe cases are marked clinically by respiratory failure and pathologically by peribronchial and interstitial inflammation, with airways often occluded by cellular debris and mucus (18). The host response to RSV infection is complex, involving multiple cellular and molecular factors, overall promoting viral clearance but often causing significant pathogen-associated lung pathology (19). Although anti-inflammatory agents such as steroids suppress inflammation, they do not improve RSV outcomes and are limited by immunosuppressive risks including secondary bacterial infection and impaired viral clearance (20). While monoclonal antibodies can prevent severe RSV infection in high-risk infants (21), no therapies are available for active infection, making new approaches to RSV treatment urgently necessary (22).

The relationship between SPMs and viral-mediated acute lung inflammation is of interest. PCTR1 promotes resolution of bacterial inflammation (4); the role of PCTR1 in viral infection remains to be determined. During influenza infection, strain virulence is associated with impaired SPM signaling in mice, and PD1 limits viral replication *via* inhibition of viral RNA nuclear export *in vitro*, improving survival when administered *in vivo* in a mouse model (23). During RSV infection, enzymatic activity of 5-lipoxygenase, necessary for biosynthesis of the lipoxin and resolvin families of SPMs, promotes resolution of lung injury *via* alternative activation of macrophages (24); however, the roles of PCTR1 and PD1 from the protectin pathway remain to be determined in RSV infection.

Here, we investigated PCTR1 and PD1's actions in RSV infections and identified temporal regulation of protectins in the lung after RSV infection. When given post-infection, these protectins attenuated lung inflammation, reduced viral burden, and regulated interferon and anti-microbial peptide expression.

MATERIALS AND METHODS

Viral Propagation and Quantification

Respiratory Syncytial Virus, strain Line 19, was originally isolated from a sick infant and generously provided by Dr. Nicholas Lukacs (University of Michigan, MI). Virus was propagated in HEp-2 cells (ATCC, Manassas, VA) and quantified by plaque assay, similar to prior publications (25) using NY3.2 $STAT1^{-/-}$ murine fibroblast cells (26) generously provided by Dr. Jennifer Bomberger (University of Pittsburgh, PA). Cells were cultured at 37°C in 5% CO_2 in Dulbecco's Modified Eagle's Medium (DMEM) with L-glutamine (Lonza, Mapleton, IL) supplemented with 10% Fetal Bovine Serum (Denville Scientific, Metuchen, NJ), 100 U/mL penicillin with 100 μg/mL streptomycin (Lonza), and 10 μg/mL gentamycin (Sigma-Aldrich, St. Louis, MO).

Animals and Infection

Experimental protocols were approved by the Institutional Animal Care and Use Committee at Harvard Medical School/ Brigham and Women's Hospital. 6-8 week old C57BL/6 male mice (Jackson Laboratory, Bar Harbor, ME) were housed in specific pathogen-free conditions at 25°C with regular light and dark cycles at the Center for Comparative Medicine at Brigham and Women's Hospital. Mice were fed *ad libitum* with a standard commercial diet including approximately 13.1% total fat and 0.5% omega-3 fatty acids (ScottPharma, Marlborough, MA). Under inhaled isoflurane anesthesia, mice were infected with 10^5 Plaque Forming Units (PFU) of viral stock in 30-50 μL of Hep2 cell culture media. In some experiments, isoflurane-anesthetized mice were administered 15 μL of SPM (100 ng) or vehicle (Phosphate Buffered Saline, PBS) intranasally (i.n.) on days 3, 4, 5 post infection (p.i.) and harvested on day 6 or day 8 p.i.

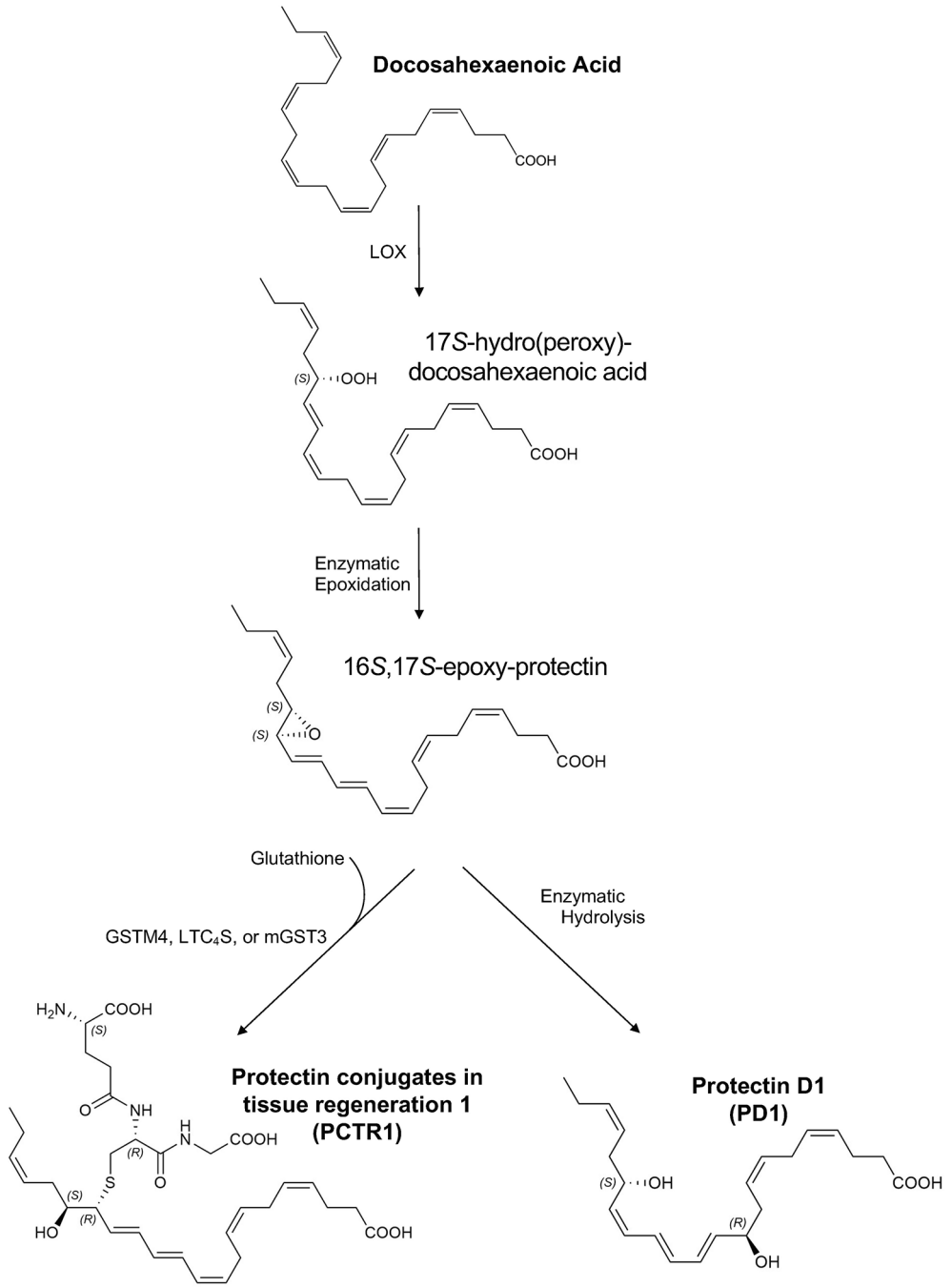

FIGURE 1 | Proposed biosynthesis of protectin conjugates in tissue regeneration 1 (PCTR1) and protectin D1 (PD1). Docosahexaenoic acid (DHA) is converted to 17*S*-hydro(peroxy)-docosahexaenoic acid (17*S*-H(p)DHA) *via* 15-lipoxygenase (LOX) in human cells and 12/15-LOX in mice (5, 6). Enzymatic epoxidation of 17*S*-H(p) DHA produces the 16*S*,17*S*-epoxy-protectin intermediate (5, 6). Enzymatic hydrolysis of the 16*S*,17*S*-epoxy-protectin intermediate generates protectin D1 (PD1) (5, 6) and glutathione S-transferase-mediated (LTC_4S, leukotriene C_4 synthase; GSTM4, glutathione S-transferase Mu 4; mGST3, microsomal glutathione S-transferase 3) S_N2 reaction with glutathione produces protectin conjugates in tissue regeneration 1 (PCTR1) (4, 7, 8). The products and intermediates are depicted in their assigned complete stereochemical configurations (4–6).

Specialized Pro-Resolving Mediators

PCTR1 (16*R*-glutathionyl, 17*S*-hydroxy-4*Z*,7*Z*,10*Z*,12*E*,14*E*,19*Z*-docosahexaenoic acid), $^{13}C_2^{15}N$-PCTR1, and $^{13}C_3^{15}N$-MCTR3 were each synthesized by total organic synthesis and provided by Dr. Nicos A. Petasis (University of Southern California) *via* subcontract for P01GM095467 to CNS. PCTR1, PD1 (10*R*,17*S*-dihydroxy-4*Z*,7*Z*,11*E*,13*E*,15*Z*,19*Z*-docosahexaenoic acid), 17-HDHA, d_4-LTB_4, d_8-5*S*-HETE, d_5-LTC_4, d_5-LTD_4, LTC_4, LTD_4,

and LTE_4 were purchased from Cayman Chemical (Ann Arbor, MI). For cellular administration, PCTR1, PD1, or vehicle (ethanol) was diluted in media to a final ethanol concentration <0.1%. For mouse administration, PCTR1, PD1, or vehicle (ethanol) was brought to dryness with a gentle stream of nitrogen gas prior to resuspension in PBS. Before experiments, each SPM was authenticated and validated using an unbiased library search (Sciex OS Version 1.7.0.36606) and was in accordance with its reported physical properties established earlier (4, 5).

Quantitative Polymerase Chain Reaction

Perfused left lungs or cell monolayers were homogenized in TRIzol (Invitrogen, Carlsbad, CA) and total RNA was extracted using a chloroform extraction method as previously described (27). After DNAse treatment (Invitrogen), cDNA was generated using the Taqman Reverse Transcription Kit (Thermo Fisher Scientific, Waltham, MA). Samples were quantified on AriaMx real-time qPCR system (Agilent Technologies, Santa Clara, CA) using EvaGreen supermix (Bio-Rad, Hercules, CA) and primers as described (Integrated DNA Technologies, Coralville, IA) (**Table S1**). Quantification was performed using the $2^{-\Delta\Delta Ct}$ method, using *18s* housekeeping gene to calculate fold change relative to naïve control or RSV-infected vehicle control as specified. Mouse and human mRNA expression of the PD1 receptor GPR37 (11) in sorted lung cells was obtained from the public LungMAP Database (https://lungmap.net).

Histopathology

Right lungs were fixed by inflation with Zinc Fixative (BD Biosciences) *via* tracheostomy at a transpulmonary pressure of 20 cm H_2O. Lung sections were stained by the Rodent Histopathology Core at Harvard Medical School. Images were obtained using a CX33 microscope with EP50 camera (Olympus Life Science, Tokyo, Japan).

Lung Cell Preparation

Lungs were perfused with 5mL PBS *via* right ventricular puncture, extracted and maintained on ice in PBS with 0.7 mg/mL Collagenase A (Roche, Cambridge MA), 30 μg/mL DNase I (Sigma-Aldrich) and 2% FBS. Lung tissue was dissociated into a single cell suspension using a gentleMACS dissociator (Miltenyi Biotec, Somerville, MA) according to the manufacturer's instructions. Lung cells were filtered through a 70 μm strainer (Thermo Fisher Scientific) and counted in Trypan Blue (Sigma-Aldrich) *via* hemocytometer (eFluor 506, Thermo Fisher Scientific). Cells were stained with viability dye (eFluor 506, Thermo Fisher Scientific), fixed and permeabilized using the FoxP3 kit (eBioscience San Diego, CA) according to the manufacturer's instructions prior to staining for flow cytometry. In some cases, cells were stimulated in a commercial cocktail of phorbol 12-myristate 13-acetate, ionomycin, brefeldin A and monensin (Tonbo Biosciences, San Diego CA) for 4 hours prior to viability dye, fixing, permeabilization, and staining.

Flow Cytometry

The following antibodies were used to identify cellular subsets and intracellular cytokines in whole lung homogenates: from BioLegend (San Diego, CA) CD45-PerCP, CD11c-FITC, Ly6G-AF700, MHC class II-BV421, CD4-FITC, CD8a-APC-Cy7, CD3-Q655, NKG2D-PE, NK1.1-PE-Cy7, IFNγ-PE; from eBioscience, CD11b-APC; from BD Biosciences (San Jose, CA) SiglecF-PE. Samples were obtained using an LSR Fortessa flow cytometer (BD Biosciences) and analyzed using FlowJo software version 10 (Ashland, OR). Cells of interest were identified after exclusion of debris, dead cells and doublets (**Figure S2**).

Bronchoalveolar Lavage and Enzyme-Linked Immunosorbent Assay (ELISA)

Lungs were lavaged with two separated volumes of 1 mL each of 0.6 mM EDTA in PBS, *via* an intratracheal catheter. ELISA for murine interferon-alpha (PBL Assay Science, Piscataway, NJ), interferon-beta and interferon-lambda 2/3 (R&D Systems, Minneapolis, MN) in BAL samples was performed according to manufacturer's instructions. Interferon levels were normalized to total protein content in BAL fluid as measured by bicinchoninic acid assay (Thermo Fisher Scientific).

Human Airway Epithelial Cells

Calu-3 (ATCC) and A549 (ATCC) human airway epithelial cell lines were cultured in Eagle's Minimum Essential Media (ATCC) or Dulbecco's Modified Eagle's Medium (Lonza), respectively, with 10% FBS, penicillin, and streptomycin as above. Cell monolayers were grown to >80% confluency, washed with PBS and infected in media with 0% FBS at a multiplicity of infection of 0.05 or 0.1 for 2 hours. Viral inoculum was replaced by 10% FBS media with PCTR1 or PD1 (10 nM) or vehicle (ethanol) and cells were incubated at 37°C in 5% CO_2 for 24 hours.

Lipid Mediator Metabololipidomics

Un-perfused lung tissue was snap-frozen in liquid nitrogen, prior to addition of ice-cold liquid chromatography/mass spectrometry-grade methanol (Thermo Fisher Scientific) containing 500 pg of each of the following deuterium-labeled internal standards: d_8-5*S*-HETE (Cayman Chemical), d_4-LTB_4 (Cayman Chemical), d_5-LTC_4 (Cayman Chemical), d_5-LTD_4 (Cayman Chemical), $^{13}C_3^{15}N$-MCTR3, and $^{13}C_2^{15}N$-PCTR1 for calculating extraction and recovery of endogenous material. Lungs were gently dispersed using a glass tissue grinder (Kimble Chase Life Science and Research Products, Vineland, NJ) and protein precipitation occurred at -20°C for 30 minutes. Lung suspensions were centrifuged at 1000 g for 10 minutes at 4°C, supernatants were collected, and products were solid phase extracted per optimized methods using an automated extractor (Extrahera, Biotage, Charlotte, NC) as in reference (8). Samples were brought to an apparent pH 3.5 with acidified water (9 mL), and rapidly loaded onto 3 mL-SPE Isolute C18 100 mg cartridges (Biotage) and neutralized with double-distilled water (4 mL). The columns were washed once with hexane (Supelco, Bellefonte, PA) (4 mL). Next, the methyl formate fraction (Sigma-Aldrich) (4 mL) eluted SPMs, prostaglandins, leukotrienes, and thromboxane. The methanol fraction (Thermo Fisher Scientific) (4 mL) eluted cys-SPMs and cys-LTs. Both the methyl formate and methanol fractions were separately brought to dryness with a gentle stream of nitrogen

gas using an automated evaporation system (TurboVap LV, Biotage), and immediately suspended in a methanol-water mixture (50:50, *v/v*) for injection on liquid chromatography tandem mass spectrometer (LC-MS/MS). Samples were injected and data acquired using a LC-MS/MS 6500$^+$ QTRAP in low mass mode (Sciex, Framingham, MA) equipped with an ExionLC (Shimadzu, Tokyo, Japan).

A Kinetex Polar C18 column (100 mm x 4.6 mm x 2.6 µm; Phenomenex, Torrance, CA, USA) was kept in a column heat jacket maintained at 50°C. (**Table S2**) specifies polarity, retention time (min), Q1 (*m/z*), Q3 (*m/z*), dwell time (msec), declustering potential (DP, V), entrance potential (EP, V), collision energy (CE, V), collision cell exit potential (CXP, V), calibration correlation coefficient (r^2), and lower limit of detection (LLOD, pg) for each mediator. The mobile phase gradient, multiple reaction monitoring (MRM), and enhanced product ion (EPI) mode settings are described in (**Table S3**). For each mediator, linear calibration curves were obtained using synthetic material with r^2 values of ≥0.98. Identification of each mediator included unbiased MS/MS matching (>70% fit score) to authentic and synthetic material in a MS/MS library (library matching parameters: precursor mass tolerance ± 0.8 Da, fragment mass tolerance ± 0.4 Da, collision energy ± 5 eV, use polarity, intensity threshold = 0.05, minimal purity = 5.0%, and intensity factor = 100) and a matching retention time to those of the authentic and synthetic material. Data was acquired with Analyst 1.7.1 software (Sciex). The MS/MS spectral library was created in LibraryView version 1.4.0 (Sciex). LC-MS/MS MRM trace data and EPI spectral data are shown as screen captures from Sciex OS version 1.7.0.36606 (Sciex).

Statistics

Statistical analysis was performed using GraphPad Prism software, version 9 (San Diego, CA) or RStudio (Boston, MA). One-way ANOVA with Holm-Sidak's correction for multiple comparisons was used for parametric data, and Kruskall-Wallis test with Dunn's correction for multiple comparisons was used for non-parametric data. Findings were considered significant when $p \leq 0.05$ and not significant when $p > 0.10$. Statistical outliers were excluded by Rout's outlier analysis (Q = 1%). For qPCR experiments, statistical analysis was performed on ΔCT values for time-course data, and on ΔCT values normalized to each experiment (ΔCT of sample/average ΔCT of the RSV-infected vehicle control group) for replicate experiments of RSV-infected mice.

RESULTS

RSV Pneumonia Resolves Spontaneously in C57/BL6 Mice

In order to investigate mechanisms of resolution of RSV infection and associated inflammation, we generated a self-limited RSV pneumonia model: C57/BL6 mice were infected intranasally with 10^5 Plaque Forming Units (PFU) of a clinically-isolated strain of RSV, Line 19 (28). Lung weight and RNA copies of RSV genes were measured serially after infection (**Figure 2**). Weight of the right lung was significantly increased 3 days post infection (p.i.) (189.0 ± 15.1 mg) compared to pre-infection lung weight (92.6 ± 2.0 mg, $p<0.001$) and to lung weights at 6 days p.i. (93.5 ± 4.9 mg, $p<0.001$) and 12 days p.i. (110.0 ± 1.78 mg, $p<0.001$). Simultaneously, viral load, as measured by quantitative PCR (qPCR) of the RSV nucleoprotein (*N*) gene RNA in whole left lung, was increased day 3 p.i. (mean fold change of 3.79 ± 2.41 x10^4, $p=0.010$) and day 6 p.i. (mean fold change of 1.52 ± 0.56 x10^4, $p=0.010$), with no remaining difference by day 12 p.i. Similarly, RNA copies of the RSV Large polymerase (*L*) gene, which correlate with active viral replication (29), were increased at day 3 p.i. (mean fold change of 4.63 ± 2.66 x10^3, $p=0.001$) and day 6 p.i. (mean fold change of 3.27 ± 1.05 x10^3, $p=0.001$), with no remaining difference by day 12 p.i.

PCTR1 and PD1 Decrease Viral Burden During RSV Infection

Because PCTR1 and PD1 are present in lung tissue (13, 14) and PD1 reduced viral burden of influenza (23), we evaluated whether PCTR1 or PD1 could facilitate host resolution of RSV infection in this model. C57/BL6 mice were infected intranasally (i.n.) with 10^5 PFU of RSV as above, prior to i.n. treatment with PCTR1 (100 ng), PD1 (100 ng), or vehicle on days 3, 4, and 5 p.i., and lungs were harvested at day 6 or day 8 p.i. (**Figure 3A**). RSV *N gene* RNA was significantly decreased in PCTR1 and PD1 cohorts (mean fold changes of 0.40 ± 0.11 and 0.21 ± 0.10, respectively; $p=0.032$ and $p<0.001$, respectively) relative to vehicle control 6 days after RSV infection (**Figure 3B**). In addition, RSV *L gene* RNA transcripts were also decreased in PCTR1- and PD1-exposed lungs (mean fold changes of 0.68 ± 0.29 and 0.21 ± 0.07, respectively; $p=0.057$ and $p=0.004$, respectively) compared to vehicle control at day 6 p.i. (**Figure 3C**). These trends continued at day 8 p.i., with lower viral RNA transcripts of RSV *N gene* and RSV *L gene* in lung tissue of PCTR1 and PD1 cohorts compared to vehicle control. At day 8 relative to day 6 p.i., the vehicle mean fold change was 0.010 ± 0.006 for RSV *N* gene and 0.010 ± 0.007 for RSV *N gene* (**Figures 3D, E**). PCTR1 and PD1 treatment each further decreased RSV *N gene* viral transcripts on day 8 relative to vehicle control (mean fold change 0.001 ± <0.001 and <0.001 ± <0.001, respectively; $p=0.191$ and $p=0.062$, respectively) (**Figure 3D**). Similarly, PCTR1 and PD1 treatment each also decreased RSV *L gene* transcripts on day 8 relative to vehicle control (mean fold changes 0.003 ± 0.001 and 0.001 ± <0.001, respectively; $p=0.653$ and $p=0.100$) (**Figure 3E**).

Of note, mRNA copies of the recently identified RSV entry receptor, Insulin-like Growth Factor 1 Receptor (*Igf1r*), were not significantly changed after PCTR1 or PD1 exposure in mice at day 6 p.i. (ΔCT values of 13.9 ± 0.5 and 13.6 ± 0.7 respectively, compared to 13.6 ± 0.4 for vehicle control; *p*=ns for both). Calu-3 human airway epithelial cells express the PD1 receptor gene *GPR37* (11) (**Figure 5F**). Exposure to PCTR1 or PD1 did not significantly change RSV *N gene* or RSV *L gene* copies (**Figure S1**) or *IGF1R* expression (ΔCT values of 11.9 ± 0.1 and 11.8 ± 0.4 respectively, compared to 11.1 ± 0.7 for vehicle control; *p*=ns for both) in directly infected Calu-3 airway epithelial cells *in vitro* at

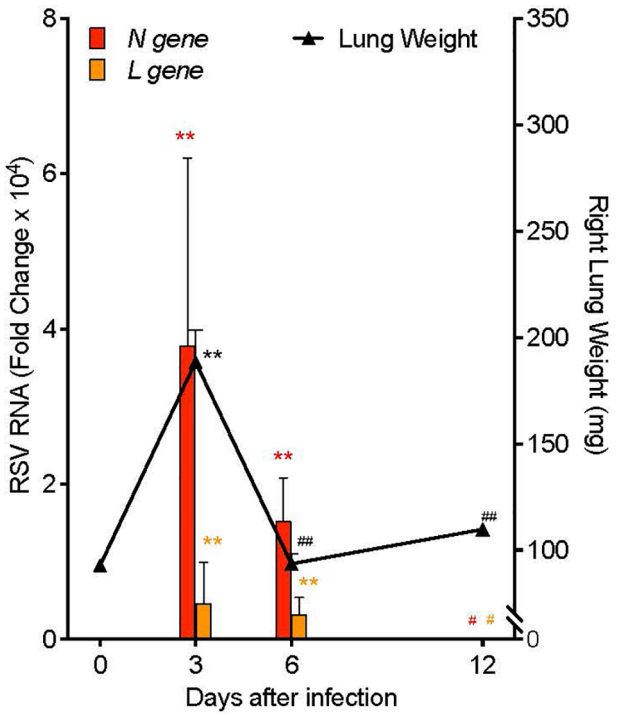

FIGURE 2 | Mouse RSV pneumonia resolves spontaneously. Mice were infected with 10^5 PFU of the RSV Line19 strain. Left axis: RSV *N gene* and *L gene* viral RNA expression in left lung tissue. Right axis: weight of right lung. Values are mean of n=3-4 per time point ± SEM and are representative of 2 separate experiments. $^{**}p < 0.01$ vs Day 0, $^{\#}p \leq 0.05$ vs Day 3, $^{\#\#}p < 0.01$ vs Day 3 by One-way ANOVA with Holm-Sidak's multiple comparison correction.

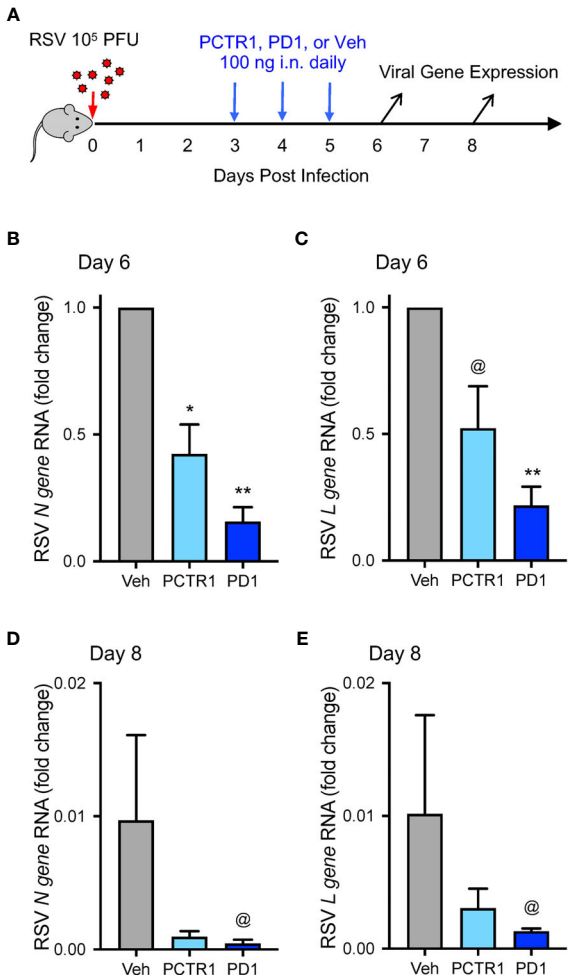

FIGURE 3 | PCTR1 and PD1 decrease viral transcripts during mouse RSV infection. **(A)** Schema of experimental mouse infection with intranasal 10^5 PFU of RSV, administration of PCTR1 or PD1 (100 ng intranasal) or vehicle daily on days 3-5 post infection, and measurement of viral gene expression on day 6 and day 8. **(B–E)** Relative RNA expression of **(B)** RSV *N gene* or **(C)** RSV *L gene* in the mouse lung tissue at day 6 after RSV infection or of **(D)** RSV *N gene* or **(E)** RSV *L gene* at day 8. Values are mean of n=4-9 per group ± SEM and include >4 separate experiments **(B, C)** or 1 experiment **(D, E)**. $^{*}p < 0.05$, $^{**}p < 0.01$, $^{@}p \leq 0.10$ vs vehicle by Kruskall-Wallis test with Dunn's multiple comparison correction.

24h p.i. The human airway epithelial cell line A549 also expressed *GPR37* RNA and was infected similarly without significant changes in viral gene expression after exposure to PCTR1 or PD1 (ΔCT values of 7.7 ± 0.1 and 7.9 respectively, compared to 8.1 ± 0.3 for vehicle control; *p*=ns for both).

PCTR1 and PD1 Decrease Lung Inflammation During RSV Infection

Given the decreases in viral load with *in vivo* PCTR1 or PD1 treatment, we evaluated effects of these SPMs on leukocyte responses to RSV. Mice were treated as in **Figure 3A**. At day 6 p.i., representative histology revealed alveolitis and peribronchial inflammation in RSV-infected mice exposed to vehicle control, with attenuation of these findings in infected mice exposed to PCTR1 or PD1 (**Figure 4A**). Given the predominantly interstitial nature of lung inflammation observed in this C57/BL6 mouse model, we evaluated single-cell lung homogenates by flow cytometry analysis for quantification of cellular subtypes (**Figures 4B–D**, **Figure S2**). Compared to vehicle, PCTR1 and PD1 significantly decreased lung $CD11c^{hi}CD11b^{lo}$ macrophages (2.24 ± 0.22 and 2.79 ± 0.26, respectively, vs 6.03 ± 1.44 cells $x10^5$ [vehicle], *p*=0.012 and 0.019) (**Figure 4E**) and lung eosinophils (0.41 ± 0.08 and 0.45 ± 0.09, respectively, vs 1.25 ± 0.37 cells $x10^5$ [vehicle], *p*=0.041 for both) (**Figure 4F**). PCTR1 significantly decreased lung neutrophils (0.95 ± 0.17 vs 3.72 ± 1.29 cells $x10^5$ [vehicle], *p*=0.044), with a similar trend for PD1 (1.60 ± 0.33 cells $x10^5$, *p*=0.082 vs vehicle) (**Figure 4G**).

Because skewing of cytokine and adaptive immune responses from type 1 to type 2 is associated with more severe RSV disease (29, 30), we evaluated the type 2 gene *Il-13* mRNA transcripts. *Il-13* expression was significantly decreased in infected mice exposed to PD1 relative to vehicle control (fold change 0.47 ± 0.22 vs vehicle, *p*=0.037) (**Figure 4H**). No significant changes in *Il-13* expression were present in mice exposed to PCTR1. Of note, neither PCTR1 nor PD1 increased *Il-13* expression or eosinophilia (**Figures 4F, H**).

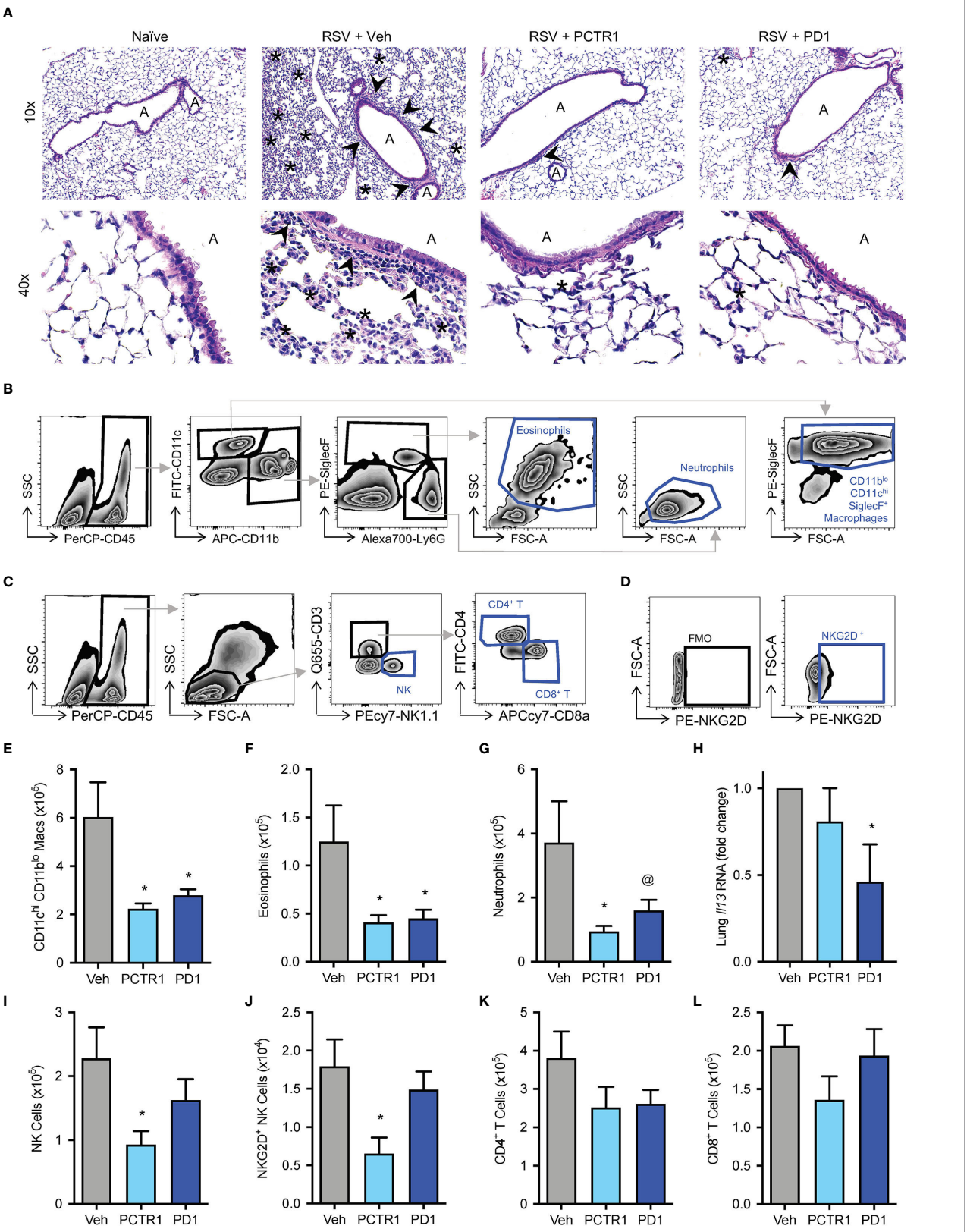

FIGURE 4 | Continued

FIGURE 4 | PCTR1 and PD1 decrease inflammatory responses to mouse RSV infection. Mice were infected with 10^5 PFU of RSV, followed by administration of PCTR1 or PD1 (100 ng intranasal) or vehicle daily on days 3-5 post infection and harvest of lungs at day 6. **(A)** Representative hematoxylin- and eosin-stained histology of mouse lung tissue at 10x and 40x magnification. "A" identifies airway lumen; arrowheads denote areas of peri-bronchiolitis; Asterix denotes area of interstitial alveolitis. **(B, C)** Gating strategy for identification of **(B)** macrophage and granulocyte or **(C)** lymphocyte subsets, after doublet and dead cell exclusion. **(D)** The NKG2D$^+$ NK cell population was determined by comparison to Fluorescence Minus One (FMO) staining. **(E–G)** Populations of **(E)** CD11c^{hi} CD11b^{lo} macrophages, **(F)** Eosinophils and **(G)** Neutrophils per right lung by flow cytometry. **(H)** Relative *Il-13* RNA expression in lung tissue. **(I–L)** Populations of **(I)** NK cells, **(J)** NKG2D$^+$ NK cells, **(K)** CD4$^+$ T cells, **(L)** CD8$^+$ T cells per right lung by flow cytometry. Values are mean of n ≥ 4 per group ± SEM and include >4 separate experiments **(B, C, E–I, K, L)** or 2 separate experiments **(D, J)**. $^*p < 0.05$ vs vehicle, $^@p < 0.10$ vs vehicle by one-way ANOVA with Holm-Sidak's multiple comparisons correction.

Additionally, PCTR1 decreased the number of Natural Killer (NK) cells in the lung (0.93 ± 0.21 vs 2.28 ± 0.49 cells x10^5 [vehicle], p=0.023) (**Figure 4I**), including NK cells expressing the NKG2D activating receptor (0.65 ± 0.21 vs 1.79 ± 0.35 cells x10^4 [vehicle], p=0.033) (**Figure 4J**), with a similar trend for CD4$^+$ and CD8$^+$ T cells (**Figures 4K, L**).

PCTR1 and PD1 Regulate Host Antiviral Responses During RSV Infection

Since PCTR1 and PD1 decreased viral load and inflammatory parameters *in vivo*, we next investigated whether PCTR1 or PD1 regulated anti-microbial peptide expression or interferon (IFN) signaling as potential mechanisms for enhanced viral clearance distinct from cellular inflammation. Expression of murine Cathelicidin Anti-Microbial Peptide (*Camp*, the human ortholog of which is also called *LL-37*) was significantly increased in the PCTR1 cohort compared to vehicle (fold change 2.48 ± 0.51, p=0.036) (**Figure 5A**). As measured by intracellular flow cytometric staining of stimulated CD4$^+$ T lymphocytes, PCTR1 significantly decreased interferon-gamma (IFNγ) expression compared to vehicle, as measured by IFNγ$^+$ CD4$^+$ T cells (1.08 ± 0.15 vs 2.82 ± 0.72 x10^4, p=0.029), returning

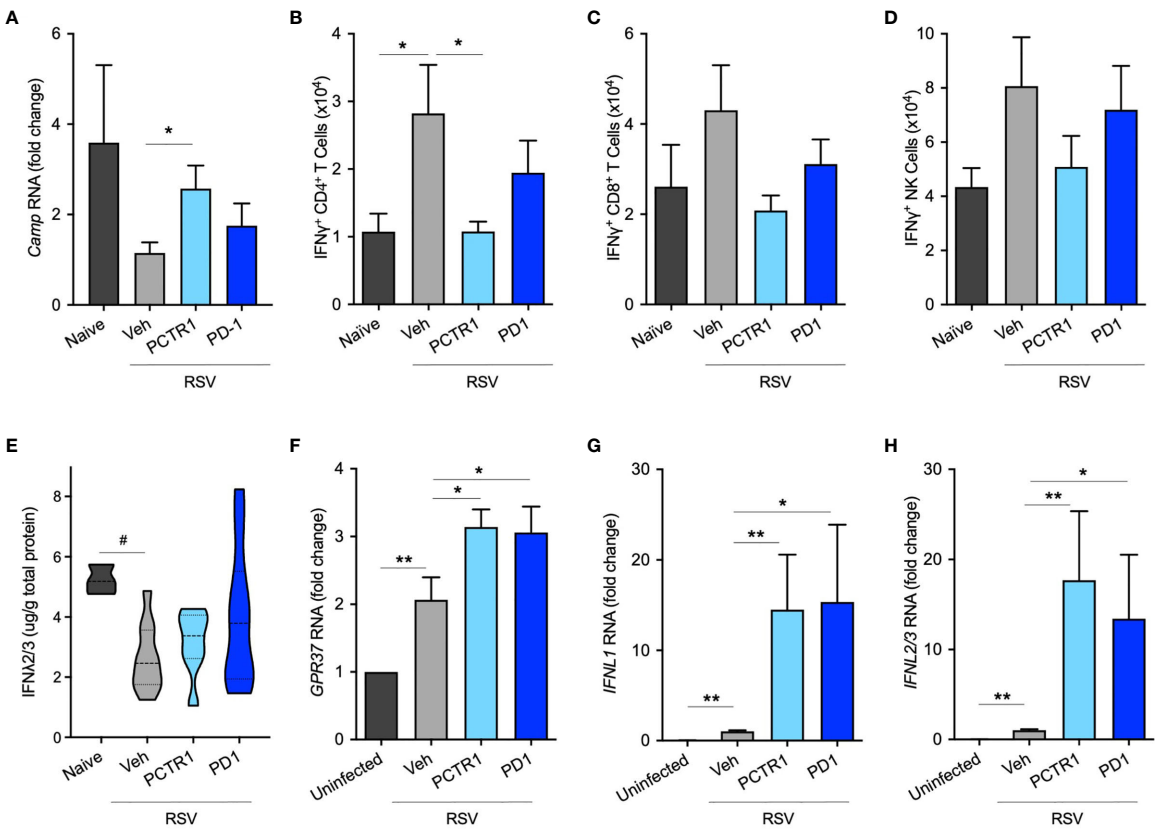

FIGURE 5 | PCTR1 and PD1 regulate host antiviral responses after RSV infection in mice. **(A)** Cathelicidin Anti-Microbial Peptide (*Camp)* RNA expression in mouse lung tissue at day 6 post infection with RSV 10^5 PFU. **(B–D)** Intracellular IFNγ expression in **(B)** CD4$^+$ T, **(C)** CD8$^+$ T, and **(D)** NK cells. **(E)** IFNλ2/3 protein concentrations in bronchoalveolar lavage fluid. **(F–H)** Relative RNA expression of **(F)** *GPR37*, **(G)** *IFNL1*, and **(H)** *IFNL2/3* in human airway epithelial cells. Values are mean of n = 4-11 per RSV group, n = 3-4 per naïve or uninfected group, ± SEM and include ≥3 separate experiments **(A–E)** or 2 separate experiments **(F–H)**. $^*p \leq 0.05$, $^{**}p < 0.01$ by one-way ANOVA with Holm-Sidak's multiple comparisons correction; $^\#p \leq 0.05$ by Kruskall-Wallis test with Dunn's multiple comparisons correction.

expression to pre-infection baseline (**Figure 5B**), with a similar trend for IFNγ$^+$ CD8$^+$ T cells and IFNγ$^+$ NK cells (**Figures 5C, D**). Concurrent with attenuation of IFNγ production, PCTR1 and PD1 increased expression of interferon-lambda (IFNλ) during RSV infection. RSV infection significantly decreased IFNλ protein levels in bronchoalveolar lavage (BAL) fluid relative to naïve controls (2.64 ± 0.35 [RSV + vehicle] vs 5.23 ± 0.28 [naïve] μg/g total protein, p=0.029). Of note, PCTR1 and PD1 prevented the RSV-induced decreases in IFNλ, maintaining the protective levels of IFNλ concentrations as those of uninfected mice (3.96 ± 0.68 and 3.15 ± 0.42 μg/g, respectively, p=ns for both) (**Figure 5E**). Type I interferons, interferon-alpha (IFNα) and -beta (IFNβ), were undetectable in BAL fluid at day 6 p.i.

In human airway epithelial cells directly infected with RSV, RNA expression of the PD1 receptor gene, *GPR37*, increased during RSV infection (2.07 ± 0.33 fold change compared to uninfected controls, p=0.007) and increased further with PCTR1 or PD1 exposure (fold changes 3.14 ± 0.26 and 3.06 ± 0.38, respectively, vs uninfected control, p<0.001 for both) (**Figure 5F**). Of note, RNA sequencing data from the LungMAP database (31) indicate that *GPR37* is expressed by epithelial cells in lung tissue throughout development in mice and humans (**Figure S3**). Exposure of RSV-infected human airway epithelial cells to either PCTR1 or PD1 significantly increased RNA expression of two isoforms of IFNλ, *IFNL1* (mean fold increases of 14.51 ± 6.07 and 15.35 ± 8.54, respectively, p=0.010 and p=0.016) and *IFNL2/3* (mean fold increases of 17.70 ± 7.64 and 13.43 ± 7.10, p=0.003 and p=0.016) compared to the RSV-infected vehicle cohort (**Figures 5G, H**). mRNA transcripts of *IFNα* and *IFNβ* were not detectable in these samples 24 hours after infection.

PCTR1 and PD1 Axes Are Temporally Regulated During RSV Infection

Since exogenous PCTR1 and PD1 administered on day 3 p.i. led to reduced genomic viral load and decreased interstitial lung inflammation when measured on day 6 p.i., we next evaluated whether endogenous production of protectins was altered during this self-limited model of RSV infection. Mice were infected with 10^5 PFU of RSV and lung tissue was subjected to multiple reaction monitoring (MRM) by liquid chromatography coupled with tandem mass spectrometry (LC-MS/MS) for evaluation of targeted lipid mediators at specified timepoints over the course of RSV infection.

Both PCTR1 and PD1 were detected in naïve and RSV-infected lung tissue in mice (**Figures 6A, C**), identified by an 80.1% unbiased library fit score and a 100.0% unbiased library fit score, respectively, as well as matching retention times to authentic and synthetic material (**Figures 6B, D**). PCTR1 and PD1 were significantly decreased at day 3 p.i. compared to naïve control (1.3 ± 0.8 pg/50 mg of lung tissue vs 12.4 ± 1.6 for PCTR1, p=0.001; 14.3 ± 1.4 vs 49.1 ± 3.7 for PD1, p=0.007) (**Table 1**) and increased significantly by day 12 p.i. (17.5 ± 0.9 pg/50 mg of lung tissue and 52.8 ± 3.7, respectively, compared to day 3 values; p<0.001 and p=0.004) (**Table 1**). Identification of the PD1 isomer protectin Dx (PDx, 10*S*,17*S*-dihydroxy-4*Z*,7*Z*,11*E*,13*Z*,15*E*,19*Z*-docosahexaenoic acid) and the separation between PD1 and PDx was also confirmed by unbiased library matching and retention time matching to authentic and synthetic material (data not shown). PCTR2 and PCTR3 were not detected in lungs during mouse RSV infection. Of interest, the DHA lipoxygenase product 17-hydroxy-docosahexaenoic acid (17-HDHA), a marker of the protectin biosynthetic pathway (**Figure 1**), was also significantly decreased at day 3 p.i. compared to naïve control (355.5 ± 46.2 pg/50 mg of lung tissue vs 1152.1 ± 61.9, respectively, p=0.004) and significantly increased by day 12 p.i. (1711.9 ± 128.7 pg/50 mg of lung tissue, p<0.001 compared to day 3 p.i.) (**Table 1**).

In addition to members of the protectin pathway, cys-LTs were also identified and detected in mouse lung tissue by LC-MS/MS and targeted MRM for each product (**Figure 7A**). Leukotriene C_4 (LTC_4) and D_4 (LTD_4) significantly increased in lung tissue at day 3 p.i. compared to that of naïve mice (1441 ± 296 pg/50 mg of lung tissue vs 3.74 ± 1.87 for LTC_4, p<0.001; 72.50 ± 7.25 vs 0.03 ± <0.01 for LTD_4, p<0.001) (**Figure 7B**). Both mediators significantly decreased by day 6 p.i. (5.48 ± 0.45 pg/50 mg lung tissue and 0.03 ± <0.01, respectively; p=0.001 and p<0.001 for each compared to day 3 p.i. values) (**Figure 7B**). Leukotriene E_4 was not significantly changed over the course of infection. As visualized in a Principal Components Analysis, the array of protectin and leukotriene mediators (PCTR1, PD1, 17-HDHA, LTC_4, LTD_4, and LTE_4) deviated from naïve baseline at day 3 p.i. and returned towards baseline over the subsequent time points during the resolution of infection (**Figure 7C**).

To investigate potential mechanisms for these temporal changes in SPM concentrations during RSV infection, we evaluated mRNA transcript copies of enzymes known to catalyze the production of PCTR1 and PD1 from DHA (**Figure 1**). Lung mRNA expression of 15-Lipoxygenase (gene *Alox15*) was not significantly changed at days 3 or 6 p.i. (mean fold changes of 1.30 ± 0.41 and 1.20 ± 0.43 compared to naïve control, p=0.255 and p=0.223, respectively) but was significantly reduced at 12 days p.i. (mean fold change 0.33 ± 0.10 compared to naïve control, p<0.001) in the setting of viral clearance (**Figure 8A**). We next explored RNA expression of identified glutathione S-transferases that convert epoxy intermediates to PCTR1 and LTC_4 (8). *Gstm4* transcripts were significantly decreased at day 3, day 6, and day 12 p.i. (mean fold changes of 0.26 ± 0.07, 0.43 ± 0.20, and 0.18 ± 0.09 respectively compared to naïve control, p=0.003 for all) (**Figure 8B**). RNA expression of *mGst2* was suppressed to a lesser extent at day 3 and day 12 p.i. (mean fold changes of 0.37 ± 0.08 and 0.32 ± 0.09 compared to naïve control, p=0.009 and p=0.007 respectively) (**Figure 8C**). *mGst3* transcripts were significantly decreased in mouse lung tissue at day 3 and day 12 p.i. (mean fold changes of 0.032 ± 0.11 and 0.11 ± 0.03 compared to naïve control, p=0.015 and p<0.001 respectively) (**Figure 8D**). *Ltc$_4$s* was significantly decreased to a similar extent as *Gstm4* at day 3 and day 12 p.i. (mean fold changes of 0.18 ± 0.06 and 0.21 ± 0.06, respectively, compared to naïve control; p<0.001 for both) (**Figure 8E**).

Expression of the PD1 receptor gene *Gpr37* (11) did not change significantly over the 12 days of infection (**Figure 8F**). RNA sequencing data from the LungMAP database (31) suggests

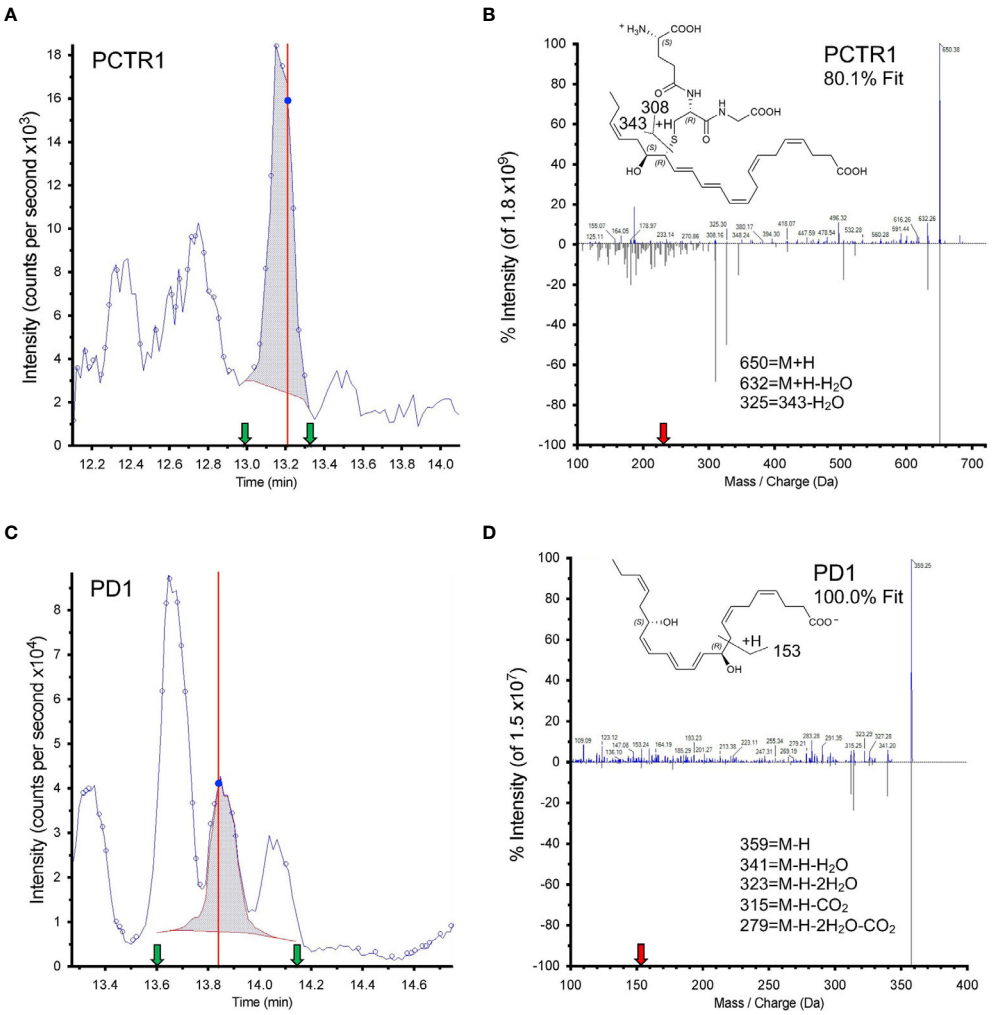

FIGURE 6 | Identification of PCTR1 and PD1 from RSV-infected mouse lung. **(A, C)** Screen captures from Sciex software of **(A)** PCTR1 and **(C)** PD1 targeted multiple reaction monitoring (MRM). Dark blue data-point indicates where the spectra for **(B, D)** were collected; vertical red line indicates the retention time for that data point. Shaded blue area denotes the area under the curve used for quantitation. Green arrows denote retention time at start and finish of quantitation. **(B, D)** Structure and tandem mass spectrometry fragmentation for **(B)** PCTR1 (*m/z* 650>231) with 80.1% unbiased fit to library and matching retention time and **(D)** PD1 (*m/z* 359>153) with 100% unbiased fit to library and matching retention time, analyzed with Sciex software. Upper MS/MS denotes sample spectrum; mirrored lower MS/MS denotes library spectrum obtained for synthetic PCTR1 and PD1. The red arrow on the x axis indicates Q3 used for quantitation. Insets show structures and proposed ion fragments.

TABLE 1 | Members of the protectin pathway of SPMs are temporally regulated by RSV infection in mice.

pg/50 mg tissue	Naïve	Day 3 p.i.	Day 6 p.i.	Day 12 p.i.
PCTR1	12.4 ± 1.6	1.3 ± 0.8*	8.3 ± 2.0#	17.5 ± 0.9
PD1	49.1 ± 3.7	14.3 ± 1.4*	31.0 ± 8.6	52.8 ± 3.7#
17-HDHA	1152.1 ± 61.9	355.5 ± 46.2*	965.0 ± 168.3#	1711.9 ± 128.7#

*Mice were infected with 10^5 PFU of RSV and lung was obtained at the specified time points post infection (p.i.). Values are mean of n = 3-4 mice per time point ± SEM. *p < 0.01 vs naïve, #p < 0.01 vs day 3 post-infection by one-way ANOVA with Holm-Sidak's multiple comparisons correction.*

that, within murine lung, *Gpr37* is most abundantly expressed on epithelial and mesenchymal cells by 4 weeks of age (**Figure S3A**) and in humans, persists in epithelial cells throughout life (**Figure S3B**).

DISCUSSION

Here, exogenous PCTR1 and PD1 decreased viral burden of RSV and concurrently decreased inflammation. Specifically, PCTR1

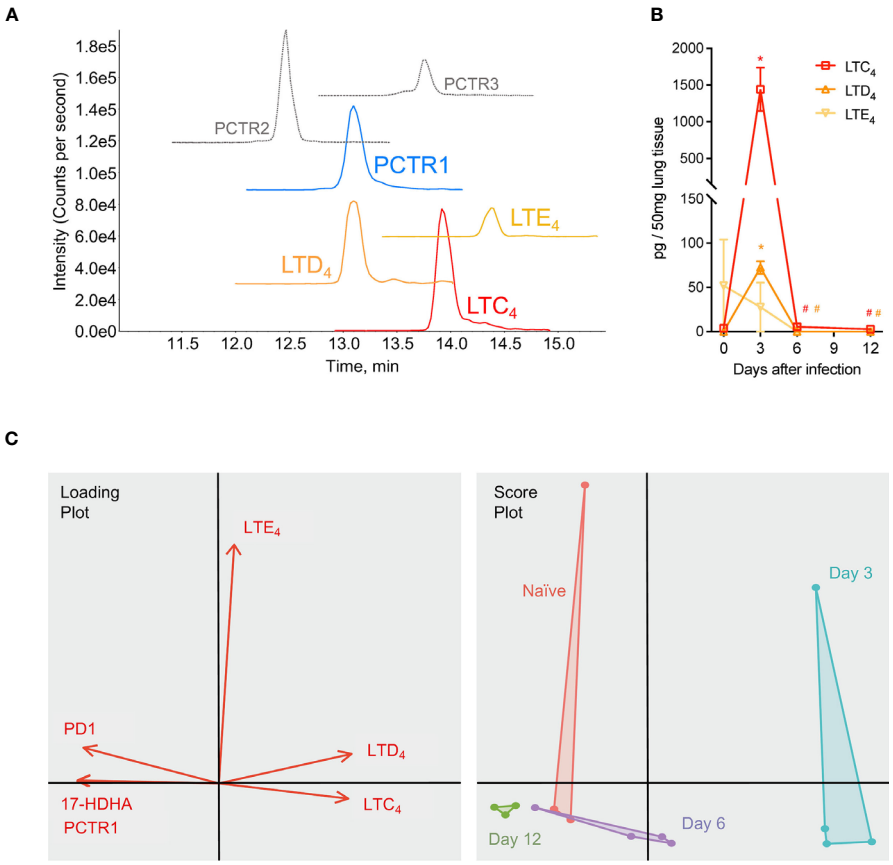

FIGURE 7 | Protectins and cysteinyl-leukotrienes (cys-LTs) are temporally regulated during mouse RSV infection. Mice were infected with 10^5 PFU of RSV and right lung was harvested at the time points stated. **(A)** Targeted multiple reaction monitoring (MRM) for PCTR1-3, LTC_4, LTD_4, and LTE_4 (1.0-point Gaussian smoothed) synthetic material, using Sciex ExionLC and 6500$^+$ Triple Quadrupole QTRAP operated in positive mode (see **Table S3** for details). **(B)** Time course of cys-LTs from RSV infections; data from LC-MS/MS quantitation expressed as pg/50 mg of mouse lung tissue. **(C)** Principal component analysis plots for PCTR1, PD1, 17-HDHA, LTC_4, LTD_4, and LTE_4 in lung tissues of naïve mice (red) or mouse lung tissues at day 3 (blue), day 6 (purple), and day 12 (green) post-infection with RSV. Values are mean of n = 3-4 mice per group ± SEM. $^*p < 0.01$ vs naïve, $^\#p < 0.01$ vs day 3 post-infection by one-way ANOVA with Holm-Sidak's multiple comparisons correction.

and PD1 decreased lung eosinophils, neutrophils and macrophages, with PCTR1 also decreasing both total and NKG2D$^+$ activated NK cells. This attenuated inflammation was associated with decreased *Il-13* expression with PD1, decreased IFNγ and increased anti-microbial peptide expression with PCTR1 *in vivo*, and increased IFNλ expression with either PCTR1 or PD1 *in vitro*. Of interest, endogenous levels of PCTR1 and PD1 were noted to be decreased in the early phase of RSV infection, with associated decreases in biosynthetic enzyme expression, during a concurrent increase in cys-LTs. These changes in lung lipid mediator profiles were most divergent from baseline at day 3 p.i., returning to baseline levels by day 12.

Since PCTR1 (13) and PD1 (14) are present in lung tissue and PD1 has been noted to suppress propagation of influenza virus (23), we examined the viral response to exogenous PCTR1 or PD1 and found that each molecule decreased genomic viral load during RSV infection *in vivo*, without evidence of a delay in viral clearance. Of interest, we did not find evidence of direct inhibition of viral replication in an *in vitro* model of airway epithelial cell infection with RSV, as has been observed with PD1 and PDx during influenza infection (23, 32). This difference suggested that innate and/or adaptive immune responses were relevant to PCTR1- or PD1-mediated control of RSV.

Immune responses to RSV are necessary for viral clearance but can also cause significant immunopathology (19). The pathology of fatal cases of human RSV infection suggests that host responses to limit viral replication also contribute to injury of 'innocent bystander' lung tissue, with inflammation present despite lack of detectable viral antigen in some cases (18). At a cellular level, NK cells, CD8$^+$ T cells, CD4$^+$ T cells and eosinophils have been implicated in promoting viral clearance and exacerbating pathogen-initiated lung injury in murine models of RSV infection (19). Here, PCTR1 and PD1 were associated with decreased lung inflammation and decreased viral burden, suggesting pro-resolving rather than immunosuppressive mechanisms. Both PCTR1 and PD1 decreased lung granulocytes and alveolar macrophages, and PCTR1 reduced both total and activated NK cells in the lung,

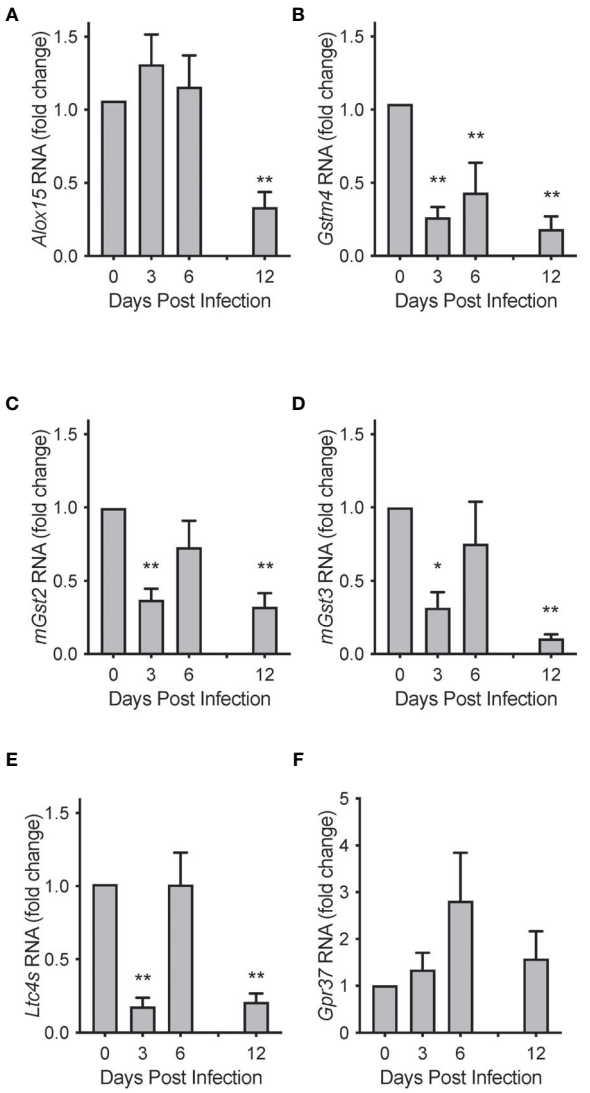

FIGURE 8 | Biosynthetic enzymes for protectins are temporally regulated during mouse RSV infection. Relative RNA expression of **(A)** *Alox15*, **(B)** *Gstm4*, **(C)** *mGst2*, **(D)** *mGst3*, and **(E)** *Ltc$_4$s* in mouse lung tissue over the course of RSV infection, compared to naïve control. **(F)** Protectin D1 receptor *Gpr37* relative RNA expression in mouse lung tissue over the course of RSV infection. Values are mean of n = 3-4 per group ± SEM and represent 2 separate experiments. *$p < 0.05$, **$p < 0.01$ vs naïve by one-way ANOVA with Holm-Sidak's multiple comparisons correction.

suggesting that control of viral burden was not due to an exuberant inflammatory response. A similar trend was seen with $CD4^+$ T and $CD8^+$ T cells, possibly reflecting later timing of the adaptive immune response in this model, as has been appreciated with similar models (19). Additionally, building on the identification of PD1 decreases in IFNγ secretion from human T cells *ex vivo* (15), the reduction of IFNγ expression in $CD4^+$ and $CD8^+$ T cells observed here suggests that PCTR1, and to some extent PD1, regulated type 1 inflammation in this model. This attenuation – rather than obliteration – of type 1 inflammation is important because knock-out and early neutralization experiments suggest that resolution of RSV infection depends on IFNγ signaling and leukocyte responses (33, 34). The regulation of inflammation by PCTR1 and PD1 – without evidence of immunosuppression – highlights a unique property, differentiating these protectins from current anti-inflammatory therapies for RSV that are clinically limited by infectious risks (35, 36).

Both clinical studies of hospitalized infants and mechanistic studies of infected mice have shown that skewing of the immune response from type 1 cytokines (including IFNγ) to type 2 cytokines (such as IL-4 and IL-13) is associated with severe RSV-induced immunopathology (19, 29, 30, 33). Of note, the decreased type 1 inflammation seen in this model was not related to skewing of the immune response to type 2 inflammation because lung eosinophils were suppressed by PCTR1 and PD1; moreover, lung *Il-13* expression was stable or decreased. Notably, PD1 has been shown to be produced by T helper type 2 skewed leukocytes in human blood (15), supporting a possible negative feedback mechanism for type 2 inflammation in this model. Decreases in neutrophils and macrophages observed in the lungs of mice treated with PCTR1 or PD1 suggest against skewing of the immune response towards IL-17 mediated immunity, as well. Of importance in models of non-infectious lung inflammation, SPMs promote resolution by multiple mechanisms (36). PCTR1 promotes the resolution of tissue injury by decreasing neutrophil infiltration and pro-inflammatory cytokines while enhancing macrophage phagocytosis, efferocytosis and planaria tissue regeneration (4). In murine models, PD1 reduces granulocyte migration into areas of inflammation, decreases pro-inflammatory cytokine production and enhances macrophage efferocytosis (2, 14, 15). Together, these provide possible mechanisms for the lower granulocyte counts seen in these PCTR1- and PD1-treated mice.

The concurrent decreases in both viral burden and lung inflammation, without evidence of direct inhibition of RSV replication in epithelial cells, suggested that mucosal host defense mechanisms may play a role in PCTR1- and PD1-mediated *in vivo* actions to promote the resolution of RSV infection and inflammation. Indeed, PCTR1 increased expression of *Camp*. This action adds to prior findings that members of the lipoxin family of SPMs induce lung *Camp* expression during infection (3). Cathelicidins can attenuate RSV infections by directly damaging the virus envelope, hence decreasing viral binding and cellular entry, and promoting an antiviral state in surrounding airway epithelial cells (37). PCTR1 induction of *Camp* in this model would thus be expected to enhance viral host defense. Of note, cathelicidins can induce pro-inflammatory leukotriene production (38); however, PCTR1 decreased the inflammatory response to RSV at day 6 p.i. in this model. Cathelicidin binds to the lipoxin receptor ALX/FPR2 to induce LTB_4 production from human neutrophils, yet SPMs can effectively interrupt this mechanism for leukotriene induction to control inflammatory responses (3, 38).

Type I interferons (primarily IFNα, IFNβ) and type III interferons (isoforms of IFNλ) also promote an antiviral state

through intracellular signaling cascades leading to induction of interferon-stimulated genes. While the type I interferon receptor is present on many cell types including leukocytes, IFNλ's effects are limited to those cells expressing its heterodimeric receptor: primarily epithelial cells. This differential receptor expression may contribute to the particular importance of IFNλ to airway mucosal host responses, with IFNλ less likely to promote inflammation than IFNα/β (39, 40) but still able to reduce RSV infection of epithelial cells (40). The ability of RSV proteins to suppress these antiviral interferons is an important component of RSV pathogenicity, with more severe infant RSV infections associated with relatively lower expression of interferon-related genes (41). The RSV NS1, NS2 and G proteins can suppress IFNα and IFNβ production and signaling *via* multiple mechanisms (19); RSV NS1 and NS2 proteins suppress IFNλ expression (40) and the RSV F protein has been implicated in EGFR-mediated suppression of IFNλ production (42).

Here, PCTR1 and PD1 increased IFNλ expression during RSV infection of human airway epithelial cells and each mediator blunted RSV-mediated suppression of murine IFNλ *in vivo*. Of interest, IFNλ has been noted to enhance macrophage phagocytosis and efferocytosis as well as drive macrophage stimulation of NK cell and $CD8^+$ T cell cytotoxicity (43) – all critical components of host anti-viral responses. Indeed, PCTR1 and PD1 increase macrophage phagocytosis in other models (2, 4). These data and prior literature suggest possible mechanisms for PCTR1 and PD1 control of viral burden in the airway without exacerbating inflammation. Additionally, combined with the identification of Protectin D1 receptor *GPR37* expression in mouse lung tissue and human airway epithelial cells (31) and PD1 effects noted on airway epithelial cells *in vitro* (23), this regulation suggests that PCTR1 and PD1 act directly on airway epithelial cells during viral infection. This induction of IFNλ by protectins appears to be the first evidence for endogenous inducers of host IFNλ expression. While IFNα and IFNβ were undetectable at day 6 p.i. of this model, it is possible that these interferons could also be regulated by PD1 or PCTR1 at earlier timepoints, thereby facilitating the viral clearance seen at day 6 p.i.

Given these actions of PCTR1 and PD1, we investigated whether endogenous levels of these SPMs were affected by RSV infection. While PD1 is transiently decreased during influenza infection in mouse lung (23), the impact of other viral infections on PD1 synthesis in the lung – and of any viral infection on PCTR1 synthesis – has been unknown. Here, mRNA expression of the enzymes for PCTR1 and PD1 synthesis was suppressed by RSV infection, and levels of protectins in the lung were transiently decreased, ultimately increasing concurrent with RSV clearance.

RSV Long strain induces mRNA expression of *Alox15*, the first enzyme in the conversion of DHA to PCTR1 or PD1, at days 1-4 post infection in mouse lungs (24). Here, using the Line 19 strain of RSV, we observed steady *Alox15* expression 3-6 days after infection, followed by a significant decrease in expression at day 12 p.i. In contrast to *Alox15* expression, we observed significantly decreased mRNA transcripts of Ltc_4s, *mGst3*, and *Gstm4* – biosynthetic enzymes downstream of *Alox15* for PCTR1 synthesis – when viral titers were highest at day 3 p.i. These transcriptional changes and the decreased lung tissue concentrations of protectins suggest that the biosynthetic pathway for protectins was suppressed by RSV in this model.

Of interest, leukotriene synthesis was increased at day 3 p.i. compared to naïve control. This increase in cys-LTs despite decreases in mRNA expression of rate-limiting enzymes (Ltc_4s, *mGst2*, *mGst3*, or *Gstm4*) may have been secondary to persistent enzyme function after initial changes in mRNA transcripts or changes in mediator degradation. Additionally, lipid mediator levels are subject to spatial regulation of biosynthetic enzymes relative to substrate availability and to differences in enzyme-substrate affinity (8). Expression of *Gpr37*, a cellular receptor for PD1 (11), was not significantly changed over the course of RSV infection. Together, these data suggest that the signaling pathways thus far identified for PCTR1 and PD1 are temporally regulated during RSV infection. Notably, the pattern of temporal regulation of PCTR1 and PD1 observed here during RSV infection appears similar to that of PD1 during influenza infection (23), suggesting a possible shared mechanism for viral host responses.

RSV is an important human pathogen for which there are currently no effective treatments. While this mouse model faithfully replicates aspects of human RSV infection including interstitial mononuclear alveolitis, peribronchial inflammation and eosinophilia, it does not incorporate all features of human infection (18). Further determination of relationships between protectins and interferons will involve translation to human subjects in ongoing studies.

In conclusion, PCTR1 and PD1 engaged host protective mechanisms and decreased lung inflammation in this RSV pneumonia model. These each stimulated decreased viral burden, notably without apparent host immunosuppression, suggesting pro-resolving more than anti-inflammatory actions. As such, PCTR1 and PD1 may serve as investigational tools to better understand both the pathogenesis of viral lung infection and the possibility of harnessing host pro-resolving mechanisms for new therapeutic benefits.

DATA AVAILABILITY STATEMENT

The original contributions presented in the study are included in the article/**Supplementary Material**. Further inquiries can be directed to the corresponding authors.

ETHICS STATEMENT

The animal study was reviewed and approved by Institutional Animal Care and Use Committee at Harvard Medical School.

AUTHOR CONTRIBUTIONS

KW conceived of the study, designed experiments, performed experiments, analyzed data and wrote and edited the manuscript. NK designed experiments, performed experiments, analyzed data, supervised the study and edited the manuscript. TB performed experiments, analyzed data and edited the manuscript. AS performed experiments, analyzed data and edited the manuscript. CS designed experiments, analyzed data and edited the manuscript. BL conceived of the study, designed experiments, analyzed data, supervised the study and edited the manuscript. All authors contributed to the article and approved the submitted version.

FUNDING

This work was supported by National Institutes of Health F32AI134019-01 (to KW), Harvard Catalyst | The Harvard Clinical and Translational Science Center | National Center for Advancing Translational Sciences, National Institutes of Health Award UL 1TR002541 (to KW), T32HL007633-31 (to BL), and P01GM095467 (to CS and BL). The content is solely the responsibility of the authors and does not necessarily represent the official views of Harvard Catalyst, Harvard University and its affiliated academic healthcare centers, or the National Institutes of Health.

ACKNOWLEDGMENTS

We thank Dr. Nicholas Lukacs (University of Michigan, Ann Arbor MI) for providing the RSV clinical isolate strain Line 19, Dr. Jennifer Bomberger (University of Pittsburgh, Pittsburgh PA) for providing the STAT1$^{-/-}$ cell line for RSV plaque assays, Dr. Bakr Jundi for assistance with principal component analysis, and Julie Nijmeh for thoughtful review of the manuscript. The graphical abstract was created with BioRender.com. The LungMAP consortium and the LungMAP Data Coordinating Center (1U01HL122638) are funded by the National Heart, Lung, and Blood Institute (NHLBI).

SUPPLEMENTARY MATERIAL

The Supplementary Material for this article can be found online at: https://www.frontiersin.org/articles/10.3389/fimmu.2021.704427/full#supplementary-material

REFERENCES

1. Serhan CN. Pro-Resolving Lipid Mediators Are Leads for Resolution Physiology. *Nature* (2014) 510(7503):92–101. doi: 10.1038/nature13479
2. Schwab JM, Chiang N, Arita M, Serhan CN. Resolvin E1 and Protectin D1 Activate Inflammation-Resolution Programmes. *Nature* (2007) 447 (7146):869–74. doi: 10.1038/nature05877
3. Sham HP, Walker KH, Abdulnour RE, Krishnamoorthy N, Douda DN, Norris PC, et al. 15-Epi-Lipoxin A4, Resolvin D2, and Resolvin D3 Induce NF-kappaB Regulators in Bacterial Pneumonia. *J Immunol* (2018) 200 (8):2757–66. doi: 10.4049/jimmunol.1602090
4. Ramon S, Dalli J, Sanger JM, Winkler JW, Aursnes M, Tungen JE, et al. The Protectin PCTR1 Is Produced by Human M2 Macrophages and Enhances Resolution of Infectious Inflammation. *Am J Pathol* (2016) 186(4):962–73. doi: 10.1016/j.ajpath.2015.12.012
5. Serhan CN, Gotlinger K, Hong S, Lu Y, Siegelman J, Baer T, et al. Anti-Inflammatory Actions of Neuroprotectin D1/protectin D1 and Its Natural Stereoisomers: Assignments of Dihydroxy-Containing Docosatrienes. *J Immunol* (2006) 176(3):1848–59. doi: 10.4049/jimmunol.176.3.1848
6. Hong S, Gronert K, Devchand PR, Moussignac RL, Serhan CN. Novel Docosatrienes and 17S-Resolvins Generated From Docosahexaenoic Acid in Murine Brain, Human Blood, and Glial Cells. Autacoids in Anti-Inflammation. *J Biol Chem* (2003) 278(17):14677–87. doi: 10.1074/jbc.M300218200
7. Dalli J, Ramon S, Norris PC, Colas RA, Serhan CN. Novel Proresolving and Tissue-Regenerative Resolvin and Protectin Sulfido-Conjugated Pathways. *FASEB J* (2015) 29(5):2120–36. doi: 10.1096/fj.14-268441
8. Jouvene CC, Shay AE, Soens MA, Norris PC, Haeggstrom JZ, Serhan CN. Biosynthetic Metabolomes of Cysteinyl-Containing Immunoresolvents. *FASEB J* (2019) 33(12):13794–807. doi: 10.1096/fj.201902003R
9. Dalli J, Vlasakov I, Riley IR, Rodriguez AR, Spur BW, Petasis NA, et al. Maresin Conjugates in Tissue Regeneration Biosynthesis Enzymes in Human Macrophages. *Proc Natl Acad Sci USA* (2016) 113(43):12232–7. doi: 10.1073/pnas.1607003113
10. Dalli J, Colas RA, Arnardottir H, Serhan CN. Vagal Regulation of Group 3 Innate Lymphoid Cells and the Immunoresolvent PCTR1 Controls Infection Resolution. *Immunity* (2017) 46(1):92–105. doi: 10.1016/j.immuni.2016.12.009
11. Bang S, Xie YK, Zhang ZJ, Wang Z, Xu ZZ, Ji RR. GPR37 Regulates Macrophage Phagocytosis and Resolution of Inflammatory Pain. *J Clin Invest* (2018) 128(8):3568–82. doi: 10.1172/JCI99888
12. Chiang N, de la Rosa X, Libreros S, Pan H, Dreyfuss JM, Serhan CN. Cysteinyl-Specialized Proresolving Mediators Link Resolution of Infectious Inflammation and Tissue Regeneration *via* TRAF3 Activation. *Proc Natl Acad Sci USA* (2021) 118(10):1–11. doi: 10.1073/pnas.2013374118
13. Levy BD, Abdulnour RE, Tavares A, Bruggemann TR, Norris PC, Bai Y, et al. Cysteinyl Maresins Regulate the Prophlogistic Lung Actions of Cysteinyl Leukotrienes. *J Allergy Clin Immunol* (2020) 145(1):335–44. doi: 10.1016/j.jaci.2019.09.028
14. Levy BD, Kohli P, Gotlinger K, Haworth O, Hong S, Kazani S, et al. Protectin D1 Is Generated in Asthma and Dampens Airway Inflammation and Hyperresponsiveness. *J Immunol* (2007) 178(1):496–502. doi: 10.4049/jimmunol.178.1.496
15. Ariel A, Li PL, Wang W, Tang WX, Fredman G, Hong S, et al. The Docosatriene Protectin D1 Is Produced by TH2 Skewing and Promotes Human T Cell Apoptosis *via* Lipid Raft Clustering. *J Biol Chem* (2005) 280 (52):43079–86. doi: 10.1074/jbc.M509796200
16. Shi T, McAllister DA, O'Brien KL, Simoes EAF, Madhi SA, Gessner BD, et al. Global, Regional, and National Disease Burden Estimates of Acute Lower Respiratory Infections Due to Respiratory Syncytial Virus in Young Children in 2015: A Systematic Review and Modelling Study. *Lancet* (2017) 390 (10098):946–58. doi: 10.1016/S0140-6736(17)30938-8
17. Shi T, Denouel A, Tietjen AK, Campbell I, Moran E, Li X, et al. Global Disease Burden Estimates of Respiratory Syncytial Virus-Associated Acute Respiratory Infection in Older Adults in 2015: A Systematic Review and Meta-Analysis. *J Infect Dis* (2020) 222(Suppl 7):S577–83. doi: 10.1093/infdis/jiz059
18. Neilson KA, Yunis EJ. Demonstration of Respiratory Syncytial Virus in an Autopsy Series. *Pediatr Pathol* (1990) 10(4):491–502. doi: 10.3109/15513819009067138
19. Openshaw PJM, Chiu C, Culley FJ, Johansson C. Protective and Harmful Immunity to RSV Infection. *Annu Rev Immunol* (2017) 35:501–32. doi: 10.1146/annurev-immunol-051116-052206

20. Buckingham SC, Jafri HS, Bush AJ, Carubelli CM, Sheeran P, Hardy RD, et al. A Randomized, Double-Blind, Placebo-Controlled Trial of Dexamethasone in Severe Respiratory Syncytial Virus (RSV) Infection: Effects on RSV Quantity and Clinical Outcome. *J Infect Dis* (2002) 185(9):1222–8. doi: 10.1086/340024
21. IMpact-RSV. Palivizumab, A Humanized Respiratory Syncytial Virus Monoclonal Antibody, Reduces Hospitalization From Respiratory Syncytial Virus Infection in High-Risk Infants. The IMpact-RSV Study Group. *Pediatrics* (1998) 102(3 Pt 1):531–7. doi: 10.1542/peds.102.3.531
22. Mazur NI, Martinon-Torres F, Baraldi E, Fauroux B, Greenough A, Heikkinen T, et al. Lower Respiratory Tract Infection Caused by Respiratory Syncytial Virus: Current Management and New Therapeutics. *Lancet Respir Med* (2015) 3(11):888–900. doi: 10.1016/S2213-2600(15)00255-6
23. Morita M, Kuba K, Ichikawa A, Nakayama M, Katahira J, Iwamoto R, et al. The Lipid Mediator Protectin D1 Inhibits Influenza Virus Replication and Improves Severe Influenza. *Cell* (2013) 153(1):112–25. doi: 10.1016/j.cell.2013.02.027
24. Shirey KA, Lai W, Pletneva LM, Karp CL, Divanovic S, Blanco JC, et al. Role of the Lipoxygenase Pathway in RSV-Induced Alternatively Activated Macrophages Leading to Resolution of Lung Pathology. *Mucosal Immunol* (2014) 7(3):549–57. doi: 10.1038/mi.2013.71
25. Miller AL, Bowlin TL, Lukacs NW. Respiratory Syncytial Virus-Induced Chemokine Production: Linking Viral Replication to Chemokine Production *In Vitro* and *In Vivo*. *J Infect Dis* (2004) 189(8):1419–30. doi: 10.1086/382958
26. Durbin JE, Hackenmiller R, Simon MC, Levy DE. Targeted Disruption of the Mouse Stat1 Gene Results in Compromised Innate Immunity to Viral Disease. *Cell* (1996) 84(3):443–50. doi: 10.1016/s0092-8674(00)81289-1
27. Chomczynski P, Sacchi N. The Single-Step Method of RNA Isolation by Acid Guanidinium Thiocyanate-Phenol-Chloroform Extraction: Twenty-Something Years on. *Nat Protoc* (2006) 1(2):581–5. doi: 10.1038/nprot.2006.83
28. Lukacs NW, Moore ML, Rudd BD, Berlin AA, Collins RD, Olson SJ, et al. Differential Immune Responses and Pulmonary Pathophysiology Are Induced by Two Different Strains of Respiratory Syncytial Virus. *Am J Pathol* (2006) 169(3):977–86. doi: 10.2353/ajpath.2006.051055
29. Culley FJ, Pollott J, Openshaw PJ. Age at First Viral Infection Determines the Pattern of T Cell-Mediated Disease During Reinfection in Adulthood. *J Exp Med* (2002) 196(10):1381–6. doi: 10.1084/jem.20020943
30. Siefker DT, Vu L, You D, McBride A, Taylor R, Jones TL, et al. Respiratory Syncytial Virus Disease Severity Is Associated With Distinct CD8(+) T-Cell Profiles. *Am J Respir Crit Care Med* (2020) 201(3):325–34. doi: 10.1164/rccm.201903-0588OC
31. LungMAP. *LungMAP Database (https://Lungmap.Net)* (2020). Available at: https://lungmap.net (Accessed 06/09/2020).
32. Imai Y. Role of Omega-3 PUFA-Derived Mediators, the Protectins, in Influenza Virus Infection. *Biochim Biophys Acta* (2015) 1851(4):496–502. doi: 10.1016/j.bbalip.2015.01.006
33. Durbin JE, Johnson TR, Durbin RK, Mertz SE, Morotti RA, Peebles RS, et al. The Role of IFN in Respiratory Syncytial Virus Pathogenesis. *J Immunol* (2002) 168(6):2944–52. doi: 10.4049/jimmunol.168.6.2944
34. Ostler T, Davidson W, Ehl S. Virus Clearance and Immunopathology by CD8 (+) T Cells During Infection With Respiratory Syncytial Virus Are Mediated by IFN-Gamma. *Eur J Immunol* (2002) 32(8):2117–23. doi: 10.1002/1521-4141(200208)32:8<2117::AID-IMMU2117>3.0.CO;2-C
35. Fernandes RM, Bialy LM, Vandermeer B, Tjosvold L, Plint AC, Patel H, et al. Glucocorticoids for Acute Viral Bronchiolitis in Infants and Young Children. *Cochrane Database Syst Rev* (2010) (10):CD004878. doi: 10.1002/14651858.CD004878.pub3
36. Krishnamoorthy N, Abdulnour RE, Walker KH, Engstrom BD, Levy BD. Specialized Proresolving Mediators in Innate and Adaptive Immune Responses in Airway Diseases. *Physiol Rev* (2018) 98(3):1335–70. doi: 10.1152/physrev.00026.2017
37. Currie SM, Gwyer Findlay E, McFarlane AJ, Fitch PM, Bottcher B, Colegrave N, et al. Cathelicidins Have Direct Antiviral Activity Against Respiratory Syncytial Virus *In Vitro* and Protective Function *In Vivo* in Mice and Humans. *J Immunol* (2016) 196(6):2699–710. doi: 10.4049/jimmunol.1502478
38. Wan M, Godson C, Guiry PJ, Agerberth B, Haeggstrom JZ. Leukotriene B4/antimicrobial Peptide LL-37 Proinflammatory Circuits Are Mediated by BLT1 and FPR2/ALX and Are Counterregulated by Lipoxin A4 and Resolvin E1. *FASEB J* (2011) 25(5):1697–705. doi: 10.1096/fj.10-175687
39. Donnelly RP, Kotenko SV. Interferon-Lambda: A New Addition to an Old Family. *J Interferon Cytokine Res* (2010) 30(8):555–64. doi: 10.1089/jir.2010.0078
40. Syedbasha M, Egli A. Interferon Lambda: Modulating Immunity in Infectious Diseases. *Front Immunol* (2017) 8:119. doi: 10.3389/fimmu.2017.00119
41. Rodriguez-Fernandez R, Tapia LI, Yang CF, Torres JP, Chavez-Bueno S, Garcia C, et al. Respiratory Syncytial Virus Genotypes, Host Immune Profiles, and Disease Severity in Young Children Hospitalized With Bronchiolitis. *J Infect Dis* (2017) 217(1):24–34. doi: 10.1093/infdis/jix543
42. Kalinowski A, Galen BT, Ueki IF, Sun Y, Mulenos A, Osafo-Addo A, et al. Respiratory Syncytial Virus Activates Epidermal Growth Factor Receptor to Suppress Interferon Regulatory Factor 1-Dependent Interferon-Lambda and Antiviral Defense in Airway Epithelium. *Mucosal Immunol* (2018) 11(3):958–67. doi: 10.1038/mi.2017.120
43. Read SA, Wijaya R, Ramezani-Moghadam M, Tay E, Schibeci S, Liddle C, et al. Macrophage Coordination of the Interferon Lambda Immune Response. *Front Immunol* (2019) 10:2674. doi: 10.3389/fimmu.2019.02674

Conflict of Interest: CS and BL are inventors on patents (protectins) assigned to Brigham and Women's Hospital.

The remaining authors declare that the research was conducted in the absence of any commercial or financial relationships that could be construed as a potential conflict of interest.

Publisher's Note: All claims expressed in this article are solely those of the authors and do not necessarily represent those of their affiliated organizations, or those of the publisher, the editors and the reviewers. Any product that may be evaluated in this article, or claim that may be made by its manufacturer, is not guaranteed or endorsed by the publisher.

Copyright © 2021 Walker, Krishnamoorthy, Brüggemann, Shay, Serhan and Levy. This is an open-access article distributed under the terms of the Creative Commons Attribution License (CC BY). The use, distribution or reproduction in other forums is permitted, provided the original author(s) and the copyright owner(s) are credited and that the original publication in this journal is cited, in accordance with accepted academic practice. No use, distribution or reproduction is permitted which does not comply with these terms.

frontiers in Immunology

ORIGINAL RESEARCH
published: 31 August 2021
doi: 10.3389/fimmu.2021.733019

Dysregulated Maresin Concentrations in Plasma and Nasal Secretions From Patients With Chronic Rhinosinusitis

Issa Beegun[1], *Duco S. Koenis*[1], *Ghassan Alusi*[1] *and Jesmond Dalli*[1,2]*

[1] *William Harvey Research Institute, Barts and The London School of Medicine and Dentistry, Queen Mary University of London, London, United Kingdom,* [2] *Centre for Inflammation and Therapeutic Innovation, Queen Mary University of London, London, United Kingdom*

The mechanisms that lead to disease onset and propagation in patients with chronic rhinosinusitis (CRS) are not fully elucidated. Maresins (MaR) are a family of essential fatty acid-derived lipid mediators that play a central role in the regulation of inflammation with several studies demonstrating that these mediators display protective activities in airway inflammation. Therefore, in the present studies we evaluated whether concentrations of these mediators were altered in both peripheral blood and nasal secretions from CRS patients. Herein, we focused on patients with CRS that also develop nasal polyps (CRSwNP), given that therapeutic options for the treatment of these patients are limited. Thereby, insights into disease mechanisms in these patients may help design more effective treatments. For this purpose, we compared maresin concentrations from CRSwNP patients with those found in healthy volunteers or patients with an upper respiratory tract infection (URTI), as a self-resolving inflammatory condition. Using liquid chromatography tandem mass spectrometry, we found that MaR concentrations were significantly decreased in plasma from patients with CRSwNP when compared to healthy volunteers. MaR concentrations were observed to be significantly upregulated in nasal secretions from patients with CRSwNP when compared with both healthy volunteers and URTI subjects. Concentration of these mediators in both plasma and nasal secretions from CRSwNP patients were positively correlated with quality-of-life scores in these patients. Assessment of the concentrations of other pro-resolving and pro-inflammatory lipid mediators (LM) demonstrated that there was a general shift in LM levels in both plasma and nasal secretions from CRSwNP when compared with healthy volunteers and URTI subjects. Of note, incubation of peripheral blood cells from CRSwNP patients with MaR1 downregulated the expression of activation markers on peripheral blood phagocytes, including CD41 and CD62P, markers of platelet-leukocyte heterotypic aggregates. Together these findings demonstrate that both local and systemic LM concentrations, in particularly those of the MaR family, become altered in patients with CRSwNP. They also suggest that therapeutics designed around MaR1 may be useful in

OPEN ACCESS

Edited by:
Janos G. Filep,
Université de Montréal, Canada

Reviewed by:
Joan Clària,
Hospital Clínic de Barcelona, Spain
Antonio Recchiuti,
University of Studies G. d'Annunzio Chieti and Pescara, Italy

****Correspondence:***
Jesmond Dalli
j.dalli@qmul.ac.uk

Specialty section:
This article was submitted to Inflammation, a section of the journal Frontiers in Immunology

Received: *29 June 2021*
Accepted: *09 August 2021*
Published: *31 August 2021*

Citation:
Beegun I, Koenis DS, Alusi G and Dalli J (2021) Dysregulated Maresin Concentrations in Plasma and Nasal Secretions From Patients With Chronic Rhinosinusitis. Front. Immunol. 12:733019. doi: 10.3389/fimmu.2021.733019

regulating the activation of phagocytes in patients with CRSwNP thereby potentially also limiting the local inflammatory response in these patients.

Keywords: resolving, resolution, inflammation, phagocytes, omega-3, chronic rhinosinusitis, airway inflammation

INTRODUCTION

Chronic rhinosinusitis (CRS) is a common inflammatory disorder of the respiratory tract resulting in symptoms of nasal blockage, discharge, loss of smell and facial pain lasting for over 12 weeks (1). It is estimated that 2.1% of the adult population in the USA suffer with CRS (2). In Europe studies estimate the prevalence of CRS to be between 2.1% and 4.3% (3–5). Approximately 20% of patients with CRS develop nasal polyps (CRSwNP) (6). This condition affects 11% of the UK adult population with 120,000 secondary care outpatient encounters and 40,000 sinus operations per year in England and Wales alone (7). Morbidity is considerable, affecting physical, social and emotional health. In addition to nasal symptoms, patients suffering from CRS report lower quality of life scores with adverse effects on sleep quality, sexual function, work productivity and mental health. The quality of life for patients suffering with CRS is thought to be worse than patients suffering with back pain or heart failure (8–10).

CRS with nasal polyps (CRSwNP) is a particularly difficult to treat aggressive phenotype associated with asthma and aspirin intolerance (11). It remains uncertain whether this population of patients represent the severe end of the CRSwNP disease spectrum or whether a unique mechanism underlies the pathogenesis of this aggressive form of disease (1). Importantly, to date establishing whether a patient with CRSwNP is intolerant to NSAIDs remains a challenging task (1, 12, 13). Several approaches including systemic and local NSAID challenges are available (14, 15). However, medical supervision with access to resuscitation equipment and overnight hospital admission are recommended, highlighting the need for further research to identify biomarkers and the development of better diagnostic tests for the identification and stratification of patients with CRSwNP. One key aspect that has hindered the development of such tests is our limited understanding of the cellular and molecular mechanism operative in patients with CRSwNP.

Chronic inflammation arises from the inability of the host's immune response to limit the production of inflammatory factors. It is now well established that the specialised pro-resolving mediators (SPM) are central in orchestrating the cessation of inflammation (16–18). These autacoids are formed *via* the conversion of essential fatty acids, including docosahexaenoic acid and n-3 docosapentaenoic acid by specific biosynthetic enzymes to yield structurally distinct mediators. The SPM are divided into four main families the resolvins, protectins maresins and lipoxins (16–18). These autacoids families share defining biological actions that contribute to the resolution of inflammation. These include: 1) counter-regulating the production of inflammatory mediators, 2) limiting of leukocyte trafficking to the site of inflammation and 3) upregulating the clearance of apoptotic cells and cellular debris by macrophages (16–18). Furthermore, each of these autacoids displays characteristic biological actives, for example resolvin (Rv) D2 regulates nitric oxide formation in endothelial cells (19), whereas the DHA-derived protectins limit viral replication (20). Findings made in both experimental systems and humans demonstrate that disruptions in the formation and activity of these autacoids contribute to the exacerbation of inflammation (16–18).

Recent studies assessing the levels of select SPM in sinus tissues from patients with CRSwNP suggest that the production of RvD2 and Lipoxin A_4 may become altered in these patients when compared to either CRS patients without polyps or healthy volunteers and correlates to disease severity (21). Chronic inflammatory conditions are characterized by systemic inflammation and recent findings suggest that plasma SPM concentrations may reflect disease activity in peripheral tissues (22). Therefore, in the present study, we sought to establish whether systemic SPM concentrations are also altered in patients with CRSwNP. Furthermore, several reports suggest that an infective stimulus in the form of an upper respiratory tract infection (URTI) may act as a trigger (23). Thus, to gain insights into the mechanisms that lead to the transition from a healthy state to CRSwNP we compared SPM levels with those from both healthy volunteers and patients with an active URTI.

METHODS

After informed consent was obtained each participant completed a copy of the Sino-Nasal Outcome Test-22 (SNOT-22), Nasal Obstruction Symptom Evaluation (NOSE) and 36-Item Short Form Survey (SF-36). The SNOT-22 is a questionnaire consisting of 22 questions evaluating a range of symptoms experienced by suffers of nasal disease (24). The NOSE questionnaire consists of five questions which predominantly focus on evaluating breathing difficulties (25). The SF-36 has been reported as the most widely used health-related quality of life survey instrument in the world (26). It is comprised of 36 items that assess eight health concepts has been used to determine the cost-effectiveness of a health treatments.

Ethics

Participants with a history of CRSwNP with failed medical management, healthy controls with no previous ear, nose and throat disease as well as those undergoing nasal cavity surgery due to non-inflammatory conditions (cosmetic or post traumatic deformity; septoplasty or septorhinoplasty) and participants with URTI were recruited. (Research Ethics Committee Number: 17/EM/0447).

Blood Collection for Lipid Mediator Profiling

Whole blood was collected from a peripheral vein of the upper limb using a 21g butterfly needle connected to a Becton Dickinson Vacutainer® containing 3.2% trisodium citrate. Samples were then centrifuged at 2500 x g for 10 minutes and 1.5 ml of the plasma supernatant transferred to 15 ml Falcon® tubes containing 6 ml of ice-cold methanol with internal standards (500 pg of each; 5S-HETE-d_8, LTB_4-d_4, LXA_4-d_5, RvD2-d_5 and PGE_2-d_4).

Nasal Secretion Lipid Mediator Profiling

Nasal secretions were collected using a polyurethane sponge (RG 27 grau, Gummi-Welz GmbH & Co., Germany), pre-cut into 20 × 15 × 5 mm pieces and sterilized by autoclaving for 20 min at 121°C prior to use. One sponge piece was placed into the anterior nasal cavity under direct vision using a head mounted light and Tilley's nasal dressing forceps. Sponges were left in place for 10 minutes, removed and placed into 1 ml of ice-cold methanol with internal standards. Samples were stored at -80°C until further analysis.

Prior to lipid mediator extraction, stored sponges were placed into a modified 1.5 ml Eppendorf™ tube. Modification consisted of removing 5 mm from the lower portion of the tube. This was accomplished by cutting the tube at an angle using a pair of Mayo scissors. The modified Eppendorf containing the sponge was suspended in a 15 ml Falcon® tube using Prolene® 4-0 suture (Ethicon Polypropylene Suture). The cap of the Falcon® tube was used to secure the sutured modified Eppendorf during centrifugation at 2000 x g for 10 minutes. Post centrifugation the supernatant was transferred to 15 ml Falcon® tubes and stored at -80°C for subsequent lipid mediator profiling. The pellet was allowed to stand under a sterile hood for ten minutes to allow evaporation of any remaining methanol. The pellet was then suspended in 400 µl of Milli-Q® water and stored at -80°C until protein quantification was performed.

Lipid Mediator Profiling

Samples were extracted and lipid mediators were identified and quantified as described (22). In brief, plasma was collected as described above and immediately placed on dry ice in 4 volumes of ice-cold methanol containing deuterated internal standards (d_4-LTB_4, d_5-LXA_4, d_4-PGE_2, d_5-RvD2) representing each chromatographic region of identified LM. Following protein precipitation (-20°C for a minimum of 45 min), supernatants were extracted on an ExtraHera instrument (Biotage) using solid-phase extraction with Isolute C18 500mg columns (Biotage). Methyl formate and methanol fractions were collected, brought to dryness and resuspended in phase (methanol/water, 1:1, vol/vol) for injection on a Shimadzu LC-20AD HPLC and a Shimadzu SIL-20AC autoinjector, paired with a QTrap 5500 or QTrap 6500+ (Sciex). In the analysis of mediators eluted in the methyl formate fraction, the QTRAP 5500 was operated in negative ion mode using a multiple reaction monitoring method. An Agilent Poroshell 120 EC-C18 column (100 mm × 4.6 mm × 2.7 µm) was kept at 50°C and mediators eluted using a mobile phase consisting of methanol/water/acetic acid of 20:80:0.01 (vol/vol/vol) that was ramped to 50:50:0.01 (vol/vol/vol) over 0.5 min and then to 80:20:0.01 (vol/vol/vol) from 2 min to 11 min, maintained till 14.5 min and then rapidly ramped to 98:2:0.01 (vol/vol/vol) for the next 0.1 min. This was subsequently maintained at 98:2:0.01 (vol/vol/vol) for 5.4 min, and the flow rate was maintained at 0.5 ml/min. In the analysis of mediators eluted in the methanol fraction, the QTrap 6500+ was operated in positive ion mode using a multiple reaction monitoring method. An Agilent Poroshell 120 EC-C18 column (100 mm × 4.6 mm × 2.7 µm) was kept at 50°C and mediators eluted using a mobile phase consisting of methanol/water/acetic acid 55:45:0.5 (vol:vol:vol) over 5 min, that was ramped to 80:20:0.5 (vol:vol:vol) for 2 min, maintained at 80:20:0.5 (vol:vol:vol) for the successive 3 min and ramped to 98:2:0.5 (vol:vol:vol) over 3 min. This condition was maintained for 3 min. Each lipid mediator was identified using established criteria, including: (1) presence of a peak with a minimum area of 2000 counts, (2) matching retention time to synthetic or authentic standards, (3) >4 data points, (4) signal to noise ratio ≥ 3. Furthermore, to confirm the identity of these mediators in representative samples we obtained MS/MS spectra, matching of at least 6 diagnostic ions to that of reference standard, with a minimum of one backbone fragment being identified. Calibration curves were obtained for each mediator using synthetic compound mixtures at 0.78, 1.56, 3.12, 6.25, 12.5, 25, 50, 100, and 200 pg that gave linear calibration curves with R^2 values of 0.98–0.99. These calibration curves were then used to calculate the abundance of each mediator per 1mL of plasma for each individual sample.

Whole Blood Assays

Participants with a history of failed medical and surgical management of CRSwNP were recruited and peripheral blood was collected between 10 am and 12 pm (Research Ethics Committee Number: 17/EM/0447) from a peripheral vein of the upper limb as described above. Forty-five microliters of whole blood were transferred to a 15 ml Falcon® tube and incubated with MaR1 at either 1 nM or 10 nM or vehicle (PBS +0.01% Ethanol). Whole blood samples were kept at 37 ^{0}C for 45 minutes. The blood was then washed using PBS $^{-/-}$ containing 0.02% BSA and then incubated with the following antibodies: APC-Cy7 conjugated mouse anti human CD16 (Clone 3G8, Biolegend), BV785 conjugated mouse anti human CD14 (Clone M5E2, Biolegend)m BV711 conjugated mouse anti human CD11b (Clone ICRF44, Biolegend), conjugated mouse anti human CD16 (Clone 3G8, Biolegend), AF700 conjugated mouse anti human CD45 (Clone 2D1, Biolegend), PerCP-Cy7 conjugated mouse anti human CD66b (Clone G10F5, Biolegend), PE conjugated mouse anti human Siglec 8 (Clone 7C9, Biolegend), eFluor 450 conjugated mouse anti human CD41 (Clone H1P8, Biolegend), PE-Cy5 conjugated mouse anti human CD62P (Clone AK4, Biolegend) and PE-CD594 conjugated mouse anti human CD49d (Clone 3G8, Biolegend) at room temperature for 15 minutes. Ten microliters of counting beads were then added and samples washed with PBS $^{-/-}$ containing 0.02% BSA. Red Blood cells were then lysed and

fixed using Red-Blood Cells lysis and fixation buffers (Beckman Coulter). Cells were then suspended in PBS $^{-/-}$ containing 0.02% BSA and staining evaluated using LSR Fortessa cell analyser (BD Biosciences) and analysed using FlowJo software (Tree Star Inc., V10).

In select experiments blood was first incubated with MaR1 as detailed above for 15 minutes at 37°C, then with platelet activating factor (PAF; 100nM) for 30 minutes at 37°C. Cells were stained, fixed and staining was evaluated as detailed above.

Data Analysis and Statistical Testing

Flow cytometry data was analysed using FlowJo v10.4. For Partial Least Square Discriminant analyses (PLS-DA), missing values were replaced by 1/5th of the minimum value of each variable across the samples, and features with a constant or single value across samples were removed. Data was then auto-scaled, 2D plots of Component 1 and 2 from each PLS-DA with their 95% confidence intervals (CI) were constructed, Variable Importance in Projection (VIP) scores were calculated, and internal validation by leave-one-out cross-validation and calculation of a coefficient of determination (R^2) for each model was performed using MetaboAnalyst (27). Mahalanobis distances between group centers and Hotelling's T-squared test p-values were calculated for Component 1 and 2 scores of the PLS-DA models using *pca-utils* (28). All other statistical tests were performed using GraphPad Prism 9 and Microsoft Excel

RESULTS

Increased Disease Severity and Decreased QoL in Patients With CRSwNP

A total of 51 participants were recruited into the present study. 16 of these participants were healthy volunteers, 27 had CRSwNP and 8 had an active URTI. None of the 8 participants with an active URTI required medical attention or prescription medication. The 27 participants with CRSwNP all had a history of failed medical treatment requiring surgical intervention (see **Table 1** for patient information).

We first evaluated parameters linked with both quality of life (QoL) and disease severity and found that, in line with previous findings (8, 23), patients with CRSwNP reported increased disease severity scores and reduced QoL. This is characterized by increased NOSE scores and SNOT22 scores (**Figures 1A, B**, Dunn's multiple comparisons test, p= 0.029; Dunn's multiple comparisons test, p = <0.0001) when compared with healthy volunteers and/or patients with URTI. Physical functioning, physical health, emotional and energy levels were also reduced in participants with CRSwNP when compared to controls (**Figures 1C–F**). Compared with controls CRSwNP participants also reported increased pain scores (**Figure 1G**) and reduced general health scores (**Figures 1H, I**). Of note, while we also observed trends towards a reduction in a number of the parameters evaluated in patients with URTI, these did not reach statistical significance.

Plasma Maresin Concentrations Correlate With Quality-of-Life Measures and Disease Severity Scores

Maresins display potent immune regulatory activities with members of this family also exerting protective actions in airway inflammation (29, 30). Therefore, we next evaluated whether plasma concentrations of these protective autacoids were altered in plasma and nasal secretions from CRSwNP patients when compared to both healthy volunteers and patients with URTI. We also sought to evaluate whether the

TABLE 1 | Participant demographics.

Group median age	Control n=16		CRSwNP n=27		URTI n=8
	31		51		32
	Plasma n=15	Nasal secretions n=4	Plasma n=24	Nasal secretions =16	Plasma & nasal secretions n=8
Median age	31	29	47	49	32
Gender F:M	F7:M8	F1:M3	F9:M14	F6:M10	F4:M4
Allergies			2	1	
Asthma			4	2	
Aspirin Sensitivity			2	1	
Previous Surgery			23	2	1
Smoking					
Saline Wash			4	2	
Topical Steroids			3	1	
Systemic Steroids			1		
Antibiotics			1		
Regular medication			3	2	1
PRN medication			3	2	

Participant demographics. Of the 16 healthy participants none were on regular medication or had a past medical history involving the ear, nose and throat region of the body. Of participants with CRSwNP all required surgical intervention as a result of persistent disease with poor quality of life following medical intervention. 8 of the CRSwNP participants used topical treatments. One participant had received a course of systemic steroids and antibiotics in the preceding 8 weeks prior to recruitment. Seven participants had a history of asthma and 4 reported aspirin sensitivity.

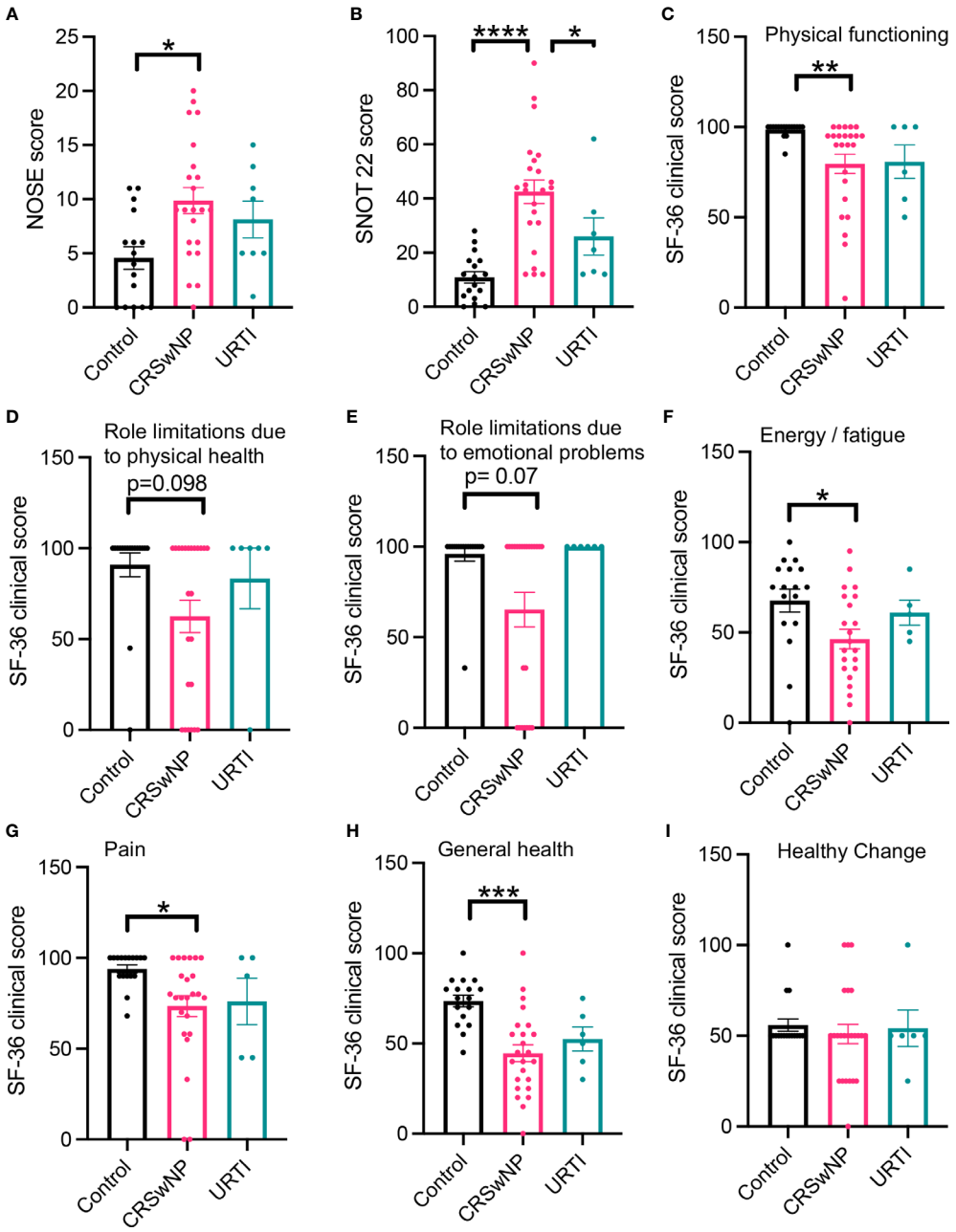

FIGURE 1 | Participants with CRSwNP have increased nasal cavity clinical scores and report poor quality of life. Compared with healthy participants and those who have recovered from an URTI, CRSwNP report worse nasal cavity complaints **(A, B)**. CRSwNP also report comparatively lower QoL scores **(C–I)**. Kruskal-Wallis test used to identify differences between the mean ranks of at least one pair of the groups. Dunn's pairwise tests was carried out to identify differences between group pairs. *p < 0.05, **p = < 0.01, ***P < 0.001, ****p < 0.0001.

concentrations of these molecules were linked with disease severity scores and QoL measures in these patients.

In plasma from all three groups, we identified mediators from the DHA and n-3 DPA maresin families that included the DHA-derived MaR1 and the n-3 DPA derived $MaR2_{n\text{-}3\ DPA}$ (**Table 2**). Assessment of overall plasma concentrations for this SPM family (i.e., the sum of MaR1, 7S,14S-diHDHA, MaR2, 22-OH-MaR1, 22-COOH-MaR1, 14-oxo-MaR1, 4,14-diHDHA, $MaR1_{n\text{-}3\ DPA}$, $MaR2_{n\text{-}3\ DPA}$ and 7S,14S-diHDPA) demonstrated a significant decreased in plasma concentrations of these mediators in the CRSwNP cohort when compared to healthy controls (**Figure 2A**). Furthermore, concentrations of this SPM family were observed to be negatively correlated with both SNOT 22 scores as well as SF-36 general health measures in patients with CRSwNP (**Figures 2B, C**).

TABLE 2 | Plasma Lipid mediator concentrations.

	Control (pg/mL)			CRSwNP (pg/mL)			URTI (pg/mL)		
DHA metabolome	mean	±	sem	mean	±	sem	mean	±	sem
RvD1	0.05	±	0.06	0.12	±	0.08	1.17	±	0.41
17R-RvD1		–		0.04	±	0.03	0.21	±	0.21
RvD2	133.94	±	86.45	30.44	±	18.38	465.20	±	194.48
RvD3	0.03	±	0.02		–			–	
17R-RvD3	1.49	±	1.20	0.01	±	0.01		–	
RvD4		–			–			–	
RvD5	0.19	±	0.11	0.03	±	0.03	1.48	±	1.22
RvD6		–			–		0.18	±	0.18
PD1	0.29	±	0.25	0.61	±	0.27	0.78	±	0.58
10S,17S-diHDAH	0.59	±	0.35		–		0.66	±	0.43
22-OH-PD1	2.05	±	2.12		–			–	
17R-PD1	0.32	±	0.29	0.32	±	0.26	0.24	±	0.18
MaR1	2.25	±	1.33	0.75	±	0.41	1.95	±	0.97
7S,14S-diHDHA	0.84	±	0.73	0.18	±	0.18		–	
MaR2		–		0.08	±	0.06		–	
22-OH-MaR1	0.65	±	0.46		–			–	
22-COOH-MaR1		–			–			–	
14-oxo-MaR1		–			–			–	
4,14-diHDHA		–			–			–	
n-3 DPA metabolome									
RvT1		–		0.36	±	0.26		–	
RvT2	0.04	±	0.04	0.03	±	0.02	0.06	±	0.06
RvT3	0.07	±	0.07	1.29	±	0.95	0.53	±	0.26
RvT4	0.66	±	0.35	0.05	±	0.03	2.37	±	1.89
RvD1 $_{n\text{-}3\ DPA}$	0.55	±	0.57	1.26	±	1.01	0.20	±	0.20
RvD2 $_{n\text{-}3\ DPA}$	0.21	±	0.15	0.04	±	0.04		–	
RvD5 $_{n\text{-}3\ DPA}$	0.55	±	0.35	0.39	±	0.28		–	
PD1 $_{n\text{-}3\ DPA}$	0.90	±	0.87		–			–	
PD2 $_{n\text{-}3\ DPA}$		–			–			–	
10S, 17S-diHDPA	0.47	±	0.49		–			–	
22-OH-PD1$_{n\text{-}3\ DPA}$		–			–			–	
MaR1 $_{n\text{-}3\ DPA}$	0.09	±	0.09		–		0.61	±	0.40
MaR2 $_{n\text{-}3\ DPA}$	7.05	±	2.38		–			–	
7S,14S-diHDPA		–			–			–	
EPA metabolome									
RvE1	4.39	±	4.37	0.04	±	0.04		–	
RvE2		–		0.19	±	0.07	0.10	±	0.10
RvE3		–			–		1.41	±	1.41
AA metabolome									
LXA_4		–		0.04	±	0.02	1.20	±	0.92
LXB_4	5.76	±	4.44		–		5.69	±	5.69
5S,15S-diHETE	0.13	±	0.09	13.40	±	9.04		–	
13,14-dehydro-15-oxo-LXA_4									
15-oxo-LX_4				0.02	±	0.01	0.39	±	0.39
15-epi-LXA_4	0.22	±	0.17	0.06	±	0.03	1.49	±	1.49
15-epi-LXB_4	2.28	±	1.76	0.08	±	0.08	5.69	±	5.69
LTB_4	7.96	±	4.97	7.56	±	1.87	8.53	±	3.84
5S,12S-diHETE	7.41	±	5.19	3.19	±	1.91	2.48	±	1.76
6-trans-LTB_4	1.57	±	1.18	2.13	±	1.10	2.36	±	1.61
6-trans-12-epi LTB_4	0.06	±	0.07	0.14	±	0.07		–	
20-OH-LTB_4	0.00	±	0.00	0.94	±	0.42	0.59	±	0.59
20-COOH-LTB_4	0.43	±	0.30	0.62	±	0.26	2.08	±	2.08
PGE_2	2.47	±	1.60	4.24	±	0.96	5.43	±	2.34
PGD_2	5.72	±	3.53	3.39	±	0.80	3.39	±	1.15
PGF_{2a}	1.05	±	0.84	3.45	±	1.03	3.89	±	1.56
TxB_2	28.68	±	23.94	71.19	±	28.47	29.88	±	15.95

Plasma was collected from patients with CRSwNP (n = 24) healthy volunteers (n =15) and subjects with URTI and LM were extracted using C18 SPE and LM concentrations determined using LC-MS/MS based LM profiling. - = Below limits.

In nasal secretions we also identified members of this SPM family, including the DHA-derived MaR1 and MaR2 (**Table 2**). Notably, we observed that in nasal secretions, Maresin concentrations were significantly upregulated when compared with levels observed in secretions from both healthy volunteers and patients with a URTI (**Figure 2D**). We also observed that concentrations of these mediators were positively correlated with SF36 general health measures in patients with CRSwNP (**Figure 2E**).

Distinct Lipid Mediator Profiles in Patients With CRSwNP When Compared to Healthy Volunteers and Patients With URTI

Having found changes in plasma Maresin concentrations in patients with CRSwNP we next set out to evaluate whether plasma concentrations of other SPM families together with those of the arachidonic acid (AA)-derived eicosanoids were differentially regulated in patients with CRSwNP when compared with those found in healthy volunteers. Using a targeted LC-MS/MS approach we identified mediators from all four essential fatty acid metabolomes, i.e., DHA, n-3 DPA, eicosapentaenoic acid (EPA) and AA, in plasma from patients with CRSwNP as well as in plasma from healthy volunteers (**Table 2**). To evaluate the relationship between peripheral blood LM concentrations we employed partial least squares discriminant analysis (PLS-DA). PLS-DA is a dimensionality-reducing multivariate analysis that creates a linear regression model accounting for multicollinearity and identifies the relationship between samples based on LM concentrations. Using PLS-DA we found that LM concentrations in plasma from participants with CRSwNP were distinguishable from those identified in healthy controls (**Figure 3A** and **Table 2**). The robustness of this model was evaluated by assessing the coefficient-of-determination (R^2) which gave a value of 0.84. The separation between these two groups was statistically evaluated using the Mahalanobis distance between groups, which gave a value of 4.62, and Hotelling's T-squared test which gave a p value of 3.8×10^{-15} (**Figure 3A**). To assess which of the identified mediators contributed to the observed separation between the groups we assessed the variable importance in projection (VIP) scores that identified mediators contributing the most to the observed separation. Here we found that 9 mediators displayed a VIP score greater than 1. These included both pro-resolving, e.g., $MaR2_{n\text{-}3\ DPA}$ and RvT4, and pro-inflammatory, e.g. $PGF_{2a,}$ autacoids. This analysis also highlighted an overall downregulation in SPM biosynthesis in plasma from patients with CRSwNP whereby out of the 13 SPM found to be differentially regulated between the two groups, 11 were found to be reduced in the CRSwNP. This was linked with an increase in both the pro-inflammatory and smooth muscle contracting agent PGF_{2a} and an increase in 20-OH-LTB_4, the further metabolite of the potent leukocyte chemoattractant LTB_4. These observations highlight a shift in plasma lipid mediator profile of patients with CRSwNP towards a pro-inflammatory profile.

We next assessed whether plasma LM concentrations were differentially regulated in patients with a URTI when compared to CRSwNP. Assessment of the clustering obtained with the lipid mediator profile from these patients demonstrated that plasma lipid mediator concentrations between the two patient groups was different, as observed from the distinct clustering (**Figure 3B**). This separation was observed to be statistically significant as demonstrated by a p value of 5.2×10^{-11} (**Figure 3B**). Evaluation of the VIP scores demonstrated that the differences observed were primarily related to 10 SPM, which included RvD2, RvD1, RvT4 and 15-epi-LXA_4. Intriguingly the concentrations of all these mediators were upregulated in patients with URTI, in line with the clinical observation that this a self-limited inflammatory response (**Figure 3B**).

It is now appreciated that distinct drugs can impact directly or indirectly on SPM production. Therefore, we next evaluated whether those patients that at time of sample collection we receiving treatment displayed a distinct lipid mediator profile to those that were not receiving medication. Results from this analysis demonstrated that there was a statistically significant shift in the lipid mediator profiles between these two groups (**Figure 3C**). This shift in lipid mediator profiles was linked with the upregulation of lipid mediator production in patients that were not receiving medication at the time of sample collection. This suggests that the therapeutics being administered, which included topical and systemic steroids as well as antibiotics, may impact lipid mediator pathway in these patients.

Nasal Secretions From Patients With CRSwNP Display an Altered Lipid Mediator Profile

Having found that SPM concentrations were altered in plasma from patients with CRSwNP we next sought to evaluate whether this was also true for nasal secretions obtained from these patients in comparison with levels found in healthy volunteers. In these secretions we also identified mediators from the lipoxygenase and cyclooxygenase metabolomes of all four fatty acids, including the DHA-derived 22-OH-MaR1, n-3 DPA-derived $MaR2_{n\text{-}3\ DPA}$, EPA-derived RvE2 and AA-derived LXB_4 (**Table 3**). PLS-DA analysis demonstrated a separation in the LM profiles of nasal secretions from patients with CRSwNP from those obtained from healthy volunteers (**Figure 4A**). This was primarily linked with an upregulation of PGE_2 and PGF_{2a} in healthy volunteers compared to patients with CRSwNP (**Figure 4A**).

To gain further insights into the regulation of LM at the site of inflammation, we next compared nasal secretion LM profiles from patients with URTI. Here we observed a separation in the cluster representing URTI patients when compared with that representing LM profiles from patients with CRSwNP (**Figure 4B**). The separation in these clusters was primarily linked with the differential regulation of 12 lipid mediators that included the pro-resolving mediators RvD5 and $RvD5_{n\text{-}3\ DPA}$ and pro-inflammatory eicosanoids, including PGE_2 and PGF_{2a}. Assessment of relative levels of these mediators demonstrated an upregulation of PGD_2, PGE_2 and PGF_{2a} in patients with URTI together with that of a number of pro-resolving mediators including 15-epi-LXA_4, $PD2_{n\text{-}3\ DPA}$ and RvD3 (**Figure 4B**).

Maresin 1 Regulates CRSwNP Circulating Monocyte Activation

Having observed that Maresin concentrations were significantly reduced in plasma from patients with CRSwNP and given that circulating phagocytes become activated in chronic inflammatory conditions we next assessed whether addback of MaR1, which exerts potent leukocyte-directed activities (31), may regulates phagocyte activation in peripheral blood cells from these patients. Incubation of peripheral blood cells with

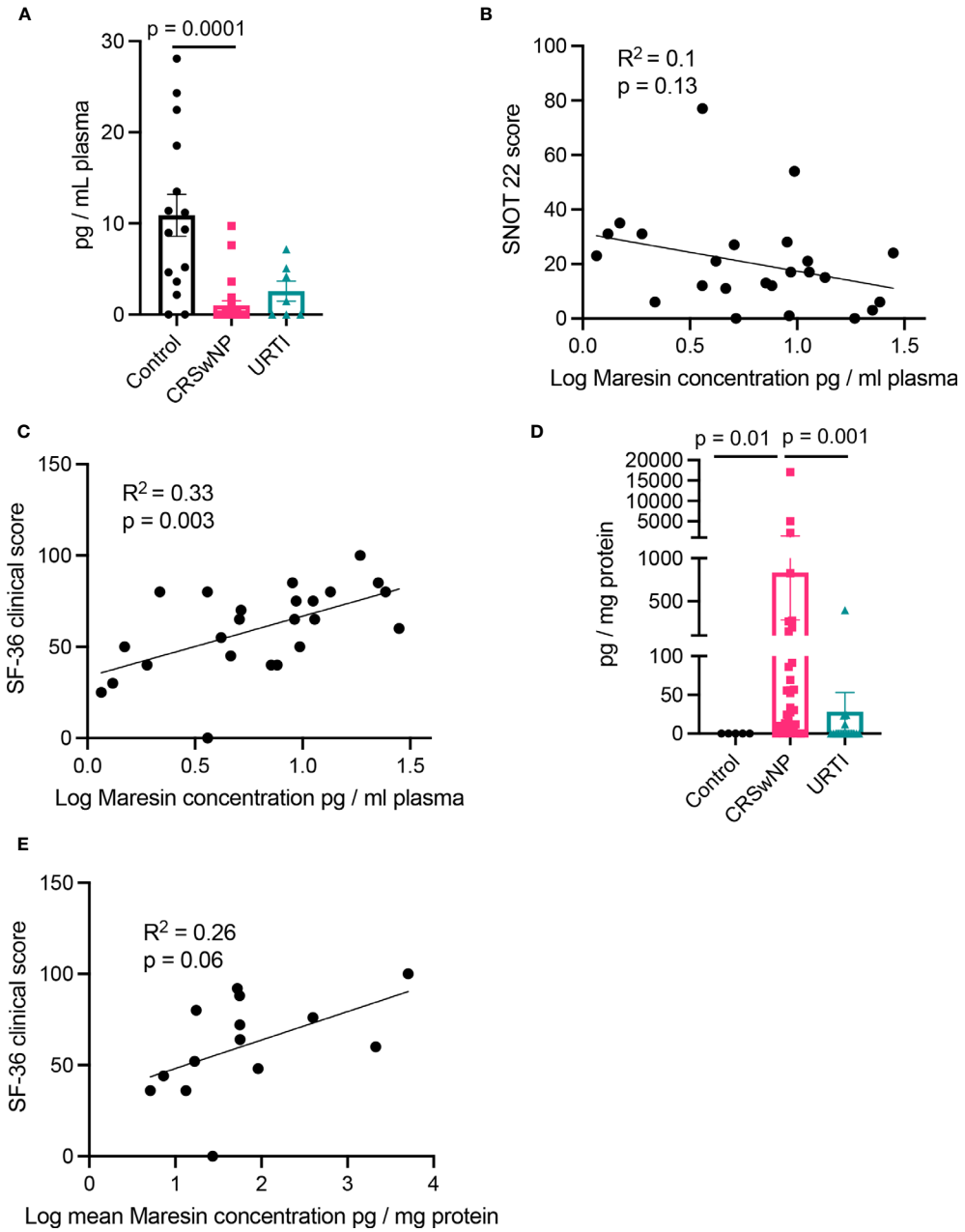

FIGURE 2 | Plasma Maresin levels correlate with clinical scores. **(A)** Plasma Maresin levels (i.e., sum of MaR1, 7S,14S-diHDHA, MaR2, 22-OH-MaR1, 22-COOH-MaR1, 14-oxo-MaR1, 4,14-diHDHA, $MaR1_{n\text{-}3\ DPA}$, $MaR2_{n\text{-}3\ DPA}$ and 7S,14S-diHDPA) for healthy volunteers (n = 15), CRSwNP (n = 24), URTI (n = 8) patients. **(B, C)** Linear regression analysis of Maresins levels in plasma in relation to **(B)** SNOT 22 scores **(C)** 36-Item Short Form Health Survey general health measures. **(D)** Maresin concentrations in nasal secretions. **(E)** Linear regression analysis of Maresins levels in plasma in relation to 36-Item Short Form Health Survey general health measures. **(A, D)** Kruskal-Wallis test used to identify differences between the mean ranks of at least one pair of the groups. Dunn's pairwise tests was carried out to identify differences between group pairs.

MaR1 led to a down regulation in the expression of activation markers on classical and intermediate monocytes and eosinophils reaching statistical significance in intermediate monocytes for CD41 expression, a marker of platelet-monocyte activation (**Figures 5A–E** and **Supplementary Figures 1**, **2**).

We next evaluated whether the leukocyte directed activities of MaR1 were retailed in the presence an inflammatory challenge. For this purpose, we incubated whole blood with platelet activating factor (PAF) together with MaR1. Here we found that MaR1 decreased the expression of activation markers, including CD41, CD11, CD62P and CD162 on monocyte subsets, neutrophils, and

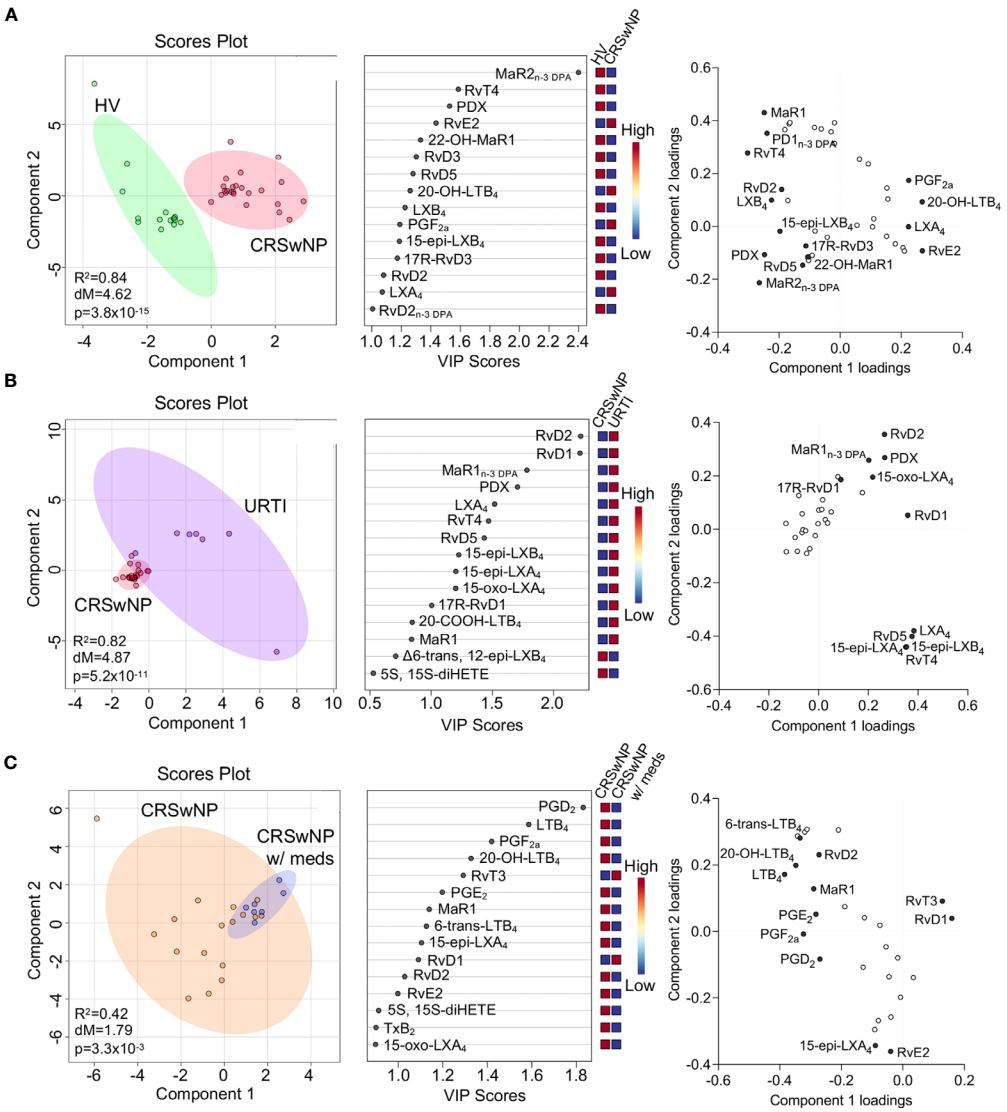

FIGURE 3 | Dysregulated lipid mediator profiles in plasma from CRSwNP when compared to both healthy volunteers and URTI. **(A)** Plasma was collected from patients with CRSwNP (n = 24) and healthy volunteers (HV, n = 15) LM concentrations were determined using LC-MS/MS based LM profiling (see methods for details). Differences in LM concentrations were evaluated using PLS-DA. (*Left panel*) 2-dimensional scores plot and (*centre panel*) corresponding VIP plot of plasma LM. (*right panel*) loading plot where mediators with VIP score >1 are annotated. **(B)**. Plasma was collected from patients with CRSwNP (n = 24) and patients with URTI (n = 7) LM concentrations were determined using LC-MS/MS based LM profiling (see methods for details). Differences in LM concentrations were evaluated using PLS-DA. (*Left panel*) 2-dimensional scores plot and (*centre panel*) corresponding VIP plot of plasma LM. (*right panel*) loading plot where mediators with VIP score >1 are annotated. **(C)** Plasma lipid mediator concentrations were evaluated in patients receiving medication and those that were not. (*Left panel*) 2-dimensional scores plot and (*centre panel*) corresponding VIP plot of plasma LM. (*right panel*) loading plot where mediators with VIP score >1 are annotated. N = 7 for patients receiving medications (CRSwNP w/meds) and n = 17 for patients not receiving medications (CRSwNP). Shaded areas represent 95% confidence interval (CI), R^2 = coefficient-of-determination, p = p-value from Hotelling's T-squared test, dM = Mahalanobis distance between groups.

eosinophils (**Figures 6A–E** and **Supplementary Figures 1**, **3**) reaching statistical significance for CD62P on classical monocytes and CD41 on intermediate monocytes. We also observed a significant upregulation of CD49d expression on classical monocytes following MaR1 incubation (**Figures 6A–D**). Together these findings indicate that MaR1 regulates the expression of phagocytes from patients with CRSwNP.

DISCUSSION

In the present study we explored whether disruption in SPM production, and in particularly that of Maresins, were linked to disease in patients with CRSwNP. In peripheral blood from patients with CRSwNP we observed a significant downregulation in concentration of Maresins when compared with healthy volunteers.

TABLE 3 | Lipid mediator profiles from nasal secretions.

	Control (pg/mg protein)			CRSwNP (pg/mg protein)			URTI (pg/mg protein)		
DHA metabolome	mean	±	sem	mean	±	sem	mean	±	sem
RvD1		–			–		0.03	±	0.03
17R-RvD1		–			–			–	
RvD2		–			–			–	
RvD3		–			–		1.86	±	1.56
17R-RvD3		–		0.42	±	0.23		–	
RvD4		–			–			–	
RvD5	103.06	±	85.45	398.47	±	143.36	975.15	±	493.43
RvD6		–			–			–	
PD1		–		10.71	±	3.41	1.62	±	0.93
10S,17S-diHDAH	9.41	±	8.59	25.30	±	25.70	56.49	±	40.33
22-OH-PD1		–			–			–	
17R-PD1		–		0.91	±	0.70		–	
MaR1		–		788.95	±	559.54	26.22	±	25.47
7S,14S-diHDHA		–		26.74	±	11.86	1.57	±	1.19
MaR2		–		16.13	±	12.97	0.62	±	0.46
22-OH-MaR1		–			–			–	
22-COOH-MaR1		–			–			–	
14-oxo-MaR1		–			–			–	
4,14-diHDHA		–		0.33	±	0.34		–	
n-3 DPA metabolome									
RvT1		–			–		0.37	±	0.32
RvT2		–			–			–	
RvT3		–			–			–	
RvT4		–			–			–	
$RvD1_{n\text{-}3\ DPA}$		–		0.02	±	0.01		–	
$RvD2_{n\text{-}3\ DPA}$		–		0.04	±	0.04		–	
$RvD5_{n\text{-}3\ DPA}$		–		21.26	±	10.23	0.93	±	0.65
$PD1_{\ n\text{-}3\ DPA}$	4.98	±	4.54		–			–	
$PD2_{\ n\text{-}3\ DPA}$	44.61	±	40.72		–		29.21	±	23.99
10S, 17S-diHDPA		–		0.06	±	0.06	0.10	±	0.11
22-OH-PD1n $_{n\text{-}3\ DPA}$		–			–			–	
$MaR1_{n\text{-}3\ DPA}$		–			–			–	
$MaR2_{n\text{-}3\ DPA}$		–			–			–	
7S,14S-diHDPA		–			–			–	
AA metabolome									
RvE1		–			–			–	
RvE2		–			–			–	
RvE3	104.09	±	95.02	78.40	±	79.65	48.23	±	29.01
AA metabolome									
LXA_4		–		3.22	±	2.00	149.68	±	154.44
LXB_4		–		32.75	±	15.98	37.82	±	13.93
5S,15S-diHETE	146.84	±	134.05	96.91	±	98.46	135.93	±	84.12
13,14-dehydro-15-oxo-LXA_4		–			–			–	
15-oxo-LXA_4		–		1.57	±	0.88	0.04	±	0.03
15-epi-LXA_4		–					2.46	±	1.97
15-epi-LXB_4	263.41	±	240.46	0.15	±	0.16	0.00	±	0.00
LTB_4	71.93	±	42.07	161.59	±	56.43	157.18	±	80.03
5S,12S-diHETE		–		0.32	±	0.32		–	
6-trans-LTB_4	38.19	±	33.42	85.22	±	39.31	124.85	±	60.29
6-trans-12-epi-LTB_4		–		94.39	±	44.69	52.73	±	49.82
20-OH-LTB_4		–		501.80	±	373.60	26.16	±	21.46
20-COOH-LTB_4		–		10.17	±	4.71	13.50	±	6.26
PGE_2	1926.04	±	1110.20	265.65	±	54.78	1408.65	±	411.74
PGD_2	1.81	±	1.65	37.97	±	19.05	489.73	±	236.24
PGF_{2a}	718.47	±	501.80	96.36	±	18.92	434.53	±	148.98
TxB_2	7.69	±	4.45	5.96	±	4.75	3.18	±	1.46
LTC_4		–			–			–	
LTD_4		–			–			–	
LTE_4		–		9.73	±	2.95	2.55	±	1.45

Plasma was collected from patients with CRSwNP (n = 16) healthy volunteers (n = 5) and subjects with URTI (8) and LM were extracted using C18 SPE and LM concentrations determined using LC-MS/MS based LM profiling. - = Below limits.

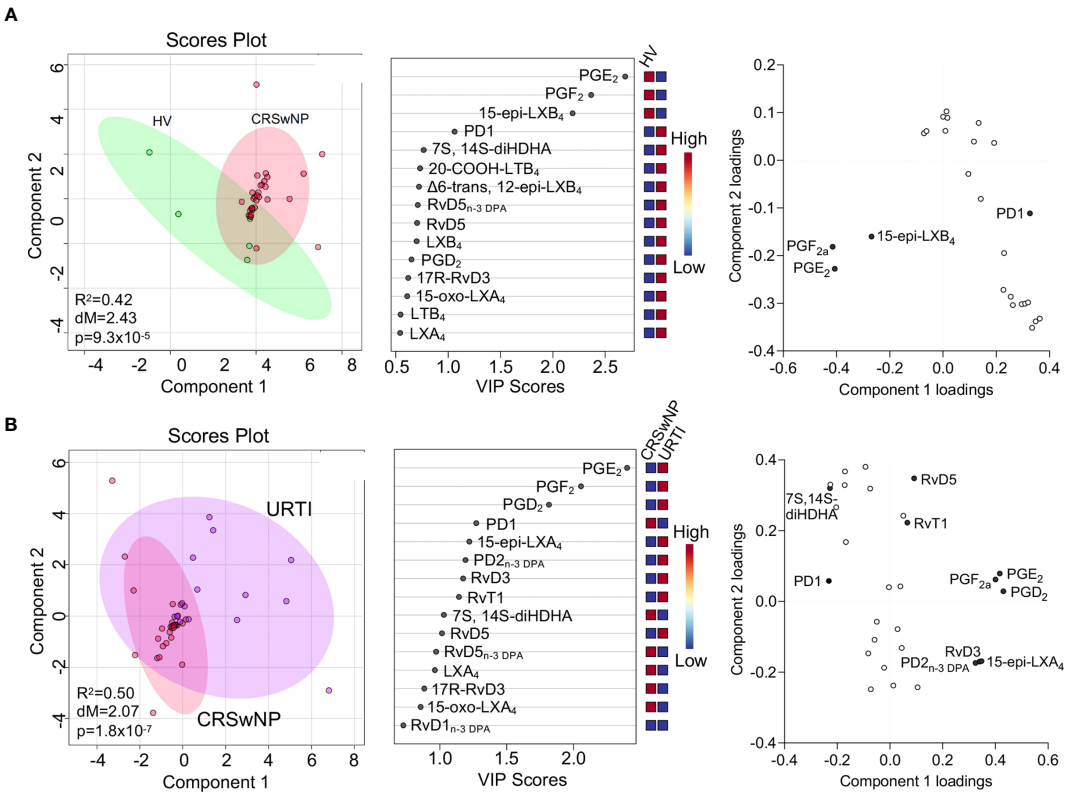

FIGURE 4 | Nasal secretions from patients with CRSwNP display a distinct LM profile to those from both healthy volunteers and URTI patients. **(A)** Nasal secretions were collected from patients with CRSwNP (n = 16) and healthy volunteers (HV, n = 5) LM concentrations were determined using LC-MS/MS based LM profiling (see methods for details). Differences in LM concentrations were evaluated using PLS-DA. (*Left panel*) 2-dimensional scores plot and (*centre panel*) corresponding VIP plot of plasma LM (*right panel*) loading plot where mediators with VIP score >1 are annotated. **(B)** Nasal secretions were collected from patients with CRSwNP (n = 16) and patients with URTI (n = 8) LM concentrations were determined using LC-MS/MS based LM profiling (see methods for details). Differences in LM concentrations were evaluated using PLS-DA. (*Left panel*) 2-dimensional scores plot and (*centre panel*) corresponding VIP plot of plasma LM (*right panel*) loading plot where mediators with VIP score >1 are annotated. Shaded areas represent 95% confidence interval (CI), R^2 = coefficient-of-determination, p = p-value from Hotelling's T-squared test, dM = Mahalanobis distance between groups.

These changes were linked with an overall downregulation of other SPM in plasma from these patients when compared with concentrations observed in healthy volunteers and patients with URTI. Interestingly, we found that Maresin concentrations in nasal secretions from these patients were significantly upregulated when compared to both healthy volunteers and patients with URTI. Of note, nasal secretion, and plasma Maresin concentrations were positively correlated with SF36 scores in patients with CRSwNP. Furthermore, incubation of peripheral blood with MaR1 reduced circulating phagocyte activation as evidenced by a downregulation of adhesion molecule expression.

It is estimated that 100 million people worldwide are affected by chronic rhinosinustits[4]. Longitudinal data from the Clinical Practice Research Datalink suggests that 1% of British adults receive treatment each year in primary care, resulting in multiple GP consultations and medical prescriptions (32). In the secondary care setting, this translates into 120,000 out-patient consultations and 40,000 operations in England and Wales annually (7). The difficulties in initiating and maintaining appropriate treatments for CRSwNP are reliant upon an accurate diagnosis, which in the primary care setting is challenging as the symptoms associated with CRSwNP (nasal obstruction, discharge, loss of smell and facial pain) are identifiable in all nasal cavity ailments. In addition, limited ENT training for medical professionals (33) and lack of diagnostic equipment available in primary care are recognised contributing factors (32). In the present studies we observed that LM profiles in both plasma and nasal secretions from patients with CRSwNP were distinct from those obtained in both healthy volunteers and patients with URTI. Our findings are also in accord with recent studies demonstrating that lipid mediator concentrations were different in sinus tissues from patients with CRSwNP when compared to both control subjects and CRS patients without polyps (21).

Adhesion molecules play a central role in phagocyte recruitment into tissues as well as in the formation of platelet-phagocyte heterotypic aggregates which are involved in the propagation of both systemic and airway inflammation (31, 34). Flow cytometric assessment of peripheral blood phagocytes demonstrated that MaR1 displayed potent phagocyte-directed

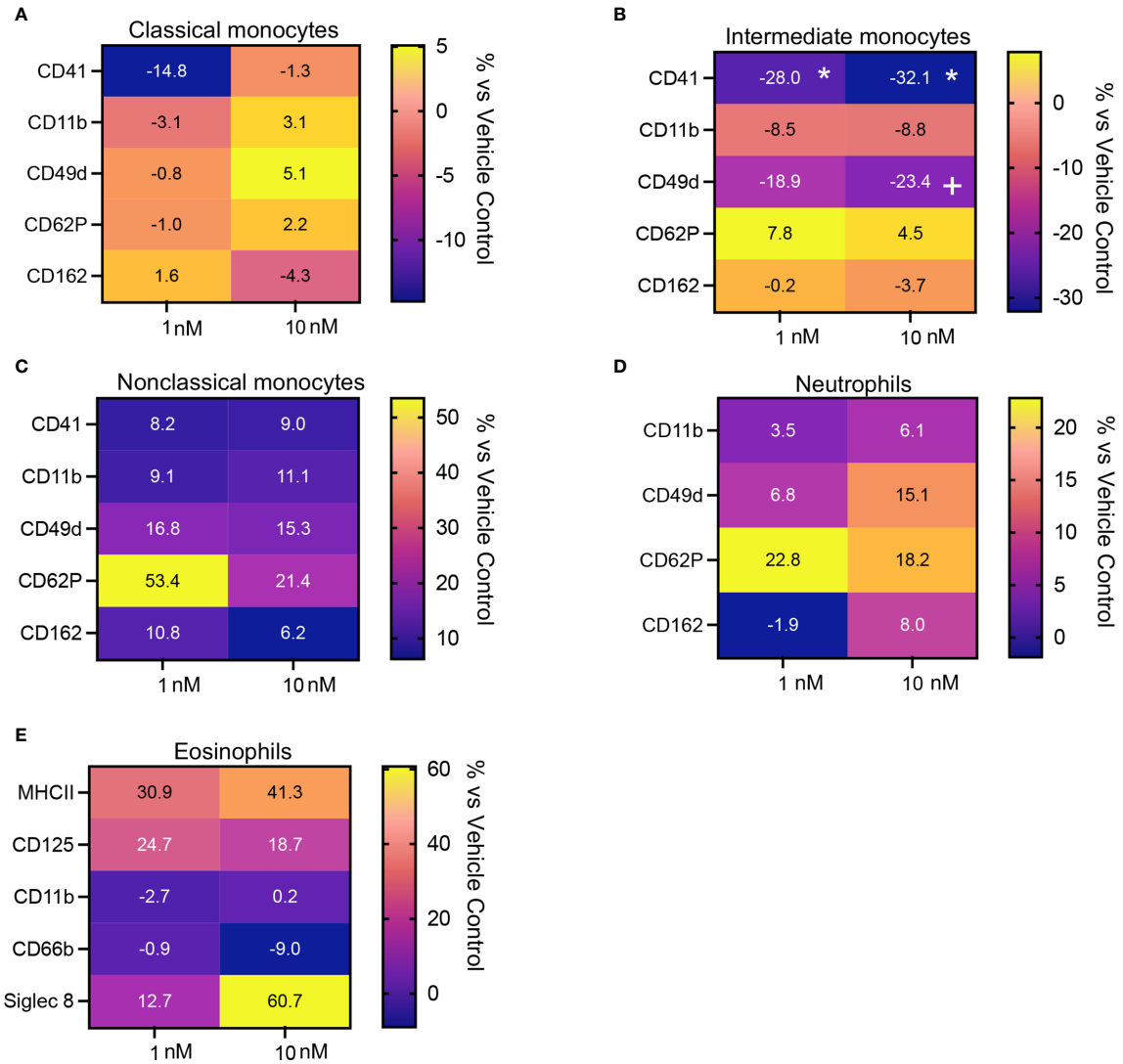

FIGURE 5 | MaR1 regulates the expression of activation markers on peripheral blood phagocytes from patients with CRSwNP. **(A–E)** peripheral blood from CRSwNP patients was incubated with vehicle or MaR1 (1 or 10nM) for 45 minutes at 37°C and the expression of the indicated activation markers was evaluated on **(A)** CD14++CD16+ Classical monocytes, **(B)** CD14++CD16++ Intermediate monocytes, **(C)** CD14+CD16++ Non-Classical monocytes, **(D)** CD16+ neutrophils and **(E)** Siglec 8+ eosinophils using flow cytometry. Results are means of percentage (%) change from values obtained in vehicle controls for each patient. N = 7 patients for **(A–D)** and 10 patients for **(E)**. *$p < 0.05$.

actions regulating the expression of adhesion molecules, including CD162 and CD11b on neutrophils and eosinophils, two proteins involved in the recruitment of phagocytes into inflamed tissues. Furthermore, we observed that MaR1 significantly downregulated the expression of markers for platelet-leukocyte heterotypic aggregates, namely CD41 and CD62P, on classical and intermediate monocytes, with a trend for the reduction in the expression of CD41 also observed in neutrophils and non-classical monocytes. These heterotypic aggregates are linked with both an increased phagocyte recruitment and activation in various acute and chronic inflammatory conditions, including COVID-19 (35). Together these observations are also in accord with previous studies demonstrating that MaR1 regulates leukocyte trafficking to the site of inflammation.

The integrated approach employed in the present studies evaluating lipid mediator profiles in both peripheral blood and tissues and linking these to quality-of-life scores and phagocyte responses provides novel insights into the role of SPM in the pathophysiology of CRSwNP. There are a number of limitations that should be noted, the first being that due to the small number of patients recruited we were unable to evaluate the impact of different drugs on lipid mediator production in patients with CRSwNP. This is of relevance given that in our analysis we observed that patients receiving some form of medication displayed distinct lipid mediator profiles when compared with

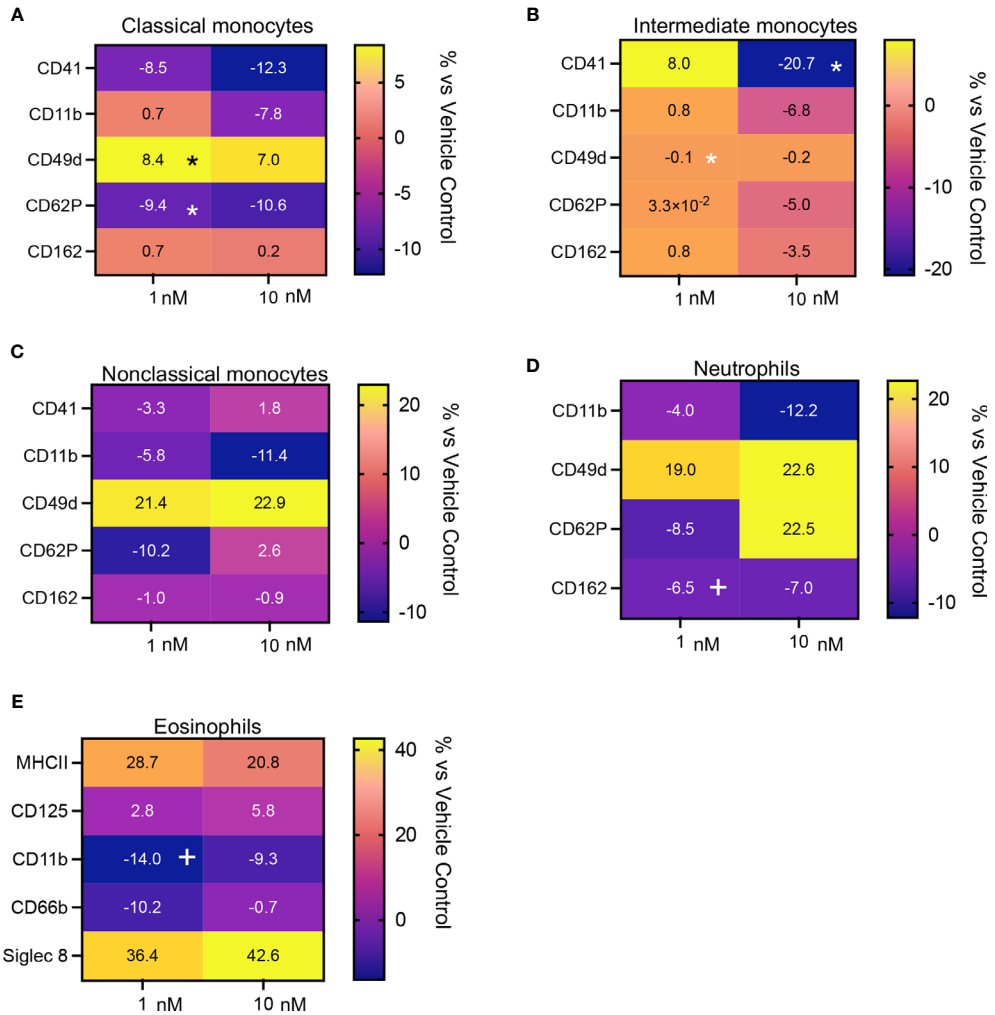

FIGURE 6 | Regulation of activation marker expression in peripheral blood from CRSwNP patients incubated with PAF by MaR1. Peripheral blood from CRSwNP patients was incubated with vehicle or MaR1 (1 or 10nM) for 15 minutes at 37°C then with PAF 100 (nM) for a further 30 minutes at 37°C and the expression of the indicated activation markers was evaluated on **(A)** CD14++CD16+ Classical monocytes, **(B)** CD14++CD16++ Intermediate monocytes, **(C)** CD14+CD16++ Non-Classical monocytes, **(D)** CD16+ neutrophils and **(E)** Siglec 8+ eosinophils using flow cytometry. Results are means of percentage (%) change from values obtained in vehicle controls for each patient. N = 7 patients for **(A–D)** and 10 patients for **(E)**. *$p < 0.05$.

those not receiving medication at time of study enrolment. Therefore, future studies will need to evaluate the impact that distinct treatments have on lipid mediator production and how this links with outcome. A second limitation of this study is that patients with CRSwNP enrolled in this study were on average older than those with URTI. Since SPM production is reduced with age this might have potentially contributed to the higher SPM levels reported in patients with URTI. Thus, future studies comparing these two groups would need to exclude the impact of age on the observed differences in SPM production observed herein. Another aspect that requires further evaluation is the mechanisms leading to the alteration of maresin production in both peripheral blood and tissues and whether maresin signalling and function in extravasated leukocyte is impaired, contributing to dysregulated phagocyte responses.

In summation, in the present studies we observed that lipid mediator concentrations in both plasma and nasal secretions from patients with CRSwNP were markedly different to those obtained from either healthy volunteer and patients with a URTI. We also found that cumulative Maresin concentrations were markedly reduced in plasma from patients with CRSwNP whilst being significantly increased in nasal secretions when compared to both healthy volunteers and patients with URTI. Furthermore, concentrations of these mediators were correlated with quality-of-life scores supporting the hypothesis that lipid mediators, potentially Maresins, may be useful diagnostics in patients with CRSwNP. We also observed that MaR1 regulated phagocyte activation suggesting that pro-resolving therapeutics may be useful in limiting chronic inflammation in these patients.

DATA AVAILABILITY STATEMENT

The original contributions presented in the study are included in the article/**Supplementary Material**. Further inquiries can be directed to the corresponding author.

ETHICS STATEMENT

The studies involving human participants were reviewed and approved by NHS Research Ethics Committee. The patients/participants provided their written informed consent to participate in this study. Participants with a history of CRSwNP with failed medical management, healthy controls with no previous ear, nose and throat disease as well as those undergoing nasal cavity surgery due to non-inflammatory conditions (cosmetic or post traumatic deformity; septoplasty or septorhinoplasty) and participants with URTI were recruited. (Research Ethics Committee Number: 17/EM/0447).

AUTHOR CONTRIBUTIONS

JD and IB designed the experiments. IB and DSK conducted the experiments and/or analysed results. All authors contributed to the article and approved the submitted version. JD and GA contributed to supervision of the work JD, GA, and IB conceived overall research plan.

FUNDING

JD received funding from the European Research Council (ERC) under the European Union's Horizon 2020 research and innovation programme (grant no: 677542) and the Barts Charity (grant no: MGU0343). JD is also supported by a Sir Henry Dale Fellowship jointly funded by the Wellcome Trust and the Royal Society (grant 107613/Z/15/Z).

ACKNOWLEDGMENTS

We would like to thank all participants for the samples provided. We would also like to thank Dr Patricia Souza for assistance with flow cytometry experiments and Drs Romain Colas, Francesco Palmas and Charlotte Jouvene for assistance with lipid mediator profiling experiments.

SUPPLEMENTARY MATERIAL

The Supplementary Material for this article can be found online at: https://www.frontiersin.org/articles/10.3389/fimmu.2021.733019/full#supplementary-material

REFERENCES

1. Fokkens WJ, Lund VJ, Hopkins C, Hellings PW, Kern R, Reitsma S, et al. European Position Paper on Rhinosinusitis and Nasal Polyps 2020. *Rhinology* (2020) 58:1–464. doi: 10.4193/Rhin20.401
2. Bhattacharyya N, Gilani S. Prevalence of Potential Adult Chronic Rhinosinusitis Symptoms in the United States. *Otolaryngol Head Neck Surg* (2018) 159:522–5. doi: 10.1177/0194599818774006
3. Bachert C, Bhattacharyya N, Desrosiers M, Khan AH. Burden of Disease in Chronic Rhinosinusitis With Nasal Polyps. *J Asthma Allergy* (2021) 14:127–34. doi: 10.2147/JAA.S290424
4. Hedman J, Kaprio J, Poussa T, Nieminen MM. Prevalence of Asthma, Aspirin Intolerance, Nasal Polyposis and Chronic Obstructive Pulmonary Disease in a Population-Based Study. *Int J Epidemiol* (1999) 28:717–22. doi: 10.1093/ije/28.4.717
5. Klossek JM, Neukirch F, Pribil C, Jankowski R, Serrano E, Chanal I, et al. Prevalence of Nasal Polyposis in France: A Cross-Sectional, Case-Control Study. *Allergy* (2005) 60:233–7. doi: 10.1111/j.1398-9995.2005.00688.x
6. Benjamin MR, Stevens WW, Li N, Bose S, Grammer LC, Kern RC, et al. Clinical Characteristics of Patients With Chronic Rhinosinusitis Without Nasal Polyps in an Academic Setting. *J Allergy Clin Immunol Pract* (2019) 7:1010–6. doi: 10.1016/j.jaip.2018.10.014
7. Philpott C, Erskine S, Smith R, Hopkins C, Kara N, Farboud A, et al. Current Use of Baseline Medical Treatment in Chronic Rhinosinusitis: Data From the National Chronic Rhinosinusitis Epidemiology Study (CRES). *Clin Otolaryngol* (2018) 43:509–24. doi: 10.1111/coa.13012
8. Gliklich RE, Metson R. The Health Impact of Chronic Sinusitis in Patients Seeking Otolaryngologic Care. *Otolaryngol Head Neck Surg* (1995) 113:104–9. doi: 10.1016/S0194-5998(95)70152-4
9. Rudmik L. Economics of Chronic Rhinosinusitis. *Curr Allergy Asthma Rep* (2017) 17:20. doi: 10.1007/s11882-017-0690-5
10. Vennik J, Eyles C, Thomas M, Hopkins C, Little P, Blackshaw H, et al. Chronic Rhinosinusitis: A Qualitative Study of Patient Views and Experiences of Current Management in Primary and Secondary Care. *BMJ Open* (2019) 9:e022644. doi: 10.1136/bmjopen-2018-022644
11. Widal F, Abrami P, Lermoyez J. Anaphylaxie Et Idiosyncrasie. 1992 [Anaphylaxis and Idiosyncrasy. 1992]. *Allergy Proc* (1993) 14:373–6; discussion 371-2. doi: 10.2500/108854193778774065
12. Kowalski ML, Agache I, Bavbek S, Bakirtas A, Blanca M, Bochenek G, et al. Diagnosis and Management of NSAID-Exacerbated Respiratory Disease (N-ERD)-A EAACI Position Paper. *Allergy* (2019) 74:28–39. doi: 10.1111/all.13599
13. Orlandi RR, Kingdom TT, Smith TL, Bleier B, DeConde A, Luong AU, et al. International Consensus Statement on Allergy and Rhinology: Rhinosinusitis 2021. *Int Forum Allergy Rhinol* (2021) 11:213–739. doi: 10.1002/alr.22741
14. Milewski M, Mastalerz L, Nizankowska E, Szczeklik A. Nasal Provocation Test With Lysine-Aspirin for Diagnosis of Aspirin-Sensitive Asthma. *J Allergy Clin Immunol* (1998) 101:581–6. doi: 10.1016/S0091-6749(98)70163-0
15. Miller B, Mirakian R, Gane S, Larco J, Sannah AA, Darby Y, et al. Nasal Lysine Aspirin Challenge in the Diagnosis of Aspirin - Exacerbated Respiratory Disease: Asthma and Rhinitis. *Clin Exp Allergy* (2013) 43:874–80. doi: 10.1111/cea.12110
16. Kim AS, Conte MS. Specialized Pro-Resolving Lipid Mediators in Cardiovascular Disease, Diagnosis, and Therapy. *Adv Drug Deliv Rev* (2020) 159:170–9. doi: 10.1016/j.addr.2020.07.011
17. Recchiuti A, Mattoscio D, Isopi E. Roles, Actions, and Therapeutic Potential of Specialized Pro-Resolving Lipid Mediators for the Treatment of Inflammation in Cystic Fibrosis. *Front Pharmacol* (2019) 10:252. doi: 10.3389/fphar.2019.00252
18. Serhan CN, Chiang N, Dalli J. New Pro-Resolving N-3 Mediators Bridge Resolution of Infectious Inflammation to Tissue Regeneration. *Mol Aspects Med* (2018) 64:1–17. doi: 10.1016/j.mam.2017.08.002
19. Spite M, Norling LV, Summers L, Yang R, Cooper D, Petasis NA, et al. Resolvin D2 Is a Potent Regulator of Leukocytes and Controls Microbial Sepsis. *Nature* (2009) 461:1287–91. doi: 10.1038/nature08541
20. Morita M, Kuba K, Ichikawa A, Nakayama M, Katahira J, Iwamoto R, et al. The Lipid Mediator Protectin D1 Inhibits Influenza Virus Replication and Improves Severe Influenza. *Cell* (2013) 153:112–25. doi: 10.1016/j.cell.2013.02.027
21. Vickery TW, Armstrong M, Kofonow JM, Robertson CE, Kroehl ME, Reisdorph NA, et al. Altered Tissue Specialized Pro-Resolving Mediators in Chronic Rhinosinusitis. *Prostaglandins Leukot Essent Fatty Acids* (2021) 164:102218. doi: 10.1016/j.plefa.2020.102218

22. Gomez EA, Colas RA, Souza PR, Hands R, Lewis MJ, Bessant C, et al. Blood Pro-Resolving Mediators Are Linked With Synovial Pathology and Are Predictive of DMARD Responsiveness in Rheumatoid Arthritis. *Nat Commun* (2020) 11:5420. doi: 10.1038/s41467-020-19176-z
23. Fokkens WJ, Lund VJ, Mullol J, Bachert C, Alobid I, Baroody F, et al. EPOS 2012: European Position Paper on Rhinosinusitis and Nasal Polyps 2012. A Summary for Otorhinolaryngologists. *Rhinology* (2012) 50:1–12. doi: 10.4193/Rhino50E2
24. Rudmik L, Soler ZM, Hopkins C. Using Postoperative SNOT-22 to Help Predict the Probability of Revision Sinus Surgery. *Rhinology* (2016) 54:111–6. doi: 10.4193/Rhino15.284
25. Stewart MG, Witsell DL, Smith TL, Weaver EM, Yueh B, Hannley MT. Development and Validation of the Nasal Obstruction Symptom Evaluation (NOSE) Scale. *Otolaryngol Head Neck Surg* (2004) 130:157–63. doi: 10.1016/j.otohns.2003.09.016
26. Hays RD, Morales LS. The RAND-36 Measure of Health-Related Quality of Life. *Ann Med* (2001) 33:350–7. doi: 10.3109/07853890109002089
27. Pang Z, Chong J, Zhou G, de Lima Morais DA, Chang L, Barrette M, et al. MetaboAnalyst 5.0: Narrowing the Gap Between Raw Spectra and Functional Insights. *Nucleic Acids Res* (2021) 49(W1):W388–96. doi: 10.1093/nar/gkab382
28. Worley B, Halouska S, Powers R. Utilities for Quantifying Separation in PCA/PLS-DA Scores Plots. *Anal Biochem* (2013) 433:102–4. doi: 10.1016/j.ab.2012.10.011
29. Levy BD, Abdulnour RE, Tavares A, Bruggemann TR, Norris PC, Bai Y, et al. Cysteinyl Maresins Regulate the Prophlogistic Lung Actions of Cysteinyl Leukotrienes. *J Allergy Clin Immunol* (2020) 145:335–44. doi: 10.1016/j.jaci.2019.09.028
30. Nordgren TM, Bauer CD, Heires AJ, Poole JA, Wyatt TA, West WW, et al. Maresin-1 Reduces Airway Inflammation Associated With Acute and Repetitive Exposures to Organic Dust. *Transl Res* (2015) 166:57–69. doi: 10.1016/j.trsl.2015.01.001
31. Abdulnour RE, Dalli J, Colby JK, Krishnamoorthy N, Timmons JY, Tan SH, et al. Maresin 1 Biosynthesis During Platelet-Neutrophil Interactions Is Organ-Protective. *Proc Natl Acad Sci USA* (2014) 111:16526–31. doi: 10.1073/pnas.1407123111
32. Vennik J, Eyles C, Thomas M, Hopkins C, Little P, Blackshaw H, et al. Management Strategies for Chronic Rhinosinusitis: A Qualitative Study of GP and ENT Specialist Views of Current Practice in the UK. *BMJ Open* (2018) 8:e022643. doi: 10.1136/bmjopen-2018-022643
33. Bhalla S, Beegun I, Awad Z, Tolley N. Simulation-Based ENT Induction: Validation of a Novel Mannequin Training Model. *J Laryngol Otol* (2020) 134:74–80. doi: 10.1017/S0022215119002639
34. Colas RA, Souza PR, Walker ME, Burton M, Zaslona Z, Curtis AM, et al. Impaired Production and Diurnal Regulation of Vascular RvDn-3 DPA Increase Systemic Inflammation and Cardiovascular Disease. *Circ Res* (2018) 122:855–63. doi: 10.1161/CIRCRESAHA.117.312472
35. Hottz ED, Azevedo-Quintanilha IG, Palhinha L, Teixeira L, Barreto EA, Pao CRR, et al. Platelet Activation and Platelet-Monocyte Aggregate Formation Trigger Tissue Factor Expression in Patients With Severe COVID-19. *Blood* (2020) 136:1330–41. doi: 10.1182/blood.2020007252

Conflict of Interest: JD is Scientific founder and director of Resolomics Ltd and Inventor on several patents and patent applications assigned to Brigham and Women's Hospital (Boston, MA) and Queen Mary University of London (London, UK) for the therapeutic and diagnostic use of specialized pro-resolving mediators.

The remaining authors declare that the research was conducted in the absence of any commercial or financial relationships that could be construed as a potential conflict of interest.

Publisher's Note: All claims expressed in this article are solely those of the authors and do not necessarily represent those of their affiliated organizations, or those of the publisher, the editors and the reviewers. Any product that may be evaluated in this article, or claim that may be made by its manufacturer, is not guaranteed or endorsed by the publisher.

Copyright © 2021 Beegun, Koenis, Alusi and Dalli. This is an open-access article distributed under the terms of the Creative Commons Attribution License (CC BY). The use, distribution or reproduction in other forums is permitted, provided the original author(s) and the copyright owner(s) are credited and that the original publication in this journal is cited, in accordance with accepted academic practice. No use, distribution or reproduction is permitted which does not comply with these terms.

frontiers in Immunology

SYSTEMATIC REVIEW
published: 01 September 2021
doi: 10.3389/fimmu.2021.720221

CNS-Spleen Axis – a Close Interplay in Mediating Inflammatory Responses in Burn Patients and a Key to Novel Burn Therapeutics

Noorisah Khan[1], *Supreet Kaur*[1], *Carly M. Knuth*[1,2] *and Marc G. Jeschke*[1,2*]

[1] Ross Tilley Burn Centre, Sunnybrook Health Sciences Centre, Toronto, ON, Canada, [2] Institute of Medical Science, University of Toronto, Toronto, ON, Canada

Severe burn-induced inflammation and subsequent hypermetabolic response can lead to profound infection and sepsis, resulting in multiple organ failure and high mortality risk in patients. This represents an extremely challenging issue for clinicians as sepsis is the leading cause of mortality in burn patients. Since hyperinflammation and immune dysfunction are a result of an immune imbalance, restoring these conditions seem to have promising benefits for burn patients. A key network that modulates the immune balance is the central nervous system (CNS)-spleen axis, which coordinates multiple signaling pathways, including sympathetic and parasympathetic pathways. Modulating inflammation is a key strategy that researchers use to understand neuroimmunomodulation in other hyperinflammatory disease models and modulating the CNS-spleen axis has led to improved clinical outcomes in patients. As the immune balance is paramount for recovery in burn-induced sepsis and patients with hyperinflammatory conditions, it appears that severe burn injuries substantially alter this CNS-spleen axis. Therefore, it is essential to address and discuss the potential therapeutic techniques that target the CNS-spleen axis that aim to restore homeostasis in burn patients. To understand this in detail, we have conducted a systematic review to explore the role of the CNS-spleen axis and its impact on immunomodulation concerning the burn-induced hypermetabolic response and associated sepsis complications. Furthermore, this thorough review explores the role of the spleen, CNS-spleen axis in the ebb and flow phases following a severe burn, how this axis induces metabolic factors and immune dysfunction, and therapeutic techniques and chemical interventions that restore the immune balance *via* neuroimmunomodulation.

Keywords: trauma, CNS, spleen, burns, sepsis

OPEN ACCESS

Edited by:
Janos G. Filep,
Université de Montréal, Canada

Reviewed by:
Andrea Baragetti,
University of Milan, Italy
Bin Gong,
University of Texas Medical Branch at Galveston, United States

***Correspondence:**
Marc G. Jeschke
marc.jeschke@sunnybrook.ca

Specialty section:
This article was submitted to Inflammation, a section of the journal Frontiers in Immunology

Received: *03 June 2021*
Accepted: *16 August 2021*
Published: *01 September 2021*

Citation:
Khan N, Kaur S, Knuth CM and Jeschke MG (2021) CNS-Spleen Axis – a Close Interplay in Mediating Inflammatory Responses in Burn Patients and a Key to Novel Burn Therapeutics. Front. Immunol. 12:720221. doi: 10.3389/fimmu.2021.720221

INTRODUCTION

Severe burns (>20% total body surface area) are one of the most devastating traumas and are a global public health concern (1–3). The World Health Organization estimates that burn injuries account for approximately 11 million injuries and 180,000 deaths per annum globally (4). Severe burns trigger a complex pattern of responses, such as inflammation and stress hormone signaling

induced hypermetabolism, that persists for years after the initial injury. One of the initial consequences is a systemic inflammatory response, which occurs within hours after the initial insult to promote recovery. However, the inflammatory response to burn injury, unlike other forms of trauma, is highly dysregulated and may be repeatedly activated throughout recovery. Repeated and uncontrolled immune activation and stress hormone signaling greatly increases the susceptibility to infections and sepsis that often lead to multiorgan failure and have a high associated risk of mortality in patients. Hypermetabolism, sepsis, and consequent multiorgan failure are mediated through the immune system. Thus, immune dysfunction is a major contributor to these adverse outcomes. This poses a significant challenge to patient care, as controlling sepsis in burn patients requires a multifaceted approach that differs from sepsis in the general population. Although sepsis is the primary cause of death in burn patients that survive the initial phase of burn shock, there are currently no effective interventions as the sepsis syndrome remains poorly understood.

The CNS-spleen axis has a central role in immune function modulation with its sympathetic and parasympathetic pathways. In light of this, we propose that the CNS-spleen axis plays an important role in mediating the inflammatory response in burn patients. Given the challenges noted above, there is a growing need to understand the key players of the inflammatory response in burn patients to determine effective treatment strategies. Furthermore, we suggest that targeting this underappreciated CNS-spleen axis may lead to identifying new treatment strategies, which may improve the outcome of septic burn patients. The spleen plays a prominent role in blood filtration and regulating systemic immune responses (5). The spleen is unique to other secondary lymphoid organs given that it filters debris directly from the blood rather than through lymphatic drainage. Circulating blood first enters the splenic artery and is dispersed into the marginal zone (MZ), which separates the white pulp (WP) from the red pulp (RP). The MZ acts as a connection between circulating blood and immune cells. Macrophages within the MZ express a diverse set of surface markers to capture and process antigens to present to B cells (6, 7). Surrounding the central arterioles of the spleen is the WP, which is composed of the periarteriolar lymphoid sheath (PALS) and follicles. T cells and B cells are concentrated in the PALS and follicular zones, respectively, where they respond to presented antigens and coordinate the innate and adaptive immune responses. On the opposite side of the MZ is the RP, which is the primary site of blood filtration. Here, RP macrophages play a crucial role in filtering aged, dead, or opsonized cells from systemic circulation (6). Furthermore, myeloid cells, including granulocytes, monocytes, and macrophages are primarily located within the RP region (8). Granulocytes like neutrophils, eosinophils, basophils, and mast cells are mainly localized in the RP region, with some cells in transition through the MZ into RP (9). When neutrophils are recruited to inflammatory sites, they have short life spans and originate from the bone marrow (10). A neutrophil-intrinsic program, like a timer, allows neutrophils to mount an efficient defense while preserving vascular health (11). However, neutrophil activity doesn't rise homogeneously throughout the entire hematopoietic system (10). Instead, the marrow-derived neutrophils that are located closest to the inflammation site migrate, rather than marrow-derived neutrophils that are further away in the body (10). Monocytes develop in the bone marrow from a common myeloid/dendritic cell progenitor and continuously migrate into blood and spleen as mature cells (12). When monocytes enter distant organs, they differentiate into macrophages upon inflammatory insult. Swirski et al. identified that there are also bona fide undifferentiated monocytes (Ly-6C^{high}) that reside in the spleen and that are larger in number than their blood monocyte equivalents (13). These reservoir monocytes assemble in clusters in the cords of the subcapsular RP and are different from macrophages and dendritic cells (13). Splenic Ly-6C^{high} monocytes can migrate from the subcapsular RP to distant sites under inflammation conditions such as ischemic stroke, even though there is no change in the bone marrow monocytes (13). This shows that the splenic monocytes increase motility, exit the spleen in bulk, and participate in rapid wound healing (13). Splenic monocytes are deployed through a variety of receptors on monocyte surfaces such as angiotensin type I (AT-1) and angiotensin type II (AT-2) receptors (13).

Not only is the spleen highly vascularized, but it is also extensively innervated. This allows for a crucial communication pathway between the CNS and the spleen to mediate systemic inflammatory responses. Specifically, the CNS aids the spleen in modulating inflammatory responses through both branches of the autonomic nervous system, *via* the sympathetic nervous system (SNS) and parasympathetic nervous system (PNS) pathways (14, 15). The spleen is innervated by efferent sympathetic and splenic fibers that originate in the celiac-superior mesenteric plexus ganglion. Most nerve fibers that innervate the spleen are catecholaminergic, hence under the control of the SNS. Indeed, tyrosine hydroxylase (TH)-positive sympathetic fibers are often observed within proximity to lymphocytes in the WP and macrophages in the RP, as demonstrated by immunostaining (14, 15). Furthermore, it is presumed that direct synaptic contact exists between sympathetic axons and B cells in the WP (15, 16). Activation of the SNS suppresses the activity of innate immune cells while promoting the activity of adaptive immune cells (17). Through the sympathetic fibers, the primary sympathetic neurotransmitters epinephrine and norepinephrine primarily bind to the beta-2 adrenergic receptors (β_2AR) on immune, vasculature, and connective tissue cells. This activates splenic cytokines such as Tumor necrosis factor α (TNFα), and Human mobility group B1 (HMGB1), which increases pro-inflammation in the body. In fact, not only does the SNS communicate with the spleen, but the cytokines released by the spleen also communicate with the SNS in a negative feedback loop (18, 19). Neurotransmitters released by the neuronal network affect the immune cell activity by either inhibiting or inducing inflammation (18, 20, 21). The classic opposing branch of the autonomic nervous system that regulates communication from the CNS to the spleen is through the PNS, specifically through its primary neurotransmitter acetylcholine

(ACh) and the vagus nerve. This is known as the cholinergic anti-inflammatory pathway (22). Neuronal tracing studies have demonstrated the absence of direct cholinergic innervation by vagus nerve fibers in the spleen (17). However, the cholinergic pathway mediates cytokine production through a two-step neuronal process in which information is transmitted from the preganglionic neurons originating in the vagus nerve and projected through the postganglionic neurons in the splenic nerve (17). Moreover, ACh derived from the vagus nerve inhibits the release of proinflammatory cytokines in the spleen and thereby decreases systemic inflammation (17). The actions of ACh are heavily dependent on the nicotinic acetylcholine α7 subunit receptor (23). Therefore, not only do sympathetic nerve fibers control spleen immune cell function but these effects can also be attributed to the cholinergic anti-inflammatory pathway *via* the vagus nerve.

As a result, many cross-communicative networks exist between the SNS and PNS pathways to maintain an immunologic balance in the body. One network is cytokine receptor regulation of immunity, specifically, the cytokines released through SNS neurotransmitter, norepinephrine, can influence the function of neurons in the PNS pathway *via* cognate receptors on the neuronal cell surfaces (6). These cytokines such as interleukin-1β (IL-1β), interact with their associated receptors as well as the N-methyl-d-aspartate (NMDA-R) receptor (24). These receptors in turn activate the PNS pathway and secrete ACh to inhibit these cytokines and subsequent hyperinflammation by way of the vagus nerve. Furthermore, T cells are also able to modulate the SNS pathway by reducing sympathetic fibers in the spleen and affecting the pituitary-adrenal axis in the CNS through diminished hypothalamic norepinephrine concentrations, thereby decreasing cytokine release (21).

A second network is the catecholaminergic regulation of immunity. Sensory neuron activation by the soleus muscle causes activation of catecholaminergic signaling to dorsal blood vessels of the fifth lumbar cord (25). This is mechanistically related to increased expression of cytokines such as CCL20 which leads to increased accumulation of pathogenic T cells and inflammation (25). After inflammation, the release of norepinephrine from catecholaminergic nerve endings in the SNS modulates the activity of invariant natural killer T cells (iNKT) (25). This modulation involves suppression of T_H1-type release of cytokines such as interferon-γ and enhancement of T_H2-type cytokine release, including IL-10, leading to immunosuppression, as done by the PNS (25).

A third network is Pavlovian conditioning and reward system regulation of immunity which functions through catecholaminergic signaling. Specifically, Goebel et al. found that after repeated pairing of a flavored drink (conditioned stimulus) and cyclosporin A (unconditioned stimulus), the drink alone mimicked the effects of cyclosporin A and resulted in suppression of immune function, by way of the PNS, including impaired T_H1 cytokine production and reduced T cell proliferation (26). Furthermore, by stimulating dopamine receptors in a brain reward region (ventral tegmental area), there was an enhanced peripheral immune response as indicated by increased phagocytic activity of dendritic cells and macrophages, and activation of monocytes (27).

A fourth cross-communicative network is through the axon reflex-like regulation of immunity. An axon-reflex is a type of reflex in which receptor activation of peripheral axonal branches of sensory neurons triggers signals transmitted to the bodies of the neurons and diverted to other peripheral axonal endings with the generation of a response (28). Specifically, in an axon reflex-like way, sensory neurons specialized in pain perception (nociceptors) modulate the local immune response to inflammation caused by specific pathogens such as *Staphylococcus aureus*. The pathogen activates nociceptors by releasing N-formyl peptides and pore forming toxin α-hemolysin, inducing action potentials (25). In turn, these neurons release neuroimmunomodulatory peptides, including calcitonin gene-related peptide, galanin, and somatostatin at the site of infection, which inhibit innate immune activation *via* interaction with neutrophils, monocytes, and macrophages like the PNS (29).

Therefore, it seems evident that the CNS-spleen axis plays a crucial role in regulating systemic immune responses (**Figure 1**). It has been postulated that patients with inflammatory diseases have a dysfunctional autonomic nervous system, leading to the overproduction of proinflammatory cytokines, such as TNFα and IL-1β. Targeting this axis has proven to be beneficial in patients with ongoing inflammatory conditions, such as Crohn's disease, rheumatoid arthritis, and sepsis (19, 30, 31). Given the clinical efficacy in treating patients with chronic inflammatory conditions by modulating the CNS-spleen axis, it is intriguing to consider whether restoring autonomic-immune homeostasis may be effective in treating the septic burn population.

This review is the first to highlight the importance of the CNS-spleen axis in modulating the response to sepsis in the severe burn patient population. We will first discuss the role of the CNS-spleen axis during the ebb and flow stages of recovery. Next, we distinguish the changes that are evident in septic burn patients that survive compared to those that succumb to their injury with regards to the CNS-spleen axis. Finally, we will address and discuss the potential therapeutic techniques that target the CNS-spleen axis, which has demonstrated efficacy in inflammatory diseases but has not yet been explored in the context of sepsis and burns. Overall, this review aims to 1) critically analyze the potential contribution of the CNS-spleen axis in modulating the immune response in the severe burn patient population, and 2) discuss the therapeutic advances made thus far along with areas of improvement in targeting the CNS-spleen axis to treat the septic burn population.

THE ROLE OF THE CNS-SPLEEN AXIS DURING THE POST-BURN HYPOMETABOLIC "EBB" PHASE

After a severe burn injury, patients undergo a biphasic metabolic response to burn injury. The acute response is known as to as the

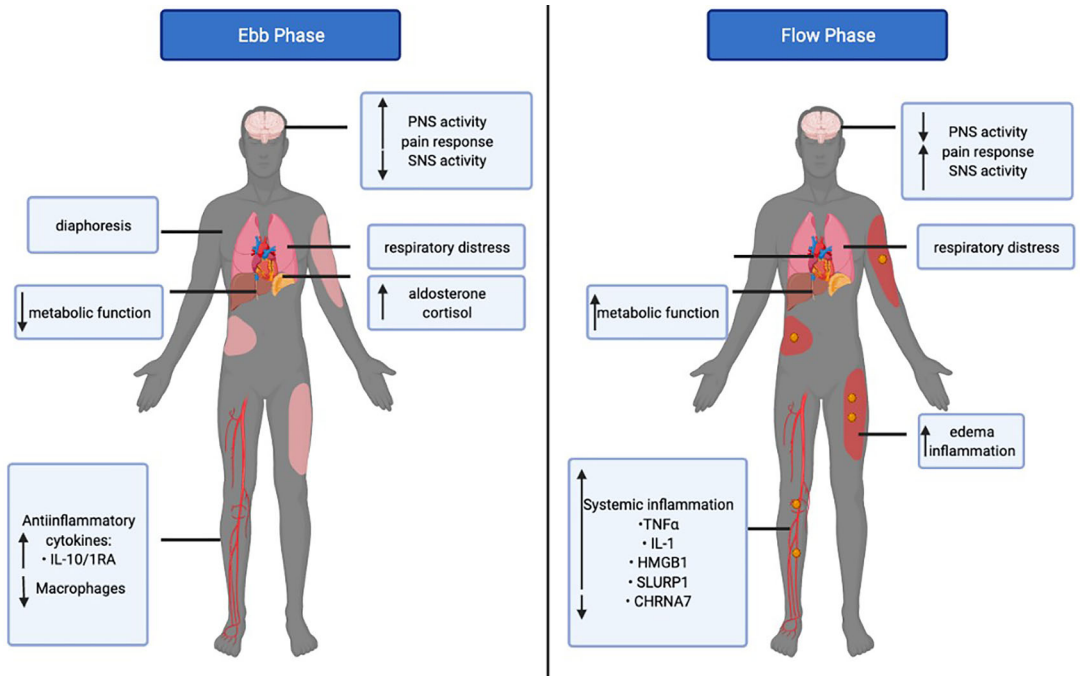

FIGURE 1 | The bi-directional communication between the central nervous system (CNS) and the spleen. The parasympathetic nervous system (PNS) uses acetylcholine and the vagus nerve to decrease burn-induced inflammation *via* the spleen. The sympathetic nervous system (SNS) uses norepinephrine and the hypothalamus, pituitary, and adrenal axis (HPA axis) to increase burn-induced inflammation *via* the spleen. In turn, the CNS is regulated by the cytokines released from the immune cells of the spleen in a negative feedback loop.

ebb (or shock) phase and the chronic response is referred to as the flow phase (**Figure 2**) (32, 33). The ebb phase develops immediately post-burn, lasting approximately 72-96h (34). The ebb phase is characterized as a hypodynamic state whereby respiratory distress occurs and the metabolic rate is depressed to reduce energy depletion (32). The ebb phase is present for a limited duration and is a period that dictates whether a patient will survive or succumb to burn injury-associated complications. Chen et al. previously showed that patients demonstrating abnormally high levels of proinflammatory IL-1β and decreased macrophages at the site of injury are highly susceptible to the development of sepsis (35). Furthermore, septic patients also had increased anti-inflammatory plasma cytokines such as interleukin-10 (IL-10) and interleukin-1RA (IL-1RA) (35). The Septic Predictor Index (SPI), which describes the ratio of IL-1β from stromal vascular fraction-derived macrophages and macrophage proportion (i.e., the proportion of CD14+ IL-1β+ cells/proportion of CD14 high CD16 low cells), was generated for the determination of macrophage and IL-1β production at the site of injury (35). All patients who developed sepsis had SPI values of >0.5, meaning that their sepsis had a later onset (<12 days). The onset of sepsis in patients SPI values of >1 occurred within 12 days post-injury, whereas a delayed onset of sepsis (>12 days)_occurred in patients with SPI values between 0.5–1 (35). During the ebb phase, some inflammatory mediators, such as cortisol, catecholamines, and aldosterone are elevated immediately post-burn (36). Furthermore, serum cytokines such as IL-6, IL-8, granulocyte colony-stimulating factor (G-CSF), and monocyte chemoattractant protein-1(MCP-1) demonstrated up to a 2000-fold increase immediately upon burn trauma (36). Mast cells (MC) are key contributors in blood coagulation as well as innate and acquired immunity (37). Evidence suggests that MCs play an important role in tissue repair and while MCs initially promote healing, they can be detrimental if activated chronically (37). Burn trauma has a direct effect on MCs leading to the secretion of histamine (38). Bankova et al. provided evidence that MC degranulation is an instantaneous response following thermal injury in the ebb phase (39). This leads to an increased xanthine oxidase activity and enhanced production of reactive oxygen species (ROS); the latter being produced after burns through differing mechanisms (39). Nonetheless, sepsis and extreme hyperinflammation do not occur in the ebb phase of burn injury (32). Concerning the CNS-spleen axis, there is decreased SNS activity and increased PNS activity in efforts to decrease inflammation. Under healthy conditions, the SNS and PNS work in opposition to the body to maintain homeostasis. However, during this bi-directional communication between the CNS and the spleen, the SNS and PNS work complementary to one another (40). During the ebb phase of burn injury, sepsis is not evident, however when the ebb phase is overcome by the flow phase, sepsis becomes a grave challenge (3).

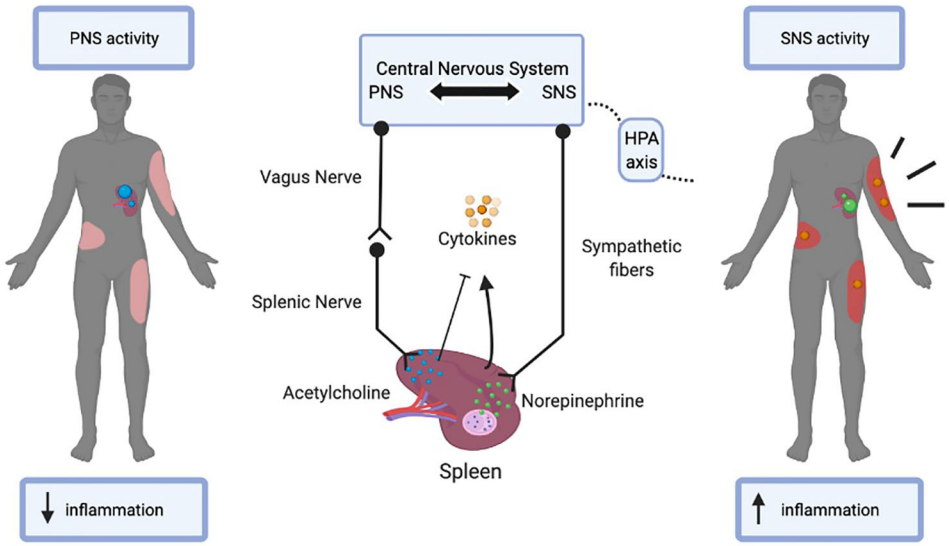

FIGURE 2 | The Ebb and Flow phases of burn injury. The Ebb phase lasts for 24-48 post-burn injury whereas the flow phase may last up to 2 years. The figure illustrates the differential systemic and metabolic response in the ebb versus flow phase in burn patients. Tumor necrosis factor-alpha (TNFα), Interleukin 1 (IL-1), High mobility group box 1 (HMGB1), Secreted Ly-6/uPAR-related protein 1 (SLURP1), Cholinergic Receptor Nicotinic Alpha 7 Subunit (CHRNA7).

THE ROLE OF THE CNS-SPLEEN AXIS DURING THE POST-BURN HYPERMETABOLIC "FLOW" PHASE

The post-burn hypermetabolic "flow" phase occurs after the ebb phase, which leads to an increased metabolic turnover and activation of the immune system and may last up to several years (**Figure 2**). Concerning the CNS-spleen axis, SNS activity is persistently elevated in the flow phase (3). As a result, increased circulating concentrations of cytokines and persistent inflammation may contribute to the development of sepsis (32). Given the increase in SNS activity, this results in a hypermetabolic stress response, which causes severe catabolism, immune dysfunction and profound physiological perturbations that may also contribute to the development of sepsis (3). It is evident that these changes in the body in response to the flow phase of burn injuries are a major cause for concern in patient care and if left untreated, physiologic exhaustion may occur and the injury becomes fatal (3). Sepsis in the general population has many differences from sepsis in the burn population as the primary barrier (skin) is absent, and infection persists as long as the skin is absent (41). Additionally, the systemic dysfunctional state decreases intestinal barrier permeability, increasing the risk of sepsis (42). In severe burn patients, the SNS stimulates pro-inflammatory responses leading to persistently high circulating cytokine concentrations, which cause hyperactive inflammation for which the spleen plays a major role in regulating. The CNS-spleen axis is therefore a major target of clinical research in trying to decipher the ability to control the body's response to immunological issues such as burn-induced inflammation and sepsis. A severe burn injury results in enhanced systemic inflammation, and to effectively manage this, it is important to decipher the role of the CNS in modulating the systemic levels of inflammation and its role in maintaining homeostasis. In the flow phase of burn injuries, the spleen is one of the major sources of mediators that contribute to an exaggerated inflammatory response. Myeloid-derived suppressor cells (MDSCs) are immature myeloid cells with simultaneous proinflammatory and immunosuppressive properties (43). MDSCs are potent producers of TNFα and ROS, which are released from splenic macrophages in response to injury (43). TNFα is a necessary and sufficient mediator of local and systemic inflammation with regards to burns (44–47). TNFα enhances and prolongs an inflammatory response by activating other cells to release pro-inflammatory cytokines such as IL-1 and HMGB1 (48). IL-1 is released by macrophages, lymphocytes, and monocytes during infection, injury and inflammation (49). HMGB1 is secreted into the extracellular space and acts as a proinflammatory cytokine, like IL-1. As such, a persistent elevation in HMGB1 and IL-1 cytokine concentrations are evident in the flow phase of burn patients (49, 50). TNFα also activates other cells to release mediators such as eicosanoids, nitric oxide, and ROS, which further promote inflammation and tissue injury (51). In the flow phase, persistent MDSC expansion exerts harmful effects by propagating persistent inflammation while dampening the adaptive immune response *via* T-cell suppression (43).

The α7 nicotinic acetylcholine receptor (CHRNA7) is important in the signaling performed by the vagus nerve to inhibit proinflammatory cytokines. ACh, released by the vagus nerve and immune cells, acts as a ligand for the CHRNA7 receptor and induces inhibition of proinflammatory cytokines

in the spleen. Holmes et al. found a >70% reduction of protein levels of the CHRNA7 in burn patients despite significantly elevated ACh (52). Additionally, proinflammatory cytokines were persistently active in burn patients as ACh signaling by the vagus nerve was not effective. Furthermore, the gene and protein levels of an endogenous allosteric modulator of CHRNA7, secreted mammalian Ly-6/urokinase-type plasminogen activator receptor-related protein-1 (SLURP1), were significantly elevated in efforts to elevate CHRNA7 numbers although to no avail (52). In the flow phase, although ACh levels were significantly elevated, CHRNA7 protein levels remained low, and inflammation was not impeded. Furthermore, SLURP1 failed to increase CHRNA7 levels, thereby leading to excessive proinflammation.

Additionally, extramedullary hematopoiesis occurs in the flow phase in which hematopoietic stresses mobilize hematopoietic stem cells from the bone marrow to the spleen (53). Splenic tissue weight increased significantly at post-burn day 7 in mice, indicating splenomegaly, presumably to support extramedullary hematopoiesis (54). Furthermore, MDSC expansion is associated with extramedullary hematopoiesis, suggesting that erythropoiesis in the spleen and liver are components of emergency myelopoiesis (43).

It is important to note that much of the criteria for sepsis in the general population is already present in the burn patient population, however, without septic infection (41). Therefore, treatment for sepsis within the burn patient population is difficult given the lack of specific and effective diagnostic criteria. Moreover, classic antibiotic cocktails used for sepsis in the general population are ineffective in burn patients. Therefore, prior to discussing therapeutic options between the general septic and the septic burn populations, it is important to distinguish the physiological changes that are evident in septic burn patients that survive compared to those that succumb to their injury with regards to the CNS-spleen axis.

SURVIVAL *VS.* DEATH IN SEPTIC BURN PATIENTS

The post-recovery phases of burn injuries in patients who survive septic burns are not fully independent of post-septic symptoms. Post-sepsis syndrome is a condition that affects sepsis survivors, in which they have a range of physical, psychological, and emotional challenges while recovering. The categories of long-term effects of sepsis include immunometabolic, neurocognitive, psychiatric, and physical derangements (55). These effects lead to enhanced mortality risk and severely impaired quality of life. In burn patients, the SNS is hyper-activated in post-sepsis syndrome, which leads to increased levels of proinflammatory cytokines such as HMGB1 (55). Patients and murine models who have survived burn-induced sepsis and inflammation have systemic changes such as extreme splenocyte dysfunction (56). HMGB1 plays a key role in mediating the immune dysfunction of splenocytes in sepsis survivors (56). Because of excess cytokines such as HMGB1, sepsis survivors have altered adaptive immune cells, such as T cells and B cells, that do not function normally in eradicating further systemic inflammation (56). Specifically, the population of cytotoxic T cells (CD8+ T cells), helper T cells (CD4+ Th cells), regulatory T cells (Treg cells), and B cells declines in a post-septic mouse model of sepsis as compared to sham controls (57).

Since much of the criteria for sepsis in the general population is already present in the burn patient population, it is important to explore the pathophysiological changes evident in the general post-septic populations (41). In a murine model of sepsis-induced by experimental cecal ligation and puncture (CLP), mice developed splenomegaly (58). This was due to a higher-than-normal activity of the spleen in secreting inflammatory cytokines such as TNFα and HMGB1. This occurred due to the sympathetic fibers innervating the spleen in the CNS-spleen axis and the SNS signaling to the spleen *via* norepinephrine to secrete more cytokines. Serum HMGB1 levels in septic mice were found to be significantly elevated for 4-6 weeks, and administration of an anti-HMGB1 monoclonal antibody significantly attenuated splenomegaly as well as splenocyte priming since the effects of cytokines produced *via* the SNS were inhibited (58). It is possible that in survivors of sepsis, HMGB1 may be a mediator of the initial over-reactivity of the immune response, but later leading to late immunosuppression in sepsis survivors. Therefore, HMGB1 is hyperactivated in post-septic survivors due to the overactive SNS and lack of effective control by the PNS. These data could be implicated towards the septic burn population however further research is needed to identify whether targeting HMGB1 would effectively mitigate splenomegaly in this population.

Jeremias et al. have identified the key role of ACh in the inflammatory response 15 days following CLP-induced sepsis in a murine model. The authors developed a murine model of dysfunctional ACh transporters (ACh KO) to determine the post-septic effects on the PNS response of the CNS-spleen axis. ACh KO mice with CLP-induced sepsis demonstrated a decreased CD8+ cytotoxic T cells and CD4+ Th and an increase in Th17 cells compared to the control (57). Th17 cells are pro-inflammatory cells that secrete inflammatory cytokines such as interleukin-17A, IL-21, and IL-22 (59). Since the ACh transporter was not present, vagus nerve activity was not being carried out properly by the PNS and as such, proinflammatory cytokine levels were high due to lack of inhibition of the SNS. This led to increased inflammation in post septic mouse survivors compared to the sham controls because of the downregulated PNS.

Burn survivors and post-septic deceased patients have multiple similarities in the bodily changes that have occurred because of septic burns. However, post-septic deceased patients have some distinguishing characteristics. Patients who die as a result of burn-induced systemic sepsis have a marked loss of noradrenergic nerves, which occurs due to the apoptosis of splenic cells (50). Nerve loss in patients may be attributed to reduced availability of neurotrophic factors that support sympathetic neurites or enhanced production of chemicals and inflammatory cytokines, which injure nerves (50). For example,

TH, which is the rate-limiting enzyme in the synthesis of norepinephrine, is also lacking in patients who die from general sepsis (50). Since norepinephrine synthesis is decreased, the SNS pathway communication is hindered, and inflammation is low in deceased septic patients. WP is also greatly reduced in patients who die as a result of septic burns (60). Moreover, germinal centers, the area responsible for initially mounting an immune response, are also greatly reduced or completely lacking in post-septic burn patients (61). These factors indicate a strong correlation of CNS-spleen axis response in modulating the inflammatory response in sepsis alone or burn sepsis patients that improves survival. Although a dearth of literature is present for general post-septic survivors and deceased models/patients, further research is required to disseminate the alterations relative to burn-induced sepsis. Moreover, it is imperative to address the potential therapeutic techniques that target the CNS-spleen axis, which has demonstrated efficacy in inflammatory diseases, such as general sepsis, but have not yet been explored in the context of burn-induced sepsis.

THERAPEUTIC TECHNIQUES FOR NEUROIMMUNOMODULATION IN BURN-INDUCED SEPSIS

The CNS-spleen axis may be of great importance in combating burn-induced sepsis as it regulates systemic inflammation. Various novel therapies that target the CNS-spleen axis exist for the treatment of the general sepsis population. These therapies may be effective in the septic burn population too. Here, we will discuss the potential use of vagus nerve stimulation (VNS), agonists and antagonists of major molecules in the CNS-spleen axis, approaches targeting proinflammatory cytokines and approaches targeting catecholamines to mitigate burn-induced sepsis (**Table 1**).

Vagus Nerve Stimulation

VNS is the most extensively studied and successful neuroimmunomodulation technique in treating burn patients (71, 74–76). As discussed previously, the vagus nerve plays a key role in suppressing inflammation as it inhibits pro-inflammatory cytokine release through ACh. Vagus nerve stimulation leads to the release of Ach in organs of the reticuloendothelial system, including the liver, heart, spleen, and gastrointestinal tract. ACh interacts with α-bungarotoxin-sensitive nicotinic CHRNA7 receptors on tissue macrophages, which inhibit the release of TNFα, IL-1, HMGB1 and other proinflammatory cytokines (77). Researchers have identified several VNS techniques, which support the use of VNS in the clinical setting for sepsis patients (60). Experimental studies have shown that invasive VNS, involving a direct electrical stimulation, significantly reduces pro-inflammatory cytokines (62). Furthermore, systemic inflammation can be attenuated by using a non-invasive method of VNS that is based on carotid sinus massage used for the treatment of rhythmic disturbances (78). This method of VNS involves massaging the vagus nerve pressure point along the neck for 5-7 seconds (79). VNS has been shown in a dose-dependent manner to reduce systemic TNFα levels during lethal endotoxemia (78). Another method of VNS is transcutaneous VNS, which acts on the afferent auricular branch of the vagus nerve through electrodes placed on the skin of the left ear (80). The electrical signal, starting in the auricular branch of the vagus nerve, reaches the nucleus tractus solitarius, which is a crucial structure that projects to a variety of brain areas (81). One such area is the locus coeruleus, which is a primary source of norepinephrine (81). A study by Huston et al. determined the effects of transcutaneous VNS on serum HMGB1 levels and survival in murine sepsis (63). Following 3 weeks of transcutaneous VNS treatment, the survival rate improved by 30% in comparison to controls. VNS also attenuated serum HMGB1 levels by 50% as compared to the control mice (63). Transcutaneous VNS carried out through electrodes inhibits

TABLE 1 | Techniques for the treatment of Burn induced Sepsis and inflammation.

Categories of Major Treatment Strategy	Type of Treatment Strategy	Description	Study Conducted in
Vagus Nerve Stimulation	Vagus Nerve stimulation	Similar to carotid sinus massage in which a pressure point on the neck is pressed for 5-7 seconds	Mice (62)
	Transcutaneous vagus nerve stimulation	Electrically stimulates the vagus nerve	Mice (63)
	CNI-1493	Vagus nerve stimulator	Mice (64)
	Amiodarone and MSH	Vagus nerve stimulator	Mice (65)
Agonists and antagonists of major mediators in the CNS-spleen axis	CNI-1493	Inhibitor of macrophage activation and TNF release	Mice (64)
	Amiodarone and MSH	Inhibitor of TNF synthesis, and suppresses edema	Mice (65)
	GTS-21	A small molecule agonist for CHRNA7 and reduces sepsis	Mice (66)
	CHRNA7 agonists	Reduces sepsis	Mice (67)
	α-chemokine receptor inhibitors	Decreases inflammation by inhibiting cytokines	Mice (68, 69)
	Stearoyl lysophosphatidylcholine	• Stimulates neutrophils to eliminate invading pathogens • Suppresses HMGB1 release from macrophages	Mice (70)
Approaches targeting proinflammatory responses	Antibodies against proinflammatory cytokines	• Anti-TNF decreased inflammation • Anti-HMGB1(ethyl pyruvate) decreased inflammation	Mice (41, 52, 71, 72)
Catecholamines	Epinephrine, Norepinephrine, and dopamine	• Along with cortisol decrease inflammation	Mice (73)

norepinephrine and subsequently reduces pro-inflammatory cytokine production through the CNS-spleen axis (63). The therapeutic potential of transcutaneous VNS has not yet been assessed in burn septic models. However, its potential efficacy in this population makes transcutaneous VNS an intriguing avenue to explore.

There are several limitations to consider with the use of VNS treatments in septic burn patients, including the absence of healthy skin. Additionally, the hypermetabolic response persists far past wound closure, indicating that further treatment is necessary following the wound healing process. However, since VNS stimulation can attenuate HMGB1 levels and therefore reduce inflammation in septic patients, it may succeed in the burn sepsis population.

Approaches Using Agonists and Antagonists of Major Mediators in the CNS-Spleen Axis

Agonists and antagonists are molecules that can target major mediators in the CNS-spleen axis. The goal in utilizing these pharmacologics is to alter the CNS-spleen axis activity to decrease pro-inflammatory cytokine production

Some of these molecules, namely, CNI-1493, Amiodarone and MSH, target cytokine production by interacting with the vagus nerve. CNI-1493, a tetravalent guanylhydrazone, is an antagonist towards macrophage activation and TNFα release in local and systemic inflammation models (64). Similarly, Amiodarone and α-melanocyte-stimulating hormone (MSH) are antagonists of TNFα synthesis *in vitro* and suppress the development of swelling and edema by decreased exposure to TNFα (65). CNI-1493 and Amiodarone both function as pharmacological stimulators of the vagus nerve (60, 65). Therefore, these treatments may be effective in the burn sepsis population.

Some molecules, rather than directly targeting the vagus nerve, focus on relieving inflammation through the cholinergic pathway, specifically through CHRNA7 receptors. GTS-21 is a small molecule partial agonist for CHRNA7, which has been used to study cholinergic anti-inflammatory mechanisms in mice (66). Treatment with GTS-21 in a mouse model of burn injury completely abolished mortality at 7-days post-burn in comparison to their untreated burn-injured counterparts, which demonstrated a 25% survival rate (66). GTS-21, along with other small molecules such as CNI-1493, which initiate signals in proximal components of the pathway in the CNS-spleen axis, were found to be beneficial in mediating the effects of sepsis and inflammation. However, clinical efficacy remains to be determined.

The CHRNA7 gene was originally found to be effective in controlling inflammation by modulating CHRNA7 expression on cytokine-producing cells during infection and tissue damage (67). CHRNA7 protein levels were found to be low in burn patients during hyperinflammatory states (52). Moreover, Holmes et al. assessed the impact of activating CHRNA7 on keratinocytes and found it to be a successful alternative to block inflammatory cytokine induction and HMGB1 release (52). In general, it has been shown that α-chemokine receptor antagonists increase survival in sepsis patients in a clinically relevant time frame (68). On the other hand, CHRNA7 agonists attenuate systemic inflammation and improve survival in experimental sepsis in murine models. One limitation of these treatments is that they also act as sedatives (69). However, given that these treatments work through the CNS-spleen axis, specifically through the PNS to decrease inflammation, activators of CHRNA7 may be promising for the burn sepsis population.

Apart from acting on the vagus nerve or cholinergic pathway, some molecules work directly on the innate immune cells. In particular, neutrophils are the most plentiful in the blood and are the first line of defense of the immune system (82). Stearoyl lysophosphatidylcholine (LPC), a class of chemical compounds that are derived from phosphatidylcholine, have recently been shown to be protective against lethal sepsis by stimulating neutrophils to eliminate invading pathogens by reducing reactive oxygen species (70). Stearoyl LPCs significantly attenuates circulating HMGB1 in sepsis by suppressing HMGB1 release from macrophages/monocytes (70). As such, neutrophils may be an indirect way to combat burn-induced sepsis.

Approaches Targeting Proinflammatory Cytokines

Previously, anti-TNFα antibodies have been shown to reduce septic inflammation, however, TNFα antibodies have not been found to be successful in the late stages of sepsis given that antibodies are not effective if therapy is started after serum clearance of TNFα (45, 72, 83). However, researchers have found that the usage of antibodies targeting HMGB1, which is produced in the late stages of sepsis, is much more promising (44, 84, 85). Moreover, HMGB1 levels can also be controlled through ethyl pyruvate, a simple aliphatic ester of pyruvic acid, which has been shown to protect against lethal septic shock even if treatment begins after a TNFα response has been elicited (72). By administering ethyl pyruvate (24h after the onset of sepsis) mouse models were rescued from lethality despite suffering from the physiological effects of sepsis, leading to severe morbidity yet reduced mortality (72). Overall, antibodies against HMGB1 and administration of ethyl pyruvate have shown promising results in the sepsis population and could potentially be translated to the septic burn population.

Approaches Targeting Catecholamines and Adrenergic Receptors

Catecholamines (epinephrine and norepinephrine) and dopamine act as vital hormones that are produced, in part, by the adrenal medulla and secreted into the circulation in response to stress or injury. Catecholamines influence and modulate sympathetic neural modulation of immune responsiveness (86). Specifically, epinephrine and other stress hormones such as cortisol have been found to inhibit cytokine synthesis and therefore, inhibit a pro-inflammatory response through the SNS pathway (86). Myeloid cells express α- and β-ARs while

lymphocytes primarily express β-ARs (87). Catecholamine receptor signaling in macrophages has significant effects on the inflammatory response. Specifically, β-AR inhibition using β–blockers led to increased TNFα secretion following lipopolysaccharide (LPS) induced inflammation in murine models (88). Compared to the pro-inflammatory effect of the β-AR blockade, α-AR inhibition of murine macrophages using α-blockers led to decreased TNFα and IL-1β expression compared with LPS alone (87, 89). Together, these observations suggest that the differential roles of catecholamines on macrophages may depend on the targeted adrenergic receptor. Therefore, in septic burns, catecholamines and their associated receptors may be used to inhibit cytokine release and inhibit inflammatory responses.

CONCLUSION

Sepsis is a major concern, not only in the general patient population but aggressively so in burn patients. The CNS-spleen axis pathway may be a crucial aspect to consider when developing treatments for burn patients as this bidirectional pathway communication leads to hyperinflammation in the body in response to burns and sepsis. Specifically, the SNS has been shown to increase pro-inflammatory cytokines in patients using epinephrine/norepinephrine, and the PNS has been shown to decrease inflammation in the body using ACh and the vagus nerve. Since targeting this axis has demonstrated clinical efficacy in patients with many ongoing inflammatory conditions (19, 30, 31), it is very intriguing to consider whether restoring autonomic-immune homeostasis may be effective in treating the septic burn population. Because sepsis onset occurs during the flow phase, it is a major target in burn patients. Methods such as VNS have shown promising results as they attenuate pro-inflammatory cytokines leading to decreased inflammation and increased survivability. However, further research is necessary to determine the effectiveness of using combination therapies in septic burn patients. Furthermore, it is also possible to activate neural anti-inflammatory mechanisms using small molecules that initiate signals in proximal components of the pathway in the CNS, such as CNI-1493. Important findings, such as with the use of GTS-21, has only been studied in murine burn sepsis models and should be translated to human patients to determine clinical efficacy (73). Furthermore, an important, but difficult implication in attempting to reduce systemic inflammation is deciphering whether beneficial inflammation is also being suppressed. Controlled inflammation by the CNS-spleen axis is a normal response to recruit immune cells to the site of infection or trauma to restore homeostasis and promote healing. Therefore, in burn injuries, inflammation should not be suppressed to the point in which wound healing is impaired. Although further research is required to find the balance between suppressing the beneficial versus harmful inflammation, research over the past few decades has made great advancements in developing methods to decrease burn-induced inflammation. Overall, the purpose of this review was to highlight the importance of the bidirectional communication of the CNS-spleen axis given the regulatory role in immunogenic responses, which can be targeted to reduce sepsis and inflammation. Failure of the body in regulating these immunogenic responses needs the intervention of external stimuli to help the body restore homeostasis and prevent lethality.

DATA AVAILABILITY STATEMENT

The original contributions presented in the study are included in the article/supplementary material. Further inquiries can be directed to the corresponding author.

AUTHOR CONTRIBUTIONS

NK has done primary research and wrote major portions of the manuscript. SK and CK both wrote portions of the manuscript and proofread the manuscript. MJ conceptualized the idea, guided the research, and proofread the manuscript. All authors contributed to the article and approved the submitted version.

FUNDING

The research work of this review article is supported by the national institute of health (NIH R01GM133961) grant.

REFERENCES

1. Forjuoh SN. Burns in Low- and Middle-Income Countries: A Review of Available Literature on Descriptive Epidemiology, Risk Factors, Treatment, and Prevention. *Burns* (2006) 32(5):529–37. doi: 10.1016/j.burns.2006.04.002
2. Schaefer TJ, Nunez Lopez O. *Burn Resuscitation And Management*. Treasure Island (FL: StatPearls (2021).
3. Williams FN, Herndon DN, Jeschke MG. The Hypermetabolic Response to Burn Injury and Interventions to Modify This Response. *Clin Plast Surg* (2009) 36(4):583–96. doi: 10.1016/j.cps.2009.05.001
4. Burns. Available at: https://www.who.int/news-room/fact-sheets/detail/burns.
5. Tarantino G, Savastano S, Capone D, Colao A. Spleen: A New Role for an Old Player? *World J Gastroenterol* (2011) 17(33):3776–84. doi: 10.3748/wjg.v17.i33.3776
6. Lori A, Perrotta M, Lembo G, Carnevale D. The Spleen: A Hub Connecting Nervous and Immune Systems in Cardiovascular and Metabolic Diseases. *Int J Mol Sci* (2017) 18(6). doi: 10.3390/ijms18061216
7. Vida G, Pena G, Deitch EA, Ulloa L. Alpha7-Cholinergic Receptor Mediates Vagal Induction of Splenic Norepinephrine. *J Immunol* (2011) 186(7):4340–6. doi: 10.4049/jimmunol.1003722
8. Hey YY, Quah B, O'Neill HC. Antigen Presenting Capacity of Murine Splenic Myeloid Cells. *BMC Immunol* (2017) 18(1):4. doi: 10.1186/s12865-016-0186-4
9. Nolte MA, Hoen EN, van Stijn A, Kraal G, Mebius RE. Isolation of the Intact White Pulp. Quantitative and Qualitative Analysis of the Cellular Composition of the Splenic Compartments. *Eur J Immunol* (2000) 30(2):626–34. doi: 10.1002/1521-4141(200002)30:2<626::AID-IMMU626>3.0.CO;2-H

10. Herisson F, Frodermann V, Courties G, Rohde D, Sun Y, Vandoorne K, et al. Direct Vascular Channels Connect Skull Bone Marrow and the Brain Surface Enabling Myeloid Cell Migration. *Nat Neurosci* (2018) 21(9):1209–17. doi: 10.1038/s41593-018-0213-2
11. Adrover JM, Del Fresno C, Crainiciuc G, Cuartero MI, Casanova-Acebes M, Weiss LA, et al. A Neutrophil Timer Coordinates Immune Defense and Vascular Protection. *Immunity* (2019) 50(2):390–402.e10. doi: 10.1016/j.immuni.2019.01.002
12. Geissmann F, Auffray C, Palframan R, Wirrig C, Ciocca A, Campisi L, et al. Blood Monocytes: Distinct Subsets, How They Relate to Dendritic Cells, and Their Possible Roles in the Regulation of T-Cell Responses. *Immunol Cell Biol* (2008) 86(5):398–408. doi: 10.1038/icb.2008.19
13. Swirski FK, Nahrendorf M, Etzrodt M, Wildgruber M, Cortez-Retamozo V, Panizzi P, et al. Identification of Splenic Reservoir Monocytes and Their Deployment to Inflammatory Sites. *Science* (2009) 325(5940):612–6. doi: 10.1126/science.1175202
14. Felten DL, Ackerman KD, Wiegand SJ, Felten SY. Noradrenergic Sympathetic Innervation of the Spleen: I. Nerve Fibers Associate With Lymphocytes and Macrophages in Specific Compartments of the Splenic White Pulp. *J Neurosci Res* (1987) 18(1):28–36, 118-21. doi: 10.1002/jnr.490180107
15. Noble BT, Brennan FH, Popovich PG. The Spleen as a Neuroimmune Interface After Spinal Cord Injury. *J Neuroimmunol* (2018) 321:1–11. doi: 10.1016/j.jneuroim.2018.05.007
16. Taylor RB, Weaver LC. Spinal Stimulation to Locate Preganglionic Neurons Controlling the Kidney, Spleen, or Intestine. *Am J Physiol* (1992) 263(4 Pt 2): H1026–33. doi: 10.1152/ajpheart.1992.263.4.H1026
17. Rosas-Ballina M, Tracey KJ. Cholinergic Control of Inflammation. *J Intern Med* (2009) 265(6):663–79. doi: 10.1111/j.1365-2796.2009.02098.x
18. Carnevale D, Perrotta M, Pallante F, Fardella V, Iacobucci R, Fardella S, et al. A Cholinergic-Sympathetic Pathway Primes Immunity in Hypertension and Mediates Brain-to-Spleen Communication. *Nat Commun* (2016) 7:13035. doi: 10.1038/ncomms13035
19. Straub RH, Antoniou E, Zeuner M, Gross V, Scholmerich J, Andus T. Association of Autonomic Nervous Hyperreflexia and Systemic Inflammation in Patients With Crohn's Disease and Ulcerative Colitis. *J Neuroimmunol* (1997) 80(1-2):149–57. doi: 10.1016/S0165-5728(97)00150-1
20. Viviani B, Bartesaghi S, Gardoni F, Vezzani A, Behrens MM, Bartfai T, et al. Interleukin-1beta Enhances NMDA Receptor-Mediated Intracellular Calcium Increase Through Activation of the Src Family of Kinases. *J Neurosci* (2003) 23 (25):8692–700. doi: 10.1523/JNEUROSCI.23-25-08692.2003
21. Jouda J, Wildmann J, Schafer M, Roggero E, Besedovsky HO, del Rey A. T Cells Affect Central and Peripheral Noradrenergic Mechanisms and Neurotrophin Concentration in the Spleen and Hypothalamus. *Ann N Y Acad Sci* (2012) 1261:18–25. doi: 10.1111/j.1749-6632.2012.06642.x
22. Straub RH. Complexity of the Bi-Directional Neuroimmune Junction in the Spleen. *Trends Pharmacol Sci* (2004) 25(12):640–6. doi: 10.1016/j.tips.2004.10.007
23. Wang H, Yu M, Ochani M, Amella CA, Tanovic M, Susarla S, et al. Nicotinic Acetylcholine Receptor Alpha7 Subunit is an Essential Regulator of Inflammation. *Nature* (2003) 421(6921):384–8. doi: 10.1038/nature01339
24. Suhs KW, Gudi V, Eckermann N, Fairless R, Pul R, Skripuletz T, et al. Cytokine Regulation by Modulation of the NMDA Receptor on Astrocytes. *Neurosci Lett* (2016) 629:227–33. doi: 10.1016/j.neulet.2016.07.016
25. Pavlov VA, Tracey KJ. Neural Regulation of Immunity: Molecular Mechanisms and Clinical Translation. *Nat Neurosci* (2017) 20(2):156–66. doi: 10.1038/nn.4477
26. Goebel MU, Trebst AE, Steiner J, Xie YF, Exton MS, Frede S, et al. Behavioral Conditioning of Immunosuppression is Possible in Humans. *FASEB J* (2002) 16(14):1869–73. doi: 10.1096/fj.02-0389com
27. Ben-Shaanan TL, Azulay-Debby H, Dubovik T, Starosvetsky E, Korin B, Schiller M, et al. Activation of the Reward System Boosts Innate and Adaptive Immunity. *Nat Med* (2016) 22(8):940–4. doi: 10.1038/nm.4133
28. Yaprak M. The Axon Reflex. *Neuroanatomy* (2008) 7:17–9.
29. Chiu IM, Heesters BA, Ghasemlou N, Von Hehn CA, Zhao F, Tran J, et al. Bacteria Activate Sensory Neurons That Modulate Pain and Inflammation. *Nature* (2013) 501(7465):52–7. doi: 10.1038/nature12479
30. Syngle V, Syngle A, Garg N, Krishan P, Verma I. Predictors of Autonomic Neuropathy in Rheumatoid Arthritis. *Auton Neurosci* (2016) 201:54–9. doi: 10.1016/j.autneu.2016.07.008
31. Munford RS, Tracey KJ. Is Severe Sepsis a Neuroendocrine Disease? *Mol Med* (2002) 8(8):437–42. doi: 10.1007/BF03402023
32. Simsek T, Simsek HU, Canturk NZ. Response to Trauma and Metabolic Changes: Posttraumatic Metabolism. *Ulus Cerrahi Derg* (2014) 30(3):153–9. doi: 10.5152/UCD.2014.2653
33. Stahel PF, Flierl MA, Moore EE. "Metabolic Staging" After Major Trauma - a Guide for Clinical Decision Making? *Scand J Trauma Resusc Emerg Med* (2010) 18:34. doi: 10.1186/1757-7241-18-34
34. Jeschke MG, van Baar ME, Choudhry MA, Chung KK, Gibran NS, Logsetty S. Burn Injury. *Nat Rev Dis Primers* (2020) 6(1):11. doi: 10.1038/s41572-020-0145-5
35. Chen P, Stanojcic M, Jeschke MG. Septic Predictor Index: A Novel Platform to Identify Thermally Injured Patients Susceptible to Sepsis. *Surgery* (2018) 163 (2):409–14. doi: 10.1016/j.surg.2017.08.010
36. Jeschke MG, Gauglitz GG, Kulp GA, Finnerty CC, Williams FN, Kraft R, et al. Long-Term Persistance of the Pathophysiologic Response to Severe Burn Injury. *PloS One* (2011) 6(7):e21245. doi: 10.1371/journal.pone.0021245
37. Douaiher J, Succar J, Lancerotto L, Gurish MF, Orgill DP, Hamilton MJ, et al. Development of Mast Cells and Importance of Their Tryptase and Chymase Serine Proteases in Inflammation and Wound Healing. *Adv Immunol* (2014) 122:211–52. doi: 10.1016/B978-0-12-800267-4.00006-7
38. Santos FX, Arroyo C, Garcia I, Blasco R, Obispo JM, Hamann C, et al. Role of Mast Cells in the Pathogenesis of Postburn Inflammatory Response: Reactive Oxygen Species as Mast Cell Stimulators. *Burns* (2000) 26(2):145–7. doi: 10.1016/S0305-4179(99)00021-2
39. Bankova LG, Lezcano C, Pejler G, Stevens RL, Murphy GF, Austen KF, et al. Mouse Mast Cell Proteases 4 and 5 Mediate Epidermal Injury Through Disruption of Tight Junctions. *J Immunol* (2014) 192(6):2812–20. doi: 10.4049/jimmunol.1301794
40. Jung WC, Levesque JP, Ruitenberg MJ. It Takes Nerve to Fight Back: The Significance of Neural Innervation of the Bone Marrow and Spleen for Immune Function. *Semin Cell Dev Biol* (2017) 61:60–70. doi: 10.1016/j.semcdb.2016.08.010
41. Greenhalgh DG. Sepsis in the Burn Patient: A Different Problem Than Sepsis in the General Population. *Burns Trauma* (2017) 5:23. doi: 10.1186/s41038-017-0089-5
42. Kumar M, Leon Coria A, Cornick S, Petri B, Mayengbam S, Jijon HB, et al. Increased Intestinal Permeability Exacerbates Sepsis Through Reduced Hepatic SCD-1 Activity and Dysregulated Iron Recycling. *Nat Commun* (2020) 11(1):483. doi: 10.1038/s41467-019-14182-2
43. Loftus TJ, Mohr AM, Moldawer LL. Dysregulated Myelopoiesis and Hematopoietic Function Following Acute Physiologic Insult. *Curr Opin Hematol* (2018) 25(1):37–43. doi: 10.1097/MOH.0000000000000395
44. Tracey KJ, Fong Y, Hesse DG, Manogue KR, Lee AT, Kuo GC, et al. Anti-Cachectin/TNF Monoclonal Antibodies Prevent Septic Shock During Lethal Bacteraemia. *Nature* (1987) 330(6149):662–4. doi: 10.1038/330662a0
45. Tracey KJ, Beutler B, Lowry SF, Merryweather J, Wolpe S, Milsark IW, et al. Shock and Tissue Injury Induced by Recombinant Human Cachectin. *Science* (1986) 234(4775):470–4. doi: 10.1126/science.3764421
46. Liu J, Marino MW, Wong G, Grail D, Dunn A, Bettadapura J, et al. TNF is a Potent Anti-Inflammatory Cytokine in Autoimmune-Mediated Demyelination. *Nat Med* (1998) 4(1):78–83. doi: 10.1038/nm0198-078
47. Wang H, Bloom O, Zhang M, Vishnubhakat JM, Ombrellino M, Che J, et al. HMG-1 as a Late Mediator of Endotoxin Lethality in Mice. *Science* (1999) 285 (5425):248–51. doi: 10.1126/science.285.5425.248
48. Sunden-Cullberg J, Norrby-Teglund A, Rouhiainen A, Rauvala H, Herman G, Tracey KJ, et al. Persistent Elevation of High Mobility Group Box-1 Protein (HMGB1) in Patients With Severe Sepsis and Septic Shock. *Crit Care Med* (2005) 33(3):564–73. doi: 10.1097/01.CCM.0000155991.88802.4D
49. Wang H, Vishnubhakat JM, Bloom O, Zhang M, Ombrellino M, Sama A, et al. Proinflammatory Cytokines (Tumor Necrosis Factor and Interleukin 1) Stimulate Release of High Mobility Group Protein-1 by Pituicytes. *Surgery* (1999) 126(2):389–92. doi: 10.1016/S0039-6060(99)70182-0

50. Hoover DB, Brown TC, Miller MK, Schweitzer JB, Williams DL. Loss of Sympathetic Nerves in Spleens From Patients With End Stage Sepsis. *Front Immunol* (2017) 8:1712. doi: 10.3389/fimmu.2017.01712
51. Abdulkhaleq LA, Assi MA, Abdullah R, Zamri-Saad M, Taufiq-Yap YH, Hezmee MNM. The Crucial Roles of Inflammatory Mediators in Inflammation: A Review. *Vet World* (2018) 11(5):627–35. doi: 10.14202/vetworld.2018.627-635
52. Holmes CJ, Plichta JK, Gamelli RL, Radek KA. Burn Injury Alters Epidermal Cholinergic Mediators and Increases HMGB1 and Caspase 3 in Autologous Donor Skin and Burn Margin. *Shock* (2017) 47(2):175–83. doi: 10.1097/SHK.0000000000000752
53. Inra CN, Zhou BO, Acar M, Murphy MM, Richardson J, Zhao Z, et al. A Perisinusoidal Niche for Extramedullary Haematopoiesis in the Spleen. *Nature* (2015) 527(7579):466–71. doi: 10.1038/nature15530
54. Hasan S, Johnson MC, Kini AR, Baldea AJ, Muthumalaiappan K. A Shift in Myeloid Cell Phenotype *via* Down Regulation of Siglec-1 in Island Macrophages of Bone Marrow Is Associated With Decreased Late Erythroblasts Seen in Anemia of Critical Illness. *Front Med (Lausanne)* (2019) 6:260. doi: 10.3389/fmed.2019.00260
55. Mostel Z, Perl A, Marck M, Mehdi SF, Lowell B, Bathija S, et al. Post-Sepsis Syndrome - an Evolving Entity That Afflicts Survivors of Sepsis. *Mol Med* (2019) 26(1):6. doi: 10.1186/s10020-019-0132-z
56. Valdes-Ferrer SI, Rosas-Ballina M, Olofsson PS, Lu B, Dancho ME, Li J, et al. High-Mobility Group Box 1 Mediates Persistent Splenocyte Priming in Sepsis Survivors: Evidence From a Murine Model. *Shock* (2013) 40(6):492–5. doi: 10.1097/SHK.0000000000000050
57. Jeremias IC, Victorino VJ, Barbeiro HV, Kubo SA, Prado CM, Lima TM, et al. The Role of Acetylcholine in the Inflammatory Response in Animals Surviving Sepsis Induced by Cecal Ligation and Puncture. *Mol Neurobiol* (2016) 53(10):6635–43. doi: 10.1007/s12035-015-9538-y
58. Valdes-Ferrer SI, Rosas-Ballina M, Olofsson PS, Lu B, Dancho ME, Ochani M, et al. HMGB1 Mediates Splenomegaly and Expansion of Splenic CD11b+ Ly-6C(High) Inflammatory Monocytes in Murine Sepsis Survivors. *J Intern Med* (2013) 274(4):381–90. doi: 10.1111/joim.12104
59. Tesmer LA, Lundy SK, Sarkar S, Fox DA. Th17 Cells in Human Disease. *Immunol Rev* (2008) 223:87–113. doi: 10.1111/j.1600-065X.2008.00628.x
60. Song XM, Li JG, Wang YL, Liang H, Huang Y, Yuan X, et al. Effect of Vagus Nerve Stimulation on Thermal Injury in Rats. *Burns* (2010) 36(1):75–81. doi: 10.1016/j.burns.2009.02.002
61. Good RA, Finstad J, Gewurz H, Cooper MD, Pollara B. The Development of Immunological Capacity in Phylogenetic Perspective. *Am J Dis Child* (1967) 114(5):477–97. doi: 10.1001/archpedi.1967.02090260065004
62. Howland RH. Vagus Nerve Stimulation. *Curr Behav Neurosci Rep* (2014) 1 (2):64–73. doi: 10.1007/s40473-014-0010-5
63. Huston JM, Gallowitsch-Puerta M, Ochani M, Ochani K, Yuan R, Rosas-Ballina M, et al. Transcutaneous Vagus Nerve Stimulation Reduces Serum High Mobility Group Box 1 Levels and Improves Survival in Murine Sepsis. *Crit Care Med* (2007) 35(12):2762–8. doi: 10.1097/01.CCM.0000288102.15975.BA
64. Bianchi M, Bloom O, Raabe T, Cohen PS, Chesney J, Sherry B, et al. Suppression of Proinflammatory Cytokines in Monocytes by a Tetravalent Guanylhydrazone. *J Exp Med* (1996) 183(3):927–36. doi: 10.1084/jem.183.3.927
65. Dias Da Silva VJ, Gnecchi-Ruscone T, Lavelli B, Bellina V, Manzella D, Porta A, et al. Opposite Effects of Iv Amiodarone on Cardiovascular Vagal and Sympathetic Efferent Activities in Rats. *Am J Physiol Regul Integr Comp Physiol* (2002) 283(2):R543–8. doi: 10.1152/ajpregu.00608.2001
66. Garg BK, Loring RH. GTS-21 has Cell-Specific Anti-Inflammatory Effects Independent of Alpha7 Nicotinic Acetylcholine Receptors. *PloS One* (2019) 14 (4):e0214942. doi: 10.1371/journal.pone.0214942
67. Hoover DB. Cholinergic Modulation of the Immune System Presents New Approaches for Treating Inflammation. *Pharmacol Ther* (2017) 179:1–16. doi: 10.1016/j.pharmthera.2017.05.002
68. Lin X, Yang H, Sakuragi T, Hu M, Mantell LL, Hayashi S, et al. Alpha-Chemokine Receptor Blockade Reduces High Mobility Group Box 1 Protein-Induced Lung Inflammation and Injury and Improves Survival in Sepsis. *Am J Physiol Lung Cell Mol Physiol* (2005) 289(4):L583–90. doi: 10.1152/ajplung.00091.2005
69. Ulloa L, Deitch EA. Neuroimmune Perspectives in Sepsis. *Crit Care* (2009) 13 (2):133. doi: 10.1186/cc7758
70. Huston JM, Ochani M, Rosas-Ballina M, Liao H, Ochani K, Pavlov VA, et al. Splenectomy Inactivates the Cholinergic Antiinflammatory Pathway During Lethal Endotoxemia and Polymicrobial Sepsis. *J Exp Med* (2006) 203(7):1623–8. doi: 10.1084/jem.20052362
71. Niederbichler AD, Papst S, Claassen L, Jokuszies A, Steinstraesser L, Hirsch T, et al. Burn-Induced Organ Dysfunction: Vagus Nerve Stimulation Attenuates Organ and Serum Cytokine Levels. *Burns* (2009) 35(6):783–9. doi: 10.1016/j.burns.2008.08.023
72. Ulloa L, Ochani M, Yang H, Tanovic M, Halperin D, Yang R, et al. Ethyl Pyruvate Prevents Lethality in Mice With Established Lethal Sepsis and Systemic Inflammation. *Proc Natl Acad Sci USA* (2002) 99(19):12351–6. doi: 10.1073/pnas.192222999
73. Seok J, Warren HS, Cuenca AG, Mindrinos MN, Baker HV, Xu W, et al. Host Response to Injury, Genomic Responses in Mouse Models Poorly Mimic Human Inflammatory Diseases. *Proc Natl Acad Sci USA* (2013) 110(9):3507–12. doi: 10.1073/pnas.1222878110
74. de Jonge WJ, Ulloa L. The Alpha7 Nicotinic Acetylcholine Receptor as a Pharmacological Target for Inflammation. *Br J Pharmacol* (2007) 151(7):915–29. doi: 10.1038/sj.bjp.0707264
75. Huston JM. The Vagus Nerve and the Inflammatory Reflex: Wandering on a New Treatment Paradigm for Systemic Inflammation and Sepsis. *Surg Infect (Larchmt)* (2012) 13(4):187–93. doi: 10.1089/sur.2012.126
76. Niederbichler AD, Papst S, Claassen L, Jokuszies A, Ipaktchi K, Reimers K, et al. Burn-Induced Organ Dysfunction: Vagus Nerve Stimulation Improves Cardiac Function. *Eplasty* (2010) 10:e45.
77. Bencherif M, Lippiello PM, Lucas R, Marrero MB. Alpha7 Nicotinic Receptors as Novel Therapeutic Targets for Inflammation-Based Diseases. *Cell Mol Life Sci* (2011) 68(6):931–49. doi: 10.1007/s00018-010-0525-1
78. Borovikova LV, Ivanova S, Zhang M, Yang H, Botchkina GI, Watkins LR, et al. Vagus Nerve Stimulation Attenuates the Systemic Inflammatory Response to Endotoxin. *Nature* (2000) 405(6785):458–62. doi: 10.1038/35013070
79. Schweitzer P, Teichholz LE. Carotid Sinus Massage. Its Diagnostic and Therapeutic Value in Arrhythmias. *Am J Med* (1985) 78(4):645–54. doi: 10.1016/0002-9343(85)90408-5
80. Borges U, Laborde S, Raab M. Influence of Transcutaneous Vagus Nerve Stimulation on Cardiac Vagal Activity: Not Different From Sham Stimulation and No Effect of Stimulation Intensity. *PloS One* (2019) 14(10):e0223848. doi: 10.1371/journal.pone.0223848
81. Foote SL, Bloom FE, Aston-Jones G. Nucleus Locus Ceruleus: New Evidence of Anatomical and Physiological Specificity. *Physiol Rev* (1983) 63(3):844–914. doi: 10.1152/physrev.1983.63.3.844
82. Segal AW. How Neutrophils Kill Microbes. *Annu Rev Immunol* (2005) 23:197–223. doi: 10.1146/annurev.immunol.23.021704.115653
83. O'Riordain MG, O'Riordain DS, Molloy RG, Mannick JA, Rodrick ML. Dosage and Timing of Anti-TNF-Alpha Antibody Treatment Determine Its Effect of Resistance to Sepsis After Injury. *J Surg Res* (1996) 64(1):95–101. doi: 10.1006/jsre.1996.0312
84. Huang LF, Yao YM, Dong N, Yu Y, He LX, Sheng ZY. Association of High Mobility Group Box-1 Protein Levels With Sepsis and Outcome of Severely Burned Patients. *Cytokine* (2011) 53(1):29–34. doi: 10.1016/j.cyto.2010.09.010
85. Wang H, Yang H, Czura CJ, Sama AE, Tracey KJ. HMGB1 as a Late Mediator of Lethal Systemic Inflammation. *Am J Respir Crit Care Med* (2001) 164(10 Pt 1):1768–73. doi: 10.1164/ajrccm.164.10.2106117
86. Madden KS, Sanders VM, Felten DL. Catecholamine Influences and Sympathetic Neural Modulation of Immune Responsiveness. *Annu Rev Pharmacol Toxicol* (1995) 35:417–48. doi: 10.1146/annurev.pa.35.040195.002221
87. Barnes MA, Carson MJ, Nair MG. Non-Traditional Cytokines: How Catecholamines and Adipokines Influence Macrophages in Immunity, Metabolism and the Central Nervous System. *Cytokine* (2015) 72(2):210–9. doi: 10.1016/j.cyto.2015.01.008
88. Guirao X, Kumar A, Katz J, Smith M, Lin E, Keogh C, et al. Catecholamines Increase Monocyte TNF Receptors and Inhibit TNF Through Beta 2-Adrenoreceptor Activation. *Am J Physiol* (1997) 273(6):E1203–8. doi: 10.1152/ajpendo.1997.273.6.E1203

89. Scanzano A, Cosentino M. Adrenergic Regulation of Innate Immunity: A Review. *Front Pharmacol* (2015) 6:171. doi: 10.3389/fphar.2015.00171

Conflict of Interest: The authors declare that the research was conducted in the absence of any commercial or financial relationships that could be construed as a potential conflict of interest.

Publisher's Note: All claims expressed in this article are solely those of the authors and do not necessarily represent those of their affiliated organizations, or those of the publisher, the editors and the reviewers. Any product that may be evaluated in this article, or claim that may be made by its manufacturer, is not guaranteed or endorsed by the publisher.

Copyright © 2021 Khan, Kaur, Knuth and Jeschke. This is an open-access article distributed under the terms of the Creative Commons Attribution License (CC BY). The use, distribution or reproduction in other forums is permitted, provided the original author(s) and the copyright owner(s) are credited and that the original publication in this journal is cited, in accordance with accepted academic practice. No use, distribution or reproduction is permitted which does not comply with these terms.

frontiers in Immunology

REVIEW
published: 03 September 2021
doi: 10.3389/fimmu.2021.715894

Critical Role of Synovial Tissue–Resident Macrophage and Fibroblast Subsets in the Persistence of Joint Inflammation

Samuel Kemble and Adam P. Croft *

Rheumatology Research Group, Institute of Inflammation and Ageing (IIA), University of Birmingham, Queen Elizabeth Hospital, Birmingham, United Kingdom

OPEN ACCESS

Edited by:
Sylvain Perruche, Institut National de la Santé et de la Recherche Médicale (INSERM), France

Reviewed by:
Eric Toussirot, INSERM CIC1431 Centre d'Investigation Clinique Besançon, France
Erik Lubberts, Erasmus University Rotterdam, Netherlands

***Correspondence:**
Adam P. Croft
a.p.croft@bham.ac.uk

Specialty section:
This article was submitted to Inflammation, a section of the journal Frontiers in Immunology

Received: *27 May 2021*
Accepted: *17 August 2021*
Published: *03 September 2021*

Citation:
Kemble S and Croft AP (2021) Critical Role of Synovial Tissue–Resident Macrophage and Fibroblast Subsets in the Persistence of Joint Inflammation. Front. Immunol. 12:715894. doi: 10.3389/fimmu.2021.715894

Rheumatoid arthritis (RA) is a chronic prototypic immune-mediated inflammatory disease which is characterized by persistent synovial inflammation, leading to progressive joint destruction. Whilst the introduction of targeted biological drugs has led to a step change in the management of RA, 30-40% of patients do not respond adequately to these treatments, regardless of the mechanism of action of the drug used (ceiling of therapeutic response). In addition, many patients who acheive clinical remission, quickly relapse following the withdrawal of treatment. These observations suggest the existence of additional pathways of disease persistence that remain to be identified and targeted therapeutically. A major barrier for the identification of therapeutic targets and successful clinical translation is the limited understanding of the cellular mechanisms that operate within the synovial microenvironment to sustain joint inflammation. Recent insights into the heterogeneity of tissue resident synovial cells, including macropahges and fibroblasts has revealed distinct subsets of these cells that differentially regulate specific aspects of inflammatory joint pathology, paving the way for targeted interventions to specifically modulate the behaviour of these cells. In this review, we will discuss the phenotypic and functional heterogeneity of tissue resident synovial cells and how this cellular diversity contributes to joint inflammation. We discuss how critical interactions between tissue resident cell types regulate the disease state by establishing critical cellular checkpoints within the synovium designed to suppress inflammation and restore joint homeostasis. We propose that failure of these cellular checkpoints leads to the emergence of imprinted pathogenic fibroblast cell states that drive the persistence of joint inflammation. Finally, we discuss therapeutic strategies that could be employed to specifically target pathogenic subsets of fibroblasts in RA.

Keywords: single cell transcriptomics, macrophage, fibroblasts, tissue resident cells, rheumatoid arthritis

INTRODUCTION

Rheumatoid arthritis (RA) is a chronic immune-mediated inflammatory disease (IMID) affecting approximately 1% of the UK population (1). Unlike osteoarthritis (OA) (a predominately non-inflammatory joint disease characterized by destruction of articular cartilage), RA is associated with systemic immune dysfunction resulting in persistent inflammation that localizes to synovial joints (2). If untreated, RA leads to irreversible joint damage and functional disability (3).

The introduction of biological, disease-modifying anti-rheumatic drugs (bDMARDs) has led to significant improvements in the treatment of RA. Current therapies target either specific immune cells, their secretory products or specific signaling pathways using small molecule inhibitors (4–9). The etiology and pathophysiology of RA is highly heterogeneous and despite advances in treatment, there is a ceiling of therapeutic response observed in which 30-40% of patients do not respond to currently available treatments regardless of the mechanism of action of the drug used (10). In addition, those individuals that achieve clinical remission often relapse once treatment is tapered or withdrawn (11, 12).

As more biological and targeted synthetic DMARDs are introduced into clinical practice, we are observing the emergence of a population of patients that have failed to respond to multiple drugs. This disease state is termed treatment refractory or difficult to treat RA (13, 14) and has recently been defined by a EULAR taskforce as the failure to respond to two bDMARDs of different mechanisms of action (15). However, the molecular and cellular basis of treatment refractory RA is yet to be determined and research strategies to address this area of unmet clinical need are urgently required (16). A key determinant of refractory RA is unidentified drivers of disease that modulate of the local synovial microenvironment (17–19). The failure to neutralize these pathways leads to disease persistence and inflammatory flare following treatment withdrawal. The next generation of therapeutics in RA will need to identify and target these cellular drivers of disease persistence, if we are to develop effective therapies for those individuals with treatment refractory RA (20).

Tissue resident cells such as synovial fibroblasts and macrophages form the underlying basis of the joint microenvironment and have been shown to contibue to tissue homeostasis, but also regulate the timing and duration of local inflammatory responses (21–26). Recent evidence suggests that such tissue resident cells are associated with significant phenotypic heterogeneity. These phenotypes are reflected at the transcriptional and functional level within distinct anatomical compartments of the synovial membrane determined by site-specific signaling cues (27–29). Whilst significant research has focused on the role of infiltrating leukocytes in the pathogenesis of RA, little prominence has been given to the cells which reside within the joint microenvironment.

Response to therapy is thought to depend on the "synovial signature" or tissue heterogeneity. In early RA, three major synovial pathotypes have been described with distinct underlying transcriptional signatures, including: lympho-myeloid (predominantly B cells with myeloid presence), diffuse-myeloid (predominantly myeloid without T and B cells) and pauci immune (30). Compared to other synovial pathotypes, treatment naïve lympho-myeloid patients have greater levels of disease activity, synovitis, immune cell infiltration and T and B cell activity and were more likely to require biological therapy at 12 month follow up (30, 31). Interestingly, anti-TNFα therapy was less effective in patients with a pauci-immune pathotype – a signature characterized by a prevalence of stromal cells (fibroblasts) (30). Thus, understanding the synovial pathology has the potential to stratify treatment interventions in the future (31, 32).

In this review, we will discuss the phenotypic and functional heterogeneity of tissue resident synovial cells in the context of joint homeostasis, inflammation and resolution. Furthermore, we will focus on important cross-talk which exist between different synovial tissue cells and finally, we will discuss potential new therapeutic strategies that target tissue resident synovial cells which could potentially restore homeostasis following chronic disease.

ROLE OF TISSUE RESIDENT SYNOVIAL CELLS IN JOINT HOMEOSTASIS

The articular capsule is a bulbous structure that consists of a fibrous mesenchymal tissue termed the synovium which encapsulates all diarthrodial joints. The synovium forms a barrier around the synovial cavity containing synovial fluid (~1-2mL of highly viscous liquid) that is rich in hyaluronic acid and lubricin (encoded by the *HAS1* and *PGR4* gene respectively) (33–35). The function of synovial fluid is to maintain viscosity and elasticity of articular cartilage and to form a layer of lubrication to reduce friction between adjacent cartilage surfaces as well as adjacent surfaces of the synovium and cartilage (34). Within the synovial cavity, type I collagen and cartilage containing collagen type II, coat the articular surface of the bones (36).

The synovium is a connective tissue structure which contains two regions: a continuous, tightly packed lining or intima layer comprised of tissue resident fibroblasts and macrophages (1-3 cell layers thick), and an underlying connective tissue called the sub-lining layer or subintima which includes sparsely distributed tissue resident fibroblasts and macrophages, adipose cells and blood and lymphatic vessels (situated in deep regions) and minimal infiltrating inflammatory cells (35, 37). Under resting conditions, tissue resident fibroblasts and macrophages form a tightly organized immunological barrier isolating the joint cavity (37). As the joint cavity lacks associated blood vessels, leukocytes are believed to migrate from the sub-lining and through the lining layer barrier however, under resting conditions this process is highly regulated with very few immune cells present in the synovial fluid (33, 35).

The joint microenvironment is constantly exposed to minor trauma as a result of locomotion. To compensate, this dynamic tissue must be continuously re-modelled and repaired to

maintain homeostasis. Recent evidence suggests, in RA, fibroblasts are transcriptionally heterogenous and have specialized functions depending on their anatomical location within the synovium (38–42). However, whether these specialized subsets of fibroblasts exist under resting conditions is yet to be fully elucidated. This is due to the challenges of acquiring healthy synovial biopsies, although the human joint cell atlas will soon provide an extensive characterization of the developing and normal musculoskeletal human tissues (43).

Given their location within the synovium, it is highly likely $HAS1^+$ $PRG4^+$ lining layer fibroblasts secrete hyaluronic acid and lubricin into the joint space, providing lubrication and nourishment to facilitate joint locomotion. *In vitro* evidence has also shown synovial fibroblasts exhibit the ability to control ion transport and maintain and re-model the joint architecture by secreting extra cellular matrix (ECM) components such as type II, IV, V and VI collagens, proteoglycans, fibronectin, laminin and tenascin, and proteases such as matrix metalloproteinases (MMPs) and cathepsins (44–47). Such processes permit nutrient exchange between the synovial fluid and the synovial membrane (48).

Tissue resident macrophages are distributed throughout the lining and sparsely in the sub-lining region of the healthy synovium and have been shown to play an essential role in normal tissue physiology (26, 27, 37). Historically, it was hypothesized that synovial macrophages derive from the bone marrow *via* circulating monocytes entering the joint tissue through blood vessels located within the sub-lining layer (49). However, it is now recognized that specialized tissue resident macrophages are seeded into tissues during embryonic development and can undergo self-renewal within the tissue (37).

Synovial tissue macrophages were previously identified by highly expressing CD68 and CD163 (50). From these populations, lining synovial macrophages were discriminated from sub-lining cells by their expression of FcγRIIIa suggesting that macrophages in the lining layer play an important role in cellular clearance (51, 52). However, contradictory findings (53–55) suggest these markers are inadequate to discriminate tissue resident from blood borne macrophages, prompting the discovery of alternative markers through the employment of single cell profiling technologies such as single cell RNA sequencing (scRNAseq).

Until recently, it was proposed the synovial lining layer surrounding the joint cavity consisted of an interwoven network of fibroblasts and macrophages. However, Culemann et al. (2019) (37) using advanced super-high resolution fluorescence microscopy in conjunction with scRNAseq transcriptomic profiling of mouse synovial macrophages, have revealed the lining layer consists of a highly organized population of epithelial-like (expressing tight junction proteins such as JAM1, ZO-1 & CLDN5 and genes associated with planar cell polarity *Fat4* and *Vangl2*) CX_3CR1^+ macrophages which form a physical (mediated by tight junctions) and immunological barrier between the synovial cavity and the synovial membrane. These lining macrophages sit directly adjacent to lining layer fibroblasts and express a gene signature related to an immune-regulatory phenotype expressing *Trem2* and Tam receptor genes such as *Axl* and *Mfge4*. Importantly, deletion of *Cx₃cr1* expressing synovial macrophages caused barrier breakdown and uncontrolled joint inflammation. These studies challenge our previous understanding of the synovial microanatomy and function, instead emphasizing the primacy of the lining macrophage as a master regulator of joint homeostasis, functioning to suppress joint inflammation.

CX_3CR1^+ $TREM2^+$ lining macrophages are long-lived with a lifespan of ~5 weeks. Under normal resting conditions this barrier is maintained through a pool of locally proliferating CX_3CR1^- $MHCII^{High}$ mononuclear cells that are embedded within the interstitial regions of the synovial sub-lining layer. In addition to CX_3CR1^+ $TREM2^+$ macrophages, CX_3CR1^- $MHCII^{High}$ macrophages also give rise to CX_3CR1^- RELMα+ expressing macrophages. These cells however are situated in the sub-lining and express CD206 and CD163. Macrophages expressing such markers have been shown to play an important role in M2 alternative activation supporting immune-regulation (56) and wound healing (57). In RA, this ultimately promotes the phagocytosis of apoptotic cells through *MERTK* expression (58). Collectively, these data suggest that under steady state conditions, immune-regulatory RELMα+ macrophages also support joint homeostasis.

In agreement with Culemann et al. (37), other studies in both mice and humans have shown under resting conditions two long-lived tissue resident macrophage subsets exist which express: in mice, $F4/80^{High}$ $MHCII^-$ and $F4/80^{High}$ $MHCII^+$ (59) and in humans, $MERTK^+$ $TREM2^+$ lining and $MERTK^+$ $LVYE1^+$ sub-lining macrophages (60). It is possible these populations are analogous to CX_3CR1^+ $TREM2^+$ and CX_3CR1^- $RELM\alpha^+$ macrophages, respectively. See diagram in **Figure 1A** for a summary of the role in which tissue resident synovial cells play in joint homeostasis.

In summary, tissue resident synovial cells not only provide the architecture of the joint but also play an important functional role in joint homeostasis. Heterogeneity has been reported within synovial macrophage and fibroblast subsets and this appears to be dependent on anatomical location within the joint microenvironment. Although these subsets of synovial cells differ in their transcriptomic signatures, the functional characteristics of these subsets under resting conditions remains to be fully elucidated.

PERSISTENT JOINT INFLAMMATION IN RA RENDERS NORMAL JOINT HOMEOSTASIS INEFFECTIVE

During established RA, the synovium becomes hyperplasic with an increase in cellularity, resulting in an expansion of the synovial membrane between 10-20 cell layers thick. In the sub-lining, extensive angiogenesis occurs supporting a mass influx of infiltrating immune cells, such as lymphocytes, plasma cells and monocyte-derived macrophages (3, 61). For the purpose of this review, the role in which infiltrating cells play in RA [reviewed in (5, 62)] will not be discussed further. The hyperplasic synovium

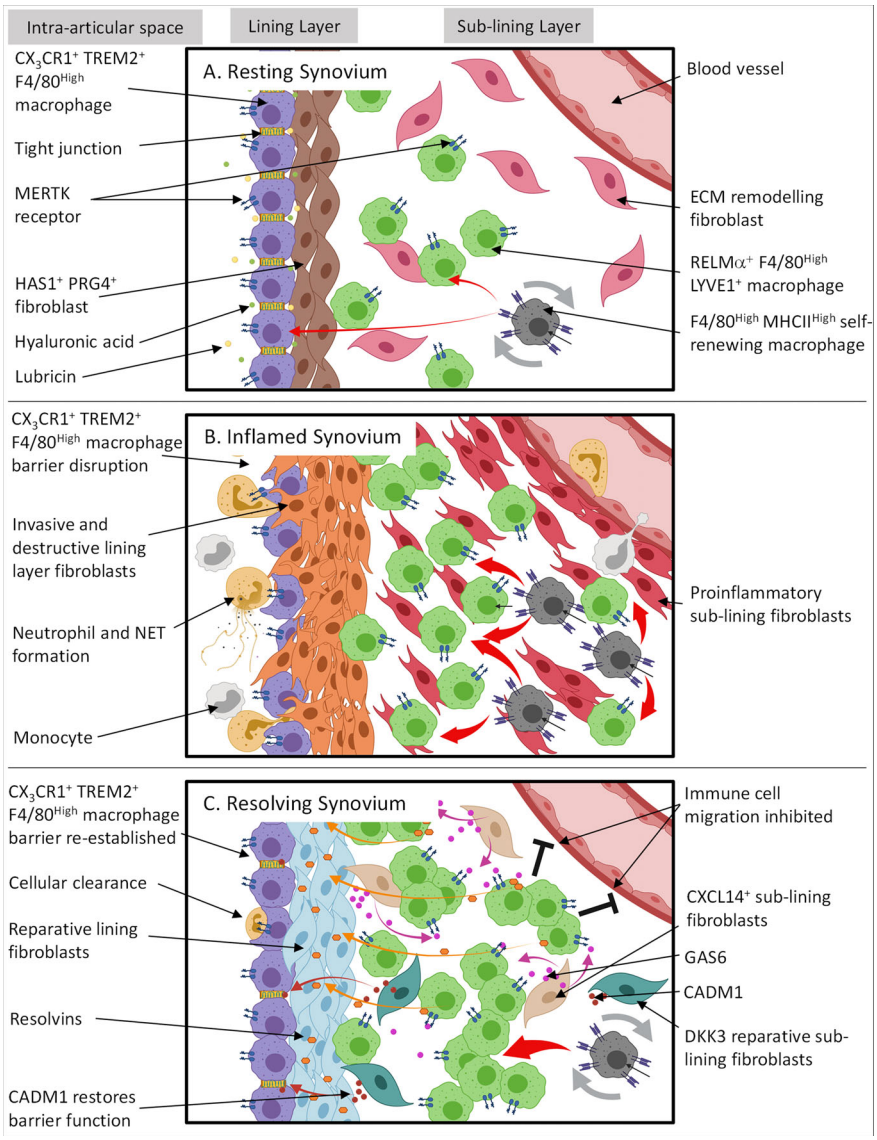

FIGURE 1 | The spatial and temporal coupling between tissue resident synovial cells determines joint homeostasis, inflammation and resolution in RA. **(A)** Resting synovial tissue consists of both tissue resident macrophages and fibroblasts. Tissue macrophages contain an immune-regulatory population expressing MERTK and are repopulated by CX_3CR1^- $F4/80^{High}$ $MHCII^{High}$ interstitial macrophages in the sub-lining. The lining layer is composed of highly organized, tight junction-mediated CX_3CR1^+ $TREM2^+$ $F4/80^{High}$ macrophages, forming an immunological barrier. Lining layer fibroblasts sit directly under CX_3CR1^+ $TREM2^+$ $F4/80^{High}$ barrier and secrete hyaluronic acid and lubricin into the intra-articular space *via* tight junctions to lubricate the joint cavity. The sub-lining is composed of sparsely distributed fibroblasts and $RELM\alpha^+$ $LYVE1^+$ $F4/80^{High}$ macrophages where the former is thought to constantly remodel ECM following mechanical trauma. **(B)** Although during arthritis the $CX3CR1^+$ $TREM2^+$ $F4/80^{High}$ macrophage barrier becomes dysfunctional allowing migrating inflammatory myeloid cells and activated lining fibroblasts to invade the intra-articular space, these lining macrophages support resolution by retaining an immune-regulating phenotype and clearing apoptotic cells from the synovial cavity. $RELM\alpha^+$ $LYVE1^+$ $F4/80^{High}$ macrophages also expand in the sub-lining. However, it is unknown if this is to actively trigger resolution or drive inflammation. **(C)** For arthritis to resolve, cellular infiltration must cease. In conjunction, it is proposed that sub-lining $CXCL14^+$ fibroblasts secrete GAS6 which interacts with MERTK on $RELMa^+$ $LYVE1^+$ $F4/80^{High}$ macrophages causing the release of resolvins. Resolvins then switch lining fibroblasts from a proinflammatory to a reparative state to restore homeostasis. Also situated in the sub-lining are $DKK3^+$ fibroblasts. The exact function of these cells is unknown; however, transcriptional evidence suggests they release proteins such as CADM1 which may promote the repair of CX_3CR1^+ $TREM2^+$ $F4/80^{High}$ macrophage barrier function. This figure is based on human and mouse data. Image created with (BioRender.com).

contains a heterogeneous population of tissue resident fibroblasts and macrophages that play differing roles in regulating and promoting joint inflammation and damage (63–68). While synovial macrophage numbers have been shown to positively correlate with disease severity (69, 70), synovial hyperplasia is predominantly a result of increases in fibroblast cell numbers thought to be due to proliferation (71), increased survival (72) and potentially migration (73).

In chronically inflamed joints the hypertrophied synovium forms pannus tissue (74) that adheres and degrades the articular cartilage (the cartilage-pannus junction) as a result of fibroblast secreted proteases (75). These proteases [such as matrix metalloproteinases (MMPs)] activate chondrocytes which in turn secrete additional proteases forming a positive endogenous feedback loop (76). For pannus formation to occur, the synovium must be re-organized into selectively expanded regions which support immune or non-immune processes (48). This re-modeling of the synovial membrane into distinct microenvironmental niches is thought to be the result of ECM remodeling by tissue fibroblasts. For example, Cadherin-11 (CDH11) is an adhesion molecule expressed by synovial fibroblasts during RA (77) and is critical for synovial hyperplasia (78). The genetic deletion of *Cdh11* impairs pannus formation and attenuates inflammation *in vivo (*78, 79). Thus, formation of hyperplasic synovial tissue is essential for supporting joint inflammation and pathogenic fibroblast behaviour in arthritis.

Fibroblast migration may also be an important contributor to fibroblast expansion in the joint and thus synovial hyperplasia. Mouse synovial fibroblasts exhibit the ability to transmigrate *in vivo* through blood vessels and spread arthritis to unaffected joints, through mesenchymal precursors (80). These fibroblasts were found to be indispensable for inducing onset of arthritis in non-inflamed joints suggesting they may be directly arthrogenic (81). Fibroblasts implanted into a cartilage/sponge matrix in an immune deficient mouse also exhibit the ability to migrate from the engraftment site to a distant cartilage implant (82). Work from our group has shown these migrating fibroblasts express podoplanin (PDPN) and not sub-lining fibroblast markers such as CD248 (38). However, as migration progressed, the synovial tissue architecture developed both lining and sub-lining regions suggesting to some extent fibroblasts are plastic and respond to micro-environmental cues.

Recent evidence in humans, supports the notion fibroblasts might migrate to non-inflamed tissue through pre-inflammatory mesenchymal cells (PRIME cells) (73). PRIME cells are detectable in human blood prior to arthritis flare and are therefore a potential biomarker for predicting relapse in RA. It is hypothesized that PRIME cells are recruited by naïve B cells, a process which is reduced following the onset of joint symptoms. Transcriptomic analysis shows that PRIME cells may represent an analogous gene signature to proinflammatory fibroblasts identified in the sub-lining layer (42). Further work is required to determine whether PRIME cells truly migrate into the joint and if so, the mechanism by which these cells induce local disease flare within the joint itself.

Although pannus formation is hypothesized to be predominantly a fibroblast mediated process, key alterations of the synovial structure are initially driven by a failure of the synovial macrophage barrier. Using 3D light-sheet fluorescence microscopy, Culemann et al. (37), showed immune complex mediated synovial lining barrier dysfunction occurs in response to serum transfer induced arthritis (STIA) (37). Although these CX_3CR1^+ $TREM2^+$ lining macrophages remained in the same position they changed orientation and morphology and permitted proliferating fibroblasts to invade the lining space and neutrophils and monocytes to migrate into the intra-articular space (**Figure 1B**). Although the fraction of CX_3CR1^+ $TREM2^+$ macrophages did not expand in response to different types of experimental arthritis, they did maintain an immune-regulatory phenotype expressing Tam receptors such as Axl and Mfge4, clearing apoptotic cell bodies from the synovial space. In conjunction, sub-lining CX_3CR1^- $RELM\alpha^+$ macrophages expand.

We propose that CX_3CR1^+ $TREM2^+$ lining macrophages can be considered as the first cellular checkpoint in the synovium that attempts to suppress joint inflammation and restore normal joint homeostasis following an inflammatory challenge. The functional purpose of the spatial coupling between lining layer macrophages and lining fibroblasts (which are functionally, spatially and anatomically distinct from sub-lining fibroblasts) is currently unknown, but we hypothesize that the loss of this spatial coupling during inflammation may lead to the emergence of a compensatory repair like phenotype in lining fibroblasts, however this remains to be definitely proven.

Lining CX_3CR1^+ $TREM2^+$ and sub-lining CX_3CR1^- $RELM\alpha$+ macrophages differentiate from tissue resident, self-renewing CX_3CR1^- $MHCII^{High}$ interstitial macrophages (37). Under resting conditions, CX_3CR1^- $RELM\alpha^+$ macrophages express genes associated with alternative activation, suggesting an immunosuppressive phenotype that is protective. However, the expansion of this population of macrophages in arthritis, suggests that either there is a compensatory response in which these macrophages attempt to suppress inflammation and reinstate homeostasis or unknown signals from within the tissue switch their phenotype to a proinflammatory cell state. The latter is controversial as unlike highly plastic monocyte-derived macrophages, it is hypothesized resident macrophages are less plastic (83). However, investigators combining fate mapping, scRNAseq and epigenetic studies and investigating the role of macrophage subsets in the pathogenesis of pulmonary fibrosis have suggested plastic monocyte-derived macrophages can differentiate into tissue resident macrophages, giving rise to inflammation-imprinted, tissue resident macrophages which drive and sustain an inflammatory response (83).

In addition to the above, synovial fibroblasts are known to modulate macrophage gene expression profiles (84) and therefore, could determine macrophage phenotype in RA. In support of this, a recent study showed scRNAseq transcriptomics of CD14+ macrophages in the RA synovium revealed a unique expanded subset of HBEGF+ macrophages and when co-cultured with TNFα-activated synovial fibroblasts these macrophages were transcriptionally modified (85). This change in polarization was shown to be similar to classically activated pro-inflammatory macrophages, however as the HBEGF+ macrophage phenotype was dependent on fibroblast-derived $prostaglandin_2$ (PGE_2) it was considered distinct from classical or alternative polarization and altered the way these macrophages could respond to standard treatments used in RA. These inflammatory macrophages were able to promote fibroblast invasiveness in an epidermal growth factor dependent manner. It is therefore possible that they play a role in determining the success or failure of the immune-regulatory

$TREM2^+$ CX_3CR1^+ macrophage barrier. Also, fibroblast-derived mediators such as PGE_2 may alter the transcriptional profile of CX_3CR1^- $RELM\alpha^+$ sub-lining macrophages favoring a proinflammatory phenotype in response to the inflammatory joint milieu in RA. These concepts have yet to be fully tested.

To answer the above questions, it is important to understand the mechanism in which CX_3CR1^- $MHCII^{High}$ macrophages give rise to anatomically distinct synovial subsets under normal and perturbed states and how interactions with fibroblasts alter these immunophenotypes. Is there a pool of CX_3CR1^- $MHCII^{High}$ macrophages which is primed but readily depleted in response to an inflammatory stimulus? If CX_3CR1^- $RELM\alpha^+$ macrophages are proinflammatory, what might switch these cells from an immunosuppressive to proinflammatory state? These are important questions that remain to be answered.

TISSUE RESIDENT SYNOVIAL CELLS RE-ESTABLISH JOINT HOMEOSTASIS IN RA PATIENTS

The recent identification of distinct tissue resident synovial macrophage (37) and fibroblast (39–42, 86) subsets in various disease states in RA, suggests the function of these cells is dependent on both their anatomical location within the synovium and the tissue disease state. Furthermore, it appears that tissue resident macrophage phenotype may be more stable than the fibroblast state. Thus, dysregulated association between these two tissue resident cell types may not only determine the timing of inflammation but also its duration.

Another possible cellular immune checkpoint may exist between type I tyrosine kinase receptor (members of the TAM family) expressing synovial macrophages and sub-lining fibroblast subsets through the release of endogenously produced GAS6 (60). Macrophage type I tyrosine kinase receptors consist of TYRO3, AXL and MER. The role in which these receptors may play in regulating joint inflammation in arthritis was first demonstrated in *Tam* deficient mice where spontaneous arthritis (amongst other inflammatory manifestations) was reported (87). In agreement with Culemann et al. (2019) (37), an investigation in humans by Alivernini et al. (2020) (60) has shown two general subsets of synovial macrophages (tissue resident $MERTK^+$ and infiltrating $MERTK^-$) with differential enrichment of these populations within the synovium depending on tissue stage where risk of disease flare was determined by the ratio of these two subpopulations in the synovium.

The above authors investigated synovial biopsy tissue from healthy individuals, patients with active RA and those individuals in sustained clinical remission under methotrexate combined with TNF inhibition (60). Monocyte-derived $MERTK^-$ macrophages were expanded during active RA and identified as proinflammatory, expressing either alarmins (S100A12 and IL-1β), bone remodelling proteins (CD48 and SPP1), interferons (HLA and ISG15) or molecules related to antigen presentation (HLA and CLEC10A). In contrast, tissue resident $MERTK^+$ macrophages were enriched in healthy synovial tissue and synovial tissue from those individuals in clinical remission. As others have shown *Mertk-/-* mice exhibit exacerbated arthritis in response to STIA (88), This suggests, a dysregulation in macrophage TAM signaling appears to determine autoimmunity and drive chronic inflammation in RA.

Immune-regulatory $MERTK^+$ macrophages consisted of high expression of either TREM2 or LYVE1 demarking their lining or sub-lining location, respectively (60). Culemann et al. (2019) also reported CX_3CR1+ lining macrophages express TREM2 (37). *Trem2* expression has proven to inhibit inflammation in mouse microglia by suppressing NF-κB signaling (89). In contrast, LYVE1+ macrophages have been shown to engage with hyaluronan on smooth muscle cells and induced MMP-9 dependent degradation of collagen to prevent its deposition and therefore vascular stiffness (90). This suggests, under resting and resolving states, that $MERTK^+$ macrophage subsets may not only regulate inflammation but potentially also fibroblast collagen production and tissue stiffness of the joint.

Endogenous pro-resolving mediators such as resolvins are cardinal biomarkers and active regulators of resolution in RA and are now considered a potentially useful biomarker of DMARD therapy (91). *In vitro* functional assays performed by Alivernini et al. (2020) showed $MERTK^+$ macrophages released resolvin D1 and induced a reparative phenotype in lining fibroblasts (increasing the expression of collagen genes such as *COL1A*) driven by GAS6 secretion from a sub-lining fibroblast subset expressing THY1 and CXCL14 (**Figure 1C**). GAS6 acts as a bridging molecule to promote the binding of MERTK with exposed phosphatidylserine (PS) on apoptotic cells and induces phagocytosis (92, 93). This anti-inflammatory/pro-resolving process ultimately causes suppression of NFκB (94). Furthermore, cleavage of the ectodomain of MERTK by ADAM metallopeptidase domain 17 (ADAM17) has been shown to exacerbate tissue inflammation by limiting the production of specialized pro-resolving mediators (95, 96).

The MERTK/GAS6 axis has been shown to suppress proinflammatory cytokine production (97) and induce IL-10 production by alternatively activating anti-inflammatory macrophages (98). Importantly, GAS6 production by synovial fibroblasts and within synovial fluid is reduced in RA joint and increased in the synovium of patients in sustained remission (60, 99, 100). Together these findings suggest diminished MERTK/GAS6 association is essential for resolution of RA and re-establishing joint homeostasis. In contrast, the loss of the MERTK/GAS6 axis following persistent proinflammatory stimuli might contribute to chronic inflammation.

Intriguingly, the transcriptional cassettes of $MERTK^+$ macrophages from healthy synovial tissue and the synovial tissue of those individuals with RA in sustained clinical remission were reported to differ (60). $MERTK^+$ macrophages in patients in stable remission expressed genes which encode Kruppel-like factor 4 (KLF4) and nuclear receptor subfamily 4 group a member 2 (NR4A2). Historical evidence shows KLF4 is expressed in the differentiating layers of the epidermis and has been shown to play an important role in establishing barrier function (101). Furthermore, both of these transcription factors have been shown to be regulators of macrophage polarization where mice lacking macrophage- or myeloid-specific

KLF4 expression demonstrate increased proinflammatory characteristics and delayed wound healing (102), whereas NR4A2 (a target of macrophage migration inhibitory factor (MIF) signaling) expression has proven to curb inflammation and promote an anti-inflammatory phenotype by reducing IL-6 production (103). More recently, a study demonstrates KLF4 and KLF2 expression in macrophages regulates immune cell apoptosis as well as suppressing toll-like receptor (TLR) responses to nucleic acids to ensure maintenance of homeostasis (104).

In addition to immune-regulatory tissue resident macrophages, sub-lining fibroblasts expressing markers such as dickkopf WNT signaling pathway inhibitor 3 (DKK3), osteoglycin (OGN), cell adhesion molecule 1 (CADM1) & microfibrillar-associated protein 2 (MFAP2) are present in inflamed murine and RA synovium (39, 42). *DKK3* encodes DickKopf3 and overexpression of this protein in keloid fibroblasts has been shown to suppress cell proliferation and promote apoptosis *via* TGF-β1/SMAD signaling (105) as well as impairing tumor growth by promoting IL-7 production (106). Interestingly, *DKK3* expression is upregulated in OA and inhibits cartilage degradation *in vitro (*107). In contrast, OGN supports ectopic bone formation and its expression increases in the RA synovium in response to low-level laser therapy (108). The relationship between the fraction of DKK3+ fibroblasts and RA pathology, duration of disease and tendency of patients to remain in clinical remission is yet to be explored however, it is possible that DKK3+ fibroblasts could play a role in promoting resolution by supporting the re-establishment of joint homeostasis through modulation of joint repair pathways. Furthermore, DKK3+ fibroblasts also express CADM1 and MFAP2 which have been shown to be involved in enhancing intestinal barrier function in rats with inflammatory bowel disease (109) and fibroblast-mediated elastic fiber formation (110), respectively. As there is evidence suggesting DKK3+ embryonic cell lineages remain in joint tissue at maturity (111) it is possible DKK3+ fibroblasts have a suppressive role in healthy joint tissue supporting the synovial macrophage barrier, but this is yet to be investigated. The role tissue resident synovial cells play in resolution of inflammation and restoration of joint homeostasis is summarized in **Figure 1C**.

In summary, these studies demonstrate that both tissue resident macrophages and fibroblasts play an important role in supporting the resolution of joint inflammation in RA. The coupling of these cell types and outcome of their cross-talk appears to be critical in determining whether inflammation persists or resolves. We propose that these tissue resident cells form critical cellular checkpoints within the synovium that attempt to regulate the local inflammatory response. In this way macrophages can act as critical off switches by suppressing the phenotype of pathogenic fibroblasts. As a result, the maintenance of these cellular checkpoints facilitates resolution of joint inflammation and maintains disease remission, whereas their failure leads to the persistence of joint inflammation. The reasons such cellular checkpoints could fail include either quantitative changes to the proportions of the cellular subsets within the tissue that make up these checkpoints or the failure of the inter-cellular communication pathways between the two cell types. It is probable that persistently activated fibroblasts in chronic disease undergo epigenetic modifications which give rise to pathogenic subsets and ultimately render tissue resident stroma-macrophage checkpoints ineffective. As macrophages and fibroblasts appear to play an important role in homeostasis and disease progression, we will need to focus on understanding how these cells communicate in the context of inflammation and resolution. This will unravel the functional networks established by these tissue resident synovial cells at different stages of disease and in response to treatment, allowing us to develop novel therapeutic approaches to treat refractory RA and restore joint homeostasis resulting in sustained clinical remission.

PATHOLOGIC SYNOVIAL FIBROBLASTS AS CELLULAR DRIVERS OF TREATMENT REFRACTORY RA

Fibroblasts provide the architectural and functional landscape for tissue microenvironments (21, 22). In arthritis, synovial fibroblasts amplify inflammation and tissue damage driving multiple aspects of pathology including production of chemokines, cytokines and proteases which affect the recruitment, retention and differentiation of infiltrating leukocytes as well as the erosion of cartilage and bone (19, 46, 63, 112–114).

Historical studies regarding synovial fibroblast heterogeneity in RA have focused mainly on tissue topography, positional identity, surface protein expression of candidate cell markers and identifying the lining and sub-lining layers as distinct anatomical regions (79, 115–117). Recent efforts through the use of scRNAseq transcriptomics have defined the cellular diversity at the transcriptional level and research is ongoing to link this heterogeneity to cellular function and role in disease pathology (39–42). The first study to utilize this strategy was by Stephenson et al. (2018) (41) and showed two transcriptionally distinct human fibroblast subsets in RA which were demarcated by anatomical location – $CD55^+$ lining and $THY1^+$ ($CD90^+$) sub-lining fibroblasts. Bulk RNA sequencing of these two populations with gene-set enrichment analysis, confirmed $CD55^+$ lining fibroblasts highly expressed *HAS1* whereas $THY1^+$ sub-lining fibroblasts expressed genes associated with ECM degradation and remodeling. $THY1^+$ fibroblasts could be further defined by $PDPN^{+/-}$ populations where the former was considered a perivascular marker suggesting $THY1^+$ fibroblasts associate with blood vessels in the sub-lining.

Since Stephenson et al. (41), multiple researchers have attempted to unravel the phenotypic difference between fibroblast subsets in RA using sort purified, enzymatically digested human and mouse synovial tissue samples (39, 40, 42, 86). For example, Mizoguchi et al. (2019) (40) sorted synovial fibroblasts from human RA biopsies using markers which are upregulated in active RA synovium: PDPN, CDH11, CD34 and THY1 (38, 79, 116, 118). Using microarray analysis with bulk sequencing and principle component analysis, three unique

PDPN+ fibroblast gene signatures were identified: 1) *CD34*$^-$ *THY1*$^-$ lining layer fibroblasts expressing *MMP1*, *MMP3*, *PRG4* and *HAS1*; 2) *CD34*$^+$ *THY1*$^+$ perivascular fibroblasts associated with sub-lining vasculature and 3) *CD34*$^+$ *THY1*$^-$ distributed in superficial lining layer and throughout deep sub-lining. *CDH11* expression was observed in most fibroblasts with the greatest expression in the lining subset matching previous findings that *CDH11* expression promotes invasive and destructive behavior (79). Interestingly, of these populations, the *CD34*$^+$ *THY1*$^+$ perivascular subset was expanded in RA and not OA and correlated with leukocyte infiltration and histological scores of synovitis and hypertrophy, whereas *CD34*$^-$ *THY1*$^-$ lining were expanded in OA and not RA, suggesting synovial fibroblast subset expansion is dependent on disease type and context.

Expansion of pathological fibroblast subsets in the sub-lining of RA synovial tissue has also been demonstrated by others (39, 40, 42, 86). Zhang et al. (2019) integrated scRNAseq transcriptomics and mass cytometry of RA synovial biopsies and based on *CD45*$^-$ *CD31*$^-$ *PDPN*$^+$ expression identified three *THY1*$^+$ sub-lining fibroblasts subsets: *CD34*$^+$, *HLA-DR*^{High} and a unique subset expressing *DKK3*$^+$ (42). Of the sub-lining subsets the *HLA-DR*^{High} and *CD34*$^+$ populations were expanded in leukocyte-rich RA synovial tissue where the former was as high as a 15-fold increase. In agreement with Mizoguchi et al. (2019) (40) lining layer fibroblast in this study were also determined by *CD34*$^-$ *THY1*$^-$ *PRG4*$^+$ as well as *CD55*$^+$.

Findings from our group show in the synovium of acute and chronic experimental arthritis models in mice and human RA synovial biopsy tissue, fibroblasts significantly increase expression of FAPα (fibroblast activation protein alpha), a cell membrane dipeptidyl peptide which was absent under resting conditions (39, 117). This led to the hypothesis that FAPα is a marker of pathogenic fibroblasts subsets in inflammatory disease. Deletion of FAPα expressing fibroblasts in mice not only suppressed inflammation but also reduced tissue damage thus confirming its pathogenic role in arthritis. FAPα fibroblasts could be broadly separated into THY1$^-$ and THY1$^+$ clusters reflective of their anatomical location in the joint synovium: THY1$^-$ lining and THY1$^+$ sub-lining layer fibroblasts. Furthermore, scRNAseq demonstrated THY1$^-$ fibroblasts contained a lining layer gene signature expressing *Cd55*, *Prg4* and Clic5, whereas a THY1$^+$ sub-lining signature expressed other markers such as *Cd34* and *Clec3b*. When comparing our mouse THY1+ scRNAseq data with human subsets identified by Zhang et al. (2019) (42), we found three transcriptionally analogous fibroblasts subsets: 1) *CD34*$^+$ *C3*$^+$ *MFAP5*$^+$ associated with blood vessels in the sub-lining perivascular space, expressing genes related to immuno-inflammatory processes and stromal memory and 2) *COL1A1*$^+$ *COL8A1*$^+$ *MDK*$^+$ expressing genes involved in bone, cartilage and ECM re-modelling. In addition, a single THY1$^-$ lining subset was identified across species containing a transcriptional profile of *CLIC5*$^+$, *TSPAN15*$^+$ and *PRG4*$^+$. Importantly, re-analysis of Zhang et al. (2019) (42) data confirmed pathogenic *HLA-DR*^{High} fibroblasts were also positive for FAPα.

From the above studies it is clear FAPα$^+$ THY1$^+$ sub-lining fibroblasts contain distinct fibroblast subsets with non-overlapping effector functions. For example, *THY1*$^+$ *CD34*$^+$ fibroblasts reported in all studies were shown to cluster in the perivascular region of the sub-lining tissue and from gene-set enrichment analysis and *in vitro* assays were shown to express inflammatory mediators such as IL-6, CXCL12 and CCL2 with the potential to facilitate immune cell infiltration. These subsets also express complement C3 and are responsible for stromal memory and tissue priming (39, 40, 42). Therefore, these populations can be generally grouped into *THY1*$^+$ *CD34*$^+$ *C3*$^+$ perivascular proinflammatory fibroblasts and importantly their expansion in RA has been shown to correlate with histopathological observations including synovial hypertrophy and inflammation (40). Recent work has shown that following repeated inflammatory stimuli, *CD34*$^+$ *C3*$^+$ synovial fibroblasts become metabolically rewired and express high amounts of complement proteins to support local, inflammation driven tissue priming (113). This robust tissue response could define the switch from resolving to chronic joint inflammation observed in RA. In contrast, *CD34*$^-$ fibroblasts can be separated into two populations: *HLA-DR*^{High} comprised of a similar proinflammatory phenotype as above as well as expressing genes associated with antigen presentation and IFNγ signaling (42), and *RANKL*^{High} expressing fibroblasts which also express low osteoprotegerin (OPG) and exhibit the ability to drive osteoclast differentiation *in vitro* (40). An enhanced migratory and invasive behavior has been reported in this subset following exposure to platelet derived growth factor BB (PDGFBB) in a trans-well matrix invasion assay (40), therefore these cells may play an important role in cartilage and bone destruction. In addition to sub-lining fibroblasts, work from our group and others has shown that lining FAPα$^+$ THY1$^-$ fibroblasts also express genes that associate with osteoclast formation and activity (CCL9, RANKL) as well as cartilage degradation (MMP3, MMP9 and MMP13) consistent with a role in mediating bone and cartilage destruction (39, 40). See **Figure 2** for summary of pathological fibroblast subsets in rheumatoid arthritis.

To confirm differences in RA fibroblast effector functions *in vivo*, our group adoptively transferred FAPα$^+$ THY1$^+$ sub-lining and FAPα$^+$ THY1$^-$ lining fibroblasts into the joint of STIA and collagen-induced arthritis (CIA) mice and demonstrated THY1$^+$ cells exacerbated disease by augmenting proinflammatory cytokine and chemokine production and promoting cellular infiltration. In contrast THY1$^-$ cells had no effect on inflammation *in vivo* but did enhance bone and cartilage destruction both *in vivo* and *in vitro* (39). Such findings enhance our understanding how fibroblast subsets drive chronic inflammation. Understanding how fibroblast subsets relate to the global synovial tissue pathotype and how changes in their phenotype or quantitative proportions underlie specific disease endotypes such as treatment refractory RA will be an important area of future research.

ENDOTHELIAL-DERIVED NOTCH SIGNALING INDUCES PATHOGENIC FIBROBLAST EXPANSION IN ARTHRITIS

It remains unclear whether fibroblast heterogeneity is due to developmental determinants, cellular differentiation and/or

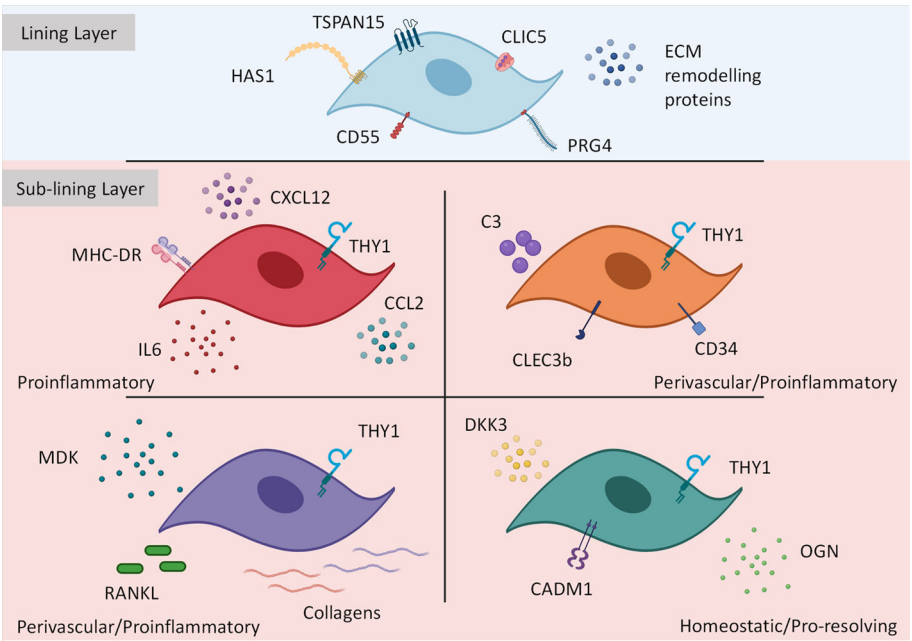

FIGURE 2 | Transcriptionally and functionally distinct synovial fibroblast subsets within the inflamed joint. Synovial fibroblasts exist as distinct subsets or activation states. Lining layer fibroblasts play an important role in tissue repair and remodelling however, in response to inflammation these fibroblasts may play a role in bone and cartilage destruction. In contrast, sub-lining fibroblasts discriminated by *THY1* expression (with a transcriptional gradient extending from the vascular loci (highest *THY1* expression) to the synovial lining) expand during inflammation Within the sub-lining tissue, four differentially activated fibroblast subsets have been identified expressing distinct transcriptional cassettes determined by anatomical location within the joint. This figure is based on human and mouse data. Image created with (BioRender.com).

epigenetic modifications. Recent studies have demonstrated differences in the expression of homeobox (*HOX*) family of transcription factors and WNT signaling pathways between fibroblasts isolated from different joints (119). The *HOX* gene signature shared similar features to the embryonic positional *HOX* gene expression pattern along the proximal–distal and anterior–posterior developmental axes. Others have shown that epigenetic modifications such as DNA methylation and histone modifications determine *HOX* gene expression in synovial fibroblasts (120, 121). It is thought that epigenetic imprinting of fibroblasts within a specific joint exists to support the unique biomechanical features of that joint. This anatomical diversity of synovial fibroblasts, while not disease specific, may underpin the tissue tropism observed in RA with positionally imprinted risk signatures of synovial fibroblasts determining the specific pattern of joint involvement in disease (122).

Synovial fibroblasts are also highly responsive to changes in the joint microenvironment with a phenotype dependent on microenvironmental instructive cues (86). In support of this, a study by Wei et al. (2020) (86) used *THY1* and *PRG4* as canonical markers of lining and sub-lining layer fibroblasts to anatomically define these regions of the synovial microanatomy and demonstrated a transcriptional *THY1/PRG4* gradient in RA synovial tissue. This suggests transcriptional intermediate fibroblast states exist between these two anatomical poles with the anatomical endpoint of the sub-lining expression signature being the mural cells (vascular smooth muscle cells and pericytes that surround microvasculature) which corresponded with the site of highest THY1 expression. Importantly, similar to Mizoguchi et al. (2018) (40), these transcriptional signatures were dependent on their positional location within the synovial tissue and were lost following ex-vivo expansion in culture. These findings collectively suggest that fibroblasts are passive responders to the joint microenvironment and their transcriptional phenotype is determined by their position in the tissue including their distance from the synovial vasculature.

Wei et al. (2020) (86) showed that THY1^{high} fibroblasts share similar anatomical sites as endothelial cell (EC) and mural cells. When cultured with or without EC in a free-floating 3D synovial tissue organoid system, fibroblasts form a lining and sub-lining layer in both conditions but only displayed a sub-lining transcriptional phenotype in the presence of EC. In the absence of EC, the fibroblast transcriptional signature became null where all fibroblasts expressed an intermediate transcriptional gene expression signature. In contrast, in the presence of EC, scRNAseq cell profiling demonstrated that 5.9% of fibroblasts were found to transcriptionally cluster with *THY1*$^{+}$ perivascular fibroblasts whereas 15.4% of fibroblasts clustered in association with mural cells suggesting signals from the EC differentiate fibroblasts into both perivascular fibroblasts and mural cells. Furthermore, receptor ligand analysis showed EC induced *THY1*$^{+}$ fibroblast and mural cell differentiation through

DLL4/JAG1:NOTCH3 signaling (86). The genetic deletion of *Notch3* or antibody mediated therapeutic blockade of NOTCH3 signaling led to attenuated arthritis (86).

Recently, Buechler et al. (2021) (123) demonstrated universal fibroblast subsets (*Pi16*$^+$ and *Col15a1*$^+$) exist across all tissue types (including the joint). These subsets express markers of stemness and are thought to give rise to specialized fibroblast subsets (dependent on tissue type and state) where *Pi16*$^+$ transition through the *Col15a1*$^+$ intermediate state. These universal fibroblasts also expressed high amounts of dermatopontin (DPT) and genetically engineered mice which express the fluorescently labelled DPT protein confirmed their transcriptional trajectory giving rise to three specialized fibroblast subsets demarked by genes *Cxcl5*, *Adamdec* and *Lrrc15*. In RA synovial tissue, *Pi16*$^+$ fibroblasts were shown to give rise to *Cxcl5*$^+$ fibroblasts which expressed high levels of proinflammatory cytokines IL-6 ad IL-1β and chemokines CCL2 and CCL7 thought to be located in the sub-lining. Co-regulated gene analysis also confirmed this activated cluster was driven by Pi3K, TNF and NFκB signaling. In summary, universal Pi16$^+$ fibroblasts are plastic and differentiate into specialized fibroblasts following a site-specific signal such as NOTCH signaling in an inflamed joint.

In agreement with the above studies, others have demonstrated similar pro-inflammatory specialized fibroblasts exist across multiple chronic inflammatory diseases: RA, inflammatory bowel disease (IBD), interstitial lung disease and Sjögren's syndrome (124). Again, using scRNAseq, this group discovered two shared fibroblast clusters exist across these diseases: *SPARC3*$^+$ *COL3A1*$^+$ and *CXCL10*$^+$ *CCL19*$^+$. The authors propose *SPARC3*$^+$ *COL3A1*$^+$ fibroblasts contain a conserved developmental pathway which drive tissue remodelling in early stages of disease to support chronic inflammation, whereas *CXCL10*$^+$ *CCL19*$^+$ fibroblasts are immune interacting and promote cellular infiltration. Thus, *SPARC3*$^+$ *COL3A1*$^+$ cells interact with blood vessels and alter the EC matrix to promote or inhibit infiltration (during early or resolving arthritis) whereas *CXCL10*$^+$ *CCL19*$^+$ fibroblast differentiation supports immune cell infiltration during active RA. In agreement with Wei et al. (2020) (86), the authors suggest that *SPARC3*$^+$ *COL3A1*$^+$ perivascular fibroblasts cross-talk with EC through DLL4:NOTCH3 signalling as well as TGF-β1, PDGFβ and angiogenic and mitogenic factors ephrin-α and -β and MDK and PTN respectively.

Furthermore, the investigators demonstrate that *CXCL10*$^+$ *CCL19*$^+$ synovial fibroblasts display a strong IFNγ response signature (124) and are therefore believed to interact directly with CD8+ T cells (IFNγ is abundantly expressed by CD8+ T cells). As a result, it is likely these immune-inflammatory fibroblasts are analogous to Zhang et al. (2019) *HLA-DR*^{High} pathogenic fibroblasts (42). Furthermore, the expression of synovial fibroblast CX_3CL1 and CX_3CR1 expressed by CD8+ T cells has been shown to positively correlate with RA severity (125) and monoclonal antibody treatment targeting CX_3CL1 has shown to be successful in early phase clinical trials in RA (126). This suggests, in conjunction with NOTCH signaling, infiltrating IFNγ producing CD8+ cells may also play a role in activating pathogenic fibroblast subsets such as *HLA-DR*^{High}. It is highly likely other signals arising from resident and infiltrating cells will evolve during disease progression that ultimately lead to modulation of fibroblast phenotype.

In summary, synovial fibroblasts demonstrate significant plasticity in response to local signals from within the joint microenvironment and give rise to transcriptionally distinct phenotypes based on their anatomical location within the synovium. These positional cues are orchestrated to create distinct synovial tissue niches that support infiltrating inflammatory cells. Under inflammatory states, the expression of transcriptional cassettes encoding the pathogenic fibroblast phenotype appear to be transient and dependent on positional cues. However, in chronically inflamed joints, fibroblasts are exposed to persistent inflammatory cues and, therefore, these signatures may become epigenetically imprinted, developing a sustained pathogenic fibroblast phenotype (29). The role in which epigenetics plays in modulating fibroblasts phenotypes in RA will be discussed below.

PATHOLOGICAL FIBROBLAST CELL STATES DRIVE THE PERSISTENCE OF JOINT INFLAMMATION

Historical evidence demonstrates fibroblasts from the RA synovium of patients with advanced disease, including those undergoing joint replacement, have an aggressive and invasive phenotype that is maintained when engrafted into a severe combined immunodefient mouse (SCID mice) (lacking B and T cells) (38, 127, 128). It is therefore hypothesized that epigenetic modifications underpin the persistently activated fibroblast cell state and the invasive phenotype observed in chronic disease.

Unlike genetic mutations, epigenetic modifications are reversible as they do not alter the genetic sequence, only the way the gene is transcribed. Thus, epigenetic modifications in the promotor region of genes suppress and exacerbate their expression. It is suggested there are three main types of epigenetic modifications reported in RA synovial fibroblasts: DNA methylation, histone modifications and micro RNA (miRNA) expression [reviewed in (29)]. Such modifications are disease specific showing different epigenetic profiles in RA compared to OA joint fibroblasts (129, 130). In addition, current investigations have now identified long non-coding RNAs (lncRNAs) as master regulators of epigenetic modifications in RA synovial fibroblasts [reviewed in (131)] which will also be discussed below.

DNA methylation is the covalent transfer of a methyl group to the 5' position within CpG islands by DNA methyltransferase (DNMT). DNA methylation silences or suppresses gene expression whereas hypomethylation (unmethylated CpG site that is normally methylated) enhances expression. In RA, the fibroblast methylome state is predominantly hypomethylated and has been shown to promote the aggressive phenotype by enriching the expression of genes associated with immuno-

inflammation, proliferation and apoptosis (132). Hypomethylation also generates destructive endogenously activated pathways in RA fibroblasts through the increased expression of CXCL12 which activates MMPs *via* CXCR7 (133).

Recent evidence suggests changes in DNA methylation occur early in RA (undifferentiated RA) and has prognostic potential (134). From this study the total number of hypermethylated CpG sites increased from 9% in undifferentiated arthritis to 84% in very early RA (symptom duration ≤3 months) and 96% established RA (≥3 months duration). Furthermore, specific hypermethylated CpG sites were observed in all stages of disease including downregulation of the *MFAP2* gene in established RA. These findings suggest, in established RA, fibroblast hypermethylation may cause a reduction in *MFAP2* expression by $DKK3^{+}$ immune-regulatory fibroblasts observed by Zhang et al. (2019) (42).

Inhibiting histone acetylation using various histone deacetlylase (HDAC) inhibitors attenuates experimental arthritis in mice (135, 136). Also, prolonged exposure to inflammatory mediators such as TNFα loosens chromatin accessibility in RA synovial fibroblasts by decreasing total histone-4 (H4) and hyperacetylating the remaining (137). Such modifications prime fibroblasts and enhance transcription of NFκB and production of proinflammatory cytokines and chemokines such as IL-6 and CXCL10, CXCL9 and CXCL11 respectively. Reports also suggest synovial fibroblast histones can be methylated which can occur on lysine and arginine residues only (with prevalence for lysine) and is regulated by histone lysine methyltransferase (HKMT) and demethylases (HKDM) (138). In response to TNFα stimulation, HKM-modifying enzymes dysregulate HKMT and HKDM activity resulting in changes in synovial fibroblast gene expression.

The production of miRNAs by synovial fibroblasts also alters their gene expression – a phenomenon driven by proinflammatory mediators which are present in the inflamed joint microenvironment. The RA synovial fibroblast miRNA signature determines the aggressive phenotype of synovial fibroblasts observed in chronic arthritis where specific miRNAs have been shown to target mechanisms that regulate methylation (139). Many synovial fibroblast miRNAs have been identified in RA synovial fibroblasts which exhibit enhanced or suppressive effects on proinflammatory gene transcription (140–142). In contrast, one study suggests miRNA expression can result in a pro-resolving state, for example resolvin D1 treatment in CIA in mice suppressed angiogenesis, pannus formation (determined by synovial expression of connective tissue growth factor) and proinflammatory cytokine levels through the upregulation of miRNA-146a-5p expression which inhibited STAT3 activation (143). So, it appears that expression of miRNAs by synovial fibroblasts has direct pathological, protective and pro-resolving outcomes which become dysregulated in chronic inflammation.

Recent findings suggest lncRNAs are also important epigenetic regulators, and in RA these non-coding RNAs are not only reduced (144) but have both suppressive and stimulatory effects on synovial fibroblast gene expression, which ultimately supports chronic inflammation by enhancing fibroblast pro-inflammatory cytokine and chemokine production, proliferation, migration and invasiveness whilst preventing apoptosis (145). Others have shown lncRNA profiles differ in normal and RA patient plasma (146). In this study, RA patient samples contained a total of 169 upregulated lncRNA and 120 downregulated compared to healthy controls, suggesting changes in lncRNA fibroblast transcription is a biomarker of RA. It is also proposed lncRNAs can regulate fibroblast miRNA expression and therefore determine RA pathogenesis (147). For example, normal expression of fibroblast lncRNA *OIP5-AS1* is protective and inhibits the expression of miR-448 (148). In contrast, dysfunctional *OIP5-AS1* expression causes upregulation of miR-448 which induces TLR3/NFκB signalling and supported pathogenesis in arthritic rats. The exact mechanism lncRNAs play in RA is still yet to be determined, however Yan et al. (2019) suggest lncRNA *HIX003209* promotes a TLR4/NFκB proinflammatory phenotype in CD14+ infiltrating macrophages in RA by sponging miR–6089 (149).

While a persistent inflammatory stimulus can induce a sustained activatory phenotype in synovial fibroblasts, tissue resident macrophages appear to respond transiently and unlike fibroblasts maintain expression of immune-regulatory proteins such as ABIN3, IRAK-M, SOCS3 and ATF3 (150). Therefore, low expression of these immune-regulatory proteins in fibroblasts determines sustained activation. A more recent study demonstrates that 280 TNFα-inducible genes are repressed in macrophages following transient activation whereas fibroblasts sustain enhanced expression of 80 of these genes (151). These 80 genes also contained hyperacetylation of H3K27 and increased chromatin accessibility in NFκB promotor, interferon regulatory factors and activating protein-1. In summary, prolonged exposure to inflammatory stimuli causes epigenetic modifications in synovial fibroblasts which promote an aggressively imprinted proinflammatory phenotype. In contrast, TNFα exposure in macrophages induces a transient response which is tolerized. In RA patients who achieve clinical remission, it is possible macrophages may rapidly alter their response and transition to a homeostatic phenotype which supports resolution of inflammation and tissue repair. However, if fibroblasts maintain a sustained pro-inflammatory phenotype, they may fail to respond to the negative suppression by tissue resident macrophages, but this is yet to be proven. Further work is required to understand how epigenetically modified fibroblasts can be targeted in RA.

TARGETING PATHOGENIC FIBROBLASTS IN REFRACTORY RA

Targeting fibroblasts directly remains an aspirational goal but one that offers the potential to be less immunosuppressive than conventional biological therapies. One approach has been to target specific fibroblast cell behavior directly such as proliferation or hypertrophy/organization. A recent multi-center study termed TRAFIC (targeting synovial fibroblast proliferation in rheumatoid arthritis) conducted a phase 1b/2a

clinical trial to determine the tolerated dose of seliciclib (152) [a cyclin-dependent kinase (CDK) inhibitor which induces expression of *p21* and suppresses expression of the pro-survival protein BCL-2] (153–156). Although the study deemed seliciclib as safe to continue forward into phase 2 trials, little is known about its therapeutic efficacy in RA currently. Similarly, the finding that *Cdh11*$^{-/-}$ mice exhibit a 50% reduction in clinical arthritis in mice (112) led to testing its therapeutic potential in RA. However, a phase I trial of a monoclonal antibody directed at CDH11 (RG6125) inflammation was completed but a phase II trial was discontinued owing to a lack of efficacy (126).

Strategies designed to directly target specific pathogenic fibroblast subsets are now being explored. Using a diphtheria toxin system in mice, we have recently shown that the selective deletion of FAPα expressing fibroblasts during inflammatory arthritis results in attenuation of synovial inflammation and reduced joint damage (39). These observations provide the rationale for therapeutic targeting of such pathogenic fibroblasts in RA. To translate these findings in humans it is important to identify such pathogenic subsets in the inflamed RA synovium and be able to effectively target these cells accurately while minimizing potential 'off target' effects. One possible approach to target FAPα+ synovial fibroblasts is the use of chimeric antigen receptor (CAR)-T cells. Local delivery of FAPα targeting CAR T cells in patients with pleural mesothelioma has been shown to be safe in a phase I clinical trial (157). Targeting FAPα expressing fibroblasts with CAR T cells following cardiac injury in mice has been shown to reduce cardiac fibrosis and restore cardiac function (158). However, further preclinical work is needed to determine the efficacy and specificity of FAPα CAR T cells in experimental arthritis.

Another potential therapeutic strategy is to inhibit local signals from within the joint which drive fibroblast activation states. For example, endothelium-derived NOTCH3 signaling inducing a pathogenic sub-lining phenotype in perivascular and interstitial fibroblasts. Genetic deletion or blockade of *Notch3* signaling has been shown to inhibit THY1^{+} sub-lining perivascular fibroblast expansion in mice and importantly attenuate experimental arthritis (86). NOTCH3 blockade has also been shown to reduce *SPARC3*$^{+}$ *COL3A1*$^{+}$ fibroblasts but not *CXCL10*$^{+}$ *CCL19*$^{+}$ fibroblasts (124). As it is hypothesized *SPARC3*$^{+}$ *COL3A1*$^{+}$ fibroblast remodel the synovial vasculature to facilitate immune cell infiltration in early disease, it is probable NOTCH3 therapy could be more effective when employed in undifferentiated or very early RA cohorts.

In chronic disease, the prolonged exposure to proinflammatory mediators causes epigenetic histone modifications in synovial fibroblasts resulting in sustained expression of TNFα inducible genes (150, 151) – a phenomenon not observed in synovial macrophages (151). As this effect is due to histone hyperacetylation, targeting histone acetylation reader proteins such as BET bromodomain proteins could modulate the sustained or persistently activated fibroblast state. In support of this, treating synovial fibroblasts with the BET inhibitor I-BET151 significantly reduces proliferation, cytokine and MMP production (159). Furthermore, the effects of I-BET151 were shown to be cell-type specific inducing anti-inflammatory effects in macrophages. As mentioned above, histone acetylation primes fibroblasts enhancing expression of proinflammatory mediators. As histone acetylation is reversible it can be deacetylated by treating with histone deacetylases (HDAC). One study demonstrates that treatment of RA synovial fibroblasts with HDAC3 significantly reduces production of inflammatory mediators such as IFNs (160). This suggests potential for using HDACs to therapeutically target synovial fibroblasts in RA. Further work is required to identify and target critical epigenetic modifications and gene regulatory pathways that sustain pathogenic fibroblast states in inflammatory joint disease.

SUMMARY

During inflammatory arthritis, the spatial and temporal cellular heterogeneity of synovial macrophages and fibroblasts sees the emergence of specialized cellular subsets that define specilised synovial tissue niches that support the pathpogenic behavior of immune cells.

Early, inflammation driven remodeling of the synovial microenvironment is associated with a disrupted macrophage lining barrier that permits the invasion of activated fibroblasts and infiltrating immune cells. The expansion of pathogenic fibroblasts and alarmin-producing MERTK^{-} macrophages in the sub-lining layer results in a pro-inflammatory microenvironment that supports the infiltration and survivial of inflammatory cells. In order for inflammation to resolve, fibroblast-derived GAS6 promotes the differentiation of MERTK^{+} macrophages which in turn induce a reparative phenotype in lining fibroblasts. At this point the lining barrier function is restored and joint homeostasis is reinstated.

We propose that these pathways are associated with critical cellular checkpoints between macropahges and fibroblasts, and the failure of these bi-directional cellular interactions to suppress pro-inflammatory pathways results in the emergence of persistently activated pathogenic cell states that drive chronic inflammation. The failure of pathogenic fibroblasts to respond to negative regulation, such as those instructive signals provided by pro-resolving macropahges may underpin chronic inflammation and treatment refractory arthritis.

Future research strategies should combine the knowledge of cellular heterogeneity scRNAseq and *in vivo* and/or *in vitro* functional assays to understand the exact biological function of tissue resident synovial cells at different stages of disease. Furthermore, employing epigenetic profiling technologies such as open chromatin sequencing will assist in deciphering the epigenetic landscape of synovial fibroblasts and identify differences in gene regulation that lead to specific programs of gene expression that underpin their phenotypic heterogeneity and how these are modulated during chronic inflammation. Such findings will enable the identification of novel fibroblast targeted therapies designed to break the ceiling of therapeutic response in RA.

AUTHOR CONTRIBUTIONS

Both authors contributed equally to the review. All authors contributed to the article and approved the submitted version.

FUNDING

AC is funded by a Kennedy Trust for Rheumatology Research Senior Clinical Research Fellowship KENN 192006.

REFERENCES

1. Lee DM, Weinblatt ME. Rheumatoid Arthritis. *Lancet* (2001) 358 (9285):903–11. doi: 10.1016/S0140-6736(01)06075-5
2. Smolen JS, Aletaha D, McInnes IB. Rheumatoid Arthritis. *Lancet* (2016) 388 (10055):2023–38. doi: 10.1016/S0140-6736(16)30173-8
3. McInnes IB, Schett G. The Pathogenesis of Rheumatoid Arthritis. *N. Engl J Med* (2011) 365(23):2205–19. doi: 10.1056/NEJMra1004965
4. Schett G, Stach C, Zwerina J, Voll R, Manger B. How Antirheumatic Drugs Protect Joints From Damage in Rheumatoid Arthritis. *Arthritis Rheum.* (2008) 58(10):2936–48. doi: 10.1002/art.23951
5. Yap HY, Tee SZ, Wong MM, Chow SK, Peh SC, Teow SY. Pathogenic Role of Immune Cells in Rheumatoid Arthritis: Implications in Clinical Treatment and Biomarker Development. *Cells* (2018) 7(10):1–19. doi: 10.3390/cells7100161
6. Guo Q, Wang Y, Xu D, Nossent J, Pavlos NJ, Xu J. Rheumatoid Arthritis: Pathological Mechanisms and Modern Pharmacologic Therapies. *Bone Res* (2018) 6:15. doi: 10.1038/s41413-018-0016-9
7. Chemin K, Gerstner C, Malmström V. Effector Functions of CD4+ T Cells at the Site of Local Autoimmune Inflammation-Lessons From Rheumatoid Arthritis. *Front Immunol* (2019) 10:353. doi: 10.3389/fimmu.2019.00353
8. Choy EHS, Miceli-Richard C, González-Gay MA, Sinigaglia L, Schlichting DE, Meszaros G, et al. The Effect of JAK1/JAK2 Inhibition in Rheumatoid Arthritis: Efficacy and Safety of Baricitinib. *Clin Exp Rheumatol* (2019) 37 (4):694–704.
9. Honda S, Harigai M. The Safety of Baricitinib in Patients With Rheumatoid Arthritis. *Expert Opin Drug Saf* (2020) 19(5):545–51. doi: 10.1080/14740338.2020.1743263
10. Liu D, Yuan N, Yu G, Song G, Chen Y. Can Rheumatoid Arthritis Ever Cease to Exist: A Review of Various Therapeutic Modalities to Maintain Drug-Free Remission? *Am J Transl Res* (2017) 9(8):3758–75.
11. Smolen JS, Aletaha D. Rheumatoid Arthritis Therapy Reappraisal: Strategies, Opportunities and Challenges. *Nat Rev Rheumatol* (2015) 11(5):276–89. doi: 10.1038/nrrheum.2015.8
12. Vittecoq O, Desouches S, Kozyreff M, Nicolau J, Pouplin S, Rottenberg P, et al. Relapse in Rheumatoid Arthritis Patients Undergoing Dose Reduction and Withdrawal of Biologics: Are Predictable Factors More Relevant Than Predictive Parameters? An Observational Prospective Real-Life Study. *BMJ Open* (2019) 9(12):e031467. doi: 10.1136/bmjopen-2019-031467
13. Malottki K, Barton P, Tsourapas A, Uthman AO, Liu Z, Routh K, et al. Adalimumab, Etanercept, Infliximab, Rituximab and Abatacept for the Treatment of Rheumatoid Arthritis After the Failure of a Tumour Necrosis Factor Inhibitor: A Systematic Review and Economic Evaluation. *Health Technol Assess* (2011) 15(14):1–278. doi: 10.3310/hta15140
14. Melville AR, Kearsley-Fleet L, Buch MH, Hyrich KL, et al. Understanding Refractory Rheumatoid Arthritis: Implications for a Therapeutic Approach. *Drugs* (2020) 80(9):849–57. doi: 10.1007/s40265-020-01309-9
15. Smolen JS, Landewé RBM, Bijlsma JWJ, Burmester GR, Dougados M, Kerschbaumer A, et al. EULAR Recommendations for the Management of Rheumatoid Arthritis With Synthetic and Biological Disease-Modifying Antirheumatic Drugs: 2019 Update. *Ann Rheum. Dis* (2020) 79(6):685–99. doi: 10.1136/annrheumdis-2019-216655
16. Buch MH, Eyre S, McGonagle D. Persistent Inflammatory and non-Inflammatory Mechanisms in Refractory Rheumatoid Arthritis. *Nat Rev Rheumatol* (2021) 17(1):17–33. doi: 10.1038/s41584-020-00541-7
17. Filer A. The Fibroblast as a Therapeutic Target in Rheumatoid Arthritis. *Curr Opin Pharmacol* (2013) 13(3):413–9. doi: 10.1016/j.coph.2013.02.006
18. Naylor AJ, Filer A, Buckley CD. The Role of Stromal Cells in the Persistence of Chronic Inflammation. *Clin Exp Immunol* (2013) 171(1):30–5. doi: 10.1111/j.1365-2249.2012.04634.x
19. Turner JD, Filer A. The Role of the Synovial Fibroblast in Rheumatoid Arthritis Pathogenesis. *Curr Opin Rheumatol* (2015) 27(2):175–82. doi: 10.1097/BOR.0000000000000148
20. Liu R, Zhao P, Tan W, Zhang M. Cell Therapies for Refractory Rheumatoid Arthritis. *Clin Exp Rheumatol* (2018) 36(5):911–9.
21. Parsonage G, Filer AD, Haworth O, Nash GB, Rainger GE, Salmon M, et al. A Stromal Address Code Defined by Fibroblasts. *Trends Immunol* (2005) 26 (3):150–6. doi: 10.1016/j.it.2004.11.014
22. Buckley CD. Why Does Chronic Inflammation Persist: An Unexpected Role for Fibroblasts. *Immunol Lett* (2011) 138(1):12–4. doi: 10.1016/j.imlet.2011.02.010
23. Filer A, Ward LSC, Kemble S, Davies CS, Munir H, Rogers R, et al. Identification of a Transitional Fibroblast Function in Very Early Rheumatoid Arthritis. *Ann Rheum. Dis* (2017) 76(12):2105–12. doi: 10.1136/annrheumdis-2017-211286
24. West NR, Hegazy AN, Owens BMJ, Bullers SJ, Linggi B, Buonocore S, et al. Oncostatin M Drives Intestinal Inflammation and Predicts Response to Tumor Necrosis Factor-Neutralizing Therapy in Patients With Inflammatory Bowel Disease. *Nat Med* (2017) 23(5):579–89. doi: 10.1038/nm.4307
25. Buckley CD, McGettrick HM. Leukocyte Trafficking Between Stromal Compartments: Lessons From Rheumatoid Arthritis. *Nat Rev Rheumatol* (2018) 14(8):476–87. doi: 10.1038/s41584-018-0042-4
26. Mosser DM, Hamidzadeh K, Goncalves R. Macrophages and the Maintenance of Homeostasis. *Cell Mol Immunol* (2021) 18(3):579–87. doi: 10.1038/s41423-020-00541-3
27. Kurowska-Stolarska M, Alivernini S. Synovial Tissue Macrophages: Friend or Foe? *RMD Open* (2017) 3(2):e000527. doi: 10.1136/rmdopen-2017-000527
28. McHugh J. Functionally Distinct Fibroblast Subsets in RA. *Nat Rev Rheumatol* (2019) 15(8):449. doi: 10.1038/s41584-019-0261-3
29. Nygaard G, Firestein GS. Restoring Synovial Homeostasis in Rheumatoid Arthritis by Targeting Fibroblast-Like Synoviocytes. *Nat Rev Rheumatol* (2020) 16(6):316–33. doi: 10.1038/s41584-020-0413-5
30. Humby F, Lewis M, Ramamoorthi N, Hackney JA, Barnes MR, Bombardieri M, et al. Synovial Cellular and Molecular Signatures Stratify Clinical Response to csDMARD Therapy and Predict Radiographic Progression in Early Rheumatoid Arthritis Patients. *Ann Rheum. Dis* (2019) 78(6):761–72. doi: 10.1136/annrheumdis-2018-214539
31. Lliso-Ribera G, Humby F, Lewis M, Nerviani A, Mauro D, Rivellese F, et al. Synovial Tissue Signatures Enhance Clinical Classification and Prognostic/Treatment Response Algorithms in Early Inflammatory Arthritis and Predict Requirement for Subsequent Biological Therapy: Results From the Pathobiology of Early Arthritis Cohort (PEAC). *Ann Rheum. Dis* (2019) 78 (12):1642–52. doi: 10.1136/annrheumdis-2019-215751
32. Humby F, Lewis M, Townsend MJ, Pitzalis C. Response to: 'Synovial Cellular and Molecular Signatures Stratify Clinical Response to csDMARD Therapy and Predict Radiographic Progression in Early Rheumatoid Arthritis Patients' by Buch Et al. *Ann Rheum. Dis* (2020) 79(11):e141. doi: 10.1136/annrheumdis-2019-215903
33. Smith MD, Barg E, Weedon H, Papengelis V, Smeets T, Tak PP, et al. Microarchitecture and Protective Mechanisms in Synovial Tissue From Clinically and Arthroscopically Normal Knee Joints. *Ann Rheum. Dis* (2003) 62(4):303–7. doi: 10.1136/ard.62.4.303
34. Rhee DK, Marcelino J, Baker M, Gong Y, Smits P, Lefebvre V, et al. The Secreted Glycoprotein Lubricin Protects Cartilage Surfaces and Inhibits Synovial Cell Overgrowth. *J Clin Invest* (2005) 115(3):622–31. doi: 10.1172/JCI200522263
35. Smith MD. The Normal Synovium. *Open Rheumatol J* (2011) 5:100–6. doi: 10.2174/1874312901105010100
36. Orr C, Vieira-Sousa E, Boyle DL, Buch MH, Buckley CD, Cañete JD, et al. Synovial Tissue Research: A State-of-the-Art Review. *Nat Rev Rheumatol* (2017) 13(8):463–75. doi: 10.1038/nrrheum.2017.115

37. Culemann S, Grüneboom A, Nicolás-Ávila J, Weidner D, Lämmle KF, Rothe T, et al. Locally Renewing Resident Synovial Macrophages Provide a Protective Barrier for the Joint. *Nature* (2019) 572(7771):670–5. doi: 10.1038/s41586-019-1471-1
38. Croft AP, Naylor AJ, Marshall JL, Hardie DL, Zimmermann B, Turner J, et al. Rheumatoid Synovial Fibroblasts Differentiate Into Distinct Subsets in the Presence of Cytokines and Cartilage. *Arthritis Res Ther* (2016) 18(1):270. doi: 10.1186/s13075-016-1156-1
39. Croft AP, Campos J, Jansen K, Turner JD, Marshall J, Attar M, et al. Distinct Fibroblast Subsets Drive Inflammation and Damage in Arthritis. *Nature* (2019) 570(7760):246–51. doi: 10.1038/s41586-019-1263-7
40. Mizoguchi F, Slowikowski K, Wei K, Marshall JL, Rao DA, Chang SK, et al. Functionally Distinct Disease-Associated Fibroblast Subsets in Rheumatoid Arthritis. *Nat Commun* (2018) 9(1):789. doi: 10.1038/s41467-018-02892-y
41. Stephenson W, Donlin LT, Butler A, Rozo C, Bracken B, Rashidfarrokhi A, et al. Single-Cell RNA-Seq of Rheumatoid Arthritis Synovial Tissue Using Low-Cost Microfluidic Instrumentation. *Nat Commun* (2018) 9(1):791. doi: 10.1038/s41467-017-02659-x
42. Zhang F, Wei K, Slowikowski K, Fonseka CY, Rao DA, Kelly S, et al. Defining Inflammatory Cell States in Rheumatoid Arthritis Joint Synovial Tissues by Integrating Single-Cell Transcriptomics and Mass Cytometry. *Nat Immunol* (2019) 20(7):928–42. doi: 10.1038/s41590-019-0378-1
43. Baldwin MJ, Cribbs AP, Guilak F, Snelling SJB. Mapping the Musculoskeletal System One Cell at a Time. *Nat Rev Rheumatol* (2021) 17(5):247–8. doi: 10.1038/s41584-021-00600-7
44. Schneider M, Voss B, Rauterberg J, Menke M, Pauly T, Miehlke RK, et al. Basement Membrane Proteins in Synovial Membrane: Distribution in Rheumatoid Arthritis and Synthesis by Fibroblast-Like Cells. *Clin Rheumatol* (1994) 13(1):90–7. doi: 10.1007/BF02229873
45. Chubinskaya S, Kuettner KE, Cole AA. Expression of Matrix Metalloproteinases in Normal and Damaged Articular Cartilage From Human Knee and Ankle Joints. *Lab Invest* (1999) 79(12):1669–77.
46. Konttinen YT, Ainola M, Valleala H, Ma J, Ida H, Mandelin J, et al. Analysis of 16 Different Matrix Metalloproteinases (MMP-1 to MMP-20) in the Synovial Membrane: Different Profiles in Trauma and Rheumatoid Arthritis. *Ann Rheum. Dis* (1999) 58(11):691–7. doi: 10.1136/ard.58.11.691
47. Kragstrup TW, Sohn DH, Lepus CM, Onuma K, Wang Q, Robinson WH, et al. Fibroblast-Like Synovial Cell Production of Extra Domain A Fibronectin Associates With Inflammation in Osteoarthritis. *BMC Rheumatol* (2019) 3:46. doi: 10.1186/s41927-019-0093-4
48. Buckley CD, Ospelt C, Gay S, Midwood KS. Location, Location, Location: How the Tissue Microenvironment Affects Inflammation in RA. *Nat Rev Rheumatol* (2021) 17(4):195–212. doi: 10.1038/s41584-020-00570-2
49. van Furth R, Cohn ZA. The Origin and Kinetics of Mononuclear Phagocytes. *J Exp Med* (1968) 128(3):415–35. doi: 10.1084/jem.128.3.415
50. Tu J, Wang X, Gong X, Hong W, Han D, Fang Y, et al. Synovial Macrophages in Rheumatoid Arthritis: The Past, Present, and Future. *Mediators Inflamm. 2020* (2020) 1583647. doi: 10.1155/2020/1583647
51. De Rycke L, Baeten D, Foell D, Kruithof E, Veys EM, Roth J, et al. Differential Expression and Response to Anti-TNFalpha Treatment of Infiltrating Versus Resident Tissue Macrophage Subsets in Autoimmune Arthritis. *J Pathol* (2005) 206(1):17–27. doi: 10.1002/path.1758
52. Magnusson SE, Engström M, Jacob U, Ulfgren AK, Kleinau S, et al. High Synovial Expression of the Inhibitory FcgammaRIIb in Rheumatoid Arthritis. *Arthritis Res Ther* (2007) 9(3):R51. doi: 10.1186/ar2206
53. Jeong JH, Hong S, Kwon OC, Ghang B, Hwang I, Kim YG, et al. CD14(+) Cells With the Phenotype of Infiltrated Monocytes Consist of Distinct Populations Characterized by Anti-Inflammatory as Well as Pro-Inflammatory Activity in Gouty Arthritis. *Front Immunol* (2017) 8:1260. doi: 10.3389/fimmu.2017.01260
54. Fonseca JE, Edwards JC, Blades S, Goulding NJ, et al. Macrophage Subpopulations in Rheumatoid Synovium: Reduced CD163 Expression in CD4+ T Lymphocyte-Rich Microenvironments. *Arthritis Rheum.* (2002) 46 (5):1210–6. doi: 10.1002/art.10207
55. Greisen SR, Moller HJ, Stengaard-Pedersen K, Hetland ML, Hørslev-Petersen K, Jørgensen A, et al. Soluble Macrophage-Derived CD163 is a Marker of Disease Activity and Progression in Early Rheumatoid Arthritis. *Clin Exp Rheumatol* (2011) 29(4):689–92.
56. Tarique AA, Logan J, Thomas E, Holt PG, Sly PD, Fantino E. Phenotypic, Functional, and Plasticity Features of Classical and Alternatively Activated Human Macrophages. *Am J Respir Cell Mol Biol* (2015) 53(5):676–88. doi: 10.1165/rcmb.2015-0012OC
57. Qing L, Fu J, Wu P, Zhou Z, Yu F, Tang J, et al. Metformin Induces the M2 Macrophage Polarization to Accelerate the Wound Healing via Regulating AMPK/mTOR/NLRP3 Inflammasome Singling Pathway. *Am J Transl Res* (2019) 11(2):655–68.
58. Degboé Y, Rauwel B, Baron M, Boyer JF, Ruyssen-Witrand A, Constantin A, et al. Polarization of Rheumatoid Macrophages by TNF Targeting Through an IL-10/STAT3 Mechanism. *Front Immunol* (2019) 10:3. doi: 10.3389/fimmu.2019.00003
59. Huang QQ, Doyle R, Chen SY, Sheng Q, Misharin AV, Mao Q, et al. Critical Role of Synovial Tissue-Resident Macrophage Niche in Joint Homeostasis and Suppression of Chronic Inflammation. *Sci Adv* (2021) 7(2)1–15. doi: 10.1126/sciadv.abd0515
60. Alivernini S, MacDonald L, Elmesmari A, Finlay S, Tolusso B, Gigante MR, et al. Distinct Synovial Tissue Macrophage Subsets Regulate Inflammation and Remission in Rheumatoid Arthritis. *Nat Med* (2020) 26(8):1295–306. doi: 10.1038/s41591-020-0939-8
61. Henderson B, Revell PA, Edwards JC. Synovial Lining Cell Hyperplasia in Rheumatoid Arthritis: Dogma and Fact. *Ann Rheum. Dis* (1988) 47(4):348–9. doi: 10.1136/ard.47.4.348
62. Rana AK, Li Y, Dang Q, Yang F. Monocytes in Rheumatoid Arthritis: Circulating Precursors of Macrophages and Osteoclasts and, Their Heterogeneity and Plasticity Role in RA Pathogenesis. *Int Immunopharmacol.* (2018) 65:348–59. doi: 10.1016/j.intimp.2018.10.016
63. Bartok B, Firestein GS. Fibroblast-Like Synoviocytes: Key Effector Cells in Rheumatoid Arthritis. *Immunol Rev* (2010) 233(1):233–55. doi: 10.1111/j.0105-2896.2009.00859.x
64. Mor A, Abramson SB, Pillinger MH. The Fibroblast-Like Synovial Cell in Rheumatoid Arthritis: A Key Player in Inflammation and Joint Destruction. *Clin Immunol* (2005) 115(2):118–28. doi: 10.1016/j.clim.2004.12.009
65. Qi W, Lin C, Fan K, Chen Z, Liu L, Feng X, et al. Hesperidin Inhibits Synovial Cell Inflammation and Macrophage Polarization Through Suppression of the PI3K/AKT Pathway in Complete Freund's Adjuvant-Induced Arthritis in Mice. *Chem Biol Interact* (2019) 306:19–28. doi: 10.1016/j.cbi.2019.04.002
66. Fernandes TL, Gomoll AH, Lattermann C, Hernandez AJ, Bueno DF, Amano MT. Macrophage: A Potential Target on Cartilage Regeneration. *Front Immunol* (2020) 11:111. doi: 10.3389/fimmu.2020.00111
67. Zhang H, Lin C, Zeng C, Wang Z, Wang H, Lu J, et al. Synovial Macrophage M1 Polarisation Exacerbates Experimental Osteoarthritis Partially Through R-Spondin-2. *Ann Rheum. Dis* (2018) 77(10):1524–34. doi: 10.1136/annrheumdis-2018-213450
68. Hannemann N, Cao S, Eriksson D, Schnelzer A, Jordan J, Eberhardt M, et al. Transcription Factor Fra-1 Targets Arginase-1 to Enhance Macrophage-Mediated Inflammation in Arthritis. *J Clin Invest* (2019) 129(7):2669–84. doi: 10.1172/JCI96832
69. Edilova MI, Akram A, Abdul-Sater AA. Innate Immunity Drives Pathogenesis of Rheumatoid Arthritis. *BioMed J* (2020). doi: 10.1016/j.bj.2020.06.010
70. Mulherin D, Fitzgerald O, Bresnihan B. Synovial Tissue Macrophage Populations and Articular Damage in Rheumatoid Arthritis. *Arthritis Rheum.* (1996) 39(1):115–24. doi: 10.1002/art.1780390116
71. Matsuo Y, Mizoguchi F, Saito T, Kawahata K, Ueha S, Matsushima K, et al. Local Fibroblast Proliferation But Not Influx is Responsible for Synovial Hyperplasia in a Murine Model of Rheumatoid Arthritis. *Biochem Biophys Res Commun* (2016) 470(3):504–9. doi: 10.1016/j.bbrc.2016.01.121
72. Shin YJ, Han SH, Kim DS, Lee GH, Yoo WH, Kang YM, et al. Autophagy Induction and CHOP Under-Expression Promotes Survival of Fibroblasts From Rheumatoid Arthritis Patients Under Endoplasmic Reticulum Stress. *Arthritis Res Ther* (2010) 12(1):R19. doi: 10.1186/ar2921
73. Orange DE, Yao V, Sawicka K, Fak J, Frank MO, Parveen S, et al. RNA Identification of PRIME Cells Predicting Rheumatoid Arthritis Flares. *N. Engl J Med* (2020) 383(3):218–28. doi: 10.1056/NEJMoa2004114
74. O'Sullivan FX, Fassbender HG, Gay S, Koopman WJ. Etiopathogenesis of the Rheumatoid Arthritis-Like Disease in MRL/l Mice. I.

The Histomorphologic Basis of Joint Destruction. *Arthritis Rheum.* (1985) 28(5):529–36. doi: 10.1002/art.1780280511
75. Ainola MM, Mandelin JA, Liljeström MP, Li TF, Hukkanen MV, Konttinen YT. Pannus Invasion and Cartilage Degradation in Rheumatoid Arthritis: Involvement of MMP-3 and Interleukin-1beta. *Clin Exp Rheumatol* (2005) 23(5):644–50.
76. Peck Y, Leom LT, Low PFP, Wang DA. Establishment of an *In Vitro* Three-Dimensional Model for Cartilage Damage in Rheumatoid Arthritis. *J Tissue Eng Regener Med* (2018) 12(1):e237–49. doi: 10.1002/term.2399
77. Chang SK, Noss EH, Chen M, Gu Z, Townsend K, Grenha R, et al. Cadherin-11 Regulates Fibroblast Inflammation. *Proc Natl Acad Sci U.S.A.* (2011) 108 (20):8402–7. doi: 10.1073/pnas.1019437108
78. Kiener HP, Lee DM, Agarwal SK, Brenner MB. Cadherin-11 Induces Rheumatoid Arthritis Fibroblast-Like Synoviocytes to Form Lining Layers *In Vitro*. *Am J Pathol* (2006) 168(5):1486–99. doi: 10.2353/ajpath.2006.050999
79. Kiener HP, Niederreiter B, Lee DM, Jimenez-Boj E, Smolen JS, Brenner MB. Cadherin 11 Promotes Invasive Behavior of Fibroblast-Like Synoviocytes. *Arthritis Rheum.* (2009) 60(5):1305–10. doi: 10.1002/art.24453
80. Marinova-Mutafchieva L, Williams RO, Funa K, Maini RN, Zvaifler NJ. Inflammation is Preceded by Tumor Necrosis Factor-Dependent Infiltration of Mesenchymal Cells in Experimental Arthritis. *Arthritis Rheum.* (2002) 46 (2):507–13. doi: 10.1002/art.10126
81. Armaka M, Ospelt C, Pasparakis M, Kollias G. The P55tnfr-IKK2-Ripk3 Axis Orchestrates Arthritis by Regulating Death and Inflammatory Pathways in Synovial Fibroblasts. *Nat Commun* (2018) 9(1):618. doi: 10.1038/s41467-018-02935-4
82. Lefèvre S, Knedla A, Tennie C, Kampmann A, Wunrau C, Dinser R, et al. Synovial Fibroblasts Spread Rheumatoid Arthritis to Unaffected Joints. *Nat Med* (2009) 15(12):1414–20. doi: 10.1038/nm.2050
83. Guilliams M, Svedberg FR. Does Tissue Imprinting Restrict Macrophage Plasticity? *Nat Immunol* (2021) 22(2):118–27. doi: 10.1038/s41590-020-00849-2
84. Donlin LT, Jayatilleke A, Giannopoulou EG, Kalliolias GD, Ivashkiv LB. Modulation of TNF-Induced Macrophage Polarization by Synovial Fibroblasts. *J Immunol* (2014) 193(5):2373–83. doi: 10.4049/jimmunol.1400486
85. Kuo D, Ding J, Cohn IS, Zhang F, Wei K, Rao DA, et al. HBEGF(+) Macrophages in Rheumatoid Arthritis Induce Fibroblast Invasiveness. *Sci Transl Med* (2019) 11(491):1–13. doi: 10.1126/scitranslmed.aau8587
86. Wei K, Korsunsky I, Marshall JL, Gao A, Watts GFM, Major T, et al. Notch Signalling Drives Synovial Fibroblast Identity and Arthritis Pathology. *Nature* (2020) 582(7811):259–64. doi: 10.1038/s41586-020-2222-z
87. Lu Q, Lemke G. Homeostatic Regulation of the Immune System by Receptor Tyrosine Kinases of the Tyro 3 Family. *Science* (2001) 293(5528):306–11. doi: 10.1126/science.1061663
88. Waterborg CEJ, Beermann S, Broeren MGA, Bennink MB, Koenders MI, van Lent P, et al. Protective Role of the MER Tyrosine Kinase *via* Efferocytosis in Rheumatoid Arthritis Models. *Front Immunol* (2018) 9:742. doi: 10.3389/fimmu.2018.00742
89. Li C, Zhao B, Lin C, Gong Z, An X, et al. TREM2 Inhibits Inflammatory Responses in Mouse Microglia by Suppressing the PI3K/NF-κb Signaling. *Cell Biol Int* (2019) 43(4):360–72. doi: 10.1002/cbin.10975
90. Lim HY, Lim SY, Tan CK, Thiam CH, Goh CC, Carbajo D, et al. Hyaluronan Receptor LYVE-1-Expressing Macrophages Maintain Arterial Tone Through Hyaluronan-Mediated Regulation of Smooth Muscle Cell Collagen. *Immunity* (2018) 49(2):326–41.e7. doi: 10.1016/j.immuni.2018.12.009
91. Gomez EA, Colas RA, Souza PR, Hands R, Lewis MJ, Bessant C, et al. Blood Pro-Resolving Mediators are Linked With Synovial Pathology And are Predictive of DMARD Responsiveness in Rheumatoid Arthritis. *Nat Commun* (2020) 11(1):5420. doi: 10.1038/s41467-020-19176-z
92. Lemke G. Phosphatidylserine Is the Signal for TAM Receptors and Their Ligands. *Trends Biochem Sci* (2017) 42(9):738–48. doi: 10.1016/j.tibs.2017.06.004
93. Lemke G, Burstyn-Cohen T. TAM Receptors and the Clearance of Apoptotic Cells. *Ann N. Y. Acad Sci* (2010) 1209:23–9. doi: 10.1111/j.1749-6632.2010.05744.x
94. Novitskiy SV, Zaynagetdinov R, Vasiukov G, Gutor S, Han W, Serezani A, et al. Gas6/MerTK Signaling is Negatively Regulated by NF-κb and Supports Lung Carcinogenesis. *Oncotarget* (2019) 10(66):7031–42. doi: 10.18632/oncotarget.27345
95. Thorp E, Vaisar T, Subramanian M, Mautner L, Blobel C, Tabas I. Shedding of the Mer Tyrosine Kinase Receptor is Mediated by ADAM17 Protein Through a Pathway Involving Reactive Oxygen Species, Protein Kinase Cδ, and P38 Mitogen-Activated Protein Kinase (MAPK). *J Biol Chem* (2011) 286 (38):33335–44. doi: 10.1074/jbc.M111.263020
96. Cai B, Thorp EB, Doran AC, Subramanian M, Sansbury BE, Lin CS, et al. MerTK Cleavage Limits Proresolving Mediator Biosynthesis and Exacerbates Tissue Inflammation. *Proc Natl Acad Sci U.S.A.* (2016) 113 (23):6526–31. doi: 10.1073/pnas.1524292113
97. Alciato F, Sainaghi PP, Sola D, Castello L, Avanzi GC. TNF-Alpha, IL-6, and IL-1 Expression is Inhibited by GAS6 in Monocytes/Macrophages. *J Leukoc Biol* (2010) 87(5):869–75. doi: 10.1189/jlb.0909610
98. Zizzo G, Hilliard BA, Monestier M, Cohen PL. Efficient Clearance of Early Apoptotic Cells by Human Macrophages Requires M2c Polarization and MerTK Induction. *J Immunol* (2012) 189(7):3508–20. doi: 10.4049/jimmunol.1200662
99. Bassyouni IH, El-Wakd MM, Azab NA, Bassyouni RH. Diminished Soluble Levels of Growth Arrest Specific Protein 6 and Tyrosine Kinase Receptor Axl in Patients With Rheumatoid Arthritis. *Int J Rheum. Dis* (2017) 20(1):53–9. doi: 10.1111/1756-185X.12367
100. Nerviani A, Humby F, Kelly S, Bombardieri M, Pitzalis C. A Functional Inhibitory Role for the GAS6/MERTK Axis in Modulating Synovial Inflammation in Rheumatoid Arthritis. *Ann Rheum. Dis* (2015) 74(Suppl 2):204. doi: 10.1136/annrheumdis-2015-eular.5727
101. Segre JA, Bauer C, Fuchs E. Klf4 is a Transcription Factor Required for Establishing the Barrier Function of the Skin. *Nat Genet* (1999) 22(4):356–60. doi: 10.1038/11926
102. Liao X, Humby F, Kelly S, Bombardieri M, Pitzalis C, et al. Krüppel-Like Factor 4 Regulates Macrophage Polarization. *J Clin Invest* (2011) 121 (7):2736–49. doi: 10.1172/JCI45444
103. Kobayashi EH, Suzuki T, Funayama R, Nagashima T, Hayashi M, Sekine H, et al. Nrf2 Suppresses Macrophage Inflammatory Response by Blocking Proinflammatory Cytokine Transcription. *Nat Commun* (2016) 7:11624. doi: 10.1038/ncomms11624
104. Roberts AW, Lee BL, Deguine J, John S, Shlomchik MJ, Barton GM. Tissue-Resident Macrophages Are Locally Programmed for Silent Clearance of Apoptotic Cells. *Immunity* (2017) 47(5):913–927.e6. doi: 10.1016/j.immuni.2017.10.006
105. Li Y, Liu H, Liang Y, Peng P, Ma X, Zhang X. DKK3 Regulates Cell Proliferation, Apoptosis and Collagen Synthesis in Keloid Fibroblasts *via* TGF-β1/Smad Signaling Pathway. *BioMed Pharmacother* (2017) 91:174–80. doi: 10.1016/j.biopha.2017.03.044
106. Sakaguchi M, Kataoka K, Abarzua F, Tanimoto R, Watanabe M, Murata H, et al. Overexpression of REIC/Dkk-3 in Normal Fibroblasts Suppresses Tumor Growth via Induction of Interleukin-7. *J Biol Chem* (2009) 284 (21):14236–44. doi: 10.1074/jbc.M808002200
107. Snelling SJ, Davidson RK, Swingler TE, Le LT, Barter MJ, Culley KL, et al. Dickkopf-3 is Upregulated in Osteoarthritis and has a Chondroprotective Role. *Osteoarthritis Cartilage* (2016) 24(5):883–91. doi: 10.1016/j.joca.2015.11.021
108. Bálint G, Barabás K, Zeitler Z, Bakos J, Kékesi KA, Pethes A, et al. Ex Vivo Soft-Laser Treatment Inhibits the Synovial Expression of Vimentin and α-Enolase, Potential Autoantigens in Rheumatoid Arthritis. *Phys Ther* (2011) 91(5):665–74. doi: 10.2522/ptj.20100065
109. Sun S, Liu W, Li Y. CADM1 Enhances Intestinal Barrier Function in a Rat Model of Mild Inflammatory Bowel Disease by Inhibiting the STAT3 Signaling Pathway. *J Bioenerg. Biomembr.* (2020) 52(5):343–54. doi: 10.1007/s10863-020-09850-8
110. Rock MJ, Cain SA, Freeman LJ, Morgan A, Mellody K, Marson A, et al. Molecular Basis of Elastic Fiber Formation. Critical Interactions and a Tropoelastin-Fibrillin-1 Cross-Link. *J Biol Chem* (2004) 279(22):23748–58. doi: 10.1074/jbc.M400212200
111. Decker RS, Um HB, Dyment NA, Cottingham N, Usami Y, Enomoto-Iwamoto M, et al. Cell Origin, Volume and Arrangement are Drivers of Articular Cartilage Formation, Morphogenesis and Response to Injury in Mouse Limbs. *Dev Biol* (2017) 426(1):56–68. doi: 10.1016/j.ydbio.2017.04.006
112. Lee DM, Kiener HP, Agarwal SK, Noss EH, Watts GF, Chisaka O, et al. Cadherin-11 in Synovial Lining Formation and Pathology in Arthritis. *Science* (2007) 315(5814):1006–10. doi: 10.1126/science.1137306

113. Friščić J, Böttcher M, Reinwald C, Bruns H, Wirth B, Popp SJ, et al. The Complement System Drives Local Inflammatory Tissue Priming by Metabolic Reprogramming of Synovial Fibroblasts. *Immunity* (2021) 54:1002–21. doi: 10.1016/j.immuni.2021.03.003
114. Liu H, Zhu Y, Gao Y, Qi D, Zhao L, Zhao L, et al. NR1D1 Modulates Synovial Inflammation and Bone Destruction in Rheumatoid Arthritis. *Cell Death Dis* (2020) 11(2):129. doi: 10.1038/s41419-020-2314-6
115. Fassbender HG. Histomorphological Basis of Articular Cartilage Destruction in Rheumatoid Arthritis. *Coll Relat Res* (1983) 3(2):141–55. doi: 10.1016/S0174-173X(83)80040-5
116. Middleton J, Americh L, Gayon R, Julien D, Mansat M, Mansat P, et al. A Comparative Study of Endothelial Cell Markers Expressed in Chronically Inflamed Human Tissues: MECA-79, Duffy Antigen Receptor for Chemokines, Von Willebrand Factor, CD31, CD34, CD105 and CD146. *J Pathol* (2005) 206(3):260–8. doi: 10.1002/path.1788
117. Ramirez-Montagut T, Blachere NE, Sviderskaya EV, Bennett DC, Rettig WJ, Garin-Chesa P, et al. FAPalpha, a Surface Peptidase Expressed During Wound Healing, is a Tumor Suppressor. *Oncogene* (2004) 23(32):5435–46. doi: 10.1038/sj.onc.1207730
118. Bauer S, Jendro MC, Wadle A, Kleber S, Stenner F, Dinser R, et al. Fibroblast Activation Protein is Expressed by Rheumatoid Myofibroblast-Like Synoviocytes. *Arthritis Res Ther* (2006) 8(6):R171. doi: 10.1186/ar2080
119. Frank-Bertoncelj M, Trenkmann M, Klein K, Karouzakis E, Rehrauer H, Bratus A, et al. Epigenetically-Driven Anatomical Diversity of Synovial Fibroblasts Guides Joint-Specific Fibroblast Functions. *Nat Commun* (2017) 8:14852. doi: 10.1038/ncomms14852
120. Ai R, Hammaker D, Boyle DL, Morgan R, Walsh AM, Fan S, et al. Joint-Specific DNA Methylation and Transcriptome Signatures in Rheumatoid Arthritis Identify Distinct Pathogenic Processes. *Nat Commun* (2016) 7:11849. doi: 10.1038/ncomms11849
121. den Hollander W, Ramos YF, Bos SD, Bomer N, van der Breggen R, Lakenberg N, et al. Knee and Hip Articular Cartilage Have Distinct Epigenomic Landscapes: Implications for Future Cartilage Regeneration Approaches. *Ann Rheum. Dis* (2014) 73(12):2208–12. doi: 10.1136/annrheumdis-2014-205980
122. Hub LC, Distler O, Tarner I, Gay RE, Gay S, Pap T. Synovial Fibroblasts: Key Players in Rheumatoid Arthritis. *Rheumatol (Oxford)* (2006) 45(6):669–75. doi: 10.1093/rheumatology/kel065
123. Buechler MB, Pradhan RN, Krishnamurty AT, Cox C, Calviello AK, Wang AW, et al. Cross-Tissue Organization of the Fibroblast Lineage. *Nature* (2021) 593:575–9. doi: 10.1038/s41586-021-03549-5
124. Korsunsky I, Wei K, Pohin M, Kim EI, Barone F, Kang JB, et al. Cross-Tissue, Single-Cell Stromal Atlas Identifies Shared Pathological Fibroblast Phenotypes in Four Chronic Inflammatory Diseases. *BioRxiv* (2021). doi: 10.1101/2021.01.11.426253
125. Jones B, Koch AE, Ahmed S. Pathological Role of Fractalkine/CX3CL1 in Rheumatic Diseases: A Unique Chemokine With Multiple Functions. *Front Immunol* (2011) 2:82. doi: 10.3389/fimmu.2011.00082
126. Tanaka Y, Takeuchi T, Umehara H, Nanki T, Yasuda N, Tago F, et al. Safety, Pharmacokinetics, and Efficacy of E6011, an Antifractalkine Monoclonal Antibody, in a First-in-Patient Phase 1/2 Study on Rheumatoid Arthritis. *Mod. Rheumatol* (2018) 28(1):58–65. doi: 10.1080/14397595.2017.1337056
127. Geiler T, Kriegsmann J, Keyszer GM, Gay RE, Gay S. A New Model for Rheumatoid Arthritis Generated by Engraftment of Rheumatoid Synovial Tissue and Normal Human Cartilage Into SCID Mice. *Arthritis Rheum.* (1994) 37(11):1664–71. doi: 10.1002/art.1780371116
128. Müller-Ladner U, Kriegsmann J, Franklin BN, Matsumoto S, Geiler T, Gay RE, et al. Synovial Fibroblasts of Patients With Rheumatoid Arthritis Attach to and Invade Normal Human Cartilage When Engrafted Into SCID Mice. *Am J Pathol* (1996) 149(5):1607–15.
129. Maeshima K, Stanford SM, Hammaker D, Sacchetti C, Zeng LF, Ai R, et al. Abnormal PTPN11 Enhancer Methylation Promotes Rheumatoid Arthritis Fibroblast-Like Synoviocyte Aggressiveness and Joint Inflammation. *JCI Insight* (2016) 1(7):1–13. doi: 10.1172/jci.insight.86580
130. Nakano K, Whitaker JW, Boyle DL, Wang W, Firestein GS. DNA Methylome Signature in Rheumatoid Arthritis. *Ann Rheum. Dis* (2013) 72(1):110–7. doi: 10.1136/annrheumdis-2012-201526
131. Wang J, Yan S, Yang J, Lu H, Xu D, Wang Z. Non-Coding RNAs in Rheumatoid Arthritis: From Bench to Bedside. *Front Immunol* (2019) 10:3129. doi: 10.3389/fimmu.2019.03129
132. Karouzakis E, Gay RE, Michel BA, Gay S, Neidhart M. DNA Hypomethylation in Rheumatoid Arthritis Synovial Fibroblasts. *Arthritis Rheum.* (2009) 60(12):3613–22. doi: 10.1002/art.25018
133. Karouzakis E, Rengel Y, Jüngel A, Kolling C, Gay RE, Michel BA, et al. DNA Methylation Regulates the Expression of CXCL12 in Rheumatoid Arthritis Synovial Fibroblasts. *Genes Immun* (2011) 12(8):643–52. doi: 10.1038/gene.2011.45
134. Karouzakis E, Raza K, Kolling C, Buckley CD, Gay S, Filer A, et al. Analysis of Early Changes in DNA Methylation in Synovial Fibroblasts of RA Patients Before Diagnosis. *Sci Rep* (2018) 8(1):7370. doi: 10.1038/s41598-018-24240-2
135. Lin HS, Hu CY, Chan HY, Liew YY, Huang HP, Lepescheux L, et al. Anti-Rheumatic Activities of Histone Deacetylase (HDAC) Inhibitors *In Vivo* in Collagen-Induced Arthritis in Rodents. *Br J Pharmacol* (2007) 150(7):862–72. doi: 10.1038/sj.bjp.0707165
136. Cantley MD, Fairlie DP, Bartold PM, Marino V, Gupta PK, Haynes DR. Inhibiting Histone Deacetylase 1 Suppresses Both Inflammation and Bone Loss in Arthritis. *Rheumatol (Oxford)* (2015) 54(9):1713–23. doi: 10.1093/rheumatology/kev022
137. Sohn C, Lee A, Qiao Y, Loupasakis K, Ivashkiv LB, Kalliolias GD. Prolonged Tumor Necrosis Factor α Primes Fibroblast-Like Synoviocytes in a Gene-Specific Manner by Altering Chromatin. *Arthritis Rheumatol* (2015) 67(1):86–95. doi: 10.1002/art.38871
138. Araki Y, Aizaki Y, Sato K, Oda H, Kurokawa R, Mimura T. Altered Gene Expression Profiles of Histone Lysine Methyltransferases and Demethylases in Rheumatoid Arthritis Synovial Fibroblasts. *Clin Exp Rheumatol* (2018) 36(2):314–6.
139. Gaur N, Karouzakis E, Glück S, Bagdonas E, Jüngel A, Michel BA, et al. MicroRNAs Interfere With DNA Methylation in Rheumatoid Arthritis Synovial Fibroblasts. *RMD Open* (2016) 2(2):e000299. doi: 10.1136/rmdopen-2016-000299
140. Yang Y, Wang Y, Liang Q, Yao L, Gu S, Bai X. MiR-338-5p Promotes Inflammatory Response of Fibroblast-Like Synoviocytes in Rheumatoid Arthritis *via* Targeting Spry1. *J Cell Biochem* (2017) 118(8):2295–301. doi: 10.1002/jcb.25883
141. Najm A, Masson FM, Preuss P, Georges S, Ory B, Quillard T, et al. MicroRNA-17-5p Reduces Inflammation and Bone Erosions in Mice With Collagen-Induced Arthritis and Directly Targets the JAK/STAT Pathway in Rheumatoid Arthritis Fibroblast-Like Synoviocytes. *Arthritis Rheumatol* (2020) 72(12):2030–9. doi: 10.1002/art.41441
142. Stanczyk J, Ospelt C, Karouzakis E, Filer A, Raza K, Kolling C, et al. Altered Expression of microRNA-203 in Rheumatoid Arthritis Synovial Fibroblasts and its Role in Fibroblast Activation. *Arthritis Rheum.* (2011) 63(2):373–81. doi: 10.1002/art.30115
143. Sun W, Ma J, Zhao H, Xiao C, Zhong H, Ling H, et al. Resolvin D1 Suppresses Pannus Formation via Decreasing Connective Tissue Growth Factor Caused by Upregulation of miRNA-146a-5p in Rheumatoid Arthritis. *Arthritis Res Ther* (2020) 22(1):61. doi: 10.1186/s13075-020-2133-2
144. Zou Y, Xu S, Xiao Y, Qiu Q, Shi M, Wang J, et al. Long Noncoding RNA LERFS Negatively Regulates Rheumatoid Synovial Aggression and Proliferation. *J Clin Invest* (2018) 128(10):4510–24. doi: 10.1172/JCI97965
145. Hu X, Tang J, Hu X, Bao P, Deng W, Wu J, et al. Silencing of Long Non-Coding RNA HOTTIP Reduces Inflammation in Rheumatoid Arthritis by Demethylation of SFRP1. *Mol Ther Nucleic Acids* (2020) 19:468–81. doi: 10.1016/j.omtn.2019.11.015
146. Qin W, Wang TH, Xie BH, Sun QQ, Huang H, Zhao BJ, et al. Plasma Long Non-Coding RNA Expression Profiles in Patients With Rheumatoid Arthritis. *Clin Lab* (2019) 65(8):1–15. doi: 10.7754/Clin.Lab.2019.190144
147. Tang J, Yi S, Liu Y. Long non-Coding RNA PVT1 can Regulate the Proliferation and Inflammatory Responses of Rheumatoid Arthritis Fibroblast-Like Synoviocytes by Targeting microRNA-145-5p. *Hum Cell* (2020) 33(4):1081–90. doi: 10.1007/s13577-020-00419-6
148. Qing P, Liu Y. Inhibitory Role of Long non-Coding RNA OIP5-AS1 in Rheumatoid Arthritis Progression Through the microRNA-448-Paraoxonase 1-Toll-Like Receptor 3-Nuclear Factor κb Axis. *Exp Physiol* (2020) 105(10):1708–19. doi: 10.1113/EP088608

149. Yan S, Wang P, Wang J, Yang J, Lu H, Jin C, et al. Long Non-Coding RNA HIX003209 Promotes Inflammation by Sponging miR-6089 *via* TLR4/NF-κb Signaling Pathway in Rheumatoid Arthritis. *Front Immunol* (2019) 10:2218. doi: 10.3389/fimmu.2019.02218
150. Lee A, Qiao Y, Grigoriev G, Chen J, Park-Min KH, Park SH, et al. Tumor Necrosis Factor α Induces Sustained Signaling and a Prolonged and Unremitting Inflammatory Response in Rheumatoid Arthritis Synovial Fibroblasts. *Arthritis Rheum.* (2013) 65(4):928–38. doi: 10.1002/art.37853
151. Loh C, Park SH, Lee A, Yuan R, Ivashkiv LB, Kalliolias GD. TNF-Induced Inflammatory Genes Escape Repression in Fibroblast-Like Synoviocytes: Transcriptomic and Epigenomic Analysis. *Ann Rheum. Dis* (2019) 78 (9):1205–14. doi: 10.1136/annrheumdis-2018-214783
152. Pratt AG, Siebert S, Cole M, Stocken DD, Yap C, Kelly S, et al. Targeting Synovial Fibroblast Proliferation in Rheumatoid Arthritis (TRAFIC): An Open-Label, Dose-Finding, Phase 1b Trial. *Lancet Rheumatol* (2021) 3 (5):337–46. doi: 10.1016/S2665-9913(21)00061-8
153. Liu H, Huang Q, Shi B, Eksarko P, Temkin V, Pope RM. Regulation of Mcl-1 Expression in Rheumatoid Arthritis Synovial Macrophages. *Arthritis Rheum.* (2006) 54(10):3174–81. doi: 10.1002/art.22132
154. Alessi F, Quarta S, Savio M, Riva F, Rossi L, Stivala LA, et al. The Cyclin-Dependent Kinase Inhibitors Olomoucine and Roscovitine Arrest Human Fibroblasts in G1 Phase by Specific Inhibition of CDK2 Kinase Activity. *Exp Cell Res* (1998) 245(1):8–18. doi: 10.1006/excr.1998.4216
155. Okada Y, Wu D, Trynka G, Raj T, Terao C, Ikari K, et al. Genetics of Rheumatoid Arthritis Contributes to Biology and Drug Discovery. *Nature* (2014) 506(7488):376–81. doi: 10.1038/nature12873
156. Perlman H, Bradley K, Liu H, Cole S, Shamiyeh E, Smith RC, et al. IL-6 and Matrix Metalloproteinase-1 are Regulated by the Cyclin-Dependent Kinase Inhibitor P21 in Synovial Fibroblasts. *J Immunol* (2003) 170(2):838–45. doi: 10.4049/jimmunol.170.2.838
157. Hiltbrunner S, Britschgi C, Schuberth P, Bankel L, Nguyen-Kim TDL, Gulati P, et al. Local Delivery of CAR T Cells Targeting Fibroblast Activation Protein is Safe in Patients With Pleural Mesothelioma: First Report of FAPME, a Phase I Clinical Trial. *Ann Oncol* (2021) 32(1):120–1. doi: 10.1016/j.annonc.2020.10.474
158. Aghajanian H, Kimura T, Rurik JG, Hancock AS, Leibowitz MS, Li L, et al. Targeting Cardiac Fibrosis With Engineered T Cells. *Nature* (2019) 573 (7774):430–3. doi: 10.1038/s41586-019-1546-z
159. Klein K, Kabala PA, Grabiec AM, Gay RE, Kolling C, Lin LL, et al. The Bromodomain Protein Inhibitor I-BET151 Suppresses Expression of Inflammatory Genes and Matrix Degrading Enzymes in Rheumatoid Arthritis Synovial Fibroblasts. *Ann Rheum. Dis* (2016) 75(2):422–9. doi: 10.1136/annrheumdis-2014-205809
160. Angiolilli C, Kabala PA, Grabiec AM, Van Baarsen IM, Ferguson BS, García S, et al. Histone Deacetylase 3 Regulates the Inflammatory Gene Expression Programme of Rheumatoid Arthritis Fibroblast-Like Synoviocytes. *Ann Rheum. Dis* (2017) 76(1):277–85. doi: 10.1136/annrheumdis-2015-209064

Conflict of Interest: The authors declare that the research was conducted in the absence of any commercial or financial relationships that could be construed as a potential conflict of interest.

Publisher's Note: All claims expressed in this article are solely those of the authors and do not necessarily represent those of their affiliated organizations, or those of the publisher, the editors and the reviewers. Any product that may be evaluated in this article, or claim that may be made by its manufacturer, is not guaranteed or endorsed by the publisher.

Copyright © 2021 Kemble and Croft. This is an open-access article distributed under the terms of the Creative Commons Attribution License (CC BY). The use, distribution or reproduction in other forums is permitted, provided the original author(s) and the copyright owner(s) are credited and that the original publication in this journal is cited, in accordance with accepted academic practice. No use, distribution or reproduction is permitted which does not comply with these terms.

frontiers in Immunology

ORIGINAL RESEARCH
published: 10 September 2021
doi: 10.3389/fimmu.2021.712948

High Na^+ Environments Impair Phagocyte Oxidase-Dependent Antibacterial Activity of Neutrophils

Luka Krampert[1†], Katharina Bauer[1†], Stefan Ebner[1,2†], Patrick Neubert[1], Thomas Ossner[1], Anna Weigert[1], Valentin Schatz[1], Martina Toelge[1], Agnes Schröder[3], Martin Herrmann[4], Markus Schnare[5], Anca Dorhoi[6,7] and Jonathan Jantsch[1]*

[1] Institute of Clinical Microbiology and Hygiene, University Hospital of Regensburg and University of Regensburg, Regensburg, Germany, [2] Max Planck Institute (MPI) of Biochemistry, Martinsried, Germany, [3] Institute of Orthodontics, University Hospital of Regensburg, Regensburg, Germany, [4] Department of Internal Medicine 3-Rheumatology and Immunology and Deutsches Zentrum für Immuntherapie, Friedrich-Alexander-University Erlangen-Nürnberg, University Hospital Erlangen, Erlangen, Germany, [5] Department of Immunology, Philipps University Marburg, Marburg, Germany, [6] Institute of Immunology, Friedrich-Loeffler Institut, Greifswald, Germany, [7] Faculty of Mathematics and Natural Sciences, University of Greifswald, Greifswald, Germany

Infection and inflammation can augment local Na^+ abundance. These increases in local Na^+ levels boost proinflammatory and antimicrobial macrophage activity and can favor polarization of T cells towards a proinflammatory Th17 phenotype. Although neutrophils play an important role in fighting intruding invaders, the impact of increased Na^+ on the antimicrobial activity of neutrophils remains elusive. Here we show that, in neutrophils, increases in Na^+ (high salt, HS) impair the ability of human and murine neutrophils to eliminate *Escherichia coli* and *Staphylococcus aureus*. High salt caused reduced spontaneous movement, degranulation and impaired production of reactive oxygen species (ROS) while leaving neutrophil viability unchanged. High salt enhanced the activity of the p38 mitogen-activated protein kinase (p38/MAPK) and increased the interleukin (IL)-8 release in a p38/MAPK-dependent manner. Whereas inhibition of p38/MAPK did not result in improved neutrophil defense, pharmacological blockade of the phagocyte oxidase (PHOX) or its genetic ablation mimicked the impaired antimicrobial activity detected under high salt conditions. Stimulation of neutrophils with phorbol-12-myristate-13-acetate (PMA) overcame high salt-induced impairment in ROS production and restored antimicrobial activity of neutrophils. Hence, we conclude that high salt-impaired PHOX activity results in diminished antimicrobial activity. Our findings suggest that increases in local Na^+ represent an ionic checkpoint that prevents excessive ROS production of neutrophils, which decreases their antimicrobial potential and could potentially curtail ROS-mediated tissue damage.

Keywords: sodium, phagocyte oxidase, infection, neutrophils, reactive oxygen species

OPEN ACCESS

Edited by:
Sylvain Perruche, Institut National de la Santé et de la Recherche Médicale (INSERM), France

Reviewed by:
Cristián A. Amador, Autonomous University of Chile, Chile
Pedro Elias Marques, KU Leuven, Belgium

****Correspondence:***
Jonathan Jantsch
Jonathan.Jantsch@ukr.de

[†]These authors have contributed equally to this work

Specialty section:
This article was submitted to Inflammation, a section of the journal Frontiers in Immunology

Received: *21 May 2021*
Accepted: *04 August 2021*
Published: *10 September 2021*

Citation:
Krampert L, Bauer K, Ebner S, Neubert P, Ossner T, Weigert A, Schatz V, Toelge M, Schröder A, Herrmann M, Schnare M, Dorhoi A and Jantsch J (2021) High Na^+ Environments Impair Phagocyte Oxidase-Dependent Antibacterial Activity of Neutrophils. Front. Immunol. 12:712948. doi: 10.3389/fimmu.2021.712948

INTRODUCTION

High salt diets (1, 2), renal impairment (3–6), inflammation, and infection (7–11) can induce Na^+ accumulation in skin tissues that can be simulated by addition of approximately 40 mM NaCl to standard cell culture media (= high salt condition, HS) (2, 8, 12, 13). In addition to skin, other organs such as liver, spleen and thymus can display enhanced Na^+ levels [reviewed in: (14)]. Although the mechanisms that govern local Na^+ accumulation are still elusive [reviewed in: (14)], it became clear in the last years that these increases in Na^+ and other ions impact the biology of various immune cells [reviewed in: (14–19)] and serve as 'ionic checkpoints' (20) in immunity.

Increases in Na^+ favor the polarization of T cells towards an inflammatory Th17 phenotype (10, 21–23). In macrophages, HS in combination with inflammatory stimuli leads to enhanced pro-inflammatory activation and increased antimicrobial capacity (8, 12, 13, 24, 25), while limiting their regulatory features (26–29). Mechanistically, this HS-boosted proinflammatory macrophage activation requires osmoprotective signaling involving the mitogen-activated protein kinase (MAPK) p38 and the transcription factor 'nuclear factor of activated T cells 5' (NFAT5/TonEBP), an emerging modulator in immunity [reviewed in: (30, 31)]. This signaling circuit is crucial in renal defenses against uropathogenic *Escherichia coli* [UPEC, (32)] under regular diet conditions as well as in cutaneous macrophage-driven antimicrobial responses against the protozoan parasite *Leishmania major* under experimental HS diet (8).

Effects of HS on polymorphonuclear leukocytes (PMN) are less clear. PMN are promptly recruited to the site of infection and contribute to warding off pathogens [reviewed in: (33)] but also to pathology [reviewed in: (34)]. Several studies reveal that HS can boost PMN activity (35–37), whereas other results indicate impairment in inflammatory activity and activation of PMN (35, 38–45). In line with the disparate findings regarding the impact of HS on neutrophil activation, the effects of HS on antibacterial capacity of PMN are not fully understood. Increases in extracellular Na^+ either impair (46, 47), augment (36) or do not affect the antimicrobial activity of neutrophils (25). Moreover, the underlying mechanisms contributing to these divergent outcomes remain elusive.

Here, we show that HS diminishes the antimicrobial activity of human and murine PMN against *E. coli*. Mechanistically, reduced bactericidal activity is due to impairment of the neutrophil enzyme nicotinamide adenine dinucleotide phosphate (NADPH) oxidase (PHOX) and subsequently reduced ROS production.

MATERIAL AND METHODS

Reagents and Antibodies

NaCl was purchased from Merck. *E. coli* (HB101 laboratory strain) (48) and *E. coli-GFP* harboring pWRG167 (12) were kept on Mueller Hinton agar II plates. *S. aureus* (ATCC 29213) was kept on Columbia sheep blood plus agar plates. Bacterial overnight liquid cultures were generated in LB media. All *in vitro* experiments were performed in RPMI media (Gibco; # 618700044) containing 10% fetal calf serum (FCS; Sigma, #F7524). We purchased phorbol-12-myristate-13-acetate (PMA; #P1585), N-formylmethionyl-leucyl-phenylalanine (fMLP; #F3506), and diphenyleneiodonium chloride (DPI; #D2926) from Sigma and SB203580 (#tlrl-sb20) from Invivogen. For western blotting, we used rabbit-anti-phospho-p38 mouse (Cell Signaling Technology, #4511S) and mouse-anti-Vinculin (BioRad, #V284) primary antibodies. As secondary antibody, we used HRP-conjugated swine-anti-rabbit and goat-anti-mouse antibodies (Dako). For flow cytometry, we stained cells using Brilliant violet 421 anti-human CD62L (BioLegend, #304828), APC anti-human CD11b (BioLegend, #301350), Pacific-Blue anti-human CD66b (BioLegend, #305112), PE anti-human CD35 (BioLegend, #333406) antibodies. For confocal microscopy, we used the rabbit-anti-myeloperoxidase (Agilent, #A039829-2) primary antibody, the donkey-anti-rabbit-Cy5 conjugated (Dianova, #711-606-152) secondary antibody and the Phalloidin AF-647 (Thermo Fisher, #A22287) marker.

PMN Isolation and Infection

We obtained peripheral blood from healthy donors and employed established standard procedures (49–51) in order to isolate PMN from peripheral blood by density gradient centrifugation using Lymphoflot (Bio-Rad, #824012). After hypotonic lysis of erythrocytes, the remaining PMN were adjusted to 250 000 cells per well and incubated for 1 h at 37°C, 5% CO_2 in 24-well plates. If DPI was used, 3 µM of DPI was added 30 min prior to stimulation. Subsequently, 40 mM NaCl (= high salt, HS) or mannitol was added where indicated. Together with the standard cell culture media conditions (= normal salt, NS), they were additionally incubated for 1 h. Cells were infected with *E. coli* at a multiplicity of 1 (MOI 1) and centrifuged to synchronize the infection. For infection with *S. aureus* (MOI 1), bacteria were opsonized with 20% human serum AB male (Biowest). Where indicated, 10 ng/ml PMA was added at this stage. Infection was terminated after 1 h - 1.5 h by addition of 400 µl cold PBS. Subsequently, serial dilutions were generated and plated on Mueller Hinton agar II plates. After overnight incubation, colony forming units (CFU) were counted and normalized to the mean of the respective NS group.

PBMC Isolation and Infection

We obtained peripheral blood from healthy donors and isolated peripheral blood mononuclear cells (PBMC) by density gradient centrifugation using Lymphoflot (Bio-Rad). PBMC were washed twice with PBS and adjusted to 250 000 cells per well in 24-well plates. PBMC infection was performed as described previously in murine macrophages (12). Briefly, cells were infected with *E. coli* (MOI 100) and subjected to gentamicin protection assays. After 2 h of infection, cells were lysed with PBS containing 0.1% Triton-X (PanReac AppliChem, #9036-19-5) and 0.05% Tween-80 (Sigma, #8.22187.0500) and serial dilutions were plated on Mueller Hinton agar II plates. CFU were counted and normalized to the mean of the respective NS group.

Murine Granulocyte Isolation and Infection

We obtained femurs and tibiae from C57BL/6 wildtype (WT) and *Cybb*$^{-/-}$ mice (including the respective controls) (52) and flushed the bone marrow using microlances (13 gauge, BD) and syringes (BD). Erythrocyte lysis was performed using ACK buffer (0.1 mM EDTA, 10 mM $KHCO_3$, 150 mM NH_4Cl, pH 7.3-7.5 in H_2O_{dd}) for 10 min at room temperature. Subsequently, cells were washed and passed through a 100 µm cell strainer, before they were resuspended in MACS buffer (0.5% BSA, 2 mM EDTA, pH 7.2 in PBS). We purified neutrophils by negative magnetic selection using the 'Neutrophil isolation Kit' (Miltenyi Biotec, #130-097-658) according to the manufacturer's instructions. Infection of murine granulocytes was performed as described above but with MOI 0.1.

BMDM Generation and Infection

Bone marrow-derived macrophages (BMDM) were generated in Teflon-bags using L929 supernatant as described earlier (53). Infection experiments (MOI 100) were performed as described above or previously (12).

Peritoneal Cell Purification and Infection

We induced a sterile inflammatory response by injecting thioglycollate (Sigma, #B2551) in the peritoneal cavity (54, 55). PMN were isolated with cold PBS from the peritoneum one day after injection. Erythrocyte lysis was performed using ACK buffer for 10 min at room temperature. Subsequently, cells were washed and PMN infection experiments were performed as described earlier. 4 days after induction of peritoneal inflammation by injection of thioglycollate, peritoneal macrophages (pMΦ) were obtained essentially as described earlier (56, 57). After 10 min of erythrocyte lysis using ACK buffer at room temperature, peritoneal cells were washed, seeded and incubated for 1-2 h before we eliminated nonadherent cells by washing. Then macrophage infection experiments were performed as described previously (12).

Immunofluorescence Microscopy

PMN were isolated as described above and seeded on gelatin/fibronectin (Sigma, #F1141) pre-coated coverslips. After 2 h of incubation, cells were infected as described earlier, but with *E. coli-GFP* (MOI 1). 1 h post infection, cells were fixed with 4% PFA (Sigma, #1.04003.1000; diluted in PBS) overnight. The next day, cells were permeabilized (PBS with 2% BSA and 0.1% Saponin) and stained with anti-Phalloidin AF-647 antibody for 1 h, followed by 30 min incubation with the secondary antibody and subsequent mounting of the slides with Prolong Gold containing DAPI (Invitrogen, #P36931). Images were collected with a Leica TCS SP5 confocal laser scanning microscope and processed using the Leica Application Suite (version 2.7.3.9723). Bacterial load was analyzed in Fiji (58).

Analysis of Neutrophil Extracellular Traps

Formation of neutrophil extracellular traps (NETs) was analyzed *via* confocal microscopy, as described elsewhere (59) with minor modifications. PMN were isolated and seeded on gelatin/fibronectin pre-coated coverslips. Subsequently, 40 mM NaCl was added to the HS conditions and, together with the NS conditions, cells were additionally incubated for 1 h. Then, cells were infected as described above, but with MOI 10, and further incubated for 1 or 4 h. Infection was terminated and cells were fixed with 4% PFA overnight. The next day, cells were blocked in PBS containing 10% FCS and stained with anti-myeloperoxidase (MPO) antibody for 1 h, followed by 30 min incubation with the secondary antibody and subsequent mounting of the slides as described above. Images were collected with a Leica TCS SP5 confocal laser scanning microscope and processed using the Leica Application Suite (version 2.7.3.9723). Analysis of NET formation was performed by Fiji (58), calculating the ratio of MPO-positive (NET marker) and DAPI-positive (cellular DNA) signal in each condition.

Cytokine Release Measurements

PMN were isolated and infected as described above. In these experiments, supernatants were kept and analyzed by Luminex® (Austin, USA) for quantification of bactericidal/permeability increasing protein (BPI) and IL-8 as described earlier (60, 61). Mean fluorescence intensities (MFI) were acquired using the Luminex xMAP 100 system (Luminex Corp).

Cell Viability Assays

Cell viability was assessed by Annexin V (BD Biosciences, #550475)/Propidium iodide (PI, Sigma-Aldrich, P4864) staining. PMN were isolated and infected as described above. Then, cells were washed and stained with Annexin V/PI, according to 'BD Biosciences' protocol. In detail, PMN were washed with cold PBS, adjusted to 10^6 cells/ml in 1x Binding Buffer (10x, BD Biosciences, #556 454) and stained for 15 min. Analysis was performed using a FACS Canto II flow cytometer (BD). MFI were calculated by FlowJo software (version 10).

Western Blotting

For analysis of pp38 abundance, PMN were lysed in RIPA buffer (25 mM sodium deoxycholate, 1% SDS, 0.4% EDTA, 10 mM NaF, 1% NP 40 in H_2O_{dd}) containing complete protease inhibitors (Roche, #1183617001) and PhosphoStop (Roche, #04906837001). After homogenization, proteins were separated on a 13% polyacrylamide gel and subsequently blotted on PVDF membranes (Merck, IPFL 00010). Images were acquired using Luminata Forte HRP substrate (Millipore, #WBLUF0500) on a Chemo Star imager (Intas).

Mobility Assays

For the detection of spontaneous (undirected) movement, PMN were isolated as described above and seeded in 8-well IBIDI live cell chamber slides (200 000 cells per well). Chambers were incubated at 37°C, 5% CO_2 for 1 h. Subsequently, 40 mM NaCl was added where indicated (= high salt, HS). After 1 h of additional incubation, cells were infected with *E. coli* at a multiplicity of 1 (MOI 1) and 10 ng/ml PMA was added where indicated. The chamber was immediately placed on a Leica SP5 confocal laser scanning microscope in a pre-heated (37°C) environment. Prior to and during the measurement,

temperature was controlled by 'The cube' (Life Imaging Services), keeping the cell environment at 37°C. Cells were recorded for 30 min by acquiring pictures in 10 s intervals. Assessment of cell mobility was performed by Fiji plugin 'manual cell tracker' analyzing 19-20 cells per video which showed at least a minimal movement. PMN migration was not given in µm but in arbitrary units (a. u.) since our experimental setup does not allow for reliable detection of cell movement in the z-axis.

Direct PMN migration towards fMLP was analyzed with the QCM Chemotaxis Cell Migration Assay (Sigma, #ECM504) according to the manufacturers' instructions. Briefly, PMN were isolated as described above and seeded in 24-well plates (500 000 cells per well) in serum-free medium. After 30 min incubation at 37°C, 5% CO_2, 40 mM NaCl was added where indicated and cells were incubated further for 1 h. Subsequently, PMN were washed twice in RPMI medium containing 0.5% BSA and adjusted to 10^6 cells/ml. Based on the Boyden chamber assay principle (62, 63), 250 µl cell suspension were added into each insert and 300 µl serum-free media ± 1 µM fMLP were added into the lower chamber. HS was added where indicated to each insert and lower chamber. The plate was incubated for 4 h at 37°C, 5% CO_2, then the inserts were removed and 200 µl cell suspension with migrated cells was transferred from the lower chamber to a 96-well plate. 20 µl of WST-1 dye solution was added to each well and PMN were incubated for 2 h before fluorescence was measured using a microplate reader (Bio-Rad).

Quantification of Reactive Oxygen Species

We used luminol-enhanced chemiluminescence for ROS quantification as described earlier (49). PMN were isolated as described above, seeded in 24-well plates (250 000 cells per well) and incubated for 30 min at 37°C, 5% CO_2. Subsequently, where indicated, cells were treated with 3 µM DPI for additional 30 min. After that incubation period, 40 mM NaCl was added to the media and incubated for additional 1 h. Following this step, cells were transferred into FACS tubes, washed and resuspended in HBSS containing luminol (Sigma, #A8511) ± 40 mM NaCl and incubated for additional 15 min at 37°C, 5% CO_2. ROS formation was induced upon stimulation with 1 µM fMLP and the measurement of ROS production using a Lumat^3 LB 9507 Tube Luminometer (Berthold Technologies) was started (2 s interval). Where indicated, 10 ng/ml PMA was added simultaneously with fMLP.

Flow Cytometry

After PMN isolation, 250 000 cells per well were seeded in 24-well plates and incubated at 37°C, 5% CO_2 for 1 h. 40 mM NaCl was added to the HS condition and cells were incubated again for 1 h. Cells were subsequently infected with *E. coli* (MOI 1) for 1 h. Infection was stopped by addition of 500 µl cold PBS. Media including cells and bacteria were transferred into FACS tubes and centrifuged. Cells were resuspended in 500 µl FACS buffer (PBS containing FCS, EDTA and NaN_3) and stained either with anti-CD35 (also known as complement receptor type 1, CR1) and anti-CD66b (carcinoembryonic antigen-related cell adhesion molecule 8, CEACAM8) or with anti-CD11b (complement receptor type 3, CR3) and anti-CD62L (L-Selectin) antibodies for 30 min at 4°C, respectively. Cells were washed and resuspended in 200 µl FACS buffer and recorded using a FACS Canto II flow cytometer (BD). MFI were calculated by FlowJo software (version 10).

Statistics

All data are presented as means ± standard error of mean (s.e.m.) unless indicated otherwise. In all experiments (unless indicated otherwise), 'n' denotes separate wells from at least two independent experiments. Graphs and statistics were carried out by GraphPad Prism (v.6.0 or 8.0). In IL-8 quantifications and Boyden chamber assays, we used ROUT to identify outliers. Data was analyzed regarding normal distribution using the Kolmogorov-Smirnov test and compared by Student's two-tailed t tests with Welch's correction (for normally distributed data sets) or Mann-Whitney U tests (for non-normally distributed data sets), respectively. When two or more groups were compared, normally distributed data sets were analyzed by one-way ANOVA with Bonferroni's multiple-comparison test, whereas the Kruskal-Wallis test with subsequent Dunn multiple-comparison test was used for non-normally distributed data. Area under the curve (AUC) calculations were carried out with the AUC tool of GraphPad Prism (v.6.0 or 8.0), as described earlier by Gagnon et al. (64). We considered p-values < 0.05 as statistically significant (*).

RESULTS

High Extracellular Na^+ Impairs Antibacterial Activity of Murine and Human Neutrophils

As demonstrated earlier (8, 12, 13, 65), addition of 40 mM NaCl to standard cell culture media (= high salt, HS) increased the antimicrobial activity of murine BMDM against *E. coli* (**Figure 1A**). In contrast, however, HS conditions impaired the antibacterial activity of bone marrow-derived murine neutrophils (BMN) (**Figure 1B**). Likewise, HS boosted antimicrobial activity of murine peritoneal macrophages (pMΦ; **Figure 1C**) and diminished the bactericidal activity of murine peritoneal elicited neutrophils (pPMN; **Figure 1D**). In accordance with these findings obtained from murine cells, HS augmented the antibacterial activity of human peripheral blood mononuclear cells (PBMC; **Figure 1E**) and, again, decreased the antibacterial activity of human PMN isolated from peripheral blood (**Figure 1F**). Moreover, HS not only impaired PMN clearance of *E. coli*, but also of Gram-positive *S. aureus* (**Figure 1G**). Of note, increases of osmolality and tonicity using mannitol did not impair the antibacterial activity of human PMN directed against *E. coli* or *S. aureus* (**Figure S1**). Annexin V/propidium iodide (PI) stainings of uninfected and infected PMN revealed no differences in the fraction of viable (Annexin V^-/PI^-) cells between NS or HS conditions (**Figure 1H**), suggesting that HS did not affect the cellular viability. In line with this, confocal microscopy revealed more GFP-labelled *E. coli* in infected PMN under HS conditions

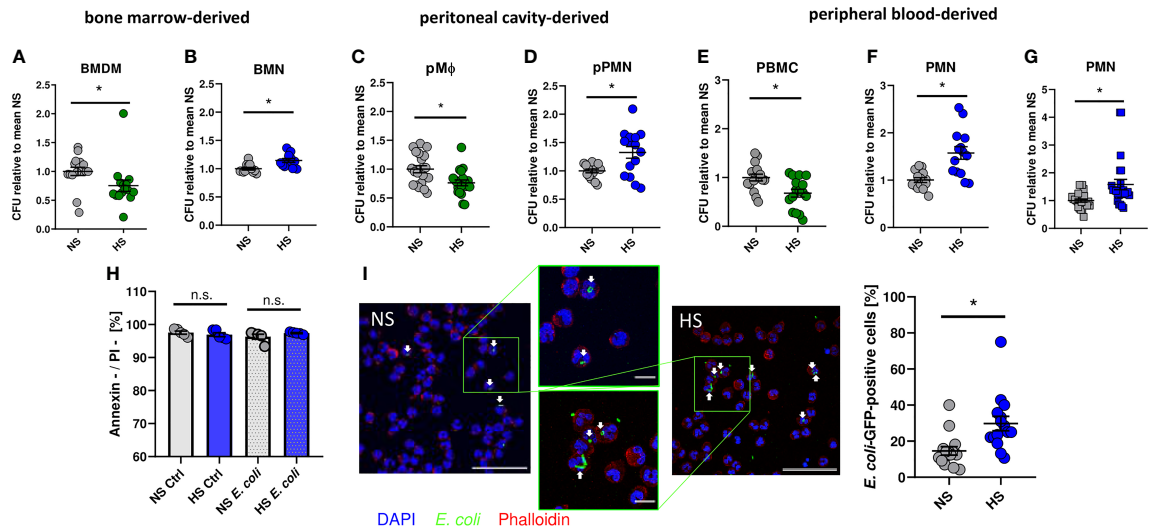

FIGURE 1 | High salt impairs bacterial killing of neutrophils. Antibacterial activity of **(A)** murine bone marrow-derived macrophages (BMDM; means ± s.e.m.; n = 15-16; Mann-Whitney test; *p < 0.05), **(B)** murine bone marrow-derived neutrophils (BMN; means ± s.e.m.; n = 12; Mann-Whitney test; *p < 0.05), **(C)** murine peritoneal macrophages (pMΦ; means ± s.e.m.; n = 20; Student's t test; *p < 0.05), **(D)** murine peritoneal neutrophils (pPMN; means ± s.e.m.; n = 15; Student's t test with Welch's correction; *p < 0.05), **(E)** human peripheral blood mononuclear cells (PBMC; means ± s.e.m.; n = 16; Student's t test; *p < 0.05) and **(F)** human peripheral blood neutrophils (PMN, means ± s.e.m.; n = 14; Student's t test with Welch's correction; *p < 0.05) infected with *E. coli* under NS or HS (NS + 40 mM NaCl) conditions. **(G)** Antibacterial activity of PMN infected with *S. aureus* (means ± s.e.m.; n = 24; Mann-Whitney test; *p < 0.05). **(H)** Cell viability by Annexin/PI staining in uninfected (Ctrl) and *E.coli*-infected PMNs (means ± s.e.m.; n = 5; Student's t test and Mann-Whitney test; n.s., not significant; *p < 0.05). **(I)** Infection rate in PMN 1 h after *E. coli*-infection; Bacterial load under NS or HS conditions, intracellular bacteria marked by arrowheads. A representative image out of three independent experiments is displayed. *E. coli-GFP*, green; Phalloidin, red; DAPI (DNA), blue. Scale bar: 50 µm (means ± s.e.m.; n = 15; Mann-Whitney test; *p < 0.05).

(**Figure 1I**). This indicates that, in contrast to macrophages, HS impairs the antibacterial activity of murine and human PMN.

HS Exposure Impairs Neutrophil Mobility and Activation

In a next step, we investigated if the suppressive effect of HS is limited to their antimicrobial capacity or whether HS impairs additional PMN functions. For that purpose, we analyzed the expression of well-established cell surface markers to characterize neutrophil degranulation and activation status (66–70), which had been shown to be modified under HS conditions (40, 41, 43). HS interfered with the surface expression of CD35 (**Figure 2A**) and CD66b (**Figure 2B**), which are both markers for PMN degranulation (66, 67, 71, 72). This resulted in a reduced frequency of degranulated PMN under HS conditions (**Figure S2**). In line with this, HS conditions reduced the release of bactericidal/permeability increasing protein (BPI; **Figure 2C**), which is stored in primary (azurophilic) granules (73). HS conditions additionally diminished the expression of the complement receptor 3 (CR3, CD11b, **Figure 2D**), which is linked to PMN activation (68, 70, 74, 75). Moreover, HS-treated PMN displayed a higher surface expression of CD62L (**Figure 2E**; L-selectin), whose expression inversely correlates with the activation and migratory potential of PMN (76).

To analyze the impact of HS on the spontaneous movement capacity of PMN, we monitored the migratory trajectories of PMN using live cell imaging. Visualization and quantification of the migrated distance over 30 min revealed that HS conditions compromised the spontaneous movement of PMN (**Figure 2F**). Next, we performed Boyden chamber assays (62). In line with our previous findings, we found less spontaneous transmigration of HS-exposed PMN in the absence of a chemoattractant stimulus into the lower chamber. Interestingly, HS conditions did not impair the directed movement of PMN towards N-formylmethionyl-leucyl-phenylalanine (fMLP; **Figure 2G**) which is an established chemoattractant and proinflammatory activator of PMN (77–82). Taken together, these findings demonstrate that HS conditions not only interfere with the antimicrobial activity, but also diminish the overall activation status and spontaneous migratory capacity of PMN.

Elevated Extracellular Na^+ Levels Diminish ROS Production in Neutrophils

Next, we set out to identify how HS alters the antimicrobial effector function of PMN. Neutrophils can trap and kill bacteria within neutrophil extracellular traps (NETs) [reviewed in: (83, 84)]. NETs are composed of neutrophil-derived cellular DNA, which serves as a scaffold for antimicrobial granule proteins such as the myeloperoxidase (MPO) (85). Extracellular MPO abundance can be used as a measure of NET formation (86). By confocal microscopy, we quantified extracellular MPO levels in infected PMN. In line with earlier findings (87), we did not detect NET formation at early time points (**Figure 3A**) under NS and HS conditions, while there was robust NET formation at 4 h after infection which was independent of extracellular Na^+ levels

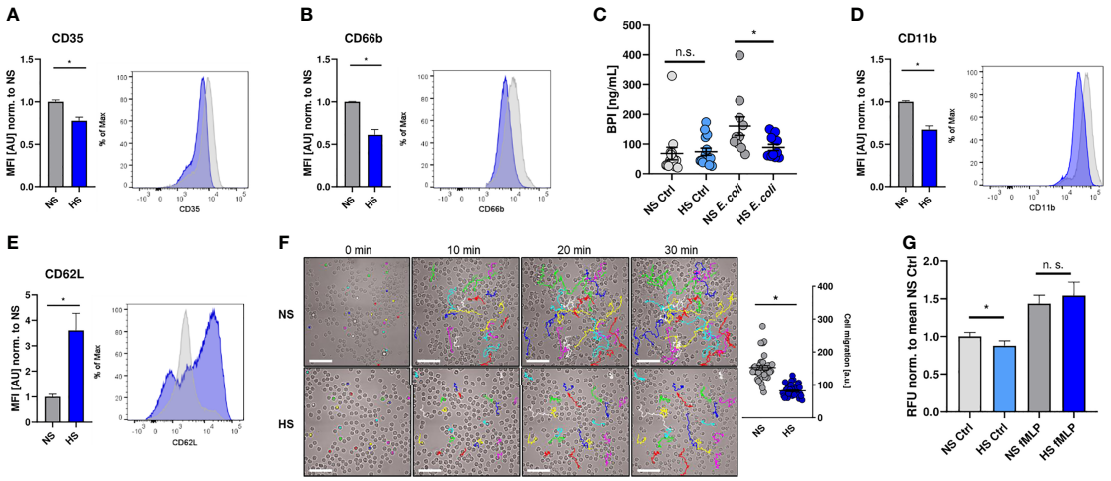

FIGURE 2 | High salt diminishes cell activation and migration. **(A, B)** Flow cytometry analysis of surface expression of CD35 and CD66b on infected PMN 1 h post infection (means ± s.e.m.; n = 10; Student's t test with Welch's correction and Mann-Whitney test; *p < 0.05). **(C)** Extracellular bactericidal/permeability increasing protein (BPI) levels of control and infected (*E. coli*) PMN under NS or HS conditions (means ± s.e.m, n = 10-15; Mann-Whitney test; n.s., not significant; *p < 0.05). **(D, E)** As **(A, B)**, but surface expression of CD11b and CD62L was analyzed (means ± s.e.m.; n = 10; Student's t test with Welch's correction and Mann-Whitney test; *p < 0.05). **(F)** Spontaneous movement of PMN [given in arbitrary units (a. u.)] upon *E. coli*-infection under NS or HS conditions. Scale bar: 50 µm (means ± s.e.m.; n = 40; each dot represents individual cell traces from two independent experiments; Mann-Whitney test; *p < 0.05). **(G)** Spontaneous and directed movement towards fMLP of PMN measured by Boyden chamber assays (means ± s.e.m.; n = 15-17; Student's t test and Mann-Whitney test; n.s., not significant; *p < 0.05).

(**Figure 3B**). Hence, we conclude that HS conditions did not affect NET-dependent antimicrobial activity of PMN.

In macrophages and PMN, exposure to HS augments the activation of the osmoprotective p38/MAPK signaling pathway (8, 35). In accordance to these reports, we found that HS enhanced the phosphorylation of p38/MAPK in neutrophils (**Figure 3C**). HS-boosted p38/MAPK was linked to IL-8 release in PBMC (88). In line with this, we found that HS increased the IL-8 release from PMN (**Figure 3D**). Since p38/MAPK was required for HS-boosted antimicrobial function in macrophages (8, 12), we wanted to

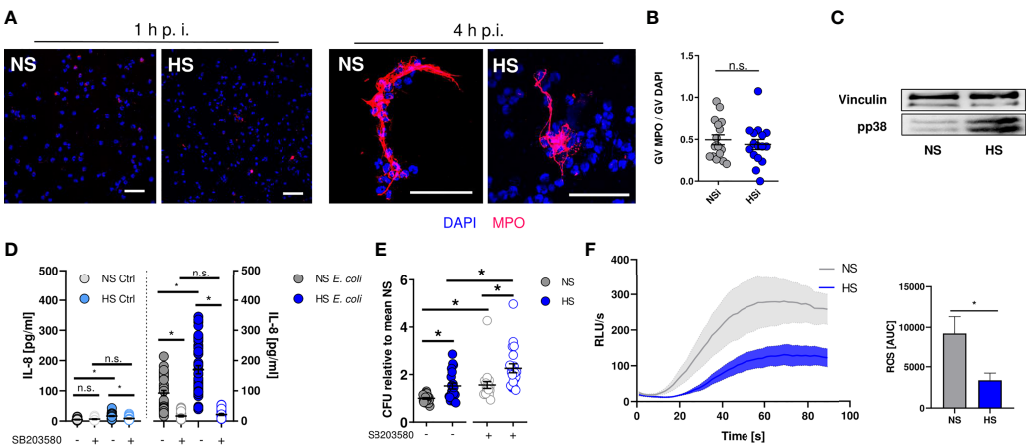

FIGURE 3 | Elevated Na^+ decreases ROS production, independent of NET formation or p38/MAPK signaling. **(A, B)** Staining of extracellular myeloperoxidase (MPO) **(A)** 1 h or **(B)** 4 h after *E. coli*-infection of PMN. A representative image out of three independent experiments is displayed. MPO, red; DAPI (DNA), blue. Scale bar: 50 µm. Gray value analysis of MPO positive NETs (means ± s.e.m.; n = 16; each dot represents an individual confocal image from three independent experiments; Student's t test; n.s., not significant). **(C)** Representative phospho-p38/MAPK and vinculin immunoblot of PMN 30 min after *E. coli* infection out of three independent experiments. **(D)** IL-8 in the supernatant of control and infected PMN under NS or HS conditions ± p38-inhibitor SB203580 (means ± s.e.m.; n = 25-45; Kruskal-Wallis test with subsequent Dunn multiple-comparison test; n.s., not significant; *p < 0.05). **(E)** Antibacterial activity of PMN 1.5 h after *E. coli*-infection ± p38 inhibitor SB203580 (means ± s.e.m.; n = 21; Kruskal-Wallis test with subsequent Dunn multiple-comparison test; *p < 0.05). **(F)** ROS production upon fMLP stimulation; Luminometric ROS detection; time curve and AUC values (means ± s.e.m.; n = 5; Student's t test; *p < 0.05).

assess bacterial elimination in PMN in the absence or presence of the pharmacological p38-inhibitor SB203580. Inhibition of p38/MAPK largely abolished HS-boosted IL-8 release (**Figure 3D**) and, in line with earlier findings (89, 90), impaired the antimicrobial activity of PMN under NS and HS conditions (**Figure 3E**). However, inhibition of p38/MAPK did not abolish the blunted antimicrobial activity under HS conditions (**Figure 3E**). This suggests that p38/MAPK-dependent signaling does not play a role in HS-impaired antimicrobial activity of PMN.

PHOX-dependent ROS production critically contributes to the antimicrobial activity of neutrophils [reviewed in: (33, 91)]. We measured ROS production for 90 s after fMLP-stimulation using continuous luminol measurements that allow for immediate detection of ROS over time (49). These assays revealed that HS conditions substantially diminished fMLP-triggered ROS production (**Figure 3F**), demonstrating that HS-mediated impairment of antibacterial PMN activity is independent of osmoprotective signaling and NET formation, possibly due to reduced ROS production.

Disturbed ROS Production Underlies Impaired Antimicrobial Activity in PMN Under HS Conditions

Therefore, we analyzed whether blocking ROS production in PMN using diphenyleneiodonium chloride (DPI) (92) mimics HS-induced attenuation of antibacterial activity. DPI-treatment diminished ROS production in PMN stimulated with fMLP under NS conditions (**Figure 4A**) and reduced the antibacterial activity of PMN under NS to levels obtained for PMN exposed to HS conditions (**Figure 4B**). Of note, HS did not further compromise the ability of PMN to fight *E. coli* (**Figure 4B**). This suggests that HS-triggered impairment of PHOX activity underlies the blunted antimicrobial PMN response. To corroborate this finding, we purified neutrophils from bone marrow of mice lacking the cytochrome b-245 subunit of PHOX (*Cybb*$^{-/-}$). We infected these cells with *E. coli* and analyzed their bactericidal activity. These experiments confirmed the previous findings using the pharmacological inhibitor DPI (**Figure 4C**). In a second approach, we wanted to test if increasing ROS production using phorbol-12-myristate-13-acetate (PMA) is able to rescue HS-impaired antimicrobial capacity of PMN. PMA is known to boost ROS production in PMN (92, 93). After additional stimulation with PMA, there was a robust increase in ROS production which was unaffected by HS exposure (**Figure 4D**). PMA-treatment normalized the blockade of HS on the migratory potential of PMN (**Figure 4E**). Of utmost importance, addition of PMA abolished the inhibitory effect of HS on the antimicrobial activity of PMN (**Figure 4F**). We conclude that HS-triggered impairment of ROS production in PMN underlies their disturbed antimicrobial activity under HS conditions.

DISCUSSION

Here, we demonstrate that a Na^+-rich environment curtails the expression of activation markers, spontaneous movement, and ROS production of PMN upon exposure to bacteria and bacterial

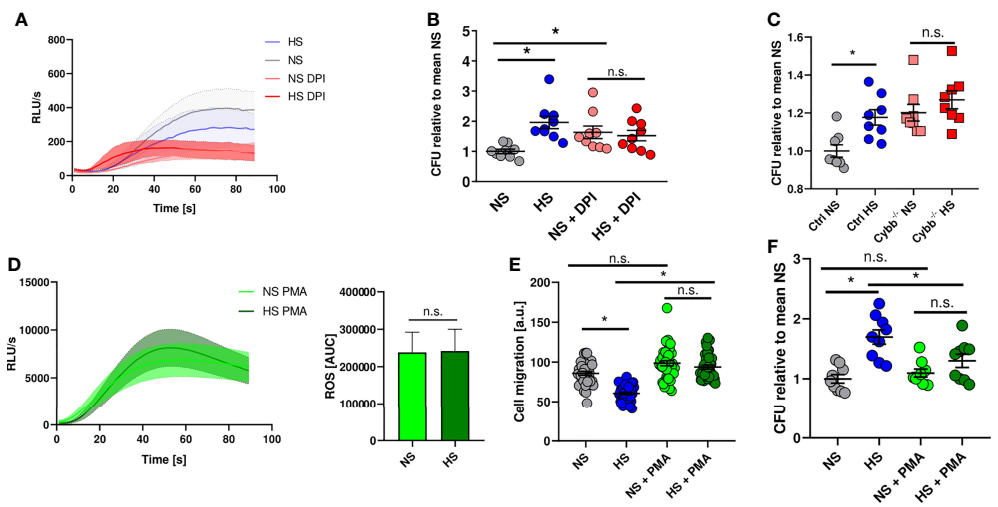

FIGURE 4 | NADPH oxidase inhibition mimics high salt effect while PMA abrogates high salt-induced killing deficiency. **(A)** ROS production in DPI pre-treated PMN under NS or HS conditions, stimulated with fMLP (means ± s.e.m.; n = 4-5). **(B)** Antibacterial activity of PMN 1.5 h after *E. coli*-infection ± PHOX-inhibitor (DPI; means ± s.e.m.; n = 9; Kruskal-Wallis test with subsequent Dunn multiple-comparison test; n.s., not significant; *p < 0.05). **(C)** Antibacterial activity of neutrophils from PHOX-deficient (*Cybb*$^{-/-}$) and control mice 1.5 h after *E. coli*-infection (means ± s.e.m.; n = 8; Mann-Whitney test; n.s., not significant; *p < 0.05). **(D)** ROS production in fMLP/PMA-stimulated PMN (PMA) under NS and HS conditions; time curve and AUC values (means ± s.e.m.; n = 8; Student's t test; n.s., not significant). **(E)** Cell migration (given as arbitrary units) upon PMA stimulation of *E. coli*-infected PMN under NS and HS conditions (means ± s.e.m.; n = 39-40; Kruskal-Wallis test with subsequent Dunn multiple-comparison test; n.s., not significant; *p < 0.05). **(F)** Antibacterial activity of PMN 1.5 h after *E. coli*-infection ± PMA-stimulation under NS or HS conditions (means ± s.e.m.; n = 9; ordinary one-way ANOVA with Bonferroni's *post hoc* test; n.s., not significant; *p < 0.05).

products which ultimately leads to diminished antimicrobial capacities of PMN. In contrast, simultaneous infection and increase of extracellular Na^+ reportedly triggers more ROS production in PMN and enhances antibacterial activity of PMN in this experimental system (36). Moreover, Junger et al. reported that exposure of PMN to HS after fMLP-stimulation did not affect ROS production (35). However, in line with our findings, other groups showed that stimulation of PMN after exposure to HS conditions caused disturbed assembly of PHOX (38), reduced ROS production (35, 37, 39), decreased expression of various surface markers related to human neutrophil activation (39–41, 43), and bacterial killing (46, 47). These findings suggest that the sequence of stimulation and Na^+ exposure critically influences the outcome of PMN activation.

If PMN are exposed to very high Na^+ environments (addition of 130 mM NaCl) this reportedly impaired migration towards an established chemoattractant (44). We, however, increased the Na^+ concentrations by addition of 40 mM NaCl in order to simulate Na^+ conditions that can be encountered in inflamed and infected skin tissues (7, 8, 10, 11). Although we found a reduced spontaneous migration of PMN upon exposure to increases in Na^+, these HS conditions did not affect chemotaxis. This indicates that local Na^+-rich environments that can be present in infected skin still allow for PMN infiltration into tissues if a chemoattractant such as fMLP is present. Since inflamed and infected skin tissues can display increased Na^+ levels (7, 8, 10, 11), it is likely that PMN pass through Na^+-rich environments before reaching the invading pathogen. Therefore, our findings might have relevance in migration of PMN through Na^+-rich environments and PMN-dependent clearance of bacteria from tissues.

Here, we confirm findings that HS impairs the antibacterial activity of PMN (46, 47). These studies (46, 47), however, assessed the effects of very high Na^+ levels that are present in the renal medulla (94). We, however, simulated moderate increases in Na^+ that can be encountered in inflamed and infected skin tissues (7, 8, 10, 11). Moreover, our studies provide mechanistic insights into how HS impairs antibacterial responses in PMN by pinning down antibacterial effectors disturbed by the addition of Na^+. In contrast to an earlier report (95), we did not detect any difference in viability upon HS exposure in our experimental setup. Therefore, we exclude cytotoxicity as cause of reduced antimicrobial activity. Further we interrogated processes and pathways relevant for microbial disposal in PMN. Oxidative killing is promptly triggered in PMN following microbial internalization. We observed reduced ROS release in HS-exposed PMN. Using pharmacological PHOX inhibitors, neutrophils from *Cybb*$^{-/-}$ mice, and pharmacological means to rescue HS-blunted ROS production, we demonstrated that HS impairs the antibacterial activity by dampening PHOX-dependent ROS production. From this finding, we would predict that the role of HS on the outcome of PMN-pathogen interaction depends on the susceptibility of the pathogen to ROS-dependent killing mechanisms. Indeed, HS did not affect the *in vitro* antimicrobial activity of PMN isolated from bone marrow directed against an uropathogenic *E. coli* (UPEC) (25), which is known to suppress oxidative burst in PMN and to be more resistant to reactive oxygen species than commensal strains (96). Moreover, in line with this reasoning, we found that HS diminished the antimicrobial control of PMN directed against *S. aureus*, whose control depends on PHOX-dependent ROS production (97).

NADPH oxidase-dependent ROS production [reviewed in: (98)] may trigger NET production or alternatively NETs require p38/MAPK (89, 99). Nadesalingam et al, who also demonstrated that increasing Na^+ availability decreases ROS production in PMN, showed that this is linked to impairment of NET formation (45). In our study, however, HS did not affect generation of NETs in PMN 4 h after *E. coli*-infection, indicating that ROS levels are not critical for casting of NETs in our experimental setup. Thus, a direct link of NET formation to HS-impaired antibacterial activity in our experiments is unlikely.

p38/MAPK activation contributes to cytokine release (including IL-8) by neutrophils (100), NADPH oxidase-dependent ROS production (101, 102) and subsequent antimicrobial activity of neutrophils under NS conditions (89, 90). In line with this, we found that p38/MAPK inhibition reduced antimicrobial activity of PMN and diminished HS-triggered or boosted IL-8 release. However, HS conditions diminished the antimicrobial activity of PMN in the absence or presence of pharmacological p38/MAPK blockade. This strongly suggests that the HS-impaired antimicrobial activity is not linked to HS-triggered modulation of p38/MAPK activity in PMN.

In sum, HS-mediated impairment of antimicrobial activity is due to blunted PHOX-dependent ROS production. The molecular mechanism that results in impaired PHOX-dependent ROS production requires further investigation. Our data strongly suggest that impaired ROS production is uncoupled from HS-modified p38/MAPK. It is possible that increases in Na^+ directly impair enzymatic PHOX activity. Since increases in Na^+ are known to affect the dynamics of the actin cytoskeleton (41) and Rac proteins that interact with the actin cytoskeleton [reviewed in: (103)] are required for proper PHOX activity [reviewed in: (104)], it is also possible that molecules involved in PHOX assembly, e.g. Rho GTPases, or rearrangement of the actin cytoskeleton could underlie our finding.

We published earlier that HS conditions led to impaired ROS production upon *E. coli* infection in macrophages as well, which nevertheless showed increased antibacterial activity under HS conditions (12). In contrast to PMN, PHOX-dependent ROS production was dispensable in HS-augmented antibacterial activity in macrophages (12). Instead, HS boosted autophagy and autolysosomal targeting of bacteria for degradation into these highly acidic compartments (12, 13). This demonstrates that HS differentially alters antibacterial responses in distinct phagocytes.

Macrophages play an important role in controlling tissue integrity and resolution of inflammation by eliminating intruding invaders and fostering the degradation of debris (105–107). Neutrophils are the first responders that are

attracted to tissue injuries, which cannot be managed by local tissue-resident macrophages already on site (108). While neutrophil accumulation helps in warding off infections, this comes at a cost of collateral tissue damage. Although it is established that in inflamed and infected tissue Na^+-rich microdomains can be present (7, 8, 10), it is unclear which mechanisms orchestrate Na^+ accumulation [reviewed in: (14)] and when Na^+ accumulation in tissues appears in the course of inflammation and infection. It is very tempting to speculate that Na^+-rich environments are a signature of prolonged inflammatory processes. Likewise it is possible that within inflamed/infected tissues Na^+ gradients exist that modulate immune cell activity. Therefore, interstitial Na^+-accumulation could represent an 'ionic checkpoint' (20) which shapes a niche that ensures tissue integrity by dampening PMN function on the one hand, while boosting macrophage-dependent antibacterial activity and clearance of tissue debris on the other hand.

In line with this hypothesis, several reports showed that hypertonic saline infusion is linked to reduced lung injury and concomitant decreased neutrophil activation (37, 109, 110) as well as increased bacterial removal by immune cells in the peritoneal cavity (37). Further studies are required to systematically assess the role of local tissue Na^+ in the resolution of inflammatory diseases. Our findings provide new views on the resolution process, which have direct clinical relevance, and open new lines of investigations.

DATA AVAILABILITY STATEMENT

The raw data supporting the conclusions of this article will be made available by the authors, without undue reservation.

ETHICS STATEMENT

The studies involving human participants were reviewed and approved by Ethikkommission bei der Universität Regensburg. The patients/participants provided their written informed consent to participate in this study. The animal study was reviewed and approved by Animal Welfare Committee of the local governmental authorities (Regierung von Unterfranken Würzburg, Germany).

AUTHOR CONTRIBUTIONS

LK, KB, SE, PN, TO, AW, VS, MT, and AS acquired, analyzed, and interpreted data. MH, MS, and AD interpreted data and contributed to the design of experiments. JJ interpreted data, designed, conceptualized and oversaw the study. LK provided the first draft of the manuscript. Manuscript was revised by TO, AS, VS, SE, KB, PN, MH, MS, AD, and JJ. All authors contributed to the article and approved the submitted version.

FUNDING

JJ was supported by Deutsche Forschungsgemeinschaft [German Research Foundation, DFG, JA 1993/4-1, SFB1350 (project nr. 387509280, TPB5)] and by the Bavarian Ministry of Science and the Arts in the framework of the Bavarian Research Network 'New Strategies Against Multi-Resistant Pathogens by Means of Digital Networking–bayresq.net'. MH received funding from the DFG (DFG-FOR2886 PANDORA Project B3).

ACKNOWLEDGMENTS

We are indebted to the excellent technical assistance provided by Monika Nowottny and Christine Lindner.

SUPPLEMENTARY MATERIAL

The Supplementary Material for this article can be found online at: https://www.frontiersin.org/articles/10.3389/fimmu.2021.712948/full#supplementary-material

REFERENCES

1. Titze J, Lang R, Ilies C, Schwind KH, Kirsch KA, Dietsch P, et al. Osmotically Inactive Skin Na+ Storage in Rats. *Am J Physiol Renal Physiol* (2003) 285:F1108–17. doi: 10.1152/ajprenal.00200.2003
2. Machnik A, Neuhofer W, Jantsch J, Dahlmann A, Tammela T, Machura K, et al. Macrophages Regulate Salt-Dependent Volume and Blood Pressure by a Vascular Endothelial Growth Factor-C-Dependent Buffering Mechanism. *Nat Med* (2009) 15:545–52. doi: 10.1038/nm.1960
3. Dahlmann A, Dörfelt K, Eicher F, Linz P, Kopp C, Mössinger I, et al. Magnetic Resonance-Determined Sodium Removal From Tissue Stores in Hemodialysis Patients. *Kidney Int* (2015) 87:434–41. doi: 10.1038/ki.2014.269
4. Kopp C, Linz P, Maier C, Wabel P, Hammon M, Nagel AM, et al. Elevated Tissue Sodium Deposition in Patients With Type 2 Diabetes on Hemodialysis Detected by 23Na Magnetic Resonance Imaging. *Kidney Int* (2018) 93:1191–7. doi: 10.1016/j.kint.2017.11.021
5. Dahlmann A, Linz P, Zucker I, Haag V, Jantsch J, Dienemann T, et al. Reduction of Tissue Na+ Accumulation After Renal Transplantation. *Kidney Int Rep* (2021). doi: 10.1016/j.ekir.2021.06.022
6. Schneider MP, Raff U, Kopp C, Scheppach JB, Toncar S, Wanner C, et al. Skin Sodium Concentration Correlates With Left Ventricular Hypertrophy in CKD. *J Am Soc Nephrol* (2017) 28:1867–76. doi: 10.1681/ASN.2016060662
7. Schwartz L, Guais A, Pooya M, Abolhassani M. Is Inflammation a Consequence of Extracellular Hyperosmolarity? *J Inflamm (Lond)* (2009) 6:21. doi: 10.1186/1476-9255-6-21
8. Jantsch J, Schatz V, Friedrich D, Schröder A, Kopp C, Siegert I, et al. Cutaneous Na+ Storage Strengthens the Antimicrobial Barrier Function of the Skin and Boosts Macrophage-Driven Host Defense. *Cell Metab* (2015) 21:493–501. doi: 10.1016/j.cmet.2015.02.003
9. Kopp C, Beyer C, Linz P, Dahlmann A, Hammon M, Jantsch J, et al. Na+ Deposition in the Fibrotic Skin of Systemic Sclerosis Patients Detected by 23Na-Magnetic Resonance Imaging. *Rheumatol (Oxf)* (2017) 56:556–60. doi: 10.1093/rheumatology/kew371
10. Matthias J, Maul J, Noster R, Meinl H, Chao Y-Y, Gerstenberg H, et al. Sodium Chloride Is an Ionic Checkpoint for Human TH2 Cells and Shapes the Atopic Skin Microenvironment. *Sci Transl Med* (2019) 11(480): eaau0683. doi: 10.1126/scitranslmed.aau0683

11. Maifeld A, Wild J, Karlsen TV, Rakova N, Wistorf E, Linz P, et al. Skin Sodium Accumulates in Psoriasis and Reflects Disease Severity. *J Invest Dermatol* (2021). doi: 10.1016/j.jid.2021.06.013
12. Neubert P, Weichselbaum A, Reitinger C, Schatz V, Schröder A, Ferdinand JR, et al. HIF1A and NFAT5 Coordinate Na+-Boosted Antibacterial Defense *via* Enhanced Autophagy and Autolysosomal Targeting. *Autophagy* (2019) 15:1899–916. doi: 10.1080/15548627.2019.1596483
13. Neubert P, Homann A, Wendelborn D, Bär A-L, Krampert L, Trum M, et al. NCX1 Represents an Ionic Na+ Sensing Mechanism in Macrophages. *PloS Biol* (2020) 18:e3000722. doi: 10.1371/journal.pbio.3000722
14. Jobin K, Müller DN, Jantsch J, Kurts C. Sodium and Its Manifold Impact on Our Immune System. *Trends Immunol* (2021) 42(6):469–79. doi: 10.1016/j.it.2021.04.002
15. Neubert P, Schröder A, Müller DN, Jantsch J. Interplay of Na+ Balance and Immunobiology of Dendritic Cells. *Front Immunol* (2019a) 10:599. doi: 10.3389/fimmu.2019.00599
16. Schatz V, Neubert P, Schröder A, Binger K, Gebhard M, Müller DN, et al. Elementary Immunology: Na+ as a Regulator of Immunity. *Pediatr Nephrol* (2017) 32:201–10. doi: 10.1007/s00467-016-3349-x
17. Wilck N, Balogh A, Markó L, Bartolomaeus H, Müller DN. The Role of Sodium in Modulating Immune Cell Function. *Nat Rev Nephrol* (2019) 15:546–58. doi: 10.1038/s41581-019-0167-y
18. Müller DN, Wilck N, Haase S, Kleinewietfeld M, Linker RA. Sodium in the Microenvironment Regulates Immune Responses and Tissue Homeostasis. *Nat Rev Immunol* (2019) 19:243–54. doi: 10.1038/s41577-018-0113-4
19. Gurusamy D, Clever D, Eil R, Restifo NP. Novel "Elements" of Immune Suppression Within the Tumor Microenvironment. *Cancer Immunol Res* (2017) 5:426–33. doi: 10.1158/2326-6066.CIR-17-0117
20. Eil R, Vodnala SK, Clever D, Klebanoff CA, Sukumar M, Pan JH, et al. Ionic Immune Suppression Within the Tumour Microenvironment Limits T Cell Effector Function. *Nature* (2016) 537:539–43. doi: 10.1038/nature19364
21. Kleinewietfeld M, Manzel A, Titze J, Kvakan H, Yosef N, Linker RA, et al. Sodium Chloride Drives Autoimmune Disease by the Induction of Pathogenic TH17 Cells. *Nature* (2013) 496:518–22. doi: 10.1038/nature11868
22. Wu C, Yosef N, Thalhamer T, Zhu C, Xiao S, Kishi Y, et al. Induction of Pathogenic TH17 Cells by Inducible Salt-Sensing Kinase SGK1. *Nature* (2013) 496:513–7. doi: 10.1038/nature11984
23. Matthias J, Heink S, Picard F, Zeiträg J, Kolz A, Chao Y-Y, et al. Salt Generates Antiinflammatory Th17 Cells But Amplifies Pathogenicity in Proinflammatory Cytokine Microenvironments. *J Clin Invest* (2020) 130:4587–600. doi: 10.1172/JCI137786
24. Zhang W-C, Zheng X-J, Du L-J, Sun J-Y, Shen Z-X, Shi C, et al. High Salt Primes a Specific Activation State of Macrophages, M(Na). *Cell Res* (2015) 25:893–910. doi: 10.1038/cr.2015.87
25. Jobin K, Stumpf NE, Schwab S, Eichler M, Neubert P, Rauh M, et al. A High-Salt Diet Compromises Antibacterial Neutrophil Responses Through Hormonal Perturbation. *Sci Transl Med* (2020) 12(536):eaay3850. doi: 10.1126/scitranslmed.aay3850
26. Binger KJ, Gebhardt M, Heinig M, Rintisch C, Schroeder A, Neuhofer W, et al. High Salt Reduces the Activation of IL-4- and IL-13-Stimulated Macrophages. *J Clin Invest* (2015) 125:4223–38. doi: 10.1172/JCI80919
27. Hucke S, Eschborn M, Liebmann M, Herold M, Freise N, Engbers A, et al. Sodium Chloride Promotes Pro-Inflammatory Macrophage Polarization Thereby Aggravating CNS Autoimmunity. *J Autoimmun* (2016) 67:90–101. doi: 10.1016/j.jaut.2015.11.001
28. He W, Xu J, Mu R, Li Q, Lv D-L, Huang Z, et al. High-Salt Diet Inhibits Tumour Growth in Mice *via* Regulating Myeloid-Derived Suppressor Cell Differentiation. *Nat Commun* (2020) 11:1732. doi: 10.1038/s41467-020-15524-1
29. Willebrand R, Hamad I, van Zeebroeck L, Kiss M, Bruderek K, Geuzens A, et al. High Salt Inhibits Tumor Growth by Enhancing Anti-Tumor Immunity. *Front Immunol* (2019) 10:1141. doi: 10.3389/fimmu.2019.01141
30. Choi SY, Lee-Kwon W, Kwon HM. The Evolving Role of TonEBP as an Immunometabolic Stress Protein. *Nat Rev Nephrol* (2020) 16:352–64. doi: 10.1038/s41581-020-0261-1
31. Aramburu J, López-Rodríguez C. Regulation of Inflammatory Functions of Macrophages and T Lymphocytes by NFAT5. *Front Immunol* (2019) 10:535. doi: 10.3389/fimmu.2019.00535
32. Berry MR, Mathews RJ, Ferdinand JR, Jing C, Loudon KW, Wlodek E, et al. Renal Sodium Gradient Orchestrates a Dynamic Antibacterial Defense Zone. *Cell* (2017) 170:860–74.e19. doi: 10.1016/j.cell.2017.07.022
33. Nauseef WM, Borregaard N. Neutrophils at Work. *Nat Immunol* (2014) 15:602–11. doi: 10.1038/ni.2921
34. Ackermann M, Anders H-J, Bilyy R, Bowlin GL, Daniel C, de Lorenzo R, et al. Patients With COVID-19: In the Dark-NETs of Neutrophils. *Cell Death Differ* (2021) 1–15. doi: 10.1038/s41418-021-00805-z
35. Junger WG, Hoyt DB, Davis RE, Herdon-Remelius C, Namiki S, Junger H, et al. Hypertonicity Regulates the Function of Human Neutrophils by Modulating Chemoattractant Receptor Signaling and Activating Mitogen-Activated Protein Kinase P38. *J Clin Invest* (1998) 101:2768–79. doi: 10.1172/JCI1354
36. Shields CJ, O'Sullivan AW, Wang JH, Winter DC, Kirwan WO, Redmond HP. Hypertonic Saline Enhances Host Response to Bacterial Challenge by Augmenting Receptor-Independent Neutrophil Intracellular Superoxide Formation. *Ann Surg* (2003) 238:249–57. doi: 10.1097/01.sla.0000080827.77985.fc
37. Chen L-W, Huang H-L, Lee I-T, Hsu C-M, Lu P-J. Hypertonic Saline Enhances Host Defense to Bacterial Challenge by Augmenting Toll-Like Receptors. *Crit Care Med* (2006) 34:1758–68. doi: 10.1097/01.CCM.0000218810.66485.01
38. Sheppard FR, Moore EE, McLaughlin N, Kelher M, Johnson JL, Silliman C, et al. Clinically Relevant Osmolar Stress Inhibits Priming-Induced PMN NADPH Oxidase Subunit Translocation. *J Trauma* (2005) 58:752–7; discussion 757. doi: 10.1097/01.TA.0000159246.33364.72
39. Ciesla DJ, Moore EE, Zallen G, Biffl WL, Silliman CC. Hypertonic Saline Attenuation of Polymorphonuclear Neutrophil Cytotoxicity: Timing Is Everything. *J Trauma* (2000) 48:388–95. doi: 10.1097/00005373-200003000-00004
40. Rizoli SB, Kapus A, Parodo J, Rotstein OD. Hypertonicity Prevents Lipopolysaccharide-Stimulated CD11b/CD18 Expression in Human Neutrophils *In Vitro*: Role for P38 Inhibition. *J Trauma* (1999) 46:794–8. doi: 10.1097/00005373-199905000-00006
41. Rizoli SB, Rotstein OD, Parodo J, Phillips MJ, Kapus A. Hypertonic Inhibition of Exocytosis in Neutrophils: Central Role for Osmotic Actin Skeleton Remodeling. *Am J Physiol Cell Physiol* (2000) 279:C619–33. doi: 10.1152/ajpcell.2000.279.3.C619
42. Ciesla DJ, Moore EE, Musters RJ, Biffl WL, Silliman CA. Hypertonic Saline Alteration of the PMN Cytoskeleton: Implications for Signal Transduction and the Cytotoxic Response. *J Trauma* (2001) 50:206–12. doi: 10.1097/00005373-200102000-00004
43. Thiel M, Buessecker F, Eberhardt K, Chouker A, Setzer F, Kreimeier U, et al. Effects of Hypertonic Saline on Expression of Human Polymorphonuclear Leukocyte Adhesion Molecules. *J Leukoc Biol* (2001) 70:261–73.
44. Matsumoto T, Takahashi K, Kubo S, Haraoka M, Mizunoe Y, Tanaka M, et al. Suppression of Chemotactic Activity of Neutrophils in Hyperosmotic Conditions Comparable to the Renal Medulla: Partial Preservation by Phosphoenolpyruvate. *Urol Int* (1993) 50:1–5. doi: 10.1159/000282438
45. Nadesalingam A, Chen JHK, Farahvash A, Khan MA. Hypertonic Saline Suppresses NADPH Oxidase-Dependent Neutrophil Extracellular Trap Formation and Promotes Apoptosis. *Front Immunol* (2018) 9:359. doi: 10.3389/fimmu.2018.00359
46. Hampton MB, Chambers ST, Vissers MCM, Winterbourn CC, Margret CMV, Winterbourn CC. Bacterial Killing by Neutrophils in Hypertonic Environments. *J Infect Dis* (1994) 169(4):839–46. doi: 10.1093/infdis/169.4.839
47. Matsumoto T, Kumazawa J, van der Auwera P. Suppression of Leukocyte Function and Intracellular Content of ATP in Hyperosmotic Condition Comparable to the Renal Medulla. *J Urol* (1989) 142:399–402. doi: 10.1016/S0022-5347(17)38772-4
48. Cheminay C, Schoen M, Hensel M, Wandersee-Steinhäuser A, Ritter U, Körner H, et al. Migration of Salmonella Typhimurium –Harboring Bone Marrow–Derived Dendritic Cells Towards the Chemokines CCL19 and CCL21. *Microb Pathog* (2002) 32:207–18. doi: 10.1006/mpat.2002.0497
49. Kuhns DB, Priel DAL, Chu J, Zarember KA. Isolation and Functional Analysis of Human Neutrophils. *Curr Protoc Immunol* (2015) 111:7.23.1–7.23.16. doi: 10.1002/0471142735.im0723s111

50. Schorn C, Janko C, Latzko M, Chaurio R, Schett G, Herrmann M. Monosodium Urate Crystals Induce Extracellular DNA Traps in Neutrophils, Eosinophils, and Basophils But Not in Mononuclear Cells. *Front Immunol* (2012) 3:277. doi: 10.3389/fimmu.2012.00277
51. Steffen U, Koeleman CA, Sokolova MV, Bang H, Kleyer A, Rech J, et al. IgA Subclasses Have Different Effector Functions Associated With Distinct Glycosylation Profiles. *Nat Commun* (2020) 11:120. doi: 10.1038/s41467-019-13992-8
52. Pollock JD, Williams DA, Gifford MA, Li LL, Du X, Fisherman J, et al. Mouse Model of X-Linked Chronic Granulomatous Disease, An Inherited Defect in Phagocyte Superoxide Production. *Nat Genet* (1995) 9:202–9. doi: 10.1038/ng0295-202
53. Schleicher U, Bogdan C. Generation, Culture and Flow-Cytometric Characterization of Primary Mouse Macrophages. *Methods Mol Biol* (2009) 531:203–24. doi: 10.1007/978-1-59745-396-7_14
54. Swamydas M, Luo Y, Dorf ME, Lionakis MS. Isolation of Mouse Neutrophils. *Curr Protoc Immunol* (2015) 110:3.20.1–3.20.15. doi: 10.1002/0471142735.im0320s110
55. Metcalf D, Robb L, Dunn AR, Mifsud S, Di Rago L. Role of Granulocyte-Macrophage Colony-Stimulating Factor and Granulocyte Colony-Stimulating Factor in the Development of an Acute Neutrophil Inflammatory Response in Mice. *Blood* (1996) 88:3755–64. doi: 10.1182/blood.V88.10.3755.bloodjournal88103755
56. Newell SL, Atkinson JP. Biosynthesis of C4 by Mouse Peritoneal Macrophages. II. Comparsion of C4 Synthesis by Resident and Elicited Cell Populations. *J Immunol* (1983) 130:834–8.
57. Zhang X, Goncalves R, Mosser DM. The Isolation and Characterization of Murine Macrophages. *Curr Protoc Immunol* (2008) Chapter 14:Unit 14.1. doi: 10.1002/0471142735.im1401s83
58. Schindelin J, Arganda-Carreras I, Frise E, Kaynig V, Longair M, Pietzsch T, et al. Fiji: An Open-Source Platform for Biological-Image Analysis. *Nat Methods* (2012) 9:676–82. doi: 10.1038/nmeth.2019
59. Carmona-Rivera C, Kaplan MJ. Induction and Quantification of NETosis. *Curr Protoc Immunol* (2016) 115:14.41.1–14.41.14. doi: 10.1002/cpim.16
60. Bülow S, Heyd R, Toelge M, Ederer KU, Schweda A, Blaas SH, et al. Lipopolysaccharide Binding Protein and Bactericidal/Permeability-Increasing Protein as Biomarkers for Invasive Pulmonary Aspergillosis. *J Fungi (Basel)* (2020) 6(4):304. doi: 10.3390/jof6040304
61. Fulton RJ, McDade RL, Smith PL, Kienker LJ, Kettman JR. Advanced Multiplexed Analysis With the FlowMetrix System. *Clin Chem* (1997) 43:1749–56. doi: 10.1093/clinchem/43.9.1749
62. Boyden S. The Chemotactic Effect of Mixtures of Antibody and Antigen on Polymorphonuclear Leucocytes. *J Exp Med* (1962) 115:453–66. doi: 10.1084/jem.115.3.453
63. Chen H-C. Boyden Chamber Assay. *Methods Mol Biol* (2005) 294:15–22. doi: 10.1385/1-59259-860-9:015
64. Gagnon RC, Peterson JJ. Estimation of Confidence Intervals for Area Under the Curve From Destructively Obtained Pharmacokinetic Data. *J Pharmacokinet Biopharm* (1998) 26:87–102. doi: 10.1023/A:1023228925137
65. Geisberger S, Bartolomaeus H, Neubert P, Willebrand R, Zasada C, Bartolomaeus T, et al. Salt Transiently Inhibits Mitochondrial Energetics in Mononuclear Phagocytes. *Circulation* (2021) 144(2):144–58. doi: 10.1161/CIRCULATIONAHA.120.052788
66. Sengeløv H, Kjeldsen L, Borregaard N. Control of Exocytosis in Early Neutrophil Activation. *J Immunol* (1993) 150:1535–43.
67. Sengeløv H, Kjeldsen L, Kroeze W, Berger M, Borregaard N. Secretory Vesicles are the Intracellular Reservoir of Complement Receptor 1 in Human Neutrophils. *J Immunol* (1994) 153:804–10.
68. Berger M, O'Shea J, Cross AS, Folks TM, Chused TM, Brown EJ, et al. Human Neutrophils Increase Expression of C3bi as Well as C3b Receptors Upon Activation. *J Clin Invest* (1984) 74:1566–71. doi: 10.1172/JCI111572
69. Stocks SC, Kerr MA, Haslett C, Dransfield I. CD66-Dependent Neutrophil Activation: A Possible Mechanism for Vascular Selectin-Mediated Regulation of Neutrophil Adhesion. *J Leukoc Biol* (1995) 58:40–8. doi: 10.1002/jlb.58.1.40
70. Borregaard N, Kjeldsen L, Sengeløv H, Diamond MS, Springer TA, Anderson HC, et al. Changes in Subcellular Localization and Surface Expression of L-Selectin, Alkaline Phosphatase, and Mac-1 in Human Neutrophils During Stimulation With Inflammatory Mediators. *J Leukoc Biol* (1994) 56:80–7. doi: 10.1002/jlb.56.1.80
71. Stojkov D, Amini P, Oberson K, Sokollik C, Duppenthaler A, Simon H-U, et al. ROS and Glutathionylation Balance Cytoskeletal Dynamics in Neutrophil Extracellular Trap Formation. *J Cell Biol* (2017) 216:4073–90. doi: 10.1083/jcb.201611168
72. Deree J, Lall R, Melbostad H, Grant M, Hoyt DB, Coimbra R. Neutrophil Degranulation and the Effects of Phosphodiesterase Inhibition. *J Surg Res* (2006) 133:22–8. doi: 10.1016/j.jss.2006.02.031
73. Weiss J, Olsson I. Cellular and Subcellular Localization of the Bactericidal/Permeability-Increasing Protein of Neutrophils. *Blood* (1987) 69:652–9. doi: 10.1182/blood.V69.2.652.652
74. Kishimoto TK, Jutila MA, Berg EL, Butcher EC. Neutrophil Mac-1 and MEL-14 Adhesion Proteins Inversely Regulated by Chemotactic Factors. *Science* (1989) 245:1238–41. doi: 10.1126/science.2551036
75. Kuijpers TW, Tool AT, van der Schoot CE, Ginsel LA, Onderwater JJ, Roos D, et al. Membrane Surface Antigen Expression on Neutrophils: A Reappraisal of the Use of Surface Markers for Neutrophil Activation. *Blood* (1991) 78:1105–11. doi: 10.1182/blood.V78.4.1105.1105
76. Griffin JD, Spertini O, Ernst TJ, Belvin MP, Levine HB, Kanakura Y, et al. Granulocyte-Macrophage Colony-Stimulating Factor and Other Cytokines Regulate Surface Expression of the Leukocyte Adhesion Molecule-1 on Human Neutrophils, Monocytes, and Their Precursors. *J Immunol* (1990) 145:576–84.
77. Torres M, Hall FL, O'Neill K. 1993//Stimulation of Human Neutrophils With Formyl-Methionyl-Leucyl-Phenylalanine Induces Tyrosine Phosphorylation and Activation of Two Distinct Mitogen-Activated Protein-Kinases. *J Immunol* (1993) 150:1563–77.
78. Petroski RJ, Naccache PH, Becker EL, Sha'afi RI. Effect of the Chemotactic Factor Formyl Methionyl-Leucyl-Phenylalanine and Cytochalasin B on the Cellular Levels of Calcium in Rabbit Neutrophils. *FEBS Lett* (1979) 100:161–5. doi: 10.1016/0014-5793(79)81155-2
79. Palmblad J, Gyllenhammar H, Lindgren JA, Malmsten CL, et al. 1984// Effects of Leukotrienes and F-Met-Leu-Phe on Oxidative Metabolism of Neutrophils and Eosinophils. *J Immunol* (1984) 132:3041–5.
80. Showell HJ, Freer RJ, Zigmond SH, Schiffmann E, Aswanikumar S, Corcoran B, et al. The Structure-Activity Relations of Synthetic Peptides as Chemotactic Factors and Inducers of Lysosomal Secretion for Neutrophils. *J Exp Med* (1976) 143:1154–69. doi: 10.1084/jem.143.5.1154
81. Kreutzer DL, O'Flaherty JT, Orr W, Showell HJ, Ward PA, Becker EL. Quantitative Comparisons of Various Biological Responses of Neutrophils to Different Active and Inactive Chemotactic Factors. *Immunopharmacology* (1978) 1:39–47. doi: 10.1016/0162-3109(78)90007-3
82. Becker EL. Chemotaxis. *J Allergy Clin Immunol* (1980) 66:97–105. doi: 10.1016/0091-6749(80)90055-X
83. Fuchs TA, Abed U, Goosmann C, Hurwitz R, Schulze I, Wahn V, et al. Novel Cell Death Program Leads to Neutrophil Extracellular Traps. *J Cell Biol* (2007) 176:231–41. doi: 10.1083/jcb.200606027
84. Sollberger G, Tilley DO, Zychlinsky A. Neutrophil Extracellular Traps: The Biology of Chromatin Externalization. *Dev Cell* (2018) 44:542–53. doi: 10.1016/j.devcel.2018.01.019
85. Brinkmann V, Reichard U, Goosmann C, Fauler B, Uhlemann Y, Weiss DS, et al. Neutrophil Extracellular Traps Kill Bacteria. *Science* (2004) 303:1532–5. doi: 10.1126/science.1092385
86. Gavillet M, Martinod K, Renella R, Harris C, Shapiro NI, Wagner DD, et al. Flow Cytometric Assay for Direct Quantification of Neutrophil Extracellular Traps in Blood Samples. *Am J Hematol* (2015) 90:1155–8. doi: 10.1002/ajh.24185
87. van der Linden M, Westerlaken GHA, van der Vlist M, van Montfrans J, Meyaard L. Differential Signalling and Kinetics of Neutrophil Extracellular Trap Release Revealed by Quantitative Live Imaging. *Sci Rep* (2017) 7:6529. doi: 10.1038/s41598-017-06901-w
88. Shapiro L, Dinarello CA. Osmotic Regulation of Cytokine Synthesis. *vitro Proc Natl Acad Sci USA* (1995) 92:12230–4. doi: 10.1073/pnas.92.26.12230
89. Keshari RS, Verma A, Barthwal MK, Dikshit M. Reactive Oxygen Species-Induced Activation of ERK and P38 MAPK Mediates PMA-Induced NETs Release From Human Neutrophils. *J Cell Biochem* (2013) 114:532–40. doi: 10.1002/jcb.24391

90. Kamikawa Y, Sakai N, Miyake T, Sagara A, Shinozaki Y, Kitajima S, et al. Involvement of P38mapk in Impaired Neutrophil Bactericidal Activity of Hemodialysis Patients. *Ther Apher Dial* (2018) 22:345–54. doi: 10.1111/1744-9987.12651
91. Nauseef WM. The Phagocyte NOX2 NADPH Oxidase in Microbial Killing and Cell Signaling. *Curr Opin Immunol* (2019) 60:130–40. doi: 10.1016/j.coi.2019.05.006
92. Ellis JA, Mayer SJ, Jones OT. The Effect of the NADPH Oxidase Inhibitor Diphenyleneiodonium on Aerobic and Anaerobic Microbicidal Activities of Human Neutrophils. *Biochem J* (1988) 251:887–91. doi: 10.1042/bj2510887
93. Rice CM, Davies LC, Subleski JJ, Maio N, Gonzalez-Cotto M, Andrews C, et al. Tumour-Elicited Neutrophils Engage Mitochondrial Metabolism to Circumvent Nutrient Limitations and Maintain Immune Suppression. *Nat Commun* (2018) 9:5099. doi: 10.1038/s41467-018-07505-2
94. Dantzler WH, Layton AT, Layton HE, Pannabecker TL. Urine-Concentrating Mechanism in the Inner Medulla: Function of the Thin Limbs of the Loops of Henle. *Clin J Am Soc Nephrol* (2014) 9:1781–9. doi: 10.2215/CJN.08750812
95. Kim JY, Hong YS, Choi SH, Yoon YH, Moon SW, Lee SW. Effect of Hypertonic Saline on Apoptosis of Polymorphonuclear Cells. *J Surg Res* (2012) 178:401–8. doi: 10.1016/j.jss.2012.01.055
96. Loughman JA, Hunstad DA. Attenuation of Human Neutrophil Migration and Function by Uropathogenic Bacteria. *Microbes Infect* (2011) 13:555–65. doi: 10.1016/j.micinf.2011.01.017
97. Jackson SH, Gallin JI, Holland SM. The P47phox Mouse Knock-Out Model of Chronic Granulomatous Disease. *J Exp Med* (1995) 182:751–8. doi: 10.1084/jem.182.3.751
98. Thiam HR, Wong SL, Wagner DD, Waterman CM. Cellular Mechanisms of NETosis. *Annu Rev Cell Dev Biol* (2020) 36:191–218. doi: 10.1146/annurev-cellbio-020520-111016
99. Tatsiy O, McDonald PP. Physiological Stimuli Induce PAD4-Dependent, ROS-Independent NETosis, With Early and Late Events Controlled by Discrete Signaling Pathways. *Front Immunol* (2018) 9:2036. doi: 10.3389/fimmu.2018.02036
100. Nick JA, Young SK, Arndt PG, Lieber JG, Suratt BT, Poch KR, et al. Selective Suppression of Neutrophil Accumulation in Ongoing Pulmonary Inflammation by Systemic Inhibition of P38 Mitogen-Activated Protein Kinase. *J Immunol* (2002) 169:5260–9. doi: 10.4049/jimmunol.169.9.5260
101. Nick JA, Avdi NJ, Young SK, Knall C, Gerwins P, Johnson GL, et al. Common and Distinct Intracellular Signaling Pathways in Human Neutrophils Utilized by Platelet Activating Factor and FMLP. *J Clin Invest* (1997) 99:975–86. doi: 10.1172/JCI119263
102. Rane MJ, Carrithers SL, Arthur JM, Klein JB, McLeish KR. Formyl Peptide Receptors are Coupled to Multiple Mitogen-Activated Protein Kinase Cascades by Distinct Signal Transduction Pathways: Role in Activation of Reduced Nicotinamide Adenine Dinucleotide Oxidase. *J Immunol* (1997) 159:5070–8.
103. Ridley AJ. Rho GTPase Signalling in Cell Migration. *Curr Opin Cell Biol* (2015) 36:103–12. doi: 10.1016/j.ceb.2015.08.005
104. Bedard K, Krause K-H. The NOX Family of ROS-Generating NADPH Oxidases: Physiology and Pathophysiology. *Physiol Rev* (2007) 87:245–313. doi: 10.1152/physrev.00044.2005
105. Martin CJ, Peters KN, Behar SM. Macrophages Clean Up: Efferocytosis and Microbial Control. *Curr Opin Microbiol* (2014) 17:17–23. doi: 10.1016/j.mib.2013.10.007
106. Kumaran Satyanarayanan S, El Kebir D, Soboh S, Butenko S, Sekheri M, Saadi J, et al. IFN-β Is a Macrophage-Derived Effector Cytokine Facilitating the Resolution of Bacterial Inflammation. *Nat Commun* (2019) 10:3471. doi: 10.1038/s41467-019-10903-9
107. Bonnefoy F, Gauthier T, Vallion R, Martin-Rodriguez O, Missey A, Daoui A, et al. Factors Produced by Macrophages Eliminating Apoptotic Cells Demonstrate Pro-Resolutive Properties and Terminate Ongoing Inflammation. *Front Immunol* (2018) 9:2586. doi: 10.3389/fimmu.2018.02586
108. Uderhardt S, Martins AJ, Tsang JS, Lämmermann T, Germain RN. Resident Macrophages Cloak Tissue Microlesions to Prevent Neutrophil-Driven Inflammatory Damage. *Cell* (2019) 177:541–55.e17. doi: 10.1016/j.cell.2019.02.028
109. Angle N, Hoyt DB, Coimbra R, Liu F, Herdon-Remelius C, Loomis W, et al. Hypertonic Saline Resuscitation Diminishes Lung Injury by Suppressing Neutrophil Activation After Hemorrhagic Shock. *Shock* (1998) 9:164–70. doi: 10.1097/00024382-199803000-00002
110. Pascual JL, Khwaja KA, Ferri LE, Giannias B, Evans DC, Razek T, et al. Hypertonic Saline Resuscitation Attenuates Neutrophil Lung Sequestration and Transmigration by Diminishing Leukocyte-Endothelial Interactions in a Two-Hit Model of Hemorrhagic Shock and Infection. *J Trauma* (2003) 54:121–30; discussion 130-2. doi: 10.1097/00005373-200301000-00015

Conflict of Interest: The authors declare that the research was conducted in the absence of any commercial or financial relationships that could be construed as a potential conflict of interest.

Publisher's Note: All claims expressed in this article are solely those of the authors and do not necessarily represent those of their affiliated organizations, or those of the publisher, the editors and the reviewers. Any product that may be evaluated in this article, or claim that may be made by its manufacturer, is not guaranteed or endorsed by the publisher.

Copyright © 2021 Krampert, Bauer, Ebner, Neubert, Ossner, Weigert, Schatz, Toelge, Schröder, Herrmann, Schnare, Dorhoi and Jantsch. This is an open-access article distributed under the terms of the Creative Commons Attribution License (CC BY). The use, distribution or reproduction in other forums is permitted, provided the original author(s) and the copyright owner(s) are credited and that the original publication in this journal is cited, in accordance with accepted academic practice. No use, distribution or reproduction is permitted which does not comply with these terms.

frontiers in Immunology

ORIGINAL RESEARCH
published: 14 September 2021
doi: 10.3389/fimmu.2021.712781

The Antimicrobial Peptide Human β-Defensin-3 Accelerates Wound Healing by Promoting Angiogenesis, Cell Migration, and Proliferation Through the FGFR/JAK2/STAT3 Signaling Pathway

Miho Takahashi[1,2], *Yoshie Umehara*[1], *Hainan Yue*[1,2], *Juan Valentin Trujillo-Paez*[1], *Ge Peng*[1,2], *Hai Le Thanh Nguyen*[1,2], *Risa Ikutama*[1,2], *Ko Okumura*[1], *Hideoki Ogawa*[1,2], *Shigaku Ikeda*[1,2] *and François Niyonsaba*[1,3]*

[1] Atopy (Allergy) Research Center, Juntendo University Graduate School of Medicine, Tokyo, Japan, [2] Department of Dermatology and Allergology, Juntendo University Graduate School of Medicine, Tokyo, Japan, [3] Faculty of International Liberal Arts, Juntendo University, Tokyo, Japan

In addition to its antimicrobial activity, the skin-derived antimicrobial peptide human β-defensin-3 (hBD-3) promotes keratinocyte proliferation and migration to initiate the wound healing process; however, its effects on fibroblasts, which are the major cell type responsible for wound healing, remain unclear. We investigated the role of hBD-3 in cell migration, proliferation and production of angiogenic growth factors in human fibroblasts and evaluated the *in vivo* effect of hBD-3 on promoting wound healing and angiogenesis. Following hBD-3 treatment, the mouse wounds healed faster and showed accumulation of neutrophils and macrophages in the early phase of wound healing and reduction of these phagocytes 4 days later. hBD-3-treated wounds also displayed an increased number of fibroblasts and newly formed vessels compared to those of the control mice. Furthermore, the expression of various angiogenic growth factors was increased in the hBD-3-treated wounds. Additionally, *in vitro* studies demonstrated that hBD-3 enhanced the secretion of angiogenic growth factors such as fibroblast growth factor, platelet-derived growth factor and vascular endothelial growth factor and induced the migration and proliferation of human fibroblasts. The hBD-3-mediated activation of fibroblasts involves the fibroblast growth factor receptor 1 (FGFR1)/Janus kinase 2 (JAK2)/signal transducer and activator of transcription 3 (STAT3) pathways, as evidenced by the inhibitory effects of pathway-specific inhibitors. We indeed confirmed that hBD-3 enhanced the phosphorylation of FGFR1, JAK2 and STAT3. Collectively, the current study provides novel evidence that hBD-3 might be a potential candidate for the treatment of wounds through its ability to promote wound healing, angiogenesis and fibroblast activation.

Keywords: angiogenesis, human β-defensin, fibroblast, migration, proliferation, wound healing

OPEN ACCESS

Edited by:
Amiram Ariel,
University of Haifa, Israel

Reviewed by:
Bruno Rivas-Santiago,
Unidad de Investigación Biomédica de Zacatecas (IMSS), Mexico
Stefania Madonna,
Istituto di Dermatologia Immacolata (IRCCS), Italy

***Correspondence:**
François Niyonsaba
francois@juntendo.ac.jp

Specialty section:
This article was submitted to Inflammation, a section of the journal Frontiers in Immunology

Received: *21 May 2021*
Accepted: *27 August 2021*
Published: *14 September 2021*

Citation:
Takahashi M, Umehara Y, Yue H, Trujillo-Paez JV, Peng G, Nguyen HLT, Ikutama R, Okumura K, Ogawa H, Ikeda S and Niyonsaba F (2021) The Antimicrobial Peptide Human β-Defensin-3 Accelerates Wound Healing by Promoting Angiogenesis, Cell Migration, and Proliferation Through the FGFR/JAK2/STAT3 Signaling Pathway. Front. Immunol. 12:712781. doi: 10.3389/fimmu.2021.712781

INTRODUCTION

The skin is the most external organ that protects the body from physical and chemical environmental challenges. Therefore, once skin injury occurs, an immediate and coordinated response is initiated to repair the wound. The skin wound healing process consists of three distinct but overlapping stages, denoted as the inflammatory phase, proliferative phase, and remodeling phase, and involves several mediators, such as inflammatory cells, growth factors and cellular and extracellular elements (1). In the inflammatory phase, both neutrophils and macrophages are attracted to the wound site to ingest and kill microbes, remove damaged tissues and release proinflammatory cytokines and growth factors that recruit and activate fibroblasts and keratinocytes. In the proliferative phase, keratinocytes and fibroblasts proliferate and migrate to the wound site, where fibroblasts synthesize extracellular matrix (ECM) to form granulation tissues. In this phase, angiogenesis also plays an important role by supplying newly formed tissue. In the remodeling phase, ECM maturation and turnover and homeostasis are regulated by metalloproteinases (MMPs). In addition to the ECM, MMPs cleave many cytokines, growth factors and cytokine/growth factor receptors that regulate several steps of the wound healing process (2).

Angiogenesis is tightly regulated by a complex of angiogenic growth factors, such as epidermal growth factor (EGF), fibroblast growth factor (FGF), platelet-derived growth factors (PDGF), and vascular endothelial growth factor (VEGF). During the wound healing process, these angiogenic growth factors promote angiogenesis by binding to their respective receptors, such as EGF receptor (EGFR), FGF receptor (FGFR), PDGF receptor (PDGFR), and VEGF receptor (VEGFR). Following binding to their corresponding ligands, these receptors undergo phosphorylation, resulting in activation of the downstream signaling pathways, therefore leading to cell proliferation, migration, angiogenesis, and wound healing (3–6). Among the various downstream signaling pathways of angiogenic receptors, Janus kinase (JAK)/signal transducer and activator of transcription (STAT) pathway transmits extracellular signals to the nucleus for the transcription of numerous genes that promote cell proliferation, differentiation and angiogenesis. JAKs belong to the tyrosine kinase family of enzymes, and their activation leads to the transfer of extracellular signals provided by growth factors, cytokines, and chemokines (7). The JAK family comprises JAK1, JAK2, JAK3 and TYK2. Activation of STATs is typically mediated *via* the cytokine receptor associated with the JAK family of nonreceptor tyrosine kinases (8). To date, seven mammalian STAT family members, STAT1, STAT2, STAT3, STAT4, STAT5a, STAT5b and STAT6, have been identified (9, 10). In nonhealing chronic wounds, the levels of many angiogenic growth factors and their receptors are downregulated, therefore delaying wound healing (11–13). Consequently, there is an unmet need for the development of drugs capable of activating angiogenic growth factor receptors and their downstream cascades to promote wound healing.

Antimicrobial peptides not only kill invading pathogenic microorganisms but also contribute to host defense and homeostasis by exhibiting a wide range of immunomodulatory functions (14). Several types of antimicrobial peptides, including human β-defensins (hBDs), cathelicidin LL-37, psoriasin (S100A7), and ribonuclease RNase-7, have been identified in human skin. Some are permanently expressed in healthy skin, and some are increased following infections, injury, proinflammatory cytokines and ultraviolet B irradiation (14). The hBD family is one of the most important antimicrobial peptide families found in human skin, and these peptides are well known for their wide range of microbicidal activities and immunomodulatory properties. To date, six members of hBDs, namely, hBD-1 to hBD-6, have been identified in the human body. Among them, hBD-1 to hBD-4 are primarily found in the epithelia of the skin, eyes, and oral, respiratory and urogenital tracts, while hBD-5 and hBD-6 are only present in the epididymis (15, 16). Among hBDs present in the skin, only hBD-1 is constitutively expressed, whereas the expression of hBD-2 to hBD-4 is enhanced upon infection or inflammation (17). In addition to killing a broad spectrum of invading microorganisms such as bacteria, viruses and fungi, hBDs also act as immunoregulators and represent a link between innate and adaptive immune responses. Various hBD-mediated immunomodulatory functions include the regulation of pro- and anti-inflammatory responses, neutralization of lipopolysaccharide, chemoattraction and activation of numerous immune cells, induction of cell proliferation, promotion of wound healing and maintenance of the skin barrier (17). It has been documented that hBDs activate various cell types, such as mast cells, neutrophils, macrophages and keratinocytes, which largely contribute to wound healing (14). Furthermore, hBD-2 and hBD-3 expression levels are upregulated by keratinocytes at skin wound sites and promote cell migration and proliferation (14, 18). hBD-induced keratinocyte proliferation and migration are mediated through phosphorylation of the EGFR and STAT proteins (19). Notably, the accelerating effects of hBDs on wound healing are not restricted to the skin but extend to other tissues, such as the eye and gut (20–22). To date, the effects of hBDs on fibroblasts, which play a crucial role in wound healing, have not been reported.

In the present study, among the hBDs tested, only hBD-3 showed the strongest stimulatory effect on human fibroblasts. hBD-3 induced the production of various angiogenic growth factors, such as FGF, PDGF and VEGF, promoted fibroblast migration and proliferation and accelerated *in vitro* wound healing. hBD-3-mediated activation of fibroblasts involved the FGFR1/JAK2/STAT3 signaling pathway. Moreover, hBD-3 markedly accelerated *in vivo* wound healing, increased the number of neutrophils, macrophages and fibroblasts at the wound site, and enhanced the formation of vessels and the expression of angiogenic growth factors in mice. These findings provide novel evidence that hBD-3 may contribute to wound healing *via* activation of fibroblasts.

MATERIALS AND METHODS

Reagents

Antimicrobial peptide hBD-3 was purchased from Peptide Institute (Osaka, Japan), whereas recombinant mouse β-defensin 14 (mBD-14) was obtained from ProSpec (Rehovot, Israel). Fruquintinib, imatinib mesylate and mitomycin C were

obtained from Sigma-Aldrich (St Louis, MO). Cryptotanshinone and AZD1480 were purchased from Selleck Chemicals (Houston, TX). SSR 128129E was purchased from Cayman Chemical (Ann Arbor, MI), recombinant basic FGF and VEGF were purchased from Peprotech (Cranbury, NJ). Antibodies against phosphorylated and unphosphorylated FGFR1, JAK1, JAK2, JAK3, STAT1 and STAT3 and RIPA buffer that consisted of 20 mM Tris-HCl (pH 7.5), 150 mM NaCl, 1 mM Na_2 EDTA, 1 mM EGTA, 1% NP-40, 1% sodium deoxycholate, 2.5 mM sodium pyrophosphate, 1 mM β-glycerophosphate, 1 mM Na_3VO_4 and 1 μg/ml leupeptin were obtained from Cell Signaling Technology (Beverly, MA). Type 1 collagen was purchased from Calbiochem (La Jolla, CA). Rabbit polyclonal antibody against ionized calcium-binding adapter molecule 1 (Iba1) was purchased from Fujifilm Wako Pure Chemical Corporation (Tokyo, Japan). Rabbit polyclonal antibody against myeloperoxidase (MPO) was obtained from CiteAb (Bath, United Kingdom). Mouse monoclonal antibody against heat shock protein 47 (HSP47) was obtained from Santa Cruz Biotechnology (Dallas, TX), whereas rabbit polyclonal antibody against mBD-14 was purchased from MyBioSource (San Diego, CA). Rabbit polyclonal antibody against CD163 was obtained from Proteintech (Rosemont, IL). Rabbit polyclonal antibody against CD80 was obtained from Abcam (Cambridge, UK).

Animal Experiments

Eight-week-old male C57BL/6 mice (Japan SLC, Inc., Ibaraki, Japan) were maintained under specific pathogen-free conditions and fed a standard diet and water *ad libitum*. All procedures were approved and performed in accordance with the Institutional Animal Care and Use Committee of Juntendo University School of Medicine (approval number: 2021255) and complied with the National Institutes of Health Guide for the Care and Use of Laboratory Animals. Following anesthesia with 2.5% isoflurane, hairs of the dorsal skin were shaved, and two 6-mm-diameter full-thickness wounds were created in the dorsal skin of mice using a circular biopsy punch under aseptic conditions. Ring-shaped silicone splints were sutured to the wound perimeter to avoid and prevent contraction. The mice were randomized into a control group that was treated with 0.01% acetic acid (solvent) and an hBD-3 group. In total, 200 μg/ml hBD-3 or mBD-14 in 20 μl of 0.01% acetic acid was topically applied every 2 days until the wounds were completely healed. After surgery, the wounds were covered with a hydrocolloid dressing (Tegaderm; 3 M Health Care, Tokyo, Japan) and cleaned with normal saline before each treatment. Digital photographs of each wound were taken, and the wound areas were calculated using ImageJ software (NIH, Bethesda, MD). After anesthesia, the mice were sacrificed, and wound skin samples were collected for further experiments.

Immunohistochemistry

Wound skin tissues were obtained after fixation with 10% paraformaldehyde (pH 7.4) in phosphate-buffered saline (PBS), processed and embedded in paraffin. The sections were deparaffinized, hydrated and blocked with normal goat serum (1:20 dilution) for 30 minutes at room temperature before being incubated at 4°C overnight with anti-MPO antibody (1:1000 dilution) for neutrophil identification, anti-Iba1 antibody (1:2000 dilution) for macrophage detection, anti-HSP47 antibody (1:1000 dilution) for fibroblast identification, anti-mBD-14 antibody (1:500 dilution), anti-CD80 antibody (1:100 dilution) and anti-CD163 (1:100 dilution) for M1 and M2 identification, respectively. After three washes in PBS, the sections were allowed to react with horseradish peroxidase-conjugated streptavidin (1:300 dilution) for 30 minutes at room temperature. Diaminobenzidine tetrahydrochloride solution was then added and incubated at room temperature for 1 minute (for anti-Iba-1 antibody, anti-CD163 antibody), 2 minutes (for anti-MPO antibody and for anti-mBD-14 antibody), and 3 minutes (for anti-HSP47 antibody) and 5 minutes (for anti-CD80 antibody). Sections were stained with hematoxylin, dehydrated in an ethanol gradient, cleared in dimethyl benzene, and mounted. Images were acquired using a phase-contrast microscope (Keyence, Osaka, Japan) at 400× magnification, and images were recorded. The wound tissue areas were measured using ImageJ software. The number of MPO-, Iba1-, HSP47-, CD80- and CD163-positive cells was counted in three microscopic fields for each sample in the fields with the highest numbers of target cell.

Cell Culture

Normal human dermal fibroblasts were purchased from Lifeline Cell Technology (Osaka, Japan) and cultured in FibroLife serum-free medium (Lifeline Cell Technology) containing L-glutamine (7.5 mM), human basic FGF (5 ng/ml), insulin (5 μg/ml), ascorbic acid (50 μg/ml), hydrocortisone (1 μg/ml), gentamycin (30 μg/ml), amphotericin B (15 ng/ml) and fetal bovine serum (2% vol/vol). All experiments were performed using subconfluent cells (from 60% to 80% confluence) grown in FibroLife serum-free medium without supplements but with antibiotics.

RNA Extraction and Real-Time PCR

Wound skin tissues were immediately stored in RNAlater solution (Ambion, Austin, TX) to stabilize and protect the RNA integrity before disruption in QIAzol Lysis Reagent (Qiagen, Hilden, Germany). Total RNA from wound tissues was extracted using the RNeasy Plus Universal Mini kit (Qiagen, Hilden, Germany), while RNA extraction from fibroblasts was performed using an RNeasy Plus Micro kit (Qiagen) according to the manufacturer's instructions. cDNA was synthesized from 1 μg of total RNA using the ReverTra Ace qPCR RT kit (Toyobo, Osaka, Japan). Real-time PCR was performed using a QuantiNova SYBR Green PCR kit (Qiagen), and cDNA was amplified and detected using the StepOne Plus Real-time PCR System (Applied Biosystems). The primer sequences used for *Pdgfc* were forward: 5′-GTGGAGGAAATT GTGCCTGT-3′ and reverse: 5′-TCCAGAGCCACATCAG TGAG-3′, for *Fgf2* were forward: 5′-GGACGGCTGCTGGCTT CTAA-3′ and reverse: 5′-CCAGTTCGTTTCAGTGCCACA TAC-3′, for *Vegfa* were forward: 5′-GTGCACTGGACCCTGGC TTTA-3′ and reverse: 5′-GGTCTCAATCGGACGGCAGTA-3′, for *Rps18* were forward: 5′-TTCTGGCCAACGGTCTAGAC AAC-3′ and reverse: 5′-CCAGTGGTCTTGGTGTGCTGA-3′,

and for *Defb14* were forward: 5′-ATCTTGTTCTTGGTGCC TGC-3′, and reverse: 5′-CTTCTTTCGGCAGCATTTTC-3′. All primers were obtained from Thermo Fisher Scientific (Waltham, MA). The target RNA level was normalized to the endogenous *Rps18* reference, and the changes in gene expression were reported as fold increases relative to vehicle.

Enzyme-Linked Immunosorbent Assay

Subconfluent fibroblasts were stimulated with 10-20 μg/ml hBD-3 for 3-48 hours, and the cell-free supernatants from cultures of stimulated cells or nonstimulated control cells were collected and used for the quantification of FGF, PDGF and VEGF by appropriate ELISA kits obtained from R&D Systems (Minneapolis, MN). ELISAs were performed following the recommendations of the supplier. In some experiments, cells were pretreated with cryptotanshinone, AZD1480 or SSR 1281289E for 2 hours before stimulation with hBD-3, and ELISA was performed as described above.

Chemotaxis Assay

Fibroblast migration was assayed using a modified Boyden chamber consisting of a 48-well microchamber (Neuro Probe, Gaithersburg, MD). Subconfluent fibroblasts were trypsinized, and a volume of 50 μl containing 5.0×10^4 cells was loaded into the upper chambers, which were separated from the lower chambers by a polyvinylpyrrolidone-free polycarbonate membrane with an 8-μm pore size (Neuro Probe) and precoated with 10 μg/ml type I collagen at 37°C for 2 hours. The lower chambers contained 27 μl of various doses of hBD-3 or vehicle. After a 6-hour incubation at 37°C in a CO_2 incubator, the membrane was removed from the chamber, and the cell side was rinsed in PBS drawn across with a wiper blade to remove the nonmigrated cells. The membrane was then stained with Diff-Quick (Kokusai Shiyaku, Kobe, Japan) according to the manufacturer's instructions. Cells that had migrated and adhered to the lower side of the membrane were counted in 3 randomly selected high-power fields under a laser scanning microscope 700 (Zeiss, Jena, Germany). In some experiments, cells were pretreated with various inhibitors for 2 hours before being added to the upper chambers, and the chemotaxis assay was performed as described above.

In Vitro Scratching Assay

Fibroblasts were seeded in a collagen I-coated 96-well plate at a density of 5×10^4 cells/well for 6 hours at 37°C. Confluent fibroblast monolayers were then wounded using a wound maker (Essen BioScience, Ann Arbor, MI) to create a uniform cell-free zone in each well and washed with PBS to remove the detached cells. In all experiments, fibroblasts were pretreated with 10 μg/ml mitomycin C for 2 hours before stimulation with hBD-3 for 24-48 hours to exclude the influence of hBD-3-mediated cell proliferation on migration. After stimulation, fibroblasts were stained with 0.5% crystal violet (Fujifilm, Tokyo, Japan), and images were recorded using a phase-contrast microscope (Keyence). Wound area was measured using ImageJ software. In some experiments, cells were pretreated with inhibitors for 2 hours before stimulation with hBD-3.

Cell Proliferation Assay

Cell proliferation was assessed by Cell Counting Kit-8 (CCK-8) purchased from Dojindo Laboratories (Kumamoto, Japan) following instructions from the manufacturer. Fibroblasts were seeded into 96-well plates at a density of 1.0×10^4 cells/well and cultured for 24 hours before stimulation with hBD-3 for 72 hours. After stimulation, 10 μl of CCK-8 solution was added to each well, and the cells were incubated for 1 hour at 37°C. The amount of formazan dye was measured by absorbance at 450 nm using a microplate reader. In some experiments, cells were pretreated with various inhibitors for 2 hours before stimulation with hBD-3.

Western Blot

Following stimulation, fibroblasts were lysed with RIPA buffer, and the proteins were extracted from the cells and quantified using Precision Red Protein Assay Reagent (Cytoskeleton, Denver, CO). Equal amounts of protein were separated in an 8% to 12% SDS-PAGE gel followed by transfer to methanol-preactivated polyvinylidene difluoride membranes (Millipore, Billerica, MA) for 50 minutes. The membranes were then blocked in Immuno-Block buffer (KAC, Hyogo, Japan.) for 1 hour at room temperature and incubated with primary antibodies against MMP-2 (1:1000 dilution), MMP-9 (1:2000 dilution), phosphorylated FGFR1 (1:500 dilution), STAT1 (1:500 dilution), STAT3 (1:1000 dilution), JAK1 (1:500 dilution), JAK2 (1:500 dilution), JAK3 (1:500 dilution), unphosphorylated FGFR1, STAT1, STAT3, JAK1, JAK2 and JAK3 (each 1:1000 dilution) overnight at 4°C, according to the manufacturer's instructions. After washing, the membranes were developed with Luminata Forte Western HRP substrate (Millipore, Billerica, MA) for detection and visualized using Fujifilm LAS-4000 Plus (Fujifilm). The intensity of bands was quantified using the software program ImageJ Gauge (LAS-1000plus, Fujifilm) to allow correction for protein loading.

Statistical Analysis

Statistical analysis was performed by one-way or two-way analysis of variance (ANOVA) with multiple comparisons test or Student's *t*-test using GraphPad Prism version 6.0 (San Diego, CA). Values are presented as the mean ± standard deviation (SD). $P < 0.05$ was considered significant.

RESULTS

hBD-3 Accelerates Wound Healing *In Vivo*

To investigate the effect of hBD-3 on skin wound healing, we first used an excisional wound model to observe the healing process for 16 consecutive days in C57BL/6 mice. We used a wound splinting model to prevent local contraction because with this model, the wound heals through granulation and re-epithelization, similar to the wound healing process in humans. In the preliminary dose-dependent experiments using 40–400 μg/ml hBD-3, we observed that 200 μg/ml was the most effective concentration for accelerating wound healing.

Therefore, this concentration was used in further *in vivo* experiments. As shown in **Figure 1A**, the wounds treated with hBD-3 displayed considerable signs of wound healing and healed faster than the vehicle-treated wounds. The hBD-3-treated wounds started to heal on day 6 and completely healed on day 12 post-injury. **Figure 1B** shows the percentage of wound area. The wound percentage was significantly lower in the hBD-3-treated groups than in the vehicle groups on days 6, 8 and 10 post-injury, suggesting that hBD-3 accelerated wound healing *in vivo*. We confirmed that mBD-14, a mouse ortholog of hBD-3 (23), also accelerated wound healing in mice with almost the same potency as seen for hBD-3 (**Figure S1**).

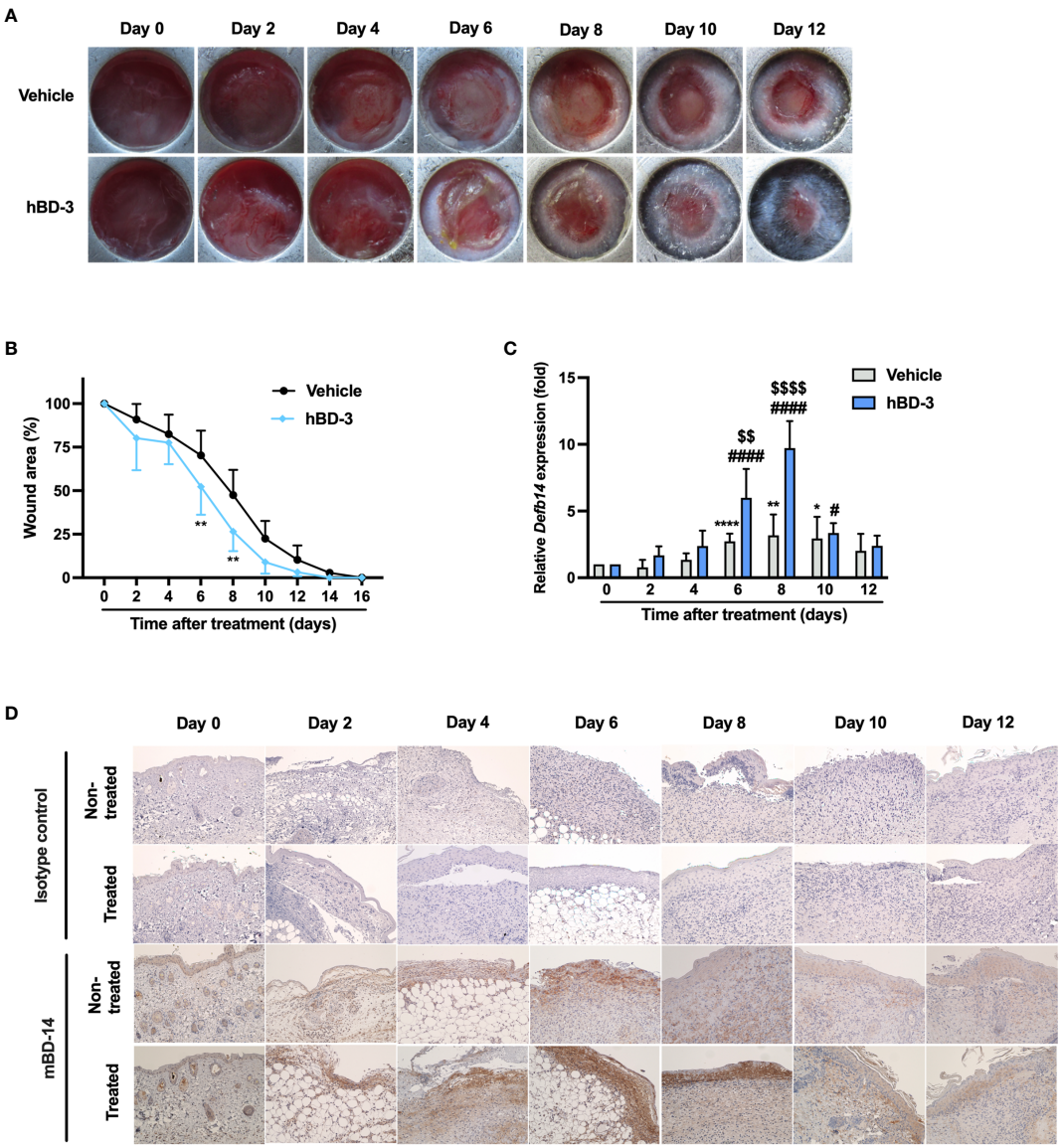

FIGURE 1 | hBD-3 accelerates wound closure *in vivo*. Dorsal full-thickness skin wounds were created on mice and then topically treated with 0.01% acetic acid (vehicle) and 200 μg/ml hBD-3. **(A)** Representative images of skin wounds from day 0 to day 12. **(B)** The average wound area was calculated using ImageJ software. The *P* value was evaluated using one-way ANOVA with Tukey's multiple comparisons test. $^{*}P < 0.05$ and $^{**}P < 0.01$ between the vehicle-treated wounds and the hBD-3-treated wounds. $n = 3$ wound areas/group. **(C)** mRNA was extracted from the wound tissues and the mRNA expression of Defb14 (mBD-14) was detected by quantitative real-time PCR analysis using SYBR Premix Ex Taq. The *P* value was determined by one-way ANOVA with Tukey's multiple comparisons test. $^{*}P < 0.05$, $^{**}P < 0.01$ and $^{****}P < 0.0001$ for comparisons between the vehicle-treated wounds. $^{\#}P < 0.05$ and $^{\#\#\#\#}P < 0.0001$ for comparisons between hBD-3-treated wounds. $^{\$\$}P < 0.01$ and $^{\$\$\$\$}P < 0.0001$ for comparisons between the vehicle-treated and hBD-3-treated wounds. $n = 3$. **(D)** Representative images of mBD-14 staining and isotype control staining in treated and nontreated wounds from day 0 to 12. Original magnification: 20×.

A previous study reported that skin injury induces hBD-3 expression (24). Therefore, we evaluated the basal expression of mBD-14/hBD-3 at both mRNA and protein levels. As seen in **Figure 1C**, the basal mRNA expression of mBD-14 was markedly increased from day 6 to day 10 in nontreated groups compared to day 0, and this expression was further enhanced in hBD-3-treated wounds. Meanwhile, immunohistochemical analysis showed that nontreated wounds had the highest basal expression of mBD-14 on day 4 and day 6, and the treatment of wounds with hBD-3 further increased this expression from day 2 to day 10, with wounds on day 6 and day 8 showing the stronger staining of mBD-14 compared to vehicle groups (**Figure 1D**).

hBD-3 Promotes Angiogenesis and Increases the Production of Angiogenic Growth Factors

Angiogenesis is one of the critical processes for wound healing. Given that hBD-3 accelerated wound healing *in vivo*, we hypothesized that this peptide might also contribute to the promotion of angiogenesis during wound healing. The analysis of subcutaneous wound tissues collected on days 6, 8 and 10 post-injury revealed that the wounds treated with hBD-3 had remarkably increased new vessel formation. Compared to the vehicle-treated groups, the hBD-3-treated groups displayed increased vessel size and number of vessels in subcutaneous tissues (**Figure 2A**).

Given that angiogenesis is tightly regulated by various angiogenic growth factors, the effect of hBD-3 on the expression of angiogenic growth factors was investigated. As observed in **Figure 2B**, hBD-3-treated wound tissues showed significantly higher mRNA expression of FGF on day 6, PDGF on days 6 and 8 and VEGF on day 8 post-injury than that of the control tissues. hBD-3 treatment did not have any effect on other growth factors, such as epidermal growth factor and transforming growth factor (data not shown).

hBD-3 Initiates the Inflammatory Phase of Wound Healing and Decreases Inflammatory Responses

In the inflammatory phase, inflammatory cells such as neutrophils and macrophages are recruited to the wound site

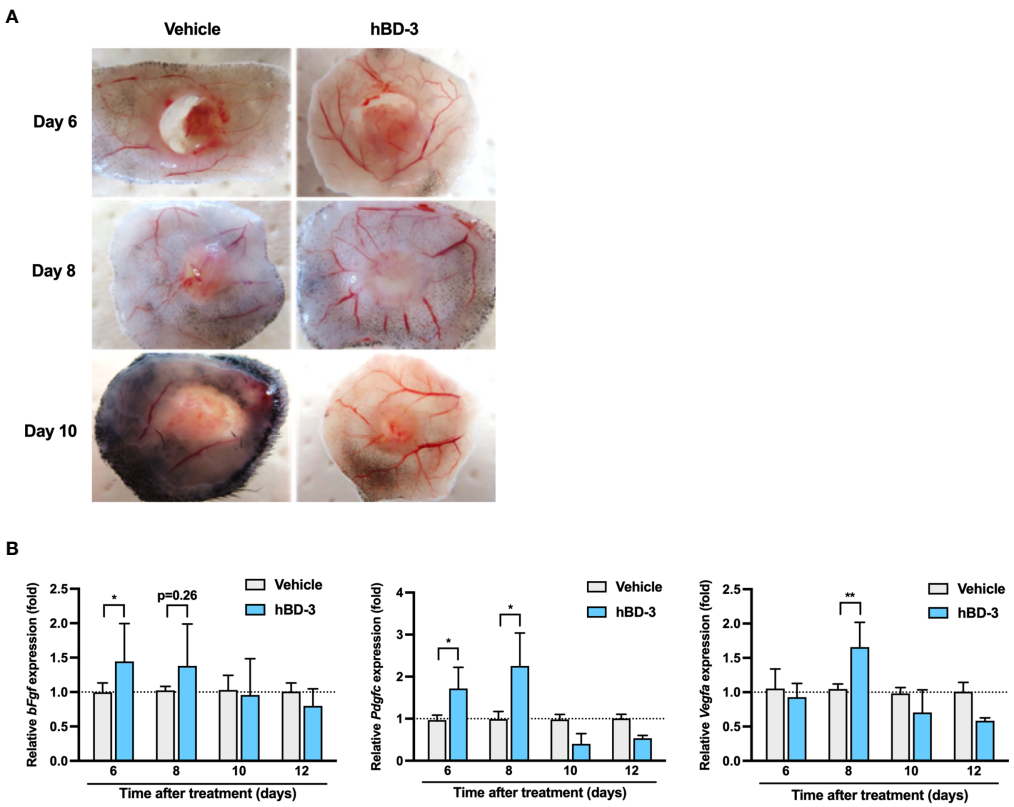

FIGURE 2 | hBD-3 promotes angiogenesis and induces the production of angiogenic growth factors. **(A)** Representative images of the macroscopic appearance of newly formed blood vessels at the wound sites on days 6, 8 and 10 post-injury in the mice treated with 0.01% acetic acid (vehicle) and 200 μg/ml hBD-3. **(B)** Biopsies were obtained from the dorsal skin wound tissues, and the mRNA expression of *bFgf, Pdgf*, and *Vegfa* was evaluated by quantitative real-time PCR analysis using SYBR Premix Ex Taq. The *P* value was calculated using one-way ANOVA with Tukey's multiple comparisons test. $^{*}P < 0.05$ and $^{**}P < 0.01$ for comparisons between the vehicle-treated and hBD-3-treated wounds. $n = 3$.

to cleanse the wound (25). In this study, we chose MPO and Iba1 as markers of neutrophils and macrophages, respectively. Iba1 is recognized as a panmacrophage marker and has been widely used to identify macrophages within skin (26, 27). As observed in **Figure 3A**, immunohistochemistry showed that on day 2 post-injury, a higher number of neutrophils was observed in the wound areas treated with hBD-3 than in those of the control groups treated with vehicle alone. Interestingly, on day 4 after injury, the number of neutrophils was significantly reduced in the hBD-3-treated groups compared with the control groups. Quantification is shown in right panel. Similarly, as observed in **Figure 3B** (quantification shown in right panel), the number of macrophages at the wound site treated with hBD-3 was higher on day 2 post-injury, and this number decreased on day 4 compared to that of the vehicle-treated wounds. Macrophages have been divided into M1 and M2 subtypes. We used CD80 as a marker of pro-inflammatory M1 phenotype (28), and CD163 for identification of anti-inflammatory M2 phenotype (29). While M1 positive macrophages were not detected neither at nontreated nor treated wound areas (**Figure 3C**, upper panels), M2 positive cells noticeably increased at the wound sites treated with hBD-3 on day 2 and this number declined on day 4 (**Figure 3C**, lower panels, quantification shown in right panel). Successful wound healing requires the shifting of macrophages from pro-inflammatory M1 phenotype to anti-inflammatory M2 phenotype with wound healing capacity (30, 31). Overall, this observation suggests that hBD-3 initiates the inflammatory phase of the wound healing process by inducing the infiltration of neutrophils and macrophages and decreases inflammation by later eliminating these cells during wound healing.

hBD-3 Promotes Fibroblast Accumulation *In Vivo* and Migration and Proliferation *In Vitro*

The second phase of the wound healing process consists of the proliferative phase, which mainly involves fibroblast migration and proliferation (6). HSP47, rather than α-smooth muscle actin (α-SMA), was used as a marker of fibroblasts because we aimed to identify all fibroblasts instead of only myofibroblasts that express α-SMA (32, 33). Notably, the α-SMA antibody may be less specific, as it also stains vascular smooth muscle cells in granulation tissue (34). Immunohistochemistry showed that on day 4 and day 6 post-injury, the wounds treated with hBD-3 displayed a higher number of fibroblasts than wounds treated with vehicle alone. Although fibroblast number was also increased on day 8 and day 10 post-injury, there was not statistically significant difference between treated and nontreated groups (**Figure 4A**, quantification shown in right panel). This finding suggests that hBD-3 might promote fibroblast proliferation and/or migration at the wound site. Therefore, we first used a scratch assay to assess the ability of hBD-3 to induce fibroblast migration *in vitro* using primary human dermal fibroblasts in the presence of mitomycin C to exclude the influence of proliferation on wound healing. Compared to the vehicle-treated cells, the cells stimulated with hBD-3 for 24 and 48 hours rapidly migrated and covered the wound area. This effect was comparable to that induced by FGF+VEGF, which was used as a positive control (**Figure 4B**). Quantification of wound closure is shown in the right panel and illustrates significantly accelerated wound closure following treatment of cells with 0.25 and 0.5 μg/ml hBD-3. We observed that high doses of hBD-3 did not further increase wound closure (data not shown).

The ability of hBD-3 to mediate cell migration was further confirmed by an *in vitro* chemotaxis assay. We found that hBD-3 markedly caused cell migration in a bell-shaped dose-response manner, with 0.5 μg/ml being the optimal concentration. Higher hBD-3 concentrations reduced fibroblast migration (**Figure 4C**). The observation that hBD-3 accelerated wound healing in the presence of mitomycin C indicates that hBD-3-promoted wound healing might be mainly attributed to cell migration. To further determine how hBD-3 promotes wound healing, we investigated the effect of hBD-3 on cell proliferation using a CCK-8 assay kit. As shown in **Figure 4D**, noticeably increased proliferation of fibroblasts was observed when cells were treated with hBD-3. An approximately twofold increase in proliferation was found in fibroblasts stimulated with hBD-3, while the positive control of FGF+VEGF resulted in a threefold increase. Thus, hBD-3 induced both cell migration and proliferation, which are indispensable steps for the promotion of wound healing.

hBD-3 Induces the Production of Angiogenic Growth Factors and the Expression of MMP-2 by Human Fibroblasts

Because hBD-3 promoted angiogenesis and elevated the expression of angiogenic growth factors *in vivo* and given that the fibroblast number was increased at the wound site, we examined the effect of hBD-3 on the production of angiogenic growth factors in human fibroblasts. Following stimulation with hBD-3 for 3 to 48 hours, the amounts of FGF, PDGF and VEGF in the cell supernatants were evaluated by ELISAs. Both 10 μg/ml and 20 μg/ml hBD-3 enhanced the production of VEGF in a dose-dependent fashion, while only 20 μg/ml hBD-3 markedly increased the production of FGF and PDGF at all time points examined (**Figure 5A**).

MMP-2 and MMP-9 are enzymes that play an important role in regulating angiogenesis during wound healing (35, 36). MMP-2 is essential for angiogenesis and prolonged matrix remodeling, while MMP-9 is involved in granulation tissue remodeling (37). Stimulation of human fibroblasts with hBD-3 resulted in significantly increased expression of MMP-2, which was detected from 24 hours and lasted until 72 hours. In contrast, MMP-9 expression was not changed by hBD-3 treatment (**Figure 5B**), suggesting that MMP-2 but not MMP-9 might be involved in hBD-3-mediated angiogenesis and wound healing.

Activation of FGFR Is Required for the hBD-3-Mediated Production of Angiogenic Growth Factors, Migration, and Proliferation in Fibroblasts

Wound healing relies on angiogenic growth factors, and degradation of these factors or downregulated expression of their receptors impairs both angiogenesis and wound healing

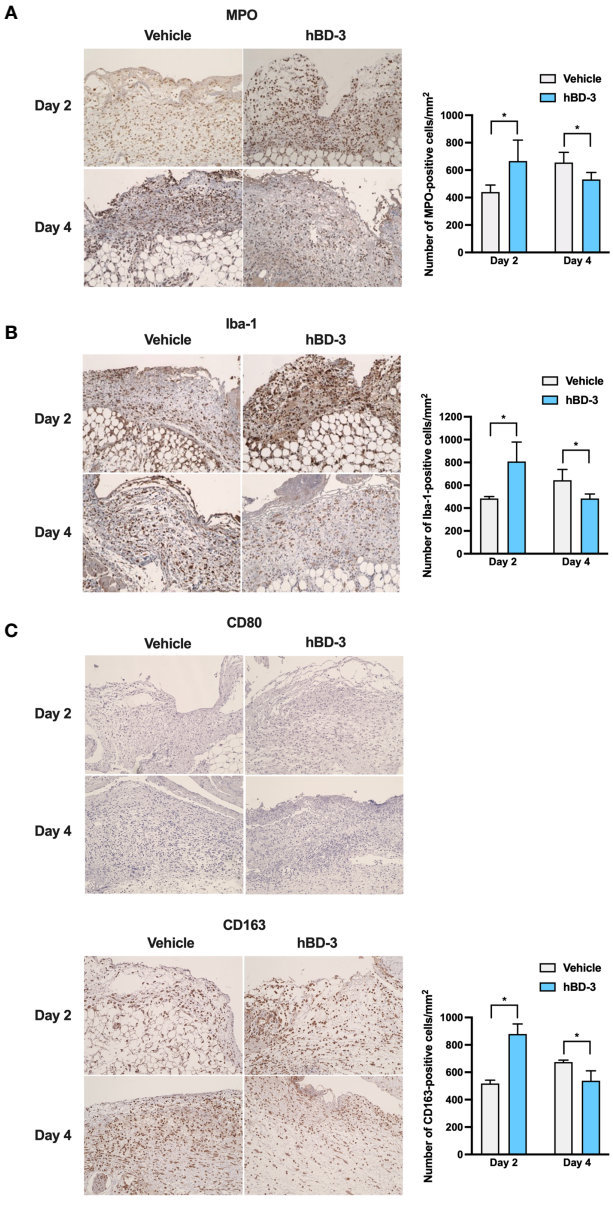

FIGURE 3 | hBD-3 accelerates the inflammatory phase of wound healing and decreases inflammatory responses. Representative images of skin wound biopsies from mice treated with 0.01% acetic acid (vehicle) and 200 μg/ml hBD-3. On day 2 and day 4 post-injury, sections were immunohistochemically stained with **(A)** anti-myeloperoxidase (MPO) antibody for neutrophil detection, **(B)** with anti-Iba-1 antibody for macrophage detection, and **(C)** with anti-CD80 (upper panels) and anti-CD163 (lower panels) antibodies for M1 and M2 macrophage detection followed by counterstaining with hematoxylin. MPO-, Iba-1- and CD163-positive cells were detected in both the epidermis and dermis of the wounds. Original magnification: 20×. Number of MPO-, Iba-1- and CD163-positive cells were counted and shown in right panels. The *P* value was calculated using Student's *t* test. $^*P < 0.05$ for comparisons between the vehicle-treated and hBD-3-treated wounds. $n = 3$.

(3,6). To verify whether hBD-3 mediated angiogenesis *via* angiogenic factor receptors, we pretreated fibroblasts with SSR 128129E (FGFR inhibitor), fruquintinib (VEGFR inhibitor) and imatinib mesylate (PDGFR inhibitor) and tested production of FGF, PDGF and VEGF after hBD-3 stimulation. Interestingly, among the above inhibitors tested, the FGFR inhibitor SSR 128129E exhibited the most significant inhibitory effect on PDGF and VEGF production but failed to inhibit FGF production (**Figure 6A**). Pretreating fibroblasts with various concentrations of fruquintinib and imatinib mesylate for 2 to 24 hours did not significantly reduce hBD-3-induced production of the tested angiogenic growth factors, suggesting that VEGFR and PDGFR were not involved in hBD-3-mediated production of angiogenic growth factors by fibroblasts (**Figures S2, S3**).

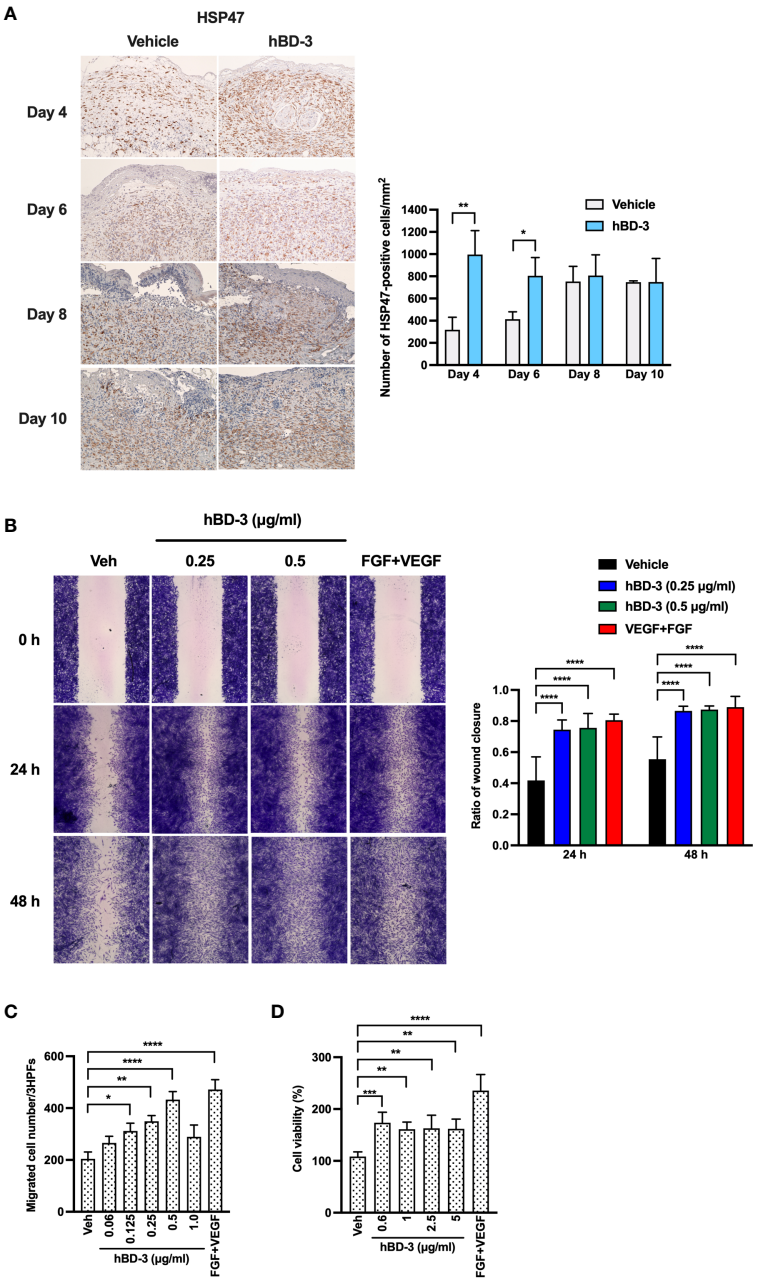

FIGURE 4 | hBD-3 enhances fibroblast accumulation *in vivo* and migration and proliferation *in vitro*. **(A)** Representative images of skin wound biopsies from mice treated with 0.01% acetic acid (vehicle) and 200 μg/ml hBD-3. On day 4, 6, 8 and 10 post-injury, sections were immunohistochemically stained with anti-heat shock protein 47 (HSP47) antibody for fibroblast detection and then counterstained with hematoxylin. HSP47-positive cells were detected in both the epidermis and dermis of the wounds. Original magnification: 20×. Number of HSP47-positive cells were counted and shown in right panel. The *P* value was calculated using Student's *t* test. $^{*}P < 0.05$ and $^{**}P < 0.01$ for comparisons between the vehicle-treated and hBD-3-treated wounds. $n = 3$. **(B)** Human primary fibroblasts were treated with 10 μg/ml mitomycin C for 2 hours, and a scratch assay was performed. Following treatment with 0.01% acetic acid (vehicle) and 0.25 and 0.5 μg/ml hBD-3 and FGF+VEGF (100 ng/ml each) for 24 and 48 hours, fibroblasts were stained with crystal violet, and images were recorded. Left panels are representative images of the scratch assay, and right panels show average data calculated using ImageJ software. **(C)** Various doses of hBD-3 were added to the lower chambers, and fibroblasts were added in the upper chambers of the chemotaxis microchamber. Following a 6-hour incubation, the membrane was stained, and migrated cells attached to the bottom surface were fixed and then stained with Diff-Quick. Migrated cells were counted in 3 random high-power fields (HPFs) under a light microscope. **(D)** Cells were stimulated with the indicated doses of hBD-3 or FGF+VEGF (100 ng/ml each) for 72 hours. Cell proliferation was assessed using a CCK-8 kit. The *P* value was calculated using one-way ANOVA with Tukey's multiple comparisons test. $^{*}P < 0.05$, $^{**}P < 0.01$, $^{***}P < 0.001$, and $^{****}P < 0.0001$ for comparison with vehicle and hBD-3. $n = 3$.

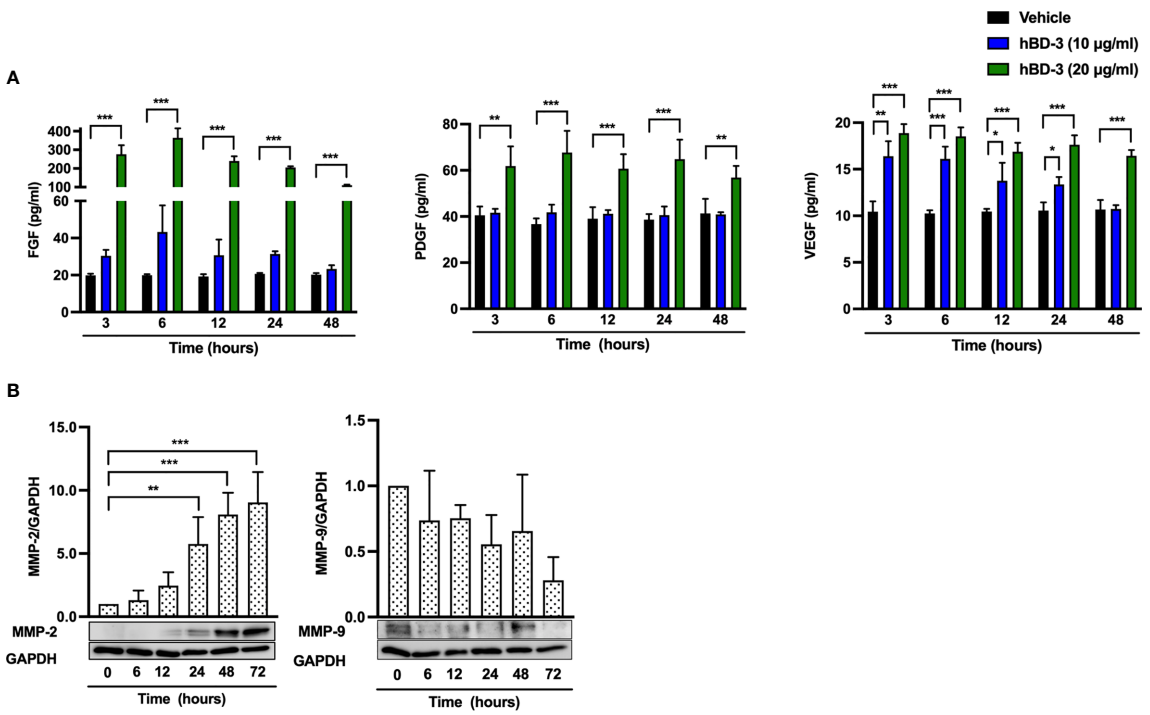

FIGURE 5 | hBD-3 increases the production of angiogenic growth factors and the expression of MMP-2 in fibroblasts. **(A)** Fibroblasts were stimulated with 10-20 μg/ml hBD-3 or 0.01% acetic acid (vehicle) for 48 hours, and the amounts of VEGF (left panel), PDGF (middle panel) and FGF (right panel) released in the culture supernatants were determined by ELISAs. **(B)** Fibroblasts were stimulated with 20 μg/ml hBD-3 for 6 to 72 hours and subjected to Western blotting using antibodies against MMP-2 and MMP-9. Bands were quantified using densitometry. The *P* value was calculated using one-way ANOVA with Tukey's multiple comparisons test. $^{*}P < 0.05$, $^{**}P < 0.01$, and $^{***}P < 0.001$ for comparisons between vehicle and hBD-3. $n = 3$.

Next, we examined the effect of the FGFR pathway on cell migration and proliferation. Pretreatment of fibroblasts with SSR 128129E markedly delayed *in vitro* wound healing (**Figure 6B**) and suppressed fibroblast chemotaxis (**Figure 6C**) and cell proliferation (**Figure 6D**) induced by hBD-3. These results suggest that the FGFR pathway mediates the hBD-3-induced promotion of angiogenesis and wound healing. Indeed, we confirmed that hBD-3 induced FGFR activation. As shown in **Figure 6E**, stimulation of fibroblasts with hBD-3 showed that this peptide significantly induced the phosphorylation of FGFR1 threefold and fourfold following stimulation for 60 minutes and 120 minutes, respectively. This result suggests that hBD-3 upregulates the activity of the FGFR1 receptor mainly through phosphorylation.

hBD-3 Induces Phosphorylation of JAK2 and STAT3

Because the FGFR/JAK/STAT pathway is known to contribute to cell proliferation, angiogenesis and migration during wound healing (38), we hypothesized that hBD-3 might activate the JAK and STAT pathways, in addition to the FGFR pathway. Using Western blotting, we observed that hBD-3 induced phosphorylation of both JAK2 and STAT3. Following stimulation with hBD-3, JAK2 underwent rapid phosphorylation, which was already detectable after 5 minutes of stimulation. This phosphorylation peaked at 15 minutes before decreasing to basal levels within 2 hours (**Figure 7A**). In contrast to JAK2, hBD-3-induced STAT3 phosphorylation was slightly detected at 60 minutes and strongly elevated at 120 minutes (**Figure 7B**). These results indicate that JAK2 and STAT3 are part of the molecular pathways involved in hBD-3-mediated activation of fibroblasts. We observed that hBD-3 did not affect the phosphorylation of JAK1, JAK3, or STAT1 (**Figure S4**).

Both JAK2 and STAT3 Are Necessary for the hBD-3-Mediated Production of Angiogenic Growth Factors, Migration, and Proliferation in Fibroblasts

To determine whether the JAK2/STAT3 pathways are indeed required for hBD-3-induced angiogenic growth factor secretion, migration and proliferation of fibroblasts, cells were pretreated with AZD1480 (JAK2 inhibitor) or cryptotanshinone (STAT3 inhibitor) for 2 hours before stimulation with hBD-3 for 24 hours. As shown in **Figure 8A**, the presence of AZD1480 markedly reduced the hBD-3-induced production of PDGF and VEGF by approximately 60% and 50%, respectively.

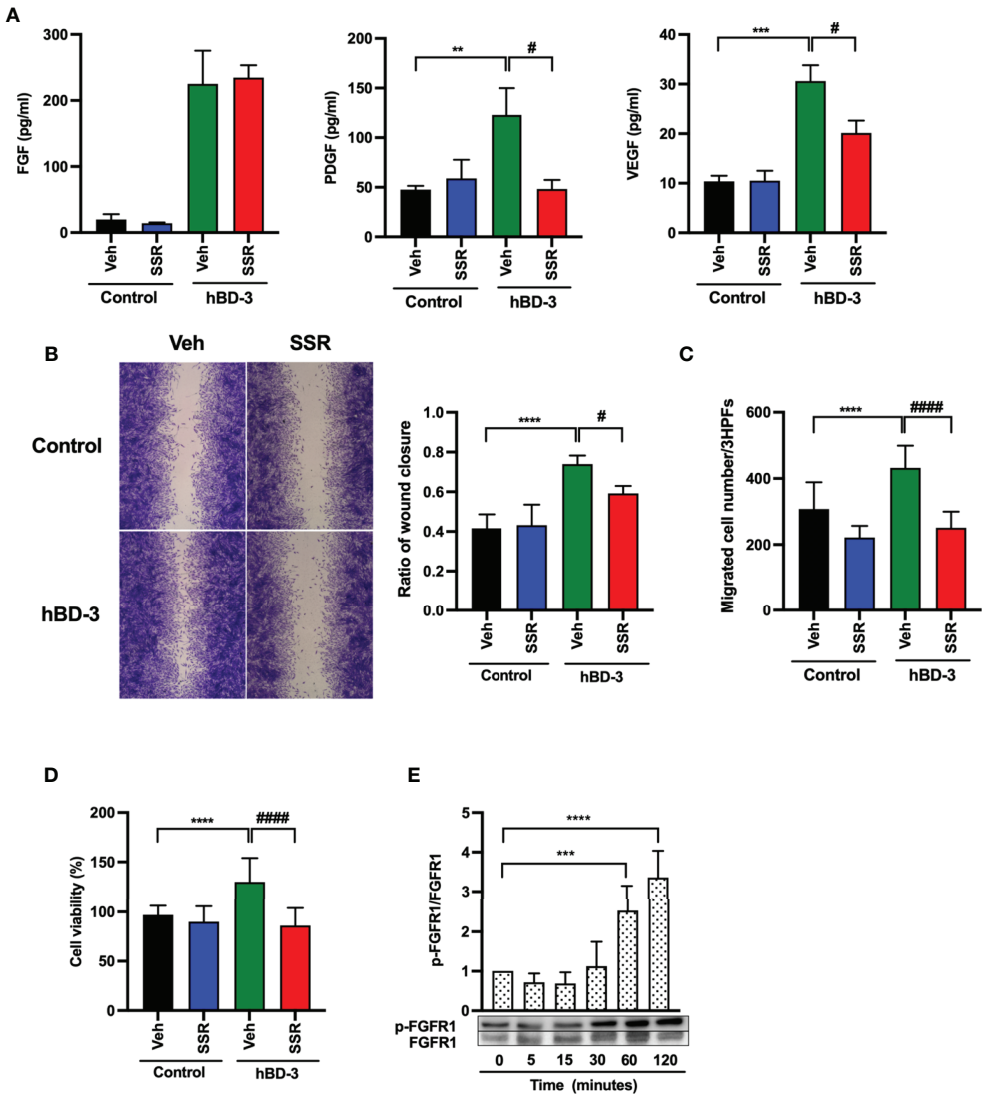

FIGURE 6 | Activation of FGFR1 is required for hBD-3-mediated production of angiogenic growth factors, migration and proliferation of fibroblasts. Human dermal fibroblasts were pretreated with 0.1% DMSO (vehicle) or 1 μM SSR 128129E (SSR) for 2 hours and then exposed to 0.01% acetic acid (control) or hBD-3. **(A)** The levels of VEGF, PDGF and FGF in the culture supernatants from pretreated cells stimulated for 48 hours with 20 μg/ml hBD-3 were measured by appropriate ELISAs. **(B)** An *in vitro* wound scratch assay in pretreated fibroblasts stimulated with solvent (control) or 0.25 μg/ml hBD-3 for 48 hours was performed. Left panels show representative images, while the right panel represents the average of wound areas analyzed using ImageJ software. **(C)** Pretreated fibroblasts were also added to the upper wells of the microchamber and allowed to migrate for 6 hours towards solvent (control) or 0.5 μg/ml hBD-3. Migrated cells were counted in 3 random high-power fields (HPFs) under a light microscope. **(D)** Pretreated fibroblasts were stimulated with 1 μg/ml hBD-3 for 72 hours, and cell proliferation was assessed using the CCK-8 kit. **(E)** Fibroblasts were stimulated with 20 μg/ml hBD-3 for 5 minutes to 120 minutes and subjected to Western blotting using antibodies against phosphorylated or unphosphorylated FGFR1. Bands were quantified using densitometry. The *P* value was determined using one-way ANOVA with Tukey's multiple comparisons test. $^{**}P < 0.01$, $^{***}P < 0.001$ and $^{****}P < 0.0001$ for comparisons between the nonstimulated cells (0 minutes) and the hBD-3-stimulated cells without inhibitors. $^{\#}P < 0.05$ and $^{\#\#\#\#}P < 0.0001$ for comparisons between the hBD-3-stimulated cells in the presence or absence of inhibitor, $n = 3$.

However, the presence of AZD1480 did not affect hBD-3-mediated FGF production. AZD1480 had no significant effect on the spontaneous production of FGF, PDGF and VEGF. Similarly, we observed that pretreatment of fibroblasts with the STAT3 inhibitor cryptotanshinone suppressed the hBD-3-mediated production of both VEGF and PDGF to basal levels and reduced the production of FGF by approximately 50% (**Figure 8B**).

We next evaluated the inhibitory effects of JAK2 and STAT3 inhibitors on fibroblast migration and proliferation. Pretreatment of fibroblasts with either AZD1480 or cryptotanshinone noticeably suppressed the *in vitro* wound healing promoted by hBD-3 by approximately 40% or 50%, respectively (**Figure 8C**). Moreover, both AZD1480 and cryptotanshinone reduced fibroblast chemotaxis and proliferation induced by hBD-3 at the basal levels (**Figures 8D, E**). Collectively, these data demonstrated

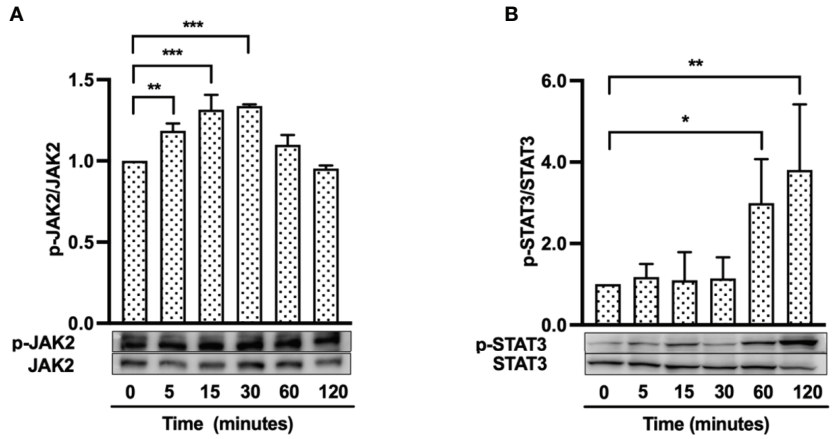

FIGURE 7 | hBD-3 enhances phosphorylation of JAK2 and STAT3. Fibroblasts were stimulated with 20 μg/ml hBD-3 for 5 minutes to 120 minutes and subjected to Western blotting using antibodies against phosphorylated or unphosphorylated JAK2 **(A)** and STAT3 **(B)**. Bands were quantified using densitometry. The *P* value was calculated using one-way ANOVA with Tukey's multiple comparisons test. $^{*}P < 0.05$, $^{**}P < 0.01$, and $^{***}P < 0.001$ for comparisons between the nonstimulated (0 minutes) and hBD-3-stimulated cells. $n = 3$.

that hBD-3 promotes angiogenesis and wound healing through the FGFR1/JAK2/STAT3 pathways. Indeed, we confirmed that the FGFR inhibitor also inhibited hBD-3-induced phosphorylation of JAK2 and STAT3, suggesting that the JAK2/STAT3 pathways function downstream of FGFR1 (**Figure S5**).

DISCUSSION

Previous studies showed that the skin-derived antimicrobial peptide hBD-3 chemoattracts macrophages, mast cells and keratinocytes that contribute to the wound healing process (19, 39); however, the effects of hBD-3 on fibroblasts have not been reported thus far. In this investigation, following hBD-3 treatment, the wounds created in C57BL/6 mice healed faster, showed accumulation of inflammatory cells in the early stage of wound healing, and increased the number of fibroblasts and newly formed vessels. Additionally, *in vitro* studies demonstrated that hBD-3 enhanced the production of various angiogenic growth factors and induced the migration and proliferation of human fibroblasts through the FGFR1/JAK2/STAT3 pathways (**Figure 9**). These observations suggest that hBD-3 might accelerate skin wound healing *via* activation of fibroblasts.

Although we used mice as an animal model to investigate the therapeutic effects of hBD-3 on wound healing, wound healing in mice is basically different from that in humans because it mainly occurs *via* contraction (40). To avoid and prevent contraction, we used ring-shaped silicone splints, thus allowing the repair process to be dependent on epithelialization, cellular proliferation and angiogenesis, a process similar to that in humans (41). In the inflammatory phase of wound healing, innate immune cells such as macrophages and neutrophils accumulate at the wound site to attack invading pathogens and remove dead tissues (42, 43). In this phase, the number of infiltrating macrophages reaches a peak 3 days post-injury and persists until day 7, whereas the number of neutrophils peaks 1 day post-wounding before declining gradually (44). Moreover, macrophages are divided into M1 and M2 phenotypes. M1 phenotype appears in the very early stage of inflammation with pro-inflammatory properties, whereas M2 phenotype is predominant in the latter stage of inflammation with anti-inflammatory effects (30, 31). Additionally, M2 macrophages are involved in wound healing by promoting angiogenesis *via* the production of VEGF and remodeling (45). Transition of macrophages from M1 to M2 phenotype occurs during acute wound healing process, and failure of this transition leads to the persistence of pro-inflammatory macrophages at the wound site, resulting in chronic wound (30, 31, 46). In our study, we observed that in hBD-3-treated wounds, the number of both neutrophils and macrophages, mostly M2 but not M1 phenotype, at the wound site was higher in the early stage of wound healing (day 2 post-injury) and declined on day 4, whereas the number of these cells increased at day 4 in the control groups. This observation suggested that hBD-3 initiates the inflammatory phase and contributes to inflammatory resolution, leading to acceleration of the wound healing process. Chronic wounds, including diabetic foot ulcers are often linked to prolonged inflammation, which may be caused by various factors such as dysfunction of neutrophils and macrophages, the failure of macrophages to switch from M1 to M2 phenotype, reduction of anti-inflammation cytokines and overproduction of reactive oxygen species (47–50). The ability of hBDs to induce the migration and activation of neutrophils and macrophages (51–53) might be one of the mechanisms by which it accelerates the infiltration of phagocytes, leading to wound healing.

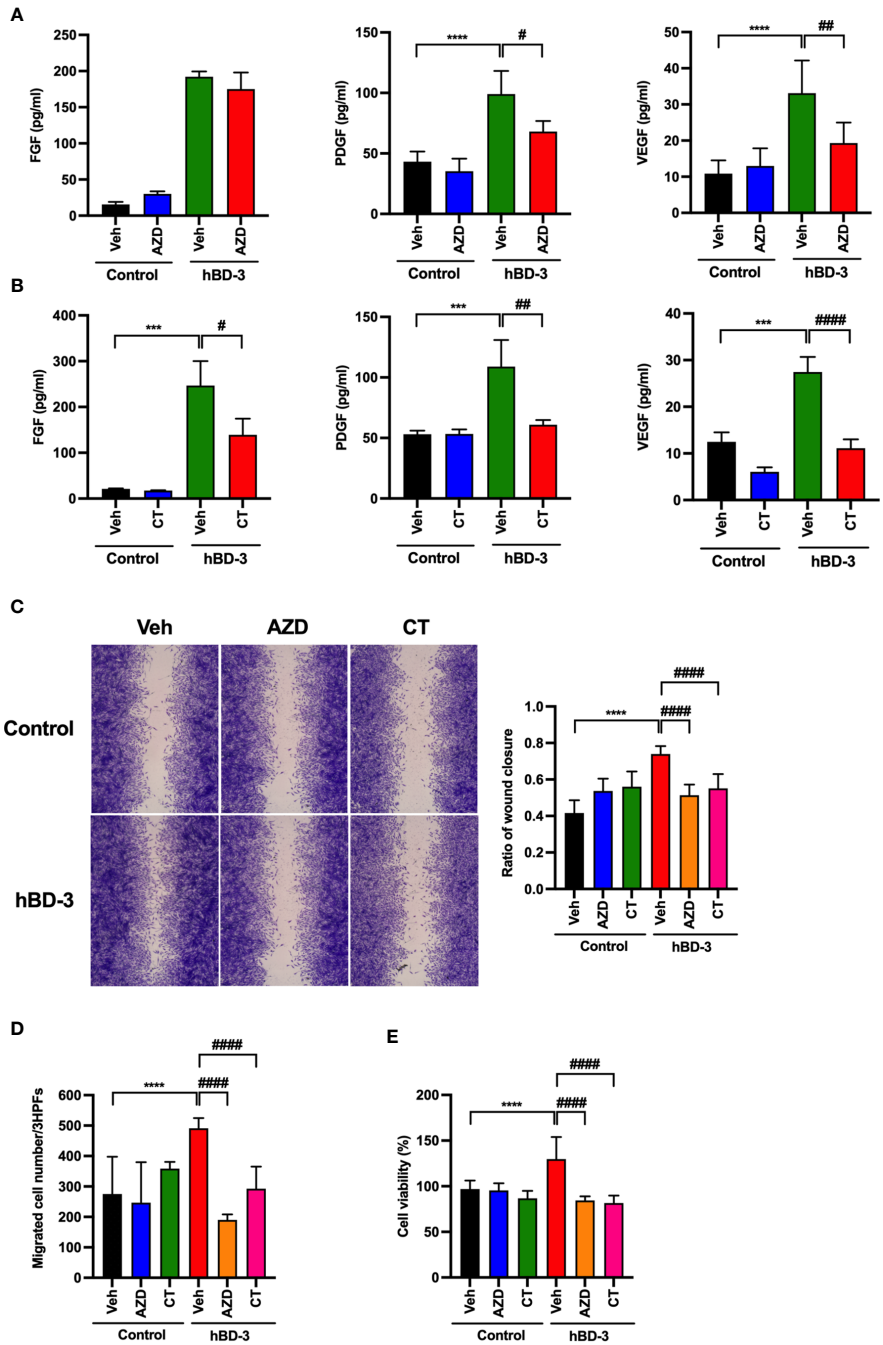

FIGURE 8 | Both JAK2 and STAT3 are necessary for the hBD-3-mediated production of angiogenic growth factors, migration and proliferation of fibroblasts. Fibroblasts were pretreated with **(A)** 10 μM AZD1480 (AZD) or **(B)** 8 μM cryptotanshinone (CT) or 0.1% DMSO (vehicle) for 2 hours and then exposed to hBD-3. The levels of VEGF, PDGF and FGF in the culture supernatants from pretreated cells stimulated for 48 hours with 20 μg/ml hBD-3 were measured by appropriate ELISAs. **(C)** An *in vitro* wound scratch assay in pretreated fibroblasts stimulated with solvent (control) or 0.25 μg/ml hBD-3 for 24 hours was performed. Left panels show representative images, while the right panel represents the average of wound areas analyzed using ImageJ software. **(D)** Pretreated fibroblasts were also added to the upper wells of the microchamber and allowed to migrate for 6 hours towards solvent (control) or 0.5 μg/ml hBD-3. Migrated cells were counted in 3 random high-power fields (HPFs) under a light microscope. **(E)** Pretreated fibroblasts were stimulated with 1.0 μg/ml hBD-3 for 72 hours, and cell proliferation was assessed using the CCK-8 kit. The *P* value was determined using one-way ANOVA with Tukey's multiple comparisons test. $^{***}P < 0.001$ and $^{****}P < 0.0001$ for comparisons between the nonstimulated cells (control) and the hBD-3-stimulated cells without inhibitors. $^{\#}P < 0.05$, $^{\#\#}P < 0.01$ and $^{\#\#\#}P < 0.001$ for comparisons between the hBD-3-stimulated cells in the presence or absence of inhibitor, $n = 3$.

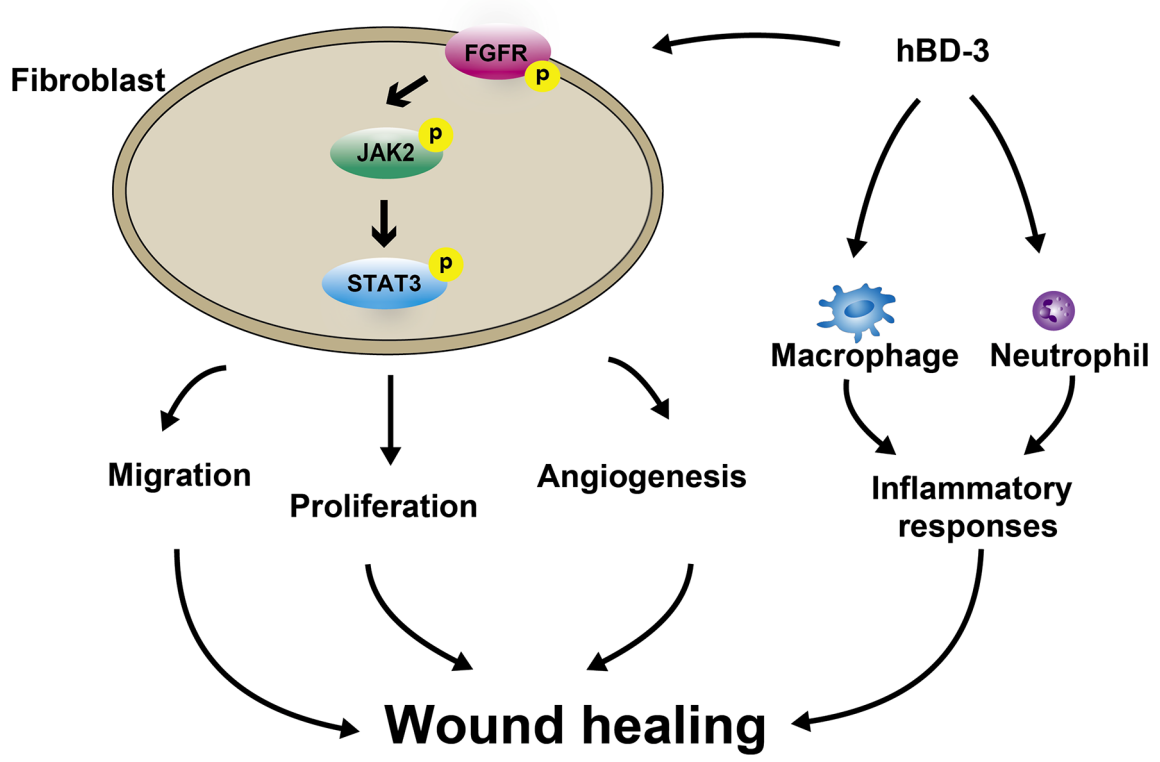

FIGURE 9 | Schematic illustrating how hBD-3 is involved in wound healing. hBD-3 induces accumulation of neutrophils and macrophages in the early phase of wound healing and reduction of these phagocytes in the latter phase, leading to regulation of inflammatory responses during the wound healing process. hBD-3 also stimulates fibroblasts to migrate, proliferate and promote angiogenesis *via* activation FGFR/JAK2/STAT3 pathways.

Among the cells involved in the wound healing process, fibroblasts play a crucial role from the late inflammatory phase until the remodeling phase through migration, proliferation, and secretion of growth factors, cytokines, collagens and other ECM components (54). In the current study, hBD-3-treated wounds displayed an increased number of fibroblasts compared with those of the control mice and showed increased expression of angiogenic growth factors such as FGF, PDGF and VEGF. These growth factors were also significantly secreted in human fibroblasts following hBD-3 stimulation. Notably, VEGF is the most effective angiogenic factor that accelerates neovascularization, angiogenesis and epithelialization (6, 55). FGF is a key regulator of angiogenesis and contributes to re-epithelialization, whereas PDGF promotes cell migration and proliferation (6, 55, 56). hBD-3-stimulated fibroblasts also showed improved migration and proliferation, the two most essential steps responsible for wound closure (57). In addition to growth factors, fibroblasts generate various MMPs. Among the MMPs, MMP-2 and MMP-9 cleave ECM, cytokines, growth factors, and cytokine/growth factor receptors, which control and coordinate signaling pathways in cell proliferation, migration, inflammation, and angiogenesis (37, 58). We found that hBD-3 increased the expression of MMP-2 but not MMP-9. MMP-2 has been shown to be indispensable for angiogenesis and prolonged matrix remodeling, while MMP-9 is involved in keratinocyte migration and granulation tissue remodeling (2).

Wound healing relies on interactions of various growth factors and cytokines that regulate cellular responses. Angiogenic growth factors promote cell proliferation, migration, and angiogenesis by binding to their corresponding receptors and activating multiple downstream signaling pathways (59). Previous studies have shown that the levels of angiogenic growth factors such as FGF, PDGF and VEGF and their respective receptors are downregulated in nonhealing chronic wounds (11–13). Therefore, it is presumed that activation of angiogenic factor receptors along with their downstream pathways may represent a promising novel approach for the treatment of nonhealing chronic wounds. Indeed, some angiogenic growth factors, including FGF, PDGF and VEGF, have been used in clinical trials to promote tissue repair (60–62). Based on this evidence, we investigated the role of hBD-3 in promoting angiogenesis, cell proliferation, and migration of fibroblasts through activation of growth factor receptors such as FGFR, PDGFR and VEGFR. Among the specific inhibitors of the above receptors tested, only the FGFR inhibitor suppressed hBD-3-mediated fibroblast activation, suggesting an important role of FGFR in hBD-3-mediated fibroblast activation. Following binding to FGF, FGFR undergoes autophosphorylation to initiate angiogenesis and tissue remodeling through downstream

signaling pathways (3, 4, 6). Our study revealed that hBD-3 significantly increased FGFR1 phosphorylation and that blocking this receptor with a specific inhibitor markedly suppressed the secretion of angiogenic growth factors, cell migration and proliferation in human fibroblasts.

The JAK/STAT pathway constitutes a major signaling mechanism for various growth factors and cytokines in mammals (63) and plays roles in processes such as cellular proliferation, differentiation, immune regulation, inflammatory response and angiogenesis (64, 65). Among the JAK members, JAK1, 2, and 3 are broadly detected in various tissues and cells, whereas TYK3 is only found in the bone marrow and lymph system (63). After their activation, JAKs induce the phosphorylation of STAT molecules. In this study, hBD-3 induced the phosphorylation of JAK2 but not that of JAK1 and JAK3 and enhanced the phosphorylation of STAT3 but not that of STAT1. Among STAT members, STAT3 has been shown to be important in wound healing through its ability to promote angiogenesis under both physiological and pathological conditions in addition to cell survival, proliferation, and differentiation (66). In this study, the upstream cascade of the JAK2/STAT3 pathway involved FGFR1, as evidenced by the inhibitory effect of an FGFR inhibitor on JAK2 and STAT3 phosphorylation by hBD-3. This inhibitor also suppressed fibroblast migration, proliferation, and secretion of angiogenic growth factors. In a previous study, an association between FGFR and STAT3 activation was demonstrated and was dependent on JAK2 (67).

Following tissue injury, the wound site becomes hypoxic due to the disruption of blood vessels. Hypoxia is a crucial moderator of normal wound healing as it influences every wound healing stage, from fibroblast proliferation to tissue growth and remodeling (68). Therefore, a failure to respond to hypoxic stimuli due to the deficiency of hypoxia-inducible factor (HIF)-1α may lead to the formation of chronic wounds (68). Although there is no direct evidence demonstrating hBD-3-induced activation HIF-1α to accelerate wound healing, the findings that major antimicrobial peptides such as defensins and cathelicidins are downregulated in HIF-1α-deficient mice suggest a correlation between antimicrobial peptides and HIF-1α activation (69). Furthermore, the fact that hBD-3 activates the nuclear factor-kappa B (NF-κB) pathway (70), which interacts with HIF-1α pathway (71) further suggests possible contribution of hBD-3 to HIF-1α activation.

In conclusion, the findings of our study suggest the therapeutic effect of the skin-derived antimicrobial peptide hBD-3 in wounds through its ability to promote wound healing, angiogenesis, cell proliferation and migration in fibroblasts. The effects of hBD-3 on fibroblasts were mediated *via* the FGFR1/JAK2/STAT3 signaling pathways.

DATA AVAILABILITY STATEMENT

The raw data supporting the conclusions of this article will be made available by the authors, without undue reservation.

ETHICS STATEMENT

The animal study was reviewed and approved by Institutional Review Committee of Juntendo University, Juntendo University Graduate School of Medicine.

AUTHOR CONTRIBUTIONS

MT and YU performed experiments and data analysis, and wrote the manuscript. HY, JT-P, GP, LN, and RI assisted with data acquisition and analyses. KO, HO, SI, and FN contributed to conceptualization, methodology, and writing the manuscript. All authors contributed to the article and approved the submitted version.

FUNDING

Parts of the work presented here were supported by a Grant-in-Aid for Scientific Research from the Ministry of Education, Culture, Sports, Science and Technology, Japan (Grant number: 21K08309 to FN) and by the Atopy (Allergy) Research Center, Juntendo University, Tokyo, Japan.

ACKNOWLEDGMENTS

The authors wish to thank the members of Atopy (Allergy) Research Center and Department of Dermatology and Allergology for their comments and Michiyo Matsumoto for secretarial assistance.

SUPPLEMENTARY MATERIAL

The Supplementary Material for this article can be found online at: https://www.frontiersin.org/articles/10.3389/fimmu.2021.712781/full#supplementary-material

REFERENCES

1. Witte MB, Barbul A. General Principles of Wound Healing. *Surg Clin North Am* (1997) 77(3):509–28. doi: 10.1016/s0039-6109(05)70566-1
2. Tombulturk FK, Soydas T, Sarac EY, Tuncdemir M, Coskunpinar E, Polat E, et al. Regulation of MMP 2 and MMP 9 Expressions Modulated by AP-1 (C-Jun) in Wound Healing: Improving Role of Lucilia Sericata in Diabetic Rats. *Acta Diabetol* (2019) 56(2):177–86. doi: 10.1007/s00592-018-1237-5
3. Galiano RD, Tepper OM, Pelo CR, Bhatt KA, Callaghan M, Bastidas N, et al. Topical Vascular Endothelial Growth Factor Accelerates Diabetic Wound Healing Through Increased Angiogenesis and by Mobilizing and Recruiting Bone Marrow-Derived Cells. *Am J Pathol* (2004) 164(6):1935–47. doi: 10.1016/S0002-9440(10)63754-6
4. Qi M, Zhou Q, Zeng W, Wu L, Zhao S, Chen W, et al. Growth Factors in the Pathogenesis of Diabetic Foot Ulcers. *Front Biosci (Landmark Ed)* (2018) 23:310–7. doi: 10.2741/4593

5. Ishihara J, Ishihara A, Fukunaga K, Sasaki K, White MJV, Briquez PS, et al. Laminin Heparin-Binding Peptides Bind to Several Growth Factors and Enhance Diabetic Wound Healing. *Nat Commun* (2018) 9(1):2163. doi: 10.1038/s41467-018-04525-w
6. Barrientos S, Stojadinovic O, Golinko MS, Brem H, Tomic-Canic M. Growth Factors and Cytokines in Wound Healing. *Wound Repair Regener* (2008) 16 (5):585–601. doi: 10.1111/j.1524-475X.2008.00410.x
7. Ghoreschi K, Laurence A, O'Shea JJ. Janus Kinases in Immune Cell Signaling. *Immunol Rev* (2009) 228(1):273–87. doi: 10.1111/j.1600-065X.2008.00754.x
8. Jatiani SS, Baker SJ, Silverman LR, Reddy EP. Jak/STAT Pathways in Cytokine Signaling and Myeloproliferative Disorders: Approaches for Targeted Therapies. *Genes Cancer* (2010) 1(10):979–93. doi: 10.1177/1947601910397187
9. Glosson NL, Bruns HA, Kaplan MH. Wheezing and Itching: The Requirement for STAT Proteins in Allergic Inflammation. *JAKSTAT* (2012) 1(1):3–12. doi: 10.4161/jkst.19086
10. Verhoeven Y, Tilborghs S, Jacobs J, De Waele J, Quatannens D, Deben C, et al. The Potential and Controversy of Targeting STAT Family Members in Cancer. *Semin Cancer Biol* (2020) 60:41–56. doi: 10.1016/j.semcancer.2019.10.002
11. Jacobi J, Tam BY, Sundram U, von Degenfeld G, Blau HM, Kuo CJ, et al. Discordant Effects of a Soluble VEGF Receptor on Wound Healing and Angiogenesis. *Gene Ther* (2004) 11(3):302–9. doi: 10.1038/sj.gt.3302162
12. Stadelmann WK, Digenis AG, Tobin GR. Physiology and Healing Dynamics of Chronic Cutaneous Wounds. *Am J Surg* (1998) 176(2A Suppl):26S–38S. doi: 10.1016/s0002-9610(98)00183-4
13. Dinh T, Braunagel S, Rosenblum BI. Growth Factors in Wound Healing: The Present and the Future? *Clin Podiatr Med Surg* (2015) 32(1):109–19. doi: 10.1016/j.cpm.2014.09.010
14. Niyonsaba F, Kiatsurayanon C, Chieosilapatham P, Ogawa H. Friends or Foes? Host Defense (Antimicrobial) Peptides and Proteins in Human Skin Diseases. *Exp Dermatol* (2017) 26(11):989–98. doi: 10.1111/exd.13314
15. Niyonsaba F, Nagaoka I, Ogawa H, Okumura K. Multifunctional Antimicrobial Proteins and Peptides: Natural Activators of Immune Systems. *Curr Pharm Des* (2009) 15(21):2393–413. doi: 10.2174/138161209788682271
16. Niyonsaba F, Nagaoka I, Ogawa H. Human Defensins and Cathelicidins in the Skin: Beyond Direct Antimicrobial Properties. *Crit Rev Immunol* (2006) 26 (6):545–76. doi: 10.1615/critrevimmunol.v26.i6.60
17. Niyonsaba F, Kiatsurayanon C, Ogawa H. The Role of Human Beta-Defensins in Allergic Diseases. *Clin Exp Allergy* (2016) 46(12):1522–30. doi: 10.1111/cea.12843
18. Mangoni ML, McDermott AM, Zasloff M. Antimicrobial Peptides and Wound Healing: Biological and Therapeutic Considerations. *Exp Dermatol* (2016) 25(3):167–73. doi: 10.1111/exd.12929
19. Niyonsaba F, Ushio H, Nakano N, Ng W, Sayama K, Hashimoto K, et al. Antimicrobial Peptides Human Beta-Defensins Stimulate Epidermal Keratinocyte Migration, Proliferation and Production of Proinflammatory Cytokines and Chemokines. *J Invest Dermatol* (2007) 127(3):594–604. doi: 10.1038/sj.jid.5700599
20. Otte JM, Werner I, Brand S, Chromik AM, Schmitz F, Kleine M, et al. Human Beta Defensin 2 Promotes Intestinal Wound Healing *In Vitro*. *J Cell Biochem* (2008) 104(6):2286–97. doi: 10.1002/jcb.21787
21. Sheng Q, Lv Z, Cai W, Song H, Qian L, Mu H, et al. Human Beta-Defensin-3 Promotes Intestinal Epithelial Cell Migration and Reduces the Development of Necrotizing Enterocolitis in a Neonatal Rat Model. *Pediatr Res* (2014) 76 (3):269–79. doi: 10.1038/pr.2014.93
22. Baxter SA, Laibson PR. Punctal Plugs in the Management of Dry Eyes. *Ocul Surf* (2004) 2(4):255–65. doi: 10.1016/s1542-0124(12)70113-1
23. Hinrichsen K, Podschun R, Schubert S, Schroder JM, Harder J, Proksch E. Mouse Beta-Defensin-14, an Antimicrobial Ortholog of Human Beta-Defensin-3. *Antimicrob Agents Chemother* (2008) 52(5):1876–9. doi: 10.1128/AAC.01308-07
24. Sorensen OE, Thapa DR, Roupe KM, Valore EV, Sjobring U, Roberts AA, et al. Injury-Induced Innate Immune Response in Human Skin Mediated by Transactivation of the Epidermal Growth Factor Receptor. *J Clin Invest* (2006) 116(7):1878–85. doi: 10.1172/JCI28422
25. Wang PH, Huang BS, Horng HC, Yeh CC, Chen YJ. Wound Healing. *J Chin Med Assoc* (2018) 81(2):94–101. doi: 10.1016/j.jcma.2017.11.002
26. Erez N, Truitt M, Olson P, Arron ST, Hanahan D. Cancer-Associated Fibroblasts are Activated in Incipient Neoplasia to Orchestrate Tumor-Promoting Inflammation in an NF-kappaB-Dependent Manner. *Cancer Cell* (2010) 17(2):135–47. doi: 10.1016/j.ccr.2009.12.041
27. Ishida Y, Gao JL, Murphy PM. Chemokine Receptor CX3CR1 Mediates Skin Wound Healing by Promoting Macrophage and Fibroblast Accumulation and Function. *J Immunol* (2008) 180(1):569–79. doi: 10.4049/jimmunol.180.1.569
28. Raggi F, Pelassa S, Pierobon D, Penco F, Gattorno M, Novelli F, et al. Regulation of Human Macrophage M1-M2 Polarization Balance by Hypoxia and the Triggering Receptor Expressed on Myeloid Cells-1. *Front Immunol* (2017) 8:1097. doi: 10.3389/fimmu.2017.01097
29. Barros MH, Hauck F, Dreyer JH, Kempkes B, Niedobitek G. Macrophage Polarisation: An Immunohistochemical Approach for Identifying M1 and M2 Macrophages. *PloS One* (2013) 8(11):e80908. doi: 10.1371/journal.pone.0080908
30. Hesketh M, Sahin KB, West ZE, Murray RZ. Macrophage Phenotypes Regulate Scar Formation and Chronic Wound Healing. *Int J Mol Sci* (2017) 18(7):1545. doi: 10.3390/ijms18071545
31. Krzyszczyk P, Schloss R, Palmer A, Berthiaume F. The Role of Macrophages in Acute and Chronic Wound Healing and Interventions to Promote Pro-Wound Healing Phenotypes. *Front Physiol* (2018) 9:419. doi: 10.3389/fphys.2018.00419
32. Akasaka Y, Ono I, Tominaga A, Ishikawa Y, Ito K, Suzuki T, et al. Basic Fibroblast Growth Factor in an Artificial Dermis Promotes Apoptosis and Inhibits Expression of Alpha-Smooth Muscle Actin, Leading to Reduction of Wound Contraction. *Wound Repair Regener* (2007) 15(3):378–89. doi: 10.1111/j.1524-475X.2007.00240.x
33. Ishiguro S, Akasaka Y, Kiguchi H, Suzuki T, Imaizumi R, Ishikawa Y, et al. Basic Fibroblast Growth Factor Induces Down-Regulation of Alpha-Smooth Muscle Actin and Reduction of Myofibroblast Areas in Open Skin Wounds. *Wound Repair Regener* (2009) 17(4):617–25. doi: 10.1111/j.1524-475X.2009.00511.x
34. Tomasek JJ, McRae J, Owens GK, Haaksma CJ. Regulation of Alpha-Smooth Muscle Actin Expression in Granulation Tissue Myofibroblasts is Dependent on the Intronic CArG Element and the Transforming Growth Factor-Beta1 Control Element. *Am J Pathol* (2005) 166(5):1343–51. doi: 10.1016/s0002-9440(10)62353-x
35. Caley MP, Martins VL, O'Toole EA. Metalloproteinases and Wound Healing. *Adv Wound Care (New Rochelle)* (2015) 4(4):225–34. doi: 10.1089/wound.2014.0581
36. Stetler-Stevenson WG. Matrix Metalloproteinases in Angiogenesis: A Moving Target for Therapeutic Intervention. *J Clin Invest* (1999) 103(9):1237–41. doi: 10.1172/JCI6870
37. Salo T, Makela M, Kylmaniemi M, Autioharmainen H, Larjava H. Expression of Matrix Metalloproteinase-2 and Metalloproteinase-9 During Early Human Wound-Healing. *Lab Invest* (1994) 70(2):176–82.
38. Czyz M. Fibroblast Growth Factor Receptor Signaling in Skin Cancers. *Cells* (2019) 8(6):540. doi: 10.3390/cells8060540
39. Chen X, Niyonsaba F, Ushio H, Hara M, Yokoi H, Matsumoto K, et al. Antimicrobial Peptides Human Beta-Defensin (hBD)-3 and hBD-4 Activate Mast Cells and Increase Skin Vascular Permeability. *Eur J Immunol* (2007) 37 (2):434–44. doi: 10.1002/eji.200636379
40. Fang RC, Mustoe TA. Animal Models of Wound Healing: Utility in Transgenic Mice. *J Biomater Sci Polym Ed* (2008) 19(8):989–1005. doi: 10.1163/156856208784909327
41. Wang X, Ge J, Tredget EE, Wu Y. The Mouse Excisional Wound Splinting Model, Including Applications for Stem Cell Transplantation. *Nat Protoc* (2013) 8(2):302–9. doi: 10.1038/nprot.2013.002
42. Sorg H, Tilkorn DJ, Hager S, Hauser J, Mirastschijski U. Skin Wound Healing: An Update on the Current Knowledge and Concepts. *Eur Surg Res* (2017) 58 (1-2):81–94. doi: 10.1159/000454919
43. Canedo-Dorantes L, Canedo-Ayala M. Skin Acute Wound Healing: A Comprehensive Review. *Int J Inflam* (2019) 2019:3706315. doi: 10.1155/2019/3706315
44. Marsolais D, Cote CH, Frenette J. Neutrophils and Macrophages Accumulate Sequentially Following Achilles Tendon Injury. *J Orthop Res* (2001) 19 (6):1203–9. doi: 10.1016/S0736-0266(01)00031-6
45. Koh TJ, DiPietro LA. Inflammation and Wound Healing: The Role of the Macrophage. *Expert Rev Mol Med* (2011) 13:e23. doi: 10.1017/S1462399411001943

46. Boniakowski AE, Kimball AS, Jacobs BN, Kunkel SL, Gallagher KA. Macrophage-Mediated Inflammation in Normal and Diabetic Wound Healing. *J Immunol* (2017) 199(1):17–24. doi: 10.4049/jimmunol.1700223
47. Loots MA, Lamme EN, Zeegelaar J, Mekkes JR, Bos JD, Middelkoop E. Differences in Cellular Infiltrate and Extracellular Matrix of Chronic Diabetic and Venous Ulcers Versus Acute Wounds. *J Invest Dermatol* (1998) 111 (5):850–7. doi: 10.1046/j.1523-1747.1998.00381.x
48. Davis FM, Kimball A, Boniakowski A, Gallagher K. Dysfunctional Wound Healing in Diabetic Foot Ulcers: New Crossroads. *Curr Diabetes Rep* (2018) 18 (1):2. doi: 10.1007/s11892-018-0970-z
49. Sindrilaru A, Peters T, Wieschalka S, Baican C, Baican A, Peter H, et al. An Unrestrained Proinflammatory M1 Macrophage Population Induced by Iron Impairs Wound Healing in Humans and Mice. *J Clin Invest* (2011) 121 (3):985–97. doi: 10.1172/JCI44490
50. Yeh CJ, Chen CC, Leu YL, Lin MW, Chiu MM, Wang SH. The Effects of Artocarpin on Wound Healing: *In Vitro* and *In Vivo* Studies. *Sci Rep* (2017) 7 (1):15599. doi: 10.1038/s41598-017-15876-7
51. Niyonsaba F, Ogawa H, Nagaoka I. Human Beta-Defensin-2 Functions as a Chemotactic Agent for Tumour Necrosis Factor-Alpha-Treated Human Neutrophils. *Immunology* (2004) 111(3):273–81. doi: 10.1111/j.0019-2805.2004.01816.x
52. Lyu J, Bian T, Chen B, Cui D, Li L, Gong L, et al. Beta-Defensin 3 Modulates Macrophage Activation and Orientation During Acute Inflammatory Response to Porphyromonas Gingivalis Lipopolysaccharide. *Cytokine* (2017) 92:48–54. doi: 10.1016/j.cyto.2016.12.015
53. Konradi S, Yasmin N, Haslwanter D, Weber M, Gesslbauer B, Sixt M, et al. Langerhans Cell Maturation is Accompanied by Induction of N-Cadherin and the Transcriptional Regulators of Epithelial-Mesenchymal Transition ZEB1/2. *Eur J Immunol* (2014) 44(2):553–60. doi: 10.1002/eji.201343681
54. Zielins ER, Atashroo DA, Maan ZN, Duscher D, Walmsley GG, Hu M, et al. Wound Healing: An Update. *Regener Med* (2014) 9(6):817–30. doi: 10.2217/rme.14.54
55. Bao P, Kodra A, Tomic-Canic M, Golinko MS, Ehrlich HP, Brem H. The Role of Vascular Endothelial Growth Factor in Wound Healing. *J Surg Res* (2009) 153(2):347–58. doi: 10.1016/j.jss.2008.04.023
56. Chen X, Zhang M, Chen S, Wang X, Tian Z, Chen Y, et al. Peptide-Modified Chitosan Hydrogels Accelerate Skin Wound Healing by Promoting Fibroblast Proliferation, Migration, and Secretion. *Cell Transplant* (2017) 26(8):1331–40. doi: 10.1177/0963689717721216
57. desJardins-Park HE, Foster DS, Longaker MT. Fibroblasts and Wound Healing: An Update. *Regener Med* (2018) 13(5):491–5. doi: 10.2217/rme-2018-0073
58. Bauvois B. New Facets of Matrix Metalloproteinases MMP-2 and MMP-9 as Cell Surface Transducers: Outside-in Signaling and Relationship to Tumor Progression. *Biochim Biophys Acta* (2012) 1825(1):29–36. doi: 10.1016/j.bbcan.2011.10.001
59. Kumar I, Staton CA, Cross SS, Reed MW, Brown NJ. Angiogenesis, Vascular Endothelial Growth Factor and its Receptors in Human Surgical Wounds. *Br J Surg* (2009) 96(12):1484–91. doi: 10.1002/bjs.6778
60. Steed DL. Clinical Evaluation of Recombinant Human Platelet-Derived Growth Factor for the Treatment of Lower Extremity Ulcers. *Plast Reconstr Surg* (2006) 117(7 Suppl):143S–149S; discussion 150S-151S. doi: 10.1097/01.prs.0000222526.21512.4c
61. Makinen K, Manninen H, Hedman M, Matsi P, Mussalo H, Alhava E, et al. Increased Vascularity Detected by Digital Subtraction Angiography After VEGF Gene Transfer to Human Lower Limb Artery: A Randomized, Placebo-Controlled, Double-Blinded Phase II Study. *Mol Ther* (2002) 6(1):127–33. doi: 10.1006/mthe.2002.0638
62. Hui Q, Jin Z, Li X, Liu C, Wang X. FGF Family: From Drug Development to Clinical Application. *Int J Mol Sci* (2018) 19(7):1875. doi: 10.3390/ijms19071875
63. Guo H, Zhou H, Lu J, Qu Y, Yu D, Tong Y. Vascular Endothelial Growth Factor: An Attractive Target in the Treatment of Hypoxic/Ischemic Brain Injury. *Neural Regener Res* (2016) 11(1):174–9. doi: 10.4103/1673-5374.175067
64. Jere SW, Abrahamse H, Houreld NN. The JAK/STAT Signaling Pathway and Photobiomodulation in Chronic Wound Healing. *Cytokine Growth Factor Rev* (2017) 38:73–9. doi: 10.1016/j.cytogfr.2017.10.001
65. Owen KL, Brockwell NK, Parker BS. JAK-STAT Signaling: A Double-Edged Sword of Immune Regulation and Cancer Progression. *Cancers (Basel)* (2019) 11(12):2002. doi: 10.3390/cancers11122002
66. Chen Z, Han ZC. STAT3: A Critical Transcription Activator in Angiogenesis. *Med Res Rev* (2008) 28(2):185–200. doi: 10.1002/med.20101
67. Dudka AA, Sweet SM, Heath JK. Signal Transducers and Activators of Transcription-3 Binding to the Fibroblast Growth Factor Receptor Is Activated by Receptor Amplification. *Cancer Res* (2010) 70(8):3391–401. doi: 10.1158/0008-5472.CAN-09-3033
68. Hong WX, Hu MS, Esquivel M, Liang GY, Rennert RC, McArdle A, et al. The Role of Hypoxia-Inducible Factor in Wound Healing. *Adv Wound Care (New Rochelle)* (2014) 3(5):390–9. doi: 10.1089/wound.2013.0520
69. Berger EA, McClellan SA, Vistisen KS, Hazlett LD. HIF-1alpha is Essential for Effective PMN Bacterial Killing, Antimicrobial Peptide Production and Apoptosis in Pseudomonas Aeruginosa Keratitis. *PloS Pathog* (2013) 9(7): e1003457. doi: 10.1371/journal.ppat.1003457
70. Funderburg N, Lederman MM, Feng Z, Drage MG, Jadlowsky J, Harding CV, et al. Human -Defensin-3 Activates Professional Antigen-Presenting Cells *via* Toll-Like Receptors 1 and 2. *Proc Natl Acad Sci USA* (2007) 104(47):18631–5. doi: 10.1073/pnas.0702130104
71. D'Ignazio L, Bandarra D, Rocha S. NF-kappaB and HIF Crosstalk in Immune Responses. *FEBS J* (2016) 283(3):413–24. doi: 10.1111/febs.13578

Conflict of Interest: The authors declare that the research was conducted in the absence of any commercial or financial relationships that could be construed as a potential conflict of interest.

Publisher's Note: All claims expressed in this article are solely those of the authors and do not necessarily represent those of their affiliated organizations, or those of the publisher, the editors and the reviewers. Any product that may be evaluated in this article, or claim that may be made by its manufacturer, is not guaranteed or endorsed by the publisher.

Copyright © 2021 Takahashi, Umehara, Yue, Trujillo-Paez, Peng, Nguyen, Ikutama, Okumura, Ogawa, Ikeda and Niyonsaba. This is an open-access article distributed under the terms of the Creative Commons Attribution License (CC BY). The use, distribution or reproduction in other forums is permitted, provided the original author(s) and the copyright owner(s) are credited and that the original publication in this journal is cited, in accordance with accepted academic practice. No use, distribution or reproduction is permitted which does not comply with these terms.

frontiers in Immunology

ORIGINAL RESEARCH
published: 30 September 2021
doi: 10.3389/fimmu.2021.718191

Apoptotic Cells for Therapeutic Use in Cytokine Storm Associated With Sepsis– A Phase Ib Clinical Trial

Peter Vernon van Heerden[1†], Avraham Abutbul[2†], Sigal Sviri[2], Eitan Zlotnick[3], Ahmad Nama[4], Sebastian Zimro[1], Raja el-Amore[3], Yehudit Shabat[5], Barak Reicher[5], Batla Falah[6] and Dror Mevorach[3,7]*

[1] General Intensive Care Unit, Hadassah-Hebrew University Medical Center, Jerusalem, Israel, [2] Medical Intensive Care Unit, Hadassah-Hebrew University Medical Center, Jerusalem, Israel, [3] Rheumatology and Rare Disease Research Center, The Wohl Institute for Translational Medicine, Hadassah-Hebrew University Medical Center and School, Jerusalem, Israel, [4] Department of Emergency Medicine, Hadassah-Hebrew University Medical Center and School, Jerusalem, Israel, [5] Department of Research, Enlivex Therapeutics Ltd., Ness-Ziona, Israel, [6] Department of Cardiology, Hadassah-Hebrew University Medical Center, Jerusalem, Israel, [7] Department of Medicine, Hadassah-Hebrew University Medical Center, Jerusalem, Israel

OPEN ACCESS

Edited by:
Sylvain Perruche, Institut National de la Santé et de la Recherche Médicale (INSERM), France

Reviewed by:
Hendrik Jan Leonard Ankersmit, Medical University of Vienna, Austria
Arnaud Millet, INSERM U1209 Institut pour l'Avancée des Biosciences (IAB), France

***Correspondence:**
Dror Mevorach
mevorachd@hadassah.org.il

†These authors have contributed equally to this work

Specialty section:
This article was submitted to Inflammation, a section of the journal Frontiers in Immunology

Received: *31 May 2021*
Accepted: *14 September 2021*
Published: *30 September 2021*

Citation:
van Heerden PV, Abutbul A, Sviri S, Zlotnick E, Nama A, Zimro S, el-Amore R, Shabat Y, Reicher B, Falah B and Mevorach D (2021) Apoptotic Cells for Therapeutic Use in Cytokine Storm Associated With Sepsis– A Phase Ib Clinical Trial. Front. Immunol. 12:718191. doi: 10.3389/fimmu.2021.718191

Background: Sepsis has no proven specific pharmacologic treatment and reported mortality ranges from 30%–45%. The primary aim of this phase IB study was to determine the safety profile of Allocetra™-OTS (early apoptotic cell) infusion in subjects presenting to the emergency room with sepsis. The secondary aims were to measure organ dysfunction, intensive care unit (ICU) and hospital stays, and mortality. Exploratory endpoints included measuring immune modulator agents to elucidate the mechanism of action.

Methods: Ten patients presenting to the emergency room at the Hadassah Medical Center with sepsis were enrolled in this phase Ib clinical study. Enrolled patients were males and females aged 51–83 years, who had a Sequential Organ Failure Assessment (SOFA) score ≥2 above baseline and were septic due to presumed infection. Allocetra™-OTS was administered as a single dose (day +1) or in two doses of 140×10^6 cells/kg on (day +1 and +3), following initiation of standard-of-care (SOC) treatment for septic patients. Safety was evaluated by serious adverse events (SAEs) and adverse events (AEs). Organ dysfunction, ICU and hospital stays, and mortality, were compared to historical controls. Immune modulator agents were measured using Luminex® multiplex analysis.

Results: All 10 patients had mild-to-moderate sepsis with SOFA scores ranging from 2–6 upon entering the study. No SAEs and no related AEs were reported. All 10 study subjects survived, while matched historical controls had a mortality rate of 27%. The study subjects exhibited rapid resolution of organ dysfunction and had significantly shorter ICU stays compared to matched historical controls ($p<0.0001$). All patients had both elevated

pro- and anti-inflammatory cytokines, chemokines, and additional immune modulators that gradually decreased following treatment.

Conclusion: Administration of apoptotic cells to patients with mild-to-moderate sepsis was safe and had a significant immuno-modulating effect, leading to early resolution of the cytokine storm.

Clinical Trial Registration: ClinicalTrials.gov Identifier: NCT03925857. (https://clinicaltrials.gov/ct2/show/study/NCT03925857).

Keywords: sepsis, Inflammation, pneumonia, apoptotic cells, cell therapeutics, cytokine storm

1 INTRODUCTION

Sepsis, identified by the World Health Organization (WHO) as a global health priority, has no specific proven pharmacologic treatment other than appropriate antibiotics, intravenous fluids, vasopressors as needed, and possibly corticosteroids (1–4). The reported death rate from sepsis in hospitalized patients ranges between 30% and 45% (5–10).

In sepsis, binding of either pathogen-associated molecular patterns (PAMPs) or damage-associated molecular patterns (DAMPs) to complement, toll-like receptors (TLRs), nucleotide-binding oligomerization domain (NOD) like receptors, retinoic acid-inducible gene (RIG)like receptors, mannose-binding lectin, and scavenger receptors, among others, induces a complex intracellular signaling system with redundant and complementary activities (11, 12). Triggering of innate immunity assures a common response pattern, regulated by the level and variation of the repertoire of PAMPs and DAMPs, and the resulting signaling pathways that are activated. This sequence of events leads to the expression of several common classes of genes that are involved in inflammation, adaptive immunity, and cellular metabolism. The complementary nature of the pathways explains the overlapping yet unique early inflammatory response to common Gram-negative and Gram-positive bacterial, fungal, and viral infections, as well as tissue injury.

Interestingly, and as summarized recently, apoptotic cells in general, and Allocetra-OTS (Enlivex Therapeutics Ltd, Nes Ziona, Israel) specifically, were shown to have a modulating effect on cytokine storms, with downregulation of both anti- and pro-inflammatory cytokines derived from PAMPs and DAMPs, in both animal and human *in vitro* models (13). Therefore, the current study was designed to examine the safety and the possible beneficial immuno-modulating effects of early apoptotic cells (Allocetra-OTS, Enlilvex Therapeutics Ltd., Nes-Ziona, Israel) administered to patients presenting with sepsis. In a previous dose-escalating clinical study enrolling patients undergoing bone marrow transplantation who had an elevated cytokine profile, matched apoptotic cells were shown to be safe and efficacious with a dose-dependent effect starting at 140×10^6 cells/kg (14). This dose, administered in either one or two treatments, was chosen for the current study. In addition, the outcome of study subjects in this safety trial were compared to historical matched controls to compare outcomes at 28 days.

2 MATERIALS AND METHODS

2.1 Study Design

This was a company (Enlivex Therapeutics)-sponsored study (ClinicalTrials.gov Identifier: NCT03925857). The primary aim of this phase Ib study was to determine the safety profile and tolerability (dose-limiting toxicity) of Allocetra-OTS infusion in subjects presenting to the emergency room with sepsis. The secondary aims were to determine the preliminary efficacy on reducing organ dysfunction; intensive care unit (ICU), intermediate care unit (IMU), and hospital stays; and mortality.

Adult males and females aged 18–85 years, weighing at least 40 kg and with a predicted life expectancy of at least 6 months at the time of the screening, who had a SOFA score >2 above baseline and had sepsis from presumed infection were included. Exclusion criteria included pregnancy, positive serology for HIV, performance status less than 80%, or serious organ dysfunction (e.g. left ventricular ejection fraction <40%, pulmonary forced vital capacity <60% of predicted, liver transaminases >2.5× the upper limit of normal, serum bilirubin >3 mg/dL, or creatinine >2.5 mg/dL.

Sequential Organ Failure Assessment (SOFA) scores were measured at enrollment and at each study time point. We also obtained blood samples for exploratory biological tests including pro- and anti-inflammatory cytokines, chemokines, growth factors, leptin, ghrelin, neutrophil gelatinase-associated lipocalin (NGAL), Triggering Receptor Expressed on Myeloid Cells 1 (TREM1), an endocrinology panel, cortisol, adrenocorticotropic hormone (ACTH), free triiodothyronine (FT3), free throxine (FT4), thyroid stimulating hormone (TSH), growth hormone, glucagon, and insulin. An autoimmune serology panel that included antinuclear antibody (ANA), anti-DNA, anti-RNP, anti-Sjögren's-syndrome-related antigen A (SSA), anti-Sjögren's-syndrome-related antigen B (SSB), cardiolipin IgG, and cardiolipin IgM was also taken.

Allocetra-OTS was administered as a single dose (cohort 1) of 140×10^6 cells/kg on day +1 (day 0 was time of diagnosis at the ER) or in two doses (cohort 2) of 140×10^6 cells/kg on days +1 and +3, following initiation of standard-of-care (SOC) treatment for septic patients, as outlined by the Surviving Sepsis Campaign (14, 15). Interim safety analyses were performed by the Data and Safety Monitoring Board (DSMB) after three and six patients from cohort 1 had completed study day 14, and after four additional patients from cohort 2 had completed study day 28.

2.2 Alloctera-OTS Preparation

Enlivex Therapeutics Ltd. has developed a product named Allocetra-OTS based on the known activity of naturally occurring apoptotic cells to induce a pro-homeostatic state for both macrophages and dendritic cells (DCs) (13, 14, 16–18) that contributes to the maintenance of peripheral homeostasis of almost all immune-triggered mechanisms in sepsis. Allocetra-OTS is composed of frozen non-human leukocyte antigen (HLA)-matched mononuclear enriched leukocytes derived from one donor to each patient, containing at least 40% early apoptotic cells, in the form of a liquid suspension that is administered intravenously (IV). Following controlled thawing, cells are incubated with corticosteroids that are washed in order to achieve an early apoptotic state. The cells are then washed again, eliminating both corticosteroid residues as well as material that may have been secreted by apoptotic cells. Once the cells are in an early apoptotic state, they are preserved at 2-8°C. They are further Gamma or X-ray irradiated at 4000cGy to prevent T cell proliferation of potentially viable cells, and therefore avoid the possible development of an acute GvHD-like response. Following irradiation, the product is stable for up to 96 hours and kept at 2-8°C to avoid progression of apoptosis.

2.3 Matched Historical Controls

The local ethics committee also approved (#0267-19-HMO) a search for matched controls that were selected from the digital records of all hospitalized patients treated in the same units as the study patients. Controls were selected from patients who were hospitalized only in an ICU or an IMU at the Hadassah-Hebrew University Medical Center, Ein Kerem, Jerusalem, during the years 2014–2019 (the standard of care was very similar during these years), and matched by gender, age (± 7 years), source of infection (i.e., pneumonia, urinary tract, biliary tract, or endovascular), and SOFA score (± 2) at diagnosis. Outcomes for the matched controls were compared to those for the study cohort at 28 days.

The total number of potential controls was 24,172 patients including 18,078 pneumonia patients, 5,370 UTI patients, 629 patients with biliary tract infection, and 95 patients with endovascular infection. Matching the characteristics of each of the 10 sepsis patients that were treated with Allocetra was done with a full match to the source of infection, SOFA score ±2, age ±7 years, and gender. A total of 37 matched historical control patients were identified, of whom 19 had pneumonia (**Table 1**). The process of identifying suitable controls was done by two physicians and reviewed by a third. All data was found in patients' charts and SOFA scores were calculated retrospectively. Outcomes for the matched controls were compared to those of the study cohorts at 28 days. Source data was verified to confirm that the reported qualified data provided in the report matched the source.

2.4 Luminex® Cytokine/ Chemokine Analysis

Serum cytokine/chemokine measurement was performed using the Luminex MAGPIX system (Luminex Corp, Texas, USA) and analyzed with Milliplex analysis software (Millipore MA, USA).

2.5 ELISA Analysis

The following cytokines/chemokines were measured by sandwich ELISA kits: IL-18 (R&D Systems, Minneapolis, MN, USA), MCP-3 (R&D), TNFR1 (R&D), TREM-1 (R&D), procalcitonin (PCT) (IBL-America, Minneapolis, MN, USA).

2.6 Autoantibodies and Anti-HLA Antibodies

Autoantibodies and anti-HLA antibodies were analyzed by the central laboratory of the Hadassah-Hebrew University Medical Center.

2.7 Statistics

2.7.1 Clinical Data

Mortality was analyzed as time-to-event measurement and comparisons between treatment arms were presented using Kaplan Meier curves and the log rank test. Expected mortality estimation was based on patients' Acute Physiology and Chronic Health Evaluation (APACHE) II scores (19). Changes in SOFA score from entry into research to days 5, 7, and 28, maximum increase in SOFA score, and duration of hospitalization and ICU/IMU stays were analyzed as continuous variables. Means, standard deviations, medians, interquartile ranges, and ranges in each treatment group were presented and compared using the t-test or Wilcoxon rank sum test, as appropriate. Area under the curve for change in SOFA score was calculated using the trapezoidal rule and also analyzed as a continuous variable. Duration of hospitalization and ICU/IMU stays were analyzed as time to first discharge, presented in the Kaplan-Meier curves and treatment groups compared using the log rank test. All analyses were repeated for the entire population as well as for subgroups receiving one or two Allocetra-OTS doses, and for pneumonia alone. Statistical analysis was performed using R 3.5.1 (R Statistical Data Analysis).

2.7.2 Laboratory and Exploratory Tests

Correlation of any parameter to clinical score was evaluated by the Pearson correlation or by Spearman's rank correlation coefficient, with a coefficient ≥ 0.7 or ≤ -0.7 considered a strong correlation. Statistical analyses for laboratory tests were performed using GraphPad (Prism, San Diego, CA, USA).

3 RESULTS

Sepsis was defined based on the Third International Consensus Definitions for Sepsis and Septic Shock (20). Twelve patients were screened, and ten were included in the study; patients 04 and 05 did not meet inclusion criteria. The DSMB met following inclusion of three (patients 01–03) and six patients (patients 01–03 and 06–08) for safety reviews and approval to continue the study, and for final review after 10 patients. Allocetra-OTS infusion in the first three patients met the protocol for defined safety criteria at day 14 and the study proceeded to the second round of patient recruitment (patients 06–08) at the same dose, which also met the protocol-defined criteria for safety. The study

TABLE 1 | Characteristics of patients and historical matched-controls.

	Total Sepsis Treated patients ***(n = 10, 100%)***	**Total Sepsis Matched-Controls** ***(n = 37, 100%)***	**Sepsis source: Pneumonia Treated Patients** ***(n=5, 50%)***	**Sepsis source: Pneumonia Matched Controls** ***(n=19, 51.3%)***	
Mean age (range)	71.5 (51–83)	73.1 (50-79)	67.8 (51–79)	67.8 (50–79)	
Male/female	8/2	31/6	4/1	15/4	
Mortality	0/10	10/37 (27%)	0/5	6/19 (31.5%)	
Patient	**SOFA score at screening**	**Predicted mortality (%) based on SOFA at presentation**	**APACHE II Score**	**Predicted mortality %) based on APACHE II**	**28-day outcome in patients treated with Allocetra-OTS**
01-001 Pneumonia	2	7	12	15	Alive. Sepsis and organ dysfunction resolved
01-002 Pneumonia	3	8	9	8	Alive. Sepsis and organ dysfunction resolved
01-003 Pneumonia	6	15	15	24	Alive. Sepsis and organ dysfunction resolved
01-006 Pneumonia	3	8	11	15	Alive. Sepsis and organ dysfunction resolved
01-007 Endovascular	6	15	21	40	Alive. Sepsis and organ dysfunction resolved
01-008 UTI	3	8	9	8	Alive. Sepsis and organ dysfunction resolved
01-009 Biliary	3	8	13	15	Alive. Sepsis and organ dysfunction resolved
01-010 Biliary	5	12	16	24	Alive. Sepsis and organ dysfunction resolved
01-011 Biliary	2	7	8	12	Alive. Sepsis and organ dysfunction resolved
01-012 Pneumonia	2	7	15	35	Alive. Sepsis and organ dysfunction resolved
Average (range)	3.4 (2–6)	9.5 (7–15) %	12.3 (8–21)	20 (8–40) %	
	SOFA score at presentation [Average (range)]	**Predicted mortality (%) based on SOFA at presentation [Average (range)]**	**APACHE II Score [Average (range)]**	**Predicted mortality (%) based on APACHE II [Average (range)]**	
Allocetra–OTS-treated patients (n=10)	3.4 (2–6)	9.5 (7–15) %	12.3 (8–21)	20 (8–40) %	
All Historical Controls (n=37)	3.8 (1–7)	9.9 (4.5–19) %	15 (5–35)	23 (8–85) %	
Historical; pneumonia (n=19)	3.6 (2–7)	9.5 (7–19) %	14 (5–24)	20 (8–40) %	
Historical; Endovascular (n=3)	6 (5–7)	14 (8–19) %	24 (17–35)	50 (24–85) %	
Historical; UTI (n=5)	3.8 (2–5)	9.8 (7–12) %	15 (12–21)	22 (15–40) %	
Historical; Biliary (n=10)	3.4 (2–5)	9.2 (4.5–12) %	14 (6–20)	20 (8–40) %	

then proceeded to recruit four additional patients (cohort 2, patients 09–12), who received two doses of Allocetra-OTS. Patient characteristics are presented in **Table 1**.

3.1 Clinical Course

All study subjects fitted the definition of sepsis and inclusion criteria and were hospitalized on admission in either the ICU or the IMU. All patients had a Glasgow Coma Score (GCS) of at least 13 (verbal 5/5) at enrollment due to the requirement to obtain consent directly from the study subject. At enrollment, the average APACHE II score was 12.9 (range 8–21) and the average SOFA score upon entry into the study was 3.4 (range 2–6). All patients fulfilled inclusion and exclusion criteria and met the 2016 definition of sepsis (20). In this study, any source of infection was included, and the patients presented with four types of infections: pneumonia (five patients treated with I.V. ceftriaxone), biliary tract infection (three patients treated with ceftriaxone), endovascular (one treated with I.V. vancomycin), and UTI (one treated with I.V. ceftriaxone) and received standard-of-care treatment for septic patients, as outlined by the Surviving Sepsis Campaign (1–3).

All patients had at least two organ systems involved (range 2–5 systems). Acute kidney injury (three patients), cardiovascular involvement (three patients), hepatic involvement (seven

patients), hematological (eight patients), and pulmonary involvement (five patients) were seen in the treated patients before investigational product (IP) administration. All patients recovered from the septic condition and were discharged alive from the hospital following the resolution of sepsis and were alive at completion of 28 days of follow-up.

3.2 Laboratory Results

Laboratory evaluation included complete blood count (CBC), biochemistry, blood gases, C-reactive protein (CRP), and lactate. **Figure 1** shows their levels during the study period. In 5/10 patients, elevated white blood cells (WBC) counts were evident in the first days, with gradual return to normal levels (**Figure 1A**). Neutrophilia was observed on admission in 6/10 patients (**Figure 1B**) and lymphopenia in 9/10 patients (**Figure 1C**). All patients had a gradual increase in lymphocyte numbers and 6/9 (66%) recovered to normal levels whereas 3/9 (33%, patients 03, 06, 07) had moderate recovery levels. Elevated CRP declined in parallel with resolution of inflammation (**Figure 1D**). Two patients (07 and 12) had a slower decline of CRP. The first (patient 07) was a patient on chronic dialysis presenting with an endovascular infection that needed antibiotics for 6 weeks, and the second (12) was a patient with pneumonia and pleural effusion. Lactate levels were elevated in 3/10 patients upon admission (01, 02, 08) and were normal or near normal in the following days. Three patients had higher lactate levels on day 28 (01, 03, 09) despite clinical and laboratory resolution of sepsis, in the range of 3.4 to 6.5 mmol/L (normal value up to 2.2 mmol/L).

3.3 Safety Parameters

Safety was evaluated by SAEs and AEs. All patients survived 28 days of follow-up. Of note, efficacy parameters (presented below),

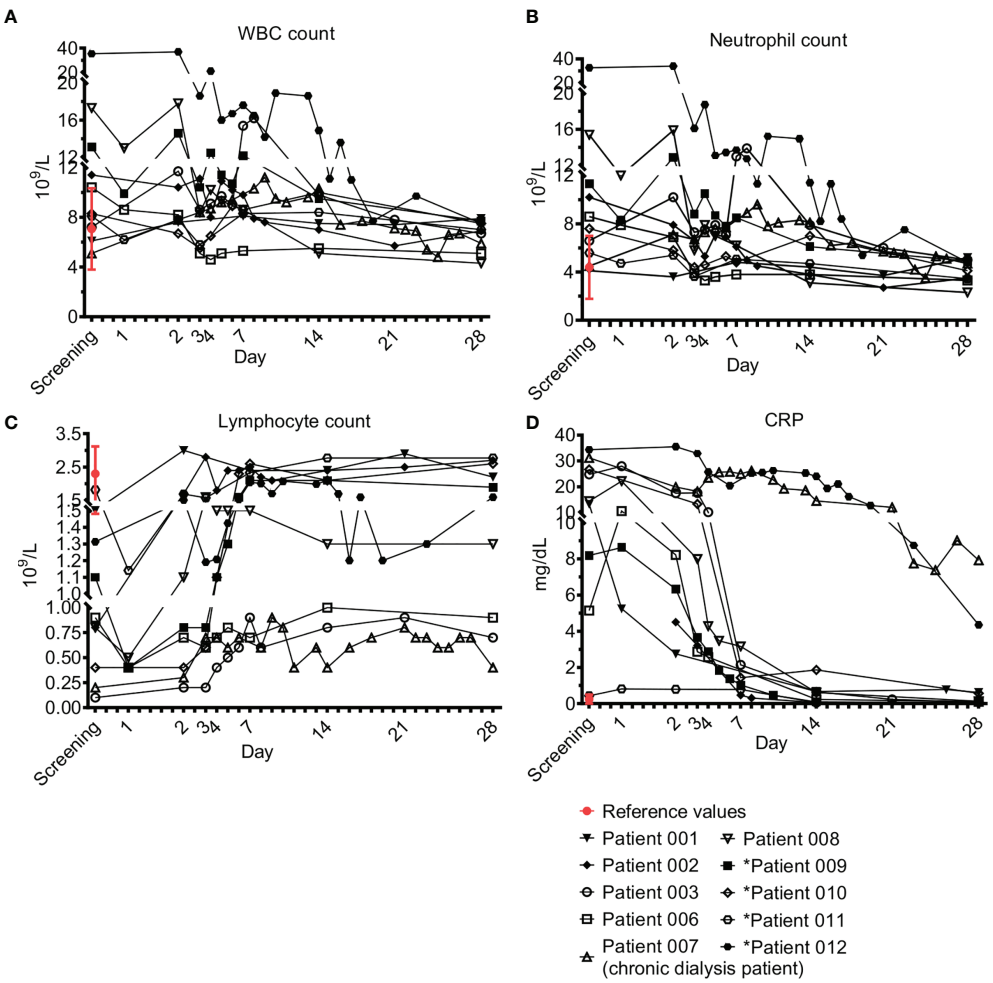

FIGURE 1 | Acute phase markers. Complete blood count (CBC) and C-reactive protein (CRP). Blood counts of fresh peripheral patient blood ethylenediamine tetraacetic acid (EDTA) samples were performed using blood analyzer. The differential of white blood cells (WBC), i.e. WBC subpopulations, was calculated. 'Screening' is a time point with a blood count that was performed 24 ± 6h before treatment with Allocetra-OTS, to test for the patient's eligibility for Allocetra-OTS treatment. 'Day 1' is a blood sample just prior to Allocetra-OTS infusion. Numbers (10^9 cells/L) of **(A)** WBCs, **(B)** neutrophils, and **(C)** lymphocytes, are shown. **(D)** CRP levels of all patients in the indicated time points. *Patients 09–12 received two doses of Allocetra-OTS (days 1 and 3).

like survival, overlapped with additional safety parameters. There were no serious unexpected serious adverse reactions (SUSARs) and none of the subjects experienced an SAE, severe or moderate AE, or discontinued the study due to an AE. Nearly all subjects (9/10; 90%) experienced at least 1 AE and on average 4.4 AEs; The most common AEs were associated with laboratory investigations (**Table 2**). All were mild in intensity, and most were unrelated to IP. The six possibly related AEs were transiently elevated temperature, mild transient tachycardia, transient hypoglycemia, and transient dizziness, each in one patient, and rigor episodes in two patients receiving one dose. All these AEs could have been related to the septic condition. However, since the two episodes of rigors occurred in patients receiving a high infusion rate (>150 mL/h), the last 8 IP administrations were given at a slower infusion rate (up to 108 mL/hr) with no rigors documented.

3.4 Autoimmunity, Anti-HLA Antibodies, and Autoantibodies

No anti-HLA antibodies developed within 28 days following one dosage in the first 6 patients. Autoantibodies and autoimmunity were evaluated at initial screening and on day 28. No autoimmunity developed in any of the study subjects during the study period. The ANA screen, which is considered a major screening tool for autoantibodies, was negative at presentation in 8/10 patients and remained negative in all eight at day 28. In two patients it was low-positive before IP administration; it remained low-positive in one and disappeared in the second. IgM and IgG anticardiolipin were negative in 10/10 patients at screening and remained negative in all.

Anti-DNA was not examined at initial screening, due to negative ANA in most patients, but was negative in all patients examined at day 28. Anti-SSA/SSB/RNP/Sm were examined mainly on day 28 and in some patients at initial screening. Only one patient (08) had very low positive RNP (20.61 vs 20, which is defined as negative) on day 28. This was considered non-significant.

In conclusion, after administration of 14 IV doses of Allocetra-OTS in 10 patients, there was no evidence of autoimmunity or autoantibodies.

3.5 Preliminary Efficacy Results

3.5.1 Mortality

No deaths occurred among the 10 study subjects. APACHE II scores for subjects in the current study are presented in **Table 1**. The average score at diagnosis was 12.9 (range 8–21). Overall probability of mortality was 20% (range 8–40%), with no significant differences between the subgroups of patients.

In patients with sepsis, an elevated SOFA score at presentation also reflects an increased risk of mortality. In one study that included >180,000 patients hospitalized with sepsis, a SOFA score of 2–6 at presentation (**Table 1**) corresponded to predicted mortality of 7–15% (21).

In addition, a total of 37 matched controls were identified for the 10 patients in the study based on the criteria of sepsis, admission to ICU/IMU, source of infection, SOFA score ±2, age ±7 years, and gender. **Table 1** shows the characteristics of controls compared to study subjects. A comparison of survival between the study group and historical controls, in all the patients and in the subgroup of patients with pneumonia, is shown in **Figure 2**. Among the 37 matched historical control patients, 10 died (27%, p-value using log rank test=0.078). Although a larger sample is needed to draw definite statistical conclusions regarding survival, predicted mortality based on the APACHE II and SOFA scores at presentation would have been a high probability of at least one death in these 10 patients.

3.5.2 Organ Dysfunction

Organ dysfunction improvement was a preliminary efficacy parameter tested in this study. No residual organ dysfunction was seen in any of the 10 study subjects at 28 days.

3.5.2.1 CNS

All patients finished 28 days of follow-up with a GCS of 15/15.

3.5.2.2 Kidneys

Apart from patient 07, who was on chronic dialysis at admission, 3/9 patients (33%) had new-onset renal injury, and all had completely recovered to baseline kidney function as measured by creatinine level at 28 days.

3.5.2.3 Lungs

5/10 (50%) of patients had lung involvement. No patient required mechanical ventilation. All patients recovered from lung dysfunction, had normal oxygen saturation, and needed no oxygen supplement at discharge.

3.5.2.4 Cardiovascular

Three patients had mean arterial pressure <70mmHg but none needed vasopressors. Cardiac evaluation was based on clinical evaluation, ECG in all patients, troponin if indicated, and echocardiogram as indicated (needed in one patient). All patients had normal sinus rhythm or tachycardia upon screening, with no evidence of ischemia during their illness. One patient with known paroxysmal atrial fibrillation had a transient episode of atrial fibrillation. Troponin was measured in four patients and was normal in all. One patient (01) underwent transthoracic echocardiography during his admission for the investigation of chest pain and elevated troponin levels following an episode of supraventricular tachycardia and electrical shock (DC cardioversion) before screening and entry to the study. Follow-up echocardiography in this patient was performed at day 28. The results were comparable to the first evaluation.

3.5.2.5 Hematological

Significant thrombocytopenia occurred in 8/10 patients (80%) with complete recovery in all.

3.5.2.6 Liver

Hyperbilirubinemia occurred in four patients (40%) and three patients had a biliary tract infection; all four had a complete recovery. Elevated liver enzymes, aspartate transaminase (AST) and alanine aminotransferase (ALT) in the range of >×3 of normal range were seen in 5/10 patients with a complete recovery in all.

3.5.2.7 SOFA Score

In the absence of days on respirator and days on vasopressors, we used SOFA score to evaluate organ dysfunction. The SOFA score

TABLE 2 | Complete list of adverse events.

No	Patient no./Gender/ Age group	Adverse Event	Severity/ Intensity	Relationship to Study Drug	Action Taken with Study Treatment	Outcome of Adverse Event
1	01/M/60–69	Rigors	Not serious/ Mild	Possibly related	Drug interrupted; rate changed. Dose unchanged	Recovered/Resolved
2	02/M/50–59	Tachycardia	Not serious/ Mild	Possibly related	Dose not changed	Recovered/Resolved
3	02/M/50–59	Temperature elevation to 37.9 C	Not serious/ Mild	Possibly related	Dose not changed	Recovered/Resolved
4	03M/70–79	Elevated liver enzymes	Not serious/ Mild	Not related	Not applicable	Recovered/Resolved
5	07/M/60–69	Dizziness	Not serious/ Mild	Possibly related	Dose not changed	Recovered/Resolved
6	07/M/60–69	Anemia	Not serious/ Mild	Not related	Not applicable	Not recovered/Not resolved
7	07/M/60–69	Gamma-glutamyl transferase out of range - high	Not serious/ Mild	Not related	Not applicable	Not recovered/Not resolved
8	07/M/60–69	Lactic dehydrogenase out of range - high	Not serious/ Mild	Not related	Not applicable	Recovered/Resolved
9	07M/60–69	Creatine phosphokinase out of range - high	Not serious/ Mild	Not related	Not applicable	Recovered/Resolved
10	07/M60–69	Alkaline phosphatase out of range - high	Not serious/ Mild	Not related	Not applicable	Not recovered/Not resolved
11	07/M/60–69	WBC out of range - high	Not serious/ Mild	Not related	Not applicable	Recovered/Resolved
12	07/M/60–69	Neutrophils out of range - high	Nor serious/ Mild	Not related	Not applicable	Recovered/Resolved
13	07/M/60–69	Lactic dehydrogenase out of range - high	Not serious/ Mild	Not related	Not applicable	Recovered/Resolved
14	08/M/80–89	Rigors	Not serious/ Mild	Possibly related	Not applicable	Recovered/Resolved
15	08/M/80–89	Glucose out of range	Not serious/ Mild	Not related	Not applicable	Recovered/Resolved
16	08/M/80–89	Sodium out of range	Not serious/ Mild	Not related	Not applicable	Recovered/Resolved
17	08/M/80–89	General atopy	Not serious/ Mild	Not related	Not applicable	Recovered/Resolved
18	08/M/80–89	Lymphocytes out of normal range - high	Not serious/ Mild	Not related	Not applicable	Recovered/Resolved
19	08/M/80–89	Lactic dehydrogenase out of range - high	Not serious/ Mild	Not related	Not applicable	Recovered/Resolved
20	08/M/80–89	Bilirubin out of range	Not serious/ Mild	Not related	Not applicable	Recovered/Resolved
21	08/M/80–89	Glucose out of range	Not serious/ Mild	Not related	Not applicable	Recovered/Resolved
22	09/M/80–89	Elevated ALK.P	Not serious/ Mild	Not related	Not applicable	Recovered/Resolved
23	09/M/80–89	Elevated LDH	Not serious/ Mild	Not related	Not applicable	Recovered/Resolved
24	09/M/80–89	Elevated WBC	Not serious/ Mild	Not related	Not applicable	Recovered/Resolved
25	09/M/80–89	Lymphocyte ABS decrease	Not serious/ Mild	Not related	Not applicable	Recovered/Resolved
26	09/M/80–89	Low glucose level	Not serious/ Mild	Possibly related	Not applicable	Not recovered/Not resolved
27	10/M/70–79	Diarrhea	Not serious/ Mild	Unlikely related	Dose not changed	Recovered/Resolved
28	11/F/70–79	Low total protein blood level	No	Mild	Not related	Dose not changed
29	11/F/70–79	Low albumin blood level	No	Mild	Not related	Dose not changed
30	11/F/70–79	Elevated LDH blood level	No	Mild	Not related	Not applicable
31	11/F/70–79	Low CPK blood level	No	Mild	Not related	Not applicable
32	11/F/70–79	Low potassium blood level	No	Mild	Not related	Dose not changed
33	11/F/70–79	Elevated CRP blood level	No	Mild	Not related	Dose not changed
34	11/F/70–79	Elevated lactate blood level	No	Mild	Not related	Not applicable

(Continued)

TABLE 2 | Continued

No	Patient no./Gender/ Age group	Adverse Event	Severity/ Intensity	Relationship to Study Drug	Action Taken with Study Treatment	Outcome of Adverse Event
35	11/F/70–79	Elevated alkaline phosphatase blood level	No	Mild	Not related	Not applicable
36	12/F/60–69	Elevated lactate blood level	No	Mild	Not related	Not applicable
37	12/F/60–69	Low total bilirubin blood level	No	Mild	Not related	Not applicable
38	12/F/60–69	Elevated ALT blood level	No	Mild	Not related	Not applicable
39	12/F/60–69	Low ALT blood level	No	Mild	Not related	Not applicable
40	12/F/60–69	Elevated AST blood level	No	Mild	Not related	Not applicable
41	12/F/60–69	Elevated LDH blood level	No	Mild	Not related	Not applicable
42	12/F/60–69	Elevated alkaline phosphatase blood level	No	Mild	Not related	Not applicable
43	12/F/60–69	Low BUN blood level	No	Mild	Not related	Not applicable
44	12/F/60–69	Elevated lactate blood level	No	Mild	Not related	Not applicable

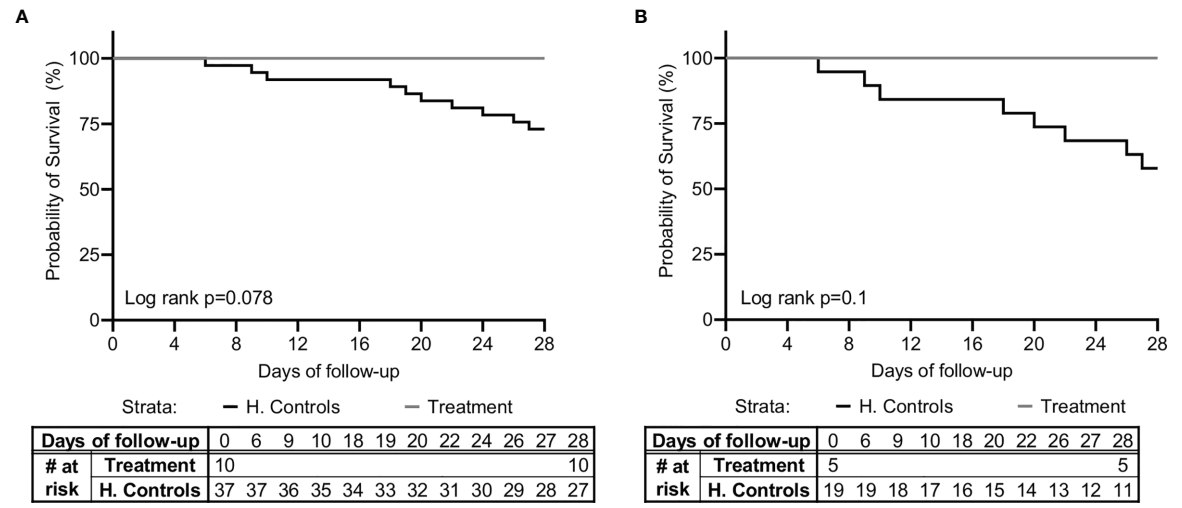

FIGURE 2 | Kaplan-Meier survival curve. A comparison of survival between the study group (*n*=10) and matched-historical controls from the same hospital (*n*=37) for **(A)** all patients, and **(B)** patients with pneumonia (*n*=5 for the study group, *n*=19 for the historical controls), is shown. Matched controls were selected from all patients admitted to ICU with a diagnosis of sepsis between 2014–2019 and were matched by gender, age ± 7, Sequential Organ Failure Assessment (SOFA) score ±2 at presentation, and source of infection.

was introduced to describe organ failure severity in patients with sepsis, including a 4-point assessment of dysfunction in each of six organ systems (17, 19, 22). In patients with sepsis, a SOFA score ≥2 at presentation reflects clinically relevant organ dysfunction and an increased risk of adverse outcomes (21). Apart from acute organ injury, we measured changes in the SOFA score from just before IP administration, maximal SOFA score, AUC of SOFA score above baseline, and time to SOFA score <2, and compared findings to those of the matched-historical controls. As shown in **Table 1** and **Figure 3**, patients had SOFA scores correlating to mild-to-moderate sepsis. However, despite the similarity to SOFA scores at entry for historical-matched controls of (average of 3.4 versus 3.47), the enrollment SOFA score was the highest for the treated patients and it did not progress further (0 points) following treatment, while it progressed with a mean maximal increase of 3.57 (range 0–15, median 1) in the historical control population (**Figure 3A**; p<0.0001, t-test and Wilcoxon), suggesting inhibition of organ dysfunction deterioration with Allocetra-OTS treatment. In historical matched controls with pneumonia, it went even higher, to a mean of +4.42 (range 0–15, median 4) (p<0.0001, t-test, and 0.0166, Wilcoxon).

We further measured the change in mean SOFA score between day 1 before treatment with Allocetra-OTS and at days 5, 7, and 28. At these time points, the scores were significantly higher in the historical-matched controls compared to patients in the current study (**Figures 3B–D**; average delta SOFA score between day 1–5, day 1–7, and day 1–28, p<0.0001, t test for all, and 0.0035, 0.001, and 0.0019, Wilcoxon, respectively). We also measured the average change in the area under the curve (AUC) between days 1 and 5 and between days 1 and 7 (**Figures 3E, F**); all changes showed significant amelioration (average AUC between day 1–5 and day 1–7, both p<0.0001, t test, and 0.0011, Wilcoxon). In

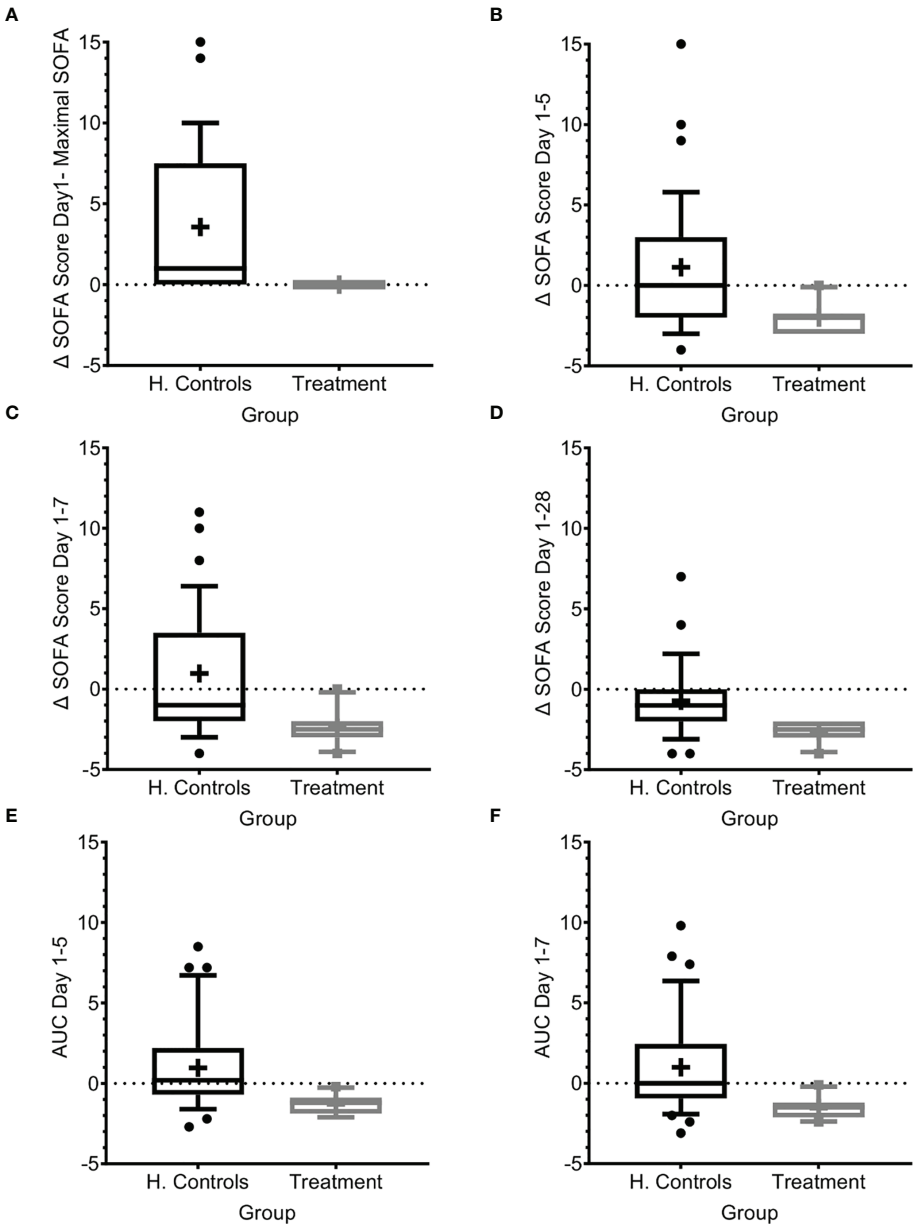

FIGURE 3 | SOFA score progression during sepsis. **(A)** SOFA score at presentation compared to maximal SOFA score. **(B–D)** Change in SOFA score before administration of Allocetra-OTS and day 5 **(B)**, day 7 **(C)**, and day 28 **(D)**. Average delta area under the curve (AUC) in the first **(E)** five days, and **(F)** seven days. Matched controls were selected from all patients admitted to ICU under the diagnosis of sepsis between 2014–2019 and were matched by gender, age ±7 years, SOFA score ±2 at presentation, and source of infection. Data is presented as the median within the interquartile range (IQR); mean values are marked with a '+' sign; error bars represent the 10-90 percentile, with outliers presented.

historical matched controls with pneumonia, it went even higher, to a mean increase of 4.42 (range 0–15, median 4; $p<0.0001$ t-test, and 0.0166 Wilcoxon). These data suggest that the favorable clinical outcomes are reflected by lack of SOFA score progression as manifested by maximal SOFA score, delta SOFA score, and the average change in AUC. We must emphasize the limitation of using historical controls that were matched as possible in demographic characteristics and SOFA score upon entry. Yet, the historical controls had a slightly increased APACHE II score (15 versus 12.3, **Table 1**) that could predict worse prognosis.

3.5.3 Time in ICU/IMU and Hospital

Since organ dysfunction was significantly improved and no mortality occurred, we were next interested to verify that these promising results were expressed in the duration of ICU/IMU and hospital stay. Since all patients in the study group survived,

we analyzed duration of stay in the hospital and in ICU/IMU for all patients in the study and for all surviving patients in the matched historical control group (**Figure 4**).

The mean hospital length-of-stay was significantly shorter for all sepsis patients treated with Allocetra-OTS (11.4 ± 7.57 days, range 4–28, median 9), and for patients with pneumonia (11.2 ± 6.38 days, range 6–22, median 10), compared to the averages for matched-historical controls of for all patients (**Figure 4A**; 17.3 ± 8.8 days, 3–28, median 17; p< 0.0488 t-test, p<0.042 Wilcoxon), and for patients with pneumonia, average 18.84 days (range 6–28, median 19; p< 0.0552 t-test, p< 0.0484, Wilcoxon). The ICU length-of-stay was significantly shorter for all treated patients, average 4.7 days (range 2–8, median 4), and for patients with pneumonia, average 3.4 days (range 2–6, median 2) compared to averages for all matched controls, 11.1 days (**Figure 4B**; 1–28, median 8; p< <0.0001 t-test, p< 0.092, Wilcoxon) and patients with pneumonia, 13.89 days (range 1–28, median 11; p<0.0001 t-test, p< 0.0233 Wilcoxon).

In addition, time-to-discharge from the hospital and/or ICU/IMU (**Figures 4C, D**) was compared. Length of hospitalization was analyzed as a time-to-event variable, comparing time to discharge from the general hospital and the ICU between treatment groups. In this analysis, events of mortality were referred to as no discharge event and the length of follow-up was censored at time of death. Times to hospital and ICU/IMU discharge were significantly shorter for the treated group (log rank p=0.00085 and p=0.00096, respectively).

3.6 Exploratory Endpoints. Effect of Allocetra-OTS on Cytokines/Chemokines/Growth Factors and Immuno-Modulating Agents

3.6.1 Pro-Inflammatory Cytokines

Pro-inflammatory cytokines regulate early responses to bacterial infection and mediate the early acute phase in sepsis. Cytokines like IL-1, IL-6, and TNF-α act as endogenous pyrogens, upregulate the synthesis of secondary mediators and other pro-inflammatory cytokines by both macrophages and mesenchymal cells such as fibroblasts, epithelial, and endothelial cells, and

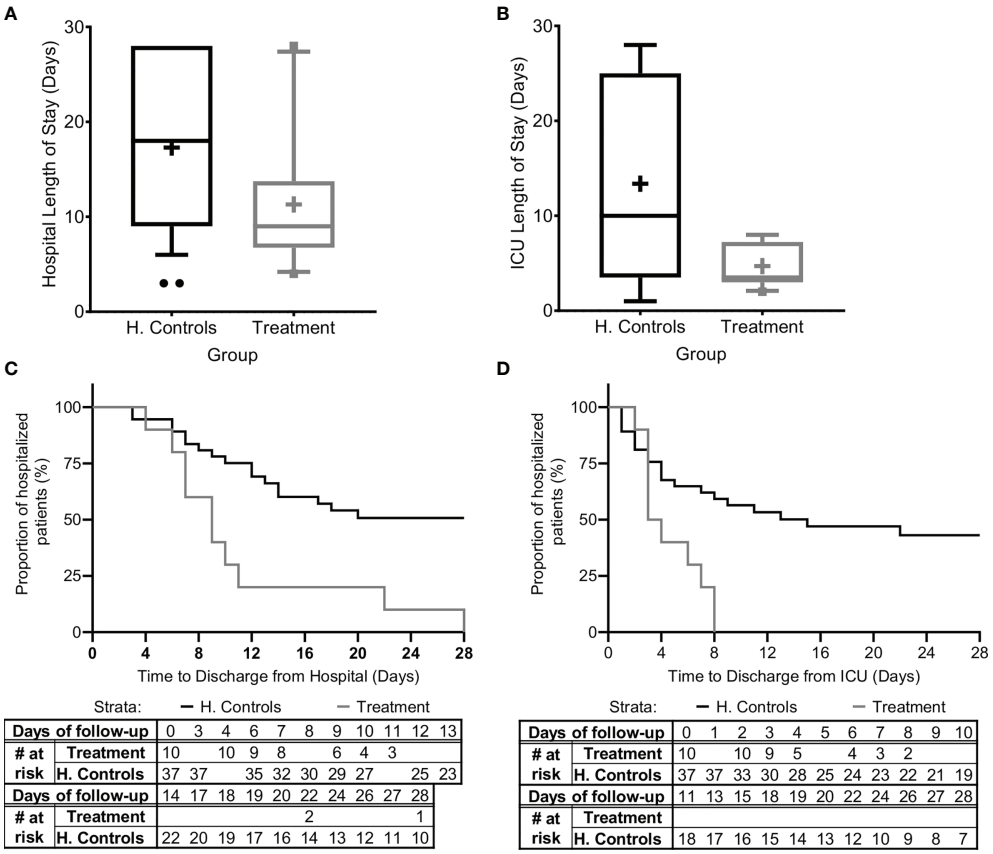

FIGURE 4 | Hospital and ICU/IMU duration of stay. The duration of stay for all patients in the study and for all patients in the matched historical control group who survived is presented **(A)** in the hospital and **(B)** in the Intensive Care Unit (ICU) or the Intermediate Medical Unit (IMU). Kaplan-Meier curves describing time-to-discharge from the **(C)** hospital and **(D)** ICU/IMU are presented. Matched controls were selected from all patients admitted to ICU/IMU with the diagnosis of sepsis between 2014–2019 and were matched by gender, age ±7, SOFA score ±2 at presentation, and source of infection. Data is presented as the median within the interquartile range (IQR); mean values are marked with a '+' sign; error bars represent the 10–90 percentile, with outliers presented.

stimulate the production of acute-phase proteins or attract inflammatory cells (23). Eight pro-inflammatory cytokines were tested, including IL-6, TNF-α, IL-1β, IL-12p70, IL-18, IL-23, IFN-γ and IL-13; five of those were detectable (IL-6, TNF-α, IL-1β, IL, IL-18, IFN-γ) and are presented here (**Figure 5**).

Overall, all patients had elevated TNF-a and IL-6 levels at initial screening, and most had elevated IL-1β and IL-18, while some had elevated IFN-γ; however, a gradual decrease in levels of all of the cytokines studied was observed upon resolution of sepsis. These trends of pro-inflammatory cytokines were characteristic of most of the patients.

3.6.2 Anti-Inflammatory Cytokines

Interestingly, anti-inflammatory cytokines are also upregulated in sepsis in parallel to pro-inflammatory cytokines (**Figure 6**) and are suggested to have a late contribution to sepsis-related immunosuppression (24). Four anti-inflammatory cytokines were tested, including IL-10 (**Figure 6A**), IL-1Ra (**Figure 6B**), IL-27, and soluble TNFR-1 (**Figure 6C**). IL-27 was not detected in our patients. Overall, the trend of the anti-inflammatory cytokines resembled that of the pro-inflammatory cytokines. Most patients had elevated IL-10, IL-1Ra, and TNFR-1, which gradually decreased as sepsis resolved.

3.6.3 Hematopoietic Growth Factors (HGFs)

During sepsis, immune cells undergo profound phenotypic modifications in their activation state, response to stimuli, and localization. These phenomena are finely regulated by various cytokines and HGFs. An HGF is a relatively stable, secreted, or membrane-bound glycoprotein that causes immune cells to mature and/or proliferate and also have profound effects on cell functions and behaviors. HGFs are deeply involved in sepsis pathophysiology both in the initial and the late phases (25). Four growth factors were tested in the study, including G-CSF (**Figure 6D**), VEGF (**Figure 6E**), GM-CSF (**Figure 6F**) and LIF (a growth factor-like cytokine), which was undetected. Overall, the trend of the HGFs resembled that of the pro- and anti-inflammatory cytokines and chemokines. Most patients presented with elevated G-CSF, VEGF, and to a lesser extent GM-CSF, at initial screening; for all, a gradual decrease upon resolution of sepsis was observed. These trends of HGFs were characteristic of most patients that received a single dose of Allocetra-OTS.

3.6.4 Chemokines

Chemokines play pivotal roles in regulating the migration and infiltration of monocytes/macrophages and neutrophils to sites of inflammation, and as such, they are usually involved in sepsis (26). Six chemokines were tested and are presented here, including monocyte chemoattractant protein 1 (MCP-1), interferon gamma-induced protein 10 (IP-10), macrophage inflammatory protein-1 alpha (MIP-1α), IL-8, growth regulated protein beta (Gro-β), and regulated upon activation, normal T cell

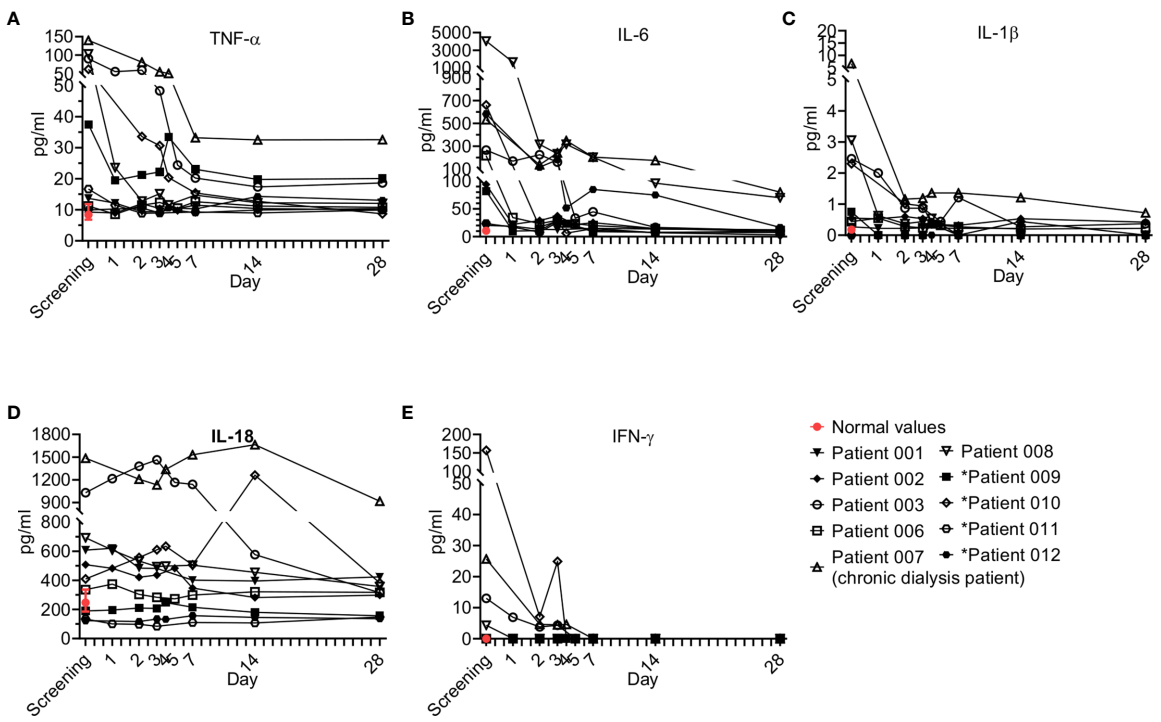

FIGURE 5 | Pro-inflammatory cytokine kinetics during sepsis. Serum was obtained from patients at the indicated times and cytokine analysis was performed as described in Methods. The serum of three healthy volunteers was analyzed using the same methods and values are presented as the normal range (median ± range). Serum concentrations of **(A)** IL-6, **(B)** TNF-α, **(C)** IL-1β, **(D)** IL-18, and **(E)** IFN-γ are presented. Patients 01–08 received one dose of Allocetra-OTS on day 1 and patients 09–12 received two doses on days 1 and 3.

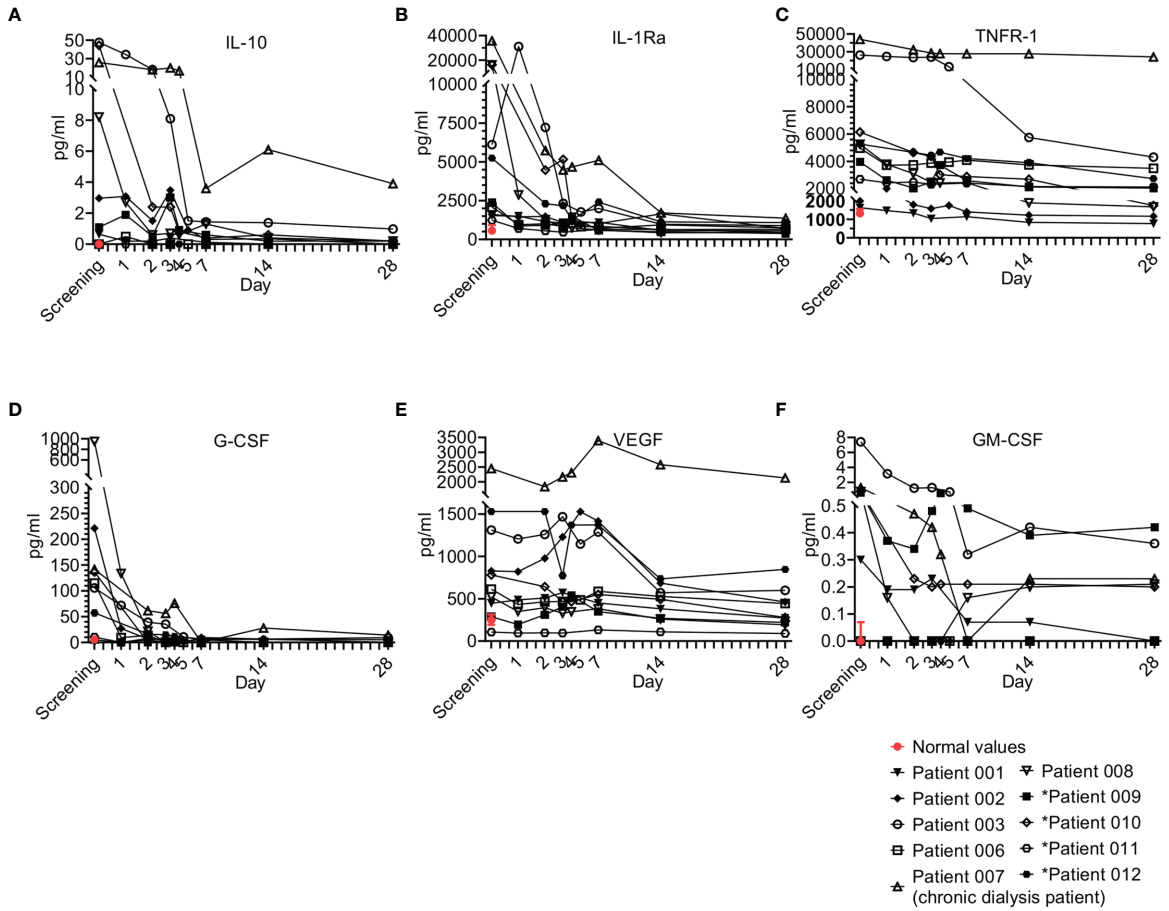

FIGURE 6 | Anti-Inflammatory cytokine and growth factor kinetics during sepsis. Serum was obtained from patients at the indicated times and cytokine/growth factor analysis was performed as described in Methods. The serum of three healthy volunteers was analyzed using the same methods and values are presented as the normal range (median ± range). Serum concentrations of **(A)** IL-10, **(B)** IL-1Ra, **(C)** TNFR-1 are presented in the upper panel, **(D)** G-CSF, **(E)** VEGF, and **(F)** GM-CSF are presented in the lower panel. Patients 01–08 received one dose of Allocetra-OTS on day 1 and patients 09–12 received two doses on days 1 and 3.

expressed and secreted (RANTES). Overall, most patients were screened with elevated MCP-1, IP-10, MIP-1α and IL-8; for all, a gradual decrease upon resolution of sepsis was observed (**Figure 7**). Of exception were Gro-β and RANTES, which were detected in most patients below the normal levels and increased upon resolution of sepsis. These trends of chemokines were characteristic to most of the patients that received a single dose of Allocetra-OTS.

3.6.5 Other Immuno-Modulating Agents

Other factors were also tested as part of the immune modulating effect of Allocetra-OTS on the resolution of sepsis (**Figure 8**). These factors included TREM-1, osteopontin, NGAL, gherlin, and leptin (**Figures 8A–E**), and several endocrinological hormones (**Figures 8F–H**).

3.6.5.1 Miscellaneous Immuno-Modulating Factors

Overall, all the patients presented with elevated TREM-1 and OPN and most had elevated NGAL and leptin levels; for all, a gradual decrease upon resolution of sepsis was observed. Of exception is ghrelin, which was below the normal levels in all the patients at presentation and increased upon resolution of sepsis. These trends of immuno-modulating factors were characteristic of most of the patients that received a single dose of Allocetra-OTS.

3.6.6 Endocrinology Kinetics

Five hormones were tested in all subjects: cortisol, FT3, FT4, glucagon and insulin. Additional hormones (TSH, ACTH and GH) were tested in some subjects. Sepsis is considered an acute stress response with a release of stress hormones including cortisol and glucagon (27). There were elevated cortisol levels in 7/10 patients at presentation, with the average of all patients being above normal (752 nmol/L, normal range of 140–690 nmol/L). Patients 03 and 12 (both with pneumonia) had the highest levels of cortisol at screening. Following Allocetra-OTS infusion, cortisol levels were downregulated (including Patient 03), reaching normal concentrations by Day 28 (**Figure 8G**). Interestingly, serum glucagon had similar kinetics to cortisol, and 7/10 patients had high glucagon at screening (average level

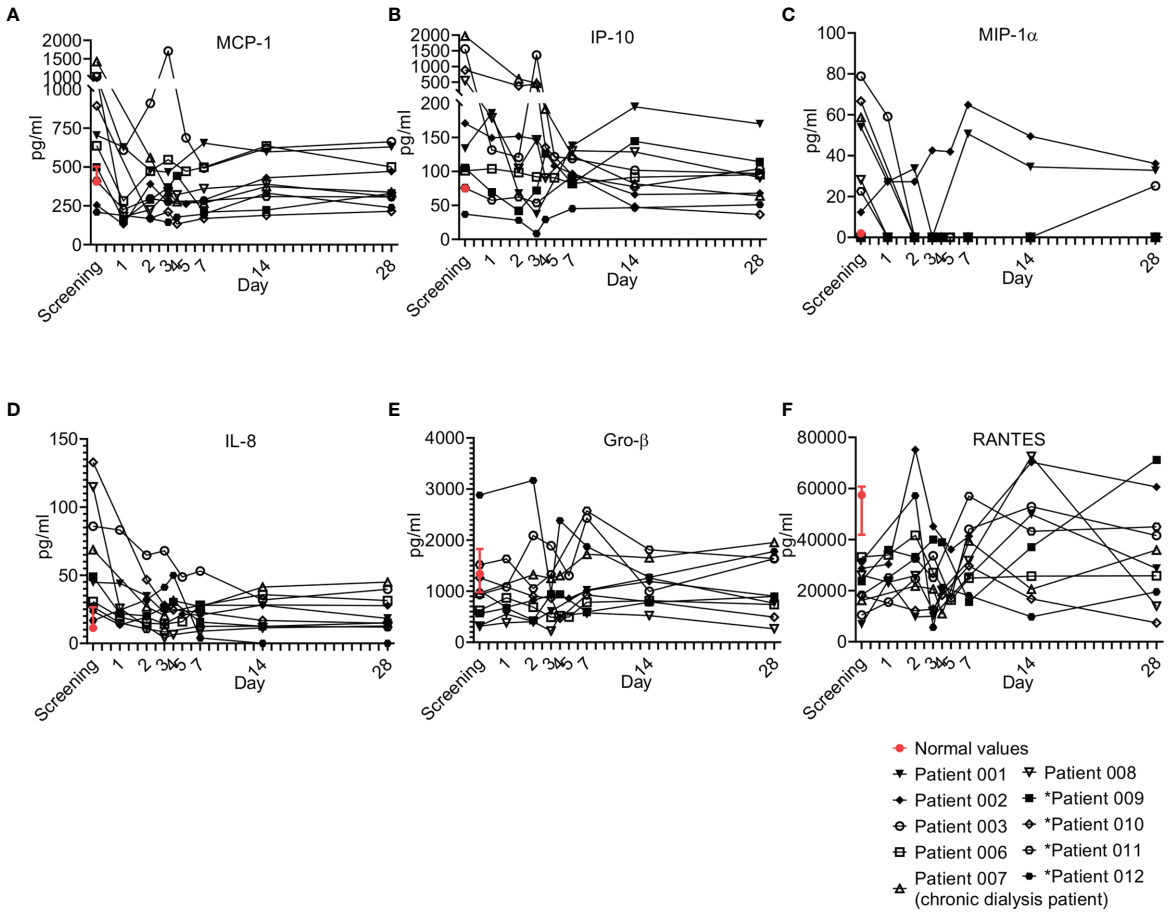

FIGURE 7 | Chemokine kinetics during sepsis. Serum was obtained from patients at the indicated times and cytokine/growth factor analysis was performed as described in Methods. The serum of three healthy volunteers was analyzed using the same methods and values are presented as the normal range (median ± range). Serum concentrations of **(A)** MCP-1, **(B)** IP-10, **(C)** MIP-1α, **(D)** IL-8, **(E)** GRO-β, and **(F)** RANTES are presented. Patients 01–08 received one dose of Allocetra-OTS on day 1 and patients 09–12 received two doses on days 1 and 3.

of all patients = 150pg/ml, range 32–285 pg/ml) compared to normal (average of 73 pg/ml, range 30–115 pg/ml), with a rapid decline in the first 2–3 days reaching low levels on day 28 (**Figure 8F**). Insulin levels were in the low normal range upon presentation (opposite to glucagon) and the levels were normalized upon resolution of sepsis. ACTH and GH were tested in some subjects and were within the normal range throughout the study, except for patient 07 (chronic dialysis) who had elevated ACTH levels on day 28 (21.5 pMol/L versus normal levels up to 13.5). All patients were screened for FT3 and FT4 levels and all had low normal or below normal FT3 levels (**Figure 8H**) with gradual increase thereafter as sepsis resolved, but normal FT4 and TSH levels at presentation and during the resolution of sepsis. These changes in serum thyroid function associated with acute illness have been termed 'sick euthyroid syndrome' or 'low T3 syndrome'. FT3 production during the acute stress response in sepsis is inhibited by both cortisol and IL-6 (28–30). We therefore tested whether the recovery of FT3 seen in the patients was linked to the downregulation of IL-6 and/or cortisol. Indeed, a strong negative correlation was found between FT3 and IL-6 (ρ-Spearman= -0.73) and an intermediate negative correlation was found between FT3 and cortisol and FT3 and glucagon (ρ-Spearman= -0.54, -0.56, respectively). The euthyroid sick syndrome should thus not be viewed as an isolated pathologic event but as part of a coordinated systemic reaction to sepsis involving both the immune and endocrine systems.

3.7 Summary

In summary, most patients had elevated pro-, and anti-inflammatory cytokines/chemokines/immune modulators/stress factors, with a gradual normalization upon resolution of sepsis (**Figures 5**–**8**). The physiological responses to acute stress in sepsis results from the activation of an array of factors, including immunological, neural, and hormonal pathways that pose a threat to the homeostasis of the organism and elicit a common series of adaptive physiological responses. We created a heat map (**Figure 9**), correlating the different immunological components of the response to stress to blood counts and SOFA score. As

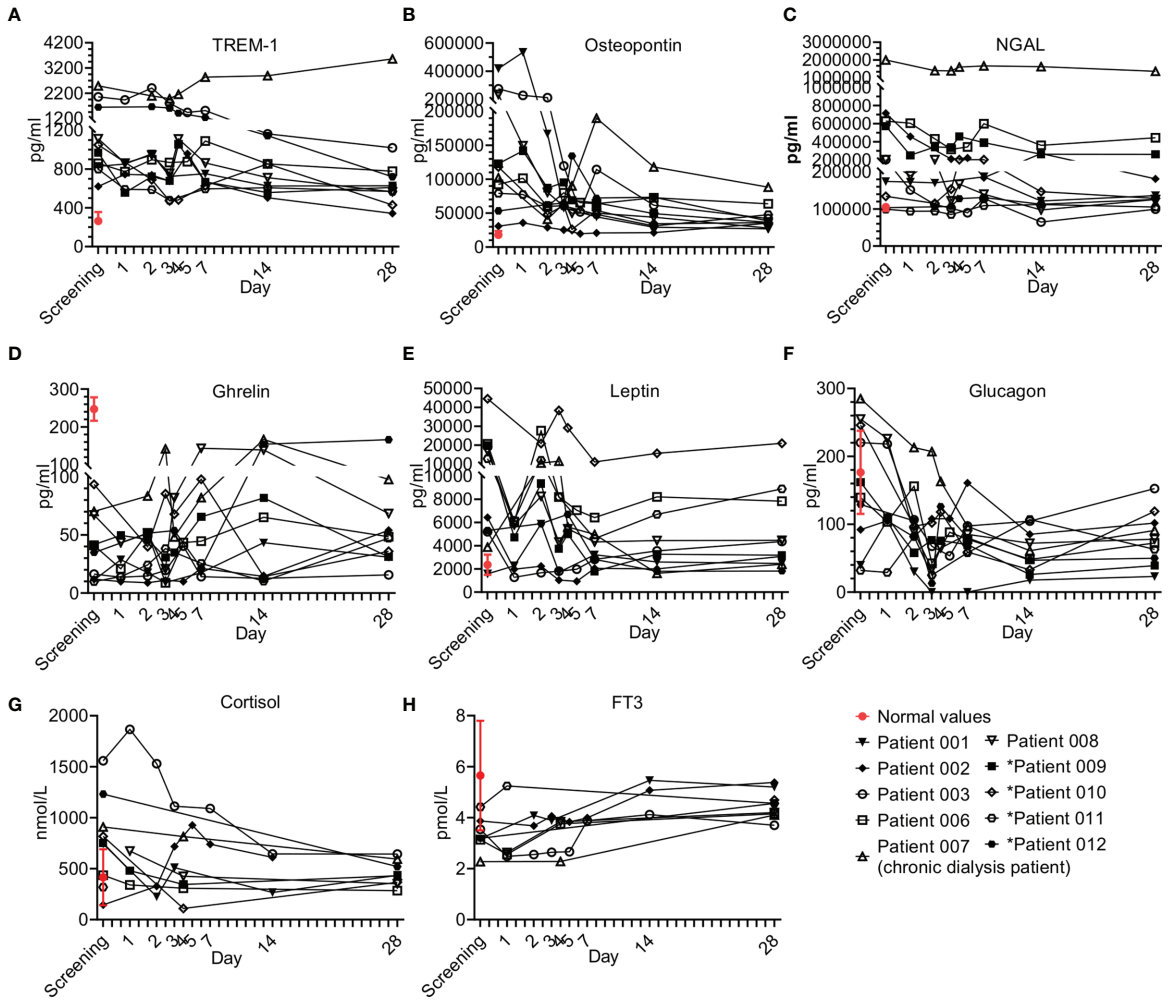

FIGURE 8 | Immune modulator and endocrine hormone kinetics during sepsis. Serum was obtained from patients at the indicated times and cytokine/growth factors analysis was performed as described in Methods. The serum of three healthy volunteers was analyzed using the same methods and values presented as the normal range (median ± range). Serum concentrations of **(A)** TREM-1, **(B)** osteopontin, **(C)** N-GAL, **(D)** ghrelin, **(E)** leptin, and **(F)** glucagon, **(G)** cortisol, and **(H)** FT3 are presented in the lower panel. Patients 01–08 received one dose of Allocetra-OTS on day 1 and patients 09–12 received two doses on days 1 and 3.

shown, high correlation is seen between pro- and anti-inflammatory cytokines, chemokines, HGFs with WBC counts, neutrophils, CRP, and most importantly with SOFA score. Inverse characteristic correlation is shown with lymphocyte counts and the chemokines Gro-β and RANTES.

4 DISCUSSION

Apoptotic cells have immunomodulatory functions *via* their interaction with macrophages and dendritic cells, and their administration as a potential therapeutic intervention has been suggested (13, 14, 31–33). In addition to physical interaction, immunomodulation by apoptotic cell-secretion of various paracrine factors was suggested by us (34) and others (35) and was used in treatments for myocardial infarction (36–38) and dermal wound-healing (39). Unlike stressed PBMC-derived secretomes, the preparation of Allocetra-OTS is unique, with an emphasis on cells in the early stages of apoptosis (i.e. apoptotic cells are Annexin V^+ propidium $iodide^-$) to avoid any effect by necrotic cells. Preparation includes several washing steps, yielding only a cellular active fraction, reducing the content of potential secreted factors.

Although not all the molecular events underlying the potential immune-regulating function of apoptotic cells are clear, changes in macrophages and dendritic cells towards a homeostatic phenotype have been investigated by several authors and implicated in apoptotic cell-mediated immune modulation [reviewed by (13, 32, 33)]. Local administration of apoptotic cells has been used to attenuate both bleomycin- and lipopolysaccharide (LPS)-induced lung inflammation, with reduced neutrophil recruitment into the lung, enhanced phagocytosis by alveolar

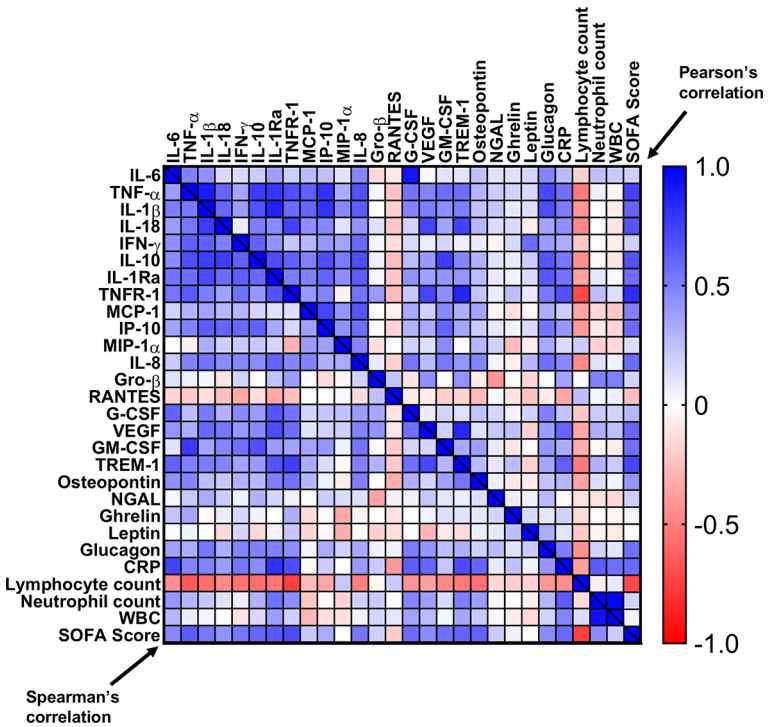

FIGURE 9 | Correlation matrix of cytokines, chemokines, and immunomodulators with SOFA score, CRP, and blood counts. A correlation heat-map of the tested cytokines/chemokines, HGFs, and immunomodulators with CRP, SOFA score, and blood counts. Pearson's r values are on the top right and the Spearman's ρ values are on the bottom left.

macrophages, and reduced pro-inflammatory cytokine production (40). Infusion of apoptotic cells 24 hours after initiation of sepsis has also been shown to protect against mortality in a mouse model of sepsis, with reduced pro-inflammatory cytokine and neutrophil recruitment into organs (41).

We cannot exclude an antimicrobial effect by apoptotic cells as suggested by Kasiri et al. that was observed in an *in-vitro* study (42). However, since Allocetra-OTS was given in addition to antibiotics, we think the main antimicrobial effect was by antibiotics.

Many of the measured cytokines/chemokines/immune-modulators were proven to be pathogenic in sepsis and septic shock; however, single targeting of cytokines did not ameliorate sepsis in many trials using anti-TNF, anti-IL-1β, and other cytokines (43).

Interestingly, and as suggested elsewhere, anti-inflammatory cytokines are also elevated early in the course of sepsis. This supported the notion that secretion of pro- and anti-inflammatory mediators in septic shock occurs as a simultaneous immune response program initiated early in the course of the disease (44), and in severe sepsis the IL-10/lymphocyte ratio was significantly correlated with the APACHE II score and strongly predicted 28-day mortality (45). Apoptotic cell infusion represents a more holistic approach, leading to rebalancing of all pro- and anti-inflammatory cytokines and chemokines, growth factors, and other immuno-modulating agents, and reprogramming of monocytes/macrophages and dendritic cells (13).

In the first few days of clinically apparent infection, there is an innate immune response in all patients. Gene expression studies have shown that transcripts from sepsis and severe viral infections involve pathways associated with signaling through TLRs, IL-27, IL-12, IFN-γ, type I IFN-inducible transcripts, and the JAK-STAT pathway. These molecules are overabundant in the acute phase. These elevated levels persist until defervescence occurs and may lead to endothelial dysfunction (45). The mechanism through which cytokines such as TNF might mediate endothelial dysfunction are not clear, though changes in the integrity of inter-endothelial cell junctions is a possible cause. Most permeability-inducing factors bind to endothelial cell plasma membrane receptors, activate heterotrimeric G proteins, and cause an increase in intracellular $Ca2^{+}$. This results in myosin-driven endothelial contraction and opening of tight junctions. In some viral diseases, increased capillary permeability occurs when viremia is in steep decline and serum cytokine concentrations are at or near their peak levels (46). In addition, pathogen-induced lung injury can progress into acute lung injury or its more severe form, acute respiratory distress syndrome (ARDS), as seen with sepsis and SARS-CoV or viral influenza infections.

4.1 Conclusions

These results may reflect a novel and safe mechanism for treatment of sepsis and diseases associated with cytokine storm

such as flu complications, acute lung injury, acute respiratory distress syndrome as seen in SARS-CoV and influenza virus infections (47), CAR-T therapy (48, 49), and the more recently described COVID-19 (50, 51). To further evaluate Allocetra™-OTS effectiveness, a randomized-controlled trial is needed.

DATA AVAILABILITY STATEMENT

The raw data supporting the conclusions of this article will be made available by the authors upon reasonable request. Requests to access the datasets should be directed to DM, (mevorachd@hadassah.org.il).

ETHICS STATEMENT

The studies involving human participants were reviewed and approved by Human Subjects Review Board, The Helsinki Committee, Hadassa Medical Center, Jerusalem, Israel. The patients/participants provided their written informed consent to participate in this study.

AUTHOR CONTRIBUTIONS

PvH performed the study and wrote the manuscript. AA and SS performed the study and participated in writing. EZ, AN, SZ, and BF performed the study and collected data. Re-A and YS analyzed blood samples. BR prepared figures and participated in writing. DM designed the study and wrote the manuscript. All authors contributed to the article and approved the submitted version.

FUNDING

The study received funding from Enlivex Therapeutics Ltd. The funder was not involved in the study design, collection, analysis, interpretation of data, the writing of this article or the decision to submit it for publication.

REFERENCES

1. Martin-Loeches I, Levy MM, Artigas A. Management of Severe Sepsis: Advances, Challenges, and Current Status. *Drug Des Devel Ther* (2015) 9:2079–88. doi: 10.2147/DDDT.S78757
2. Rello J, Valenzuela-Sanchez F, Ruiz-Rodriguez M, Moyano S. Sepsis: A Review of Advances in Management. *Adv Ther* (2017) 34(11):2393–411. doi: 10.1007/s12325-017-0622-8
3. Venkatesh B, Finfer S, Cohen J, Rajbhandari D, Arabi Y, Bellomo R, et al. Adjunctive Glucocorticoid Therapy in Patients With Septic Shock. *N Engl J Med* (2018) 378(9):797–808. doi: 10.1056/NEJMoa1705835
4. Vincent JL, Grimaldi D. Novel Interventions: What's New and the Future. *Crit Care Clin* (2018) 34(1):161–73. doi: 10.1016/j.ccc.2017.08.012
5. Finfer S, Bellomo R, Lipman J, French C, Dobb G, Myburgh J. Adult-Population Incidence of Severe Sepsis in Australian and New Zealand Intensive Care Units. *Intensive Care Med* (2004) 30(4):589–96. doi: 10.1007/s00134-004-2157-0
6. Fleischmann C, Scherag A, Adhikari NK, Hartog CS, Tsaganos T, Schlattmann P, et al. Assessment of Global Incidence and Mortality of Hospital-Treated Depsis. Current Estimates and Limitations. *Am J Respir Crit Care Med* (2016) 193(3):259–72. doi: 10.1164/rccm.201504-0781OC
7. Liu V, Escobar GJ, Greene JD, Soule J, Whippy A, Angus DC, et al. Hospital Deaths in Patients With Sepsis From 2 Independent Cohorts. *JAMA* (2014) 312(1):90–2. doi: 10.1001/jama.2014.5804
8. Machado FR, Cavalcanti AB, Bozza FA, Ferreira EM, Angotti Carrara FS, Sousa JL, et al. The Epidemiology of Sepsis in Brazilian Intensive Care Units (the Sepsis Prevalence Assessment Database, SPREAD): An Observational Study. *Lancet Infect Dis* (2017) 17(11):1180–9. doi: 10.1016/S1473-3099(17)30322-5
9. Reinhart K, Daniels R, Kissoon N, Machado FR, Schachter RD, Finfer S. Recognizing Sepsis as a Global Health Priority — a WHO Resolution. *N Engl J Med* (2017) 377(5):414–7. doi: 10.1056/NEJMp1707170
10. Rhee C, Dantes R, Epstein L, Murphy DJ, Seymour CW, Iwashyna TJ, et al. Incidence and Trends of Sepsis in US Hospitals Using Clinical vs Claims Data, 2009-2014. *JAMA* (2017) 318(13):1241–9. doi: 10.1001/jama.2017.13836
11. Hotchkiss RS, Moldawer LL, Opal SM, Reinhart K, Turnbull IR, Vincent JL. Sepsis and Septic Shock. *Nat Rev Dis Primers* (2016) 2:16045. doi: 10.1038/nrdp.2016.45
12. Tang D, Kang R, Coyne CB, Zeh HJ, Lotze MT. Pamps and Damps: Signal 0s That Spur Autophagy and Immunity. *Immunol Rev* (2012) 249(1):158–75. doi: 10.1111/j.1600-065X.2012.01146.x
13. Trahtemberg U, Mevorach D. Apoptotic Cells Induced Signaling for Immune Homeostasis in Macrophages and Dendritic Cells. *Front Immunol* (2017) 8:1356. doi: 10.3389/fimmu.2017.01356
14. Mevorach D, Zuckerman T, Reiner I, Shimoni A, Samuel S, Nagler A, et al. Single Infusion of Donor Mononuclear Early Apoptotic Cells as Prophylaxis for Graft-Versus-Host Disease in Myeloablative HLA-Matched Allogeneic Bone Marrow Transplantation: A Phase I/Iia Clinical Trial. *Biol Blood Marrow Transplant* (2014) 20(1):58–65. doi: 10.1016/j.bbmt.2013.10.010
15. Rowan KM, Kerr JH, Major E, McPherson K, Short A, Vessey MP. Intensive Care Society's APACHE II Study in Britain and Ireland–I: Variations in Case Mix of Adult Admissions to General Intensive Care Units and Impact on Outcome. *BMJ* (1993) 307(6910):972–7. doi: 10.1136/bmj.307.6910.972
16. Knaus WA, Draper EA, Wagner DP, Zimmerman JE. APACHE II: A Severity of Disease Classification System. *Crit Care Med* (1985) 13(10):818–29. doi: 10.1097/00003246-198510000-00009
17. Minne L, Abu-Hanna A, de Jonge E. Evaluation of SOFA-Based Models for Predicting Mortality in the ICU: A Systematic Review. *Crit Care* (2008) 12(6):R161. doi: 10.1186/cc7160
18. Moon BH, Park SK, Jang DK, Jang KS, Kim JT, Han YM. Use of APACHE II and SAPS II to Predict Mortality for Hemorrhagic and Ischemic Stroke Patients. *J Clin Neurosci* (2015) 22(1):111–5. doi: 10.1016/j.jocn.2014.05.031
19. Vincent JL, Moreno R. Clinical Review: Scoring Systems in the Critically Ill. *Crit Care* (2010) 14(2):207. doi: 10.1186/cc8204
20. Singer M, Deutschman CS, Seymour CW, Shankar-Hari M, Annane D, Bauer M, et al. The Third International Consensus Definitions for Sepsis and Septic Shock (Sepsis-3). *JAMA* (2016) 315(8):801–10. doi: 10.1001/jama.2016.0287
21. Raith EP, Udy AA, Bailey M, McGloughlin S, MacIsaac C, Bellomo R, et al. Prognostic Accuracy of the SOFA Score, SIRS Criteria, and Qsofa Score for in-Hospital Mortality Among Adults With Suspected Infection Admitted to the Intensive Care Unit. *JAMA* (2017) 317(3):290–300. doi: 10.1001/jama.2016.20328
22. Vincent JL, Moreno R, Takala J, Willatts S, De Mendonca A, Bruining H, et al. The SOFA (Sepsis-Related Organ Failure Assessment) Score to Describe Organ Dysfunction/Failure. On Behalf of the Working Group on Sepsis-Related Problems of the European Society of Intensive Care Medicine. *Intensive Care Med* (1996) 22(7):707–10. doi: 10.1007/BF01709751
23. Chaudhry H, Zhou J, Zhong Y, Ali MM, McGuire F, Nagarkatti PS, et al. Role of Cytokines as a Double-Edged Sword in Sepsis. *In Vivo* (2013) 27(6):669–84.
24. Chousterman BG, Swirski FK, Weber GF. Cytokine Storm and Sepsis Disease Pathogenesis. *Semin Immunopathol* (2017) 39(5):517–28. doi: 10.1007/s00281-017-0639-8
25. Chousterman BG, Arnaud M. Is There a Role for Hematopoietic Growth Factors During Sepsis? *Front Immunol* (2018) 9:1015. doi: 10.3389/fimmu.2018.01015

26. Aziz M, Jacob A, Yang WL, Matsuda A, Wang P. Current Trends in Inflammatory and Immunomodulatory Mediators in Sepsis. *J Leukoc Biol* (2013) 93(3):329–42. doi: 10.1189/jlb.0912437
27. Jones BJ, Tan T, Bloom SR. Minireview: Glucagon in Stress and Energy Homeostasis. *Endocrinology* (2012) 153(3):1049–54. doi: 10.1210/en.2011-1979
28. Meyer S, Schuetz P, Wieland M, Nusbaumer C, Mueller B, Christ-Crain M. Low Triiodothyronine Syndrome: A Prognostic Marker for Outcome in Sepsis? *Endocrine* (2011) 39(2):167–74. doi: 10.1007/s12020-010-9431-4
29. Plikat K, Langgartner J, Buettner R, Bollheimer LC, Woenckhaus U, Scholmerich J, et al. Frequency and Outcome of Patients With Nonthyroidal Illness Syndrome in a Medical Intensive Care Unit. *Metabolism* (2007) 56(2):239–44. doi: 10.1016/j.metabol.2006.09.020
30. Wiersinga WJ, Seymour CW. *Handbook of Sepsis*. Cham, Switzerland: Springer Int. Publ. AG (2018).
31. Bonnefoy F, Gauthier T, Vallion R, Martin-Rodriguez O, Missey A, Daoui A, et al. Factors Produced by Macrophages Eliminating Apoptotic Cells Demonstrate Pro-Resolutive Properties and Terminate Ongoing Inflammation. *Front Immunol* (2018) 9:2586. doi: 10.3389/fimmu.2018.02586
32. Poon IK, Lucas CD, Rossi AG, Ravichandran KS. Apoptotic Cell Clearance: Basic Biology and Therapeutic Potential. *Nat Rev Immunol* (2014) 14(3):166–80. doi: 10.1038/nri3607
33. Saas P, Daguindau E, Perruche S. Concise Review: Apoptotic Cell-Based Therapies-Rationale, Preclinical Results and Future Clinical Developments. *Stem Cells* (2016) 34(6):1464–73. doi: 10.1002/stem.2361
34. Krispin A, Bledi Y, Atallah M, Trahtemberg U, Verbovetski I, Nahari E, et al. Apoptotic Cell Thrombospondin-1 and Heparin-Binding Domain Lead to Dendritic-Cell Phagocytic and Tolerizing States. *Blood* (2006) 108(10):3580–9. doi: 10.1182/blood-2006-03-013334
35. Beer L, Mildner M, Gyöngyösi M, Ankersmit HJ. Peripheral Blood Mononuclear Cell Secretome for Tissue Repair. *Apoptosis* (2016) 21(12):1336–53. doi: 10.1007/s10495-016-1292-8
36. Hoetzenecker K, Assinger A, Lichtenauer M, Mildner M, Schweiger T, Starlinger P, et al. Secretome of Apoptotic Peripheral Blood Cells (APOSEC) Attenuates Microvascular Obstruction in a Porcine Closed Chest Reperfused Acute Myocardial Infarction Model: Role of Platelet Aggregation and Vasodilation. *Basic Res Cardiol* (2012) 107(5):292–2. doi: 10.1007/s00395-012-0292-2
37. Lichtenauer M, Mildner M, Baumgartner A, Hasun M, Werba G, Beer L, et al. Intravenous and Intramyocardial Injection of Apoptotic White Blood Cell Suspensions Prevents Ventricular Remodelling by Increasing Elastin Expression in Cardiac Scar Tissue After Myocardial Infarction. *Basic Res Cardiol* (2011) 106(4):645–55. doi: 10.1007/s00395-011-0173-0
38. Lichtenauer M, Mildner M, Hoetzenecker K, Zimmermann M, Podesser BK, Sipos W, et al. Secretome of Apoptotic Peripheral Blood Cells (APOSEC) Confers Cytoprotection to Cardiomyocytes and Inhibits Tissue Remodelling After Acute Myocardial Infarction: A Preclinical Study. *Basic Res Cardiol* (2011) 106(6):1283–97. doi: 10.1007/s00395-011-0224-6
39. Hacker S, Mittermayr R, Nickl S, Haider T, Lebherz-Eichinger D, Beer L, et al. Paracrine Factors From Irradiated Peripheral Blood Mononuclear Cells Improve Skin Regeneration and Angiogenesis in a Porcine Burn Model. *Sci Rep* (2016) 6(1):25168. doi: 10.1038/srep25168
40. Lee YJ, Moon C, Lee SH, Park HJ, Seoh JY, Cho MS, et al. Apoptotic Cell Instillation After Bleomycin Attenuates Lung Injury Through Hepatocyte Growth Factor Induction. *Eur Respir J* (2012) 40(2):424–35. doi: 10.1183/09031936.00096711
41. Ren Y, Xie Y, Jiang G, Fan J, Yeung J, Li W, et al. Apoptotic Cells Protect Mice Against Lipopolysaccharide-Induced Shock. *J Immunol* (2008) 180(7):4978–85. doi: 10.4049/jimmunol.180.7.4978
42. Kasiri MM, Beer L, Nemec L, Gruber F, Pietkiewicz S, Haider T, et al. Dying Blood Mononuclear Cell Secretome Exerts Antimicrobial Activity. *Eur J Clin Invest* (2016) 46:853–63. doi: 10.1111/eci.12667
43. Cohen J, Opal S, Calandra T. Sepsis Studies Need New Direction. *Lancet Infect Dis* (2012) 12(7):503–5. doi: 10.1016/S1473-3099(12)70136-6
44. Tamayo E, Fernandez A, Almansa R, Carrasco E, Heredia M, Lajo C, et al. Pro- and Anti-Inflammatory Responses Are Regulated Simultaneously From the First Moments of Septic Shock. *Eur Cytokine Netw* (2011) 22(2):82–7. doi: 10.1684/ecn.2011.0281
45. Li X, Xu Z, Pang X, Huang Y, Yang B, Yang Y, et al. Interleukin-10/Lymphocyte Ratio Predicts Mortality in Severe Septic Patients. *PloS One* (2017) 12(6):e0179050. doi: 10.1371/journal.pone.0179050
46. Libraty DH, Endy TP, Houng HS, Green S, Kalayanarooj S, Suntayakorn S, et al. Differing Influences of Virus Burden and Immune Activation on Disease Severity in Secondary Dengue-3 Virus Infections. *J Infect Dis* (2002) 185(9):1213–21. doi: 10.1086/340365
47. Pugin J, Ricou B, Steinberg KP, Suter PM, Martin TR. Proinflammatory Activity in Bronchoalveolar Lavage Fluids From Patients With ARDS, a Prominent Role for Interleukin-1. *Am J Respir Crit Care Med* (1996) 153(6 Pt 1):1850–6. doi: 10.1164/ajrccm.153.6.8665045
48. Gauthier J, Turtle CJ. Insights Into Cytokine Release Syndrome and Neurotoxicity After CD19-Specific CAR-T Cell Therapy. *Curr Res Transl Med* (2018) 66(2):50–2. doi: 10.1016/j.retram.2018.03.003
49. Giavridis T, van der Stegen SJC, Eyquem J, Hamieh M, Piersigilli A, Sadelain M. CAR T Cell-Induced Cytokine Release Syndrome Is Mediated by Macrophages and Abated by IL-1 Blockade. *Nat Med* (2018) 24(6):731–8. doi: 10.1038/s41591-018-0041-7
50. Huang R, Xia J, Chen Y, Shan C, Wu C. A Family Cluster of SARS-CoV-2 Infection Involving 11 Patients in Nanjing, China. *Lancet Infect Dis* (2020) 20(5):534–5. doi: 10.1016/S1473-3099(20)30147-X
51. Mehta P, McAuley DF, Brown M, Sanchez E, Tattersall RS, Manson JJ, et al. COVID-19: Consider Cytokine Storm Syndromes and Immunosuppression. *Lancet* (2020) 395(10229):1033–4. doi: 10.1016/S0140-6736(20)30628-0

Conflict of Interest: PvH received honoraria from Enlivex Ltd as a consultant. DM is the founder, and CMO of Enlivex Therapeutics Ltd. YS and BR are part of the research team of Enlivex Therapeutics Ltd.

The remaining authors declare that the research was conducted in the absence of any commercial or financial relationships that could be construed as potential conflicts of interest.

Publisher's Note: All claims expressed in this article are solely those of the authors and do not necessarily represent those of their affiliated organizations, or those of the publisher, the editors and the reviewers. Any product that may be evaluated in this article, or claim that may be made by its manufacturer, is not guaranteed or endorsed by the publisher.

Copyright © 2021 van Heerden, Abutbul, Sviri, Zlotnick, Nama, Zimro, el-Amore, Shabat, Reicher, Falah and Mevorach. This is an open-access article distributed under the terms of the Creative Commons Attribution License (CC BY). The use, distribution or reproduction in other forums is permitted, provided the original author(s) and the copyright owner(s) are credited and that the original publication in this journal is cited, in accordance with accepted academic practice. No use, distribution or reproduction is permitted which does not comply with these terms.

frontiers in Immunology

ORIGINAL RESEARCH
published: 30 September 2021
doi: 10.3389/fimmu.2021.756321

Desmoglein2 Regulates Claudin2 Expression by Sequestering PI-3-Kinase in Intestinal Epithelial Cells

*Natalie Burkard[1], Michael Meir[1], Felix Kannapin[1], Christoph Otto[1], Maximilian Petzke[1], Christoph-Thomas Germer[1], Jens Waschke[2] and Nicolas Schlegel[1]**

[1] Department of General, Visceral, Transplant, Vascular and Pediatric Surgery University Hospital Würzburg, Würzburg, Germany, [2] Institute of Anatomy and Cell Biology, Department I, Ludwig-Maximilians-Universität München, Munich, Germany

Inflammation-induced reduction of intestinal desmosomal cadherin Desmoglein 2 (Dsg2) is linked to changes of tight junctions (TJ) leading to impaired intestinal epithelial barrier (IEB) function by undefined mechanisms. We characterized the interplay between loss of Dsg2 and upregulation of pore-forming TJ protein Claudin2. Intraperitoneal application of Dsg2-stablising Tandem peptide (TP) attenuated impaired IEB function, reduction of Dsg2 and increased Claudin2 in DSS-induced colitis in C57Bl/6 mice. TP blocked loss of Dsg2-mediated adhesion and upregulation of Claudin2 in Caco2 cells challenged with TNFα. In Dsg2-deficient Caco2 cells basal expression of Claudin2 was increased which was paralleled by reduced transepithelial electrical resistance and by augmented phosphorylation of AKT^{Ser473} under basal conditions. Inhibition of phosphoinositid-3-kinase proved that PI-3-kinase/AKT-signaling is critical to upregulate Claudin2. In immunostaining PI-3-kinase dissociated from Dsg2 under inflammatory conditions. Immunoprecipitations and proximity ligation assays confirmed a direct interaction of Dsg2 and PI-3-kinase which was abrogated following TNFα application. In summary, Dsg2 regulates Claudin2 expression by sequestering PI-3-kinase to the cell borders in intestinal epithelium.

Keywords: Claudin2, Dsg2, inflammation, intestinal barrier, PI-3-kinase, inflammatory bowel disease, desmosome, tight junction

OPEN ACCESS

Edited by:
Janos G Filep, Université de Montréal, Canada

Reviewed by:
Tsaffrir Zor, Tel Aviv University, Israel
Bin Gong, University of Texas Medical Branch at Galveston, United States

****Correspondence:***
Nicolas Schlegel
Schlegel_N@ukw.de
orcid.org/0000-0001-5705-3945

Specialty section:
This article was submitted to Inflammation, a section of the journal Frontiers in Immunology

Received: *10 August 2021*
Accepted: *10 September 2021*
Published: *30 September 2021*

Citation:
Burkard N, Meir M, Kannapin F, Otto C, Petzke M, Germer C-T, Waschke J and Schlegel N (2021) Desmoglein2 Regulates Claudin2 Expression by Sequestering PI-3-Kinase in Intestinal Epithelial Cells. Front. Immunol. 12:756321. doi: 10.3389/fimmu.2021.756321

INTRODUCTION

The intestinal epithelium provides a selective barrier which separates the gut lumen containing nutrients, commensal bacteria and pathogens from the inner part of the body (1). Loss of intestinal epithelial barrier (IEB) integrity is known to contribute to the pathogenesis of inflammatory bowel diseases (2, 3).

Under basal condition the intestinal mucosa is lined by a single layer of polarized epithelial cells (enterocytes) that are sealed by tight junctions (TJ) and held together by adherens junctions and desmosomes (3–5). Adherens junctions are composed of E-cadherins which are tethered to the actin cytoskeleton while desmosomes in the intestine are composed of the desmocadherins desmoglein2 (Dsg2) and desmocollin2 (Dsc2) (3, 6). Both are linked to the intermediate filament system *via*

various adapter proteins. Previously, it was reported that desmosomal integrity is not only essential to maintain the intestinal epithelial barrier under basal conditions but it is meanwhile established that loss of Dsg2 significantly contributes to inflammation-induced breakdown of the gut barrier in inflammatory bowel diseases (6–11). Desmosomes are known to stabilize IEB function by strengthening intercellular adhesion. In addition they are increasingly recognized as signaling hubs that mediate a variety of signals linked to cell proliferation, apoptosis and barrier regulation (3, 11–16).

Beside the growing evidence for the importance of desmosomal integrity to maintain the IEB in health and disease, it is well established that the main diffusion barrier within the junctional complex is formed by tight junctions that consist of various transmembrane proteins including claudins and occludin which are typically found at the most apical part of the membranes (5). The majority of the claudins that are typically present in the intestine such as claudin1, 3, 4, 5, 7, and 8 exert barrier-sealing properties. In contrast, Claudin2 which is strongly upregulated in intestinal inflammation is a pore-forming claudin which increases the permeability for cations like Na^+, K^+, Li^+ and water (9, 10, 17–19). Upregulation of Claudin2 has been linked to diarrhea as typical clinical symptom of gut barrier changes. Under basal conditions Claudin2 is largely absent in the adult colon tissue whereas it has been described to be expressed in the human small intestine along the crypt-villus axis especially in the crypts (20). It is known that Claudin2 is increased following stimulation of enterocytes with cytokines such as TNFα, which is also regarded as a key cytokine contributing to mucosal injury in inflammatory bowel diseases (18, 21, 22).

Many studies meanwhile described a close correlation between the integrity of desmosomes and tight junctions (23–25). In line with this, we found a correlation between inflammation-induced loss of Dsg2 and increased Claudin2 expression in patients with Crohn's disease and *in vitro* in a previous study. Interestingly, we observed that restoration of Dsg2-mediated adhesion using a Dsg-linking tandem peptide (TP) blocked TNFα-induced upregulation of Claudin2 (10). Based on this, we tested here whether Dsg2-mediated adhesion/signalling may be directly involved in the regulation of Claudin2.

MATERIALS AND METHODS

Test Reagents

TNFα (Biomol, Hamburg, Germany) was used at 100 ng/ml (10). Tandem Peptide was used at 20 μM *in vitro* and 10 μM *in vivo* (Bachem, Bubendorf, Switzerland). The PI-3-kinase inhibitor LY294002 was used at 20 μM (Millipore, Darmstadt, Germany). Dsg2 binding was blocked by using a Dsg2 specific monoclonal mouse antibody directed against the third extracellular repeat domains of Dsg2 (anti-$Dsg2^{EC}$) (clone 10G11, sodium azide free, Progen, Heidelberg, Germany) applied 1:50 (14). If not indicated otherwise cells were incubated with the mediators for 24h alone or in combination. When combinations of different reagents were used, they were applied simultaneously.

Animal Experiments

After approval by the animal care committee (Laboratory Animal Care and Use Committee of the District of Unterfranken; AZ 2-272), experiments were performed in male C57BL6/J mice (Janvier Labs, Le Genest Saint Isle, France). Animals were kept under conditions that complied with the NIH *Guide for the Care and Use of Laboratory Animals*, and studies were approved by the governments of Unterfranken and Germany. Animals were kept on a standard diet and 12-hour day and night cycles.

Experimental Setup

We used dextran sulfate sodium (DSS)-induced colitis in mice as (a murine) model for inflammatory bowel disease. Eight-week-old male mice received 2.5% DSS in autoclaved drinking water ad libitum for 4 days. The control group received normal drinking water *ad libitum*. Mice were monitored daily to evaluate the disease activity index (DAI) as described previously (8). Animals were randomized in different groups. One group received intraperitoneally (i.p.) 10 μM TP dissolved in 100μl 0.9% NaCl (DSS+TP) whereas the other group received 100μl 0.9% NaCl i.p. (DSS group). Injections were administered daily up from day 4 onwards every 24 hours for 3 days. Endpoint of the experiment was defined after 6 days.

Measurement of Intestinal Permeability, Colon Length, and Tissue Harvesting

Intestinal permeability was measured as described previously (8): After 6 days, mice were anaesthetized mice using isoflurane (Forene, Abbott, Wiesbaden, Germany). Following laparotomy, the colon was mobilized and opened at the ileocaecal valve and at the upper rectum. After flushing the colon with PBS at RT to remove blood and stool, the colon was ligated at the cutted ends without compromising the blood supply. To determine intestinal permeability 200μl of 4kDa FITC dextran diluted in PBS (1 mg/ml) was injected in the ligated colon. After 1h blood from the inferior vena cava was taken to measure the concentration of 4 kDa FITC dextran translocated from the colonic lumen into the blood. The blood samples were centrifuged at 13.400 rpm for 10 minutes at 4°C, and the luminescence of the serum was quantified by using Genios Pro Reader (Tecan, Maennedorf, Switzerland). After blood collection mice were euthanized by exsanguination, the colon was harvested and the length was measured.

The ligations of the colon were removed and the colon was cut longitudinally into two pieces. One part was fixed in 4% paraformaldehyde embedded in paraffin and sectioned. The other half of the colon was lyzed and homogenized with a Tissue Lyzer (Quiagen, Hilden, Germany) in a SDS lysis buffer and used for Western Blot analysis.

Histological Injury Score

Two blinded investigators quantified the inflammation of the tissue in H.E.-stained sections of the colon using the following inflammation score (26): Extent of inflammatory cell infiltration (none =1, mucosal infiltration =2, submucosal infiltration =3 transmural infiltration =4) and severity of epithelial damage (no epithelial damage =1, focal lesions =2, multiple lesions =3,

extended ulcerations =4), resulting in a total scoring range from 2 – 8 per mouse.

Immunostaining

Animal tissue samples were embedded in paraffin and sectioned in 1µm slices. Immunostaining was performed after removal of paraffin as described for CaCo2 cells.

Cultured cell monolayers were prepared for immunostaining as described previously (27). In brief, CaCo2 cells were grown to confluence on coverslips. After incubation with or without different mediators, cells were fixated with 2% formaldehyde for 10 minutes and permeabilized with 0.1% Triton-X100 for 15 minutes afterwards, at room temperature. The coverslips were incubated at 4°C overnight using following primary antibodies at 1:100 in phosphate-buffered saline (PBS): rabbit anti-Desmoglein2 (MyBiosource, Kampenhout, Belgium); mouse anti-Claudin2 (ThermoFisher, Schwerte, Germany); mouse anti-PI-3-kinase (Santa Cruz, Heidelberg, Germany). As secondary antibodies, we used Cy3- or 488- labeled goat anti-mouse, goat anti-rabbit (all diluted 1:600, Dianova, Hamburg, Germany). Coverslips were mounted on glass slides with Vector Shield Mounting Medium as anti-fading compound, which included DAPI to visualize cell nuclei additionally (Vector Laboratories, Burlingham, CA). Representative experiments were documented with a confocal microscope (Leica LSM 780) (Zeiss, Oberkochen, Germany).

Western Blot

For Western blot analyses of mouse tissue, the specimens were lyzed in a SDS lysis buffer using TissueLyzer (Quiagen, Hilden Germany). CaCo2 cells were grown on 6-well plates, incubated with different mediators for 24h and finally homogenized in sodium dodecyl sulfate (SDS) lysis buffer containing 25 mmol/l HEPES, 2 mmol/l EDTA, 25 mmol/l NaF and 1% SDS. SDS gel electrophoresis and blotting were carried out after normalization of the protein amount using BCA assay (Thermo Fisher, Waltham, MA), as described previously (27). The following antibodies were used: mouse anti-Desmoglein 2 diluted 1:1000 (ThermoFisher, Schwerte, Germany); mouse anti-Claudin 2 diluted 1:700 (ThermoFisher, Schwerte, Germany); rabbit anti-PI-3-kinase diluted 1:500 (abcam, Cambridge, UK); rabbit anti-Phospho Akt (Ser473) diluted 1:1000 (Cell Signaling, Leiden, Netherlands); rabbit anti-Phospho Akt (Thr308) diluted 1:700 (Cell Signaling, Leiden, Netherlands), rabbit anti-Akt diluted 1:1000 (Cell signaling, Leiden, Netherlands) in 5% bovine serum albumin (BSA) and 0.1% Tween. As secondary antibodies horseradish peroxidase-labeled goat anti-rabbit IgG, goat anti-mouse IgG (all Santa Cruz Biotechnology, Heidelberg, Germany) were used (1:3000 in 5% BSA, 0.1% Tween). To validate equal loading of the gels peroxidase-labeled β-Actin or GAPDH (both Sigma-Aldrich, Munich, Germany) antibodies were applied. Chemiluminescence signal detection and quantification were performed by densitometry (ChemicDoc Touch Bio-Rad Laboratories GmbH, Munich, Germany). Optical densities (OD) were quantified in each Western Blot using Image Lab ChemicDoc Touch (Bio-Rad Laboratories GmbH, Munich, Germany) for statistical evaluation.

Cell Culture

Caco2 cells (Caco2 $Dsg2^{WT}$) were acquired from ATCC (Wesel, Germany) and were cultured in Eagle's Minimum Essential Medium (EMEM, ATCC, Wesel, Germany) supplemented with 50 U/ml Penicillin-G, 50 µg Streptomycin and 10% fetal calf serum (FCS, Biochrom, Berlin, Germany). Cultures were used for experiments when grown to confluent monolayers. For experiments, cells were serum-starved for 24h. In addition, our Dsg2-deficient Caco2 cell line (Caco2 $Dsg2^{-/-}$) was used as described in detail previously (8).

Dispase-Based Enterocyte Dissociation Assays

As described previously (10), confluent cells in 24-well plates were exposed to the test reagents as indicated above, washed with Hank's buffered saline solution plus (HBSS, Sigma-Aldrich, Munich, Germany) and incubated with Dispase-II (Sigma-Aldrich, Munich, Germany) for 30 minutes to release the monolayer from the well bottom. Afterwards, the cell sheet was exposed to shear stress by pipetting 5 times. Four fields of view were photographed with BZ-9000 (BIOREVO, Keyence, Osaka, Japan) and numbers were quantified.

Measurement of FITC-Dextran Flux Across Monolayers of Cultured Epithelial Cells

As described previously (27), Caco2 cells were seeded on top of transwell filter chambers on 12-well plates (0.4µm pore size; Falcon, Heidelberg, Germany). After reaching confluence, cells were rinsed with PBS, and incubated with fresh DMEM without phenol red (Sigma) containing 10 mg/ml FITC-dextran (4 kDa). Paracellular flux was assessed by taking 100µl aliquots from the outer chamber over 2 h of incubation. Fluorescence was measured using a Tecan GENios Microplate Reader (MTX Lab systems, Bradenton, USA) with excitation and emission at 485 and 535 nm, respectively. For all experimental conditions, permeability coefficients (P_E) were calculated by the following formula (28): $P_E = [(\Delta C_A/\Delta t) \times V_A]/S \times \Delta C_L$, where P_E = diffusive permeability (cm/s), ΔC_A = change of FITC-dextran concentration, Δt = change of time, V_A = volume of the abluminal medium, S = surface area, and ΔC_L = constant luminal concentration. Experiments were performed in triplicates for each conditions and mean values of each triplicates were taken together as one independent experiment.

Measurements of Transepithelial Electrical Resistance (TER)

To measure transepithelial electrical resistance (TER) we used ECIS trans-Filter Adapter for ECIS 1600R across cell monolayers (Applied Biophysics, Ibidi GmBH, Martinsried, Germany). Cells were seeded on 8 well arrays with 40 electrodes per well (Applied Biophysics, Ibidi GmBH, Martinsried, Germany) as described previously (8). At confluency of monolayers cells were treated with different mediators and measurements were started immediately after application of the reagents.

Real Time Quantitative (q)RT-PCR

RNA from CaCo2 wildtype and CaCo2 Dsg2 knock-out cells was isolated using TRIZOL and cDNA was synthesized with iScript™ cDNA Synthesis Kit (Biorad, Munich, Germany). Quantitative

PCR was performed using MESA GREEN qPCR MasterMix Plus for SYBR® Assay No ROX (Eurogentec, Cologne, Germany) on the CFX96 Touch Real-Time PCR Detection System (Biorad, Munich, Germany). Gene expression was analyzed *via* the Bio-Rad CFX Manager software with β-actin as a reference gene. All reactions were done in duplicates at 60.0°C annealing temperature. Primers were applied at a concentration of 5 µM. Primer sequences: humanDSG2 f: 5`- AACGACAACTGTCCCACACT -3`, humanDSG2 r: 5`- TTTCTTGGCGTGCTATTTTC -3`; human claudin2 f: 5`- CTCCCTGGCCTGCATTATCTC -3`; human claudin2 r: 5`- ACCTGCTACCGCCACTCTGT -3`

Membrane Protein Extraction Assay

Protein fractionation was carried out using Mem-Per Plus Kit (Thermo Fischer, Waltham, MA, USA) as described previously (8). Cells were harvested in growth media by scraping them from the bottom with a cell scraper. After centrifugation at 300 rpm for 5 minutes and washing three times, cells were permeabilized with a permeabilization buffer to release the cytosolic fraction. The cytosolic fraction was separated by centrifugation at 16.000 rpm for 15 minutes. The pellet containing the membrane-associated proteins was then re-suspended in a solubilization buffer. The suspension was centrifuged another time at 16.000 rpm for 15 minutes to remove particulate material. Then the cytosolic and membrane-associated supernatants were used for Western Blot analysis.

Co-Immunoprecipitation Experiments

Cells were seeded on 6-well plates. Monolayer cells at confluency were treated with different mediators and harvested after different incubation times in RIPA-buffer (ThermoFisher). Samples were steamed for 1min and centrifuged for 15min at 15.000g and 4°C. Total protein concentration was determined by measuring absorbance at 280nm.

The Co-IP experiments were done using the immunoprecipitation Starter Pack (GE Healthcare, Germany). The amount of 300-600 µg protein was used. After an initial preclearing step of one hour at 4°C (500µl of whole cell lysate with respectively 25µl protein G/A sepharose beads), antigens were coupled overnight at 4°C to 2.5 µg purified antibody rabbit anti-PI-3-kinase (Santa Cruz Biotechnology, Heidelberg, Germany). Protein-antibody complexes were precipitated with a mix of 25µl protein A and G sepharose beads for one hour at 4°C. The beads were washed three times with isotonic salt buffer (RIPA-buffer), once with wash-buffer (50 mM TRIS, pH 8) and suspended in 50µl Laemmli buffer. After denaturation for 5min at 95°C and a following centrifugation step, the supernatant was analyzed by western Blot analyses as described above. Detection was performed with mouse anti-Dsg2 diluted 1:1000 (Invitrogen, Carlsbad, CA, USA). Optical densities (OD) were quantified in each Western Blot using Image Lab ChemicDoc Touch (Bio-Rad Laboratories GmbH, Munich, Germany) for statistical evaluation. A ratio of the co-immununoprecipitated proteins was calculated to determine the potential changes detected under different conditions.

Proximity Ligation Assay

Proximity ligation assays (PLA) were carried out as recommended by the manufacturer ((Sigma-Aldrich, Munich, Germany): In brief, cells were seeded on coverslips and treated with TNFα for 24h when reached confluency. Two primary antibodies from different species were selected. Following antibodies were used: mouse anti-Dsg2 (Invitrogen, Carlsbad, CA, USA) at a dilution of 1:100, rabbit anti-PI-3-kinase 1:100 (Cell signaling, Leiden, Netherlands), mouse anti-Plakoglobin 1:100 (Progen, Heidelberg, Germany) and rabbit anti-Dsg2 1:100 (abcam, Cambrige, UK). After blocking of unspecific binding sites, slides were incubated with the mentioned primary antibodies. Next, a pair of oligonucleotide-labeled secondary antibodies (PLUS and MINUS Probes) which bind to the primary antibody were applied. When the PLA probes are in close proximity, connector oligos join the PLA probes and become ligated by addition of ligase at a dilution of 1:40. As a consequence, a closed circle DNA template is formed and acts as a primer for a DNA polymerase. Finally, labeled oligos hybridize to the complementary sequences within the amplicon, which are then visualized as discrete spots (PLA signals) by microscopy analysis. As negative controls, the same procedure was carried without application of primary antibodies as recommended by the manufacturer.

Quantification of Immunostaining

Quantification of immunostaining was carried out as described previously (9). In brief, 10µm line was placed orthogonal to the cell border with the cell border representing the middle of this line. The fluorescence pixel intensity was measured using ImageJ, which resulted in a graph with a maximum peak in the middle of the curve if the staining pattern was at the cell border. Loss of staining intensity at the cell borders resulted in a flattening of the curve. Indicating a redistribution of the proteins in the cytoplasm. For each sample at least ten randomly chosen junctions were measured by a blinded observer. For merge images the position and length of each line was then saved and also measured in the corresponding image field, thus resulting in 60 measurements at 30 distinct junctions per condition. After calculating the average and subtracting the gray value of the backgrounds three lane profiles per protein and condition were analyzed using a Two-way ANOWA with multiple comparisons.

Statistics

Statistical analysis was performed using Prism (GraphPad Software, La Jolla, CA, USA). Data are presented as means ± SE. Statistical significance was assumed for $p<0.05$. Paired Student's t-test was performed for two-sample group analysis after checking for a Gaussian distribution. Analysis of variance (ANOVA) followed by Tukey's multiple comparisons test and Bonferroni correction was used for multiple sample groups. The tests applied for each of the different experiments are indicated in the figure legends.

RESULTS

DSS-Induced Colitis and Increased Intestinal Permeability in Mice Were Attenuated by Application of Dsg-Linking Tandem Peptide (TP)

Previously, we demonstrated that Dsg-linking tandem peptide (TP) restored TNFα-induced loss of intestinal epithelial barrier

function in Caco2 cells *in vitro* by increasing Dsg2-mediated adhesion (10). To test the effects of TP on IEB in an *in vivo* model of intestinal inflammation, we induced acute colonic injury with 2.5% dextran sulfate sodium (DSS) in mice. C57Bl/6 mice (n=17) received 2.5% DSS (n=6) in autoclaved drinking water ad libitum, whereas control mice (n=5) received normal drinking water. One group of mice (DSS + TP, n=6) were injected intraperitoneally beginning at day 4 with 10 µM of TP in 100µl 0.9% sodium chloride whereas the other group (DSS) received 100µl 0.9% sodium chloride i.p daily.

Following DSS application, the disease activity index (DAI) and the stool index were increased to 2.0 ± 0.75 and 2.33 ± 0.89 (**Figures 1A, B**). Both were significantly reduced at day 6 (endpoint of the experiment) in animals treated with TP. The bodyweight was reduced in the DSS group compared to controls and following treatment with TP (**Figure 1C**). In the control group, the colon length was 75.4 ± 3.54mm which was reduced to 48.17 ± 2.72mm in the DSS group. Reduction of colon length was attenuated by TP application (60.0 ± 3.55mm; **Figure 1D**). Intestinal permeability as revealed by measurements of 4 kDa FITC–dextran flux across the IEB was increased in DSS animals compared to control animals whereas treatment with TP attenuated inflammation-induced increase of intestinal permeability (**Figure 1E**). Histological analyses of H&E-stained colon sections showed a severe inflammation pattern after treatment with DSS (**Figure 2Ab**) which was attenuated by injection of TP (**Figure 2Ac**). TP application alone did not have an obvious effect on crypt architecture in colon sections (data not shown). Histological injury score also revealed an acute inflammation following DSS administration (control 2.00 ± 0.01 *vs.* DSS 7.13 ± 0.48, $p<0.0001$). Again, TP reduced inflammation (histological score DSS+TP 5.63 ± 0.52, $p<0.05$ compared to DSS) (data not shown).

To verify the close correlation between the integrity of Dsg2 and Claudin2 that we had previously observed *in vitro* (10), immunostaining was carried out for both proteins from the gut specimens of the different experimental groups of the *in vivo* experiments. In the control group, Dsg2 in colon sections showed a regular staining pattern along the cell borders of enterocytes whereas Claudin2 was hardly detectable (**Figure 2Ba–c**). In DSS-colitis, Dsg2 was reduced in intestinal epithelium whereas Claudin2 was present along virtually all enterocytes (**Figure 2Bd–f**). Both the reduction of Dsg2 and the strong increase of Claudin2 were attenuated when TP was applied to animals with DSS-colitis (**Figure 2Bg–i**). In line with this, in Western blot analyses DSS-induced reduction of Dsg2 compared to control conditions ($p<0.05$, n=6) was restored after TP treatment ($p<0.01$, n=6) (**Figures 2C, D**). Moreover, DSS-induced increase of Claudin2 compared to controls ($p<0.05$, n=6) was decreased after TP application ($p<0.01$, n=6) (**Figure 2E**). In summary, these data confirmed a critical role of Dsg2 for intestinal barrier stabilization and accordingly TP is effective to stabilize intestinal barrier function *in vivo*. Additionally, the close correlation between the integrity of Dsg2 and Claudin2 strengthened our hypothesis of a causal interaction between both proteins in the regulation of intestinal permeability.

TNFα-Induced Loss of Dsg2-Mediated Adhesion Augmented Claudin2 Expression in Caco2 Monolayers

Next, we used our *in vitro* system of differentiated Caco2 cells and performed immunostaining following TNFα application to mimic inflammation. In Caco2 cells, TNFα resulted in reduced Dsg2 at the cell borders compared to untreated controls (**Figure 3A**). TNFα-induced loss of Dsg2 was completely blocked when TP was applied while TP application alone did not have an effect on Dsg2 staining (**Figure 3Ac, d**). Claudin2 staining was augmented when TNFα was applied to epithelial monolayers (**Figure 3Ae, f**), which was attenuated following TP application (**Figure 3Ag, h**). Western blot analyses confirmed a strong increase of Claudin2 expression in Caco2 cells following application of TNFα, which was blocked even below control levels when TNFα and TP were applied together (**Figure 3Ag, h, B, C**). Dsg2 expression did not change significantly in Western blot analysis under the different conditions (data not shown). However, in line with the observed loss of Dsg2 at the cell borders, dispase-based enterocyte dissociation assays demonstrated that TNFα led to a 2.5-fold increased fragmentation of epithelial monolayers (**Figure 3D**). Application of TP blocked TNFα-induced cell dissociation which confirmed the significant role of Dsg2 in this context (**Figure 3D**) (n=4, $p<0.05$). Measurements of 4kDa FITC dextran flux across CaCo2 monolayers showed augmented epithelial permeability following incubation with TNFα (**Figure 3E**) (n=16, $p<0.01$). This was attenuated when TP was applied together with TNFα (n=16, $p<0.05$). Taken together, the *in vitro* experiments in CaCo2 monolayers confirmed that TNFα-induced loss of Dsg2 at the cell borders led to increased epithelial permeability, cell dissociation and Claudin2 expression. All of these effects were attenuated when Dsg-stabilising TP was applied, suggesting a direct link between Dsg2 integrity and Claudin2 expression.

Loss of Dsg2 Integrity Increased Claudin2 Expression

To directly interfere with Dsg2-mediated adhesion, we applied a monoclonal antibody directed against the extracellular second and third extracellular repeat domains of Dsg2 (anti-Dsg2^{EC}) on Caco2 monolayers as described previously (6, 14). This resulted in a reduction of Dsg2 at the cell borders after 6h and 12h of incubation with anti-Dsg2^{EC} in immunostaining (**Figure 4Aa–c**). The loss of Dsg2 at the cell borders was paralleled with a strong increase of Claudin2 which was sparsely seen under control conditions and regularly present at the cell borders after 6h and after 12h of incubation with anti-Dsg2^{EC} (**Figure 4Ad–f**). In contrast, the staining pattern of barrier-sealing TJ protein Claudin1 was modestly changed when compared to Claudin2 staining pattern after 6h and 12h of incubation with anti-Dsg2 ^{EC} (**Figure 4Aj–l**). In line with this, application of anti-Dsg2^{EC} led to decreased Transepithelial Electrical Resistance (TER) after 6h and 12h to 0.87 ± 0.04-fold and 0.88 ± 0.03-fold of control (**Figure 4B**) whereas measurements of 4 kDa FITC dextran flux remained unaltered under these conditions (**Figure 5B**).

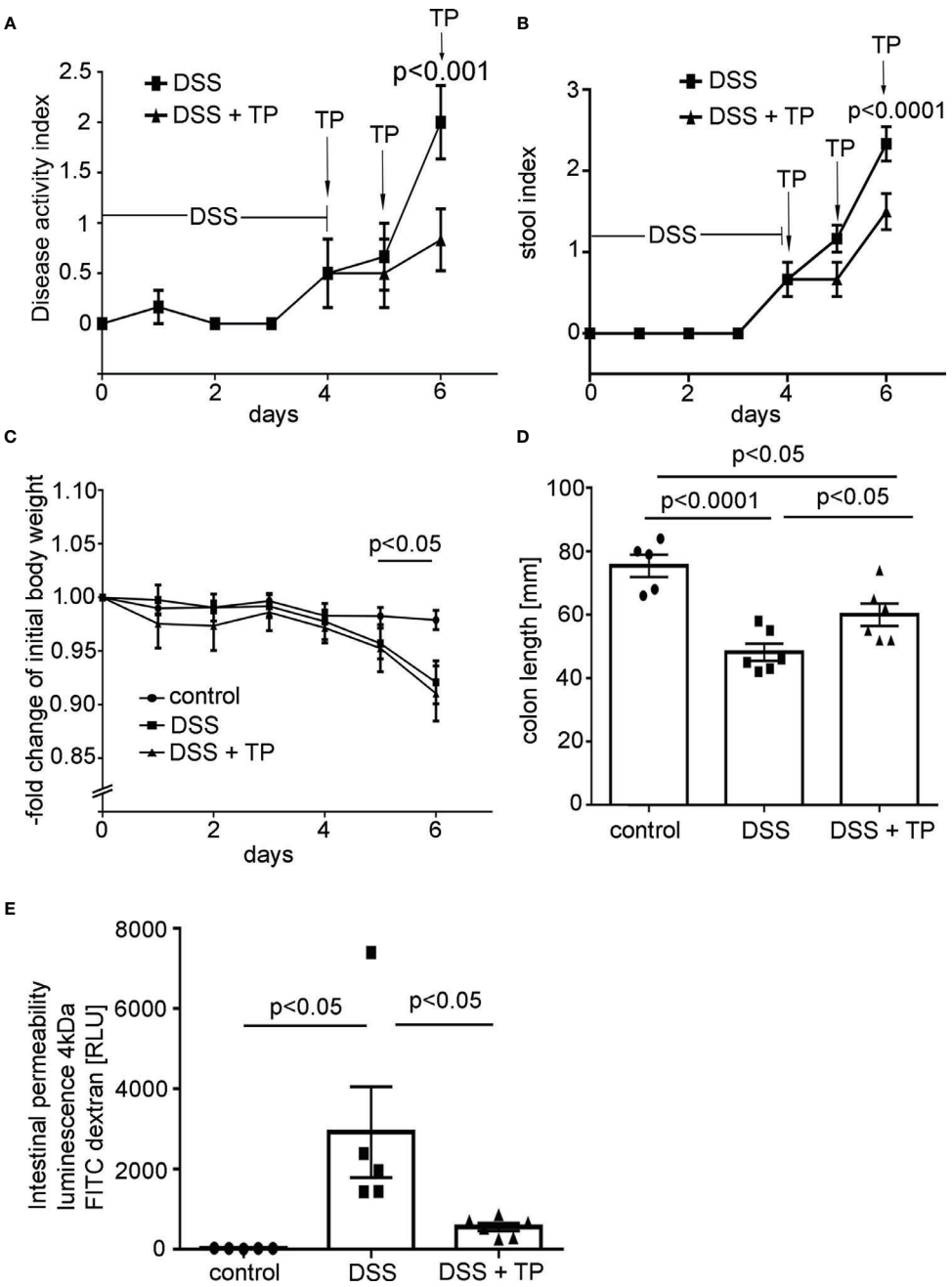

FIGURE 1 | DSS- induced colitis in mice was attenuated by application of Tandem peptide (TP). **(A)** Disease activity index (DAI) is shown for C57/Bl6 mice receiving 2.5% DSS alone or in combination with TP at 10 μM i.p. (n= 6) for each group. DAI was significantly reduced in mice treated with TP ($p<0.0001$; unpaired t-test for each time point). **(B)** The stool index was increased in DSS colitis and significantly reduced ($p<0.0001$) at day 6 in mice treated with TP (unpaired t-test for each time point). **(C)** Body weight of control animals was unchanged in the course of experiments whereas in mice with DSS colitis body weight was significantly reduced ($p<0.05$; unpaired t-test for each time point). **(D)** DSS treatment resulted in a significantly reduced colon length ($p<0.0001$, n=8) compared to controls. Treatment with TP attenuated colon length reduction compared to DSS animals ($p<0.05$, n=8) (ordinary 1-way ANOVA). **(E)** Measurements of 4 kDa FITC dextran flux across the IEB show increased levels of luminescence in the blood compared to controls (n=5, $p<0.05$). Treatment of DSS animals with TP attenuated increased intestinal permeability compared to DSS induced colitis (n=5, $p<0.05$) (ordinary one-way ANOVA).

In cell compartment separation assays application of anti-$Dsg2^{EC}$ or TNFα reduced Dsg2 in the membrane-bound fraction compared to controls (**Figure 4C**). This was paralleled with an increase of Claudin2 in the membrane-bound fraction both after application of anti-$Dsg2^{EC}$ and after incubation with TNFα. In line with these observations, application of anti-$Dsg2^{EC}$ and TNFα augmented Claudin2 mRNA-levels in Caco2 $Dsg2^{WT}$ (**Figure 4D**) whereas Dsg2 mRNA levels were not affected (**Figure 4E**).

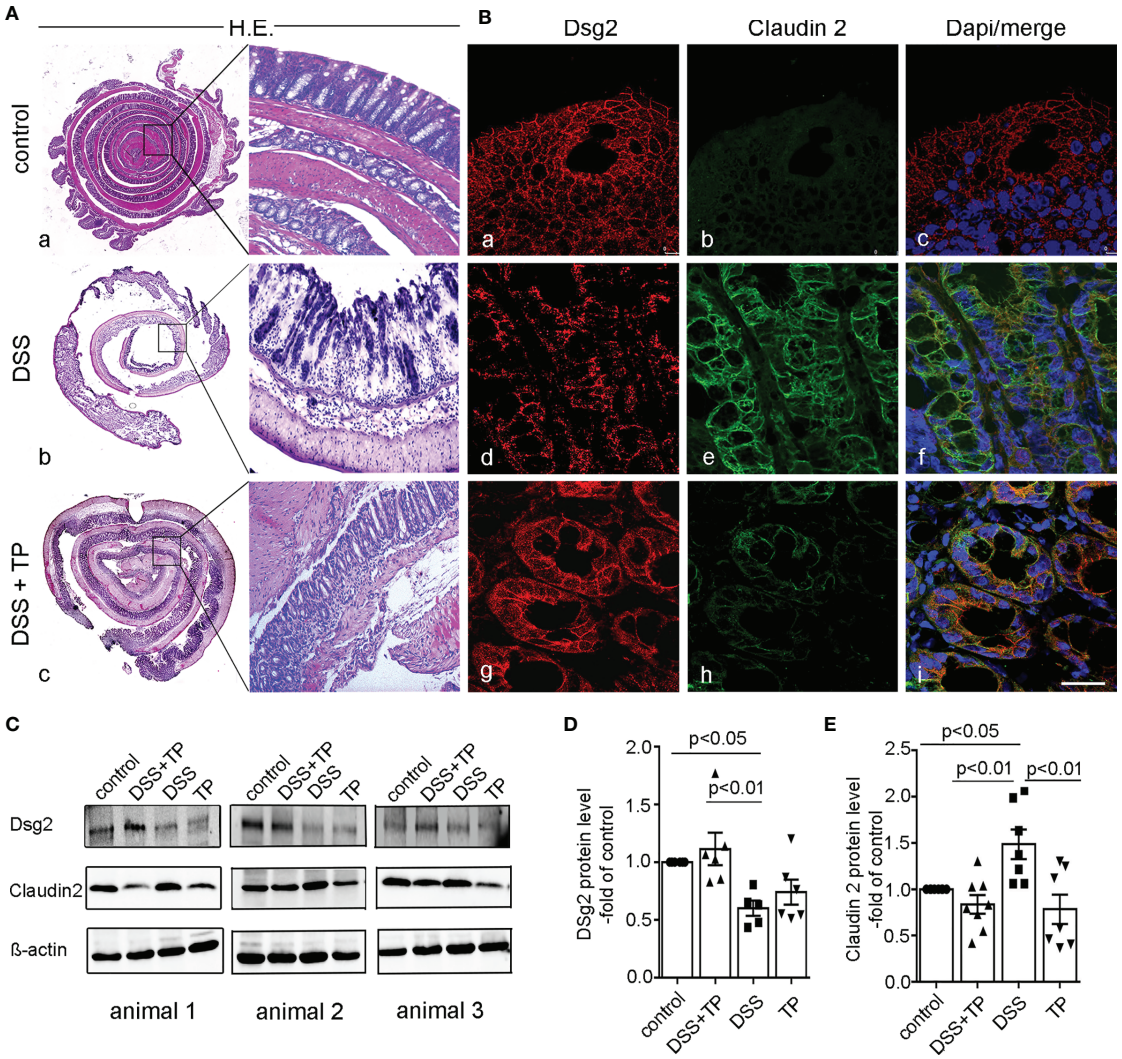

FIGURE 2 | TP affected DSS-induced redistribution of Dsg2 and Cld2 at the cell border *in vivo*. **(A)** Representative H&E staining of mouse colon are shown (left overview; right magnification). Controls (a) show a normal morphology of the gut whereas DSS (2.5% DSS) animals (b) show signs of severe inflammation with mucosal damage. Treatment of animals with 10 µM TP (c; DSS+TP) attenuated inflammation-induced changes in the colon. Images shown are representatives for n=6 in each group. **(B)** Immunostaining for Dsg2 (a, d, g), Claudin2 (b, e, h) or merged images with staining of cell nuclei using DAPI (c, f, i) are shown for the same conditions. The loss of Dsg2 in DSS animals (d) compared to controls (a) is attenuated by TP treatment (g). This is paralleled by augmented Claudin2 staining (e) in DSS colitis compared to controls (b) whereas TP blocked inflammation-induced increase of Claudin2 (h). Images shown are representatives of n=6 in each group. Scale bar is 25 µm. **(C)** Western Blots from colon lysates of control animals, animals with DSS colitis treated with TP (DSS+TP), DSS colitis alone and with TP alone are shown for Dsg2 and Claudin2 and β-actin. A set of 3 different animals is shown. **(D)** Quantitative analyses of the optical densities for Dsg2 Western blot bands normalized to β-actin showed reduced Dsg2 compared to DSS-colitis. This reduction was not observed in DSS+TP-treated animals ($p<0.05$ compared to the control group, n=6; $p<0.01$ compared to DSS+TP-treated mice; TP showed no significant change compared to all other groups; n=6 for each group, ordinary 1-way ANOVA). **(E)** Quantitative analyses of the optical densities for Claudin2 Western Blot bands normalized to β-actin showed significantly increase of Claudin2 in DSS mice compared to control mice ($p<0.05$) which was blocked by TP ($p<0.01$) (n=6 for each group; ordinary one-way ANOVA).

To further determine a causal relationship between loss of Dsg2 and increased Claudin2 we used our Dsg2-deficient Caco2 cell line (Caco2 Dsg2$^{-/-}$) (8). Measurements of TER values across differentiated monolayers revealed a significantly higher basal resistance in Caco2^{WT} of 238 ± 20 Ω*cm² compared to Caco2 Dsg2$^{-/-}$ with 110 ± 5 Ω*cm² when cultured under the exact same conditions (**Figure 5A**). However, Permeability coefficient-values as revealed by measurements of 4 kDa FITC dextran flux across epithelial monolayers showed that basal permeability was not different when Caco2^{WT} and Caco2 Dsg2$^{-/-}$ were compared (**Figure 5B**). Incubation of monolayers with TNFα increased permeability in both cell lines (**Figure 5B**). In immunostaining of differentiated Caco2 Dsg2^{WT} monolayers Dsg2 was regularly distributed at the cell borders whereas Claudin2 was sparsely found (**Figure 5Da–d**). In Caco2 Dsg2$^{-/-}$ no Dsg2 (**Figure 5Dm**) was detected in immunostaining whereas Claudin2 (**Figure 5Do**)

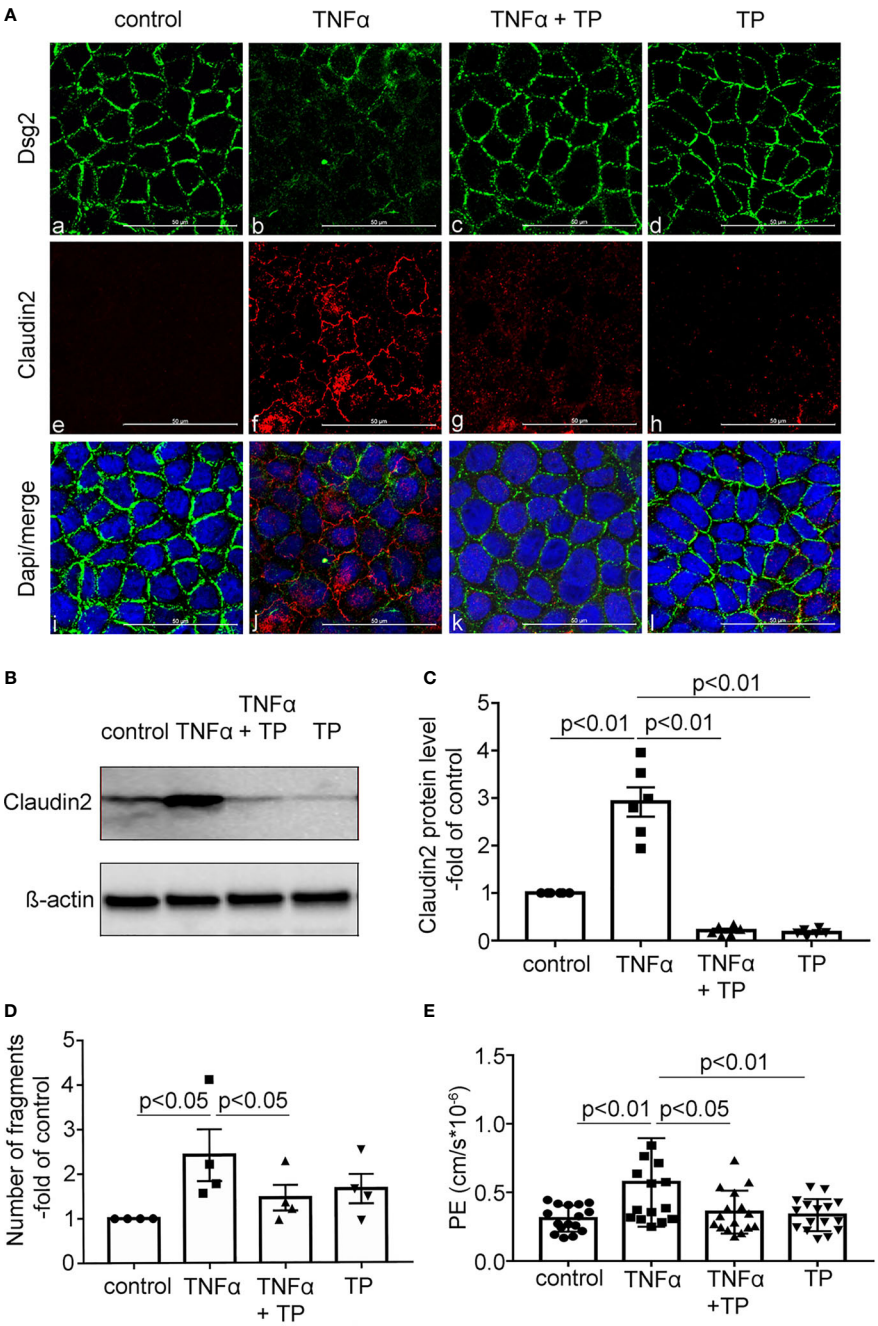

FIGURE 3 | TP attenuated TNFα-induced redistribution of Dsg2 and Cld2 *in vitro*. **(A)** Representative immunofluorescence staining of Caco2 cells after 24h treatment with either TNFα (100 ng/ml) or TP (20 μM) or both (TNFα+TP) are shown for Dsg2 (green; a-d), Claudin2 (red; e-h) or merged images with DAPI staining (blue; i-l) to visualize cell nuclei. Compared to controls (a,e,i) application of TNFα resulted in reduced Dsg2 (b) and increased Claudin2 (f) at the cell borders. TNFα-induced changes were blunted by application of TP (c,g,k). TP alone had no effect on Dsg2 and Claudin2 (d,h,l) compared to controls. Images shown are representative for n=7, scale bar is 50 μm. **(B)** Representative Western Blot from Caco2 lysates under the conditions outlined in A for Claudin 2 is shown; ß-actin is shown as loading control. **(C)** Quantitative analyses of the optical densities for Claudin2 Western Blot bands normalized to β-actin showed a significant increase of Claudin2 protein levels compared to controls which is attenuated following incubation of cells with TNFα+TP. TP alone has no effect on Claudin2 expression. N= 4 for controls and n=6 for all other experimental conditions; ordinary 1-way ANOVA **(D)** Results from enterocyte dissociation assays are shown for the same conditions outlined in **(A)** Incubation of Caco2 cells with TNFα results in increased fragmentation of monolayers whereas TNFα+TP blocked this effect. Effects of TP alone on Caco2 monolayers were absent ($p<0.05$, n=4, ordinary 1-way ANOVA). **(E)** Permeability coefficient (P_E) measured as 4 kDa FITC dextran flux across confluent Caco2 monolayers are shown. TNFα-induced increase of epithelial permeability compared to controls ($p<0.01$) was blocked by application of TP ($p<0.05$, compared to TNFα); n=16 for each group; ordinary 1-way ANOVA.

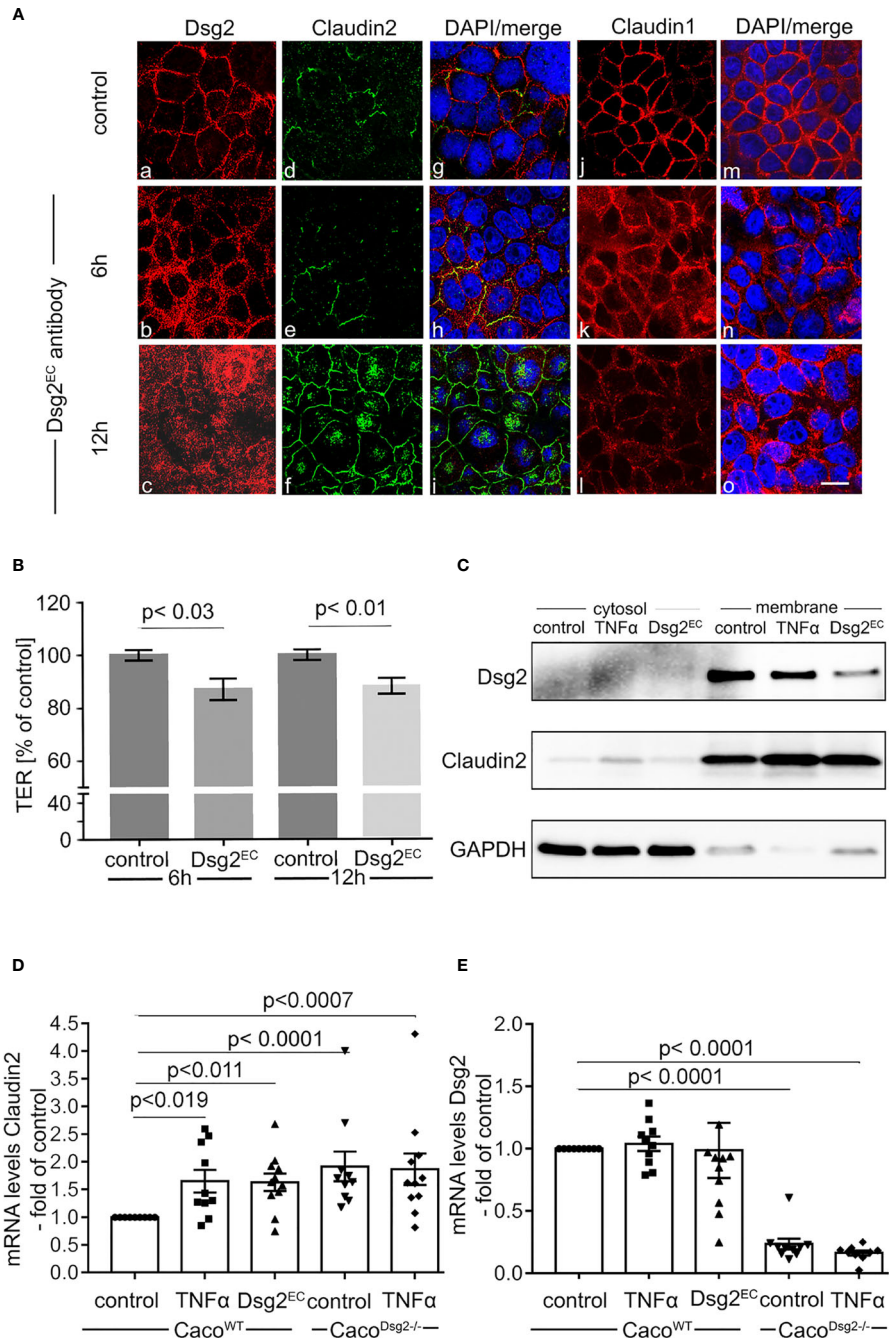

FIGURE 4 | Antibody-induced loss of Dsg2 increased Claudin2 at the cell borders.**(A)** Immunostaining of Caco2 monolayers for Dsg2 (a-c) Claudin2 (d-f), Claudin1 (j-l) following incubation with a Dsg2 antibody directed against parts of the extracellular domain of Dsg2 ($Dsg2^{EC;}$ 1:50) for 6h (b, e, h, k, n) and 12h (c, f, i, o) are shown. Application of $Dsg2^{EC}$ results in loss of Dsg2 at the cell borders (b,c) compared to controls (a). This was paralleled by increased Claudin2 (e,f) whereas changes of Claudin1 staining following $Dsg2^{EC}$ application are modest (k,l). Images are representative for n=8; scale bar is 20 µm. **(B)** Application of $Dsg2^{EC}$ antibody decreases Transepithelial Electrical Resistance (TER) after 6h ($p<0.03$, n=14, ordinary 1-way ANOVA) and 12h ($p<0.01$, n=14, ordinary 1-way ANOVA) and 12h compared to untreated CaCo2 cells .**(C)** Representative Western Blot after cell compartment separation assay is shown for Dsg2 and Claudin2 after incubation of Caco2 with TNFα (24h) or $Dsg2^{EC}$ (12h). GAPDH served to document the separation in cytosolic and membrane fraction. Both TNFα and $Dsg2^{EC}$ decrease Dsg2 and augment Claudin2 the membrane-bound fraction; n=5. **(D)** Quantitative (q)RT-PCR showed that Claudin2 expression was elevated in Dsg2-deficient Caco2 cells ($Dsg2^{-/-}$) under basal conditions compared to $CaCo2^{WT}$ ($p<0.0001$, n=10, ordinary 1-way ANOVA). Application of TNFα (24h) increased Claudin2 mRNA levels in $Caco2^{WT}$ compared to untreated cells ($p<0.019$, n=10, ordinary 1-way ANOVA) but not in $CaCo2^{Dsg2-/-}$. **(E)** qRT-PCR shows that mRNA levels of Dsg2 are not altered following application of $Dsg2^{EC}$ antibody and no Dsg2 was detectable in Caco2 $Dsg2^{-/-}$ (n=10, ordinary 1-way ANOVA).

was found to be regularly present at the cell borders under basal conditions. Application of TNFα resulted in reduced Dsg2 (**Figure 5Dg**) and significantly augmented Claudin2 staining at the cell borders in Caco2 $Dsg2^{WT}$ (**Figure 5Di**). In Caco2 $Dsg2^{-/-}$, Claudin2 was located at the cell borders under both conditions (untreated and TNFα) (**Figure 5Do, u**). Claudin1 was regularly distributed at the cell borders of Caco2 $Dsg2^{WT}$ and Caco2 $Dsg2^{-/-}$ under basal conditions (**Figure 5Do, u**) which was reduced by application of TNFα (**Figure 5Dk, w**).

In Western blot analyses Dsg2 was equally expressed under basal conditions and following application of TNFα in $Caco2^{WT}$ (**Figure 5C**) whereas no Dsg2 was found in Caco2 $Dsg2^{-/-}$ (**Figure 5C**). In WT cells Claudin2 was augmented following application of TNFα (**Figure 5C**). In Caco2 $Dsg2^{-/-}$ basal expression of Claudin2 was increased compared to $Caco2^{WT}$ and was further augmented after incubation with TNFα (**Figure 5C**).

In line with this, qRT-PCR showed similar results indicating changes of Claudin2 at the level of protein expression rather than on changes in protein turnover (**Figure 4D**).

Loss of Dsg2 Augmented Basal Activation of PI-3/AKT-Signaling

Previously it was reported that inflammation-induced Claudin2 upregulation in intestinal epithelial cells is dependent on PI-3-kinase/AKT signaling (29–31). Based on this, we first verified that inhibition of PI-3-kinase using LY294002 blocked TNFα-induced upregulation of Claudin2 (**Figure 6**). In line with previous data, LY294002 attenuated the TNFα-induced phosphorylation of AKT at Ser 473 in Caco2 $Dsg2^{WT}$ and upregulation of Claudin2 (**Figure 6**). In Caco2 $Dsg2^{-/-}$ where basal Claudin2 expression was increased, augmented basal phosphorylation of AKT^{Ser473} was observed (**Figures 6A–C**). Application of TNFα strongly increased phosphorylation of AKT^{Ser473} which was diminished after application by LY294002 (**Figures 6A, B**). Phosphorylation of AKT^{Thr308} was unaffected under all experimental conditions (**Figure 6A**).

Taken together these data confirmed a critical role of PI-3/AKT signaling in the regulation of Claudin2. Furthermore the increased basal phosphorylation of AKT^{Ser473} followed by an exaggerated phosphorylation pattern after TNFα incubation in Dsg2-deficient cells pointed to a potential role for Dsg2 in modulating PI-3-kinase. To substantiate this conclusion we tested whether application of TP would affect phosphorylation of AKT^{Ser473}. As outlined above incubation of Caco2 monolayers resulted in augmented phosphorylation of AKT^{Ser473} to 1.6 ± 0.1-fold of controls. This effect was blocked when Caco2 cells were incubated with TNFα together with TP (1.1 ± 0.1-fold of controls), (**Figures 6D, E**).

Dsg2 Sequesters PI-3-Kinase Under Basal Conditions

To further resolve the potential contribution of Dsg2 to regulate both Claudin2 expression and PI-3-kinase signaling we next performed co-immunostaining of Dsg2 and PI-3-kinase under basal conditions and following stimulation with TNFα in $Caco2^{WT}$ cells (**Figure 7A**). Under basal conditions both Dsg2 and PI-3-kinase p110ß were found at the cell borders where they co-localized (**Figure 7Aa–c**). Incubation with TNFα resulted in loss of Dsg2 at the cell borders and redistribution of PI-3-kinase into the cytoplasm (**Figure 7Ad–f**). Accordingly, the co-localization of Dsg2 and PI-3-kinase was abrogated following application of TNFα (**Figure 7Af**). This visual impression was confirmed when quantifications of the immunostaining were carried out. Under basal conditions the mean peak of the staining intensity was found at the cell borders for both Dsg2 and PI-3-kinase. Application of TNFα resulted in a flattening of the curves for Dsg2 and PI-kinase indicating a redistribution of both proteins from the cell borders in the cytoplasm (**Figures 7B, C**).

Since this suggested a direct interaction of Dsg2 and PI-3-kinase we performed proximity ligation assays and co-immunoprecipitation studies. Proximity ligation assays revealed a direct interaction of Dsg2 and PI-3-kinase under basal conditions as revealed by the fluorescent spots throughout the cytoplasm (**Figure 8Aa**) and at the cell periphery (**Figure 8Ab**; inset). This interaction was reduced following incubation of $Caco2^{WT}$ cells with TNFα (**Figure 8Ac, d**). To ensure the staining specificity, the same experiments were carried out using Caco2 $Dsg2^{-/-}$ cells, where no spots i.e. no interaction between Dsg2 and PI-3-kinase was detectable both under basal conditions (**Figure 8Ae, f**) and after incubation with TNFα (**Figure 8Ag,h**). PLAs were also performed in $Caco2^{WT}$ with Dsg2 and the desmosomal plaque protein plakoglobin which is a known interaction partner of Dsg2 (32) (**Figure 8i–l**). This confirmed an interaction between Dsg2 and Plakogblobin (**Figure 8i**, inset in j) under basal conditions which was reduced following incubation of Caco2 cells with TNFα. Negative controls to exclude unspecific staining patterns induced by the duolink fluorescent detection reagent (**Figure 8Am–p**) were performed without application of primary antibodies. This did not result in the visualization of any spots.

Co-immunoprecipitation (IP) using cell lysates from Caco2 $Dsg2^{WT}$ confirmed the interaction of Dsg2 and PI-3-kinase under basal conditions (**Figures 8B–D**) whereas application of TNFα led to decreased interaction of these two proteins. In quantifications of the IPs TNFα reduced the interaction between TNFα and PI-3-kinase to 0.34 ± 0.06-fold of controls whereas incubation of TP with TNFα restored the interaction to control levels (0.99 ± 0.05-fold of controls) and TP alone had no effect (0.92 ± 0.11-fold of control). LY294002 blocked even augmented the interaction between Dsg2 and PI-3-kinase when applied alone (1.6 ± 0.27-fold of control) and when applied together with TNFα (1.5 ± 0.16-fold of control) (**Figure 8D**). Quantification of PI-3-kinase protein levels in whole cell lysates of Caco2 Dsg^{WT} showed no significant differences under the different experimental conditions (**Figures 8C, E**).

DISCUSSION

The present study extends our previous investigations on the role of desmosomal adhesion and signaling in the regulation of IEB integrity. Here, we show that Dsg2 at the cell borders is required to inhibit upregulation of pore-forming tight junction protein

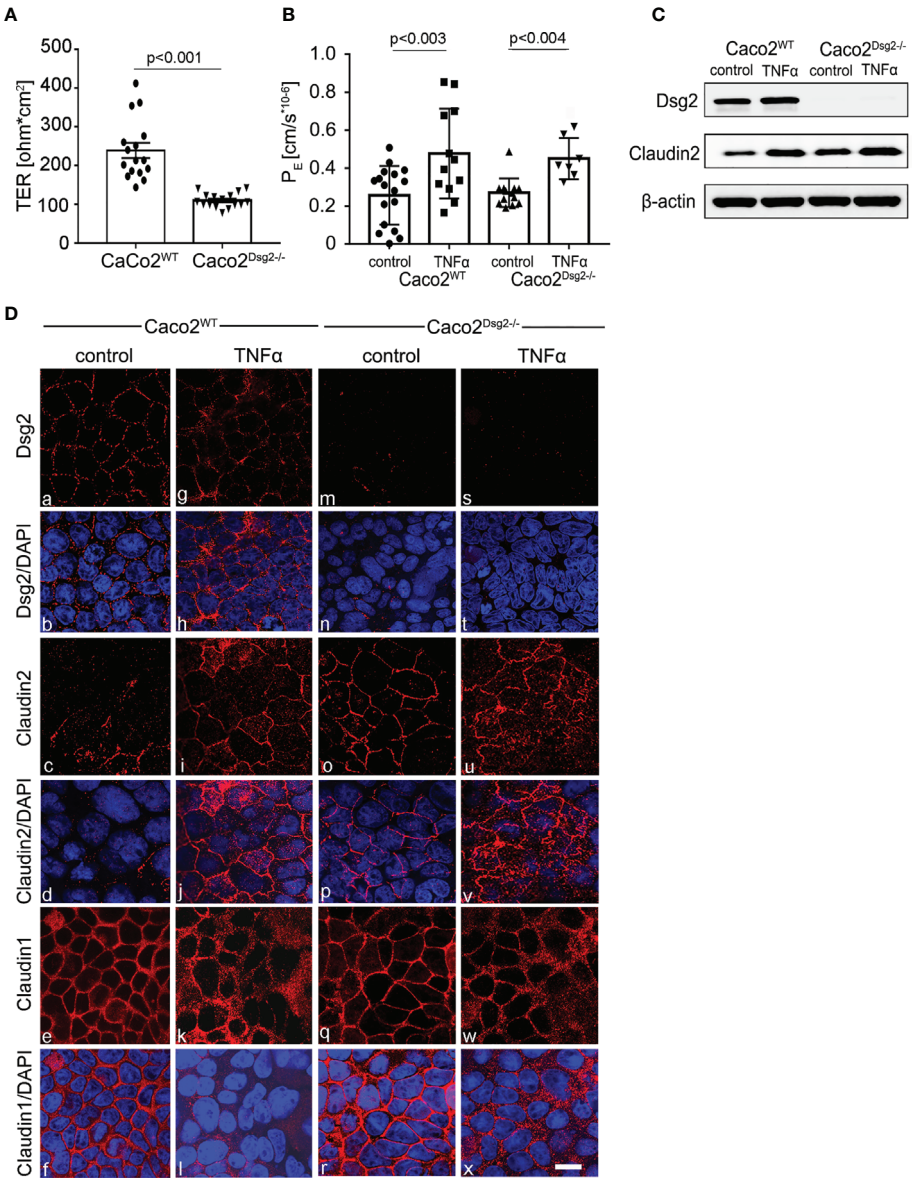

FIGURE 5 | Claudin2 was increased following Dsg2 knockout in Caco2 cells. **(A)** Measurements of Transepithelial Electrical Resistance (TER) of $CaCo2^{WT}$ compared to CaCo2 $Dsg2^{-/-}$ monolayers under baseline conditions demonstrate reduced baseline TER in Dsg2-deficient cells ($p<0.001$, n=13, ordinary 1-way ANOVA). **(B)** Permeability coefficient (P_E) of 4kDa FITC Dextran on $Caco2^{WT}$ cells ($p<0.003$ compared to control, n=12, ordinary 1-way ANOVA) and in Caco2 $Dsg2^{-/-}$ cells ($p<0.004$ compared to Caco2 $Dsg2^{-/-}$ control, n=12, ordinary 1-way ANOVA) show increased permeability after incubation with TNFα whereas no differences under baseline conditions are obvious (n=12, ordinary 1way ANOVA). **(C)** Western Blot experiments of $CaCo2^{WT}$ and CaCo2 $Dsg2^{-/-}$ monolayers is shown for Dsg2, Claudin2 and for ß-actin to verify equal loading of the Western Blots. This confirms loss of Dsg2 in CaCo2 $Dsg2^{-/-}$ cells and augmented basal expression of Claudin2 compared to $CaCo2^{WT}$; the experiment shown is representative for n=8. **(D)** Immunostaining of $Caco2^{WT}$ and Caco2 $Dsg2^{-/-}$ for Dsg2 (a, g, m, s), Claudin2 (c, i, o, u) and Claudin1 (e, k, q, w) are shown under baseline (control) conditions (a-f, m-r) and following application of TNFα (g-l, s-x) for 24h. Dsg2 is found at the cells borders in $Caco2^{WT}$ under control conditions (a). TNFα leads to a loss of Dsg2 at the cell borders (g) and in Caco2 $Dsg2^{-/-}$ no Dsg2 was detectable (m, s). Claudin2 is hardly detectable in $Caco^{WT}$ under control conditions (c) but can be found at the cell membrane after TNFα incubation (i). In Caco2 $Dsg2^{-/-}$ cells Claudin2 staining pattern shows a distribution at the cell borders in both control and after TNFα treatment (o, u). Claudin1 is found at the membrane in both Caco2WT and Caco2Dsg2-/- cells under control conditions (e, q), which is reduced following application of TNFα (k, w) (n=4; scale bar is 20 µm).

Claudin2. Loss of Dsg2-mediated adhesion induced by antibodies, TNFα or knock-out of Dsg2 induces the activation of PI-3-kinase/AKT signaling which results in the upregulation of Claudin2. This can be explained by the observation that Dsg2 sequesters PI-3-kinase under basal conditions keeping PI-3-kinase/AKT signaling axis in an inactive state. This shows a new mechanism how desmosomal integrity is involved in the regulation of tight junctions in intestinal epithelium.

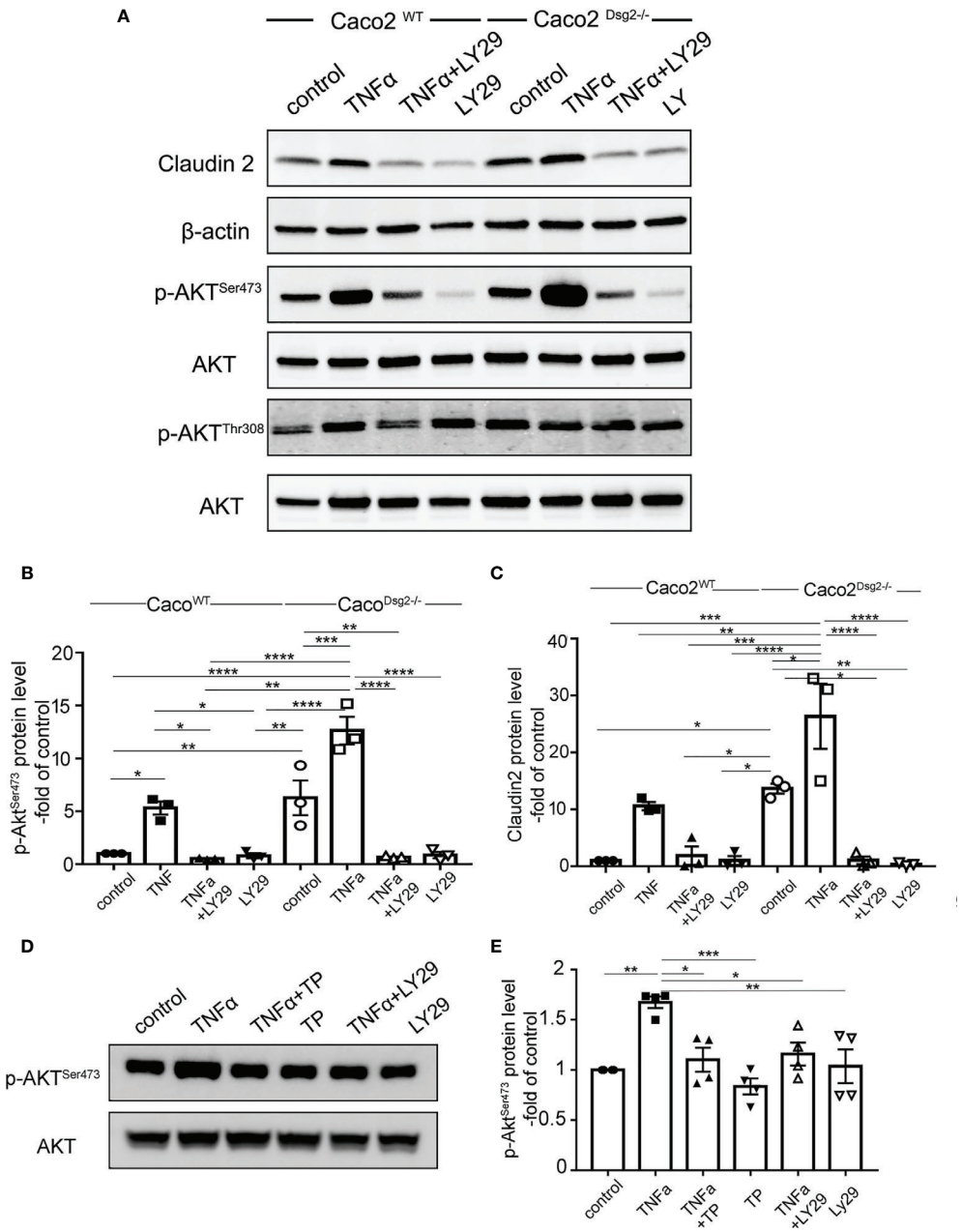

FIGURE 6 | PI-3K/Akt pathway is involved in the regulation of Claudin2. **(A)** Western Blot of Caco2^{WT} and Caco2 Dsg$^{-/-}$ are shown for Claudin2, p-AKT^{Ser473},p-AKT^{Thr308}, total AKT and ß-actin as loading control under the different experimental conditions. Experiment shown is representative for n=3. **(B)** Quantitative analyses of the optical densities for p-AKTSer473/total AKT; ordinary 1-way ANOVA are presented. **(C)** Quantitative analyses of the optical densities for Claudin2 Western Blot bands normalized to β-actin are shown; ordinary 1-way ANOVA. **(D)** Western Blot of Caco2^{WT} for p-AKT^{Ser473} and total AKT for the different experimental conditions are shown. Experiment shown is representative for n=4. **(E)** Quantitative analyses of the optical densities for p-AKT^{Ser473}/total AKT; ordinary 1-way ANOVA. Asterisks mark significant difference *p < 0.01, **p < 0.001, ***p < 0.0001, ****p < 0.00001). Comparisons are indicated by the lines above the columns.

Stabilization of Dsg2 by TP Reduced Intestinal Permeability in Acute DSS Colitis *In Vivo*

The stability of intestinal barrier function has been increasingly reported to be dependent on desmosomal integrity in particular by Dsg2-mediated adhesion and signaling (6, 7, 10, 13). Based on this, it has also been proposed that strengthening Dsg2-mediated adhesion between enterocytes might be an attractive target for intestinal barrier stabilization under conditions of inflammation (3). This notion is now substantiated by our present data using the acute DSS-colitis

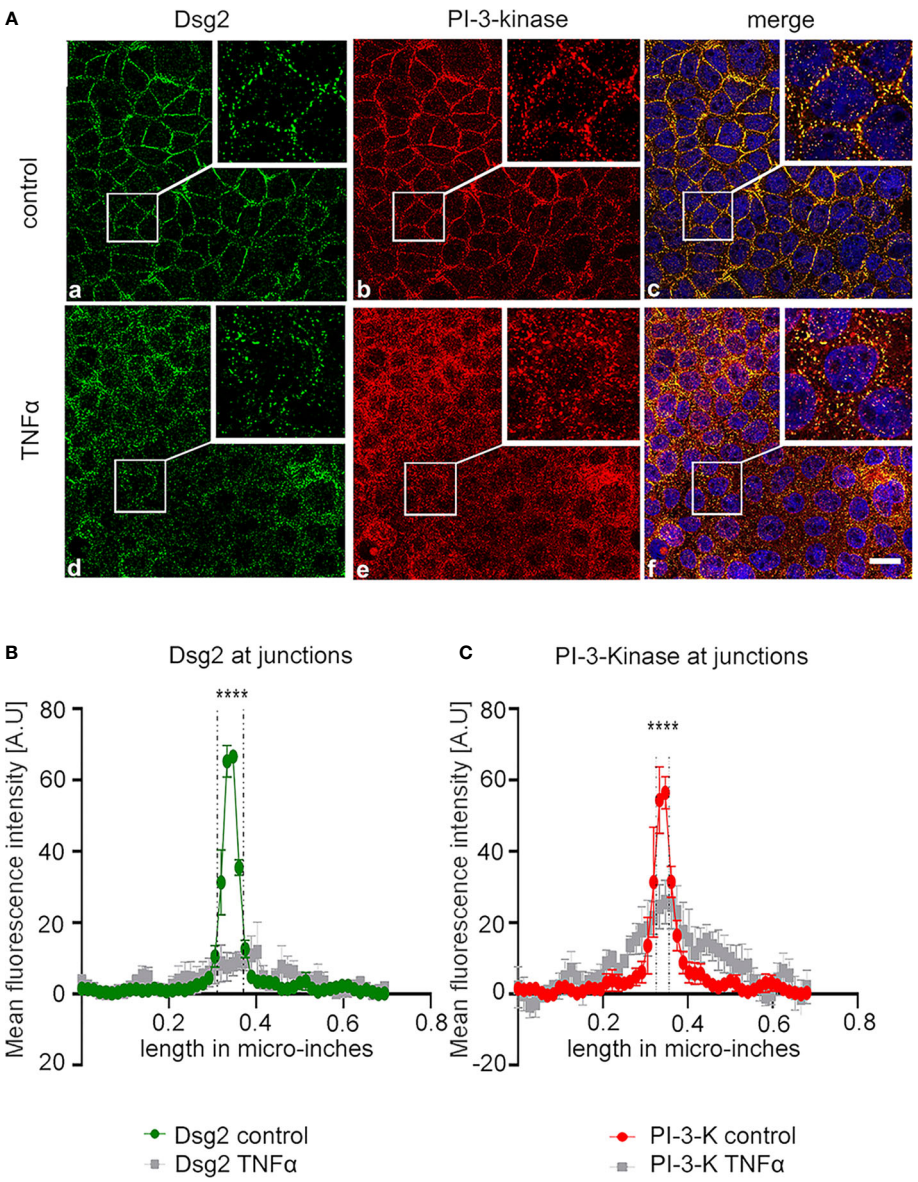

FIGURE 7 | Dsg2 sequesters PI3-kinase under basal conditions. **(A)** Immunostaining for Dsg2 (a,d)=and PI-3-kinase Caco2 cells under control conditions (a-c) and following treatment with TNFα for 24h at 100 ng/ml (d-f) are shown. Merge images include staining with DAPI to visualize cell nuclei (c,f). Images shown are representative for n=4 experiments, scale bar is 2 βμm. **(B, C)** Quantification of all experiments for the conditions of the immunostaining images shown in A are presented; dashed lines in the graphs indicate the area of cell junctions; Asteriks mark significant difference ****p < 0.00001; two way ANOVA.

model in which we clearly demonstrate a barrier-protective effect following application of TP *in vivo*. This was accompanied by an improved disease activity score *in vivo* and by reduced overall inflammation as revealed by H.E.-staining. The observation that TP effectively strengthens IEB function and thereby reduces intestinal inflammation supports the overall clinical importance of intestinal barrier integrity and the impact of Dsg2-mediated adhesion as an important player in this context (2, 3, 33).

TP was originally designed as 2 cyclized peptides connected through a flexible amino hexan linker to bind to Dsg1 and was later confirmed to bind Dsg2 as well because of its high sequence homology (10, 34). Since it has been shown that E-cadherin binds Dsg2 on the E-cadherin cis binding interface which appears to be important for desmosome assembly (35) it is possible that TP also binds E-cadherin and thereby strengthens cellular adhesion. On the other hand previous data demonstrated that TP did not modulate homophilic binding of classical cadherins such as E-cadherin or N-cadherin (34, 36). The fact that loss of Dsg2 was attenuated using TP both in immunostaining and in Western blot analyses suggests that crosslinking of neighboring Dsg2 proteins may already be sufficient to prevent loss of intercellular adhesion and the induction of barrier-compromising

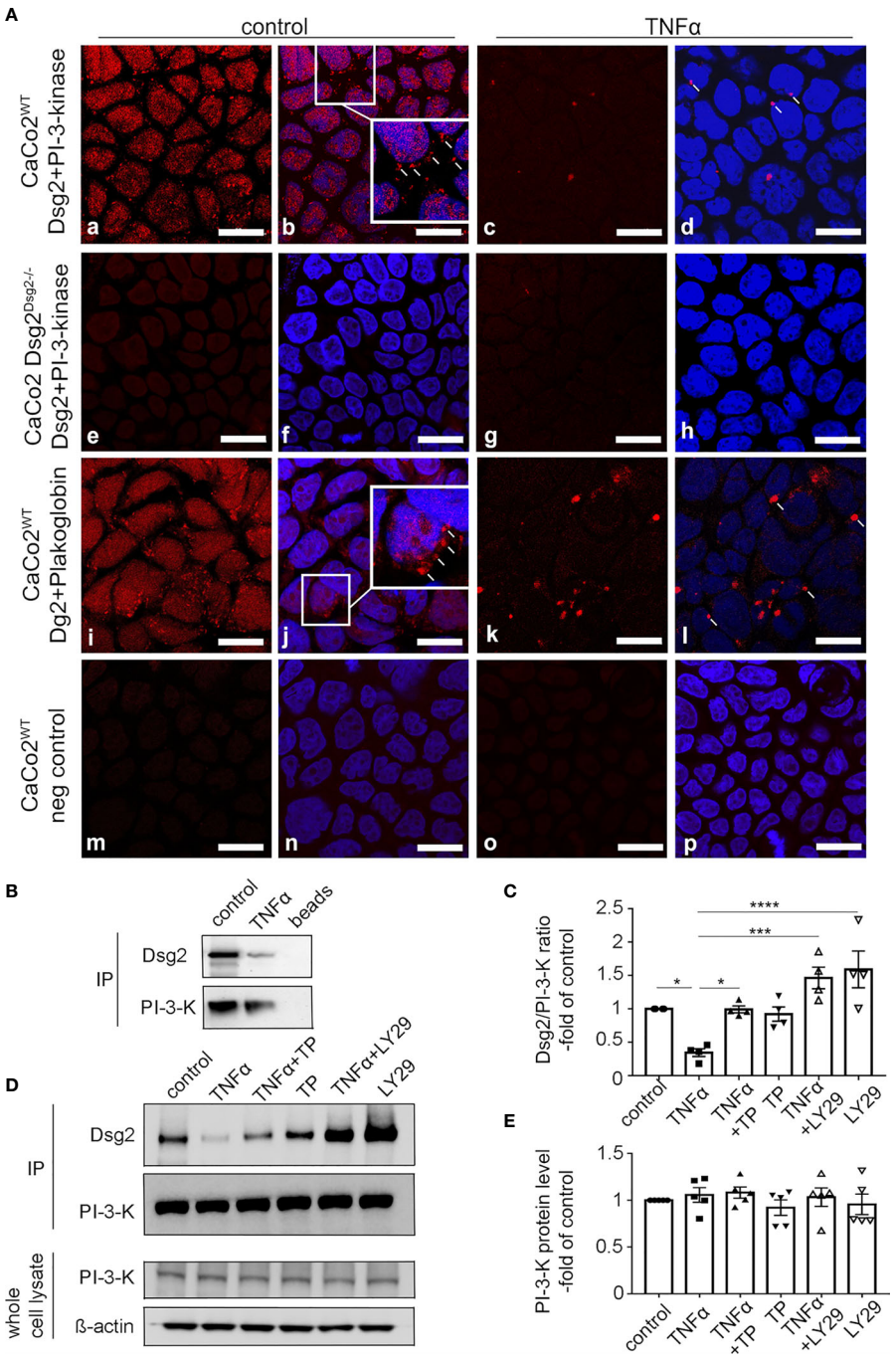

FIGURE 8 | Dsg2 and PI-3-K show direct interaction. **(A)** Images following Proximity ligation assays (PLA) are shown. Images were stained with DAPI to visualize cell nuclei (b, f, j, n, d, h, l). In Caco^{WT} (a-d) red fluorescent spots within cells are shown after incubation of cells with antibodies directed against Dsg2 and PI-3-kinase under basal conditions (a, b). Insert in (b) highlights spots at the cell periphery. Incubation of monolayers with TNFα reduced the number of spots (c, d). PLAs using Caco$^{Dsg2-/-}$ (e-h) under the same conditions and Caco^{WT} without primary antibodies (m-p) served as negative controls. Caco^{WT} were stained with Dsg2 and Plakoglobin as positive control (i-l); images shown are representative for n=5 experiments. Scale bar is10μm. **(B)**, **(C)** Co-Immunoprecipitations (IP) are shown that were performed with 2.5μg PI-3-kinase antibody in Caco2^{WT} cells under control conditions, incubated for 24h with TNFα (100 ng/ml), TP (20 μM), LY294002 (20 μM, PI-3-kinase inhibitor) or in combination. Beads without primary antibody served as negative controls. Western Blot of PI-3-kinase from whole cell lysates of Caco2 Dsg2^{WT} is also shown. ß-actin served as loading control. **(D)** Quantifications of all IPs from **(C)** are presented. Quantifications were carried out by calculating Dsg2/PI-3-kinase ratio from the ODs; n= 4 experiments, Ordinary 1-way ANOVA Asteriks mark significant differences *p < 0.01, ***p < 0.0001, ****p < 0.00001; comparisons are indicated by the lines above the columns. **(E)** Quantification of PI-3-kinase protein level showed no significant difference, n=5, Ordinary 1-way ANOVA.

signaling events. This is supported by our *in vitro* data in Caco2 cells, where TP attenuated loss of intercellular adhesion in dispase-based enterocyte dissociation assays and by the fact that loss of intercellular adhesion induced by the application of antibodies directed against the extracellular domain of Dsg2 was sufficient to increase permeability of Caco2 monolayers. Comparable observations were made in previous studies (6, 11).

Loss of Dsg2 and of Dsg-2-Mediated Adhesion Are Directly Linked With Claudin2 Expression

An interplay between desmosomes and tight junction integrity has been discussed in the recent years although detailed mechanistic insights remained absent (37). It has been proposed that the control of microtubule stabilization by desmosomes could promote the trafficking of tight junction proteins (38). In the intestine, it can be assumed that a mechanical break of tight junctions as a consequence of reduced Dsg2-mediated adhesion may induce increased intestinal permeability. Given the close correlation between loss of tight junctions in general and Dsg2 at the cell borders this appears to be reasonable (6–8, 10). However, the fact that the Claudin2 is upregulated on both, RNA- and protein levels following loss of Dsg2 indicates a mechanistic interplay between these two proteins instead of only a passive interplay of tight junctions. Following this, Dsg2 may serve as a scaffold protein to modulate downstream signaling either in response to other upstream signaling events and/or to changes in cell adhesion. The observation that loss of Dsg2 induced by TNFα, by gene knock out and by antibody-induced loss of intercellular adhesion resulted in increased Claudin2 levels demonstrates that all of these events are sufficient to induce Dsg2-dependent signaling. The role of Dsg2 as a protein critically involved in cellular signaling events has been recognized earlier in the context of apoptosis, where a fragment of the intracellular domain of Dsg2 contributed to the induction of cell death under certain experimental conditions (12, 13, 15). In addition is has been observed that Dsg2 or desmosomes in general contribute to the regulation of Rho GTPase activity by the modulation of Rho GEF and regulate the activity of protein kinase C which was observed in the context of plakophilin2 in keratinocytes and in cardiomyocytes (39–44).

Dsg2-Mediated Sequestering of PI-3-Kinase Regulates Activity of the PI-3-Kinase/AKT Signaling Axis

Increased Claudin2 levels are a typical hallmark in response to inflammatory stimuli in the intestine (45, 46). According to this, Claudin2 is upregulated under conditions of acute inflammation in DSS-induced colitis in mice (47) and in patients with IBD (9, 10, 48). On a functional level Claudin2 as a pore-forming tight junction protein is critically involved in symptoms such as diarrhea in intestinal inflammation (49). On a mechanistic level it has been demonstrated earlier that upregulation of Claudin2 is dependent on PI-3-kinase activation leading to phosphorylation of AKT. Accordingly, inhibition of PI-3-kinase using LY294002 was effective to attenuate inflammation-induced upregulation in previous studies (30, 31, 50, 51). This supports our current observation where LY294002 blocked TNFα-induced upregulation of claudin2 in Caco2 cells. The TNFα-induced activation of PI-3-kinase may lead to Cdx2 expression as described previously for IL-6 (30). The enhanced expression of the transcription factor Cdx2 may then activate the claudin2 promotor resulting in the increased Claudin2 expression (29). The fact that LY294002 completely blocked both AKT phosphorylation and increased Claudin2 expression indicates that the critical event is upstream of AKT i.e. at the level of PI-3-kinase activation.

The novel observation here is that Dsg2 sequesters PI-3-kinase in intestinal epithelial cells. The finding that we observed increased phosphorylation of AKT^{Ser473} in Dsg2-deficient cells when compared to WT cells under basal conditions and highly increased phosphorylation following application of TNFα led to the assumption that the sequestering of PI-3-kinase by Dsg2 may regulate its activity. On the other hand, the fact that TNFα application still results in increased Claudin2 expression and AKT phosphorylation in Dsg2-deficient cells also points to the presence of Dsg2-independent pathways in addition to the proposed mechanism here. The Dsg2-independent pathways may involve direct AKT phosphorylation by TNFα-induced activation of src kinase (52) by miRNAs (53) and also by integrins as has been observed in platelets (54) upstream of PI-3-kinase. Nonetheless, the experiments using TP to stabilize Dsg2-mediated adhesion showed that this was sufficient to block TNFα-induced AKT-phosphorylation and Claudin2 upregulation which overall supports the notion that Dsg2 is critically involved in the regulation of the PI-3-kinase/AKT signaling axis.

Application of TNFα not only resulted in loss of Dsg2 at the cell borders but also remarkably removed PI-3-kinase to the cytoplasm in immunostaining. The direct interaction of PI-3-kinase and Dsg2 was proven by PLA-assays and co-immunoprecipitation. However, when taking into account the staining pattern in PLA-assays it appears that not only desmosomal Dsg2 at the cell borders but also extradesmosomal Dsg2 which can be found apically in enterocytes also appears to be involved in sequestering PI-3-kinase (11). The presence of extradesmosmal Dsg2 may also explain the dotted staining pattern across the whole cells in PLAs. Interestingly, both TP and LY294002 blocked the dissociation of PI-3-kinase and Dsg2. According to the quantifications of the co-immunoprecipitation assays, LY294002 even increased the interaction between Dsg2 and PI-3-kinase above baseline levels both when applied alone and following application of TNFα. This suggests that activation of PI-3-kinase causes disassembly of both proteins leading to increased Claudin2 expression. On the other hand as outlined above the stabilization of Dsg2 by TP blocked the dissociation of Dsg2 and PI-3-kinase and thereby attenuated AKT phosphorylation. Taking all these observations together, it is conceivable that the sequestering of PI-3-kinase to Dsg2 is required to prevent further downstream signaling in response to PI-3-kinase activation. Therefore, loss of the interaction triggers further downstream signaling. In addition, it can be speculated that loss of Dsg2 may further promote the susceptibility PI-3-kinase to be further activated. Based on this, we suggest that Dsg2 recruits PI-3-kinase under basal conditions. Loss of Dsg2 or Dsg2-mediated adhesion promotes the activation of PI-3-kinase and/or downstream signaling leading to AKT phosphorylation which then results in the upregulation of Claudin2.

In summary, our current data not only show a novel and important mechanism by which Dsg2 i.e. desmosomes are directly involved in the regulation of tight junction proteins but also strengthen the potential role of Dsg2 as a promising therapeutic target to stabilize intestinal barrier function in intestinal inflammation.

DATA AVAILABILITY STATEMENT

The raw data supporting the conclusions of this article will be made available by the authors, without undue reservation.

ETHICS STATEMENT

The animal study was reviewed and approved by Regierung von Unterfranken.

AUTHOR CONTRIBUTIONS

NB: Conceptualization, Investigation, Data analysis, Methodology, and Writing original draft. MM: Investigation, Data analysis, and Methodology. FK: Investigation and Data analysis. CO: Investigation and Data analysis. MP: Investigation and Data analysis. C-TG: Supervision, Data analysis, and Resources. JW: Conceptualization, Supervision, Data analysis, and funding acquisition. NS: Conceptualization, Supervision, Data analysis, Funding acquisition, Writing original draft, and review and editing. All authors contributed to the article and approved the submitted version.

FUNDING

These studies were funded by Deutsche Forschungsgemeinschaft (DFG) Priority Programm SPP 1782 to NS and JW.

REFERENCES

1. Chelakkot C, Ghim J, Ryu SH. Mechanisms Regulating Intestinal Barrier Integrity and Its Pathological Implications. *Exp Mol Med* (2018) 50(8):1–9. doi: 10.1038/s12276-018-0126-x
2. Martini E, Krug SM, Siegmund B, Neurath MF, Becker C. Mend Your Fences: The Epithelial Barrier and Its Relationship With Mucosal Immunity in Inflammatory Bowel Disease. *Cell Mol Gastroenterol Hepatol* (2017) 4 (1):33–46. doi: 10.1016/j.jcmgh.2017.03.007
3. Schlegel N, Boerner K, Waschke J. Targeting Desmosomal Adhesion and Signalling for Intestinal Barrier Stabilization in Inflammatory Bowel Diseases —Lessons From Experimental Models and Patients. *Acta Physiologica* (2021) 231(1):e13492. doi: 10.1111/apha.13492
4. Farquhar MG, Palade GE. Junctional Complexes in Various Epithelia. *J Cell Biol* (1963) 17:375–412. doi: 10.1083/jcb.17.2.375
5. Luissint A-C, Parkos CA, Nusrat A. Inflammation and the Intestinal Barrier: Leukocyte–Epithelial Cell Interactions, Cell Junction Remodeling, and Mucosal Repair. *Gastroenterology* (2016) 151(4):616–32. doi: 10.1053/j.gastro.2016.07.008
6. Schlegel N, Meir M, Heupel W-M, Holthöfer B, Leube RE, Waschke J. Desmoglein 2-Mediated Adhesion Is Required for Intestinal Epithelial Barrier Integrity. *Am J Physiol-Gastrointestinal Liver Physiol* (2010) 298(5): G774–83. doi: 10.1152/ajpgi.00239.2009
7. Gross A, Pack LAP, Schacht GM, Kant S, Ungewiss H, Meir M, et al. Desmoglein 2, But Not Desmocollin 2, Protects Intestinal Epithelia From Injury. *Mucosal Immunol* (2018) 11(6):1630–9. doi: 10.1038/s41385-018-0062-z
8. Meir M, Burkard N, Ungewiß H, Diefenbacher M, Flemming S, Kannapin F, et al. Neurotrophic Factor GDNF Regulates Intestinal Barrier Function in Inflammatory Bowel Disease. *J Clin Invest* (2019) 129(7):2824–40. doi: 10.1172/jci120261
9. Meir M, Salm J, Fey C, Schweinlin M, Kollmann C, Kannapin F, et al. Enteroids Generated From Patients With Severe Inflammation in Crohn's Disease Maintain Alterations of Junctional Proteins. *J Crohn's Colitis* (2020) 14(10):1473–87. doi: 10.1093/ecco-jcc/jjaa085
10. Spindler V, Meir M, Vigh B, Flemming S, Hütz K, Germer C-T, et al. Loss of Desmoglein 2 Contributes to the Pathogenesis of Crohn's Disease. *Inflammatory Bowel Dis* (2015) 21(10):2349–59. doi: 10.1097/mib.0000000000000486
11. Ungewiß H, Vielmuth F, Suzuki ST, Maiser A, Harz H, Leonhardt H, et al. Desmoglein 2 Regulates the Intestinal Epithelial Barrier *via* P38 Mitogen-Activated Protein Kinase. *Sci Rep* (2017) 7(1):6329. doi: 10.1038/s41598-017-06713-y
12. Kamekura R, Kolegraff KN, Nava P, Hilgarth RS, Feng M, Parkos CA, et al. Loss of the Desmosomal Cadherin Desmoglein-2 Suppresses Colon Cancer Cell Proliferation Through EGFR Signaling. *Oncogene* (2014) 33(36):4531–6. doi: 10.1038/onc.2013.442
13. Kamekura R, Nava P, Feng M, Quiros M, Nishio H, Weber DA, et al. Inflammation-Induced Desmoglein-2 Ectodomain Shedding Compromises the Mucosal Barrier. *Mol Biol Cell* (2015) 26(18):3165–77. doi: 10.1091/mbc.e15-03-0147
14. Ungewiß H, Rötzer V, Meir M, Fey C, Diefenbacher M, Schlegel N, et al. Dsg2 *via* Src-Mediated Transactivation Shapes EGFR Signaling Towards Cell Adhesion. *Cell Mol Life Sci* (2018) 75(22):4251–68. doi: 10.1007/s00018-018-2869-x
15. Yulis M, Quiros M, Hilgarth R, Parkos CA, Nusrat A. Intracellular Desmoglein-2 Cleavage Sensitizes Epithelial Cells to Apoptosis in Response to Pro-Inflammatory Cytokines. *Cell Death Dis* (2018) 9(3):389. doi: 10.1038/s41419-018-0380-9
16. Jiang K, Rankin CR, Nava P, Sumagin R, Kamekura R, Stowell SR, et al. Galectin-3 Regulates Desmoglein-2 and Intestinal Epithelial Intercellular Adhesion. *J Biol Chem* (2014) 289(15):10510–7. doi: 10.1074/jbc.M113.538538
17. Venugopal S, Anwer S, Szászi K. Claudin-2: Roles Beyond Permeability Functions. *Int J Mol Sci* (2019) 20(22):5655. doi: 10.3390/ijms20225655
18. Luettig J, Rosenthal R, Barmeyer C, Schulzke JD. Claudin-2 as a Mediator of Leaky Gut Barrier During Intestinal Inflammation. *Tissue Barriers* (2015) 3(1-2):e977176. doi: 10.4161/21688370.2014.977176
19. Barrett KE. Claudin-2 Pore Causes Leak That Breaches the Dam in Intestinal Inflammation. *J Clin Invest* (2020) 130(10):5100–1. doi: 10.1172/jci140528
20. Escaffit F, Boudreau F, Beaulieu JF. Differential Expression of Claudin-2 Along the Human Intestine: Implication of GATA-4 in the Maintenance of Claudin-2 in Differentiating Cells. *J Cell Physiol* (2005) 203(1):15–26. doi: 10.1002/jcp.20189
21. Zhang C, Yan J, Xiao Y, Shen Y, Wang J, Ge W, et al. Inhibition of Autophagic Degradation Process Contributes to Claudin-2 Expression Increase and Epithelial Tight Junction Dysfunction in TNF-α Treated Cell Monolayers. *Int J Mol Sci* (2017) 18(1):157. doi: 10.3390/ijms18010157
22. Amasheh M, Grotjohann I, Amasheh S, Fromm A, Söderholm JD, Zeitz M, et al. Regulation of Mucosal Structure and Barrier Function in Rat Colon Exposed to Tumor Necrosis Factor Alpha and Interferon Gamma *In Vitro*: A Novel Model for Studying the Pathomechanisms of Inflammatory Bowel Disease Cytokines. *Scandinavian J Gastroenterol* (2009) 44(10):1226–35. doi: 10.1080/00365520903131973
23. Niessen CM. Tight Junctions/Adherens Junctions: Basic Structure and Function. *J Invest Dermatol* (2007) 127(11):2525–32. doi: 10.1038/sj.jid.5700865
24. Tunggal JA, Helfrich I, Schmitz A, Schwarz H, Günzel D, Fromm M, et al. E-Cadherin Is Essential for *In Vivo* Epidermal Barrier Function by Regulating

Tight Junctions. *EMBO J* (2005) 24(6):1146–56. doi: 10.1038/sj.emboj.7600605
25. Campbell HK, Maiers JL, DeMali KA. Interplay Between Tight Junctions & Adherens Junctions. *Exp Cell Res* (2017) 358(1):39–44. doi: 10.1016/j.yexcr.2017.03.061
26. Erben U, Loddenkemper C, Doerfel K, Spieckermann S, Haller D, Heimesaat MM, et al. A Guide to Histomorphological Evaluation of Intestinal Inflammation in Mouse Models. *Int J Clin Exp Pathol* (2014) 7(8):4557–76.
27. Meir M, Flemming S, Burkard N, Bergauer L, Metzger M, Germer CT, et al. Glial Cell Line-Derived Neurotrophic Factor Promotes Barrier Maturation and Wound Healing in Intestinal Epithelial Cells *In Vitro*, American Journal of Physiology. *Gastrointestinal liver Physiol* (2015) 309(8):G613–24. doi: 10.1152/ajpgi.00357.2014
28. Hollander D. Intestinal Permeability, Leaky Gut, and Intestinal Disorders. *Curr Gastroenterol Rep* (1999) 1(5):410–6. doi: 10.1007/s11894-999-0023-5
29. Mankertz J, Amasheh M, Krug SM, Fromm A, Amasheh S, Hillenbrand B, et al. Tnfalpha Up-Regulates Claudin-2 Expression in Epithelial HT-29/B6 Cells *via* Phosphatidylinositol-3-Kinase Signaling. *Cell Tissue Res* (2009) 336 (1):67–77. doi: 10.1007/s00441-009-0751-8
30. Suzuki T, Yoshinaga N, Tanabe S. Interleukin-6 (IL-6) Regulates Claudin-2 Expression and Tight Junction Permeability in Intestinal Epithelium*. *J Biol Chem* (2011) 286(36):31263–71. doi: 10.1074/jbc.M111.238147
31. Yamamoto T, Kojima T, Murata M, K.-i. Takano M, Chiba H, Sawada N. IL-1β Regulates Expression of Cx32, Occludin, and Claudin-2 of Rat Hepatocytes *via* Distinct Signal Transduction Pathways. *Exp Cell Res* (2004) 299(2):427–41. doi: 10.1016/j.yexcr.2004.06.011
32. Schlegel N, Boerner K, Waschke J. Targeting Desmosomal Adhesion and Signalling for Intestinal Barrier Stabilization in Inflammatory Bowel Diseases-Lessons From Experimental Models and Patients. *Acta Physiol (Oxf)* (2021) 231(1):e13492. doi: 10.1111/apha.13492
33. Ananthakrishnan AN, Bernstein CN, Iliopoulos D, Macpherson A, Neurath MF, Ali RAR, et al. Environmental Triggers in IBD: A Review of Progress and Evidence, Nature Reviews. *Gastroenterol Hepatol* (2018) 15(1):39–49. doi: 10.1038/nrgastro.2017.136
34. Heupel WM, Muller T, Efthymiadis A, Schmidt E, Drenckhahn D, Waschke J. Peptides Targeting the Desmoglein 3 Adhesive Interface Prevent Autoantibody-Induced Acantholysis in Pemphigus. *J Biol Chem* (2009) 284 (13):8589–95. doi: 10.1074/jbc.M808813200
35. Shafraz O, Rubsam M, Stahley SN, Caldara AL, Kowalczyk AP, Niessen CM, et al. E-Cadherin Binds to Desmoglein to Facilitate Desmosome Assembly. *Elife* (2018) 7:e37629. doi: 10.7554/eLife.37629
36. Schlipp A, Schinner C, Spindler V, Vielmuth F, Gehmlich K, Syrris P, et al. Desmoglein-2 Interaction is Crucial for Cardiomyocyte Cohesion and Function. *Cardiovasc Res* (2014) 104(2):245–57. doi: 10.1093/cvr/cvu206cvu206
37. Green KJ, Jaiganesh A, Broussard JA. Desmosomes: Essential Contributors to an Integrated Intercellular Junction Network. *F1000Res* (2019) 8:F1000 Faculty Rev-2150. doi: 10.12688/f1000research.20942.1
38. Patel DM, Dubash AD, Kreitzer G, Green KJ. Disease Mutations in Desmoplakin Inhibit Cx43 Membrane Targeting Mediated by Desmoplakin-EB1 Interactions. *J Cell Biol* (2014) 206(6):779–97. doi: 10.1083/jcb.201312110
39. Rasmussen TB, Nissen PH, Palmfeldt J, Gehmlich K, Dalager S, Jensen UB, et al. Truncating Plakophilin-2 Mutations in Arrhythmogenic Cardiomyopathy Are Associated With Protein Haploinsufficiency in Both Myocardium and Epidermis. *Circulation: Cardiovasc Genet* (2014) 7(3):230–40. doi: 10.1161/CIRCGENETICS.113.000338
40. Chen X, Bonné S, Hatzfeld M, van Roy F, Green KJ. Protein Binding and Functional Characterization of Plakophilin 2: Evidence for Its Diverse Roles in Desmosomes and β-Catenin Signaling*. *J Biol Chem* (2002) 277(12):10512–22. doi: 10.1074/jbc.M108765200
41. Bass-Zubek AE, Hobbs RP, Amargo EV, Garcia NJ, Hsieh SN, Chen X, et al. Plakophilin 2: A Critical Scaffold for PKC Alpha That Regulates Intercellular Junction Assembly. *J Cell Biol* (2008) 181(4):605–13. doi: 10.1083/jcb.200712133
42. Gerull B, Heuser A, Wichter T, Paul M, Basson CT, McDermott DA, et al. Mutations in the Desmosomal Protein Plakophilin-2 Are Common in Arrhythmogenic Right Ventricular Cardiomyopathy. *Nat Genet* (2004) 36 (11):1162–4. doi: 10.1038/ng1461
43. Bendrick JL, Eldredge LA, Williams EI, Haight NB, Dubash AD. Desmoplakin Harnesses Rho Gtpase and P38 Mitogen-Activated Protein Kinase Signaling to Coordinate Cellular Migration. *J Invest Dermatol* (2019) 139(6):1227–36. doi: 10.1016/j.jid.2018.11.032
44. Hartlieb E, Rötzer V, Radeva M, Spindler V, Waschke J. Desmoglein 2 Compensates for Desmoglein 3 But Does Not Control Cell Adhesion *via* Regulation of P38 Mitogen-Activated Protein Kinase in Keratinocytes. *J Biol Chem* (2014) 289(24):17043–53. doi: 10.1074/jbc.M113.489336
45. Weber CR, Nalle SC, Tretiakova M, Rubin DT, Turner JR. Claudin-1 and Claudin-2 Expression is Elevated in Inflammatory Bowel Disease and may Contribute to Early Neoplastic Transformation. *Lab Invest* (2008) 88 (10):1110–20. doi: 10.1038/labinvest.2008.78
46. Zeissig S, Burgel N, Gunzel D, Richter J, Mankertz J, Wahnschaffe U, et al. Changes in Expression and Distribution of Claudin 2, 5 and 8 Lead to Discontinuous Tight Junctions and Barrier Dysfunction in Active Crohn's Disease. *Gut* (2007) 56(1):61–72. doi: 10.1136/gut.2006.094375
47. Xiao YT, Yan WH, Cao Y, Yan JK, Cai W. Neutralization of IL-6 and TNF-α Ameliorates Intestinal Permeability in DSS-Induced Colitis. *Cytokine* (2016) 83:189–92. doi: 10.1016/j.cyto.2016.04.012
48. Barmeyer C, Schulzke JD, Fromm M. Claudin-Related Intestinal Diseases. *Semin Cell Dev Biol* (2015) 42:30–8. doi: 10.1016/j.semcdb.2015.05.006
49. Burgel N, Bojarski C, Mankertz J, Zeitz M, Fromm M, Schulzke JD. Mechanisms of Diarrhea in Collagenous Colitis. *Gastroenterology* (2002) 123(2):433–43. doi: 10.1053/gast.2002.34784. S001650850200121X.
50. Prasad S, Mingrino R, Kaukinen K, Hayes KL, Powell RM, MacDonald TT, et al. Inflammatory Processes Have Differential Effects on Claudins 2, 3 and 4 in Colonic Epithelial Cells. *Lab Invest* (2005) 85(9):1139–62. doi: 10.1038/labinvest.3700316
51. Ahmad R, Chaturvedi R, Olivares-Villagómez D, Habib T, Asim M, Shivesh P, et al. Targeted Colonic Claudin-2 Expression Renders Resistance to Epithelial Injury, Induces Immune Suppression, and Protects From Colitis. *Mucosal Immunol* (2014) 7(6):1340–53. doi: 10.1038/mi.2014.21
52. Amasheh M, Fromm A, Krug SM, Amasheh S, Andres S, Zeitz M, et al. Tnfalpha-Induced and Berberine-Antagonized Tight Junction Barrier Impairment *via* Tyrosine Kinase, Akt and Nfkappab Signaling. *J Cell Sci* (2010) 123(Pt 23):4145–55. doi: 10.1242/jcs.070896
53. Ghafouri-Fard S, Abak A, Tondro Anamag F, Shoorei H, Majidpoor J, Taheri M. The Emerging Role of non-Coding Rnas in the Regulation of PI3K/AKT Pathway in the Carcinogenesis Process. *BioMed Pharmacother* (2021) 137:111279. doi: 10.1016/j.biopha.2021.111279
54. Laurent PA, Hechler B, Solinhac R, Ragab A, Cabou C, Anquetil T, et al. Impact of PI3Kα (Phosphoinositide 3-Kinase Alpha) Inhibition on Hemostasis and Thrombosis. *Arterioscler Thromb Vasc Biol* (2018) 38 (9):2041–53. doi: 10.1161/atvbaha.118.311410

Conflict of Interest: The authors declare that the research was conducted in the absence of any commercial or financial relationships that could be construed as a potential conflict of interest.

Publisher's Note: All claims expressed in this article are solely those of the authors and do not necessarily represent those of their affiliated organizations, or those of the publisher, the editors and the reviewers. Any product that may be evaluated in this article, or claim that may be made by its manufacturer, is not guaranteed or endorsed by the publisher.

Copyright © 2021 Burkard, Meir, Kannapin, Otto, Petzke, Germer, Waschke and Schlegel. This is an open-access article distributed under the terms of the Creative Commons Attribution License (CC BY). The use, distribution or reproduction in other forums is permitted, provided the original author(s) and the copyright owner(s) are credited and that the original publication in this journal is cited, in accordance with accepted academic practice. No use, distribution or reproduction is permitted which does not comply with these terms.

frontiers in Immunology

REVIEW
published: 01 October 2021
doi: 10.3389/fimmu.2021.727861

Monocyte Chemotactic Protein-Induced Protein 1 (MCPIP-1): A Key Player of Host Defense and Immune Regulation

Zhuqing Jin[1], *En Zheng*[2], *Candice Sareli*[3], *Pappachan E. Kolattukudy*[4] *and Jianli Niu*[3,4]*

[1] School of Basic Medical Sciences, Zhejiang Chinese Medical University, Hangzhou, China, [2] Department of Chemistry, Zhejiang University, Hangzhou, China, [3] Office of Human Research, Memorial Healthcare System, Hollywood, FL, United States, [4] Burnett School of Biomedical Sciences, University of Central Florida College of Medicine, Orlando, FL, United States

OPEN ACCESS

Edited by:
Sylvaine You,
Institut National de la Santé et de la Recherche Médicale (INSERM), France

Reviewed by:
Dong Li,
Jilin University, China
Dipyaman Ganguly,
Indian Institute of Chemical Biology (CSIR), India

***Correspondence:**
Jianli Niu
jniu@mhs.net

Specialty section:
This article was submitted to Inflammation, a section of the journal Frontiers in Immunology

Received: 19 June 2021
Accepted: 08 September 2021
Published: 01 October 2021

Citation:
Jin Z, Zheng E, Sareli C, Kolattukudy PE and Niu J (2021) Monocyte Chemotactic Protein-Induced Protein 1 (MCPIP-1): A Key Player of Host Defense and Immune Regulation. Front. Immunol. 12:727861. doi: 10.3389/fimmu.2021.727861

Inflammatory response is a host-protective mechanism against tissue injury or infections, but also has the potential to cause extensive immunopathology and tissue damage, as seen in many diseases, such as cardiovascular diseases, neurodegenerative diseases, metabolic syndrome and many other infectious diseases with public health concerns, such as Coronavirus Disease 2019 (COVID-19), if failure to resolve in a timely manner. Recent studies have uncovered a superfamily of endogenous chemical molecules that tend to resolve inflammatory responses and re-establish homeostasis without causing excessive damage to healthy cells and tissues. Among these, the monocyte chemoattractant protein-induced protein (MCPIP) family consisting of four members (MCPIP-1, -2, -3, and -4) has emerged as a group of evolutionarily conserved molecules participating in the resolution of inflammation. The focus of this review highlights the biological functions of MCPIP-1 (also known as Regnase-1), the best-studied member of this family, in the resolution of inflammatory response. As outlined in this review, MCPIP-1 acts on specific signaling pathways, in particular NFκB, to blunt production of inflammatory mediators, while also acts as an endonuclease controlling the stability of mRNA and microRNA (miRNA), leading to the resolution of inflammation, clearance of virus and dead cells, and promotion of tissue regeneration *via* its pleiotropic effects. Evidence from transgenic and knock-out mouse models revealed an involvement of MCPIP-1 expression in immune functions and in the physiology of the cardiovascular system, indicating that MCPIP-1 is a key endogenous molecule that governs normal resolution of acute inflammation and infection. In this review, we also discuss the current evidence underlying the roles of other members of the MCPIP family in the regulation of inflammatory processes. Further understanding of the proteins from this family will provide new insights into the identification of novel targets for both host effectors and microbial factors and will lead to new therapeutic treatments for infections and other inflammatory diseases.

Keywords: inflammation, viral infection, ischemic inflammation, resolution, MCPIP-1

INTRODUCTION

Inflammatory response is an immunological defense mechanism of the host to infections and tissue damage (e.g., ischemic insults) or stress (1). Damaged or stressed cells are thought to release danger-associated molecular patterns (DAMPs) that can trigger the innate immune system in the same manner as microbial components, the so-called pathogen-associated molecular patterns (PAMPs), by binding to host pattern-recognition receptors (PRRs) presented on various cells, including immune cells (T-cells, B-cells and NK cells) and the tissue cells such as endothelial cells, cardiomyocytes, and even neurons (1). This recognition triggers a series of signaling cascades that initiate the activation of transcriptional factor nuclear factor-κB (NFκB) and NLRP3 inflammasome, leading to the release of inflammatory mediators, like tumor necrosis factor-alpha (TNFα), monocyte chemoattractant protein-1 (MCP-1), interleukin-1 (IL-1) and IL-6 (2, 3). The inflammatory response is beneficial to the host by eliminating the harmful agents (PAMPs or DAMPs) and is usually resolved in a timely manner; however, failure to resolve can cause excessive or persistent inflammation that is often disruptive and can cause marked tissue damage (4).

The resolution of inflammation is a programmed active process that involves the biosynthesis of a variety of active molecules that act on key events of inflammatory response to terminate the production of pro-inflammatory mediators and restore tissue homeostasis (5). There is an increasing body of evidence that many pro-inflammatory mediators produced during the inflammatory phase can simultaneously initiate a program for active resolution (6). For example, TNFα can effectively induce A20 (also known as tumor necrosis factor-α-induced protein 3 or TNFAIP3), an ubiquitin editing enzyme that negatively regulates the inflammatory response by interfering with NFκB signaling pathway, leading to the resolution of inflammation (7). The newly synthesized molecules not only act as signals for the termination of the inflammatory response, but also promote the clearance of dead cells to accelerate the resolution of inflammation (4, 8).

A major contribution of our group to the field was the discovery of the novel zinc-finger protein, named MCP-1–induced protein (MCPIP), which was originally detected in MCP-1 treated human peripheral blood monocytes (9, 10). Subsequent studies demonstrated that MCPIP belongs to a new Zc3h12 family consisting of four members (MCPIP-1, -2, -3, and -4) that are encoded by Zc3h12a, Zc3h12b, Zc3h12c, and Zc3h12d, respectively (11). MCPIP-1 is the most-studied protein that contains an N-terminal domain, a PilT N-terminus like (PIN) domain, a zinc finger domain, and a C-terminal domain (12). Emerging evidence indicates that MCPIP-1 plays an essential role in the regulation of inflammatory response, with additional roles in defense against viruses and various stresses, cellular differentiation, and apoptosis (13, 14), all of these are key cellular and molecular components that contribute to the successful resolution of inflammation (9, 10, 15–18). The focus of this review is to present evidence illustrating that the role played by MCPIP-1 is important in the resolution of inflammation initiated by virus infections or ischemic injuries and highlight recent advances on the actions of this protein and its potential clinical significance. We also discuss the available evidence regarding the role of other members (MCPIP-2, -3, and -4) from this family in the regulation of inflammatory processes.

EXPRESSION AND DYNAMIC REGULATION OF MCPIP-1

MCPIP-1 was originally identified in human peripheral blood monocytes stimulated with MCP-1 (9). Subsequent studies demonstrated that MCPIP-1 is produced in many other cell types, either constitutively or after induction by a wide range of stimuli, such as inflammatory cytokines (e.g., IL-1β, IL-17 and TNFα) and oxidative stress (13, 19, 20). Further studies demonstreated that the expression of MCPIP-1 can be induced by ischemia in the heart and the brain (21, 22). Infections by virus such as hepatitis C virus (HCV), hepatitis B virus (HBV), influenza A virus (IAV), Japanese encephalitis virus (JEV) and Dengue virus as well as by bacteria and fungal increase the expression of MCPIP-1 (23–25). The extracellular high mobility group box 1 (HMGB1), a non-histone DNA-binding protein released from dying cells in response to tissue injuries, also increases microglium expression of MCPIP-1 that negatively regulates HMGB-1-mediated neuroinflammation and neuronal toxicity (26). Minocycline, a member of tetracycline antibiotics with anti-inflammatory properties, also induces MCPIP-1 expression in the heart and the brain (27, 28).

Although the molecular mechanisms responsible for MCPIP-1 expression are still poorly understood, MCP-1 binding to its cognate receptor CCR2 was thought to activate ERK or AKT pathways, leading to the expression of MCPIP-1 (9). Activation of NFκB signaling was suggested to induce the expresion of MCPIP-1 by inflammatory cytokines such as IL-1β (29). Transcription factors Elk-1 and SRF were also reported to mediate IL-1-dependent expression of MCPIP-1 by binding to the promoter region of MCPIP-1 (30). Activation of JAK/STAT3 signaling was also reported to mediate MCPIP-1 expression in epithelial cells (31). At the post-transcriptional level, MCPIP-1 mRNA was found to be downregulated by miR-9 in LPS-activated microglial cells (32). MCPIP-1 also cleaves its own transcript (33, 34). Moreover, the translated MCPIP-1 protein can be phosphorylated by IκB kinase (IKK) β and then undergoes ubiquitination and degradation (35) or cleaved by the paracaspase Malt-1 (33, 36). These data indicate that MCPIP-1expression is tightly controlled by an autoregulatory feedback mechanism, which ensures an appropriate level of MCPIP-1 aimed to minimize any disruption of immune homeostasis.

FUNCTIONAL FEATURES OF MCPIP-1

MCPIP-1 was first described as a transcriptional activator owing to the structural feature of a potential DNA binding zinc finger domain (9). Subsequent studies indicate that MCPIP is localized to both the cytoplasmic and nuclear compartments, depending on the distinct functions it plays in different cell types

(11, 37, 38). Mutational analysis of MCPIP-1 has identified the two regions of the primary structure that are critical for its biological activity (12, 39–41). The first region consists of the ubiquitin-associated domain from 43-89, which is associated with the control of protein ubiquitination; whereas the second region consists of PIN domain from 133–270, which is associated with RNA-cleaving function and is why it was later renamed as Regnase-1 (regulatory RNase-1) (40, 42). In addition to these two regions, the C-terminal region of the NYN domain is crucial for suppressing microRNA (miRNA) biogenesis *via* cleavage of the terminal loops of precursor miRNAs (16, 40–44).

MCPIP-1 Regulates Protein Ubiquitination

Ubiquitination has emerged as a crucial mechanism that regulates signal transduction in the inflammatory response (3, 45). The use of MCPIP-1-deficient mice has revealed the crucial role of MCPIP-1 in the regulation of inflammatory cytokine signaling pathways. Mice lacking MCPIP-1 are normal at birth but suffer growth retardation and die prematurely due to massive multi-organ inflammation, indicative of a key role for MCPIP in immune homeostasis of the host (41). Macrophages from MCPIP-1-deficient mice showed up-regulation of pro-inflammatory mediators together with a greatly increased ubiquitination of TRAFs (TNF receptor–associated factors) and the receptor-interacting protein (RIP) kinases, both of which play a central role in the LPS-, IL-1β- and TNF-induced activation of NFκB signaling pathway (46). The purified MCPIP-1 protein was shown to cleave K48- or K63-linked polyubiquitin chain, while this action of MCPIP-1 was inhibited by N-ethyl maleimide, a known inhibitor of cysteine proteinases (41). Consistent with this finding, treatment of high-molecular-weight K63-linked polyubiquitin with purified MCPIP-1 caused hydrolysis of the polyubiquitin, leading to the inhibition of phosphorylation of TAK1 (47), a critical factor for activation of the downstream kinase IKK, thereby mediating IκBα phosphorylation and NFκB activation (48). Accordingly, deletion of the ubiquitin association domain of MCPIP-1 resulted in the loss of inhibition of TNFα-induced NFκB activation (41). These results indicate that MCPIP-1 can act as a deubiquitinase to hydrolyze K63-, K48-linked polyubiquitin chains and inhibits NFκB transcriptional activity, thus contributing to suppression of the pro-inflammatory response (**Figure 1**). MCPIP-1 has also been reported to stabilize NFκB essential modulator by promoting deubiquitination, resulting in subsequent inhibition of NFκB activation induced by DNA damage (49). MCPIP-1 was also shown to stabilize the hypoxia-inducible factor 1alpha protein that is required for macrophage maturation under hypoxic conditions, in which deubiquitination plays a key regulatory role (50).

MCPIP-1 Regulates Inflammatory mRNA Stability

MCPIP-1 can also act as an RNase to regulate mRNA stability (19, 33, 40, 51). MCPIP-1 can directly bind the 3′-untranslated region (UTR) of IL-6 mRNA and manifested RNase activity to degrade

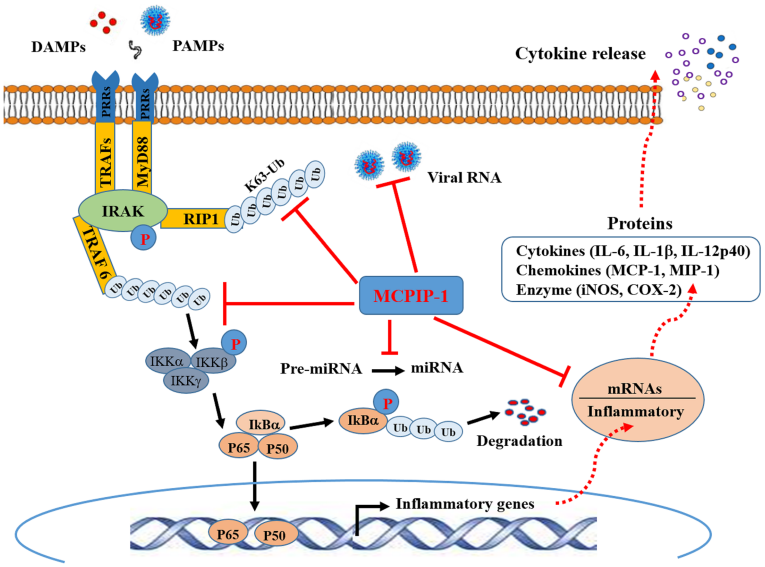

FIGURE 1 | Schematic representation of anti-inflammatory activity of MCPIP-1. Binding of molecules (DAMPs) derived from tissue damage or pathogens (PAMPs) to PRRs triggers interactions between the cytoplasmic adaptor proteins and the kinases IRAK. This engages the ubiquitin ligase TRAF6 to make polyubiquitin chains that activate the IKK complex, leading to phosphorylation and subsequent ubiquitination IKBα. This releases P50/p65 dimer for entry into the nucleus to cause transcriptional activation of NFκB-dependent genes encoding inflammatory cytokines. Ubiquitylation of RIP1, and potentially other components of the complex, recruits IKKγ and TAK1 for NFκB and MAPK activation (not shown). MCPIP-1 hydrolyzes all of these K48- and K63-linked polyubiquitins to block NFκB activation. The RNase activity of MCPIP-1 also degrades viral RNA and some mRNAs encoding for inflammatory cytokines, leading to dampening of protein expression of the inflammatory cytokines. The anti-Dicer activity of MCPIP-1 can cleave the terminal loops of pre-miRNAs leading to destabilization of pre-miRNAs and suppression of the miRNA biogenesis.

IL-6 transcripts (40). A similar finding was demonstrated in the expression of IL-1β mRNA that was degraded by the increased level of MCPIP-1 in HepG2 and U937 cells (19). Genome-wide association studies showed that the PIN domain of MCPIP-1 contains the RNase catalytic center that requires an interaction with the N-terminus for its full RNase activity and the zinc-finger domain is responsible for the recognition and direct binding of the mRNAs (12, 39, 51). With the cooperation of its domains, MCPIP-1 recognizes and degrades target mRNAs by recognizing stem-loop structures at the 3′-UTRs of these genes (40, 51). In T cells, MCPIP-1 downregulates a set of genes by cooperating with roquin, another CCCH type zinc finger protein (36, 51). However, a recent study in other type of cells indicates that, although roquin and MCPIP-1 control shared mRNAs, they do so in different mechanisms within different subcellular compartments (51). Thus, the co-operation between MCPIP-1 and roquin remains incompletely understood. In different cell types, MCPIP-1 recognizes and degrades target mRNAs may be cell-specific.

To date, MCPIP-1-dependent degradation of inflammatory mRNAs has been increasingly identified. In addition to IL-6 and IL-1β, mRNAs encoding for IL-2, IL-12 and IL-17 have been identified as direct targets of MCPIP-1 (51, 52). Both CXCL1 and CXCL2, two important chemokines contributing to early stage neutrophil recruitment during tissue inflammation (53), are also direct targets of MCPIP-1 (51). MCPIP-1 also degrades mRNAs encoding T-cell co-stimulatory receptors such as ICOS, TNFR2 and OX40 as well as T-cell activation marker CD44 (33), all of which play a key role in permitting T cell mature and activation. Importantly, MCPIP-1 degrades mRNA encoding for the anti-apoptotic immediate early response 3 (IER3) protein (54), resulting in apoptosis of macrophages that contributes to resolution of inflammation. Thus, MCPIP-1 controls inflammatory response not only by preventing the transcription of the inflammatory cytokines, but also by dampening of the protein expression of the inflammatory cytokines at the post-transcriptional level as well (**Figure 1**).

MCPIP-1 Regulates miRNA Processing

Emerging studies have shown that miRNAs modulate many aspects of the immune responses such as proliferation, differentiation, cell fate determination, immune cell function, and cytokine responses (55, 56). when miRNAs are aberrantly expressed they contributes to the pathogenesis of inflammatory and autoimmune diseases by regulating their cellular and molecular targets (55). Besides targeting mRNA, MCPIP-1 was shown to regulate miRNA biogenesis by counteracting Dicer, a central ribonuclease in miRNA biosynthesis (42, 57). MCPIP-1 can cleave the terminal loop of pre-miRNAs, thereby inhibiting their maturation (41). Studies have shown that miRNA-146a and miRNA-155 are specifically down-regulated by MCPIP-1 (42, 58). Both miR-146a and miR-155 have been proposed to regulate the macrophage activation by forming a combined negative and positive regulatory loop that alters NFκB activity (59). miR-155 is highly transcribed upon an inflammatory stimulus, which can amplify NFκB activity, while as an inflammatory response develops, miR-146a levels accumulate, which causes suppression of IRAK1 and TRAF6, leading to the inhibition of NFκB activation (59). However, a study by Mino et al. indicated that expression of both miR-155 and miR-146 was not altered in mouse embryonic fibroblasts from MCPIP-1-deficient mice (51). Therefore, MCPIP appears to utilize distinct mechanisms to keep the inflammatory signaling suppressed and to re-establish immune hemostasis (**Figure 1**).

The Pro-Apoptotic Activity of MCPIP-1

Apoptosis is an evolutionarily conserved cell death program that is tightly regulated by the Bcl-2 family of proteins, which contains both pro-apoptotic and pro-survival members that balance the decision between cellular life and death (60). Microarray analysis revealed that MCPIP-1 upregulates the pro-apoptotic genes and downregulates the anti-apoptotic genes in the myocardium (9). Along this line, MCPIP-1 was found to mediate endothelial cell apoptosis and dysfunction upon MCP-1 treatment (61). The pro-apoptotic activity of MCPIP-1 was further documented *in vitro* assays in HEK 293 cells (9), H9c2 cardiomyoblasts (62), neonatal rat cardiomyocytes (63), macrophages (64, 65), neutrophils (66), T cells (67), and even cancer cells (68). Mechanistically, MCPIP-1 selectively binds and cleaves the mRNAs of anti-apoptotic genes, such as Bcl-2A1, Bcl-2L1, and RELB, leading to down-regulation of anti-apoptotic proteins and upregulation of pro-apoptotic proteins (66, 68). The inhibition of miRNA biogenesis by MCPIP-1 is also linked to its pro-apoptotic activity. MCPIP-1 has been shown to downregulate miR-3613-3p expression in neuroblastoma cells, which in turn upregulates apoptotic protease activating factor 1, causing apoptosis by caspase-9 proteolysis (69). The pro-apoptotic activity of MCPIP-1 was found to be associated with its influence on the formation of stress granules (SGs), one kind of non-membranous ribonucleoprotein complexes containing untranslated mRNA formed in response to stress exposure (70). MCPIP-1 can completely block SG formation and promote macrophage apoptosis (71).

It is well documented that the amount of reactive oxygen species (ROS) produced and the extent of oxidative stress in a cell determine the fate of the cell to die or survive (72). The pro-apoptotic activity of MCPIP-1 was strongly correlated with its ability to induce intracellular ROS that cause endoplasmic reticulum (ER) stress, resulting in autophagy and apoptosis in cardiomyocytes (62, 63), macrophages (64, 73), endothelial cells (74, 75), and in renal cell carcinoma (76). Deubiquitination of RIP1 by CYLD or A20 has been suggested to facilitate cell death (77, 78). As a new member of the deubiquitinase family, however, the role of the deubiquitinating activity of MCPIP-1 in cell death remains to be determined. While it has been reported that MG-132, a proteasome inhibitor, effectively upregulates MCPIP-1 expression, potently activating the apoptosis of cancer cells (79). Further research is needed to fully understand its significance in regulating cell death.

ROLES OF MCPIP-1 IN THE RESOLUTION OF INFLAMMATION

Resolution of inflammation is a coordinated and active process that involves the suppression of pro-inflammatory reaction,

apoptosis and subsequent clearance of activated inflammatory cells, and repolarization of macrophages towards a resolving phenotype aimed at restoration of tissue integrity and function (5, 6). As mentioned above, the functions of MCPIP-1 support the notion that MCPIP-1 has critical roles in restricting inflammation (**Figure 2**). In the following we present the experimental findings to provide an overview of MCPIP-1 that drives these resolution processes.

MCPIP-1 Restricts Virus Replication and Inflammation

Acute inflammation occurs in response to pathogen infection. This process involves the activation of innate responses that enhance innate microbial killing and clearance to protect organ structure and function (80). MCPIP-1 has been evident in cells infected with various viruses and exerts antiviral activity (23–25, 81, 82). MCPIP-1 can distinguish mRNAs from the host genome and can selectively degrade foreign mRNAs through its RNase activity (83). Indeed, MCPIP-1 is activated upon viral infections and has been shown to restrict virus replication by directly binding and subsequently degrading viral RNAs, such as JEV, IAV, DEN, coxsackievirus B3, encephalomyocarditis virus, and HIV (23, 81, 84). The deubiquitinase activity has not been shown to play a role in the antiviral effect of MCPIP-1, even though ubiquitination has been implicated in virus replication (85, 86). MCPIP-1 also restricts HCV replication by directly degrading HCV RNA and inhibits HCV-mediated expression of pro-inflammatory response (23, 24). In patients with chronic hepatitis C, the expression of MCPIP-1 in the liver has been suggested to have a protective role in antiviral responses (87). Type I interferons (IFNs) are recognized as the first line of defense against viral infection (88). MCPIP-1 has been proven to be a positive feedback amplifier of IFN signaling and promotes innate antiviral immunity independently of its RNase and deubiquitinase activities (82). Therefore, MCPIP-1 seems to be a very promising target for antiviral infections by degrading viral genomes, suppressing virus-mediated expression of pro-inflammatory cytokines or through the induction of antiviral effector molecules, resulting in the resolution of inflammation. These findings also reveal an exciting possibility for MCPIP-1 protecting against the infection caused by the SARS-CoV-2, an RNA virus that may cause severe acute respiratory distress syndrome due to "cytokine storms" induced by a hyper-activation of inflammatory cytokine response (89, 90).

MCPIP-1 Regulates Post-Ischemic Inflammation

Inflammatory response represents one of the first immune processes following ischemic injury, which is usually self-limiting, followed by tissue repair and healing responses (91, 92). Ischemic preconditioning is a well-established phenomenon, in which brief episodes of sub-lethal ischemia and reperfusion elicit strong cellular protection against the subsequently sustained ischemia in the heart and the brain (93, 94). There is increasing evidence that ischemic preconditioning induces a powerful anti-inflammatory response (94–96), which has been well illustrated by 'endotoxin tolerance' and is thought to be an adaptive response conferring protection by suppression of the hyper-activation of the innate immune system through auto-regulatory network of cytokines (94, 97). Preconditioning stimuli with low doses of LPS, a primary ligand for TLR4, provides protection against subsequent challenges with injurious focal ischemia in the brain that is similar to ischemic preconditioning (98). Diminished activation of cellular inflammatory responses to ischemia by LPS preconditioning has been suggested to play an important role for protection against ischemic injury (98, 99). In a mouse model of middle cerebral artery (MCA) occlusion, LPS induces upregulation of MCPIP-1 in the brain and the neuroprotection offered by LPS preconditioning was diminished due to MCPIP-1 deficiency, suggesting MCPIP-1 expression initiated by LPS preconditioning may be an intrinsic cellular defense mechanism against the sustained ischemic injury (100). Consistently, mice lacking MCPIP-1 showed an enhanced leakage of blood–brain barrier, increased production of cytokines and a larger infarct

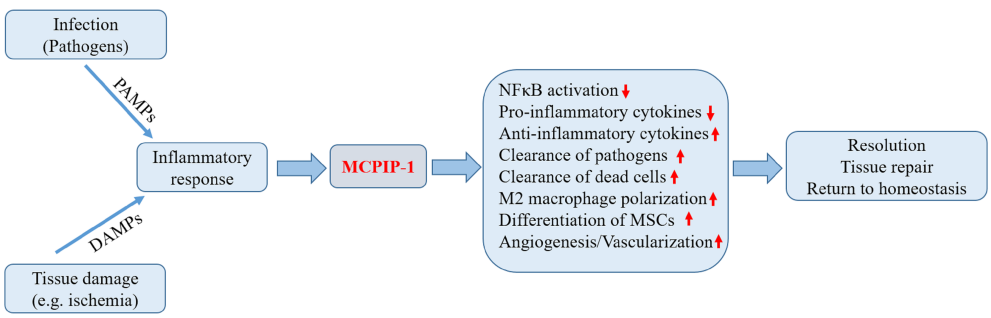

FIGURE 2 | Biological roles of MCPIP-1 associated with resolution of inflammation. During the early phase of inflammation, inflammatory response initiated by infection or tissue injury activates the endogenous defense mechanisms aimed to bring about proper resolution. The expression of MCPIP-1 induced by the inflammatory response modulates a wide range of cellular and molecular events associated with the resolution of inflammation. The expression of MCPIP-1 results in the suppression of NFκB activation and reduced pro-inflammatory cytokines. MCPIP-1 is able to induce apoptosis of infected or damaged cells, leading to their clearance by macrophages. In addition, MCPIP-1 promotes M2 macrophage polarization and enhances angiogenic differentiation of mesenchymal stem cells (MSCs). These events will create a favorable environment contributing to the resolution and tissue homeostasis.

volume after MCA occlusion (21, 101). This scenario was further demonstrated in the heart, where cardiac-specific expression of MCPIP-1 protected against LPS-induced myocardial inflammation and dysfunction (44). Consistently, mice with cardiac-specific expression of MCPIP-1 showed cardioprotective effects against myocardial infarction, as evidenced by the improved cardiac function, mitigated interstitial myocardial fibrosis, increased apoptosis of inflammatory cells, and decreased myocardial inflammation (22). In cardiomyocytes, NFκB activity was increased in response to LPS but suppressed by forced expression of MCPIP-1, thus linking MCPIP-1 to the suppression of myocardial inflammation in response to cardiac stress (22, 44). Consistent with this findings, NFκB activity initiated by myocardial infarction was inhibited by forced expression of MCPIP-1, suggesting that the preconditioning-like effects of MCPIP-1 probably involve its ability to inhibit NFκB activation (22, 44). The murine hearts expressing MCPIP-1 also displayed lower expression of inflammation-associated miR-126,-146,-155 and -199a when compared to those seen in the wild type mice (22). Preconditioning by minocycline is a pharmacological alternative to ischemic preconditioning, which enhances neuroprotection after ischemic stroke (102). Minocycline preconditioning inhibits the inflammatory cytokine response to ischemia through preferential induction of MCPIP-1, and the protective role of minocycline was diminished in the MCPIP-1-deficient mice subjected to focal cerebral ischemia/reperfusion (I/R) injury (27). Similar findings were observed in a mouse model of myocardial I/R injury, in which minocycline attenuated myocardial I/R injury *via* upregulating MCPIP-1 that subsequently inhibited NFκB activation and pro-inflammatory cytokine secretion (28). These findings are in agreement with the previous reports that MCPIP-1 deficiency results in massive multi-organ inflammation and premature death in mice (40, 41, 43).

The mechanisms underlying the preconditioning-like cellular protection by MCPIP-1 need further investigation. MCPIP-1 is likely to alter the immune responses to the ischemic insults by limiting pro-inflammatory cytokine transcription, dampening of protein expression of pro-inflammatory cytokines, regulating synthesis of pro-inflammatory miRNAs or enhancing clearance of the infiltrated inflammatory cells (44, 100). The combination of these mechanisms may result in an effective resolution of inflammation, pointing to MCPIP-1 as a promising target for the development of new therapeutic strategies to treat post-ischemic inflammation, and therefore warrant future studies on the molecular mode of action of MCPIP-1 in inflammatory diseases.

Pleiotropic Effects of MCPIP-1 On Inflammation

Resolution of inflammation is a coordinated process that requires a tight interplay between macrophages, stem and progenitor cells, together with stromal cells to restoration of tissue integrity and function (5, 6). Beyond its anti-inflammatory activity, MCPIP-1 has also shown some beneficial pleiotropic effects, contributing to the resolution of inflammation and the restoration of tissue homeostasis.

MCPIP-1 was shown to induce angiogenesis by promoting the migration and apoptosis of human umbilical vein endothelial cells (HUVECs) and the expression of angiogenesis-related gene CDH12 and CDH19 (103). Moreover, MCPIP-1 inhibits the production of anti-angiogenetic miR-20b and miR-34a, which repress the translation of HIF-1α and SIRT-1 respectively, leading to promoting angiogenesis in the HUVECs (50). These findings agree with the animal data showing that forced expression of MCPIP-1 induces angiogenesis of bone marrow monocytic cells and accelerates post-ischemic neovascularization (104). Mesenchymal stem cells (MSCs) are candidates for cellular therapies aimed at promoting tissue repair or immunoregulation (105). MCPIP-1 was shown to increase angiogenic and cardiac differentiation capacity of bone marrow-derived MSCs, contributing to repair and regeneration of ischemic myocardium (106). Vascular endothelial and smooth muscle cells play critical roles in the stability and tonic regulation of vascular homeostasis. MCPIP-1 was shown to regulate the phenotypic switching of both endothelial and smooth muscle cells *via* suppression of synthesis of miRNAs, such as miR-126, 145, -146a, and -223 (43, 107). However, Marona et al. reported that MCPIP-1 reduces tumor vascularity in clear cell renal cell carcinoma by inhibiting the recruitment of bone marrow-derived endothelial progenitor cells (EPCs) and phosphorylation of VE-cadherin *via* the degradation of mRNAs encoding for IL8, VEGF and CXCL12 (108).

A key event required for resolution of inflammation is efferocytosis of apoptotic and necrotic cells, mostly by macrophages acquiring an alternative M2 phenotype (109). We reported the ability of MCPIP-1 to control macrophage reprogramming toward a M2 phenotype, resulting in reduced production of pro-inflammatory cytokines and increased release of anti-inflammatory and reparative mediators (16). With MCPIP-1 mutants that have only one of the two catalytic activities, both the deubiquitinase and RNase activities of MCPIP-1 were shown to play a critical role in M2 macrophage polarization (16, 110). MCPIP-1was also reported to suppress the synthesis of miR155 and upregulate miR-223 and miR-146 expression, contributing to M2 polarization (111). By its RNase activity, MCPIP-1 is capable of suppressing the expression of a group of mRNAs encoding factors involved in Th1 differentiation (36, 112). Similar effects were observed in Th17 differentiation, MCPIP-1 works cooperatively with roquin to suppress the differentiation of pro-inflammatory Th17 cells (36). IL-17, a cytokine produced by Th17 cells, has been indicated in the pathogenesis of chronic inflammatory and autoimmune diseases such as psoriasis (113). MCPIP-1 is induced by IL-17A *via* the phosphorylation of STAT3 (31) and negatively regulate IL-17-dependent inflammation through the degradation of IL-17A-induced target gene transcripts and IL-17RA mRNA (112). Ablation of MCPIP-1 in keratinocytes resulted in the upregulated expression of transcripts encoding factors related to inflammation and keratinocyte differentiation (114). Similar to the results obtained with Th17 cells, MCPIP-1 was shown to play a role in Th2 cell differentiation by dampening of Gata3 expression through the degradation of Gata3 mRNA (115). Mice lacking MCPIP-1 suffered severe airway inflammation, with increased numbers of airway Th2 cells and elevated level of IL-5 (115). These findings

suggest MCPIP-1 has pleiotropic effects that contributes to maintaining homeostasis under inflammatory conditions.

The involvement of MCPIP-1 in adipogenesis was also reported, in which MCPIP-1 was thought to induce p47phox, a critical component of NADPH oxidase that contributes to the increase of ROS, which initiates the sequential differentiation process (116, 117). Other studies, however, reported an opposite effect of MCPIP-1 on adipogenesis (118), which shows that forced expression of MCPIP-1 decreases mRNA levels of the C/EBPβ and PPARγ, two key transcription factors controlling adipogenesis, leading to the impairment of adipogenesis (118). Although the evidence described above suggests that MCPIP-1 may exhibit diverse actions according to normal or pathological conditions and the types of cells, it should be noted that most of the evidence regarding the pleiotropic effects of MCPIP-1 were observed *in vitro*. In addition, most of the studies dissecting the effects of MCPIP-1 were associative and further investigations are warranted to address the pleiotropic effects of MCPIP-1.

ROLES OF MCPIP-2, -3, AND -4 IN THE REGULATION OF INFLAMMATION

Compared to MCPIP-1, the biological roles played by other three members of the Zc3h12 family are less characterized, although it appears that these members are also involved in inflammatory processes. Similar to MCPIP-1, MCPIP-2 has been shown to regulate the course of inflammation. MCPIP-2 participates in the degradation of IL-6 mRNA, resulting in reduced production of IL-6 protein upon stimulation with IL-1β (119). MCPIP-2 also interacts with other known substrates of MCPIP-1 and MCPIP-4, such as the 3'UTR of IER3 mRNA, leading to the degradation of the target mRNAs (119). In a separate study by Huang et al. (120) indicated that IL-6 mRNA is not a direct target of MCPIP-2, which could not exclusively attributable to the different cell line used. In addition, Suzuki et al. (42) showed that MCPIP-2 lacks the miRNA silencing activity, which is attributed to the lack of the proline-rich domain important for this activity. The biological roles of MCPIP-2 remain completely unknown, and further investigations are warranted to address this issue.

MCPIP-3 also contains an RNase domain at the N-terminus before the CCCH-zinc finger domain. Liu et al. (121) showed that MCPIP-3 is able to inhibit the endothelial cell inflammatory response *in vitro* by suppressing NFκB activation in human endothelial cells. Mice with MCPIP-3 deficiency developed hypertrophic lymph nodes and a higher proportion of immature B cells and innate immune cells, particularly macrophages, by regulating IFN signaling (122). Like MCPIP-1, MCPIP-3 is an RNase essential for immune homeostasis, which binds, degrades and regulates mRNAs, such as MCPIP-1 and IL-6, as observed by reduction in luciferase activity (123). Further comparative structural analysis of MCPIP-3 suggests that the RNA substrate is cooperatively recognized by the PIN and Zinc finger domains of MCPIP-3 (123). Unlike MCPIP-1, MCPIP-3 is specifically expressed in macrophages and is transcriptionally controlled by IFN signaling (122). In humans, MCPIP-3 has been linked with chronic immune disorders like psoriasis *via* regulating TNFα and Th1 activation (124, 125). Recently, Liu et al. reported that MCPIP-3 expression is positively associated with psoriasisform lesions, and highly expressed in macrophages and plasmacytoid dendritic cells (126). In the same study, the authors demonstrated that MCPIP-3 may promote TNFα/IL-12 *via* the degradation of MCPIP-1 and IL-6 *via* direct mRNA degradation, contributing to psoriatic skin inflammation. Consistently, mice with MCPIP-3 deficiency are protected from imiquimod-induced psoriasiform lesions. These data suggest that MCPIP-3 could be a potential inhibitory target to treat psoriasis and other autoimmune diseases (126).

MCPIP-4 was originally reported as a putative tumor suppressor that is deregulated in transformed follicular lymphoma in human (127). A single nucleotide polymorphism analysis indicated that MCPIP-4 is associated with the suppression of tumor cell growth both *in vitro* and *in vivo* (128). Similar to MCPIP-1, the expression of MCPIP-4 was markedly induced by TLR ligands through the activation of JNK and NFκB signal pathways, while forced expression of MCPIP-4 inhibited the activation of JNK, ERK, and NFκB signaling in macrophages (129). The latter is achieved by the inhibition of global protein ubiquitination, a key event in the regulation of NFκB activation, suggesting MCPIP-4 is a novel negative feedback regulator of TLR signaling and macrophage activation (129). MCPIP-4 also participates in the degradation of pro-inflammatory mRNAs, such as the mRNAs of IL-2, IL-6, IL-10, TNFα, IER3, and MCPIP-1 (130, 131). Mechanistically, it was demonstrated that MCPIP-4 interacts with MCPIP-1 to form a protein complex, but acts independently in the regulation of IL-6 mRNA degradation (120). To test the *in vivo* effect of MCPIP-4 in determining host immunity, Minagawa et al. generated a model with MCPIP-4 deletion in mice that displayed normal phenotypes under normal condition, but exhibited more activated lymphocytes, particularly Th17 cells, upon inflammatory stimulation (132). In experimental autoimmune encephalitis induced in the MCPIP-4-deficient mice, a higher proportion of Th17 cells with increased IL-17A mRNA levels were observed in the brain of MCPIP-4 deficient mice than did those in MCPIP-4 wild-type mice, suggesting MCPIP-4 may suppress excessive inflammation in the brain by inhibiting the infiltration and activation of Th17 cells in the experimental autoimmune encephalitis (132).

CONCLUSIONS AND PERSPECTIVES

In this review, we summarized the relevant literature about the role of MCPIP family proteins, in particular MCPIP-1, in the regulation of inflammatory response in different stress conditions. *In vivo* and *in vitro* studies revealed that MCPIP-1 expression by immune and non-immune cells contributes to the resolution of inflammation through distinct cellular and molecular programs. Overall, the expression of MCPIP-1 may be a promising target for the prevention and treatment of inflammatory disorders. Besides its crucial role the regulation

of inflammation, MCPIP-1 appeared to play a significant role in diverse cellular functions in a variety of cell types, including macrophages, T cells, MSCs, endothelial progenitor cells and adipocytes, as we discussed above in this review. Macrophages are a major source of active inflammation associated with various chronic inflammatory diseases, such as cardiovascular disease, obesity, atherosclerosis, bone loss, and cancer. Understanding how MCPIP-1 regulates macrophage phenotype and modulates nflammatory response may offer promising opportunities for the development of novel therapeutic approach for these disorders. In addition, MCPIP-1 processes antiviral cellular response by degrading the genomic nucleic acids of both positive-sense and negative-sense RNA viruses and DNA viruses. There is a clear potential for MCPIP-1 to be considered as a therapeutic target to prevent the deleterious effects of cytokine storms caused by SARS–CoV−2 infection, although much remains to be investigated. On the other hand, other MCPIP members appear to be involved in the regulation of inflammatory processes. Additional studies are needed to elucidate the effects of other members on the regulation of inflammation, which would include the crosstalk of the proteins from this family and the mechanisms of their actions, especially those related to the resolution of inflammation. Finally, it should be assessed in the future whether the modulation of these proteins should contribute to the discovery of new pharmacological targets that allow us to design specific strategies to resolve inflammation, especially in the context of acute or chronic inflammatory diseases.

AUTHOR CONTRIBUTIONS

ZJ wrote the manuscript. EZ conducted literature collection and summary. JN prepared the final version of the manuscript. CS and PK critically reviewed the manuscript. All authors contributed to the article and approved the submitted version.

FUNDING

This work was supported in part by the National Natural Science Foundation of China (Grant No. 81774010).

ACKNOWLEDGMENTS

We apologize to those investigators whose work was not cited due to space constraints.

REFERENCES

1. Amarante-Mendes GP, Adjemian S, Branco LM, Zanetti LC, Weinlich R, Bortoluci KR. Pattern Recognition Receptors and the Host Cell Death Molecular Machinery. *Front Immunol* (2018) 9:2379. doi: 10.3389/fimmu.2018.02379
2. Kelley N, Jeltema D, Duan Y, He Y. The NLRP3 Inflammasome: An Overview of Mechanisms of Activation and Regulation. *Int J Mol Sci* (2019) 20(13):3328. doi: 10.3390/ijms20133328
3. Liu T, Zhang L, Joo D, Sun SC. NF-kappaB Signaling in Inflammation. *Signal Transduct Target Ther* (2017) 2:17023. doi: 10.1038/sigtrans.2017.23
4. Chen L, Deng H, Cui H, Fang J, Zuo Z, Deng J, et al. Inflammatory Responses and Inflammation-Associated Diseases in Organs. *Oncotarget* (2018) 9(6):7204–18. doi: 10.18632/oncotarget.23208
5. Sugimoto MA, Sousa LP, Pinho V, Perretti M, Teixeira MM. Resolution of Inflammation: What Controls Its Onset? *Front Immunol* (2016) 7:160. doi: 10.3389/fimmu.2016.00160
6. Serhan CN, Savill J. Resolution of Inflammation: The Beginning Programs the End. *Nat Immunol* (2005) 6(12):1191–7. doi: 10.1038/ni1276
7. Coornaert B, Carpentier I, Beyaert R. A20: Central Gatekeeper in Inflammation and Immunity. *J Biol Chem* (2009) 284(13):8217–21. doi: 10.1074/jbc.R800032200
8. Liu J, Cao X. Cellular and Molecular Regulation of Innate Inflammatory Responses. *Cell Mol Immunol* (2016) 13(6):711–21. doi: 10.1038/cmi.2016.58
9. Zhou L, Azfer A, Niu J, Graham S, Choudhury M, Adamski FM, et al. Monocyte Chemoattractant Protein-1 Induces a Novel Transcription Factor That Causes Cardiac Myocyte Apoptosis and Ventricular Dysfunction. *Circ Res* (2006) 98(9):1177–85. doi: 10.1161/01.RES.0000220106.64661.71
10. Uehata T, Takeuchi O. Regnase-1 Is an Endoribonuclease Essential for the Maintenance of Immune Homeostasis. *J Interferon Cytokine Res* (2017) 37(5):220–9. doi: 10.1089/jir.2017.0001
11. Liang J, Wang J, Azfer A, Song W, Tromp G, Kolattukudy PE, et al. A Novel CCCH-Zinc Finger Protein Family Regulates Proinflammatory Activation of Macrophages. *J Biol Chem* (2008) 283(10):6337–46. doi: 10.1074/jbc.M707861200
12. Xu J, Peng W, Sun Y, Wang X, Xu Y, Li X, et al. Structural Study of MCPIP1 N-Terminal Conserved Domain Reveals a PIN-Like RNase. *Nucleic Acids Res* (2012) 40(14):6957–65. doi: 10.1093/nar/gks359
13. Mao R, Yang R, Chen X, Harhaj EW, Wang X, Fan Y. Regnase-1, a Rapid Response Ribonuclease Regulating Inflammation and Stress Responses. *Cell Mol Immunol* (2017) 14(5):412–22. doi: 10.1038/cmi.2016.70
14. Uehata T, Akira S. mRNA Degradation by the Endoribonuclease Regnase-1/ZC3H12a/MCPIP-1. *Biochim Biophys Acta* (2013) 1829(6-7):708–13. doi: 10.1016/j.bbagrm.2013.03.001
15. Schett G, Neurath MF. Resolution of Chronic Inflammatory Disease: Universal and Tissue-Specific Concepts. *Nat Commun* (2018) 9(1):3261. doi: 10.1038/s41467-018-05800-6
16. Kapoor N, Niu J, Saad Y, Kumar S, Sirakova T, Becerra E, et al. Transcription Factors STAT6 and KLF4 Implement Macrophage Polarization *via* the Dual Catalytic Powers of MCPIP. *J Immunol* (2015) 194(12):6011–23. doi: 10.4049/jimmunol.1402797
17. Li Y, Huang X, Huang S, He H, Lei T, Saaoud F, et al. Central Role of Myeloid MCPIP1 in Protecting Against LPS-Induced Inflammation and Lung Injury. *Signal Transduct Target Ther* (2017) 2:17066. doi: 10.1038/sigtrans.2017.66
18. Cui X, Mino T, Yoshinaga M, Nakatsuka T, Hia F, Yamasoba D, et al. Regnase-1 and Roquin Nonredundantly Regulate Th1 Differentiation Causing Cardiac Inflammation and Fibrosis. *J Immunol* (2017) 199(12):4066–77. doi: 10.4049/jimmunol.1701211
19. Mizgalska D, Wegrzyn P, Murzyn K, Kasza A, Koj A, Jura J, et al. Interleukin-1-Inducible MCPIP Protein has Structural and Functional Properties of RNase and Participates in Degradation of IL-1beta mRNA. *FEBS J* (2009) 276(24):7386–99. doi: 10.1111/j.1742-4658.2009.07452.x
20. Dhamija S, Winzen R, Doerrie A, Behrens G, Kuehne N, Schauerte C, et al. Interleukin-17 (IL-17) and IL-1 Activate Translation of Overlapping Sets of mRNAs, Including That of the Negative Regulator of Inflammation, MCPIP1. *J Biol Chem* (2013) 288(26):19250–9. doi: 10.1074/jbc.M113.452649
21. Jin Z, Liang J, Wang J, Kolattukudy PE. Delayed Brain Ischemia Tolerance Induced by Electroacupuncture Pretreatment Is Mediated *via* MCP-Induced Protein 1. *J Neuroinflamm* (2013) 10:63. doi: 10.1186/1742-2094-10-63
22. Niu J, Jin Z, Kim H, Kolattukudy PE. MCP-1-Induced Protein Attenuates Post-Infarct Cardiac Remodeling and Dysfunction Through Mitigating NF-kappaB Activation and Suppressing Inflammation-Associated microRNA Expression. *Basic Res Cardiol* (2015) 110(3):26. doi: 10.1007/s00395-015-0483-8

23. Lin RJ, Chien HL, Lin SY, Chang BL, Yu HP, Tang WC, et al. MCPIP1 Ribonuclease Exhibits Broad-Spectrum Antiviral Effects Through Viral RNA Binding and Degradation. *Nucleic Acids Res* (2013) 41(5):3314–26. doi: 10.1093/nar/gkt019
24. Lin RJ, Chu JS, Chien HL, Tseng CH, Ko PC, Mei YY, et al. MCPIP1 Suppresses Hepatitis C Virus Replication and Negatively Regulates Virus-Induced Proinflammatory Cytokine Responses. *J Immunol* (2014) 193 (8):4159–68. doi: 10.4049/jimmunol.1400337
25. Li M, Yang J, Zhao Y, Song Y, Yin S, Guo J, et al. MCPIP1 Inhibits Hepatitis B Virus Replication by Destabilizing Viral RNA and Negatively Regulates the Virus-Induced Innate Inflammatory Responses. *Antiviral Res* (2020) 174:104705. doi: 10.1016/j.antiviral.2020.104705
26. Liu XX, Wang C, Huang SF, Chen Q, Hu YF, Zhou L, et al. Regnase-1 in Microglia Negatively Regulates High Mobility Group Box 1-Mediated Inflammation and Neuronal Injury. *Sci Rep* (2016) 6:24073. doi: 10.1038/srep24073
27. Jin Z, Liang J, Wang J, Kolattukudy PE. MCP-Induced Protein 1 Mediates the Minocycline-Induced Neuroprotection Against Cerebral Ischemia/Reperfusion Injury *In Vitro* and *In Vivo*. *J Neuroinflamm* (2015) 12:39. doi: 10.1186/s12974-015-0264-1
28. Yi Q, Tan FH, Tan JA, Chen XH, Xiao Q, Liu YH, et al. Minocycline Protects Against Myocardial Ischemia/Reperfusion Injury in Rats by Upregulating MCPIP1 to Inhibit NF-kappaB Activation. *Acta Pharmacol Sin* (2019) 40 (8):1019–28. doi: 10.1038/s41401-019-0214-z
29. Skalniak L, Mizgalska D, Zarebski A, Wyrzykowska P, Koj A, Jura J. Regulatory Feedback Loop Between NF-kappaB and MCP-1-Induced Protein 1 RNase. *FEBS J* (2009) 276(20):5892–905. doi: 10.1111/j.1742-4658.2009.07273.x
30. Kasza A, Wyrzykowska P, Horwacik I, Tymoszuk P, Mizgalska D, Palmer K, et al. Transcription Factors Elk-1 and SRF Are Engaged in IL1-Dependent Regulation of ZC3H12A Expression. *BMC Mol Biol* (2010) 11:14. doi: 10.1186/1471-2199-11-14
31. Ruiz-Romeu E, Ferran M, Gimenez-Arnau A, Bugara B, Lipert B, Jura J, et al. MCPIP1 RNase Is Aberrantly Distributed in Psoriatic Epidermis and Rapidly Induced by IL-17a. *J Invest Dermatol* (2016) 136(8):1599–607. doi: 10.1016/j.jid.2016.04.030
32. Yao H, Ma R, Yang L, Hu G, Chen X, Duan M, et al. MiR-9 Promotes Microglial Activation by Targeting MCPIP1. *Nat Commun* (2014) 5:4386. doi: 10.1038/ncomms5386
33. Uehata T, Iwasaki H, Vandenbon A, Matsushita K, Hernandez-Cuellar E, Kuniyoshi K, et al. Malt1-Induced Cleavage of Regnase-1 in CD4(+) Helper T Cells Regulates Immune Activation. *Cell* (2013) 153(5):1036–49. doi: 10.1016/j.cell.2013.04.034
34. Wawro M, Kochan J, Kasza A. The Perplexities of the ZC3H12A self-mRNA Regulation. *Acta Biochim Pol* (2016) 63(3):411–5. doi: 10.18388/abp.2016_1325
35. Iwasaki H, Takeuchi O, Teraguchi S, Matsushita K, Uehata T, Kuniyoshi K, et al. The IkappaB Kinase Complex Regulates the Stability of Cytokine-Encoding mRNA Induced by TLR-IL-1R by Controlling Degradation of Regnase-1. *Nat Immunol* (2011) 12(12):1167–75. doi: 10.1038/ni.2137
36. Jeltsch KM, Hu D, Brenner S, Zoller J, Heinz GA, Nagel D, et al. Cleavage of Roquin and Regnase-1 by the Paracaspase MALT1 Releases Their Cooperatively Repressed Targets to Promote T(H)17 Differentiation. *Nat Immunol* (2014) 15(11):1079–89. doi: 10.1038/ni.3008
37. Chan FK, Luz NF, Moriwaki K. Programmed Necrosis in the Cross Talk of Cell Death and Inflammation. *Annu Rev Immunol* (2015) 33:79–106. doi: 10.1146/annurev-immunol-032414-112248
38. Koenig U, Robenek H, Barresi C, Brandstetter M, Resch GP, Groger M, et al. Cell Death Induced Autophagy Contributes to Terminal Differentiation of Skin and Skin Appendages. *Autophagy* (2020) 16(5):932–45. doi: 10.1080/15548627.2019.1646552
39. Yokogawa M, Tsushima T, Noda NN, Kumeta H, Enokizono Y, Yamashita K, et al. Structural Basis for the Regulation of Enzymatic Activity of Regnase-1 by Domain-Domain Interactions. *Sci Rep* (2016) 6:22324. doi: 10.1038/srep22324
40. Matsushita K, Takeuchi O, Standley DM, Kumagai Y, Miyake T, Satoh T, et al. Zc3h12a Is an RNase Essential for Controlling Immune Responses by Regulating mRNA Decay. *Nature* (2009) 458(7242):1185–90. doi: 10.1038/nature07924
41. Liang J, Saad Y, Lei T, Wang J, Qi D, Yang Q, et al. MCP-Induced Protein 1 Deubiquitinates TRAF Proteins and Negatively Regulates JNK and NF-kappaB Signaling. *J Exp Med* (2010) 207(13):2959–73. doi: 10.1084/jem.20092641
42. Suzuki HI, Arase M, Matsuyama H, Choi YL, Ueno T, Mano H, et al. MCPIP1 Ribonuclease Antagonizes Dicer and Terminates microRNA Biogenesis Through Precursor microRNA Degradation. *Mol Cell* (2011) 44 (3):424–36. doi: 10.1016/j.molcel.2011.09.012
43. Jin Z, Niu J, Kapoor N, Liang J, Becerra E, Kolattukudy PE. Essential Role of Endothelial MCPIP in Vascular Integrity and Post-Ischemic Remodeling. *Int J Mol Sci* (2019) 20(1):172. doi: 10.3390/ijms20010172
44. Niu J, Wang K, Graham S, Azfer A, Kolattukudy PE. MCP-1-Induced Protein Attenuates Endotoxin-Induced Myocardial Dysfunction by Suppressing Cardiac NF-Small Ka, CyrillicB Activation *via* Inhibition of Ismall Ka, CyrillicB Kinase Activation. *J Mol Cell Cardiol* (2011) 51(2):177–86. doi: 10.1016/j.yjmcc.2011.04.018
45. Hu H, Sun SC. Ubiquitin Signaling in Immune Responses. *Cell Res* (2016) 26 (4):457–83. doi: 10.1038/cr.2016.40
46. Wu Y, Kang J, Zhang L, Liang Z, Tang X, Yan Y, et al. Ubiquitination Regulation of Inflammatory Responses Through NF-kappaB Pathway. *Am J Transl Res* (2018) 10(3):881–91.
47. Kolattukudy PE, Niu J. Inflammation, Endoplasmic Reticulum Stress, Autophagy, and the Monocyte Chemoattractant Protein-1/CCR2 Pathway. *Circ Res* (2012) 110(1):174–89. doi: 10.1161/CIRCRESAHA.111.243212
48. Sato S, Sanjo H, Takeda K, Ninomiya-Tsuji J, Yamamoto M, Kawai T, et al. Essential Function for the Kinase TAK1 in Innate and Adaptive Immune Responses. *Nat Immunol* (2005) 6(11):1087–95. doi: 10.1038/ni1255
49. Niu J, Shi Y, Xue J, Miao R, Huang S, Wang T, et al. USP10 Inhibits Genotoxic NF-kappaB Activation by MCPIP1-Facilitated Deubiquitination of NEMO. *EMBO J* (2013) 32(24):3206–19. doi: 10.1038/emboj.2013.247
50. Roy A, Zhang M, Saad Y, Kolattukudy PE. Antidicer RNAse Activity of Monocyte Chemotactic Protein-Induced Protein-1 Is Critical for Inducing Angiogenesis. *Am J Physiol Cell Physiol* (2013) 305(10):C1021–32. doi: 10.1152/ajpcell.00203.2013
51. Mino T, Murakawa Y, Fukao A, Vandenbon A, Wessels H, Ori D, et al. Regnase-1 and Roquin Regulate a Common Element in Inflammatory mRNAs by Spatiotemporally Distinct Mechanisms. *Cell* (2015) 161 (5):1058–73. doi: 10.1016/j.cell.2015.04.029
52. Li M, Cao W, Liu H, Zhang W, Liu X, Cai Z, et al. MCPIP1 Down-Regulates IL-2 Expression Through an ARE-Independent Pathway. *PloS One* (2012) 7 (11):e49841. doi: 10.1371/journal.pone.0049841
53. De Filippo K, Dudeck A, Hasenberg M, Nye E, Rooijen NV, Hartmann K, et al. Mast Cell and Macrophage Chemokines CXCL1/CXCL2 Control the Early Stage of Neutrophil Recruitment During Tissue Inflammation. *Blood* (2013) 121(24):4930–7. doi: 10.1182/blood-2013-02-486217
54. Kochan J, Wawro M, Kasza A. IF-Combined smRNA FISH Reveals Interaction of MCPIP1 Protein With IER3 mRNA. *Biol Open* (2016) 5 (7):889–98. doi: 10.1242/bio.018010
55. Singh RP, Massachi I, Manickavel S, Singh S, Rao NP, Hasan S, et al. The Role of miRNA in Inflammation and Autoimmunity. *Autoimmun Rev* (2013) 12(12):1160–5. doi: 10.1016/j.autrev.2013.07.003
56. Zhou X, Li X, Wu M. miRNAs Reshape Immunity and Inflammatory Responses in Bacterial Infection. *Signal Transduct Target Ther* (2018) 3:14. doi: 10.1038/s41392-018-0006-9
57. Song MS, Rossi JJ. Molecular Mechanisms of Dicer: Endonuclease and Enzymatic Activity. *Biochem J* (2017) 474(10):1603–18. doi: 10.1042/BCJ20160759
58. Qu B, Cao J, Zhang F, Cui H, Teng J, Li J, et al. Type I Interferon Inhibition of MicroRNA-146a Maturation Through Up-Regulation of Monocyte Chemotactic Protein-Induced Protein 1 in Systemic Lupus Erythematosus. *Arthritis Rheumatol* (2015) 67(12):3209–18. doi: 10.1002/art.39398
59. Mann M, Mehta A, Zhao JL, Lee K, Marinov GK, Garcia-Flores Y, et al. An NF-kappaB-microRNA Regulatory Network Tunes Macrophage Inflammatory Responses. *Nat Commun* (2017) 8(1):851. doi: 10.1038/s41467-017-00972-z
60. Singh R, Letai A, Sarosiek K. Regulation of Apoptosis in Health and Disease: The Balancing Act of BCL-2 Family Proteins. *Nat Rev Mol Cell Biol* (2019) 20(3):175–93. doi: 10.1038/s41580-018-0089-8

61. He M, Liang X, He L, Wen W, Zhao S, Wen L, et al. Endothelial Dysfunction in Rheumatoid Arthritis: The Role of Monocyte Chemotactic Protein-1-Induced Protein. *Arterioscler Thromb Vasc Biol* (2013) 33(6):1384–91. doi: 10.1161/ATVBAHA.113.301490
62. Younce CW, Kolattukudy PE. MCP-1 Causes Cardiomyoblast Death *via* Autophagy Resulting From ER Stress Caused by Oxidative Stress Generated by Inducing a Novel Zinc-Finger Protein, MCPIP. *Biochem J* (2010) 426 (1):43–53. doi: 10.1042/BJ20090976
63. Younce CW, Wang K, Kolattukudy PE. Hyperglycaemia-Induced Cardiomyocyte Death Is Mediated *via* MCP-1 Production and Induction of a Novel Zinc-Finger Protein MCPIP. *Cardiovasc Res* (2010) 87(4):665–74. doi: 10.1093/cvr/cvq102
64. Wang X, Zhang Y, Zhang W, Liu H, Zhou Z, Dai X, et al. MCPIP1 Regulates Alveolar Macrophage Apoptosis and Pulmonary Fibroblast Activation After *In Vitro* Exposure to Silica. *Toxicol Sci* (2016) 151(1):126–38. doi: 10.1093/toxsci/kfw029
65. Shu S, Zhang Y, Li W, Wang L, Wu Y, Yuan Z, et al. The Role of Monocyte Chemotactic Protein-Induced Protein 1 (MCPIP1) in Angiotensin II-Induced Macrophage Apoptosis and Vulnerable Plaque Formation. *Biochem Biophys Res Commun* (2019) 515(2):378–85. doi: 10.1016/j.bbrc.2019.05.145
66. Dobosz E, Wadowska M, Kaminska M, Wilamowski M, Honarpisheh M, Bryzek D, et al. MCPIP-1 Restricts Inflammation *via* Promoting Apoptosis of Neutrophils. *Front Immunol* (2021) 12:627922. doi: 10.3389/fimmu.2021.627922
67. Wei J, Long L, Zheng W, Dhungana Y, Lim SA, Guy C, et al. Targeting REGNASE-1 Programs Long-Lived Effector T Cells for Cancer Therapy. *Nature* (2019) 576(7787):471–6. doi: 10.1038/s41586-019-1821-z
68. Lu W, Ning H, Gu L, Peng H, Wang Q, Hou R, et al. MCPIP1 Selectively Destabilizes Transcripts Associated With an Antiapoptotic Gene Expression Program in Breast Cancer Cells That Can Elicit Complete Tumor Regression. *Cancer Res* (2016) 76(6):1429–40. doi: 10.1158/0008-5472.CAN-15-1115
69. Boratyn E, Nowak I, Horwacik I, Durbas M, Mistarz A, Kukla M, et al. Monocyte Chemoattractant Protein-Induced Protein 1 Overexpression Modulates Transcriptome, Including MicroRNA, in Human Neuroblastoma Cells. *J Cell Biochem* (2016) 117(3):694–707. doi: 10.1002/jcb.25354
70. Kedersha N, Anderson P. Mammalian Stress Granules and Processing Bodies. *Methods Enzymol* (2007) 431:61–81. doi: 10.1016/S0076-6879(07)31005-7
71. Qi D, Huang S, Miao R, She ZG, Quinn T, Chang Y, et al. Monocyte Chemotactic Protein-Induced Protein 1 (MCPIP1) Suppresses Stress Granule Formation and Determines Apoptosis Under Stress. *J Biol Chem* (2011) 286(48):41692–700. doi: 10.1074/jbc.M111.276006
72. Circu ML, Aw TY. Reactive Oxygen Species, Cellular Redox Systems, and Apoptosis. *Free Radic Biol Med* (2010) 48(6):749–62. doi: 10.1016/j.freeradbiomed.2009.12.022
73. Liu H, Fang S, Wang W, Cheng Y, Zhang Y, Liao H, et al. Macrophage-Derived MCPIP1 Mediates Silica-Induced Pulmonary Fibrosis *via* Autophagy. *Part Fibre Toxicol* (2016) 13(1):55. doi: 10.1186/s12989-016-0167-z
74. Chao J, Wang X, Zhang Y, Zhu T, Zhang W, Zhou Z, et al. Role of MCPIP1 in the Endothelial-Mesenchymal Transition Induced by Silica. *Cell Physiol Biochem* (2016) 40(1-2):309–25. doi: 10.1159/000452547
75. Xie X, Zhu T, Chen L, Ding S, Chu H, Wang J, et al. MCPIP1-Induced Autophagy Mediates Ischemia/Reperfusion Injury in Endothelial Cells *via* HMGB1 and CaSR. *Sci Rep* (2018) 8(1):1735. doi: 10.1038/s41598-018-20195-6
76. Lee CH, Hung PF, Lu SC, Chung HL, Chiang SL, Wu CT, et al. MCP-1/MCPIP-1 Signaling Modulates the Effects of IL-1beta in Renal Cell Carcinoma Through ER Stress-Mediated Apoptosis. *Int J Mol Sci* (2019) 20(23):6101. doi: 10.3390/ijms20236101
77. Ganjam GK, Terpolilli NA, Diemert S, Eisenbach I, Hoffmann L, Reuther C, et al. Cylindromatosis Mediates Neuronal Cell Death *In Vitro* and *In Vivo*. *Cell Death Differ* (2018) 25(8):1394–407. doi: 10.1038/s41418-017-0046-7
78. Garcia-Carbonell R, Wong J, Kim JY, Close LA, Boland BS, Wong TL, et al. Elevated A20 Promotes TNF-Induced and RIPK1-Dependent Intestinal Epithelial Cell Death. *Proc Natl Acad Sci U S A* (2018) 115(39):E9192–200. doi: 10.1073/pnas.1810584115
79. Skalniak L, Koj A, Jura J. Proteasome Inhibitor MG-132 Induces MCPIP1 Expression. *FEBS J* (2013) 280(11):2665–74. doi: 10.1111/febs.12264
80. Serhan CN. Treating Inflammation and Infection in the 21st Century: New Hints From Decoding Resolution Mediators and Mechanisms. *FASEB J* (2017) 31(4):1273–88. doi: 10.1096/fj.201601222R
81. Liu S, Qiu C, Miao R, Zhou J, Lee A, Liu B, et al. MCPIP1 Restricts HIV Infection and Is Rapidly Degraded in Activated CD4+ T Cells. *Proc Natl Acad Sci U S A* (2013) 110(47):19083–8. doi: 10.1073/pnas.1316208110
82. Qian L, Zuo Y, Deng W, Miao Y, Liu J, Yuan Y, et al. MCPIP1 Is a Positive Regulator of Type I Interferons Antiviral Activity. *Biochem Biophys Res Commun* (2018) 498(4):891–7. doi: 10.1016/j.bbrc.2018.03.076
83. Qian Y, Li X, Miao R, Liu S, Xin HB, Huang X, et al. Selective Degradation of Plasmid-Derived mRNAs by MCPIP1 RNase. *Biochem J* (2019) 476 (19):2927–38. doi: 10.1042/BCJ20190646
84. Li M, Yan K, Wei L, Yang Y, Qian Q, Xu W. MCPIP1 Inhibits Coxsackievirus B3 Replication by Targeting Viral RNA and Negatively Regulates Virus-Induced Inflammation. *Med Microbiol Immunol* (2018) 207 (1):27–38. doi: 10.1007/s00430-017-0523-0
85. Liao TL, Wu CY, Su WC, Jeng KS, Lai MM. Ubiquitination and Deubiquitination of NP Protein Regulates Influenza A Virus RNA Replication. *EMBO J* (2010) 29(22):3879–90. doi: 10.1038/emboj.2010.250
86. Si X, Gao G, Wong J, Wang Y, Zhang J, Luo H. Ubiquitination Is Required for Effective Replication of Coxsackievirus B3. *PloS One* (2008) 3(7):e2585. doi: 10.1371/journal.pone.0002585
87. Ge D, Fellay J, Thompson AJ, Simon JS, Shianna KV, Urban TJ, et al. Genetic Variation in IL28B Predicts Hepatitis C Treatment-Induced Viral Clearance. *Nature* (2009) 461(7262):399–401. doi: 10.1038/nature08309
88. McNab F, Mayer-Barber K, Sher A, Wack A, O'Garra A. Type I Interferons in Infectious Disease. *Nat Rev Immunol* (2015) 15(2):87–103. doi: 10.1038/nri3787
89. Hirano T, Murakami M. COVID-19: A New Virus, But a Familiar Receptor and Cytokine Release Syndrome. *Immunity* (2020) 52(5):731–3. doi: 10.1016/j.immuni.2020.04.003
90. Zhou F, Yu T, Du R, Fan G, Liu Y, Liu Z, et al. Clinical Course and Risk Factors for Mortality of Adult Inpatients With COVID-19 in Wuhan, China: A Retrospective Cohort Study. *Lancet* (2020) 395(10229):1054–62. doi: 10.1016/S0140-6736(20)30566-3
91. Shichita T, Sakaguchi R, Suzuki M, Yoshimura A. Post-Ischemic Inflammation in the Brain. *Front Immunol* (2012) 3:132. doi: 10.3389/fimmu.2012.00132
92. Wu MY, Yiang GT, Liao WT, Tsai AP, Cheng YL, Cheng PW, et al. Current Mechanistic Concepts in Ischemia and Reperfusion Injury. *Cell Physiol Biochem* (2018) 46(4):1650–67. doi: 10.1159/000489241
93. Tomai F, Crea F, Chiariello L, Gioffre PA. Ischemic Preconditioning in Humans: Models, Mediators, and Clinical Relevance. *Circulation* (1999) 100 (5):559–63. doi: 10.1161/01.CIR.100.5.559
94. Smith RM, Lecour S, Sack MN. Innate Immunity and Cardiac Preconditioning: A Putative Intrinsic Cardioprotective Program. *Cardiovasc Res* (2002) 55(3):474–82. doi: 10.1016/S0008-6363(02)00288-2
95. McDonough A, Weinstein JR. Neuroimmune Response in Ischemic Preconditioning. *Neurotherapeutics* (2016) 13(4):748–61. doi: 10.1007/s13311-016-0465-z
96. Obrenovitch TP. Molecular Physiology of Preconditioning-Induced Brain Tolerance to Ischemia. *Physiol Rev* (2008) 88(1):211–47. doi: 10.1152/physrev.00039.2006
97. Sullivan PJ, Sweeney KJ, Hirpara KM, Malone CB, Curtin W, Kerin MJ. Cyclical Ischaemic Preconditioning Modulates the Adaptive Immune Response in Human Limb Ischaemia-Reperfusion Injury. *Br J Surg* (2009) 96(4):381–90. doi: 10.1002/bjs.6554
98. Rosenzweig HL, Lessov NS, Henshall DC, Minami M, Simon RP, Stenzel-Poore MP. Endotoxin Preconditioning Prevents Cellular Inflammatory Response During Ischemic Neuroprotection in Mice. *Stroke* (2004) 35 (11):2576–81. doi: 10.1161/01.STR.0000143450.04438.ae
99. Dong JW, Vallejo JG, Tzeng HP, Thomas JA, Mann DL. Innate Immunity Mediates Myocardial Preconditioning Through Toll-Like Receptor 2 and TIRAP-Dependent Signaling Pathways. *Am J Physiol Heart Circ Physiol* (2010) 298(3):H1079–1087. doi: 10.1152/ajpheart.00306.2009
100. Liang J, Wang J, Saad Y, Warble L, Becerra E. Kolattukudy PE. Participation of MCP-Induced Protein 1 in Lipopolysaccharide Preconditioning-Induced

Ischemic Stroke Tolerance by Regulating the Expression of Proinflammatory Cytokines. *J Neuroinflamm* (2011) 8:182. doi: 10.1186/1742-2094-8-182
101. Jin Z, Liang J, Li J, Kolattukudy PE. Absence of MCP-Induced Protein 1 Enhances Blood-Brain Barrier Breakdown After Experimental Stroke in Mice. *Int J Mol Sci* (2019) 20(13):3214. doi: 10.3390/ijms20133214
102. Sakata H, Niizuma K, Yoshioka H, Kim GS, Jung JE, Katsu M, et al. Minocycline-Preconditioned Neural Stem Cells Enhance Neuroprotection After Ischemic Stroke in Rats. *J Neurosci* (2012) 32(10):3462–73. doi: 10.1523/JNEUROSCI.5686-11.2012
103. Niu J, Azfer A, Zhelyabovska O, Fatma S, Kolattukudy PE. Monocyte Chemotactic Protein (MCP)-1 Promotes Angiogenesis *via* a Novel Transcription Factor, MCP-1-Induced Protein (MCPIP). *J Biol Chem* (2008) 283(21):14542–51. doi: 10.1074/jbc.M802139200
104. Niu J, Wang K, Zhelyabovska O, Saad Y, Kolattukudy PE. MCP-1-Induced Protein Promotes Endothelial-Like and Angiogenic Properties in Human Bone Marrow Monocytic Cells. *J Pharmacol Exp Ther* (2013) 347(2):288–97. doi: 10.1124/jpet.113.207316
105. Uccelli A, Moretta L, Pistoia V. Mesenchymal Stem Cells in Health and Disease. *Nat Rev Immunol* (2008) 8(9):726–36. doi: 10.1038/nri2395
106. Labedz-Maslowska A, Lipert B, Berdecka D, Kedracka-Krok S, Jankowska U, Kamycka E, et al. Monocyte Chemoattractant Protein-Induced Protein 1 (MCPIP1) Enhances Angiogenic and Cardiomyogenic Potential of Murine Bone Marrow-Derived Mesenchymal Stem Cells. *PloS One* (2015) 10(7): e0133746. doi: 10.1371/journal.pone.0133746
107. Shu B, Zhuo M, Liu Z, Lu Z, Qian M. Cholesterol Induces Dedifferentiation of Vascular Smooth Muscle Cells by Regulating Monocyte Chemotactic Protein-1-Induced Protein 1. *Int J Clin Exp Pathol* (2019) 12(9):3258–67.
108. Marona P, Gorka J, Mazurek Z, Wilk W, Rys J, Majka M, et al. MCPIP1 Downregulation in Clear Cell Renal Cell Carcinoma Promotes Vascularization and Metastatic Progression. *Cancer Res* (2017) 77 (18):4905–20. doi: 10.1158/0008-5472.CAN-16-3190
109. Watanabe S, Alexander M, Misharin AV, Budinger GRS. The Role of Macrophages in the Resolution of Inflammation. *J Clin Invest* (2019) 129 (7):2619–28. doi: 10.1172/JCI124615
110. Xu R, Li Y, Yan H, Zhang E, Huang X, Chen Q, et al. CCL2 Promotes Macrophages-Associated Chemoresistance *via* MCPIP1 Dual Catalytic Activities in Multiple Myeloma. *Cell Death Dis* (2019) 10(10):781. doi: 10.1038/s41419-019-2012-4
111. Miao R, Huang S, Zhou Z, Quinn T, Van Treeck B, Nayyar T, et al. Targeted Disruption of MCPIP1/Zc3h12a Results in Fatal Inflammatory Disease. *Immunol Cell Biol* (2013) 91(5):368–76. doi: 10.1038/icb.2013.11
112. Garg AV, Amatya N, Chen K, Cruz JA, Grover P, Whibley N, et al. MCPIP1 Endoribonuclease Activity Negatively Regulates Interleukin-17-Mediated Signaling and Inflammation. *Immunity* (2015) 43(3):475–87. doi: 10.1016/j.immuni.2015.07.021
113. Beringer A, Noack M, Miossec P. IL-17 in Chronic Inflammation: From Discovery to Targeting. *Trends Mol Med* (2016) 22(3):230–41. doi: 10.1016/j.molmed.2016.01.001
114. Konieczny P, Lichawska-Cieslar A, Kwiecinska P, Cichy J, Pietrzycka R, Szukala W, et al. Keratinocyte-Specific Ablation of Mcpip1 Impairs Skin Integrity and Promotes Local and Systemic Inflammation. *J Mol Med (Berl)* (2019) 97(12):1669–84. doi: 10.1007/s00109-019-01853-2
115. Peng H, Ning H, Wang Q, Lu W, Chang Y, Wang TT, et al. Monocyte Chemotactic Protein-Induced Protein 1 Controls Allergic Airway Inflammation by Suppressing IL-5-Producing TH2 Cells Through the Notch/Gata3 Pathway. *J Allergy Clin Immunol* (2018) 142(2):582–94. doi: 10.1016/j.jaci.2017.09.031
116. Younce CW, Azfer A, Kolattukudy PE. MCP-1 (Monocyte Chemotactic Protein-1)-Induced Protein, a Recently Identified Zinc Finger Protein, Induces Adipogenesis in 3T3-L1 Pre-Adipocytes Without Peroxisome Proliferator-Activated Receptor Gamma. *J Biol Chem* (2009) 284 (40):27620–8. doi: 10.1074/jbc.M109.025320
117. Younce C, Kolattukudy P. MCP-1 Induced Protein Promotes Adipogenesis *via* Oxidative Stress, Endoplasmic Reticulum Stress and Autophagy. *Cell Physiol Biochem* (2012) 30(2):307–20. doi: 10.1159/000339066
118. Lipert B, Wegrzyn P, Sell H, Eckel J, Winiarski M, Budzynski A, et al. Monocyte Chemoattractant Protein-Induced Protein 1 Impairs Adipogenesis in 3T3-L1 Cells. *Biochim Biophys Acta* (2014) 1843(4):780–8. doi: 10.1016/j.bbamcr.2014.01.001
119. Wawro M, Wawro K, Kochan J, Solecka A, Sowinska W, Lichawska-Cieslar A, et al. ZC3H12B/MCPIP2, a New Active Member of the ZC3H12 Family. *RNA* (2019) 25(7):840–56. doi: 10.1261/rna.071381.119
120. Huang S, Liu S, Fu JJ, et al. Monocyte Chemotactic Protein-Induced Protein 1 and 4 Form a Complex But Act Independently in Regulation of Interleukin-6 mRNA Degradation. *J Biol Chem* (2015) 290(34):20782–92. doi: 10.1074/jbc.M114.635870
121. Liu L, Zhou Z, Huang S, Tony Wang T, Yao X, Kumar A, et al. Zc3h12c Inhibits Vascular Inflammation by Repressing NF-kappaB Activation and Pro-Inflammatory Gene Expression in Endothelial Cells. *Biochem J* (2013) 451(1):55–60. doi: 10.1042/BJ20130019
122. von Gamm M, Schaub A, Jones AN, Wolf C, Behrens G, Lichti J, et al. Immune Homeostasis and Regulation of the Interferon Pathway Require Myeloid-Derived Regnase-3. *J Exp Med* (2019) 216(7):1700–23. doi: 10.1084/jem.20181762
123. Garg A, Roske Y, Yamada S, Uehata T, Takeuchi O, Heinemann U. PIN and CCCH Zn-Finger Domains Coordinate RNA Targeting in ZC3H12 Family Endoribonucleases. *Nucleic Acids Res* (2021) 49(9):5369–81. doi: 10.1093/nar/gkab316
124. Tsoi LC, Spain SL, Knight J, Ellinghaus E, Stuart PE, Capon F, et al. Identification of 15 New Psoriasis Susceptibility Loci Highlights the Role of Innate Immunity. *Nat Genet* (2012) 44(12):1341–8. doi: 10.1038/ng.2467
125. Munir S, ber Rahman S, Rehman S, Saba N, Ahmad W, Nilsson S, et al. Association Analysis of GWAS and Candidate Gene Loci in a Pakistani Population With Psoriasis. *Mol Immunol* (2015) 64(1):190–4. doi: 10.1016/j.molimm.2014.11.015
126. Liu B, Huang J, Ashraf A, Rahaman O, Lou J, Wang L, et al. The RNase MCPIP3 Promotes Skin Inflammation by Orchestrating Myeloid Cytokine Response. *Nat Commun* (2021) 12(1):4105. doi: 10.1038/s41467-021-24352-w
127. Minagawa K, Yamamoto K, Nishikawa S, Ito M, Sada A, Yakushijin K, et al. Deregulation of a Possible Tumour Suppressor Gene, ZC3H12D, by Translocation of IGK@ in Transformed Follicular Lymphoma With T(2;6)(P12;Q25). *Br J Haematol* (2007) 139(1):161–3. doi: 10.1111/j.1365-2141.2007.06752.x
128. Wang M, Vikis HG, Wang Y, Jia D, Wang D, Bierut LJ, et al. Identification of a Novel Tumor Suppressor Gene P34 on Human Chromosome 6q25.1. *Cancer Res* (2007) 67(1):93–9. doi: 10.1158/0008-5472.CAN-06-2723
129. Huang S, Qi D, Liang J, Miao R, Minagawa K, Quinn T, et al. The Putative Tumor Suppressor Zc3h12d Modulates Toll-Like Receptor Signaling in Macrophages. *Cell Signal* (2012) 24(2):569–76. doi: 10.1016/j.cellsig.2011.10.011
130. Zhang H, Wang WC, Chen JK, Zhou L, Wang M, Wang ZD, et al. ZC3H12D Attenuated Inflammation Responses by Reducing mRNA Stability of Proinflammatory Genes. *Mol Immunol* (2015) 67(2 Pt B):206–12. doi: 10.1016/j.molimm.2015.05.018
131. Wawro M, Kochan J, Krzanik S, Jura J, Kasza A. Intact NYN/PIN-Like Domain Is Crucial for the Degradation of Inflammation-Related Transcripts by ZC3H12D. *J Cell Biochem* (2017) 118(3):487–98. doi: 10.1002/jcb.25665
132. Minagawa K, Wakahashi K, Kawano H, Nishikawa S, Fukui C, Kawano Y, et al. Posttranscriptional Modulation of Cytokine Production in T Cells for the Regulation of Excessive Inflammation by TFL. *J Immunol* (2014) 192 (4):1512–24. doi: 10.4049/jimmunol.1301619

Conflict of Interest: The authors declare that the research was conducted in the absence of any commercial or financial relationships that could be construed as a potential conflict of interest.

Publisher's Note: All claims expressed in this article are solely those of the authors and do not necessarily represent those of their affiliated organizations, or those of the publisher, the editors and the reviewers. Any product that may be evaluated in this article, or claim that may be made by its manufacturer, is not guaranteed or endorsed by the publisher.

Copyright © 2021 Jin, Zheng, Sareli, Kolattukudy and Niu. This is an open-access article distributed under the terms of the Creative Commons Attribution License (CC BY). The use, distribution or reproduction in other forums is permitted, provided the original author(s) and the copyright owner(s) are credited and that the original publication in this journal is cited, in accordance with accepted academic practice. No use, distribution or reproduction is permitted which does not comply with these terms.

frontiers in Immunology

ORIGINAL RESEARCH
published: 04 October 2021
doi: 10.3389/fimmu.2021.744477

Syndecan-1 Amplifies Ovalbumin-Induced Airway Remodeling by Strengthening TGFβ1/Smad3 Action

Dong Zhang[1], *Xin-rui Qiao*[1], *Wen-Jing Cui*[1], *Jin-tao Zhang*[1], *Yun Pan*[1], *Xiao-fei Liu*[1] *and Liang Dong*[1,2]*

[1] Department of Respiratory, Shandong Qianfoshan Hospital, Cheeloo College of Medicine, Shandong University, Jinan, China, [2] Department of Respiratory, Shandong Institute of Respiratory Diseases, The First Affiliated Hospital of Shandong First Medical University, Shandong Provincial Qianfoshan Hospital, Shandong University, Jinan, China

OPEN ACCESS

Edited by:
Sylvain Perruche, Institut National de la Santé et de la Recherche Médicale (INSERM), France

Reviewed by:
Samira Alliouachene, Queen Mary University of London, United Kingdom
Michael Roth, University Hospital of Basel, Switzerland

***Correspondence:**
Liang Dong
dl5506@126.com

Specialty section:
This article was submitted to Inflammation, a section of the journal Frontiers in Immunology

Received: 20 July 2021
Accepted: 17 September 2021
Published: 04 October 2021

Citation:
Zhang D, Qiao X-r, Cui W-J, Zhang J-t, Pan Y, Liu X-f and Dong L (2021) Syndecan-1 Amplifies Ovalbumin-Induced Airway Remodeling by Strengthening TGFβ1/Smad3 Action. Front. Immunol. 12:744477. doi: 10.3389/fimmu.2021.744477

Syndecan-1 (SDC-1) is a transmembrane proteoglycan of heparin sulfate that can regulate various cell signal transduction pathways in the airway epithelial cells and fibroblasts. Airway epithelial cells and human bronchial fibroblasts are crucial in airway remodeling. However, the importance of SDC-1 in the remodeling of asthmatic airways has not been confirmed yet. The present study was the first to uncover SDC-1 overexpression in the airways of humans and mice with chronic asthma. This study also validated that an increase in SDC-1 expression was correlated with TGFβ1/Smad3-mediated airway remodeling *in vivo* and *in vitro*. A small interfering RNA targeting SDC-1 (SDC-1 siRNA) and homo-SDC-1 in pcDNA3.1 (pc-SDC-1) was designed to assess the effects of SDC-1 on TGFβ1/Smad3-mediated collagen I expression in Beas-2B (airway epithelial cells) and HLF-1 (fibroblasts) cells. Downregulation of the SDC-1 expression by SDC-1 siRNA remarkably attenuated TGFβ1-induced p-Smad3 levels and collagen I expression in Beas-2B and HLF-1 cells. In addition, SDC-1 overexpression with pc-SDC-1 enhanced TGFβ1-induced p-Smad3 level and collagen I expression in Beas-2B and HLF-1 cells. Furthermore, the levels of p-Smad3 and collagen I induced by TGFβ1 were slightly increased after the addition of the recombinant human SDC-1 protein to Beas-2B and HLF-1 cells. These findings *in vitro* were also confirmed in a mouse model. A short hairpin RNA targeting SDC-1 (SDC-1 shRNA) to interfere with SDC-1 expression considerably reduced the levels of p-Smad3 and remodeling protein (α-SMA, collagen I) in the airways induced by ovalbumin (OVA). Similarly, OVA-induced p-Smad3 and remodeling protein levels in airways increased after mice inhalation with the recombinant mouse SDC-1 protein. These results suggested that SDC-1 of airway epithelial cells and fibroblasts plays a key role in the development of airway remodeling in OVA-induced chronic asthma.

Keywords: syndecan-1, ovalbumin, airway remodeling, TGFβ1/Smad3 signaling, asthma

INTRODUCTION

Asthma is an inflammatory disease of the airways induced by allergens, gastroesophageal reflux, and genetic factors with complex pathogenesis (1). The normal structures and functions of bronchial epithelial cells and human fibroblasts are necessary to the standard functioning of lung tissues. Epithelial cells in the airways undergo interstitial transformation with disease progression, and fibroblasts are activated and differentiated into myofibroblasts (2). These cells produce numerous extracellular matrix proteins, including type I collagen and α-smooth muscle actin (α-SMA) (2). These changes in airway composition transform normal repairable injury responses to pathologic consequences, such as loss of epithelial integrity and excessive matrix deposition in interstitial, which, in turn, accelerate the structural remodeling of the airways (3).

Transforming growth factor β1 (TGFβ1), an important cytokine, mediates and regulates cellular transformation in various diseases (4). Large amounts of TGFβ1 are secreted after cell injury and other factors, which then participate in the regulation of various transcription factors and the synthesis of protein components of the extracellular matrix, thereby accelerating changes in cellular structures (5). Smad3, a member of the Smad protein family, is a TGFβ1 signaling downstream activator (6). TGFβ1/Smad3 signaling transduction plays a key regulatory role in the progression of liver fibrosis (7), pulmonary fibrosis (8), renal fibrosis (9), airway remodeling (10), cardiac structural remodeling (11), skin scar hyperplasia (12), and other diseases.

SDC-1 is a transmembrane heparin sulfate proteoglycan that carries various side chains, such as heparin sulfate (HS), chondroitin sulfate (CS), and hyaluronic acid (HA) (13). The SDC-1 core protein comprises extracellular, transmembrane, and intracellular regions (14). SDC-1 shedding has been widely studied in septic-related lung and kidney injury models (15). SDC-1 abscission is affected by many factors, such as inflammation and oxidative stress. In addition, Filla et al. (16) found that the cell surface proteoglycan SDC-1 mediates fibroblast growth factor-2 binding and activity. Hayashida et al. (17) reported that SDC-1 expression in epithelial cells can be induced by TGFβ1 through a PKA-dependent pathway. The special structural functions of SDC-1 in various physiological and pathological processes, such as cell proliferation (18), cell adhesion (19), and cell scarring (12), have been extensively studied. However, the exact role of SDC-1 in patients with asthma remains unclear.

The acute and chronic asthma models induced by OVA are respectively dominated by inflammation (20) and airway remodeling (21). SDC-1 has not been clearly described in OVA-induced acute or chronic asthma models. Therefore, the changes in SDC-1 in airway epithelium and alveolar lavage fluid (BALF) were further observed in OVA-induced acute or chronic asthma models. SDC-1 is hypothesized to be involved in airway remodeling by affecting TGFβ1/Smad3 signal transduction due to its role in regulating multiple cellular signal transduction pathways. Results suggested that SDC-1 is an important regulatory factor in the development of TGFβ1/Smad3 signal-mediated airway remodeling. Therefore, SDC-1 might be a novel therapeutic target in the pathologic form of airway remodeling in patients with asthma.

MATERIALS AND METHODS

Reagents

Ovalbumin (OVA) and 4, 6-diamino-2-phenylindole dihydrochloride (DAPI) were purchased from Sigma-Aldrich (USA). The rabbit monoclonal antibodies SDC-1, p-Smad3, Smad3, and collagen I were prepared by Abcam (USA). Meanwhile, the rabbit monoclonal antibody GAPDH, HRP-conjugated goat anti-rabbit IgG, Alexa Fluor goat anti-rabbit, recombinant human TGFβ1, recombinant mouse SDC-1, and recombinant human SDC-1 were acquired from RD Biotechnology Ltd. Small interfering RNA targeting SDC-1 (SDC-1 siRNA), homo-SDC-1 in PCDNA3.1 (pc-SDC-1), and SDC-1 short hairpin RNA (SDC-1 shRNA) were synthesized by Gene Chem Co., Ltd. (Jinan, China).

Human Subject

Human subjects were diagnosed with chronic asthma following the criteria of the 2019 Edition Global Asthma Initiative, and age-matched healthy subjects were enrolled at Qianfoshan Hospital (Jinan, China). The characteristics of patients with asthmatic and healthy subjects are shown in **Table 1**. This study was approved by the Human Research Ethics Review Committee of Qianfoshan Hospital of Shandong University.

Cell Culture and Treatment

Beas-2B and HLF-1 cells (Cell Line Bank, Shanghai, China) were cultured in different DMEM containing 10% fetal bovine serum. The cells were seeded in 6- or 24-well culture plates under the following conditions: an incubator at 37°C, 95% air, 5% CO_2, and a humid atmosphere. Serum-free synchronization was conducted for 24 h before the experiment and then used in all tests.

Beas-2B and HLF-1 cells were stimulated by 10 ng/mL TGFβ1 at different times (1, 2, 3, and 4 days), and changes in the cells were observed. The appropriate stimulating time point of TGFβ1 for Beas-2B or HLF-1 cells was selected by observing the protein levels of SDC-1, p-Smad3, Smad3, and collagen I.

The cell experiment was divided into four groups: 1) NC siRNA group: serum-free culture+siRNA negative control; 2) SDC-1 siRNA 1: cells cultured in serum-free culture and transfected with SDC-1 siRNA 1; 3) SDC-1 siRNA 2: cells cultured in serum-free culture and transfected with SDC-1 siRNA 2; 4) SDC-1 siRNA 3: cells cultured in serum-free culture and transfected with SDC-1 siRNA 3. Lipofectamine 3000 and NC siRNA or SDC-1 siRNA were added into the cell culture dishes for transfection according to the transfection manual. The SDC-1 siRNA and NC siRNA sequences were as follows: 1) SDC-1 siRNA 1: 5′-CCAAAUUGUGGCUACUAA UTT-3′; 2) SDC-1 siRNA 2: 5′-GCAGGACUUCACCUUUGAA TT-3′; 3) SDC-1 siRNA 3: 5′-CCACCAAACAGGAGGAA UUTT-3′; 4) NC siRNA: 5′-UUCUCCGAACGUGU CACGUTT-3′. The effectiveness of SDC-1 siRNA in silencing SDC-1 protein expression was used for further studies.

Cells were then further divided into five groups: 1) Control group: cells cultured in serum-free culture without any stimulus factor; 2) NC siRNA group: serum-free culture+siRNA negative control; 3) SDC-1 siRNA: cells cultured in serum-free culture

TABLE 1 | Characteristics and physiologies of asthmatic patients and the normal.

Characteristic	Normal	Asthmatic
Number	24	24
Age (years)	63.8 ± 6.4	60.7 ± 7.0
Gender (male/female)	12/12	11/13
FEV1 (% of predicted)	114.6 ± 8.5	42.3± 14.6
BDT	Negative	Positive
Past history of cough	Occasional	Always
Other diseases: COPD, lung tumors, coronary heart disease, rheumatic heart disease, allergic rhinitis, bronchitis	NO	NO

Data are depicted as means ± SD. FEV1, forced expiratory volume in one second; FEV1/FVC, the ratio of forced expiratory volume in the first second to forced vital capacity; BDT, bronchial dilation test.

and transfected with SDC-1 siRNA. 4) NC siRNA+TGFβ1 group: cells cultured in serum-free culture with 10 ng/mL TGFβ1 and transfected with NC siRNA; 5) SDC-1 siRNA+TGFβ1: cells cultured in serum-free culture with 10 ng/mL TGFβ1 and transfected with SDC-1 siRNA. Lipofectamine 3000 and NC siRNA or SDC-1 siRNA were also transfected with cells according to the transfection manual.

The experiment was further divided into the following groups to observe the effects of pc-SDC-1: 1) Control group: cultured in serum-free culture without any stimulus factor; 2) pcDNA3.1 group: serum-free culture+pcDNA3.1 negative control; 3) pc-SDC-1 group: cells cultured in serum-free culture and transfected with pc-SDC-1; 4) TGFβ1 group: cells cultured in serum-free culture with 10 ng/mL TGFβ1; 5) pc-SDC-1+TGFβ1: cells cultured in serum-free culture with 10 ng/mL TGFβ1 and transfected with pc-SDC-1 for SDC-1 overexpression. The CDS region of the NM_002997 transcript of the SDC-1 gene was constructed into the pcDNA3.1 plasmid vector (**Figure 5A**), and pcSDC-1 was transferred into cells to generate SDC-1 overexpression according to the transfection manual. The effective of pc-SDC-1 in overexpressing SDC-1 protein was used for further studies.

Then, cells were divided into the following groups to investigate the effects of human recombinant SDC-1 protein: 1) Control group; 2) TGFβ1 group; 3) TGFβ1+recombinant SDC-1 (500 ng/mL); 4) TGFβ1+recombinant SDC-1 (1000 ng/mL); 5) TGFβ1+recombinant SDC-1 (2000 ng/mL). The cells in the TGFβ1+recombinant SDC-1 groups were c-ultured with 10 ng/mL TGFβ1 and the different dosages of human recombinant SDC-1 protein.

Animals and Grouping

C57BL/6 female mice (18–20 g) were purchased from Pengyue Animal Breeding Co., Ltd. (Jinan, China). The mice were raised on an OVA-free diet without pathogens. The mice were then studied in accordance with the National Institutes of Health guidelines for the care and use of laboratory animals and approved by the Institutional Review Committee of Shandong University–Qianfoshan Hospital.

The mice were randomly divided into four groups to observe the dynamic changes in each index (n = 8/group): 1) Control-4 weeks group; 2) OVA-4 weeks group; 3) Control-8 weeks group; 4) OVA-8 weeks group. The sensitization, challenges, and atomization processes are shown in **Figure 2A**.

The Control-8 weeks and OVA-8 weeks groups were selected as the research object to further study SDC-1. The mice were randomly divided into four groups (n = 8/group): 1) Control group; 2) LV2NC group; 3) OVA group; 4) OVA+SDC-1 shRNA group. The specific process is outlined in **Figures 8A1, A2**. The LV2NC or SDC-1 shRNA sequences were as follows: 1) LV2NC: 5′-TTCTCCGAACGTGTCACACGT-3′; 2) SDC-1 shRNA: 5′-GAACAAGACTTCACCTTTGAA-3′.

Then, mice were divided into four groups to asses the effects of mouse recombinant SDC-1 protein on OVA-induced chronic asthma (n = 8/group): 1) Control group; 2) Recombinant SDC-1 group; 3) OVA group; 4) OVA+ recombinant SDC-1 group. The mice in the OVA+ recombinant SDC-1 group were inhaled with recombinant SDC-1 (2000 ng/mL) after preatment with OVA (3% g/mL). The specific process is outlined in **Figure 8A3**.

Morphological Changes in the Airways

Lung tissues were fixed with 4% paraformaldehyde for 2 days, dehydrated with alcohol, embedded with paraffin, and finally cut into 5 μm thick paraffin sections. Airway inflammation was assessed by hematoxylin and eosin staining (HE). Collagen deposition was evaluated by Masson staining. The tissue sections were scored in accordance with the method described by Mohammadtursun et al. (22).

Immunohistochemistry Assay

The 5 μm thick paraffin sections were antigenically repaired and endogenous peroxidase was removed, and then SDC-1 antibody was incubated at 4°C for 15 h. Subsequently, the lung tissue sections were washed with PBS solution and incubated with goat anti-rabbit antibody in the dark for 40 min. The lung tissue sections were washed with PBS solution and then incubated with DAB solution for 4 min. Finally, the tissue sections were dehydrated with alcohol, dewaxed until transparent with xylene, and photographed under a microscope. Protein expression was evaluated using Image J.

Western Blot Analysis

The protein samples were added to 12% SDS polyacrylamide gel for electrophoresis separation, and then the proteins were transferred to a PVDF membrane, which was incubated with 5% skim milk for 90 min at room temperature. The primary antibodies (SDC-1, p-Smad3, Smad3, collagen I, α-SMA, and GAPDH) were incubated at 4°C for 15 h after washing with TBST solution. The PVDF membrane was washed with TBST and then incubated with HRP-conjugated goat anti-rabbit IgG for 1.5 h. The PVDF

membrane was washed three times with TBST and then visualized using an enhanced chemiluminescence reagent.

Immunofluorescence

The lung tissues were repaired with citric acid antigen and washed with PBS and then incubated with the antibodies of SDC-1, TGFβ1, p-Smad3, collagen I, and α-SMA at 4°C for 15 h. The lung tissues were washed with PBS and then stained with Alexa Fluor goat anti-rabbit and DAPI. Finally, the lung tissues were observed and photographed under a fluorescence microscope (Olympus, Japan).

The Beas-2B or HLF-1 cells were seeded on soul plates in 24-well plates. The cells were fixed with 4% paraformaldehyde after different pretreatments and treatments and incubated with the antibody of SDC-1 overnight at 4°C. The soul plates were washed with PBS and then stained with Alexa Fluor goat anti-rabbit and DAPI. Finally, the cell images were photographed under a fluorescence microscope (Olympus, Japan).

Measurement Inflammatory Cytokine and SDC-1 Level in BALF

The mice were anesthetized with 4% chloral hydrate and intubated. BALF was obtained *via* multiple intratracheal injections of PBS (a total of 1.0 mL PBS). BALF was centrifuged at 3500 rpm at 4°C; for 15 min, and the supernatant was collected. Levels of SDC-1 (Zcibio Biotechnology, China), IL-4 (70-EK204/2, Multisciences), IL-5 (70-EK205, Multisciences), and IL-13 (70-EK213, Multisciences) in BALF were detected using an ELISA kit.

Statistical Analysis

All data were expressed as the mean ± standard deviation, and differences among groups were analyzed by one-way ANOVA and SNK test. $p < 0.05$ was considered statistically significant. All statistical analyses were performed using SPSS19.0.

RESULTS

SDC-1 Is Overexpressed in the Bronchial Epithelium of Human Chronic Asthma

The protein level of SDC-1 in the human subjects with chronic asthma was detected by immunohistochemistry. Results showed that SDC-1 was overexpressed in the lung airways of the asthmatic subjects, and the degree of overexpression in the tracheal epithelium was considerably higher than that around the trachea (**Figures 1A, C**). In addition, Masson staining indicated that substantial amounts of collagen were deposited around the bronchial duct in the subjects with chronic asthma, suggesting the possible involvement of SDC-1 in airway remodeling (**Figures 1B, D**).

Syndecan-1 Is Upregulated in the Bronchial Epithelium of OVA-Induced Chronic Asthma

Changes in SDC-1 expression in the airways of mice with acute and chronic asthma were detected by immunofluorescence. Results showed that SDC-1 expression slightly decreased in the tracheal epithelium and periductal of OVA-induced acute asthma compared with normal mice (**Figures 2B, C**). However, SDC-1 expression remarkably increased in the tracheal epithelium and periductal of OVA-induced chronic asthma (**Figures 2B, C**). In addition, SDC-1 levels in the BALF were higher in chronic asthma than in acute asthma (**Figure 2D**)

The results of masson staining and α-SMA indicated that airway remodeling induced by OVA-induced was considerably higher in chronic asthma than in acute asthma (**Figures 2E-H**).

HE staining and ELISA detection results of inflammatory factors (IL-4, IL-5, and IL-13) showed that the inflammatory response was substantially higher in OVA-induced acute asthma (OVA-4 weeks group) than that in chronic asthma (OVA-8 weeks group) (**Figures 2I-L**). These findings suggested that SDC-1 was overexpressed in human subjects with chronic asthma and mice with OVA-induced chronic asthma.

TGFβ1/Smad3 and Collagen I Are Upregulated in the Bronchial Epithelium of OVA-Induced Acute and Chronic Asthma

Moreover, collagen I expression in the airways of mice with OVA-induced acute asthma was higher than that in normal mice (**Figures 3A, D**). Meanwhile, collagen I expression in the airways of mice with chronic asthma induced by OVA sharply increased compared with that in the acute asthma group (**Figures 3A, D**).

TGFβ1/Smad3 signaling plays an important role in airway remodeling. Accordingly, changes in the expression of TGFβ1/Smad3 and collagen I in the airways with acute and chronic asthma were detected *via* immunofluorescence. Results showed that TGFβ1 and p-Smad3 expression substantially increased in the airways of mice with acute asthma induced by OVA compared with normal mice (**Figures 3B, C, E, F**). However, TGFβ1 and p-Smad3 expression slightly decreased in the OVA-induced chronic asthma compared with the acute asthma group.

SDC-1 siRNA Deletion of SDC-1 Suppresses Collagen I Expression by TGFβ1/Smad Signaling in Beas-2B Cells

The siRNA targeting SDC-1 was used to knock out SDC-1 expression to evaluate the role of SDC-1 in Beas-2B cells. Immunofluorescence revealed that three kinds of SDC-1 siRNA downregulated SDC-1 expression, and the most remarkable downregulation of SDC-1 expression was observed after SDC-1 siRNA 3 interference (**Figures 4A, B**). Therefore, SDC-1 siRNA 3 was selected for downstream studies to target the knockout of SDC-1 expression.

TGFβ1/Smad3 signaling plays an important role in collagen deposition. Therefore, changes in the expression of SDC-1, p-Smad3, and collagen I over time under TGFβ1 stimulation were detected by Western blot analysis. Results showed that SDC-1, p-Smad3, and collagen I expressions substantially increased after 2 days of TGFβ1 stimulation (**Figures 4C-E, L-N**). Therefore, TGFβ1 stimulation for 2 days was selected in the downstream study.

Interestingly, Western blot analysis revealed that TGFβ1 stimulation substantially induced the levels of SDC-1, p-Smad3

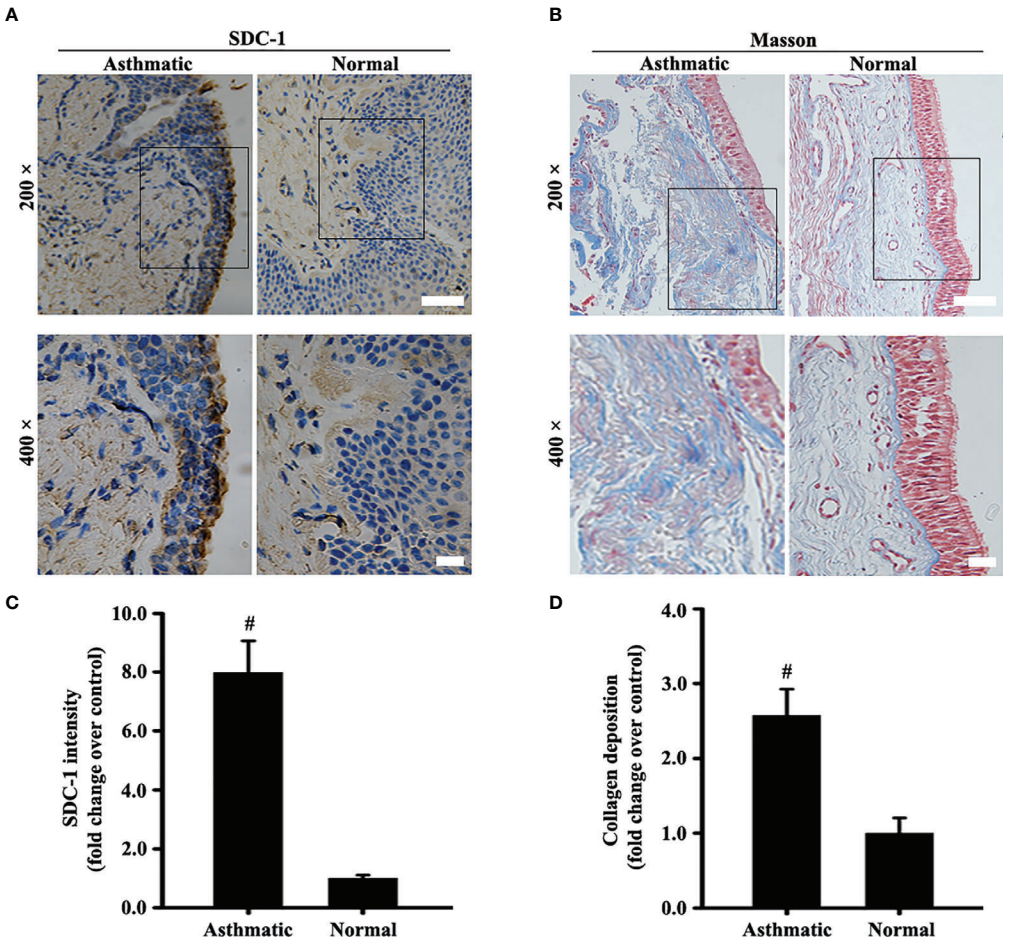

FIGURE 1 | SDC-1 levels in the asthmatic and normal human bronchial samples were evaluated by immunohistochemical staining **(A)**. Collagen deposition in the asthmatic and normal human bronchial samples was evaluated by Masson staining **(B)**. **(C)** SDC-1 intensity analysis of **(A)**. **(D)** Collagen intensity analysis of **(B)** Data are shown as the means ± SD of three independent experiments. $^{\#}p < 0.05$ *versus* the control group.

and collagen I in Beas-2B cells compared with those in the control group (**Figures 4F-H, O-Q**). However, SDC-1 downregulation by SDC-1 siRNA strongly inhibited the levels of p-Smad3 and collagen I induced by TGFβ1 stimulation in Beas-2B cells (**Figures 4F-H, O-Q**). In addition, SDC-1 intervention alone had no significant difference in p-Smad3 and Collagen I compared with those in the control group (**Figures 4I-K, R-T**).

These results suggested that SDC-1 siRNA might improve collagen deposition by inhibiting TGFβ1/Smad3 signaling.

SDC-1 Overexpression Aggravates Collagen I Expression by TGFβ1/Smad Signaling in Beas-2B Cells

A plasmid vector was constructed to overexpress SDC-1 and further explore the role of SDC-1 in p-Smad3 and collagen I expressions. Interestingly, the pc-SDC-1 considerably increased TGFβ1-induced SDC-1 expression compared with the TGFβ1 group (**Figures 5B, I**). The pc-SDC-1 upregulation of SDC-1 expression also notably enhanced the level of TGFβ1-induced p-Smad3 and collagen I expressions in Beas-2B cells (**Figures 5C, D, J, K**). In addition, SDC-1 overexpression alone had no significant difference in p-Smad3 and Collagen I compared with those in the control group (**Figures 5E, F, L, M**).

The effects of exogenous recombinant human SDC-1 addition on p-Smad3 and collagen I expressions were also investigated. Results demonstrated that high concentrations of recombinant human SDC-1 slightly increased the levels of p-Smad3 and collagen I induced by TGFβ1 compared with those in the TGFβ1 group (**Figures 5G, H, N, O**).

These results suggested that SDC-1 overexpression and SDC-1 detachment might aggravate collagen deposition by enhancing TGFβ1/Smad3 signaling.

SDC-1 siRNA Deletion of SDC-1 Suppresses Collagen I Expression by TGFβ1/Smad Signaling in HLF-1 Cells

Fibroblasts play an important role in airway remodeling. SDC-1 expression in fibroblasts was obtained through database retrieval (www.proteinatlas.org). Therefore, the effects of SDC-1 on TGFβ1/Smad3 signal in fibroblasts were further explored.

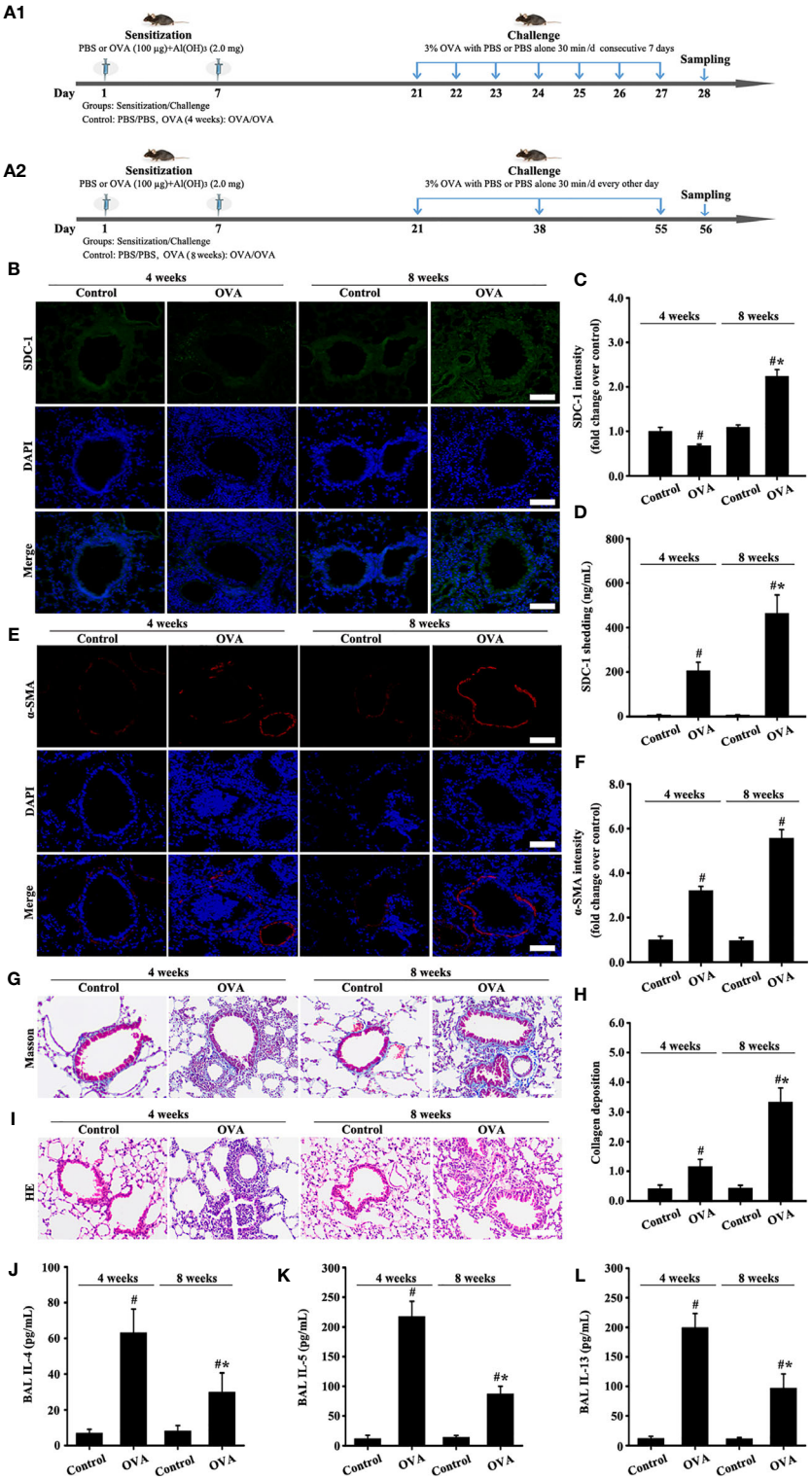

FIGURE 2 | Animal experimental schedule is shown in **(A)**. SDC-1 **(B)** and α-SMA **(E)** levels were detected by immunofluorescence. Collagen deposition was evaluated by Masson staining **(G)**. Histopathologic changes were detected by HE staining **(I)**. Levels of SDC-1 shedding **(D)**, IL-4 **(J)**, IL-5 **(K)**, and IL-13 **(L)** in BALF were measured by ELISA. **(C, F)** immunofluorescence intensity analysis of **(B, E). (H)** collagen deposition intensity analysis of **(G)** Data are shown as the means ± SD of three independent experiments. $^{\#}p < 0.05$ *versus* the control group. $^{\#*}p < 0.05$ *versus* the OVA (4 weeks) or control group.

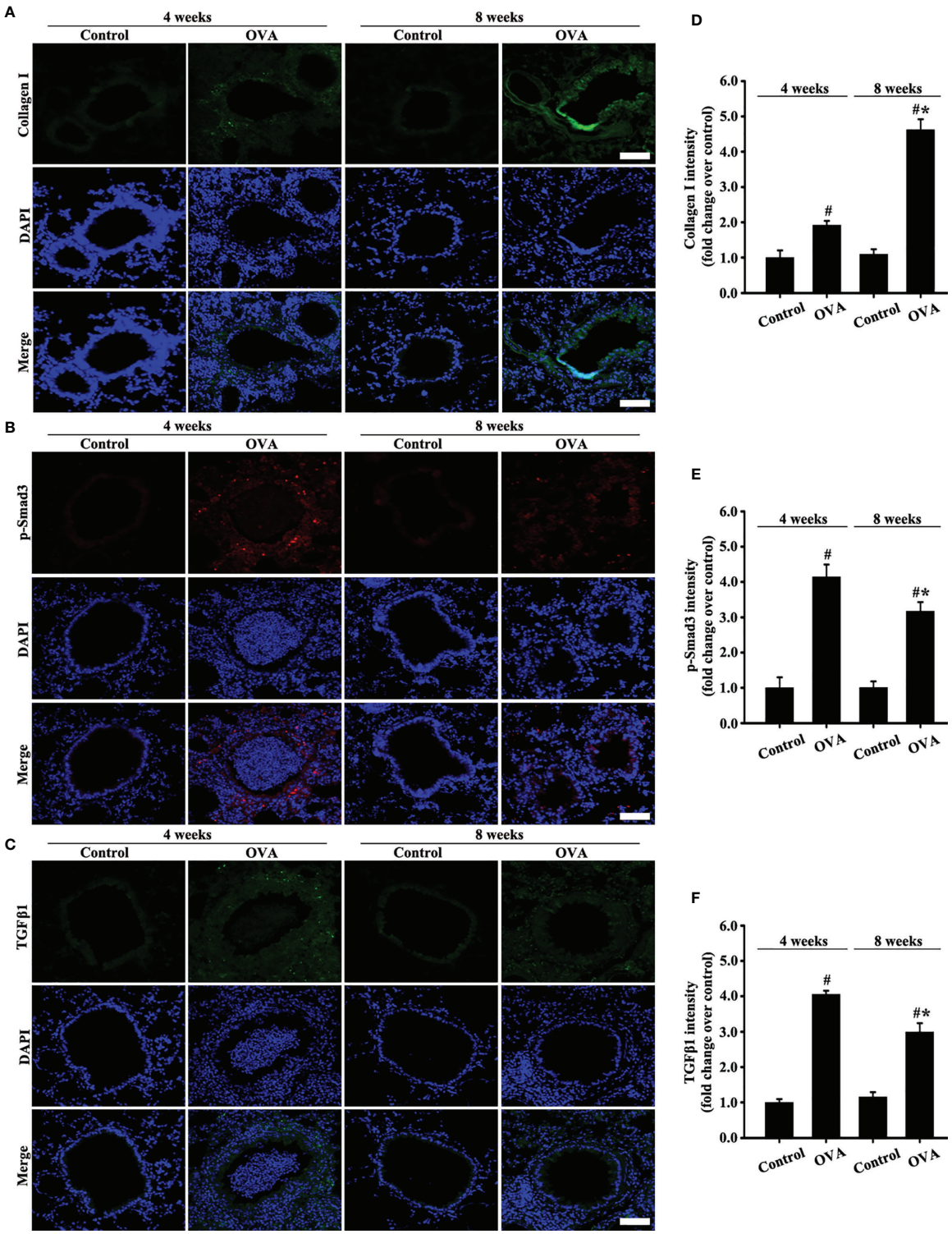

FIGURE 3 | Animal experimental schedule is shown in **Figures 2A**. Collagen I **(A)**, p-Smad3 **(B)**, and TGFβ1 **(C)** were detected by immunofluorescence. **(D–F)** Immunofluorescence intensity analysis of **(A–C)**, respectively. Data are shown as the means ± SD of three independent experiments. $^{\#}p < 0.05$ *versus* the control group. $^{\#*}p < 0.05$ *versus* the OVA (4 weeks) or control group.

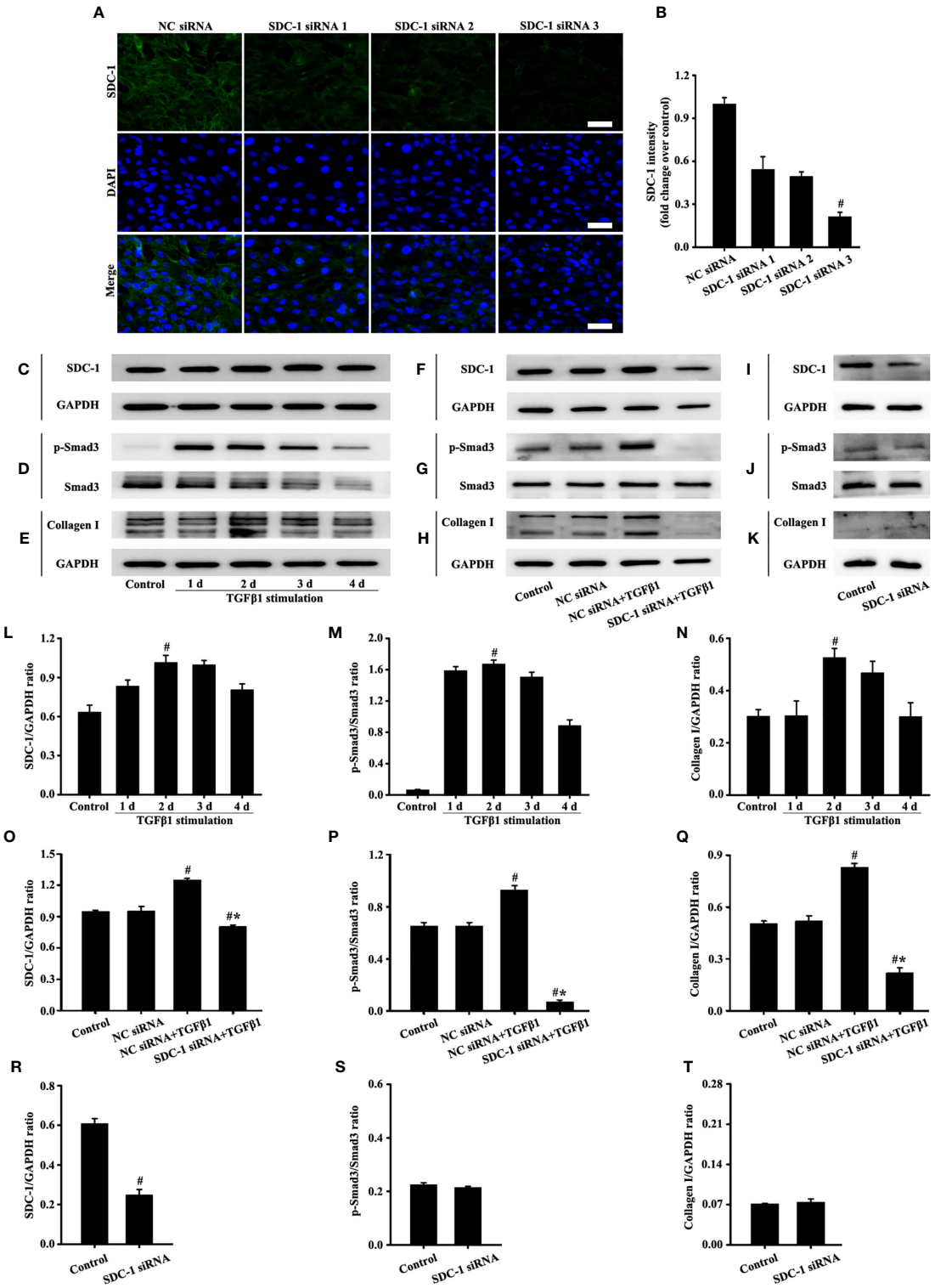

FIGURE 4 | Effects of SDC-1 siRNA on collagen I and p-Smad3 in Beas-2B cells were observed. Deletion effects of SDC-1 siRNA 1, SDC-1 siRNA 2, and SDC-1 siRNA 3 on SDC-1 expression **(A)** were detected by immunofluorescence. Changes in SDC-1 **(C)**, p-Smad3 **(D)**, and collagen I **(E)** under TGFβ1 stimulation at different periods were detected by Western blot. Effects of SDC-1 siRNA 3 on SDC-1 **(F, I)**, p-Smad3 **(G, J)**, and collagen I **(H, K)** were detected by Western blot. **(B)** SDC-1 immunofluorescence intensity analysis of **(A)**. **(L–T)** Protein intensity analysis of **(C-K)**, respectively. Data are shown as the means ± SD of three independent experiments. $^{\#}p < 0.05$ *versus* the control group. $^{\#*}p < 0.05$ *versus* the NC siRNA+TGFβ1 group.

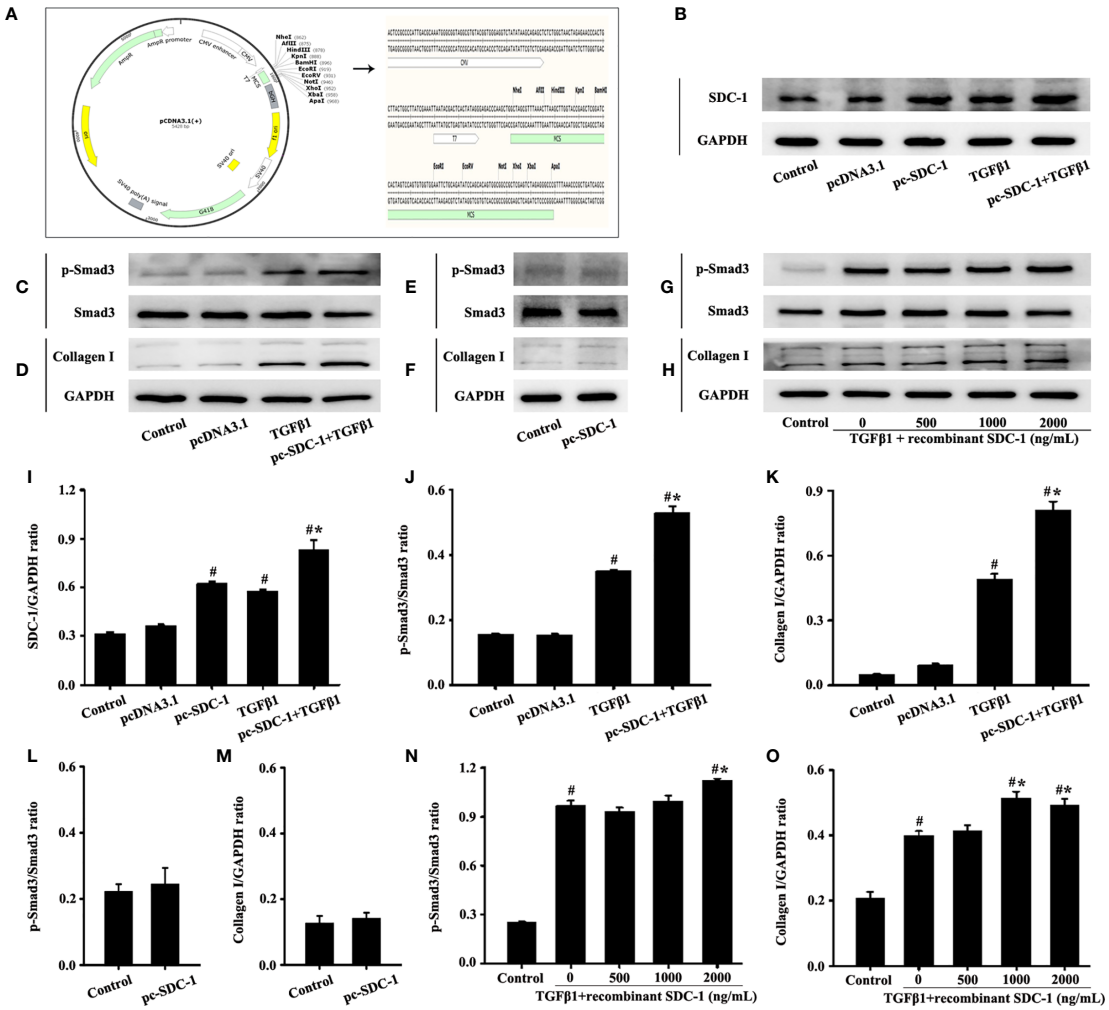

FIGURE 5 | Effects of SDC-1 overexpression by pc-SDC-1 or addition of the recombinant human SDC-1 protein on the levels of collagen I and p-Smad3 in Beas-2B cells were observed. Plasmid vector atlas of SDC-1 overexpression **(A)**. Effect of pc-SDC-1 overexpression on TGFβ1-stimulated SDC-1 expression **(B)** was detected by Western blot. Effect of SDC-1 overexpression on the levels of p-Smad3 **(C, E)** and collagen I **(D, F)** were detected. Effects of the addition of different concentrations of the recombinant human SDC-1 protein on TGFβ1-stimulated p-Smad3 **(G)** and collagen I **(H)** were detected by Western blot. **(I–O)** Protein intensity analysis of **(B–H)**, respectively. Data are shown as the means ± SD of three independent experiments. $^{\#}p < 0.05$ *versus* the control group. $^{\#*}p < 0.05$ *versus* the TGFβ1 group.

The role of three SDC-1 siRNAs in HLF-1 cells was reevaluated to analyze the effects of SDC-1 on HLF-1 cells. Immunofluorescence results confirmed that SDC-1 expression was most notably downregulated after SDC-1 siRNA 3 interference (**Figures 6A, B**). Therefore, SDC-1 siRNA 3 was also selected for the downstream study to target the knockout of SDC-1 expression in HLF-1 cells.

Western blot analysis revealed that SDC-1, p-Smad3 and collagen I substantially increased after 1 day of TGFβ1 stimulation (**Figures 6C-E, L-N**). Therefore, TGFβ1 stimulation for 1 day was selected in the downstream study of HLF-1 cells.

Western blot analysis revealed that SDC-1 downregulation by SDC-1 siRNA strongly inhibited the levels of TGFβ1-induced p-Smad3 and collagen I in HLF-1 cells compared with those in the TGFβ1-treated group (**Figures 6F-H, O-Q**). While downregulation SDC-1 alone had no significant difference in p-Smad3 and Collagen I compared with those in the control group (**Figures 6I-K, R-T**).

SDC-1 Overexpression Aggravates Collagen I Deposition by TGFβ1/Smad Signaling in HLF-1 cells

Interestingly, the pc-SDC-1 substantially increased TGFβ1-induced SDC-1 expression in the pc-SDC-1+TGFβ1 group compared with that in the TGFβ1 group (**Figures 7A, H**). The pc-SDC-1 also notably enhanced the level of TGFβ1-induced p-Smad3 and collagen I in the pc-SDC-1+TGFβ1 group compared with that in the TGFβ1 group (**Figures 7B, C, I, J**). However, SDC-1 overexpression by pc-SDC-1 alone had no significant difference in p-Smad3 and Collagen I compared with those in the control group (**Figures 7D, E, K, L**).

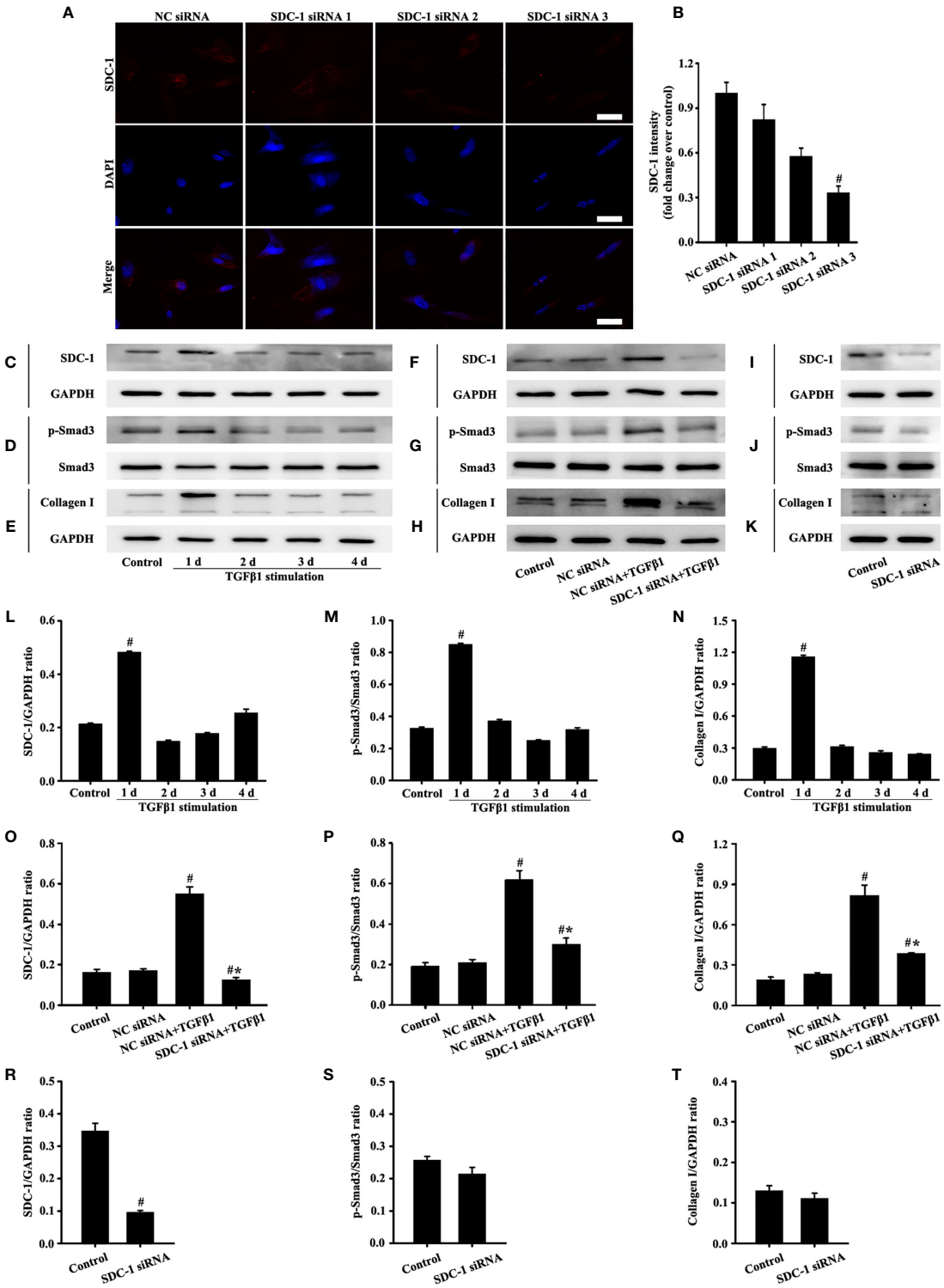

FIGURE 6 | Effects of SDC-1 siRNA on HLF-1 cells were detected. Deletion effects of SDC-1 siRNA 1, 2, or 3 on SDC-1 expression **(A)** were observed by immunofluorescence. Changes in levels of SDC-1 **(C)**, p-Smad3 **(D)**, and collagen I **(E)** under TGFβ1 stimulation were detected by Western blot. Effect of SDC-1 siRNA 3 on the levels of SDC-1 **(F, I)**, p-Smad3 **(G, J)**, and collagen I **(H, K)** were detected by Western blot. **(B)** SDC-1 immunofluorescence intensity analysis of **(A). (L–T)** Protein intensity analysis of **(C–K)**, respectively. Data are shown as the means ± SD of three independent experiments. $^{\#}p < 0.05$ *versus* the control group. $^{\#*}p < 0.05$ *versus* the NC siRNA+ TGFβ1 group.

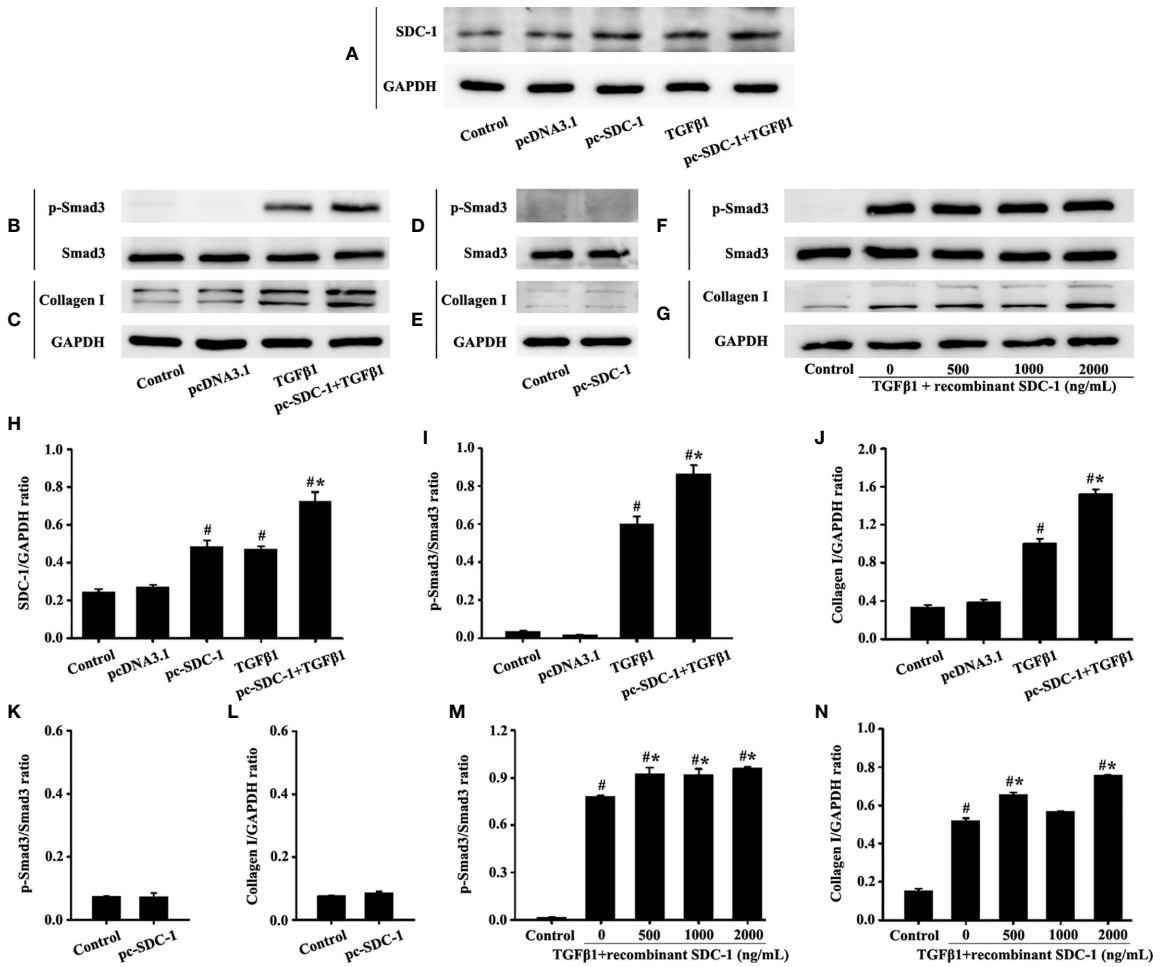

FIGURE 7 | Effects of SDC-1 overexpression by pc-SDC-1 or the addition of the recombinant human SDC-1 protein on the collagen I and p-Smad3 in HLF-1 cells were observed. Effects of pc-SDC-1 overexpression on TGFβ1-stimulated SDC-1 expression **(A)** were detected. Effects of pc-SDC-1 on the levels of p-Smad3 **(B**, **D)** and collagen I **(C**, **E)** were detected by Western blot. Effects of the recombinant human SDC-1 protein addition on TGFβ1-stimulated p-Smad3 **(F)** and collagen I **(G)** expression were detected by Western blot. **(H**-**N)** Protein intensity analysis of **(A**-**G)**, respectively. Data are shown as the means ± SD of three independent experiments. $^{\#}p < 0.05$ *versus* the control group. $^{\#*}p < 0.05$ *versus* the TGFβ1 group.

p-Smad3 and collagen I expression in the TGFβ1 +recombinant human SDC-1 group increased compared with that in the TGFβ1 group (**Figures 7F, G, M, N**). These results indicated that SDC-1 overexpression might transfuse signaling to fibroblasts to enhance collagen expression.

SDC-1 Overexpression Accelerates Airway Remodeling-Induced by OVA in Chronic Asthma

The similarities in SDC-1 overexpression in mice and humans with chronic asthma suggested that airway remodeling had a conserved effect across species. Therefore, SDC-1 deficient mice with lentivirus were constructed to determine the functional role of SDC-1 in airway remodeling.

No difference in the airway of control and LV2NC mice was found (**Figures 8B, C, F**). The mice with OVA-induced chronic asthma showed higher levels of inflammation and collagen deposition (**Figures 8B–G**) as well as SDC-1, p-Smad3, collagen I and α-SMA expression than the control group (**Figures 9A–P**). However, SDC-1 downregulation by SDC-1 shRNA in the OVA+SDC-1 shRNA group remarkably alleviated OVA-induced p-Smad3, collagen deposition, and collagen I and α-SMA expression compared with that in the OVA group (**Figures 8C, F** and **9A–P**).

These findings collectively clarify the mechanism of SDC-1 overexpression in airway remodeling in mice and humans.

Inhalation With Recombinant Mouse SDC-1 Protein Accelerates Airway Remodeling-Induced by OVA in Chronic Asthma

ELISA detected the presence of shedding SDC-1 in the BALF, and the concentration of SDC-1 in mice with chronic asthma was

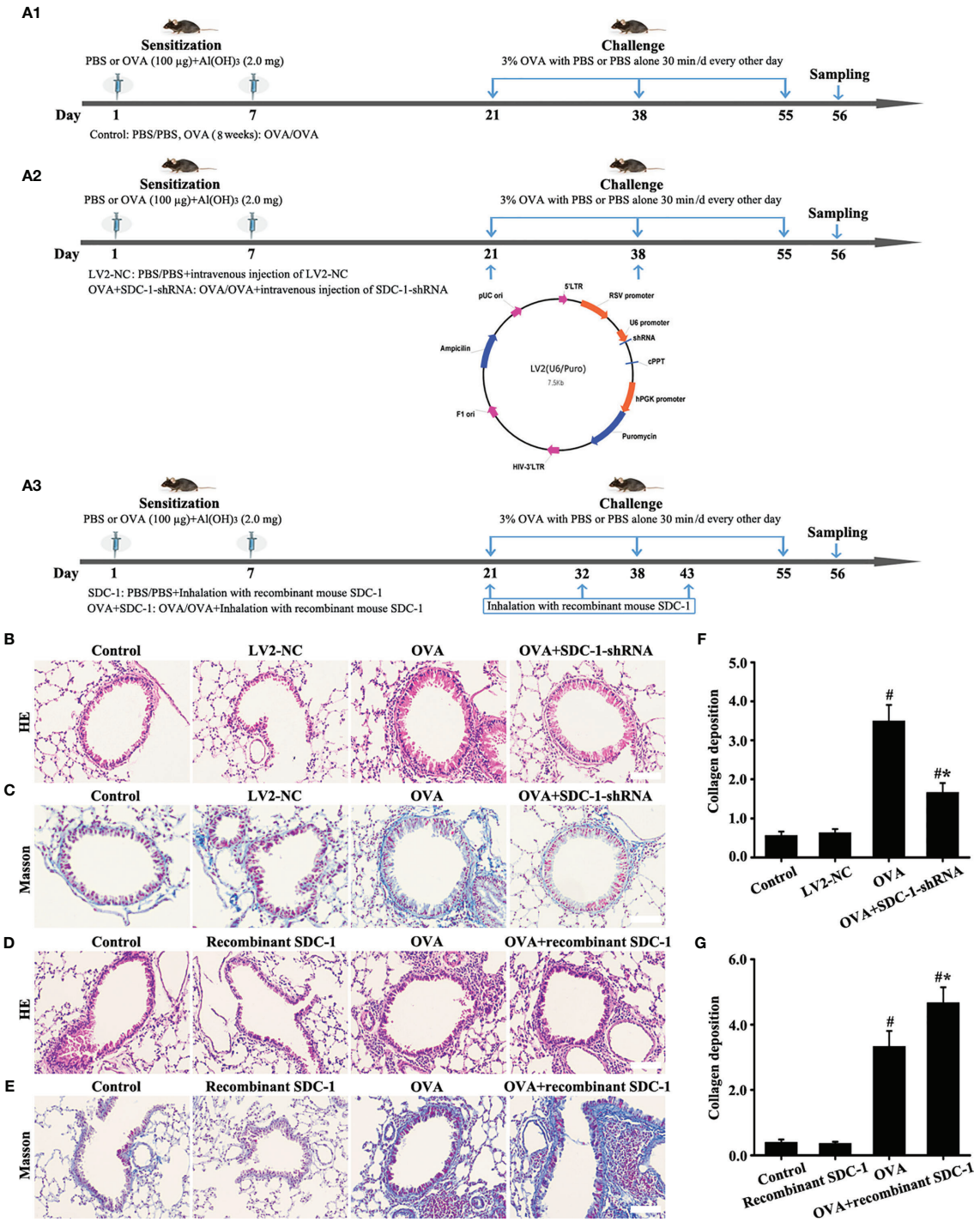

FIGURE 8 | Animal experimental intervention schedule is shown in **(A)**. Effects of SDC-1 deletion by SDC-1 shRNA or inhalation with the recombinant mouse SDC-1 protein on collagen deposition **(C**, **E)** and pathological changes **(B**, **D)** were observed. **(F, G)** Collagen intensity analysis of **(C, E)**, respectively. Data are shown as the means ± SD of three independent experiments. $^{\#}p < 0.05$ *versus* the control group. $^{\#*}p < 0.05$ *versus* the OVA group.

higher than that in mice with acute asthma (**Figure 2D**). Thus, the mice were induced to inhale the recombinant mouse SDC-1 protein to investigate the effects of shedding SDC-1 on airway remodeling.

No difference was found in pathological form, Smad3 phosphorylation, collagen deposition, and α-SMA and collagen I expression in the airways of the control and inhalation with the recombinant mouse SDC-1 protein mice (**Figures 8D, E, G**, **10A–L**).

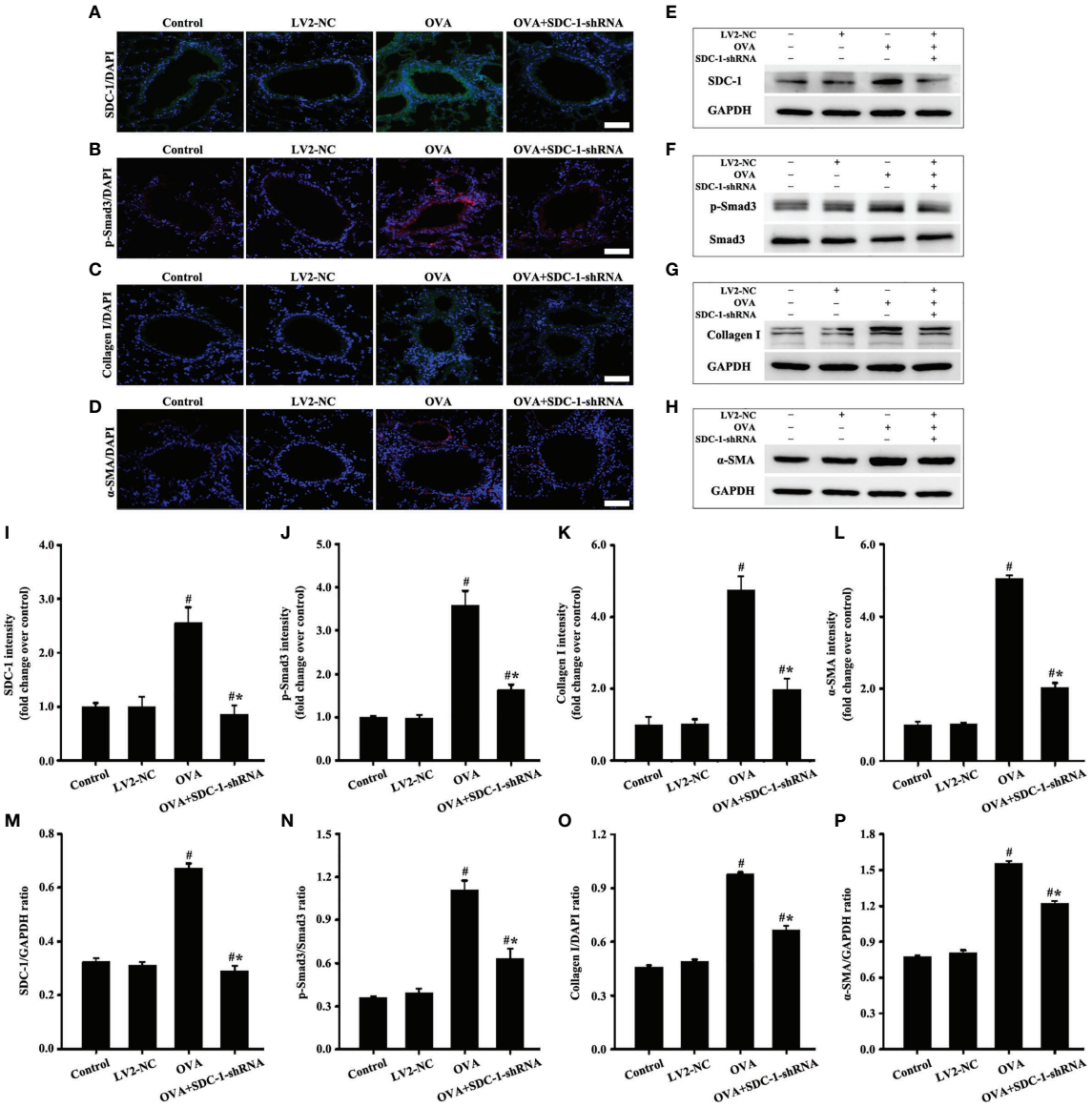

FIGURE 9 | Animal experimental intervention schedule is shown in **Figures 8A1, A3**. Effects of SDC-1 deletion by SDC-1 shRNA on the levels of SDC-1 **(A, E)**, p-Smad3 **(B, F)**, collagen I **(C, G)**, and α-SMA **(D, H)** in mice were observed by immunofluorescence and Western blot. **(I–L)** Immunofluorescence intensity analysis of **(A–D)**, respectively. **(M–P)** Gray intensity analysis of **(E–H)**, respectively. Data are shown as the means ± SD of three independent experiments. $^{\#}p < 0.05$ *versus* the control group. $^{\#*}p < 0.05$ *versus* the OVA group.

Smad3 phosphorylation and collagen I and α-SMA expression induced by OVA increased compared with those in the control mice (**Figures 10A-L**). However, inhalation with the recombinant mouse SDC-1 protein in the OVA+SDC-1 group increased collagen deposition and the expression levels of p-Smad3, α-SMA, and collagen I compared with those in the OVA group (**Figures 8E, G**, and **10A-L**). These findings were consistent with the results of *in vitro* experiments.

These results suggested that shedding SDC-1 might strengthen TGFβ1/Smad3 signaling to participate in the airway remodeling of mice and humans.

DISCUSSION

Airway remodeling is an important feature in the development of chronic asthma. Blocking or slowing down airway remodeling has become a hot topic in the research on asthma (23, 24). The present study was the first to demonstrate the involvement of SDC-1 in airway remodeling in chronic asthma *in vivo* and *in vitro*. The primary finding of this study was that SDC-1 may mediate TGFβ1/Smad3 signaling to participate in airway remodeling (**Figure 11**).

SDC-1, a major component of glycocalyx, is an important signaling transmembrane protein molecule. SDC-1 has an

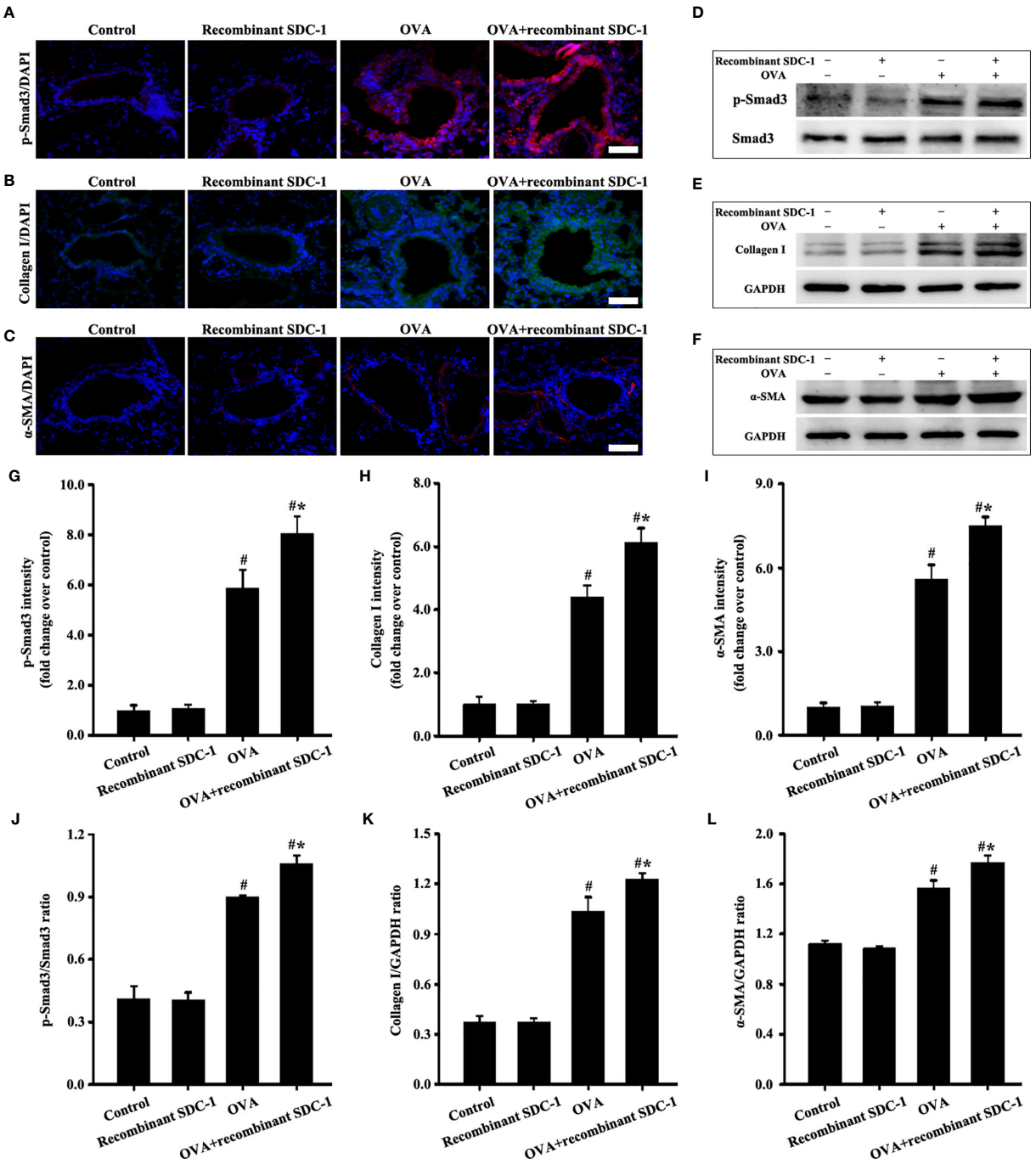

FIGURE 10 | Animal experimental intervention schedule is shown in **Figures 8A1, A3**. Effects of inhalation with the recombinant mouse SDC-1 protein on the levels of p-Smad3 **(A**, **D)**, collagen I **(B**, **E)**, and α-SMA **(C**, **F)** in mice were observed. **(G–I)** Immunofluorescence intensity analysis of **A–C)**, respectively. **(J–L)** Gray intensity analysis of **(D–F)**, respectively. Data are shown as the means ± SD of three independent experiments. $^{\#}p < 0.05$ *versus* the control group. $^{\#*}p < 0.05$ *versus* the OVA group.

extracellular glycosaminoglycan chain comprising HS, HA, and CS (13, 15). First, SDC-1 protrudes from extracellular structural features and functions as a physical barrier, capturing signal molecules and directing them to receptors on the membrane (14). Second, the transmembrane structure and cytoplasmic region of SDC-1 can transmit extracellular signals into cells and then mediate a series of intracellular reactions (25). The previous study confirmed the role of SDC-1 as a barrier against permeability in the LPS-induced ARDS model (15). Parimon et al. (26) confirmed that SDC-1 promotes lung fibrosis by

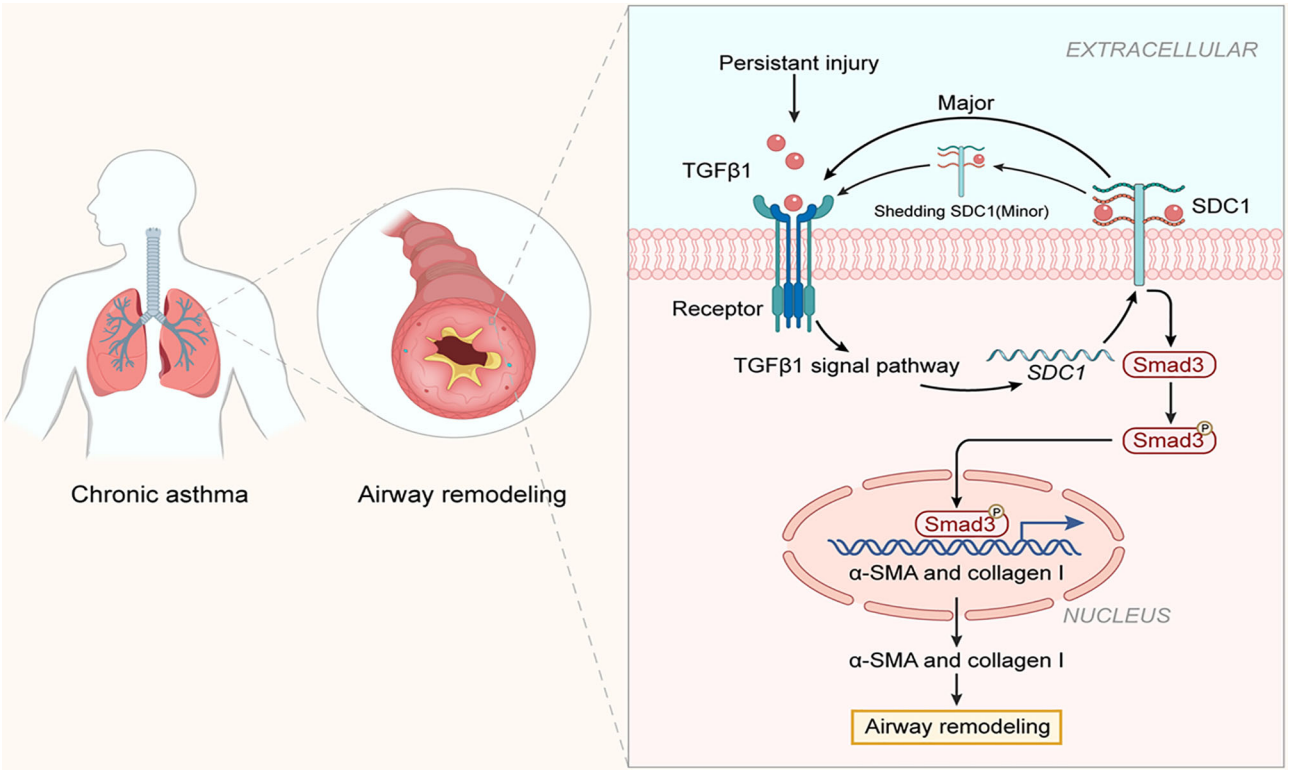

FIGURE 11 | Structure of SDC-1 overexpression with aggravated airway remodeling by strengthening TGFβ1/Smad3 signaling in OVA-induced chronic asthma.

regulating epithelial reprogramming through extracellular vesicles. The present results showed that SDC-1 and collagen deposition synchronously increased in humans and mice with chronic asthma, whereas that after SDC-1 shRNA intervention in mice or SDC-1 siRNA intervention in cells synchronously decreased to reduce SDC-1 level. To a certain extent, this study also supported the idea that SDC-1 enhances intracellular signal transduction through the recruitment of its external domain amplification ligand.

The present study also found an interesting phenomenon that SDC-1 expression in bronchial epithelial and periductal cells decreased in humans and mice with acute asthma stage, whereas that in humans and mice with chronic asthma stage substantially increased. These results led to speculation that SDC-1 has different mechanisms of action in various disease stages. The inflammatory damage caused by inflammatory responses can lead to a certain increase in SDC-1 shedding (27, 28). Xu et al. (29) reported that the SDC-1 ectodomains of the airway epithelium are closely related to the inflammatory response of acute asthma. Changes in inflammatory cytokines, such as IL-4, IL-5, and IL-13 in BALF, were further detected in the present study. ELISA results showed that the levels of IL-4, IL-5, and IL-13 sharply increased in mice with acute asthma compared with normal mice. However, the levels of IL-4, IL-5, and IL-13 substantially decreased in mice with chronic asthma compared with those in mice with acute asthma. These results indicated the possible relation of shedding of the SDC-1 ectodomains of the airway epithelium in mice with acute asthma to acute inflammatory response. By contrast, the persistence of chronic inflammatory response had minimal effect on SDC-1 expression in chronic asthma.

The SDC-1 ectodomains of epithelial cells have anti-inflammatory, antipermeability, and other barrier effects. However, the shedding of the SDC-1 exodomain has different roles in various models. Li et al. (30) found that the abdication of the SDC-1 exogenous domain regulates bleomycin-induced intrapulmonary transport of neutrophils in acute lung injury. Xu et al. (29) uncovered that the shedding of the SDC-1 exodomain has anti-inflammatory properties in acute asthma. Different degrees of SDC-1 exodomain shedding in acute and chronic asthma were observed in the present study, and inhalation with SDC-1 promoted collagen deposition in OVA-induced chronic asthma models. These findings suggested that SDC-1 shedding has different regulatory functions in various disease models.

TGFβ1 is a kind of factor with multiple effects on the different disease models, such as pro-airway remodeling, as well as anti-inflammatory or pro-inflammatory effects (31, 32). Hogan et al. (33) reported that the TGFβ1 pathway is required for NF-κB signaling in mouse keratinocytes. However, TGFβ1 plays an anti-inflammatory, pro-inflammatory, and pro-airway remodeling role in the pathogenesis of asthma at different stages (34–36). TGFβ1 was substantially higher in mice with acute asthma than those with chronic asthma in the present

study. These results led to speculation regarding the possible role of TGFβ1 levels in the production of IL-4, IL-5, and IL-13. In addition, TGFβ1 stimulates epithelial or fibroblast transcription and suppresses collagenase transcription, thus allowing TGFβ1/Smad3 signaling to play a key role in collagen deposition (37, 38). TGFβ1/Smad3 is crucial in promoting airway remodeling in chronic asthma, and this phenomenon was also verified in this study. Therefore, these results strongly suggested that SDC-1 overexpression played an important role in collagen I expression in the epithelial cells or fibroblasts through TGFβ1/Smad3 signaling.

Overall, the present study was the first to demonstrate that the high expression of SDC-1 in the trachea of patients with chronic asthma is closely related to airway remodeling, and SDC-1 may regulate collagen deposition in epithelial cells or fibroblasts through the TGFβ1/Smad signaling pathway. This study provides a theoretical basis for the treatment of asthma in the future.

DATA AVAILABILITY STATEMENT

The original contributions presented in the study are included in the article/**Supplementary Material**. Further inquiries can be directed to the corresponding author.

ETHICS STATEMENT

The studies involving human participants were reviewed and approved by Human Research Ethics Review Committee of Qianfoshan Hospital. Written informed consent for participation was not required for this study in accordance with the national legislation and the institutional requirements. The animal study was reviewed and approved by Institutional Review Committee of Shandong University–Qianfoshan Hospital. Written informed consent was obtained from the individual(s) for the publication of any potentially identifiable images or data included in this article.

AUTHOR CONTRIBUTIONS

LD conceived the idea and proofread the manuscrift. DZ conceived the idea, conducted the study, drafted the figures, and wrote the original draft. J-TZ, W-JC, and X-RQ interpreted the data and drafted the figures. YP and X-FL proofread the manuscript. DZ contributed mainly to the article. All authors contributed to the article and approved the submitted version.

FUNDING

This work was supported by the National Natural Science Foundation of China (81770029).

SUPPLEMENTARY MATERIAL

The Supplementary Material for this article can be found online at: https://www.frontiersin.org/articles/10.3389/fimmu.2021.744477/full#supplementary-material

REFERENCES

1. Frey A, Lunding LP, Ehlers JC, Weckmann M, Zissler UM, Wegmann M. More Than Just a Barrier: The Immune Functions of the Airway Epithelium in Asthma Pathogenesis. *Front Immunol* (2020) 11:761. doi: 10.3389/fimmu.2020.00761
2. Paw M, Wnuk D, Jakieła B, Bochenek G, Sładek K, Madeja Z, et al. Responsiveness of Human Bronchial Fibroblasts and Epithelial Cells From Asthmatic and Non-Asthmatic Donors to the Transforming Growth Factor-Beta(1) in Epithelial-Mesenchymal Trophic Unit Model. *BMC Mol Cell Biol* (2021) 22:19. doi: 10.1186/s12860-021-00356-8
3. Zhang H, Yan HL, Li XY, Guo YN. TNFSF14, a Novel Target of MiR-326, Facilitates Airway Remodeling in Airway Smooth Muscle Cells *via* Inducing Extracellular Matrix Protein Deposition and Proliferation. *Kaohsiung J Med Sci* (2020) 36:508–14. doi: 10.1002/kjm2.12197
4. Li X, Yang N, Cheng Q, Zhang H, Liu F, Shang Y. MiR-21-5p in Macrophage-Derived Exosomes Targets Smad7 to Promote Epithelial Mesenchymal Transition of Airway Epithelial Cells. *J Asthma Allergy* (2021) 14:513–24. doi: 10.2147/JAA.S307165
5. Han L, Luo H, Huang W, Zhang J, Wu D, Wang J, et al. Modulation of the EMT/MET Process by E-Cadherin in Airway Epithelia Stress Injury. *Biomolecules* (2021) 11:669. doi: 10.3390/biom11050669
6. Zou H, Ming B, Li J, Xiao Y, Lai L, Gao M, et al. Extracellular HMGB1 Contributes to the Chronic Cardiac Allograft Vasculopathy/Fibrosis by Modulating TGF-Beta1 Signaling. *Front Immunol* (2021) 12:641973. doi: 10.3389/fimmu.2021.641973
7. Yang L, Han B, Zhang M, Wang YH, Tao K, Zhu MX, et al. Activation of BK Channels Prevents Hepatic Stellate Cell Activation and Liver Fibrosis Through the Suppression of Tgfbeta1/SMAD3 and JAK/STAT3 Profibrotic Signaling Pathways. *Front Pharmacol* (2020) 11:165. doi: 10.3389/fphar.2020.00165
8. Wang W, Liu Z, Niu J, Yang H, Long Q, Liu H, et al. Feibi Recipe Reduced Pulmonary Fibrosis Induced by Bleomycin in Mice by Regulating BRP39/IL-17 and Tgfbeta1/Smad3 Signal Pathways. *Evid Based Complement Alternat Med* (2020) 2020:5814658. doi: 10.1155/2020/5814658
9. Yu C, Xiong C, Tang J, Hou X, Liu N, Bayliss G, et al. Histone Demethylase JMJD3 Protects Against Renal Fibrosis by Suppressing Tgfbeta and Notch Signaling and Preserving PTEN Expression. *Theranostics* (2021) 11:2706–21. doi: 10.7150/thno.48679
10. Wang Z, Li L, Wang C, Piao Y, Jiang J, Li L, et al. Recombinant Pyrin Domain Protein Attenuates Airway Inflammation and Alleviates Epithelial-Mesenchymal Transition by Inhibiting Crosstalk Between Tgfbeta1 and Notch1 Signaling in Chronic Asthmatic Mice. *Front Physiol* (2020) 11:559470. doi: 10.3389/fphys.2020.559470
11. Albadrani GM, BinMowyna MN, Bin-Jumah MN, El-Akabawy G, Aldera H, Al-Farga AM. Quercetin Prevents Myocardial Infarction Adverse Remodeling in Rats by Attenuating TGF-Beta1/Smad3 Signaling: Different Mechanisms of Action. *Saudi J Biol Sci* (2021) 28:2772–82. doi: 10.1016/j.sjbs.2021.02.007
12. Meng X, Gao X, Chen X, Yu J. Umbilical Cord-Derived Mesenchymal Stem Cells Exert Anti-Fibrotic Action on Hypertrophic Scar-Derived Fibroblasts in Co-Culture by Inhibiting the Activation of the TGF Beta1/Smad3 Pathway. *Exp Ther Med* (2021) 21:210. doi: 10.3892/etm.2021.9642
13. Javadi J, Heidari-Hamedani G, Schmalzl A, Szatmári T, Metintas M, Aspenström P, et al. Syndecan-1 Overexpressing Mesothelioma Cells Inhibit Proliferation, Wound Healing, and Tube Formation of Endothelial Cells. *Cancers (Basel)* (2021) 13:655. doi: 10.3390/cancers13040655

14. Schellings MW, Vanhoutte D, van Almen GC, Swinnen M, Leenders JJ, Kubben N, et al. Syndecan-1 Amplifies Angiotensin II-Induced Cardiac Fibrosis. *Hypertension* (2010) 55:249–56. doi: 10.1161/HYPERTENSIONAHA.109.137885
15. Zhang D, Han SS, Zhou Y, Qi BY, Wang XZ. Therapeutic Effects of Mangiferin on Sepsis-Associated Acute Lung and Kidney Injuries *via* the Downregulation of Vascular Permeability and Protection of Inflammatory and Oxidative Damages. *Eur J Pharm* (2020) 152:105400. doi: 10.1016/j.ejps.2020.105400
16. Filla MS, Dam P, Rapraeger AC. The Cell Surface Proteoglycan Syndecan-1 Mediates Fibroblast Growth Factor-2 Binding and Activity. *J Cell Physiol* (1998) 174:310–21. doi: 10.1002/(SICI)1097-4652(199803)174:3<310::AID-JCP5>3.0.CO;2-R
17. Hayashida K, Johnston DR, Goldberger O, Park PW. Syndecan-1 Expression in Epithelial Cells is Induced by Transforming Growth Factor Beta Through a PKA-Dependent Pathway. *J Biol Chem* (2006) 281:24365–74. doi: 10.1074/jbc.M509320200
18. Shen X, Wang X. The Function Role and Synergic Effect of Syndecan-1 for Mifepristone in Uterine Leiomyoma. *Cytotechnology* (2021) 73:179–87. doi: 10.1007/s10616-021-00455-6
19. Couchman JR. Syndecan-1 (CD138), Carcinomas and EMT. *Int J Mol Sci* (2021) 22:4227. doi: 10.3390/ijms22084227
20. Casaro M, Souza VR, Oliveira FA, Ferreira CM. OVA-Induced Allergic Airway Inflammation Mouse Model. *Methods Mol Biol* (2019) 1916:297–301. doi: 10.1007/978-1-4939-8994-2_28
21. Kianian F, Karimian SM, Kadkhodaee M, Takzaree N, Seifi B, Sadeghipour HR. Protective Effects of Ascorbic Acid and Calcitriol Combination on Airway Remodelling in Ovalbumin-Induced Chronic Asthma. *Pharm Biol* (2020) 58:107–15. doi: 10.1080/13880209.2019.1710218
22. Mohammadtursun N, Li QP, Abuduwaki M, Jiang S, Zhang H, Sun J, et al. Loki Zupa Alleviates Inflammatory and Fibrotic Responses in Cigarette Smoke Induced Rat Model of Chronic Obstructive Pulmonary Disease. *Chin Med* (2020) 15:92. doi: 10.1186/s13020-020-00373-3
23. Huang J, Pansare M. New Treatments for Asthma. *Pediatr Clin North Am* (2019) 66:925–39. doi: 10.1016/j.pcl.2019.06.001
24. Propp P, Becker A. Prevention of Asthma: Where are We in the 21st Century? *Expert Rev Clin Immunol* (2013) 9:1267–78. doi: 10.1586/1744666X.2013.858601
25. Tkachenko E, Rhodes JM, Simons M. Syndecans: New Kids on the Signaling Block. *Circ Res* (2005) 96:488–500. doi: 10.1161/01.RES.0000159708.71142.c8
26. Parimon T, Yao C, Habiel DM, Ge L, Bora SA, Brauer R, et al. Syndecan-1 Promotes Lung Fibrosis by Regulating Epithelial Reprogramming Through Extracellular Vesicles. *JCI Insight* (2019) 5:e129359. doi: 10.1172/jci.insight.129359
27. Zhang Y, Wang Z, Liu J, Zhang Z, Chen Y. Suppressing Syndecan-1 Shedding Ameliorates Intestinal Epithelial Inflammation Through Inhibiting NF-KappaB Pathway and TNF-Alpha. *Gastroenterol Res Pract* (2016) 2016:6421351. doi: 10.1155/2016/6421351
28. Dogné S, Flamion B. Endothelial Glycocalyx Impairment in Disease: Focus on Hyaluronan Shedding. *Am J Pathol* (2020) 190:768–80. doi: 10.1016/j.ajpath.2019.11.016
29. Xu J, Park PW, Kheradmand F, Corry DB. Endogenous Attenuation of Allergic Lung Inflammation by Syndecan-1. *J Immunol* (2005) 174:5758–65. doi: 10.4049/jimmunol.174.9.5758
30. Li Q, Park PW, Wilson CL, Parks WC. Matrilysin Shedding of Syndecan-1 Regulates Chemokine Mobilization and Transepithelial Efflux of Neutrophils in Acute Lung Injury. *Cell* (2002) 111:635–46. doi: 10.1016/s0092-8674(02)01079-6
31. Wang N, Yan D, Liu Y, Liu Y, Gu X, Sun J, et al. A Hur/TGF-Beta1 Feedback Circuit Regulates Airway Remodeling in Airway Smooth Muscle Cells. *Respir Res* (2016) 17:117. doi: 10.1186/s12931-016-0437-1
32. Sugiura Y, Niimi T, Sato S, Yoshinouchi T, Banno S, Naniwa T, et al. Transforming Growth Factor Beta1 Gene Polymorphism in Rheumatoid Arthritis. *Ann Rheum Dis* (2002) 61:826–8. doi: 10.1136/ard.61.9.826
33. Hogan KA, Ravindran A, Podolsky MA, Glick AB. The Tgfbeta1 Pathway Is Required for Nfkappab Dependent Gene Expression in Mouse Keratinocytes. *Cytokine* (2013) 64:652–9. doi: 10.1016/j.cyto.2013.09.004
34. Camoretti-Mercado B, Solway J. Transforming Growth Factor-Beta1 and Disorders of the Lung. *Cell Biochem Biophys* (2005) 43:131–48. doi: 10.1385/CBB:43:1:131
35. Lambrecht BN, Hammad H. The Immunology of Asthma. *Nat Immunol* (2015) 16:45–56. doi: 10.1038/ni.3049
36. Hammad H, Lambrecht BN. The Basic Immunology of Asthma. *Cell* (2021) 184:1469–85. doi: 10.1016/j.cell.2021.02.016
37. Fang L, Wu J, Huang T, Zhang P, Xin X, Shi Y. TGF-Beta1 Stimulates Epithelial-Mesenchymal Transition Mediated by ADAM33. *Exp Ther Med* (2018) 15:985–92. doi: 10.3892/etm.2017.5478
38. Liu P, Miao K, Zhang L, Mou Y, Xu Y, Xiong W, et al. Curdione Ameliorates Bleomycin-Induced Pulmonary Fibrosis by Repressing TGF-Beta-Induced Fibroblast to Myofibroblast Differentiation. *Respir Res* (2020) 21:58. doi: 10.1186/s12931-020-1300-y

Conflict of Interest: The authors declare that the research was conducted in the absence of any commercial or financial relationships that could be construed as a potential conflict of interest.

Publisher's Note: All claims expressed in this article are solely those of the authors and do not necessarily represent those of their affiliated organizations, or those of the publisher, the editors and the reviewers. Any product that may be evaluated in this article, or claim that may be made by its manufacturer, is not guaranteed or endorsed by the publisher.

Copyright © 2021 Zhang, Qiao, Cui, Zhang, Pan, Liu and Dong. This is an open-access article distributed under the terms of the Creative Commons Attribution License (CC BY). The use, distribution or reproduction in other forums is permitted, provided the original author(s) and the copyright owner(s) are credited and that the original publication in this journal is cited, in accordance with accepted academic practice. No use, distribution or reproduction is permitted which does not comply with these terms.

frontiers in Immunology

ORIGINAL RESEARCH
published: 06 October 2021
doi: 10.3389/fimmu.2021.763379

LN Monocytes Limit DC-Poly I:C Induced Cytotoxic T Cell Response *via* IL-10 and Induction of Suppressor CD4 T Cells

Anita Tewari[1†], *Miglena G. Prabagar*[2†], *Sophie L. Gibbings*[2†], *Kavita Rawat*[1] *and Claudia V. Jakubzick*[1*]

[1] Department of Microbiology and Immunology, Geisel School of Medicine, Hanover, NH, United States, [2] Department of Pediatrics, National Jewish Health, Denver, CO, United States

OPEN ACCESS

Edited by:
Amiram Ariel,
University of Haifa, Israel

Reviewed by:
Philippe Saas,
U1098 Interactions Hôte-Greffon-Tumeur & Ingénierie Cellulaire et Génique (INSERM), France
Flavio Andres Salazar Onfray,
University of Chile, Chile

***Correspondence:**
Claudia V. Jakubzick
claudia.jakubzick@dartmouth.edu

[†]*These authors have contributed equally to this work*

Specialty section:
This article was submitted to Inflammation, a section of the journal Frontiers in Immunology

Received: *23 August 2021*
Accepted: *20 September 2021*
Published: *06 October 2021*

Citation:
Tewari A, Prabagar MG, Gibbings SL, Rawat K and Jakubzick CV (2021) LN Monocytes Limit DC-Poly I:C Induced Cytotoxic T Cell Response via IL-10 and Induction of Suppressor CD4 T Cells. Front. Immunol. 12:763379. doi: 10.3389/fimmu.2021.763379

Every immune response has accelerators and brakes. Depending on the pathogen or injury, monocytes can play either role, promoting or resolving immunity. Poly I:C, a potent TLR3 ligand, licenses cross-presenting dendritic cells (DC1) to accelerate a robust cytotoxic T cells response against a foreign antigen. Poly I:C thus has promise as an adjuvant in cancer immunotherapy and viral subunit vaccines. Like DC1s, monocytes are also abundant in the LNs. They may act as either immune accelerators or brakes, depending on the inflammatory mediator they encounter. However, little is known about their contribution to adaptive immunity in the context of antigen and Poly I:C. Using monocyte-deficient and chimeric mice, we demonstrate that LN monocytes indirectly dampen a Poly I:C induced antigen-specific cytotoxic T cell response, exerting a "braking" function. This effect is mediated by IL-10 production and induction of suppressor $CD4^+$ T cells. In a metastatic melanoma model, we show that a triple-combination prophylactic treatment consisting of anti-IL-10, tumor peptides and Poly I:C works because removing IL-10 counteracts the monocytic brake, resulting in significantly fewer tumors compared to mice treated with tumor peptides and Poly I:C alone. Finally, in human LN tissue, we observed that monocytes (unlike DCs) express high levels of IL-10, suggesting that anti-IL-10 may be an important addition to treatments. Overall, our data demonstrates that LN monocytes regulate the induction of a robust DC1-mediated immune response. Neutralization of either IL-10 or monocytes can augment Poly I:C-based treatments and enhance T cell cytotoxicity.

Keywords: dendritic cells, Ly6C$^+$ monocytes, antigen-presentation, IL-10, cytotoxic T cells, Poly I:C, suppressor CD4$^+$ T cells, double-stranded RNA

INTRODUCTION

The mononuclear phagocyte (MP) system in the healthy lung is comprised of tissue-specific alveolar macrophages, interstitial macrophages, dendritic cells (DCs) and monocytes (1). Of these MPs, DCs and monocytes can acquire antigen in the lung, migrate to the lung-draining lymph node (LLN), and present antigen to induce T cell differentiation. The induction of naïve T cells into effector T

cells is mainly attributed to two DC subtypes, DC1 and DC2, with further subdivision of DC2 into subsets (2–5). In a previous publication, we demonstrated that DC1 is the main driver of a Poly I:C-induced CTL response (6). When lung was stimulated with Poly I:C and antigen, DC1 was shown to be essential for differentiating cytotoxic T cells (CTL) (6). DC2 could cross-present the antigen and induce T cell proliferation but could not differentiate the antigen-specific T cells to become effector T cells. In addition to DCs, the LN contains monocytes, which are as abundant as any DC subset (1, 7–9), so in this study we ask, what role are the LN monocytes playing.

Monocytes represent ~5-10% of circulating PBMCs and have a half-life of ~20 hours (7, 10). They are continuously trafficking into tissue and LNs and are often referred to as inflammatory monocytes or macrophages. This is a misnomer, as $Ly6C^+$ monocytes continuously enter tissue and LNs in healthy animals (during steady state) to survey the environment (7). The rapid migration into tissue is illustrated in parabiotic mice where $Ly6C^+CD62L^+$ monocytes never reach 50:50 equilibrium regardless of the amount of time the mice share circulation (7, 11–13). Most importantly, the trafficking of monocytes, like DCs, into tissue and LNs does not require commensals (7), suggesting that monocytes are critical players in immune regulation both in steady state and inflammation. Based on the turnover, number and surveying property of monocytes, many questions arise for the role of monocytes; particularly after it has been shown that monocytes are not readily replacing steady state macrophages in some cases, such as alveolar macrophages and microglia, while in others this replacement occurs regularly such as intestinal and liver macrophages (7, 11, 14–22).

Once monocytes enter tissue, they can display phagocytic properties and secrete inflammatory mediators such as TNF and NO, or anti-inflammatory mediators such as IL-10 and VEGF (8, 17, 23, 24). Although these examples suggest that monocytes can have macrophage-like properties, monocytes can also display DC-like properties, upregulating CCR7 and migrating down afferent lymphatics from tissue to LNs (7, 25). Upon entering the LNs, monocytes present exogenous antigen to cognate T cells and induce their differentiation into effector CD4 or CD8 T cell (i.e., Th1, Th2, Th17, T reg, CTL etc.) (9, 19, 26–32). All in all, the stimulus (i.e., pathogen associated molecular pattern) and environment (i.e., growth factors) dictate the outcome and role of monocytes during an immune response, highlighting their plasticity.

The importance of understanding how LN monocytes contribute to the adaptive immune response is largely based on the growing number of clinical trials that use DC-based vaccine designs containing tumor-associated antigens or personalized neoantigens with Poly I:C (33, 34). The efficacy of such vaccines was demonstrated in recent studies in which treatment of stage III melanoma patients with personalized neoantigens and Poly I:C resulted in complete tumor regression, with no recurrence at 2-year follow-up (33, 34). Since monocytes contribute to the development of effector T cells or suppressor T cells and are highly present in the draining LNs, we set out to address the role of monocytes in the context of antigen and Poly I:C vaccination, and perhaps provide insight on how to enhance the efficacy of this promising cancer and viral vaccine.

MATERIALS AND METHODS

Mice

Six to eight-week-old C57BL/6 Ly5.1 (CD45.1), Ly5.2 (CD45.2), WT mice were purchased from Charles River or Jackson Laboratory. $CCR2^{-/-}$, $IL\text{-}10^{-/-}$, $H\text{–}2K^{bm1}$, OTI, OTII, $MHCII^{-/-}$ and IL-10 GFP (Tiger) mice were purchased from Jackson Laboratory. $PDL1/2^{-/-}$ mice were kindly provided by Dr. Daniel Barber and Keith Kauffman. OTII mice were crossed with IL-10 GFP to generate OTIl IL-10 GFP reporter mice. All mice were genotyped upon arrival and prior to their use in experiments. Mice were housed in a specific pathogen-free environment at National Jewish Health and Dartmouth Hitchcock Medical College, an AAALAC accredited institution, and used in accordance with protocols approved by the Institutional Animal Care and Utilization Committee.

Bone Marrow Chimera Mice

Eight-week-old CD45.1 or CD45.2 C57BL/6 mice were lethally irradiated with 900 rads and reconstituted intravenously at a bone marrow (BM) cell ratio of 80:20 from $CCR2^{-/-}$ and either WT, $H\text{–}2K^{bm1}$, $PDL1/2^{-/-}$, or $IL\text{-}10^{-/-}$ mice. Six to eight weeks post-reconstitution, mice were assessed for chimerism prior to use.

Flow Cytometry and LN Digestion

Lung-draining LNs were teased with 26G needles and digested in 1ml of 2.5 mg ml^{-1} collagenase D (Roche) solution in 1X RPMI at 37°C for 30 min. After incubation, 100 µl of 100 mM EDTA was added to stop the enzymatic reaction. The cells were pipetted up and down with glass Pasteur pipets and then passed through a 70 µm nylon filter. Single cell suspensions were collected and centrifuged at 300 g for 5 min. Cells were stained with the following monoclonal Abs: Phycoerythrin (PE)-conjugated to Vα2, CD4 and CD64; PerCP-Cy5.5- conjugated to CD11b and CD4; PE-Cy7-conjugated to CD11c and CD44; BUV395-conjugated to CD11b; BUV805-conjugated to CD8a, fluorescein isothiocyanate (FITC)-conjugated to CD4, CD45.1 and CD103; allophycocyanin (APC)-conjugated to Vβ51, CD45.2, CD45 and CD103; APC-Cy7-conjugated to CD45.2 and MHCII; and BV510 conjugated to Ly6C and MHCII. The PE-conjugated MHC Tetramer H-2kb OVA SIINFEKL was purchased from MBL international. The viability dye 4',6-diamidino-2-phenylindole (DAPI) (#D9542, Sigma) was added immediately before each sample acquisition on a BD Symphony A3 analyzer (BD Biosciences). Data were analyzed using FlowJo (Tree Star, Ashland, OR). Antigen-specific antibodies and isotype controls were obtained from BioLegend, eBioscience and BD Biosciences.

Proliferation of OVA-Specific Transgenic OTI or OTII T Cells

Spleen cells from OTI or OTII GFP mice, in which the TCR of $CD8^+$ or $CD4^+$ T cells are restricted to an OVA peptide, were

labeled with 10 μM carboxyfluorescein succinimidyl ester (CFSE) for 10 mins. Half a million of these cells were transferred intravenously into recipient mice 1 day before intranasal delivery of 2 μg soluble OVA and 20 μg Poly I:C. Mice were sacrificed 3 days after intranasal deliveries for analysis of T cell proliferation (CFSE dye dilution) in the LLN. For OTI: Isolated cells were cultured 5 hours in RPMI 10% FCS containing 10 μM OVA peptide (257-264) and Brefeldin A 10 μg/ml. Following surface staining, BD Foxp3 intracellular staining kit was used. Cells were stained with APC-conjugated to IFNγ, PerCP-Cy5.5-TNFα, or isotype controls (BD Pharmingen). For OTII: Isolated cells were cultured 5 hours in RPMI 10% FCS containing 10 μM OVA peptide (323-339) and Brefeldin A 10 μg/ml. Following stimulation, cells were stained with PE-conjugated to CD4, APC-conjugated to Vβ51, PE-Cy7-conjugated to Vα2, APC-Cy7-conjugated to CD44, BUV805-conjugated to CD8 (BD Pharmingen, eBioscience or Biolegend).

Quantitative Reverse-Transcription PCR

Monocytes from CD11b enriched cell suspension (Miltenyi) were sorted (FACSAriaIII sorter). Total RNA was extracted using the RNeasy Minikit (Qiagen). Equal amounts of total RNA from each sample were reverse transcribed into cDNA using SuperScript™ VILO™ Master Mix (Invitrogen). qPCR was set up using PowerUp SYBR Green PCR Master Mix (Applied Biosystems) and analyzed on Bio-Rad C-1000 CFX96. RT-PCR primers for IL-10: Forward-GGTTGCCAAGCCTTATCGGA; Reverse-ACCTGCTCCACTGCCTTGCT. Relative quantification of gene expression was performed by normalizing expression levels of genes of interest over housekeeping (Thoc1) gene within each sample followed by relative expression to control (mean of triplicate).

B16F10 Lung Melanoma Model

B16F10 melanoma cells were purchased from ATCC (CRL-6475) and maintained in RPMI with 10% FCS, 1% Pen/Strep/L-glutamine (Sigma), 1% non-essential amino acids (Sigma), 1% sodium pyruvate (Sigma), 10 mM HEPES (Sigma) and 0.1 mM β-mercaptoethanol.

Immunization With B16F10 Peptides, Poly I:C, and Anti-IL-10

Melanoma vaccine was freshly prepared prior to inoculation. Vaccine consisted of 10 μg each peptide premelanosome protein (Pmel17 or gp100) (25-30; seq: EGSRNQDWL, Anaspec) and tyrosinase-related protein-2 (TRP-2) (180-188; seq: SVYDFFVWL, Anaspec), and 50 μg Poly I:C (TLR3 agonists). To deplete IL-10, some mice were given three i.p. injections of anti-IL-10 (JES5-2A5 clone, BioXcell) at days 2 (300μg), 5 (100μg) and 22 (100μg).

Tumor Assessment Post Prophylactic Therapy

After treatment, mice were intravenously challenged with 2×10^5 viable B16F10 cells and euthanized 16 days post injection. Lungs of mice were perfused with PBS and then inflated with 1% agarose. Experimentally blind laboratory member counted the B16F10 lung surface metastases.

Human Lung-Draining LNs

We received de-identified non-diseased human lung with attached LLNs from the International Institute for the Advancement of Medicine (Edison, NJ, USA). We selected donors without a history of chronic lung disease and with reasonable lung function with a P_aO_2/F_iO_2 ratio of >225, a clinical history and X-ray that did not indicate infection, and limited time on a ventilator. Lungs were removed en bloc in the operating room and included the trachea, LNs and pulmonary vessels. Pulmonary arteries were perfused in the operating room with cold histidine-tryptophan-ketoglutarate (HTK) solution to preserve endothelial cell function and prevent intravascular clot formation. The lungs were submerged in HTK, and immediately shipped on ice. All lungs were processed within 24 hours of removal. The lungs were visually inspected for lesions or masses and were eliminated from the study if grossly abnormal. Peribronchial LNs were identified and removed. Procedure additionally described in (35, 36). The Committee for the Protection of Human Subjects at National Jewish Health approved this research. RNA sequencing was completed as previously described (11).

Statistics

Statistical analysis was conducted using Prism software. All bar graphs are expressed as the mean ± SEM. Statistical tests were performed using two-tailed Student's t-test and ANOVA. $P < 0.05$ was considered statistically significant.

RESULTS

The Absence of LN Monocytes Significantly Increases Poly I:C Induced Antigen-Specific CTL Response

Monocytes require CCR2 to exit the bone marrow and enter tissue under steady-state and inflammatory conditions (7, 37). As anticipated, 24 hours post intranasal delivery of antigen and Poly I:C, the total number of migratory DCs in the LLN was similar between WT and $CCR2^{-/-}$ mice (**Figure 1A**). In contrast, monocytes are substantially deficient in the $CCR2^{-/-}$ mice compared to WT mice (17, 23, 37).

To examine the role of LN monocytes in a Poly I:C-induced antigen-specific CTL response, CFSE labeled naïve OVA-specific $CD8^+$ T cells (OTI) were adoptively transferred into WT and $CCR2^{-/-}$ mice. Three days post inoculation of antigen and Poly I:C, LLN OTI T cells were analyzed for the production of CTL cytokines, IFNγ and TNFα. Although we observed a relatively similar number of proliferating $CFSE^+$ OTI T cells between WT and $CCR2^{-/-}$ mice (**Figure 1B**), the frequency of IFNγ and TNFα producing OTI T cell was significantly greater in $CCR2^{-/-}$ mice compared to WT mice (**Figure 1C**), showing that monocytes downregulate the intensity of cytokine production in proliferated OTI T cells.

Temporary Depletion of LN Monocytes Significantly Increases Poly I:C Induced Antigen-Specific CTL Response

To support the findings in the $CCR2^{-/-}$ mice, where LN monocytes are continually deficient, we examined whether temporary depletion

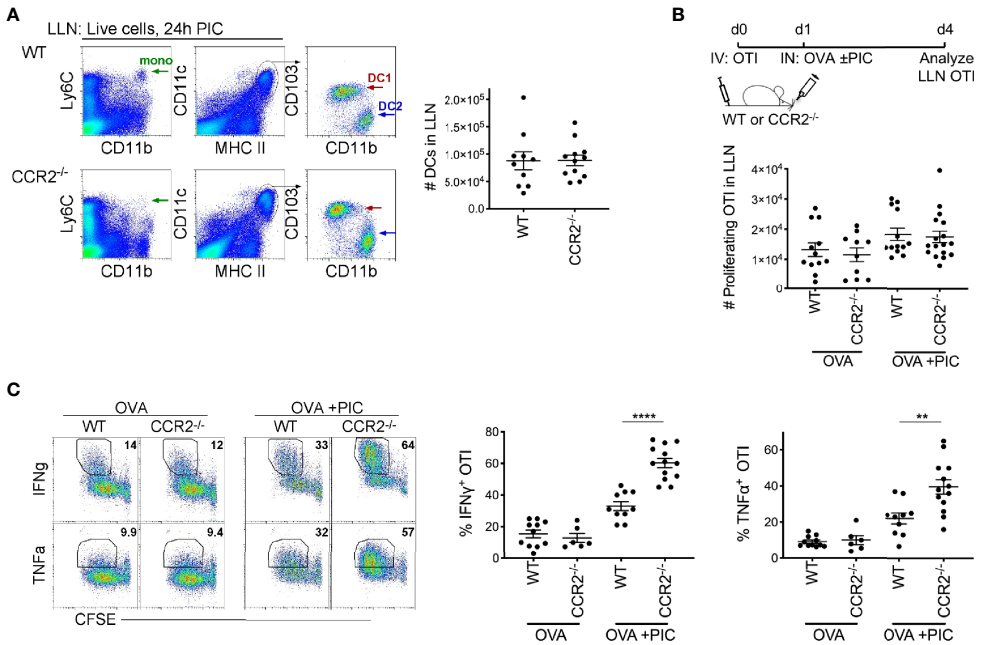

FIGURE 1 | Lymph node monocytes suppress Poly IC-induced antigen-specific cytotoxic CD8$^+$ T cells. **(A)** Flow plots of LLN from WT and CCR2$^{-/-}$ mice were isolated 24 hours postimmunization with OVA and Poly IC. Gated live cells illustrate Ly6C$^+$CD11b$^+$ monocytes (left plots) and CD11c$^+$MHCII^{high} population (middle plots), CD103$^+$ DC1 and CD11b$^+$ DC2 (right plots). Scatter plot, each dot represents a mouse. Total number of migratory DCs in the LLN 24 hours post immunization. Data are 2 independent experiments. **(B)** Immunization protocol for CTL response, top. Total number of proliferating OTI T cells 3 days post- immunization. Data are cumulative from 3 independent experiments with n = 4 per group. **(C)** Representative flow plots display gating strategy of cytokine production from WT and CCR2$^{-/-}$ mice, left. Scatter plot analysis of cytokine frequency from individual mice, right. Data are cumulative from 2-3 independent experiments of n = 3,4 per group. Data are shown as mean ± SEM. Each dot represents a mouse. ****P < 0.0001. **P value < 0.01.

of monocytes would also result in an increased Poly I:C induced CTL response. Using anti-Gr1, monocytes were temporarily depleted in WT mice on the same day as the inoculation of antigen and Poly I:C. A caveat to note is that in addition to monocytes, anti-Gr1 depletes neutrophils, plasmacytoid DCs and Ly6C$^+$ T cells but not DCs for up to 2-3 days (6, 38). As observed in CCR2$^{-/-}$ mice, WT mice with transiently depleted monocytes displayed a significant increase in IFNγ and TNFα producing antigen-specific CD8$^+$ T cells compared to mice treated with control antibody (**Supplementary Figure 1**). Collectively, data from mice either constitutively (CCR2$^{-/-}$) or temporarily (*via* anti-Gr1 treatment) depleted of LN monocytes suggest that the role of monocytes is to restrict an exaggerated CTL response in the context of antigen and Poly I:C.

IL-10 Production by LN Monocytes Is Required to Dampen an Enhanced CTL Response

We investigated three possible mechanisms by which monocytes could dampen a Poly I:C induced CTL response. First, we hypothesized that monocytes directly interfere with the cross-presentation and cross-priming of CTLs by TLR3 stimulated DC1s. To address this hypothesis, we took advantage of the H–2K^{bm1} mice which have mutations to the antigen binding site of MHCI, rendering antigen presenting cells incapable of inducing proliferation of OTI T cells (39). Lethally irradiated CD45.1 C57BL/6 mice were reconstituted with a mixture of 80% CCR2$^{-/-}$ and 20% H–2K^{bm1} bone marrow (BM) cells or with 20% CD45.1 WT BM in control mice. In this competitive setting, CCR2-sufficient BM cells will outcompete CCR2-deficent cells in the reconstitution of CCR2 dependent cell types, resulting in the complete repopulation of LN monocytes by H–2K^{bm1}-derived BM cells (or CD45.1 WT BM cells in control mice). Importantly DCs, which do not depend on CCR2 for their migration into tissue, are found at a ratio of 80:20 CD45.2:CD45.1 in the LNs of control mice, reflecting the ratio of transferred BM cells (**Figure 2A**). Thus, in chimeric mice, 100% of LN monocytes are incapable of directly presenting antigen to OTI T cells while antigen presentation by DCs is minimally affected.

In BM chimeras where the LN monocytes were derived from WT or H–2K^{bm1} BM, we observed no difference in the cytokine production in Poly I:C induced CTLs (**Figure 2C**). Therefore, we examined our second hypothesis that PDL1 expression on monocytes directly dampen the CTL response. In the LLN, PDL1 is highly expressed in steady-state and inflamed monocytes (**Figure 2B**). However, in the lung, monocytes and not DCs upregulate PDL1 after Poly I:C exposure (**Figure 2B**) (7). When we created BM chimeric mice where monocytes lacked PDL1/2 expression, there was a slight decrease in cytokine production from proliferating antigen-specific T cells compared to PDL1/2 expressing monocytes (**Figure 2D**). In summary, the mechanism of action that LN monocytes use to

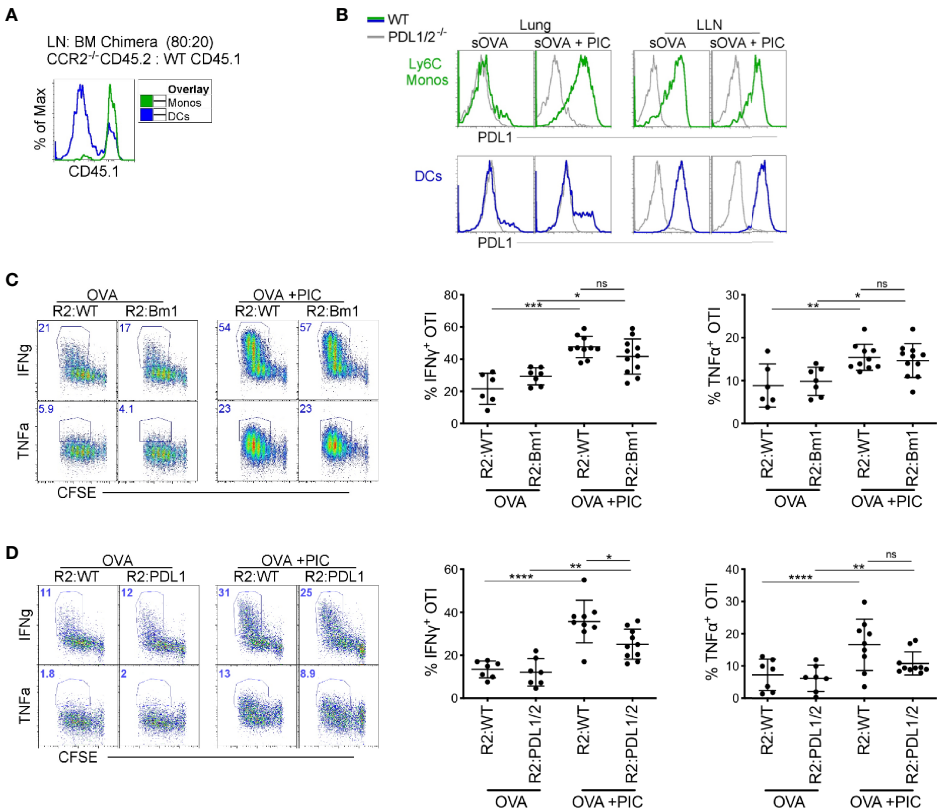

FIGURE 2 | Direct antigen presentation and PDL1 expression by monocytes are dispensable for suppression of cytokine production in antigen-specific CD8$^+$ T cells **(A)** Lethally irradiated mice were reconstituted 80:20 with CCR2$^{-/-}$ CD45.2 or WT CD45.1 BM cells. Six weeks post-reconstitution, LNs were assessed for monocyte BM derivation. Flow plots illustrate monocyte derivation was ~100% derived from CCR2 sufficient, WT CD45.1 BM cells compared to DC subtypes which were mainly derived from CCR2$^{-/-}$ CD45.2 BM with a portion from WT CD45.1 BM. **(B)** WT and PDL1/2$^{-/-}$ mice were treated with OVA or OVA and Poly IC, 24 h post treatment, PDL1 protein expression was examined on lung and LN monocytes (top) and total migratory DCs (bottom). **(C)** Lethally irradiated mice were reconstituted 80:20 with CCR2$^{-/-}$ and H–2K^{bm1} BM cells: R2:Bm1 chimeric mice. Control mice were reconstituted 80:20 with CCR2$^{-/-}$ and WT BM cells: R2:WT chimeric mice. Six-eight weeks after reconstitution, mice were immunized as described in **Figure 1B** and cytokine production was examined in OTI proliferating T cells. Right panels represent flow plots demonstrate gating strategy for cytokine production by proliferating OTI T cells. Left, scatter plot analysis of cytokine frequency from R2:WT and R2:Bm1 chimeric mice. Data are 3-4 independent experiments n=3-5 mice per group. Each dot represents a mouse. **(D)** Lethally irradiated mice were reconstituted 80:20 with CCR2$^{-/-}$ and PDL1/2$^{-/-}$ BM cells: R2:PDL1/2 chimeric mice. Control mice were reconstituted 80:20 with CCR2$^{-/-}$ and WT BM cells: R2:WT chimeric mice. Scatter plot analysis of cytokine frequency from R2:WT and R2:PDL1/2 chimeric mice. Data are 2 independent experiments, n=3-5 mice per group. Data are shown as mean ± SEM. Each dot represents a mouse. ****P <0.0001. ***P value < 0.001. **P value < 0.01. *P value < 0.05. Non-significant (ns).

regulate a Poly I:C-induced antigen-specific CTL response is not mediated *via* cross-presentation or PDL1 expression.

Thirdly, we hypothesized that the production of IL-10, a well-described anti-inflammatory cytokine secreted by monocytes and macrophages in response to PAMP stimulation, might provide the mechanism by which monocytes dampen a Poly I:C-induced CTL response. First, we confirmed that monocytes produce IL-10 after an intranasal bolus of antigen and Poly I:C using IL-10 reporter mice (**Figure 3A**). Among extravascular CD11b$^+$ cells, CD64$^+$Ly6C$^+$ monocytes uniquely expressed IL-10 after exposure to Poly I:C; intravascular cells were excluded by labeling with injection of anti-CD45 antibody given 5 minutes prior to harvest. Moreover, in the LLN, monocytes increased their mRNA expression of IL-10 after nasal inoculation of antigen and Poly I:C (**Figure 3B**). Using the same bone marrow chimera approach described previously (**Figure 2**), we created mice with IL-10 deficient LN monocytes. Compared to IL-10 sufficient LN monocytes, IL-10 deficient LN monocytes were unable to dampen the CTL response induced by antigen and Poly I:C (**Figure 3C**). In conclusion, these data suggest that monocytes require IL-10 production to dampen a CTL response. However, whether this effect is direct or indirect is unclear.

Monocytes Are Required for the Induction of Suppressor Antigen-Specific T Cells

Next, we investigated whether other immune cell populations were involved in the modulation of adaptive immune response promoted by monocytes. Suppressor T cells (Treg) are known for their critical role in controlling autoimmunity and suppressing inflammatory responses. They also promote tumor development and progression by dampening the anti-tumor immune response. Therefore, we examined whether there was an

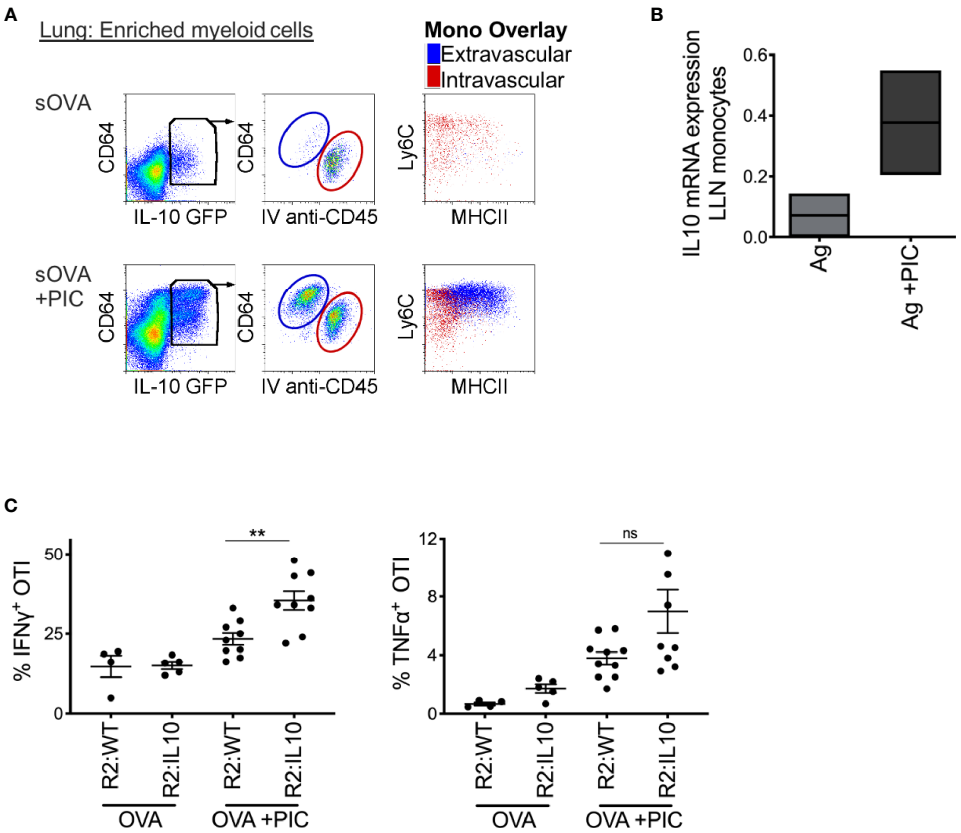

FIGURE 3 | Poly IC-induced IL-10 production by monocytes is required to suppress antigen-specific CTL response. **(A)** IL-10 GFP reporter mice were inoculated i.n. with 2 μg OVA ±20 μg Poly IC. Five minutes prior to sacrifice and tissue harvest, 5 ul of anti-CD45 antibody was given intravenously. Lung monocytes were isolated and analyzed by flow cytometry for IL-10 expression, left plots. Middle plots illustrate gated IL-10 producing cells, where all extravascular IL-10 producing cells were $CD64^+$ cells. Right plots display overlay of intravascular (red) and extravascular (blue) IL-10 producing cells, which were all $CD64^+$ $Ly6C^+$ monocytes with extravascular monocytes displaying signs of maturation, up-regulation of MHCII. **(B)** Normalized mRNA expression of IL-10 in LLN of WT mice after i.n. immunization with 2 μg OVA ±20 μg Poly IC as outlined in **Figure 1B**. Box plot is the mean of two independent experiments. **(C)** Lethally irradiated mice were reconstituted 80:20 with $CCR2^{-/-}$ and $IL\text{-}10^{-/-}$ BM cells: R2:IL-10. Control mice were reconstituted 80:20 with $CCR2^{-/-}$ and WT BM cells: R2:WT chimeric mice. Scatter plot analysis of cytokine frequency from R2:WT and R2:IL-10 chimeric mice. Datum is representative of two independent experiments. Data are shown as mean ± SEM. Each dot represents a mouse. **P value < 0.01. Non-significant (ns).

increase in suppressor T cells in WT mice compared to $CCR2^{-/-}$ mice. Suppressor T cells can be either $Foxp3^+$ or $Foxp3^-$ (35). We observed no difference in the frequency of $Foxp3^+$ regulatory T cells between WT and $CCR2^{-/-}$ mice (**Supplementary Figure 2**). Then, we examined the frequency of endogenous $CD44^+CD4^+$ IL-10 producing T cells post antigen and Poly I:C exposure and observed an increase in IL-10 producing $CD4^+$ T cells in WT mice compared to $CCR2^{-/-}$ mice (**Supplementary Figure 2**). Since these data do not convey antigen-specificity, OTII OVA-specific CD4 T cells were crossed with an IL-10 reporter and transferred these into WT or $CCR2^{-/-}$ mice. After delivery of antigen with Poly I:C, WT mice displayed a significant increase in IL-10 producing antigen-specific $CD4^+$ T cells compared to $CCR2^{-/-}$ monocyte deficient mice (**Figure 4A**).

Based on this finding, we examined *ex vivo* whether endogenous $CD4^+$ T cells from antigen and Poly I:C treated WT mice are more suppressive than those from $CCR2^{-/-}$ mice. We isolated $CD4^+$ T cells from the LLNs of WT and $CCR2^{-/-}$ mice treated with antigen and Poly I:C and co-cultured them with antigen-specific CD8 T cells and stimulants (splenic DCs, antigen and Poly I:C). After five days in culture, antigen-specific $CD8^+$ T cells co-cultured with $CD4^+$ T cells from WT mice compared to $CCR2^{-/-}$ mice produced significantly less IFNγ (**Figure 4B**). This suggests that LN monocytes are required for the induction of an antigen-specific $CD4^+$ T cell that suppresses the Poly I:C induced CTL response.

To clearly demonstrate that antigen presentation by monocytes is required for the induction of suppressor T cells, we created BM chimeric mice where monocytes lacked MHCII expression (80:20, $CCR2^{-/-}MHCII^{-/-}$ BM). First, we examined whether endogenous Poly I:C-induced antigen-specific $CD8^+$ T cells were significantly increased when monocytes lacked the ability to differentiate suppressor CD4 T cells. Indeed, when monocytes lacked MHCII expression, tetramer staining illustrated a significant increase in endogenous Poly I:C induced antigen-specific $CD8^+$ T cells (**Figure 5A**). When $CCR2^{-/-}$:$MHCII^{-/-}$ BM chimeras were challenged with antigen, Poly I:C, and antigen-specific $CD8^+$ T

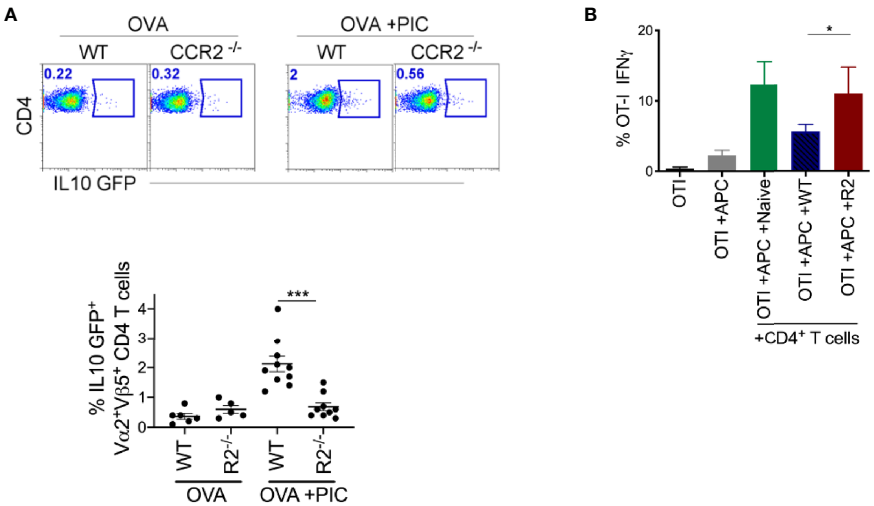

FIGURE 4 | Monocytes are required for the induction of suppressive $CD4^+$ T cells. **(A)** After immunization as outlined in **Figure 1B** and adoptive transfer of OTII IL-10 GFP^+ cells, LLN antigen-specific OTII IL-10 GFP^+ T cells was examined in WT and $CCR2^{-/-}$ mice. Representative flow plots display OTII population gated on $V\alpha2^+V\beta5^+CD4^+$IL-10 GFP^+ from WT and $CCR2^{-/-}$ mice, top. Scatter plot analysis of targeted population frequency from individual mice, Bottom. Combined set of 2 independent experiment. **(B)** WT splenic DCs and CFSE-labeled OTI cells were co-cultured with $CD4^+$ T cells isolated from LLN of either naïve mice or WT and $CCR2^{-/-}$ mice immunized with OVA ± Poly IC as outlined in **Figure 1B**. Bar graph demonstrates IFNγ (left) and TNFα (right) producing OTI T cells after 5 days of co-culture. Data are representative of two independent experiments, n=4 mice per group. Data are shown as mean ± SEM. ***P value < 0.001. *P < 0.05.

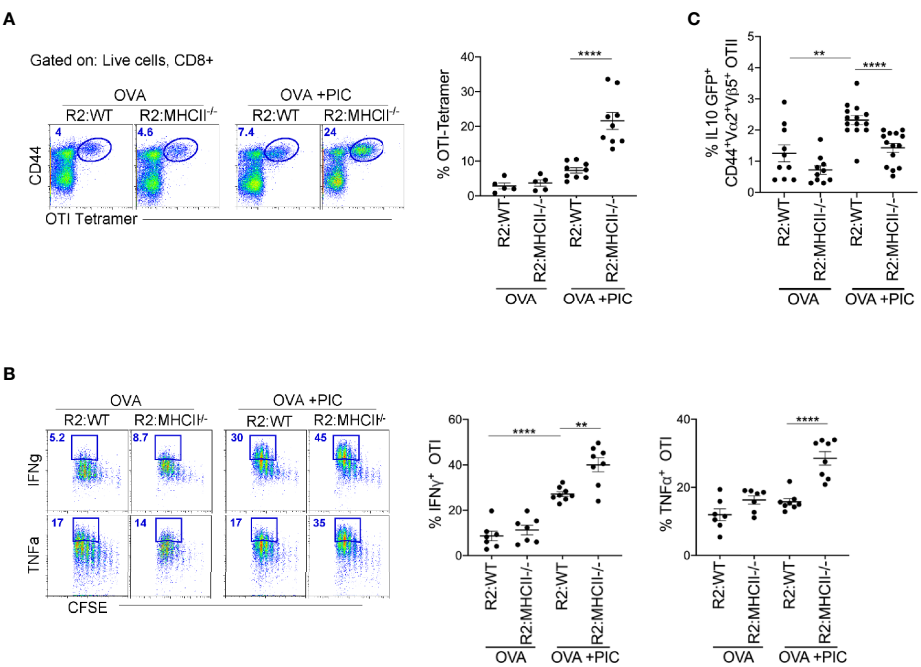

FIGURE 5 | Poly IC-induced IL-10 production to suppress antigen-specific CTL response is done by $MHCII^+$ monocytes. **(A)** OTI SIINFEKL $tetramer^+$ T cells was examined in BM Chimeric mice after immunization and adoptive transfer (i.v.) of OTI cells. Scatter plot shows analysis of targeted population frequency from individual mice (right) and flow panel illustrate the representative $CD44^+$ $Tetramer^+$ OTI cells (left). Combined set of 2 independent experiment, n=3-5 mice per group. **(B)** After immunization as outlined in **Figure 1B**, LLN antigen-specific OTII IL-10 GFP^+ T cells was examined in BM Chimeric mice. Combined set of 3 independent experiments, n=3-5 mice per group**. (C)** Lethally irradiated mice were reconstituted 80:20 with $CCR2^{-/-}$ and $MHCII^{-/-}$ BM cells: R2:MHCII chimeric mice. Control mice were reconstituted 80:20 with $CCR2^{-/-}$ and WT BM cells: R2:WT chimeric mice. Flow and Scatter plot analysis of cytokine frequency from respective BM chimeric mice. Representative data of 2 independent experiments, n=3-5 mice per group. Data are shown as mean ± SEM. Each dot represents a mouse. ****P value < 0.0001. **P < 0.01.

cells, as in **Figure 1**, mice lacking MHCII expression on monocytes, displayed significantly enhanced cytokine production in Poly I:C-induced antigen-specific T cells (**Figure 5B**). Finally, we demonstrated in MHCII sufficient monocyte BM chimeras that the differentiation of IL-10 producing antigen-specific $CD4^+$ T cells was significantly greater than in MHCII deficient monocyte BM chimeras (**Figure 5C**). Overall, these data suggest that MHCII expression on monocytes and not DCs is required for the differentiation of IL-10 suppressor antigen-specific $CD4^+$ T cells that regulate the Poly I:C induced CTL response.

Blocking IL-10 Improves Prophylactic Treatment in Metastatic Melanoma Model

Next, the relevance of these findings was demonstrated in a prophylactic metastatic melanoma model. Treatment with anti-IL-10 was performed instead of monocyte depletion, as there are currently no human monocyte specific depleting antibodies. A triple combination therapy of anti-IL-10, tumor peptides and Poly I:C, was compared to tumor peptides +/- Poly I:C, types of therapy already known to promote anti-tumor immunity. Although the tumor peptides with Poly I:C alone displayed a robust anti-tumor immune response, the triple combination therapy of melanoma challenged mice displayed the greatest anti-tumor immunity (**Figure 6** and **Supplementary Figure 3**). This finding demonstrates that an anti-tumor immune response can be significantly enhanced in combination with IL-10 neutralization.

Human Lung-Draining LN Monocytes Selectively Express IL-10

Finally, to translate our findings to clinical practice, we examined whether human LN monocytes, like mice, express IL-10. Indeed, like mice, human LLNs contained a similar number of $CD14^+CD11c^{hi}HLADR^+$ monocytes as $CD14^-CD11c^{hi}HLADR^{++}$ DCs (**Figure 7A**) (36, 40), and expressed significantly more IL-10.

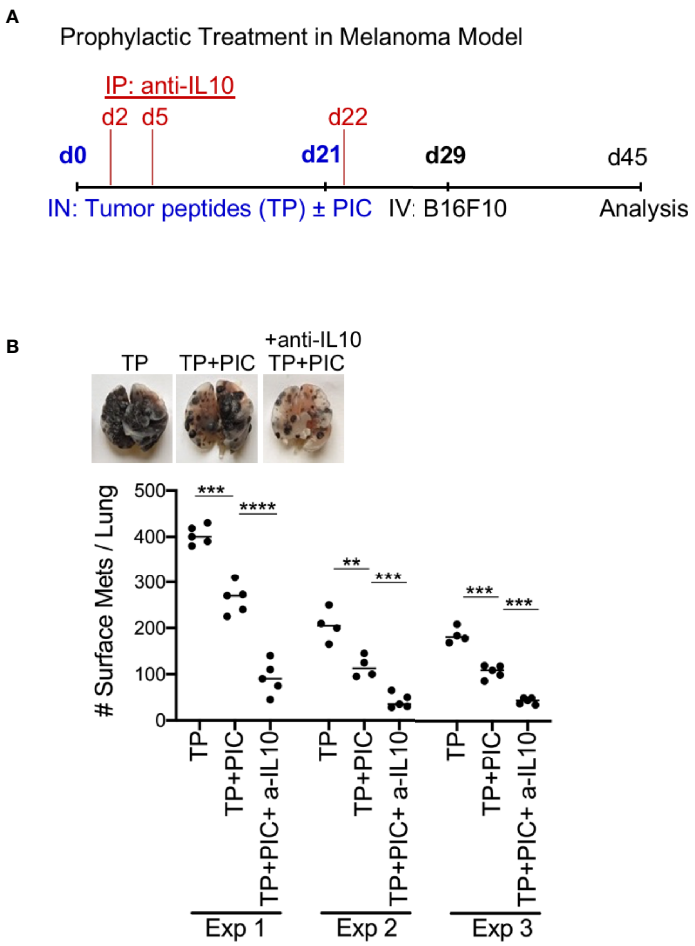

FIGURE 6 | Immunization with B16F10 Peptides (TP) +Poly IC +anti IL-10 subunit vaccine produces anti-tumor effect in metastatic B16F10 melanoma model. **(A)** Schematic protocol for vaccination and B16F10 i.v. injection in WT mice for anti-tumor effect. **(B)** WT with TP (peptides) only, with TP +Poly IC and with TP +Poly IC +anti-IL-10 were harvested after i.v. B16F10 challenge and mouse lungs were inflated. Pics depict total surface metastases (mets) per lung (top), which were enumerated and illustrated by scatter plot, each dot represents one mouse (bottom). Combined data of three independent experiments with 4-5 mice per group. Data are shown as mean ± SEM. ****P value < 0.0001. ***P < 0.001. **P < 0.01.

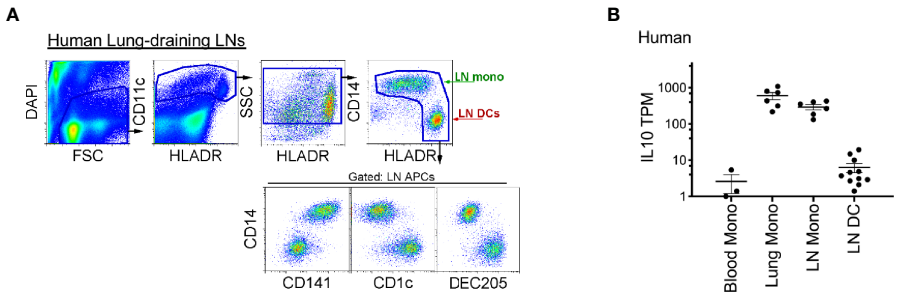

FIGURE 7 | Compared to LN DCs, human lung and lung-draining LN monocytes express IL-10. **(A)** Top, flow cytometry gating strategy to identify human lung-draining LN monocytes and DCs: live cell gate, DAPI$^-$, followed by CD11c$^+$ cells and intermediate-high side scatter with the final HLADR$^{+/high}$ APC gate: displaying CD14$^+$CD141$^{low/+}$ monocytes and DC subsets (CD14$^-$CD141$^-$, CD1c$^+$, DEC205$^+$). Flow plot is representative of over 30 human LLNs analyzed (36, 40). **(B)** RNA sequencing, transcripts per million (TPM) of monocytes and DCs sorted from human blood, lung and lung-draining LN (40). Data are shown as mean ± SEM.

Transcriptionally, the lung and LLN monocytes expressed ~10 to 100-fold greater amounts of IL-10 compared to LN DCs and immature blood monocytes (**Figure 7B**). This demonstrates that human monocytes produce IL-10 after extravasation into tissue and LN and perhaps, play a continuous role of regulating immunity.

DISCUSSION

In this study, we found that monocytes regulate Poly I:C-induced antigen-specific CTL response. First, we demonstrated that in the absence of LN monocytes (in CCR2$^{-/-}$ mice), there was an enhanced Poly I:C-induced CTL response compared to WT mice. Second, using BM chimeric mice that lack key functional properties of monocytes—MHCI antigen cross-presentation, PDL1, IL-10, and MHCII antigen presentation—we found that the absence of IL-10 production and MHCII expression impaired monocyte function, resulting in enhanced CTL response. Third, we demonstrated that the production of IL-10 by monocytes was required to promote the differentiation of suppressor CD4$^+$ T cells. When CD4$^+$ T cells were isolated from WT mice inoculated with antigen and Poly I:C, and co-cultured with stimulated OTI T cells, CTL cytokines were significantly suppressed compared to CD4$^+$ T cells isolated from monocyte deficient mice. These results demonstrate that the presence of monocytes is required to develop antigen-specific suppressor CD4$^+$ T cells. Fourth, in a metastatic melanoma model, we examined the importance of removing the monocytic brake in a prophylactic treatment consisting of anti-IL-10, tumor peptides and Poly I:C. The triple combination therapy resulted in significantly fewer tumors compared to mice treated with tumor peptides and Poly I:C alone. Finally, we found that like mice, only human LN monocytes (but not DCs) expressed IL-10. This finding converges with other studies of human orthologs of splenic APCs, which show that monocytes (compared to other cell types) have strong transcriptional correspondence across species (1, 41). Overall, our findings suggest that monocytes exert a braking function on Poly I:C-induced CTL responses through the production of IL-10 and indirectly *via* the induction of suppressor CD4+ T cells. This novel function of LN monocytes limits the potential for DC-mediated over-exuberant CTL responses that might be damaging to the host. The development of a suppressor CD4+ T cell population is likely important in returning the immune system to homeostasis after an inflammatory response.

Our findings have implications for the development of vaccines and other therapeutics that depend on Poly I:C. The future of personalized medicine is here, and the synthesis of personalized neoantigens with Poly I:C and immune checkpoint blockade is currently in clinical trials. Although these trials appear to be efficacious, understanding what may potentiate or limit the efficiency is critical in developing additional treatments for combination therapy, such as IL-10 as demonstrated here. In addition, the tumor microenvironment contains suppressive monocyte-derived cells which can be targeted in a similar fashion as illustrated here for LN monocytes. Thus, defining the role each antigen-presenting cell subtype may play during the induction of the desired cancer or pathogen vaccine is imperative and may enhance our ability to develop immunotherapies for cancer and other diseases.

DATA AVAILABILITY STATEMENT

The raw data supporting the conclusions of this article will be made available by the authors, without undue reservation.

ETHICS STATEMENT

The animal study was reviewed and approved by National Jewish Health and Dartmouth Hitchcock Medical College, an AAALAC accredited institution, and used in accordance with protocols approved by the Institutional Animal Care and Utilization Committee.

AUTHOR CONTRIBUTIONS

AT, MP, SG, and CJ contributed to concept, experimental design, and wrote the manuscript. AT, MP, SG, and KR performed the animal experiments and analyzed the data. All authors contributed to the article and approved the submitted version.

FUNDING

National Institutes of Health supported this work CJ grants: R01 HL115334, R01 HL135001 and R35 HL155458 (CJ).

ACKNOWLEDGMENTS

We would like to thank Dr. Shaikh M. Atif for experimental assistance. Madeline Morrison and Dina K. Rabadi for their critical feedback.

SUPPLEMENTARY MATERIAL

The Supplementary Material for this article can be found online at: https://www.frontiersin.org/articles/10.3389/fimmu.2021.763379/full#supplementary-material

REFERENCES

1. Leach SM, Gibbings SL, Tewari AD, Atif SM, Vestal B, Danhorn T, et al. Human and Mouse Transcriptome Profiling Identifies Cross-Species Homology in Pulmonary and Lymph Node Mononuclear Phagocytes. *Cell Rep* (2020) 33(5):108337. doi: 10.1016/j.celrep.2020.108337
2. Edelson BT, Kc W, Juang R, Kohyama M, Benoit LA, Klekotka PA, et al. Peripheral CD103+ Dendritic Cells Form a Unified Subset Developmentally Related to CD8alpha+ Conventional Dendritic Cells. *J Exp Med* (2010) 207 (4):823–36. doi: 10.1084/jem.20091627
3. Tussiwand R, Everts B, Grajales-Reyes GE, Kretzer NM, Iwata A, Bagaitkar J, et al. Klf4 Expression in Conventional Dendritic Cells Is Required for T Helper 2 Cell Responses. *Immunity* (2015) 42(5):916–28. doi: 10.1016/j.immuni.2015.04.017
4. Murphy KM. Transcriptional Control of Dendritic Cell Development. *Adv Immunol* (2013) 120:239–67. doi: 10.1016/B978-0-12-417028-5.00009-0
5. Bosteels C, Neyt K, Vanheerswynghels M, van Helden MJ, Sichien D, Debeuf N, et al. Inflammatory Type 2 cDCs Acquire Features of Cdc1s and Macrophages to Orchestrate Immunity to Respiratory Virus Infection. *Immunity* (2020) 52(6):1039–56 e9. doi: 10.1016/j.immuni.2020.04.005
6. Desch AN, Gibbings SL, Clambey ET, Janssen WJ, Slansky JE, Kedl RM, et al. Dendritic Cell Subsets Require Cis-Activation for Cytotoxic CD8 T-Cell Induction. *Nat Commun* (2014) 5:4674. doi: 10.1038/ncomms5674
7. Jakubzick C, Gautier EL, Gibbings SL, Sojka DK, Schlitzer A, Johnson TE, et al. Minimal Differentiation of Classical Monocytes as They Survey Steady-State Tissues and Transport Antigen to Lymph Nodes. *Immunity* (2013) 39 (3):599–610. doi: 10.1016/j.immuni.2013.08.007
8. Hohl TM, Rivera A, Lipuma L, Gallegos A, Shi C, Mack M, et al. Inflammatory Monocytes Facilitate Adaptive CD4 T Cell Responses During Respiratory Fungal Infection. *Cell Host Microbe* (2009) 6(5):470–81. doi: 10.1016/j.chom.2009.10.007
9. Kim TS, Braciale TJ. Respiratory Dendritic Cell Subsets Differ in Their Capacity to Support the Induction of Virus-Specific Cytotoxic CD8+ T Cell Responses. *PloS One* (2009) 4(1):e4204. doi: 10.1371/journal.pone.0004204
10. Yona S, Kim KW, Wolf Y, Mildner A, Varol D, Breker M, et al. Fate Mapping Reveals Origins and Dynamics of Monocytes and Tissue Macrophages Under Homeostasis. *Immunity* (2013) 38(1):79–91. doi: 10.1016/j.immuni.2012.12.001
11. Gibbings SL, Thomas SM, Atif SM, McCubbrey AL, Desch AN, Danhorn T, et al. Three Unique Interstitial Macrophages in the Murine Lung at Steady State. *Am J Respir Cell Mol Biol* (2017) 57(1):66–76. doi: 10.1165/rcmb.2016-0361OC
12. Liu K, Waskow C, Liu X, Yao K, Hoh J, Nussenzweig M. Origin of Dendritic Cells in Peripheral Lymphoid Organs of Mice. *Nat Immunol* (2007) 8(6):578–83. doi: 10.1038/ni1462
13. Jakubzick C, Tacke F, Ginhoux F, Wagers AJ, van Rooijen N, Mack M, et al. Blood Monocyte Subsets Differentially Give Rise to CD103+ and CD103- Pulmonary Dendritic Cell Populations. *J Immunol* (2008) 180(5):3019–27. doi: 10.4049/jimmunol.180.5.3019
14. Ginhoux F, Greter M, Leboeuf M, Nandi S, See P, Gokhan S, et al. Fate Mapping Analysis Reveals That Adult Microglia Derive From Primitive Macrophages. *Science* (2010) 330(6005):841–5. doi: 10.1126/science.1194637
15. Schulz C, Gomez Perdiguero E, Chorro L, Szabo-Rogers H, Cagnard N, Kierdorf K, et al. A Lineage of Myeloid Cells Independent of Myb and Hematopoietic Stem Cells. *Science* (2012) 336(6077):86–90. doi: 10.1126/science.1219179
16. Scott CL, Henri S, Guilliams M. Mononuclear Phagocytes of the Intestine, the Skin, and the Lung. *Immunol Rev* (2014) 262(1):9–24. doi: 10.1111/imr.12220
17. Jakubzick CV, Randolph GJ, Henson PM. Monocyte Differentiation and Antigen-Presenting Functions. *Nat Rev Immunol* (2017) 17(6):349–62. doi: 10.1038/nri.2017.28
18. Atif SM, Gibbings SL, Redente EF, Camp FA, Torres RM, Kedl RM, et al. Immune Surveillance by Natural IgM Is Required For Early Neoantigen Recognition and Initiation of Adaptive Immunity. *Am J Respir Cell Mol Biol* (2018) 59(5):580–91. doi: 10.1165/rcmb.2018-0159OC
19. Larson SR, Atif SM, Gibbings SL, Thomas SM, Prabagar MG, Danhorn T, et al. Ly6C(+) Monocyte Efferocytosis and Cross-Presentation of Cell-Associated Antigens. *Cell Death Differ* (2016) 23(6):997–1003. doi: 10.1038/cdd.2016.24
20. Misharin AV, Morales-Nebreda L, Reyfman PA, Cuda CM, Walter JM, McQuattie-Pimentel AC, et al. Monocyte-Derived Alveolar Macrophages Drive Lung Fibrosis and Persist in the Lung Over the Life Span. *J Exp Med* (2017) 214(8):2387–404. doi: 10.1084/jem.20162152
21. Ravichandran KS, Lorenz U. Engulfment of Apoptotic Cells: Signals for a Good Meal. *Nat Rev Immunol* (2007) 7(12):964–74. doi: 10.1038/nri2214
22. Henson PM, Bratton DL. *Recogntion and Removal of Apopotic Cells*. DG Russell, S Gordon, editors. Washington: ASM Press (2009) p. 341–65.
23. Serbina NV, Salazar-Mather TP, Biron CA, Kuziel WA, Pamer EG. TNF/iNOS-Producing Dendritic Cells Mediate Innate Immune Defense Against Bacterial Infection. *Immunity* (2003) 19(1):59–70. doi: 10.1016/S1074-7613(03)00171-7
24. Guilliams M, Mildner A, Yona S. Developmental and Functional Heterogeneity of Monocytes. *Immunity* (2018) 49(4):595–613. doi: 10.1016/j.immuni.2018.10.005
25. Randolph GJ, Inaba K, Robbiani DF, Steinman RM, Muller WA. Differentiation of Phagocytic Monocytes Into Lymph Node Dendritic Cells *In Vivo*. *Immunity* (1999) 11(6):753–61. doi: 10.1016/S1074-7613(00)80149-1
26. Nakano H, Lin KL, Yanagita M, Charbonneau C, Cook DN, Kakiuchi T, et al. Blood-Derived Inflammatory Dendritic Cells in Lymph Nodes Stimulate Acute T Helper Type 1 Immune Responses. *Nat Immunol* (2009) 10 (4):394–402. doi: 10.1038/ni.1707
27. Cheong C, Matos I, Choi JH, Dandamudi DB, Shrestha E, Longhi MP, et al. Microbial Stimulation Fully Differentiates Monocytes to DC-SIGN/CD209(+) Dendritic Cells for Immune T Cell Areas. *Cell* (2010) 143(3):416–29. doi: 10.1016/j.cell.2010.09.039
28. Langlet C, Tamoutounour S, Henri S, Luche H, Ardouin L, Gregoire C, et al. CD64 Expression Distinguishes Monocyte-Derived and Conventional Dendritic Cells and Reveals Their Distinct Role During Intramuscular Immunization. *J Immunol* (2012) 188(4):1751–60. doi: 10.4049/jimmunol.1102744
29. Leon B, Lopez-Bravo M, Ardavin C. Monocyte-Derived Dendritic Cells Formed at the Infection Site Control the Induction of Protective T Helper 1 Responses Against Leishmania. *Immunity* (2007) 26(4):519–31. doi: 10.1016/j.immuni.2007.01.017

30. Yi H, Guo C, Yu X, Zuo D, Wang XY. Mouse CD11b+Gr-1+ Myeloid Cells can Promote Th17 Cell Differentiation and Experimental Autoimmune Encephalomyelitis. *J Immunol* (2012) 189(9):4295–304. doi: 10.4049/jimmunol.1200086
31. Ko HJ, Brady JL, Ryg-Cornejo V, Hansen DS, Vremec D, Shortman K, et al. GM-CSF-Responsive Monocyte-Derived Dendritic Cells Are Pivotal in Th17 Pathogenesis. *J Immunol* (2014) 192(5):2202–9. doi: 10.4049/jimmunol.1302040
32. Croxford AL, Lanzinger M, Hartmann FJ, Schreiner B, Mair F, Pelczar P, et al. The Cytokine GM-CSF Drives the Inflammatory Signature of CCR2+ Monocytes and Licenses Autoimmunity. *Immunity* (2015) 43(3):502–14. doi: 10.1016/j.immuni.2015.08.010
33. Ott PA, Hu Z, Keskin DB, Shukla SA, Sun J, Bozym DJ, et al. An Immunogenic Personal Neoantigen Vaccine for Patients With Melanoma. *Nature* (2017) 547(7662):217–21. doi: 10.1038/nature22991
34. Ott PA, Hu-Lieskovan S, Chmielowski B, Govindan R, Naing A, Bhardwaj N, et al. A Phase Ib Trial of Personalized Neoantigen Therapy Plus Anti-PD-1 in Patients With Advanced Melanoma, Non-Small Cell Lung Cancer, or Bladder Cancer. *Cell* (2020) 183(2):347–62 e24. doi: 10.1016/j.cell.2020.08.053
35. Vieira PL, Christensen JR, Minaee S, O'Neill EJ, Barrat FJ, Boonstra A, et al. IL-10-Secreting Regulatory T Cells do Not Express Foxp3 But Have Comparable Regulatory Function to Naturally Occurring CD4+CD25+ Regulatory T Cells. *J Immunol* (2004) 172(10):5986–93. doi: 10.4049/jimmunol.172.10.5986
36. Desch AN, Gibbings SL, Goyal R, Kolde R, Bednarek J, Bruno T, et al. Flow Cytometric Analysis of Mononuclear Phagocytes in Non-Diseased Human Lung and Lung-Draining Lymph Nodes. *Am J Respir Crit Care Med* (2015) 193(6):614–26. doi: 10.1164/rccm.201507-1376OC
37. Serbina NV, Pamer EG. Monocyte Emigration From Bone Marrow During Bacterial Infection Requires Signals Mediated by Chemokine Receptor CCR2. *Nat Immunol* (2006) 7(3):311–7. doi: 10.1038/ni1309
38. Daley JM, Thomay AA, Connolly MD, Reichner JS, Albina JE. Use of Ly6G-Specific Monoclonal Antibody to Deplete Neutrophils in Mice. *J Leukoc Biol* (2008) 83(1):64–70. doi: 10.1189/jlb.0407247
39. Wakim LM, Bevan MJ. Cross-Dressed Dendritic Cells Drive Memory CD8+ T-Cell Activation After Viral Infection. *Nature* (2011) 471(7340):629–32. doi: 10.1038/nature09863
40. Gibbings SL, Jakubzick CV. A Consistent Method to Identify and Isolate Mononuclear Phagocytes From Human Lung and Lymph Nodes. *Methods Mol Biol* (2018) 1799:381–95. doi: 10.1007/978-1-4939-7896-0_28
41. Ingersoll MA, Spanbroek R, Lottaz C, Gautier EL, Frankenberger M, Hoffmann R, et al. Comparison of Gene Expression Profiles Between Human and Mouse Monocyte Subsets. *Blood* (2010) 115(3):e10–9. doi: 10.1182/blood-2009-07-235028

Conflict of Interest: The authors declare that the research was conducted in the absence of any commercial or financial relationships that could be construed as a potential conflict of interest.

Publisher's Note: All claims expressed in this article are solely those of the authors and do not necessarily represent those of their affiliated organizations, or those of the publisher, the editors and the reviewers. Any product that may be evaluated in this article, or claim that may be made by its manufacturer, is not guaranteed or endorsed by the publisher.

Copyright © 2021 Tewari, Prabagar, Gibbings, Rawat and Jakubzick. This is an open-access article distributed under the terms of the Creative Commons Attribution License (CC BY). The use, distribution or reproduction in other forums is permitted, provided the original author(s) and the copyright owner(s) are credited and that the original publication in this journal is cited, in accordance with accepted academic practice. No use, distribution or reproduction is permitted which does not comply with these terms.

frontiers in Immunology

ORIGINAL RESEARCH
published: 12 October 2021
doi: 10.3389/fimmu.2021.701675

The Transcription Factor FRA-1/AP-1 Controls Lipocalin-2 Expression and Inflammation in Sepsis Model

Shan Cao[1†], *Anne Schnelzer*[1†], *Nicole Hannemann*[1,2], *Georg Schett*[1], *Didier Soulat*[3*‡] *and Aline Bozec*[1*‡]

[1] Department of Internal Medicine 3, Rheumatology and Immunology, Universitätsklinikum Erlangen, Friedrich-Alexander-Universität (FAU) Erlangen-Nürnberg, Erlangen, Germany, [2] Institute of Regenerative Medicine and Biotherapies (IRMB), University of Montpellier, INSERM U1183, Montpellier, France, [3] Mikrobiologisches Institut – Klinische Mikrobiologie, Immunologie und Hygiene, Universitätsklinikum Erlangen, Friedrich-Alexander-Universität (FAU) Erlangen-Nürnberg, Erlangen, Germany

OPEN ACCESS

Edited by:
Amiram Ariel,
University of Haifa, Israel

Reviewed by:
Esther G. Meyron-Holtz,
Technion Israel Institute of Technology, Israel
Verena Link,
National Institutes of Health (NIH), United States

***Correspondence:**
Didier Soulat
Didier.Soulat@uk-erlangen.de
Aline Bozec
Aline.Bozec@uk-erlangen.de

[†]*These authors have contributed equally to this work*

[‡]*These authors have contributed equally to this work*

Specialty section:
This article was submitted to Inflammation, a section of the journal Frontiers in Immunology

Received: *28 April 2021*
Accepted: *24 September 2021*
Published: *12 October 2021*

Citation:
Cao S, Schnelzer A, Hannemann N, Schett G, Soulat D and Bozec A (2021) The Transcription Factor FRA-1/AP-1 Controls Lipocalin-2 Expression and Inflammation in Sepsis Model. Front. Immunol. 12:701675. doi: 10.3389/fimmu.2021.701675

Sepsis is a life-threatening condition characterized by excessive inflammation in its early phase. This is followed by an aberrant resolution phase associated to a prolonged period of immune suppression that can ultimately lead to multiple organ dysfunctions. This immunosuppression can be mediated by the functional reprogramming of gene transcription in monocytes/macrophages in response to prolonged lipopolysaccharide (LPS) exposure. Surprisingly, there is no report on the role of AP-1 transcription factors in this reprogramming process. Herein, we used the endotoxin tolerance model on murine bone marrow-derived macrophages in which tolerant cells stimulated twice with LPS were compared to naïve cells stimulated once. Out of all AP-1 transcription factors tested, *Fosl1* gene stood out because of its unique regulation in tolerized cells. Moreover, we could correlate FRA-1 expression to the expression of an essential anti-inflammatory molecule involved in sepsis response, Lipocalin 2 aka NGAL. Identical results were obtained in human PBMC following the endotoxin tolerance model. When using FRA-1 deficient macrophages, we could confirm that FRA-1 regulates NGAL expression during the tolerant state. Interestingly, ChIP-seq and ChIP-qPCR revealed the binding of FRA-1 on *Lcn2* promoter after LPS stimulation in these cells. Finally, we used an *in vivo* septic model of consecutive injection of LPS, in which the second stimulation is performed before the resolution of inflammation, in wild type and FRA-1 deficient mice. NGAL secretion was elevated in lung, spleen and serum of wild type tolerant mice, whereas it was significantly lower in tolerant FRA-1 deficient mice. Moreover, an increased inflammatory state likely dependent of the low level of NGAL was observed in these FRA-1 deficient mice. This was characterized by an increase of neutrophil infiltration in lung and an increase of apoptotic follicular cells in spleen. This suggests that FRA-1 expression supports resolution of

inflammation in this model. Collectively, our data indicate that FRA-1 is involved in myeloid cell tolerance responses by mediating the functional reprogramming of *Lcn2* transcription in response to prolonged LPS exposure. In conclusion, FRA-1 may have a protective role in the tolerance response of sepsis through the regulation of NGAL, leading to resolution of inflammation.

Keywords: sepsis, transcription factor, AP-1/Fra-1, lipocalin-2, macrophage, endotoxin tolerance

INTRODUCTION

Sepsis is a life-threatening condition, which represents the leading cause of death in intensive care units (ICUs) worldwide (1). In the last decades, numerous treatments to ameliorate sepsis outcome have failed in clinical trials. There is therefore a strong need to better understand the underlying sepsis mechanism to develop new therapeutic strategies (2). Sepsis is caused by a dysregulated host response to infection that consists of two dynamic phases. The initial and uncontrolled systemic inflammatory response (SIRS) is followed by an unchecked compensatory anti-inflammatory response (CARS). This latter phase often fails to adequately resolve the systemic inflammation and predisposes to immune dysfunction. The failure of resolution process can lead to collateral tissue destruction and multiple organ dysfunction often lethal (3).

The most prominent feature of sepsis-induced immunosuppression is the diminished capacity of innate immune cells, especially monocytes and macrophages, to release pro-inflammatory cytokines in response to pathogen associated molecular patterns (PAMP) (3). Ultimately, these deactivated macrophages adopt an immunosuppressive phenotype making them unresponsive to secondary infections, but prone to resolve inflammation and regenerate tissue. In the case of sepsis, this tolerization process can be studied in the context of endotoxin tolerance induced by consecutive LPS stimulations (4).

Two classes of genes have been categorized in tolerant macrophages in previous studies: genes not inducible described as 'tolerizable' genes and genes still inducible named 'non-tolerizable' genes (5). Interleukin-6 (*Il6*), known as a classical pro-inflammatory cytokine in sepsis, is a typical tolerizable gene. Despite being a TLR inducible gene, the induction of IL-6 expression by macrophages was abolished after a second LPS stimulation. On the other side, non-tolerizable genes such as lipocalin-2 (*Lcn2*) were found to be significantly elevated in tolerant macrophages (5). Also known as neutrophil gelatinase-associated lipocalin, NGAL is a mammalian protein expressed by myeloid and epithelial cells in response to TLR activation during infections. NGAL plays an anti-microbial role by inhibiting bacterial siderophores and therefore depriving bacteria of iron (6). In parallel to this anti-microbial function, NGAL expression is also important for the immune response. In a LPS-induced sepsis model, *Lcn2* knockout mice showed a dysregulated iron metabolism that resulted in an increased apoptosis of leukocytes, an increased release of pro-inflammatory cytokines and a higher mortality (7). Similarly, NGAL has been shown to induce the production of the anti-inflammatory cytokine IL-10 in macrophages during *Streptococcus pneumoniae* infection, making NGAL not only a marker of macrophages deactivation but also a deactivator of macrophages (8). Interestingly, a feed forward regulation between IL-10 and NGAL has been suggested in another sepsis model, in which NGAL expression correlates with IL-10 level and a better outcome after polymicrobial sepsis (9). Collectively, these researches imply that NGAL plays a role in controlling inflammation and thereby contributes to the resolution of severe inflammation (7). However, its transcriptional regulation, especially in the tolerant cells remains to be defined since regulating the expression of NGAL may provide novel therapy for the resolution of sepsis.

Recent investigations have focused on the mechanisms underlying the functional reprogramming of the gene transcription in macrophages in response to prolonged LPS exposure. Up-regulation of hypoxia-inducible factor-α (HIF-1α) and subsequent elevation of the negative regulator of TLR signaling IRAKM have been involved in the establishment of an endotoxin-tolerant state in monocytes which interestingly possess anti-bacterial and wound-healing properties (10). At the transcriptional level, the cyclin-dependent kinase inhibitor p21 has been shown to tune NF-κB pathway that controls part of the macrophages reprogramming happening during endotoxin tolerance. A high level of p21 favors p50-p50 over p65-p50 for binding to NF-κB sites on DNA, resulting in lower IFN-β production and a hypo-responsive phenotype of macrophage (11). Surprisingly, no data has been reported on the role of AP-1 transcription factors in this reprogramming process. AP-1 family is mainly composed of c-Fos and c-Jun related transcription factors. Depending on stimuli and cell type, they can be activated by phosphorylation or methylation, promptly assembled into homodimers or heterodimers through their leucine-zipper domain and bound to AP-1 sites on target gene promoter, resulting in the promotion or inhibition of gene expression (12).

In the present work, we studied AP-1 transcription factors role using the endotoxin tolerance model in both murine bone marrow-derived macrophages (BMDM) and human peripheral blood mononuclear cell (PBMC). We found that the expression of FRA-1 and NGAL were positively correlated in response to LPS, both in tolerant murine and human cells *in vitro*. With the help of FRA-1 deficient BMDM, we showed that FRA-1 positively regulates NGAL expression especially in the tolerant state. Using ChIP-seq and ChIP-qPCR, FRA-1 was shown to bind *Lcn2* promoter, especially in the tolerant state. Finally, *in vivo* septic model using consecutive injection of LPS showed a decreased resolution as well as an increased inflammation in

FRA-1 depleted conditions, likely dependent on the low level of NGAL in these mice. Collectively, our results indicate that FRA-1 transcription factor is involved in myeloid cell tolerant responses by mediating the functional reprogramming of *Lcn2* transcription in response to prolonged LPS exposure.

METHODS AND MATERIALS

Animals

Wild type C57Bl/6NCrl mice were purchased from Charles River. The generation of *Fosl1* floxed and *Mx*-Cre mice has been described before (13). Briefly, the *Fosl1* gene knockout in *Fosl1*$^{\Delta Mx}$ mice was induced 2 weeks before the experiment by 3 consecutive injections of 250 µg poly(I:C) per mouse every other day. Littermate *Fosl1*$^{fl/fl}$ mice were used as controls and were treated with poly (I:C) like the deficient mice. Mice were bred and maintained on a 129/B6 mixed background. All experiments were performed with 8-12-week-old mice (both male and female). Animals were kept under standardized conditions. A 12-hour light/12-hour dark cycle was maintained, and standard diet and water were provided ad libitum. All animal experiments were discussed and approved by the University of Friedrich-Alexander-Universität Erlangen-Nürnberg ethics committee and carried out in accordance with protocols approved by the German law.

Cell Preparation

Bone marrow-derived macrophages (BMDM) were generated from total bone marrow cells flushed out from 8-12 weeks old mice. The total bone marrow cells were then incubated within 10 cm petri dishes in 5% CO_2 at 37°C in DMEM and GlutaMAX (Gibco, Thermo Fisher Scientific) supplemented with 10% (v/v) FCS (Gibco, Thermo Fisher Scientific), 1% (v/v) penicillin/streptomycin (Gibco, Thermo Fisher Scientific), and 20% (v/v) supernatant from L929 fibroblast cultures [ATCC clone CCL-1] as a source of macrophage colony-stimulating factor (M-CSF) (14). After overnight incubation, the non-adherent cells were then harvested and reseeded into 10 cm petri dishes supplemented with the medium above at the concentration of $5x10^6$ cells/dish. 7 days later, BMDM were carefully harvested, counted and replated into 12-well plates at the concentration of $1x10^6$ cells/well in RPMI-1640 (Gibco, Thermo Fisher Scientific) supplemented with 10% (v/v) FCS (Gibco, Thermo Fisher Scientific) and 1% (v/v) penicillin/streptomycin (Gibco, Thermo Fisher Scientific). After overnight incubation, the adherent cells were stimulated with 10 ng/mL LPS (Naïve) or stimulated with 100 ng/mL LPS for 24 h, washed twice with warm PBS and stimulated again with 10 ng/mL LPS (Tolerant) as described in previous study (5).

Human peripheral blood mononuclear cells (PBMCs) were isolated from EDTA-blood of normal, healthy donors, using a Ficoll gradient (Lymphoflot, Bio-Rad). PBMCs were then incubated overnight in RPMI-1640 (Gibco, Thermo Fisher Scientific) supplemented with 10% (v/v) FCS (Gibco, Thermo Fisher Scientific) and 1% (v/v) penicillin/streptomycin (Gibco, Thermo Fisher Scientific) and adherent cells were stimulated with once or twice LPS as described above.

Isolation of CD11b$^+$ Cells

The single cell suspensions from the organs were created by using gentleMACS dissociation tubes (Miltenyi Biotec). CD11b$^+$ cells were then isolated *via* CD11b microbeads (Miltenyi Biotec) under the manufacturer's instructions.

Real-Time PCR Analysis

A standard phenol-chloroform extraction was performed with Trizol reagent to isolate total RNA from cells. cDNA was synthesized from 1 µg of total RNA with a High-Capacity cDNA Reverse Transcription Kit (ThermoFisher). Real-time PCR analysis was then performed and analysed with a SYBR label (SYBR Select Mastermix, Applied Biosystems) in QuantStudio™ 6 Flex Real-Time PCR System. The real-time PCR primer sequences are listed in **Supplementary Table 1**. The relative expression of the gene of interest (GOI) was calculated with the ΔΔCt method using β-actin (*Actb*) expression as normalizer (norm) and the not-stimulated naïve control as calibrator: relative expression = $2^{-\Delta\Delta Ct}$ where $\Delta\Delta Ct = (Ct_{GOI} - Ct_{norm})_{unknown} - (Ct_{GOI} - Ct_{norm})_{calibrator}$.

ELISA

The IL-6 and NGAL concentrations in the relevant supernatant or serum were quantified with the Mouse IL-6 DuoSet ELISA Kit and Mouse Lcn2 DuoSet ELISA Kit following the manufacturer's instructions (R&D Systems).

Western Blot Analysis

Proteins from BMDM stimulated once or twice with LPS were collected at 0, 0.5, 1, 2 or 4 h with RIPA buffer supplied with protease inhibitors (Roche, cOmplete™ ULTRA Tablets, 05892970001). The protein extracts were then separated by SDS-PAGE electrophoresis and semi-dry transferred to a PVDF membrane. The membrane was incubated with antibodies against FRA-1 (sc-605, Santa-Cruz, 1: 200) and GAPDH (#2118, Cell Signalling, 1:1000) overnight at 4°C.

Chromatin Immunoprecipitation-seq and ChIP-qPCR

The ChIP-seq results have been deposited online in the GEO datatabase (GSE178865) along with our previous publication (13). The raw ChIP-seq data were re-analyzed with GALAXY (15) to explore the binding of FRA-1 on the promoter sites of *Il6* and *Lcn2*, with or without stimulation with LPS. In brief, the data sets were firstly trimmed by Trimmomatic to remove adapters and trim reads to improve the overall quality. The sequenced reads were mapped using Bowtie2. The peak-calling step was then performed by MACS2 to identify significantly enriched loci in the genome. Finally, the output files were visualized with the help of Integrated Genome Browser (16).

For further promoter analysis, the 4.000 bp nucleotide sequences upstream of the transcription start sequence (TSS) of *Il6* and *Lcn2* genes were identified thanks to the NCBI Gene database. The putative AP-1 binding sites on *Il6* and *Lcn2*

promoters were predicted *via* an online tool TFBIND (17) and relative primers to detect each site were designed accordingly.

ChIP-qPCR on peritoneal macrophages and BMDM was performed with the ChIP-IT High Sensitivity® (HS) Kit (Active Motif) following the manufacturer's instructions. Briefly, thioglycollate-elicited macrophages were generated by injecting mice i.p. with 2.5 mL of 4% (w/v) Brewer's thioglycolate medium (Sigma-Aldrich). FRA-1 deficient mice and littermates were sacrificed 72 hours after injection. Peritoneal cavity cells were harvested by lavage, and cells were washed and plated in RPMI-1640 (Gibco, Thermo Fisher Scientific) supplemented with 10% (v/v) FCS (Gibco, Thermo Fisher Scientific) and 1% (v/v) penicillin/streptomycin (Gibco, Thermo Fisher Scientific). BMDM were prepared as described above (Cell Preparation). After overnight incubation, adherent cells were stimulated with 10 ng/mL LPS for 1h (Naïve) or stimulated with 100 ng/mL LPS for 24 h, washed twice with warm PBS and stimulated again with 10 ng/mL LPS for 1h (Tolerant). The cells were fixed with 1% formaldehyde for 15 min to cross-link the proteins to the DNA and then washed for 3 times. The pellet was re-suspended in ChIP lysis buffer and lysate was sonicated to shear DNA to an average fragment size of 200–1000 bp. 30 μg chromatins were incubated with antibodies against FRA-1 (sc-605 from Santa-Cruz for peritoneal macrophages, since the production of this antibody has been discontinued by the company, we used PA5-81175 from Invitrogen for BMDM, 5μg/sample) or Normal Rabbit IgG (#2729, Cell Signalling, 5μg/sample) overnight at 4°C. On the second day, samples were incubated with protein A/G beads for 3 hours. DNA was then eluted, de-crosslinked overnight and purified. 25 μl starting chromatins without incubation with antibodies were also de-crosslinked and purified, named as Input. The enrichment of each binding site was evaluated by ChIP-qPCR. The data was normalized and calculated with Percent Input Method: Adjust Input=Ct_{Input}-log2 ($V_{Chromatin}/V_{Input}$), V means volume. % Input= $100*2^{(Adjusted\ Input\ -\ Ct\ Chromatin)}$. The ChIP-qPCR primer sequences are listed in **Supplementary Table 1**.

In Vivo Endotoxin Tolerance Model

The *in vivo* endotoxin tolerance model was established by consecutive i.p. injection of LPS. Briefly, mice were rendered tolerant to LPS by an initial injection of 25 μg of LPS and stimulated 3 days later with another similar dose of LPS for 2 h. The naïve group injected only once with LPS and sacrificed 2h after (**Figure 5A**). PBS-injected mice served as control.

Histological Analysis

Mice were sacrificed with CO_2 at indicated time point under respective treatment. The organs were then harvested and fixed in 4% formaldehyde for 12 h. Then, the samples were embedded in paraffin, cut to 1 μm thickness and mounted onto glass slides. For HE staining, the slides were stained with Hematoxylin and Eosin as common procedure. To quantify the LPS-induced changes in the spleen, the follicular areas were measured with ImageJ in 4-fold magnified images. For the evaluation of pulmonary inflammation in response to LPS, the categories "cellular infiltration" and "alveolar wall thickening" were used as described in previous study (18). Briefly, for cellular infiltration, 0 means no immune cell infiltration, 1 means moderate infiltration and 2 means massive infiltration. For alveolar wall thickening, 0 is normal, 1 represents thickening fewer than 50% while 2 is over 50%. Four representative images in 20-fold magnification per slide were analyzed and the respective values for each sample were summed up and then compared among diverse treatments.

TUNEL Staining

TUNEL staining of the spleen slides were performed with the In Situ Cell Death Detection-Kit (POD) following the manufacturer's instructions. Four representative images in 20-fold magnification per slide were analyzed and the apoptotic splenocytes within the follicular area were counted and compared among diverse treatments.

Data Analysis

GraphPad Prism version 8.0 (GraphPad Software, San Diego, CA) was used for statistical treatment. Experimental data was shown as mean ± s.e.m. Two-tailed unpaired student's t-test for two groups or ANOVA with multiple comparisons test were used as indicated in respective experiments. For kinetic expression of genes and proteins, repeated measures two-way ANOVA (two-way RM ANOVA) was used in which the time factors are matched, to account for the nestedness of the data.

RESULTS

Fosl1 Expression Is Altered After Induction of Endotoxin Tolerance in Murine Macrophages

To evaluate the AP-1 expression within the two phases of sepsis, we first set up the endotoxin tolerance model in wild type murine bone marrow-derived macrophages (BMDM) by consecutive stimulation of LPS (**Figure 1A**) (5). The adherent BMDM were stimulated with 10 ng/mL LPS (Naïve) or stimulated with 100 ng/mL LPS for 24 h, washed twice with warm PBS and stimulated again with 10 ng/ml LPS (Tolerant). The cells were then harvested at 0, 0.5, 1, 2 or 4 h after the stimulation. The validity of our experimental model was confirmed by analyzing the kinetic expression of genes previously known as tolerizable or non-tolerizable (5) at the indicated time point in naïve and tolerant macrophages. The tolerizable genes (*Il6, Il12b* and *Mmp13*) were significantly up-regulated in the naïve cells, while significantly diminished in the tolerant cells compared to the naïve one. Meanwhile, the non-tolerizable genes (*Saa3, Lcn2*) were only weakly induced by LPS in naïve cells but showed a strong and sustained expression in stimulated tolerant cells (**Figure 1B**). The analysis of the protein secretion for IL-6 and NGAL (neutrophil gelatinase-associated lipocalin, protein name of *Lcn2*) in the supernatant of murine BMDM further confirmed the mRNA results (**Figure 1C**). IL-6 cytokine levels in the supernatant were significantly elevated after the first LPS stimulation, and abolished after the second stimulation, while

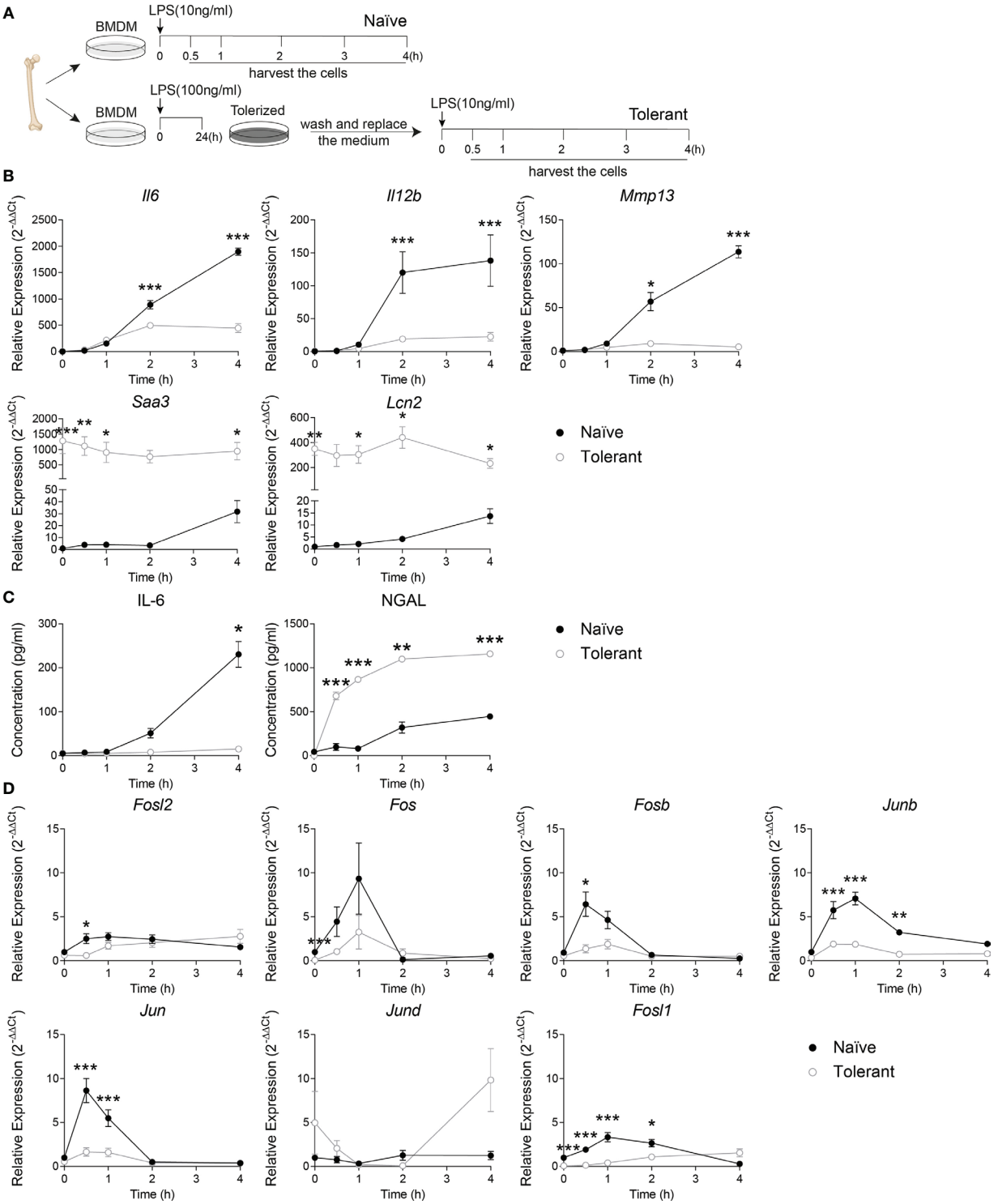

FIGURE 1 | *Fosl1* expression is altered after induction of endotoxin tolerance in murine macrophages. **(A)** Experimental scheme of the induction of endotoxin tolerance in wild type murine BMDM. A kinetic analysis of genes and proteins expression was performed at the indicated time point in macrophages harvested following one (Naïve) or two (Tolerant) LPS stimulations. **(B)** Quantitative RT-PCR analysis of the expression of tolerizable genes (*Il6, Il12b Mmp13*) and non-tolerizable genes (*Saa3, Lcn2*), normalized to the expression of *Actb*. **(C)** Quantification of IL-6 and NGAL protein secretion in cell culture supernatant. **(D)** Quantitative RT-PCR analysis of AP-1 transcription factor genes, normalized to the expression of *Actb*. Data are shown as mean ± s.e.m. *p < 0.05; **p < 0.01; ***p < 0.001 by two-way RM ANOVA with Tukey's multiple comparisons test. The data shown are from one experiment representative of three independent biological replicates.

the NGAL protein expression was still increased in the tolerant state. After this confirmation, we studied the expression kinetic of AP-1 transcription factor genes in murine BMDM in both naïve and tolerant state. The expression of *Fosl2, Fos, Fosb, Junb* and *Jun* peaked shortly (0.5-1h) after LPS stimulation in naïve cells, whereas the induction of these genes was strongly diminished in tolerant cells (**Figure 1D**). In this homogenous family picture, two AP-1 members stood out: *Jund* was unresponsive to LPS stimulation and was therefore not considered further, whereas *Fosl1* response was more interesting. In naïve cells, *Fosl1* responded alike the other AP-1 transcription factors. However, in tolerant cells, *Fosl1* did not show the small expression peak observed for the other AP-1 members but an initial level of expression dramatically reduced (6% of the unstimulated naïve cells) that slowly and steadily increased after LPS re-stimulation. Therefore, our results in wild type BMDM suggested that the induction of AP-1 gene expression by LPS stimulation in naïve cells was strongly reduced in tolerant cells, and Fra-1 expression seemed unique compared to the other members.

Fosl1 Expression Is Altered After Induction of Endotoxin Tolerance in PBMC

To verify whether our findings on AP-1 response in tolerant state can be transposed in human, the endotoxin tolerance was studied in isolated human PBMC (**Figure 2A**). Alike in murine cells, the tolerizable genes (*TNF, IL6*) were up-regulated by LPS stimulation in naïve cells, but could not be induced similarly in the tolerant cells. As expected, the expression of *LCN2* was higher in the tolerant state compared to the naïve one (**Figure 2B**). These data demonstrate a response of human PBMC to endotoxin tolerance consistent with the one observed in mouse macrophages. Next, AP-1 gene transcriptions were analyzed. Alike in mouse cells, the peak expression of *FOS, JUNB* and

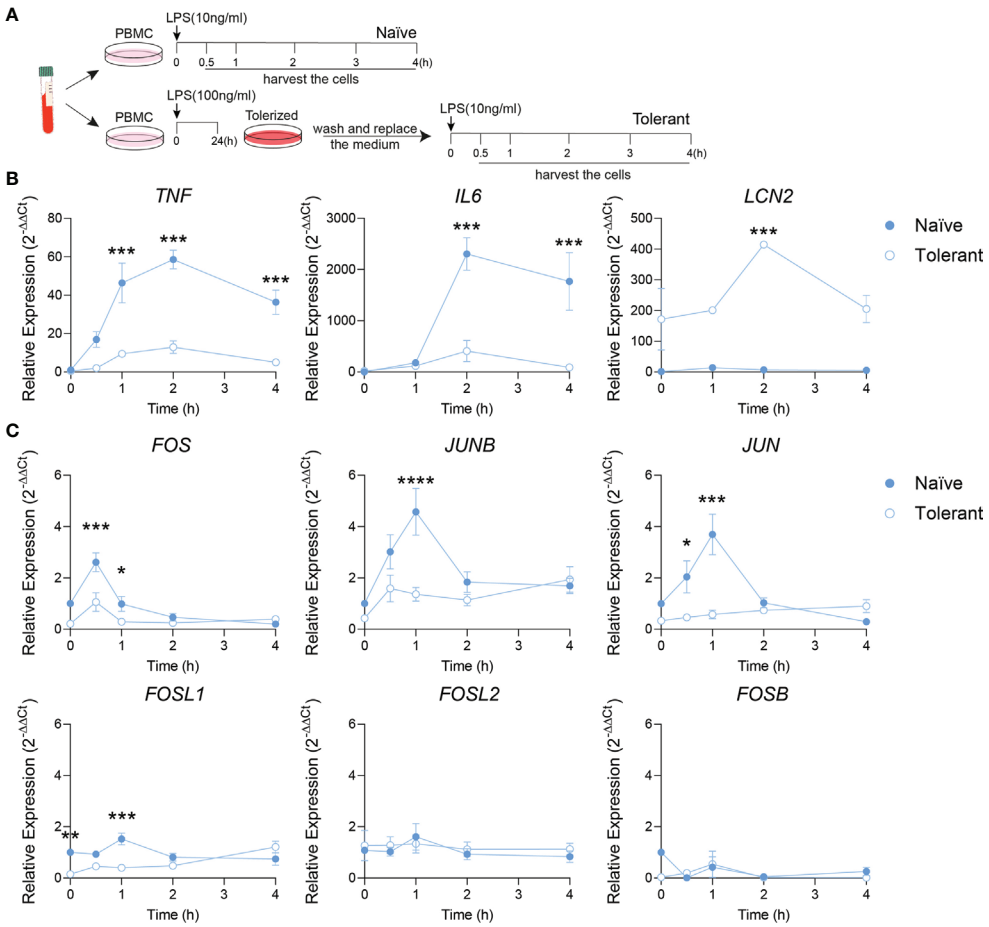

FIGURE 2 | *Fosl1* expression is altered after induction of endotoxin tolerance in human peripheral blood mononuclear cells. **(A)** Experimental scheme of the induction of endotoxin tolerance response in human PBMC. A kinetic analyses of gene expression was performed at the indicated time point in PBMC harvested following one (Naïve) or two (Tolerant) LPS stimulations. **(B)** Quantitative RT-PCR analysis of tolerizable genes (*TNF, IL6*) and non-tolerizable genes (*LCN2*), normalized to the expression of *Actb*. **(C)** Quantitative RT-PCR analysis of AP-1 transcription factor genes, normalized to the expression of *Actb*. Data are shown as mean ± s.e.m. *p < 0.05; **p < 0.01; ***p < 0.001; ****p < 0.0001 by two-way RM ANOVA with Tukey's multiple comparisons test. The data shown are from one experiment representative of three independent biological replicates.

JUN observed in naïve cells after 0.5-1 h of LPS stimulation diminished in stimulated tolerant cells. Here again, *FOSL1* expression was initially strongly decreased in tolerant cells and could be gradually increased up to 8-fold (1.21/0.15) by LPS stimulation (**Figure 2C**). Despite that this pattern was reproduced by other AP-1 transcription factors gene like *JUNB* (4.6-fold, 1.94/0.43) and *JUN* (2.7-fold, 0.90/0.33), *FOSL1* was the most LPS responsive AP-1 gene. Therefore, these results established that the data obtained with the mouse macrophages can be confidently transposed to human PBMC.

Increased Expression of NGAL in Tolerant Macrophages Depends on FRA-1 Expression

Considering the significantly different expression of *Fosl1* in naïve and tolerant state in both murine and human phagocytes, we speculated that FRA-1 could play an important role in regulating the tolerance induced transcriptional reprogramming. To evaluate how FRA-1 influenced the inflammatory response in endotoxin tolerance, inducible FRA-1 deficient mice were generated by crossing *Fosl1* lox mice to *Mx*-Cre mice. After the induction of FRA-1 deficiency by consecutive poly (I: C) injection, BMDM were isolated from the FRA-1 deficient mice and their littermates to study their response to the endotoxin tolerance model *in vitro*. After LPS stimulation, naïve macrophages from littermates induced *Fosl1* expression following a similar pattern as wild type macrophages but to a higher extent. This slightly increased *Fosl1* expression might be due to the heterogeneity of their genetic background. The up-regulation of *Fosl1* by LPS was abolished in the naïve and tolerant FRA-1 deficient BMDM (**Figure 3A**). The mRNA expression profiles of other AP-1 members such as *Fosb, Junb* and *Jun* were not significantly altered by the absence of *Fosl1* and responded similarly to the LPS stimulation (**Figure 3A**). This transcriptional data could be correlated at the translational level: FRA-1 expression after LPS stimulation is reduced in wild type cells after tolerance induction and is strongly diminished in FRA-1 deficient cells (**Figure 3B**).

To determine the influence of FRA-1 on the regulation of the tolerizable and non-tolerizable genes, we next investigated the expression pattern of *Il6* and *Lcn2* in FRA-1 deficient cells. In absence of *Fosl1*, expression of *Il6* mRNA was strongly decreased, especially in naïve state (**Figure 3C**, black hash sign), without significantly altering the early secretion of IL-6 protein (**Figure 3D**). Interestingly, the elevated expression of *Lcn2* in the tolerant cells was significantly reduced in FRA-1 knockout macrophages both at mRNA and protein levels (**Figures 3C, D**). This data suggested that expression of FRA-1 and NGAL are positively correlated, especially in tolerant cells.

FRA-1 Transcriptionally Regulates *Il6* and *Lcn2* at the Promoter Level

Considering the fundamental role of FRA-1 as a transcription factor, we hypothesized that FRA-1 can regulate directly the transcription of *Il6* and/or *Lcn2* in the context of endotoxin tolerance. Using our previously published ChIP-seq analyses performed in peritoneal macrophages with or without LPS stimulation (13), we discovered that FRA-1 can bind to the promoter sites of *Il6* and *Lcn2*, especially after LPS stimulation. For further analysis of these promoters, we considered the 4.000 bp upstream of their transcription start (TSS) (gray area depicted in **Supplementary Figures 1A, B**). The putative AP-1 binding sites on *Il6* and *Lcn2* promoters were predicted *in silico* (**Figures 4A, B**) (17). To confirm this analysis, ChIP-qPCR were then performed with anti-FRA-1 antibody in BMDM from FRA-1 deficient mice and littermates under naïve or tolerant conditioning and compared to not stimulated cells. In this experiment, *Fosl1*$^{\Delta Mx}$ BMDMs expressing minimal amount of FRA-1 were used as control for the anti-FRA-1 antibody specificity. ChIP-seq data were partly confirmed by our new ChIP-qPCR experiment: FRA-1 could be detected on the promoter of *Il6* at the loci 1, 4, 5 and 6 in all conditions including non-stimulated cells. Upon LPS stimulation, naïve cells showed an increase of FRA-1 binding on most of the *Il6* promoter locus (all but 1). A similar pattern was observed upon re-stimulation of tolerant cells and diminished in FRA-1 deficient tolerant cells (**Figure 4C**). Interestingly, FRA-1 could not be detected on most of the loci of *Lcn2* promoter in resting cells. However, LPS stimulation strongly mobilized FRA-1 loci 1 to 8 on this promoter in naive cells. Moreover, this binding could be increased for loci 7 and 8 in tolerant cells (**Figure 4D**). This FRA-1 binding pattern on *Il6* and *Lcn2* promoter was confirmed by performing a similar analysis in peritoneal macrophages (**Supplementary Figures 1C, D**). Therefore, our data implies important transcriptional regulation of the *Lcn2* promoter by FRA-1 especially in the tolerant state.

Increased Inflammation in the Immunosuppressive Phase of Sepsis in *Fosl1*$^{\Delta Mx}$ Mice Compared to Littermates

Once established the role of FRA-1 in endotoxin tolerance *in vitro*, we decided to investigate if this finding could be transposed *in vivo* in a model mimicking the induction of endotoxin tolerance observed during sepsis. To do so, we applied consecutive injection of LPS to *Fosl1*$^{\Delta Mx}$ and the littermate control mice (**Figure 5A**). Mice were rendered tolerant to LPS by an initial i.p. injection of 25 μg of LPS and stimulated 3 days later with another similar dose of LPS for 2 h. These mice were compared to naive mice injected only once with LPS. PBS-injected mice served as control. Lungs and spleens were then harvested to quantify the inflammation induced by LPS in these organs. *In vivo* injection of LPS in mice is characterized by a recruitment of immune cells to the lung and an increase of the thickness of the alveolar walls. In littermate control mice, LPS injection significantly thickens the lung alveolar walls of naïve mice. Interestingly, this thickening was decreased in tolerant mice despite a similar immune cell infiltration in the lung when compared to naïve mice (**Figure 5B**). This acute inflammatory response could also be observed in *Fosl1*$^{\Delta Mx}$ mice but to a lower extend. Tolerant FRA-1 deficient mice showed thickening of their alveolar walls similar to the tolerant littermate control mice but a significantly decreased infiltration of their lung by immune cells (**Figure 5C**). We further investigated the inflammatory conditions in the spleen of these mice. Even though the

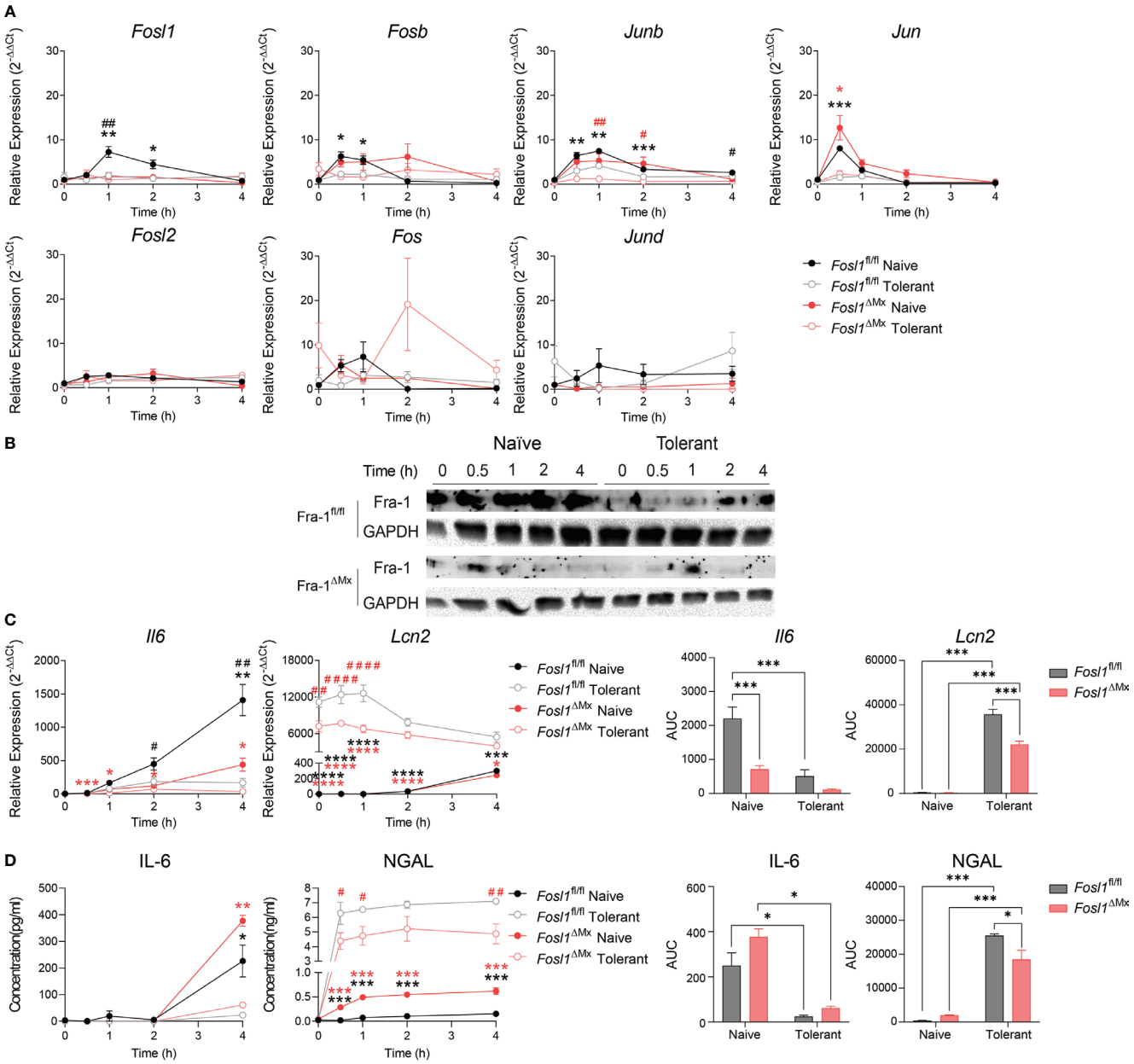

FIGURE 3 | Increased expression of *Lcn2* after induction of endotoxin tolerance is reduced in *Fosl1* knockout murine macrophages. **(A)** Quantitative RT-PCR analysis of AP-1 transcription factor gene expression in littermate control and Fra-1 deficient BMDM after LPS stimulation in both naïve and tolerant state, normalized to the expression of *Actb*. **(B)** Western blot detection of FRA-1 protein after LPS stimulation in littermate control and FRA-1 deficient BMDM in both naïve and tolerant state. GAPDH was used as loading control. **(C)** Quantitative RT-PCR analysis of *Il6* and *Lcn2* in littermate control and FRA-1 deficient BMDM after LPS stimulation in both naïve and tolerant state. Left panels represent the kinetic of gene expression normalized to the expression of *Actb* and right panels represent the area under curve (AUC) for the respective genes. **(D)** IL-6 and NGAL protein levels in the supernatant of wild type and FRA-1 deficient BMDM after LPS stimulation in both naïve and tolerant state. Left panels represent the kinetic of protein secretion and right panels represent the area under curve (AUC) for the respective protein. The data shown are from one experiment representative of three independent biological replicates and they are shown as mean ± s.e.m. *$p < 0.05$; **$p < 0.01$; ***$p < 0.001$; ****$p < 0.0001$ by two-way RM ANOVA with Tukey's multiple comparisons test. Black asterisks indicated significant difference between naïve (n=6) versus tolerant (n=9) state in littermate control mice; red asterisk indicated significant difference between naïve (n=3) versus tolerant (n=9) state in FRA-1 deficient mice; $^{\#}p < 0.05$; $^{\#\#}p < 0.01$; $^{\#\#\#\#}p < 0.0001$ by two-way RM ANOVA with Tukey's multiple comparisons test. Black hash sign indicated significant difference between FRA-1 deficient and littermate cells in naïve state; red hash sign indicated significant difference between FRA-1 deficient and littermate cells in tolerant state.

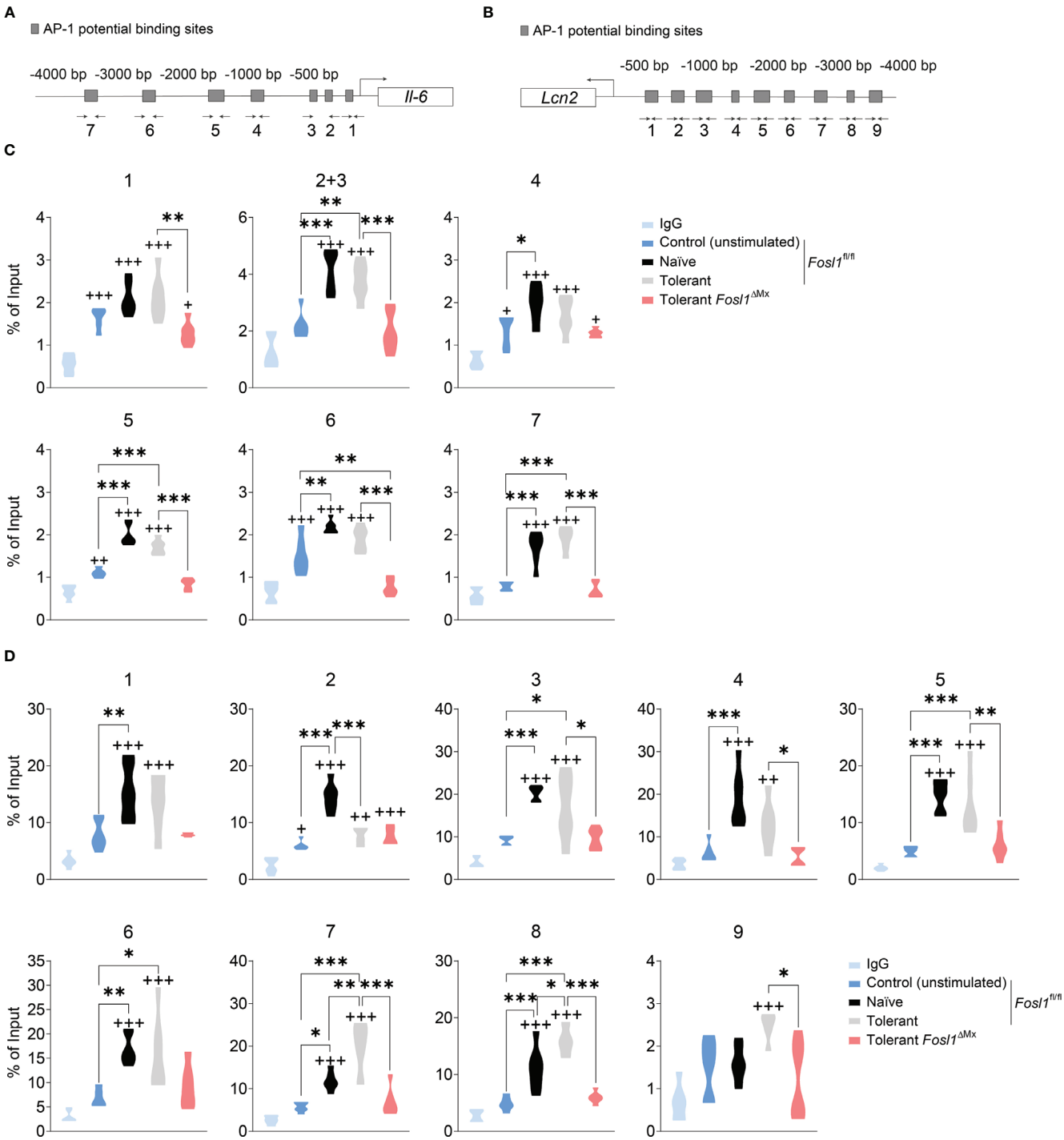

FIGURE 4 | FRA-1 binds stronger to the promoter of *Lcn2* after induction of endotoxin tolerance in murine BMDM. **(A, B)** Prediction of the AP-1 binding sites by the online tool TFBIND and the locations of the primers for each site on *Il6* **(A)** and *Lcn2* **(B)** promoters. **(C, D)** ChIP assays showing the recruitment of the endogenous FRA-1 on the AP-1 binding sequence of *Il6* **(C)** and *Lcn2* **(D)** promoters after one (naïve) or two (tolerant) stimulations with LPS in bone marrow-derived macrophages isolated from *Fosl1*$^{\Delta Mx}$ or littermate mice. $^{+}p < 0.05$; $^{++}p < 0.01$; $^{+++}p < 0.001$ by one-way ANOVA with Sidak's multiple comparisons test. + means compared to the IgG group. $^{*}p < 0.05$; $^{**}p < 0.01$; $^{***}p < 0.001$ by one-way ANOVA with Sidak's multiple comparisons test.

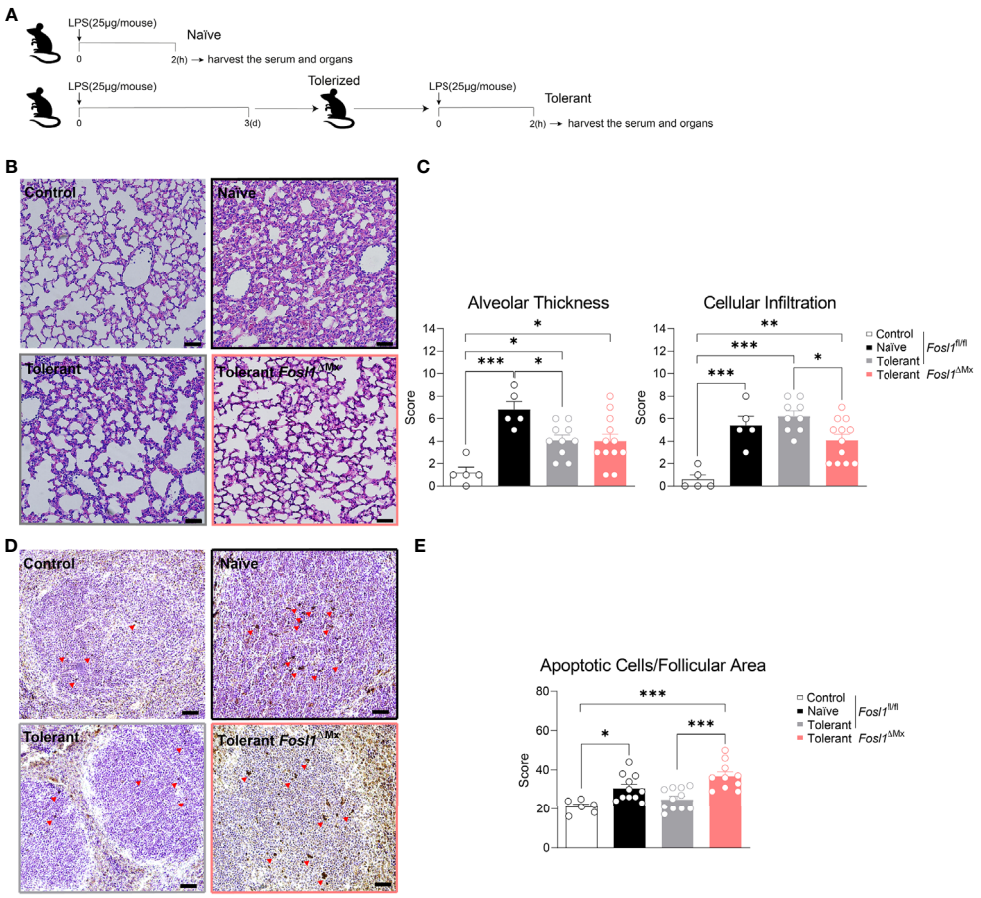

FIGURE 5 | Increased inflammation in the immunosuppressive phase of sepsis is observed in *Fosl1*$^{\Delta Mx}$ mice compared to littermates. **(A)** Experimental scheme of the induction of endotoxin tolerance response *in vivo*. **(B, C)** Representative H&E microscopy images and quantification of alveolar thickness and immune cell infiltration in the lung of *Fosl1*$^{\Delta Mx}$ and the littermate mice 2 h after once (Naïve) or twice (Tolerant) LPS stimulation. Scale bar = 200µm. **(D, E)** Representative TUNEL staining images and quantification of apoptotic cells adjusted to follicular area in the spleen of *Fosl1*$^{\Delta Mx}$ and the littermate mice after once (Naïve) or twice (Tolerant) LPS stimulation. Scale bar = 40µm. Graph points indicate individual mice. Data are shown as mean ± s.e.m. *p < 0.05; **p < 0.01; ***p < 0.001 by one-way ANOVA with Sidak's multiple comparisons test.

follicular area of the spleen was significantly increased by LPS injection in the naïve wild type mice, it appears that this criterion went back to normal and became unresponsive to LPS in tolerant wild type mice. No significant difference was observed between the *Fosl1*$^{\Delta Mx}$ mice and the littermates in the tolerant state (**Supplementary Figure 2**). Another consequence of systemic inflammatory response induced by LPS is the induction of apoptosis in leukocyte (7). Our TUNEL staining confirmed that LPS injection increased the number of apoptotic cells in the splenic follicular area of naïve mice (control vs naïve, p=0.0224). Interestingly, this induction of apoptosis by LPS was not observed in tolerant mice (control vs tolerant, p=0.7671). This tolerance seems to be dependent on *Fosl1* expression as tolerant FRA-1 deficient mice showed a higher number of apoptotic leukocytes compared to littermate control tolerant mice (tolerant vs tolerant FRA-1 deficient mice, p=0.0005) (**Figures 5D, E**). Altogether, our data suggested that a more severe inflammation as well as a weaker resolution in lung and spleen occurred in tolerant FRA-1 deficient mice compared to their wild type littermates.

Increased Expression of NGAL in the Immunosuppressive Phase of Sepsis Is Reduced in *Fosl1*$^{\Delta Mx}$ Mice

To understand how AP-1 transcription factors and particularly FRA-1 are involved in our endotoxin tolerance model, we investigated their gene expression profile in murine sepsis model. *Fosl1, Junb* and *Jun* were significantly increased by LPS in both lung and spleen of naïve mice. However, establishment of endotoxin tolerance in wild type mice strongly reduced the increased of *Fosl1* and *Junb* in lung and of *Jun* in spleen by LPS (**Figure 6A**). In the same line, we measured the expression of *Il6* and *Lcn2* as standard tolerizable and non-tolerizable genes respectively, in lung and spleen of the control, naïve and tolerant mice. As expected, *Il6* was strongly induced only in naïve mice whereas *Lcn2* was induced in naive and even more in tolerant

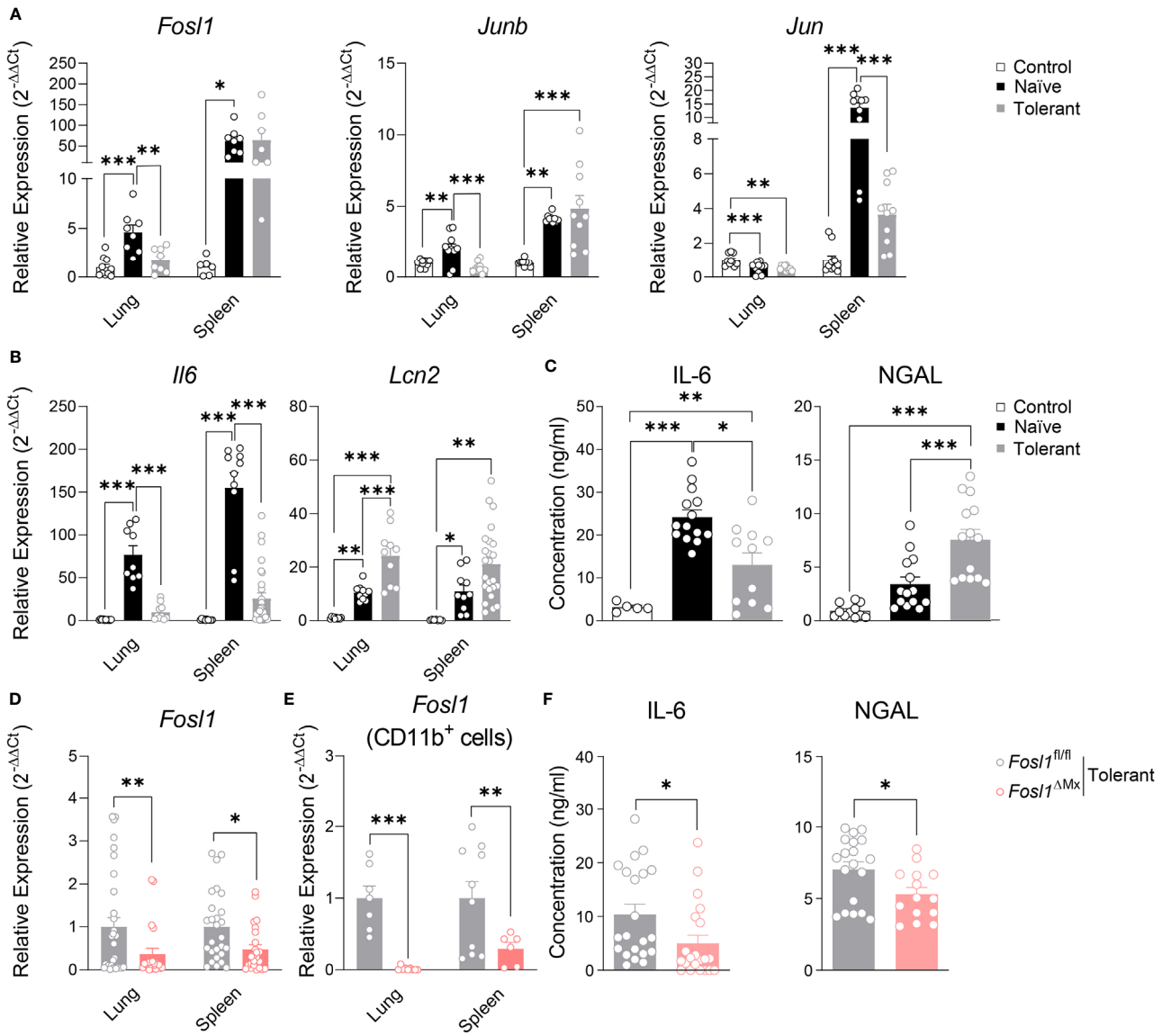

FIGURE 6 | Increased expression of *Lcn2* in the immunosuppressive phase of sepsis is reduced in *Fosl1*$^{\Delta Mx}$ mice. **(A, B)** Quantitative RT-PCR analysis of AP-1 transcription factors **(A)** and *Il6* and *lcn2* genes **(B)** in lung and spleen of control, naïve or tolerant wild type mice 2 h after LPS infection. **(C)** IL-6 and NGAL levels in serum of control, naïve or tolerant wild type mice 2 h after LPS infection. **(D, E)** Quantitative RT-PCR analysis of *Fosl1* transcription factor genes in total organ **(D)** or CD11b$^+$ cells **(E)** from lungs and spleens of *Fosl1*$^{\Delta Mx}$ and the littermate mice in tolerant state, normalized to the expression of *Actb*. **(F)** IL-6 and NGAL levels in serum of *Fosl1*$^{\Delta Mx}$ and the littermate mice in tolerant state. Graph points indicate individual mice. Data are shown as mean ± s.e.m. *p < 0.05; **p < 0.01; ***p < 0.001 by one-way ANOVA with Tukey's multiple comparisons in **(A–C)** and student t test in **(D–F)**.

mice. For these two genes, protein secretion in the serum fully matched the mRNA data obtained in lung and spleen (**Figures 6B, C**). For the *Fosl1*$^{\Delta Mx}$ and littermate control mice, we first quantified the knockout efficiency within the organs and found that *Fosl1* expressions were significantly decreased in lung and spleen in the tolerant state, especially in CD11b$^+$ cells (**Figures 6D, E**). Alongside, we could confirm the influence of FRA-1 on the cytokine secretion as FRA-1 deficient mice have a lower level of circulating IL-6 and NGAL (**Figure 6F**). Altogether, our *in vivo* experiments confirm that NGAL expression is controlled by FRA-1 during tolerance induction.

DISCUSSION

In the present study, we delineated the expressions of the AP-1 transcription factor family *in vitro* with an endotoxin tolerance model applied to murine BMDM and human PBMC and *in vivo*

with a murine LPS induced sepsis model. These experiments revealed that the AP-1 transcription factor FRA-1 regulates NGAL expression during the establishment of tolerance in myeloid cells. Interestingly, ChIP-qPCR data further demonstrated a direct regulation on *Lcn2* expression by FRA-1, through its binding on *Lcn2* promoter in tolerant macrophages. This observation could be transposed in the *in vivo* septic model of consecutive injection of LPS. FRA-1 deficient mice showed a decreased resolution of inflammation likely dependent on their low level of circulating NGAL. Thus, our data indicates that FRA-1 is involved in myeloid cell tolerance responses by mediating the functional reprogramming of *Lcn2* transcription in response to prolonged LPS exposure. In addition, FRA-1 may have a protective role in the tolerance response and resolution of inflammation in sepsis through the regulation of NGAL.

Sepsis is a lethal systemic inflammatory response. Due to the high mortality rate and the lack of efficient therapy, the main mechanisms sustaining this disease are still under investigation. Although initially not appreciated, the rapid display of profound immunosuppression in most patients with sepsis is now a well-established phenomenon (4, 19). However, the immunological and molecular mechanism of the immunosuppression is still poorly understood. Here, we used the endotoxin tolerance model as described previously (5) *in vitro* and *in vivo* to mimic the prolonged LPS stimulation that can induce immunosuppression during sepsis. Endotoxin tolerance model is a convenient model for analyzing macrophage hyporesponsiveness. It is induced after exposure of macrophages or mice to a non-lethal low dose of LPS that induces hyperinflammation and then with a second exposure to LPS deactivates the macrophages, resulting in the establishment of immunosuppression (20). With endotoxin tolerance model, we could observe an increase of pro-inflammatory genes upon the first LPS stimulation, and diminished significantly after the second LPS stimulation as shown by Simmie L. Foster and her colleagues (5). We also observed *in vivo* a significantly increased alveolar wall thickness and neutrophil infiltration in the lung and more follicular apoptotic cells in the spleen in the naïve state, while this phenotype was ameliorated in the tolerant state as shown by Frank M. Davis et al. (21), vividly illustrating the whole process of sepsis..

After the tolerance induction, macrophages undergo functional reprogramming and change to an anti-inflammatory phenotype that activates resolution and regeneration programs, promoting a return to tissue homeostasis (11). Scientific advances have highlighted the role of transcriptional regulation in this functional reprogramming process underlying the immunosuppressive phase (10, 11, 22). The AP-1 transcription factor family is involved in numerous processes such as cell proliferation, differentiation and death, depending on the stimulus, the microenvironment and the cell type (12). The wide range of possible combinations and the occurrence of post-translational modifications explain the great functional heterogeneity of AP-1 transcription factors (12, 23). The function of FRA-1 is clearly established in bone and tumor biology (24, 25). There, FRA-1 needs to heterodimerize with another AP-1 transcription to function. This peculiarity makes FRA-1 an interesting transcription factor as its deletion alters the functions of its partners on their shared target genes. Nonetheless, the role of FRA-1 in the context of inflammation, especially concerning *Il6* expression, is still controversial. Mimicking the tumor microenvironment *in vitro*, the 4T1 mammary carcinoma cells promoted *de novo* overexpression of *Fosl1* in RAW264. 7 cells, and the subsequent binding of FRA-1 on the *Il6* promoter and an increase of IL-6 production in response to LPS (26). On the contrary, Morishita et al. reported that IL-6 production after LPS stimulation could be inhibited in RAW264.7 macrophages by overexpressing FRA-1 thanks to a lentiviral vector. This phenotype could be reversed by knockdown of *Fosl1* in this cell line (27). In parallel, no significant difference was observed on *Il6* expression in FRA-1 deficient alveolar macrophages in a LPS triggered acute lung injury model, even though the KO mice exhibited lower mortality rates compared to the control (28). Thus, the function of FRA-1 on IL-6 expression upon inflammation appears to vary depending on the stimulating strategy, the initial intracellular concentration of FRA-1 and the cell type. This multi-factorial context probably influences the non–AP1 transcription factors and the nature of the partner of FRA-1 in the AP-1 heterodimer binding to the *Il6* promoter. This ambivalent function of FRA-1 should rely on opposite regulatory mechanisms. Indeed, FRA-1 has been described as a positive regulator of transcription for genes involved in innate immunity (13) as well as a mediator to repress gene expression in related context (29). In the present study, we could first confirm that *Il6* was a strongly tolerizable gene. In addition, we showed that *Il6* mRNA expression upon LPS stimulation was dependent on the *de novo* expression of Fra-1 in naïve macrophages. If our limited kinetic could not illustrate this FRA-1 dependency for the IL-6 protein secretion *in vitro*, we observed *in vivo* that circulating IL-6 level were decreased in tolerant mice subjected to our sepsis model.

The role of FRA-1 on *Lcn2* expression has yet to be reported. NGAL has been described as a marker of deactivated macrophages and was initially characterized as an anti-microbial protein targeting bacterial siderophore (6, 8). In addition, NGAL supports the establishment of hypoferremia during inflammation to restrict iron availability for the pathogens and thus contributes to the resolution of sepsis (7). Therefore, expression of NGAL promotes microbicidal activities of the immune system and would ultimately contribute to the resolution of sepsis. In our results, the elevated expression of *Lcn2* in the tolerant state was significantly reduced in the *Fosl1* knockout macrophages, at both mRNA and protein level. This correlation between FRA-1 and *Lcn2* expression suggest that this transcription factor offers an additional layer of regulation to the already tightly controlled *Lcn2* promoter. Indeed, transcription factors classically activated under inflammatory conditions such as STAT1 or NF-kB have been previously linked to the regulation of *Lcn2* expression (30, 31). Strikingly, we also observed this correlation *in vivo*. FRA-1 deficient mice subjected to endotoxin tolerance had a significantly decreased level of circulating NGAL. These mice also showed less neutrophil infiltration in the lung and more apoptotic cells in the spleen, implying a higher level of inflammation. Altogether, we propose that FRA-1 have a protective role in response endotoxin induced sepsis through the regulation of NGAL.

Therefore, a better understanding of how AP-1, especially FRA-1, expression and functions in tolerant macrophages can provide

valuable insights into the fundamental mechanisms underlying sepsis. Characterizing the regulation of the downstream targets of these transcription factors could open new avenue for the development of therapeutic options against sepsis.

DATA AVAILABILITY STATEMENT

The datasets presented in this study can be found in online repositories. The names of the repository/repositories and accession number(s) can be found below: https://www.ncbi.nlm.nih.gov/geo/, GSE178865.

ETHICS STATEMENT

The animal study was reviewed and approved by University of Friedrich-Alexander-Universität Erlangen-Nürnberg ethics committee.

AUTHOR CONTRIBUTIONS

SC, NH, and AB designed the study. SC, DS, and AB wrote the manuscript. NH contributed to the ChIP-sequencing analysis. SC and AS performed the *in vitro* and *in vivo* experiments. GS supervised the study and edited the manuscript. All authors contributed to the article and approved the submitted version.

FUNDING

This work was supported by the Deutsche Forschungsgemeinschaft: BO-3811/5-1; BO-3811/6-1; FOR 2886-TP02; CRC 1181 project A01; SPP2084 μBone; Erlangen-Nuremberg University ELAN-Program P044; Interdisciplinary Centre for Clinical Research (IZKF) grant F1-04; European Research Council (ERC) Synergy Grant 4D Nanoscope and ERC consolidator - ODE.

SUPPLEMENTARY MATERIAL

The Supplementary Material for this article can be found online at: https://www.frontiersin.org/articles/10.3389/fimmu.2021.701675/full#supplementary-material

Supplementary Figure 1 | FRA-1 binds to the promoters of *Il6* and *Lcn2*. **(A, B)** ChIP-seq data (13) of thioglycollate-elicited macrophages from wild type mice, unstimulated or stimulated with LPS were used to identify FRA-1 target genes. Bindings of FRA-1 on the *Il6* **(A)** and *Lcn2* **(B)** promoter are indicated **(C, D)** ChIP assays showing the recruitment of the endogenous FRA-1 on the AP-1 binding sequence of *Il6* **(C)** and *Lcn2* **(D)** promoters in thioglycollate-elicited macrophages isolated from *Fosl1*$^{\Delta Mx}$ or littermate mice after once (naïve) or twice (tolerant) stimulation of LPS. Data are shown as mean ± s.e.m. *p < 0.05; **p < 0.01; ***p < 0.001 by one-way ANOVA with Tukey's multiple comparisons test.

Supplementary Figure 2 | Follicular area is not significantly altered in the immunosuppressive phase of sepsis in *Fosl1*$^{\Delta Mx}$ mice compared to littermates. Representative H&E microscopy images and quantification of follicular area in the spleen of *Fosl1*$^{\Delta Mx}$ and the littermate mice after once (naïve) or twice (tolerant) stimulation of LPS. Scale bar = 200μm. Graph points indicate individual mice. Data are shown as mean ± s.e.m. *p < 0.05 by one-way ANOVA with Sidak's multiple comparisons test.

Supplementary Figure 3 | Uncropped blots results of (**Figure 3B**) Western blot detection of FRA-1 protein after LPS stimulation in littermate control and FRA-1 deficient BMDM in both naïve and tolerant state. GAPDH was used as loading control.

Supplementary Table 1 | Primers sequences used for Real-Time PCR and ChIP-qPCR.

REFERENCES

1. Singer M, Deutschman CS, Seymour CW, Shankar-Hari M, Annane D, Bauer M, et al. The Third International Consensus Definitions for Sepsis and Septic Shock (Sepsis-3). *Jama* (2016) 315(8):801–10. doi: 10.1001/jama.2016.0287
2. Cavaillon JM, Singer M, Skirecki T. Sepsis Therapies: Learning From 30 Years of Failure of Translational Research to Propose New Leads. *EMBO Mol Med* (2020) 12(4):e10128. doi: 10.15252/emmm.201810128
3. Venet F, Monneret G. Advances in the Understanding and Treatment of Sepsis-Induced Immunosuppression. *Nat Rev Nephrol* (2018) 14(2):121. doi: 10.1038/nrneph.2017.165
4. Hotchkiss RS, Monneret G, Payen D. Sepsis-Induced Immunosuppression: From Cellular Dysfunctions to Immunotherapy. *Nat Rev Immunol* (2013) 13(12):862–74. doi: 10.1038/nri3552
5. Foster SL, Hargreaves DC, Medzhitov R. Gene-Specific Control of Inflammation by TLR-Induced Chromatin Modifications. *Nature* (2007) 447(7147):972–8. doi: 10.1038/nature05836
6. Moschen AR, Gerner RR, Wang J, Klepsch V, Adolph TE, Reider SJ, et al. Lipocalin 2 Protects From Inflammation and Tumorigenesis Associated With Gut Microbiota Alterations. *Cell Host Microbe* (2016) 19(4):455–69. doi: 10.1016/j.chom.2016.03.007
7. Srinivasan G, Aitken JD, Zhang B, Carvalho FA, Chassaing B, Shashidharamurthy R, et al. Lipocalin 2 Deficiency Dysregulates Iron Homeostasis and Exacerbates Endotoxin-Induced Sepsis. *J Immunol* (2012) 189(4):1911–9. doi: 10.4049/jimmunol.1200892
8. Warszawska JM, Gawish R, Sharif O, Sigel S, Doninger B, Lakovits K, et al. Lipocalin 2 Deactivates Macrophages and Worsens Pneumococcal Pneumonia Outcomes. *J Clin Invest* (2013) 123(8):3363–72. doi: 10.1172/JCI67911
9. Vazquez DE, Nino DF, De Maio A, Cauvi DM. Sustained Expression of Lipocalin-2 During Polymicrobial Sepsis. *Innate Immun* (2015) 21(5):477–89. doi: 10.1177/1753425914548491
10. Shalova IN, Lim JY, Chittezhath M, Zinkernagel AS, Beasley F, Hernández-Jiménez E, et al. Human Monocytes Undergo Functional Re-Programming During Sepsis Mediated by Hypoxia-Inducible Factor-1α. *Immunity* (2015) 42(3):484–98. doi: 10.1016/j.immuni.2015.02.001
11. Rackov G, Hernández-Jiménez E, Shokri R, Carmona-Rodríguez L, Mañes S, Álvarez-Mon M, et al. P21 Mediates Macrophage Reprogramming Through Regulation of P50-P50 NF-κb and IFN-β. *J Clin Invest* (2016) 126(8):3089–103. doi: 10.1172/JCI83404
12. Hess J, Angel P, Schorpp-Kistner M. AP-1 Subunits: Quarrel and Harmony Among Siblings. *J Cell Sci* (2004) 117(25):5965–73. doi: 10.1242/jcs.01589
13. Hannemann N, Cao S, Eriksson D, Schnelzer A, Jordan J, Eberhardt M, et al. Transcription Factor Fra-1 Targets Arginase-1 to Enhance Macrophage-Mediated Inflammation in Arthritis. *J Clin Invest* (2019) 129(7):2669–84. doi: 10.1172/JCI96832
14. Schleicher U, Bogdan C. Generation, Culture and Flow-Cytometric Characterization of Primary Mouse Macrophages. *Methods Mol Biol* (2009) 531:203–24. doi: 10.1007/978-1-59745-396-7_14
15. Afgan E, Baker D, Batut B, Van Den Beek M, Bouvier D, Čech M, et al. The Galaxy Platform for Accessible, Reproducible and Collaborative Biomedical

Analyses: 2018 Update. *Nucleic Acids Res* (2018) 46(W1):W537–44. doi: 10.1093/nar/gky379
16. Freese NH, Norris DC, Loraine AE. Integrated Genome Browser: Visual Analytics Platform for Genomics. *Bioinformatics* (2016) 32(14):2089–95. doi: 10.1093/bioinformatics/btw069
17. Tsunoda T. And Takagi, T. Estimating Transcription Factor Bindability on DNA. *Bioinformatics (Oxford England)* (1999) 15(7):622–30. doi: 10.1093/bioinformatics/15.7.622
18. Madtes DK, Elston AL, Hackman RC, Dunn AR, Clark J. G. Transforming Growth Factor-α Deficiency Reduces Pulmonary Fibrosis in Transgenic Mice. *Am J Respir Cell Mol Biol* (1999) 20(5):924–34. doi: 10.1165/ajrcmb.20.5.3526
19. Hotchkiss RS, Monneret G, Payen D. Immunosuppression in Sepsis: A Novel Understanding of the Disorder and a New Therapeutic Approach. *Lancet Infect Dis* (2013) 13(3):260–8. doi: 10.1016/S1473-3099(13)70001-X
20. West MA, Heagy W. Endotoxin Tolerance: A Review. *Crit Care Med* (2002) 30(1):S64–73. doi: 10.1097/00003246-200201001-00009
21. Davis FM, Schaller MA, Dendekker A, Joshi AD, Kimball AS, Evanoff H, et al. Sepsis Induces Prolonged Epigenetic Modifications in Bone Marrow and Peripheral Macrophages Impairing Inflammation and Wound Healing. *Arteriosclerosis Thrombosis Vasc Biol* (2019) 39(11):2353–66. doi: 10.1161/ATVBAHA.119.312754
22. Rackov G, Shokri R, De Mon MÁ, Balomenos D. The Role of IFN-β During the Course of Sepsis Progression and Its Therapeutic Potential. *Front Immunol* (2017) 8:493. doi: 10.3389/fimmu.2017.00493
23. Zenz R, Eferl R, Scheinecker C, Redlich K, Smolen J, Schonthaler HB, et al. Activator Protein 1 (Fos/Jun) Functions in Inflammatory Bone and Skin Disease. *Arthritis Res Ther* (2008) 10(1):1–10. doi: 10.1186/ar2338
24. Jochum W, David J-P, Elliott C, Wutz A, Plenk H, Matsuo K, et al. Increased Bone Formation and Osteosclerosis in Mice Overexpressing the Transcription Factor Fra-1. *Nat Med* (2000) 6(9):980–4. doi: 10.1038/79676
25. Belguise K, Kersual N, Galtier F, Chalbos D. FRA-1 Expression Level Regulates Proliferation and Invasiveness of Breast Cancer Cells. *Oncogene* (2005) 24(8):1434–44. doi: 10.1038/sj.onc.1208312
26. Wang Q, Ni H, Lan L, Wei X, Xiang R, Wang Y. Fra-1 Protooncogene Regulates IL-6 Expression in Macrophages and Promotes the Generation of M2d Macrophages. *Cell Res* (2010) 20(6):701–12. doi: 10.1038/cr.2010.52
27. Morishita H, Saito F, Kayama H, Atarashi K, Kuwata H, Yamamoto M, et al. Fra-1 Negatively Regulates Lipopolysaccharide-Mediated Inflammatory Responses. *Int Immunol* (2009) 21(4):457–65. doi: 10.1093/intimm/dxp015
28. Mishra RK, Potteti HR, Tamatam CR, Elangovan I, Reddy SP. C-Jun Is Required for Nuclear Factor-κb–Dependent, LPS-Stimulated Fos-Related Antigen-1 Transcription in Alveolar Macrophages. *Am J Respir Cell Mol Biol* (2016) 55(5):667–74. doi: 10.1165/rcmb.2016-0028OC
29. Mittelstadt ML, Patel RC. AP-1 Mediated Transcriptional Repression of Matrix Metalloproteinase-9 by Recruitment of Histone Deacetylase 1 in Response to Interferon β. *PLoS One* (2012) 7(8):e42152. doi: 10.1371/journal.pone.0042152
30. Zhao P, Elks CM, Stephens JM. The Induction of Lipocalin-2 Protein Expression *In Vivo* and *In Vitro*. *J Biol Chem* (2014) 289(9):5960–9. doi: 10.1074/jbc.M113.532234
31. Jung M, Ören B, Mora J, Mertens C, Dziumbla S, Popp R, et al. Lipocalin 2 From Macrophages Stimulated by Tumor Cell–Derived Sphingosine 1-Phosphate Promotes Lymphangiogenesis and Tumor Metastasis. *Sci Signaling* (2016) 9(434):ra64–4. doi: 10.1126/scisignal.aaf3241

Conflict of Interest: The authors declare that the research was conducted in the absence of any commercial or financial relationships that could be construed as a potential conflict of interest.

Publisher's Note: All claims expressed in this article are solely those of the authors and do not necessarily represent those of their affiliated organizations, or those of the publisher, the editors and the reviewers. Any product that may be evaluated in this article, or claim that may be made by its manufacturer, is not guaranteed or endorsed by the publisher.

Copyright © 2021 Cao, Schnelzer, Hannemann, Schett, Soulat and Bozec. This is an open-access article distributed under the terms of the Creative Commons Attribution License (CC BY). The use, distribution or reproduction in other forums is permitted, provided the original author(s) and the copyright owner(s) are credited and that the original publication in this journal is cited, in accordance with accepted academic practice. No use, distribution or reproduction is permitted which does not comply with these terms.

frontiers in Immunology

ORIGINAL RESEARCH
published: 26 October 2021
doi: 10.3389/fimmu.2021.740562

Pharmacological Activation Of Aldehyde Dehydrogenase 2 Protects Against Heatstroke-Induced Acute Lung Injury by Modulating Oxidative Stress and Endothelial Dysfunction

Hsiao-Ya Tsai[1], Yu-Juei Hsu[2,3], Cheng-Yo Lu[1], Min-Chien Tsai[4], Wan-Chu Hung[4], Po-Chuan Chen[1], Jen-Chun Wang[1], Lung-An Hsu[5], Yung-Hsin Yeh[5], Pauling Chu[2,3] and Shih-Hung Tsai[1,4]**

[1] Department of Emergency Medicine, Tri-Service General Hospital, National Defense Medical Center, Taipei, Taiwan, [2] Division of Nephrology, Department of Internal Medicine, Tri-Service General Hospital, National Defense Medical Center, Taipei, Taiwan, [3] Center for the Prevention and Treatment of Heat Stroke, Tri-Service General Hospital, National Defense Medical Center, Taipei, Taiwan, [4] Department of Physiology and Biophysics, Graduate Institute of Physiology, National Defense Medical Center, Taipei, Taiwan, [5] Cardiovascular Department, Chang-Gung Memorial Hospital and School of Medicine, Chang-Gung University, Taoyuan, Taiwan

OPEN ACCESS

Edited by:
Sylvaine You,
Institut National de la Santé et de la Recherche Médicale (INSERM), France

Reviewed by:
Jingbo Pang,
University of Illinois at Chicago, United States
Arturo Briva,
Universidad de la República, Uruguay

***Correspondence:**
Yu-Juei Hsu
yujuei@mail2000.com.tw
Shih-Hung Tsai
tsaishihung@ndmctsgh.edu.tw

Specialty section:
This article was submitted to Inflammation, a section of the journal Frontiers in Immunology

Received: 13 July 2021
Accepted: 11 October 2021
Published: 26 October 2021

Citation:
Tsai H-Y, Hsu Y-J, Lu C-Y, Tsai M-C, Hung W-C, Chen P-C, Wang J-C, Hsu L-A, Yeh Y-H, Chu P and Tsai S-H (2021) Pharmacological Activation Of Aldehyde Dehydrogenase 2 Protects Against Heatstroke-Induced Acute Lung Injury by Modulating Oxidative Stress and Endothelial Dysfunction. Front. Immunol. 12:740562. doi: 10.3389/fimmu.2021.740562

Heatstroke (HS) can cause acute lung injury (ALI). Heat stress induces inflammation and apoptosis *via* reactive oxygen species (ROS) and endogenous reactive aldehydes. Endothelial dysfunction also plays a crucial role in HS-induced ALI. Aldehyde dehydrogenase 2 (ALDH2) is a mitochondrial enzyme that detoxifies aldehydes such as 4-hydroxy-2-nonenal (4-HNE) protein adducts. A single point mutation in ALDH2 at E487K (ALDH2*2) intrinsically lowers the activity of ALDH2. Alda-1, an ALDH2 activator, attenuates the formation of 4-HNE protein adducts and ROS in several disease models. We hypothesized that ALDH2 can protect against heat stress-induced vascular inflammation and the accumulation of ROS and toxic aldehydes. Homozygous ALDH2*2 knock-in (KI) mice on a C57BL/6J background and C57BL/6J mice were used for the animal experiments. Human umbilical vein endothelial cells (HUVECs) were used for the *in vitro* experiment. The mice were directly subjected to whole-body heating (WBH, 42°C) for 1 h at 80% relative humidity. Alda-1 (16 mg/kg) was administered intraperitoneally prior to WBH. The severity of ALI was assessed by analyzing the protein levels and cell counts in the bronchoalveolar lavage fluid, the wet/dry ratio and histology. ALDH2*2 KI mice were susceptible to HS-induced ALI *in vivo*. Silencing ALDH2 induced 4-HNE and ROS accumulation in HUVECs subjected to heat stress. Alda-1 attenuated the heat stress-induced activation of inflammatory pathways, senescence and apoptosis in HUVECs. The lung homogenates of mice pretreated with Alda-1 exhibited significantly elevated ALDH2 activity and decreased ROS accumulation after WBH. Alda-1 significantly decreased the WBH-induced accumulation of 4-HNE and p65 and p38 activation. Here, we demonstrated the crucial roles of ALDH2 in protecting against heat stress-induced

ROS production and vascular inflammation and preserving the viability of ECs. The activation of ALDH2 by Alda-1 attenuates WBH-induced ALI *in vivo*.

Keywords: heatstroke, heat stress, aldehyde dehydrogenase 2 (ALDH2), Alda-1, acute lung injury (ALI), reactive oxygen species (ROS)

HIGHLIGHTS

- Mice carrying the human ALDH2*2 variant were susceptible to whole-body heating-induced acute lung injury.
- Silencing ALDH2 induced 4-HNE and ROS accumulation in endothelial cells subjected to heat stress.
- Alda-1 attenuated the heat stress-induced activation of inflammatory pathways, senescence and apoptosis *in vitro*.
- Activation of ALDH2 by Alda-1 attenuated whole-body heating-induced acute lung injury *in vivo*.

INTRODUCTION

Heat-related illness (HRI) affects a large number of people and is an increasing cause of health issues, as climate change results in elevated global temperatures (1, 2). The heatstroke (HS) -related inflammatory response is akin to the systemic inflammatory response syndrome and lead to a rapid deterioration in clinical status, resulting in disseminated intravascular coagulation, acute lung injury (ALI), multiorgan failure syndrome (MODS) and death (3, 4). Heat stress induces several inflammatory and apoptotic pathways and increases the production of reactive oxygen species (ROS) and endogenous reactive aldehydes (5–9). As an inducible transcription factor, nuclear factor-kappa B (NF-κB) can be activated by ROS, cytokines, and endotoxin and is associated with the pathophysiological changes associated with heat stress and strenuous exercise (10–12). Endothelial cells (ECs) play an essential role in maintaining the stability of microvascular permeability. Heat stress induces cellular senescence, apoptosis and pyroptosis in a variety of cell types, and endothelial activation/dysfunction with hyperpermeability play crucial roles in HS-induced ALI (13–17). The accumulation of toxic aldehydes and oxidative stress and upregulation of the NF-κB signaling pathway have been found in the hippocampus and lung tissues of rats subjected to HS (18, 19). Scavenging ROS significantly inhibited HS-induced necroptosis, suggesting that preventing necroptosis could alleviate HS-induced small intestinal tissue injury and cell death (20).

Mitochondrial aldehyde dehydrogenase 2 (ALDH2) is an enzyme that detoxifies aldehydes by converting toxic exogenous and endogenous aldehydes such as 4-hydroxy-2-nonenal (4-HNE) protein adducts and lipoperoxides such as malondialdehyde (MDA) to form nontoxic carboxylic acids. Although ALDH2 was initially known for its crucial role in ethanol metabolism in the liver, it has since been implicated in a variety of diseases, such as cardiovascular diseases (CVDs), diabetes, neurologic dysfunctions and ischemia reperfusion injury (IRI), in several organs (21–25). Endogenous aldehydic products, such as 4-HNE and MDA, can be formed by lipid peroxidation of mitochondrial and plasma membranes under oxidative stress conditions (26, 27). ALDH2 deficiency is known to increase oxidative stress due to an imbalance in antioxidant defense and ROS generation (8, 28). A single point mutation in ALDH2 at E487K, which is known as ALDH2*2, intrinsically lowers ALDH2 activity in approximately 40% of East Asian individuals. The ALDH2 activator Alda-1 binds to ALDH2 and restores ALDH2 activity by acting as a structural chaperone (29). Previous studies indicated that Alda-1 attenuated the formation of 4-HNE protein adducts and inactivated the NF-κB pathway in several disease models (30–34). Pretreatment with Alda-1 had been shown to have beneficial effects on hyperoxia and acrolein induced ALI through preserving the endothelial barrier and mitochondrial dysfunction (35–37).

While ALDH2 protects against oxidative damage through the oxidation of toxic aldehydes, few studies have investigated the role of ALDH2 in the pathogenesis of HS. We hypothesized that ALDH2 can protect against heat stress-induced vascular inflammation and ROS and the accumulation of toxic aldehydes. We further tested whether the ALDH2 activator Alda-1 could be an adjunctive therapy for HS-induced ALI.

MATERIALS AND METHODS

Cell Culture and Reagents

Human umbilical vein endothelial cells (HUVECs) were obtained from Cell Applications (San Diego, CA, USA) and Taiwan Medical Cell and Bioresource Collection and Research Center (BCRC, Taiwan). Cells at passages 3-5 were used for the experiments with ALDH2-silencing RNA (siALDH2, Santa Cruz, sc-60147) and Alda-1 (Adooq Bioscience, A15805, 20 mM in DMSO as stock solution, 1:1,000 dilution (20μM) for the *in vitro* experiments). According to previous published literatures and our own experiences (24–26, 38), we believe that DMSO in such concentration would not exert obvious toxic or protective effects on endothelial cells. HUVECs were cultured in M200 medium supplemented with endothelial growth factor (Gibco, Medium 200 and LSGS) and maintained in a humidified atmosphere at 37°C and 5% CO_2. The control cells were maintained in an incubator at 37°C. For heat stress induction, cells were subjected to 42°C for 2 h and then at 37°C overnight, as previously described (11, 15).

Immunoblotting

Protein lysates from the cells and lung tissues were subjected to SDS-PAGE followed by electroblotting onto PVDF membranes.

The membranes were probed with monoclonal antibodies against ALDH2 (Abcam, ab108306), cytochrome c (Santa Cruz, sc-7159), caspase 3 (CST, #9662), 4-HNE (Abcam, ab46545), p-p38 (CST, #9215), p38 (CST, #9212), p-p65 (CST, #3033), p65 (CST, #3034), NOX1 (GeneTex, GTX103888), NOX4 (GeneTex, GTX121929) and GAPDH (Santa Cruz, sc-32233). Bands were visualized by chemiluminescence detection reagents, and densitometric analysis was conducted with imaging processing software (Multi Gauge, Fujifilm). These data are expressed as the fold changes relative to the controls.

Determination of ALDH2 Activity

ALDH2 activity was measured using an ALDH2 activity assay kit according to the manufacturer's protocol (Abcam, ab115348, Cambridge, UK). In brief, the activity was estimated by measuring the conversion of oxidized nicotinamide adenine dinucleotide (NAD^+) to reduced nicotinamide adenine dinucleotide (NADH) at an absorbance of 450 nm every 5 minutes for 2 hours period in the lung tissues and every 30 minutes for a 6 hours period (39).

Measurement of ROS

ROS measurement was performed according to the manufacturer's recommendations (OxiSelecte *in vitro* ROS/reactive nitrogen species (RNS) assay kit, Green Fluorescence; Catalog #STA-347, Cell Biolabs, Inc., San Diego, CA, USA). This *in vitro* assay measured total ROS/RNS free radical activity. Unknown ROS or RNS samples or standards were added to the wells with a catalyst that helps accelerate the oxidative reaction. Samples were measured fluorometrically against hydrogen peroxide. The free radical content in the samples was determined by comparison with a hydrogen peroxide standard curve. In brief, the cell lysates were stained with 2',7'-dichlorofluorescein diacetate (DCFH-DA), which is oxidized by ROS to form fluorescent 2',7'-dichlorofluorescein and were measured at an excitation wavelength of 488 nm and an emission wavelength of 535 nm. In addition, the dihydroethidium (DHE) method was also used to detect superoxide production at an excitation wavelength of 518 nm and an emission wavelength of 606 nm. The samples were loaded onto black 96-well plates and incubated for 30 min at 37°C, and the relative fluorescence units (RFUs) were determined by a fluorescence microplate reader (BMG Labtech, Ortenberg, Germany).

ALDH2*2 Gene-Targeted Knock-In Mice

Knock-in mice on a C57BL/6J background with an inactivating point mutation in ALDH2 (ALDH2*2) were generated by homologous recombination, as previously described (34). There were no significant phenotypic changes in ALDH2*2 KI mice. Homozygous ALDH2*2 KI mice were used for the experiments.

Murine Model of Whole-Body Hyperthermia

C57BL/6J mice and homozygous ALDH2*2 KI mice with a C57BL/6J background were used for the animal experiments. The mice were directly exposed to whole-body heating (WBH) at 42°C for 1 h at 80% relative humidity using a temperature-controlled environmental chamber from room temperature and then returned to room temperature for 6-hour recovery period. Rectal temperature was measured using a copper-constantan thermocouple probe inserted into the rectum and connected to a thermometer. After the 1-h heating period, the mice were returned to their home cages and given food and water ad libitum (40). These mice were treated with either vehicle control (20% DMSO and 20% PEG 400 in 100μl PBS) or Alda-1 [16 mg/kg in 100 μl in PBS with 20% DMSO and 20% PEG 400 (Sigma, 06855)] intraperitoneally 30 minutes prior to WBH as previously described with some modification (34, 41). Previous literatures had showed that there were no obvious toxic or protective effects of this DMSO preparation on animal experiments (34, 42). Mice were considered adequately anesthetized when no attempt to withdraw the limb after pressure was observed. At the end of the study, the mice were euthanized by exsanguination under anesthesia. Bronchioalveolar lavage fluid (BALF) was collected at the end of the experiment by slowly irrigating the right lung with two separate 0.7-ml aliquots of PBS, of which 1.2 ml could be retrieved consistently. To avoid overdistention, the pressure should be kept less than 20 mmH_2O. All experimental protocols and procedures were approved by the Institutional Animal Care Committee of the National Defense Medical Center (Taipei, Taiwan) (43).

Assessment of ALI

Lungs were collected after the mice were sacrificed following WBH. The wet weights of the organs were measured, and their dry weights were determined after the tissues were fully dried in an oven at 105°C. The water content was calculated as a percentage according to the following formula: 100×(wet weight-dry weight)/wet weight. One BALF aliquot was used immediately to measure the total cell counts. Erythrocytes were lysed using erythrocyte lysis buffer (Sigma, 1814389001), and the BALF was centrifuged at 400 g for 5 min and the supernatant was discarded. The pelleted cells were resuspended in 1.0 ml of PBS for the total leukocyte count by using a hemocytometer as previously described (44). The protein concentration in the supernatant was determined using bicinchoninic acid (BCA) method (Pierce, Rockford, IL, USA).

Histology and Immunohistochemistry

Lung injury was evaluated by histological analysis as described previously. In brief, lung tissue was fixed in 10% formalin solution for 24 h and stained with hematoxylin and eosin (H&E). Lung injury was scored based on (1) the infiltration or accumulation of neutrophils in the airspace or vessel wall and on (2) the thickness of the alveolar wall. These two observations were scored from 0 (normal) to 5 (most severe injury or greatest thickness, respectively) (45).

Cell Viability

Cell proliferation was analyzed by the MTT assay (Sigma, #11465007001) in accordance with the manufacturer's protocols. Briefly, 5,000 cells/well were grown in 96-well plates, exposed to heat stress at 42°C for 2 h and recovered at 37°C

overnight. Then, the cells were incubated with MTT medium in a 5% CO_2 incubator at 37°C. After 4 h, the absorbance was measured at 570 nm using a Clariostar microplate reader (BMG Labtech, Ortenberg, Germany).

Terminal Deoxynucleotidyl Transferase-Mediated dUTP Nick End-Labeling Assay

Cell apoptosis was evaluated by a TUNEL assay using a fluorescein direct *in situ* apoptosis detection kit (Millipore, S7110) according to the manufacturer's recommended protocol. Apoptosis was determined as the percentage of positive cells per 1,000 DAPI-stained nuclei, and the cells were visualized under a fluorescence microscope (Nikon Eclipse 50i) at a magnification of 100×.

Senescence Assay

Cellular aging was assessed with a senescence cell staining kit according to the manufacturer's instructions (Sigma, CS0030). Cultured HUVECs were fixed and then incubated with fresh X-gal staining solution (1 mg/ml, 5 mmol/l potassium ferrocyanide, 5 mmol/l potassium ferricyanide, and 2 mmol/l $MgCl_2$; pH 6). After the cells were stained, the numbers of blue-stained and total cells were determined, and the percentage of β-galactosidase-positive cells was calculated.

Assessment of Mitochondrial Injury

The mitochondrial membrane potential (ΔΨm) has been used as a parameter of mitochondrial function (46). To assess mitochondrial function in HUVECs after HS, JC-1 (5,5',6,6'-tetrachloro-1,1',3,3'- tetraethylbenzimidazolcarbocyanine iodide) staining (BD Biosciences, 551302) was performed and assessed by fluorescence microscopy (Nikon Eclipse 50i) at a magnification of 200×. The images represent the merging of red and green channels. In addition, the fluorescence intensity of the cells was measured by a fluorescence microplate reader (BMG Labtech, Ortenberg, Germany). The data are expressed as the ratio of red fluorescence to green fluorescence intensity.

Serum Levels of Organ Injuries

The serum levels of creatine kinase (CK), aspartate transferase (AST), and blood urea nitrogen (BUN) were measured by a FUJI Dri-chem slide on a FUJIDRI-CHEM 4000i instrument.

Statistical Analysis

All experiments were performed independently at least 3 times, and all continuous variables are presented as the mean ± standard deviation (SD). The F test for equal variance was performed before the differences among groups were analyzed. Comparisons between two groups were analyzed using Student's t test. For multiple groups, the data were analyzed using one-way ANOVA. For *post hoc* analysis, the Tukey test was used to correct for multiple comparisons, and the Fisher Least Significant Difference test was used for planned comparisons. Target protein expression measured by immunoblotting was analyzed by densitometry and is expressed as percent changes relative to an internal control or as the phosphorylated protein level relative to the total protein expression. Statistical significance was defined as a P value less than 0.05. Analyses were performed using a statistical software package (SPSS version 16.0 for Windows; SPS, Inc; Chicago, IL, USA) and GraphPad software.

RESULTS

ALDH2*2 KI Mice Are Susceptible to HS-Induced ALI *In Vivo*

There were no significant differences in body temperature between wild-type (WT) and ALDH2*2 KI mice after WBH (**Supplementary Figure 1**). Compared to WT mice, ALDH2*2 KI mice were more vulnerable to WBH with increased mortality rates (**Figure 1A**). ALDH2*2 mice were susceptible to WBH-induced ALI, there was a significant increase in the wet/dry ratio of lung tissue in WBH-induced mice (**Figure 1B**). WBH significantly induced pathological fluid accumulation and inflammatory cell infiltration in the lung (**Figure 1C**). Increased inflammatory cells, protein levels and ROS production were observed in the BALF of ALDH2*2 KI mice subjected to WBH compared with WT mice (**Figures 1D–F**). In lung homogenates, the ROS production was increased in ALDH2*2 KI mice subjected to WBH compared with that in WT mice (**Figure 1G**). ALDH2 activity was decreased in the livers of ALDH2*2 KI mice compared with WT mice (**Figure 1H**). WBH significantly induced the accumulation of 4-HNE, NOX1, the phosphorylated-p65:p65 ratio and the phosphorylated-p38:p38 ratio (**Figure 1I**). There were no significant differences in NOX4 expression between the groups. In addition, there were significantly elevated serum levels of AST, CK and BUN in ALDH2*2 KI mice subjected to WBH compared with WT mice (**Supplementary Figure 2**). Taken together, these results indicate that ALDH2*2 KI mice are susceptible to WBH-induced ALI.

Silencing ALDH2 Exacerbates Heat Stress Induced Inflammatory Pathways and Reduced the Viability of HUVECs *In Vitro*

To further confirm the effect of ALDH2 on heat stress *in vitro*, silencing ALDH2 was used in HUVECs with or without heat stress. As expected, the protein and activity of ALDH2 were decreased by silencing ALDH2 (**Figures 2A, B**). There was increased ROS accumulation in HUVECs subjected to 42°C for 2 h (**Figures 2C, D**). Silencing ALDH2 reduced the viability and exaggerated apoptosis and senescence of HUVECs subjected to heat stress (**Figures 2E–G**). Consistent with the results of previous studies (5, 47), heat stress induced mitochondrial dysfunction and apoptosis. We found silencing ALDH2 attenuated the level of ΔΨm (**Figure 2H**) and increased the expression of cytochrome c and cleaved caspase 3 relative to the HS in HUVECs (**Figure 2I**). Meanwhile, the phosphorylated-p65:p65 ratio, the phosphorylated-p38:p38 ratio, the expression of NOX1 and the toxic 4-HNE were accumulated in the silencing ALDH2 subjected to HS in HUVECs (**Figure 2I**). NOX4 expression was not significantly different between the group. These results suggest that reduced ALDH2 exacerbates heat stress induced NF-kB inflammatory pathways, ROS production, mitochondrial dysfunction and reduces the viability of HUVECs *in vitro*.

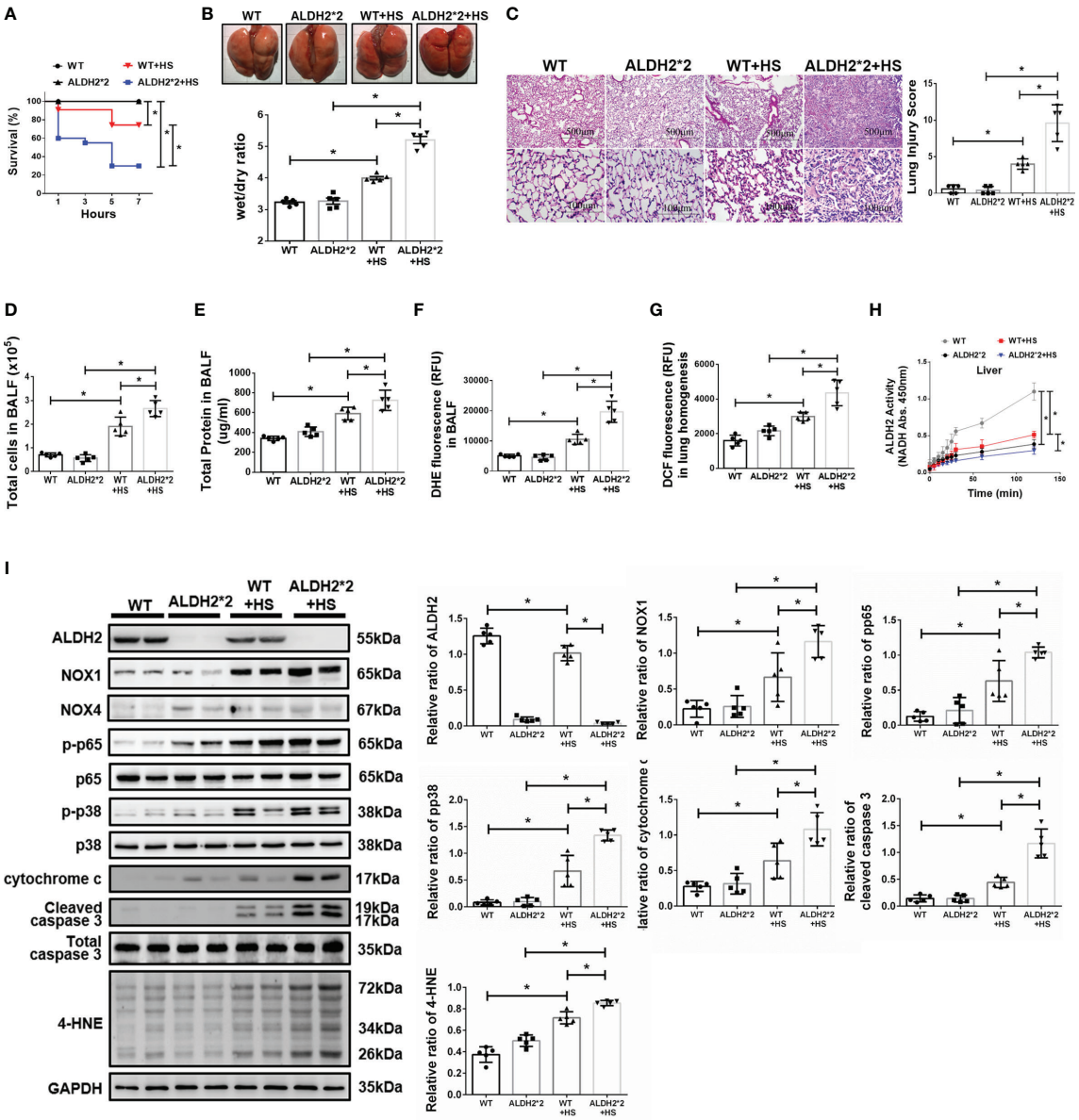

FIGURE 1 | Effects of ALDH2 on HS-induced ALI *in vivo*. C57BL/6J WT and ALDH2*2 KI mice were exposed to WBH (42°C, 80% RH for 1 h) and then analyzed. **(A)** Survival of mice subjected to WBH (n = 20 in each group). **(B)** Representative images of the lungs and wet/dry ratio of the lungs (n = 5). **(C)** H&E stain of the lungs (n = 5). **(D)** Total cells in the BALF (n = 5). **(E)** Total protein in the BALF (n = 5). **(F)** ROS production in the BALF as determined by DHE fluorescence measurement using a fluorescence microplate reader with an excitation wavelength of 518 nm and an emission wavelength of 606 nm (n = 5). **(G)** ROS production in lung homogenates as determined by DCF fluorescence measurement using a fluorescence microplate reader with an excitation wavelength of 488 nm and an emission wavelength of 535 nm (n = 5). **(H)** The ALDH2 activity in liver homogenates was measured by NADH production using the O.D. absorbance at 450 nm in a microplate reader (n = 5). **(I)** The protein and 4-HNE levels in lung homogenates were measured by immunoblotting. Densitometric analysis was conducted with imaging processing software. The data were quantified by normalization to GAPDH; phosphorylated proteins were normalized to total proteins (n = 5). The data are expressed as the mean ± SD. Statistical significance is indicated as $^*p < 0.05$.

Alda-1 Attenuates Heat Stress-Induced Activation of Inflammatory Pathways and Preserved Viability in HUVECs *In Vitro*

To understand the effect of ALDH2 activation on HS, Alda-1 was pretreated in HS induced HUVECs. Consistent with previous studies (29, 31, 48), Alda-1 (20μM) significantly augmented ALDH2 activity (**Figure 3A**) and reduced heat stress-induced ROS accumulation (**Figures 3B, C**). Alda-1 ameliorated the heat stress-induced cell death (**Figure 3D**) and reduced heat stress-induced apoptosis (**Figure 3E**) and senescence (**Figure 3F**) in HUVECs. Alda-1 reversed the heat stress-reduced ΔΨm (**Figure 3G**). Alda-1 attenuated the heat stress-induced

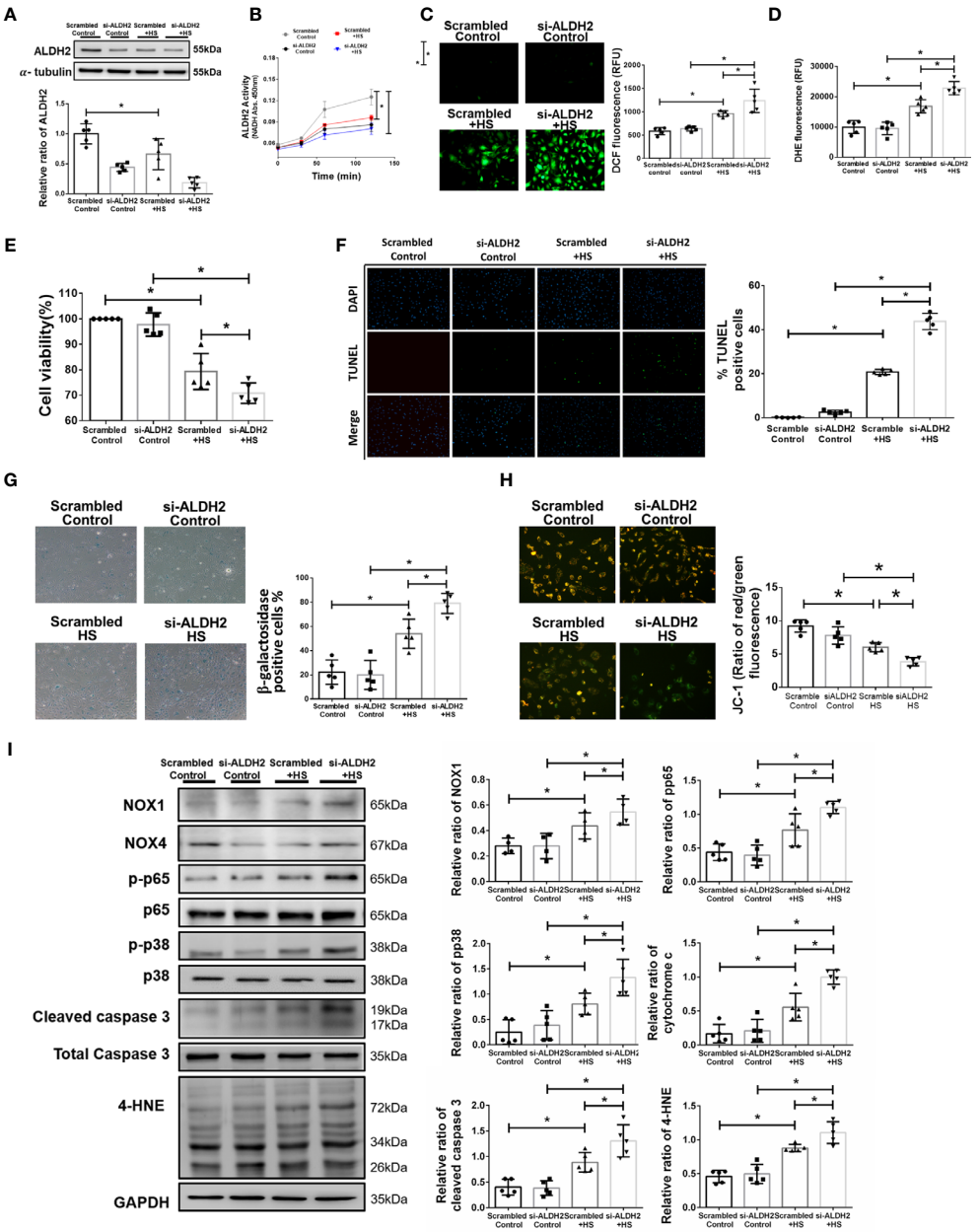

FIGURE 2 | Silencing ALDH2 augmented heat stress-induced activation of NF-κB, ROS production and apoptosis in HUVECs *in vitro.* HUVECs were transfected with ALDH2 siRNA or control siRNA (scramble) before heat stress induction (42°C for 2 h). **(A)** ALDH2 protein expression was measured by immunoblotting ($n = 5$). **(B)** The ALDH2 activity in cell lysate was determined by measuring NADH production based on the O.D. absorbance at 450 nm in a microplate reader ($n = 5$). **(C)** Measurement of ROS production based on DCF fluorescence using a fluorescence microplate reader with an excitation wavelength of 488 nm and an emission wavelength of 535 nm ($n = 5$). **(D)** Measurement of cellular ROS production based on DHE fluorescence using a fluorescence microplate reader with an excitation wavelength of 518 nm and an emission wavelength of 606 nm ($n = 5$). **(E)** The viability of HUVECs was measured by the MTT assay based on the O.D. absorbance at 570 nm in a microplate reader ($n = 5$). **(F)** The levels of apoptosis were measured by the TUNEL assay as determined fluorescence microscopy. The percentage of apoptotic cells was determined based on the number of TUNEL-positive cells among the total number of cells ($n = 5$). **(G)** The levels of senescence were measured by β-galactosidase activity detection using bright field microscopy ($n = 5$). **(H)** Detection of mitochondrial dysfunction by the JC-1 assay, revealing a decrease in the mitochondrial membrane potential ($\Delta\Psi m$) in live cells as determined by fluorescence microscopy and fluorescence microplate reader. The $\Delta\Psi m$ level is expressed as the merge of the red and green channels, and the data were quantified as the ratio of red fluorescence intensity to the green fluorescence intensity ($n = 5$). **(I)** The protein and 4-HNE levels in lung homogenates were measured by immunoblotting. Densitometric analysis was conducted with imaging processing software. The data were quantified by normalization to GAPDH; phosphorylated proteins were normalized to total proteins ($n = 5$). The data are expressed as the mean ± SD. Statistical significance is indicated as $^*p < 0.05$.

phosphorylated-p65:p65 ratio, phosphorylated-p38:p38 ratio, cytochrome c, cleaved caspase 3, NOX1 and 4-HNE accumulation (**Figure 3H**). There were no significant differences regarding NOX4 expression. These results suggest that activation of ALDH2 by Alda-1 reduces heat stress induced mitochondrial dysfunction and ROS accumulation of HUVECs *in vitro*.

Alda-1 Ameliorates WBH-Induced ALI *In Vivo*

We then tested the protective effects of Alda-1 on WBH-induced ALI *in vivo*. Pretreatment with Alda-1 significantly increased HS-related survival rates by 25% (**Figure 4A**). Alda-1 ameliorated WBH-induced ALI, there was a significant decrease in wet/dry ratio of lung tissue in mice that received WBH exposure with Alda-1 pretreatment (**Figure 4B**). In addition, Alda-1 significantly reduced pathological fluid accumulation and inflammatory cell infiltration in the lung (**Figure 4C**). There were decreased inflammatory cell protein levels and ROS production in the BALF of Alda-1-pretreated mice subjected to WBH (**Figures 4D–F**). In lung homogenates, mice subjected to WBH increased ROS accumulation by 2.8-fold relative to the control, whereas pretreatment with Alda-1 reduced the level by 2.9-fold (**Figure 4G**). As expected, Alda-1-treated mice had significantly elevated ALDH2 activity (**Figure 4H**) in liver homogenates. Alda-1 significantly decreased the WBH-induced accumulation of 4-HNE, NOX1 expression, the phosphorylated-p65:p65 ratio, the phosphorylated-p38:p38 ratio, cytochrome c expression and cleaved caspase 3 expression (**Figure 4I**). NOX4 expression was not significantly different between the groups. Alda-1 attenuated HS-induced elevations in serum levels of AST, CK, and BUN (**Supplementary Figure 2**). These results suggest that pretreatment with Alda-1 ameliorates WBH-induced ALI *in vivo* through reduced activation of NF-kB and apoptotic pathways and ROS accumulation.

DISCUSSION

In this study, we demonstrated the protective role of ALDH2 in HS-induced ALI. Alda-1 attenuated HS-induced ALI by reducing the accumulation of ROS and toxic aldehydes and alleviating vascular inflammation and endothelial dysfunction. A schematic is shown in **Figure 5**.

In this study, we highlight 4-HNE and ROS production as a vicious cycle in heatstroke-induced ALI and the roles of ALDH2 in breaking the vicious cycle. Activation of NF-κB-induced NOXs activation and ROS production (34, 49, 50). Previous studies indicated that 4-HNE increased the production of ROS through NOX and 5-lipoxygenase (5-LO) (51). 5-LO expression induced by HNE is regulated by activation of the p38 MAPK and NF-κB pathways in macrophages (52). The activation of 5-LO by HNE enhanced the CD36 expression and MMP-2 production and led to macrophage foam cell formation and atherosclerotic plaque instability (53, 54). Nicotinamide adenine dinucleotide phosphate oxidases (NOX) are transmembrane enzymes that catalyze the generation of superoxide anions through the transfer of electrons from NADPH to molecular oxygen and NOXs-derived ROS induce endothelial dysfunction (55). NOX1 is a major source of ROS that induces p38 and NF-kB activation and 4-HNE expression, thereby causing inflammation and oxidative stress (56, 57). In addition, NF-kB and p38 activation upregulate NOX-1 overexpression in ECs (38, 58). NOX-derived ROS causes a decrease in the $\Delta\Psi m$, resulting in an increase in mitochondrial-derived ROS, whereas mitochondrial ROS production cause a secondary activation of NOXs (59). NOX-derived ROS are mediators of endogenous biological changes under HS (60), consistently, we also found that acute HS induces NOX1 overexpression but not NOX4. Using mice carrying the human ALDH2*2 dysfunctional polymorphism, we demonstrated that this ALDH2*2 variant conferred susceptibility to HS, as evidenced by increased ROS and 4-HNE accumulation, vascular inflammation and endothelial dysfunction. Previous studies have shown increased inflammatory markers in patients with HS and in animal models of HS. HS resembles sepsis in several aspects, and increasing evidence suggests that endotoxemia and cytokines may be implicated in HS pathogenesis (16). HS significantly elevates the levels of cytokines in BALF and activates the NF-κB signaling pathway in lung tissue (61). HS induces p38 activation and inflammatory signaling, apoptosis and pyroptosis in vascular cells (14, 15, 17, 62). Consistent with previous studies, we also found that mice subjected to HS had increased accumulation of ROS and 4-HNE (18). ALDH2*2 variants are associated with the increased incidence of several neurodegenerative, cardiovascular and endocrinological diseases as well as lung and alimentary tract cancers (62). The accumulation of 4-HNE has been implicated in the pathogenesis of numerous oxidative stress-related diseases and in the development and progression of CVDs (63–65). The rs671 polymorphism in ALDH2 promotes macrophage foam cell formation and vascular inflammation in atherosclerosis (65, 66). Patients with ALDH2 deficiency have higher postoperative oxidative stress levels and are susceptible to cisplatin-induced cytotoxicity *via* the overproduction of ROS (67, 68). Genetic ALDH2-deficient mice are prone to ethanol-induced liver inflammation and fibrosis by paracrine activation of IL-6 in Kupffer cells (69). Consistent with previous studies, we also found that decreased ALDH2 activity resulted in enhanced phosphorylation of p65 and p38 and apoptosis in ECs (40, 70, 71).

The primary treatment for HS is the alleviation of hyperthermia. Adjunctive therapies for organ injury are still limited (3). We provided a rationale for the use of an ALDH2 activator as an adjunctive HS treatment in this study. ALDH2 was shown to protect against oxidative stress and the subsequent accumulation of toxic aldehydes and adducts in IRI (24). ALDH2 protects against heat shock and is involved in the pathogenesis of sepsis (72). ALDH2 overexpression prevented acetaldehyde-induced cell injury and decreased apoptosis in ECs and oxidative stress-induced endothelial dysfunction (73–75). Alda-1 binds to ALDH2 and restores ALDH activity by acting as a structural chaperone (29). Previous studies demonstrated decreased ALDH2 expression due to increased ALDH2 protein

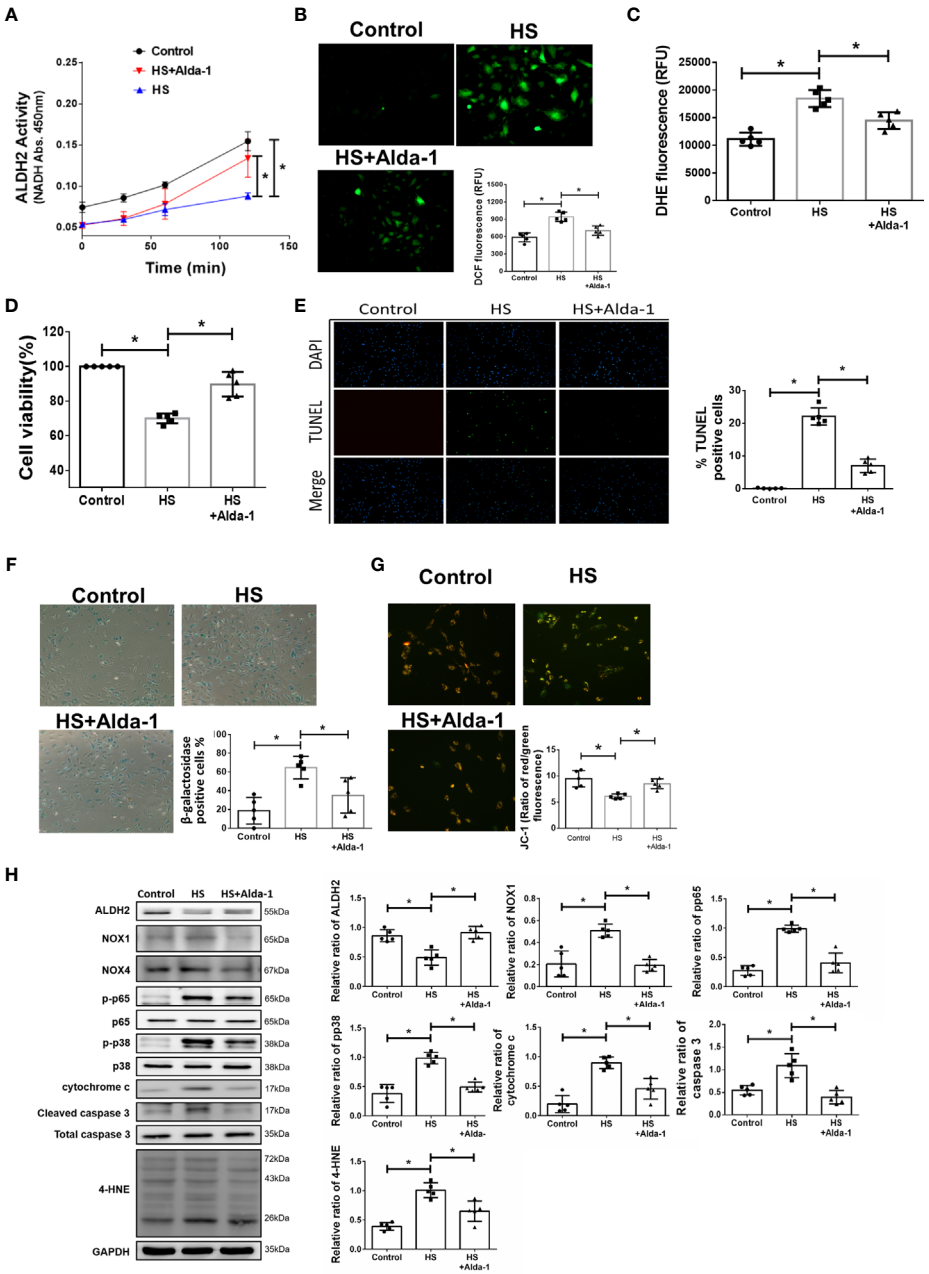

FIGURE 3 | Effects of Alda-1 on HS-induced vascular inflammation, ROS and apoptosis *in vitro*. Alda-1 (20 μM) was added to HUVECs for 6 h before HS (42°C for 2 h). **(A)** The ALDH2 activity in cell lysate was determined by measuring NADH production based on the O.D. absorbance at 450 nm in a microplate reader ($n = 5$). **(B)** Measurement of ROS production based on DCF fluorescence as determined by using a fluorescence microplate reader with an excitation wavelength of 488 nm and an emission wavelength of 535 nm ($n = 5$). **(C)** Measurement of cellular ROS production based on DHE fluorescence as determined using a fluorescence microplate reader with an excitation wavelength of 518 nm and an emission wavelength of 606 nm ($n = 5$). **(D)** The viability of HUVECs was measured by the MTT assay based on the O.D. absorbance at 570 nm in a microplate reader ($n = 5$). **(E)** The levels of apoptosis were measured by the TUNEL assay as determined by fluorescence microscopy. The percentage of apoptotic cells was determined based on the number of TUNEL-positive cells among the total number of cells. **(F)** The levels of senescence were measured by β-galactosidase activity detection using bright field microscopy ($n = 5$). **(G)** Detection of mitochondrial dysfunction by the JC-1 assay, revealing that the mitochondrial membrane potential ($\Delta\Psi m$) was decreased in live cells as determined by fluorescence microscopy and a fluorescence microplate reader. The $\Delta\Psi m$ level is expressed as the merge of the red and green channels, and the data were quantified as the ratio of red fluorescence intensity to green fluorescence intensity ($n = 5$). **(H)** The protein and 4-HNE levels in lung homogenates were measured by immunoblotting. Densitometric analysis was conducted with imaging processing software. The data were quantified by normalization to GAPDH; phosphorylated proteins were normalized to total proteins ($n = 5$). The data are expressed as the mean ± SD. Statistical significance is indicated as $^*p < 0.05$.

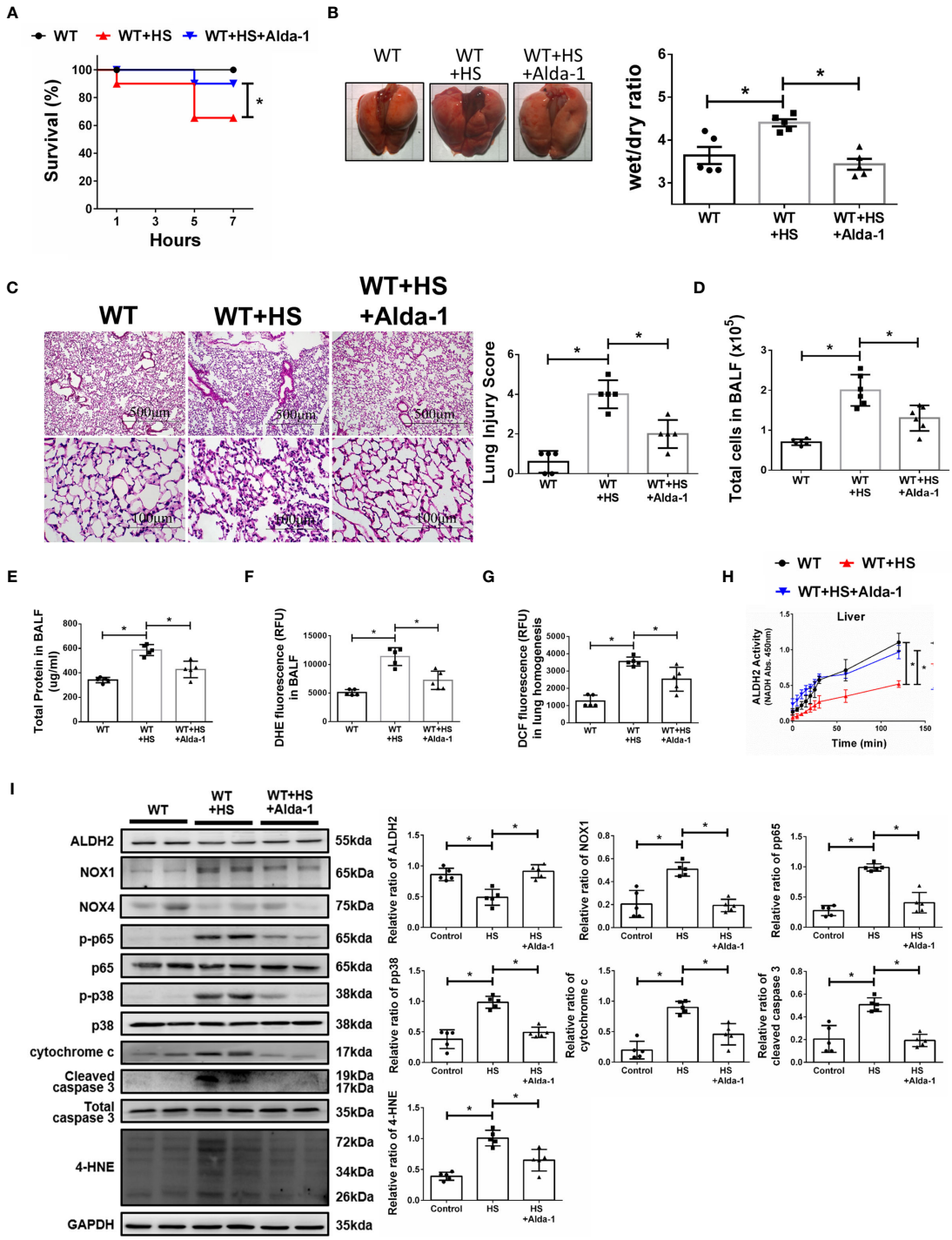

FIGURE 4 | Alda-1 attenuates HS-induced ALI *in vivo*. Alda-1-pretreated C57BL/6J mice were exposed to WBH (42°C, 80% RH for 1 h) and then analyzed. **(A)** Survival of mice subjected to WBH (n = 20 in each group). **(B)** Representative images of the lungs and wet/dry ratio of the lungs (n = 5). **(C)** H&E stain of the lungs (n = 5). **(D)** Total cells in the BALF (n = 5). **(E)** Total protein in the BALF (n = 5). **(F)** Measurement of ROS production in BALF based on DHE fluorescence as determined using a fluorescence microplate reader with an excitation wavelength of 518 nm and an emission wavelength of 606 nm (n = 5). **(G)** Measurement of ROS production in lung homogenates based on DCF fluorescence as determined using a fluorescence microplate reader with an excitation wavelength of 488 nm and an emission wavelength of 535 nm (n = 5). **(H)** The ALDH2 activity in lung homogenates was measured by NADH production based on the O.D. absorbance at 450 nm in a microplate reader (n = 5). **(I)** The protein and 4-HNE levels in lung homogenates were measured by immunoblotting. Densitometric analysis was conducted with imaging processing software. The data were quantified by normalization to GAPDH; phosphorylated proteins were normalized to total proteins (n = 5). The data are expressed as the mean ± SD. Statistical significance is indicated as $^*p < 0.05$.

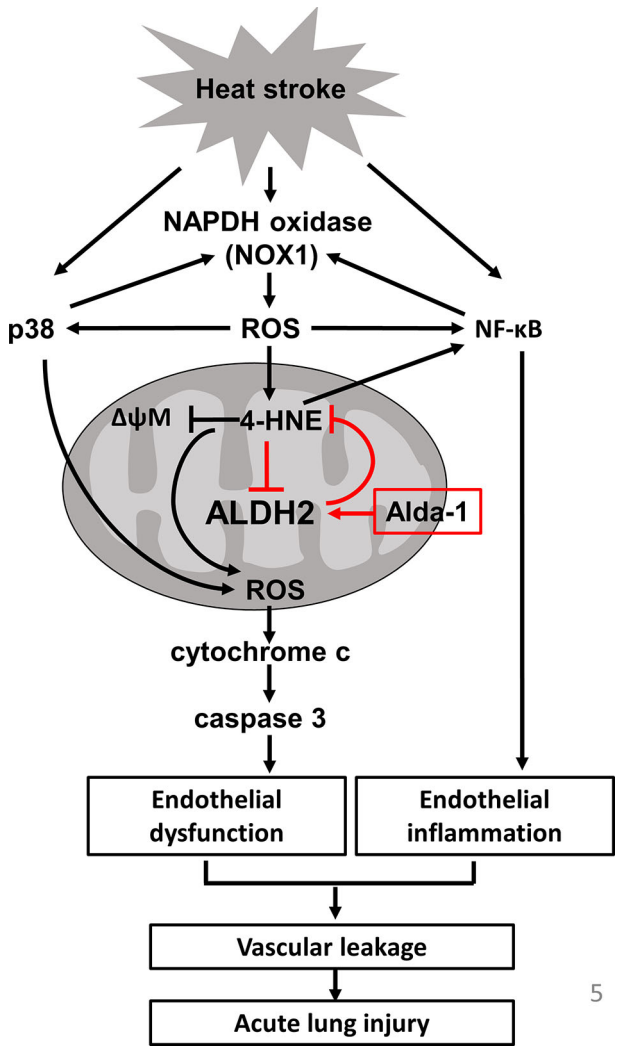

FIGURE 5 | Schematic of the role of ALDH2 in HS.

turnover in both humans with the ALDH2*2 variant and in ALDH2*2 KI mice (76, 77). Aldehydes and 4-HNE also inactivate ALDH2 itself and the mitochondrial electron transport chain (64). Alda-1 restored the high-glucose-induced decrease in ALDH2 protein expression and activity in rat cardiomyocytes (78). Consistently, we also found that Alda-1 increased ALDH2 activities and protein expression under heat stress. Nonetheless, Alda-1 increased the ALDH2 activity but not its protein expression in the control cells. We speculated that Alda-1 stabilizes heat stress-induced ALDH2 degradation by acting as a chemical chaperone (29). ALDH2 protects against angiotensin II-induced ROS generation and prevents ROS-induced vessel contraction (28). Pretreatment with Alda-1 upregulated ALDH2 activity and reduced 4-HNE and MDA accumulation in various models of intestinal IRI (32). Accelerated aldehyde degradation by Alda-1 also decreased bile duct ligation-induced liver necrosis, inflammation and fibrosis (33). Alda-1 attenuated 4-HNE-induced vascular smooth muscle cell proliferation and migration by regulating NF-κB activation, ameliorated vascular remodeling in a mouse model of pulmonary hypertension and inhibited atherosclerosis and fatty liver in hyperlipidemic mice (30, 31). Alda-1 inhibits oxidized low-density lipoprotein-induced priming and activation of the NLRP3 inflammasome by reducing oxidative stress in macrophages (79). Alda-1 attenuated high-glucose-induced mitochondrial injury in H9c2 cells (80). In this study, we found that Alda-1 attenuated HS-induced accumulation of 4-HNE and ROS and further prevented HS-induced ALI. Our previous study also demonstrated that Alda-1 attenuated AngII-induced abdominal aortic aneurysm (AAA) in ApoE-KO mice (34).

Increased immune cells in BALF could be due to endothelial activation/dysfunction and recruitment of inflammatory cells. Consistent with previous studies (14, 17), We have found that there were increased total cells in the BALF in mice subjected to HS. A recent study regarding hyperoxia induced ALI also revealed that pretreatment with Alda-1 reduced hyperoxia induced immune cell infiltration, alveolar damage and lung inflammation and preserved alveolar permeability through the activation of Akt and mTOR pathways (35). Here we demonstrated that pretreatment with Alda-1 prevented HS-induced ALI by reducing ROS production, toxic aldehydes and mitochondrial injury and preserving the viability of ECs.

Through HS clearly induces endothelial barrier dysfunction and hyperpermeability (13–17), the potential role of hydrostatic lung edema formation in HS induced ALI models are otherwise limited. Accumulated ROS also induced lung edema formation through downregulation of alveolar epithelial Na/K-ATPase activity with impaired alveolar fluid reabsorption (81).

Limitations

We are aware that the development of HS could be multifactorial in nature, including other cell types, mediators and pathways. Infiltrated immune cells in BALF could be determined to further elucidate the roles of ALDH2 on HS. The roles of ALDH2 in other inflammatory cells as well HS-induced changes in pulmonary hemodynamics, lung endothelial permeability and the alveolar fluid resorption should be further investigated. Heat shock response systems, including the heat shock factor-1 (HSF-1) and heat shock protein (HSP) stress systems, provide protection against thermal insult by regulating the transcription of several HSPs and promoting chaperone activities to alleviate proteotoxic stresses in eukaryotic cells. The interplay among HSF-1, HSPs and ALDH2 should be further explored. HSF-1 can upregulate the expression of ALDH2 *via* protein kinase C (82). 4-HNE targets and impairs the function of HSP70 and the endoplasmic reticulum homolog of HSP70, glucose-regulated protein 78 (83, 84).

CONCLUSION

We demonstrated the crucial role of ALDH2 in protecting against heat stress-induced ROS production and vascular

inflammation and preserving the viability of ECs. ALDH2 activation by Alda-1 attenuated WBH-induced ALI *in vivo*.

DATA AVAILABILITY STATEMENT

The original contributions presented in the study are included in the article/**Supplementary Material**. Further inquiries can be directed to the corresponding authors.

ETHICS STATEMENT

The animal study was reviewed and approved by Tri-Service General Hospital, National Defense Medical Center, Taipei, Taiwan.

AUTHOR CONTRIBUTIONS

S-HT and Y-JH participated in the design and planning of the study. H-YT, W-CH, and C-YL performed and analyzed experiments. J-CW wrote the article. L-AH, Y-HY, and PC prepared the figures. All authors have read, edited, and approved the manuscript.

FUNDING

This study was supported by grants from Tri-Service General Hospital, National Defense Medical Center, Taipei, Taiwan (TSGH-D-109071, TSGH-D-109125, TSGH-E-110222 and TSGH-E-110223), the Ministry of National Defense-Medical Affairs Bureau (MAB-108-018 and MAB-110-121) and the Ministry of Science and Technology (MOST 108-2314-B-016-047-MY3 and MOST 110-2314-B-016-054).

SUPPLEMENTARY MATERIAL

The Supplementary Material for this article can be found online at: https://www.frontiersin.org/articles/10.3389/fimmu.2021.740562/full#supplementary-material

Supplementary Figure 1 | The core temperature of the experimental animals. Body temperature changes in WT and ALDH2*2 KI mice subjected to WBH.

Supplementary Figure 2 | The serum levels of AST, CK, and BUN in experimental animals. ALDH2*2 KI mice and their littermates **(A)** and Alda-1-treated mice **(B)** subjected to WBH. The data are expressed as the mean ± SD. Statistical significance is indicated as $*p < 0.05$.

Supplementary Figure 3 | Alda-1 increased the ALDH2 activity but not its expression in HUVECs. **(A)** ALDH2 protein expression was measured by immunoblotting ($n = 5$). **(B)** ALDH2 activity was measured by NADH production as determined by the O.D. absorbance at 450 nm in a microplate reader ($n = 5$). The data are expressed as the mean ± SD. Statistical significance is indicated as $*p < 0.05$.

REFERENCES

1. Sankoff J. Heat Illnesses: A Hot Topic in the Setting of Global Climate Change. *Aust Fam Physician* (2015) 44(1-2):22–6.
2. Hess JJ, Saha S, Luber G. Summertime Acute Heat Illness in U.S. Emergency Departments From 2006 Through 2010: Analysis of a Nationally Representative Sample. *Environ Health Perspect* (2014) 122(11):1209–15. doi: 10.1289/ehp.1306796
3. Epstein Y, Yanovich R. Heatstroke. *N Engl J Med* (2019) 380(25):2449–59. doi: 10.1056/NEJMra1810762
4. Leon LR, Bouchama A. Heat Stroke. *Compr Physiol* (2015) 5(2):611–47. doi: 10.1002/cphy.c140017
5. Ganesan S, Volodina O, Pearce SC, Gabler NK, Baumgard LH, Rhoads RP, et al. Acute Heat Stress Activated Inflammatory Signaling in Porcine Oxidative Skeletal Muscle. *Physiol Rep* (2017) 5(16):e13397–406. doi: 10.14814/phy2.13397
6. Stallings JD, Ippolito DL, Rakesh V, Baer CE, Dennis WE, Helwig BG, et al. Patterns of Gene Expression Associated With Recovery and Injury in Heat-Stressed Rats. *BMC Genomics* (2014) 15(1):1058. doi: 10.1186/1471-2164-15-1058
7. Chauhan NR, Kapoor M, Prabha Singh L, Gupta RK, Chand Meena R, Tulsawani R, et al. Heat Stress-Induced Neuroinflammation and Aberration in Monoamine Levels in Hypothalamus Are Associated With Temperature Dysregulation. *Neuroscience* (2017) 358:79–92. doi: 10.1016/j.neuroscience.2017.06.023
8. Wang C, Fan F, Cao Q, Shen C, Zhu H, Wang P, et al. Mitochondrial Aldehyde Dehydrogenase 2 Deficiency Aggravates Energy Metabolism Disturbance and Diastolic Dysfunction in Diabetic Mice. *J Mol Med (Berl)* (2016) 94(11):1229–40. doi: 10.1007/s00109-016-1449-5
9. Zhang M, Zhu X, Tong H, Lou A, Li Y, Li Y, et al. AVE 0991 Attenuates Pyroptosis and Liver Damage After Heatstroke by Inhibiting the ROS-NLRP3 Inflammatory Signalling Pathway. *BioMed Res Int* (2019) 2019:1806234. doi: 10.1155/2019/1806234
10. Lawrence T. The Nuclear Factor NF-KappaB Pathway in Inflammation. *Cold Spring Harb Perspect Biol* (2009) 1(6):a001651. doi: 10.1101/cshperspect.a001651
11. Park S, Lim Y, Lee D, Elvira R, Lee JM, Lee MR, et al. Modulation of Protein Synthesis by Eif2alpha Phosphorylation Protects Cell From Heat Stress-Mediated Apoptosis. *Cells* (2018) 7(12):1–15. doi: 10.3390/cells7120254
12. Selkirk GA, McLellan TM, Wright HE, Rhind SG. Mild Endotoxemia, NF-kappaB Translocation, and Cytokine Increase During Exertional Heat Stress in Trained and Untrained Individuals. *Am J Physiol Regul Integr Comp Physiol* (2008) 295(2):R611–23. doi: 10.1152/ajpregu.00917.2007
13. Mundhara N, Majumder A, Panda D. Hyperthermia Induced Disruption of Mechanical Balance Leads to G1 Arrest and Senescence in Cells. *Biochem J* (2020) 478(1):179–96. doi: 10.1042/bcj20200705
14. Chen Y, Tong H, Pan Z, Jiang D, Zhang X, Qiu J, et al. Xuebijing Injection Attenuates Pulmonary Injury by Reducing Oxidative Stress and Proinflammatory Damage in Rats With Heat Stroke. *Exp Ther Med* (2017) 13(6):3408–16. doi: 10.3892/etm.2017.4444
15. Pei Y, Geng Y, Su L. Pyroptosis of HUVECs can be Induced by Heat Stroke. *Biochem Biophys Res Commun* (2018) 506(3):626–31. doi: 10.1016/j.bbrc.2018.10.051
16. Lu KC, Wang JY, Lin SH, Chu P, Lin YF. Role of Circulating Cytokines and Chemokines in Exertional Heatstroke. *Crit Care Med* (2004) 32(2):399–403. doi: 10.1097/01.ccm.0000108884.74110.d9
17. Zhou G, Chen Z, Li J, Guo X, Qin K, Luo J, et al. Role of the Receptor for Advanced Glycation End Products in Heat Stress-Induced Endothelial Hyperpermeability in Acute Lung Injury. *Front Physiol* (2020) 11:1087. doi: 10.3389/fphys.2020.01087
18. Tao Z, Cheng M, Wang SC, Lv W, Hu HQ, Li CF, et al. JAK2/STAT3 Pathway Mediating Inflammatory Responses in Heatstroke-Induced Rats. *Int J Clin Exp Pathol* (2015) 8(6):6732–9.
19. Liu Z, Chen J, Hu L, Li M, Liang M, Chen J, et al. Expression Profiles of Genes Associated With Inflammatory Responses and Oxidative Stress in Lung After

Heat Stroke. *Biosci Rep* (2020) 40(6):BSR2019048-62. doi: 10.1042/bsr20192048
20. Li L, Tan H, Zou Z, Gong J, Zhou J, Peng N, et al. Preventing Necroptosis by Scavenging ROS Production Alleviates Heat Stress-Induced Intestinal Injury. *Int J Hyperthermia* (2020) 37(1):517–30. doi: 10.1080/02656736.2020.1763483
21. Chen C-H, Ferreira JCB, Gross ER, Mochly-Rosen D. Targeting Aldehyde Dehydrogenase 2: New Therapeutic Opportunities. *Physiol Rev* (2014) 94 (1):1–34. doi: 10.1152/physrev.00017.2013
22. Zhang Y, Ren J. ALDH2 in Alcoholic Heart Diseases: Molecular Mechanism and Clinical Implications. *Pharmacol Ther* (2011) 132(1):86–95. doi: 10.1016/j.pharmthera.2011.05.008
23. Zhang Y, Babcock SA, Hu N, Maris JR, Wang H, Ren J. Mitochondrial Aldehyde Dehydrogenase (ALDH2) Protects Against Streptozotocin-Induced Diabetic Cardiomyopathy: Role of GSK3beta and Mitochondrial Function. *BMC Med* (2012) 10:40. doi: 10.1186/1741-7015-10-40
24. Panisello-Rosello A, Lopez A, Folch-Puy E, Carbonell T, Rolo A, Palmeira C, et al. Role of Aldehyde Dehydrogenase 2 in Ischemia Reperfusion Injury: An Update. *World J Gastroenterol* (2018) 24(27):2984–94. doi: 10.3748/wjg.v24.i27.2984
25. Hao P-P, Chen Y-G, Wang J-L, Wang XL, Zhang Y. Meta-Analysis of Aldehyde Dehydrogenase 2 Gene Polymorphism and Alzheimer's Disease in East Asians. *Can J Neurol Sci Le J Canadien Des Sci Neurologiques* (2011) 38 (3):500–6. doi: 10.1017/s0317167100011938
26. Schneider C, Porter NA, Brash AR. Routes to 4-Hydroxynonenal: Fundamental Issues in the Mechanisms of Lipid Peroxidation. *J Biol Chem* (2008) 283(23):15539–43. doi: 10.1074/jbc.R800001200
27. Mali VR, Palaniyandi SS. Regulation and Therapeutic Strategies of 4-Hydroxy-2-Nonenal Metabolism in Heart Disease. *Free Radical Res* (2014) 48(3):251–63. doi: 10.3109/10715762.2013.864761
28. Choi H, Tostes RC, Webb RC. Mitochondrial Aldehyde Dehydrogenase Prevents ROS-Induced Vascular Contraction in Angiotensin-II Hypertensive Mice. *J Am Soc Hypertens* (2011) 5(3):154–60. doi: 10.1016/j.jash.2011.02.005
29. Perez-Miller S, Younus H, Vanam R, Chen CH, Mochly-Rosen D, Hurley TD. Alda-1 Is an Agonist and Chemical Chaperone for the Common Human Aldehyde Dehydrogenase 2 Variant. *Nat Struct Mol Biol* (2010) 17(2):159–64. doi: 10.1038/nsmb.1737
30. Xu T, Liu S, Ma T, Jia Z, Zhang Z, Wang A. Aldehyde Dehydrogenase 2 Protects Against Oxidative Stress Associated With Pulmonary Arterial Hypertension. *Redox Biol* (2017) 11:286–96. doi: 10.1016/j.redox.2016.12.019
31. Stachowicz A, Olszanecki R, Suski M, Wisniewska A, Toton-Zuranska J, Madej J, et al. Mitochondrial Aldehyde Dehydrogenase Activation by Alda-1 Inhibits Atherosclerosis and Attenuates Hepatic Steatosis in Apolipoprotein E-Knockout Mice. *J Am Heart Assoc* (2014) 3(6):e001329. doi: 10.1161/jaha.114.001329
32. Zhu Q, He G, Wang J, Wang Y, Chen W. Pretreatment With the ALDH2 Agonist Alda-1 Reduces Intestinal Injury Induced by Ischaemia and Reperfusion in Mice. *Clin Sci (Lond)* (2017) 131(11):1123–36. doi: 10.1042/cs20170074
33. Wimborne HJ, Takemoto K, Woster PM, Rockey DC, Lemasters JJ, Zhong Z. Aldehyde Dehydrogenase-2 Activation by Alda-1 Decreases Necrosis and Fibrosis After Bile Duct Ligation in Mice. *Free Radic Biol Med* (2019) 145:136–45. doi: 10.1016/j.freeradbiomed.2019.09.026
34. Tsai SH, Hsu LA, Tsai HY, Yeh YH, Lu CY, Chen PC, et al. Aldehyde Dehydrogenase 2 Protects Against Abdominal Aortic Aneurysm Formation by Reducing Reactive Oxygen Species, Vascular Inflammation, and Apoptosis of Vascular Smooth Muscle Cells. *FASEB J* (2020) 34(7):9498–511. doi: 10.1096/fj.201902550RRR
35. Sidramagowda Patil S, Hernández-Cuervo H, Fukumoto J, Krishnamurthy S, Lin M, Alleyn M, et al. Alda-1 Attenuates Hyperoxia-Induced Acute Lung Injury in Mice. *Front Pharmacol* (2020) 11:597942. doi: 10.3389/fphar.2020.597942
36. Lu Q, Mundy M, Chambers E, Lange T, Newton J, Borgas D, et al. Alda-1 Protects Against Acrolein-Induced Acute Lung Injury and Endothelial Barrier Dysfunction. *Am J Respir Cell Mol Biol* (2017) 57(6):662–73. doi: 10.1165/rcmb.2016-0342OC
37. Patil SS, Hernández-Cuervo H, Fukumoto J, Narala VR, Saji S, Borra M, et al. Alda-1 Attenuates Hyperoxia-Induced Mitochondrial Dysfunction in Lung Vascular Endothelial Cells. *Aging (Albany NY)* (2019) 11(12):3909–18. doi: 10.18632/aging.102012
38. Huang J, Li L, Yuan W, Zheng L, Guo Z, Huang W. NEMO-Binding Domain Peptide Attenuates Lipopolysaccharide-Induced Acute Lung Injury by Inhibiting the NF-κb Signaling Pathway. *Mediators Inflamm* (2016) 2016:7349603. doi: 10.1155/2016/7349603
39. Chen C-H, Budas GR, Churchill EN, Disatnik M-H, Hurley TD, Mochly-Rosen D. Activation of Aldehyde Dehydrogenase-2 Reduces Ischemic Damage to the Heart. *Sci (New York NY)* (2008) 321(5895):1493–5. doi: 10.1126/science.1158554
40. Lin CY, Hsu CC, Lin MT, Chen SH. Flutamide, an Androgen Receptor Antagonist, Improves Heatstroke Outcomes in Mice. *Eur J Pharmacol* (2012) 688(1-3):62–7. doi: 10.1016/j.ejphar.2012.05.002
41. Sun L, Ferreira JC, Mochly-Rosen D. ALDH2 Activator Inhibits Increased Myocardial Infarction Injury by Nitroglycerin Tolerance. *Sci Transl Med* (2011) 3(107):107ra11. doi: 10.1126/scitranslmed.3002067
42. Pan G, Roy B, Palaniyandi SS. Diabetic Aldehyde Dehydrogenase 2 Mutant (ALDH2*2) Mice Are More Susceptible to Cardiac Ischemic-Reperfusion Injury Due to 4-Hydroxy-2-Nonenal Induced Coronary Endothelial Cell Damage. *J Am Heart Assoc* (2021) 10(18):e021140. doi: 10.1161/jaha.121.021140
43. National Research Council Committee for the Update of the Guide for the C, Use of Laboratory A. The National Academies Collection: Reports Funded by National Institutes of Health. In: *Guide for the Care and Use of Laboratory Animals*. Washington (DC: National Academies Press (US) Copyright © 2011, National Academy of Sciences (2011).
44. Tang SE, Wu CP, Wu SY, Peng CK, Perng WC, Kang BH, et al. Stanniocalcin-1 Ameliorates Lipopolysaccharide-Induced Pulmonary Oxidative Stress, Inflammation, and Apoptosis in Mice. *Free Radic Biol Med* (2014) 71:321–31. doi: 10.1016/j.freeradbiomed.2014.03.034
45. Lin HJ, Wu CP, Peng CK, Lin SH, Uchida S, Yang SS, et al. With-No-Lysine Kinase 4 Mediates Alveolar Fluid Regulation in Hyperoxia-Induced Lung Injury. *Crit Care Med* (2015) 43(10):e412–9. doi: 10.1097/ccm.0000000000001144
46. Chou SH, Lan J, Esposito E, Ning M, Balaj L, Ji X, et al. Extracellular Mitochondria in Cerebrospinal Fluid and Neurological Recovery After Subarachnoid Hemorrhage. *Stroke* (2017) 48(8):2231–7. doi: 10.1161/strokeaha.117.017758
47. Gu ZT, Wang H, Li L, Liu YS, Deng XB, Huo SF, et al. Heat Stress Induces Apoptosis Through Transcription-Independent P53-Mediated Mitochondrial Pathways in Human Umbilical Vein Endothelial Cell. *Sci Rep* (2014) 4:4469. doi: 10.1038/srep04469
48. Zhang R, Liu B, Fan X, Wang W, Xu T, Wei S, et al. Aldehyde Dehydrogenase 2 Protects Against Post-Cardiac Arrest Myocardial Dysfunction Through a Novel Mechanism of Suppressing Mitochondrial Reactive Oxygen Species Production. *Front Pharmacol* (2020) 11:373. doi: 10.3389/fphar.2020.00373
49. Echizen K, Horiuchi K, Aoki Y, Yamada Y, Minamoto T, Oshima H, et al. NF-κb-Induced NOX1 Activation Promotes Gastric Tumorigenesis Through the Expansion of SOX2-Positive Epithelial Cells. *Oncogene* (2019) 38(22):4250–63. doi: 10.1038/s41388-019-0702-0
50. Tsai SH, Wang JC, Liao WI, Hsu YJ, Lin CY, Liao MT, et al. Fucoidan Attenuates Angiotensin II-Induced Abdominal Aortic Aneurysms Through the Inhibition of C-Jun N-Terminal Kinase and Nuclear Factor κb Activation. *J Vasc Surg* (2018) 68(6s):72S–81S.e1. doi: 10.1016/j.jvs.2017.09.042
51. Yun MR, Park HM, Seo KW, Lee SJ, Im DS, Kim CD. 5-Lipoxygenase Plays an Essential Role in 4-HNE-Enhanced ROS Production in Murine Macrophages *via* Activation of NADPH Oxidase. *Free Radic Res* (2010) 44(7):742–50. doi: 10.3109/10715761003758122
52. Lee SJ, Kim CE, Seo KW, Kim CD. HNE-Induced 5-LO Expression Is Regulated by NF-{Kappa}B/ERK and Sp1/p38 MAPK Pathways *via* EGF Receptor in Murine Macrophages. *Cardiovasc Res* (2010) 88(2):352–9. doi: 10.1093/cvr/cvq194
53. Seo KW, Lee SJ, Kim CE, Yun MR, Park HM, Yun JW, et al. Participation of 5-Lipoxygenase-Derived LTB(4) in 4-Hydroxynonenal-Enhanced MMP-2 Production in Vascular Smooth Muscle Cells. *Atherosclerosis* (2010) 208 (1):56–61. doi: 10.1016/j.atherosclerosis.2009.06.012
54. Yun MR, Im DS, Lee SJ, Park HM, Bae SS, Lee WS, et al. 4-Hydroxynonenal Enhances CD36 Expression on Murine Macrophages *via* P38 MAPK-

Mediated Activation of 5-Lipoxygenase. *Free Radic Biol Med* (2009) 46 (5):692–8. doi: 10.1016/j.freeradbiomed.2008.12.013
55. Wenzel P, Mollnau H, Oelze M, Schulz E, Wickramanayake JM, Müller J, et al. First Evidence for a Crosstalk Between Mitochondrial and NADPH Oxidase-Derived Reactive Oxygen Species in Nitroglycerin-Triggered Vascular Dysfunction. *Antioxid Redox Signal* (2008) 10(8):1435–47. doi: 10.1089/ars.2007.1969
56. Ho CC, Chen YC, Tsai MH, Tsai HT, Weng CY, Yet SF, et al. Ambient Particulate Matter Induces Vascular Smooth Muscle Cell Phenotypic Changes *via* NOX1/ROS/NF-κb Dependent and Independent Pathways: Protective Effects of Polyphenols. *Antioxid (Basel)* (2021) 10(5):742–50. doi: 10.3390/antiox10050782
57. Choi H, Dikalova A, Stark RJ, Lamb FS. C-Jun N-Terminal Kinase Attenuates Tnfα Signaling by Reducing Nox1-Dependent Endosomal ROS Production in Vascular Smooth Muscle Cells. *Free Radic Biol Med* (2015) 86:219–27. doi: 10.1016/j.freeradbiomed.2015.05.015
58. Song W, Wei L, Du Y, Wang Y, Jiang S. Protective Effect of Ginsenoside Metabolite Compound K Against Diabetic Nephropathy by Inhibiting NLRP3 Inflammasome Activation and NF-κb/P38 Signaling Pathway in High-Fat Diet/Streptozotocin-Induced Diabetic Mice. *Int Immunopharmacol* (2018) 63:227–38. doi: 10.1016/j.intimp.2018.07.027
59. Masselli E, Pozzi G, Vaccarezza M, Mirandola P, Galli D, Vitale M, et al. ROS in Platelet Biology: Functional Aspects and Methodological Insights. *Int J Mol Sci* (2020) 21(14):692–8. doi: 10.3390/ijms21144866
60. Habashy WS, Milfort MC, Rekaya R, Aggrey SE. Expression of Genes That Encode Cellular Oxidant/Antioxidant Systems Are Affected by Heat Stress. *Mol Biol Rep* (2018) 45(3):389–94. doi: 10.1007/s11033-018-4173-0
61. Geng Y, Li R, He SX, Yang HH, Deng QT, Shao XY, et al. Dexmedetomidine Attenuates Acute Lung Injury Induced by Heatstroke and Improve Outcome. *Shock* (2018) 10(5):782–803. doi: 10.1097/shk.0000000000001289
62. Gross ER, Zambelli VO, Small BA, Ferreira JC, Chen CH, Mochly-Rosen D. A Personalized Medicine Approach for Asian Americans With the Aldehyde Dehydrogenase 2*2 Variant. *Annu Rev Pharmacol Toxicol* (2015) 55:107–27. doi: 10.1146/annurev-pharmtox-010814-124915
63. Zhong H, Yin H. Role of Lipid Peroxidation Derived 4-Hydroxynonenal (4-HNE) in Cancer: Focusing on Mitochondria. *Redox Biol* (2015) 4:193–9. doi: 10.1016/j.redox.2014.12.011
64. Chen C-H, Sun L, Mochly-Rosen D. Mitochondrial Aldehyde Dehydrogenase and Cardiac Diseases. *Cardiovasc Res* (2010) 88(1):51–7. doi: 10.1093/cvr/cvq192
65. Zhong S, Li L, Zhang Y-L, Zhang L, Lu J, Guo S, et al. Acetaldehyde Dehydrogenase 2 Interactions With LDLR and AMPK Regulate Foam Cell Formation. *J Clin Invest* (2018) 129(1):389–94. doi: 10.1172/JCI122064
66. Guo YJ, Chen L, Bai YP, Li L, Sun J, Zhang GG, et al. The ALDH2 Glu504Lys Polymorphism Is Associated With Coronary Artery Disease in Han Chinese: Relation With Endothelial ADMA Levels. *Atherosclerosis* (2010) 211(2):545–50. doi: 10.1016/j.atherosclerosis.2010.03.030
67. Gong D, Zhang L, Zhang Y, Wang F, Zhou X, Sun H. East Asian Variant of Aldehyde Dehydrogenase 2 Is Related to Worse Cardioprotective Results After Coronary Artery Bypass Grafting. *Interact Cardiovasc Thorac Surg* (2019) 28(1):79–84. doi: 10.1093/icvts/ivy204
68. Kim J, Chen CH, Yang J, Mochly-Rosen D. Aldehyde Dehydrogenase 2*2 Knock-in Mice Show Increased Reactive Oxygen Species Production in Response to Cisplatin Treatment. *J BioMed Sci* (2017) 24(1):33. doi: 10.1186/s12929-017-0338-8
69. Kwon HJ, Won YS, Park O, Chang B, Duryee MJ, Thiele GE, et al. Aldehyde Dehydrogenase 2 Deficiency Ameliorates Alcoholic Fatty Liver But Worsens Liver Inflammation and Fibrosis in Mice. *Hepatology* (2014) 60(1):146–57. doi: 10.1002/hep.27036
70. Pan C, Xing JH, Zhang C, Zhang YM, Zhang LT, Wei SJ, et al. Aldehyde Dehydrogenase 2 Inhibits Inflammatory Response and Regulates Atherosclerotic Plaque. *Oncotarget* (2016) 7(24):35562–76. doi: 10.18632/oncotarget.9384
71. Zhang P, Xu D, Wang S, Fu H, Wang K, Zou Y, et al. Inhibition of Aldehyde Dehydrogenase 2 Activity Enhances Antimycin-Induced Rat Cardiomyocytes Apoptosis Through Activation of MAPK Signaling Pathway. *BioMed Pharmacother* (2011) 65(8):590–3. doi: 10.1016/j.biopha.2009.12.001
72. Chen HW, Kuo HT, Hwang LC, Kuo MF, Yang RC. Proteomic Alteration of Mitochondrial Aldehyde Dehydrogenase 2 in Sepsis Regulated by Heat Shock Response. *Shock* (2007) 28(6):710–6. doi: 10.1097/shk.0b013e318050c8c2
73. Hu XY, Fang Q, Ma D, Jiang L, Yang Y, Sun J, et al. Aldehyde Dehydrogenase 2 Protects Human Umbilical Vein Endothelial Cells Against Oxidative Damage and Increases Endothelial Nitric Oxide Production to Reverse Nitroglycerin Tolerance. *Genet Mol Res* (2016) 15(2):gmr7822. doi: 10.4238/gmr.15027822
74. Li SY, Gomelsky M, Duan J, Zhang Z, Gomelsky L, Zhang X, et al. Overexpression of Aldehyde Dehydrogenase-2 (ALDH2) Transgene Prevents Acetaldehyde-Induced Cell Injury in Human Umbilical Vein Endothelial Cells: Role of ERK and P38 Mitogen-Activated Protein Kinase. *J Biol Chem* (2004) 279(12):11244–52. doi: 10.1074/jbc.M308011200
75. Zhong Z, Ye S, Xiong Y, Wu L, Zhang M, Fan X, et al. Decreased Expression of Mitochondrial Aldehyde Dehydrogenase-2 Induces Liver Injury *via* Activation of the Mitogen-Activated Protein Kinase Pathway. *Transpl Int* (2016) 29(1):98–107. doi: 10.1111/tri.12675
76. Xiao Q, Weiner H, Crabb DW. The Mutation in the Mitochondrial Aldehyde Dehydrogenase (ALDH2) Gene Responsible for Alcohol-Induced Flushing Increases Turnover of the Enzyme Tetramers in a Dominant Fashion. *J Clin Invest* (1996) 98(9):2027–32. doi: 10.1172/JCI119007
77. Jin S, Chen J, Chen L, Histen G, Lin Z, Gross S, et al. ALDH2(E487K) Mutation Increases Protein Turnover and Promotes Murine Hepato carcinogenesis. *Proc Natl Acad Sci USA* (2015) 112(29):9088–93. doi: 10.1073/pnas.1510757112
78. Kang P, Wang J, Fang D, Fang T, Yu Y, Zhang W, et al. Activation of ALDH2 Attenuates High Glucose Induced Rat Cardiomyocyte Fibrosis and Necroptosis. *Free Radic Biol Med* (2020) 146:198–210. doi: 10.1016/j.freeradbiomed.2019.10.416
79. Xu Y, Yuan Q, Cao S, Cui S, Xue L, Song X, et al. Aldehyde Dehydrogenase 2 Inhibited Oxidized LDL-Induced NLRP3 Inflammasome Priming and Activation *via* Attenuating Oxidative Stress. *Biochem Biophys Res Commun* (2020) 529(4):998–1004. doi: 10.1016/j.bbrc.2020.06.075
80. Liu M, Lu S, He W, Zhang L, Ma Y, Lv P, et al. ULK1-Regulated Autophagy: A Mechanism in Cellular Protection for ALDH2 Against Hyperglycemia. *Toxicol Lett* (2018) 283:106–15. doi: 10.1016/j.toxlet.2017.11.008
81. Comellas AP, Briva A, Dada LA, Butti ML, Trejo HE, Yshii C, et al. Endothelin-1 Impairs Alveolar Epithelial Function *via* Endothelial ETB Receptor. *Am J Respir Crit Care Med* (2009) 179(2):113–22. doi: 10.1164/rccm.200804-540OC
82. Ji E, Jiao T, Shen Y, Xu Y, Sun Y, Cai Z, et al. Molecular Mechanism of HSF1-Upregulated ALDH2 by PKC in Ameliorating Pressure Overload-Induced Heart Failure in Mice. *BioMed Res Int* (2020) 2020:3481623. doi: 10.1155/2020/3481623
83. Yang LL, Chen H, Wang J, Xia T, Sun H, Yuan CH, et al. 4-HNE Induces Apoptosis of Human Retinal Pigment Epithelial Cells by Modifying Hsp70. *Curr Med Sci* (2019) 39(3):442–8. doi: 10.1007/s11596-019-2057-8
84. Galligan JJ, Fritz KS, Backos DS, Shearn CT, Smathers RL, Jiang H, et al. Oxidative Stress-Mediated Aldehyde Adduction of GRP78 in a Mouse Model of Alcoholic Liver Disease: Functional Independence of ATPase Activity and Chaperone Function. *Free Radic Biol Med* (2014) 73:411–20. doi: 10.1016/j.freeradbiomed.2014.06.002

Conflict of Interest: The authors declare that the research was conducted in the absence of any commercial or financial relationships that could be construed as a potential conflict of interest.

Publisher's Note: All claims expressed in this article are solely those of the authors and do not necessarily represent those of their affiliated organizations, or those of the publisher, the editors and the reviewers. Any product that may be evaluated in this article, or claim that may be made by its manufacturer, is not guaranteed or endorsed by the publisher.

Copyright © 2021 Tsai, Hsu, Lu, Tsai, Hung, Chen, Wang, Hsu, Yeh, Chu and Tsai. This is an open-access article distributed under the terms of the Creative Commons Attribution License (CC BY). The use, distribution or reproduction in other forums is permitted, provided the original author(s) and the copyright owner(s) are credited and that the original publication in this journal is cited, in accordance with accepted academic practice. No use, distribution or reproduction is permitted which does not comply with these terms.

frontiers in Immunology

REVIEW
published: 16 November 2021
doi: 10.3389/fimmu.2021.768133

Regulation of T-Cell Immune Responses by Pro-Resolving Lipid Mediators

Javier Perez-Hernandez[1,2†], *Valerio Chiurchiù*[3,4†], *Sylvain Perruche*[5,6] *and Sylvaine You*[1*]

[1] Université de Paris, Institut Cochin, CNRS, Institut National de la Santé et de le Recherche Médicale (INSERM), Paris, France, [2] Departament of Nutrition and Health, Valencian International University (VIU), Valencia, Spain, [3] Institute of Translational Pharmacology, National Research Council, Rome, Italy, [4] Laboratory of Resolution of Neuroinflammation, European Center for Brain Research, Istituto di Ricovero e Cura a Carattere Scientifico (IRCCS) Santa Lucia Foundation, Rome, Italy, [5] Université de Bourgogne Franche-Comté, INSERM, Etablissement Français du Sang (EFS) Bourgogne-Franche Comté (BFC), Unité Mixte de Recherche (UMR)1098 Research on Interaction between Graft, Host and Tumor (RIGHT), Interactions Hôte Greffon-Tumeur/Ingénierie Cellulaire et Génique, Fédération Hospitalo-Universitaire Integrated Center for REsearch in inflammatory diseASes (InCREASe), Besançon, France, [6] MED'INN'Pharma, Besançon, France

Both the initiation and the resolution of inflammatory responses are governed by the sequential activation, migration, and control/suppression of immune cells at the site of injury. Bioactive lipids play a major role in the fine-tuning of this dynamic process in a timely manner. During inflammation and its resolution, polymorphonuclear cells (PMNs) and macrophages switch from producing pro-inflammatory prostaglandins and leukotrienes to specialized pro-resolving lipid mediators (SPMs), namely, lipoxins, resolvins, protectins, and maresins, which are operative at the local level to limit further inflammation and tissue injury and restore homeostasis. Accumulating evidences expand now the role and actions of these lipid mediators from innate to adaptive immunity. In particular, SPMs have been shown to contribute to the control of chronic inflammation, and alterations in their production and/or function have been associated with the persistence of several pathological conditions, including autoimmunity, in human and experimental models. In this review, we focus on the impact of pro-resolving lipids on T cells through their ability to modulate T-cell responses. In particular, the effects of the different families of SPMs to restrain effector T-cell functions while promoting regulatory T cells will be reviewed, along with the underlying mechanisms. Furthermore, the emerging concept of SPMs as new biological markers for disease diagnostic and progression and as putative therapeutic tools to regulate the development and magnitude of inflammatory and autoimmune diseases is discussed.

Keywords: resolution, adaptive immunity, autoimmunity, T cell, therapy, specialized pro-resolving lipid mediators (SPMs), chronic inflammation

OPEN ACCESS

Edited by:
Heiko Mühl,
Goethe University Frankfurt, Germany

Reviewed by:
Antonio Recchiuti,
University of Studies G. d'Annunzio Chieti and Pescara, Italy
Alpdogan Kantarci,
The Forsyth Institute, United States

***Correspondence:**
Sylvaine You
sylvaine.you@inserm.fr

[†]*These authors have contributed equally to this work*

Specialty section:
This article was submitted to Inflammation, a section of the journal Frontiers in Immunology

Received: *31 August 2021*
Accepted: *26 October 2021*
Published: *16 November 2021*

Citation:
Perez-Hernandez J, Chiurchiù V, Perruche S and You S (2021) Regulation of T-Cell Immune Responses by Pro-Resolving Lipid Mediators. Front. Immunol. 12:768133. doi: 10.3389/fimmu.2021.768133

INTRODUCTION

The natural resolution of inflammation is a tightly controlled dynamic process that engages several molecular and cellular mediators to prevent excessive and/or chronic immune responses and tissue damage that may compromise organ function. Indeed, a dysregulation of this process has been incriminated in many inflammatory disorders (1–5). While the mechanisms regulating the onset of

inflammation have been well characterized for almost a century and are mainly carried out by innate immune cells, which release pro-inflammatory lipids (i.e., eicosanoids: prostaglandins, leukotrienes, and thromboxanes) and cytokines/chemokines, the first endogenous mechanisms that terminate the inflammatory response have been identified exactly 20 years ago and now comprise over 25 lipid mediators derived from polyunsaturated fatty acids (PUFAs) and collectively termed specialized pro-resolving mediators (SPMs). The biosynthesis of all SPMs identified to date is initiated by the enzymatic addition of oxygen to four dietary PUFAs, namely, ω-6 arachidonic acid (AA), ω-3 eicosapentaenoic acid (EPA), ω-3 docosahexaenoic acid (DHA), and ω-3 docosapentaenoic acid (DPA), by means of the stereoselective and concerted action of the very same enzymes used for eicosanoid production, namely, the lipoxygenase (LOX) isozymes, the cyclooxygenase-2 (COX-2), and, to a minor extent, the cytochrome P450 (6).

SPMs include distinct families of bioactive lipids: AA-derived lipoxins (LXA_4 and LXB_4), EPA-derived E-series resolvins (RvE1-RvE4), DHA-derived D-series resolvins (RvD1-RvD6), protectins (PD1 and PDX), and maresins (MaR1-MaR2), together with their respective sulfide-conjugates in tissue regeneration (RCTR1-3, PCTR1-3, and MCTR1-3), DPA-derived 13-series resolvins (RvT1-RvT4), and $RvD_{n\text{-}3DPA}$ (**Figure 1**). These lipid mediators, identified between 2001 and 2021 in the laboratory of Prof. Serhan in many tissues during acute inflammation (inflammatory exudates, plasma, brain, lymph nodes, etc.), are mostly produced locally by professional phagocytes [tissue-resident macrophages, recruited monocytes, immature dendritic cells (DCs)] and also by vascular endothelial cells and fibroblasts, to some extent. They act as "immunoresolvents," i.e., immune-pharmacological agents of resolution (distinct from immunosuppressive agents), and induce (i) cessation of leukocyte infiltration and stimulation of nonphlogistic recruitment of mononuclear cells, (ii) macrophage-mediated phagocytosis of apoptotic polymorphonuclear cells (efferocytosis) and cellular debris, (iii) killing and clearance of pathogens, (iv) production of anti-inflammatory mediators while inhibiting secretion of pro-inflammatory cytokines and reactive oxygen species, (v) shortening time of resolution and activation of endogenous resolution programs, and (vi) promotion of tissue regeneration and healing (5–7).

SPMs trigger their pro-resolving signals *via* specific transmembrane G protein-coupled receptors (GPCRs) that display a variable level of redundancy and include FPR2 (or ALX), GPR32 (or DRV1), GPR18 (or DRV2), ChemR23 (or ERV), BLT1 (or LTB4R/GPR16), LGR6, GPR37, RORα, and GPR101 (8, 9). Of note, each SPM can act by activating different receptors, and each receptor is often engaged by several SPMs, which can also compete with pro-inflammatory lipids for binding. For instance, leukotriene B4 (LTB4) and RvE1/E2 are both ligands for BLT1 but exert opposite effects by respectively acting as an agonist (i.e., favoring neutrophil survival) or an antagonist (promoting neutrophils apoptosis) (10, 11).

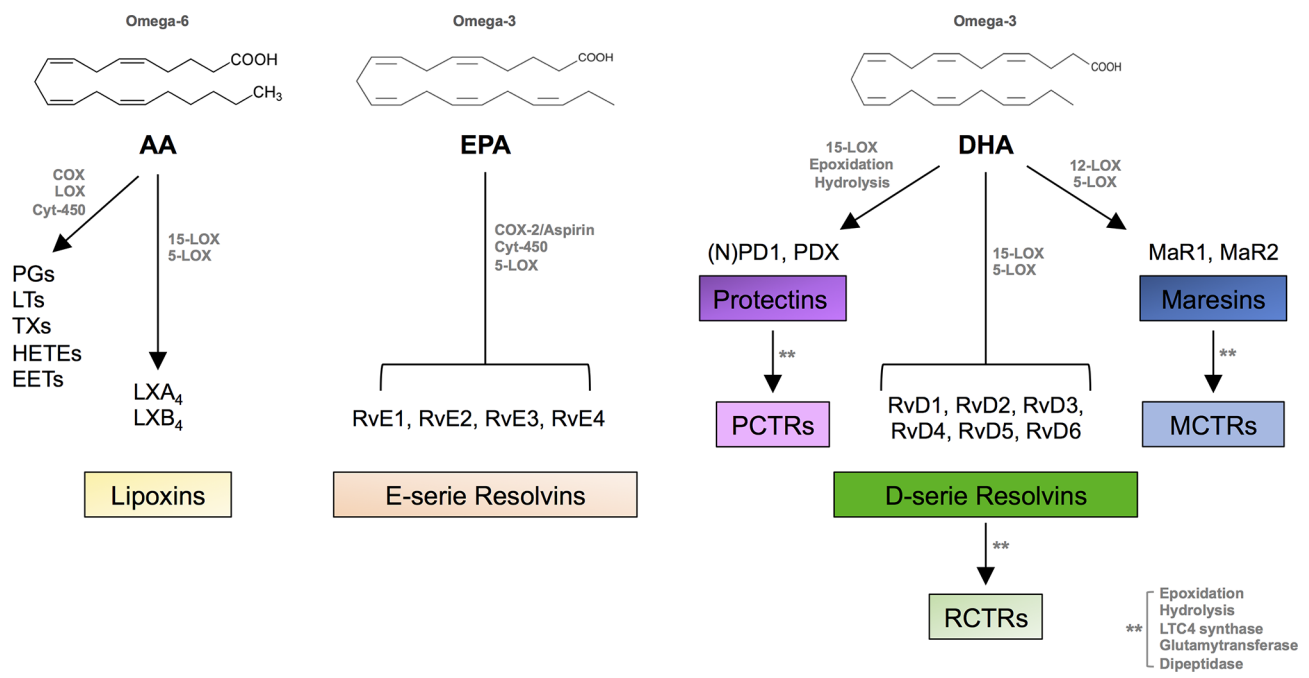

FIGURE 1 | SPM biosynthesis. Chemical structures of AA, EPA, and DHA and outline of the individual families of the main pro-inflammatory eicosanoids and SPMs biosynthesized from these PUFAs. AA, arachidonic acid; COX, cyclooxygenase; LOX, lipoxygenase; Cyt, cytochrome; PGs, prostaglandins; LTs, leukotrienes; TXs, thromboxanes; EETs, epoxy eicosatrienoic acids; HETEs, hydroxy eicosatetraenoic acids; Rv, resolvin; PD, protectin; MaR, maresin; PCTR, protectin conjugates in tissue regeneration; RCTR, resolvin conjugates in tissue regeneration; MCTR, maresin conjugates in tissue regeneration.

The role of SPMs has been extensively explored in the context of inflammation-resolution operated by innate immune cells (mainly neutrophils and monocytes/macrophages) to resolve acute inflammatory diseases and infections (12, 13). However, accumulating evidence now pleads for an additional direct action of SPMs on the adaptive immune system and highlights their capacity to prevent the transition into chronic inflammation (5, 14, 15). Indeed, T lymphocytes express SPM receptors and are sensitive to omega-3- and omega-6-derived bioactive lipids, which, in the local microenvironment, can exert pro- or anti-inflammatory actions and thus influence T-cell fate and functions. More generally, it becomes increasingly clear that the mechanisms controlling T-cell responses and resolution of inflammation are tightly linked.

In this review, we will present in both human and mouse the evidence highlighting the role of SPMs, in comparison to their pro-inflammatory lipid counterparts, in the regulation of T-cell responses and T-cell-mediated immunity and autoimmunity. We will also discuss their putative usage as biomarkers of disease development or progression as well as therapeutic agents to restore tissue and immune homeostasis through their direct and/or indirect targeting of T cells.

PRO-INFLAMMATORY LIPID MEDIATORS AND T CELLS

The first evidence for a role and action of bioactive lipids on T cells has been documented in the early 2000s by studies uncovering the capacity of pro-inflammatory leukotrienes (LTs), especially of LTB4, to mediate effector T-cell (Teff) recruitment to inflammatory sites. Indeed, activated $CD4^+$ and $CD8^+$ Teff express the LTB4 high affinity receptor BLT1 but not naïve T cells (16, 17). LTB4 chemoattractant property was demonstrated in experimental models of peritonitis (16), asthma (18), transplantation (19), airway hyperresponsiveness (20, 21), and oxazolone (OXA)-induced contact dermatitis (22). T-cell trafficking into peripheral tissues was impaired in BTL1-deficient mice or in mice treated with a BLT1 antagonist, leading to the reduction of inflammation, graft rejection (19), and airway responsiveness (21). Adoptive transfer models using $BLT1^{+/+}$ versus $BLT1^{-/-}$ $CD8^+$ T cells further strengthened the key role of the LTB4-BLT1 pathway in the migration of Teff to inflamed tissues or tumoral niches and the development of immune responses (16, 20, 21, 23). *In vitro* studies on mouse and human T cells confirmed the capacity of LTB4 to promote effector function by increasing Th1 (IFN-γ), Th2 (IL-4), and Th17 (IL-17) cell migration and responses while decreasing $Foxp3^+$ regulatory T cells (Tregs) in polarization assays (17, 24, 25). LTB4 was also shown to induce the differentiation of T follicular helper (Tfh) cells from naïve T cells, which activate naïve B cells to form germinal centers (26).

Prostaglandins (PGs) also affect T-cell responses through binding to the E-prostanoid receptors (EP)1-4 (27). Notably, PGE2 boosts and expands Th1 and Th17 cells, which express EP2 and EP4, while inhibiting Th2 cells (28). T cells deficient for EP4 are insensitive to PGE2 and downregulate IL-12 and IFN-γ receptor expression, reducing their *in vivo* pathogenicity (28). Similarly, administration of EP antagonists impaired the development of experimental arthritis, psoriasis, and multiple sclerosis through the inhibition of Th1 and Th17 responses (29–31). These pro-inflammatory effects are in line with the capacity of PGE2 to dampen the differentiation of type 1 regulatory T cells (Tr1) (32) and $Foxp3^+$ Tregs (33), although some contradictory results were reported (34). Overall, both LTs and PGs, being central in the perpetuation of inflammatory signals that are at the basis of the transition from acute to chronic inflammation, act as "cytokine amplifiers" by stimulating almost all Teff subsets (**Figure 2**).

IMMUNOMODULATORY ROLE OF SPMs ON PATHOGENIC T CELLS

T-cell activation and differentiation into T helper (i.e., Th1, Th2, Th17, Th22 cells) or cytotoxic subsets is instrumental to fight pathogens. They must, however, be controlled and limited in space and time to avoid T-cell hyperactivation, a hallmark of chronic inflammation and autoimmunity. Accordingly, an increasing number of recent studies in mice and humans now document the capacity of several families of SPMs to inhibit pathogenic T cells (**Figure 2**), thereby contributing to the resolution of inflammation.

Initial studies on the effect of SPMs on T cells came from lipoxins, whereby LXA4 and LXB4 inhibited ERK-dependent TNF-α secretion from peripheral T cells stimulated with anti-CD3 antibody (35). These effects were mediated by the LXA4 receptor FPR2/ALX, expressed at a higher level on activated $CD25^+$ and memory $CD45RO^+CD4^+$ T cells, with respect to their $CD25^-$ and naïve $CD45RA^+CD4^+$ counterparts (35, 36). Accordingly, treatment with LXA4 inhibited Th1 and Th17 activation, as observed *in vivo* in the cervical draining lymph nodes of mice with dry eye disease (37), and *in vitro* using peripheral blood from healthy donors (38). LXA4 was also reported to differentiate naïve $CD4^+$ T cells from tonsils and peripheral blood into Tfh cells in an FPR2-dependent manner (26).

The evidence that the other SPM families were capable of modulating T-cell responses was first unveiled through indirect studies showing reduced T-cell migration into target organs and decreased production of inflammatory cytokines after SPM *in vivo* administration in various experimental models of inflammation (detailed in the last section and **Table 1**). The capacity of SPMs to directly impact T-cell response was demonstrated by Chiurchiù and colleagues, who extended these observations to RvD1, RvD2, MaR1, and aspirin-triggered RvD3. Indeed, these SPMs were able to reduce the pro-inflammatory activity of both human $CD4^+$ and $CD8^+$ T cells upon stimulation of their T-cell receptor, to inhibit cytokine production by circulating Th1 and Th17 cells, and to prevent Th1 and Th17 commitment of naïve $CD4^+$ T cells, without, however, impacting T-cell viability and proliferative capacity (52). These findings

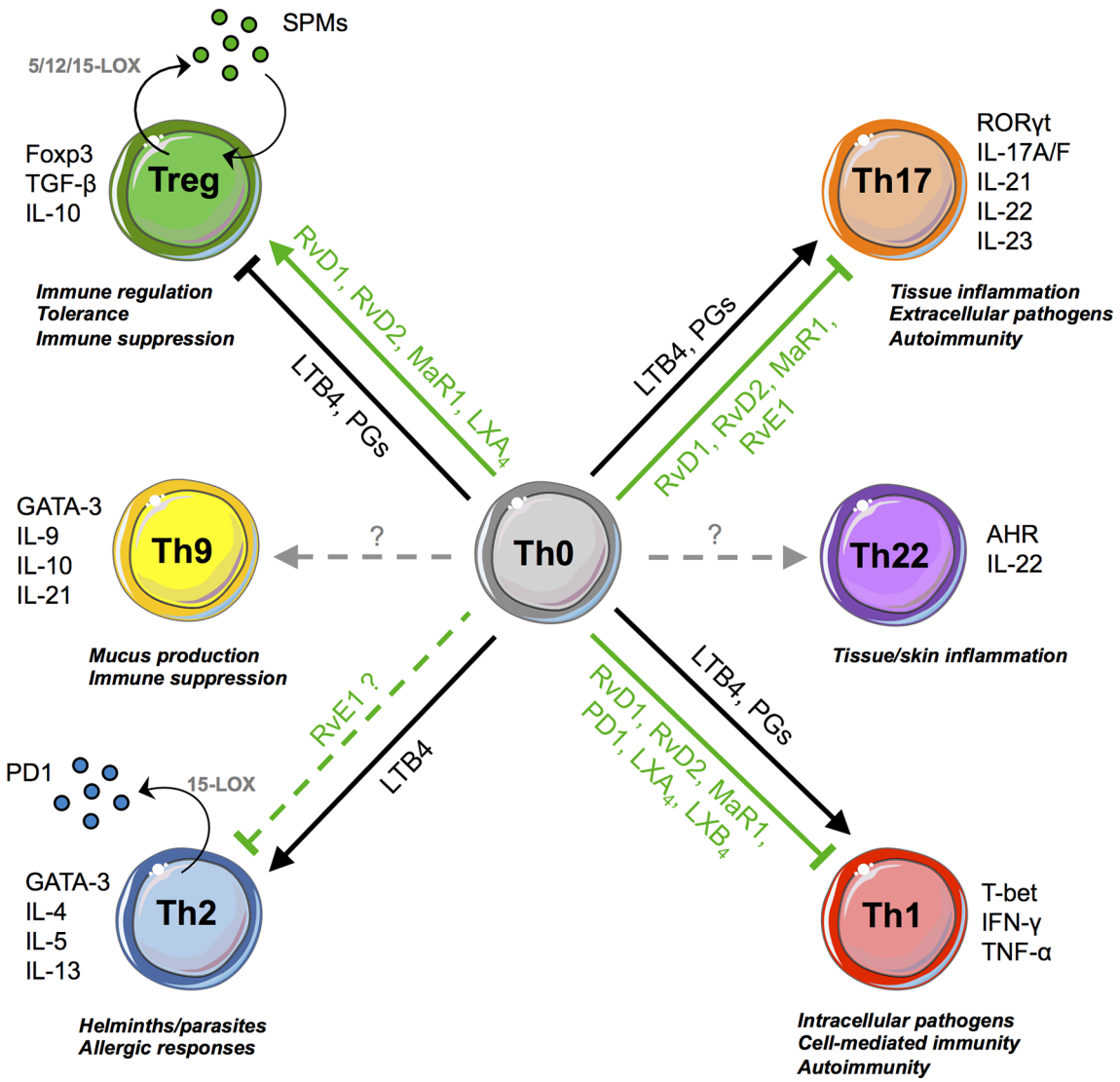

FIGURE 2 | SPMs and T-cell responses. SPMs and pro-inflammatory lipids promote or inhibit, in opposite ways, T-cell differentiation (from Th0 precursors to Tregs, Th1, Th2, Th17). Th2 and Treg cells are also able to biosynthesize few SPMs, such as 17R-RvD3, RvD4, MaRn-3DPA, and PD1, respectively.

were also supported by the *in vivo* evidence that mice deficient for elongase 2, the key enzyme involved in the biosynthesis of DHA, the precursor of D-resolvins, protectins, and maresins, showed increased percentages of Th1 and Th17 cells, which were reduced upon dietary supplementation with DHA or *in vivo* treatment with RvD1 (52). Of note, the capacity of SPMs to prevent Th17 polarization was also observed in patients with inflammatory diseases such as rheumatoid arthritis or systemic lupus erythematosus (59, 63). Interestingly, RvD1, RvD2, and MaR1 were not capable to modulate IL-4 production and Th2-cell development *in vitro* (which may, however, not reflect *in vivo* processes) (52). These results are in line with studies reporting that, in Th2-driven pathologies and mouse models, DHA-derived SPMs like RvD1 and PD1 do not affect IL-4 release and might ameliorate clinical outcome by acting on different cellular targets (64, 65).

In contrast, RvE1, which is derived from EPA, was reported to promote resolution of asthmatic airway inflammation and atopic dermatitis by reducing Th2 cytokines; however, evidence of a direct T-cell targeting is missing (66–68). Although data supporting the suppressive effect of RvE1 on Th1, Th2, and Th17 cells are mostly indirect, obtained either upon *in vivo* administration or *in vitro* stimulation of dendritic cells (39, 40, 42, 66–71), a very recent study showed that this bioactive lipid can directly impact Th17 development by inhibiting their IL-6 and TGF-β-induced polarization (72). The effect of SPMs on other T helper subsets like Th22 and Th9, either direct or indirect, is still unknown.

TABLE 1 | *In vivo* treatment with SPMs and impact on T-cell subsets and functions.

SPM	Disease/*Model*	Treatment	Therapeutic efficacy and MOA	Ref.
RvE1	Allergic airway-inflammation/*mouse*	5,000 ng/kg/day for 3 days (iv)	Airway inflammation resolution: ↓ IL-23 and IL-6 and cell infiltrate within the bronchoalveolar lavage fluid. ↑ Th1/Th17 ratio.	(39)
	HSV-induced stromal keratitis (SK)/*mouse*	60,000 ng/kg/day for 8 days(topical, eye)	↓ SK severity ↓ cornea influx of neutrophils, Th1 and Th17 cells, IFN-γ, and IL-6.	(40)
	Imiquimod (IMQ) challenge-induced psoriasis/*mouse*	8,000 ng/kg/day (iv)	↓ psoriasis severitySuppression of IL-23-producing DCs and γδ T cells.	(41)
	Corneal allograft/*mouse*	50,000 ng/kg at day 0 and 7 (subconjunctival)	↑ graft survival ↓ Th1 and Th17 infiltration and edema into the graft and draining lymph nodes	(42)
	Ligature-induced periodontitis/*mouse*	140 ng/kg/day for 10 days (topical)	↓ bone loss ↓ T-cell infiltrate and preservation of Tregs.	(43)
	Hypersensitivity skin model/*mouse*	10,000 ng/kg/day at day -1, 0, and 5 (iv)	↓ ear swelling ↓ IFN-γ-producing $CD8^+$ T cells in the skin	(44)
	Femoral artery wire injury/*mouse*	8,000 ng/kg/day (ip) (2 days before surgery)	↓ T-cell recruitment to perivascular areas. ↓ IFN-γ and IL-2 mRNA levels in injured arteries.	(45)
RvD1	Endotoxin-induced uveitis/*rat*	10 to 1,000 ng/kg (iv/intravitreal)	↓ uveitis. ↓ neutrophils, T and B cells, M1 macrophages infiltration ↓ TNF-α, CXCL8, and RANTES in the eye.	(46, 47)
	Experimental autoimmune encephalomyelitis/*mouse*	5,000 ng/kg/day for 40 days (oral)or during 15 days starting at day 7 (ip)	↓ disease severity ↓ autoreactive T cell infiltration	(48)
	OVA-induced allergic eye disease (AED)/*mouse*	1,000 ng/kg/day for 7 days (topical)	↓ AED score ↓ conjunctival immune cells (except macrophages).	(49)
	Experimental autoimmune neuritis (EAN)/*rat*	5,000 ng/kg/day for 12 days (ip)	Enhanced EAN recovery ↓ effector T cells. ↑ Tregs and IL-10, TGF-β.	(50)
	Ischemia/reperfusion-induced acute kidney injury/*mouse*	5,000 ng/kg/day for 3 days (iv)	↑ Tregs and alleviated renal tubular injury. ↓ serum levels of IFN-γ, TNF-α, and IL-6 in a ALX/FPR2-dependent pathway.	(51)
	DHA deficiency ($Elovl2^{-/-}$)/*mouse*	5,000 ng/kg/day with 50 μg of anti-CD3 (ip)	↓ IFN-γ and IL-17 by peripheral blood $CD4^+$ T cells	(52)
RvD1/ RvE1	Concanavalin A-induced hepatitis/*mouse*	10,000 ng/kg/day (iv)	↓ liver injury ↓ $CD4^+$ and $CD8^+$ T-cell liver infiltration, inflammatory cytokines, and NF-κB/AP-1 activity.	(53)
RvD2	Porphyromonas gingivalis-induced experimental periodontitis/*mouse*	25,000 ng for 3 days plus 5,000 ng for 6 days (over 2 weeks) (ip)	Prevent alveolar bone loss ↓Th1 priming and chronic IFN-γ secretion. ↑ pro-resolving macrophages in the gingiva. ↓Tregs.	(54)
PD1	Zymosan A-induced peritonitis/*mouse*	5,000 ng/kg, 2 h prior to challenge (iv)	↓ T-cell infiltration in the peritoneum	(55)
	IMQ-induced psoriasis/*mouse*	10–1,000 ng/kg/day for 7 days (sc)	↓ psoriasis severity↓ inflammatory cytokines in lesion and serum ↓ Th1/Th17 cells in spleen	(56)
	HSV-induced stromal keratitis (SK)/*mouse*	15,000 ng/kg twice/day for 10 days(topical, eye)	↓ SK severity ↓ infiltration of neutrophils and pathogenic $CD4^+$ T cells ↓ inflammatory cytokines, chemokines, and angiogenic factors in the cornea	(57)
MaR1	OVA-induced allergic inflammation/*mouse*	50 ng/kg/day for 4 days (iv)	↑ Tregs ↓ IL-13 secretion by ILC2 in the bronchoalveolar lavage fluid	(58)
	Collagen-induced arthritis/*mouse*	5,000 ng/kg/day for 16 days (iv)	↓ arthritis severity↑ Treg/Th17 ratio (draining lymph node)	(59)
	IMQ-induced psoriasis/*mouse*	8,000 ng/kg/day for 5 days (topical)	↓ skin inflammation ↓ IL-17-producing $CD4^+$ and γδ T cells in the skin.	(60)

(Continued)

TABLE 1 | Continued

SPM	Disease/*Model*	Treatment	Therapeutic efficacy and MOA	Ref.
	Spontaneous colitis/*IL-10*$^{-/-}$ *mouse*	50 ng/kg/day for 14 days (ip)	↓ $CD4^+$ T cells in colon *lamina propia* ↓ TNF-α, IFN-γ, IL-6, and IL-17 levels in colon	(61)
LXA4	Autoimmune dry eye/*mouse*	5,000–50,000 ng/kg/day for 10 days(topical/systemic)	↓ Th1 and Th17 cells in draining lymph nodes↑ Treg	(37)
	Experimental autoimmune encephalomyelitis (EAE)/*mouse*	5,000 ng/kg/day, daily (ip)	↓ EAE severity ↓ Th1 and Th17 cell infiltration into the central nervous system ↓ levels of pro-inflammatory lipids in spinal cord fluid.	(38)
	Experimental autoimmune uveitis (EAU)/*mouse*	40,000 ng/kg (mouse; ip)/day, daily	↓ EAU severity ↓ Th1 and Th17 cell infiltration ↓$CD4^+$ T cell glycolytic responses and IFN-γ production	(62)

CD, cluster of differentiation; DC, dendritic cell; HSV, herpes simplex virus; IFN, interferon; IL, interleukin; ILC, innate lymphoid cells; ip, intraperitoneal; iv, intravenous; LXA4, lipoxin A4; MaR1, maresin 1; MOA, mode of action; OVA, ovalbumin; PD1, protectin 1; RANTES, regulated upon activation, normal T cell expressed and secreted; RvD1, resolvin D1; RvD2, resolvin D2; RvE1, resolvin E1; sc, subcutaneous; TCR, T-cell receptor; Th, T helper; TNF, transforming necrosis factor; Treg, regulatory $CD4^+$ T cell.

SPM-mediated modulation of T-cell fate and function is associated with the expression of several SPM receptors, including ALX/FPR2, GPR32, GPR18, BLT1, and ChemR23, with higher levels reported on activated and effector cells (albeit at significantly lower levels compared to innate immune cells), indicating that activated T cells are more responsive to SPMs in general (35, 36, 52). However, clear data on their expression and signaling pathway in the different T-cell subsets remain currently very limited and deserve further investigations. Accordingly, human Th1 express higher mRNA levels of ALX/FPR2 and also higher protein levels of GPR32 compared to Th0 (52), while Th17 express higher protein levels of both GPR32 and ChemR23 (52, 72). These receptors account for the reported effects of RvD1 and RvE1 in reducing Th1 and Th17 responses. The role of the other SPM-binding receptors in mediating the effects of RvD2, PD1, and MaR1 remains to be explored. This may be related to their more recent discovery, such as GPR37 that was identified as the PD1 receptor in 2018 and investigated only in macrophages (73) or LGR6, the surface receptor for MaR1, identified in 2019 and mainly expressed in neutrophils and macrophages, with little expression on total $CD3^+$ T cells (74). Thus, additional thorough studies are necessary at the systemic and tissue levels to better decipher the expression profile and activity of SPM receptors on T cells, which may account for their activation, migration, and control.

Lastly, while it is now well documented that T cells can respond to several SPMs, little information is known about their capacity to produce pro-resolving lipids. As yet, only one study reported that human Th2-polarized peripheral blood mononuclear cells (PBMCs) with IL-4, but not IL-12/IFNγ-polarized Th1 cells, produced PD1 in a 15-LOX-dependent manner (55). However, due to likely cellular contaminants in the experimental setting using total PBMC and not highly purified naïve CD4 T cells, the possibility that other IL-4-responding cell types (i.e., monocytes and dendritic cells) were the source of PD1 cannot be ruled out.

IMPACT OF SPMs ON REGULATORY T CELLS

Among all T-cell subsets, Tregs are arguably the one that fits the most with the concept of resolution of inflammation due to their crucial role in maintaining immune equilibrium and homeostasis (75). They not only play a vital role in the prevention of autoimmunity and the maintenance of self-tolerance but have also been shown to promote macrophage pro-resolving functions, i.e., efferocytosis through an IL-13/IL-10/Vav1 pathway, expression of SPM receptors, and SPM production in target tissues (76, 77). Of note, recent studies suggest that the abundance and function of Tregs change during inflammation and that the pool of peripheral Tregs is diverse and can derive from other pathogenic T helper cells; for instance, Th17 can transdifferentiate into Tregs during the resolution of inflammation (78).

Despite the key role of Tregs in regulating immune and tissue homeostasis, the experimental evidence reporting the impact of SPMs on these tolerogenic T cells dates back only to 2015, first with the *in vitro* demonstration of the direct effect of MaR1 in amplifying the TGF-β-induced *de novo* generation of Foxp3$^+$ Tregs (iTregs) (58), and second with the *in vivo* observation of an increased frequency of Foxp3-expressing T cells after LXA_4 treatment (37). These findings were extended to RvD1, RvD2, and MaR1 in the human setting, with iTregs showing increased CTLA-4 expression, IL-10 release, and suppressive capacity (52). However, although mice genetically unable to produce SPMs (Elovl2$^{-/-}$ mice) displayed decreased proportion of Foxp3$^+$ Tregs, none of the tested SPMs was capable, *per se*, to induce Foxp3 expression and convert naïve CD4$^+$ T cells into Tregs without the required TGF-β-enriched polarizing milieu (52).

The positive impact of SPMs on Foxp3$^+$ Tregs was further corroborated *in vivo* upon administration of SPMs (mainly RvD1, LXA4, and MaR1) in several experimental models of chronic inflammatory or neurodegenerative diseases, although the enhanced Treg proportion observed in these contexts may be due to both direct and indirect effect on T cells (50, 51, 59, 63, 79) (**Table 1**). Of note, a majority of these studies also reported an improved Treg/Th17-Th1 balance in the target tissue or draining lymph nodes, associated with SPM therapeutic efficacy. Concerning PD1, its *in vivo* administration has recently been associated with increased frequency of IL-10-producing CD4$^+$ T cells in the colon, suggesting an impact on Tr1 cells (80). Yet, no evidence has been reported for a role of this DHA-derived SPM on Foxp3$^+$ Tregs.

Only two studies have examined which receptor might be involved in mediating the SPM-induced Treg generation. Both studies focused on RvD1 and, by using neutralizing antibodies, they demonstrated that GPR32 was responsible for the Foxp3$^+$ Treg differentiation in humans (52), while ALX/FPR2 was at play in mice (51).

Interestingly, a recent work reported that human and mouse Foxp3$^+$ Tregs express the 5/12/15-lipoxygenases and are able to biosynthetize several SPMs from all four major bioactive metabolomes, but only 17R-RvD3, RvD4, and MaRn-3DPA were significantly produced at a higher amount compared to naïve CD4$^+$ T cells (81). Genetic ablation of ALOX15 in Tregs decreased Foxp3 expression and altered their transcriptional and metabolic programs, resulting in impaired suppressive function and increased effector pathways. Also, Foxp3 binding elements were identified in the ALOX15 promoter region, allowing a direct positive regulation of ALOX15 expression by Foxp3 (81).

Collectively, these findings demonstrate that SPMs can target different T-cell subsets to modulate their development and functions, and emphasize the pro-resolving and homeostatic actions of SPMs (**Figure 2**). They also pinpoint that mechanisms driving immune regulation and resolution of inflammation are complementary and interconnected, which supports the potential of new therapeutic opportunities. Additionally, SPMs may be produced not only by innate immune cells but also by T cells, possibly exerting autocrine and paracrine anti-inflammatory actions, ultimately contributing to immune regulation.

DEFECTIVE PRO-RESOLVING PATHWAYS ASSOCIATED WITH PATHOGENIC T-CELL RESPONSES

Chronic diseases are characterized by excessive inflammation and impairment of natural resolution mechanisms. Bioactive lipids are implicated in the pathologic processes, with an unbalanced production of inflammatory over pro-resolving lipids, driving the aberrant recruitment and activation of immune cells, including effector T lymphocytes, leading to tissue damage and ultimately disease symptoms (5). Pathogenic T-cell responses have been associated with defective resolution pathways and disease progression. However, so far, few studies have investigated and demonstrated a direct link between a deficient SPM pathway and exacerbated T-cell reactivity.

In experimental models of autoimmune dry eye disease or autoimmune neuritis (mimicking human inflammatory demyelinating polyradiculoneuropathy), reduced RvD1 or LXA4 amounts correlated with decreased proportion of Foxp3$^+$ Tregs in the inflamed tissues, respectively (37, 50). In humans, the BLT1 receptor was found upregulated on T cells isolated from the airways of patients presenting obliterative bronchiolitis after lung transplantation (19), or from the blood of asthmatic patients (82). These data suggest an increased T-cell sensitivity to pro-inflammatory LTB4 and a critical role of BLT1 in T-cell recruitment into target organs as evidenced in animal models. Conversely, T cells from patients with chronic heart failure expressed reduced levels of GPR32 as compared to healthy subjects, correlating with an impaired responsiveness of CD4$^+$ and CD8$^+$ T cells to RvD1 and RvD2 (assessed by the inhibition of inflammatory cytokine production) (83). In the context of multiple sclerosis (MS), ALX/FPR2, GPR32, GPR18, and ChemR23 were differentially expressed on PBMCs according to disease activity, with decreased mRNA levels in patients with progressive MS as compared to patients presenting relapsing or remitting MS (84). Of note, while BLT1 showed similar expression in all donor groups, these SPM receptors were globally upregulated in relapsing or remitting MS compared to healthy donors, which may reflect the engagement of resolution mechanisms in immune cells, including T cells, in response to inflammation and autoimmunity. Lastly, a recent study showed that LXA4 modulated *in vitro* activation, TNF-α, IFN-γ, IL-17 production, and transendothelial migration capacity of CD4$^+$ and CD8$^+$ T cells from both healthy donors and patients with relapsing–remitting MS (38). However, we have to keep in mind that these analyses were performed on circulating T cells, not on tissue-infiltrating T cells, which may exhibit distinct functional characteristics and behavior influenced by the local inflammatory/resolving lipid balance.

Of interest, in the last years, lipidomic analysis of plasma or serum recovered from patients with chronic inflammatory disorders implicating pathogenic T-cell responses constantly showed decreased SPM concentrations at the time of active disease, compared with healthy and/or inactive disease status. This was reported for MaR1 and PD1 in rheumatoid arthritis (RA) (59, 85) and for RvD1 in SLE, MS, and chronic heart failure

(63, 83, 84). Lower levels of RvD3, RvD4, and RvE3 were also observed in a small cohort of stage III RA patients, with concomitant increase in inflammatory TBX2 (86). In some instances, SPM abundance negatively correlated with disease severity (63, 84, 85). Similarly, patients with leprosy and acute Th1-mediated inflammatory episodes showed reduced plasma levels of RvD1 as compared to patients without Th1 hyperreactivity (87). In most cases, opposite patterns were observed for arachidonic acid-derived inflammatory lipids (LTB4, PGs), which were found in higher abundance at the time of progressive disease.

However, available information is overall limited, and caution should be brought on the interpretation of these results. Indeed, depending on the clinical context, higher levels of plasmatic SPMs can be detected in patients presenting inactive/controlled inflammatory and autoimmune pathologies as compared to healthy individuals, which may reflect perturbed resolution processes related to an attempt to counteract inflammation. In addition, systemic levels of bioactive lipids may not coincide with tissue abundance, and a decrease in the SPM level could result from higher consumption, reduced production, or both conditions. Lastly, expression of SPM receptors on T cells and their responsiveness to SPMs have so far been explored in few pathological contexts. These investigations need to be extended to additional immune disorders to better understand the impact of resolutive pathways on effector and regulatory T-cell subsets and to identify putative failures at the systemic and tissue levels, which may contribute to the defective immune regulation leading to disease progression.

Thus, these findings call for further deciphering, in mice and humans, the impact of resolution mechanisms and the SPM pathway on adaptive immunity, in particular their role in the dysregulated effector/regulatory T-cell responses responsible for the progression and chronicity of immune and autoimmune diseases.

IN VIVO THERAPEUTIC EFFICACY OF SPMs THROUGH T-CELL REPROGRAMMING

The potent pro-resolving properties of SPMs have encouraged their therapeutic application in various experimental models of inflammation (**Table 1** and **Figure 3**). Particularly, RvD1 and RvE1, but also RvD2, MaR1, PDX, and LAX4, have been tested in a number of pathological contexts presenting resolution defects accentuated by effector T-cell infiltration and activity in target organs.

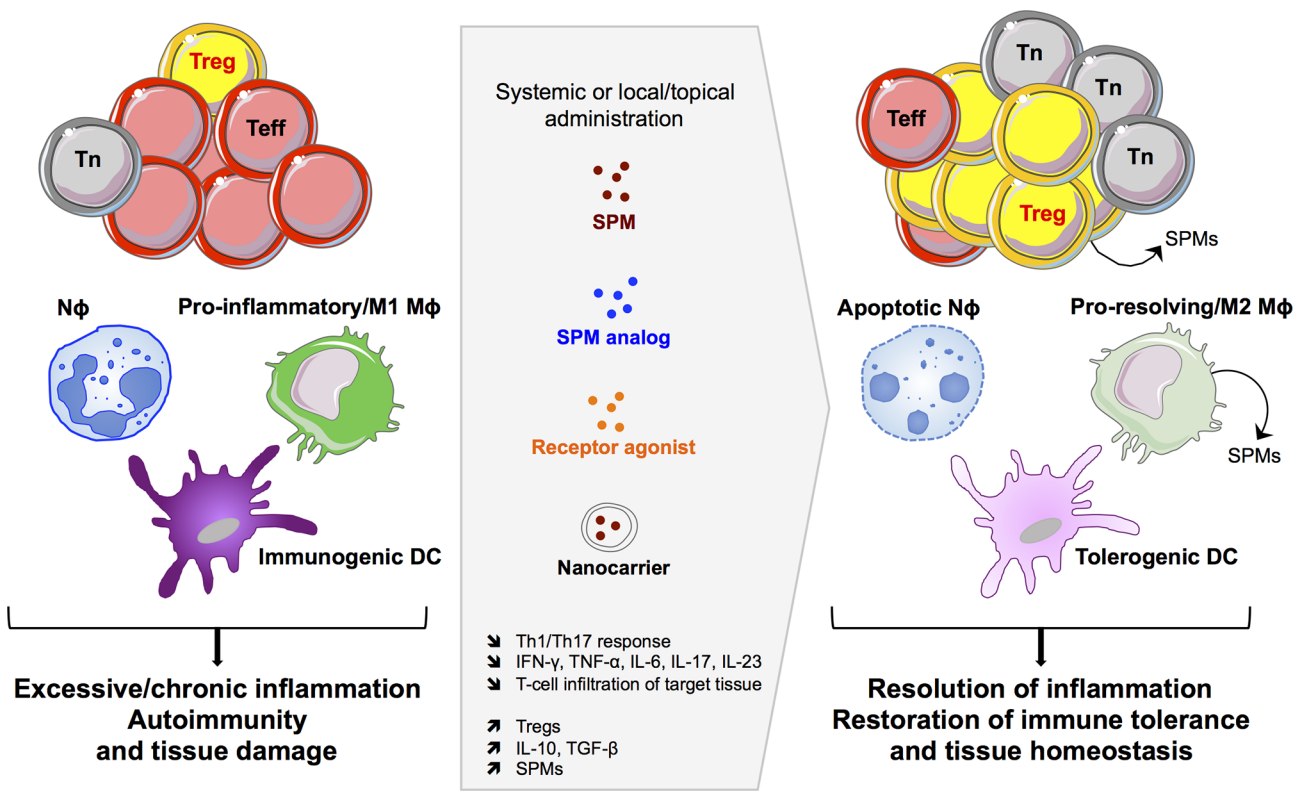

FIGURE 3 | SPM-based therapeutic opportunities. Targeting the SPM pathway can impact innate and adaptive immune cells to induce efficient resolution of excessive inflammatory responses and to restore immune tolerance and tissue homeostasis. Nϕ, neutrophil; Mϕ, macrophage; DC, dendritic cell; Teff, effector T cell; Tn, naïve T cell; Treg, regulatory T cell.

The protocols used were very variable depending on the model: SPMs were administered through systemic (intravenous, intraperitoneal) or local (topical application on the eye, intravitreal, subconjunctival) routes, at an average dose of 5 μg/kg, i.e., approximately 100 ng/mouse (ranging from 20 to 500 ng/injection), with single or repeated injections over several weeks.

Overall, SPM treatment reduced the severity of inflammatory diseases (in most cases experimentally induced in animal models), marked by decreased tissue damage, immune cell infiltration, and inflammatory cytokines. Indeed, Th1 and Th17 cells were repeatedly found in lower numbers in target organs and draining lymph nodes, together with less *in situ* expression (mRNA and/or protein) of IFN-γ, TNF-α, IL-17, IL-6, and IL-1β in the context of endotoxic uveitis (46, 47), concanavalin-A-induced hepatitis (53), sepsis-induced lung injury (88), stromal keratitis (herpes simplex virus-induced ocular inflammatory lesions) (40, 57, 89), periodontitis (43, 54), and rheumatoid arthritis (59, 85). Similar positive outcomes were observed in allergic manifestations such as chronic allergic eye disease (49), allergic airway inflammation (39), and psoriatic dermatitis (41). SPM therapy has been explored in few autoimmune diseases, i.e., RvD1 in Sjögren's syndrome (90) and SLE (63), and LXA4 in experimental autoimmune uveitis (EAU) (62) and encephalomyelitis (EAE) (38), with here again the amelioration of symptoms and reduction of pathogenic T-cell trafficking to target tissues and inflamed responses. Of note, the metabolic program of $CD4^+$ T cells was found modulated in LXA4-teated mice, marked by decreased glycolytic responses associated with reduced IFN-γ production (62). Lastly, RvE1 has been applied in a model of corneal transplantation, promoting graft survival associated with diminished Th1 and Th17 $CD4^+$ T cells and inflammatory cytokines in the allogeneic transplant (42, 91).

In some studies, the decrease in effector T lymphocytes observed after SPM treatment was paralleled by an increase in $Fox3^+$ Treg frequency and associated immunomodulatory cytokines such as IL-10 and TGF-β (50, 51, 54, 59, 63, 85). Administration of SD-208, a TGF-β receptor antagonist, reversed the RvD1 therapeutic effect in autoimmune neuritis, showing the closed relationship between these two modulatory pathways (50). The cross-talk between SPMs and Tregs was highlighted in a model of ischemia/reperfusion-induced acute kidney injury (IRI-AKI mice) by the abrogation of RvD1 therapeutic effect after the administration of the anti-CD25 PC61 monoclonal antibody, which preferentially depletes Tregs (51). Furthermore, the beneficial effect of RvD1 on Treg frequency was suppressed after *in vivo* blockade of FPR2 with a specific antagonist (Boc-1), leading to severe renal tubular injury (51).

Therefore, these experimental data support SPM-based therapy as a promising avenue for the treatment of a wide range of T-cell-mediated immune and autoimmune diseases. Especially, the *in vivo* therapeutic efficacy of SPMs and associated dampening of effector T-cell responses can benefit from both a direct effect on T cells and an indirect action through antigen-presenting cells (APCs: DCs, macrophages), expressing SPM receptors, as SPMs downregulate APC activation, expression of costimulatory molecules, and secretion of inflammatory cytokines, which subsequently prime effector T cells (72).

In terms of clinical application, a pilot study has been launched in patients undergoing total knee arthroplasty to investigate the impact of preoperative supplementation with Lipinova® (Solutex), described as a concentrate of EPA, DHA, and SPMs (NCT03434236). However, the clinical use of SPMs as therapeutic agents is impeded by their metabolically labile and unstable state, restricted bioavailability, and rapid clearance, and thus calls for the development of SPM synthetic analogs displaying pharmacokinetic properties in compliance with *in vivo* usage (92, 93). In this line, a RvE1 mimetic, RX-10045, has been tested as an ophthalmic solution for dry eye symptoms (NCT00799552), allergic conjunctivitis (NCT01639846), and in patients undergoing cataract surgery (NCT02329743). Promising results were recently reported in a phase 1 trial evaluating the safety and efficacy of BLXA4, a LXA4 analog, to treat periodontitis (NCT02342691): daily rinsing with mouthwash containing BLXA4 reduced gingival inflammation, and this was associated with a shift in serum lipid mediators toward a pro-resolving profile (94).

The development of SPM receptor agonists is also in the pipeline, as recently documented by the study of Trilleaud et al. who tested a new anti-ChemR23 agonist antibody in models of acute and chronic colitis (induced by DSS or adoptive transfer of $CD4^+CD45RB^{high}$ T cells, respectively) and inflammation-driven cancers (95). This antibody was able to activate the pro-resolving ChemR23 pathway and trigger the resolution of inflammatory responses.

CONCLUSION

SPMs display a wide range of anti-inflammatory actions, which are increasingly explored in adaptive immunity, notably through their ability to bind several GPCRs expressed by T cells, to regulate T-cell functions, and to trigger the resolution of inflammatory and immune-mediated diseases in animal models. Of note, a number of studies also report SPM activity on humoral responses, with, however, some discrepant results, as RvD1 increased the production of IgM and IgG (96) while decreasing the secretion of IgE by activated B lymphocytes (97, 98). IgM and IgG production and antigen-specific memory B-cell responses were similarly reduced by LXA4 (99). Building on the potent immunoresolvent properties of SPMs and their multiple targets, these findings open a new field of investigations that may provide a better understanding of the physiological regulation of adaptive immune response and its failure in pathophysiological contexts. SPM lipidomic analyses are indeed performed in the frame of several clinical studies as a read-out of disease diagnosis and progression, inflammatory profile [for instance in COVID19 patients (100)], as well as response to therapeutic interventions (NCT04698291, NCT04452942, NCT04697719, NCT01865448, NCT04308889, NCT04377334, and NCT02719665) (101).

In addition, the pathways governing immune regulation and resolution programs are interrelated and provide the mechanistic rationale for developing SPM-based therapeutic strategies that can be beneficial for the treatment of chronic inflammatory disorders, autoimmune diseases, and organ transplantation, notably through the control of effector T cells and boost of Tregs. This is reinforced by the positive outcomes observed in various pathological settings after dietary intervention using SPM precursors, DHA and EPA, or omega-3 lipids, which enhance SPM levels and help in controlling excessive inflammation and autoimmunity in both humans and mice (102–104). Thus, the multiple actions of SPMs on innate and adaptive immunity provide novel opportunities for SPM-based biomarker and drug development (**Figure 3**). The production of metabolically stable SPM analogs or receptor agonist with increased half-life, together with the design of nanocarriers to protect SPMs from degradation, may accelerate the way toward clinical translation.

AUTHOR CONTRIBUTIONS

JP-H, VC, SP, and SY wrote and revised the manuscript. All authors contributed to the article and approved the submitted version.

FUNDING

The laboratory of SY and JP-H is supported by grants from the EFSD/JDRF/Lilly European Programme in Type 1 Diabetes Research 2019, the *Agence Nationale de la Recherche* (ANR-17-CE17-0004, ANR-18-IDEX-0001), the *Fondation pour la Recherche Médicale* (EQU20193007831), the *Association des Jeunes Diabétiques*, and the Innovative Medicines Initiative 2 Joint Undertaking under grant agreements 115797 and 945268 (INNODIA and INNODIA HARVEST), which receive support from the EU Horizon 2020 program, the European Federation of Pharmaceutical Industries and Associations, JDRF, and The Leona M. and Harry B. Helmsley Charitable Trust. VC is funded by the Italian Ministry of Health (grant GR-2016-02362380), the Italian Foundation of Multiple Sclerosis (FISM 2017/R/08), and the MAI Award Grant (MAI-VC-2021). SP is funded by the *Conseil Régional de Franche-Comté* (AAP 2019), the *Agence Nationale de la Recherche* (ANR-11-LABX-0021 and ANR-17-CE17-0004), BPI France (grant No. DOS0060162/00), and the European Union through the European Regional Development Fund of the Région Bourgogne-Franche-Comte (FC0013440).

REFERENCES

1. Lawrence T, Gilroy DW. Chronic Inflammation: A Failure of Resolution? *Int J Exp Pathol* (2007) 88(2):85–94. doi: 10.1111/j.1365-2613.2006.00507.x
2. Nathan C, Ding A. Nonresolving Inflammation. *Cell* (2010) 140(6):871–82. doi: 10.1016/j.cell.2010.02.029
3. Nagata S, Hanayama R, Kawane K. Autoimmunity and the Clearance of Dead Cells. *Cell* (2010) 140(5):619–30. doi: 10.1016/j.cell.2010.02.014
4. Szondy Z, Garabuczi E, Joos G, Tsay GJ, Sarang Z. Impaired Clearance of Apoptotic Cells in Chronic Inflammatory Diseases: Therapeutic Implications. *Front Immunol* (2014) 5:354. doi: 10.3389/fimmu.2014.00354
5. Chiurchiù V, Leuti A, Maccarrone M. Bioactive Lipids and Chronic Inflammation: Managing the Fire Within. *Front Immunol* (2018) 9:38. doi: 10.3389/fimmu.2018.00038
6. Serhan CN. Pro-Resolving Lipid Mediators Are Leads for Resolution Physiology. *Nature* (2014) 510(7503):92–101. doi: 10.1038/nature13479
7. Serhan CN. Discovery of Specialized Pro-Resolving Mediators Marks the Dawn of Resolution Physiology and Pharmacology. *Mol Aspects Med* (2017) 58:1–11. doi: 10.1016/j.mam.2017.03.001
8. Chiang N, Serhan CN. Structural Elucidation and Physiologic Functions of Specialized Pro-Resolving Mediators and Their Receptors. *Mol Aspects Med* (2017) 58:114–29. doi: 10.1016/j.mam.2017.03.005
9. Tiberi M, Chiurchiù V. Specialized Pro-Resolving Lipid Mediators and Glial Cells: Emerging Candidates for Brain Homeostasis and Repair. *Front Cell Neurosci* (2021) 15:673549. doi: 10.3389/fncel.2021.673549
10. Arita M, Ohira T, Sun Y-P, Elangovan S, Chiang N, Serhan CN. Resolvin E1 Selectively Interacts With Leukotriene B4 Receptor BLT1 and ChemR23 to Regulate Inflammation. *J Immunol* (2007) 178(6):3912–7. doi: 10.4049/jimmunol.178.6.3912
11. Kebir DE, Gjorstrup P, Filep JG. Resolvin E1 Promotes Phagocytosis-Induced Neutrophil Apoptosis and Accelerates Resolution of Pulmonary Inflammation. *PNAS* (2012) 109(37):14983–8. doi: 10.1073/pnas.1206641109
12. Buckley CD, Gilroy DW, Serhan CN. Proresolving Lipid Mediators and Mechanisms in the Resolution of Acute Inflammation. *Immunity* (2014) 40 (3):315–27. doi: 10.1016/j.immuni.2014.02.009
13. Serhan CN, Gupta SK, Perretti M, Godson C, Brennan E, Li Y, et al. The Atlas of Inflammation Resolution (AIR). *Mol Aspects Med* (2020) 74:100894. doi: 10.1016/j.mam.2020.100894
14. Serhan CN, Levy BD. Resolvins in Inflammation: Emergence of the Pro-Resolving Superfamily of Mediators. *J Clin Invest* (2018) 128(7):2657–69. doi: 10.1172/JCI97943
15. Leuti A, Fazio D, Fava M, Piccoli A, Oddi S, Maccarrone M. Bioactive Lipids, Inflammation and Chronic Diseases. *Advanced Drug Deliv Rev* (2020) 159:133–69. doi: 10.1016/j.addr.2020.06.028
16. Goodarzi K, Goodarzi M, Tager AM, Luster AD, von Andrian UH. Leukotriene B4 and BLT1 Control Cytotoxic Effector T Cell Recruitment to Inflamed Tissues. *Nat Immunol* (2003) 4(10):965–73. doi: 10.1038/ni972
17. Islam SA, Thomas SY, Hess C, Medoff BD, Means TK, Brander C, et al. The Leukotriene B4 Lipid Chemoattractant Receptor BLT1 Defines Antigen-Primed T Cells in Humans. *Blood* (2006) 107(2):444–53. doi: 10.1182/blood-2005-06-2362
18. Tager AM, Bromley SK, Medoff BD, Islam SA, Bercury SD, Friedrich EB, et al. Leukotriene B4 Receptor BLT1 Mediates Early Effector T Cell Recruitment. *Nat Immunol* (2003) 4(10):982–90. doi: 10.1038/ni970
19. Medoff BD, Seung E, Wain JC, Means TK, Campanella GSV, Islam SA, et al. BLT1-Mediated T Cell Trafficking is Critical for Rejection and Obliterative Bronchiolitis After Lung Transplantation. *J Exp Med* (2005) 202(1):97–110. doi: 10.1084/jem.20042481
20. Miyahara N, Takeda K, Miyahara S, Taube C, Joetham A, Koya T, et al. Leukotriene B4 Receptor-1 Is Essential for Allergen-Mediated Recruitment of CD8 $^+$ T Cells and Airway Hyperresponsiveness. *J Immunol* (2005) 174 (8):4979–84. doi: 10.4049/jimmunol.174.8.4979
21. Taube C, Miyahara N, Ott V, Swanson B, Takeda K, Loader J, et al. The Leukotriene B4 Receptor (BLT1) Is Required for Effector CD8 $^+$ T Cell-Mediated, Mast Cell-Dependent Airway Hyperresponsiveness. *J Immunol* (2006) 176(5):3157–64. doi: 10.4049/jimmunol.176.5.3157
22. Lv J, Zou L, Zhao L, Yang W, Xiong Y, Li B, et al. Leukotriene B_4-Leukotriene B_4 Receptor Axis Promotes Oxazolone-Induced Contact Dermatitis by Directing Skin Homing of Neutrophils and CD8$^+$ T Cells. *Immunol* (2015) 146(1):50–8. doi: 10.1111/imm.12478
23. Sharma RK, Chheda Z, Jala VR, Haribabu B. Expression of Leukotriene B4 Receptor-1 on CD8+ T Cells Is Required for Their Migration Into Tumors To Elicit Effective Antitumor Immunity. *J Immunol* (2013) 191(6):3462–70. doi: 10.4049/jimmunol.1300967
24. Chen H, Qin J, Wei P, Zhang J, Li Q, Fu L, et al. Effects of Leukotriene B4 and Prostaglandin E2 on the Differentiation of Murine Foxp3+ T Regulatory

Cells and Th17 Cells. *Prostaglandins Leukot Essent Fatty Acids* (2009) 80 (4):195–200. doi: 10.1016/j.plefa.2009.01.006
25. Lee W, Su Kim H, Lee GR. Leukotrienes Induce the Migration of Th17 Cells. *Immunol Cell Biol* (2015) 93(5):472–9. doi: 10.1038/icb.2014.104
26. Nagaya T, Kawata K, Kamekura R, Jitsukawa S, Kubo T, Kamei M, et al. Lipid Mediators Foster the Differentiation of T Follicular Helper Cells. *Immunol Lett* (2017) 181:51–7. doi: 10.1016/j.imlet.2016.11.006
27. Maseda D, Ricciotti E, Crofford LJ. Prostaglandin Regulation of T Cell Biology. *Pharmacol Res* (2019) 149:104456. doi: 10.1016/j.phrs.2019.104456
28. Yao C, Hirata T, Soontrapa K, Ma X, Takemori H, Narumiya S. Prostaglandin E_2 Promotes Th1 Differentiation *via* Synergistic Amplification of IL-12 Signalling by cAMP and PI3-Kinase. *Nat Commun* (2013) 4:1685. doi: 10.1038/ncomms2684
29. Chen Q, Muramoto K, Masaaki N, Ding Y, Yang H, Mackey M, et al. A Novel Antagonist of the Prostaglandin E(2) EP(4) Receptor Inhibits Th1 Differentiation and Th17 Expansion and is Orally Active in Arthritis Models. *Br J Pharmacol* (2010) 160(2):292–310. doi: 10.1111/j.1476-5381.2010.00647.x
30. Lee J, Aoki T, Thumkeo D, Siriwach R, Yao C, Narumiya S. T Cell–Intrinsic Prostaglandin E2-EP2/EP4 Signaling Is Critical in Pathogenic TH17 Cell–Driven Inflammation. *J Allergy Clin Immunol* (2019) 143(2):631–43. doi: 10.1016/j.jaci.2018.05.036
31. Esaki Y, Li Y, Sakata D, Yao C, Segi-Nishida E, Matsuoka T, et al. Dual Roles of PGE2-EP4 Signaling in Mouse Experimental Autoimmune Encephalomyelitis. *Proc Natl Acad Sci USA* (2010) 107(27):12233–8. doi: 10.1073/pnas.0915112107
32. Hooper KM, Kong W, Ganea D. Prostaglandin E2 Inhibits Tr1 Cell Differentiation Through Suppression of C-Maf. *PloS One* (2017) 12(6): e0179184. Kim CH, editor. doi: 10.1371/journal.pone.0179184
33. Li H, Chen H-Y, Liu W-X, Jia X-X, Zhang J-G, Ma C-L, et al. Prostaglandin E2 Restrains Human Treg Cell Differentiation *via* E Prostanoid Receptor 2-Protein Kinase A Signaling. *Immunol Lett* (2017) 191:63–72. doi: 10.1016/j.imlet.2017.09.009
34. Baratelli F, Lin Y, Zhu L, Yang S-C, Heuzé-Vourc'h N, Zeng G, et al. Prostaglandin E2 Induces FOXP3 Gene Expression and T Regulatory Cell Function in Human CD4+ T Cells. *J Immunol* (2005) 175(3):1483–90. doi: 10.4049/jimmunol.175.3.1483
35. Ariel A, Chiang N, Arita M, Petasis NA, Serhan CN. Aspirin-Triggered Lipoxin A_4 and B_4 Analogs Block Extracellular Signal-Regulated Kinase-Dependent TNF-α Secretion From Human T Cells. *J Immunol* (2003) 170 (12):6266–72. doi: 10.4049/jimmunol.170.12.6266
36. Spurr L, Nadkarni S, Pederzoli-Ribeil M, Goulding NJ, Perretti M, D'Acquisto F. Comparative Analysis of Annexin A1-Formyl Peptide Receptor 2/ALX Expression in Human Leukocyte Subsets. *Int Immunopharmacol* (2011) 11(1):55–66. doi: 10.1016/j.intimp.2010.10.006
37. Gao Y, Min K, Zhang Y, Su J, Greenwood M, Gronert K. Female-Specific Downregulation of Tissue Polymorphonuclear Neutrophils Drives Impaired Regulatory T Cell and Amplified Effector T Cell Responses in Autoimmune Dry Eye Disease. *J Immunol* (2015) 195(7):3086–99. doi: 10.4049/jimmunol.1500610
38. Derada Troletti C, Enzmann G, Chiurchiù V, Kamermans A, Tietz SM, Norris PC, et al. Pro-Resolving Lipid Mediator Lipoxin A4 Attenuates Neuro-Inflammation by Modulating T Cell Responses and Modifies the Spinal Cord Lipidome. *Cell Rep* (2021) 35(9):109201. doi: 10.1016/j.celrep.2021.109201
39. Haworth O, Cernadas M, Yang R, Serhan CN, Levy BD. Resolvin E1 Regulates Interleukin 23, Interferon-γ and Lipoxin A4 to Promote the Resolution of Allergic Airway Inflammation. *Nat Immunol* (2008) 9 (8):873–9. doi: 10.1038/ni.1627
40. Rajasagi NK, Reddy PBJ, Suryawanshi A, Mulik S, Gjorstrup P, Rouse BT. Controlling Herpes Simplex Virus-Induced Ocular Inflammatory Lesions With the Lipid-Derived Mediator Resolvin E1. *J. Immunol* (2011) 186 (3):1735–46. doi: 10.4049/jimmunol.1003456
41. Sawada Y, Honda T, Nakamizo S, Otsuka A, Ogawa N, Kobayashi Y, et al. Resolvin E1 Attenuates Murine Psoriatic Dermatitis. *Sci Rep* (2018) 8 (1):11873. doi: 10.1038/s41598-018-30373-1
42. Wang H, Zhao Q, Luo D, Yin Y, Li T, Zhao M. Resolvin E1 Inhibits Corneal Allograft Rejection in High-Risk Corneal Transplantation. *Invest Ophthalmol Vis Sci* (2018) 59(10):3911. doi: 10.1167/iovs.18-24562
43. Alvarez C, Abdalla H, Sulliman S, Rojas P, Wu Y-C, Almarhoumi R, et al. RvE1 Impacts the Gingival Inflammatory Infiltrate by Inhibiting the T Cell Response in Experimental Periodontitis. *Front Immunol* (2021) 12:664756. doi: 10.3389/fimmu.2021.664756
44. Sawada Y, Honda T, Hanakawa S, Nakamizo S, Murata T, Ueharaguchi-Tanada Y, et al. Resolvin E1 Inhibits Dendritic Cell Migration in the Skin and Attenuates Contact Hypersensitivity Responses. *J Exp Med* (2015) 212 (11):1921–30. doi: 10.1084/jem.20150381
45. Liu G, Gong Y, Zhang R, Piao L, Li X, Liu Q, et al. Resolvin E1 Attenuates Injury-Induced Vascular Neointimal Formation by Inhibition of Inflammatory Responses and Vascular Smooth Muscle Cell Migration. *FASEB J* (2018) 32(10):5413–25. doi: 10.1096/fj.201800173R
46. Settimio R, Clara DF, Franca F, Francesca S, Michele D. Resolvin D1 Reduces the Immunoinflammatory Response of the Rat Eye Following Uveitis. *Mediators Inflamm* (2012) 2012:1–9. doi: 10.1155/2012/318621
47. Rossi S, Di Filippo C, Gesualdo C, Potenza N, Russo A, Trotta MC, et al. Protection From Endotoxic Uveitis by Intravitreal Resolvin D1: Involvement of Lymphocytes, miRNAs, Ubiquitin-Proteasome, and M1/M2 Macrophages. *Mediators Inflamm* (2015) 2015:1–12. doi: 10.1155/2015/149381
48. Poisson LM, Suhail H, Singh J, Datta I, Denic A, Labuzek K, et al. Untargeted Plasma Metabolomics Identifies Endogenous Metabolite With Drug-Like Properties in Chronic Animal Model of Multiple Sclerosis. *J Biol Chem* (2015) 290(52):30697–712. doi: 10.1074/jbc.M115.679068
49. Saban DR, Hodges RR, Mathew R, Reyes NJ, Yu C, Kaye R, et al. Resolvin D1 Treatment on Goblet Cell Mucin and Immune Responses in the Chronic Allergic Eye Disease (AED) Model. *Mucosal Immunol* (2019) 12(1):145–53. doi: 10.1038/s41385-018-0089-1
50. Luo B, Han F, Xu K, Wang J, Liu Z, Shen Z, et al. Resolvin D1 Programs Inflammation Resolution by Increasing TGF- Expression Induced by Dying Cell Clearance in Experimental Autoimmune Neuritis. *J Neurosci* (2016) 36 (37):9590–603. doi: 10.1523/JNEUROSCI.0020-16.2016
51. Luan H, Wang C, Sun J, Zhao L, Li L, Zhou B, et al. Resolvin D1 Protects Against Ischemia/Reperfusion-Induced Acute Kidney Injury by Increasing Treg Percentages *via* the ALX/FPR2 Pathway. *Front Physiol* (2020) 11:285. doi: 10.3389/fphys.2020.00285
52. Chiurchiù V, Leuti A, Dalli J, Jacobsson A, Battistini L, Maccarrone M, et al. Proresolving Lipid Mediators Resolvin D1, Resolvin D2, and Maresin 1 are Critical in Modulating T Cell Responses. *Sci Transl Med* (2016) 8 (353):353ra111. doi: 10.1126/scitranslmed.aaf7483
53. Kuang H, Hua X, Zhou J, Yang R. Resolvin D1 and E1 Alleviate the Progress of Hepatitis Toward Liver Cancer in Long-Term Concanavalin A-Induced Mice Through Inhibition of NF-κb Activity. *Oncol Rep* (2016) 35(1):307–17. doi: 10.3892/or.2015.4389
54. Mizraji G, Heyman O, Van Dyke TE, Wilensky A. Resolvin D2 Restrains Th1 Immunity and Prevents Alveolar Bone Loss in Murine Periodontitis. *Front Immunol* (2018) 9:785. doi: 10.3389/fimmu.2018.00785
55. Ariel A, Li P-L, Wang W, Tang W-X, Fredman G, Hong S, et al. The Docosatriene Protectin D1 Is Produced by TH2 Skewing and Promotes Human T Cell Apoptosis *via* Lipid Raft Clustering. *J Biol Chem* (2005) 280 (52):43079–86. doi: 10.1074/jbc.M509796200
56. Park KD, Kim N, Kang J, Dhakal H, Kim JY, Jang YH, et al. Protectin D1 Reduces Imiquimod-Induced Psoriasiform Skin Inflammation. *Int Immunopharmacol* (2021) 98:107883. doi: 10.1016/j.intimp.2021.107883
57. Rajasagi NK, Reddy PBJ, Mulik S, Gjorstrup P, Rouse BT. Neuroprotectin D1 Reduces the Severity of Herpes Simplex Virus–Induced Corneal Immunopathology. *Invest Ophthalmol Vis Sci* (2013) 54(9):6269–79. doi: 10.1167/iovs.13-12152
58. Krishnamoorthy N, Burkett PR, Dalli J, Abdulnour R-EE, Colas R, Ramon S, et al. Cutting Edge: Maresin-1 Engages Regulatory T Cells To Limit Type 2 Innate Lymphoid Cell Activation and Promote Resolution of Lung Inflammation. *JI* (2015) 194(3):863–7. doi: 10.4049/jimmunol.1402534
59. Jin S, Chen H, Li Y, Zhong H, Sun W, Wang J, et al. Maresin 1 Improves the Treg/Th17 Imbalance in Rheumatoid Arthritis Through miR-21. *Ann Rheum Dis* (2018) 77(11):1644–52. doi: 10.1136/annrheumdis-2018-213511
60. Saito-Sasaki N, Sawada Y, Mashima E, Yamaguchi T, Ohmori S, Yoshioka H, et al. Maresin-1 Suppresses Imiquimod-Induced Skin Inflammation by

Regulating IL-23 Receptor Expression. *Sci Rep* (2018) 8(1):5522. doi: 10.1038/s41598-018-23623-9
61. Wang H, Shi P, Huang C, Liu Q. Maresin 1 Ameliorates Iron-Deficient Anemia in IL-10-/- Mice With Spontaneous Colitis by the Inhibition of Hepcidin Expression Though the IL-6/STAT3 Pathway. *Am J Transl Res* (2016) 8(6):2758–66.
62. Wei J, Mattapallil MJ, Horai R, Jittayasothorn Y, Modi AP, Sen HN, et al. A Novel Role for Lipoxin A4 in Driving a Lymph Node–Eye Axis That Controls Autoimmunity to the Neuroretina. *eLife* (2020) 9:e51102. doi: 10.7554/eLife.51102
63. Cheng T, Ding S, Liu S, Li X, Tang X, Sun L. Resolvin D1 Improves the Treg/Th17 Imbalance in Systemic Lupus Erythematosus Through miR-30e-5p. *Front Immunol* (2021) 12:668760. doi: 10.3389/fimmu.2021.668760
64. Levy BD, Kohli P, Gotlinger K, Haworth O, Hong S, Kazani S, et al. Protectin D1 is Generated in Asthma and Dampens Airway Inflammation and Hyperresponsiveness. *J Immunol* (2007) 178(1):496–502. doi: 10.4049/jimmunol.178.1.496
65. Rogerio AP, Haworth O, Croze R, Oh SF, Uddin M, Carlo T, et al. Resolvin D1 and Aspirin-Triggered Resolvin D1 Promote Resolution of Allergic Airways Responses. *J Immunol* (2012) 189(4):1983–91. doi: 10.4049/jimmunol.1101665
66. Aoki H, Hisada T, Ishizuka T, Utsugi M, Kawata T, Shimizu Y, et al. Resolvin E1 Dampens Airway Inflammation and Hyperresponsiveness in a Murine Model of Asthma. *Biochem Biophys Res Commun* (2008) 367(2):509–15. doi: 10.1016/j.bbrc.2008.01.012
67. Aoki H, Hisada T, Ishizuka T, Utsugi M, Ono A, Koga Y, et al. Protective Effect of Resolvin E1 on the Development of Asthmatic Airway Inflammation. *Biochem Biophys Res Commun* (2010) 400(1):128–33. doi: 10.1016/j.bbrc.2010.08.025
68. Kim T-H, Kim G-D, Jin Y-H, Park YS, Park C-S. Omega-3 Fatty Acid-Derived Mediator, Resolvin E1, Ameliorates 2,4-Dinitrofluorobenzene-Induced Atopic Dermatitis in NC/Nga Mice. *Int Immunopharmacol* (2012) 14(4):384–91. doi: 10.1016/j.intimp.2012.08.005
69. Vassiliou EK, Kesler OM, Tadros JH, Ganea D. Bone Marrow-Derived Dendritic Cells Generated in the Presence of Resolvin E1 Induce Apoptosis of Activated CD4+ T Cells. *J Immunol* (2008) 181(7):4534–44. doi: 10.4049/jimmunol.181.7.4534
70. Tian H, Lu Y, Sherwood AM, Hongqian D, Hong S. Resolvins E1 and D1 in Choroid-Retinal Endothelial Cells and Leukocytes: Biosynthesis and Mechanisms of Anti-Inflammatory Actions. *Invest Ophthalmol Vis Sci* (2009) 50(8):3613–20. doi: 10.1167/iovs.08-3146
71. Li N, He J, Schwartz CE, Gjorstrup P, Bazan HEP. Resolvin E1 Improves Tear Production and Decreases Inflammation in a Dry Eye Mouse Model. *J Ocul Pharmacol Ther* (2010) 26(5):431–9. doi: 10.1089/jop.2010.0019
72. Oner F, Alvarez C, Yaghmoor W, Stephens D, Hasturk H, Firatli E, et al. Resolvin E1 Regulates Th17 Function and T Cell Activation. *Front Immunol* (2021) 12:637983. doi: 10.3389/fimmu.2021.637983
73. Bang S, Xie Y-K, Zhang Z-J, Wang Z, Xu Z-Z, Ji R-R. GPR37 Regulates Macrophage Phagocytosis and Resolution of Inflammatory Pain. *J Clin Invest* (2018) 128(8):3568–82. doi: 10.1172/JCI99888
74. Chiang N, Libreros S, Norris PC, de la Rosa X, Serhan CN. Maresin 1 Activates LGR6 Receptor Promoting Phagocyte Immunoresolvent Functions. *J Clin Invest* (2019) 129(12):5294–311. doi: 10.1172/JCI129448
75. Smigiel KS, Srivastava S, Stolley JM, Campbell DJ. Regulatory T-Cell Homeostasis: Steady-State Maintenance and Modulation During Inflammation. *Immunol Rev* (2014) 259(1):40–59. doi: 10.1111/imr.12170
76. Proto JD, Doran AC, Gusarova G, Yurdagul A, Sozen E, Subramanian M, et al. Regulatory T Cells Promote Macrophage Efferocytosis During Inflammation Resolution. *Immunity* (2018) 49(4):666–677.e6. doi: 10.1016/j.immuni.2018.07.015
77. Sharma M, Schlegel MP, Afonso MS, Brown EJ, Rahman K, Weinstock A, et al. Regulatory T Cells License Macrophage Pro-Resolving Functions During Atherosclerosis Regression. *Circ Res* (2020) 127(3):335–53. doi: 10.1161/CIRCRESAHA.119.316461
78. Gagliani N, Amezcua Vesely MC, Iseppon A, Brockmann L, Xu H, Palm NW, et al. Th17 Cells Transdifferentiate Into Regulatory T Cells During Resolution of Inflammation. *Nature* (2015) 523(7559):221–5. doi: 10.1038/nature14452
79. Gao Y, Su J, Zhang Y, Chan A, Sin JH, Wu D, et al. Dietary DHA Amplifies LXA4 Circuits in Tissues and Lymph Node PMN and is Protective in Immune-Driven Dry Eye Disease. *Mucosal Immunol* (2018) 11(6):1674–83. doi: 10.1038/s41385-018-0070-z
80. Ariyoshi T, Hagihara M, Eguchi S, Fukuda A, Iwasaki K, Oka K, et al. Clostridium Butyricum MIYAIRI 588-Induced Protectin D1 Has an Anti-Inflammatory Effect on Antibiotic-Induced Intestinal Disorder. *Front Microbiol* (2020) 11:587725. doi: 10.3389/fmicb.2020.587725
81. Marques RM, Gonzalez-Nunez M, Walker ME, Gomez EA, Colas RA, Montero-Melendez T, et al. Loss of 15-Lipoxygenase Disrupts Treg Differentiation Altering Their Pro-Resolving Functions. *Cell Death Differ* (2021) 28(11):3140–60. doi: 10.1038/s41418-021-00807-x
82. Chung EH, Jia Y, Ohnishi H, Takeda K, Leung DYM , Sutherland ER, et al. Leukotriene B4 Receptor 1 is Differentially Expressed on Peripheral T Cells of Steroid-Sensitive and -Resistant Asthmatics. *Ann Allergy Asthma Immunol* (2014) 112(3):211–6.e1. doi: 10.1016/j.anai.2013.12.006
83. Chiurchiù V, Leuti A, Saracini S, Fontana D, Finamore P, Giua R, et al. Resolution of Inflammation is Altered in Chronic Heart Failure and Entails a Dysfunctional Responsiveness of T Lymphocytes. *FASEB J* (2019) 33 (1):909–16. doi: 10.1096/fj.201801017R
84. Kooij G, Troletti CD, Leuti A, Norris PC, Riley I, Albanese M, et al. Specialized Pro-Resolving Lipid Mediators are Differentially Altered in Peripheral Blood of Patients With Multiple Sclerosis and Attenuate Monocyte and Blood-Brain Barrier Dysfunction. *Haematologica* (2020) 105(8):2056–70. doi: 10.3324/haematol.2019.219519
85. Jin S, Sun S, Ling H, Ma J, Zhang X, Xie Z, et al. Protectin DX Restores Treg/Th17 Cell Balance in Rheumatoid Arthritis by Inhibiting NLRP3 Inflammasome *via* miR-20a. *Cell Death Dis* (2021) 12(3):280. doi: 10.1038/s41419-021-03562-6
86. Arnardottir HH, Dalli J, Norling LV, Colas RA, Perretti M, Serhan CN. Resolvin D3 Is Dysregulated in Arthritis and Reduces Arthritic Inflammation. *J Immunol* (2016) 197(6):2362–8. doi: 10.4049/jimmunol.1502268
87. Silva CAM, Webb K, Andre BG, Marques MA de M, de Carvalho FM, de Macedo CS, et al. Type 1 Reaction in Leprosy Patients Corresponds With a Decrease in Pro-Resolving and an Increase in Pro-Inflammatory Lipid Mediators. *J Infect Dis* (2016) 215(3):431–9. doi: 10.1093/infdis/jiw541
88. Xia H, Wang F, Wang M, Wang J, Sun S, Chen M, et al. Maresin1 Ameliorates Acute Lung Injury Induced by Sepsis Through Regulating Th17/Treg Balance. *Life Sci* (2020) 254:117773. doi: 10.1016/j.lfs.2020.117773
89. Rajasagi NK, Bhela S, Varanasi SK, Rouse BT. Frontline Science: Aspirin-Triggered Resolvin D1 Controls Herpes Simplex Virus-Induced Corneal Immunopathology. *J Leukoc Biol* (2017) 102(5):1159–71. doi: 10.1189/jlb.3HI1216-511RR
90. Dean S, Wang C-S, Nam K, Maruyama CL, Trump BG, Baker OJ. Aspirin Triggered Resolvin D1 Reduces Inflammation and Restores Saliva Secretion in a Sjögren's Syndrome Mouse Model. *Rheumatol* (2019) 58(7):1285–92. doi: 10.1093/rheumatology/kez072
91. Hua J, Jin Y, Chen Y, Inomata T, Lee H, Chauhan SK, et al. The Resolvin D1 Analogue Controls Maturation of Dendritic Cells and Suppresses Alloimmunity in Corneal Transplantation. *Invest Ophthalmol Vis Sci* (2014) 55(9):5944. doi: 10.1167/iovs.14-14356
92. Arita M, Oh SF, Chonan T, Hong S, Elangovan S, Sun Y-P, et al. Metabolic Inactivation of Resolvin E1 and Stabilization of its Anti-Inflammatory Actions. *J Biol Chem* (2006) 281(32):22847–54. doi: 10.1074/jbc.M603766200
93. Orr SK, Colas RA, Dalli J, Chiang N, Serhan CN. Proresolving Actions of a New Resolvin D1 Analog Mimetic Qualifies as an Immunoresolvent. *Am J Physiol Lung Cell Mol Physiol* (2015) 308(9):L904–911. doi: 10.1152/ajplung.00370.2014
94. Hasturk H, Schulte F, Martins M, Sherzai H, Floros C, Cugini M, et al. Safety and Preliminary Efficacy of a Novel Host-Modulatory Therapy for Reducing Gingival Inflammation. *Front Immunol* (2021) 12:704163. doi: 10.3389/fimmu.2021.704163
95. Trilleaud C, Gauttier V, Biteau K, Girault I, Belarif L, Mary C, et al. Agonist Anti-ChemR23 mAb Reduces Tissue Neutrophil Accumulation and Triggers Chronic Inflammation Resolution. *Sci Adv* (2021) 7(14):eabd1453. doi: 10.1126/sciadv.abd1453

96. Ramon S, Gao F, Serhan CN, Phipps RP. Specialized Proresolving Mediators Enhance Human B Cell Differentiation to Antibody-Secreting Cells. *J Immunol* (2012) 189(2):1036–42. doi: 10.4049/jimmunol.1103483
97. Kim N, Ramon S, Thatcher TH, Woeller CF, Sime PJ, Phipps RP. Specialized Proresolving Mediators (SPMs) Inhibit Human B-Cell IgE Production. *Eur J Immunol* (2016) 46(1):81–91. doi: 10.1002/eji.201545673
98. Kim N, Thatcher TH, Sime PJ, Phipps RP. Corticosteroids Inhibit Anti-IgE Activities of Specialized Proresolving Mediators on B Cells From Asthma Patients. *JCI Insight* (2017) 2(3):e88588. doi: 10.1172/jci.insight.88588
99. Ramon S, Bancos S, Serhan CN, Phipps RP. Lipoxin A_4 Modulates Adaptive Immunity by Decreasing Memory B-Cell Responses *via* an ALX/FPR2-Dependent Mechanism. *Eur J Immunol* (2014) 44(2):357–69. doi: 10.1002/eji.201343316
100. Archambault A-S, Zaid Y, Rakotoarivelo V, Turcotte C, Doré É, Dubuc I, et al. High Levels of Eicosanoids and Docosanoids in the Lungs of Intubated COVID-19 Patients. *FASEB J* (2021) 35(6):e21666. doi: 10.1096/fj.202100540R
101. Schaller MS, Chen M, Colas RA, Sorrentino TA, Lazar AA, Grenon SM, et al. Treatment With a Marine Oil Supplement Alters Lipid Mediators and Leukocyte Phenotype in Healthy Patients and Those With Peripheral Artery Disease. *J Am Heart Assoc* (2020) 9(15):e016113. doi: 10.1161/JAHA.120.016113
102. Li X, Bi X, Wang S, Zhang Z, Li F, Zhao AZ. Therapeutic Potential of ω-3 Polyunsaturated Fatty Acids in Human Autoimmune Diseases. *Front Immunol* (2019) 10:2241. doi: 10.3389/fimmu.2019.02241
103. Barry AR, Dixon DL. Omega-3 Fatty Acids for the Prevention of Atherosclerotic Cardiovascular Disease. *Pharmacotherapy* (2021). doi: 10.1002/phar.2615
104. Djuricic I, Calder PC. Beneficial Outcomes of Omega-6 and Omega-3 Polyunsaturated Fatty Acids on Human Health: An Update for 2021. *Nutrients* (2021) 13(7):2421. doi: 10.3390/nu13072421

Conflict of Interest: SP is the CEO and shareholder of MED'INN'Pharma, which develops pro-resolutive drug candidates.

The remaining authors declare that the research was conducted in the absence of any commercial or financial relationships that could be construed as a potential conflict of interest.

Publisher's Note: All claims expressed in this article are solely those of the authors and do not necessarily represent those of their affiliated organizations, or those of the publisher, the editors and the reviewers. Any product that may be evaluated in this article, or claim that may be made by its manufacturer, is not guaranteed or endorsed by the publisher.

Copyright © 2021 Perez-Hernandez, Chiurchiù, Perruche and You. This is an open-access article distributed under the terms of the Creative Commons Attribution License (CC BY). The use, distribution or reproduction in other forums is permitted, provided the original author(s) and the copyright owner(s) are credited and that the original publication in this journal is cited, in accordance with accepted academic practice. No use, distribution or reproduction is permitted which does not comply with these terms.

frontiers in Immunology

ORIGINAL RESEARCH
published: 08 December 2021
doi: 10.3389/fimmu.2021.734322

Transcriptional and Histochemical Signatures of Bone Marrow Mononuclear Cell-Mediated Resolution of Synovitis

Bruno C. Menarim[1,2], Hossam El-Sheikh Ali[2,3], Shavahn C. Loux[2], Kirsten E. Scoggin[2], Theodore S. Kalbfleisch[2], James N. MacLeod[2] and Linda A. Dahlgren[1]*

[1] Department of Large Animal Clinical Sciences, Virginia-Maryland College of Veterinary Medicine, Virginia Tech, Blacksburg, VA, United States, [2] Gluck Equine Research Center, Department of Veterinary Sciences, College of Agricultural, Food and Environment, University of Kentucky, Lexington, KY, United States, [3] Theriogenology Department, Faculty of Veterinary Medicine, Mansoura University, Mansoura, Egypt

OPEN ACCESS

Edited by:
Amiram Ariel, University of Haifa, Israel

Reviewed by:
Adam Paul Cribbs, University of Oxford, United Kingdom
Florien Jenner, University of Veterinary Medicine Vienna, Austria
Laure Campillo-Gimenez, University of California, San Diego, United States

***Correspondence:**
Bruno C. Menarim
bruno.menarim@uky.edu

Specialty section:
This article was submitted to Inflammation, a section of the journal Frontiers in Immunology

Received: *30 June 2021*
Accepted: *09 November 2021*
Published: *08 December 2021*

Citation:
Menarim BC, El-Sheikh Ali H, Loux SC, Scoggin KE, Kalbfleisch TS, MacLeod JN and Dahlgren LA (2021) Transcriptional and Histochemical Signatures of Bone Marrow Mononuclear Cell-Mediated Resolution of Synovitis. Front. Immunol. 12:734322. doi: 10.3389/fimmu.2021.734322

Osteoarthritis (OA) may result from impaired ability of synovial macrophages to resolve joint inflammation. Increasing macrophage counts in inflamed joints through injection with bone marrow mononuclear cells (BMNC) induces lasting resolution of synovial inflammation. To uncover mechanisms by which BMNC may affect resolution, in this study, differential transcriptional signatures of BMNC in response to normal (SF) and inflamed synovial fluid (ISF) were analyzed. We demonstrate the temporal behavior of co-expressed gene networks associated with traits from related *in vivo* and *in vitro* studies. We also identified activated and inhibited signaling pathways and upstream regulators, further determining their protein expression in the synovium of inflamed joints treated with BMNC or DPBS controls. BMNC responded to ISF with an early pro-inflammatory response characterized by a short spike in the expression of a NF-ĸB- and mitogen-related gene network. This response was associated with sustained increased expression of two gene networks comprising known drivers of resolution (*IL-10, IGF-1, PPARG*, isoprenoid biosynthesis). These networks were common to SF and ISF, but more highly expressed in ISF. Most highly activated pathways in ISF included the mevalonate pathway and PPAR-γ signaling, with pro-resolving functional annotations that improve mitochondrial metabolism and deactivate NF-ĸB signaling. Lower expression of mevalonate kinase and phospho-PPARγ in synovium from inflamed joints treated with BMNC, and equivalent IL-1β staining between BMNC- and DPBS-treated joints, associates with accomplished resolution in BMNC-treated joints and emphasize the intricate balance of pro- and anti-inflammatory mechanisms required for resolution. Combined, our data suggest that BMNC-mediated resolution is characterized by constitutively expressed homeostatic mechanisms, whose expression are enhanced following inflammatory stimulus. These mechanisms translate into macrophage proliferation optimizing their capacity to counteract inflammatory damage and improving their general and mitochondrial metabolism to endure oxidative stress while driving tissue

repair. Such effect is largely achieved through the synthesis of several lipids that mediate recovery of homeostasis. Our study reveals candidate mechanisms by which BMNC provide lasting improvement in patients with OA and suggests further investigation on the effects of PPAR-γ signaling enhancement for the treatment of arthritic conditions.

Keywords: macrophage, arthritis, mevalonate pathway, oxidative stress, joint therapy

INTRODUCTION

Osteoarthritis (OA) is a common and debilitating condition that similarly affects horses and people (1, 2). Because chronic synovial inflammation is a hallmark of OA and often the single driver of related degenerative changes (3–7), the use of anti-inflammatory drugs (steroidal and non-steroidal) has been a logical and long-accepted approach for the treatment of many arthritic conditions (8, 9). However, acute inflammation is not simply a clinical sign to alleviate. Acute inflammation is a critical event in promoting tissue repair and setting the stage for endogenous resolution of the inflammatory process and recovery of homeostasis (10). Importantly, anti-inflammatory and pro-resolving effects are not the same, and resolution is not merely the passive termination of the inflammatory process. Anti-inflammation is based on inhibiting key pro-inflammatory mediators, such as chemokine and cytokine production and leukocyte extravasation to the site of injury. Resolution is an active process driven primarily by macrophages and their derived cytokines and lipid mediators, which shift the phlogistic phase of inflammation into a non-phlogistic process that culminates with tissue repair and recovery of homeostasis (11, 12). Most importantly, the recruitment of macrophages and the production of pro-resolving mediators is triggered by enzymes synthesized during the acute inflammatory process (13). Macrophages play such a fundamental role in resolving inflammation and promoting tissue repair that impaired macrophage chemotaxis and/or macrophage depletion results in inefficient healing or chronic inflammation (14–16). Blocking acute inflammation with anti-inflammatory medications interferes, at least to some degree, with macrophage recruitment and the pro-resolving response, and often prevents effective resolution and recovery of homeostasis (12, 13). Targeted therapies for chronic joint inflammation should therefore have pro-resolving properties, which precisely combine pro- and anti-inflammatory mechanisms (12).

Abbreviations: OA, osteoarthritis; BMNC, bone marrow mononuclear cells; IL, interleukin; IGF-1, insulin-like growth factor 1; PGE_2, prostaglandin E_2; NF-ƙB, nuclear factor – kappa B; SF, normal synovial fluid; ISF, inflamed synovial fluid; DPBS, Dulbecco's phosphate buffered saline; LPS, lipopolysaccharide; CSF1, colony-stimulating factor 1; SDF-1, stromal derived factor-1; IL-1ra, interleukin-1 receptor antagonist; WGCNA, weighted gene co-relation analysis; FPKM, fragments per kilobase of transcript per million mapped reads; DEGs, differentially expressed genes; GO, gene ontology; IPA, ingenuity pathway analysis; PPAR-γ peroxisome proliferator-activated receptor-gamma; PPARGC1A, PPAR-γ co-activator 1-α; TLR3, toll-like receptor 3; MAFB, transcription factor MAFB; SIRT2, sirtuin 2; FN1, fibronectin 1; PCA, principal component analysis; BP, biological process; STAT, signal transducer and activator of transcription; DAMP, damage-associated molecular pattern.

Synovial macrophages are the central drivers of the inflammatory response in osteoarthritic synovium (17, 18). In fact, synovial macrophage activation is directly related to disease activity, severity, and pain in OA-affected patients (19). However, this relationship is not causative. Synovial macrophages are also essential keepers of synovial homeostasis through phagocytic clearance and secretion of anti-inflammatory and pro-resolving cytokines, chemokines, enzymes, and growth factors (20–23). Following injury, synovial macrophages proliferate to form a protective immunological barrier in the synovial lining for intra-articular structures (24, 25). When regulatory functions are overwhelmed by the amount of damage, synovial macrophages upregulate inflammation, signaling to monocytes and other leukocytes (e.g., neutrophils and lymphocytes) to help counteract the increased demands for tissue repair and restore homeostasis (17, 26). During the progression of OA, the recruitment of myeloid monocytes into joints seems to be impaired (27), which combined with continuous joint damage, overwhelms the pro-resolving mechanisms of synovial macrophages, leading to degeneration (17, 27, 28).

The mononuclear cell fraction of bone marrow aspirates (bone marrow mononuclear cells -BMNC) is a rich source of pro-resolving macrophages that have been used therapeutically to improve tissue repair and inflammation resolution (29–39). Macrophages within BMNC are the main drivers of such effect, which's documented pro-resolving functions include increased production of IL-10 (30, 33), diverse types of prostaglandins and specialized lipid mediators (13, 40, 41). The production of these molecules induce decreased production of IL-6 (33), increased phagocytic clearance of debris and apoptotic cells (efferocytosis) (30, 39) and enhanced PPAR-gamma signaling (42–47). Increasing the numbers of myeloid macrophages present in osteoarthritic knees, by injection of BMNC, restored joint homeostasis with long-lasting effects (48). Similarly, BMNC therapy increased counts of pro-resolving macrophages and induced marked resolution of joint inflammation in *in vivo* and *in vitro* models of equine synovitis (49, 50). In these models, there was a coordinated spectrum of pro-inflammatory, pro-resolving and anti-inflammatory events, including increased IL-10, IGF-1, and PGE_2 production, and self-limiting IL-1 signaling (α and β). These events are all innately required for efficient synovial homeostasis and tissue repair and are commonly antagonized by therapeutic corticosteroids (30, 51–53). While these findings partially explain the durable effects of BMNC in the treatment of OA, little is known about BMNC-related mechanisms of resolution. Therefore, our purpose was to identify cellular mechanisms from BMNC driving joint homeostasis that could

be used for developing targeted pro-resolving joint therapies and uncovering biomarkers of arthritis resolution. The aim of this study was to identify transcriptional signatures of BMNC leading to inflammation resolution using RNA-sequencing and relate these to the expression of key gene products in the synovial membrane. We hypothesized that gene networks linked to macrophage proliferation, negative regulation of inflammatory response, and to a lesser extent, NF-ƙB signaling, would be temporally upregulated in response to inflammation.

MATERIALS AND METHODS

Study Design

Samples used in the current report were obtained from two previous studies using the same horses. These *in vitro* (50) and *in vivo* (49) studies were counterparts of a larger project assessing the effects of BMNC on joint inflammation resolution. Briefly, eight skeletally mature Thoroughbred horses (3-9 years old, median 5 years; 2 females and 6 castrated males) free of OA or systemic inflammation were used under IACUC approval and oversight. General and musculoskeletal health were confirmed by clinical, hematological and orthopedic evaluations. Following sternal bone marrow aspiration for BMNC isolation, synovitis was induced in both radiocarpal joints, as a way of producing more homogeneous inflammation and inflamed synovial fluid (ISF) than could be acquired from naturally occurring OA. Normal synovial fluid (SF) was collected from healthy middle carpal joints. BMNC from each horse were cultured independently (not pooled) in neat (100%) autologous SF or ISF and harvested at 0 (uncultured), 48 and 96 hours, and 6 and 10 days for RNA isolation. RNA-seq was used to identify transcriptional signatures of BMNC in response to acute joint inflammation. The transcriptome of BMNC was assessed over time within the same group (SF or ISF), as well as comparatively between groups at each time point (**Figure 1**). The expression of 9 potential upstream regulator genes identified following bioinformatical analysis was assessed by immunohistochemistry in the synovium of inflamed joints from the same horses, 6 days after treatment with BMNC or Dulbecco's phosphate buffered saline (DPBS). Four protein coded by genes identified in key activated pathways were also assessed by IHC.

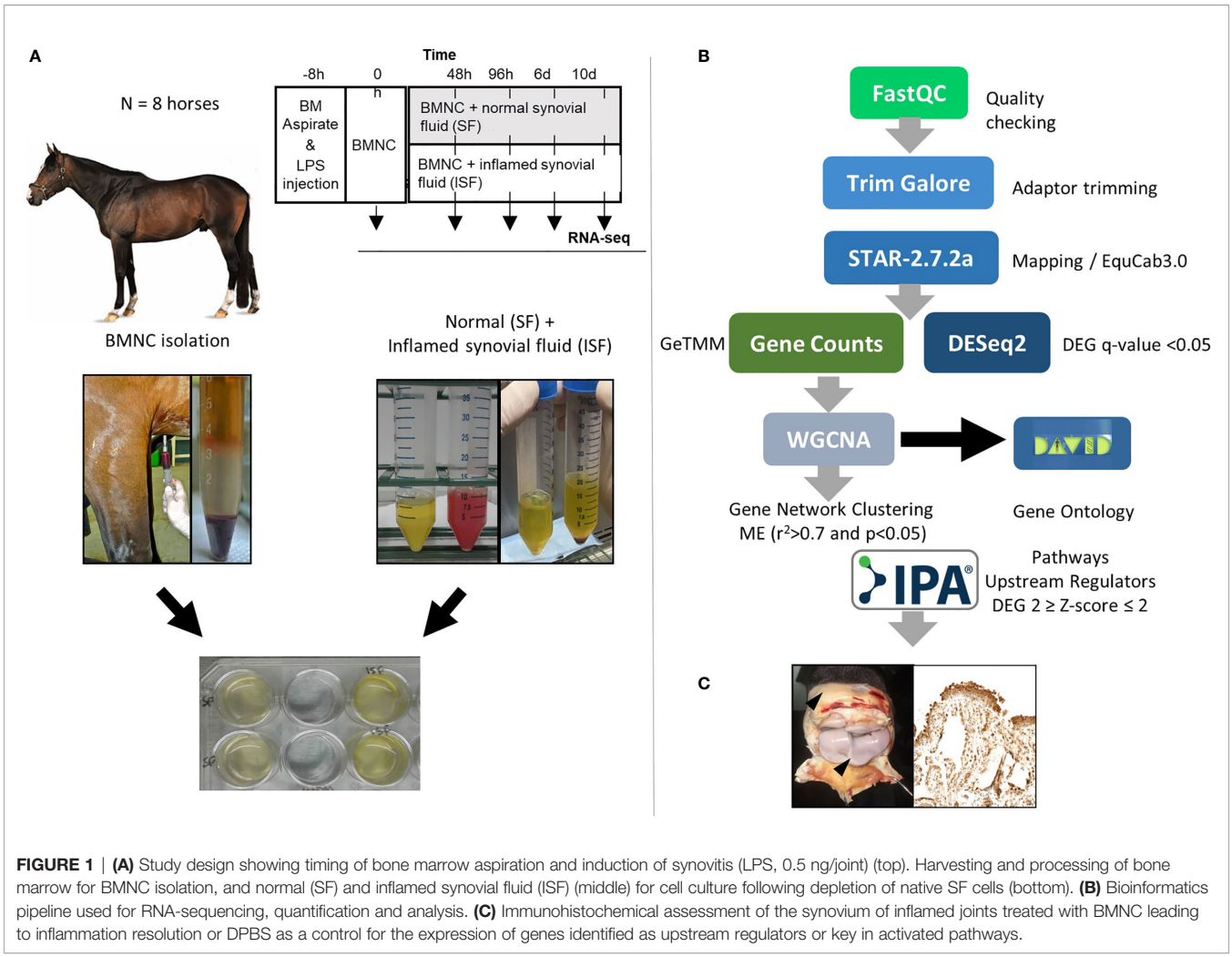

FIGURE 1 | **(A)** Study design showing timing of bone marrow aspiration and induction of synovitis (LPS, 0.5 ng/joint) (top). Harvesting and processing of bone marrow for BMNC isolation, and normal (SF) and inflamed synovial fluid (ISF) (middle) for cell culture following depletion of native SF cells (bottom). **(B)** Bioinformatics pipeline used for RNA-sequencing, quantification and analysis. **(C)** Immunohistochemical assessment of the synovium of inflamed joints treated with BMNC leading to inflammation resolution or DPBS as a control for the expression of genes identified as upstream regulators or key in activated pathways.

BMNC Isolation, Induction of Synovitis, and Synovial Fluid Harvest

Bone marrow harvest and processing of BMNC, and induction of the synovitis model were performed as previously described in our related study (49). Briefly, BMNC were isolated by density gradient centrifugation. Synovitis was induced by intra-articular injection of 0.5 ng lipopolysaccharide (LPS) into each radiocarpal joint (49, 54). At peak inflammation (8 hours following induction of the model), SF and ISF were collected using aseptic technique. Synovial fluid cytology (SF and ISF) was performed to confirm the health of normal joints and ensure LPS effectively induced synovitis. Synovial fluid was then centrifuged (5,000g; 20 min; 4°C) for cell depletion and the cell-free supernatant used as autologous growth medium. Parameters used to differentiate SF from ISF included quantification of cytokine as reported in our related study (50), total protein (<2.5 g/dL in SF and >4g/dL in ISF) and synovial fluid cytology (total nucleated cells/μL < 1,500 in SF and ~130,000 in ISF; neutrophil count <10% in SF and >80% in ISF).

BMNC Culture in SF and ISF

BMNC were plated in 24 well culture plates ($2x10^6$ viable cells/50 μL DPBS/well) and covered with 500 μL SF or ISF. Cell viability was assessed at baseline using trypan blue and ranged from 74-96% across horses. Well contents were carefully mixed and plates incubated at 37°C in 5% CO_2 and 90% humidity. Remaining SF and ISF was preserved at 4°C for later addition of medium to replenish cell nutrients (200 μL added every 48 hours). All conditions and time points were performed in duplicate wells with cells from one well used for RNA-sequencing and the other for flow cytometry (macrophage activation markers CD14, CD86, CD206 and IL-10). Conditioned medium was aspirated at the same time points of cell harvest (48 and 96 hours and 6 and 10 days) centrifuged, and the cell-free supernatant used for cytokine and growth factor quantification (FGF-2, GM-CSF, IL-1β, IL-6, MCP-1, IL-10, TNF-α, SDF-1, IGF- 1, IL-1ra, and PGE_2) using a PGE_2 ELISA kit (KGE004B; R&D Systems) and the Milliplex Map Equine chemokine/cytokine bead based array (Eqcttmag-93K,; MilliporeSigma). Details and findings from flow cytometry and cytokine and growth factor quantification are reported elsewhere (50) and were used in this study as a trait for weighted gene co-relation network analysis (WGCNA).

Transcriptome Analysis of BMNC Cultured in SF and ISF

RNA Isolation and Sequencing

Cultured cells were recovered in 10 mM EDTA, centrifuged (12,000g; 10 min; 4°C) and the cell pellet placed in guanidinium chloride-phenol (Trizol®, Life Technologies, 15596018, Carlsbad, CA). RNA was purified with on-column DNase digest (DirectZol™ RNA microprep kit, R2061, Zymo Research, Irvine, CA), quantified (Qubit® 3.0 Fluorometer, 33216, ThermoFisher Scientific, Carlsbad, CA), and stored at -80°C. RNA quality was assessed (Bioanalyzer 2100, Agilent Technologies, Santa Clara, CA) and cDNA libraries prepared using TruSeq DNA Library Preparation kits (Illumina, Inc., San Diego, CA), followed by sequencing (NovaSeq 6000 S4, Illumina) to generate an average of 34.5 (range, 24-54) million stranded paired-end reads (2 x 150 nt) per sample.

Bioinformatics Pipeline

Reads were trimmed for quality and adapters with TrimGalore 0.4.3 and mapped to the equine reference genome (EquCab 3.0) (55) using STAR (56) algorithm (version 2.7.2a) and GeneCounts, and expression values determined as gene length corrected trimmed mean of M-values (GeTMM) (57) with the Ensembl v104 annotation. Differentially expressed genes (DEGs) were determined using DESeq2 based upon a false discovery rate (FDR) adjusted *P*-value (q-value) <0.05 after Benjamini–Hochberg correction for multiple testing, by comparing datasets from consecutive time points within SF or ISF, and by comparing ISF to SF datasets at any given time point. The cutoff set for considering a transcript expressed prior to analysis was 10 fragment alignments. DEGs were represented by principal component analysis using JMP Pro 13 and by volcano plots using Origin software (version 2019, OriginLab, Northampton, MA, USA).

Functional Genomics

We adopted a multidisciplinary approach to functional genomics by employing several bioinformatics tools to tease out the biological significance of our data. We used WGCNA and DAVID in a semi-supervised analysis to identify biological processes of interest, and IPA to identify upstream regulators and activated and inhibited signaling pathways. By using this approach, we took advantage of both the superior annotation of biological processes from DAVID and the better pathway annotation of IPA. Together, these tools enabled us to make associations to our previous clinical studies to start to draw clinical translations to our findings.

Weighted gene co-relation analysis was performed using WGCNA version 1.66 package in R to construct gene co-expression networks as described elsewhere (58, 59). Gene co-expression clusters were generated from the whole transcriptome in SF and ISF datasets separately over time. Only genes expressed in at least 50% of samples in each dataset were included in the analysis (16,318 genes in SF and 18,038 genes in ISF). In order to normalize the data, the GeTMM values for each gene were log2 transformed. Next, a pairwise correlation matrix was constructed between all pairs of genes across the samples, and a matrix of weighted adjacency was generated by raising co-expression to a power $\beta = 9$, as determined for our sample set (58, 60). A topological overlap matrix (TOM) was then assembled and used as input for hierarchical clustering analysis. Then, a dynamic tree cutting algorithm was used to identify gene clusters or modules (i.e., genes with high topological overlap) in an unsupervised fashion. Gene modules were visualized by heatmap plot (TOMplot) of the gene network topological overlap. Module relationships were summarized by a hierarchical clustering dendrogram and TOMplot of module eigengenes (MEs). Associations between gene modules and traits of interest were tested by correlating MEs to trait score. Module–trait

correlations were visualized using a heatmap plot and only modules with trait relationship significance (R^2) higher than 0.7 and a p-value ≤0.05 were considered for further analysis. Traits of interest used for WGCNA included: timeline from our previous study, previously reported CD14, CD86, CD206 and IL-10 expression measured by flow cytometry, and IL-10, IGF-1, MCP-1, IL-1β, TNF-α, PGE_2 and SDF-1 concentrations quantified in conditioned SF and ISF (50). Module memberships (MM; correlation between each gene expression profile (GeTMM) and the ME of a given module as an indicator of the intramodular connectivity) and gene significance (GS; correlation between the gene expression profile (GeTMM) and the trait score (e.g. cytokine concentration in conditioned SF/ISF) as a measure of biological relevance) were calculated (58). Genes (network nodes) having MM ≥ 0.90, *P*-value < 0.05, and GS ≥ 0.5 were identified as intramodular hub genes (61). Gene ontology (GO) analysis was performed on the entire gene list derived from each module as described above using DAVID Bioinformatics Resources version 6.8 (62) to functionally annotate their biological processes (BP). Of note, no single time point was chosen to determine the module-trait correlations. The entire timeline of the study was itself a trait. Therefore, genes within each module were co-expressed at all time points and thus dominant (overrepresented) BPs for a given module were the same at all time points.

To predict upstream regulators relevant for each set of DEGs, analysis was performed using the Ingenuity Pathway Analysis software (IPA, 2018) (63). The analysis output provided a *P*-value of overlap, activation Z-scores, and the downstream targets for each predicted upstream regulator. Z-scores were used to predict activation state (activation or inhibition) of each upstream regulator/signaling pathway. Predicted upstream regulators were considered significant if they had $P < 0.05$ and activation Z-score >2 (activated) or <−2 (inhibited). Subsequently, we investigated overlap between the predicted upstream regulators for each set and the DEGs from the same set to identify potential regulators among those DEGs. Genes in common between the two analyses with Z-scores (generated by IPA) matching the direction of fold change (generated by DESeq2) were defined as potential regulators. To investigate the interaction and relationships between potential upstream regulators, all known protein–protein interactions were referenced and matched using STRING version 10.5 (64). Potential upstream regulators of high interaction were selected to have their protein expression assessed in synovium from inflamed joints treated with BMNC or DPBS, as a means of identifying candidate biomarkers of BMNC-mediated resolution. Synovial membrane samples were obtained from a related study in which BMNC therapy induced marked inflammation resolution (49) and represented inflamed joints treated with autologous BMNC or DPBS. IPA was also used to determine activated and inactivated signaling pathways, considering significance at $P < 0.05$ and activation Z-score >2 (activated) or <−2 (inhibited) and a -log(p-value > 1.3, which corresponds to p>0.05). For cases in which a large list of pathways met this criterion, those with a -log(p-value > 3 (FDR <0.01) were given priority attention.

Immunohistochemistry

Formalin-fixed paraffin-embedded synovial membrane samples from inflamed joints of 6 horses treated with either BMNC or DPBS were sectioned at 5-7 μm and baked at 38°C for 48 hours. Sectioned tissues were processed with the BOND-MAX system (Leica Microsystems, Buffalo Groove, IL) using antibodies for the following gene-products, identified as key upstream regulators or key genes from most activated pathways: peroxisome proliferator-activated receptor γ (PPARγ; rabbit anti-human, clone 16643-1-AP, ThermoFisher Scientific), phospho- PPARγ (rabbit anti-human, clone PA536763, ThermoFisher Scientific), PPARγ co-activator 1 alpha (PPARGC1A; rabbit anti-human, clone PA5-38021; ThermoFisher Scientific), mevalonate kinase (MVK; rabbit anti-human, clone PA528650, ThermoFisher Scientific), 3-Hydroxy-3-Methylglutaryl-CoA Synthase 1 (HMGCS1; rabbit anti-human, clone PA529488, ThermoFisher Scientific), colony-stimulating factor 1 (CSF1; rabbit anti-mouse, clone PA5-95279; ThermoFisher Scientific), interleukin-1β (IL-1β; rabbit anti-human, clone P420B; Invitrogen), transcription factor MAFB (MAFB; rabbit anti-human, clone PA5-40756; ThermoFisher Scientific) and sirtuin 2 (SIRT2; rabbit anti-human, clone PA3-200; ThermoFisher Scientific). Positive controls included equine liver, heart, and kidney. Negative controls were prepared with mouse (for PPARγ, phospho-PPARγ, MVK, HMGCS1, PPARGC1A, IL-1β, MAFB, SIRT2 antibodies) or goat (CSF1) IgG (Santa Cruz Biotechnology, Inc.). Photographs of representative areas were scored by 3 experienced investigators for staining intensity (0-absent, 1-mild, 2-moderate, 3-intense) and distribution (0-absent, 1-scattered, 2-focal, 3- across the entire villi lining) as previously described (49). Composite scores for immunohistochemical data were presented as median and 95% confidence interval and analyzed by paired t-tests with significance set as $p \leq 0.05$ using Prism GraphPad 7.

RESULTS

Temporal Transcriptional Changes in BMNC Following Culture in SF and ISF

Differential Gene Expression

Principal component analysis (PCA) of DEGs between BMNC cultured in SF and ISF showed clear differences in clustering patterns as early as 48 hours, and progressively diverged over time, representative of differences in BMNC response to normal and inflammatory environments (**Figure 2A**). Volcano plots depict up and downregulated DEGs when comparing ISF to SF cultures at each time point (**Figure 2B**). Vertical and horizontal comparisons were made, with the number of DEGs between any two conditions reported (**Figure 2C**). In vertical comparisons, ISF cultures were compared to their SF counterparts at each time point. Counts of upregulated genes were most remarkable at 96 hours and 6 days. In horizontal comparisons, each subset of BMNC was compared with its nearest time point to analyze gene expression variation from BMNC response along the timeline.

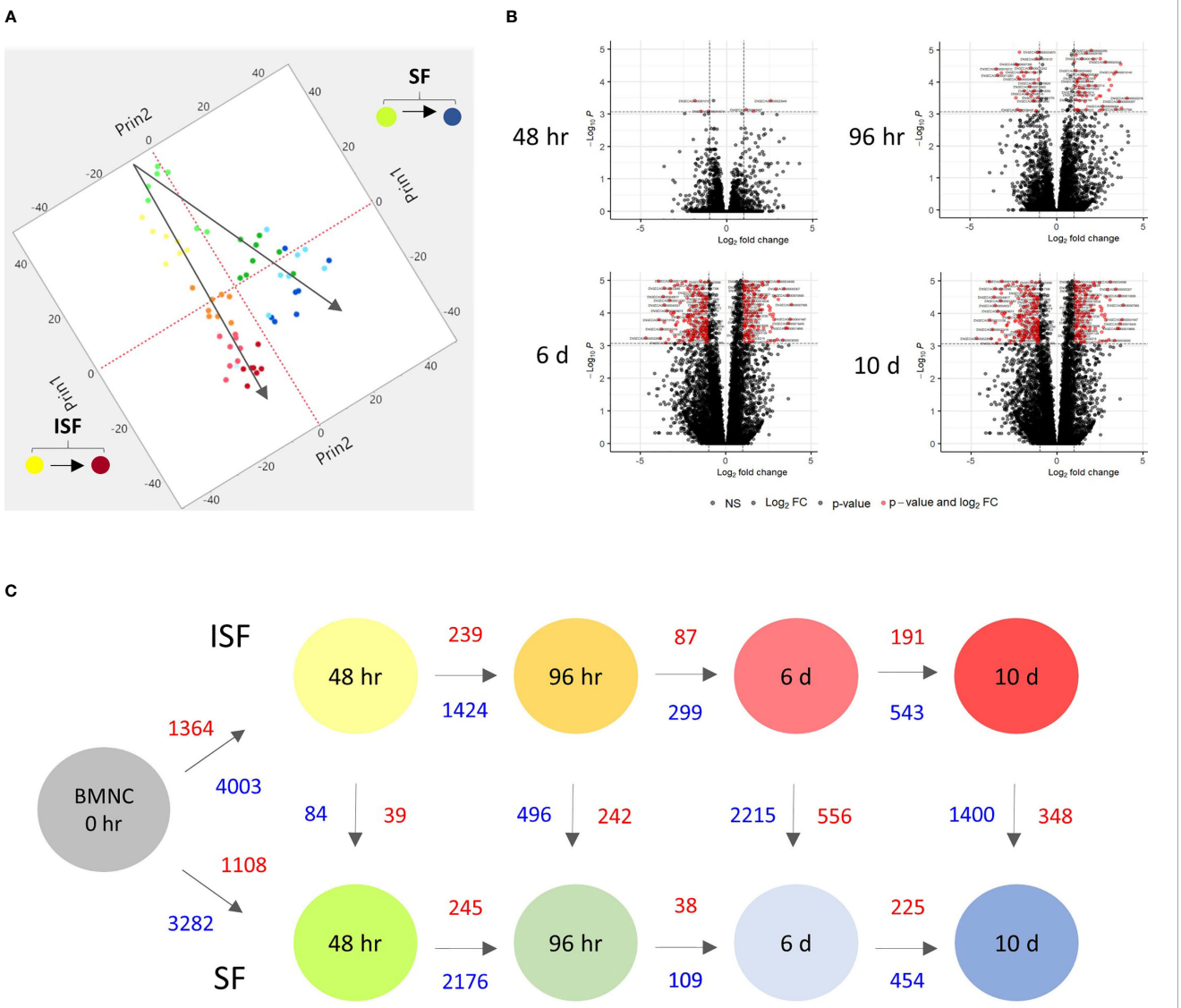

FIGURE 2 | Kinetics of transcriptional signatures of BMNC cultured in SF and ISF. **(A)** Principal Component Analysis from 8456 genes differentially expressed (DEGs) by BMNC following culture in SF (green to blue dots; top) and ISF (yellow to red dots; bottom) for 10 days shows increasing divergence in the patterns of gene expression over time. Each dot color represents a different time point and each dot represents an individual horse. **(B)** Volcano plots depicting downregulated (left red quadrant) and upregulated (right red quadrant) DEGs in ISF compared to SF cultures at each time point, showing major changes at 6 days. **(C)** Schematic of changes in gene expression of BMNC cultured in SF (bottom) and ISF (top) for 10 days, depicting the number of DEGs over consecutive time points within groups (horizontal comparisons in SF or ISF) and between groups (vertical comparisons) at each time point (FDR ≤0.05). Numbers represent upregulated (red text) and downregulated genes (blue text) between the compared conditions.

From baseline to 48 hours, when myeloid progenitors in BMNC commit to the monocyte/macrophage lineage, the number of DEGs was highest among all time points, for both SF and ISF. The expression patterns of DEGs identified in all vertical and horizontal comparisons were also visualized by heat map (**Figure 3A**). Further, Venn diagrams were used to illustrate the intersection between DEGs identified by horizontal comparisons and revealed that SF and ISF cultures shared 64.9% of DEGs over the 10 days, while those expressed exclusively in the SF or ISF dataset represented 15.0% and 20.1%, respectively (**Figure 3B**). Upset plots elucidating the intersection between DEGs identified by vertical comparisons revealed that most DEGs were exclusively expressed in ISF cultures at 6 days (**Figure 3C**). An entire list of DEGs is available at **Supplementary Table 1**.

Co-Expression Network Analysis From BMNC in Response to Inflammation

WGCNA provided further insights into the patterns of gene co-expression and the identification of genes with the highest

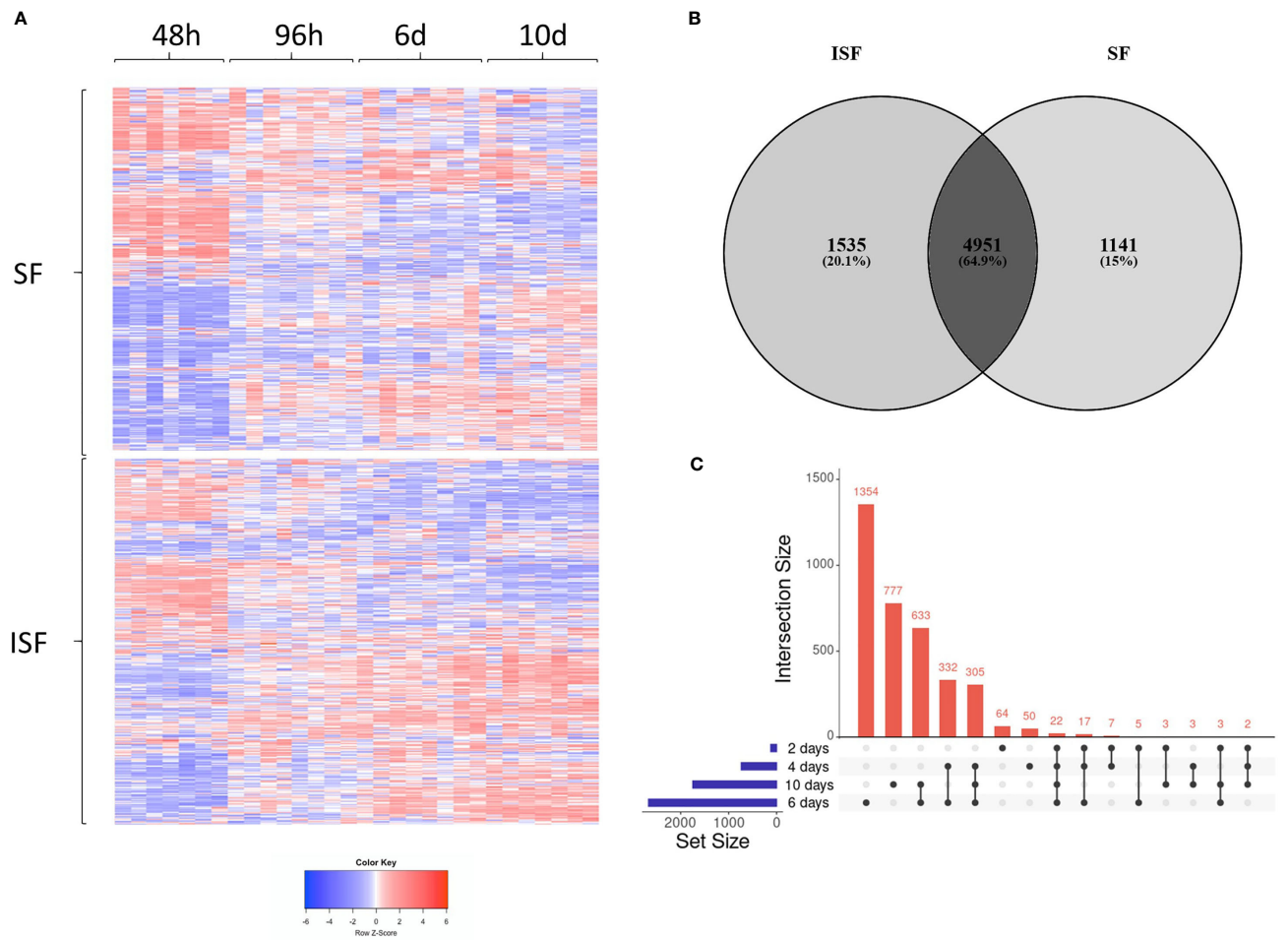

FIGURE 3 | Differentially expressed genes (DEGs) in BMNC cultured in normal (SF) and inflamed autologous synovial fluid (ISF). **(A)** Heatmap of DEGs (FDR<0.05) identified among all possible comparisons (n=8456) between SF and ISF cultures over 10 days. The heatmap was created using Log10 transformed GeTMM values expressed on a color scale denoting high (red) and low (blue) expression. Each dataset (SF and ISF) included all DEGs displayed in a fixed position for comparison of the effect of culture medium over the same genes. **(B)** Venn diagram illustrating the intersection between DEGs identified by horizontal comparisons in either SF or ISF cultures. **(C)** Upset plots elucidating the intersection between DEGs identified by vertical comparisons. The nature of each intersection is indicated by the dots under the vertical bars, which denote the number of DEGs in each intersection, while horizontal bars represent the number of DEGs in each comparison.

interaction or connectivity (hub genes) among SF and ISF datasets separately (hub genes are denoted by bold cells in **Supplementary Table 2**). Co-expression analysis of 18,038 genes in ISF identified 11 module eigengenes (i.e., clusters) (**Figure 4A**). Among these, modules turquoise, green, blue, brown, black and pink were positively associated with three of the assigned traits. The turquoise and green modules were positively associated with IL-1β concentrations in conditioned ISF, and thus interpreted as having an overall pro-inflammatory nature. Modules blue, brown, black and pink were positively associated with the timeline. The blue module was also associated with CD86 expression assessed by flow cytometry, which denotes macrophage activation (50). In the SF dataset, analysis of the 16,318 genes identified the same 11 gene modules; however, the timeline was the only trait with a positive relationship to MEs, which like ISF included the blue, brown, black and pink modules (**Figure 4B**). Thus, the IL-1β-related green and turquoise modules are the standout, inflammation-associated differences between ISF and SF cultures, while the blue module also differed in the number of positively associated traits. Since events associated with inflammation resolution would only be present in an inflammatory environment, further dissection of WGCNA findings were centered on data from ISF cultures, while data from SF cultures were used as a point of comparison.

To assess the temporal behavior of each module, the mean expression profile (mean GeTMM values for all genes) for each module was plotted over time for both SF and ISF separately (**Figure 5A**). This comparison revealed that the blue and brown modules exhibited increasing mean expression profiles that similarly dominated over time in both SF and ISF, which however, were higher in ISF. The pink and black modules had lesser expression among modules identified which completely

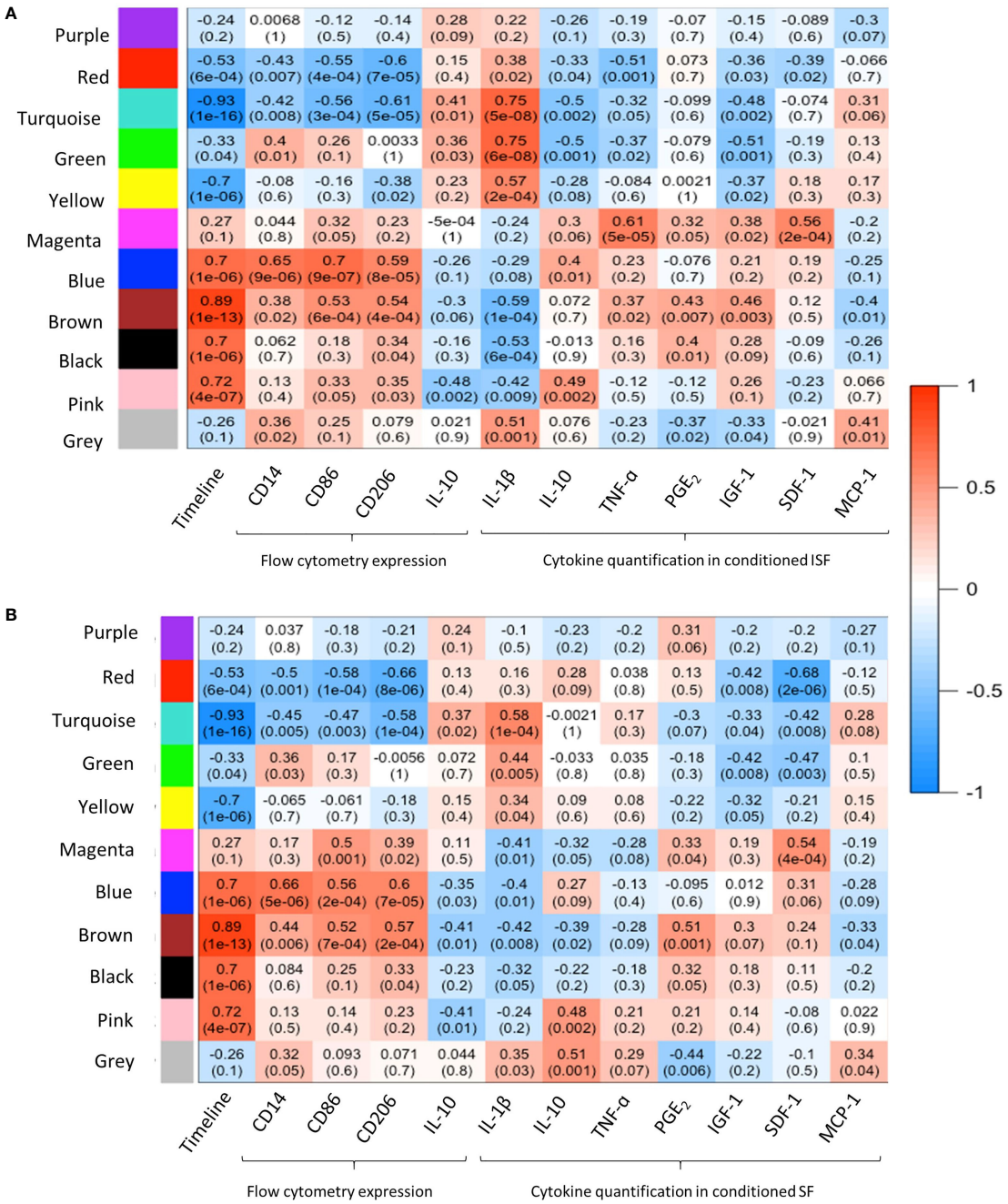

FIGURE 4 | Weighted gene co-expression network analysis (WGCNA): module-trait relationships. **(A)** WGCNA of 18,038 genes in ISF identified 11 modules eigengene (ME), of which 6 were positively associated ($R^2 \geq 0.7$, $p = \leq 005$) with the assigned traits. The turquoise and green modules were positively associated with IL-1β quantification in ISF conditioned by BMNC. MEs blue, brown, black and pink were positively associated with the timeline. The blue module was also associated with CD86 expression assessed by flow cytometry (29). **(B)** In the SF dataset, analysis of the 16,318 genes identified the same 11 gene modules; however, timeline was the only trait with a positive association to MEs blue, brown, black and pink modules, as in ISF.

overlapped between SF and ISF, and therefore are not graphically represented. Additional comparisons for a given module between ISF and its SF counterpart also included the functional annotation of the genes within such modules (**Figures 5B–E**). The blue, brown, black and pink modules completely overlapped between ISF and SF regarding their gene list, HUB genes list (**Supplementary Table 2**) and functional annotations (**Supplementary Tables 3, 4**). Exclusive to ISF, the green module peaked at 48 hours, the same time at which the blue and brown modules started to exhibit increased expression in

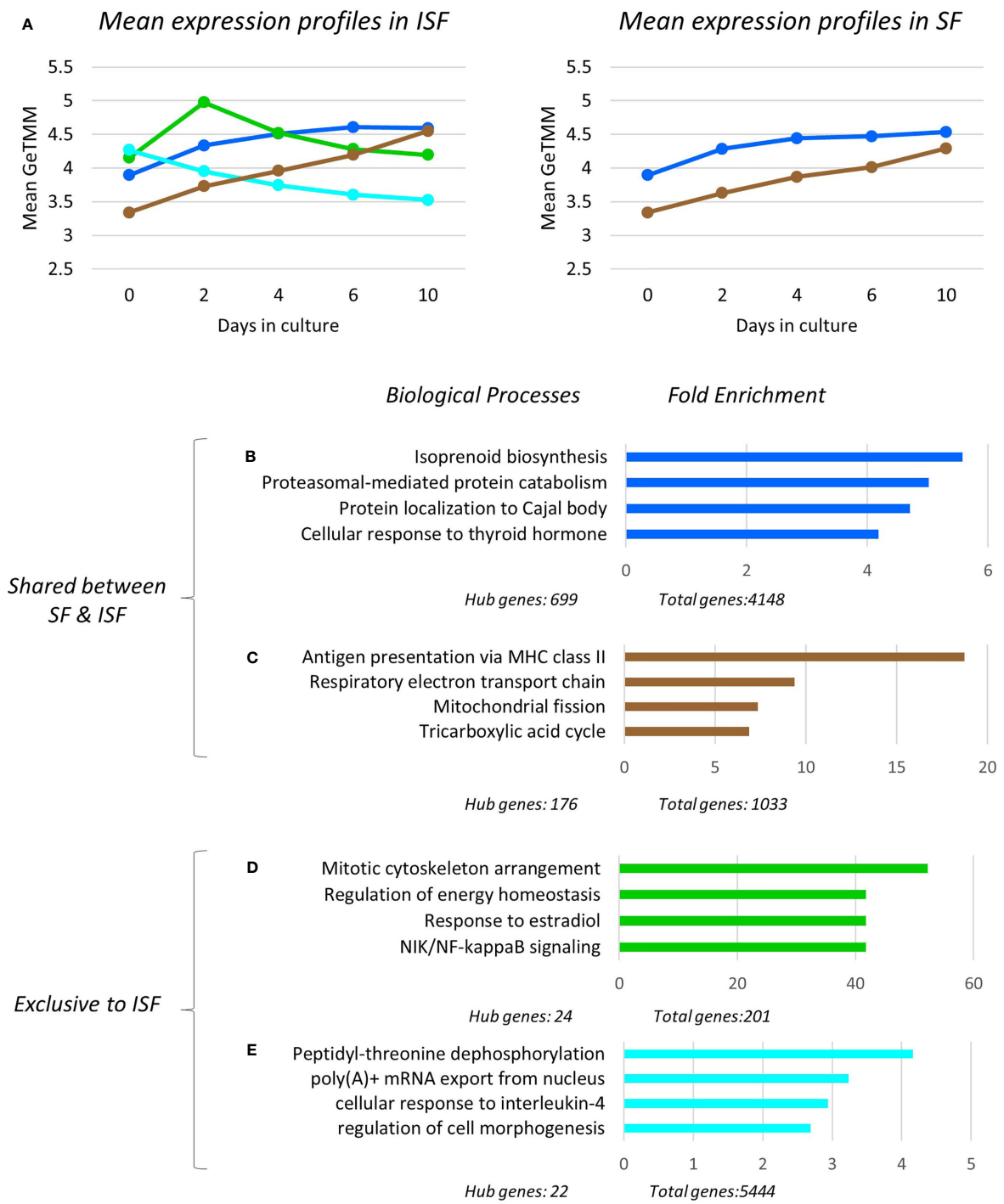

FIGURE 5 | Expression profile, gene ontology enrichment and overrepresented biological processes within dominant modules. The green and turquoise modules were only significant in ISF and positively associated with IL-1β quantification in conditioned ISF, and overall associated with pro-inflammatory mechanisms. The blue and brown modules were significantly associated to the timeline for both SF and ISF, while the blue module was positively associated to CD86 expression in ISF. **(A)** Mean expression profiles of significant modules in SF and ISF derived from all transcripts in each cluster. In ISF, the presence of the pro-inflammatory green and turquoise modules are associated to increased mean expression of the homeostatic/pro-resolving blue and brown modules. Overrepresented Biological Processes (BPs) in the blue **(B)**, brown **(C)**, green **(D)**, turquoise **(E)** modules and their corresponding fold enrichment. The complete list of significant modules, BPs and related genes for each module is presented in **Supplementary Tables 2, 3**.

comparison to its SF counterpart. The mean expression profile in the ISF's turquoise module progressively decreased from baseline. Functional annotation of genes within each module was then inspected (**Figures 5B–E**).

Modular Gene Ontology Enrichment and Overrepresented Biological Processes (BPs)

Overrepresented BPs were ranked based on fold enrichment and having an FDR <0.05 (**Supplementary Table 3**). For cases in which a large list of BPs met this criterion, BPs with FDR <0.01 were given priority attention. Fold enrichment was determined by comparing the background frequency of total genes annotated to a certain BP in the specified species to the sample frequency of genes under such BP. Overrepresentation was defined by a positive fold enrichment value (65). Since the gene list for modules blue, brown, pink and black completely overlapped between SF and ISF (**Supplementary Table 2**), overrepresented BPs in any of these modules were the same for both groups (**Figures 5B–E**). For the blue module, isoprenoid biosynthesis was the most overrepresented of the 79 BPs identified by GO. Given the high number of overall (n=4148) and hub genes (n=699) in this module, a diversity of BPs was identified within it, and is collectively discussed below. Of note, genes identified with pro-resolving functions in the related previous studies (*IL10* and *IGF1)* (49, 50) also allocated to the blue module. In the brown module, while the most overrepresented BP was "antigen presentation *via* MHC class II", most BPs in this module related to mitochondrial response to oxidative stress and energy metabolism homeostasis. Overrepresented BPs in the pink and black modules constituted a minor list and were associated with a variety of cell homeostasis and housekeeping functions.

Exclusive to ISF cultures, BPs in the IL-1β-associated green module were primarily associated with macrophage response to damage, including mitosis, adjustment of lipid and glucose metabolism following circadian distress, activation of the amphireguling-STAT3 axis (GO:0032355~response to estradiol) and noncanonical NF-κB signaling, thus, likely a module with a pro-inflammatory signature. In the turquoise module, also associated with IL-1β production, overrepresented BPs reflected the response of myeloid progenitors to stress and IL-4 signaling, a key event in the response of pro-resolving macrophages, amplifying chromatin opening for enhanced mRNA transcription (44–46). In summary, ISF triggered an early pro-inflammatory response in BMNC progenitors (green module) leading to macrophage commitment and priming (turquoise module). These events enhanced the constitutive expression of homeostatic mechanisms from macrophages (blue and brown modules) required to counteract damage and recover homeostasis (**Figures 5A–E**).

Pathway Analysis, Upstream Regulators and Their Network Interactions

Ingenuity Pathway Analysis revealed activated and inactivated pathways in SF and ISF cultures (**Table 1**, **Supplementary Table 4**). Our pathway analysis results from 0-48 hours (performed with IPA) agrees with findings from GO analysis and points repeatedly to activation of the mevalonate pathway and isoprenoid biosynthesis (superpathways of cholesterol biosynthesis, geranylgeranyl diphosphate biosynthesis, cholesterol biosynthesis I, II and III, and mevalonate pathway I). The patterns of expression of genes involved in these pathways, comparing BMNC cultured in SF and ISF (**Figure 6**), highlight the increased expression of genes such as *ACAA2, HADHA ACAT2* and *FDPS in ISF*, essential for the synthesis of isoprenoids and mitochondria beta-oxidation of fatty acids. Additional pathways activated at 0-48 hours included unfolded protein response in agreement with overrepresented BPs in the blue module, and estrogen biosynthesis, in agreement with the BP "response to estradiol" from the green module, peaking at 48 hours and progressively decreasing.

From 48-96 hours, the PPAR- signaling pathways were repeatedly identified, which agrees with the identification of *PPARG* as highly connected upstream regulator, depicting the activation of the PPAR-γ and PPAR-α signaling pathways. Comparisons for BMNC cultured in SF and ISF for the expression of genes involved in these pathways (**Figure 6**), highlight the higher expression of PPAR genes in ISF. It also highlights the higher expression of *NFKB2* and *RELB* genes, encoding for drivers of non-canonical NF-κB signaling, which has essential pro-resolving functions. After 96 hours of culture in ISF, a mix of pathways involved in cartilage metabolism (Heparan Sulfate Biosynthesis), cellular homeostasis/ inflammation resolution (Cell Cycle: G2/M DNA Damage Checkpoint Regulation, Unfolded Protein Response) and leukocyte migration during inflammation (Netrin Signaling) were observed to be activated. This mixed profile may have resulted from continuously challenging BMNC with ISF every 48 hours as performed in our model (50). Inhibited pathways included leukocyte extravasation signaling, IL-6 across the time course, IL-15 production and acute phase response signaling, key players in the development and maintenance of synovitis and degenerative processes observed in osteoarthritis. While the "Osteoarthritis Pathway" was identified as the third most activated pathway in SF at 6-10 days, neither the model used in our study, nor the list of genes involved in such functional annotation support such a finding.

Twenty-three potential upstream regulators were identified as activated ($p < 0.05$ and a Z-score ≥ 2) in ISF and 35 in SF (**Figure 7A**, **Supplementary Table 5**, **Supplementary Figure 1**). Within these, 5 transcription factors (*EIF4E, LARP1*, *MAFB, NFE2L2* and *SIRT2* genes), the transmembrane receptor *TREM2*, the enzymes *LPL* and *PIK3R1*, and the multifunctional receptor *GABARAP* were conserved between ISF and SF. Inactivated upstream regulators ($p < 0.05$ and a Z-score ≤ 2) were also identified in both ISF (n=17) and SF (n=32). Within these, *IL1B* and its downstream signaling transcription factor *RELA*, the mitochondria fission receptor *MFN2*, and the transcription factor *GATA1* were conserved between ISF and SF.

Interaction networks generated by STRING among activated and inhibited upstream regulators in ISF cultures revealed predicted interactions between upstream regulators in and outside their same module (**Figure 7B**). Among activated

TABLE 1 | Top 3 most activated or inactivated pathways (Z-score > 2.0 or < -2.0; -log (p-value) > 1.3 = p>0.05) identified by IPA from DEGs between consecutive timepoints in SF and ISF.

Time	ISF		SF	
	Activated ***z-score; -log (p-value)***	***Inhibited*** ***z-score; -log (p-value)***	***Activated*** ***z-score; -log (p-value)***	***Inhibited*** ***z-score; -log (p-value)***
0-48 hr	Superpathway of cholesterol biosynthesis (4.14; 10.3)	Signaling by Rho GTPases (-3.35; 8.00)	Superpathway of cholesterol biosynthesis (4.24; 8.74)	IL-5 production (-3.00; 4.43)
	Geranylgeranyl diphosphate Biosynthesis I (via Mevalonate) (3.31; 4.88)	Leukocyte extravasation signaling (-3.20; 14.9)	Geranylgeranyl diphosphate Biosynthesis I (via Mevalonate) (3.31; 5.83)	Apoptosis signaling (-2.55; 4.13)
	Mevalonate Pathway I (3.00; 4.54)	IL-5 production (-3.317; 5.43)	Mevalonate Pathway I (3.00; 5.34)	Signaling by Rho GTPases (-2.35; 4.12)
48-96 hr	PPAR signaling (3.41; 9.22)	Acute Phase Response signaling (-4.42; 5.96)	LRX/RXR activation (3.71; 4.08)	Natural Killer cell signaling (-5.85; 4.12)
	PPARα/RXRα activation (3.08; 9.22)	Natural Killer Cell signaling (-4.13; 6.23)	PPAR signaling (3.41; 9.89)	IL-6 signaling (-5.24; 14.9)
	LXR/RXR activation (2.67; 3.27)	IL-6 signaling (-4.01; 10.50)	PPARα/RXRα activation (2.59; 12.00)	Acute Phase Response signaling (-4.87; 7.31)
96 hr-6 d	Heparan Sulfate Biosynthesis (Late Stages) (2.0; 1.79)	IL-6 signaling (-2.23; 2.08)	————————	————————
	Heparan Sulfate Biosynthesis (2.0; 1.66)	PRRs in Pathogen Recognition (-2.0; 1.69)	————————	————————
6-10 d	Cell Cycle: G2/M DNA Damage Checkpoint Regulation (2.33; 5.27)	Cell cycle control of chromosomal replication (-3.60; 8.78)	GP6 Signaling Pathway (3.05; 4.83)	EIF2 signaling (-5.456; 41.90)
	Unfolded Protein Response (2.44; 3.23)	Kinetochore Mataphase signaling (-2.98; 16.61)	Osteoarthritis Pathway (2.53; 4.15)	Oxidative Phosphorylation (-3.00; 2.81)
	Netrin signaling (2.23; 1.39)	Mitotic Roles of Polo-Like Kinases (-2.12; 6.89)	Tumor Microenvironment Pathway (3.31; 2.80)	Autophagy (-2.23; 0.00)

In agreement with GO, dominant responses related to inflammation-derived oxidative stress and an antioxidant response relying on lipid biosynthesis and activation of the PPAR signaling pathway. While the IL-6 pathway inhibition was common to both SF and ISF, it was a more frequent in ISF cultures. A detailed list of activated and inactivated pathways is presented on ***Supplementary Table 4****.*

upstream regulators, the blue module was overrepresented in ISF (50%; including *PPARG*, *SCAP, MAFB* and *SIRT2*) followed by the brown module (*CSF1, LARP1, LPL, NFE2L1*) and turquoise module (including *CDKN1A, CDKN2A, EIF4E, TG*) equally representing 16.6% of upstream regulators, while the grey (12.5%; *CREB3L2, MEF2D, NFE2L2*) and green (8.3%; *STAT3* and *GABARAP*) modules were minimally represented. Amongst inhibited upstream regulators in ISF (**Figure 7B**), the turquoise module was overrepresented (70.5%) and largely related to the IL-1β/NF-κB signaling pathway. Overall, such interactions underscore the proliferation and differentiation (*CSF1*) of BMNC into macrophages (50), and their response to inflammation-induced oxidative stress (*PPARG, NFE2L1*) (43, 66, 67) involving changes in lipid metabolism (*LPL*) (68). Such a response likely mediates resolution, at least partially in a PPAR-γ-reliant manner, downregulating the IL-1β/NF-κB signaling pathway (*IL1B* and *RELA* genes) (43).

Tissue Expression of Upstream Regulators and Genes Central to Activated Pathways

From the patterns of gene expression for each activated upstream regulator assessed over time (GeTMM counts and fold change, **Supplementary Table 6**), those with a high network interaction and exhibiting evident fold changes over time (decreasing or increasing) were selected for immunohistochemistry. Genes identified as essential drivers of the most activated pathways, were also selected as IHC targets. Ultimately, available immunohistochemistry targets with antibodies known to cross-react with equine proteins included PPARγ, phospho-PPARγ, PPARGC1A, MVK, HMGCS1, IL-1β, MAFB, SIRT2, and CSF1. Tissue expression for phosphorylated PPARγ (*p=0.0032*) and mevalonate kinase (*p=0.0291*) were lower in BMNC-treated joints (**Figure 8**), likely because the resolution process had already been achieved, and is similar to the patterns of expression of IL-10 in our previous study using the same synovial samples (49). None of the remaining histochemical findings reached statistical significance. Tissue expression for PPARGC1A was consistently higher in BMNC-treated joints for 5/6 horses compared to those treated with DPBS. In contrast, CSF1 and MAFB tended toward higher expression in DPBS-treated joints. No differences were observed in the staining patterns for SIRT2 and IL-1β.

DISCUSSION

In this study, we identified differential transcriptional signatures of BMNC in response to ISF and SF. These same BMNC were previously shown to resolve synovitis following exposure to an inflamed synovial environment *in vivo* and *in vitro* (49, 50). We demonstrate a temporal behavior of co-expressed gene networks and their association with traits from our previous studies (49,

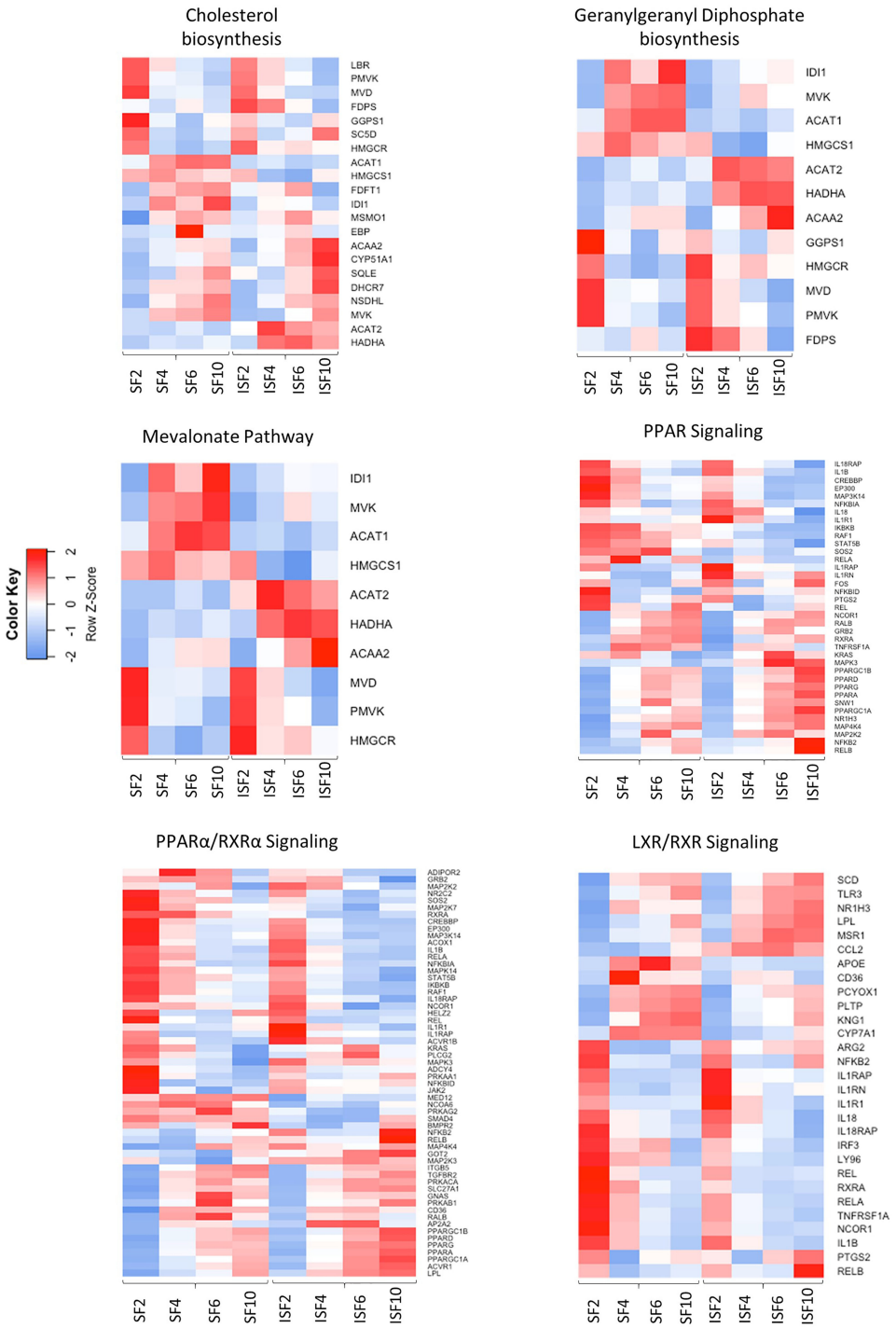

FIGURE 6 | Heatmaps depicting the patterns of expression of genes involved in the most highly activated signaling pathways associated with resolution of synovitis, comparing BMNC cultured in SF and ISF. Further details are available at **Supplementary Table 4**.

50), as well as with the expression of key proteins in the synovium by immunohistochemistry. Our findings illustrate the elaborate balance of pro- and anti-inflammatory mechanisms shifting dominance through the recovery of joint homeostasis. BMNC responded to ISF with an early pro-inflammatory response (green module), characterized by a short spike in the expression of NF-κB-related genes, coincident with the peak of IL-1β secretion in conditioned ISF

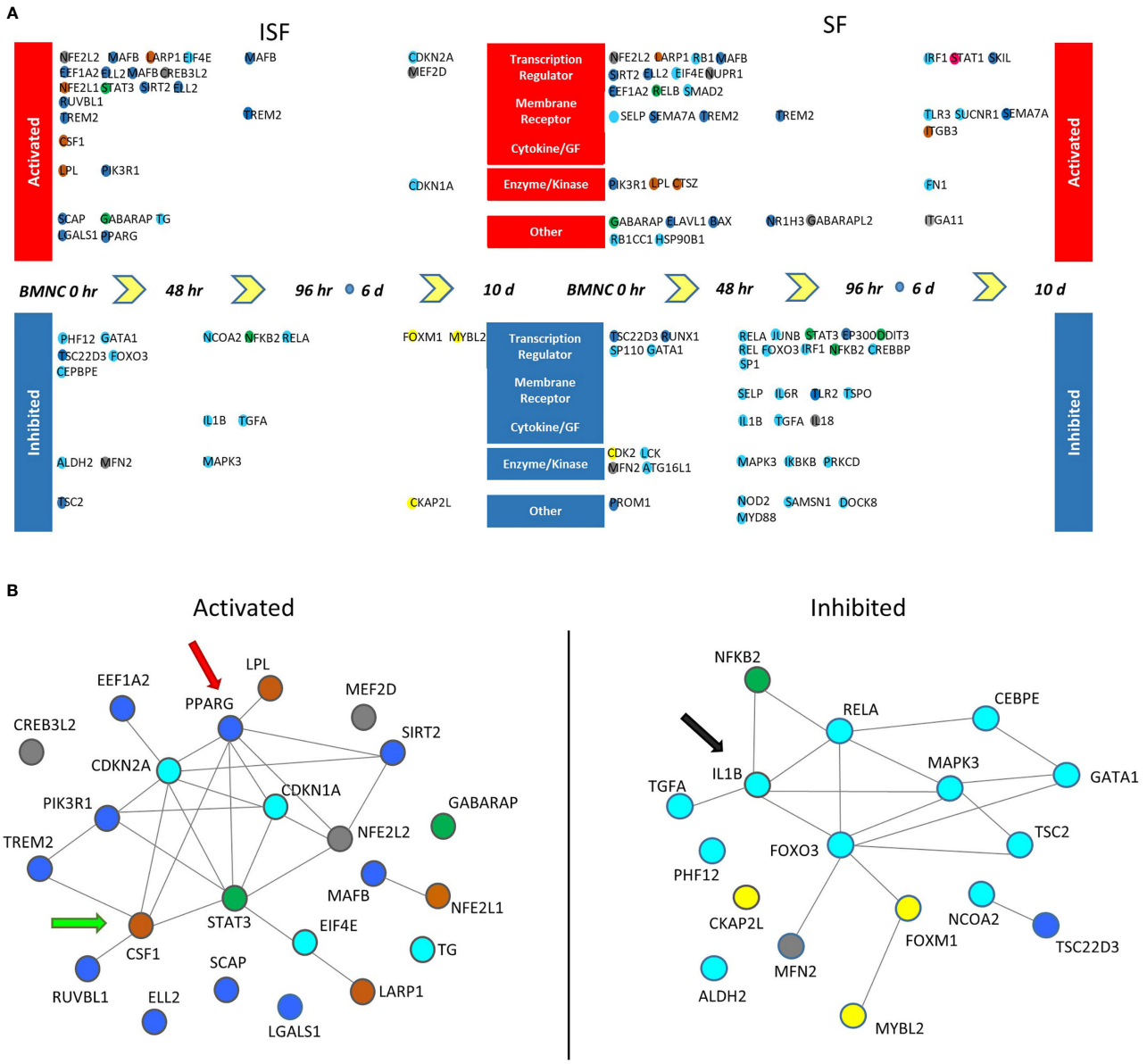

FIGURE 7 | Potential upstream regulators of genes differentially expressed between consecutive time points (DEGcts) in SF and ISF cultures. **(A)** Time window specific identification of upstream regulators analysis of the DEGcts using Ingenuity Pathway Analysis (IPA). The colored circles are upstream regulators identified for each comparison of consecutive time points with an activation or inhibition Z-score (> 2.0 or < -2.0), respectively (**Supplementary Table 5**). Colors of the circles correspond to colors of the module eigengene from WGCNA to which that specific gene associated. Activated upstream regulators are shown at the top and those inhibited at the bottom. Upstream regulators were grouped into five categories: `Transcription regulator', `Membrane receptor', `Cytokine/Growth Factor (GF)', 'Enzyme/Kinase' and `Other'. **(B)** Interaction network among activated (left) and inhibited (right) upstream regulators in BMNC cultured in ISF. Color coding of nodes relate to the corresponding module eigengene. Interaction networks reflect a response to inflammation-induced oxidative stress associated with proliferation and differentiation of BMNC into macrophages (CSF1 - green arrow), and a PPARγ-reliant inflammation resolution (red arrow), associated with inhibition of the IL-1β signaling pathway (black arrow) as suggested by complimentary analyses.

(50). This response was associated with increased expression of the blue and brown modules, 2 gene networks with homeostatic functions comprising known drivers of resolution, which were more highly expressed in ISF and were dominant among activated upstream regulators. Significant differences in the expression of phosphorylated PPARγ and mevalonate kinase in synovial membranes from inflamed joints treated with BMNC, and equivalent IL-1β staining between BMNC- and DPBS-treated joints, emphasize the fine tuning of so-called pro-inflammatory pathways that must remain active at physiological levels during the resolution process. These observations highlight the differences between the

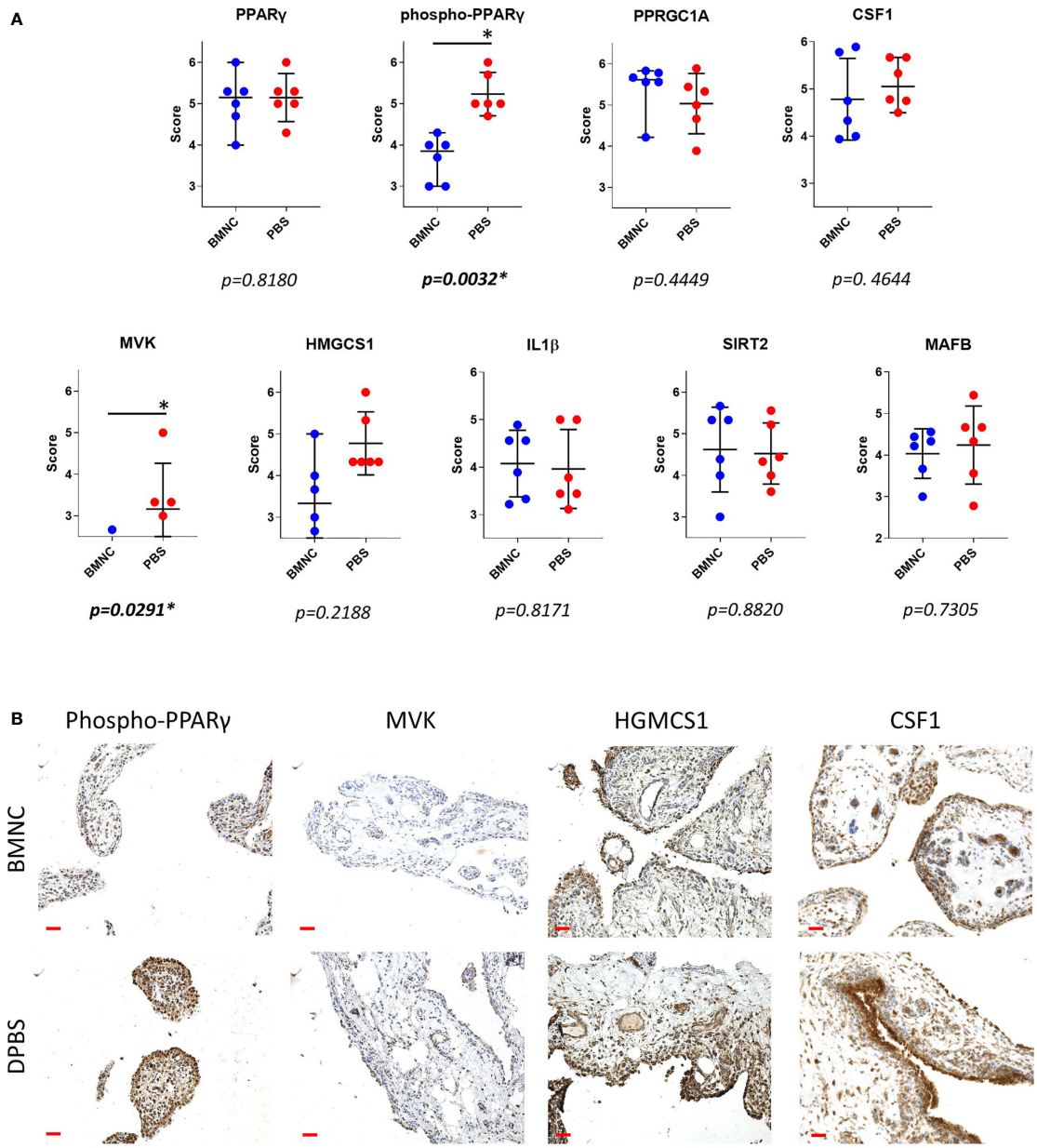

FIGURE 8 | Immunohistochemistry of synovial membranes from 6 horses with experimental synovitis treated with BMNC or DPBS. Marked resolution of inflammation was evident following BMNC therapy (31). Selected targets were potential upstream regulators of high network interaction that were differentially expressed in ISF cultures over consecutive time points, or central drivers of most activated pathways. **(A)** Scatterplots of composite staining scores (median, 95% confidence interval) for PPARγ (*PPARG gene*), phosphorylated PPARγ, PPARγ co-activator 1 alpha (*PPARGC1A gene*), colony stimulating factor 1 (*CSF1 gene*), mevalonate kinase (*MVK gene*), 3-Hydroxy-3-Methylglutaryl-Coenzyme A Synthase 1 (*HMGCS1 gene*), interleukin-1β (*IL-1β gene*), sirtuin 2 (*SIRT2 gene*), and transcription factor MAFB (*MAFB gene*). Each dot in the scatterplot represents the composite score for each individual horse. Tissue expression for phosphorylated PPARγ (*p=0.0032*) and mevalonate kinase (*p=0.0291*) were lower in BMNC-treated joints. **(B)** Representative sections of synovium from inflamed joints treated with BMNC or DPBS and stained for selected markers detailed above (scale bars 100μm).

pro-resolving effects associated with BMNC therapy compared to the anti-inflammatory effects observed following clinical treatment with corticosteroids (30, 49–51, 69, 70).

The short spike of expression of the pro-inflammatory green module observed in ISF, is essential to trigger a cascade of events that culminates in a pro-resolving response. NF-ƙB-related and mitogen genes co-expressed in the green module (**Supplementary Table 3**) play a key role in promoting the proliferation of macrophages necessary to counteract damage (24, 25). NF-ƙB-related genes also induce increased expression of

genes with anabolic and anti-inflammatory functions within the blue and brown modules, which have critical roles in driving resolution of joint inflammation. The top four overrepresented BPs in the green module relate to a group of genes sharing important mitogenic activity. Genes such as *MAD1L1* and *CHAMP1* encode proteins that interact and regulate cell structure organization preceding mitosis (71, 72). *NR4A3* and *NR1D2* encode transcriptional activators involved in proliferation, survival and differentiation of myeloid progenitor cells, and in adjusting myeloid progenitor cell metabolism to oxidative stress (73, 74). NR1D2 does so by activation of IL-6 transcription, which is also required to induce expression of the IL-4 receptor and related downstream regulatory functions of macrophages, including their self-renewal (75–77). The BP "response to estradiol" was characterized by the expression of the amphiregulin (*AREG*) and *STAT3* genes. Macrophages are an important source of amphiregulin produced during acute inflammation. The AREG/ERK/STAT3 signaling axis is required for the differentiation of progenitor cells during tissue repair and establishing a pro-resolving response (78–81). *AREG* was more highly expressed in ISF and exhibited progressively decreasing expression over time, as the resolving response progressed (**Supplementary Table 6**). Additionally, estrogen accelerates the resolution of inflammation through the regulation of IL-10/STAT3-mediated deactivation of pro-inflammatory responses, such that post-menopausal women are prone to developing chronic inflammation (82). STAT3 was the activated upstream regulator in ISF cultures with the highest connectivity. The NIK/NF-ĸB signaling in the green module was highlighted by the expression of *RELB* and *NFKB2*. Both RELB and NFKB2 are subunits of the non-canonical NF-κB signaling, which in macrophages, can exert both pro- and anti-inflammatory effects (83, 84). Non-canonical NF-κB signaling is critical to produce SDF-1α and recruit monocytes to the site of damage immediately following injury (83). Further, during monocyte-macrophage differentiation, non-canonical NF-κB signaling prevents hyperactivation of new macrophages by accelerating the removal of RelA and c-Rel (canonical NF-κB subunits) from pro-inflammatory gene promotors preventing overt inflammation. As such, blocking non-canonical NF-κB by inactivation of its IKKα subunit results in increased inflammation (84). In both SF and ISF cultures, *RELB* expression was positively regulated, with decreasing expression over time, while *RELA* was downregulated (**Figure 6**; **Supplementary Table 6**). Combined, these signatures illustrate a fraction of molecular drivers of the acute response of BMNC to inflammation, which also sets the stage for establishing a pro-resolving response.

Increased expression of the blue module in response to inflammation, in parallel with the surge of the green module, and over a timeline associated with resolution in our previous studies (49, 50), suggests a pro-resolving identity. Genes encoding established drivers of joint inflammation resolution (IL-10, IGF-1) allocated to the blue module (**Supplementary Table 2**). A major functional signature of this module was the activation of the mevalonate pathway and isoprenoids biosynthesis, comprised by the expression of genes encoding central drivers of the mevalonate/isoprenoid pathway (*COQ2, HMGCR, FDPS, HMGCS1, GGPS1, MVK, PDSS1, PDSS2, GGDPS1, FDPS, ACAA2, HADHA* and *ACAT2*. In agreement, the super pathway of cholesterol biosynthesis, geranylgeranyl biosynthesis (an isoprenoid) and mevalonate pathway had the highest activation scores in ISF cultures between 0 and 48 hours, as detected by IPA. The roles of the mevalonate pathway in steroidogenesis, counteracting oxidative stress and inflammation resolution, are well documented in the macrophage response to damage and inflammation resolution (85–88). Deficiency of mevalonate kinase (MVK), a key enzyme in the mevalonate pathway, causes reduced synthesis of isoprenoids, leading to mitochondrial damage, subsequent oxidative stress and severe inflammation (89, 90). Importantly, exogenous isoprenoid treatment in models of inflammation induces decreased oxidative stress and production of inflammatory markers, by increasing expression of the NF-κB inhibitor IκBα and antioxidant selenoproteins (86, 91–93). Gene expression for MVK and HMGCS1, key enzymes in the mevalonate pathway, exhibited a similar expression profile between themselves (**Figure 6**; **Supplementary Table 6**). These enzyme genes were more highly expressed in SF, suggesting that inflammation negatively affects this pathway. A similar pattern of gene expression for *IL10* and *IGF1* was observed in our previous study, in which both genes were more highly expressed in SF than ISF (50). However, concentrations of IL-10 and IGF-1 in ISF were higher than in SF, because the decreased relative production in ISF was compensated for by higher macrophage counts (50). Our ongoing lipidomic study on BMNC-conditioned SF and ISF from the same samples used in this study may help elucidate if a similar context applies for isoprenoid production. Interestingly, it was recently evidenced that transcriptional dysregulation of the mevalonate pathway is a key signature of the overt inflammation caused by SARS-CoV-2 infection, highlighting its importance for inflammation resolution (88). Differences in MVK expression detected in synovial membranes suggests that the *in situ* activity of MVK in synovitis resolution happens earlier in time, as suggested by our pathway analysis and *in vivo* study (49).

The second overrepresented BP in the blue module "proteasome ubiquitin-dependent protein catabolism" was comprised of genes that characterize the formation of the 26S proteasome. Inflammation-derived oxidative stress damages nascent proteins that become misfolded and targeted for degradation (94). The 26S proteasome is essential for the degradation of these proteins, preventing aggregate formation, which is part of the pathogenesis of several conditions (94). Such observation from GO analysis agrees with the IPA findings where the "Unfolded Protein Response" was identified among the most activated pathways following isoprenoid biosynthesis through the mevalonate pathway. The next overrepresented BP was "protein localization to the Cajal body". These are coiled bodies found in the nucleus of proliferating or metabolically active cells and are implicated in telomere homeostasis (95, 96). This BP was represented primarily by genes encoding chaperonin containing

tailless (CCT) proteins that are critical regulators of telomerase folding and trafficking (97). Depletion of CCT proteins cause Cajal body and telomerase mislocalization and failure of telomere elongation (97). CCTs are also required for folding of cytoskeletal proteins during cell proliferation (98). The fourth dominant BP, "response to thyroid hormone stimulus", reflects the effects of triiodothyronine on regulation of macrophage maturation and responses. Such responses include controlling cell migration and conferring protection against endotoxemia and LPS exposure, in great part through proliferation of tissue resident macrophages (99, 100). In addition, half of the genes characterizing this BP encode for cathepsins that mediate endolysosomal protein degradation. In summary, the dissection of a minute part of the blue module, illustrates the effect of isoprenoids and thyroid hormones in improving metabolism and performance of BMNC-derived macrophages to counteract the effects of inflammatory oxidative stress (85, 89, 90, 99, 100). This response is, at least partially, achieved by adjusting proteostasis through the 26S proteasome and Cajal bodies, preventing degenerative protein aggregate formation during increased cell transcription, proliferation and metabolism in response to inflammation (94, 97, 98).

The signature of the brown module were BPs that comprised of a series of gene groups encoding proteins that regulate the mitochondrial respiratory chain and mitochondria-mediated regulation of energy metabolism (101, 102). There is growing evidence of the pivotal role of mitochondria in energy metabolism adjustments required for inflammation resolution as shown in the brown module (103–105). In the face of inflammatory challenges, enhanced cell respiration induces oxidative stress, activating alternative sources of energy driving gluconeogenesis and enhancing mitochondrial fatty acid oxidation (101, 102) as denoted by the increased expression of genes such *ACAA2* and *HADHA* in ISF cultures (**Figure 6**). These genes were, however, associated with the isoprenoid biosynthetic pathway, highlighting the recently reported role of mitochondrial isoprenoid biosynthetic process (106). Enhancing the mitochondrial respiratory chain is a homeostatic mechanism that prevents mitochondrial DNA damage and its subsequent cytosolic and extracellular release signaling through damage-associated molecular pattern (DAMP) receptors (107). The peroxisome proliferator-activated receptor-gamma (PPAR-γ) co-activator 1-α (PPRGC1A; *PPRGC1A* gene), a master regulator of mitochondria biogenesis and liver gluconeogenesis was among the outstanding genes involved in mitochondrial regulatory functions listed in the brown module (101) and exhibited a trend for higher expression in BMNC treated joints (**Figure 8**).

Following interaction with PPRGC1A, PPAR-γ exhibits increased activity, interacting with a multitude of transcription factors and PPAR-γ responsive elements (43). PPAR-signaling was an important activated pathway identified by IPA in both SF and ISF cultures between 48 and 96 hours (**Table 1**, **Figure 6**), denoting its homeostatic functions. Among different PPARs, PPAR-γ was one of the most highly connected upstream regulators. In macrophages and other cells, PPAR-γ signaling is a cornerstone of tissue repair and inflammation resolution, exhibiting myriad functions that are either PPAR-γ-mediated or -dependent (43). Examples include shifting the production of pro-inflammatory cytokines towards anti-inflammatory and pro-resolving mediators, driving apoptosis and clearance of neutrophils, enhancing macrophage traffic, recruitment, phagocytosis and efferocytosis, improving mitochondrial respiratory performance, and the overall transcriptome of a regulatory response driving recovery of homeostasis (43, 47, 101, 108). Of note, some isoprenoids, the signature of the blue module, as well as some specialized pro-resolving molecules, signal through PPAR-γ, conferring increased production of IL-10, resistance to inflammatory stimuli and attenuated NF-ƙB activation following LPS stimulation (43, 81, 109–111). Gene expression for *PPARG* was higher in ISF compared to SF. Significantly lower staining for phospho-PPAR-γ expression in synovial membranes detected by IHC, combined with the timing at which *PPARG* was identified as an Upstream Regulator, suggest that its activity modeling synovitis resolution almost overlap with the acute phase of inflammation. Importantly, PPAR-signaling findings from IPA at 48-96 coincide with the time at which pro-resolving effects were observed in our previous *in vivo* and *in vitro* studies (49, 50). Histochemical findings for phospho-PPAR-γ and PPRGC1A in BMNC compared to DPBS-treated controls suggests PPAR-γ signaling was not only a BMNC response to the inflamed synovial environment, but also part of the beneficial effects of BMNC on treated joints. Moreover, there is recent evidence that *PPRGC1A* expression is required for chondrocyte metabolism and cartilage homeostasis, with *PPRGC1A* knockouts exhibiting delayed endochondral ossification, disruption of physeal morphology and severe premature osteoarthritis (112).

Also in the brown module, *CSF1* was identified as an upstream regulator gene and was more highly expressed in ISF than SF cultures. The marked proliferation of BMNC in ISF observed *in vitro* (50) may also be a response from CSF-1 signaling (50). Following a spike of proliferation, stimulation of macrophage progenitors with interferon-gamma (IFN-γ) or LPS induce maturation and cell cycle arrest, increasing MHC-II expression and developing the capability to quickly respond to inflammatory stimuli and antigen presentation (113). Given that synovitis in our model was induced by injection of LPS, it is not surprising that "antigen processing and presentation of polysaccharide antigen *via* MHC class II" was a dominant BP in the brown module, particularly considering that IFN-γ was not detected by immunoassay in conditioned SF or ISF in a preliminary screening performed in our study (50). Combined, these observations from the brown module highlight the importance of macrophage proliferation and maturation, and PPRGC1A/PPAR-γ signaling during macrophage-mediated joint homeostasis, identifying the need for further investigation of the therapeutic roles of PPAR-γ-agonists in the recovery of joint health.

The combined overrepresented BPs in the turquoise module, exclusive to ISF, reflect the dynamic of serine/threonine phosphorylation, autophosphorylation and dephosphorylation during cytokine signaling and subsequent mRNA transduction

(114). In our study, these events happened in response to IL-4 (50). IL-4 signaling regulates the establishment of a pro-resolving response in macrophages by adjusting chromatin conformation and access for RNA transcription initiation (45). It also represses the expression of classical pro-inflammatory genes, decreasing inflammasome activation, IL-1β production and pyroptosis (44). Alternatively, IL-4 signaling enhances DNA binding of RNAPII-pS2 and RNAPII-pS5, and H3K27Ac as a positive epigenetic modification that leads to increased expression of several gene networks with a pro-resolving function (44). STAT6, which also allocates to the turquoise module, is a major regulator of IL-4 (likely through IL-4r expression) and PPAR-γ signaling (46). STAT6 facilitates binding of PPAR-γ to DNA, which, like IL-4, increases the number of regulated genes and the magnitude of response from macrophages (44, 46, 47, 115). IL-4r expression was increased in BMNC cultured in both SF and ISF, but was significantly higher in ISF (50), in agreement with the overall findings in this module. We did not, however, detect gene expression for IL-4 or the IL-4r agonist IL-13. Also, neither IL-4 nor IL-13 were detected in the synovial fluid (SF or ISF) in our *in vitro* and *in vivo* studies (29,31). Collectively, these findings suggest that, if produced by cells in the joint other than BMNC, their concentrations were either below detectable limits or absent, raising the possibility of signaling by an unidentified IL4r agonist or an unconsidered pathway with equivalent gene ontology. The decreasing mean expression of the turquoise module in relationship to the increasing mean expression of the blue and brown modules, indicates that the biological processes included in the turquoise module are primarily required for priming the macrophages in BMNC towards a pro-resolving response (45).

IL1B gene expression in BMNC and protein expression in synovial fluid coincided in time and duration, peaking at 24 hours and progressively decreasing over time (49, 50). The *IL1B* gene was identified as a centerpiece among inhibited upstream regulators in ISF. Interestingly, IL-1β expression in the synovial membrane at 6 days following LPS model induction remained evident in both BMNC- and DPBS-treated joints. This finding suggests that the physiological levels of IL-1β expression required for homeostasis were conserved and not blocked, as commonly observed with the use of corticosteroids (51). Staining patterns for the other selected markers were inconclusive due to variability between individual horses. Although our experimental design was aimed at minimizing variability by including only horses of the same breed and a narrow range of age, variability is expected when working with human populations and animal models. Inbred mice poorly mimic the inflammatory reaction of people (116). While this study comprised a small cohort, the horse is an excellent model for the translation of inflammation (117) and an established model for the study of degenerative and inflammatory joint disease (1, 118). In agreement with our *in vivo* (49) and *in vitro* (50) findings using the same horses, the combined effects of gene networks comprised by each module depict a pro-resolving response, dissecting some important signatures of this process, and identifying candidate biomarkers of synovitis resolution, such as PPAR-γ and MVK expression and synovial fluid quantification of isoprenoids. The overall agreement between different analytical tools used in this study (between gene ontology of WGCNA-derived modules with IPA pathways and upstream regulator analysis) reinforce the significance of our data. However, future mechanistic studies are necessary to further determine the specific roles of pathways and biological processes identified in our study. A study of the transcriptome analysis from synovial samples from naturally inflamed joints treated with BMNC and DPBS would complement our current observations and further illustrate the molecular drivers of the synovial response to BMNC injection.

CONCLUSION

Our current data suggest that BMNC-derived mechanisms of resolution are primarily represented by constitutively expressed homeostatic mechanisms, whose expression is enhanced to counteract tissue damage. These homeostatic mechanisms translate into macrophage proliferation, enlarging the "macrophage army" to fight aggressors, also improving their general and mitochondrial metabolism to better resist the challenges of inflammatory oxidative stress. Such effect is partially achieved through the synthesis and signaling of lipid mediators that promote recovery of homeostasis. Further exploration of BPs and pathways not dissected in this study may identify additional targets for future investigations. The combined findings of our equine studies (27, 49, 50) and human clinical trials (48, 119) highlight the long-lasting and superior pro-resolving effects of BMNC in the treatment of arthritic conditions. This study reveals important transcriptional signatures of BMNC-induced resolution of synovitis and reinforce that pro-resolving macrophages do not fit within commonly described pro- or anti-inflammatory phenotypes established in artificial *in-vitro* systems (120, 121). Current knowledge, including our study, suggests that *in vivo*, macrophages are by default homeostatic cells that, following injury, drive inflammation with the purpose of counteracting tissue aggressors, further guiding inflammation resolution and recovery of homeostasis (24, 25, 39, 122–125). Our study also highlights candidate mechanisms by which BMNC provide lasting improvement in patients with OA. Therapeutic enhancement of PPAR-γ signaling in joints with chronic inflammation may represent a novel strategy for resolving joint inflammation. Defining multiple mechanisms of macrophage-mediated synovitis resolution may provide means to develop pharmacological pro-resolving therapies, bypassing the need for more invasive bone marrow aspiration and further advancing the treatment of many inflammatory arthropathies, not just OA.

DATA AVAILABILITY STATEMENT

The datasets generated for this study are available on request to the corresponding author. The current RNAseq data was deposited in the Gene Expression Omnibus (GEO; GSE18552) repository.

ETHICS STATEMENT

This study was conducted in compliance with the Animal Welfare Act and the approval of the Virginia Tech Institutional Animal Care and Use Committee.

AUTHOR CONTRIBUTIONS

BCM, JNM, and LAD designed studies. BCM obtained and processed the samples. TSK and SCL mapped and quantified the sequenced libraries. HE-SA and SCL performed DEGs analysis. BCM and HE-SA performed functional genomics, figures preparation, data interpretation and conceptualization. KES performed immunohistochemical assays, which were scored by BCM, HE-SA, and KES. BCM prepared the manuscript. All authors edited, reviewed, and approved the manuscript.

FUNDING

This study was supported by the Grayson-Jockey Club Research Foundation and the Virginia-Maryland College of Veterinary Medicine Internal Research Competition. BM received graduate assistantship support from the Interdisciplinary Graduate Education Program at Virginia Tech, the Virginia-Maryland College of Veterinary Medicine and the College of Agriculture, Food and Environment at the University of Kentucky.

SUPPLEMENTARY MATERIAL

The Supplementary Material for this article can be found online at: https://www.frontiersin.org/articles/10.3389/fimmu.2021.734322/full#supplementary-material

REFERENCES

1. McIlwraith CW, Frisbie DD, Kawcak CE. The Horse as a Model of Naturally Occurring Osteoarthritis. *Bone Joint Res* (2012) 1:297–309. doi: 10.1302/2046-3758.111.2000132
2. Murphy LB, Cisternas MG, Pasta DJ, Helmick CG, Yelin EH. Medical Expenditures and Earnings Losses Among US Adults With Arthritis in 2013. *Arthritis Care Res* (2018) 70:869–76. doi: 10.1002/acr.23425
3. Sellam J, Berenbaum F. The Role of Synovitis in Pathophysiology and Clinical Symptoms of Osteoarthritis. *Nat Rev Rheumatol* (2010) 6:625. doi: 10.1038/nrrheum.2010.159
4. Goldring MB, Otero M. Inflammation in Osteoarthritis. *Curr Opin Rheumatol* (2011) 23:471–8. doi: 10.1097/BOR.0b013e328349c2b1
5. Mathiessen A, Conaghan PG. Synovitis in Osteoarthritis: Current Understanding With Therapeutic Implications. *Arthritis Res Ther* (2017) 19:18. doi: 10.1186/s13075-017-1229-9
6. Smith MD. The Normal Synovium. *Open Rheumatol J* (2011) 5:100–6. doi: 10.2174/1874312901105010100
7. Lopes EBP, Filiberti A, Husain SA, Humphrey MB. Immune Contributions to Osteoarthritis. *Curr Osteoporos Rep* (2017) 15:593–600. doi: 10.1007/s11914-017-0411-y
8. McIlwraith C. Principles and Practices of Joint Disease Treatment. In: D S. and MW Ross, editors. *Diagnosis and Management of Lameness in the Horse*. St. Louis MO: Elsevier Saunders (2011). p. 840–52.
9. Hunter D. Treatment of Osteoarthritis. In: N Arden, editor. *Atlas of Osteoarthritis*, vol. pp . London: Springer Healthcare (2018). p. 80–99.
10. Nathan C, Ding A. Nonresolving Inflammation. *Cell* (2010) 140:871–82. doi: 10.1016/j.cell.2010.02.029
11. Serhan CN, Chiang N, Van Dyke TE. Resolving Inflammation: Dual Anti-Inflammatory and Pro-Resolution Lipid Mediators. *Nat Rev Immunol* (2008) 8:349–61. doi: 10.1038/nri2294
12. Sugimoto MA, Sousa LP, Pinho V, Perretti M, Teixeira MM. Resolution of Inflammation: What Controls Its Onset? *Front Immunol* (2016) 7. doi: 10.3389/fimmu.2016.00160
13. Buckley CD, Gilroy DW, Serhan CN. Proresolving Lipid Mediators and Mechanisms in the Resolution of Acute Inflammation. *Immunity* (2014) 40:315–27. doi: 10.1016/j.immuni.2014.02.009
14. Dingenouts CKE, Goumans M-J, Bakker W. Mononuclear Cells and Vascular Repair in HHT. *Front Genet* (2015) 6:114. doi: 10.3389/fgene.2015.00114
15. Godwin JW, Pinto AR, Rosenthal NA. Macrophages are Required for Adult Salamander Limb Regeneration. *Proc Natl Acad Sci USA* (2013) 110:9415–20. doi: 10.1073/pnas.1300290110
16. Wynn TA, Barron L. Macrophages: Master Regulators of Inflammation and Fibrosis. *Semin Liver Dis* (2010) 30:245–57. doi: 10.1055/s-0030-1255354
17. Bondeson J, Wainwright SD, Lauder S, Amos N, Hughes CE. The Role of Synovial Macrophages and Macrophage-Produced Cytokines in Driving Aggrecanases, Matrix Metalloproteinases, and Other Destructive and Inflammatory Responses in Osteoarthritis. *Arthritis Res Ther* (2006) 8:R187. doi: 10.1186/ar2099
18. Manferdini C, Paolella F, Gabusi E, Silvestri Y, Gambari L, Cattini L, et al. From Osteoarthritic Synovium to Synovial-Derived Cells Characterization: Synovial Macrophages are Key Effector Cells. *Arthritis Res Ther* (2016) 18:83–3. doi: 10.1186/s13075-016-0983-4
19. Kraus VB, McDaniel G, Huebner JL, Stabler TV, Pieper CF, Shipes SW, et al. Direct In Vivo Evidence of Activated Macrophages in Human Osteoarthritis. *Osteoarthritis Cartilage* (2016) 24:1613–21. doi: 10.1016/j.joca.2016.04.010
20. Van Weeren PR. General Anatomy and Physiology of Joints. In: D F., CW McIlwraith, CE Kawcak and PR van Weeren, editors. *Joint Disease in the Horse*. St Louis, MO: Elsevier (2016). p. 23–52.
21. Fichadiya A, Bertram KL, Ren G, Yates RM, Krawetz RJ. Characterizing Heterogeneity in the Response of Synovial Mesenchymal Progenitor Cells to Synovial Macrophages in Normal Individuals and Patients With Osteoarthritis. *J Inflamm (London England)* (2016) 13:12–2. doi: 10.1186/s12950-016-0120-9
22. Bellac CL, Dufour A, Krisinger MJ, Loonchanta A, Starr AE, Auf dem Keller U, et al. Macrophage Matrix Metalloproteinase-12 Dampens Inflammation and Neutrophil Influx in Arthritis. *Cell Rep* (2014) 9:618–32. doi: 10.1016/j.celrep.2014.09.006
23. Alivernini S, MacDonald L, Elmesmari A, Finlay S, Tolusso B, Gigante MR, et al. Distinct Synovial Tissue Macrophage Subsets Regulate Inflammation and Remission in Rheumatoid Arthritis. *Nat Med* (2020) 26:1295–306. doi: 10.1038/s41591-020-0939-8
24. Culemann S, Gruneboom A, Nicolas-Avila JA, Weidner D, Lammle KF, Rothe T, et al. Locally Renewing Resident Synovial Macrophages Provide a Protective Barrier for the Joint. *Nature* (2019) 572:670–5. doi: 10.1038/s41586-019-1471-1
25. Uderhardt S, Martins AJ, Tsang JS, Lammermann T, Germain RN. Resident Macrophages Cloak Tissue Microlesions to Prevent Neutrophil-Driven Inflammatory Damage. *Cell* (2019) 177:541–55.e17. doi: 10.1016/j.cell.2019.02.028
26. Kennedy A, Fearon U, Veale DJ, Godson C. Macrophages in Synovial Inflammation. *Front Immunol* (2011) 2:52–2. doi: 10.3389/fimmu.2011.00052
27. Menarim BC, Gillis KH, Oliver A, Ngo Y, Werre SR, Barrett SH, et al. Macrophage Activation in the Synovium of Healthy and Osteoarthritic Equine Joints. *Front Vet Sci* (2020) 7:568756–6. doi: 10.3389/fvets.2020.568756
28. Scanzello CR, Goldring SR. The Role of Synovitis in Osteoarthritis Pathogenesis. *Bone* (2012) 51:249–57. doi: 10.1016/j.bone.2012.02.012

29. Anna Paula Balesdent Barreira ALGA, Saito ME, Amorim RL, Kohayagawa A, Carvalho Menarim B, Sousa Mota L. Autologous Implant of Bone Mar-Row Mononuclear Cells as Treat-Ment of Induced Equine Tendinitis. *Intern J Appl Res Vet Med* (2008) 6:46–54.
30. Barussi FC, Bastos FZ, Leite LM, Fragoso FY, Senegaglia AC, Brofman PR, et al. Intratracheal Therapy With Autologous Bone Marrow-Derived Mononuclear Cells Reduces Airway Inflammation in Horses With Recurrent Airway Obstruction. *Respir Physiol Neurobiol* (2016) 232:35–42. doi: 10.1016/j.resp.2016.07.002
31. Chu CR, Fortier LA, Williams A, Payne KA, McCarrel TM, Bowers ME, et al. Minimally Manipulated Bone Marrow Concentrate Compared With Microfracture Treatment of Full-Thickness Chondral Defects: A One-Year Study in an Equine Model. *J Bone Joint Surg* (2018) 100:138–46. doi: 10.2106/JBJS.17.00132
32. Crovace A, Lacitignola L, Rossi G, Francioso E. Histological and Immunohistochemical Evaluation of Autologous Cultured Bone Marrow Mesenchymal Stem Cells and Bone Marrow Mononucleated Cells in Collagenase-Induced Tendinitis of Equine Superficial Digital Flexor Tendon. *Vet Med Int* (2010) 2010:250978. doi: 10.4061/2010/250978
33. Cruz FF, Borg ZD, Goodwin M, Coffey AL, Wagner DE, Rocco PR, et al. CD11b+ and Sca-1+ Cells Exert the Main Beneficial Effects of Systemically Administered Bone Marrow-Derived Mononuclear Cells in a Murine Model of Mixed Th2/Th17 Allergic Airway Inflammation. *Stem Cells Transl Med* (2016) 5:488–99. doi: 10.5966/sctm.2015-0141
34. Cuende N, Rico L, Herrera C. Concise Review: Bone Marrow Mononuclear Cells for the Treatment of Ischemic Syndromes: Medicinal Product or Cell Transplantation? *Stem Cells Transl Med* (2012) 1:403–8. doi: 10.5966/sctm.2011-0064
35. Menarim B, Fortini G, Álvarez P, Gómez J, Jarrín C, Ramírez A, et al. Autologous Implant of Bone Marrow Mononuclear Stem-Cells as Treatment for Equine Bicipital Tendonitis: Case Report. *Arch Med Vet* (2012) 44:291–5. doi: 10.4067/S0301-732X2012000300013
36. Nguyen TL, Nguyen HP, Nguyen TK. The Effects of Bone Marrow Mononuclear Cell Transplantation on the Quality of Life of Children With Cerebral Palsy. *Health Qual Life Outcomes* (2018) 16:164. doi: 10.1186/s12955-018-0992-x
37. Saw KY, Hussin P, Loke SC, Azam M, Chen HC, Tay YG, et al. Articular Cartilage Regeneration With Autologous Marrow Aspirate and Hyaluronic Acid: An Experimental Study in a Goat Model. *Arthroscopy* (2009) 25:1391–400. doi: 10.1016/j.arthro.2009.07.011
38. Song F, Tang J, Geng R, Hu H, Zhu C, Cui W, et al. Comparison of the Efficacy of Bone Marrow Mononuclear Cells and Bone Mesenchymal Stem Cells in the Treatment of Osteoarthritis in a Sheep Model. *Int J Clin Exp* (2014) 7:1415–26.
39. Giraldi-Guimarães A, de Freitas HT, Coelho B, Macedo-Ramos H, Mendez-Otero R, Cavalcante LA, et al. Bone Marrow Mononuclear Cells and Mannose Receptor Expression in Focal Cortical Ischemia. *Brain Res* (2012) 1452:173–84. doi: 10.1016/j.brainres.2012.03.002
40. Levy BD, Clish CB, Schmidt B, Gronert K, Serhan CN. Lipid Mediator Class Switching During Acute Inflammation: Signals in Resolution. *Nat Immunol* (2001) 2:612–9. doi: 10.1038/89759
41. Tsubosaka Y, Maehara T, Imai D, Nakamura T, Kobayashi K, Nagata N, et al. Hematopoietic Prostaglandin D Synthase-Derived Prostaglandin D2 Ameliorates Adjuvant-Induced Joint Inflammation in Mice. *FASEB J* (2019) 33:6829–37. doi: 10.1096/fj.201802153R
42. Gautier EL, Chow A, Spanbroek R, Marcelin G, Greter M, Jakubzick C, et al. Systemic Analysis of Pparγ in Mouse Macrophage Populations Reveals Marked Diversity in Expression With Critical Roles in Resolution of Inflammation and Airway Immunity. *J Immunol* (2012) 189:2614–24. doi: 10.4049/jimmunol.1200495
43. Croasdell A, Duffney PF, Kim N, Lacy SH, Sime PJ, Phipps RP. Pparγ and the Innate Immune System Mediate the Resolution of Inflammation. *PPAR Res* (2015) 2015:549691. doi: 10.1155/2015/549691
44. Czimmerer Z, Daniel B, Horvath A, Rückerl D, Nagy G, Kiss M, et al. The Transcription Factor STAT6 Mediates Direct Repression of Inflammatory Enhancers and Limits Activation of Alternatively Polarized Macrophages. *Immunity* (2018) 48:75–90.e6. doi: 10.1016/j.immuni.2017.12.010
45. Daniel B, Nagy G, Horvath A, Czimmerer Z, Cuaranta-Monroy I, Poliska S, et al. The IL-4/Stat6/Pparγ Signaling Axis Is Driving the Expansion of the RXR Heterodimer Cistrome, Providing Complex Ligand Responsiveness in Macrophages. *Nucleic Acids Res* (2018) 46:4425–39. doi: 10.1093/nar/gky157
46. Szanto A, Balint BL, Nagy ZS, Barta E, Dezso B, Pap A, et al. STAT6 Transcription Factor Is a Facilitator of the Nuclear Receptor Pparγ-Regulated Gene Expression in Macrophages and Dendritic Cells. *Immunity* (2010) 33:699–712. doi: 10.1016/j.immuni.2010.11.009
47. Varga T, Mounier R, Patsalos A, Gogolák P, Peloquin M, Horvath A, et al. Macrophage Pparγ, a Lipid Activated Transcription Factor Controls the Growth Factor GDF3 and Skeletal Muscle Regeneration. *Immunity* (2016) 45:1038–51. doi: 10.1016/j.immuni.2016.10.016
48. Goncars V, Kalnberzs K, Jakobsons E , En{ele I, Briede I, Blums K, et al. Treatment of Knee Osteoarthritis With Bone Marrow–Derived Mononuclear Cell Injection: 12-Month Follow-Up. *CARTILAGE* (2018) 10:26–35. doi: 10.1177/1947603517746721
49. Menarim BG, K H, Oliver A, Mason C, Ngo Y, Werre SR, et al. Dahlgren, LA Autologous Bone Marrow Mononuclear Cells Modulate Joint Homeostasis in an Equine *In Vivo* Model of Synovitis. *FASEB J* (2019) 33:14337–53. doi: 10.1096/fj.201901684RR
50. Menarim BC, Gillis KH, Oliver A, Mason C, Werre SR, Luo X, et al. Inflamed Synovial Fluid Induces a Homeostatic Response in Bone Marrow Mononuclear Cells *In Vitro*: Implications for Joint Therapy. *FASEB J* (2020) 34:4430–44. doi: 10.1096/fj.201902698R
51. Souza M. Osteoarthritis in Horses - Part 2: A Review of the Intra-Articular Use of Corticosteroids as a Method of Treatmentbraz. *Arch Biol Technol* (2016) 59:1–10. doi: 10.1590/1678-4324-2016150025
52. Behrendt P, Feldheim M, Preusse-Prange A, Weitkamp JT, Haake M, Eglin D, et al. Chondrogenic Potential of IL-10 in Mechanically Injured Cartilage and Cellularized Collagen ACI Grafts. *Osteoarthritis Cartilage / OARS Osteoarthritis Res Soc* (2018) 26:264–75. doi: 10.1016/j.joca.2017.11.007
53. Iannone F, De Bari C, Dell'Accio F, Covelli M, Cantatore FP, Patella V, et al. Interleukin-10 and Interleukin-10 Receptor in Human Osteoarthritic and Healthy Chondrocytes. *Clin Exp Rheumatol* (2001) 19:139–45.
54. Palmer JL, Bertone AL. Experimentally-Induced Synovitis as a Model for Acute Synovitis in the Horse. *Equine Vet J* (1994) 26:492–5. doi: 10.1111/j.2042-3306.1994.tb04056.x
55. Kalbfleisch TS, Rice ES, DePriest MS, Walenz BP, Hestand MS, Vermeesch JR, et al. Improved Reference Genome for the Domestic Horse Increases Assembly Contiguity and Composition. *Commun Biol* (2018) 1:197. doi: 10.1038/s42003-018-0199-z
56. Dobin A, Davis CA, Schlesinger F, Drenkow J, Zaleski C, Jha S, et al. STAR: Ultrafast Universal RNA-Seq Aligner. *Bioinformatics* (2013) 29:15–21. doi: 10.1093/bioinformatics/bts635
57. Smid M, Coebergh van den Braak RRJ, van de Werken HJG, van Riet J, van Galen A, de Weerd V, et al. Gene Length Corrected Trimmed Mean of M-Values (GeTMM) Processing of RNA-Seq Data Performs Similarly in Intersample Analyses While Improving Intrasample Comparisons. *BMC Bioinf* (2018) 19:236. doi: 10.1186/s12859-018-2246-7
58. Langfelder P, Horvath S. WGCNA: An R Package for Weighted Correlation Network Analysis. *BMC Bioinf* (2008) 9:559. doi: 10.1186/1471-2105-9-559
59. Davies CL, Patir A, McColl BW. Myeloid Cell and Transcriptome Signatures Associated With Inflammation Resolution in a Model of Self-Limiting Acute Brain Inflammation. *Front Immunol 10* (2019) 10. doi: 10.3389/fimmu.2019.01048
60. Li J, Zhou D, Qiu W, Shi Y, Yang J-J, Chen S, et al. Application of Weighted Gene Co-Expression Network Analysis for Data From Paired Design. *Sci Rep* (2018) 8:622. doi: 10.1038/s41598-017-18705-z
61. Abedi M, Gheisari Y. Nodes With High Centrality in Protein Interaction Networks are Responsible for Driving Signaling Pathways in Diabetic Nephropathy. *PeerJ* (2015) 3:e1284–4. doi: 10.7717/peerj.1284
62. Huang DW, Sherman BT, Lempicki RA. Systematic and Integrative Analysis of Large Gene Lists Using DAVID Bioinformatics Resources. *Nat Protoc* (2009) 4:44–57. doi: 10.1038/nprot.2008.211
63. Krämer A, Green J, Pollard J Jr., Tugendreich S. Causal Analysis Approaches in Ingenuity Pathway Analysis. *Bioinformatics* (2014) 30:523–30. doi: 10.1093/bioinformatics/btt703

64. Jensen LJ, Kuhn M, Stark M, Chaffron S, Creevey C, Muller J, et al. STRING 8–a Global View on Proteins and Their Functional Interactions in 630 Organisms. *Nucleic Acids Res* (2009) 37:D412–6. doi: 10.1093/nar/gkn760
65. Dalmer TRA, Clugston RD. Gene Ontology Enrichment Analysis of Congenital Diaphragmatic Hernia-Associated Genes. *Pediatr Res* (2019) 85:13–9. doi: 10.1038/s41390-018-0192-8
66. Sato T, Chang H-C, Bayeva M, Shapiro JS, Ramos-Alonso L, Kouzu H, et al. mRNA-Binding Protein Tristetraprolin is Essential for Cardiac Response to Iron Deficiency by Regulating Mitochondrial Functionproc. *Natl Acad Sci USA* (2018) 115:E6291–300. doi: 10.1073/pnas.1804701115
67. Lu SC. Regulation of Glutathione Synthesis. *Mol Aspects Med* (2009) 30:42–59. doi: 10.1016/j.mam.2008.05.005
68. Chang HR, Josefs T, Scerbo D, Gumaste N, Hu Y, Huggins LA, et al. Role of LpL (Lipoprotein Lipase) in Macrophage Polarization *In Vitro* and *In Vivo*. *Arterioscler Thromb Vasc Biol* (2019) 39:1967–85. doi: 10.1161/ATVBAHA.119.312389
69. Frisbie DD, Kawcak CE, Baxter GM, Trotter GW, Powers BE, Lassen ED, et al. Effects of 6alpha-Methylprednisolone Acetate on an Equine Osteochondral Fragment Exercise Model. *Am J Vet Res* (1998) 59:1619–28.
70. Frisbie DD, Kawcak CE, Trotter GW, Powers BE, Walton RM, McIlwraith CW. Effects of Triamcinolone Acetonide on an *In Vivo* Equine Osteochondral Fragment Exercise Model. *Equine Vet J* (1997) 29:349–59. doi: 10.1111/j.2042-3306.1997.tb03138.x
71. Garcia YA, Velasquez EF, Gao LW, Gholkar AA, Clutario KM, Cheung K, et al. Mapping Proximity Associations of Core Spindle Assembly Checkpoint Proteins. *J Proteome Res* (2021) 20:3414–27. doi: 10.1021/acs.jproteome.0c00941
72. Hara K, Taharazako S, Ikeda M, Fujita H, Mikami Y, Kikuchi S, et al. Dynamic Feature of Mitotic Arrest Deficient 2-Like Protein 2 (MAD2L2) and Structural Basis for its Interaction With Chromosome Alignment-Maintaining Phosphoprotein (CAMP). *J Biol Chem* (2017) 292:17658–67. doi: 10.1074/jbc.M117.804237
73. Duan Z, Huang H, Sun F. The Functional and Predictive Roles of miR-210 in Cryptorchidism. *Sci Rep* (2016) 6:32265. doi: 10.1038/srep32265
74. Freire PR, Conneely OM. NR4A1 and NR4A3 Restrict HSC Proliferation *via* Reciprocal Regulation of C/Ebpα and Inflammatory Signaling. *Blood* (2018) 131:1081–93. doi: 10.1182/blood-2017-07-795757
75. Mauer J, Chaurasia B, Goldau J, Vogt MC, Ruud J, Nguyen KD, et al. Signaling by IL-6 Promotes Alternative Activation of Macrophages to Limit Endotoxemia and Obesity-Associated Resistance to Insulin. *Nat Immunol* (2014) 15:423–30. doi: 10.1038/ni.2865
76. Elhage R, Clamens S, Besnard S, Mallat Z, Tedgui A, Arnal J, et al. Involvement of Interleukin-6 in Atherosclerosis But Not in the Prevention of Fatty Streak Formation by 17beta-Estradiol in Apolipoprotein E-Deficient Mice. *Atherosclerosis* (2001) 156:315–20. doi: 10.1016/S0021-9150(00)00682-1
77. Jenkins SJ, Ruckerl D, Cook PC, Jones LH, Finkelman FD, van Rooijen N, et al. Local Macrophage Proliferation, Rather Than Recruitment From the Blood, is a Signature of TH2 Inflammation. *Science* (2011) 332:1284–8. doi: 10.1126/science.1204351
78. Minutti CM, Modak RV, Macdonald F, Li F, Smyth DJ, Dorward DA, et al. A Macrophage-Pericyte Axis Directs Tissue Restoration *via* Amphiregulin-Induced Transforming Growth Factor Beta Activation. *Immunity* (2019) 50:645–654.e6. doi: 10.1016/j.immuni.2019.01.008
79. Meng C, Liu G, Mu H, Zhou M, Zhang S, Xu Y. Amphiregulin may be a New Biomarker of Classically Activated Macrophages. *Biochem Biophys Res Commun* (2015) 466:393–9. doi: 10.1016/j.bbrc.2015.09.037
80. Xu Y, Meng C, Liu G, Yang D, Fu L, Zhang M, et al. Classically Activated Macrophages Protect Against Lipopolysaccharide-Induced Acute Lung Injury by Expressing Amphiregulin in Mice. *Anesthesiology* (2016) 124:1086–99. doi: 10.1097/ALN.0000000000001026
81. Serhan CN, Gupta SK, Perretti M, Godson C, Brennan E, Li Y, et al. The Atlas of Inflammation Resolution (AIR). *Mol Aspects Med* (2020) 74:100894. doi: 10.1016/j.mam.2020.100894
82. Villa A, Rizzi N, Vegeto E, Ciana P, Maggi A. Estrogen Accelerates the Resolution of Inflammation in Macrophagic Cells. *Sci Rep* (2015) 5:15224. doi: 10.1038/srep15224
83. Noort AR, Tak PP, Tas SW. Non-Canonical NF-κb Signaling in Rheumatoid Arthritis: Dr Jekyll and Mr Hyde? *Arthritis Res Ther* (2015) 17:15. doi: 10.1186/s13075-015-0527-3
84. Lawrence T, Bebien M, Liu GY, Nizet V, Karin M. IKKalpha Limits Macrophage NF-kappaB Activation and Contributes to the Resolution of Inflammation. *Nature* (2005) 434:1138–43. doi: 10.1038/nature03491
85. Tricarico PM, Kleiner G, Valencic E, Campisciano G, Girardelli M, Crovella S, et al. Block of the Mevalonate Pathway Triggers Oxidative and Inflammatory Molecular Mechanisms Modulated by Exogenous Isoprenoid Compounds. *Int J Mol Sci* (2014) 15:6843–56. doi: 10.3390/ijms15046843
86. Marcuzzi A, Decorti G, Pontillo A, Ventura A, Tommasini A. Decreased Cholesterol Levels Reflect a Consumption of Anti-Inflammatory Isoprenoids Associated With an Impaired Control of Inflammation in a Mouse Model of Mevalonate Kinase Deficiency. *Inflamm Res* (2010) 59:335–8. doi: 10.1007/s00011-010-0168-6
87. Jin J, Qian H, Wan B, Zhou L, Chen C, Lv Y, et al. Geranylgeranyl Diphosphate Synthase Deficiency Hyperactivates Macrophages and Aggravates Lipopolysaccharide-Induced Acute Lung Injury. *Am J Physiol Lung Cell Mol Physiol* (2021) 320:L1011–l1024. doi: 10.1152/ajplung.00281.2020
88. Gomez Marti JL, Wells A, Brufsky AM. Dysregulation of the Mevalonate Pathway During SARS-CoV-2 Infection: An in Silico Study. *J Med Virol* (2021) 93:2396–405. doi: 10.1002/jmv.26743
89. Celec P, Behuliak M. The Lack of non-Steroid Isoprenoids Causes Oxidative Stress in Patients With Mevalonic Aciduria. *Med Hypotheses* (2008) 70:938–40. doi: 10.1016/j.mehy.2007.08.030
90. Buhaescu I, Izzedine H. Mevalonate Pathway: A Review of Clinical and Therapeutical Implications. *Clin Biochem* (2007) 40:575–84. doi: 10.1016/j.clinbiochem.2007.03.016
91. Marcuzzi A, Pontillo A, Leo LD, Tommasini A, Decorti G, Not T, et al. Natural Isoprenoids are Able to Reduce Inflammation in a Mouse Model of Mevalonate Kinase Deficiency. *Pediatr Res* (2008) 64:177–82. doi: 10.1203/PDR.0b013e3181761870
92. Healey GD, Collier C, Griffin S, Schuberth H-J, Sandra O, Smith DG, et al. Mevalonate Biosynthesis Intermediates Are Key Regulators of Innate Immunity in Bovine Endometritis. *J Immunol* (2016) 196:823–31. doi: 10.4049/jimmunol.1501080
93. Santoro A, Ciaglia E, Nicolin V, Pescatore A, Prota L, Capunzo M, et al. The Isoprenoid End Product N6-Isopentenyladenosine Reduces Inflammatory Response Through the Inhibition of the Nfκb and STAT3 Pathways in Cystic Fibrosis Cells. *Inflamm Res* (2018) 67:315–26. doi: 10.1007/s00011-017-1123-6
94. Kors S, Geijtenbeek K, Reits E, Schipper-Krom S. Regulation of Proteasome Activity by (Post-)Transcriptional MechanismsFront. *Mol Biosci 6* (2019) 42:297–307. doi: 10.3389/fmolb.2019.00048
95. Zhao Y, Abreu E, Kim J, Stadler G, Eskiocak U, Terns MP, et al. Processive and Distributive Extension of Human Telomeres by Telomerase Under Homeostatic and Nonequilibrium Conditions. *Mol Cell* (2011) 42:297–307. doi: 10.1016/j.molcel.2011.03.020
96. Jády BE, Richard P, Bertrand E, Kiss T. Cell Cycle-Dependent Recruitment of Telomerase RNA and Cajal Bodies to Human Telomeres. *Mol Biol Cell* (2006) 17:944–54. doi: 10.1091/mbc.e05-09-0904
97. Freund A, Zhong FL, Venteicher AS, Meng Z, Veenstra TD, Frydman J, et al. Proteostatic Control of Telomerase Function Through TRiC-Mediated Folding of TCAB1. *Cell* (2014) 159:1389–403. doi: 10.1016/j.cell.2014.10.059
98. Grantham J. The Molecular Chaperone CCT/TRiC: An Essential Component of Proteostasis and a Potential Modulator of Protein Aggregation. *Front Genet* (2020) 11. doi: 10.3389/fgene.2020.00172
99. Rosa L.F.B.P.C., Safi DA, Curi R. Effect of Hypo- and Hyperthyroidism on the Function and Metabolism of Macrophages in Rats. *Cell Biochem Funct* (1995) 13:141–7. doi: 10.1002/cbf.290130211
100. Perrotta C, Buldorini M, Assi E, Cazzato D, De Palma C, Clementi E, et al. The Thyroid Hormone Triiodothyronine Controls Macrophage Maturation and Functions: Protective Role During Inflammation. *Am J Pathol* (2014) 184:230–47. doi: 10.1016/j.ajpath.2013.10.006
101. Sanchis-Gomar F, García-Giménez JL, Gómez-Cabrera MC, Pallardó FV. Mitochondrial Biogenesis in Health and Disease. *Mol Ther Approaches Curr Pharm Des* (2014) 20:5619–33. doi: 10.2174/1381612820666140306095106
102. Anderson EJ, Thayne KA, Harris M, Shaikh SR, Darden TM, Lark DS, et al. Do Fish Oil Omega-3 Fatty Acids Enhance Antioxidant Capacity and

Mitochondrial Fatty Acid Oxidation in Human Atrial Myocardium *via* Pparγ Activation? *Antioxid Redox Signal* (2014) 21:1156–63. doi: 10.1089/ars.2014.5888
103. Hernández-Aguilera A, Rull A, Rodríguez-Gallego E, Riera-Borrull M, Luciano-Mateo F, Camps J, et al. Mitochondrial Dysfunction: A Basic Mechanism in Inflammation-Related non-Communicable Diseases and Therapeutic Opportunities. *Mediat Inflamm* (2013) 2013:135698–8. doi: 10.1155/2013/135698
104. Raoof R, van der Vlist M, Willemen HLDM, Prado J, Versteeg S, Vos M, et al. Macrophages Transfer Mitochondria to Sensory Neurons to Resolve Inflammatory Pain. *bioRxiv* (2020) 2020.02.12.940445:1–32. doi: 10.1101/2020.02.12.940445
105. Ramond E, Jamet A, Coureuil M, Charbit A. Pivotal Role of Mitochondria in Macrophage Response to Bacterial Pathogens. *Front Immunol* (2019) 10. doi: 10.3389/fimmu.2019.02461
106. Cao X, Yang S, Cao C, Zhou YJ. Harnessing Sub-Organelle Metabolism for Biosynthesis of Isoprenoids in Yeast. *Synth Syst Biotechnol* (2020) 5:179–86. doi: 10.1016/j.synbio.2020.06.005
107. Xuan W, Song D, Yan Y, Yang M, Sun Y. A Potential Role for Mitochondrial DNA in the Activation of Oxidative Stress and Inflammation in Liver Disease. *Oxid Med Cell Longev* (2020) 2020:5835910. doi: 10.1155/2020/5835910
108. Heming M, Gran S, Jauch S-L, Fischer-Riepe L, Russo A, Klotz L, et al. Peroxisome Proliferator-Activated Receptor-γ Modulates the Response of Macrophages to Lipopolysaccharide and Glucocorticoids. *Front Immunol* (2018) 9:893–3. doi: 10.3389/fimmu.2018.00893
109. Lee YJ, Kim BM, Ahn YH, Choi JH, Choi YH, Kang JL. STAT6 Signaling Mediates Pparγ Activation and Resolution of Acute Sterile Inflammation in Mice. *Cells* (2021) 10:501. doi: 10.3390/cells10030501
110. Asada K, Sasaki S, Suda T, Chida K, Nakamura H. Antiinflammatory Roles of Peroxisome Proliferator-Activated Receptor Gamma in Human Alveolar Macrophages. *Am J Respir Crit* (2004) 169:195–200. doi: 10.1164/rccm.200207-740OC
111. Giannakis N, Sansbury BE, Patsalos A, Hays TT, Riley CO, Han X, et al. Dynamic Changes to Lipid Mediators Support Transitions Among Macrophage Subtypes During Muscle Regeneration. *Nat Immunol* (2019) 20:626–36. doi: 10.1038/s41590-019-0356-7
112. Prein C, Beier F. PGC1A is Required for Chondrocyte Metabolism and Cartilage Homeostasis. *Osteoarthritis Cartilage* (2020) 28:S25–6. doi: 10.1016/j.joca.2020.02.040
113. Xaus J, Comalada M, Barrachina M, Herrero C, Goñalons E, Soler C, et al. The Expression of MHC Class II Genes in Macrophages Is Cell Cycle Dependent. *J Immunol* (2000) 165:6364–71. doi: 10.4049/jimmunol.165.11.6364
114. McCubrey JA, May WS, Duronio V, Mufson A. Serine/threonine Phosphorylation in Cytokine Signal Transduction. *Leukemia* (2000) 14:9–21. doi: 10.1038/sj.leu.2401657
115. Takeda K, Tanaka T, Shi W, Matsumoto M, Minami M, Kashiwamura S, et al. Essential Role of Stat6 in IL-4 Signalling. *Nature* (1996) 380:627–30. doi: 10.1038/380627a0
116. Seok J, Warren HS, Cuenca AG, Mindrinos MN, Baker HV, Xu W, et al. Genomic Responses in Mouse Models Poorly Mimic Human Inflammatory Diseases. *Proc Natl Acad Sci USA* (2013) 110:3507–12. doi: 10.1073/pnas.1222878110
117. Karagianni AE, Kapetanovic R, Summers KM, McGorum BC, Hume DA, Pirie RS. Comparative Transcriptome Analysis of Equine Alveolar Macrophages. *Equine Vet J* (2016) 49:375–82. doi: 10.1111/evj.12584
118. McIlwraith C. Traumatic Arthritis and Posttraumatic Osteoarthritis in the Horse. In: F D., CW McIlwraith, CE Kawcak and PR van Weeren, editors. *Joint Disease in the Horse*. St. Louis, MO: Elsevier (2016). p. 33–44.
119. Goncars V, Jakobsons E, Blums K, Briede I, Patetko L, Erglis K, et al. The Comparison of Knee Osteoarthritis Treatment With Single-Dose Bone Marrow-Derived Mononuclear Cells vs. Hyaluronic Acid Injections. *Med (Kaunas Lithuania)* (2017) 53:101–8. doi: 10.1016/j.medici.2017.02.002
120. Stables MJ, Shah S, Camon EB, Lovering RC, Newson J, Bystrom J, et al. Transcriptomic Analyses of Murine Resolution-Phase Macrophages. *Blood* (2011) 118:e192–208. doi: 10.1182/blood-2011-04-345330
121. Pietras EM, Mirantes-Barbeito C, Fong S, Loeffler D, Kovtonyuk LV, Zhang S, et al. Chronic Interleukin-1 Exposure Drives Haematopoietic Stem Cells Towards Precocious Myeloid Differentiation at the Expense of Self-Renewal. *Nat Cell Biol* (2016) 18:607–18. doi: 10.1038/ncb3346
122. Sergijenko A, Roelofs AJ, Riemen AHK, De Bari C. Bone Marrow Contribution to Synovial Hyperplasia Following Joint Surface Injury. *Arthritis Res Ther* (2016) 18:166–6. doi: 10.1186/s13075-016-1060-8
123. Ryncarz RE, Anasetti C. Expression of CD86 on Human Marrow CD34(+) Cells Identifies Immunocompetent Committed Precursors of Macrophages and Dendritic Cells. *Blood* (1998) 91:3892–900. doi: 10.1182/blood.V91.10.3892.3892_3892_3900
124. St Clair EW. Interleukin 10 Treatment for Rheumatoid Arthritis. *Ann Rheum Dis* (1999) 58:I99–I102. doi: 10.1136/ard.58.2008.i99
125. Olingy CE, San Emeterio CL, Ogle ME, Krieger JR, Bruce AC, Pfau DD, et al. Non-Classical Monocytes are Biased Progenitors of Wound Healing Macrophages During Soft Tissue Injury. *Sci Rep* (2017) 7:447. doi: 10.1038/s41598-017-00477-1

Conflict of Interest: The authors declare that the research was conducted in the absence of any commercial or financial relationships that could be construed as a potential conflict of interest.

Publisher's Note: All claims expressed in this article are solely those of the authors and do not necessarily represent those of their affiliated organizations, or those of the publisher, the editors and the reviewers. Any product that may be evaluated in this article, or claim that may be made by its manufacturer, is not guaranteed or endorsed by the publisher.

Copyright © 2021 Menarim, El-Sheikh Ali, Loux, Scoggin, Kalbfleisch, MacLeod and Dahlgren. This is an open-access article distributed under the terms of the Creative Commons Attribution License (CC BY). The use, distribution or reproduction in other forums is permitted, provided the original author(s) and the copyright owner(s) are credited and that the original publication in this journal is cited, in accordance with accepted academic practice. No use, distribution or reproduction is permitted which does not comply with these terms.

frontiers in Immunology

ORIGINAL RESEARCH
published: 22 December 2021
doi: 10.3389/fimmu.2021.754475

Pro-Resolving Factors Released by Macrophages After Efferocytosis Promote Mucosal Wound Healing in Inflammatory Bowel Disease

*Omayra Martin-Rodriguez[1], Thierry Gauthier[1], Francis Bonnefoy[1,2], Mélanie Couturier[1,2], Anna Daoui[1], Cécile Chagué[1], Séverine Valmary-Degano[3], Claire Gay[4], Philippe Saas[1] and Sylvain Perruche[1,2]**

[1] Univ. Bourgogne Franche-Comté, INSERM, EFS BFC, UMR1098 RIGHT, Interactions Hôte-Greffon-Tumeur/Ingénierie Cellulaire et Génique, Fédération Hospitalo-Universitaire INCREASE, LabEx LipSTIC, Besançon, France, [2] MED'INN'Pharma, Besançon, France, [3] Department of Pathology, University Hospital of Besançon, Besançon, France, [4] Department of Gastroenterology, University Hospital of Besançon, Besançon, France

OPEN ACCESS

Edited by:
Robson Coutinho-Silva, Federal University of Rio de Janeiro, Brazil

Reviewed by:
Jingbo Pang, University of Illinois at Chicago, United States
Claudia Farias Benjamim, Federal University of Rio de Janeiro, Brazil

***Correspondence:**
Sylvain Perruche
sylvain.perruche@inserm.fr

Specialty section:
This article was submitted to Inflammation, a section of the journal Frontiers in Immunology

Received: 06 August 2021
Accepted: 06 December 2021
Published: 22 December 2021

Citation:
Martin-Rodriguez O, Gauthier T, Bonnefoy F, Couturier M, Daoui A, Chagué C, Valmary-Degano S, Gay C, Saas P and Perruche S (2021) Pro-Resolving Factors Released by Macrophages After Efferocytosis Promote Mucosal Wound Healing in Inflammatory Bowel Disease. Front. Immunol. 12:754475. doi: 10.3389/fimmu.2021.754475

Nonresolving inflammation is a critical driver of several chronic inflammatory diseases, including inflammatory bowel diseases (IBD). This unresolved inflammation may result from the persistence of an initiating stimulus or from the alteration of the resolution phase of inflammation. Elimination of apoptotic cells by macrophages (a process called efferocytosis) is a critical step in the resolution phase of inflammation. Efferocytosis participates in macrophage reprogramming and favors the release of numerous pro-resolving factors. These pro-resolving factors exert therapeutic effects in experimental autoimmune arthritis. Here, we propose to evaluate the efficacy of pro-resolving factors produced by macrophages after efferocytosis, a secretome called SuperMApo, in two IBD models, namely dextran sodium sulfate (DSS)-induced and T cell transfer-induced colitis. Reintroducing these pro-resolving factors was sufficient to decrease clinical, endoscopic and histological colitis scores in ongoing naive T cell-transfer-induced colitis and in DSS-induced colitis. Mouse primary fibroblasts isolated from the colon demonstrated enhanced healing properties in the presence of SuperMApo, as attested by their increased migratory, proliferative and contractive properties. This was confirmed by the use of human fibroblasts isolated from patients with IBD. Exposure of an intestinal epithelial cell (IEC) line to these pro-resolving factors increased their proliferative properties and IEC acquired the capacity to capture apoptotic cells. The improvement of wound healing properties induced by SuperMApo was confirmed *in vivo* in a biopsy forceps-wound colonic mucosa model. Further *in vivo* analysis in naive T cell transfer-induced colitis model demonstrated an improvement of intestinal barrier permeability after administration of SuperMApo, an intestinal cell proliferation and an increase of α-SMA expression by fibroblasts, as well as a reduction of the transcript coding for fibronectin (*Fn1*). Finally, we identified TGF-β, IGF-I and VEGF among SuperMApo as necessary to favor mucosal healing and confirmed their role both *in vitro* (using neutralizing antibodies) and *in vivo* by depleting these factors from efferocytic macrophage secretome using

antibody-coated microbeads. These growth factors only explained some of the beneficial effects induced by factors released by efferocytic macrophages. Overall, the administration of pro-resolving factors released by efferocytic macrophages limits intestinal inflammation and enhance tissue repair, which represents an innovative treatment of IBD.

Keywords: efferocytosis, resolution of inflammation, macrophages, fibroblasts, colitis, wound healing

1 INTRODUCTION

Inflammatory bowel diseases (IBD, including Crohn's disease [CD] and ulcerative colitis [UC]) consist in a family of chronic idiopathic relapsing diseases characterized by a dysregulated response of the innate and adaptive immune system. This dysregulated response leads to the damage of the intestine and of the colonic mucosa (1). Today, the most commonly available treatments for IBD are based on immunosuppressive agents that target the deleterious effector arm of the pathogenic immune response (2). However, these current approaches are not entirely effective and not specific to pathogenic immune cells triggering IBD. They are responsible for multiple adverse effects, including an increased susceptibility to infections. In most cases, surgical resection remains the ultimate therapeutic alternative. Despite significant improvements in the management of IBD patients brought by the development of innovative drugs [such as biologic agents like anti-TNF therapy (3, 4)], new therapeutic strategies are needed.

Non-immune components of the intestinal mucosa are also involved in the pathogenesis of IBD (5). This is illustrated by intestinal epithelial cell (IEC) damage which participates in IBD pathogenesis (6). Indeed, mucosal healing is emerging as a critical endpoint in clinical trials and practice (2, 7). Under normal homeostatic conditions, once neutrophils have controlled and eliminated the mucosal insult, they undergo apoptosis at the site of inflammation (8), and then attract blood-derived monocytes through "find-me" signals (9). Together with tissue-resident phagocytes, monocyte-derived macrophages eliminate apoptotic cells through a process called efferocytosis (10). Along with a pro-inflammatory to pro-resolving lipid shift (11), efferocytosis triggers the resolution of inflammation, leading to restoration of homeostasis and regeneration of a functional tissue (12). Factors produced by efferocytic macrophages promote wound repair (13). This repair involves the migration, proliferation and differentiation of different cell types, including macrophages, fibroblasts, as well as IEC in IBD (2). The secretome of macrophages triggered by apoptotic cell removal (thereafter called SuperMApo) demonstrates its ability to terminate chronic inflammation and restore tissue homeostasis in several inflammatory situations, particularly in ongoing arthritis (14). SuperMApo contains several factors, including chemokines (CCL5, CXCL2, and CCL22) and cytokines (IL-1RA, IL-10, and TGF-β) (14). In the treatment of collagen-induced arthritis with SuperMApo, TGF-β demonstrated a critical role in association with co-factors (14). In that context, SuperMApo induced auto-antigen-specific regulatory T cells through the reprogramming of antigen-presenting cells, in particular macrophages (14).

During intestinal inflammation, the differentiation of monocytes into mature intestinal macrophages is disrupted; this delays efferocytosis and aborts the resolution phase. Neutrophils accumulate in the *lamina propria* (15), resist transiently to apoptosis (16) and generate a highly inflammatory microenvironment contributing to tissue destruction (17). This favors a pro-inflammatory macrophage profile; these activated macrophages release inflammatory mediators (18, 19) preventing neutrophil apoptosis and delaying the pro-inflammatory to pro-resolving lipid shift (20, 21). This creates a pro-inflammatory loop.

Triggering an efficient resolution of inflammation in IBD seems an innovative approach to limit inflammation and favor tissue healing (22, 23). Apoptotic cell-based approaches have been successfully evaluated to trigger resolution in two experimental models of IBD, triggering resolution through the efficient elimination of apoptotic cells by phagocytes and the consequent release of pro-resolutive factors (24, 25). We therefore addressed whether the administration of pro-resolving factors released by macrophages after efferocytosis would be able to restore intestinal mucosa homeostasis. Here, we provide evidence that reintroducing these pro-resolving factors enhances tissue repair as the colon mucosa ameliorations observed in the DSS-induced chronic colitis model, showing similarities with UC (notably the presence of crypt abscesses), and in the T cell transfer-induced colitis showing similarities with CD (notably endoscopic and histological deep ulcerations and inflammatory cell infiltration), thanks to video-endoscopy. The same pro-healing properties of SuperMApo pro-resolutive drug were also observed in absence of systemic inflammation using a model of forceps-induced intestinal wound. Pro-resolving factors modulate local fibroblasts and IEC, which then acquire pro-resolving properties. Our findings reveal that pro-resolving factors released by macrophages after efferocytosis represent important modulators of mucosal inflammation and healing. This represents a new therapeutic approach for the treatment of IBD.

2 MATERIAL AND METHODS

2.1 Mice

Four to eight-week-old C57BL/6 female mice were obtained from Charles River Laboratories (L'Arbresle, France) and kept in quarantine for at least one week before any experimental

procedure. Rag2-deficient (Rag-$2^{-/-}$) C57BL/6 mice were bred in our specific pathogen-free rodent facility. Mice were housed in this facility (#D25-056-7) in standard plastic cages with cellulose bedding in environmentally controlled and germ-free rooms at 22°C, and kept under a 12-hour light/dark cycle. Pellet food and sterile tap water (Hydropack; Plexx) were available *ad libitum*. Experimentation (#02831) was approved by the local ethic committee (#58) and the French Ministry of Higher Education and Research (*Ministère de l'Enseignement Supérieur, de la Recherche et l'Innovation*) and was conducted in accordance with the European Union Directive 2010/63.

2.2 *In Vivo* Intestinal Mucosal Injury Procedure

An intestinal mucosal wound was performed as previously described (26). To wound the C57BL/6 mouse colon, a biopsy forceps was inserted into the working channel of the endoscope (superslim 8.4 Fr, 2.8 mm, flexible video ureteroscope [URF V2; Olympus]) and introduced into the colon of a 2% isoflurane-anaesthetized 6 to 8-week-old mice. Under visual control, a small piece of mucosa was carefully removed. SuperMApo or vehicle (X-vivo) was administrated i.p. the day of the injury and 48 hrs later (1 mL per mouse/injection). The process of wound healing was subsequently monitored by daily endoscopies.

2.3 Naive T Cell Transfer-Induced Colitis

Naive $CD25^{-}CD45RB^{high}CD4^{+}$ T cells were sorted by flow cytometry (cell sorter SH800Z, SONY) from magnetically enriched $CD4^{+}$ spleen and lymph node cell suspensions (EasySep Mouse $CD4^{+}$ T Cell Isolation Kit; StemCell Technology) to a >95% purity. According to the described model (27), 5.10e5 naive T cells sorted from C57BL/6 were injected into the tail vein of 6 to 8-week-old Rag-$2^{-/-}$ C57BL/6 mice to induce colitis. Mice were monitored daily for clinical assessment of colitis and twice a week by video-endoscopy to appreciate colon mucosa. SuperMApo or vehicle (X-vivo) was administrated i.p. at day 10, after T cell transfer, and 48 hrs later (1 mL/mouse/injection). At that time (10 days post-T cell transfer) mice experimented a 6 to 7 MEICS score, out of 15. In additional *in vivo* experiments, TGF-β, IGF-I and VEGF recombinant growth factors (R&D systems), or PBS, were administrated i.p. at day 10, after T cell transfer, and 48 hrs later (1 mL per mouse/injection; TGF-β: 700 pg/mL, IGF-I: 1050 pg/mL and VEGF 350 pg/mL).

2.4 Dextran Sulfate Sodium (DSS)-Induced Colitis

Chronic DSS colitis was induced in 6 to 8-week-old C57BL/6 mice with the addition of 3% of DSS (MP Biomedicals LLC) in drinking water for seven consecutive days. Then, regular water was given for the next 10 days, and this cycle was repeated twice. Control mice were given with tap water only. Mice were monitored daily for clinical assessment of colitis and twice a week by video-endoscopy to appreciate their colon mucosa. SuperMApo or vehicle (X-vivo) were given i.p. the day of the first DSS cycle initiation, and 48 hrs later (1 mL/mouse).

2.5 Mice Monitoring and Video-Endoscopy

The mice were monitored daily for clinical assessment of colitis according to a total clinical score of 0 to 9 assigned to each animal and composed of the sum of the body weight loss (0 to 5% of weight loss = 0; 5 to 10% = 1; 10 to 15% = 2; 15 to 20% = 3; >20% = 4), the feces appearance (normal = 0; diarrhea = 1; bloody stools = 2), and the general behavior (normal = 0; mild alteration = 1; piloerection and motor activity altered = 2; severe alteration = 3). The mice were monitored twice a week by video-endoscopy under 2% isoflurane-induced anesthesia, without bowel preparation nor starving. Video-endoscopy was performed using a superslim 8.4 Fr (2.8 mm) flexible video ureteroscope (URF V2; Olympus), connected to OTV-S190 and CLV-S190 visera elite monitor system (Olympus), with a narrow band imaging system enhancing visibility of vascular structures. Endoscopic assessment of mucosal inflammation was reported with the murine endoscopic index of clinical severity (MEICS) score (28), composed of five parameters rated from 0 to 3, including: thickening of the colon, changes in the vascular pattern, fibrin deposition, granularity of the mucosal surface, and stool consistency.

2.6 Intestinal Permeability Evaluation

The mice were submitted to gavage with fluorescein isothiocynate (FITC)-dextran (MW 4000; Sigma-Aldrich) at 80 mg/kg of body weight, five hrs prior to blood collection through retro orbital puncture. Fluorescence intensity in the serum was measured at 520 nm (Perkin Elmer). FITC-dextran concentrations were determined from a standard curve generated by a serial dilution of FITC-dextran. Quantification of regenerating islet derived protein 3-γ (REG-3γ) concentrations in plasma was determined by ELISA (Cloud clone corporation) according to the manufacturer's instructions.

2.7 Generation of pro-Resolving Factors Released by Efferocytic Macrophages

Pro-resolving factors from mouse or human pro-resolving macrophages (called SuperMApo) were produced as described previously (14). Briefly, SuperMApo consisted in the supernatant of a 48-hr culture of apoptotic thymocytes (rendered apoptotic by a 35 Gy-irradiation) with thioglycolate-elicited peritoneal macrophages, in X-vivo culture medium to a 5 to 1 ratio, respectively (14). Human SuperMApo consisted in the 48-hr culture supernatant of M-CSF blood monocyte-derived macrophages cultured with apoptotic autologous peripheral blood mononuclear cells (rendered apoptotic by a 35 Gy-irradiation) to a 5 to 1 ratio in MEM medium, respectively (14). Supernatants were collected, centrifuged to eliminate debris, filtered through a 0.22 µm filter and frozen or lyophilized and frozen for conservation. SuperMApo was used directly in culture experiments (see *Functional Assays*) or injected i.p. for *in vivo* experiments (1 ml/mouse repeated 48 hrs later, in total 2 ml per mouse). In some *in vitro* experiments, VEGF (AF493NA), TGF-β (MAB240) and IGF-I (AF791) neutralizing antibodies or control anti-goat IgG (AB-108-C) or anti-mouse IgG1 antibodies (MAB002) (all from R&D systems),

were used in addition to SuperMApo. In some *in vivo* experiments, growth factors were immuno-magnetically depleted from SuperMApo. Briefly, 10 µg/ml of antibodies directed against VEGF and IGF-I (the same clones than in blocking experiments) as well as 50 µg/ml of anti-TGF-β antibody (2G7 clone; provided by Prof. L. Chatenoud) were incubated for one hour with SuperMApo at room temperature. Then, goat anti-mouse IgG (Polysciences Europe GMBH) or rabbit anti-goat IgG (Rockland) coated magnetic beads were incubated separately with a pre-formed antigen (Ag)-antibody (Ab) complex for 20 minutes or one hour respectively, at room temperature. The Ag-Ab-bead complexes were then captured using a magnetic separator. Protein levels of FGF, EGF, TGF-β, IGF-I and VEGF in SuperMApo were determined by ELISA (all from R&D systems), according to the manufacturer's protocols.

2.8 Histological Analysis and Immunofluorescence

Immediately after sacrificing the mice, tissue samples from the proximal, median and distal parts of the colon were collected and fixed overnight in 5% formalin. Paraffin inclusions were performed on the macroscopic injured area. Then, 4 µm sections were stained with hematoxylin-eosin-saffron (HES). A histological evaluation was performed by an experimented pathologist blinded to the nature of the mice being examined, using a five-degree severity score based on inflammatory cell infiltration, erosions and ulcerations, epithelial hyperplasia and mucin depletion, as previously described (29). Cytofix/Cytoperm buffer (eBioscience) was applied for the detection of nuclear staining. The primary antibodies used for immunostaining of mouse tissue and primary fibroblasts were: rabbit anti-mouse Ki-67 (clone SP6; Abcam), rabbit anti-human α-smooth muscle actin (α-SMA) (polyclonal; Abcam) and Alexa 488-conjugated rabbit anti-vimentin (Clone D21H3; Cell signaling). The secondary antibody was Alexa Fluor 555 goat anti-rabbit IgG (H+L) (Life Technologies). The nuclei were counterstained with DAPI (Sigma-Aldrich). Fluorescence analysis was performed with Olympus IX81 and Fluoview FV1000 software (Olympus). For quantitative analyses, at least four to five representative high-power fields (HPF, 40X) per section were evaluated in a blinded manner.

2.9 RNA Isolation and PCR Analysis

Total RNA were extracted from tissues or cells using the RNeasy mini kit (Qiagen) and 1 to 2 µg of RNA was reversed-transcribed into cDNA using the high capacity RNA to cDNA kit (Applied Biosystems). Then, cDNA were quantified by real time RT-PCR using the power SYBR green PCR master mix (Applied Biosystems) using *Col1a1* (Mm0080 1666_m1), *Col3a1* (Mm0125 4476_m1), *Fn1* (Mm0125 6744_m1) and *GAPDH* primers (from Applied Biosystems). Relative mRNA levels were determined using the ΔΔCt method. Values were expressed relative to *GAPDH* levels.

2.10 Cell Isolation and Culture

Fibroblasts were isolated from C57BL/6 mice colon mucosa or from human colon biopsies (30). Colon biopsies were collected according to standard procedures. This study was approved by the Ethics Committee of Besançon (#14/456; date of approval: July 13th, 2021), and all participants signed an informed consent form. Mucosal sheets were treated with 5 mM of EDTA (Life Technologies) in calcium-free HBSS (Life Technologies) five times at 37°C for 15 min to remove the epithelial layer. The mucosal sheets without epithelial cells were then cut into small pieces and cultured in completed RPMI-1640 medium (Life Technologies) containing 10% of FBS (Life technologies), 1% of penicillin/streptomycin and 10 mg/mL of collagenase D (Roche) for 60 min at 37°C, 5% CO_2. Isolated fibroblasts were cultured in RPMI-1640 medium containing 10% of FBS, 1% of penicillin/streptomycin, 10 mM of sodium pyruvate (Lonza), 1 mM of non-essential amino acids (Lonza) and 0.05 mM of 2 beta-mercaptoethanol (Sigma Aldrich). The cultured fibroblasts were used for experiments after two to four passages. The immortalized MODE-K cell line derived from mouse small IEC was obtained from INSERM U1111 (31). Cells were cultured in completed RPMI-1640 medium at 37°C, 5% CO_2.

2.11 Functional Assays

2.11.1 Proliferation and Phagocytosis

Cell proliferation was determined by mitochondrial activity using the 3-(4,5-dimethylthiazol-2yl)-2,5-diphenyltetrazolium bromide (MTT) assay according to the manufacturer's instructions. For the phagocytic assay, apoptotic cells were stained with carboxyfluorescein succinimidyl ester (CFSE; Invitrogen) according to the manufacturer's protocol, and co-cultured with MODE-K cells for six hours in 24-well plates with 1 mL of SuperMApo or X-vivo control medium. Phagocytosis was determined by FACS.

2.11.2 Wound Healing Scratch Assay and Migration Assay

For the wound-healing scratch assay, cells were seeded in 6-well plates (5.10e5 cells/well) and grown to confluence. Then, linear mechanical scratch wounds were performed in each well using a 1000-µl plastic pipette tip, and the rate of cell migration in the presence of 5 mL of SuperMApo or X-vivo control medium was measured by determining the surface empty of cells immediately after wounding (day 0) and at different times as indicated. For migration assays, 8-µm pore size transwells (Greiner) were used with cells seeded on the top of the transwells, and incubated for 24 hrs at 37°C, 5% CO_2, in the presence of 1 mL of SuperMApo or X-vivo control medium. Then, after removing cells from the top using a cotton bud, cells at the bottom of the wells were fixed with 100% of ethanol, stained with 2% of crystal violet and pictures from each membrane were taken. Finally, the invasive cells located in the lower chamber were counted manually.

2.11.3 Contraction Assay

Concerning the contraction assays, collagen culture gel was prepared as previously described (32). Briefly, collagen was prepared by mixing 0.1% of acetic acid with rat-tail type 1 collagen (Corning®) to 3 mg/mL. Then, 400 µL of cell suspension was mixed with 200 µL of collagen solution in a 24-well plate. Quickly, 1 M of NaOH was added to the well for

gel solidification. After 20 min, the gel was finally detached from the bottom of the well and incubated during 24 hrs at 37°C, 5% CO_2 in the presence of 1 mL of SuperMApo or X-vivo control medium. Gel contractions were determined by the measurement of collagen disk diameters at different time points.

2.12 Statistical Analysis

Data are expressed as mean ± standard error of the mean (s.e.m.), and were analyzed using adapted statistical tests, as indicated in figure legends, using GraphPad Prism software (5.01 version). A p-value below 0.05 was considered statistically significant.

3 RESULTS

3.1 Pro-Resolving Factors Released by Macrophages After Efferocytosis Promote the Resolution of Inflammatory Bowel Diseases

The pro-resolving functions of the factors released by macrophages after co-culture with apoptotic cells (named SuperMApo) have been described previously (14). These factors were evaluated for their capacity to stop naive T cell transfer-induced colitis. SuperMApo was injected twice (at a 48-hr interval) in mice exhibiting ongoing colitis, as attested by a MEICS score of 6 to 7 out of 15 (determined by live colonic endoscopy). The day after the last injection, colonic lesions stopped progressing in SuperMApo-treated mice, as attested by the MEICS score stagnation, whereas these lesions aggravated in vehicle-treated mice (**Figure 1A**). A thickening and increased granularity of the colon mucosa, a high fibrin deposition as well as thinner and tortuous blood vessels demonstrated lesion worsening between the last day of treatment (day 10) and day 19 in vehicle-treated mice (**Figure 1A**). MEICS score improvement after SuperMApo treatment was associated with reduced weight loss and reduced colitis clinical score (**Figures 1B, C**). Intestinal necropsy 10 days post-treatment showed an increased length of the colon in IBD mice receiving SuperMApo compared to the colon length in vehicle-treated mice. Colons of vehicle-treated mice were shorter, hyperemic and contained fewer feces due to massive diarrhea (**Figures 1A, D**). Altogether, this indicates inflamed colons. Histological examination of the intestines showed a reduced infiltration of inflammatory cells, notably in the rectum, in SuperMApo-treated mice (**Figure 1E**). Overall, these data demonstrate that the injection of pro-resolving factors released by efferocytic macrophages in mice with ongoing IBD could control IBD progression and inflammatory cell infiltration.

We further evaluated the wound healing properties of factors produced by efferocytic macrophages in DSS-induced colitis model. Administered on the day of colitis induction and 48 hrs later, SuperMApo strongly prevented colitis severity as attested by a reduced clinical score (which reached a score of 0 by day 48 following treatment), and a reduced MEICS score (**Figures 2A, B**) throughout the 50 days of the experiments. Body weight loss was not significantly improved (**Figure 2C**). Vehicle-treated mice exhibited worse colitis lesions, such as high fibrin deposition within the colon, a thickened and bleached mucosa with spontaneous bleeding, superficial ulceration and edema (**Figure 2B**). Macroscopic and histologic examinations confirmed mucosa improvement in mice receiving pro-resolving factors (**Figures 2D, E**). Overall, these factors exhibit pro-resolving properties in inflamed intestine mucosa.

3.2 Pro-Resolving Factors Released by Macrophages After Efferocytosis Induce Wound Healing Properties in Mouse Fibroblasts and Intestinal Epithelial Cells

Fibroblasts and epithelial cells are the main cells involved in tissue wound healing. Next, we addressed whether these cells are affected by pro-resolving factors released by macrophages after efferocytosis (*i.e.*, SuperMApo treatment). First, primary mouse fibroblasts extracted from colon tissues were cultured with SuperMApo. α-SMA expression was strongly increased by SuperMApo and, at the same time, mRNA levels of extracellular matrix-associated genes coding for fibronectin, type I and III collagens, were decreased (**Figures 3A, B**). SuperMApo-treated mouse fibroblasts demonstrated enhanced proliferative and migratory properties (**Supplemental Figures 1A, B**). This was further confirmed using a scratch assay where these fibroblasts showed enhanced wound healing capacities (**Figure 3C**). In addition, using floating collagen gels, SuperMApo-treated fibroblasts demonstrated increased contraction capacities (**Figure 3D**). Thus, *in vitro*, primary fibroblasts isolated from colon demonstrated higher healing properties in the presence of pro-resolving factors released by macrophages after efferocytosis.

We then analyzed the effects on IEC using the MODE-K intestinal immortalized epithelial cell line. We observed a similar improvement of healing functions, such as increased proliferative and migratory capacities, as well as increased wound closure properties (**Supplemental Figures 1D–F**). In addition to the gain in healing properties, SuperMApo allowed MODE-K epithelial cells to acquire phagocytic capacities to eliminate apoptotic cells (**Figure 3E**), as previously demonstrated in the lung mucosa (33). These data indicate that pro-resolving factors produced by efferocytic macrophages trigger wound healing properties in fibroblasts and IEC, providing IEC with phagocytic activity as well.

3.3 Pro-Resolving Factors Released by Macrophages After Efferocytosis Restores Healing Properties of Human Fibroblasts Isolated From Patients Diagnosed With IBD

SuperMApo-treated mouse fibroblasts demonstrate all the features of activated fibroblasts but without overexpressing extracellular matrix-associated genes. This suggests that fibroblasts acquired a specific pro-resolving profile. These properties were therefore evaluated on human fibroblasts isolated from colon biopsies (from inflamed lesions and control

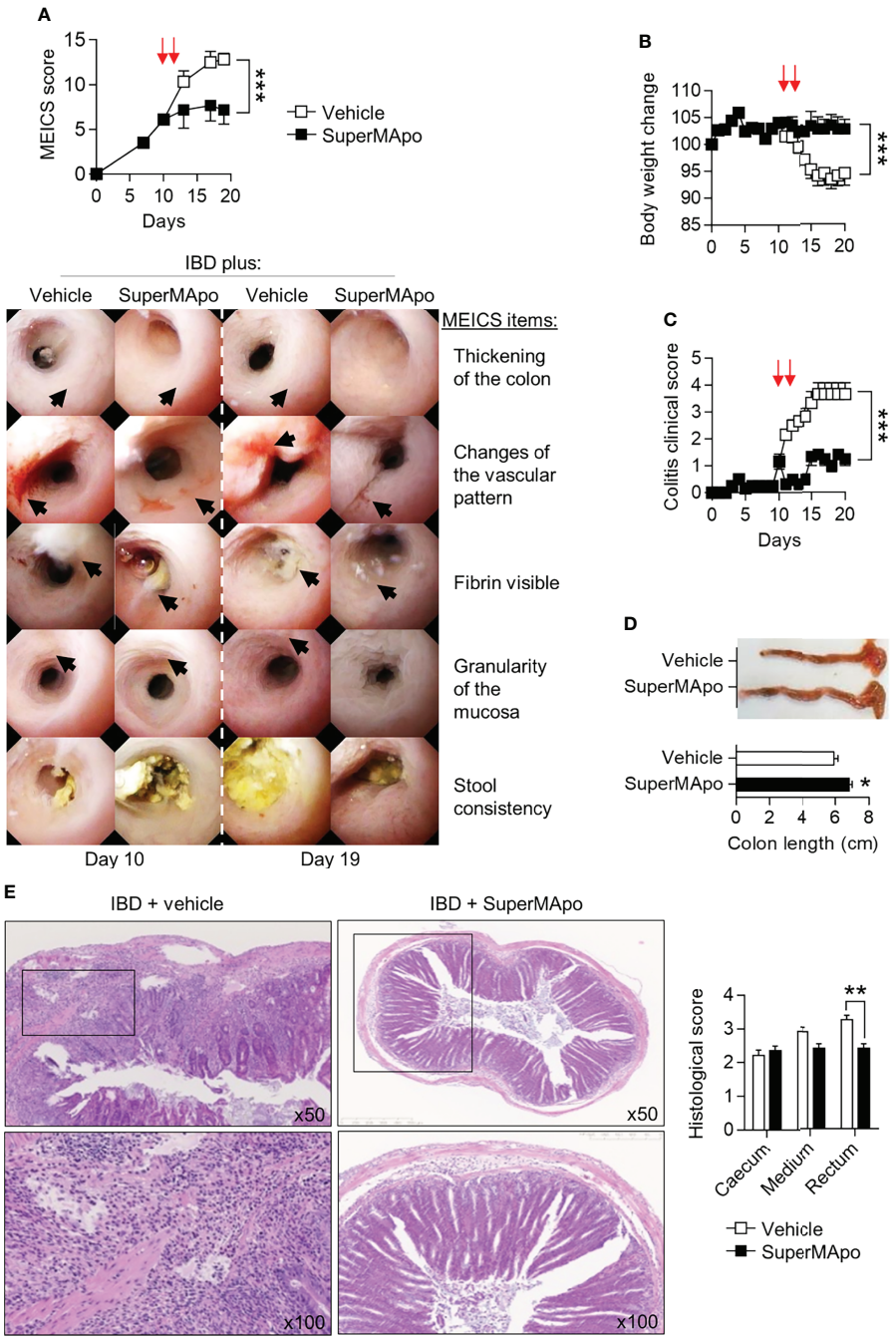

FIGURE 1 | Pro-resolving factors released by macrophages after efferocytosis promote intestine mucosal healing and limit colitis. Colitis was induced by the transfer of naïve $CD4^{+}CD25^{-}CD45RB^{hi}$ T cells into $Rag2^{-/-}$ C57BL/6 mice. **(A)** Colon examination was performed by colonoscopy and lesion quantification was assessed by the murine endoscopic index of colitis severity (MEICS) score. Mice developing colitis received twice (arrows) pro-resolving factors (SuperMApo) or vehicle (1 mL/mouse, i.p.) 10 days after the induction of colitis (*i.e.*, naïve T cell transfer) when they experimented a MEICS score of 6 to 7 out of 15, and 48 h later. Representative pictures are displayed from day 10 and 19 according to MEICS items. Black arrows identify the MEICS items on each picture. Cumulated data from one representative experiment out of three, expressed as mean ± s.e.m. (5 to 6 mice per groups) were also shown. **(B, C)** Body weight loss and clinical score changes were assessed on colitis mice. Data are expressed as mean of group ± s.e.m. (5 to 6 animals per groups) from one representative experiment out of three independent experiments; ***$p < 0.001$ (two-way ANOVA with Bonferroni post-test). **(D)** Colon length was assessed on colitis mice from a. Representative colon pictures are shown as well as cumulative data from one representative experiment out of three independent experiments (5 to 6 mice per group); *$p < 0.05$ (nonparametric Mann-Whitney test). **(E)** Representative HES staining of paraffin-embedded sections of the colonic tissues obtained from colitis mice from **(A)**, and cumulative histological scores (pooled from 3 independent experiments) are shown and expressed as mean of group ± s.e.m. (5 to 6 mice per group); **$p < 0.01$ (nonparametric Mann-Whitney test).

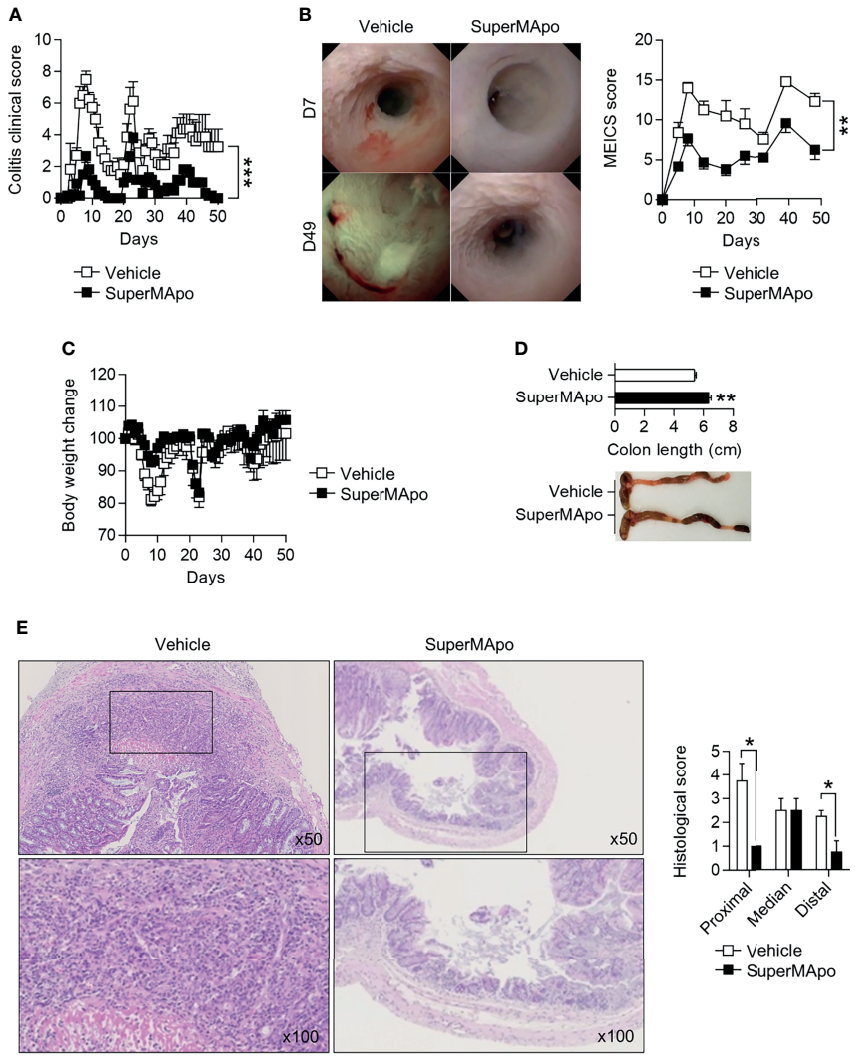

FIGURE 2 | Pro-resolving factors released by macrophages after efferocytosis promote healing of colon lesions induced by dextran sodium sulfate and limit colitis. **(A)** C57BL/6 Mice were subjected to three cycles of DSS and received at day 0 and day 2 pro-resolving factors (SuperMApo, 1 mL/mouse; i.p.) or vehicle, and were monitored daily for clinical changes over 50 days. Data are expressed as mean of group + s.e.m. (5 to 6 mice per group) and are representative of two independent experiments; ***$p < 0.001$ (two-way ANOVA with Bonferroni post-test). **(B)** Endoscopic assessment according to the MEICS score was also performed on colitis mice from **(A)** as well as body weight loss **(C)**. Representative pictures of colonoscopy at day 7 and day 49 are shown, as well as cumulated MEICS score from two independent experiments. Data are expressed as mean of group + s.e.m. (5 to 6 mice per group); **$p < 0.01$ (two-way ANOVA with Bonferroni post-test). **(D)** Colon length was assessed on the colitis mice from a, and representative colon pictures were shown as well as cumulative data from two independent experiments. Data are expressed as mean of group + s.e.m. (5 to 6 mice per group); **$p < 0.01$ (nonparametric Mann-Whitney test). **(E)** Representative HES staining of paraffin-embedded sections of the colonic tissues from colitis mice from a (at x50 and x100 magnifications). Cumulative histological scores from one experiment are shown as mean of group + s.e.m. (5 to 6 mice per group); *$p < 0.05$ (nonparametric Mann-Whitney test).

tissues of patients diagnosed with IBD). In the presence of human SuperMApo (*i.e.*, the secretome of human macrophages that have eliminated human apoptotic cells), the wound healing functions of control fibroblasts (*i.e.*, isolated from control tissue) were strongly increased including higher proliferative properties and higher wound closure capacities (**Figures 3F, G**). Concerning inflamed lesion-derived fibroblasts, proliferative properties and wound closure capacities were also increased and less modestly (**Figures 3F, G**). These data demonstrate that pro-resolving factors released by efferocytic macrophages could restore the healing functions of IBD fibroblasts, and thus support the use of SuperMApo in IBD patients.

3.4 Pro-Resolving Factors Released by Efferocytic Macrophages Limits the Loss of Intestinal Permeability by Inducing Intestinal Epithelial Cell Proliferation and Fibroblast Activation

The enhanced healing functions induced by pro-resolving factors released by efferocytic macrophages were then addressed *in vivo*

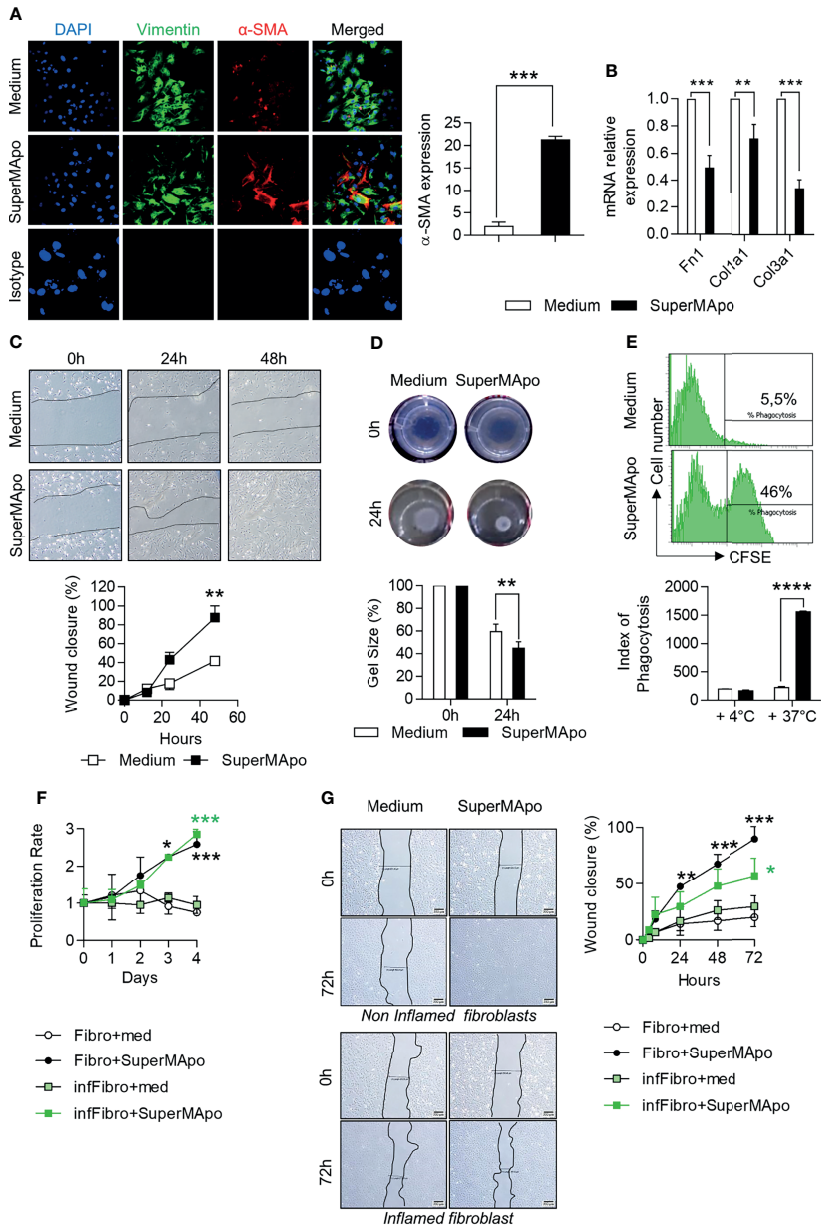

FIGURE 3 | Pro-resolving factors released by macrophages after efferocytosis trigger wound healing properties in fibroblasts and intestinal epithelial cells. **(A)** Expression of vimentin, α-smooth muscle actin (α-SMA) assessed by immunofluorescence and DAPI staining in mouse colon primary fibroblasts cultured in the presence of SuperMApo or control medium for 24 (h) Representative pictures are shown as well as cumulative data representative of α-SMA expression from three independent experiments, as mean ± s.e.m.; ***$p < 0.001$ (unpaired student's t test). **(B)** mRNA expression of genes coding for fibronectin (*Fn1*), type I (*Col1a1*) and type III (*Col3a1*) collagen in fibroblasts from **(A)**. Data are expressed as mean of duplicate per condition ± s.e.m. from three independent experiments pooled together. **$p < 0.01$, ***$p < 0.001$ (unpaired student's t test). **(C)** Migration of mouse fibroblasts in wound-healing scratch assays in the presence of SuperMApo or control medium. Data are expressed as mean of duplicates per conditions ± s.e.m. from one representative experiment out of three independent experiments. **$p <$ 0.01 (two-way ANOVA with Bonferroni post-test). **(D)** Contractility of mouse fibroblasts was assessed in floating collagen gels containing medium or SuperMApo. Representative pictures are shown, as well as cumulative data (mean ± s.e.m.) from one representative experiment out of three independent experiments. **$p < 0.01$ (two-way ANOVA with Bonferroni post-test). **(E)** Engulfment of CFSE-labelled apoptotic cells by the mouse intestinal epithelial cell line MODE-K assessed by flow cytometry after 6 h of co-culture in presence of control medium or SuperMApo. To confirm that this represents an active mechanism and to appreciate CFSE-labelled apoptotic cells stick to MODE-K cells, the same experiment was performed at +4°C instead of 37°C. Data are expressed as representative dot plots showing the percentage of $CFSE^+$ MODE-K cells and as index of phagocytosis ± s.e.m. from one representative experiment out of three independent experiments; ****$p < 0.0001$ (non-parametric Mann-Whitney test). **(F, G)** Primary human fibroblasts harvested from biopsies of non-inflamed (Fibro) or inflamed (infFibro) colon tissue were grown in the presence of medium (med) or SuperMApo. **(F)** Proliferation was determined by MTT assay and **(G)** wound closure was analyzed using the scratch assay at 0, 24, 48 and 72 h of culture. Data are expressed as mean of group ± s.e.m., and are representative of three independent experiments; *$p < 0.05$, **$p < 0.01$, ***$p < 0.001$ (two-way ANOVA with Bonferroni post-test).

using a biopsy forceps-wounded colonic mucosa model in which inflammation is localized to the injured tissue and not systemic. In this model, i.p. injection of SuperMApo on the day of mucosa injury significantly accelerated the lesion wound healing observed by video endoscopy, compared to the lesions of control vehicle-treated mice (**Figure 4A**). We addressed the integrity of the intestinal barrier after naive T cell transfer-induced colitis by using FITC-Dextran oral administration and its quantification in the mouse serum. Reduced systemic levels of FITC-Dextran were found in colitis mice receiving SuperMApo compared to control mice (**Figure 4B**). This attested for a conserved barrier permeability, further supported by a lower MEICS score (**Figure 4C**). In addition, the levels of the intestinal barrier integrity marker, the regenerating islet-derived protein 3γ (REG3γ) (34, 35), were also found reduced in colitis mice treated with SuperMApo (**Figure 4D**). These results suggest a restored intestinal barrier permeability by administration of pro-resolving factors. This was associated with a marked *in vivo* proliferation of cells within the crypts and activation of fibroblasts in the colon mucosa of colitis mice receiving SuperMApo, as attested by increased $Ki67^+$ cell number per mucosal crypt, and with an increased expression of α-SMA in colonic fibroblasts, respectively (**Figures 4E, F**). Moreover, a slight decrease of colon mRNA expression of extracellular matrix-associated genes *Fn1*, *Col1a1*, *Col3a1* and *Tgf-β* was observed in colitis mice receiving SuperMApo treatment. This decrease was significant for *Fn1* (**Figure 4G**). Overall, our data demonstrate that treatment of mice experiencing ongoing colitis with pro-resolving factors released by efferocytic macrophages restores intestinal barrier permeability by inducing IEC proliferation and activating local fibroblasts *in vivo*.

3.5 TGF-β, IGF-I and VEGF Growth Factors Participate in the Wound Healing Induced by Factors Released by Macrophages After Efferocytosis

Several pro-resolving factors have been shown to be released by macrophages after efferocytosis (36, 37). Thus, different growth factors, including EGF, FGF, TGF-β, IGF-I and VEGF, were quantified in the SuperMApo supernatant. TGF-β, IGF-I and VEGF were detected in significant higher quantities than in control supernatants, whereas EGF and FGF were not detectable (**Figure 5A**). When blocking antibodies directed against TGF-β, IGF-I and VEGF were used, we observed a non-significant decrease of SuperMApo-induced α-SMA expression (**Supplemental Figure 2A**). The reduction of SuperMApo-induced *Col1a1*, *Col3a1* and *Fn1* mRNA expression in primary fibroblasts was not significantly affected by growth factor blockade (**Supplemental Figure 2B**). The proliferative and contractive properties of mouse primary fibroblasts were not affected by antibodies blocking these growth factors (**Supplemental Figures 2C, D**). However, blockade of TGF-β or IGF-I significantly reduced the proliferation of IEC line MODE-K (**Figure 5B**). In addition, SuperMApo-enhanced cell migration of fibroblasts and IEC was reduced by the addition of blocking antibodies whatever the neutralized growth factor *(i.e.*, TGF-β, IGF-I or VEGF) (**Figure 5C**). Thus, while proliferation and migration of IEC induced by SuperMApo are sustained by TGF-β, IGF-I and VEGF growth factors, only migration of fibroblast is associated to these growth factors.

The role of TGF-β, IGF-I and VEGF growth factors was further addressed *in vivo* using the T cell-transfer colitis model in which all the growth factors tested *in vitro* were infused together. While colon lesions were not ameliorated – as attested by a similar MEICS score between growth factor-treated and control mice (**Figure 6A**), weight loss and the composite clinical score were slightly improved by the treatment with the three growth factors (**Figure 6B**). We next decided to deplete the SuperMApo supernatant from TGF-β, IGF-I and VEGF using antibody-coupled microbeads before its injection to colitis mice. Depletion of TGF-β, IGF-I and VEGF from SuperMApo inhibited the improvement of the MEICS score induced by SuperMApo (**Figure 6C**). However, the absence of TGF-β, IGF-I and VEGF in the SuperMApo supernatant partially reduced the properties of SuperMApo in terms of weight loss prevention and clinical score reduction (**Figure 6D**). These data demonstrate that TGF-β, IGF-I and VEGF participate in intestinal mucosal healing induced by SuperMApo but are not sufficient to resolve global IBD inflammation.

Altogether, these results highlight pro-resolving factors released by efferocytic macrophages as a promising therapeutic approach to both circumvent inflammation and promote lesion healing in the setting of inflammatory bowel diseases.

4 DISCUSSION

IBD is a family of inflammatory diseases that ultimately lead to damage of the distal small intestine and the colonic mucosa. Available treatments for IBD based on immunosuppressive agents try to diminish the effector response and treat the sequelae of uncontrolled/nonresolving inflammation. However, these drugs are not entirely effective, exert nonspecific functions and result in multiple adverse effects, including infections. In most cases, surgical resection is the last alternative. This illustrates the need for new therapeutic approaches that specifically modulate both components of the disease, namely uncontrolled inflammation and tissue repair. Recent studies have shown that IBD patients who achieve and maintain colonic mucosal healing have more favorable long-term outcomes than patients who do not. Thus, mucosal healing is emerging as a critical endpoint in clinical trials and practice (2, 7). Resolution pharmacology proposes to trigger the resolution phase of inflammation and initiate tissue repair (38, 39). Apoptotic cell-based therapy can be an interesting approach in this setting, since apoptotic cell infusion has been shown to improve chronic intestinal inflammation in two different experimental colitis models, naive T cell transfer- and DSS-induced colitis (24, 25, 40). These approaches are based on the triggering of the resolution phase of inflammation induced by efferocytosis. Soluble factors released by macrophages after efferocytosis play an important role in the success of apoptotic cell-based therapies (41, 42). Here, the novelty resides in the use of the cell-free whole

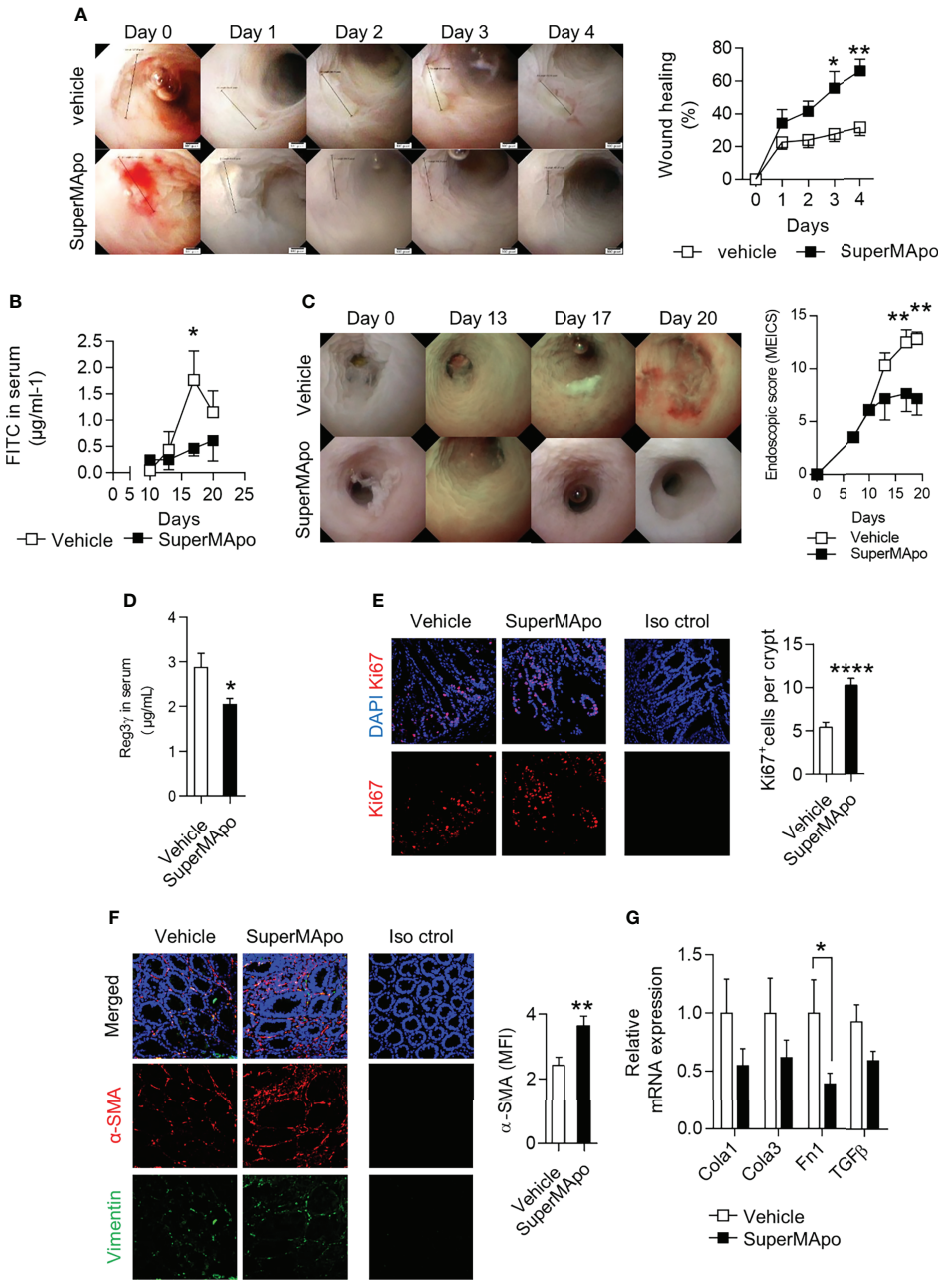

FIGURE 4 | Treatment with pro-resolving factors released by macrophages after efferocytosis maintains intestinal barrier permeability *via* intestinal epithelial cell proliferation and fibroblast activation. **(A)** Wild-type mice were monitored daily by video-endoscopy to evaluate healing of the colon mucosa, wounded at day 0 by forceps and receiving at day 0 and 2 SuperMApo or vehicle (1 mL/mouse; i.p.). Representative pictures are displayed from day 0 to day 4, as well as cumulated data (expressed as % of wound healing, right hand side panel). Data are representative of three independent experiments showing similar results, and expressed as mean of group ± s.e.m. (5 to 6 animals per group); $^{*}p < 0.05$, $^{**}p < 0.01$ (two-way analysis of variance [ANOVA] with Bonferroni post-test). **(B–D)** Colitis was induced by transfer of naive $CD4^{+}CD25^{-}CD45RB^{hi}$ T cells into $Rag2^{-/-}$ C57BL/6 mice and mice received vehicle or SuperMApo at day 10 and 12 (1 mL/mouse; i.p.). **(B)** FITC-dextran particle gavage and quantification in the serum was assessed to appreciate intestinal barrier integrity. Data are expressed as mean of group ± s.e.m. (5 to 6 mice per group) and are representative of two independent experiments; $^{*}p < 0.05$ (two-way ANOVA with Bonferroni post-test). **(C)** Colonoscopy evaluation of the mice and **(D)** regenerating islet-derived protein 3-gamma (REG3γ) quantification in the serum were also performed. Data are expressed as mean of group ± s.e.m. (5 to 6 mice per group) and representative of four independent experiments; $^{**}p < 0.01$ (two-way ANOVA with Bonferroni post-test). **(E)** Cell proliferation in the epithelial crypts and **(F)** fibroblast differentiation into myofibroblasts were determined by Ki-67 and α-SMA staining, respectively, of colon cuts from colitis mice from **(B)**. Nuclei are counterstained with DAPI and an isotype control antibody was used as control (Iso ctrol). **(G)** Expression of mRNA of genes coding for extracellular matrix proteins type I [*Col1a1*] and type III [*Col3a1*] collagen, fibronectin [*Fn1*] and TGF-β (*tgf-b*) was assessed by RT-qPCR in the colon of the colitis mice from **(B)** Data are expressed as mean of group ± s.e.m. (5 to 6 mice per group) and are representative of two; $^{*}p < 0.05$ (Unpaired student t test), $^{**}p < 0.01$; $^{****}p < 0.0001$ (nonparametric Mann-Whitney test).

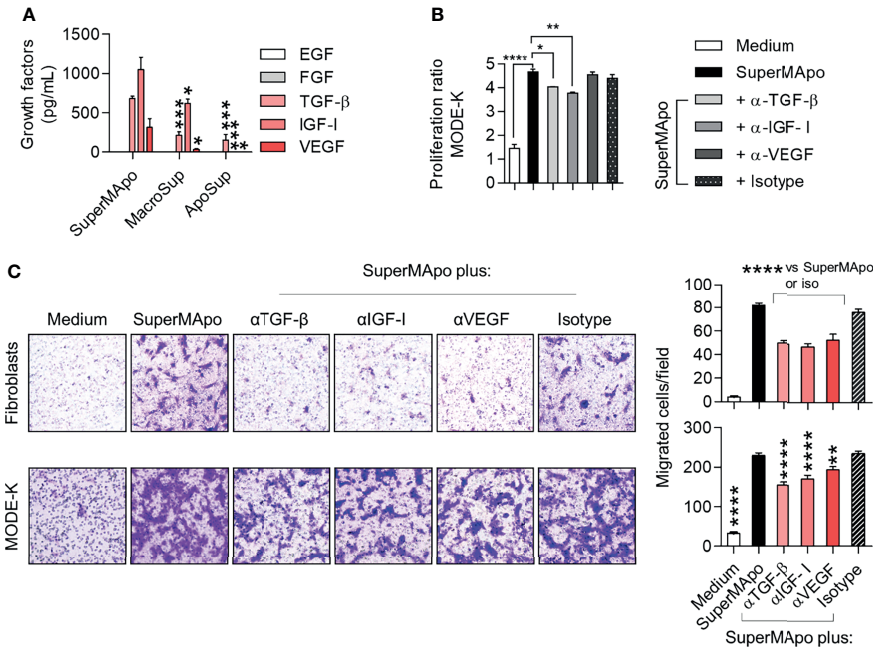

FIGURE 5 | Pro-resolving factors released by macrophages after efferocytosis include TGF-β, IGF-I and VEGF and their capacity to attract primary fibroblasts and IEC are dependent on these growth factors. **(A)** EGF, FGF, TGF-β, IGF-I and VEGF were quantified by ELISA in the supernatants of macrophages after efferocytosis (SuperMApo) and in the control supernatants of macrophages (MacroSup) cultured alone or apoptotic cells (ApoSup) cultured alone. Data represented as mean ± s.e.m. are the pool of six independents experiments; *$p < 0.05$; ***$p < 0.001$ (one-way ANOVA with Tukey's multiple comparison post-test). **(B)** Proliferation of mouse primary fibroblasts was assessed by MTT assay for 4 days with or without neutralizing antibodies to TGF-β, IGF-I or VEGF, or control isotype. Data are from one representative experiment out of three and expressed as mean + s.e.m. of 3 replicates per condition; *p < 0.05; **p < 0.01, ****p < 0.0001 (two-way ANOVA with Bonferroni post-test). **(C)** Mouse primary fibroblasts or MODE-K IEC were incubated with medium or SuperMApo, with or without neutralizing antibodies to TGF-β, IGF-I or VEGF, or control isotype, and migration was determined using a transwell assay during 24 (h). Data are shown as representative pictures and as pooled data expressed as mean of migrated cells/field of duplicates per group ± s.e.m. from one representative experiment out of three. **$p < 0.01$, ****$p < 0.0001$ (one-way ANOVA with tukey's multiple comparisons post-test).

secreted factors issued from macrophages that have eliminated apoptotic cells in order to reengage and foster the resolution of established inflammation in ongoing colitis. This new biologic complex product SuperMApo, contains all the factors released by efferocytic macrophages. These factors are involved in the resolution of inflammation and in tissue healing (14). In the present work, we wanted to focus on the healing properties of SuperMApo using colitis models in which lesions can be regularly followed up by live endoscopy in order to appreciate mucosa lesion healing (26). How SuperMApo factors affected the cells orchestrating tissue repair, namely fibroblasts and IEC, was addressed in the context of colitis and wound healing. Three *in vivo* models were used in which video-endoscopy (26) allowed us to better appreciate lesion healing. With the naive T cell-transfer model (27), we were able to address the therapeutic effect of SuperMApo injection in mice presenting colon lesions, lesions that are mostly T cell dependent. With the DSS-induced colitis model, the preventing role of SuperMApo treatment (injected at the time of DSS administration initiation) was addressed up to 50 days and, this model also helped us to determine the capacity of the drug candidate to prevent metabolite-induced microbiota alteration favoring mucosal lesion occurrence. Furthermore, using the biopsy forceps-wounded colonic mucosa model (26) we addressed mucosal wound healing in absence of systemic inflammation, focusing on the property of the product to enhance tissue healing. Collectively, the data provide several key insights. First, we demonstrated that SuperMApo stimulates the wound healing properties of colonic fibroblasts and IEC, the main cell types orchestrating the tissue repair process (43–46). *In vitro* treatment of fibroblasts with SuperMApo increases the expression of α-SMA. This is confirmed *in vivo* in naive T cell transfer-induced colitis. This suggests the differentiation of fibroblasts into myofibroblasts, but paradoxically SuperMApo decreases the expression of genes coding for extracellular matrix proteins, particularly *Fn1 in vivo*. Our observation suggests that, under this pro-resolving microenvironment (*i.e.*, exposure to SuperMApo), fibroblasts appear as activated (as attested by α-SMA expression) but with reduced pro-fibrotic functions (*i.e.*, reduced expression of extracellular matrix genes). Other fibroblast functions involved in wound healing are also stimulated *in vitro* by SuperMApo, including migratory, proliferative and contractive properties. While there is a difference between the biology of mouse and human pro-resolving macrophages (47), human pro-resolving factors (*i.e.*, SuperMApo) also increase the capacity of human fibroblasts isolated from colons of IBD patients to proliferate, migrate and

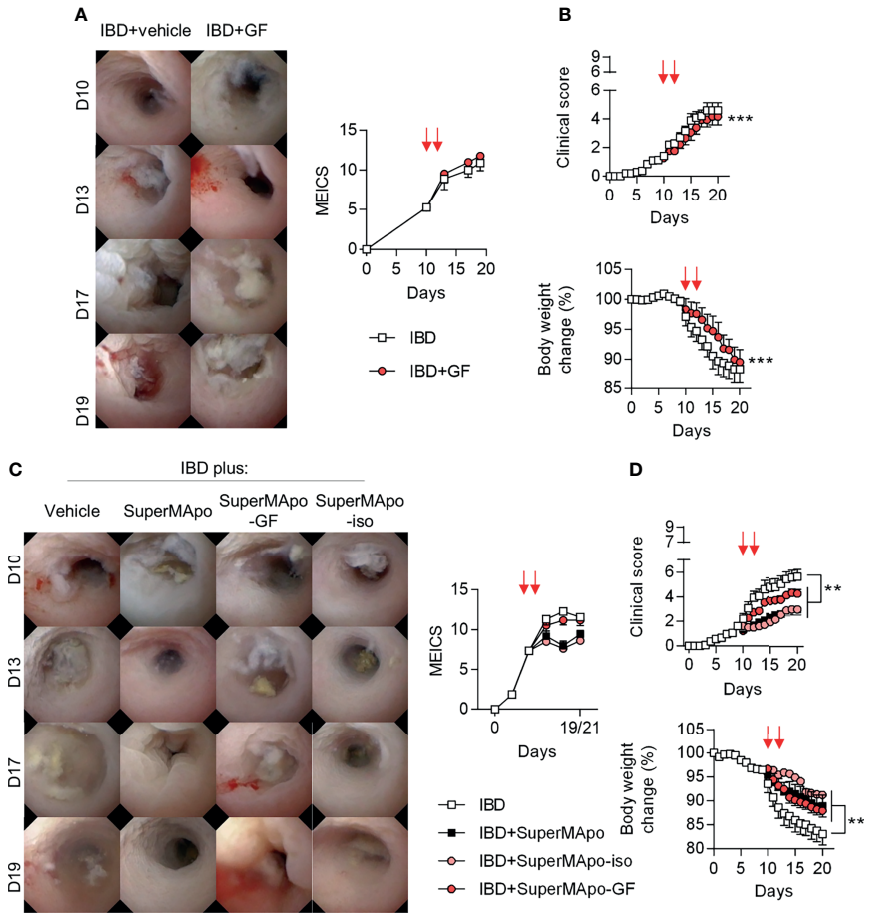

FIGURE 6 | TGF-β, IGF-I and VEGF found in the SuperMAPo supernatant participate in lesion healing. **(A, B)** Colitis was induced by the transfer of naive $CD4^{+}CD25^{-}CD45RB^{hi}$ T cells into $Rag2^{-/-}$ C57BL/6 mice and mice received at day 10 and 12 vehicle (PBS; 1 mL/mouse) or the three following recombinant growth factors: TGF-β (700 pg/mL/mouse), IGF-I (1050 pg/mL/mouse) and VEGF (350 pg/mL/mouse) (red arrows) when they exhibited a MEICS score of 6-7, and were then monitored daily. **(A)** Endoscopic assessment according to the MEICS score was performed and results are shown as representative pictures of mini-colonoscopy at day 10, 13, 17 and 19, as well as cumulated score. **(B)** Clinical score changes and body weight loss were also assessed and results are expressed as mean of groups ± s.e.m. (5 to 6 mice per group). Data are from two independent experiments pooled together; $^{***}p < 0.05$, $p < 0.001$ (one-way ANOVA with Bonferroni post-test). **(C)** Colitis was induced similarly and mice received SuperMAPo, or SuperMAPo depleted in TGF-β, IGF-I and VEGF (SuperMAPo-GF), or SuperMAPo treated similarly but using isotype control antibodies instead of antibodies against growth factors (SuperMAPo-iso), or vehicle when they exhibited a MEICS score of 6-7 and were then monitored daily. Endoscopic assessment according to the MEICS score was performed and results are shown as representative pictures of mini-colonoscopy at day 10, 13, 17 and 19, as well as cumulated score. **(D)** Clinical score changes and body weight loss were also assessed and results are expressed as mean of groups ± s.e.m. (5 to 6 mice per group). Data are from three independent experiments pooled together; $^{**}p < 0.01$ (one-way ANOVA with Bonferroni post-test).

close a wound *in vitro*. In addition, this targets human fibroblasts either from inflammatory or non-inflammatory intestinal tissues. Concerning IEC, we also observed a gain of pro-healing properties both *in vitro* and *in vivo* after the reintroduction of pro-resolving factors released by efferocytic macrophages, as well as the acquisition of efferocytic capacities. It has been previously demonstrated that a dysregulated clearance of apoptotic cells is associated with many inflammatory diseases (48, 49), and that boosting apoptotic cell clearance dampens inflammation, notably through increasing colonic epithelial cell efferocytosis of apoptotic cells (33). Therefore, an interesting extrapolation of this work is that improving apoptotic cell clearance by IEC in the early stages of IBD could potentially help to reduce the inflammatory responses seen in later stages of the disease.

Second, pro-resolving factors released by efferocytic macrophages promote mucosal healing *in vivo* in three different intestinal models whatever the initial injury (mechanical [biopsy forceps], T cell-mediated, or chemical [DSS]). SuperMAPo stimulates wound healing *via* the pro-healing properties of fibroblasts and IEC. We did not study whether efferocytosis factors also promoted extra-intestinal bone marrow-derived cell recruitment to participate in wound healing, as observed in a recent study using a parabiosis chemical-induced colitis model (50). It has been shown that colonic fibroblasts are critically involved in tissue repair in the

gastrointestinal tract (43). In the colon, based on their location (just beneath the IEC) and on their net-like structures, intestinal fibroblasts seem to be ideally located for sensing damage signals resulting from disintegration of the IEC layer (44). Following injury, adjacent IEC rapidly migrate into the damaged area to restore barrier integrity (a process called epithelial restitution). Proliferation of IEC then increases the number of enterocytes to reduce this damaged area resulting from the wound. Furthermore, differentiation of IEC is needed to restore the mucosal barrier and epithelial function (45, 51). Thus, our data confirm that pro-resolving factors contained in SuperMApo initiate these mechanisms involved in intestinal mucosal healing, including migration and activation of fibroblasts into myofibroblasts, which facilitate the wound gap closure, as well as migration and proliferation of IEC. As discussed above, a decrease in extracellular matrix gene expression in the colons of SuperMApo-treated mice has been also observed, despite a higher expression of α-SMA expression in fibroblasts. This is associated with a decrease of *tgf-b* mRNA expression in the colons of SuperMApo-treated mice. TGF-β is produced by a variety of cell types. Macrophages, as the critical source of this growth factor, have been shown to promote fibrosis (52). Thus, TGF-β is considered as fibrotic, as it contributes to myofibroblast differentiation by stimulating α-SMA expression (53) and their survival (54). It also stimulates the production of extracellular matrix proteins by myofibroblasts (54), as well as migration (55) and contraction (56) of myofibroblasts. Our data suggest that within SuperMApo, TGF-β improves myofibroblast contractility to enhance the wound gap closure without promoting extracellular matrix production and possibly fibrosis. Neutralization experiments confirmed that TGF-β in SuperMApo stimulated fibroblast proliferation and migration, as well as IEC migration. Further studies are thus necessary to elucidate whether resolving α-SMA positive "extracellular matrix negative" fibroblasts should be considered as healing myofibroblasts or as advanced healing stage fibroblasts.

Third, the different phases of wound healing are controlled by several proteins, such as chemokines, defensins, growth factors (TGF-β, EGF, FGF, or IGF-I), cytokines (e.g., IL-1β, IL-6 and IL-22), as well as trefoil peptides (57, 58). Here, we focused on 5 but 3 growth factors that were detectable in significant amounts in SuperMApo. This corresponds to TGF-β, IGF-I and VEGF that may participate, at least partially, in SuperMApo-induced wound healing *in vitro* and *in vivo*. While i.p. administration of the corresponding recombinant forms of these growth factors, at concentrations similar to those found in SuperMApo, did not ameliorate mucosal lesions, body weight loss was significantly delayed with recombinant growth factor injection. Depletion of the growth factors from SuperMApo confirm that these 3 factors exert a significant effect on wound healing. Body weight loss and clinical score amelioration were only partially affected by the depletion of these growth factors from SuperMApo. This suggests that other factors present in SuperMApo in combination with growth factors, participate in the global resolution of ongoing colitis. This is in line with what we observed *in vitro*. Growth factors induced fibroblast and IEC migration and, only TGF-β and IGF-I induced the proliferation of MODE-K IEC line. Again, this suggests that other factors in SuperMApo may participate. Whether other SuperMApo factors are directly or indirectly involved in wound healing and participate to the treatment of colitis remains to be determined.

In summary, this work demonstrates that SuperMApo improves ongoing IBD, by controlling inflammation and enhancing mucosal healing in mice. SuperMApo also targets human fibroblasts isolated from colons of IBD patients. Thus, SuperMApo emerges as a potential "bio-mimetic" drug belonging to resolution pharmacology, able to terminate ongoing IBD and achieve mucosal healing.

DATA AVAILABILITY STATEMENT

The raw data supporting the conclusions of this article will be made available by the authors, without undue reservation.

ETHICS STATEMENT

Colon biopsies were collected according to standard procedures. This study (*i.e.*, colon biopsy collection and *ex vivo* analysis of the effects of SuperMApo) was approved by the Ethics Committee of Besançon (CPP#14/456; date of final approval: July 13th 2021), and all participants signed an informed consent form. The study protocol is conformed to the ethical guidelines of the 1975 Declaration of Helsinki. The patients/participants provided their written informed consent to participate in this study. Experimentation (#02831) was approved by the local ethic committee (#58) and the French Ministry of Higher Education and Research (Ministère de l'Enseignement Supérieur, de la Recherche et l'Innovation) and was conducted in accordance with the European Union's Directive 2010/63.

AUTHOR CONTRIBUTIONS

SP conceived and supervised the study. OM-R designed and performed most of the experiments, analyzed and interpreted the data. TG, AD, FB, CC, and MC contributed to some experiments. SV-D performed the histological analysis and scoring of the tissues. CG participated to endoscopy procedures. OM-R, PS, and SP analyzed the data and wrote the manuscript. All authors discussed the results and the manuscript and approved the final manuscript.

FUNDING

The work was funded by the Etablissement Français du Sang (2016-02 to S.P.), the Conseil Régional de Franche-Comté ("Soutien au LabEX LipSTIC" 2018/2019 to PS, AAP 2013-2017 to SP and SONY SH800Z cell sorter), and by the Agence Nationale de la Recherche (ANR-11-LABX-0021 to Labex LipSTIC), as well as by the MiMedI project funded by BPI France (grant No. DOS0060162/00), and the European Union through the European Regional Development Fund of the Région Bourgogne-Franche-Comté (grant No. FC0013440).

OM-R and CC are supported by a doctoral fellowship from the Ministère de l'Enseignement Supérieur, de la Recherche et de l'Innovation, TG by a doctoral fellowship from the Etablissement Français du Sang and from the Labex LipSTIC.

ACKNOWLEDGMENTS

We thank Lucienne Chatenoud (Hopital Necker, Paris, France) for providing us with the TGF-β antibody and Dominique Kaiserlian (Inserm-U1111, Lyon, France) for providing us with the MODE-K cell line. We also thank Dominique Paris and Emmanuel Salvado for taking care of the mice.

SUPPLEMENTARY MATERIAL

The Supplementary Material for this article can be found online at: https://www.frontiersin.org/articles/10.3389/fimmu.2021.754475/full#supplementary-material

REFERENCES

1. Baumgart DC, Carding SR. Inflammatory Bowel Disease: Cause and Immunobiology. *Lancet* (2007) 369(9573):1627–40. doi: 10.1016/S0140-6736(07)60750-8
2. Neurath MF. New Targets for Mucosal Healing and Therapy in Inflammatory Bowel Diseases. *Mucosal Immunol* (2014) 7(1):6–19. doi: 10.1038/mi.2013.73
3. Rutgeerts P, Van Assche G, Sandborn WJ, Wolf DC, Geboes K, Colombel JF, et al. Adalimumab Induces and Maintains Mucosal Healing in Patients With Crohn's Disease: Data From the EXTEND Trial. *Gastroenterology* (2012) 142 (5):1102–11.e2. doi: 10.1053/j.gastro.2012.01.035
4. Nielsen OH, Ainsworth MA. Tumor Necrosis Factor Inhibitors for Inflammatory Bowel Disease. *N Engl J Med* (2013) 369(8):754–62. doi: 10.1056/NEJMct1209614
5. Danese S. Immune and Nonimmune Components Orchestrate the Pathogenesis of Inflammatory Bowel Disease. *Am J Physiol Gastrointestinal liver Physiol* (2011) 300(5):G716–22. doi: 10.1152/ajpgi.00472.2010
6. Gunther C, Neumann H, Neurath MF, Becker C. Apoptosis, Necrosis and Necroptosis: Cell Death Regulation in the Intestinal Epithelium. *Gut* (2013) 62(7):1062–71. doi: 10.1136/gutjnl-2011-301364
7. Neurath MF, Travis SP. Mucosal Healing in Inflammatory Bowel Diseases: A Systematic Review. *Gut* (2012) 61(11):1619–35. doi: 10.1136/gutjnl-2012-302830
8. de Oliveira S, Rosowski EE, Huttenlocher A. Neutrophil Migration in Infection and Wound Repair: Going Forward in Reverse. *Nat Rev Immunol* (2016) 16(6):378–91. doi: 10.1038/nri.2016.49
9. Medina CB, Ravichandran KS. Do Not Let Death do Us Part: 'Find-Me' Signals in Communication Between Dying Cells and the Phagocytes. *Cell Death Differ* (2016) 23(6):979–89. doi: 10.1038/cdd.2016.13
10. Ortega-Gomez A, Perretti M, Soehnlein O. Resolution of Inflammation: An Integrated View. *EMBO Mol Med* (2013) 5(5):661–74. doi: 10.1002/emmm.201202382
11. Serhan CN. Pro-Resolving Lipid Mediators are Leads for Resolution Physiology. *Nature* (2014) 510(7503):92–101. doi: 10.1038/nature13479
12. Greenlee-Wacker MC. Clearance of Apoptotic Neutrophils and Resolution of Inflammation. *Immunol Rev* (2016) 273(1):357–70. doi: 10.1111/imr.12453
13. Bosurgi L, Cao YG, Cabeza-Cabrerizo M, Tucci A, Hughes LD, Kong Y, et al. Macrophage Function in Tissue Repair and Remodeling Requires IL-4 or IL-13 With Apoptotic Cells. *Science* (2017) 356(6342):1072–6. doi: 10.1126/science.aai8132
14. Bonnefoy F, Gauthier T, Vallion R, Martin-Rodriguez O, Missey A, Daoui A, et al. Factors Produced by Macrophages Eliminating Apoptotic Cells Demonstrate Pro-Resolutive Properties and Terminate Ongoing Inflammation. *Front Immunol* (2018) 9:2586. doi: 10.3389/fimmu.2018.02586
15. Bressenot A, Salleron J, Bastien C, Danese S, Boulagnon-Rombi C, Peyrin-Biroulet L. Comparing Histological Activity Indexes in UC. *Gut* (2015) 64 (9):1412–8. doi: 10.1136/gutjnl-2014-307477
16. Brannigan AE, O'Connell PR, Hurley H, O'Neill A, Brady HR, Fitzpatrick JM, et al. Neutrophil Apoptosis is Delayed in Patients With Inflammatory Bowel Disease. *Shock* (2000) 13(5):361–6. doi: 10.1097/00024382-200005000-00003
17. Wéra O, Lancellotti P, Oury C. The Dual Role of Neutrophils in Inflammatory Bowel Diseases. *J Clin Med* (2016) 5(12):1–24. doi: 10.3390/jcm5120118
18. Liu H, Dasgupta S, Fu Y, Bailey B, Roy C, Lightcap E, et al. Subsets of Mononuclear Phagocytes are Enriched in the Inflamed Colons of Patients With IBD. *BMC Immunol* (2019) 20(1):42. doi: 10.1186/s12865-019-0322-z
19. Sena A, Grishina I, Thai A, Goulart L, Macal M, Fenton A, et al. Dysregulation of Anti-Inflammatory Annexin A1 Expression in Progressive Crohns Disease. *PLoS One* (2013) 8(10):e76969. doi: 10.1371/journal.pone.0076969
20. Na YR, Stakenborg M, Seok SH, Matteoli G. Macrophages in Intestinal Inflammation and Resolution: A Potential Therapeutic Target in IBD. *Nat Rev Gastroenterol Hepatol* (2019) 16(9):531–43. doi: 10.1038/s41575-019-0172-4
21. Mangino MJ, Brounts L, Harms B, Heise C. Lipoxin Biosynthesis in Inflammatory Bowel Disease. *Prostaglandins Other Lipid Mediat* (2006) 79 (1-2):84–92. doi: 10.1016/j.prostaglandins.2005.10.004
22. Sugimoto MA, Vago JP, Perretti M, Teixeira MM. Mediators of the Resolution of the Inflammatory Response. *Trends Immunol* (2019) 40(3):212–27. doi: 10.1016/j.it.2019.01.007
23. Ho GT, Cartwright JA, Thompson EJ, Bain CC, Rossi AG. Resolution of Inflammation and Gut Repair in IBD: Translational Steps Towards Complete Mucosal Healing. *Inflamm Bowel Dis* (2020) 26(8):1131–43. doi: 10.1093/ibd/izaa045
24. Ansary MM, Ishihara S, Oka A, Kusunoki R, Oshima N, Yuki T, et al. Apoptotic Cells Ameliorate Chronic Intestinal Inflammation by Enhancing Regulatory B-Cell Function. *Inflamm Bowel Dis* (2014) 20(12):2308–20. doi: 10.1097/MIB.0000000000000240
25. Grau A, Tabib A, Grau I, Reiner I, Mevorach D. Apoptotic Cells Induce NF-kappaB and Inflammasome Negative Signaling. *PLoS One* (2015) 10(3): e0122440. doi: 10.1371/journal.pone.0122440
26. Neurath MF, Wittkopf N, Wlodarski A, Waldner M, Neufert C, Wirtz S, et al. Assessment of Tumor Development and Wound Healing Using Endoscopic Techniques in Mice. *Gastroenterology* (2010) 139(6):1837–43.e1. doi: 10.1053/j.gastro.2010.10.007
27. Powrie F, Leach MW, Mauze S, Menon S, Caddle LB, Coffman RL. Inhibition of Th1 Responses Prevents Inflammatory Bowel Disease in Scid Mice Reconstituted With CD45RBhi CD4+ T Cells. *Immunity* (1994) 1(7):553–62. doi: 10.1016/1074-7613(94)90045-0
28. Becker C, Fantini MC, Wirtz S, Nikolaev A, Kiesslich R, Lehr HA, et al. *In Vivo* Imaging of Colitis and Colon Cancer Development in Mice Using High Resolution Chromoendoscopy. *Gut* (2005) 54(7):950–4. doi: 10.1136/gut.2004.061283
29. Asseman C, Mauze S, Leach MW, Coffman RL, Powrie F. An Essential Role for Interleukin 10 in the Function of Regulatory T Cells That Inhibit Intestinal Inflammation. *J Exp Med* (1999) 190(7):995–1004. doi: 10.1084/jem.190.7.995
30. Khalil H, Nie W, Edwards RA, Yoo J. Isolation of Primary Myofibroblasts From Mouse and Human Colon Tissue. *J visualized experiments: JoVE* (2013) 80):1–6. doi: 10.3791/50611
31. Vidal K, Grosjean I, evillard JP, Gespach C, Kaiserlian D. Immortalization of Mouse Intestinal Epithelial Cells by the SV40-Large T Gene. Phenotypic and Immune Characterization of the MODE-K Cell Line. *J Immunol Methods* (1993) 166(1):63–73. doi: 10.1016/0022-1759(93)90329-6
32. Su S, Chen J. *Collagen Gel Contraction Assay*. (2015). doi: 10.1038/protex.2015.082
33. Lee CS, Penberthy KK, Wheeler KM, Juncadella IJ, Vandenabeele P, Lysiak JJ, et al. Boosting Apoptotic Cell Clearance by Colonic Epithelial Cells Attenuates Inflammation. *In Vivo Immun* (2016) 44(4):807–20. doi: 10.1016/j.immuni.2016.02.005
34. Cayatte C, Joyce-Shaikh B, Vega F, Boniface K, Grein J, Murphy E, et al. Biomarkers of Therapeutic Response in the IL-23 Pathway in Inflammatory Bowel Disease. *Clin Trans Gastroenterol* (2012) 3:e10. doi: 10.1038/ctg.2012.2

35. Marafini I, Di Sabatino A, Zorzi F, Monteleone I, Sedda S, Cupi ML, et al. Serum Regenerating Islet-Derived 3-Alpha is a Biomarker of Mucosal Enteropathies. *Alimentary Pharmacol Ther* (2014) 40(8):974–81. doi: 10.1111/apt.12920
36. Saas P, Daguindau E, Perruche S. Concise Review: Apoptotic Cell-Based Therapies-Rationale, Preclinical Results and Future Clinical Developments. *Stem Cells* (2016) 34(6):1464–73. doi: 10.1002/stem.2361
37. Han CZ, Juncadella IJ, Kinchen JM, Buckley MW, Klibanov AL, Dryden K, et al. Macrophages Redirect Phagocytosis by Non-Professional Phagocytes and Influence Inflammation. *Nature* (2016) 539(7630):570–4. doi: 10.1038/nature20141
38. Perretti M, Leroy X, Bland EJ, Montero-Melendez T. Resolution Pharmacology: Opportunities for Therapeutic Innovation in Inflammation. *Trends Pharmacol Sci* (2015) 36(11):737–55. doi: 10.1016/j.tips.2015.07.007
39. Barnig C, Bezema T, Calder PC, Charloux A, Frossard N, Garssen J, et al. Activation of Resolution Pathways to Prevent and Fight Chronic Inflammation: Lessons From Asthma and Inflammatory Bowel Disease. *Front Immunol* (2019) 10:1699. doi: 10.3389/fimmu.2019.01699
40. Chen H, Kasagi S, Chia C, Zhang D, Tu E, Wu R, et al. Extracellular Vesicles From Apoptotic Cells Promote TGFbeta Production in Macrophages and Suppress Experimental Colitis. *Sci Rep* (2019) 9(1):5875. doi: 10.1038/s41598-019-42063-7
41. Poon IK, Lucas CD, Rossi AG, Ravichandran KS. Apoptotic Cell Clearance: Basic Biology and Therapeutic Potential. *Nat Rev Immunol* (2014) 14(3):166–80. doi: 10.1038/nri3607
42. Kuang R, Perruche S, Chen W. Apoptotic Cell-Linked Immunoregulation: Implications for Promoting Immune Tolerance in Transplantation. *Cell Biosci* (2015) 5:27. doi: 10.1186/s13578-015-0019-9
43. Neufert C, Becker C, Tureci O, Waldner MJ, Backert I, Floh K, et al. Tumor Fibroblast-Derived Epiregulin Promotes Growth of Colitis-Associated Neoplasms Through ERK. *J Clin Invest* (2013) 123(4):1428–43. doi: 10.1172/JCI63748
44. Stappenbeck TS, Miyoshi H. The Role of Stromal Stem Cells in Tissue Regeneration and Wound Repair. *Science* (2009) 324(5935):1666–9. doi: 10.1126/science.1172687
45. Sturm A, Dignass AU. Epithelial Restitution and Wound Healing in Inflammatory Bowel Disease. *World J Gastroenterol* (2008) 14(3):348–53. doi: 10.3748/wjg.14.348
46. Zigmond E, Bernshtein B, Friedlander G, Walker CR, Yona S, Kim KW, et al. Macrophage-Restricted Interleukin-10 Receptor Deficiency, But Not IL-10 Deficiency, Causes Severe Spontaneous Colitis. *Immunity* (2014) 40(5):720–33. doi: 10.1016/j.immuni.2014.03.012
47. Saas P, Chague C, Maraux M, Cherrier T. Toward the Characterization of Human Pro-Resolving Macrophages? *Front Immunol* (2020) 11:593300. doi: 10.3389/fimmu.2020.593300
48. Nagata S, Hanayama R, Kawane K. Autoimmunity and the Clearance of Dead Cells. *Cell* (2010) 140(5):619–30. doi: 10.1016/j.cell.2010.02.014
49. Morioka S, Maueroder C, Ravichandran KS. Living on the Edge: Efferocytosis at the Interface of Homeostasis and Pathology. *Immunity* (2019) 50(5):1149–62. doi: 10.1016/j.immuni.2019.04.018
50. Sung J, Sodhi CP, Voltaggio L, Hou X, Jia H, Zhou Q, et al. The Recruitment of Extra-Intestinal Cells to the Injured Mucosa Promotes Healing in Radiation Enteritis and Chemical Colitis in a Mouse Parabiosis Model. *Mucosal Immunol* (2019) 12(2):503–17. doi: 10.1038/s41385-018-0123-3
51. Dise RS, Frey MR, Whitehead RH, Polk DB. Epidermal Growth Factor Stimulates Rac Activation Through Src and Phosphatidylinositol 3-Kinase to Promote Colonic Epithelial Cell Migration. *Am J Physiol Gastrointestinal liver Physiol* (2008) 294(1):G276–85. doi: 10.1152/ajpgi.00340.2007
52. Wynn TA, Barron L. Macrophages: Master Regulators of Inflammation and Fibrosis. *Semin liver Dis* (2010) 30(3):245–57. doi: 10.1055/s-0030-1255354
53. Desmouliere A, Geinoz A, Gabbiani F, Gabbiani G. Transforming Growth Factor-Beta 1 Induces Alpha-Smooth Muscle Actin Expression in Granulation Tissue Myofibroblasts and in Quiescent and Growing Cultured Fibroblasts. *J Cell Biol* (1993) 122(1):103–11. doi: 10.1083/jcb.122.1.103
54. Desmouliere A. Factors Influencing Myofibroblast Differentiation During Wound Healing and Fibrosis. *Cell Biol Int* (1995) 19(5):471–6. doi: 10.1006/cbir.1995.1090
55. Postlethwaite AE, Keski-Oja J, Moses HL, Kang AH. Stimulation of the Chemotactic Migration of Human Fibroblasts by Transforming Growth Factor Beta. *J Exp Med* (1987) 165(1):251–6. doi: 10.1084/jem.165.1.251
56. Montesano R, Orci L. Transforming Growth Factor Beta Stimulates Collagen-Matrix Contraction by Fibroblasts: Implications for Wound Healing. *Proc Natl Acad Sci USA* (1988) 85(13):4894–7. doi: 10.1073/pnas.85.13.4894
57. Vannella KM, Wynn TA. Mechanisms of Organ Injury and Repair by Macrophages. *Annu Rev Physiol* (2017) 79:593–617. doi: 10.1146/annurev-physiol-022516-034356
58. Martini E, Krug SM, Siegmund B, Neurath MF, Becker C. Mend Your Fences: The Epithelial Barrier and its Relationship With Mucosal Immunity in Inflammatory Bowel Disease. *Cell Mol Gastroenterol Hepatol* (2017) 4(1):33–46. doi: 10.1016/j.jcmgh.2017.03.007

Conflict of Interest: FB, MC, PS, and SP are shareholders of MED'INN'Pharma SAS. FB, MC, and SP are employed by MED'INN'Pharma SAS which develops the SuperMApo biologic drug candidate.

The remaining authors declare that the research was conducted in the absence of any commercial or financial relationships that could be construed as a potential conflict of interest.

Publisher's Note: All claims expressed in this article are solely those of the authors and do not necessarily represent those of their affiliated organizations, or those of the publisher, the editors and the reviewers. Any product that may be evaluated in this article, or claim that may be made by its manufacturer, is not guaranteed or endorsed by the publisher.

Copyright © 2021 Martin-Rodriguez, Gauthier, Bonnefoy, Couturier, Daoui, Chagué, Valmary-Degano, Gay, Saas and Perruche. This is an open-access article distributed under the terms of the Creative Commons Attribution License (CC BY). The use, distribution or reproduction in other forums is permitted, provided the original author(s) and the copyright owner(s) are credited and that the original publication in this journal is cited, in accordance with accepted academic practice. No use, distribution or reproduction is permitted which does not comply with these terms.

frontiers in Immunology

ORIGINAL RESEARCH
published: 11 February 2022
doi: 10.3389/fimmu.2022.726153

Hypoxia Promotes Neutrophil Survival After Acute Myocardial Infarction

Maximilian Dölling[1,2,3], *Markus Eckstein*[4], *Jeeshan Singh*[1,2], *Christine Schauer*[1,2], *Janina Schoen*[1,2], *Xiaomei Shan*[1,2], *Aline Bozec*[1,2], *Jasmin Knopf*[1,2], *Georg Schett*[1,2], *Luis E. Muñoz*[1,2*†] and *Martin Herrmann*[1,2†]

[1] Department of Internal Medicine 3 - Rheumatology and Immunology, Friedrich-Alexander-University Erlangen-Nürnberg (FAU) and Universitätsklinikum Erlangen, Erlangen, Germany, [2] Deutsches Zentrum für Immuntherapie (DZI), Friedrich-Alexander-University Erlangen-Nürnberg and Universitätsklinikum Erlangen, Erlangen, Germany, [3] Department of Surgery, University Hospital Magdeburg, Magdeburg, Germany, [4] Institut für Pathologie, Universitätsklinikum Erlangen, Friedrich-Alexander-Universität Erlangen-Nürnberg, Erlangen, Germany

OPEN ACCESS

Edited by:
Amiram Ariel,
University of Haifa, Israel

Reviewed by:
Ioannis Mitroulis,
Democritus University of Thrace, Greece
Meraj Alam Khan,
Hospital for Sick Children, Canada
Michal Amit Rahat,
Technion-Israel Institute of Technology, Israel

***Correspondence:**
Luis E. Muñoz
Luis.Munoz@uk-erlangen.de

†These authors have contributed equally to this work and share senior authorship

Specialty section:
This article was submitted to Inflammation, a section of the journal Frontiers in Immunology

Received: *16 June 2021*
Accepted: *24 January 2022*
Published: *11 February 2022*

Citation:
Dölling M, Eckstein M, Singh J, Schauer C, Schoen J, Shan X, Bozec A, Knopf J, Schett G, Muñoz LE and Herrmann M (2022) Hypoxia Promotes Neutrophil Survival After Acute Myocardial Infarction. Front. Immunol. 13:726153. doi: 10.3389/fimmu.2022.726153

Phagocytosis, degranulation, and neutrophil extracellular traps (NETs) formation build the armory of neutrophils for the first line of defense against invading pathogens. All these processes are modulated by the microenvironment including tonicity, pH and oxygen levels. Here we investigated the neutrophil infiltration in cardiac tissue autopsy samples of patients with acute myocardial infarction (AMI) and compared these with tissues from patients with sepsis, endocarditis, dermal inflammation, abscesses and diseases with prominent neutrophil infiltration. We observed many neutrophils infiltrating the heart muscle after myocardial infarction. Most of these had viable morphology and only few showed signs of nuclear de-condensation, a hallmark of early NET formation. The abundance of NETs was the lowest in acute myocardial infarction when compared to other examined diseases. Since cardiac oxygen supply is abruptly abrogated in acute myocardial infarction, we hypothesized that the resulting tissue hypoxia increased the longevity of the neutrophils. Indeed, the viable cells showed increased nuclear hypoxia inducible factor-1α (HIF-1α) content, and only neutrophils with low HIF-1α started the process of NET formation (chromatin de-condensation and nuclear swelling). Prolonged neutrophil survival, increased oxidative burst and reduced NETs formation were reproduced under low oxygen tensions and by HIF-1α stabilization *in vitro*. We conclude that nuclear HIF-1α is associated with prolonged neutrophil survival and enhanced oxidative stress in hypoxic areas of AMI.

Keywords: neutrophils, acute myocardial infarction, hypoxia inducible factor 1, DNA decondensation, NET formation, neutrophil extracellular traps

INTRODUCTION

Neutrophils are the first circulating cells to respond to microbial attacks or tissue damage. They initiate and orchestrate the inflammatory response (1). Besides performing phagocytosis and degranulation, neutrophils are capable to externalize chromatin and form Neutrophil Extracellular Traps (NETs) at sites of inflammation (2). The expelled chromatin is decorated

with a plethora of nuclear and granular proteins; several of these display enzymatic activities. Initially NET formation is proinflammatory, however, at high neutrophil densities the NETs tend to aggregate and form aggregated NETs (aggNETs). The latter are endowed with robust proteolytic activities that degrade various soluble cytokine and toxic compounds in the resolution phase of inflammation (3–5).

During infection, NETs immobilize and kill bacteria, protozoa and fungi and limit their spread (6–10). Besides this beneficial, physiologic role, NETs and aggNETs reportedly also induce adverse effects. Indeed, NETs occlude Meibomian glands (11) and pancreatic ducts (12), promote formation and growth of gallstones (13) and salivary stones (14), and precipitate vasculopathy as well as immunothrombosis in COVID-19 (15). Furthermore, NETs may contribute to septic multi organ failure during tumor thrombosis (16–18) and malaria (19). Dysregulated NET metabolism and chronic persistence of circulating NETs and its degradation products, namely cell-free DNA, citrullinated Histone H3, Myeloperoxidase-/Neutrophil Elastase-DNA complexes, precipitate autoimmunity and inflammatory vessel damage (20–22).

After stimulation of the neutrophil, the NOX2-dependent oxidative burst and mitochondrial production of reactive oxygen species (ROS) are crucial in many pathways of NET formation (23). ROS initiate the disintegration of the nuclear envelope and the granular membranes (24). Although pathways independent of ROS have been described (10), conventional suicidal NET formation largely depends on the capability of the membrane-bound NADPH oxidase and myeloperoxidase (MPO) to produce hydrogen peroxide and its derivatives (25, 26). A sufficient supply with oxygen warrants the continuous formation of NETs in tissues (27). Slightly alkaline microenvironment favors the formation of NETs while acidic conditions are associated with reduced NET formation (28). Tissue hypoxia is often accompanied by a metabolic reprograming that conditions the acidification of the microenvironment. Interestingly, PMA induced NET formation was completely abolished in hypoxia but not NET formation triggered by Staphylococci (29). This indicates a fine regulation of the stimulating signals received by the neutrophil *in vitro*. Very little is known about the influence of tissue hypoxia on neutrophils *in vivo*.

Under normoxia, cytoplasmic hypoxia-inducible factor-1α (HIF-1α) is bound by hydroxyl groups and von Hippel- Lindau protein (VHL) and, consequently, degraded by the proteasome (30). In hypoxia, HIF-1α is protected from degradation by the prolyl hydroxylase domain-containing proteins (PHDs) and accumulates in the nucleus, where it induces the transcription of hypoxia-regulated genes. The most prominent transcripts are vascular endothelia growth factor (VEGF), erythropoietin (EPO) and adrenomedullin (31–33). In neutrophils, HIF-1α induces the transcription of NF-κB, which leads to reduced apoptosis and prolonged survival of neutrophils in hypoxia (34). The role of HIF-1α and hypoxia during NET formation *in vivo* has not been studied yet.

NET formation in normoxia or hypoxia setups was evaluated by (I) stimulation of isolated human peripheral blood neutrophils, and (II) collection of human tissue samples from acute myocardial infarction and other neutrophil-rich diseases without overt hypoxia through immunohistochemical analysis of HIF-1α and neutrophil elastase (NE). We sought to compare the level of expression of HIF-1α in apparently healthy neutrophils with neutrophils displaying already de-condensed nuclei on a single cell level in systematic immunofluorescence analyses of various human tissues.

Here we report that in acute myocardial infarction, a condition of pronounced hypoxia, most neutrophils showed high nuclear levels of HIF-1α and displayed a viable nuclear morphology. In contrast, the neutrophils that had started chromatin decondensation showed a low HIF-1α content. Furthermore, NET formation *in vitro* was reduced under hypoxia and HIF-1α stabilization by two PHDs inhibitors, roxadustat (RXD) and cobalt^{2+} (Co^{2+}). These observations illustrate that hypoxia modulates NET formation *in vitro* and *in vivo* deepening our understanding of the influence of the microenvironment on the biology of neutrophils during initiation and resolution of sterile inflammation.

MATERIAL AND METHODS

Patients

Investigations on human material were performed in accordance with the Declaration of Helsinki and with the approval of the ethical committee of the University Hospital Erlangen (permit 243_15 B and permit 3755). A written informed consent was given by each donor.

Neutrophil Isolation

Heparinized blood (20 U/ml) was drawn and diluted 1:1 with phosphate buffered saline (PBS) without calcium and magnesium (Thermo Fisher Scientific, Waltham, MS, US) and centrifuged at 350 RCF for 30 min at room temperature on a Ficoll (Bio-Rad, 824012, Dreieich, Germany) density gradient. The polymorphonuclear cells (PMNs) are separated from mononuclear cells forming a layer on the top of the red blood cells. PMNs were collected and subjected to 2 short cycles of hypotonic lysis with 36 ml deionized water. Osmolarity was restituted after 20 s with the addition of 4 ml 10 x PBS. Isolated PMNs containing more than 98% of neutrophils were suspended in PBS without calcium and magnesium and used for *in vitro* experiments immediately.

Normoxia and Hypoxia

Buffer medium R_0 consisting of RPMI 1640 containing 24 mM $NaHCO_3$ (Gibco Thermo Fisher Scientific) and supplemented with 1 mM $CaCl_2$ was equilibrated to pH 7.4 by incubation for 24 hours in a 5 % CO_2 atmosphere. With the addition of 24 mM of $NaHCO_3$ the pH was adjusted to 7.8. All buffers were equilibrated at 37°C, 5 % CO_2 at 20 % oxygen for normoxia and at 2 % oxygen for hypoxia for 24 hours in a Heracell CO2 Incubator (ThermoFisher Scientific, Rockford, USA) or in the Whitley H35 hypoxystation (Meintrup-DWS, Bingley, UK) before starting the experiments, respectively.

HIF-1α Stabilization

Equilibrated R_0 medium was used to incubate the isolated neutrophils in R_0 with 5μM Roxadustat for 30 min prior to the addition of the stimuli (RXD; Selleckchem, Houston, USA) or in the presence of cobalt chloride (Co^{2+}, Sigma-Aldrich C8661, Taufkirchen, Germany) at the indicated concentrations during the stimulation period. RXD is an inhibitor of the prolyl hydroxylase domain-containing proteins (PHDs) which hydroxylates HIF-1α avoiding its ubiquitination and proteasome degradation (30). Co^{2+} oxidates ascorbate which is essential to reduce Fe^{3+} to Fe^{2+} in the catalytic sites of PHDs, thus inhibiting its activity and stabilizing HIF-1α in cells (35, 36).

NET Assays

The sytox DNA externalization assay was employed to quantify the amount of DNA expelled by the neutrophils during NET-formation. Briefly, neutrophils (150,000/well) were seeded in 96-well plates (Greiner, flat bottom transparent polystyrene plate) in R_0 buffer. The membrane impermeable DNA-dye sytox green was added (3.2 μM) just before starting the incubation at the indicated conditions. Extracellular trap formation was triggered by addition of LPS from *Klebsiella pneumoniae* at 2.5 μg/ml, PMA at 10 ng/ml, Ionomycin at 5μg/ml and 24 mM bicarbonate (pH 7.8) in R_0 buffer medium. The increase of the sytox green fluorescence (ΔF) emitted at 525nm after 4 hours of incubation was recorded with the plate reader Infinite F200 Pro fluorometer (TECAN, Männedorf, Swiss). NET formation was confirmed by indirect immunofluorescence staining of neutrophils cultured on chamber slides under the same conditions. The percentage of inhibition of NET formation by various concentrations of Co^{2+} was calculated relative the ΔF of sytox green of those wells without Co^{2+}.

Indirect Immunofluorescence

Tissue samples from autopsies or biopsies were fixed in 4% formalin, dehydrated and embedded in paraffin blocks. Three μm sections were mounted and dried on Superfrost Plus slides (Thermo Fisher Scientific, Waltham, MS, US). Sections were dewaxed by incubation at 64°C for 1 hour. Paraffin residues were washed out in multiple steps with a solution containing decreasing concentrations of RotiHistol (Roth Chemie GmbH, Karlsruhe, Germany). Sections were rehydrated with Isopropanol following by incubation at 90°C for 20 min in Epitope Retrieval Solution (50 mM sodium citrate, pH 6). Chamber slides containing *in vitro* stimulated neutrophils were washed with PBS and fixed with 4% paraformaldehyde. Sections and chamber slides were then rinsed with deionized water, and permeabilized for 5 min with 0.5 % Triton X100 in PBS at RT.

The fixed slides were treated with blocking buffer (PBS supplemented with 1 % BSA; 2 % goat serum; 0.05 % Tween 20; 0.5 % Triton X100) for 2 h. Unconjugated primary antibodies (**Table 1**) were diluted in blocking buffer and incubated on the slides over night at 4°C. On the next day, the slides were washed with deionized water twice and rinsed with PBS once. Secondary antibodies (**Table 1**) were mixed with propidium iodide (PI, Sigma, P4641) for co-staining of DNA in blocking buffer. The mixture was added for 1.5 h at RT in darkness. Slides were rinsed three times with PBS, and embedded in DAKO fluorescent mounting medium (BIOZOL, Eching, Germany). Analysis was performed employing a BZ-X710 fluorescence microscope (Keyence, Neu-Isenburg, Germany) and (Nikon GmbH, Düsseldorf, Germany). We conducted Z-stacks in order to increase depth and to improve the visualization of NETs on these images. Images were post-processed using Photoshop CS6 (Adobe, München, Germany).

Apoptosis Detection by Flow Cytometry

For the quantification of cell viability and apoptosis, neutrophils incubated under normoxia and hypoxic conditions for 4 hours were stained with annexin A5 (AxA5-FITC) and propidium iodide (PI). In brief, 100 μl of cell suspension was incubated for 30 min at 4°C with 400 μl Ringer`s solution (Braun) containing 0.5 μg/ml AxA5-FITC 2 μg/ml PI (Sigma-Aldrich). Then, cells were analyzed with a Gallios™ flow cytometer (Beckman Coulter, Hialeah, FL). FITC fluorescence was excited with 488 nm and recorded on a fluorescence 1 (FL1) channel (525 nm BP 40). PI fluorescence was excited with 488 nm and recorded on a fluorescence 3 (FL3) channel (620 nm BP 30). Data were processed with Kaluza™ software, version 2.1, after electronic compensation to eliminate bleed through of fluorescence. At least three independent experiments, each in triplicates, were performed. Acquired neutrophils were classified in viable (AxA5/PI negative), apoptotic (AxA5 positive/PI negative), and necrotic (AxA5 positive/PI positive) cells, respectively.

Oxygen Saturation of Culture Medium in a Cell-Free System

In order to determine the reduction of oxygen saturation of medium, we employed 96-well microplates Oxoplates® with integrated chemical optical oxygen sensors (Pressens,

TABLE 1 | Antibodies used in immune fluorescence.

	Serial number	Company
Primary antibodies		
Rabbit anti-human neutrophil elastase; 1:100	ab68672	Abcam, United Kingdom
Rabbit anti-human anti-HIF-1α 1:100	Orb378857	Biorbyt, Cambridge, United Kingdom
Secondary antibodies		
Cy5-conjungated goat anti-rabbit IgG; 1:400	111-175-144	Jackson ImmunoResearch, Suffolk, United Kingdom
AF647-Goat anti-Rabbit IgG (H+L) Invitrogen (1:400)	ab150079	Abcam, United Kingdom

Regensburg, Germany). Oxygen saturated medium with and without 100µM ascorbate (Sigma-Aldrich, A92902, Taufkirchen, Germany) was incubated with the indicated concentrations of Co^{2+} for 1 hour. The percentage of oxygen saturation was calculated according manufacturer instructions after measuring the fluorescence from two filter pairs for the indicator (excitation: 535 nm, emission: 680 nm) and reference dye (excitation: 540 nm, emission: 590 nm).

Quantification of Reactive Oxygen Species by Flow Cytometry

For the measurement of intracellular ROS, isolated neutrophils were loaded for 20 minutes with 2 µM CM-H2DCFDA (ThermoFisher) at in PBS. For the measurement of mitochondrial ROS, isolated neutrophils were loaded for 10 minutes with 5 µM MitoSOX™ (ThermoFisher) in PBS. The ROS produced by the neutrophils was calculated as the fold increase of the fluorescence detected by the FL1 (525 nm BP 40) and FL2 (575 BP 30) channels of the Gallios Flow Cytometer upon stimulation with 100 ng/ml PMA for 30 minutes.

Cytomorphometry

Distribution and co-localization of fluorescence signals of immunofluorescence images were processed using self-generated macros for Photoshop CS6. Staining, magnification, exposure, and processing were identically performed for all samples. Positive samples and negative controls were simultaneously co-processed. Regions infiltrated with neutrophils (neutrophil elastase) of various pathologies were selected and the grey levels of Cy5 and PI were recorded. Signals with a grey level less than 4 were considered remaining background signal and not included in the analysis. Neutrophil elastase positive areas were classified according to its appearance as either condensed multilobulated neutrophils (viable neutrophils) or as diffuse extracellular NE pattern (NET aggregates). The ratio of the area of the NE-signal associated with lobulated nuclei to the total area of the elastase signal defined the % area of neutrophil elastase in viable neutrophils. The ratio of the area of the NE-signal associated with NET aggregates to the total area of the elastase signal defined the % area of neutrophil elastase of NET aggregates. Various forms of neutrophils and NETs were observed and are described and summarized in the **Table 2**. The HIF-1α fluorescence in myocardial tissues was also quantified recording the grey value (MFI) of the pixels co-localizing with PI fluorescence. The nuclear area of each leukocyte was quantified by the pixel area of PI fluorescence. A Pearson correlation analysis between the HIF-1α fluorescence intensity and the nuclear area of the leukocyte infiltrates was performed.

Data Presentation and Statistical Analysis

Quantitative results are displayed as means and individual values. If not indicated otherwise, two-way analyses of variance (ANOVAs) were used for establishing statistical differences among groups. In case of multiple comparisons, either Sidak's or Tukey´s multiple comparisons tests were applied. Statistical analysis was performed with the software GraphPad Prism 6.0 (GraphPad Software, USA).

RESULTS

Morphologies of Tissue Neutrophils

We stained tissue sections from various diseases for DNA with PI (red) and for neutrophil elastase (green). The most representative nuclei that were associated with neutrophil elastase signals were selected for a composite image showing various forms of appearance of neutrophil in tissues (**Figure 1**). The specificity of the anti-neutrophil elastase antibody was confirmed in non-infiltrated areas of the same section (**Supplementary Figure 1**). The nuclei of viable neutrophils showed a lobulated morphology with cytoplasmic neutrophil elastase (**Figure 1**, column 1). Some neutrophils had swollen nuclei and showed extracellular spreading of neutrophil elastase (signs of degranulation). In some cases neutrophil elastase remnants were found associated to the nuclear membrane (columns 2-3). Various steps of chromatin externalization of NET forming neutrophils were observed (columns 4-9): DNA decondensation, nuclear swelling and increase of cellular diameter (4), deformation of the nucleus (5, 6), and mixture of chromatin with granular enzymes (7). Finally, spreading of chromatin and aggregation of neutrophils without NETs (8) or in aggregated NETs (9). Interestingly, the predominant morphologic form of neutrophils varied among the investigated diseases. The main morphological features of tissue neutrophils are summarized in **Table 2**.

TABLE 2 | Morphological forms of tissue neutrophils and NETs.

Morphologic form	Features
Viable neutrophils	Many granules with 0.0025-0.25 µm²; granular cytoplasmic elastase not-colocalizing with nuclear chromatin; no or inactive cytoplasmic HIF-1α; 90-100 µm²
Degranulated neutrophils	Few granules; granular cytoplasmic elastase not-colocalizing with nuclear chromatin; no or inactive cytoplasmic HIF-1α; 90-100 µm²
Granules	High levels of elastase; no DNA; 0.0025-0.25 µm²
Neutrophils with decondensed chromatin in hypoxic areas	Low active nuclear HIF-1α; 100-200 µm²
Viable neutrophils in hypoxic areas	High active nuclear HIF-1α; 90-100 µm²
NETs	Granular cytoplasmic elastase colocalizing with extranuclear chromatin; 400-1000 µm²
NET aggregates	Granular cytoplasmic elastase colocalizing with extranuclear chromatin; can extend almost unlimited

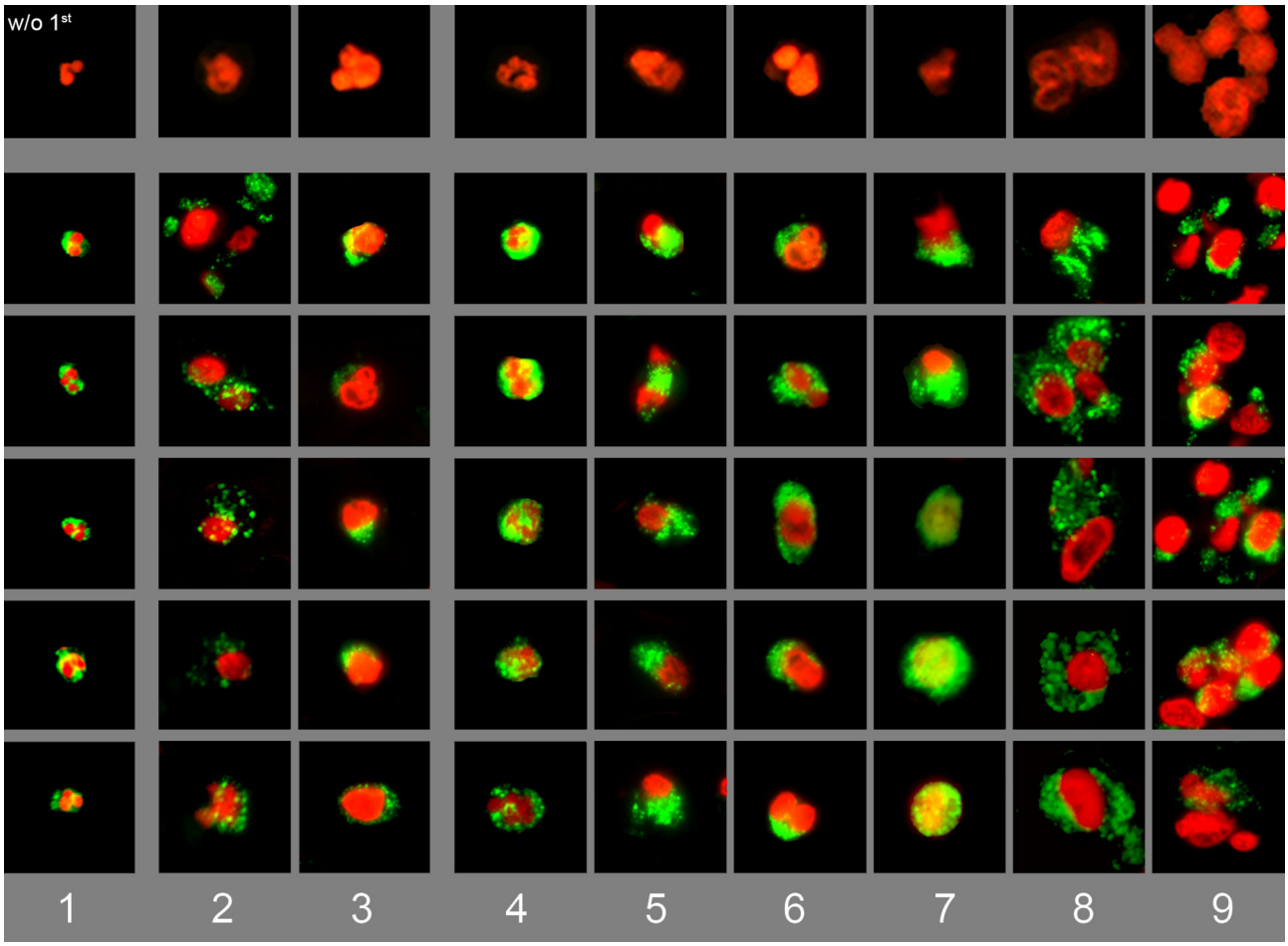

FIGURE 1 | Composite image of various stages of degranulation or NET formation of tissue neutrophils. Immunofluorescence staining of various biopsies for DNA with PI (red) and for neutrophil elastase (green). Various types of tissue neutrophils were identified and classified in a composite image showing (1) viable neutrophils, (2) chromatin decondensation and spreading of granular content, (3) highly decondensed chromatin with associated granular remnants. (4-9) various steps of chromatin externalization: (4) nuclear swelling and increase of cellular diameter, (5-6) loss of nuclear shape, (7) mixture of DNA with granular enzymes, and (8-9) aggregation of swollen neutrophils with and without chromatin externalization. The upper panel shows selected nuclei from slides lacking of the first antibody. Each individual field represent 50 x 50 µm.

A total of 145 tissue samples of 67 patients with various diseases (**Table 3**) were stained for DNA (PI) and neutrophil elastase. In acute myocardial infarction, a disease with tissue damage caused by severe hypoxia, the DNA of most neutrophils (PI; red) displayed a condensed multilobulated nuclear appearance and neutrophil elastase (immune fluorescence; green) was invariably found in the cytoplasmic granules (**Figure 2A**). We consider these cells viable neutrophils. In contrast, in abscesses (**Figures 2B, J**), acute pancreatitis (**Figure 2D**), infectious endocarditis (**Figures 2E, F**), COVID-19 (**Figure 2K**) and many more conditions (**Figures 2B–L**; **Table 3**) the neutrophil elastase appeared often diffuse and associated or not with extracellular chromatin/DNA. This suggests abundant degranulation and/or formation of neutrophil extracellular traps.

The cytomorphometric analyses showed that viable neutrophils with cytoplasmic pattern of neutrophil elastase immunostaining dominated the sections of patients with acute myocardial infarction (**Figure 3**). Whereas only few viable neutrophils were to be detected in the other diseases ($p < 0.0001$). In all other pathologies analyzed mostly diffuse neutrophil elastase immunostaining associated or not with extracellular chromatin/DNA was observed ($p < 0.0001$).

NET Formation Under Hypoxia and Stabilized HIF-1α

We aimed to quantify NET formation triggered by ionomycin, PMA, LPS and pH 7.8 in hypoxia and normoxia (2 % and 21 % O_2, respectively). We confirmed in the first instance that neutrophils treated with the mentioned stimuli formed NETs. Spread extracellular DNA were decorated with neutrophil elastase identified as NETs in immunostainings of neutrophil cultures (**Figure 4A**). In order to quantify changes in the ability to form NETs, a sytox green-based DNA-externalization assay

TABLE 3 | Neutrophil-driven diseases included in this study.

Pathology	Number of sections	Number of patients
Acute myocardial infarction	25	7
Infectious endocarditis	23	5
Abscesses*	22	6
Thrombosis in COVID-19 infection**	22	6
Acute pancreatitis	20	4
Dermal inflammation***	12	12
Infiltrated dental calculin	14	14
Granuloma	6	3
Abdominal aortic aneurysm	5	5
Sjögren Syndrome	4	4
Liver failure in COVID 19	4	1
Total	**145**	**67**

**Several abscesses were included from different sites of the body: dermal abscess (1), liver abscess (1), perianal abscess (1), perimandibular abscess (1), pharyngeal abscess (1), and sinus pilonidalis abscess (1).*

***Thrombosis in COVID-19 patients were found in central lungs (6), peripheral lungs (9) and in the kidneys (7).*

****Dermal inflammation included sections from following pathologies: pemphigoid (2), psoriasis pustulosa (4), and systemic lupus erythematodes (6).*

was employed. In normoxia, PMA, LPS, elevated pH as well as ionomycin induced robust DNA externalization when compared to the unstimulated condition ($p = 0.0093$, $p = 0.0205$, $p = 0.0116$ and $p = 0.0514$ in the ANOVA corrected by Tukey´s multiple comparisons, respectively). Under conditions of hypoxia DNA externalization was partially abrogated. Neither PMA ($p = 0.302$), LPS ($p = 0.838$), elevated pH ($p = 0.441$) nor ionomycin ($p = 0.097$) induced significant DNA externalization when compared to the unstimulated condition. Furthermore, the intensity of DNA externalization induced under hypoxia was significantly lower than those measured under normoxic conditions (**Figure 4B**). We further analyzed induced DNA externalization after treatment with RXD, an inhibitor of PHDs, which hydroxylates HIF-1α avoiding its ubiquitination and proteasome degradation. The stabilization of HIF-1α led to a partial but significant reduction of DNA release after simulation with PMA, LPS, pH 7.8 and ionomycin (**Figure 4C**). We also stabilized HIF-1α by Co^{2+} which catalyzes the oxidation of ascorbate, favouring the Fe^{3+} redox state, inactivating PHD activity and stabilizing HIF-1α (35, 36).

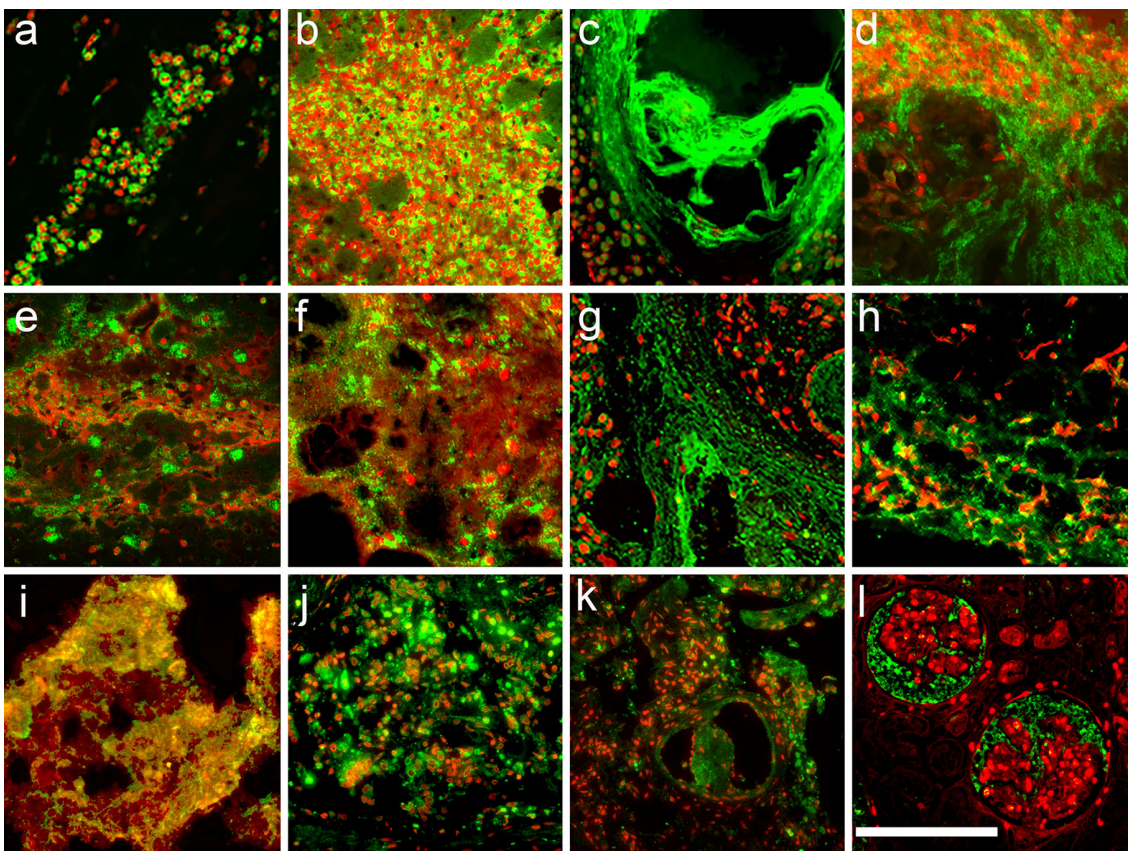

FIGURE 2 | Viable neutrophils dominate samples from acute myocardial infarction. Immunofluorescence microphotographs of histological sections of various pathologies stained for neutrophil elastase (green) and counterstained for DNA (PI; red). Note, in acute myocardial infarction **(A)** neutrophils showed lobulated nuclei, cytoplasmic granular elastase and little extracellular DNA, indicating viable neutrophils. In contrast, in hepatic abscess **(B)**, inflamed dermal tissue in systemic lupus erythematodes **(C)**, acute pancreatitis **(D)**, infectious endocarditis **(E, F)**, Sjögren syndrome **(G)**, abdominal aortic aneurysm **(H)**, infiltrated dental calculi **(I)**, sinus pilonidalis abscess **(J)**, vascular plugs in the lungs of COVID-19 **(K)**, and glomerulonephritis in COVID-19 **(L)** most neutrophils have formed NETs or NET aggregates. The size bar represents 200 µm.

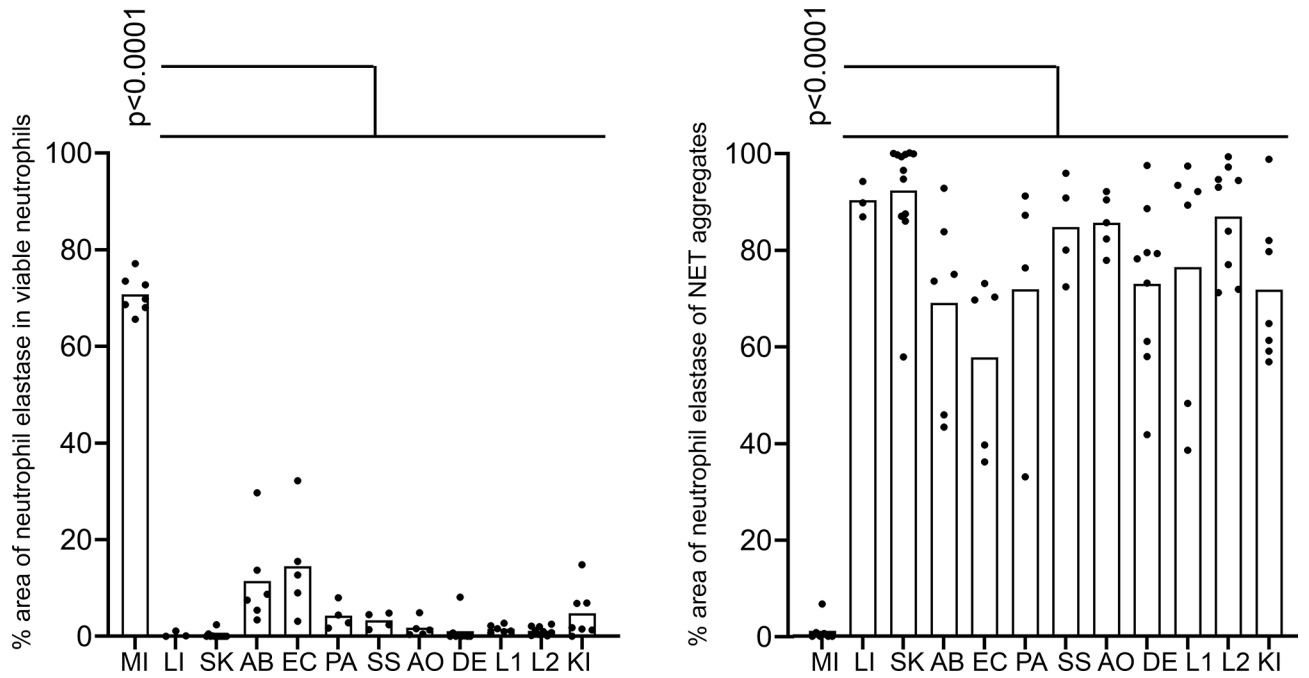

FIGURE 3 | Pattern of neutrophil elastase in various tissues. Cytomorphometry of viable neutrophils and NETs (aggregates) found in tissue sections described in **Table 1** and exemplarily shown in **Figure 2**: MI, acute myocardial infarction; LI, liver of a patient with severe COVID-19; SK, epidermal inflammation; AB, abscesses; EC, heart muscle of patients with infective endocarditis; PA, pancreatitis; SS, lip salivary glands of patients with Sjögren's syndrome; AO neutrophil infiltrates of patients with aortic aneurysms; DE, dental calculi infiltrated by neutrophils; L1, vascular plugs in the central lung of patients with COVID-19; L2, vascular plugs in the peripheral lung of patients with COVID-19; KI, renal thrombosis in patients with COVID-19. Note that in acute myocardial infarction tissue neutrophils remained predominantly viable compared to other diseases ($p < 0.0001$). Conversely, neutrophils formed large amounts of aggregates in all other diseases, but not in acute myocardial infarction ($p < 0.0001$). The p values are from a two-way ANOVA after Tukey´s multiple testing correction.

A doses-dependent inhibition by Co^{2+} of NET formation was observed in the DNA-externalization experiments (**Figure 4D**) without significant reduction of the viability of neutrophils (**Figure 4E**). Interestingly, the reduction of the oxygen saturation induced by the Co^{2+}-dependent oxidation of ascorbate in the cell-free assays fairly overlaps with the inhibition of NET formation (**Figure 4F**). Additionally, we confirmed that under hypoxic conditions neutrophils are rescued from the spontaneous apoptosis and that most of the neutrophils retained their membrane integrity during the indicated incubation times (**Figure 4G**). Notably, hypoxia not only prolonged the lifespan of neutrophils *in vitro*, it also fostered the production of ROS in the cytoplasma without affecting the oxidative burst in the mitochondria of isolated neutrophils as measured by the probes CM-H2DCFDA and MitoSOX (**Figure 4H**).

Next, serial tissue sections of patients with acute myocardial infarction were immunostained for nuclear HIF-1α, neutrophil elastase and DNA (**Figure 5A**). The cytomorphometry analysis showed that neutrophils with viable appearance contained more nuclear HIF-1α than those with decondensed nuclei (**Figures 5B, C**; $p < 0.0001$). The correlation analysis after Pearson showed a significant inverse correlation between the intensity of HIF-1α and the nuclear area of myocardial neutrophils (r -0.5574, $p < 0.0001$).

DISCUSSION

The main function of NETs is to form surrogate barriers against invading pathogens during acute phase of inflammation (8). Additionally, NETs are endowed with potent intrinsic anti-microbial and anti-inflammatory activities that result vital for tissue homeostasis (3). The formation of NETs suppose the destruction of the neutrophil and the loss of other important defensive functions like degranulation and phagocytosis. Our systematic observational study of various pathologies demonstrates that NETs are found in tissues without overt ischemia and are practically absent in the ischemic myocardium. We sought therefore to evaluate the factors contributing to the decision of the neutrophil to form NETs based on the pattern of appearance of neutrophils, NETs and HIF-1α, the key factor in cell response to hypoxia, in human tissues.

Under hypoxia, HIF-1α is stabilized and transferred into the nucleus of neutrophils. This results in an increase of NF-κB, which mediates neutrophil survival and cytokine transcription (34). Our *in vitro* data indicate that low oxygen tension and nuclear HIF-1α strongly reduce the capacity of neutrophils to form NETs, prolong survival and favor the production of cytoplasmic ROS. This is in line with previous investigations showing that elevated expression of HIF-1α in neutrophils promotes their phagocytotic capabilities and prolongs their survival (37).

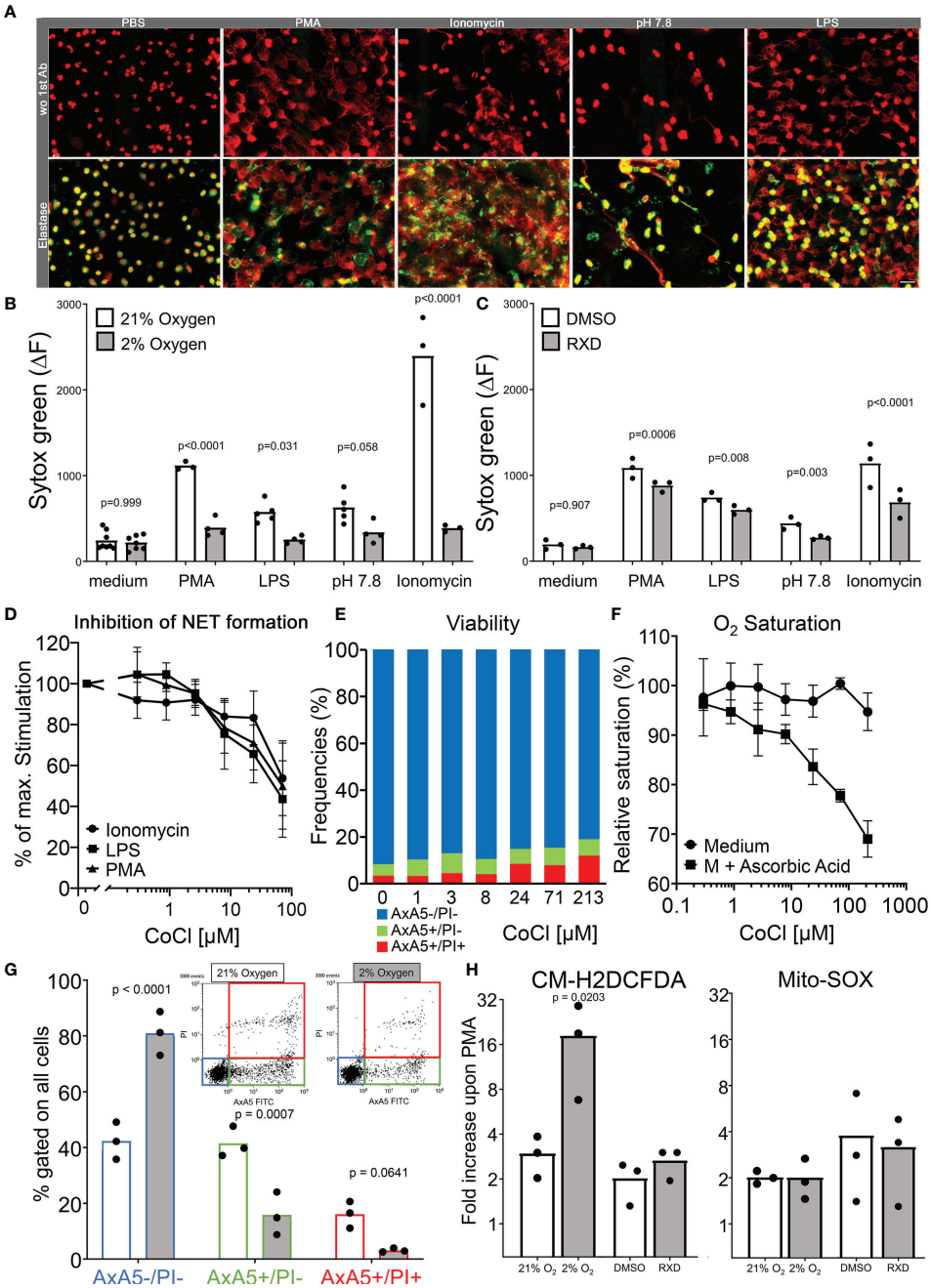

FIGURE 4 | Modulation of neutrophil functions during hypoxia. Immunofluorescence stainings of stimulated neutrophils in chamber slides showing nuclear decondensation, DNA spreading and colocalization of neutrophil elastase with extracellular DNA **(A)**. The quantification of NET formation in hypoxia and normoxia was done by DNA externalization. The delta of the Sytox green fluorescence between 0 and 4 hours of incubation in normoxia and hypoxia is shown in **(B)** and after HIF-1α stabilization (RXD) in **(C)**. Doses-dependent inhibition of NET formation by Co^{2+} in sytox assays after stimulation with Ionomycin, LPS and PMA **(D)**. Frequencies of viable (AxA5-/PI-), apoptotic (AxA5+/PI-), and necrotic (AxA5+/PI+) neutrophils after 4 hours incubation in medium with increasing concentrations of Co^{2+} **(E)**. The oxygen saturation of medium in the presence of increasing concentrations of Co^{2+} after the oxidation of ascorbic acid for 1 hour **(F)**. The proportion of viable (AxA5-/PI-), apoptotic (AxA5+/PI-), and necrotic (AxA5+/PI+) neutrophils after 4 hours incubation in normoxia and hypoxia are shown in **(G)**. The production of ROS in the cytoplasma (CM-H2DCFDA) and mitochondria (MitoSOX) of neutrophils was measured upon PMA stimulation under hypoxia and HIF-1α stabilization. Displayed are the fold increase of the fluorescence of the indicated ROS sensors upon PMN stimulation after 30 minutes incubation **(H)**. Results were obtained from at least 3 independent experiments with 3 to 4 different blood donors. The p values are from a two way ANOVA after Sidak´s multiple testing correction.

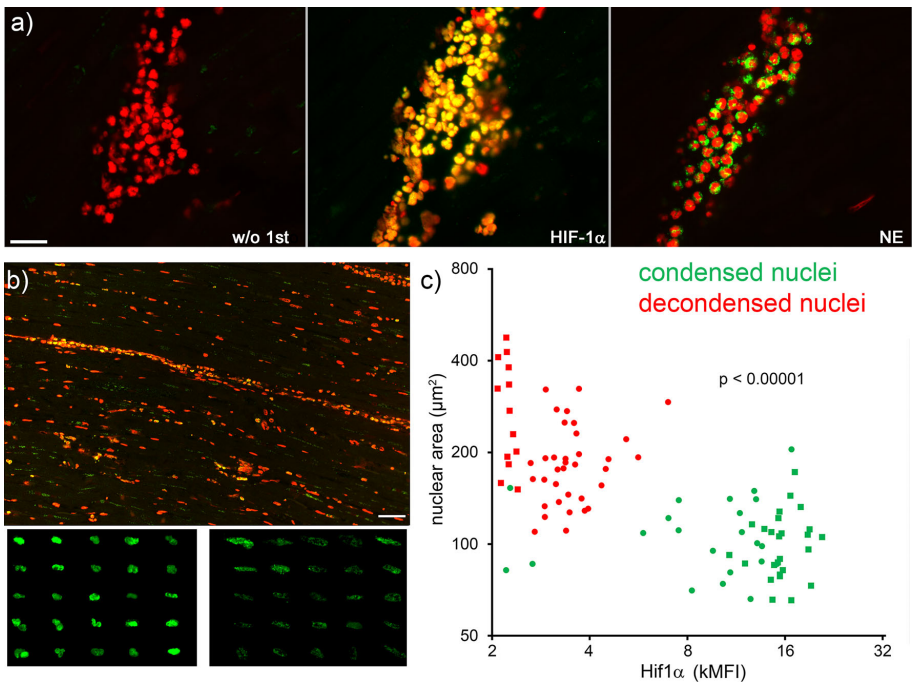

FIGURE 5 | Neutrophils with high nuclear levels of HIF-1α under hypoxia display viable morphologies. Serial slices of neutrophil infiltrates of ischemic areas of human acute myocardial infarction were stained by immunofluorescence for HIF-1α (green), neutrophil elastase (NE, green) and DNA (PI, red) **(A)**. Overview (**B**, upper panel) and composite details (B, lower panels) of HIF-1α positive nuclei. The size bar represents 400 µm. Neutrophils with condensed nuclei (viable) showed bright HIF-1α staining (**B**, left lower panel), whereas neutrophils with decondensed nuclei (early stage of NET formation) contained less HIF-1α (**B**, right lower panel). The pattern and intensity of HIF-1α inversely correlated (*Pearson r* -0.5574, p <0.0001) with the nuclear area of neutrophils **(C)**. Round and square dots distinguish the sample of AMI analyzed (two samples). MFI, mean fluorescence intensity.

We confirmed in the human AMI that neutrophils displaying a viable multilobulated nuclei express high levels of HIF-1α in their nuclei. Conversely, low levels of nuclear HIF-1α were associated with DNA decondensation, an early step NET formation. Under hypoxic conditions, neutrophils exhibit elevated release of matrix metalloproteinase-9, lactoferrin, myeloperoxidase, and elastase suggesting increased degranulation and enhanced tissue damage potential (38). Branitzki-Heinemann et al. failed detecting up-regulation of the expression of HIF-1α in neutrophils exposed to hypoxia (29). HIF-1α nuclear translocation is reportedly required to maintain degranulation and chemotaxis active in neutrophils during hypoxia (39) while cytoplasmic HIF-1α is required for LPS induced NET formation (40). We see a clear nuclear accumulation of HIF-1α in dense multilobulated neutrophil nuclei *in vivo* and inhibition of NET formation at low oxygen tension and with the chemical stabilization of HIF-1α *in vitro*.

The chemical stabilization of HIF-1α simulates transcriptional responses of cells exposed to low oxygen tensions. Oxygen, ascorbate and 2-oxoglutarate are required to maintain Fe^{2+} in PHDs in a chain of well-balanced redox reactions (41). The amount of Co^{2+} required for the oxidation of ascorbate is directly proportional to the lack of oxygen. This assumption allows us to extrapolate the level of hypoxia required to inhibit NET formation by measuring the amount of oxygen consumed in the medium during the oxidation of ascorbate by Co^{2+}. In this fashion, we observed a reduction of 20% of the NET formation by Co^{2+} with the same concentration of Co^{2+} that caused 20% reduction of the oxygen saturation of the medium. In terms of oxygen tension in the medium this would be around 120 mmHg pO_2. Further experiments are needed to confirm this approximation.

Our observations along with the published data suggest specific roles of HIF-1α according to its subcellular localization in neutrophils. The main limitation of our observational study is the natural bias derived from unilateral observations. However, we have demonstrated with standard research tools and employing appropriate controls that neutrophils have different appearances in different human tissues and diseases. The molecular mechanism behind this particular behavior of neutrophils need further investigations in both, *in vitro* and *in vivo* models of ischemic disease.

In our experiments, the ability to produce ROS in the mitochondria of neutrophils was not affected by low oxygen tensions. Cytoplasmic oxidative burst was contrarily enhanced under hypoxia. This means that atmospheric oxygen is dispensable for the oxidative metabolism of the neutrophil and suggest that compensatory metabolic pathways are engaged to maintain neutrophil functions active at sites with low oxygen availability. It has been reported that the stabilization of HIF-1α up-regulate the pentose phosphate pathway ensuring the cytoplasmic supply of NADPH (42–44). Furthermore, the pharmacological activation of the glycolytic pathway through the phosphofructokinase-1 liver type,

as it occurs during hypoxia, inhibits NET formation (45). In sum, low oxygen tensions prompt neutrophils to cause tissue damage through a sustained degranulation and secretion of reactive oxygen species and a reduction of pro-resolving NETs.

The decision between neutrophil survival and NET formation is also influenced by the equilibrium among CO_2, bicarbonate and pH. NETs are readily externalized under conditions with high pH and a high ratio between HCO_3^- and CO_2, less NETs are formed under low pH (28). During ischemia, oxygen levels are diminished and the environmental pH is decreased (46). In myocardial infarction neutrophils are attracted by cell debris and inflammatory signals released by activated neighboring cells and massively infiltrate the infarcted area in the first few hours following onset of ischemia (47). Our observations on AMI demonstrate that neutrophils do not externalize chromatin at sites of ischemia and hypothesize that they remain active being able to remove cell debris or releasing matrix-degrading enzymes and reactive oxygen species. This concurs in a weakening of myocardial extracellular matrix and enhancement of the infarct area (48). Elevated rates of complications after AMI such as ventricular wall rupture or papillary muscle disruption are associated with neutrophil infiltration (49), indicating a pivotal role of neutrophils in wound healing and scar formation (50). Since the aggregation of NETs have been reported to degrade inflammatory mediators (3) and sequester proteolytic enzymes (51), we suggest that the lack of NET formation contributes the prolonged inflammatory insult to the myocardium in AMI.

AUTHOR'S NOTE

The present work was performed in fulfillment of the requirements for obtaining the degree, Dr. med." Maximilian Dölling.

DATA AVAILABILITY STATEMENT

The original contributions presented in the study are included in the article/**Supplementary Material**. Further inquiries can be directed to the corresponding author.

ETHICS STATEMENT

Investigations on human material were performed in accordance with the Declaration of Helsinki and with the approval of the ethical committee of the University Hospital Erlangen (permit 243_15 B and permit 3755). A written informed consent was given by each donor. The patients/participants provided their written informed consent to participate in this study.

AUTHOR CONTRIBUTIONS

MD and ME conducted autopsies, performed general pathological analysis, coordinated patient sample acquisition and acquired ethical approval of the study. MD, JSc, XS and JSi performed immunofluorescence staining and performed tissue neutrophil studies. MD and MH processed the images. JSi, XS, JSc and CS performed *in vitro* hypoxia experiments. JK, AB, CS, LM and MH supervised experiments and made data and statistical analyses. LM, AB, GS and MH conceived the study. All authors provided scientific input, wrote, read and approved the manuscript.

FUNDING

This work was partially supported by the German Research Foundation (DFG) 2886 PANDORA Project-No.B3; SCHA 2040/1-1; CRC1181(C03); TRR241(B04), by the EU ERC-Synergy grant 4D Nanoscope and by H2020-FETOPEN-2018-2019-2020-01; 861878„NeutroCure", and by the Volkswagen-Stiftung (Grant 97744).

SUPPLEMENTARY MATERIAL

The Supplementary Material for this article can be found online at: https://www.frontiersin.org/articles/10.3389/fimmu.2022.726153/full#supplementary-material

REFERENCES

1. Kolaczkowska E, Kubes P. Neutrophil Recruitment and Function in Health and Inflammation. *Nat Rev Immunol* (2013) 13:159–75. doi: 10.1038/nri3399
2. Fuchs TA, Abed U, Goosmann C, Hurwitz R, Schulze I, Wahn V, et al. Novel Cell Death Program Leads to Neutrophil Extracellular Traps. *J Cell Biol* (2007) 176:231–41. doi: 10.1083/jcb.200606027
3. Schauer C, Janko C, Munoz LE, Zhao Y, Kienhofer D, Frey B, et al. Aggregated Neutrophil Extracellular Traps Limit Inflammation by Degrading Cytokines and Chemokines. *Nat Med* (2014) 20:511–7. doi: 10.1038/nm.3547
4. Knopf J, Leppkes M, Schett G, Herrmann M, Munoz LE. Aggregated NETs Sequester and Detoxify Extracellular Histones. *Front Immunol* (2019) 10:2176. doi: 10.3389/fimmu.2019.02176
5. Hahn J, Schauer C, Czegley C, Kling L, Petru L, Schmid B, et al. Aggregated Neutrophil Extracellular Traps Resolve Inflammation by Proteolysis of Cytokines and Chemokines and Protection From Antiproteases. *FASEB J* (2019) 33:1401–14. doi: 10.1096/fj.201800752R
6. Brinkmann V, Reichard U, Goosmann C, Fauler B, Uhlemann Y, Weiss DS, et al. Neutrophil Extracellular Traps Kill Bacteria. *Science* (2004) 303:1532–5. doi: 10.1126/science.1092385
7. Abi Abdallah DS, Denkers EY. Neutrophils Cast Extracellular Traps in Response to Protozoan Parasites. *Front Immunol* (2012) 3:382. doi: 10.3389/fimmu.2012.00382
8. Urban CF, Reichard U, Brinkmann V, Zychlinsky A. Neutrophil Extracellular Traps Capture and Kill Candida Albicans Yeast and Hyphal Forms. *Cell Microbiol* (2006) 8:668–76. doi: 10.1111/j.1462-5822.2005.00659.x
9. Clark SR, Ma AC, Tavener SA, McDonald B, Goodarzi Z, Kelly MM, et al. Platelet TLR4 Activates Neutrophil Extracellular Traps to Ensnare Bacteria in Septic Blood. *Nat Med* (2007) 13:463–9. doi: 10.1038/nm1565
10. Yipp BG, Kubes P. NETosis: How Vital is it? *Blood* (2013) 122:2784–94. doi: 10.1182/blood-2013-04-457671
11. Mahajan A, Hasikova L, Hampel U, Gruneboom A, Shan X, Herrmann I, et al. Aggregated Neutrophil Extracellular Traps Occlude Meibomian Glands During Ocular Surface Inflammation. *Ocul Surf* (2021) 20:1–12. doi: 10.1016/j.jtos.2020.12.005

12. Leppkes M, Maueroder C, Hirth S, Nowecki S, Gunther C, Billmeier U, et al. Externalized Decondensed Neutrophil Chromatin Occludes Pancreatic Ducts and Drives Pancreatitis. *Nat Commun* (2016) 7:10973. doi: 10.1038/ncomms10973
13. Munoz LE, Boeltz S, Bilyy R, Schauer C, Mahajan A, Widulin N, et al. Neutrophil Extracellular Traps Initiate Gallstone Formation. *Immunity* (2019) 51:443–450 e4. doi: 10.1016/j.immuni.2019.07.002
14. Schapher M, Koch M, Weidner D, Scholz M, Wirtz S, Mahajan A, et al. Neutrophil Extracellular Traps Promote the Development and Growth of Human Salivary Stones. *Cells* (2020) 9(9):2139. doi: 10.3390/cells9092139
15. Leppkes M, Knopf J, Naschberger E, Lindemann A, Singh J, Herrmann I, et al. Vascular Occlusion by Neutrophil Extracellular Traps in COVID-19. *EBioMedicine* (2020) 58:102925. doi: 10.1016/j.ebiom.2020.102925
16. Xu J, Zhang X, Pelayo R, Monestier M, Ammollo CT, Semeraro F, et al. Extracellular Histones are Major Mediators of Death in Sepsis. *Nat Med* (2009) 15:1318–21. doi: 10.1038/nm.2053
17. Engelmann B, Massberg S. Thrombosis as an Intravascular Effector of Innate Immunity. *Nat Rev Immunol* (2013) 13:34–45. doi: 10.1038/nri3345
18. Demers M, Wagner DD. NETosis: A New Factor in Tumor Progression and Cancer-Associated Thrombosis. *Semin Thromb Hemost* (2014) 40:277–83. doi: 10.1055/s-0034-1370765
19. Boeltz S, Munoz LE, Fuchs TA, Herrmann M. Neutrophil Extracellular Traps Open the Pandora's Box in Severe Malaria. *Front Immunol* (2017) 8:874. doi: 10.3389/fimmu.2017.00874
20. Hakkim A, Fuchs TA, Martinez NE, Hess S, Prinz H, Zychlinsky A, et al. Activation of the Raf-MEK-ERK Pathway is Required for Neutrophil Extracellular Trap Formation. *Nat Chem Biol* (2011) 7:75–7. doi: 10.1038/nchembio.496
21. Soderberg D, Kurz T, Motamedi A, Hellmark T, Eriksson P, Segelmark M. Increased Levels of Neutrophil Extracellular Trap Remnants in the Circulation of Patients With Small Vessel Vasculitis, But an Inverse Correlation to Anti-Neutrophil Cytoplasmic Antibodies During Remission. *Rheumatol (Oxford)* (2015) 54:2085–94. doi: 10.1093/rheumatology/kev217
22. Mahajan A, Herrmann M, Munoz LE. Clearance Deficiency and Cell Death Pathways: A Model for the Pathogenesis of SLE. *Front Immunol* (2016) 7:35. doi: 10.3389/fimmu.2016.00035
23. Stoiber W, Obermayer A, Steinbacher P, Krautgartner WD. The Role of Reactive Oxygen Species (ROS) in the Formation of Extracellular Traps (ETs) in Humans. *Biomolecules* (2015) 5:702–23. doi: 10.3390/biom5020702
24. Kirchner T, Moller S, Klinger M, Solbach W, Laskay T, Behnen M. The Impact of Various Reactive Oxygen Species on the Formation of Neutrophil Extracellular Traps. *Mediators Inflammation* (2012) 2012:849136. doi: 10.1155/2012/849136
25. Papayannopoulos V, Metzler KD, Hakkim A, Zychlinsky A. Neutrophil Elastase and Myeloperoxidase Regulate the Formation of Neutrophil Extracellular Traps. *J Cell Biol* (2010) 191:677–91. doi: 10.1083/jcb.201006052
26. Metzler KD, Goosmann C, Lubojemska A, Zychlinsky A, Papayannopoulos V. A Myeloperoxidase-Containing Complex Regulates Neutrophil Elastase Release and Actin Dynamics During NETosis. *Cell Rep* (2014) 8:883–96. doi: 10.1016/j.celrep.2014.06.044
27. Nishinaka Y, Arai T, Adachi S, Takaori-Kondo A, Yamashita K. Singlet Oxygen is Essential for Neutrophil Extracellular Trap Formation. *Biochem Biophys Res Commun* (2011) 413:75–9. doi: 10.1016/j.bbrc.2011.08.052
28. Maueroder C, Mahajan A, Paulus S, Gosswein S, Hahn J, Kienhofer D, et al. Menage-A-Trois: The Ratio of Bicarbonate to CO2 and the pH Regulate the Capacity of Neutrophils to Form NETs. *Front Immunol* (2016) 7:583. doi: 10.3389/fimmu.2016.00583
29. Branitzki-Heinemann K, Mollerherm H, Vollger L, Husein DM, de Buhr N, Blodkamp S, et al. Formation of Neutrophil Extracellular Traps Under Low Oxygen Level. *Front Immunol* (2016) 7:518. doi: 10.3389/fimmu.2016.00518
30. Cockman ME, Masson N, Mole DR, Jaakkola P, Chang GW, Clifford SC, et al. Hypoxia Inducible Factor-Alpha Binding and Ubiquitylation by the Von Hippel-Lindau Tumor Suppressor Protein. *J Biol Chem* (2000) 275:25733–41. doi: 10.1074/jbc.M002740200
31. Semenza GL. Regulation of Mammalian O2 Homeostasis by Hypoxia-Inducible Factor 1. *Annu Rev Cell Dev Biol* (1999) 15:551–78. doi: 10.1146/annurev.cellbio.15.1.551
32. Metzen E, Berchner-Pfannschmidt U, Stengel P, Marxsen JH, Stolze I, Klinger M, et al. Intracellular Localisation of Human HIF-1 Alpha Hydroxylases: Implications for Oxygen Sensing. *J Cell Sci* (2003) 116:1319–26. doi: 10.1242/jcs.00318
33. Wenger RH. Cellular Adaptation to Hypoxia: O2-Sensing Protein Hydroxylases, Hypoxia-Inducible Transcription Factors, and O2-Regulated Gene Expression. *FASEB J* (2002) 16:1151–62. doi: 10.1096/fj.01-0944rev
34. Walmsley SR, Print C, Farahi N, Peyssonnaux C, Johnson RS, Cramer T, et al. Hypoxia-Induced Neutrophil Survival is Mediated by HIF-1alpha-Dependent NF-kappaB Activity. *J Exp Med* (2005) 201:105–15. doi: 10.1084/jem.20040624
35. Kaczmarek M, Cachau RE, Topol IA, Kasprzak KS, Ghio A, Salnikow K. Metal Ions-Stimulated Iron Oxidation in Hydroxylases Facilitates Stabilization of HIF-1 Alpha Protein. *Toxicol Sci* (2009) 107:394–403. doi: 10.1093/toxsci/kfn251
36. Munoz-Sanchez J, Chanez-Cardenas ME. The Use of Cobalt Chloride as a Chemical Hypoxia Model. *J Appl Toxicol* (2019) 39:556–70. doi: 10.1002/jat.3749
37. Walmsley SR, Cowburn AS, Clatworthy MR, Morrell NW, Roper EC, Singleton V, et al. Neutrophils From Patients With Heterozygous Germline Mutations in the Von Hippel Lindau Protein (pVHL) Display Delayed Apoptosis and Enhanced Bacterial Phagocytosis. *Blood* (2006) 108:3176–8. doi: 10.1182/blood-2006-04-018796
38. Hoenderdos K, Lodge KM, Hirst RA, Chen C, Palazzo SG, Emerenciana A, et al. Hypoxia Upregulates Neutrophil Degranulation and Potential for Tissue Injury. *Thorax* (2016) 71:1030–8. doi: 10.1136/thoraxjnl-2015-207604
39. McGovern NN, Cowburn AS, Porter L, Walmsley SR, Summers C, Thompson AAR, et al. Hypoxia Selectively Inhibits Respiratory Burst Activity and Killing of Staphylococcus Aureus in Human Neutrophils. *J Immunol* (2011) 186:453–63. doi: 10.4049/jimmunol.1002213
40. McInturff AM, Cody MJ, Elliott EA, Glenn JW, Rowley JW, Rondina MT, et al. Mammalian Target of Rapamycin Regulates Neutrophil Extracellular Trap Formation *via* Induction of Hypoxia-Inducible Factor 1 Alpha. *Blood* (2012) 120:3118–25. doi: 10.1182/blood-2012-01-405993
41. Bruick RK, McKnight SL. A Conserved Family of Prolyl-4-Hydroxylases That Modify HIF. *Science* (2001) 294:1337–40. doi: 10.1126/science.1066373
42. Curi R, Levada-Pires AC, Silva EBD, Poma SO, Zambonatto RF, Domenech P, et al. The Critical Role of Cell Metabolism for Essential Neutrophil Functions. *Cell Physiol Biochem* (2020) 54:629–47. doi: 10.33594/000000245
43. Sadiku P, Walmsley SR. Hypoxia and the Regulation of Myeloid Cell Metabolic Imprinting: Consequences for the Inflammatory Response. *EMBO Rep* (2019) 20:e47388. doi: 10.15252/embr.201847388
44. Cramer T, Yamanishi Y, Clausen BE, Forster I, Pawlinski R, Mackman N, et al. HIF-1alpha is Essential for Myeloid Cell-Mediated Inflammation. *Cell* (2003) 112:645–57. doi: 10.1016/S0092-8674(03)00154-5
45. Amara N, Cooper MP, Voronkova MA, Webb BA, Lynch EM, Kollman JM, et al. Selective Activation of PFKL Suppresses the Phagocytic Oxidative Burst. *Cell* (2021) 184:4480–4494 e15. doi: 10.1016/j.cell.2021.07.004
46. Graham RM, Frazier DP, Thompson JW, Haliko S, Li H, Wasserlauf BJ, et al. A Unique Pathway of Cardiac Myocyte Death Caused by Hypoxia-Acidosis. *J Exp Biol* (2004) 207:3189–200. doi: 10.1242/jeb.01109
47. Puhl SL, Steffens S. Neutrophils in Post-Myocardial Infarction Inflammation: Damage vs. Resolution? *Front Cardiovasc Med* (2019) 6:25. doi: 10.3389/fcvm.2019.00025
48. Carbone F, Nencioni A, Mach F, Vuilleumier N, Montecucco F. Pathophysiological Role of Neutrophils in Acute Myocardial Infarction. *Thromb Haemost* (2013) 110:501–14. doi: 10.1160/TH13-03-0211
49. Zidar N, Jeruc J, Balazic J, Stajer D. Neutrophils in Human Myocardial Infarction With Rupture of the Free Wall. *Cardiovasc Pathol* (2005) 14:247–50. doi: 10.1016/j.carpath.2005.04.002
50. Ipek G, Onuk T, Karatas MB, Gungor B, Atasoy I, Murat A, et al. Relationship Between Neutrophil-To-Lymphocyte Ratio and Left Ventricular Free Wall Rupture in Acute Myocardial Infarction. *Cardiology* (2015) 132:105–10. doi: 10.1159/000431354
51. Podolska MJ, Mahajan A, Hahn J, Knopf J, Maueroder C, Petru L, et al. Treatment With DNases Rescues Hidden Neutrophil Elastase From Aggregated NETs. *J Leukoc Biol* (2019) 106:1359–66. doi: 10.1002/JLB.3AB0918-370R

Conflict of Interest: The authors declare that the research was conducted in the absence of any commercial or financial relationships that could be construed as a potential conflict of interest.

Publisher's Note: All claims expressed in this article are solely those of the authors and do not necessarily represent those of their affiliated organizations, or those of the publisher, the editors and the reviewers. Any product that may be evaluated in

this article, or claim that may be made by its manufacturer, is not guaranteed or endorsed by the publisher.

Copyright © 2022 Dölling, Eckstein, Singh, Schauer, Schoen, Shan, Bozec, Knopf, Schett, Muñoz and Herrmann. This is an open-access article distributed under the terms of the Creative Commons Attribution License (CC BY). The use, distribution or reproduction in other forums is permitted, provided the original author(s) and the copyright owner(s) are credited and that the original publication in this journal is cited, in accordance with accepted academic practice. No use, distribution or reproduction is permitted which does not comply with these terms.

Advantages of publishing in Frontiers

OPEN ACCESS
Articles are free to read for greatest visibility and readership

FAST PUBLICATION
Around 90 days from submission to decision

HIGH QUALITY PEER-REVIEW
Rigorous, collaborative, and constructive peer-review

TRANSPARENT PEER-REVIEW
Editors and reviewers acknowledged by name on published articles

Frontiers
Avenue du Tribunal-Fédéral 34
1005 Lausanne | Switzerland

Visit us: www.frontiersin.org
Contact us: frontiersin.org/about/contact

REPRODUCIBILITY OF RESEARCH
Support open data and methods to enhance research reproducibility

DIGITAL PUBLISHING
Articles designed for optimal readership across devices

FOLLOW US
@frontiersin

IMPACT METRICS
Advanced article metrics track visibility across digital media

EXTENSIVE PROMOTION
Marketing and promotion of impactful research

LOOP RESEARCH NETWORK
Our network increases your article's readership